NIST Special Publication 1246

Assessing the Predictive Capability for Real-Scale Residential Upholstered Furniture Mock-Up Fires using Cone Calorimeter Measurements. Part 1: Real-Scale Experiments

William M. Pitts
Martin Werrel
Marco Fernandez
Mary A. Long
Evan A Eisenberg
James Filliben
Cory D. Runyon

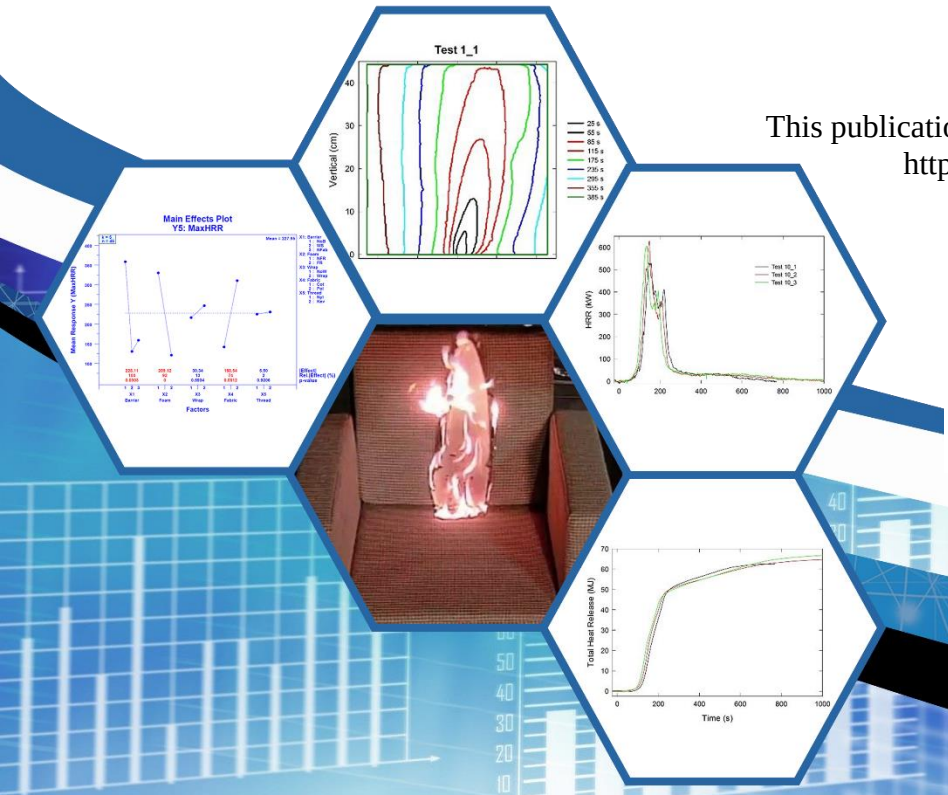

This publication is available free of charge from:
https://doi.org/10.6028/NIST.SP.1246

National Institute of Standards and Technology
U.S. Department of Commerce

NIST Special Publication 1246

Assessing the Predictive Capability for Real-Scale Residential Upholstered Furniture Mock-Up Fires using Cone Calorimeter Measurements. Part 1: Real-Scale Experiments

William M. Pitts, Martin Werrel, Marco Fernandez, Mary A. Long, and Evan A Eisenberg
Fire Research Division
Engineering Laboratory

James Filliben
Statistical Engineering Division
Information Technology Laboratory

Cory D. Runyon
PCNA Consulting Group, Inc.
205 E. Warm Springs Rd. Ste. 105 Las Vegas, NV 89119

This publication is available free of charge from:
https://doi.org/10.6028/NIST.SP.1246

February 2020

U.S. Department of Commerce
Wilbur L. Ross, Jr., Secretary

National Institute of Standards and Technology
Walter Copan, NIST Director and Undersecretary of Commerce for Standards and Technology

National Institute of Standards and Technology Special Publication 1246
Natl. Inst. Stand. Technol. Spec. Publ. 1246, 589 pages (February 2020)
CODEN: NSPUE2

This publication is available free of charge from:
https://doi.org/10.6028/NIST.SP.1246

Abstract

This is the first of three reports describing a study designed to assess the feasibility of utilizing small-scale measurements in a cone calorimeter as inputs for predicting the burning (flaming) behavior of real-scale residential upholstered furniture (RUF). Here the focus is the experimental approach and results for the real-scale experiments. A literature review provides the rationale for our interest in RUF and summarizes previous efforts to characterize and regulate its burning behavior. The RUF items considered are mock-ups consisting of four cushions arranged in a chair configuration and mounted on a metal stand. The effects on burning behavior of changes in five types of materials—Fire Barrier, Polyurethane Foam, Polyester Fiber Wrap, Upholstery Cover Fabric, and Sewing Thread—previously identified as possibly affecting RUF burning are considered. Four of the material factors have two conditions, while Barrier has three (i.e., no barrier, or one of two barrier types). A reduced factorial design utilizing 20 different material combinations is used along with a minimum of two repeats for each combination. The experimental behaviors of interest are flame spread (characterized by time-resolved flame edge contours on the back and seat cushions) and fire growth (characterized by heat release rate measurements). A variety of parameters are used to characterize the temporal variations of both. Graphical representations of the results suggest that three of the factors (Barrier, Foam, and Fabric) have easily identified effects on mock-up burning behavior. This finding is confirmed by a variety of analyses showing these three factors have statistically significant effects on mock-up burning behaviors, with Barrier and Fabric having strong and roughly equal effects and Foam somewhat weaker effects. Changes in Fiber Wrap or Thread result in no statistically significant effects on the parameters. It is also shown that interactions between Barrier and Foam are statistically significant and will need to be considered in approaches designed to predict burning behavior. In addition to characterization of flame spread and fire growth, supplementary measurements of mass and radiative heat flux at six locations around the mock-ups provide additional insights concerning mock-up burning behavior. The real-scale results are compared to previous studies to provide additional understanding of RUF burning. and its dependence on material properties.

Key Words

fire barriers; flame spread rate; flexible polyurethane foam; heat release rate; mock-ups; polyester fiber wrap; residential upholstered furniture; sewing thread; statistical analysis; thermal radiation

Table of Contents

List of Figures

List of Tables

List of Symbols and Abbreviations

Symbols

a_{bv}	Characteristic vertical flame spread acceleration on back cushion of RUF mock-up (cm/s^2)
$FIGRA_{max}$	Maximum FIGRA recorded during an experiment (kW/s)
$FIGRA_{peak1}$	FIGRA value for initial peak (kW/s)
$FWHM_{>25}$	Full width at half maximum for HHR curve between times t_{+25} and t_{-25} (s)
$HRR_{avg>25}$	Average HRR during period HRR was greater than 25 kW, i.e., $Q_{>25}/(t_{-25}-t_{+25})$ (kW)
HRR_{max}	Maximum HRR recorded during an experiment (kW)
HRR_{peak1}	HRR value for initial peak (kW)
H0	Null hypothesis of "no primary factor effect"
$\dot{m}$	Mass loss rate of burning RUF item (g/s)
m_z	Slope of line for $(q_{max})_z$ versus HRR_{max} for heat flux gauge located z cm from mock-up
n	Number of trials
Q_{25}	Heat released between t_{+25} and t_{-25} (MJ)
q_{max}	Maximum heat flux recorded by gauge during burning of a RUF mock-up (kW/m^2)
q_z	Radiative heat flux at distance z from burning RUF item (kW/m^2)
p	Probability of success in a binomial distribution
R_u	Ratio of $\bar{u}_l$ and $\bar{u}_t$
R_{ut}	Ratio of $(u_{st})_{edge}$ and $\bar{u}_t$
R^2	Coefficient of determination for linear least squares curve fit
s	Standard deviation
sm	Standard deviation of the mean
SF_t	Shape Factor #1 for HRR curves defined as the ratio of $FWHM_{>25}$ and $t_{>25}$
SF_{HRR}	Shape Factor #2 for HRR curves defined as the ratio of $HRR_{max}/HRR_{avg>25}$
t	Time (s)
t	95 % confidence interval expansion factor
t_{back}	Time required for flames to spread completely over back surface (s)
t_{FIGRA1}	Time of initial FIGRA maximum (s)
$t_{FIGRAmax}$	Time of maximum FIGRA (s)
t_{ig}	Characteristic arm ignition time given by average of t_{igl} and t_{igr} (s)
t_{igl}	Time of flame spread onto left arm of a mock-up (s)
t_{igr}	Time of flame spread onto right arm of a mock-up (s)
t_{max}	Time of maximum HRR (s)
t_p	Time of peak HHR (s)
t_{peak1}	Time of the initial HRR maximum (s)
t_{seat}	Time required for flames to spread completely over seat surface (s)
t_0	Time when line extrapolated between HRRs at t_p and t_1 equals 0 kW (s)
t_1	Time when HRR first reaches 100 kW (s)
t_2	Time when HRR first falls below 100 kW (s)
t_{-25}	Time (final) when the HRR of a burning mock-up drops below 25 kW (s)
t_{+25}	Time when the HRR of a burning mock-up first reaches 25 kW (s)
$t_{>25}$	Time period when the HRR remained above 25 kW, i.e, t_{+25} - t_{-25} (s)
t_3	Time when line extrapolated between HRRs at t_p and t_2 equals 0 kW (s)
u_{bl}	Characteristic lateral flame spread rate on back cushion of RUF mock-up (cm/s)
u_{bv}	Characteristic vertical flame spread rate on back cushion of RUF mock-up (cm/s)
u_l	Characteristic lateral velocity determined by averaging u_{bl} and u_{sl} (cm/s)
u_{sl}	Characteristic lateral flame spread rate on seat cushion of RUF mock-up (cm/s)
u_{st}	Characteristic transverse flame spread rate on seat cushion of RUF mock-up (cm/s)
$(u_{st})_{edge}$	Transverse velocity on seat cushion as fire approached cushion edge (cm/s)
$\bar{u}_t$	Average transverse velocity on seat cushion between ignition and arm flaming (cm/s)

x	Horizontal component in physical space on two-dimensional surface in image (cm)
Xi	Factor used in statistical analysis of experimental results, i = 1 to 5
y	Vertical component in physical space on two-dimensional surface in image (cm)
Yj	Experimental response considered in statistical analysis, j =1 to 13
z	Distance between the outer edge of a mock-up and a heat flux gauge (cm)
α	Statistical significance level
overbar	Average value
´	Standard deviation value

Abbreviations

78%PP/22%PE	78 % polypropylene/22 % polyester
ANOVA	Analysis of variance
ANPR	Advanced Notice of Proposed Rule Making
ASET	available safe egress time
ASTM E1537	ASTM International Standard E1537
ATF	Bureau of Alcohol, Tobacco, Firearms and Explosives
BEAR-HFTI	Bureau of Electronic and Appliance Repair, Home Furnishings and Thermal Insulation
BS-5852	British Standard 5852
CBHF	California Bureau of Home Furnishings
CBUF	Combustion Behavior of Upholstered Furniture
Cal TB-117	California Technical Bulletin 117
Cal TB-133	California Technical Bulletin 133
CMHR	Combustion-modified high resilient
CPSC	Consumer Product Safety Commission
CSIRO	Commonwealth Scientific and Industrial Research Organisation
EHOC	Effective heat of combustion
FIGRA	Fire growth rate
FPUF	Flexible polyurethane foam
FR	Fire retarded
FRFPUF	Fire-retarded flexible polyurethane foam
FRL	Fire Research Laboratory
FTIR	Fourier transform infrared
FPC	Fire Products Collector
HFG	Heat flux gauge
HR	High resilient
HRFPUF	High resilient flexible polyurethane foam
HRR	Heat release rate
ILD	Indentation load defection
ISO	International Organization for Standardization
MBR	Medium Burn Room
MLR	Mass loss rate
NASFM	National Association of State Fire Marshalls
NBS	National Bureau of Standards
NFR	Non fire retarded
NFRFPUF	Non-fire-retarded flexible polyurethane foam
NFRL	National Fire Research Laboratory
NFIRS	National Fire Incident Reporting System
NFPA	National Fire Protection Association
NIST	National Institute of Standards and Technology
NPR	Notice of Proposed Rulemaking
PEFW	Polyester fiber wrap

PHHR	Peak heat release rate
RGB	Red-green-blue (color model based on additive color primaries)
RIP	Reduced ignition propensity
RUF	Residential upholstered furniture
SI-1324	Statutory Instrument 1324
TDI	Toluene diisocyanate
UFAC	Upholstered Furniture Action Council

Executive Summary

This manuscript is the first of three planned reports describing a study of the feasibility of predicting the burning (flaming) behavior of residential upholstered furniture (RUF) mock-ups formed from four upholstered cushions using the results of small-scale experiments performed in a cone calorimeter. The current manuscript describes the results of full-scale experiments using the RUF mock-ups. The second report will provide comparable findings for the small-scale experiments. The third and final report will assess the degree of correlation between the small-scale and large-scale experiments and thus the feasibility of predicting the large-scale results based on the small-scale experiments.

Section 1 provides background material and a literature review of studies related to RUF. It begins with brief summaries of the origin of concerns regarding the contribution of RUF to fire losses starting in the 1960s and subsequent historical proposals for regulating the flammability characteristics of furniture. The focus is on the experimental approaches used, the role of material changes in RUF flammability, and fundamental understanding of RUF burning behavior. Roughly forty different studies are discussed. The last part of this section discusses recent characterizations of the RUF flammability problem in the United States with a focus on traditional measures of the losses associated with fires starting on RUF and their magnitude, the development of a new approach for estimating losses associated with fires starting on other items in a residence that act as ignition sources for RUF items that then play a major role in subsequent fire growth, and the controversy that has arisen with the recognition that many fire retardants often added to RUF to meet the original California TB-117 furniture flammability standard can have detrimental human health and environmental effects, while providing little or no practical improvement in RUF burning behavior.

Section 2 discusses the experimental design for the real-scale mock-up tests. Actual RUF incorporates literally thousands of different combinations of materials, so broad coverage was not feasible. The approach adopted is to consider five classes (referred to as factors) of possible materials: Fire Barrier Condition, Foam, use of Polyester Fiber Wrap, Cover Fabric, and Sewing Thread chosen based on previous research and known furniture manufacturing practice. Materials for use in each class are chosen with the goal of maximizing the likelihood of identifying statistically significant effects on the experimental responses chosen to characterize mock-up burning behavior.

The types of materials chosen for each factor are shown in the following table:

Upholstery Material	Polyurethane Foam	Polyester Fiber Wrap	Fire Barrier	Fire Barriers	Sewing Thread
Thermo-plastic	Standard, non-FR	Yes	Yes	High-loft, non-woven FR-fiber	Thermoplastic
Cellulosic	FR, meets British SI-1324	No	No	Fire resistant woven fabric	Fire resistant

FR=fire retarded

Note that four of the five factors have two levels, with only Fire Barrier having three, i.e., none or one of two barriers.

Based on the table, the total number of combinations possible for a full-factorial test design is 3×2×2×2×2 = 48. It is generally desirable to have a minimum of three repeated tests for each combination of factors. A full-factorial design would have required a total of 144 tests. Such an extensive test matrix was deemed

too costly in time and money, so the decision was made to reduce the number of tests by employing a balanced reduced-factorial design of 24 material combinations and only performing two repeats for each. Ultimately, it was recognized that combining a high-loft barrier and a polyester fiber wrap was impractical, and these four combinations were not tested. Thus, the final test matrix includes 20 different material combinations in a slightly unbalanced partial factorial design

Section 3 discusses experimental details. The mock-ups were formed by mounting two 45.7 cm × 45.7 cm × 10.2 cm (seat and back) and two 35.6 cm × 45.7 cm × 10.2 cm (arms) cushions in a chair configuration on a metal test stand. The specific materials used to construct the four cushions for a given mock-up based on the table above are described. Mock-ups were ignited by placing an ignition source at the center of the crevice formed by the intersection of the seat and back cushions. A small gas flame designed to represent a burning match was applied for 20 s. If substantial burning of the mock-up was not observed, this was followed by application of a somewhat stronger gas flame for forty seconds. Finally, if substantial flame spread still did not occur, a small burning wood crib was applied.

Numerous fire measurements can be used to characterize mock-up burning behavior. The decision was made to focus on the broad areas of flame spread (characterized based on time-resolved flame edge contours) and fire growth (parameters based on time-resolved heat release rate (HRR) measurements). Flame spread contours as a function of time on the seat and back cushions were derived from video recordings from the front of the mock-up (back cushion) and from a 45° overhead angle (seat cushion). Seven additional video cameras, including an infrared camera, and a still camera were used to visually record the fire behavior.

Time-resolved HRR measurements were made using the 1 MW Fire Product Collector (FPC) system located at the Bureau of Alcohol, Tobacco, Firearms, and Explosives ATF Fire Research Laboratory. This "furniture calorimeter" is designed to measure time-resolved HRRs for fires ranging in size from a few tens of kW up to 1 MW.

Mock-up mass using a load cell and radiative heat flux measurements at two distances along three orthogonal directions from the mock-ups using Schmidt-Bolter total heat flux gauges were recorded to provide supplemental characterization of mock-up burning behavior.

Section 4 discusses the data analysis procedures employed. The HRRs and time-resolved flame spread contours serve as the primary bases for analysis. Time-resolved HRRs were calculated using standard FPC protocols. The HRR data were also used to calculate the time-resolved fire growth rate (FIGRA), defined as the HRR divided by the time since ignition. Novel analysis procedures developed to determine time-resolved flame contours from videos of the burning mock-ups are described in detail. The flame contours were used to determine transverse, i.e., direction perpendicular to the crevice formed by the seat and back cushions, flame spread rate on the seat cushion, upward flame spread rate on the back cushion, and averaged lateral flame spread rates; i.e., average of the two spread rates parallel to the crevice away from the ignition location and toward the cushion edges, on the seat and back cushions as a function of time. Additional insights concerning flame spread were obtained by noting the times that flames first ignited the interiors of the mock-up arms.

Secondary time-resolved data measured or derived from measurements include mock-up mass, mass-loss rate, effective heat of combustion, defined as the HRR divided by mass loss rate, and radiative heat flux.

Section 5 summarizes the experimental results including observed ignition behavior and plots of time-resolved HRR, FIGRA, mass, mass-loss rate, effective heat of combustion, seat and back cushion flame contours, and radiative heat flux levels. The flame contours were used to generate time-resolved upward flame spread rate on the back cushion, averaged lateral flame spread rates on the seat and back cushions,

transverse flame spread rate on the seat cushion, and burned areas on the back and seat cushions. Plots of the time-resolved results for each test are included in Appendix A.

The various experimental measurements were used as the basis for subsequent analysis. Ignition behavior was characterized in terms of whether a given ignition source resulted in sustained burning of a mock-up. It became apparent that mock-ups covered with thermoplastic fabric were ignited much more easily by an open flame ignition source than those covered in the cellulosic fabric. In many cases, ignition was observed on the back cushion but not on the seat. In some of these cases, flames spreading on the back cushions would ultimately spread to the seat and continue to spread. In others, the flames burned to the top of the back cushion and extinguished, leaving the seat cushion unaffected. In such cases the next stronger ignition source was applied.

It is typical to determine one or more derived single-value parameters, generally based on the observed behaviors, to characterize experimental temporal profiles such as those described above. Comparisons showed substantial variations in the HRR profiles among the different mock-ups. In an attempt to characterize these differences, a total of 13 parameters: 1) Time required to reach 25 kW (t_{+25}), 2) Time of first HRR maximum (t_{peak1}), 3) Value of first HRR maximum (HRR_{peak1}), 4) Time of maximum HRR (t_{max}), 5) Value of maximum HRR (HRR_{max}), 6) Time HRR falls below 25 kW (t_{-25}), 7) Period during which HRR > 25 kW ($t_{>25}$), 8) Heat released while HRR > 25 kW ($Q_{>25}$), 9) Average HRR while above 25 kW ($HRR_{avg>25}$), 10) Full width at half maximum above 25 kW ($FWHM_{>25}$), 11) Shape factor #1 ($FWHM_{>25}/t_{>25}$), 12) Shape factor #2 ($HRR_{max}/HRR_{avg>25}$), and 13) Total heat released (Q_{tot}) were considered. Values of these parameters are summarized in Appendix B for individual tests along with averaged values and standard deviations for each mock-up combination.

In order to provide insights into the effects of changing materials on mock-up burning behavior, averaged values of the parameters were plotted as functions of mock-up combination number. The experimental design makes its straight forward to visually identify variations associated with changes in materials. Generally strong variations were evident in Parameters 1 to 12 with changes in Barrier Condition, Foam, and particularly Cover Fabric. Effects due to changes in the Polyester Fiber Wrap and Sewing Thread were much less evident.

Some of the largest variations in the parameters between combinations are shown to be due to variations in the burning behavior of liquid frequently observed being released from the mock-up cushions onto the substrate surface below. In some tests, very intense burning developed at this location, while in others either substantial liquid was not released or did not develop intense burning.

The results for total heat release differed substantially from the parameters based on the HRR temporal profiles. The largest variations are found for combinations differing in the Foam factor, with Barrier Condition and Fabric resulting in smaller effects.

The FIGRA temporal profiles are characterized in terms of the values and times required to reach an initial peak and the corresponding values for maximum, i.e., analogues of Parameters 2-5 for HRR. The FIGRA parameter variations between combinations have similar dependencies on Barrier Condition, Foam, and Cover Fabric, but relative changes are generally somewhat greater compared to those based on HRR.

Percentages of mockup mass loss after burning are plotted as a function of combination number. Generally, if a mock-up burned, a substantial fraction of mass was lost. There is an evident trend showing that mock-ups containing FR-FPUF were less likely to burn substantially, and when burning did occur the percentage of mass loss was lower.

The effective heats of combustions were time averaged during periods when the HHR was greater than 25 kW. In general, the variations with combination number are relatively small, with the only obvious effect being due to the Foam factor.

The second primary focus of the experiments was flame spread immediately following ignition. Several different qualitative flame spread behaviors were observed and are summarized. One involves fires in which flames spread rapidly up the back cushion in a relatively narrow band, while relatively slower spreading flames moved laterally in two directions on the seat and back cushions and transversely on the seat with comparable rates. A second type of burn pattern was observed in multiple tests where flames spread along the crevice formed by the two cushions, but spread only part way up the back cushion, while spreading more rapidly in the lateral direction than the transverse direction on the seat cushion. A third qualitative type of flame spread involved very erratic and slow spread with convoluted flame fronts.

Time-resolved measurements based on the flame contours of upward flame spread rate on the back cushion, average lateral flame spread rates on the back and seat cushions, and transverse flame spread rate on the seat cushion generally extended until the mock-up arms became involved, with the single exception being the transverse flame measurements on the seat cushion which continued until the spreading flames reached the outside seat cushion edge.

For many of the fires in which flames spread to the top of back cushion, it was observed that the rate increased roughly linearly with time. This implies a constant flame acceleration, which was calculated using linear least squares curve fits. Plots of vertical flame acceleration versus combination number reveal that most of the mock-ups where such flame spread occurred were covered with cellulosic fabric. However, the highest acceleration values, by far, are associated with the two mock-ups filled with non-FR FPUF and covered in thermoplastic. The acceleration on cushions covered with cellulosic fabric depended on the underlying substrate, with the highest values recorded for mock-ups incorporating the high-loft barrier and the lowest for mock-ups with the woven barrier. The exception was for the two mock-ups filled with non-FR FPUF and covered with layers of polyester fiber wrap and cotton, which resulted in the third highest acceleration values.

Plots of average lateral flame spread rates on the back and seat cushions as well as transverse flame spread rate on the seat are included in Appendix A. Review showed that average lateral flame spread rates on the seat and back cushions were nearly constant and equal until the spreading flames ignited the mock-up arms. Based on this observation, a single characteristic lateral flame spread rate value was calculated by averaging the individual measurements on both cushions. A plot of these values versus combination number shows that the strongest variation is associated with fabric type, with much faster flame spread over mock-ups covered with the thermoplastic. Ratios of characteristic lateral flame rates for mock-ups differing only in cover fabric varied from 2.8 to 7.5, with most values falling between 3.0 and 4.5.

A similar plot of seat cushion transverse flame spread rates again showed a strong dependence on fabric type, but also smaller variations with changes in barrier condition and foam type. Ratios of characteristic lateral and transverse flame spread rates varied with combination number, indicated that while similar, these rates were not identical. This conclusion is consistent with the variations in burned area shapes described above.

Transverse flame spread rates as the flames approached the outer edge of the seat cushion are compared with the averaged transverse flame spread rate prior to flames reaching the mock-ups arms. Generally, values at the cushion edge are two to four times higher. This is an indication that transverse flame spread accelerated after the arms became involved in flames.

The ignition times for each arm were determined visually and averaged to yield a characteristic value for each test. It is reasonable to assume that arm ignition times are inversely related to the lateral flame spread rates, which are generally roughly constant. In fact, such a relationship is evident when a plot of characteristic arm ignition times versus mock-up combination number is compared to the corresponding plot for characteristic transverse velocities.

It was noted above that more rapid fire growth, based on both visual observations and HRR measurements, is often evident after the mock-up arms become involved. Comparison of arm ignition times with times required for the HRR to reach 25 kW shows that for many combinations the times were indeed similar, and both parameters had similar variations with combination number. This provides additional evidence that ignition of the arms tends to accelerate fire growth on these mock-ups.

The flame contours are also used to calculate burned areas on the seat and back cushions as a function of time. It is possible to correlate the shapes of the resulting curves with observations concerning the flame spread. These plots also allow the periods required for flames to fully cover the back and seat cushions to be calculated. Such times provided an alternate approach for characterizing flame spread.

Temporal heat flux profiles recorded at the six locations are plotted in Appendix A for each test. These show that while fluxes in the different directions have similar appearances, there are differences in temporal shapes and magnitudes associated with thermal radiation blockage effects due to mock-up geometry as well as fire locations on the mock-ups relative to the gauge locations. A strong correlation of the maximum observed heat flux and the maximum HRR is evident for the two gauges located towards the front of the mock-ups.

Additional tests were run to supplement the test matrix results discussed up to now. One of these involved a test of a mock-up filled with non-FR FPUF treated with a proposed clay-based fire retardant developed at NIST. The thermoplastic cover fabric was used. For comparison purposes, repeated tests were also performed for mock-ups constructed using either bare non-FR or FR FPUF. Data plots and analysis results are provided in Appendices C and D.

Section 7 describes statistical analyses carried out to determine if the thirteen experimental responses chosen for consideration (see following table) depend in statistically significant ways on the five experimental factors discussed earlier. Responses considered included five parameters based on the HRR temporal behaviors, the total heat release, four parameters based on the FIGRA temporal profiles, and three parameters related to flame spread behavior on the mock-ups.

Response	Parameter	Symbol	Abbreviation
Y1	Time required to reach 25 kW	t_{+25}	T25kW
Y2	Time of first HRR maximum	t_{peak1}	T1PHRR
Y3	Value of first HRR maximum	HRR_{peak1}	1PHRR
Y4	Time of maximum HRR	t_{max}	TMaxHRR
Y5	Value of maximum HRR	HRR_{max}	MaxHRR
Y6	Total heat released	Q_{tot}	TotHR
Y7	Time of first FIGRA maximum	t_{FIGRA1}	T1Figra
Y8	Value of first FIGRA maximum	$FIGRA_{peak1}$	1Figra
Y9	Time of maximum FIGRA	$t_{FIGRAmax}$	T2Figra
Y10	Value of maximum FIGRA	$FIGRA_{max}$	2Figra
Y11	Characteristic lateral flame spread velocity	$\bar{u}_l$	LatVel
Y12	Right arm ignition time	t_{igr}	RtArmIT
Y13	Left arm ignition time	t_{igl}	LtArmIT

The statistical significance of the factors is assessed using six analysis approaches based on Main Effects Plots, Block Plots, and Ordered Data Plots. Since some analyses are more conservative than others, some minor variations are observed between the results. However, there is general agreement that only three of the primary factors; Barrier Condition, Foam, and Cover Fabric; had statistically significant effects on the responses. Each of the analysis approaches identifies Barrier Configuration and Cover Fabric as having statistically significant effects on the nine parameters derived from the HRR and FIGRA temporal profiles. Results for the Foam factor are mixed, with the most conservative approach identifying statistically significant effects for factors based on HRR and FIGRA values, but not those based on the times required to reach peak values, and less rigorous approaches indicating that some of the periods are also significant.

The analysis results also provide indications of the relative strengths of the effects on these nine factors. This leads to the conclusion that overall the effects of Barrier Condition and Cover Fabric had strong and comparable effects, while the effects due to Foam were considerably weaker, and Polyester Fiber Wrap and Sewing Thread effects were not statistically significant.

For the total heat release response only the Foam factor was found to be statistically significant.

The three responses related to the flame spread behavior, i.e., characteristic lateral flame spread rate and the arm ignition times, did not depend on the factors as strongly as the responses derived from the HRR and FIGRA temporal profiles. The more conservative Main Effects Plot-based approach only identified Cover Fabric as having statistically significant effects on the three responses. Interestingly, the less conservative analyses based on Block Plot analysis identified Barrier Condition, and, for one analysis approach, Foam as being statistically significant. Once again, Fiber Wrap and Thread did not have statistically significant effects.

Block Plot analysis also provides a means to determine whether interactions between factors have statistically significant effects on the responses. The results show that the largest numbers of responses (nine of thirteen) are dependent on the Barrier Condition:Fabric interaction. This is reasonable because these two factors have the strongest primary effects. Generally, the responses that did not show a statistically significant effect on this interaction were those expected to depend on flame spread behavior. A few additional interactions are identified as statistically significant, but no other clear patterns are evident.

Overall, the various analysis approaches used yielded consistent finding concerning the dependence of the responses on the factors. This provides high confidence in the statistical conclusions.

Section 8 discusses and summarizes the findings of the study. Where appropriate, the current results are compared with those from previous studies. Individual subsections discuss the HRR, total HRR, FIGRA, and flame spread parameters with a focus on the responses used for the statistical analysis. It is shown that the current findings are in general agreement with earlier studies of RUF and RUF mock-up burning extending back to the 1970s. On the other hand, quantitative comparisons were not generally possible due to uncertainties concerning materials used and wide variations in experimental approaches.

While not the primary focus of the current study, the experiments also provide important findings related to mock-up ignition behavior, mass loss, effective heat of combustion, and radiative heat flux. These findings are also discussed and related to earlier studies. In the case of the heat flux measurements, an attempt is made to develop a quantitative predictive tool for heat flux in terms of the maximum HRR. This approach uses the current results as well as earlier measurements available in the literature. While shown to be potentially useful, insufficient numbers of experimental measurements are available to fully develop and test the approach.

The final section, 9, provides a short wrap-up of the findings.

1 Background and Literature Review

This report describes a study of the burning behavior of real-scale (i.e., full-scale) mockups designed to mimic fire development on residential upholstered furniture (RUF). The mock-ups consist of four upholstered cushions mounted on a metal frame to form the seating area of a chair. The results (Part 1) are a portion of a wider study designed to assess the feasibility of utilizing bench-scale experiments to predict the burning (flaming) behavior of such real-scale mock-ups, with the ultimate goal being the development of a capability to predict flame spread and fire growth on RUF. Two additional reports will describe the findings of a series of small-scale experiments utilizing similar materials in the cone calorimeter (Part 2) and the potential for predicting the real-scale results based on the small-scale findings (Part 3), respectively.

RUF burning has been the focus of substantial research and regulatory activity for several decades. In this section selected background material is presented to justify interest in the principal topic of this report and to provide a foundation for discussing the burning behavior of real-scale mock-ups and actual RUF. The intent is not to provide a complete literature review or a complete summary of the associated regulatory history. Substantial older background material is summarized in an earlier monograph and subsequent book [1, 2] and in a book by Prager and Rosteck [3].

The fire safety community has been concerned about the burning behaviors of certain types of residential upholstered furniture for over half a century. As early as the 1960s there was sufficient concern with regard to RUF flammability that in 1967 the Flammability Fabrics Act dating from 1953 was updated to explicitly allow the Secretary of Commerce to issue flammability standards for RUF. [4] Note that the early focus was on the flammability of upholstery fabrics and not the cushioning materials used in upholstery or RUF as a system. In 1972 the Commerce Department published a Notice of Finding in the Federal Register indicating that a standard or other regulation may be necessary to address upholstered furniture flammability. [5, 6] The National Bureau of Standards (NBS), the predecessor organization of the National Institute of Standards and Technology (NIST), initiated research on furniture flammability in 1968. [7]

Even though responsibility for the Flammability Fabrics Act was transferred to the newly formed US Consumer Product Safety Commission (CPSC) in 1973, NBS continued research for and began development of a RUF flammability standard, delivering a draft version to CPSC in 1976. [8] The proposed standard was designed to provide a minimum level of resistance to smoldering ignition of RUF by cigarettes. It consisted of two parts. The first part utilized a real-scale mock-up of the filling materials to be used covered by a standard fabric with a similar smoldering propensity as the fabric to be used on the actual RUF. The second part utilized a small-scale mock-up with a crevice formed by horizontal and vertical sections to classify upholstery fabrics into one of four classes. The fabric was spread over either glass fiber boards or a cotton batting substrate (vertical section only). For both tests, specified cigarettes were placed on the mock-ups, and sustained smoldering behavior was determined by the appearance of apparent sustained smoldering or by the spread of smoldering to specified distances from the cigarette.

In the same timeframe that national attention was focused on fabric issues associated with RUF flammability, the state legislature of California passed a law in August,1972 requiring all furniture to be "flame retardant" and specified that all furniture sold in California after October 1, 1975 meet standards developed by the California Bureau of Home Furnishings (CBHF). [9] The test and standard that CBHF developed were designated as Technical Bulletin 117 (Cal TB-117). [10] This document focused on the flammability behavior of the cushioning materials used in RUF. These materials were required to be able to resist ignition by a match-size flame as well as covered and uncovered smoldering cigarettes. Flexible polyurethane foam (FPUF) was tested in a vertical configuration with a 38 mm flame applied for 12 s. Cigarettes were place on a horizontal slab of the material. A number of tests for different cushioning materials were also specified. Upholstery fabrics were only required to a meet a standard [11] designed to

eliminate unusually flammable fabrics. Note that not only was Cal TB-117 focused primarily on a different component of RUF than the national efforts, but that flaming ignition sources were considered in addition to a smoldering source.

Similar versions of Cal TB-117 remained in effect until 2013 (the 2013 revision will be discussed later). The focus remained on limiting the flammability of cushioning materials with regards to both flaming and smoldering ignition sources. In 1980, a cigarette ignition test similar to the small mock-up test included as the second part of the original NBS flammability test was included. The test differed in that the cushioning material to be tested was covered with a standard fabric, and a pass/fail criteria based on the remaining mass of the foam slabs after all char had been removed (mass loss not to exceed 20 %) was adopted.

In September, 1977 the CPSC commissioners reviewed the NBS proposed standard and agreed that a mandatory standard dealing with RUF flammability would be necessary. [12] At the same time, they also requested that CPSC technical staff review the test method to determine if the economic burden could be reduced, to consider various options for implementing a mandatory standard, to consider the adequacy of voluntary industry action, and consider a petition from California to adopt their state standard nationally. In November, 1978 CPSC staff recommended that the Commissioners adopt a revised version of the draft standard. [12]

Very shortly after the CPSC staff recommendation, the furniture industry's Upholstered Furniture Action Council (UFAC) proposed its own voluntary testing program and standard for cigarette ignition resistance of upholstered furniture. A test method was quickly developed and was accepted in April, 1979. [13] The method had many similarities to the NBS recommended standard, but tested individual elements including upholstery fabrics, interior fabrics, barriers, decking materials, cushioning materials, and decorative trims. These tests required the use of standard fabrics and FPUF. Manufacturers won UFAC approval by certifying that all components in a RUF item met the relevant UFAC standards. In 1981 the CPSC commissioners tentatively accepted the UFAC standard. [2] Similar approaches have been adopted by ASTM International [14] and the National Fire Protection Association (NFPA) [15] as standard tests.

During this time frame initial attempts were made to assess the role of RUF in national fire losses. Using the limited survey samples available at the time, Vickers and Tovey provided an assessment of the role of RUF in fire losses. [16] Their analysis found that the majority of fire deaths occurred in residences. A large percentage of the fires in which RUF was the first item ignited involved smoldering ignition by smoking materials. The upholstery fabrics involved were predominantly cotton, rayon, or cotton-rayon blends. The most common cushioning material was cotton batting, but FPUF was also identified as playing a role. Clarke and Ottoson published a report in 1978 in which they looked at the most common scenarios responsible for fire deaths. [17] They concluded that the most common, by far, was a fire on furnishings, which they defined as either upholstered furniture or mattresses and bedclothes, following smoldering ignition. They estimated that such fires were responsible for 27 % of fire deaths in the nation, with roughly half due to RUF. Using an estimate of 9000 deaths per year due to fire [18], resulted in an estimate of 1215 deaths per year due to RUF ignited by smoking materials. Such numbers provided a powerful justification for the early focus on smoldering ignition of RUF.

In the intervening years active research and assessment of the need for a national standard designed to limit the flammability of RUF has continued. Much of this activity was in response to a formal petition filed in 1993 from the National Association of State Fire Marshals (NASFM) that CPSC establish a nationwide flammability standard for RUF modeled on Cal TB-117. [19] Two Advance Notices of Proposed Rulemaking (ANPR) and a Notice of Proposed Rulemaking (NPR) including a proposed standard have been released, but no standard has thus far been promulgated by CPSC. [20-22] Cal TB-117 was modified several times over the years, but remained primarily a small-flame ignition test of RUF cushioning materials until December 31, 2014. After this date, Cal TB-117 was modified (now TB 117-2013) to eliminate the

flame FPUF test and replace it with a test designed to reduce the contribution of cover fabrics to cigarette-induced smoldering ignition of RUF. The test uses small mock-ups consisting of a block of FPUF covered with the upholstery fabric. This modification and some of the reasons for it are discussed further below.

Despite wide spread concern about the role of RUF in fire losses in the United States, regulations to reduce its flammability have been primarily limited to Cal TB-117 and the voluntary UFAC standards. The approaches of these standards can be viewed as reducing the likelihood of smoldering ignition by cigarettes or ensuring a minimum resistance of cushioning materials to small-flame ignition. A very different approach for controlling RUF flammability has been implemented in the United Kingdom. The legal regulations are based on a test method developed by the British Standards Institute, designated BS-5852, that was originally released in 1979. [23]

BS-5852 is designed to evaluate the ignitability of furniture composites and/or complete pieces of upholstered furniture. Eight Ignition Sources, 0 to 7, are specified. Ignition Source 0 is a smoldering cigarette. The seven flaming sources increase in intensity in steps of roughly a factor of two, with Ignition Source 1 designed to simulate a burning match and Ignition Source 7 the burning of four pieces of standard-size newsprint. Ignition Sources 1 to 3 are butane flames with nominal heights of 35 mm, 145 mm, and 240 mm applied for 20 s, 40 s, and 70 s, respectively. Ignition Sources 4 to 7 are wood cribs that use increasing sizes and numbers of elements to generate fires of increasing heat release rate and duration. These sources are applied to the center of the crevice of mock-ups formed by 7.5-cm-thick 30 cm × 45 cm horizontal and 45 cm × 45 cm vertical sections. The two sections are formed by covering layers of the interior cushioning materials with the upholstery material for the furniture item of interest. For tests involving actual RUF, the ignition sources are applied to various locations on the item including the seating area, sides, and underneath. Criteria are provided for identifying smoldering and flaming ignition. A mock-up of a furniture item passes the test when the application of a given ignition source does not result in smoldering or flaming ignition.

Legislation requiring that all RUF sold in the United Kingdom must pass BS-5852 using Ignition Sources 0 and 5 went into effect on November 1, 1988. [24] This Statutory Instrument, referred to as SI-1324, required any FPUF and other cushioning materials to be tested in a mock-up configuration with a specified fire-retarded polyester upholstery fabric. Note that the flaming ignition test is a composite test and utilizes a relatively severe ignition source compared to the original California TB-117 flaming test, which tested the foam alone and used a match-size flame ignition source.

In addition to Cal TB-117, California also developed a more severe test, designated Technical Bulletin 133 (Cal TB-133), to be applied to seating furniture intended for use in public occupancies such as jails, nursing care homes, health care facilities, public auditoriums, hotels and motels. It was explicitly stated that this regulation was not intended for RUF. This test is fundamentally different than the tests described thus far in that it considers complete items in a room with a single door and its pass/fail criteria are based on limiting the burning behavior and not on the item's ignition resistance. In its original form, the standard required the ignition of actual furniture using five sheets of crumbled newsprint. [25] To pass the test, a number of criteria had to be fulfilled: temperature near the ceiling less than 149 °C, temperature 1.2 m above the floor less than 66 °C, less than 75 % opacity 1.2 m above floor, less than 50 % opacity at floor level, carbon monoxide (CO) concentration less than 0.1 %, and less than 10 % mass loss of the test item during the initial ten minutes.

Over the following seven years several modifications and additions were made to Cal TB-133. [26] Criteria for passing the earlier Cal TB-133 version were changed such that the temperature increases near the ceiling and the 1.2 m height could not exceed 93 °C and 10 °C, respectively, the CO concentration could not exceed 0.1 % for more than five minutes, and the total mass loss of the test item could not exceed 1.4 kg during the initial ten minutes. Based on testing at NBS [27], the five sheets of newspaper as an ignition source

was replaced with a comparable 25 cm square propane burner, with multiple holes, designed to impinge on the test item. Note that the newspaper fire source was judged to be suitable for screening tests. The propane flow rate is sufficient to generate a flame with a heat release rate (HRR) of 18 kW that is applied for 80 s. A major modification was to allow HRR measurements to be made at the doorway of the test room by oxygen consumption calorimetry as an alternative to temperature measurements within the room. When HRR measurements are made, the temperature and mass loss pass/fail criteria are replaced with HRR criteria that require the maximum HRR not to exceed 80 kW and the total heat released during the first 10 min to be less than 25 MJ. Obscuration and CO requirements were unchanged. The current standard also allows for testing of real-scale mock-ups that incorporate the same materials, thickness, and configurations as the actual furniture item. A description of a test stand suitable for mock-up testing is included. As of this writing the state of California is considering the elimination of TB-133.

The ASTM International Standard E1537 (ASTM E1537) describes a fire test items for upholstered furniture that is very similar to Cal TB-133. [28]

An early investigation of RUF ignition and burning behavior, referred to as the "Fire Hazards of Plastics in Furniture and Furnishings" study, was performed in the United Kingdom during the mid-1970s. Results were summarized in a series of reports. [29-31] This study was focused on changes in the ignition and burning behavior of RUF due to the introduction of man-made plastic materials in their manufacture. It was recognized that consideration of both ignition and subsequent burning behaviors were central to understanding these changes. The study was wide ranging, investigating ignition by smoldering and flaming sources of small-scale samples, real-scale mock-ups, and actual RUF items. The burning behavior of RUF items within rooms and subsequent fire spread to other items placed nearby were also studied.

The experiments demonstrated that combinations of fabrics which were capable of smoldering over FPUF could be ignited by cigarettes. Ignition of similar combinations by match-sized flames indicated that ignition resistance as well as the strength of subsequent burning was strongly influenced by upholstery fabric type. Differences in ignition resistance and burning behavior were reduced as the flaming ignition source strength increased. Ease of ignition was influenced by the density of the polyurethane foam, with lower density foams igniting more readily. Direct comparison of RUF items constructed using "traditional" materials such as cotton fabrics and cotton batting and "modern" materials such as nylon and FPUF indicated that traditional RUF was more easily ignited than modern RUF by smoldering sources, but that the opposite was true for flaming sources. Flaming fires grew more quickly on modern furniture and burned more intensely. Experiments showed that in a room with a range of furnishings including RUF, flashover did not occur when traditional RUF was present, but flashover with complete burn out of all fuel took place when modern RUF was used. The authors concluded that when modern RUF was included "escape from the fire would need to be more rapid than with traditional furniture". By constructing RUF items using less flammable modern upholstery fabrics and cushioning, it was demonstrated that it was possible to construct items with performance similar to that of traditional furniture. Limited mock-up studies showed that "polypropylene upholstery fabrics gave no protection against fire, was readily ignited, and should be regarded as a hazardous upholstery fabric".

A second series of experiments sponsored by the International Isocyanate Institute were performed in the United Kingdom during roughly the same time frame. These studies are summarized in two publications. [32, 33] Part of these investigations considered ignition and fire spread over two side-by-side mock-ups consisting of seat, back, and two arm cushions arranged on metal test stands and located in a test room. [32] A large number of upholstery fabrics, cushioning materials, and barrier fabrics ("interliners") were used to construct the cushion mock-ups. Smoldering ignition by cigarettes was shown to take place on cushions upholstered with fabrics containing cellulosic materials such as cotton. Incorporation of certain barrier fabrics reduced the likelihood of cigarette ignition. Most material combinations were susceptible to ignition

by small- and medium-sized flaming ignition sources. The combination of modacrylic cover fabric with an interliner provided a reduced likelihood of ignition by flaming sources.

Flame spread rate measurements showed a dependence on cushioning material, upholstery fabric, and barriers. Use of thermoplastic cover fabrics generally resulted in higher flame spread rates due to peeling back of the fabric to expose the underlying material. Following ignition, the use of barrier fabrics which were not thermoplastics were shown to significantly lengthen the burning time and resulted in lower temperatures in the upper layer of the room.

During the second part of the investigation the burning behavior of upholstered furniture in a building representative of a two-story, four-bedroom home was studied. [32, 33] An upholstered settee (i.e., a small two-seat sofa) and two chairs were placed in a living room on the first floor which contained additional furniture, carpeting, and curtains. Conditions in the fire room as well as at other locations on the first and second floors were monitored. Ventilation was controlled. For some experiments the home was sealed. In others, an upstairs bedroom window was left open, and a window was opened in the fire room seven minutes after ignition to simulate fire-induced window breakage. Two material combinations were used for the upholstered furniture. The outer surfaces of the three items for both types were covered with polyvinylchloride fabric supported on cotton, while the seat cushions were covered with a cotton/nylon/rayon blend. In one set a polyether-based FPUF was used as cushioning material, while the second incorporated wool flock in the body of the chair and feathers enclosed in a nylon case in the seat cushion.

Comparison of fires in the sealed building showed that those involving the three items incorporating FPUF developed more quickly and destroyed larger fractions of the settee and chairs than those where natural cushioning materials were used. In both cases the fires died down before flashover occurred in the room of fire origin. While conditions in the fire room were life threatening after two minutes, conditions in an upstairs bedroom did not appear to become life-threatening during the tests. When the fires were ventilated the damage observed for a fire involving the furniture with natural cushioning was similar to that for the fire with limited ventilation. For the furniture containing FPUF, ventilation resulted in fire spread to items not involved during the limited-ventilation fire. When the additional items became involved, conditions in the upstairs bedroom deteriorated. As for the unventilated fires, flashover was not observed for fires with either type of RUF. The authors concluded that while fire development was somewhat more rapid and extensive with the furniture incorporating FPUF, variations in the overall hazard in the living room were relatively small, and the type of furniture had small effects on the hazard in the upstairs bedroom.

Wooley et al. reported an ignition-behavior study of upholstered cushions which included a wide range of fabrics (17), interliners (3) and filling materials (5). [34] A series of increasingly strong flaming ignition sources were applied to the base of a single vertically oriented cushion formed from a 30 cm × 30 cm × 7.5 cm foam slab covered with an upholstery fabric and an interliner (if used) until ignition was noted. The results showed that non-fire retarded FPUF (NFRFPUF) in combination with non-fire-retarded cover fabrics provided no ignition resistance to the weakest flame source used. Some increased ignition resistance, as indicated by the need to utilize stronger ignition sources, was noted when fire-retarded and fire-resistant foams and/or fire-retarded fabrics were used and when interliners were included.

Wooley et al. also investigated the burning behavior of real-scale mock-ups formed from four cushions (back: 60 cm × 47.5 cm × 7.5 cm, seat: 52.5 cm × 47.5 cm × 7.5 cm, and arms: 60 cm × 27.5 cm × 7.5 cm) mounted on a steel frame and located in a burn room attached to a corridor. For these tests the strongest of the seven sources (a wood crib) was used to ignite the mock-up. The burning behavior was characterized by temperature, carbon monoxide concentration, and carbon dioxide concentration measurements at the top of the room doorway and visual observations of the times when the spreading fire reached the far arm of the mock-up and when the mock-up was fully involved. In order to characterize the fire development these

authors introduced a temperature index defined as the product of the rate of temperature growth and the maximum temperature. The experimental results showed that this index depended on the types of upholstery fabric, interliner, and foam included in the mock-ups. The least favorable behaviors were observed for cushions containing NFRFPUF and non-fire-retarded fabrics. The inclusion of fire-retarded FPUF (FRFPUF) and/or barriers provided improved burning behavior. The use of latex foam resulted in more intense fires.

Babrauskas burned a series of specially constructed chairs for which the upholstery and cushioning materials were varied in an enclosure with a single doorway. [35] Measurements reported included temperatures at multiple locations, mass loss rates, smoke extinction, heat fluxes at multiple locations, and concentrations of oxygen (O_2), CO, and carbon dioxide (CO_2). Only one item with a particularly high fuel loading led to flashover in the room. Tenability criteria were used to determine when life threatening conditions were reached. In general, the best performance among chairs with similar size and construction was obtained for those that included cotton upholstery fabrics and cotton batting as the cushioning material. Replacing the cotton batting with FPUF resulted in the chair having one of the worst observed fire performances. Tests for chairs where only the upholstery fabrics was changed showed that the use of cotton fabrics gave noticeably better fire performance as compared to chairs with either polypropylene or nylon covering the cushioning materials.

Babrauskas reported one of the earliest studies in which oxygen consumption calorimetry [36] was used to characterize the heat release rates of upholstered furniture items. [37] The calorimeter employed a hood in a large open room to collect the fire products. A series of chairs in which the construction materials were systematically varied were burned along with several larger loveseats and a sofa. Chairs were prepared from various combinations of upholstery cover fabrics (cotton or polyolefin), cushioning (NFRFPUF, Cal TB-117-compliant FRFPUF, and fire-retarded cotton batting), and frame materials (wood, polypropylene, and polyurethane). Furniture items were ignited on the outside of the furniture with a gas burner simulating a wastebasket fire (50 kW applied for 200 s). In addition to the HRR measurements, a load cell was included to record real-time mass of the item, and a single gauge located 0.5 m in front of the furniture item was used to record heat flux from the fires.

Maximum HRR and the time required to reach this value were used to characterize the burning behavior. The times for the various chairs fell into three well defined groups, with the shortest observed for FPUF combined with thermoplastics fabrics, intermediate times occurred for cases with mixed-type materials (cotton fabrics over FPUF or thermoplastic fabric over cotton batting), and the longest growth times were for chairs with cotton fabric over cotton batting. The times needed to reach the maximum HRR ranged from 235 s to 910 s. Maximum HRRs also fell into three groups. Recognizing that slow growth times and low maximum HRRs are desirable, the maximum HRRs were grouped in nearly the same way as the times with regard to improved fire behavior. Maximum HRRs ranged from 370 kW to 1980 kW. Chairs constructed using either NFRFPUF or Cal TB-117-compliant FRFPUF covered by the polyolefin fabric displayed no significant differences in time to or maximum HRR. Fires on the loveseats and the sofa had much higher HRRs, demonstrating the importance of fuel load for the intensity of fires burning on RUF.

The availability of both HRR and mass loss data allowed values for the effective heat of combustion to be calculated for these fires. In general, the lowest values were observed for furniture incorporating cotton fabric and batting, while the highest were measured for furniture with polyolefin fabric and FPUF cushioning. Values of radiative heat flux from the fires were also measured. It was demonstrated that there was a rough correlation between the maximum observed heat fluxes and the mass loss rates at those times.

Krasny and Babrauskas described the results of burning a number of RUF mock-ups formed by placing one to six upholstered cushions on a steel stand. [38] The cushions had surface areas of 61 cm × 61 cm and were either 5.1 cm or 10.2 cm thick. A variety of materials were used to construct the cushions including

four fabrics (light- and heavy-weight cottons and polyolefins) and three types of cushioning materials (neoprene, NFRFPUF, and FRFPUF meeting the Cal TB-117 standard). Cushion configurations tested and the number of cushions in the mock-up included a single seat (1); seat and back combinations (2); seat, back, and side arm combinations (3); chair configurations (4); and loveseat configurations (6). Experimental measurements in the furniture calorimeter included HRR; CO, CO_2, and O_2 concentrations; various measures of fire spread rate including seat area involved, times to full coverage of seats and backs, and times to burn through of threads placed near the top of the vertical cushions at locations in front of and behind the cushion; and radiative heat flux at a location 0.5 m from the front and 0.2 m above the front edge of the mock-up. For most mock-ups relatively weak methenamine pills (45 W for 90 s [2]) were used as ignition sources, while cushions covered with the heavier weight cotton fabric required the use of 4.5 g of burning filter paper.

The upholstery fabric type was found to affect the ease of ignition as well as the flame spread rate. The best fire behaviors, i.e., harder to ignite and slower flame spread, were found for cushions covered with the heavy-weight cotton, and the worst were when the light-weight polyolefin was used. Values of maximum HRR varied from 310 kW to 1.5 MW when four 10.2 cm thick cushions were used. Interestingly, while HRRs on bare cushions of NFRFPUF and FRFPUF revealed a substantial improvement in HRR behavior for the Cal TB-117 FPUF, the difference was reduced substantially when the FPUF was covered with upholstery fabric. For these experiments, small improvements in burning behavior were observed when the Cal TB-117 FPUF was replaced with NFRFPUF. This conclusion differs from that reported earlier, see above, during the study on actual RUF, where only minimal differences were measured. [37] The authors concluded that the type of upholstery fabrics played the largest role in determining the fire hazards associated with burning mock-ups.

Cushion configuration had small effects on the maximum HRR observed, while the values scaled roughly linearly with the total cushion mass. The same was found to be true for flame radiation and concentrations of fire gases. Faster fire growth was observed when thinner cushions were used. As a result, values of maximum HRR normalized by the cushion total mass were higher for the thinner cushion mock-ups. Limited investigation of the effect of ignition location showed that the primary differences were observed during the early fire growth periods. Once fires exceeded 100 kW, ignition location played a minimal role.

Babrauskas compared the burning behaviors of a chair and loveseat tested previously in a furniture calorimeter [37] when burned in a 2.3 m × 3.9 m × 2.3 m room equipped with a large window opening in one of the shorter walls. [39] The height of the window was varied to change the ventilation. The test items consisted of a wood frame padded with Cal TB-117 FRFPUF covered with a polyolefin fabric and had masses of 28.3 kg (chair) and 40.0 kg (loveseat). A 285 g polyethylene waste basket filled with 390 g of milk cartons was used to ignite the furniture on the outer side. Experimental instrumentation included oxygen consumption calorimetry in the hood that collected the combustion products, bidirectional pressure probes for velocity measurements along the centerline in the window, two thermocouple trees inside the room, a heat flux gauge at the floor, and a load cell to record mass.

One chair and three loveseats were burned separately. Visual observations showed that the flow from the window was not uniform but was instead concentrated in the corners. As a result, the velocity measurements did not provide an accurate mass flow measurement. For all four tests the heat flux at the floor exceeded 20 kW, a level indicative of flashover conditions in a room. HRR curves for each type of furniture was compared with the corresponding curves for experiments run under a furniture calorimeter. For this room configuration the conclusion was that the HRR curves were independent of whether or not the item was burned in a room. This conclusion is somewhat surprising since radiative heat flux levels reached quite high levels.

Andersson and Magnusson described a large number of RUF chair and sofa mock-up experiments. [40] The chair mockups consisted of 50 cm × 50 cm × 7.5 cm seat (35 kg/m^3 FPUF) and back (25 kg/m^3 FPUF) cushions arranged on a metal stand. Either 10 g or 40 g wood cribs placed on the seat were used as ignition sources. Fourteen different fabrics combined with three interliners (FRFPUF, novaloid felt and modified neoprene foam) and three FPUFs (NFR, high resiliency, and FR) were combined into 26 different combinations. Measurements included mass loss and smoke production. The experiments showed that the ignitability of the mock-ups was strongly dependent on the fabric, interliner, and FPUF type. The most fire-resistant fabrics contained at least 50 % wool. These authors also reported that flame spread rates over the chair mock-ups varied with cover fabric and interliner.

The sofa mock-ups consisted of loose seat cushions mounted on a steel frame and burned inside a 2.4 m × 3.6 m × 2.4 m test room with a single doorway. Eleven tests were run with different combinations of three upholstery fabrics (acrylic, wool, and 61 % wool/39 % rayon) and the same interliners and FPUFs used in the chair study. Experimental measurements included mass loss, temperatures, and heat fluxes. A liquid fueled burner producing 20 kW to 30 kW served as the ignition source. Similar to results for the chair mock-ups, fire spread rates varied with the fabric and interliner types. The authors concluded "that the rate of fire spread is just as important for the development of a fire as the mass burning rate, and that choice of fabric determines not only ignitability but also to a large extent the total fire-growth process." Estimates were provided for HRRs during these fires, but it is likely that these were subject to large uncertainties.

Ohlemiller and Shields described a study of RUF mock-up burning behavior using the Cal TB-133 protocol. [41] A primary focus of this study was the effectiveness of barriers in limiting fire spread and growth. A wide range of materials were used spanning seven fabrics (polyester, nylon, 75 % modacrylic/25 % nylon, 38 % polyester/62 % cotton, cotton, and two aerial densities of polypropylene), two FPUFs (Cal TB-117 and one moderately fire retarded with melamine), and four barrier fabrics (non-woven aramid, knitted glass/charring fiber, knitted glass/charring fiber with added halogen fire retardant, and woven glass). Barrier materials were bonded to the backs of the upholstery materials. Mock-ups generally consisted of four cushions (51 cm × 51 cm × 10 cm seat, 51 cm × 37 cm × 10 cm back, and two 51 cm × 30 cm × 10 cm arms). The cushions were arranged on a Cal TB-133 test stand with seat and arms resting on the test stand and the back resting on top of the seat at a 15° angle relative to vertical. Cushions were sewn with an aramid thread. Early experiments included nylon zippers in the cushions, but experience showed that such zippers could melt and allow flame penetration. In subsequent experiments, aramid thread was used to close the seams. The mock-ups were ignited with a Cal TB-133 square burner following the test protocol. HRRs were measured in a furniture calorimeter. Extensive imagery of the tests was recorded. Heat fluxes to the mock-up surfaces were measured at limited locations using gauges raised slightly above the surface.

The primary quantification of burning behavior was in terms of HRR. All material combinations showed a peak in HRR during the 80 s application of the burner. In many cases a second, higher peak was observed after the ignition burner was removed. Maximum HRR values ranged from 35 kW to as high as 744 kW. The lowest HRRs were associated with mock-ups covered with the 75 % modacrylic/25 % nylon fabric, while the highest values were observed for cushions with polypropylene fabric. Generally, the performance (lower maximum HRR) of the barrier fabrics was ordered non-woven aramid > knitted glass/charring fiber with added halogen fire retardant > knitted glass/charring fiber ≈ knitted glass. The imagery of the fires allowed the general fire spread behavior on the interior surfaces of the mock-up to be described. Fire spread on the seating areas were quantified in terms of area burned.

A joint study between NIST and the California Bureau of Home Furnishings and Thermal Insulation (BEAR-HFTI) considered the behavior of chairs constructed from ten different material combinations burning in either of two different sized rooms (3.0 m × 3.7 m × 2.4 m and 2.4 × 3.7 m × 2.4 m) with single doorways or in a furniture calorimeter. [42] Single-style chairs were fabricated using one of four cover fabrics (wool, nylon, polyvinylchloride, and polyolefin), one of two types of FPUF (Cal TB-117 and

melamine fire retarded) and either with or without a fiberglass barrier fabric. Measurements inside the rooms included HRR, temperature, CO, CO_2, and O_2 concentrations, smoke opacity, and mass.

A wide range of burning behaviors were observed with maximum HRRs ranging from close to zero up to 2.5 MW. The lowest maximum HRRs were found for chairs constructed with wool upholstery fabric, the glass barrier fabric, and Cal TB-117 FPUF. The highest HRRs were observed for chairs constructed with Cal TB-117 FPUF and covered with the polyolefin fabric. Based on the experimental results, it was concluded that results in the two different-sized rooms were indistinguishable, a HRR of 65 kW resulted in a temperature rise of 111 °C (the maximum allowable in Cal TB-133) near the room ceiling, and burning behaviors in the furniture calorimeter and room tests were identical for HRRs up to 600 kW.

One of the most extensive studies of RUF burning behavior was the Combustion Behavior of Upholstered Furniture (CBUF) study performed in Europe. [43] This multi-laboratory study investigated a number of aspects related to small- and real-scale testing of RUF as well as modeling of the burning behavior. 225 real-scale tests were performed in rooms and furniture calorimeters. Test items included a variety of actual specimens purchased in the European marketplace as well as several series of "custom-made" furniture in which various aspects of the construction and materials were varied. A variety of upholstery fabrics (cotton, fire-retarded cotton, polyester, fire-retarded polyester, acrylic, wool, and leather), cushioning materials (polyether NFRFPUF, high resilient (HR) FPUF, full-depth impregnated FPUF, and a combustion-modified high resilient (CMHR) FPUF), barrier fabrics, referred to as interliners (non-woven Kevlar, woven glass fiber, and a knitted fire-retarded glass/cotton system), and cases with and without polyester fiber wrap were tested. Framing materials included wood and metal tubing. Various style chairs (with and without arms, varying cushion sizes and orientations) were studied. Chairs were extended to form loveseats (2 cushions) and sofas (3 cushions).

Instrumentation in the room experiments recorded HRR, temperatures, heat fluxes, and the concentrations of flame gases. Measurements during furniture calorimeter experiments included HRR using oxygen consumption calorimetry, mass using a load cell, and flame-gas composition using light extinction and Fourier Transform InfraRed (FTIR) gas species measurements. Video cameras recorded fire development and burning behavior. Experiments were carried out to assess reproducibility within a laboratory and across different laboratories. A variety of ignition sources were used in preliminary experiments. Since the main goal was to characterize burning behavior, it was decided that a large enough source to ensure ignition should be employed. For most of the tests a burner similar to that specified in the Cal TB-133 test was used, but with a propane flow rate sufficient to generate a 30 kW flame, and the burner was applied to the test item for 120 s. For test comparison purposes, the start of a burn (0 s) was defined to be when the HRR first reached 50 kW.

The experimental results showed that similar chairs covered with different fabrics gave HRR curves that developed at different rates and reached different maxima. The worst performers (faster growth, higher HRR maxima) were the thermoplastic fabrics, while the natural products performed better. By far, the best performer was the wool fabric. Experiments in which the FPUF was varied showed only minor differences when polyether NFRFPUF or FRFPUF were exchanged, but a measurable improvement when the CMHR FPUF was used. Results for cotton- and wool-covered chairs showed dramatic improvements in fire behavior with added fire barriers. Tests for chairs with and without arms showed that faster fire growth and higher HRRs occurred when arms were present. Tests comparing the burning behavior of a chair and a sofa showed faster fire growth on the chairs, but much higher maximum HRRs for the sofas. Smoke and toxic gas measurments showed that varying the chair composition had measurable, but generally small, effects on tenability in a room during fires involving upholstered furniture.

Several models were applied in the CBUF in attempts to predict the experimental findings. [43] The most widely employed of these models made two major assumptions. The first was that the initial fire growth

period was not included in the analysis, and time zero was defined as when the HRR first reached 50 kW. The second was that the HRR temporal behavior was approximated as having a triangular shape with a single peak.

Söderbom et al. investigated the effect of ignition source size on the burning behavior of six ordinary chairs chosen from the European market to cover a wide range of expected fire growth. [44] The authors first summarized the findings of a study by van Hees and Meirsschaert in which a relatively large ignition source based on the Cal TB-133 burner was applied to non-fire-retarded and fire-retarded chairs. [45] The non-fire-retarded chairs were constructed on a wood frame using 65 % acrylic/35 % rayon fabric covering polyester fiber wrap and polyether NFRFPUF (seat: 27.5 kg/m^{3,} back: 17 kg/m^3), and the fire-retarded chairs included 69 % acrylic/31 % cotton fabric fire-retarded by a back coating covering polyester fiber wrap and a CMHR FPUF (seat: 37 kg/m^2, back: 35 kg/m^2). Four sets of ignition conditions were tested in which the HRR and time of application were varied as follows: (40 kW, 120 s), (30 kW, 120 s), (30 kW, 180 s), and (20 kW, 300 s). Tabulated values of maximum HRR and total heat released following ignition showed that the results were independent of ignition source, and both measures were roughly two times larger for the fire-retarded chairs, which is likely due to the higher masses of the fire-retarded foams used. Comparison of the HRR time behaviors emphasized the good reproducibility of the burning and the absence of an effect of ignition source. The shapes of the HRR curves were different, with the fires on the non-fire-retarded chairs growing rapidly to a single peak of roughly 500 kW after 165 s and those on the fire-retarded chairs first reaching a plateau around 200 kW, before starting to grow in roughly 40 s to a peak of 1.1 MW 290 s after the ignition source was applied.

The focus of the published study was a miniaturized square ignition burner in which the dimensions were reduced from 25 cm to 11.5 cm. The size of the burner flame, application time, and its application location were varied to control the heat flux applied to the chairs. Burner HRRs of 1.7 kW and 5.8 kW were used. In addition, a small match-like flame based on standard test EN 1021-2 was applied. [46] The results were compared to tests where the original 30 kW burner applied for 120 s was used as the ignition source. The six commercial chairs contained a wide range of materials which are listed in the report. The test protocol was to start with the smallest ignition source, and if ignition did not occur, to apply the next largest ignition source all the way up to the 5.8 kW source. HRR curves were recorded for cases where sustained fires developed. In order to compare the effects of ignition source, the HRR curves were compared after the HRR had grown to 50 kW (defined as zero time). Comparisons of burning behaviors for ignitions with smaller sources and the larger 30 kW source were made by comparing the periods required for fires to grow from 50 kW to 400 kW, which was the HRR judged to be that for which a small compartment would become untenable. The results showed that while the times between the application of an ignition source and when the HRR reached 50 kW (referred to as the ignition period) varied with ignition source, the fire growth periods as well as maximum HRRs were similar and independent of ignition source size.

A long-term study on RUF flammability has been carried out at the University of Canterbury in New Zealand. Many of the results are available only as theses and reports. Much of this work has been aimed at applying the CBUF experimental procedures to New Zealand RUF. An initial study by Firestone incorporated results from an extensive series of furniture mock-up fires performed during 1993 at the Commonwealth Scientific and Industrial Research Organisation (CSIRO) in Melbourne, Australia. [47] The account of these experiments provided by Firestone is quite detailed. The mock-up tests involved placing various numbers of cushions on a metal frame and igniting with a 400 g pine wood crib placed on one of the cushions. When burned alone, the wood crib fires lasted about 500 s with a maximum HRR of roughly 25 kW. The test frame used and dimensions for the cushions were those specified in NORDTEST NT Fire 032. [48] The sofa mock-up seat and back were inclined with the rear of the mock-up located 20.5 cm above and the front 27 cm above the support base. Seat, back, and arm cushions had specified sizes of 65 cm × 55 cm × 10 cm, 42 cm × 55 cm × 10 cm, and 65 cm × 25 cm × 10 cm, respectively.

The CSIRO experiments used a number of cushion configurations supported on the NT Fire 032 test stand. These included one, two, or three combinations of seat cushions only, back cushions only, or both seat and back cushions. The wood cribs were generally placed at the center of the cushions. In cases where more than one set of cushions were side by side, two different ignition locations could be tested. A full chair configuration including a seat, back, and two arm cushions was also tested with the ignition crib place in one the corners formed by the seat, back, and an arm. Cushions were assembled using one of two upholstery fabrics (a 100 % cellulosic (cotton/linen blend), 300 g/m^2 or 100 % polypropylene, 350 g/m^2) and one of four FPUFs (standard, non-fire-retarded, 23 kg/m^3; high resilient, non-fire-retarded, 32 kg/m^3; moderately fire-retarded, 36 kg/m^3; and heavily fire-retarded, 45 kg/m^3). A total of 141 experiments were completed. The mockups were burned under a furniture calorimeter. The primary measurement reported was heat release rate. Video and still photographs were used to capture visual records of the tests.

For single-seat arrangements (i.e., one seat and one back cushion), comparisons of tests with the same FPUF and the two fabrics revealed that the mock-ups with non-fire-retarded foams generated HRR temporal profiles with single maxima, while those with added fire-retardants had double peaks. For all four FPUFs the initial HRR growth was faster for the cushions covered with polypropylene. Interestingly, while it was observed that the maximum HRR for NFRFPUF covered with polypropylene was higher than for those covered with the cotton/linen fabric, the opposite was true for those that incorporated the three other foam types. This difference was particularly striking for the two fire-retarded foams, where the second peaks in the HRR were substantial compared to the initial peak when covered with cotton/linen fabric, but much reduced when covered with polypropylene. For cushions with HRFPUF, which displayed a single maximum, the HRRs were considerably higher when covered with the cotton/linen material. Firestone speculated that the different behaviors were due to the fact the high-resilient and fire-retarded FPUFS all had some degree of fire retardancy and required some wicking type material to stabilize its burning. Similar comparisons of cases with the four types of FPUF for a single fabric showed that the fire severity decreased in the order: standard foam > high-resilience foam > moderately fire-retarded foam > highly fire-retarded foam.

Two seat configurations were run for the two fabrics and standard and high-resilient FPUFs. Single HRR maxima were observed for these fires. Substantial fires developed with both types of fabric when the NFRFPUF was used as the cushioning material. Maximum HRRs were reached sooner and were higher when the foam was covered with polypropylene fabric as compared to the cotton/linen blend. When the HRFPUF was used the burning intensity was markedly reduced and became much more erratic. For cushions covered with the cotton/linen fabric, the maximum HRRs were substantially higher and occurred much earlier than when the polypropylene fabric was used. Firestone characterized the burning on the mock-ups with HRFPUF and polypropylene as superficial since the maximum HRRs were well under 100 kW and occurred nearly 5 minutes after ignition. The reduced fire intensities with the polypropylene fabric were similar to those observed for the one-seat composites when polypropylene covered the HRFPUF.

Tests with three-seat mock-ups were run with the ignition source placed on either the center seat cushion or the right-hand seat cushion. For all of the foam/fabric combinations the highest HRRs and shortest burn times were observed for ignition at the center location. This was attributed to flame spread behavior since the fire could move in two directions when ignited at the center. Differences in fire spread behavior due to fabric type were also noted, with fire spread over the polypropylene fabric being dominated by radiation and over the cotton/line fabric by charring. Intense fires developed when NFRFPUF was used with either fabric, but the fire development was faster and the maximum HRR was higher for cushions covered with polypropylene. HRRs exceeding1 MW were observed for the three-seat mock-ups formed with cushions incorporating NFRPUF covered with polypropylene fabric. The burning intensities were considerably reduced when HRFPUF was used. For these cases the mock-ups that included the polypropylene fabric had the lowest fire intensity. Firestone concluded that the mock-ups with the cotton/linen fabric developed self-sustaining burning while those with polypropylene did not.

Firestone included an interesting discussion of the effect of the test stand on the burning behavior of the mock-ups. The test stand was open, which allowed any free liquid formed by the burning to drip to the support surface underneath the test stand. If the material on the support surface did not ignite and burn vigorously, it did not contribute to the heat release. This was deemed especially important for tests with high-resiliency and fire-retarded foams.

From visual observations it was noted that the cotton fabric tended to char when exposed to fire but remained intact, while the polypropylene quickly shrank and melted away when exposed to the flames, exposing the underlying FPUF.

In another study Enright focused primarily on characterizing the accuracy of the cone and furniture calorimeters used in the study. [49] Part of this investigation included measuring HRRs from a series of exemplary samples of commercial New Zealand RUF in a furniture calorimeter. [49, 50] Similar furniture was deconstructed, and samples were used to perform cone calorimeter measurements. Both chairs and loveseats with similar compositions were studied. Five chairs with the same nominal construction, but having different cover fabrics, were tested. HRRs curves for the five similar chairs had moderately different shapes with maximum HRRs varying from 795 kW to 1705 kW. All of the curves displayed two main peaks. The highest HRR value was for a chair covered with polypropylene fabric, while the lowest was for a chair covered with a fabric consisting of polyester mixed with other fibers. Maximum HRRs for loveseats were substantially higher than those for the corresponding chairs.

Denize studied the burning of especially constructed chairs using a furniture calorimeter. [51] The protocols developed during the CBUF project were followed, and the chair design was the base chair from the European study. [43] Ten different chairs were constructed using two fabrics (100 % polypropylene and 95 % wool/5 % synthetic) and five different foams (three NFRFPUFs of varying density and two FPUFs which were mildly and heavily fire retarded). The ignition source was a square burner with a 30 kW flame applied for two minutes. Measurements reported included HRR, total heat release, mass, heat of combustion, and CO, CO_2, and O_2 concentrations in the furniture calorimeter stack.

It was found that fires on the chairs covered with the wool/synthetic fabric grew more slowly and reached lower maximum HRRs than the corresponding test items covered with 100 % polypropylene fabric. Maximum HRRs ranged from 591 kW to 1048 kW. The HRR curves for chairs with a given fabric were found to have similar growth behaviors for each of the foams, with the exception of the most heavily fire-retarded foam covered with polypropylene. The fires on these chairs developed noticeably slower. Similarly, maximum HRRs were similar for the three non-fire-retarded and the lightly fire-retarded FPUFs, with small differences correlated with foam density. The maximum HRRs for the heavily fire-retarded foam were considerably lower. Interestingly, for chairs covered with the wool/synthetic blend, the highest HRR was measured for the chair with heavily-fire-retarded foam. Heats of combustion ranged between 29 MJ/kg and 42 MJ/kg and 16 MJ/kg and 27 MJ/kg for the polypropylene- and cotton/synthetic-covered chairs, respectively. This reflects primarily the differences in heat of combustion between the two cover fabrics.

All of the HRR curves for the tests showed two distinct peaks. Based on visual observation, Denize identified four distinct stages in the burning behavior. During Stage 1 (“Constant Growth”), which developed after the 30 kW burner was applied, fires grew linearly to a first maximum as the interior locations on the seat, back, and arms became involved in fire. For four of the chairs covered with polypropylene, the initial HRR maxima were reached about 60 s, after which time the fires began to die down slightly. The one exception was the chair with the heavily fire-retarded FPUF, for which the HRR continued to grow until the ignition burner was turned off at 120 s. The fire growth on the chairs covered with the wool/synthetic fabric also died down after the burner was shut off at 120 s. During the second stage (“Decline in HRR”) the HRRs fell to intermediate minimum values. Stage 2 burning was relatively

brief for the four chairs that reached HRR maxima 60 s after the ignition burner was applied, and the minima were shallow. For the remaining six chairs, the periods of depressed HRR were longer, and the reductions in HRR were more noticeable. At the start of Stage 3 (Rapid Growth) the HRRs rates grew rapidly to maximum values and burned intensely for brief periods. Imagery showed that during these periods there was intense burning on the floor underneath the chair as well as on remaining materials on the chair itself. Denize attributed the sudden increase in HRR to the burn through of the sides at the bases of the chairs, which allowed air to reach accumulated fuel that had dripped down underneath the chairs. The longer Phase 2 periods for the chair with heavily fire-retarded FPUF and those covered with the wool/synthetic material were attributed to the longer times required for the lower panels to burn through. During Stage 4 (Decay in HRR) the fire began to die down as the remaining fuels burned out.

Girgis burned seven similar chairs in an International Organization for Standardization (ISO) ISO-9705 room (2.4 m × 2.4 m × 3.6 m with single doorway). [52] The chairs had the same base and were covered with the same polypropylene fabric as those used by Denize. [51] Six of the chairs included the same FPUFs as well. Thus, it was possible to directly compare the burning behavior of the chairs in the enclosed room and in the open furniture calorimeter. Measurements reported included HRR, mass, temperature at multiple locations in the room, CO, CO_2, and O_2 concentrations in the exhaust stack, heat flux at the floor of the room, and video imagery. Ignition of the fires used the same CBUF burner as the earlier study.

Maximum HRRs measured for the chairs ranged from 1.3 MW to 1.8 MW. These values are considerably higher than reported by Denize for nominally the same chairs burned in the furniture calorimeter. The higher HRRs were attributed to radiative feedback from the upper layer of the test room. [51] Girgis found a different order in the variations of maximum HRR with foam type. For instance, the lowest value seen by Denize was for the heavily fire-retarded FPUF, while the lowest observed by Girgis was for the chair constructed with mildly fire-retarded foam. The same combination of materials gave the highest maximum HRR for the two types of tests. No explanation was provided for the difference. Girgis also reported the times required for the fires to grow to 500 kW. These times should be roughly independent of test configuration since limited feedback from the upper layer is expected for fires of this size. Comparison of these times with similar values from the furniture calorimeter results were in better agreement than those for the maximum HRRs.

As part of a study aimed at developing appropriate design fires to represent growing fires on upholstered furniture, Young provided an extensive review of earlier studies dealing with the topic. [53] Results were collected in a database and used to derive probability distributions of such properties as time to peak HRR, peak HRR, total heat released, and effective heat of combustion. These distributions were used as the basis for design fires representative of developing RUF fires.

Other studies available from the University of Canterbury that are relevant to the problem of upholstered furniture flammability, but which do not deal directly with the subject of the current report include the works of Coles, [54] Chen, [55] and Wong [56].

Collier and Whiting investigated the early development of flaming fires ignited by small flame sources (either a match or small gas flame) on two-cushion mock-ups mounted on a steel frame. [57] The seat FPUF (NFR, 60 cm × 60 cm × 10 cm, 28 kg/m^3) and back FPUF (NFR, 60 cm × 60 cm × 6 cm, 21 kg/m^3) were chosen to be typical of lower-end RUF in New Zealand at the time. The FPUF was covered with a layer of 2.0-cm-thick polyester fiber wrap and a 100 % polyester fabric. The primary focus of the study was whether the incipient phase would substantially change estimates for the detection times and potential escape times for fires developing on RUF as compared to assuming the initiation time was zero time for a "*t*-squared" fit to the period of rapid growth in HRR.

The effect of ignition location on the seat cushion (front edge, center, and rear edge) on the "incipient" fire growth, which they defined as the period between the application of the ignition source and the time when the fire first grew to 30 kW, was reported. By performing at least three tests for each condition, probability curves for the time to reach 30 kW and the maximum HRR were generated for each ignition source and location. The average incipient periods varied from just under 60 s to greater than 130 s. The times were reduced for the gas burner as compared to the match. The reductions were dependent on ignition location, with the largest difference observed for the ignition at the back of the seat cushion. The longest incipient times were observed for ignition at the front edge of the cushion. The mock-ups failed to ignite when matches were applied at this location. The periods required to reach maximum HRRs followed similar trends. In addition to the chair mock-up, three chairs consisting of approximately 21 kg of FPUF, polyester fiber wrap, and upholstery fabric were burned following ignition in the center of the seat. An average of 115 s was required for the fires to reach maxima HRR of just under 1 MW.

Based on their observations, the authors concluded that the best definition for the end of the incipient phase was when a fire reached a HRR of 30 kW. Using a *t*-squared fit to the period of rapid HRR increase allowed alternate values for the incipient fire period to be derived, but the results showed wider variations than those using the fixed value of 30 kW. While incipient times varied with ignition location, the overall increases in burning time were relatively minor. Since neglect of the incipient time provides a conservative estimate of the time, the authors recommended that incipient fire growth times not be incorporated into estimates of fire growth based on a t^2-growth rate.

Bwalya et al. measured HRRs and temperatures for several samples of commercial upholstered furniture burned in a room. [58] Information provided about the chairs included upholstery fabric and total mass. The chairs were covered with polyester or blends of polyester and acrylic. A square burner generating 19 kW was applied for 80 s as an ignition source. Maximum HRRs varied from 0.9 MW to 2.7 MW. The fire with the highest HRR also grew the most rapidly, reaching the peak in 185 s. A chair, a loveseat, and a sofa constructed from the same materials were also tested. The fire on the chair reached a maximum HRR the fastest, but the maximum HRRs were higher and burning periods longer for the larger items.

A test series that involved burning sixty-four specially built chairs in an ISO standard test room (2.4 m × 3.7 m × 2.4 m) with a single doorway [59] has been described by Mehta. [60] The test series was designed to investigate the effectiveness of fire barriers in reducing the fire hazard of RUF. Sixteen different combinations of materials were tested in quadruplicate using a full factorial design. Materials included four cotton fabrics, either a polyester fiber wrap (1.9 cm thick, 240 g/m^2) or a fire barrier (0.95 cm thick, 135 g/m^2 polyester fiber wrap over a needle-punched sheet of 47 % fiberglass, 50 % modacrylic, and 3 % polyester fibers), and either NFR (29 kg/m^3, indentation load deflection (ILD) 25 % to 30 %) or FR (Cal TB-117) FPUF. Two of the cotton fabrics had been shown to be highly smolder prone, and two were more smolder resistant. Three of the fabrics had area densities close to 270 g/m^2, while the fourth was considerably heavier at 680 g/m^2. Measurements reported included HRR, vertical temperature profiles at two locations in the room, CO and CO_2 concentrations at a location just outside of the door, heat flux at the floor, and visual records. The ignition source was a 240 mm high butane flame applied for 70 s at the center of the crevice formed by the seat and back cushions. This source is similar to Ignition Source 3 specified in BS-5852. [23]

Visual records showed similar fire development on each of the chairs. After ignition, there was rapid flame spread upwards along the center of the back cushion. Flames then spread concurrently outward along the crevice formed by the seat and back cushions. The fire growth began to accelerate after the flames spread to and ignited the arms, and the remainder of the seat surface then became involved. The first HRR maxima occurred around this time. Comparison of fires for chairs with and without the fire barrier showed that flame spread in the absence of the barrier was substantially faster.

The HRR time curves for all of the tests showed two peaks similar to those described by Denize. [51] Recall that Denize attributed the first peak to the end of an initial growth period in which a fire spread to cover the inside surfaces of the seat, back, and arm cushions. The second peak was attributed to rapid fire growth associated with the development of burning of a liquid underneath the chair that had dripped down from above. Mehta also attributed the first peak to the full involvement of the soft materials (cushions, fabric, and batting on arms), but attributed the second peak to involvement of the wood frame of the chair. Interestingly, burning of a liquid in the area underneath the chairs was also described by Mehta. Based on this conclusion concerning the source of the second peak, most analysis was focused on the time to and magnitude of the first peaks, even though the second peaks were generally substantially larger.

Comparison of the results showed that the initial HRR peaks were reduced by roughly a factor of two for chairs which incorporated the fire barrier as opposed to those which included the polyester fiber wrap. The periods required to reach these peaks were increased by more than a factor of three. The effect of foam type was also assessed. Statistical analysis revealed that there was an average 7 % drop in the HRR maxima when the FRFPUF was used. This was judged to be a practically insignificant change. Whether or not a fabric was smolder prone was found to have little effect on fire spread and growth. Fire development on chairs with the three fabrics of roughly constant density were very similar for chairs with the same type of interliner. However, the values of the first HRR peak were reduced, and the time required to reach the maxima were longer for chairs covered with the heavier weight fabric.

The full factorial design of the study allowed a formal statistical analysis of the results. Miller considered the response of the two dependent variables (time to initial peak HRR, and initial peak HRR) to changes in the three independent variables (presence or absence of barrier, fabric type, and foam type). [61] The analysis revealed that the maximum HRR varied in a statistically meaningful way with changes in the barrier and foam type, but not with the four types of fabric. By far, the strongest response was for the presence or absence of a barrier, with, on average, the maximum HRR reduced by a factor of 2.1 by the inclusion of the barrier. The corresponding factor for exchanging the NFRFPUF with FRFPUF was 1.07. The times needed to reach the initial HRR peak were found to be statistically dependent on each of the three independent variables. As before, the strongest response was observed when the barrier fabric was added with a 3.3 factor increase in time. The corresponding factor was 1.03 when standard FPUF was replaced with FRFPUF. The periods required to reach the HRR peak were similar for three fabrics with roughly the same areal density, but considerably longer for the heavier-weight cotton.

Miller also considered the possible two- and three-way interactions between the independent variables. For the maximum HRR the only statistically significant result was found for the fabric/fire barrier interaction. It is interesting that fabric is involved since it was not statistically significant as a main effect. The author argues that its effect may have been masked by the strong barrier/fabric interaction. When the time to maximum HRR was tested the only significant interaction was between foam and barrier with the change in foam to FRFPUF resulting in a larger increase for chairs without a barrier than those with one.

An extensive and thorough study focused on the effectiveness of three possible approaches for reducing the flammability of upholstered furniture; namely, replacing untreated FPUF with a fire-retarded version, substitution of polyester fiber wrap with a high-loft fire barrier, and inclusion of a flat fire barrier between a polyester fiber wrap layer and the upholstery fabric; has been described by Fabian. [62] The investigation included material characterization as well as studies of ignition and burning behavior of small- and real-scale mock-ups. Most of the composite experiments were performed on small three-cushion mock-ups constructed by arranging the cushions (30.5 cm × 30.5 cm × 7.6 cm (seat), 22.9 cm × 30.5 cm × 7.6 cm (back), and 22.9 cm × 22.9 cm × 7.6 cm (arm)) in a corner configuration. The mock-ups were ignited above the seat cushion in the crevice formed by the back and arm cushions using the match-flame-equivalent BS-5852 Ignition Source 1 [23]. The standard calls for a 20 s application of the flame. If a mock-up failed to ignite following the 20 s period, the same flame was applied for 60 s longer. If ignition was still not

observed, the flame would be applied for an additional 300 s. Experimental measurements included HRR and mass and qualitative determinations of whether or not ignition occurred with a given ignition source and whether burning was sustained (i.e., burned completely over the mock-up).

The cushions were constructed with combinations of two types of FPUF (NFR, 29.6 kg/m^3 and FR meeting Cal TB-117, 27.6 kg/m^3), high-loft materials (either polyester fiber wrap, 1440 g/m^2 or one of five high-loft barriers), flat fire barriers (six different types), and a single polyester upholstery fabric (718 g/m^2). Combinations tested included the two FPUFs covered with the upholstery fabric with or without the polyester fiber wrap between the fabric and foam, NFRFPUF wrapped with each of the high-loft fire barriers, i.e., as a replacement for polyester fiber wrap, and cushions that included the NFRFPUF wrapped in polyester fiber wrap with one of the flat fire barriers interposed between the polyester and the outer upholstery fabric. Details concerning compositions and physical properties of the 11 barriers tested were provided.

The findings concerning the effectiveness of the three mitigation strategies were summarized as follows. Replacing NFRFPUF with FRFPUF resulted in a decrease in the period of flame application required for mock-up ignition, a reduction in peak HRR by an average of 45 %, and a more than doubling of the total burn time. Replacing the polyester fiber wrap with the high-loft fire barriers resulted in a lengthening of the time of source application necessary to ignite the mock-up, peak HRR average reductions of between 40 % to 60 %, and fire duration increases ranging from 500 s to 1600 s. Interposing thin fire barriers between a polyester fiber wrap layer and the upholstery fabric increased the period of ignition source application required for mock-up ignition from 20 s to values ranging from 60 s to greater than 300 s, fire peak HRR average reductions between 59 % and 66 %, and lengthening of the total burn times by 800 s to 1200 s. Overall, the inclusion of flat fire barriers resulted in the largest reduction in flammability, followed by replacing polyester fiber wrap with a high-loft fire barrier, and finally using FRFPUF in place of the NFRFPUF. In constructing the cushions, the side away from the fire were not sewn and were simply folded over. Fabian noted a tendency for a fire to spread around to these sides and penetrate the cushions to the FPUF through these openings, thus emphasizing the importance of seam integrity.

Based on the small-scale mock-up results, multiple copies of four types of chairs were manufactured that incorporated some of the same soft materials. The base chair, referred to as “Chair 1,” was built on a wooden frame equipped with springs and incorporated loose seat and back cushions. The arms and the back cushion support were padded on the inside of the chair with polyester fiber wrap over FPUF and on the outside with polyester fiber wrap. The same polyester fabric used for the mock-ups covered the chair’s outer surfaces. The cushions included 10.2 cm thick NFRFPUF slabs with polyester fiber wrap and were upholstered with sewn polyester fabric. Overall cushion dimensions were not provided. Chair 2 was similar to Chair 1, with the exception that NFRFPUF was replaced with FRFPUF meeting Cal TB-117. Chair 3 was the same as Chair 1, but with the polyester fiber wrap replaced with one of the high-loft fire barriers (FB 8). Chair 4 was the same as Chair 1, but also included one of the flat fire barriers (FB 3) between the polyester fiber wrap in the seat and back cushions and in the inside and outside arms and backing the outer upholstery fabric.

A BS-5852 Ignition Source 1 was used to ignite the chairs at three different locations: interior corner formed by the seat, back, and arm cushions, at the center of the crevice formed by the seat and back cushions, and at the lower rear on the outside back of a chair near a leg. A 20 s application of the ignition source was found to be sufficient to ignite the chair at the corners and in the seat/back crevices. For tests with the ignition source located on the rear of the chair, flame extinction was frequently observed shortly after the ignition source was removed. Chair 1 ignited following the first application of the ignition source, and Chairs 2 and 3 ignited after additional applications. Chair 4 failed to sustain burning after four applications of the small flame.

Maximum measured HRRs for the 12 tests varied with the chair type and ignition location. The highest values (≈ 1.3 MW) were recorded for Chairs 1 and 2 with only moderate variations due to ignition location and the type of FPUF used. Fires on Chair 3, in which the polyester fiber wrap was replaced with high-loft fire barrier, generated maximum HRRs around 400 kW with little variation due to ignition location. The two Chair 4 tests where burning was sustained had maximum HRRs that were roughly half of those measured during Chair 3 fires. As noted above, when ignited at the rear location, Chair 3 did not sustain a fire. Fire growth behavior was characterized by recording the times required for a given fire to reach HRR levels of 100 kW, 200 kW, 500 kW, 1000 kW, and the peak HRR. The results showed that the most rapid fire development took place on Chairs 1 and 2, while growth rates on Chairs 3 and 4 were slower. Fire growth rates were comparable for ignition in the corners and in the crevices of the seat and back cushions, but was noticeably slower following ignition at the back of a chair.

Based on the experiments, Fabian concluded that "collectively these results show that the benefits of the flame retardant treatment foam utilized in this study are overwhelmed by the ignition source and application duration employed in this study and does not result in a practical benefit to occupants with respect to occupant safety and egress time."

Janssens performed an extensive study of the burning of RUF mock-ups and actual furniture with the goal of assessing the capabilities of various literature models for predicting the burning behavior (maximum HRRs and burning times). [63] Mock-up fires were studied in an open furniture calorimeter and within an enclosure (4.65 m × 3.43 m × 2.43 m) with a single doorway. Measurements reported included HRR using oxygen consumption calorimetry, mass using a load cell, temperatures at multiple locations within the room, heat flux at the floor in the center of the room and at two locations above the floor, still photography and video recordings.

A wide range of parameters were varied during the mock-up experiments. The mock-ups were constructed from seat and back cushions having dimensions of 46 cm × 46 cm × 10 cm oriented at 90°. When included, arms for the mock-ups were 46 cm × 36 cm × 10 cm cushions. The mock-ups were supported on steel frames based on those described in Cal TB-133. [25] The experiments focused on chair mock-ups formed from seat, back, and two arm cushions or sofa mock-ups incorporating three sets of seat and back cushions with arm cushions. Limited experiments were also performed for chair mock-ups without arms and for a loveseat mock-up incorporating two pairs of seat and back cushions with arms. Cushions were constructed from one of two fabrics (cotton, 355 g/m^2; heavily fire-retarded cotton, 415 g/m^2 meeting NFPA 701 [64]) and one of six padding materials (low density NFRFPUF, 17 kg/m^3; high density NFRFPUF, 45 g/m^3; a Cal TB-117 FPUF, 23 kg/m^3; polychloroprene latex foam, 103 kg/m^3; polyester wrap, 16 kg/m^3; and densified polyester, 23 kg/m^3). Three types of ignition sources (small flame, large flame, and liquid fuel) were used. The ignition sources were applied to one of three locations on the mockups—in the center of the seat cushion, at the center of the lower front edge of the seat cushion, and at the center of the lower rear edge of the seat cushion. The small flame source was generally the BS-5852 Source 1 butane flame, but Source 2 was occasionally used when an item failed to ignite. [23] The large gas flame used at the center of the seat cushion was the square burner specified in Cal TB-133. [26] When ignition was at the two lower locations on the mock-ups, the square tube burner was replaced with a square 25 cm × 25 cm sand burner employing the same butane flow rate and application time. [28] When a liquid fuel was used on the top of the seat cushion, 59 ml of gasoline were poured over the top of the seat cushion and ignited. For the two lower positions 118 ml of gasoline were poured over a 28 cm × 43 cm × 2.5 cm ceramic fiber blanket and ignited.

A series of eighteen tests were run under the furniture calorimeter in general accordance with ASTM E 1537 [28] using various combinations of the upholstery fabric and filling materials. For three of the tests the Cal TB-133 burner specified in the standard was replaced with the BS-5852 Source 1. Most tests involved the chair configuration with arms, but a single test was run using the loveseat configuration, and two with the

sofa configuration. HRR curves for repeated tests using cushions with non-fire-retarded cotton and FPUF showed excellent agreement when the Cal TB-133 ignition source was used, but much poorer agreement, due primarily to differences in fire growth behavior, when the small ignition flame was used. This difference is generally consistent with observations reported in other studies. The two tests using a sofa configuration were done with ignition on the center or right-hand cushions. After initial periods in which the fire growth was similar, the fire ignited at the center cushion grew much more rapidly and reached a HHR maximum more than twice as high as observed for the fire ignited on the edge cushion. When the fire-retarded cotton was combined with polychloroprene latex foam, the mock-up was barely ignited with the Cal TB-133 burner, and the fire rapidly died away after the burner was removed. Similar burning behaviors were observed for otherwise similar mock-ups when the lower- and higher-density polyester wraps were incorporated in the cushions.

Sixty-one mock-up burn tests were run in the test room. Thirty-six of these tests were part of a reduced-factorial-design study of the dependence of mock-up burning behavior on ignition source (small gas flame, large gas flame, and accelerant), ignition location (center of seat cushion, lower front, and lower rear), cushioning material (NFR low density FPUF, NFR high density FPUF, and Cal TB-117 FRFPUF) and mock-up size (chair or sofa). The non-fire-retarded cotton fabric was used to upholster the mock-ups for these tests. A one-third factorial model was used to reduce the 27 possible combinations for each of the mock-ups sizes to 9. Allowing for two repeats of each combination led to the requirement for 36 tests.

A novel approach was used to characterize the experimental HRR curves. The first step was to assume that the HRR had a triangular shape. By identifying the times when the HRR first went above 100 kW (t_1), reached its maximum HRR (PHHR, t_p), and first fell below 100 kW (t_2), the triangle for a given test was defined by drawing straight lines from the HRR maximum through the 100 kW levels at t_1 and t_2. The lower vertices of the triangles at HRR = 0 kW were defined to be t_0 and t_3. The four independent variables t_0, t_p-t_o, *PHRR*, t_3-t_0 were treated as the response variables for the experiments. An analysis of variance was used to determine whether a given experimental response depended on the experimental factors in a statistically significant manner. An ignition delay was defined as the period between application of the ignition source and t_0.

The analysis showed that the ignition source had a significant effect on ignition delay for both chair and sofa configurations due to significantly higher values for the small ignition sources as compared to those for the two larger sources, which yielded similar values of t_0. A significant effect of ignition location was also identified for the chair mock-ups, but was absent for the sofas. The analysis also indicated that there was a strong effect of foam type on the peak HRR. More detailed comparison showed that most of the dependence was due to the much lower values recorded for the Cal TB-117 FPUF as compared to those for the lower and higher density NFRFPUFs, which were very similar. Ignition location also affected the peak HRRs for the chair configuration, with ignition at the rear location resulting in lower values. It was also found that t_p-t_0 and t_3-t_0 values were dependent on the location of the ignition source for the chair mock-ups (with slower fire growth following ignition at the back) and by the type of ignition source for the sofas (with the large flame ignition sources resulting in slower fire growth).

Twenty-five additional mock-up tests were run in the enclosure. These were designed to investigate the effects of changes in configuration such as mock-ups with a gap introduced between the seat and back and changing to a loveseat configuration, composition such as including the fire-retarded cotton fabric or densified polyester padding, and ignition scenario such as igniting in a corner instead of at the center of a cushion that were not addressed during the factorial design experiments. The only finding based on these additional tests discussed by Janssens was that moving the ignition location from the center of the seat cushion to one of the corners formed by the seat, back, and arm resulted in faster fire growth but a reduced peak HRR for both chair and sofa mock-ups.

An additional series of tests were run in the burn room using actual RUF provided by employees of Southwest Research Institute. An important criterion was that any donated furniture had to consist of at least two matching pieces. This allowed one item to serve as a test item while the second provided materials for small-scale testing and, in some cases, for replicate testing. Twenty-two sets of furniture were collected and 27 individual items were burned in the room. Items ranged from simple chairs without arms through large sofas. Three ignition sources were used—liquid, 59 ml of gasoline poured on the seat cushion; small gas flame applied to the center of the seat cushion; and small gas flame applied in the corner formed by the seat, back, and an arm cushion.

A pair of upholstered chairs were ignited with the small flame and the liquid fuel. The fire on the chair ignited with the gasoline developed much more quickly, but the time behaviors of the primary heat release periods were very similar and matched closely when overlaid by time shifting the curve for ignition with the small flame by 170 s. Heat release rate curves for all tests are provided. The vast majority of items generated HRRs in excess of 1 MW, and in some cases the fires sizes approached 3 MW. Note that these values are considerably higher than those generated during the mock-up tests. Only one set of furniture generated maximum HRRs considerably less than 1 MW. These were three chairs without arms that were covered with vinyl fabric. Maximum HRRs for these were generally less than 100 kW.

Storesund et al. describe the burning behaviors of small RUF mock-ups, based on the three-cushion corner configuration introduced by Fabian [62], following application of either a small match-like flame source for fifteen seconds [46] or a BS-5852 Crib 5 ignition source [23].[65] The focus was the possibility of improving the flammability properties of contemporary RUF without the use of flame retardants. Materials used in the mock-ups were chosen based on their current use in RUF in Scandinavia, their potential to improve flammability properties, and commercial availability. These included seven cover fabrics (natural and man-made materials and blends), a single polyester wadding (200 g/m^2), three barrier fabrics (two fiber glass weaves (25 g/m^2, plain weave and 80 g/m^2, twill weave), and an aramid fiber (36 g/m^2)), and a single FPUF (35 kg/m^3). Measurements reported include instantaneous heat release and smoke production rates with burning behavior characterized in terms of total heat release, maximum HRR, and total smoke production.

In tests involving six different cover fabrics covering the polyester wadding over the foam, only one of the mock-ups (incorporating an 83 % cotton, 9 % modal, 8 % polyester blend) was ignited by the small-flame source. The remaining tests used the Crib 5 Ignition Source. In thirteen tests involving various combinations of fabric and barrier materials, the mock-ups were ignited by the stronger source in all but two, both of which incorporated one of the barrier fabrics.

The principal conclusion of the study was that the use of barrier fabrics generally reduced the maximum HRR and the total heat release as compared to cases without barriers, even though substantial variations in effectiveness were observed depending on the particular combinations of cover and barrier fabrics used. Based on their findings, the authors proposed that a voluntary system be created that would rate the flammability of actual RUF and allow consumers an opportunity to choose a desired level of fire performance.

As a follow up to their earlier study on the potential for barrier materials to reduce the flammability of RUF [60], researchers at CPSC investigated the burning behaviors of chairs with wooden frames that incorporated a variety of upholstery materials. [66] Both smoldering (cigarettes) and flaming ignition (BS-5852 Ignition Source 3, 240 mm butane flame applied for 70 s [23]) sources were used. Here, we focus on the results with the flaming ignition source.

The chairs ignited by the open flame incorporated one of two cover fabrics (100 % cotton, 441 g/m^2; 56 % rayon/34 % polyester/10 % cotton, 339 g/m^2), one of five barrier fabrics containing various levels of fire

retardants (cellulose based, nonwoven; glass/modacrylic/polyester, needle-punched; modacrylic/glass, knit; rayon/polyester, high-loft; and rayon/polyester, densified) and/or polyester batting (271 g/m^2, 1.9 cm thick), and a single FPUF (28.8 kg/m^3, ILD of 25 % to 30 %, some added melamine). When barriers were included they were placed over the polyester batting. The fire barriers and polyester batting fully enclosed the seat and back cushions and were also incorporated in the arms and in the side of the back support facing the back cushion. A novel aspect of the study was that half of the chairs were subjected to simulated aging by repetitively applying a 750 N force through a 25 cm plate to the center of the chair seat cushion for two hundred thousand cycles. Combining the various variables results in 24 possible combinations. The test plan called for three repeated tests or a total of 72 tests. In practice, due to a manufacturing problem, some combinations were repeated only two times, while others were tested four or five times.

The burning behavior of the chairs was characterized using time-resolved HRR measured by oxygen consumption calorimetry. Parameters used to describe the HRR curves included the peak HRR during the first fifteen minutes, the peak HRR, the time to reach the peak HRR, the time to reach a HRR of 200 kW, and the total heat released during the initial ten minutes. For each parameter, time was taken to be 0 s when the flaming ignition source was removed from the chair, i.e., nominally 70 s after the gas flame was applied.

In seven of the tests, the chairs were not ignited by the 70 s application of the butane flame. These chairs included either the glass/modacrylic/polyester or the modacrylic/glass barrier fabrics, with the majority incorporating the glass/modacrylic/polyester fabric. For those chairs that did ignite, maximum HRRs varied from a low of 470 kW to a maximum of 2.2 MW. Data plots included in the report revealed that adding the barrier fabrics to the chairs significantly improved the burning behavior compared to chairs with only the polyester batting, reducing the peak HRR by 40 % to 60 % and increasing the time to maximum HRR by 10 min to 20 min, i.e., by roughly a factor of three. In general, the chairs covered with the 100 % cotton fabric performed better than the chairs covered with the rayon/polyester/cotton blend. Fires on chairs that had undergone mechanical stressing of the seat cushion seemed to develop somewhat faster, but had similar HRR curves that were simply offset in time.

The authors provide a general description of the fire spread and growth on the chairs that developed high HRRs. Following removal of the ignition flame, the fire initially spread upward on the back cushion and more slowly radially outward on the seat cushion. As the flames spread over the cushions, they fire grew in intensity. Burn through of the back cushion and chair back occurred first and exposed the interior of the chair to increased air flow. At this point the fire HRR grew more rapidly. Eventually, liquid was observed dripping down on the floor below the chair and a strong pool fire developed here. Afterwards, the fire died down slowly.

The number of repeated tests available in the CPSC study was designed to allow a statistical analysis to be performed as described by Miller. [67] In particular, the design allowed an analysis of variance (ANOVA) on the experimental parameters of maximum HRR and time to maximum HRR due to the presence or absence of barrier fabrics. The author expressly noted that the experimental design was not intended to differentiate the relative effectiveness of individual barrier fabrics.

For the analysis based on peak HRR, Miller first considered a full model involving three main effects (barrier, fabric, age) and their two- and three-way interactions. Eliminating terms with *p*-values greater than 0.25 resulted in a model with three main interactions and two two-term interactions (barrier*fabric and fabric*age). The ANOVA itself revealed that the two remaining two-term interactions were not statistically significant. Of the three main effects, barrier and fabric had statistically significant effects while age did not. The effects of barrier and fabric were characterized as strong effects.

A similar analysis for time to maximum HRR resulted in a reduced model with the three main effects and the same two two-way interactions as for the HRR. Unlike as found for maximum HRR, the barrier*fabric

two-way interaction was shown to be statistically significant and was included in the analysis. This suggests a synergistic effect existed between these two material types. As observed in the maximum HRR analysis, the main effects of fabric and barrier were statistically significant, while aging was not.

It is apparent that the burning behavior of RUF has been a focus of fire research and regulatory concern since the mid-1960s. Despite this attention, by 2010 the only mandatory regulation for RUF flammability in the United States was Cal TB-117, which was first introduced in 1975. It was designed to limit smoldering ignition of upholstery fabrics by cigarettes and small flame ignition by reducing the small-flame ignitability of cushioning materials, primarily FPUF. As discussed above, the effectiveness of Cal TB-117 in providing practically important reductions in the small-flame ignitability for upholstered materials had been brought into question by numerous studies, starting with the work of Babrauskas. [37] The nationwide voluntary UFAC standard primarily addresses smoldering ignition of upholstery fabrics by cigarettes. [13]

Since the burning behavior of RUF was first recognized as being a national concern, there have been significant changes in the magnitude and understanding of the problem as well as the landscape surrounding current and potential regulation. Some of these changes are summarized to provide additional context for the current on-going study.

Starting in 1980, the United States has had a system in place for collecting and analyzing fire statistics. The current manifestation is known as the National Fire Incident Reporting System (NFIRS). [68] The NFPA has routinely used these statistics to assess the fire problem within the country. These studies include periodic assessments of the nature of fires in residences as well as those that begin with ignition of upholstered furniture. Two recent reports in these series provide important insights into the contribution of fires involving upholstered furniture to fire losses in homes and how they have changed with time. [69, 70] These reports consolidate fire statistics over five year periods ranging from 2010-2014 [69] and 2009-2013 [70]. Changes in various statistics over the period starting in 1980, the first year reliable statistics became available, up to the present time are discussed.

The first study focuses on fires in which RUF was identified as the initial item ignited. It shows that for the 2010-2014 period there were an average of 5,630 fires reported annually in which upholstered furniture was the first item ignited. [69] This number represents 2 % of fires reported in homes during the period. The number of civilian fire deaths due to these fires averaged 440 per year, corresponding to 18 % of the total. The statistics indicated that there were fires deaths associated with one out of every 13 reported fires that began on upholstered furniture and that such fires were nine time more likely to result in a fatality than the average for all fires in homes. These fires also resulted in 700 injuries and $269 million in fire losses annually. RUF ignition represented the highest percentage of fire deaths for all item types identified as first ignited.

Numerous ignition sources that ignite RUF were listed, but smoking materials dominated, being responsible for an average of 220 deaths per year (50 %) of the deaths resulting from direct ignition of RUF. Roughly one third of the fatal fires did not spread beyond the room of fire origin. The remaining fire deaths were distributed roughly evenly between fires ignited by intentional actions, candles, hot ember or ash, heating equipment, electrical distribution and lighting equipment, and playing with a heat source. Note that there is some ambiguity as to whether the initial burning behavior was smoldering or flaming. Smoking materials and hot ember or ash sources would be expected to induce initially smoldering fires, while intentional actions, candles, and playing with a heat source would most likely ignite flaming fires. Heating equipment and electrical distribution and lighting equipment can cause either type of ignition.

Despite the central role played by RUF in fire losses in recent times, the situation has improved dramatically since the early 1980s, with the annual number of reported fires ignited on RUF declining by 85 %, from a high of 36,900 to a low of 5,400. [69] The decline in related fire deaths over the same period, 58 %, was

not as large. These percentage changes can be compared with those for all fires of 50 % and 47 %, respectively. [71] Note that the improvement in fire losses with time is actually somewhat better than suggested by the raw numbers since the overall population and number of homes increased substantially over this period. The statistics show that the largest percentage drop of the various ignition sources identified for RUF fires was for smoking materials. In 1980 ignition by smoking materials was responsible for 62 % of RUF-ignited fires and 80 % of associated deaths. By 2014, the percentages had dropped to 27 % and 50 %. The statistics suggest that most of the gains in fire safety occurred during the 1980s, with losses tending to level off or drop more slowly after this time.

The second study is a more general discussion of structural fires in homes. [70] The 50 % drop in fires and 52 % drop in fire deaths since the 1980s was mentioned above. When weighted for population, the reduction in fires deaths becomes 64 %. Interestingly, the rate of fire deaths per reported fire remained nearly constant over the period. This suggests that most fire deaths occur when fires reach a size where it is necessary to call the fire department, and that the likelihood of fire deaths for such fires has not changed since the 1980s. Most fire losses in homes occur in one- and two-family homes, and the overall fire losses in homes resemble the profile for such residences. It also noteworthy that 92 % of all civilian structural fire deaths in the United States occur in homes. The analysis shows that the most likely cause of home fires at 45 % was cooking equipment, and such fires were also responsible for the highest percentage of injuries. In contrast, smoking materials were identified as the cause in only 5 % of the fires, but were responsible for the largest fraction of fire deaths, 22 %.

In response to the high fire losses due to cigarette ignition of RUF, laws have been passed in all fifty states requiring that burning cigarettes have a reduced ignition propensity (RIP) as compared to older cigarettes when placed on upholstered fabrics.

Not surprisingly, the most likely origin for a fire to start, 43 %, was in a kitchen even though the associated percentages of fire deaths, 16 %, and property losses, 15 %, were much lower. On the other hand, while the likelihood of a fire starting in a bedroom, 7 %, or in a living room, family room, or den, 4 %, were much lower, fires in these locations were each responsible for one quarter of all fire deaths. Note that fires in locations where upholstered furniture is expected to be concentrated are six times more likely to result in death than the average fire in a residence. The high percentages of fatal fires associated with RUF ignition are consistent with the raised likelihood of death for fires in these areas, since RUF is expected to be concentrated in these types of rooms.

Ahrens discusses the correlation of fire size with fire deaths. It was noted that only 25 % of fires spread beyond the room of fire origin, but that 81 % of fire deaths occurred in these larger fires. This finding suggests that fire deaths are strongly correlated with large flaming fires.

The studies discussed above have demonstrated that a large percentage of modern upholstered furniture can support unusually rapidly developing, high HRR fires following flaming ignition. While circumstantial in nature, the fire statistics described by Ahrens suggest that these burning characteristics of RUF are associated with the enhanced likelihood of fire deaths for fires ignited on RUF and in the areas of homes where RUF items are expected to be concentrated. There is also evidence that fire spread beyond the room of fire origin is an important component of the problem, which is also expected when fires grow rapidly. Despite the apparent central role of flaming RUF in fire losses, much of the regulatory focus has been on limiting the ignition likelihood of RUF by smoldering and match-like flame sources. Particularly with regard to smoldering sources, the focus has been on the upholstery fabrics, which can be traced back to changes in the fabric flammability act in 1967 to include RUF. [4] Very little regulatory focus in the United States has considered the potential for flaming RUF fires to accelerate fire spread and HRR growth within and from a room of fire origin.

As a first step toward improving quantification and understanding of the contribution of flaming RUF fires to fire losses in the United States, one of the authors of this report organized a workshop entitled "Quantifying the Contribution of Flaming Residential Upholstered Furniture to Fire Losses in the United States." [72] The workshop brought together experts in the analysis of fire statistics and fire scientists knowledgeable in furniture burning behavior and building fire dynamics. Major workshop findings included: 1) fires involving flaming RUF have the potential to grow very rapidly to high HRR levels capable of threatening civilians, firefighters, and property, 2) fires involving RUF are a major factor in current fire losses in the United States, contributing at much greater levels than their numbers would indicate, and 3) existing statistical analyses likely underestimate the full contribution of flaming RUF to fire losses. One of the recommendations was a possible approach for quantifying fire losses associated with fires in which RUF was not the first item ignited, but became involved after ignition from another flaming source. The approach was based on an optional field in the NFIRS data base which identifies the item contributing most to flame spread. Several recommendations for reducing the uncertainties in estimates of fire losses due to flaming RUF fires were provided. An additional important conclusion was a consensus among the participants that the vast majority of losses associated with fires in which RUF is ignited by a smoldering source occur after such fires transition from smoldering to flaming. An implication of this finding is that possible approaches for limiting fire growth rates on flaming RUF could reduce the impacts of RUF fires ignited by both smoldering and flaming sources.

John Hall of NFPA implemented the procedure proposed during the workshop to estimate the number of fire deaths associated with fires in which RUF was not the first item ignited, but was the primary contributor to fire growth once ignited. In the interest of rapid dissemination, the results of his analysis were included as an appendix in a revision of the workshop proceedings. [73] A more complete description of the work was subsequently published. [74]

The results of Hall's analysis are striking. As a first step he estimated the average annual numbers of fires and fire losses during the period from 2006 to 2010 that could be associated with various types of RUF ignition sources including, for the first time, the number of fires due to flaming ignition of RUF by fires originally ignited on other objects. Table 1 is compiled from the published work. [74] The results of the analysis show that the number of fire deaths associated with the burning behavior of RUF are increased by 32 %, and the number of fires involving RUF are increased by 27 %. Based on this new analysis, the percentage of fires due to smoking material ignition of RUF represent 21 % of RUF fires and 44 % of fire deaths. RUF fires due to ignition by smoking materials remain responsible for the largest fraction of fire deaths, but the number associated with flaming ignition by another item is nearly half as large. Combining the totals for ignition sources expected to result in flaming ignition results in values of fire deaths that are comparable in magnitude to those resulting from ignition by smoking materials.

Based on the implication of the enhanced analysis of RUF fires and losses, Hall concluded that "Strategies to address such fires would need to test resistance to ignition by a much stronger heat source (representing another burning item) than the test fire used when evaluating resistance to ignition by small open flame. In fact, such strategies might need to abandon the goal of prevention through resistance to ignition in favor of a goal of mitigation through improved fire performance (e.g., slower fire growth, lower peak intensities)."

During the 1970s concerns arose about the possible negative effects on human health and the environment of some of the chemicals being added to fabrics and plastics to reduce their flammability. One of the earliest studies focused on the flame retardant tris-(2,3-dibromoproply)phosphate, which was widely used to flame retard fabrics in children's sleepwear in order to meet flammability standards. [75] Experimental evidence was presented that this chemical was mutagenic and likely carcinogenic. Several additional flame retardant chemicals were also identified with similar concerns that they might be potentially harmful. The authors discussed the need to consider both the risk and benefits of including flame retardants in commercial

Table 1. Average number of RUF ignitions per year (2007-2011) by various direct ignition sources and by flame spread from other burning objects.

	Fires	Civilian deaths	Civilian injuries	Direct damage (in millions)
Lighted tobacco product	1,900 (21 %)	270 (45 %)	320 (29 %)	US$97 (17 %)
Open flame from other fire	2,200 (25 %)	130 (21 %)	280 (25 %)	US$138 (24 %)
Operating equipment	1,500 (17 %)	70 (12 %)	140 (13 %)	US$81 (14 %)
Small open flame	1,400 (16 %)	60 (10 %)	220 (20 %)	US$69 (12 %)
Ember, ash or other or unclassified hot or smoldering object	1,300 (15 %)	60 (10 %)	130 (11 %)	US$150 (27 %)
Unclassified, other or multiple heat source	600 (7 %)	20 (3 %)	30 (3 %)	US$31 (5 %)
Totals	8,900 (100 %)	610 (100 %)	1,120 (100 %)	US$566 (100 %)

products. A second publication from the same group identified a similar flame retardant, tris-(1,3-dichloro-2-propyl) phosphate as a mutagen. [76]

During the following decades researchers continued to generate evidence that halogenated flame retardants were accumulating in the environment and living organisms, including humans, and that they posed potential risks to the environment and human health. An understanding of the concerns and state of the science at the turn of the 21st century can be obtained by reviewing papers published in two special issues of journals dedicated to the topic. [77, 78]

One family of flame retardants that received a great deal of attention was the polybrominated diphenyl ethers. Three types were widely used as fire retardants—penta-, octa-, and decabromodiphenyl ether. Up to this time, pentabromodiphenyl ether had been widely included in FPUF used for RUF in order to meet the Cal TB-117 small-flame ignition resistance requirement. This flame retardant is a mixture of several possible isomers and can contain small amounts of additional molecules with fewer or higher numbers of bromine atoms. Due to environmental and health concerns, several states banned its use, starting with California in 2003 with a 2006 implementation date. [79] In 2004 the only US producer of the penta- and octa-forms halted production. [79] CPSC and the U. S. Environmental Protection Agency began to assess the potential toxicity of flame retardants used in RUF. [79-82]

Babrauskas et al. explicitly discussed the evidence suggesting the relative ineffectiveness of flame retardant levels incorporated in FPUF conforming to Cal TB-117 in limiting flaming ignition and fire growth on RUF and the mounting evidence concerning the potential harmful effects of the flame retardants used to meet the standard. [83] They concluded that little fire safety had been achieved while introducing harmful chemicals into homes and the environment. It was suggested that Cal TB-117 be revaluated based on their conclusions. They emphasized the need to consider the potential impacts of approaches for reducing flammability on human health and the environment when developing approaches for reducing flammability.

In 2012 Stapleton et al. published a study in which samples of FPUF collected from upholstered couches around the United State were tested for the presence and type of flame retardants. [84] Flame retardants were identified in 85 % of the 102 samples tested. For RUF purchased prior to 2005, there was no detectable flame retardant in 24 % of the items. The most common flame retardant was pentabromodiphenyl ether (39 %) followed by tris-(1,3-dichloro-2-proply) phosphate (24 %). Seventy-four percent of items purchased after the 2005 phase-out of pentabromodiphenyl were found to contain tris-(1,3-dichloro-2-propyl) phosphate and/or chemicals associated with a commercially available fire-retardant mixture (isopropylated triarylphosphates along with 2-ethylhexyl-tetrabromobenzoate and bis(2-ethylhexyl) tetrabromophthalate). tris-(1,3-dichloro-2-proply) phosphate was present in over half of the post 2005 samples. Non-halogenated organophosphate flame retardants were identified in 13 % of the couches. The percentage of non-flame-retarded couches had dropped to 7 %. While the total number of samples was limited, the findings suggest that the types of flame retardants used changed dramatically when pentabromodiphenyl ether was removed from the marketplace, and the percentage of couches which were fire retarded increased substantially. Since RUF was collected from around the country, the study concluded that flame retardants were generally included whether or not the furniture was sold in California.

Most of the discussion prior to 2012 concerning RUF flammability and the possible toxicity of the flame retardants used to meet Cal TB-117 took place in technical forums. While some specific flame retardant chemicals were no longer being added to the FPUF used in RUF, the use of others to meet Cal TB-117 remained widespread. The dynamics of the discussion changed abruptly in May 2012 when the Chicago Tribune published a four-part investigative series on the use of flame retardants in RUF and the manner by which their use had been justified. [85-88] The publication of this series led to numerous additional stories in other newspapers, magazines, and scientific venues, as well as the release of a full-length documentary movie. The total effect of the increased scrutiny was a greatly enhanced public awareness and increasingly

urgent calls for changes in the policies that led to the incorporation of flame retardants (particularly brominated flame retardants) in American RUF.

Response of governmental bodies to the publication of the Chicago Tribune investigation was rapid and intense. On June 18, 2012, Governor Brown directed the California Bureau of Electronic and Appliance Repair, Home Furnishings and Thermal Insulation to review Cal TB-117 and make recommendations for reducing or eliminating dangerous chemicals. [89] The following month BEAR-HFTI released a draft revision of Cal TB-117-2012 that eliminated small-flame testing of FPUF used in RUF and included a smoldering ignition test similar to ASTM E-1353-08a. [90] Following public hearings, public comment periods, and revision, Cal TB-117-2013 was adopted in June 2013. It went into effect in January 2014 and was fully implemented as of January 2015. [91] The United States Senate Subcommittee on Financial Services and General Government, Committee on Appropriations, chaired by Senator Richard Durbin of Illinois, held hearings on July 17, 2012, that focused on RUF flammability and the possible toxicity of flame retardant chemicals. [92]

The NFPA released a white paper on the fire problem associated with RUF in which the statistics concerning RUF fires were reviewed. [93] The emerging new understanding and increased estimates of fire losses due to RUF burning when RUF is the major item contributing to fire growth, but not the first item ignited, were emphasized. When the expanded contribution to fire deaths was considered, RUF was found to be a primary factor in 24 % home fire deaths (slightly more than 600 deaths per year). Five major scenarios for RUF fires were identified: 1) cigarette-ignition (45 % of total upholstered furniture home fire deaths), 2) open flame ignition by another fire (21 %), 3) ignition by arcing or heat from operating equipment (12 %), 4) small-open-flame ignition by candle, match or lighter (10 %), and 5) smoldering ignition by ember, ash or other or unclassified hot or smoldering object (10 %). It was estimated that between 55 % and 67 % of RUF fires start as smoldering fires with the remainder ignited by flaming sources. Smoldering fires that did not transition to flaming were estimated to be responsible for only 1 % of total home fire deaths. The white paper concluded that nearly all fire deaths and property damage from fires that start as smoldering fires "are caused by fires that transition to flaming at some point and have most of their growth after that transition."

The white paper included a discussion of the various regulations that had been put in place to address the RUF flammability problem. These primarily addressed limiting smoldering and small flame ignitions. It was argued that existing regulations (note that Cal TB-117 was about to be modified) only addressed scenarios responsible for about 55 % of fire deaths. A number of potential engineering solutions to reduce fire losses associated with RUF were discussed along with their potential to better match the ignition profiles for these fires.

Dr. Richard Gann has provided a recent overview of RUF flammability and its contribution to fire losses. [94] It includes a review of statistics for fire losses and incorporated the recent analysis of Hall that emphasized the contribution of flaming RUF as a second item ignited to fire losses, leading to a conclusion that "the number of fire deaths due to flaming of upholstered furniture is in the range of the number resulting from cigarette ignition." The analysis also indicated that a large fraction of the fire deaths associated with cigarette ignition of RUF occurred outside of the room of fire origin. Since such deaths are unlikely without flashover, this suggests that a large fraction of these deaths occurred following transition of smoldering RUF to flaming fires. The state of regulation of RUF in the United States was discussed along with the proposed changes (at that time) of Cal TB-117. The California regulation for the flammability of contract furniture, Cal TB-133, was also summarized. [26]

Thus far the role of mattresses in fire losses has not been discussed. Fire statistics show that fire deaths and fiscal losses due to fires starting on mattresses have historically been comparable in magnitude to those starting on RUF. However, as Gann discusses, the regulatory history for mattresses has been very different

from that for RUF. [94] Mattress manufacturers and their trade association worked closely with regulators to develop an approach to significantly reduce the flammability of their products. The result was CPSC 16 CFR 1633, a Federal regulation which limits the HRR of a mattress and its foundation to less than 200 kW during the 30 min following ignition by a very robust source and the total heat evolved during the initial 10 min to 15 MJ (i.e., average of 25 kW). [95] This regulation went into effect in 2007 and requires testing of all commercial mattress models. Prior to introduction of this regulation, a single flaming mattresses could routinely generate a fire of 2 MW or higher. Due to the stringent nature of the regulation and its testing requirements, it is anticipated that fire deaths associated with fires starting on mattresses will drop significantly as older models are replaced with the newer types having vastly improved fire behavior. As a result, we concluded that the mattress flammability problem has been adequately addressed and have chosen to focus our research efforts on RUF flammability.

Gann's review also provides an illuminating discussion of why the RUF flammability problem is considerably more difficult to address than that for mattresses. The reasons include the large number of relatively small manufacturers, the highly varied and rapidly changing materials used, and the extremely large number of styles and geometries. As a result, it is not feasible to consider fire testing of every single type of RUF. Gann argues that an approach is needed where manufacturers can simply estimate the flammability behavior of their furniture based on design and materials utilized. The flammability behavior is described in terms of three stages starting with smoldering, with the potential negative consequences of each stage rapidly increasing. The stages are: 1) smoldering, 2) transition, and 3) flaming involvement. Note that flaming ignition results primarily only in stage 3 burning). A number of possible approaches for improving the flammability behavior of RUF by intervening at the three stages were presented.

The following section (2) describes the partial factorial test plan used to study the burning behavior of the real-scale mock-ups. This is followed by a description of the experimental system employed (Section 3). The analysis procedures used are discussed in Section 4. Section 5 summarizes the observations and measurement results for the experiments forming the experimental test matrix. Similar results for a few supplemental experiments are included in Section 6. Section 7 summarizes the results of several statistical analyses designed to identify which measures used to characterize the flammability behavior have statistically meaningful dependencies, along with their relative magnitudes, on the mock-up properties varied in preparing the cushions. The next section (8) discusses the observations and findings and some final remarks are included in Section 9.

Table 2. General properties of materials utilized in real-scale mock-up tests.

Upholstery Material	Polyurethane Foam	Polyester Fiber Wrap	Fire Barrier	Fire Barriers	Sewing Thread
Thermo-plastic	Standard, non-FR	Yes	Yes	High-loft, non-woven FR-fiber	Thermoplastic
Cellulosic	FR, meets British SI-1324	No	No	Fire resistant woven fabric	Fire resistant

FR=Fire Retarded

2 Experimental Test Plan

This report describes fire spread and growth experiments on real-scale mockups of upholstered furniture formed by arranging four cushions in a chair configuration. This section summarizes the materials that were used in the cushions to form the mock-ups. An experimental test matrix based on a reduced factorial design incorporating the different materials is then described. Tests were run in a randomized order.

The study considered a number of possible material variations for RUF including upholstery fabric, polyurethane foam type (FR or NFR), presence or absence of a polyester fiber wrap around the polyurethane foam, presence or absence and type of fire blocking barrier, and the type of thread used to sew the cushions. In order to restrict the number of tests required, the choices for a given variable were generally limited to two, and attempts were made to choose material pairs judged likely to lead to measurable differences in fire spread and growth. These considerations along with characteristics of actual RUF guided the general choices of materials summarized in Table 2. The specific materials used are discussed below.

The chosen material types are expected to lead to measurable differences in burning behavior. During a fire thermoplastic fabrics tend to melt and pull away from a flame, thus exposing the underlying materials, while cellulosic materials tend to char and stay in place, thus providing some degree of protection for underlying materials. NFRFPUF is known to be easily ignited, highly flammable, and to be capable of generating large heat release rates, as discussed in two recent publications from this laboratory. [96, 97] On the other hand, foams meeting SI-1324 [24] typically include sufficient flame retardant(s) to resist FPUF involvement when covered with a specified flame-resistant fabric and ignited by the small wood crib fire specified as Ignition Source 5 in BS-5852 [23]. Polyester fiber wrap (PEFW) is a flammable low-density material often wrapped over FPUF to provide desired shapes for upholstered furniture and at the same time limit abrasion between an outer covering and the underlying foam. Fire barriers are materials designed to limit heat and/or mass transfer between a fire burning on the outside of upholstery and flammable interior cushioning materials. Nazaré and Davis have provided a recent review of fire barrier fabrics and their characteristics. [98] The two barriers chosen for this study differ substantially in thickness, thermal conductivity, and porosity, all parameters which have been shown to correlate with barrier effectiveness. [99] Sewn seams in upholstery using highly heat-sensitive threads are potential weak spots with regard to fire resistance. The two thread types included in Table 2 were chosen to either easily weaken upon heating (thermoplastic) or to withstand high temperatures (fire resistant).

Ideally, a test matrix based on the types of materials listed in Table 2 would include all possible combinations, i.e., a full-factorial design, and a minimum of three repeated experiments involving each combination. Such a test matrix would have required $3\times3\times2\times2\times2\times2=144$ separate experiments. Note that it has been assumed that the two characteristics in Table 2 dealing with barrier fabrics are combined into a single parameter having three possible levels. Resources for such an extensive test series were not available. In order to provide a more realistic test plan, we worked with Dr. James Filliben from the NIST Statistical Design, Analysis, and Modeling Group. He recommended a reduced-factorial design incorporating 24

Table 3. Test matrix for real-scale RUF mock-up experiments.

Index	*X1* Fire Barrier	*X2* FPUF	*X3* Polyester Fiber Wrap	*X4* Fabric	*X5* Sewing Thread
-1	High-Loft	Non-Fire-Retarded	No	Cellulosic	Standard
0	None				
+1	Fire-Resistant Fabric	Fire-Retarded	Yes	Thermo-plastic	Fire-Resistant
1	-1	-1	-1	-1	-1
2	-1	-1	-1	+1	+1
3	-1	-1	+1	-1	+1
4	-1	-1	+1	+1	-1
5	-1	+1	-1	-1	+1
6	-1	+1	-1	+1	-1
7	-1	+1	+1	-1	-1
8	-1	+1	+1	+1	+1
9	0	-1	-1	-1	-1
10	0	-1	-1	+1	+1
11	0	-1	+1	-1	+1
12	0	-1	+1	+1	-1
13	0	+1	-1	-1	+1
14	0	+1	-1	+1	-1
15	0	+1	+1	-1	-1
16	0	+1	+1	+1	+1
17	+1	-1	-1	-1	-1
18	+1	-1	-1	+1	+1
19	+1	-1	+1	-1	+1
20	+1	-1	+1	+1	-1
21	+1	+1	-1	-1	+1
22	+1	+1	-1	+1	-1
23	+1	+1	+1	-1	-1
24	+1	+1	+1	+1	+1

material combinations with two repeated tests as a reasonable compromise between the full-factorial design and the need to limit the number of real-scale tests. Table 3 shows the resulting test matrix developed by Dr. Filliben.

After the test matrix was formulated, it was recognized that it was not appropriate to combine the high-loft barrier material with the polyester fiber wrap. After consultation with Dr. Filliben, it was decided to omit the specimens containing both the high-loft barrier fabric and the fiber wrap (Combinations 3, 4, 7, and 8) from the test matrix. Note that, for consistency, the experimental indexes were left unchanged, with the combination numbering running from 1 to 24, even though only twenty material combinations were actually tested. With two repeats, the total number of real-scale tests to be run was forty. The tests were performed in random order in order to minimize any potential effects of test sequence on the results. This was achieved by associating random numbers running between 1 and 24 with each of the two sets of repeated tests. The order of testing is indicated in Table 4.

Table 4. Test series order for real-scale mock-up tests.

Test Series 1	Test Series 2
17	11
6	14
12	16
2	22
16	13
9	12
22	15
5	10
15	19
10	21
13	5
20	9
21	6
23	20
11	23
19	2
14	1
18	17
1	24
24	18

3 Experimental System

3.1 Introduction

At the time of this study, the NIST National Fire Research Laboratory (NFRL) was under construction and not available for testing. As an alternative, the experiments were performed under an Interagency Agreement at the Fire Research Laboratory (FRL) of the Bureau of Alcohol, Tobacco, Firearms and Explosives (ATF) located at the ATF National Laboratory Center in suburban Maryland. Under this agreement, NIST was to provide overall supervision of the test plan and all required materials. ATF staff were responsible for providing test facilities, performing the experiments, overall safety of the effort, recording data and initial analysis of results, providing complete data sets to NIST, and preparing a final written report.

The goal of these experiments was to characterize the fire spread and growth on real-scale furniture mock-ups formed from four upholstered cushions. Visual analysis of videos was chosen as the approach for characterizing the fire spread on the mock-up surfaces. Real-time heat release rate and mass loss measurements were utilized to characterize fire growth. Even though not directly related to mock-up fire spread and HRR growth, the radiative heat flux generated around the mock-ups was characterized using six heat flux gauges. An important characteristic of a flaming RUF item is its ability to act as an ignition source for other objects inside a room, often referred to as "second-item ignition." The heat flux measurements were intended to provide insights into this fire spread mechanism.

There are a number of standard tests available for characterizing fire growth on furnishings. While a specific standard was not followed during this test series, a number of features from several different tests were adopted for use. These tests will be identified as appropriate.

3.2 Heat Release Rate Measurements

All experiments were conducted under the 1 MW Fire Product Collector (FPC) system located in the Medium Burn Room (MBR) at the ATF FRL. [100] This system consists of a 9.1 m^2 square hood located 2.9 m above the floor of the laboratory, a fan system to exhaust the hood, and instrumentation for measuring heat release rate (HRR) using oxygen consumption calorimetry. A photograph of the hood is shown in Figure 1. The hood is connected to an exhaust system with a nominal room temperature volume flow rate of 3.75 m^3/s. Gases extracted from the exhaust duct for the hood were used to measure concentrations of oxygen, carbon dioxide, and carbon monoxide. The pressure drop over an orifice plate in conjunction with a thermocouple temperature measurement allows the actual gas volume flow rate to be determined. These measurements are sufficient to calculate the heat release rate using the well-known approach of oxygen consumption originally suggested by Huggett. [101] The relevant equations and an uncertainty analysis for a similar system have been discussed by Bryant et al. [102] Estimated uncertainties for the FPC vary with the measured HRR. Calculated values using the approach of Bryant et al. are included in Table 5. [100]

The test assembly consisted of a custom test stand with various seat cushions. The test assembly was placed on top of a weighing device and was centered under the 1 MW FPC.

3.3 Test Stand and Cushion Configuration

The upholstered cushion mock-ups used during the study consisted of two pairs of cushions having nominal sizes of 45.7 cm × 45.7 cm × 10.2 cm and 35.6 cm × 45.7 cm × 10.2 cm. The two larger cushions formed the "seat" and "back" for the mock-up, and the two smaller cushions formed the "arms". The mock-up was held in place on a stand based on the design described in Cal TB-133 [26], which is a standard for testing flame-resistant contract furniture. A drawing of the test stand with dimensions is shown in Figure 2. The exterior of the frame and adjustable arms were constructed of 2.54 cm × 2.54 cm 90°-angle iron. The

Figure 1. Photograph showing the collection hood for the 1 MW FPC used during the experiments.

Table 5. Combined standard uncertainties in heat release rate for the FPC (coverage factor of 1). [100]

Fire Size (kW)	Combined Standard Uncertainty (kW)	Relative Uncertainty (%)
50	24	42
500	25	4.6
1100	31	2.6

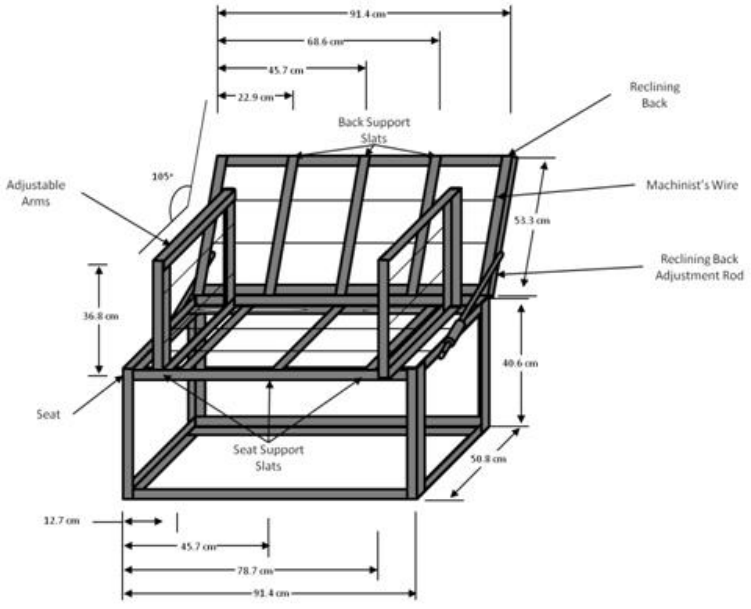

Figure 2. Schematic of the test stand used for the cushion mock-up fire tests.

support slats were formed from 2.54 cm wide iron strips. Additional support for the cushions was obtained by running narrow-gauge (28) nichrome wire between the iron supports as indicated. In order to reduce cushion movement (primarily falling over), additional lengths of the thin wire were wrapped around the back and arm cushions and attached to the frame. The back support was joined to the stand base with hinges

Figure 3. Photograph showing four cushions in place on the test stand.

that permitted rotation of the back from 0° to 90° relative to the vertical direction. Adjustment rods allowed the back to be set to any desired angle. For these tests the back cushions were inclined 15° from vertical. The arm supports were capable of sliding horizontally to provide a maximum spacing of 68.6 cm. The separation was set to 66.0 cm to accommodate the seat and arm cushions.

The cushions were arranged on the stand by placing the seat cushion on the center of the support stand against the back support and placing the arm cushions on either side with their bottom edges supported by the stand. The back cushion was then placed between the two arm cushions against the back support and rested on top of the seat cushion. Figure 3 shows a photograph of four cushions in place on the test stand.

3.4 Upholstered Cushion Materials and Assembly

The general properties of materials to be used in the assembly of the twenty different upholstered cushion combinations were described in Section 2. The specific materials used and some of their properties are summarized in the following.

3.4.1 Flexible Polyurethane Foam

Two types of FPUF were used in the core of the cushions. One was a NFRFPUF purchased from a local supplier. The foam was cut by the supplier from a single block of FPUF. The nominal density was reported to be 29.6 kg/m^3 with an ILD of 32. The latter value is the weight in pounds required to compress a 10.2 cm thick section of FPUF to 75 % of its original height. No details of the foam composition were available, but it is considered likely to have been manufactured using toluene diisocyanate (TDI) and a polyether polyol.

The second foam was fire retarded and is intended to meet the requirements of British SI-1324. [24] The foam (VE30 13) was supplied by Vitafoam (Manchester, UK). It is characterized as a combustion modified foam manufactured with an 80:20 mixture of 2,4- and 2,6-TDI and a 3000 MW polyether polyol, a density between 29 kg/m^3 and 31 kg/m^3, and a hardness value between 115 N and 150 N. Properties for the particular foam provided by the manufacturer are listed in Table 6.

Table 6. Properties of fire-retarded FPUF supplied by manufacturer.

Melamine Content	9 %
Tris (1-chloro-2-propyl) phosphate (TCPP) content	9 %
Hardness ISO 2439 Method A 40%	131 N
Density ISO 845	29.6 kg/m^3
Porosity	70 L/min
Tensile Strength BS EN ISO 1798	113 kPa
Elongation BS EN ISO 1798	254 %
Crib 5 Weight Loss	37 g

Dimensions and masses for the 160 foam blocks used in the cushions were recorded. The results were used to determine density values of 28.5 kg/m^3 ± 0.5 kg/m^3 and 29.3 kg/m^3 ± 0.4 kg/m^3 for the NFRFPUF and FRFPUF, respectively. The density for the NFRFPUF was slightly less than the nominal value, while the result for the FR foam was close to that specified.

3.4.2 Fabrics

The thermoplastic fabric was purchased from an on-line fabric supplier. It was identified as "Pontiac-Cricket." It was a low-pile chenille tweed manufactured by Swavelle/Mill Creek and consisted of 78 % polypropylene and 22 % polyester, which will be abbreviated as 78%PP/22%PE. The color was listed as sand with navy accents. A latex coating was applied to the back side of the fabric. The UFAC fire rating was reported as Class 1. Masses for ten nominally 45.7 cm × 45.7 cm sections (actual dimensions were recorded) cut from the same area of a roll were used to determine the areal density for the fabric. The result was 203 g/m^2 ± 2 g/m^2.

The cotton upholstery fabric was purchased through a local upholstery shop. It was manufactured by National Fabrics Inc and was identified as a 100 % cotton duck with natural color. Mass measurements of ten nominally 45.7 cm × 45.7 cm sections of the cloth yielded an areal density of 222 g/m^2 ± 3 g/m^2.

3.4.3 Polyester Fiber Wrap

Polyester fiber wrap is often used to cover FPUF slabs in cushions for upholstered furniture. For these experiments a nominally 1.27 cm thick fiber wrap identified as 100 % polyester was used. The packaging included a flammability warning. Inspection showed that the density and thickness varied somewhat throughout the roll of material. Eight measurements of areal density using 10 cm × 10 cm samples gave an average of 230 g/m^2 ± 30 g/m^2.

3.4.4 Fire Barrier Fabrics

As indicated in Table 2, two barrier fabrics having very different characteristics were inserted between the outer fabric and the interior of the cushions. One of these, with the trade name Omni 45, was provided by Norfab Corporation. In this manuscript Omni 45 will be referred to as "Norfab." This material is woven from threads composed of 60 % Kevlar and 40 % Basofil. Kevlar is a para-aramid synthetic fiber produced by Dupont, and Basofil is a synthetic fiber based on polymerized melamine produced by Basofil Fabrics. Relevant properties for Omni 45 taken from specifications provided by the manufacturer are summarized in Table 7. The color was Yellow Natural.

Areal density measurements on Omni 45 were made on two different types of samples. Results for three samples with 270 cm^2 area yielded values of 251 g/m^2 ± 1 g/m^2. Results for 16 samples with areas of 2330 cm^2 or 1451 cm^2 gave an average of 248 g/m^2 ± 1 g/m^2. While close to each other, the averaged values were slightly less than expected based on the value listed in Table 7.

Table 7. Manufacturer-supplied properties for Omni 45 (Norfab).

Weave Style	Rip Stop
Fabric Weight	265 g/m^2
Fabric Thickness	0.66 mm
Warp Strength	143 kg/2.54 cm
Fill Strength	136.4 kg/2.54 cm
Thermal Protection Performance	TPP > 48 cal/cm^2
Heat Char Resistance	Passes NFPA 1971

Table 8. Manufacturer-supplied properties for Whispershield Plus.

Thickness	1.02 cm ± 10%
Areal Density	153 g/m^2 ± 10%
Fire Tests Passed	Cal TB 603, Cal TB 604, Cal TB 117, FAA 25-853 A,B

The second barrier fabric was Whispershield Plus, which is a non-woven high-loft material produced by Wm. T. Burnett & Company. It is a thermally bonded nonwoven fabric containing fire-retarded rayon, polyester, and glass fibers. Table 8 includes properties of Whispershield Plus supplied by the manufacturer.

3.4.5 Sewing Threads

One of the variables included in the test matrix was sewing thread. The first thread was the nylon typically used by the upholsterer. It is a bonded thread supplied by Fil-Tec, Inc and has a linear mass density (g/1000 m) of 70 tex. The second was a flame-resistant thread manufactured from 100 % Kevlar supplied by Saunders Thread Company. It is a spun thread with a linear mass density of 70 tex. The color was SK 100 Natural.

3.4.6 Cushions

Each mock-up consisted of four cushions arranged in a chair configuration with a back, a seat, and left and right arms. The upholstery for a cushion was fabricated by sewing top and bottom sections of fabric to a sidewall section. Three sides of the sidewall were formed by a single strip of fabric, while the fourth side incorporated an aluminum zipper held in place by nylon tape. The nylon with the zipper was stitched on either side to narrow strips of upholstery fabric that together formed the fourth sidewall, which was then sewn to the top and bottom sections as well as the two ends of the remaining sidewall fabric.

The fabric for the seat and back cushions was cut with nominal dimensions of 48.3 cm × 48.3 cm, while the long sidewall section had a width of 12.7 cm. When two sections of fabrics were sewn together, the edges were overlapped and the seam placed 1.27 cm from the edges. Figure 4 shows one of the cushions being sewn. When the seams were placed on the inside of the upholstery, the nominal outside dimensions of these cushions were 45.7 cm × 45.7 cm × 10.2 cm, with a zipper extending across one of the sides. The arm cushion covers were constructed in the same way, but the nominal outside dimensions were 45.7 cm × 35.6 cm × 10.2 cm. The zipper was sewn into one of the longer sides.

Generally, in RUF construction the filling materials are sized larger than the upholstery and are compressed when "stuffed" into the upholstery. As a result, the upholstery is completely filled and develops a "plump" appearance. This approach was applied for the filling materials used in these experiments. For cases where only FPUF foam was used (see Table 3) the foam was cut with nominal dimensions of 47.0 cm × 47.0 cm × 11.4 cm for the seat and back cushions and 47.0 cm × 36.8 cm × 11.4 cm for the arms. When the cushions were wrapped with the high-loft barrier fabric or the PEFW, the FPUF dimensions were reduced to 45.7 cm × 45.7 cm × 10.2 cm and 45.7 cm × 35.6 cm × 10.2 cm.

Figure 4. Photograph showing the bottom and sidewalls for a cushion cover being sewn together. The top seam has already been completed.

The dimensions of the FPUF blocks were recorded. For the smaller seat and back cushions the average and standard deviations for the long dimensions were 46.0 cm ± 0.3 cm and 35.9 cm ± 0.2 cm for the NFRFPUF and 45.8 ± 0.2 cm and 36.3 ± 0.6 cm for the FRFPUF. Both the average and standard deviation for the short dimension are somewhat larger than expected for the FRFPUF. Inspection showed that some of the FPUF slabs were cut incorrectly, with values close to 36.8 cm. The remaining dimensions were close to their expected nominal values, and their standard deviations were smaller. The average FPUF thickness was 10.22 cm ± 0.07 cm for the NFRFPUF and 10.3 cm ± 0.1 cm for the FRFPUF. Both values agree well with their nominal values.

As outlined in Table 3, for many of the tests the FPUF in the cushions was enclosed in a barrier fabric and/or PEFW. For the high-loft barrier and PEFW this was accomplished by cutting the material in a shape that could be folded to fully enclose the FPUF slab. The template shown schematically in Figure 5 was used for 45.7 cm × 45.7 cm × 10.2 cm FPUF slabs. When folded around the slab, the edges of the high-loft barrier or PEFW overlapped by roughly 0.6 cm. Staples spaced approximately 1.2 cm apart were used to seal the edges. A similar template shortened appropriately was used for materials covering the 45.7 cm × 35.6 cm × 10.2 cm FPUF slabs. Figure 6 shows a photograph one of the FPUF slabs used in the arms covered in PEFW and stuffed into the outer cotton cover.

The properties listed in Table 7 indicate the Norfab barrier fabric was less than 1 mm thick. In order to create a covering for the filling materials, this material was sewn by the upholsterer with the same dimensions as the outer upholstery fabrics. As for the outer upholstery, aluminum zippers held by nylon tape were used to provide access.

As noted above, the PEFW and the high-loft fire barrier were not utilized together. On the other hand, the test matrix included cushions where the Norfab barrier fabric and PEFW were incorporated together. For these mock-ups the choice was made to place the PEFW inside the fire barrier. It would have also been possible to place the fiber wrap between the outer upholstery cover and the fire barrier.

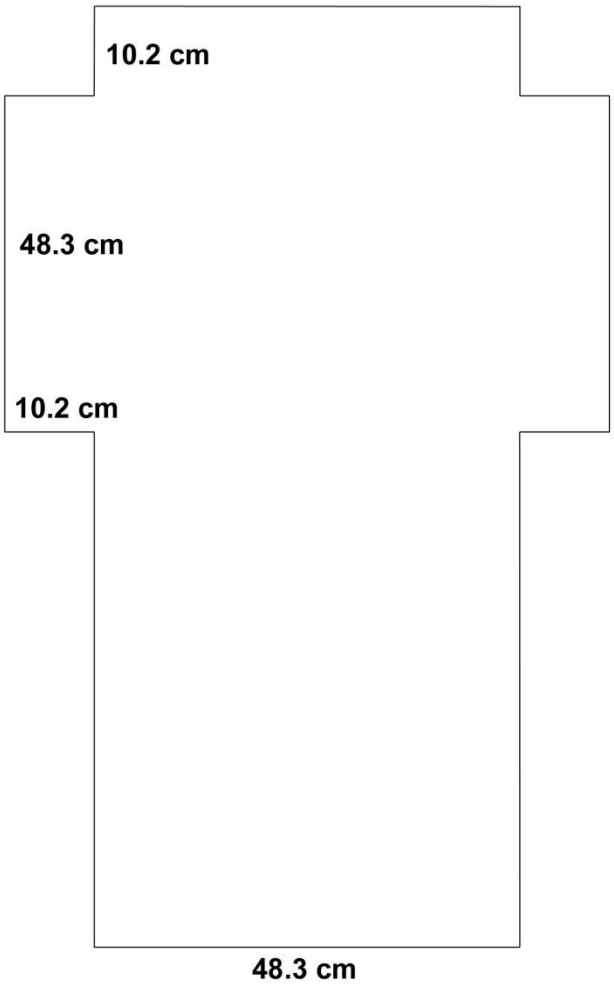

Figure 5. Drawing of template with dimensions used to size the high-loft barrier and the PEFW used to wrap 45.7 cm × 45.7 cm × 8.9 cm FPUF slabs.

Figure 6. Photograph showing the corner of an FPUF slab wrapped in PEFW and placed inside a cotton outer cover.

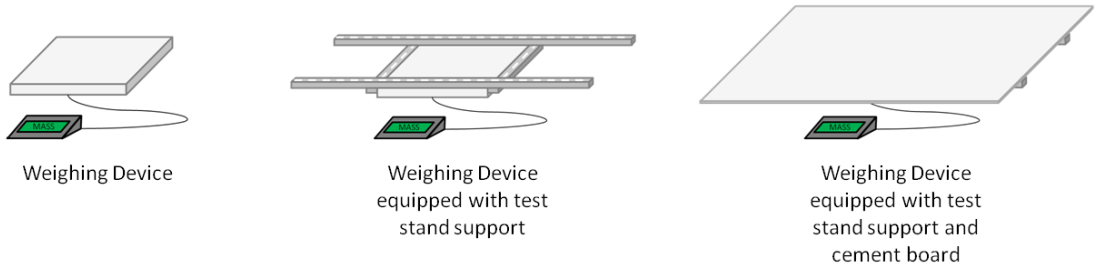

Figure 7. Drawings showing the configuration of the load cell, base frame, and overlaid cement board.

Table 9. Camera numbers, locations, views, and general information are provided for the eight video cameras.

Camera Number	Camera Location and View	Camera Type, Pixels
1	Front, looking at mock-up	Infrared, 720×480
2	Front, looking at mock-up	Standard DV, 720×480
3	Front from above, looking at mock-up	Standard DV, 720×480
4	Rear, zoomed out	Standard DV, 720×480
5	Right side, zoomed out	Standard DV, 720×480
6	Left side, near floor, looking at exterior of left cushion	Standard DV, 720×480
7	≈45° CCW from front, looking at interior of left arm	Standard DV, 720×480
8	≈45° CW from front, zoomed out	Standard DV, 720×480

3.5 Load Cell and Test Stand Support

A Sartorius-Scale-150 kg load cell was used to record mass changes during the experiments. The load cell was placed on the floor. A base to support the mock-up test stand and provide heat protection for the load cell was fabricated by placing a 91.4 cm × 152 cm sheet of 1.27 cm thick USG Durock cement board on a frame designed to fit over the load cell as shown in Figure 7. The frame was constructed from two 152 cm lengths of 3.81 cm × 3.81 cm Unistrut Framing System held in place by two 40.0 cm long cross lengths having 3.81 cm × 1.27 cm dimensions. Both the support base and mock-up support frame were carefully centered under the FPC hood prior to each test. A portion of the base support is visible in Figure 3.

Subsequent to the completion of the initial test matrix of experiments, it was discovered that the load cell did not function correctly during several of the experiments. The mass measurements were either offset, erratic, or frozen. These tests are indicated in Appendix A. In some cases, tests were repeated in order to provide at least one valid mass measurement for a given cushion combination.

3.6 Visual Characterization

Video cameras were used to qualitatively and quantitatively characterize fire spread and growth on the cushion mock-ups. Seven standard video digital cameras along with an infrared camera were used to record a range of views of the fires. Table 9 includes a list of the camera numbers along with their locations relative to the chair mock-up and indication of what each was imaging. The relative camera locations are shown by the configuration drawing (not to scale) in Figure 8. The videos from cameras viewing primarily the mock-ups and individual cushions were intended for fire spread measurements. Those looking at larger areas were not only used to image the fire spread behavior, but also to view the overall flame size and any burning which developed on the support base under the mock-up test stand.

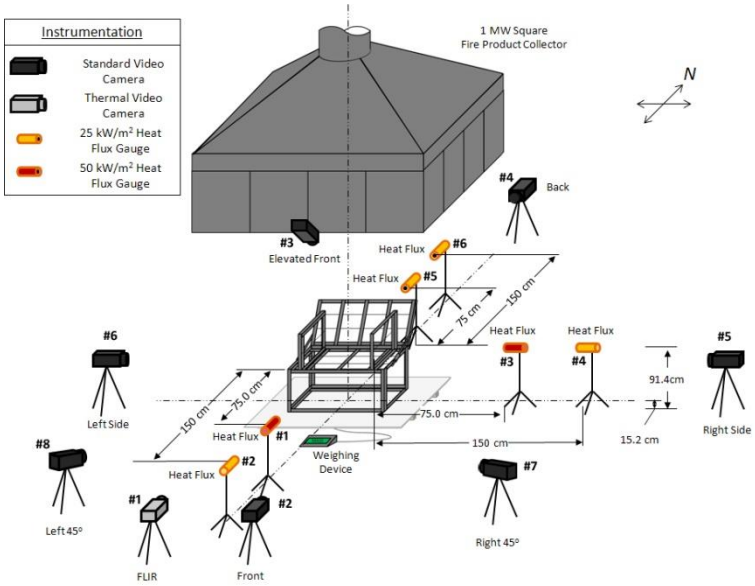

Figure 8. This drawing shows the locations of the video and infrared cameras and heat flux gauges relative to the chair mock-up test stand and the FPC.

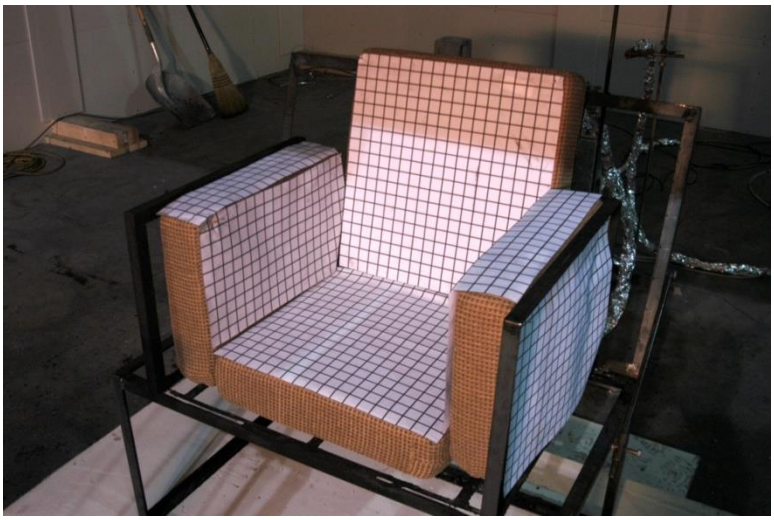

Figure 9. Photograph showing a four-cushion mock-up prior to a fire test with the scaling templates in place.

A number of supplementary tests, described below, were run following the completion of the test matrix. During these experiments, two of the cameras, numbers 2 and 7, listed in Table 9 were replaced with high definition cameras having pixel sizes of 1920 × 1080.

A series of grids printed on a cloth material were applied to the cushions before the ignition of a fire to provide templates for converting pixel locations to actual spatial locations on the cushion surfaces. The square grid spacing was nominally 2.54 cm, but measurements showed that during printing the grids were distorted slightly, and the grids were actually rectangular with sides of 2.54 cm × 2.46 cm. The templates were attached to the cushions with straight pins (where necessary) and placed on the upper surface of the seat, front side of the back, the interiors of the right and left arms, the exterior of the right arm, and the tops of both arms. Figure 9 shows a photograph of one of the cushion mock-ups with the scaling templates in

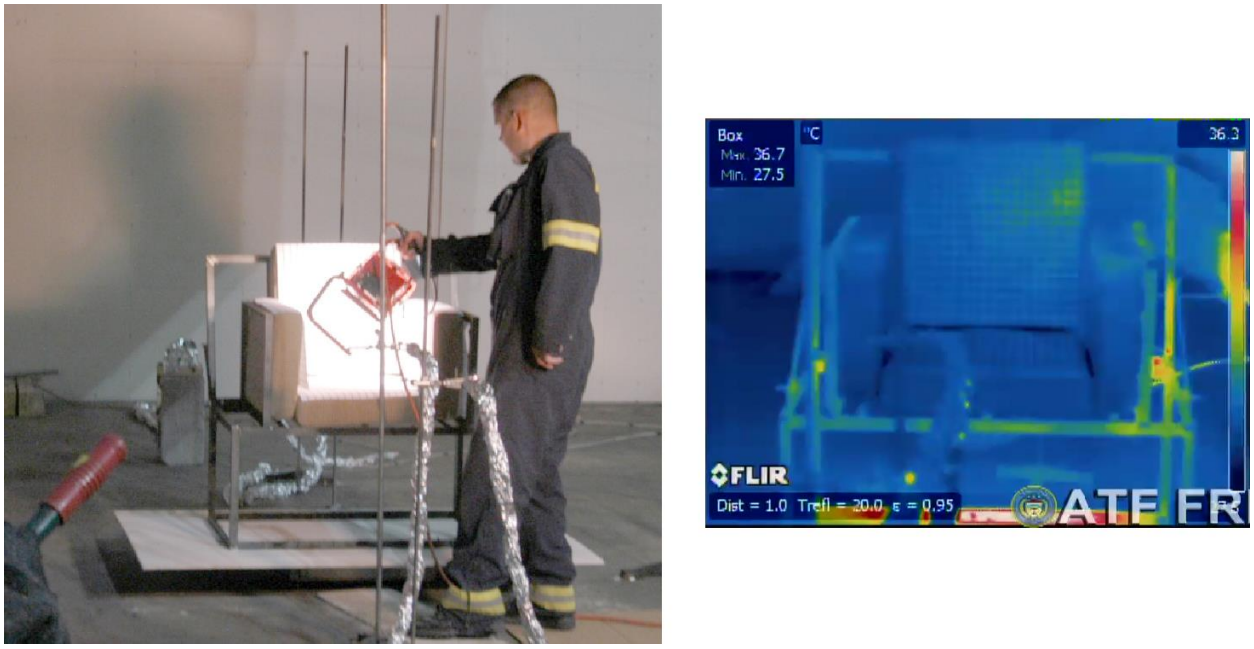

Figure 10. The right photograph shows a cushion mock-up being "painted" by a lamp, and the left panel shows a frame with a "painted" grid taken from an infrared video.

place. The mock-ups with the grids in place were recorded by all video cameras simultaneously, and the templates were then removed prior to igniting a fire.

The grids were not normally visible under infrared imaging. However, it was possible to visualize the grids by passing a high intensity light source just above the template. The heat from the lamp was preferentially absorbed by the dark grids, and these areas were heated to higher temperatures. As a result, following such "painting" of the grids with the lamp, the image of the template could be recorded in the infrared. The left side of Figure 10 shows a photograph taken while the grid on one of the cushion mock-ups was being painted with a high intensity lamp. The visualization of one of the grids taken from one of the infrared videos is shown on the right. While faint, the grid is easily discernible.

A digital still camera was used to record the experiments from a variety of directions and distances during an experiment.

3.7 Heat Flux Measurements

Thermal radiation levels from the burning mock-ups were recorded using six Medtherm Schmidt-Boelter total heat flux gauges (HFGs). Four of the gauges had ranges of 0 kW/m^2 - 25 kW/m^2 and two were 0 kW/m^2 - 50 kW/m^2. Two HFGs were placed 0.75 m and 1.5 m from the edge of the cushion mock-up test stand along each of three lines that passed through the edge centers from the front, right side, and rear. All HFGs were positioned 91.4 cm above the floor or 76.2 cm above the test stand support. Table 10 includes information about the HFGs including numbering, locations, type, model number, and operating range. The locations for the six HFGs are indicated in the apparatus drawing shown in Figure 8.

3.8 Ambient Laboratory Conditions

The ambient laboratory temperature, barometric pressure, and relative humidity were monitored during each experiment using an industrial probe and microserver. The probe measured ambient conditions using capacitive digital sensors and output a digital signal that was captured by the data acquisition system.

Table 10. Heat flux gauge designations and characteristics.

HFG Number	Direction, Distance	HFG Type	Model Number	Range
1	Front, 0.75 m	Total	64-2.5-20	0 kW/m^2-25 kW/m^2
2	Front, 1.5 m	Total	64-2.5-20	0 kW/m^2-25 kW/m^2
3	Right, 0.75 m	Total	64-5SB-20	0 kW/m^2-50 kW/m^2
4	Right, 1.5 m	Total	64-2.5-20	0 kW/m^2-25 kW/m^2
5	Rear, 0.75 m	Total	64-5SB-20	0 kW/m^2-50 kW/m^2
6	Rear, 1.5 m	Total	64-2.5SB-36-21640	0 kW/m^2-25 kW/m^2

3.9 Data Acquisition and Recording

Data acquisition in the ATF FPC was handled by a transportable modular data system connected to a central storage system. One or more data acquisition systems were combined to create a system capable of handling hundreds of data acquisition channels. The modules could record a variety of input signals. Prior to a test, a channel list was prepared that incorporated all of the measurements that were made including those for the HRR measurements, mass, and heat flux. Any additional information that had to be acquired such as Test IDs, timing information, e.g. ignition times, and other relevant information were input and stored with the appropriate test. The measurements were ultimately stored in multiple Microsoft Excel data sheets that allowed easy data processing of the raw data.

A high throughput video system recorded the eight video signals and synced them together. A central timing capability allowed the video recordings and other data to also be synced together.

3.10 Ignition Sources

Three ignition sources were utilized during the test series. These were based on, but did not exactly duplicate, three Ignition Sources (1, 2, and 5) described in BS-5852. [23] Ignition Sources 1 and 2 are gas flames that utilize a burner formed from a 200 mm length of stainless steel tubing with inner diameter of 6.5 mm and outer diameter of 8.0 mm. BS-5852 calls for the fuel to be butane. We chose instead to use propane since it was more readily available. Flexible tubing was used to connect the burner to a regulated cylinder of commercial propane.

Ignition Source 1 is designed to be equivalent to a burning match. The standard specifies that a butane flow rate of 44 mL/min be used and that the flame be applied for 20 s. The standard indicates that this flow rate will generate a flame height of 35 mm. Data summarized in Table 4-1 of Krasny et al. indicates the heat release rate of this flame is roughly 100 W. [2] For the current experiments, a microvalve was used to control the propane flow, which was adjusted to provide a 35 mm high propane flame. A Bios Definer 220 Series flow meter was used to measure the resulting volume gas flow rate. Repeated measurements over several days yielded flow rates of 57 mL/min ± 4 mL/min. This value can be compared with the recommended flow rate of butane from BS-5852 of 44 mL/min (20 ºC). The measured flow rate for propane is consistent with that expected if the burner heat release rates for both fuels are comparable, since the heats of combustion for the two fuels are nearly equal on a per mass basis, and their flow rate ratio is nearly the inverse of their molecular weight ratio. Assuming complete combustion and using the heat of combustion for propane results in an estimate of 94 W for the HRR of this flame, which is consistent with the 100 W estimate provided by Krasney et al. for the butane case.

Ignition Source 2 uses the same burner, but increases the butane flow rate to 160 mL/min. [23] The length of exposure to the flame is doubled from 20 s to 40 s. The BS-5852 documentation indicates the flame length for this source is 145 mm. Based on values listed in Krasny et al., the heat release rates for this burner is roughly 300 W. [2] Flow rates for propane were adjusted to provide the same flame length.

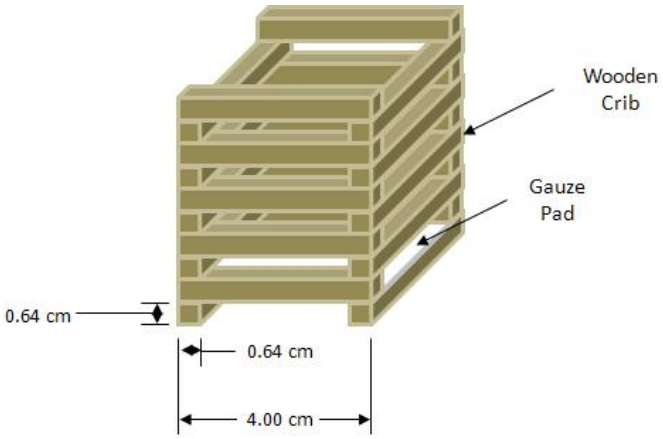

Figure 11. A drawing of the Ignition Source 5 wood crib with dimensions.

Measured propane flow rates were 188 mL/min ± 5 mL/min. The volume flow rate ratio of 1.18 is slightly less than the molecular weight ratio of 1.32 for the fuels. Assuming complete combustion, the HRR is calculated to be 288 W, which agrees well with the estimate of Krasny et al.

Ignition Source 5 is specified as a wood crib constructed from twenty Scots Pine sticks of 40 mm length and 6.5 mm square cross section. A section of surgical gauze on the bottom layer soaked with 1.4 mL of isopropanol ignited by a small flame serves as the ignition source for the crib. A drawing of the crib with dimensions is shown in Figure 11. Since Scots pine was not readily available, birch wooden dowels with 6.4 mm square cross sections were purchased from a local home improvement store and were cut to the required lengths. Small amounts of polyvinyl acetate glue were used to attach the sticks to each other and to hold the gauze in place.

According to BS-5852, the mass of the Scots Pine crib should be 17 g. [23] Measurements for five of the cribs (glued and with the gauze in place) used here gave an average mass of 14.3 g ± 0.2 g. Heat release rate measurements for two of the cribs were made using a cone calorimeter with no external heating applied. Figure 12 shows the measured HRRs and the crib mass as a function of time. The measurements are very similar for both cribs. The maximum HRRs were reached around 60 s following ignition and fell between 3.5 kW and 4.0 kW. By integrating the HRRs over time, the total heats released by the cribs were determined to be 257 kJ and 260 kJ for the two repeated tests. Krasny et al. listed the total heat release of the BS-5852 Ignition Source 5 as 285 kJ and the time to 90% mass loss as 150 s. [2] The corresponding mass loss times for the data shown in Figure 12 were 136 s and 134 s. These results suggest that the wood cribs used in these experiments released roughly 10 % less total energy than comparable Scots pine cribs and burned slightly faster. On this basis, it seems likely that the burning behaviors of the two types of wood cribs are similar.

3.11 Sample Conditioning

All of the cushions and the wood crib ignition sources were placed in a conditioning room for at least a week prior to testing. The room conditions were nominally 23 ºC with a relative humidity of 50 %. The actual conditions were monitored and were recorded several times during the test series. Measured values were 23.0 ºC ± 0.2 ºC and 49 % ± 2 %. Several months later several supplemental fire tests were done. For these the temperature was the same, but the relative humidity was slightly lower at 45 % ± 2%.

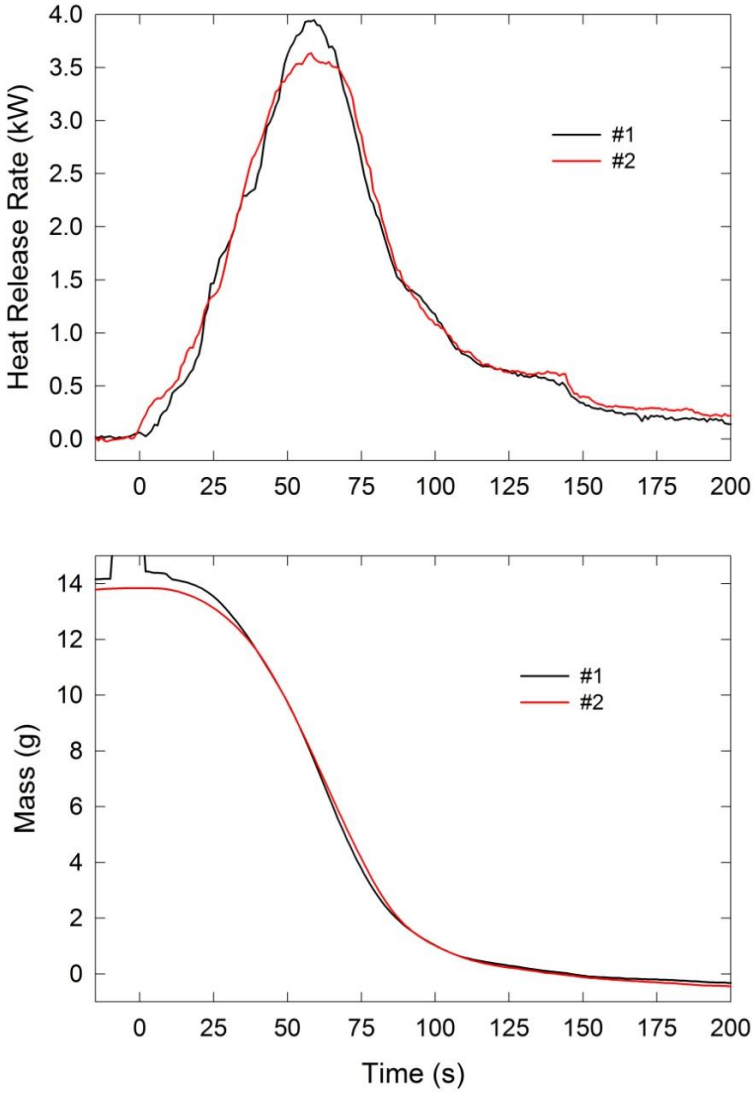

Figure 12. The heat release rate and mass of two Ignition Source 5 wood cribs are plotted as a function of time.

3.12 Test Procedure

The first step in a test was to remove the four cushions identified with tags listing material combination number (xx), iteration number (y), and location in the mock-up (seat, back, left and right arms) from the conditioning room while noting the time. The nomenclature "xx_y" is used to specify particular combination and iteration test numbers. The cushions were then configured in the test stand as shown in Figure 3, and the identification tags were removed. Wires used to support the arms and back were placed around the cushions. Next the scaling templates were positioned on the cushions as shown in Figure 9 and held in place, where necessary, by straight pins. At this point recording by the data acquisition system and video cameras was initiated. A lamp was used to visualize the templates in the infrared video as described earlier. Once the templates were recorded by the video cameras, they were removed and the mock-up was ready for ignition.

Attempts were made to limit the time between the removal of the cushions from the conditioning room and the time of ignition. Generally, fifteen minutes or less were required to arrange the cushions and record background videos of the templates. In a few cases where difficulties arose, longer periods elapsed.

Figure 13. Photograph showing ignition of a furniture mock-up with Ignition Source 1.

When the preliminary tasks were completed, a verbal countdown was started, and at "zero" Ignition Source 1 was applied near the center of the seat cushion back edge at a location immediately below the outer bottom edge of the back cushion. Figure 13 shows a photograph of Ignition Source 1 as it was applied to one of the furniture mock-ups. An event marker was activated manually and recorded by the data acquisition system as the ignition source was applied. At the same time, a stop watch was started to time when the ignition source was to be removed from the mock-up after a 20 s application. During a test the digital still camera was used to record views from a number of directions and distances.

An experiment was constantly monitored to ensure that flame spread and fire growth did not stop before a large fraction of the available cushion surface area was exposed to flames. In several cases following exposure to Ignition Source 1, only limited flame spread occurred before the flames went out. For several of these tests flame spread occurred upwards on the back cushion, but lateral flame spread was limited and stopped when the flames reached the upper edge of the cushion. For many of these cases the seat cushion surface was not ignited by Ignition Source 1. In these cases and others where limited flame spread occurred, Ignition Source 2 was applied at the same location on the seat cushion for 40 s after flame spread was no longer evident. A marker was recorded by the data acquisition system at the time of application, and the 40 s application period was determined using the stop watch. Figure 14 shows an example of a test in which Ignition Source 2 was applied to a mock-up.

Figure 14 reveals a potential limitation of the ignition approach utilized. It can be seen that a narrow vertical section on the back cushion had previously burned following the application of Ignition Source 1. It is likely that in this region ignition and flame spread would be more difficult than on a pristine mock-up. In fact, when successful ignitions took place, flame spread occurred over areas outside of the previously burned areas. Since Ignition Source 2, and also Ignition Source 5, were not applied to pristine mock-ups, it was not possible to characterize the effects of the previously burned areas on subsequent flame spread and growth. Nevertheless, in several cases Ignition Source 2 was found to induce additional substantial flame spread and fire growth on mock-ups on which Ignition Source 1 had previously been used.

For cases where Ignition Source 2 also failed to ignite sustained burning over a large fraction of the surface of a mock-up, Ignition Source 5 was applied. The wood crib was placed at the same ignition location on the mock-up as Ignition Sources 1 and 2, the small amount of isopropyl alcohol was applied to the surgical gauze, and a small flame was used to ignite the alcohol-soaked gauze. A time stamp for ignition of the wood crib was recorded by the data acquisition system as the gauze was ignited. Figure 15 shows photographs of a wood crib being ignited on one of the mock-ups and a second photograph of the crib

Figure 14. Photograph showing ignition of a furniture mock-up with Ignition Source 2.

Figure 15. Two photographs show an Ignition Source 5 wood crib on a chair mock-up as it was ignited (left) and the resulting flame 57 s later.

burning 57 s later. Based on the HRR plots in Figure 12, the second photograph was taken close to the time of maximum HRR for the crib. The area burned previously due to the applications of Ignition Sources 1 and 2 is evident in both photographs.

Once ignited, a mock-up burned until the flames had died down and only light smoke or no smoke was visible. At this point, the end of the experiment was announced, and a brief period was allowed for background data to be collected. Following the end of the background period the data acquisition system was stopped, and the data was transferred to the ATF central data storage facility for later analysis. Following a test, any substantial parts of the mock-up cushions which remained were inspected and photographed. In cases where outer shells were intact, they were slit open to inspect the condition of any FPUF or other materials on the inside.

After inspection was complete, any remaining materials were discarded, and the test stand was scraped to remove any residue. If a large amount of material had fallen onto the Durock sheet under the test stand or if substantial burning had taken place on its surface, it was replaced with a new sheet, and the Durock base and test stand were carefully centered under the collection hood. At this point, the system was ready for the next test.

Table 11. Identification numbers for a series of supplemental tests are provided along with the types of foam used.

Test ID	Foam Type
25_1	NIST Fire Retarded
26_1	SI-1324
26_2	SI-1324
27_1	NFRFPUF
27_2	NFRFPUF

3.13 Additional Tests of Material Combinations

After the mock-up burns for the original test matrix were complete, an additional five mock-ups were assembled and tested. As discussed earlier, mass measurements did not record properly during some of the experiments for the test matrix. In an effort to ensure that at least one time record of mass loss was available for each material combination, additional cushions were assembled from the appropriate materials and burned. Three fires were burned for Combinations 1, 5, 10, 20, and 22, with the repeated tests assigned an iteration number of "3".

3.14 Supplemental Tests

After the completion of the forty-five experiments involving the twenty different material combinations, an additional five tests using different material combinations were performed. A single mock-up utilizing experimental fire-retarded FPUF slabs prepared by members of the Flammability Reduction Group in the Fire Research Division of NIST was tested. Layer-by-layer assembly was utilized to coat the NFRFPUF structure with 3.5 bilayers of a nanocomposite formed by soaking the foam in alternating aqueous solutions of 0.5 mass % polyethyleneimine and 0.5 mass % polyacrylic acid/0.5 % sodium montmorillonite clay. The foam was covered with the 78 % polypropylene/22 % polyester upholstery sewn with Kevlar thread. Additional details are available in Kim et al. [103] This test was assigned an identification number of 25_1.

Finally, two repeat tests were run using only NFRFPUF or FRFPUF slabs arranged in the mock-up configuration. These tests were assigned identification numbers of 26 (SI-1324 foam) and 27 (NFRFPUF). Table 11 summarizes the supplemental tests and their assigned test IDs.

4 Data Analysis

The data acquired during a single test in the FPC were provided to NIST as a series of forty-eight separate worksheets in an Excel workbook. The worksheets contained a wide variety of information. Typically spread sheets of data as a function of time were included along with separate temporal plots of the data. The basic measurements required to calculate HRR, such as the hood mass flow rate, temperature, and oxygen, carbon dioxide, and carbon monoxide concentrations were provided. The results of HRR calculations using both convective and oxygen consumption approaches were included in a workbook along with integrated HRR values. Results of the load cell and heat flux gauge measurements were converted to sample mass and heat flux measurements. Other information provided included ambient conditions, details concerning instrumentation used, picture and video summaries, marker times (such as application of ignition source), and test start times. The times included in the ATF Excel files were not adjusted for ignition times but were based on the time when data acquisition was initiated.

An Excel macro named Template_ATFRSDatatool.xlsm was created to simplify the handling and analysis of the ATF data. It was designed to read selected information from the ATF files and combine it with additional test-specific information such as the masses of the components used in the cushions and to output the results in a single Excel worksheet containing the results of primary interest, including temporal profiles of the oxygen-consumption HRR, total heat released, sample mass, and the heat fluxes recorded at the six gauge locations. The time lines were offset so that the time when an ignition source was applied was defined to be 0 s.

In addition to the primary values listed above, two additional parameters derived from the primary measurements were calculated and included in the data table. The first of these was the time-resolved effective heat of combustion (EHOC), defined as the instantaneous HRR divided by the instantaneous mass loss rate (MLR). The MLR was obtained by differentiating the sample mass measurements. It is well known that derivatives of experimental measurements can be very sensitive to noise. The mass values were recorded with one-gram resolution. Since this was comparable to the measured mass changes during one second, the experimental resolution introduced additional uncertainty into the derivatives. In order to reduce high frequency noise and smooth the steps introduced by limited resolution, the mass signals were first smoothed with a Savitzky-Golay filter that utilizes polynomial fitting. [104] Differentiated values were then obtained at each time step by differentiating the polynomials used in the fit. The parameters used in the fitting were saved as part of the Excel file. Values for EHOC were then calculated and included in the spreadsheet.

The second derived parameter calculated by the macro was the fire growth rate (FIGRA) parameter, defined here as the instantaneous HRR divided by the elapsed time since ignition. This parameter was originally introduced as part of the European single burning item test method, Test method EN 13823 – SBI, Fire Technical Testing of Building Products. [105] Since it combines both the HRR and the time required to reach the level, it is viewed as being a measure of relative fire growth behavior.

The macro also included a capability to adjust mass loss curves for cases where problems were identified in the measurements. For some of the experiments it was noted that the mass curves were simply offset from their true values. By shifting these curves, it was possible to obtain corrected values. This feature also allowed limited numbers of noisy data points to be replaced. A plot allowed the original mass values to be compared with the adjusted values. It was possible to iterate in order to obtain the desired corrected mass data. The macro also provided a tool for quickly plotting values of HRR, total heat evolved, mass, MLR, EHOC, and FIGRA.

Three output files identified as ATFRS_xx_y, with xx = combination number and y = the test iteration number, were generated by the macro. Two contained the summary temporal profiles saved as comma-

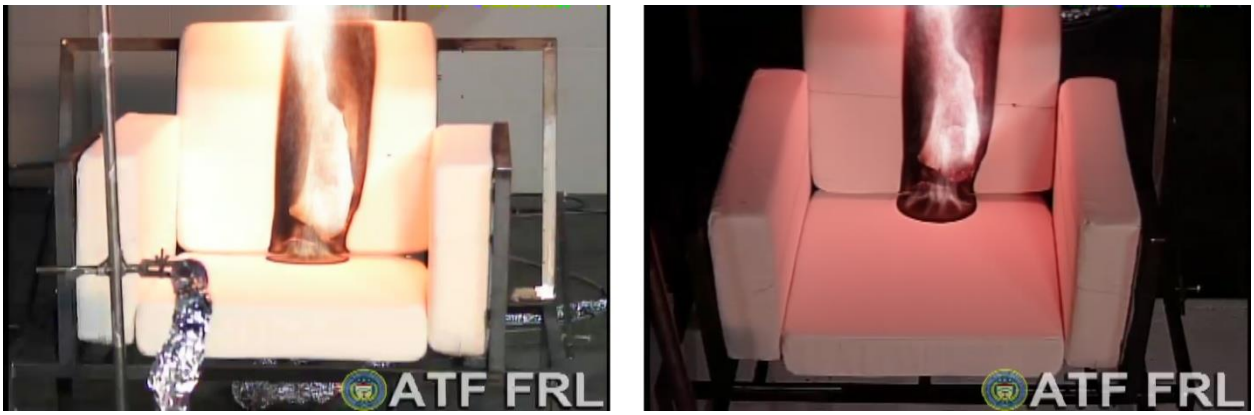

Figure 16. Frames captured from videos recorded by Cameras #2 (left) and #3 (right) 135 s following application of Ignition Source 1 are shown for a mock-up including cotton-covered cushions.

separated values (.csv) and Excel (.xls) files. Additionally, the modified macro file, containing the analysis as well as additional data about the specific test, was saved as ATFRS_xx_y - Macro Tool.xlms.

Once available, the files could be accessed to extract specific data or generate summary tables of results.

An additional goal of the experiments was to characterize the flame spread behavior on the mock-ups using videos of the fires. Ultimately, flame spread behaviors on the seat and back cushions were determined. The analysis required the development of new approaches for determining the edges of the spreading fires. Adobe Photoshop was used as the basis of the analysis.

Ideally, one would prefer to identify locations on a cushion where active burning was taking place. This proved difficult to implement. As an alternative, the total area over which fire spread had occurred was determined. The approaches adopted were slightly different for the cotton and the 78%PP/22%PE cover fabrics. As flames spread over the cotton surface they blackened the light-colored fabric. The charred cotton tended to remain in place immediately after flame passage. As a result, the flame edge was easily identified along the narrow boundary between blackened and unblackened cotton. Figure 16 shows examples of frame captures from the front- (#2) and overhead-view (#3) video cameras for a mock-up including cushions covered with cotton. These views were used for flame spread measurements on the back and seat cushions, respectively. The sharp interfaces between burned and unburned fabric are apparent. Generally, the interfaces were smooth. As can be seen in Figure 16, burned areas on seat cushions covered in cotton upholstery frequently had semi-circular shapes.

Since the 78%PP/22%PE fabric was a thermoplastic, it tended to melt and pull away from a spreading flame, exposing whatever material was below the fabric. The videos showed that flames on the underlying material (either FPUF, a barrier, or PEFW) usually either traveled with the edge of the melted material or spread rapidly over the exposed material underneath. Even though cases were observed for which the upholstery fabric had pulled away from the flame front, flames would generally catch up with the retreating fabric quickly. On this basis, the interface between the exposed material and the edge of the retreating fabric was used as a measure of the flame spread for cushions covered with the thermoplastic material. Front and overhead views of a fire spreading over a mock-up having cushions covered with 78%PP/22%PE fabric are shown in Figure 17. The fabric tended to roll up as it pulled away from the spreading fire. The edges of the melted fabric are somewhat irregular, but it is evident that they can be readily distinguished in the images.

As a fire grew larger, the fluctuating flames often instantaneously obscured the edges of the spreading fires. This was particularly the case for fires spreading upward on the back cushion. Since it was recognized that

Figure 17. Frames captured from videos recorded by Cameras #2 (left) and #3 (right) 75 s following application of Ignition Source 1 are shown for a mock-up formed from cushions covered with 78 % polypropylene/22 % polyester fabric.

Figure 18. The image on the left is a frame taken from a video recorded by Camera #2 285 s after Ignition Source 1 was applied to one of the mock-ups. The image on the right is a frame at the same time from a video generated by averaging the original video over 31 frames.

the flames fluctuated rapidly, an attempt was made to improve surface visibility using a running time average approach. An application named FlameSpread 2 was developed using LabView software to read a video file, average the $n/2$ frames on either side of a specific frame, where $n + 1$ is the total number of frames to average, and output a file of the resulting video. Averaging times were chosen to be short enough that the fire did not spread appreciably over the cushions during the period. Figure 18 shows an example of the effectiveness of this approach. The image on the left side is a single frame taken from the video 285 s after the ignition source was applied. Heavy flames are present which partially obscure the edge of the spreading fire. A frame for the same time from the video where running frame averaging has been applied is shown on the right side. The surface of the back cushion is now much easier to see, and the edges of the spreading fire can be identified. The effect of the averaged flames is indicated by the hazy orange color in front of the surface. The bright region in the middle of the darkened area is an area where the cotton has opened up, exposing the FPUF underneath. Note that the frames shown in Figure 16 and Figure 17 were averaged in the same manner.

The first step in the flame spread analysis was to choose a set of frames from videos of the spreading fires for analysis. Video from Camera #2 was used for flame spread on the back cushion and from Camera #3 for the seat cushion. The selected frames were saved as JPEG files. Attempts were made to ensure that frames were roughly equally spaced in time and that sufficient numbers were taken to adequately characterize the changing fire areas.

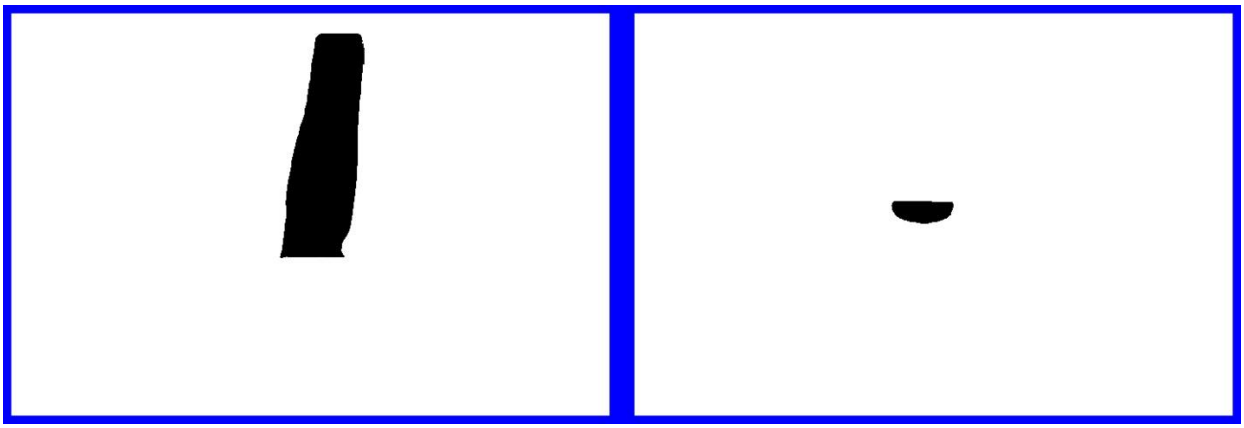

Figure 19. Burned areas for the back (left) and seat (right) cushions based on the images shown in Figure 16 for a mock-up covered with cotton upholstery fabric.

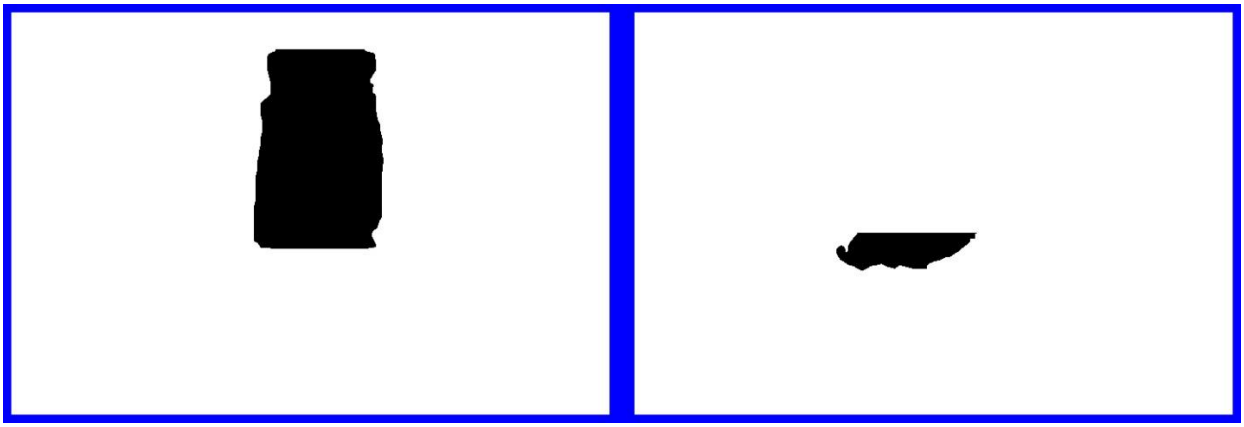

Figure 20. Burned areas for the back (left) and seat (right) cushions based on the images shown in Figure 17 for a mock-up covered with 78%PP/22%PE upholstery fabric.

The next step was to isolate the area in an image over which flame spread had already taken place. Various tools in Adobe Photoshop were used for this purpose. These included the "magnetic lasso" tool which automatically snaps to the edge of an object that is being roughly traced with a mouse, the "quick mask" tool which allows the edges of an object selected by the magnetic lasso tool to be refined, the "magic wand" tool which automatically selects pixels having similar tone and color, and the "levels adjustment" tool which adjusts levels and improves contrast. Once the burned area in the image was isolated, the "paint bucket" tool was used to fill the selected area with pure black (red,green,blue (RGB) value of 0,0,0). By applying the "inverse" command the selected area could be changed to pixels outside of the burned area. These pixels were then painted white (RGB value of 255,255,255). The result of such an analysis was a new two-color image where the black area corresponded to the burned area in the original image.

Figure 19 and Figure 20 show examples of the burned areas on the back and seat cushions identified using the above approach for the video frames shown in Figure 16 and Figure 17. Comparison shows a close correspondence between the chosen areas and the burned areas in the video frames.

Maps of burned areas such as shown in Figure 19 and Figure 20 indicate pixel locations in the image where flame spread has occurred. The last step in the analysis was to associate the pixel locations with physical locations on the cushions. Several observations concerning the nature of the images were used to aid with this analysis. It was found that recorded images of the grid templates on the back cushion were not noticeably distorted by perspective effects, i.e. the lines were parallel and equally spaced. This greatly

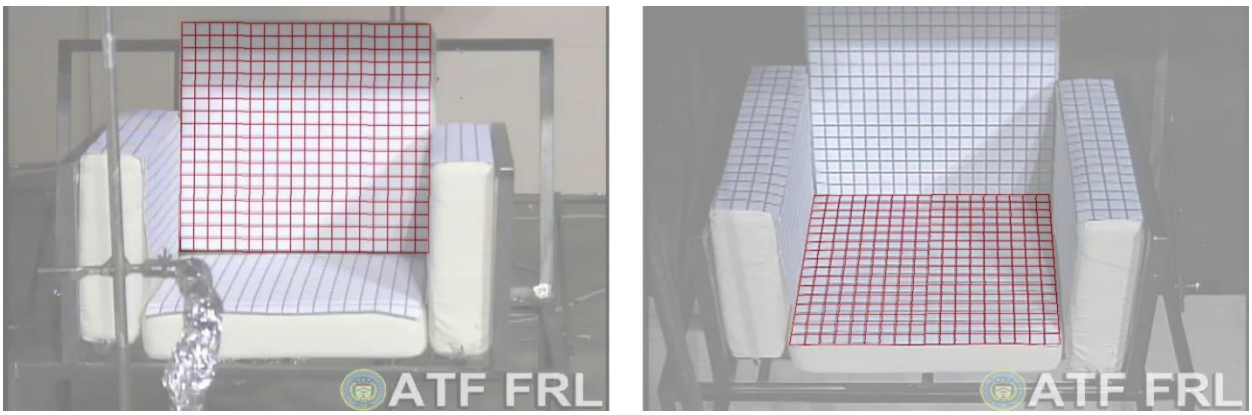

Figure 21. Frames taken from Camera #2 (left) and Camera #3 (right) show the grid templates (black lines) in place on the back and seat cushions, respectively. The superimposed red grids were calculated using the approaches described in the text.

simplified the analysis since it was only necessary to identify three locations on the grid in order to prepare a map relating the pixels to a two-dimensional axes system on the cushion surface. A Mathematica routine was developed that allowed an image of the template to be imported, selection of three corners of the grid, and the calculation of a mathematical grid in terms of pixel locations within the experimental image. Once available, the grid locations were used to calculate coordinates for and areas of individual pixels over the entire grid area. An example of a grid determined using this approach is included on the left side of Figure 21. The red calculated grid is partially transparent and has been superimposed over the black grid in the captured video frame. The close correspondence of the calculated grid with the imaged grid is apparent. Matrices including the x and y coordinates for the pixels within the grid area were saved as separate files. Once pixel coordinates were available, it was possible to calculate areas for each pixel within the grid. These values were saved in a third file.

Calculating a grid to match the template on the seat cushion based on the overhead camera view was more complicated. For these cases, perspective effects caused the grid lines to appear closer together as the distance from the video camera increased. Nonetheless, it was found that the lines perpendicular to the camera direction remained parallel. A simple iterative analysis that involved an initial estimate for the number of pixels between the two horizontal lines near the back of the seat cushion, the assumption of a linear dependence for the increase in line spacing as the grid moved toward the camera, and a determination of the pixel locations for the corners of the grid allowed the separations for the horizontal grid lines to be estimated. It is clear from the image that the vertical lines appear to "fan out" as the imaged location moves closer to the camera. The degree of spread was determined by comparing grid corner pixel locations at the far and near edges of the seat cushion. The spreading was found to be asymmetric on the left and right sides of the grid. The assumption was made that the apparent spreading with grid location was linear on either side of the template centerline, and the spreading lateral grid lines were calculated accordingly. A separate Mathematica routine was used to perform these calculations. The right side of Figure 21 shows a comparison of the calculated grid (red) and the imaged grid (black) taken from a Camera #3 view of the seat. Small deviations are evident between the calculated and imaged grids. Much of the difference is due to the fact that the seat cushion surface is slightly curved and the grid was not perfectly flat. Nonetheless, the agreement is high enough to provide confidence in pixel locations, which were determined by their positions relative to the calculated grid lines. Pixel x and y coordinates and areas were saved as separate files.

Additional Mathematica routines were written to import the image files representing the burned areas and the corresponding files containing the mapped locations and areas corresponding to the pixels covering the cushion surfaces. By convoluting these files, quantitative pixel locations for the edges of the burned areas

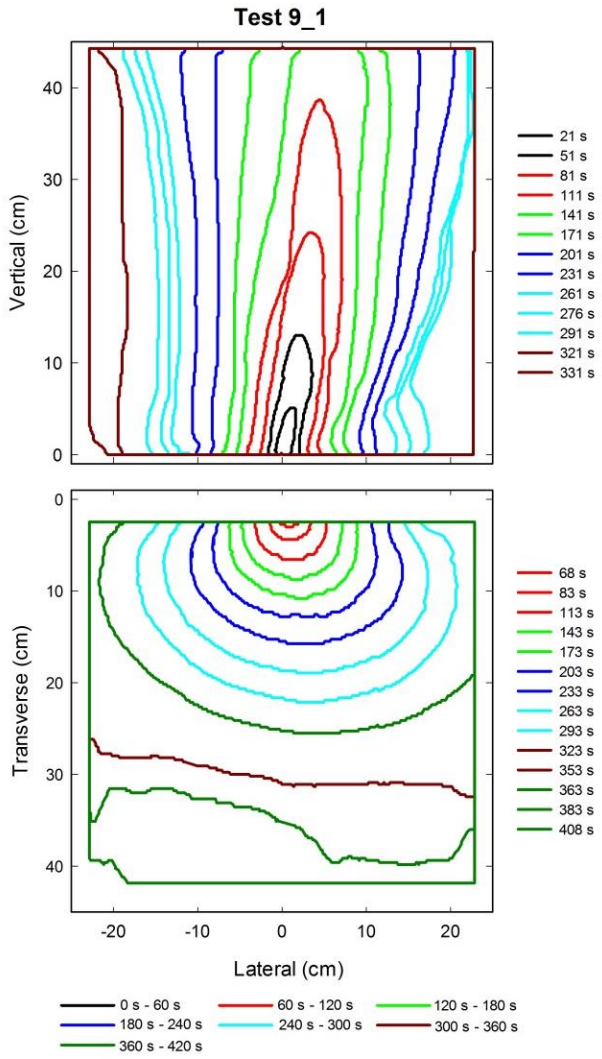

Figure 22. Flame edge contours for flame spread over the back (top) and seat (bottom) of a furniture mock-up formed using NFRFPUF and cotton upholstery.

on the seat and back were determined. When plotted on an *x-y* plot, these edge pixels provide a quantitative indication of the flame edge locations. By plotting flame edges for various times during a test, a time series of flame contours that provided quantitative indications of the flame spread behavior were generated. Contours for both the seat and back cushions were included on a single plot. When plotted in this way, the degree of correlation between flame spread behaviors on the two surfaces could be assessed visually. Figure 22 shows an example of flame spread contours for Test 9_1. Note that the times when the contours were obtained are indicated on each plot and that color coding has been used to aid time comparisons between flame spread on the seat and back cushions.

It is evident that flame edge contours as a function of time, such as those shown in Figure 22, can provide quantitative measures of flame spread rates between two time-adjacent contours since the physical locations of each edge point are known. However, it also evident that such rates can vary substantially with direction and time on both the back and seat cushions. In order to address this complication, four characteristic flame spread rates were defined. Based on observations of the spreading flames, these definitions differed somewhat for the back and seat cushions. For most cushion combinations (but not all), upward flame spread on the back cushion was observed to be much faster than the corresponding lateral flame spread. The upward flame spread was not always symmetric about the back cushion vertical centerline. To allow for this asymmetry, a characteristic flame spread rate in the vertical direction between two time contours,

symbolized as u_{bv}, was defined as the vertical distance between the highest flame-front locations on the cushion at the two times divided by the time difference. The flame movement in directions perpendicular to the vertical, here referred to as the lateral direction, varied substantially with time and height. Generally, such flame spread was in both directions away from the central region of the cushion. In order to provide a consistent definition for lateral flame spread rate on the back cushion, denoted u_{bl}, the characteristic rate was determined along a lateral line located at a height on the cushion chosen as the vertical centroid of the burned area immediately following the removal of the ignition source. The lateral extents of the flame edge on the left and right sides of the contours were determined at this height as a function of time, and the characteristic lateral flame spread rate for the period between the two contours was then calculated as the overall change in flame width at this height divided by twice the time difference between contours (the factor of two accounts for the flame spreading in two directions). Note that u_{bl} is truly a characteristic spread rate since the values in the two lateral directions were often not the same. The values of u_{bl} are also likely to depend on the height chosen for the analysis.

Similar characteristic flame spread rates as a function of time were defined for the mock-up seats. Since the flames on the seat spread laterally away from the center region of the cushion in both directions, a definition similar to that for u_{bl} was used as a characteristic spread rate, denoted u_{sl}. For most of the tests, the maximum lateral extents of the flame contours on the seat were located near the crevice where the back and seat cushions met. In order to simplify the definition, the maximum lateral flame extents on the left and right sides were determined as a function of time, and u_{sl} was defined as the increase in the difference between the two edges during the period between the two contours divided by twice the time difference. Again, the factor of two is included because the flames were usually spreading in two lateral directions simultaneously. The flame spread on the seats away from the crevice formed by the seat and back cushions where ignition took place, here referred to as the transverse direction, was not always symmetric about a line running from the ignition location. Similar to the definition of u_{bv}, a characteristic transverse spread rate, u_{st}, was defined as the difference between the maximum transverse distances from the seat-back crevice for the two contours divided by the period between contours.

Figure 23 shows plots of time behaviors of u_{bv}, u_{bl}, u_{sl}, and u_{st} for Test 9_1 based on the flame contours shown in Figure 22. Note that values were only determined until the spreading flames first reached the other side of a given cushion (top or one of lateral edges for the back, one of the lateral edges or the near edge for the seat).

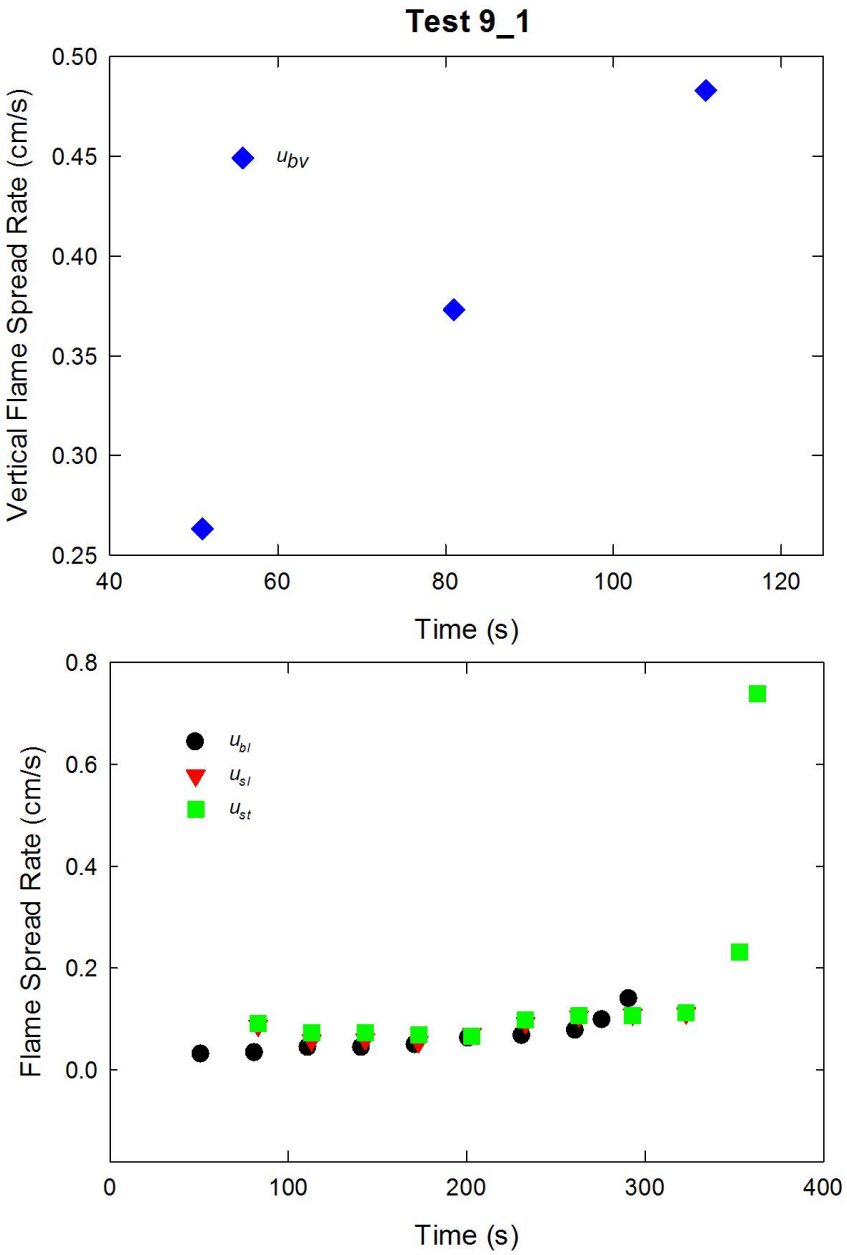

Figure 23. Plots of the four characteristic velocities as a function of time for Test 9_1 based on the flame contours in Figure 22 are shown.

5 Results for Test-matrix Mock-ups

5.1 Data Plots

A number of parameters related to the burning behavior were measured for each mock-up test. Appendix A includes graphical data summarizing results for each mock-up burned as part of the test matrix shown in Table 3. In cases where more than one ignition source was used, results are shown separately for each. Appendix A is broken into sections for each of the twenty material combinations. A section contains measurements for two tests or three tests (when the tests listed in Section 3.13 were repeated). Available results for each test are plotted on common temporal plots of HRR and total HRR, of FIGRA and mass, and MLR and EHOC. These are followed by individual contour plots for each test showing flame spread as a function of time. The data included in the contour plots are used to calculate the four characteristic flame spread rates, which are plotted as functions of time with two plots showing u_{bv} and u_{bl}, and u_{sl} and u_{st}. The burned area data were also used to determine total burned areas on the back and seat as a function of time. The results for all of the tests are included on a single plot. The last graph in a given section compares separate plots of the radiant heat fluxes recorded in orthogonal directions from the front, right side, and rear of all of the mock-ups at distances of 0.75 m and 1.5 m. Appendix C provides comparable plots for the supplemental experiments using Combinations 25, 26, and 27 listed in Table 11.

5.2 Ignition

As discussed in Sections 3.10 and 3.12, a hierarchy of ignition sources was used to ignite the chair mock-ups based on whether or not an ignition was judged successful. Initially Ignition Source 1 was applied for 20 s. If no or only limited flame spread was observed, Ignition Source 2 was next applied for 40 s. If flame spread was still limited, the Ignition Source 5 wood crib was used. Table 12 summarizes the ignition results for fifty (test matrix plus repeated and supplemental) mock-ups tested. For each test ID an "X" indicates that Ignition Source 1 was used. If only Ignition Source 1 was used, the entries under Ignition Source 2 and Ignition Source 5 are blank. If Ignition Sources 2 and 5 were applied to a mock-up, the time of application in seconds relative to the application of Ignition Source 1 (defined as 0 s) is listed in the table.

Notes included in Appendix A for individual tests provide additional details concerning observations for cases in which Ignition Sources 1 and 2 were employed. As an example, in many of the tests in which ignition by Ignition Source 1 was judged to be unsuccessful, some flame spread was observed over the back cushion of the mock-up, but the seat failed to ignite at all. It should also be noted that for at least seven of the mock-ups, Ignition Source 1 initially ignited the back cushion, and the spreading flames later moved onto the seat.

Some general observations concerning ignition behavior can be obtained by reviewing the results included in Table 12. For the tests involving the primary test matrix (tests numbered 1 to 24), the application of Ignition Source 2, and for some cases Ignition Source 5, was only necessary for odd-numbered tests, which were upholstered with cotton fabric (see Table 3). This observation suggests that the cotton fabric was more resistant to flaming ignition than the 78%PP/22%PE thermoplastic fabric.

For the cotton-fabric-covered mock-ups with no barrier fabric (Combinations 9, 11, 13, and 15), it was only necessary to apply Ignition Source 2 during three tests (Test 9_2, Test 13_1, and Test 15_2). Note that these three tests correspond to three different material combinations. One of the mock-ups (Test 9_2) included NFRFPUF, while the other two incorporated the fire-retarded foam. Review of the videos for these three tests provided some additional insights concerning the failed ignition behaviors. During Tests 9_2 and 15_2 the application of Ignition Source 1 resulted in limited charring of the cotton fabric near the flame application site as can be seen in Figure 24 for Test 9_2. These tests were two of the few in which

Table 12. Summary of ignition sources used for each mock-up test. Numbers refer to times in seconds following the application of Ignition Source 1.

Combination		Ignition Sources				Ignition Sources				Ignition Sources		
	ID	1	2	5	ID	1	2	5	ID	1	2	5
1	1_1	x			1_2	x			1_3	x		
2	2_1	x			2_2	x						
5	5_1	x	1647		5_2	x			5_3	x		
6	6_1	x			6_2	x						
9	9_1	x			9_2	x	120					
10	10_1	x			10_2	x			10_3	x		
11	11_1	x			11_2	x						
12	12_1	x			12_2	x						
13	13_1	x	1434		13_2	x						
14	14_1	x			14_2	x						
15	15_1	x			15_2	x	87					
16	16_1	x			16_2	x						
17	17_1	x	369		17_2	x	767					
18	18_1	x			18_2	x						
19	19_1	x	295	1090	19_2	x	491					
20	20_1	x			20_2	x			20_3	x		
21	21_1	x	910	1218	21_2	x	879	2239				
22	22_1	x		964*	22_2	x			22_3	x		
23	23_1	x	340	1969	23_2	x	487	2708				
24	24_1	x			24_2	x						
25	25_1	x										
26	26_1	x	105	429	26_1	x	85	275				
27	27_1	x			27_2	x						

*Ignition Source 5 was applied even though fire had previously spread over most of the outer fabric

Figure 24. This frame taken from the Video Camera #3 view of the mock-up during Test 9_2 shows the appearance of the cotton fabric immediately following the removal of Ignition Source 1.

such cotton charring was observed but where there was no additional flame spread on the back or seat cushions. The ignition behavior for Test 13_1 was different. Ignition Source 1 ignited only the back cushion and, as evident from the flame contours in Figure A-89, the flames spread upward before extinguishing. There was no evident blackening on the seat cushion.

During tests of mock-ups constructed with the Whispershield barrier (Combinations 1, 2, 5, and 6), the use of Ignition Source 2 was only required for Test 5_1. Review of the videos for this test showed that only the back cushion ignited when Ignition Source 1 was applied. The fire then spread slowly over most of the back surface (see the flame contours in Figure A-26) as well as the right arm. While the sample sizes are limited, the relative success in igniting the mock-ups containing a Whispershield barrier and cotton upholstery fabrics suggests that the likelihoods for ignition of cotton-upholstered mock-ups with and without a Whispershield barrier were similar.

Flaming ignition of the cotton-covered cushions was much less likely when Norfab fabric (Combinations 17, 19, 21, and 23) was included as a barrier material as compared to combinations that included no barrier or used Whispershield as a barrier. Ignition Source 2 was applied for each of the experiments involving these components. Following applications of Ignition Source 1 there were varying amounts of flame spread on the back cushions, but no evident flame spread on the seats. In most tests there was no obvious blackening of the seat cushion after Ignition Source 1 was removed, but, in a few cases, a small charred area was evident on the cotton.

For three of the four tests with cotton-covered mock-ups that included cushions with Norfab barrier and NFRFPUF, there was significant flame spread on the backs and seats of the mock-ups following application of Ignition Source 2, and Ignition Source 5 was not applied. During Test 19_1 Ignition Source 2 induced only limited flame spread on both the seat and back cushions. In contrast, the crib ignition source (Ignition Source 5) was used for each of the combinations that included the cotton upholstery fabric over the FRFPUF (with or without polyester fiber wrap). This suggests that the likelihood of ignition for mock-ups with Norfab barriers was reduced when NFRFPUF was replaced with the fire-retarded foam.

The results summarized in Table 12 show that there was some irreproducibility in the likelihood of ignition for mock-ups upholstered with cotton fabric. For several combinations the ignition sources necessary for ignition were different for repeated tests. These differences represent a potential source of variability since the previously burned areas on the seat and back cushions could vary substantially when Ignition Source 2 and Ignition Source 5 were used.

5.3 Heat Release Rate

The heat release rate behavior of a fire is generally recognized as the most important parameter related to fire safety. [106] Thus, assessing the feasibility of predicting various parameters related to the real-scale HRR curves based on small-scale tests is a major goal of the overall study introduced in Section 1. Temporal HRR profiles for all material combinations included in the test matrix in Table 3 are plotted in Appendix A. Review of the HRR curves reveals that their shapes varied significantly with combination as the materials in the cushions forming the mock-ups changed. Various shapes were observed, ranging from nearly flat (e.g., see Combination 5 HRR curves in Appendix A.3) to roughly symmetrical single peaks (e.g., see Combination 9 HRR curves in Appendix A.5), to curves with two or more HRR peaks (e.g., see Combination 1 HRR curves in Appendix A.1). Wide variations in maximum HRR, denoted HRR_{max} were observed with values ranging from ≈ 0 kW to ≈ 600 kW. Burning times also varied widely, with periods of measurable substantial HRRs ranging from as short as 250 s to values in excess of 3000 s. Comparisons of the HRR curves for given material combinations showed that in many cases results for repeated tests had very similar shapes, magnitudes, and burning periods, while in a few cases the curves were substantially different. The largest variations between repeated tests were found for combinations where the maximum

Table 13. Parameters used to characterize experimental HRR behaviors for four cushion mock-ups with units and symbols.

Parameter	Units	Symbol
Time required to reach 25 kW	s	t_{+25}
Time of first HRR maximum	s	t_{peak1}
Value of first HRR maximum	kW	HRR_{peak1}
Time of maximum HRR	s	t_{max}
Value of maximum HRR	kW	HRR_{max}
Time HRR falls below 25 kW	s	t_{-25}
Period HRR above 25 kW ($t_{>25}$-$t_{<25}$)	s	$t_{>25}$
Heat released while HRR > 25 kW	MJ	$Q_{>25}$
Average HRR while above 25 kW	kW	$HRR_{avg>25}$
Full width half maximum above 25 kW	s	$FWHM_{>25}$
Shape factor #1 ($FWHM_{>25}/t_{>25}$)	--	SF_t
Shape factor #2 ($HRR_{max}/HRR_{avg>25}$)	--	SF_{HRR}
Total heat released	MJ	Q_{tot}

HRR values were relatively low and burning lasted for long periods. An example of the latter type of variation is evident for the HRR curves for Combination 19 shown in Figure A-152 following application of Ignition Source 2. For Test 19_1 the HRR was minimal and the test was stopped after 800 s, while low, but measurable, HRRs were observed during Test 19_2 between 1000 s and 2600 s.

Even though some variations were observed, the differences between repeated tests for any given material combination were generally much less than the differences observed between tests with different combinations. This qualitative observation provides evidence that the choices of material combinations summarized in Table 3 resulted in observable variations in burning behavior as reflected in the HRR temporal profiles.

It is important to quantify changes in HRR behaviors in order to confirm the role of various materials on mock-up burning behavior and to provide a means for judging the effectiveness of small-scale test results for predicting the real-scale mock-up observations. There are a number of parameters that could be used for this purpose. Based on the HRR behaviors observed during the current tests, the parameters listed in Table 13 were chosen.

The parameter t_{+25} defined as the time when a fire's HRR first reached 25 kW is intended to characterize the initial HRR growth behavior of the fires. The value of 25 kW is arbitrary, but is large enough to be easily identified in the HRR data, while being far less than the HRR_{max} observed during most tests. The times and HRR values for the initial peak and maximum observed HRRs provide insights into both the fire growth rate and the overall HRR behavior. Keep in mind that for some experiments the initial HRR peak and the maximum HRR peak were the same. This can result for experiments in which there is only a single peak or ones in which there are multiple peaks, but the first peak is also the maximum.

The time when the HRR dropped back below 25 kW (t_{-25}) was used to calculate the period over which the HRR remained above 25 kW ($t_{>25}$) for a given test. Note that in a few tests the HRR went above and dropped below 25 kW two or more times. For these cases, the final occurrence was used to determine t_{-25}. By integrating the HRR between t_{+25} and t_{-25}, the quantity of heat released while the HRR remained greater than 25 kW (Q_{25}) could be determined. The average HRR during this period ($HRR_{avg>25}$) was then calculated as $Q_{>25}/(t_{-25}-t_{+25})$.

Two shape parameters were defined in order to provide insights into the variations of HRR with time. The first (SF_t) is that most commonly used to describe such curves and is given by the full width half maximum of the curve during the period when the HRR was above 25 kW ($FWHM_{>25}$) divided by the period when the HRR > 25 kW. For current purposes, the base was defined as the period between t_{+25} and t_{-25}, and the $FWHM_{>25}$ was determined for a HRR equal to (HRR_{max} – 25 kW)/2+25 kW. For cases in which the curve rose above and fell below this value multiple times, the final occurrence was used to define $FWHM_{>25}$. The second shape parameter (SF_{HRR}) was defined as $HRR_{avg>25}/HRR_{max}$. Note that values for both parameters can range from 0 to 1, with values near zero characteristic of a sharp HRR peak(s) with a trailing or following long period with HRRs below the FWHM, values near 0.5 characteristic of nearly symmetric HRR peaks, and values near 1 characteristic of HRR curves that are roughly constant between t_{+25} and t_{-25}.

Values for all of the parameters listed in Table 13 are included in Appendix B.2 for each of the individual tests (Table B-3) along with averages (symbol with overbar) and standard deviation values (symbol with ´) for the combinations (Table B-4). Bar charts are used to provide easily interpreted graphical representations of the results. In the bar charts a parameter of interest is plotted as a function of Combination Number. The heights of the bars represent average values, while standard deviations are represented by the error bars. Some conventions are used to aid interpretation. Combinations that include cotton upholstery covers are represented by red bars, while those with 78%PP/22%PE covers are green. Open bars represent combinations where NFRFPUF was used, while cross-hatched bars indicate that FRFPUF was included. The type of barrier; Whispershield (Combinations 1 to 8), no barrier (Combinations 9 to 16), and Norfab (Combinations 17 to 24); are indicated by notations above the bars. In a given group of foam and barrier type, the first two combinations did not incorporate PEFW, while the next two did. Recall that PEFW was not used with the Whispershield barrier, and Combinations 3, 4, 7, and 8 were not tested. For some parameters, values are not reported for a few of the other combinations. This generally means the values could not be determined for those cases. As an example, for some combinations of materials, no measurable HRRs were recorded, while in others the HRRs did not exceed 25 kW. The variation of sewing thread used with a given combination number was more complex. Table 3 indicates the order used.

The average times required for developing fires on the cushion mock-ups to grow to 25 kW, $\overline{t_{+25}}$, are plotted as a function of combination number in Figure 25. Note that HRRs following ignition of mock-ups with Combinations 21 and 23 materials did not grow sufficiently to reach 25 kW. In effect, values of $\overline{t_{+25}}$ for these two combinations were infinity. Two repeated tests were performed for Combination 19. Neither fire spread substantially when Ignition Source 1 was applied. For Combination 19_1 the same was true when Ignition Sources 2 and 5 were used. However, a fire did grow and exceed 25 kW following the application of Ignition Source 2 to Combination 19_2. The result for the latter is included in the plot.

From a review of Figure 25, it is obvious that for combination pairs in which the only change was the upholstery fabric, the tests for mock-ups covered with cotton material required substantially longer times to grow to 25 kW than those with the 78%PP/22%PE fabric. Similarly, $\overline{t_{+25}}$ values for cotton-covered cushions were dramatically increased when NFRFPUF was replaced with the FR foam. This trend is not nearly as evident for mock-ups covered with the thermoplastic fabric. The addition of polyester fiber wrap to a given combination of polyurethane, barrier, and upholstery fabric appeared to have had minimal effects on $\overline{t_{+25}}$. No effects of using different sewing threads are evident in these data.

The average periods required for mock-up fires to grow to an initial HRR peak ($\overline{t_{peak1}}$) are shown in Figure 26. The dependence on combination number is similar to that for $\overline{t_{+25}}$ shown in Figure 25. This suggests that these values depended on cushion materials in the same way. For most of the combinations, $\overline{t_{peak1}}$ values are slightly higher than corresponding values of $\overline{t_{+25}}$. This is explained by the observation that most often the initial peak HRR (HRR_{peak1}) is higher than 25 kW and passes through this level as the HRR is increasing. In only a few tests were HRR_{peak1} values less than 25 kW with t_{peak1} less than t_{+25}.

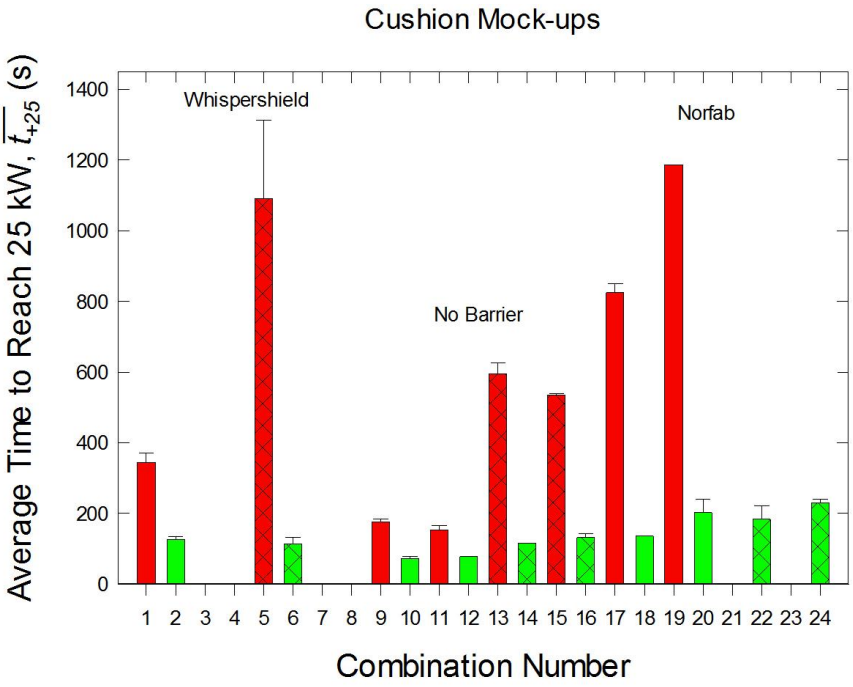

Figure 25. Average and standard deviation of the times required for fires on the mock-ups to grow to 25 kW are plotted as a function of mock-up combination number.

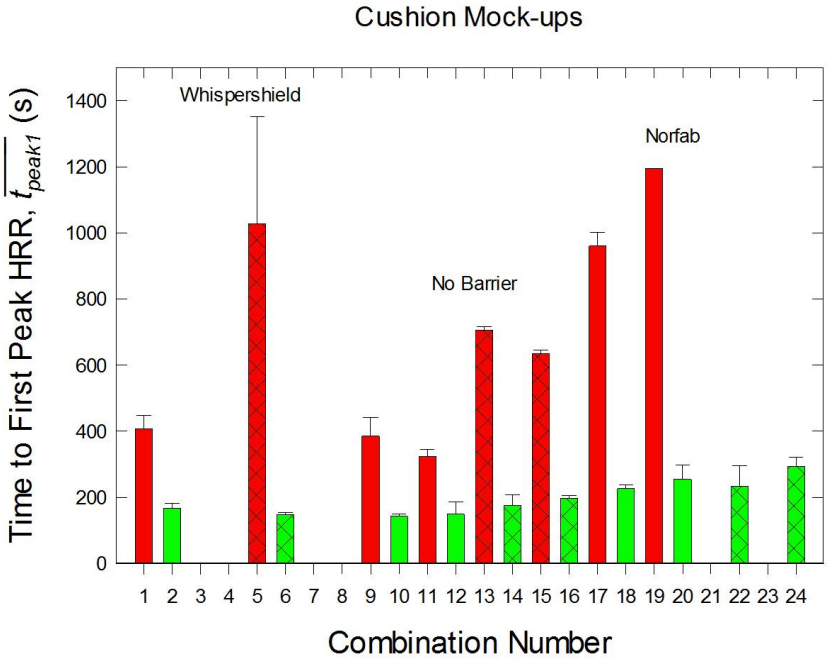

Figure 26. Average and standard deviation values for the times required for fires on the mock-ups to grow to an initial HRR peak are plotted as a function of mock-up combination number.

Average and standard deviations for HRR_{peak1} are plotted in Figure 27 for the various mock-up combinations. The apparent missing values for Combinations 21 and 23 are actually zero since measurable HRRs were not observed. Values ranged from 0 kW to 588 kW. The highest $\overline{HRR_{peak1}}$ are associated with mock-ups with cushions that did not include a barrier. Corresponding values for combinations

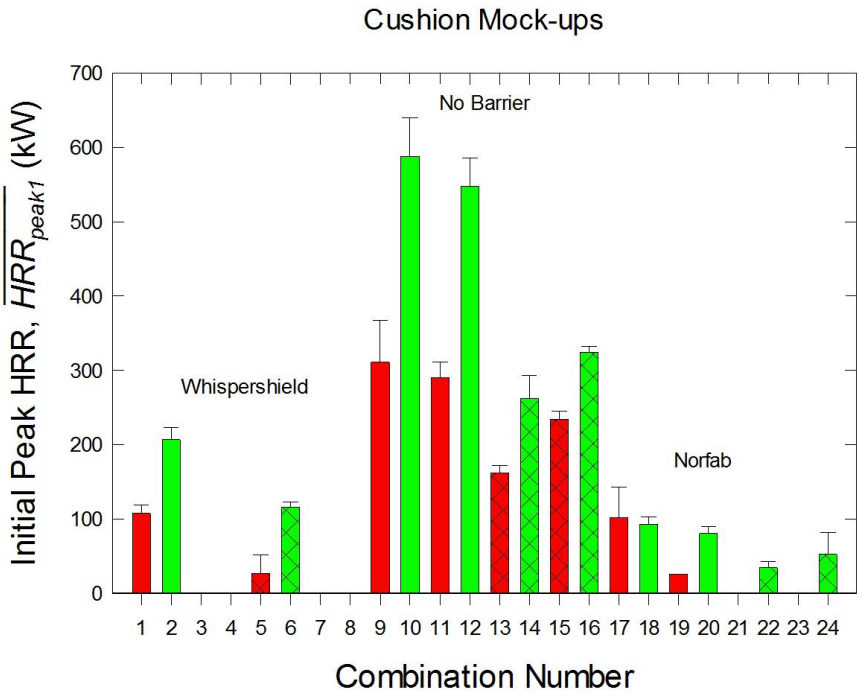

Figure 27. Average and standard deviation values of the initial peak HRR are plotted as a function of mock-up combination number.

containing either of the two barriers were reduced substantially. The reductions were somewhat larger when Norfab fabric was used.

Comparison of mock-up combinations where only the upholstery fabric changed indicates that $\overline{HRR_{peak1}}$ values were noticeably reduced when cotton cover fabric was used in place of the 78%PP/22%PE blend. The only exception was the Combination 17 and 18 pair for which values were nearly equal. In many cases, reductions in $\overline{HRR_{peak1}}$ were greater than 50 %. Comparison of combinations in which NFRFPUF was replaced with FRFPUF shows comparable reductions in $\overline{HRR_{peak1}}$. It is evident that the $\overline{HRR_{peak1}}$ values depend strongly on upholstery fabric, FPUF type, and the presence or absence and type of barrier.

The addition of PEFW to the cushions seemed to have had variable effects on $\overline{HRR_{peak1}}$. For cushions with NFRFPUF and no barrier, small reductions with overlapping standard deviations were observed. When FRFPUF was used, addition of the PEFW resulted in increases in $\overline{HRR_{peak1}}$ that were larger than the standard deviations. Keeping in mind the different behaviors observed for Tests 19_1 and 19_2, it is not possible to draw conclusions concerning the effect of adding PEFW to cushions with a Norfab barrier.

Average and standard deviations for the periods required to reach HRR_{max} (t_{max}) for the various mock-up combinations are shown in Figure 28. While the overall variations in $\overline{t_{max}}$ are similar to those in Figure 26 for $\overline{t_{peak1}}$, close inspection shows some substantial variations in the relative magnitudes. These variations are associated with changes in the HRR temporal profiles between the various combinations. Review of the HRR profiles in Appendix A and the list of t_{peak1} and t_{max} in Appendix B reveals that, with two exceptions, the two values were nearly identical for the tests in which no barrier was included in the mock-up cushions. The HRR curve for Test 13_2 (see Figure A-86) shows two distinct peaks, with the second very slightly higher. Two separate HRR peaks were identified for Test 14_1 (see Figure A-98), but the curve actually appears to have been a single peak with HRR fluctuations. The small time difference between the peaks supports this interpretation.

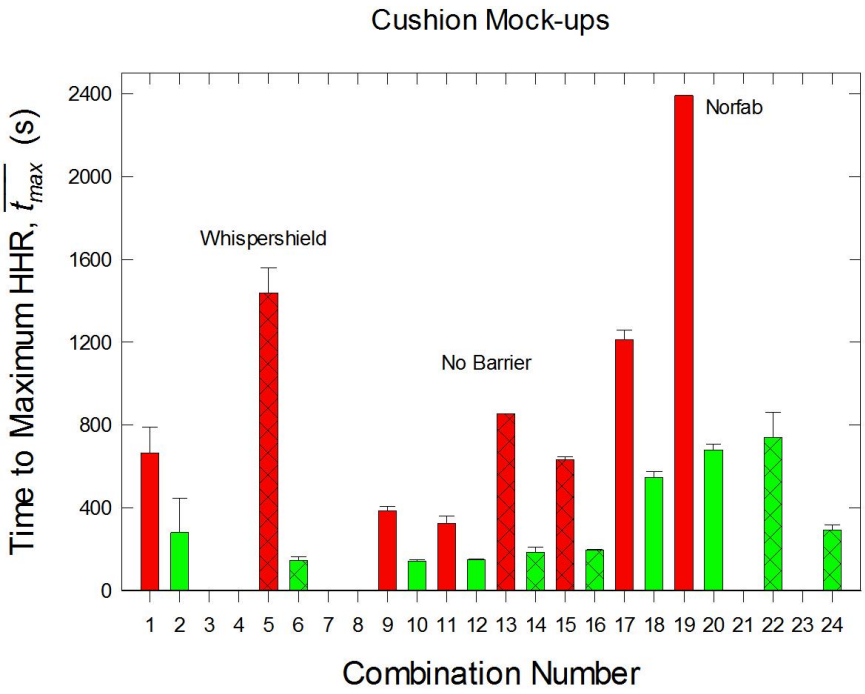

Figure 28. Average and standard deviation values of the times required for fires on the mock-ups to grow to peak HRR are plotted as a function of mock-up combination number.

The temporal HRR profiles for the tests without barriers generally showed single or double peaks. Interestingly, for combinations with NFRFPUF, single peaks were observed when the cushions were covered in cotton fabric, and two peaks were present when 78%PP/22%PE fabric was used. When NFRFPUF was replaced with SI-1324 FRFPUF, the order was reversed, and two peaks were associated with combinations containing the cotton fabric.

Comparisons of the videos for fires on mock-ups with no barrier and NFRFPUF provide an explanation for the variations in HRR curve shapes between cotton-covered (Combinations 9 and 11) and 78%PP/22%PE-covered cushions (Combinations 10 and 12). For both types of cover fabric, HRR_{peak1}s were observed when the interior surfaces of the mock-ups were fully involved in flames. In the case of the mock-ups constructed with cushions covered with the thermoplastic fabric, a large amount of liquid poured down from the mock-up onto the cement board under the support stand base shortly after HRR_{peak1} was reached and began to burn intensely. These intense pool fires were responsible for the second peaks. Figure 29 shows frames taken from a video of the fire burning on a mock-up covered with the thermoplastic fabric during Test 10_1. The video frames correspond to the times when HRR_{peak1} and the second HRR peak were recorded, 146 s on the left and 220 s on the right, respectively.

Figure 30 shows corresponding images for one of the fires (Test 9_1) burning on cushions upholstered with the cotton fabric. The image on the left was recorded at t_{max}. Videos taken from different directions showed that by this time the fire had burned through the back cushion and that this cushion had partially collapsed. Most of the flames are apparent on the seat and side cushions. The image on the right was recorded just prior to the time when the HRR dropped rapidly. It shows that while some liquid had been deposited on the cement board base, there was only limited burning taking place there. A large pool fire such as evident during Test 10_1 (see right-hand side of Figure 29) did not develop. Thus the single intense HRR peak for these tests was associated with burning constrained primarily to the cushions.

A similar review of the videos for tests with FRFPUF covered with the thermoplastic fabric showed that the HRR reached its single maximum peak when all of the interior cushion surfaces were involved. This

Figure 29. Two frames taken from a video recorded by Camera #8 show the appearance of the fire during Test 10_1 at 146 s (left) and 220 s (right) following application of Ignition Source 1.

Figure 30. Two frames taken from a video recorded by Camera #8 show the appearance of the fire during Test 9_1 at 401 s (left) and 544 s (right) following application of Ignition Source 1.

Figure 31. Two frames taken from a video recorded by Camera #8 show the appearance of the fire during Test 14_2 at 204 s (left) and 324 s (right) following application of Ignition Source 1.

is evident in the left-hand side of Figure 31, which was recorded at the peak HRR. For these tests a small amount of liquid was deposited on the cement board, but the resulting fire was much smaller than observed when NFRFPUF was used (compare with Figure 29).

The two peaks observed for mock-ups with cotton cover fabric over FRFPUF resulted from a different type of burning behavior. Figure 32 shows two views captured from a video of Test 13_2 at the time when the

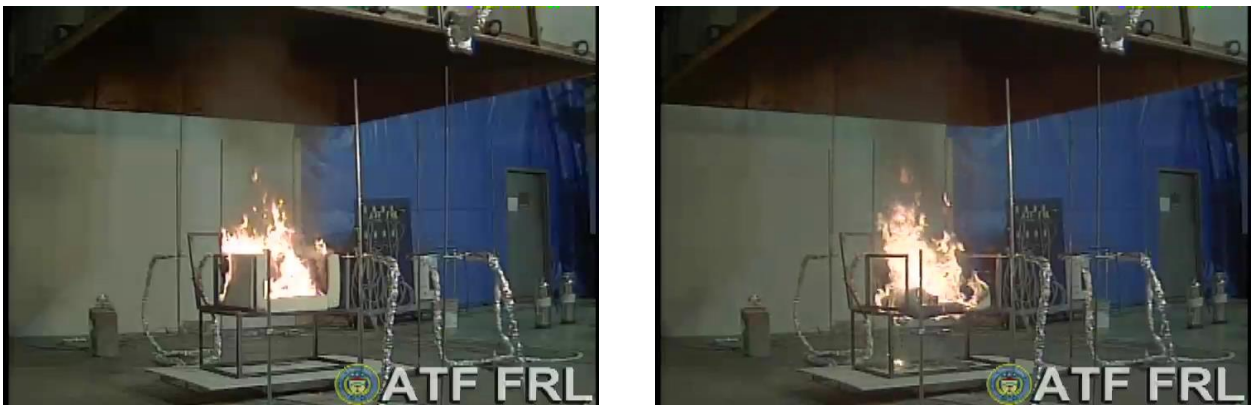

Figure 32. Two frames taken from a video recorded by Camera #8 show the appearance of the fire during Test 13_2 at 723 s (left) and 855 s (right) following application of Ignition Source 1.

first (left) and second (right) HRR maxima were recorded. Inspection of the videos associated with this mock-up combination showed that following the initial HRR maximum, the back and side cushions partially collapsed inward onto the seat, forming a more compact fuel package. One of these collapsed mock-ups is visible on the right side of Figure 32. The second HRR peak resulted from enhanced burning that developed on the collapsed fuel package. Note that very little burning was present on the test stand base under the mock-up.

Whether or not t_{peak1} and t_{max} were the same or different depended on the type of FPUF and upholstery fabric used in the four mock-ups types incorporating Whispershield barrier fabric. When cotton fabric covered the barrier and NFRFPUF (Combination 1), the HRR curves had three distinct peaks (see Figure A-1 in Appendix A) that occurred at roughly the same time during each test. For the three specimens tested, the maximum HRR was associated with either the second (Tests 1_1 and 1_2) or third (Test 1_3) peaks. Review of videos suggested that the three peaks coincided with intense burning on different sections of the mock-ups. The first HRR peak occurred after a period of rapid fire growth before the flames had spread to cover the entire seat and arm interior areas. At this time primarily the back and arms were involved. Shortly thereafter the back began to collapse, and the fire to died down in this area. Meanwhile, the fire had continued to spread over the interior portions of the seat and arms. At the time of the second HRR peak the arms appeared to be burning intensely, with weaker burning on the seat. Eventually, the arm cushions collapsed inward in a manner similar to that described above. This seemed to lead to intense burning of the seat which coincided with the third peak in the HRR curves.

The HRR curves for mock-ups containing Whispershield and NFRFPUF covered with the thermoplastic fabric had a different appearance (see Figure A-12 in Appendix A). The HRR curves for both tests had relatively sharp initial peaks followed by much longer burning periods with substantially different appearances. Review of the videos showed that the first peak was associated with rapid flame spread in combination with intense burning over the 78%PP/22%PE cover fabric. By the time of the first peak, the fire had spread over nearly all of the interior surfaces of the seat, back, and arms, as well as part of the tops of the back and arm cushions. After the initial peak, the fires died down somewhat, and it was possible to see the apparently intact cushions through the flames. The maximum HRR for Test 2_1 was a second peak that occurred 399 s following ignition, or nearly five minutes after the initial peak. The videos showed that at this time heavy flaming had developed on all four cushions, and the arms had collapsed partially inwards towards the seat. The HRR behavior following the initial peak for Test 2_2 was somewhat different, with a period of roughly constant HRR lower than HRR_{peak1} that lasted longer than the extended burning during Test 2_1. Videos of Test 2_2 showed that flames during this period appeared much weaker and more localized than during Test 2_1, with the areas of burning tending to move around on the various cushions. There was no substantial burning of liquid on the support stand base during either test.

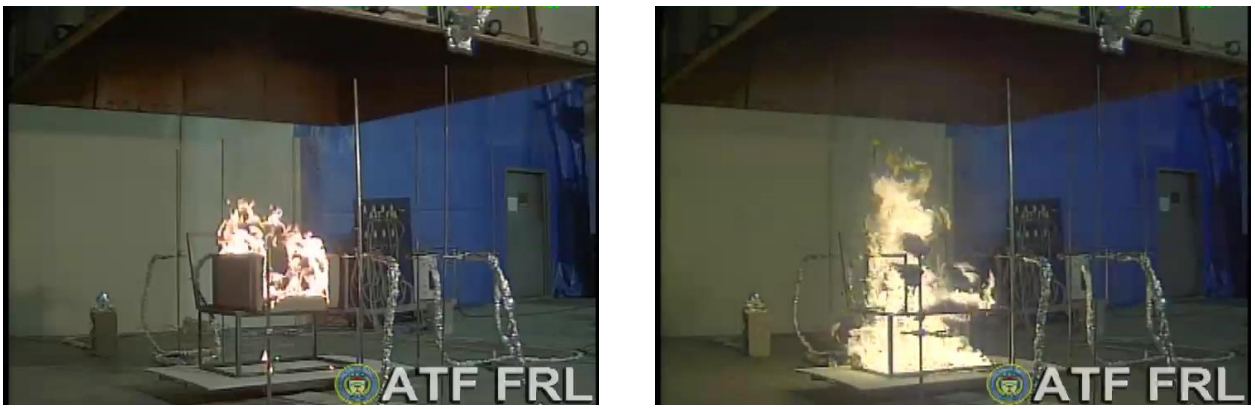

Figure 33. Two frames taken from a video recorded by Camera #8 show the appearance of the fire during Test 18_1 at 225 s (left) and 567 s (right) following application of Ignition Source 1.

Replacing the NFRFPUF with SI-1324 compliant foam dramatically changed the burning behaviors of the mock-ups protected with Whispershield barrier fabric. The HRR profiles for these cases are shown in Figure A-21 and Figure A-37 in Appendix A. For cushions upholstered with the cotton fabric, at least fifteen minutes were required for the HRR to grow above 25 kW, and for one of the three repeated tests (5_1) the fire never exceeded this value. When the fires finally began to grow, they burned for long periods, and the maximum HRRs remained well below 100 kW. Videos of these fires showed that following ignition (either Ignition Sources 1 or 2) the flame heights remained low as the flames spread. For Tests 5_2 and 5_3 more intense flames first appeared along the crevice formed by the seat and back cushions. The region of more intense burning moved around the cushions with time. For both tests, the final area of significant flaming was on the left-arm cushion.

When the 78%PP/22%PE fabric covered the Whispershield barrier and FRFPUF the burning behavior differed significantly. The HRR curves are shown in Figure A-37 of Appendix A. For Tests 6_1 and 6_2 there were initial spikes in HRR which exceeded 100 kW, followed by long, slowly decaying tails that were generally below 25 kW. Videos of these fires revealed that the HRR spike was due to rapid flame spread and burning of the cover fabric. Once the burning fabric died down, there was little or no further burning of the underlying materials.

The remaining eight combinations included a Norfab barrier placed between the upholstery fabric and the inner filling (either FPUF or FPUF covered with PEFW). With the exception of Combination 24, the maximum HRR occurred later than the initial peak. In tests 24_1 and 24_2 there were single HRR peaks. The time behaviors of the HRR for these mock-ups are summarized below.

All of the combinations covered with thermoplastic fabric ignited when Ignition Source 1 was applied. The HRR curves for Combinations 18 and 20 (see Figure A-141 and Figure A-171 in Appendix A), which included NFRFPUF were similar. There was a relatively rapid HRR increase to an initial peak around 100 kW, followed by a slightly longer growth period during which the HRR reached much higher levels between 400 kW and 500 kW. The addition of PEFW to the cushions appeared to have a slight effect on the HRR curves in that the mock-ups with the PEFW had a broader second HRR peak. Videos of these fires showed the same general behaviors. Following ignition, there was rapid flame spread and fire growth on the fabric that resulted in the initial HRR peak. After the fabric was consumed, relatively small fires remained on the mock-ups which continued to burn until a large amount of liquid poured down on the cement board under the test stand. At this point a large pool fire developed while, at the same time, the remaining mock-up material on the test stand became heavily involved in flames. This intense burning coincided with the second HRR peak. Figure 33 shows two frames taken from a video of Test 18_1 recorded at the times of the initial (left) and maximum (right) HRR peaks.

Replacing NFRFPUF with FR foam had a dramatic effect on the burning behavior of the mock-ups formed from cushions covered with thermal-plastic upholstery. The HRR curves for the three tests where the PEFW was not included (Combination 22) are shown in Figure A-203 of Appendix A. Even though the upholstery fabric ignited, and the flames spread over the cushion surfaces, HRR_{peak1} values were reduced by roughly a factor of two compared to cases where NFRFPUF was used. After the initial HRR increases, there were relatively long periods during which burning continued, but the HRR generally remained below 60 kW. Videos of these fires show that the flames spread fairly quickly over the fabric surfaces on the interior surfaces of the mock-up cushions. This fire growth was responsible for the initial HRR peak.

Afterwards, flame spread continued over other sections of the fabric which had not burned, while at the same time there was evidence for localized burning of interior materials which contributed to the HRRs measured at later times. This burning died down slowly. When PEFW was included inside the Norfab barrier (Combination 24), the initial flame spread on the cover fabric was similar to that described above, as was the HRR growth to an initial peak (see Figure A-229 in Appendix A). However, after the thermo-plastic fabric burned away, there was very little of the additional burning observed when the wrap was not present, and the HRR fell to low levels and remained barely measurable. Videos of these fires showed the outer fabric burning away followed by a period of small isolated fires at various locations on the cushions.

Exchanging the thermoplastic outer fabric with cotton in the mock-ups with Norfab fire barriers significantly modified the fire development. Consider first mock-ups that contained NFRFPUF. Ignition with Source 1 failed to fully ignite any of these mock-ups. However, application of Ignition Source 2 to the mock-ups that did not contain PEFW (Combination 17) inside the Norfab barrier did result in fires that spread over the mock-up surfaces. The HRR curves for Test 17_1 and 17_2 are shown in Figure A-127 in Appendix A. For both, initial fire growth was very slow, and the HRRs did not exceed 25 kW during the initial 800 s following ignition. However, starting around this time the HRRs began to grow quickly, and levels approaching 200 kW were reached. This relatively intense burning lasted for roughly ten minutes. This burning behavior is in strong contrast to that observed for mock-ups covered with the thermoplastic fabric, where a measurable HRR developed early in the fire, and HRRs grew to levels nearly three times as high. When PEFW was added to the cushions, the burning behavior was noticeably modified. In one case, Test 19_1, only limited flame spread was observed following application of Ignition Sources 1, 2, and 5, and HRR levels were not measurable. Following application of Ignition Source 2 during Test 19-2, flames did spread over the cushion surfaces, and after roughly 18 minutes a measurable HRR was observed that displayed several peaks with the HRR_{max} slightly higher than 100 kW. Review of videos for this fire showed that the HRR peaks developed as localized fires moved to different cushions of the mock-up. Comparison of the results for mock-ups with and without the PEFW showed that including the wrap resulted in fires with lower HRRs and longer development times, i.e., an improved fire performance. When the NFRFPUF in the cotton-upholstered cushions was replaced with the FR version in the mock-ups containing the Norfab barrier material, no measurable HRRs were recorded for mock-ups with or without PEFW.

A bar plot showing the average and standard deviations for HRR_{max} as a function of mock-up combination number is shown in Figure 34. Differences between this plot and Figure 27, which shows the corresponding plot for $\overline{HRR_{peak1}}$, arise primarily for mock-ups with an added barrier. For many of these combinations, $\overline{HRR_{max}}$ were considerably higher than $\overline{HRR_{peak1}}$. The variations in HRR temporal profiles responsible for the differences have been discussed above. The variations of $\overline{HRR_{max}}$ with cover fabric and FPUF type are evident. The values also clearly depend on whether or not a barrier fabric was included, as well as the type of barrier.

In every case in which the other materials were held the same while the upholstery fabric was varied, values of $\overline{HRR_{max}}$ were lower with cotton than when the thermoplastic was used. Replacing the NFRFPUF with

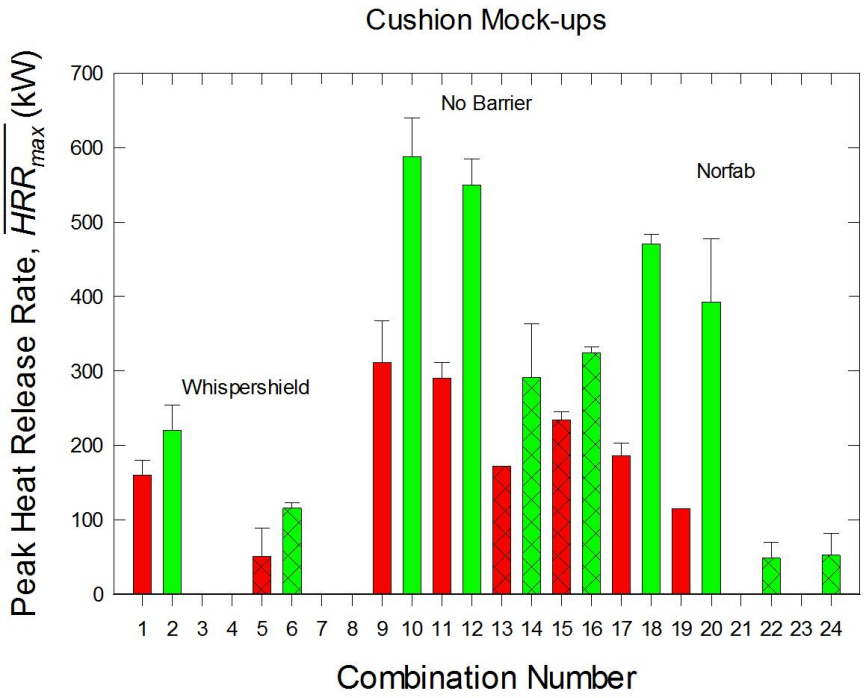

Figure 34. Average and standard deviation values of the maximum HRR are plotted as a function of mock-up combination number.

the FR version also resulted in reduced HRRs. Similarly, adding either of the two barrier fabrics to a given combination of other materials lowered the HRR.

Closer analysis reveals some differences in the effects of changing one of the materials. For instance, replacing Whispershield with Norfab fabric in mock-ups containing NFRFPUF resulted in increased values of $\overline{HRR_{max}}$, while the opposite was the case for mock-ups that included SI-1324 foam. The effect of adding PEFW on $\overline{HRR_{max}}$ also depended on the combination of materials considered. Addition of the wrap to cushions with NFRFPUF and no barrier resulted in small reductions in $\overline{HRR_{max}}$, while the opposite was true when FR foam was used. For mock-ups containing NFRFPUF with a Norfab barrier, the addition of the PEFW resulted in lower HRRs.

A number of other parameters have been determined in order to characterize the HRR curves measured for the mock-ups. These include parameters that depend on the curve shapes such as $t_{>25}$, $HRR_{avg>25}$, and $FWHM_{>25}$. The definitions for these parameters were provided in Table 13.

Averages and standard deviations for $t_{>25}$ are plotted as a function of Combination Number in Figure 35. The obvious outliers are the large values for Combinations 5 and 19. For each of these combinations, one of the tests, Test 5_1 and Test 19_1, did not reach 25 kW and was omitted from the analysis. As can be seen in Figure A-21 and Figure A-152 in Appendix A, the other tests burned for long periods with HRRs that fluctuated above and below 25 kW. These were the only combinations where such extended burning was observed. For mock-ups that included NFRFPUF, values of $\overline{t_{>25}}$ were higher when one of the barrier fabrics was added to a given combination of upholstery fabric and PEFW; with the larger increases observed with the Norfab barrier. Large, consistent changes when either the upholstery fabric or the type of FPUF was varied were generally not apparent. One exception was for mock-ups that included FRFPUF and no barrier. For combinations with and without PEFW, mock-ups that included cotton upholstery fabric burned longer above the HRR threshold than the corresponding combinations with 78%PP/22%PE fabric.

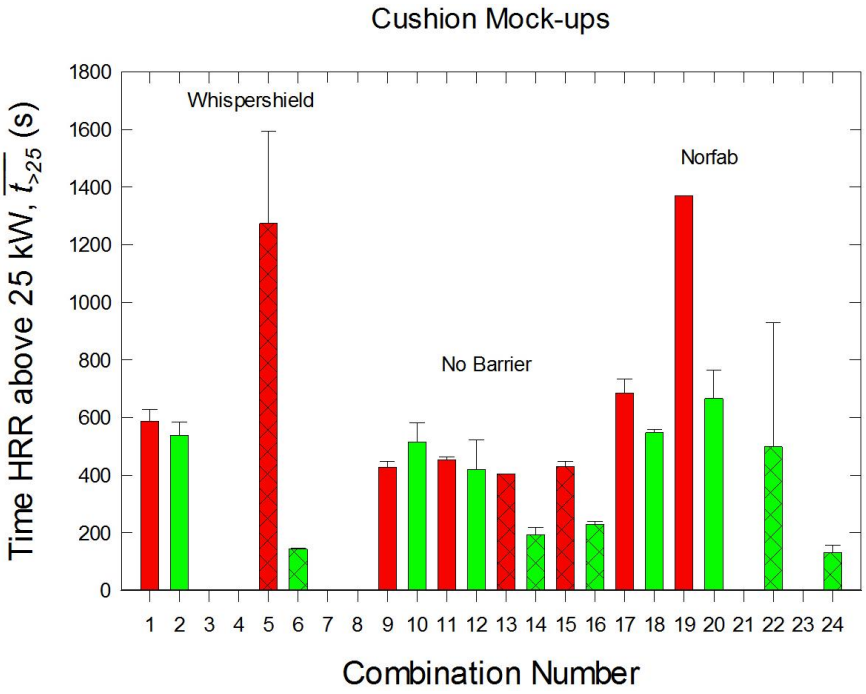

Figure 35. Average and standard deviation values of the period the HRR was above 25 kW are plotted as a function of mock-up combination number.

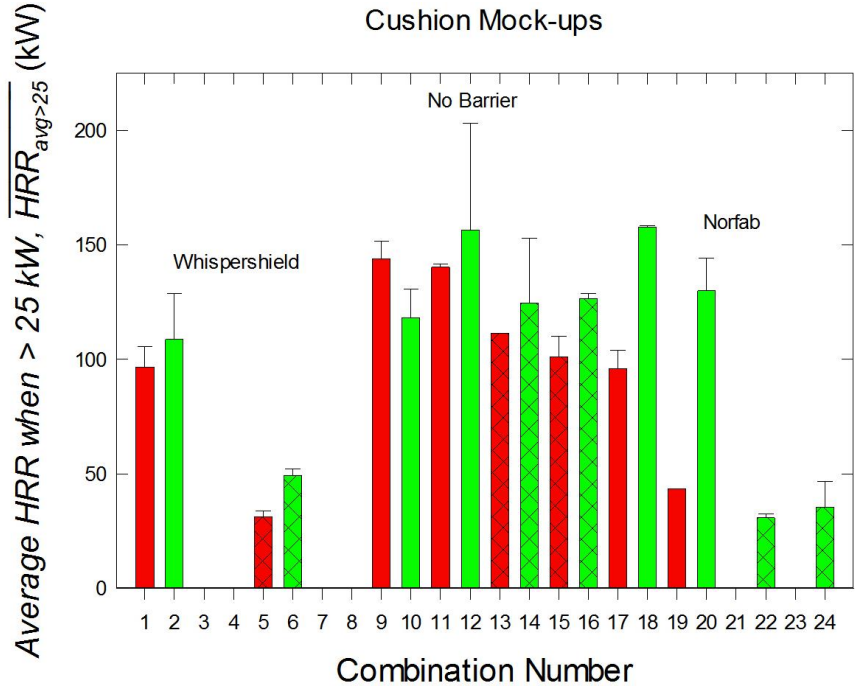

Figure 36. Averages and standard deviations of the average HRR while above 25 kW, $HHR_{avg>25}$, are plotted as a function of mock-up combination number.

The average HRRs and standard deviations during the periods when the HRRs were greater than 25 kW, $HRR_{avg>25}$, are plotted as a function of combination number in Figure 36. Generally, material combinations that did not include a barrier had higher $\overline{HHR_{avg>25}}$s than those which incorporated a barrier fabric. The primary exception was Combination 18, which had a higher value compared to combinations that did not

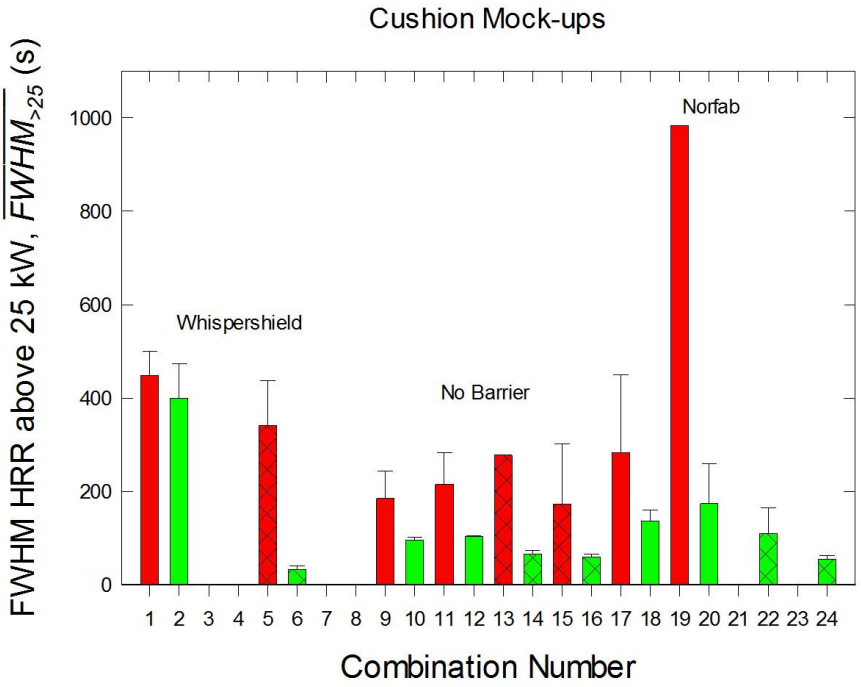

Figure 37. Averages and standard deviations of the FWHM HRR recorded while the HRR remained above 25 kW, $FWHM_{>25}$, are plotted as a function of mock-up combination number.

include a barrier. For the majority of combination pairs where the only difference was the outer upholstery material, those with the cotton cover fabric had lower $\overline{HHR_{avg>25}}$. The only exception involved Combinations 9 and 10. Even though the dependence on upholstery fabric was systematic, relative changes in $\overline{HHR_{avg>25}}$ were much less than those observed for $\overline{HRR_{max}}$ (compare Figure 34 and Figure 36). Including PEFW in mock-ups without a barrier appeared to have a minimal effect on $\overline{HHR_{avg>25}}$, while there did appear to be an effect when PEFW was added to the cushions with NFR foam and the Norfab barrier fabric, where adding the wrap seemed to significantly lower $\overline{HHR_{avg>25}}$.

Averages and standard deviations for the full width half maximum of the HRR while above 25 kW, $FWHM_{>25}$, are shown in Figure 37. The one distinct outlier is Combination 19, which has, by far, the largest value. Recall that this combination also resulted in a large value for $t_{>25}$ (see Figure 35). Interestingly, while Combination 5 also had a very large value of $\overline{t_{>25}}$, its value for $\overline{FWHM_{>25}}$ is more in line with those observed for other combinations. Comparison of the HRR curves shown in Figure A-21 and Figure A-152 for Combinations 5 and 19 reveals that the different behaviors can be traced to the shapes of the curves. The HRR curves for Combination 5 had single, relatively sharp, maximum peaks that were responsible for the reduced values of $\overline{FWHM_{>25}}$, while the curve for Test 19_2 had two nearly equally sized peaks separated by a substantial period of time.

Strong effects of upholstery material and FPUF type are evident in Figure 37. In each case where only the upholstery fabric was varied, values of $\overline{FWHM_{>25}}$ were larger when cotton fabric was used. Generally, combinations that included a barrier fabric had larger values than the comparable combinations without a barrier. The one possible exception was Combination 24, which had a similar value to Combination 16. No systematic effects of including PEFW or changing the sewing thread are discernable in the data.

The variations in HRR curve shapes with changes in mock-up materials clearly have a strong influence on the HRR parameters determined. The two shape factors defined in Table 13 are attempts to characterize such variations quantitatively. Shape factor #1, SF_t, which is defined as the FWHM for the HRR normalized

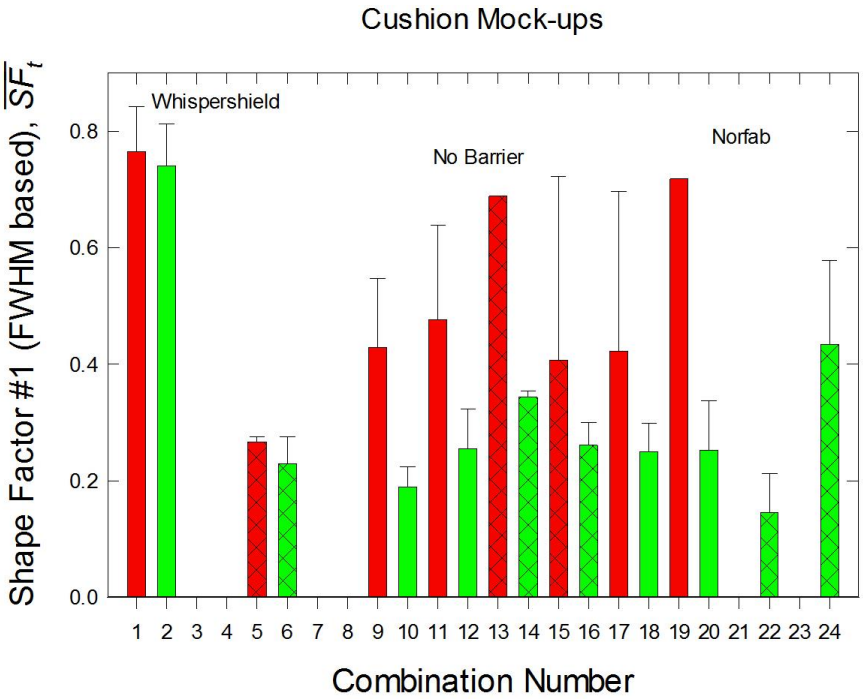

Figure 38. Averages and standard deviations of Shape Factor #1 based on measurements while the HRR remained above 25 kW, SF_t, are plotted as a function of mock-up combination number.

by $t_{>25}$, is a common measure for shape changes. Average values and standard deviations are plotted against combination number in Figure 38. A few of the standard deviations are a large fraction of the average, which indicates substantial variations between tests for these material combinations. Nonetheless, $\overline{SF_t}$ vary over a wide range. Comparisons of combinations for which only the cover fabric changed indicate that $\overline{SF_t}$ values are higher for mock-ups covered in cotton compared to those with the 78%PP/22%PE fabric. In contrast, the effects of varying the FPUF cushioning are more variable. For mock-ups with cushions including the Whispershield barrier fabric, replacing NFRFPUF with FRFPUF resulted in a drop in $\overline{SF_t}$ values from near one to well below 0.5. When no barrier fabric was included, differences between $\overline{SF_t}$ for the FPUF types were of a smaller magnitude, and the values were generally higher for mock-ups incorporating SI-1324 foam, i.e., the opposite dependence observed when the Whispershield barrier fabric was used. For mock-ups without a barrier fabric, the effects of including PEFW in the mock-ups also seems to depend on the type of FPUF, with values of $\overline{SF_t}$ increasing slightly for mock-ups incorporating NRFFPUF and decreasing when the FR version was used.

The second shape factor, SF_{HRR}, defined in Table 13 is based on the ratio of the average HRR over the period it remains above 25 kW normalized by the maximum HRR. Average and standard deviation values for SF_{HRR} are plotted as a function of mock-up combination number in Figure 39. The standard deviations for $\overline{SF_{HRR}}$ are somewhat reduced compared to those for $\overline{SF_t}$, but the variations with combination number are also reduced. Comparisons of $\overline{SF_t}$ between the different mock-up combinations show similar variations with changes in upholstery fabric, type of FPUF, and absence or presence of PEFW to those identified for $\overline{SF_t}$.

5.4 Total Heat Release

The total heat released during a fire test, Q_{tot}, is calculated simply by summing over a HRR time series since the data were collected at one second intervals. Averages and standard deviations for Q_{tot}, are plotted as a function of combination number in Figure 40. Several interesting trends are evident in the plot. Consider

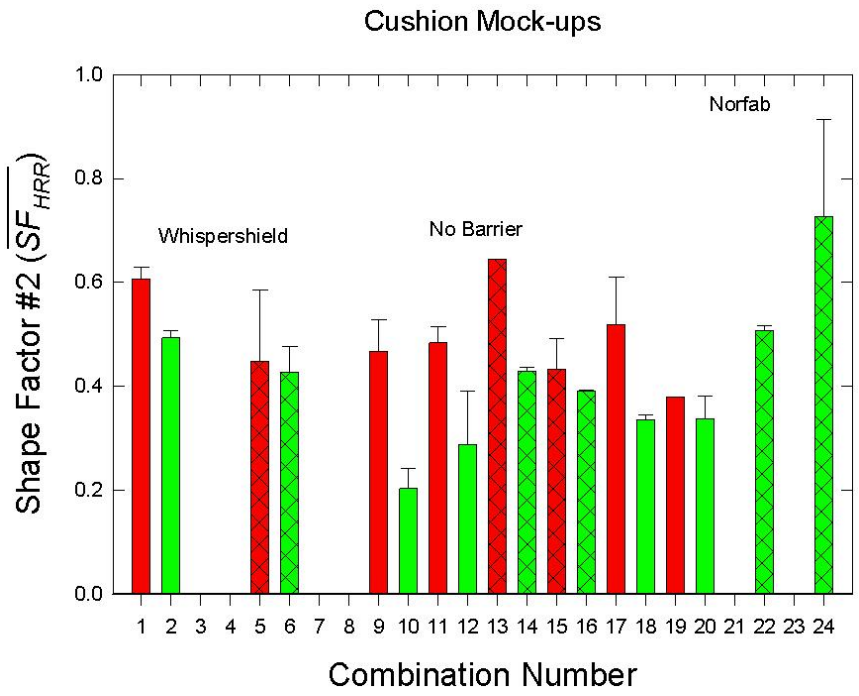

Figure 39. Averages and standard deviations of Shape Factor #2 based on measurements while the HRR remained above 25 kW, SF_{HRR}, are plotted as a function of mock-up combination number.

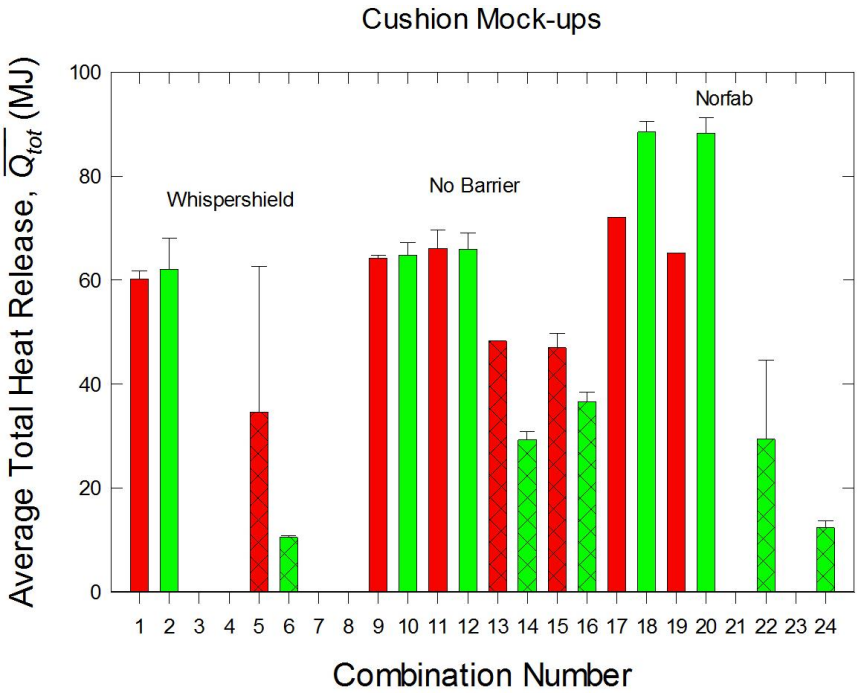

Figure 40. Averages and standard deviations for the total heat released are plotted as a function of mock-up combination number.

first the combinations which contained NFR foam. The $\overline{Q_{tot}}$ values were relatively high and nearly equal for the six combinations with either no barrier or with the Whispershield barrier. Similar values were also recorded for the two combinations with cotton fabric that incorporated the Norfab barrier fabric. However,

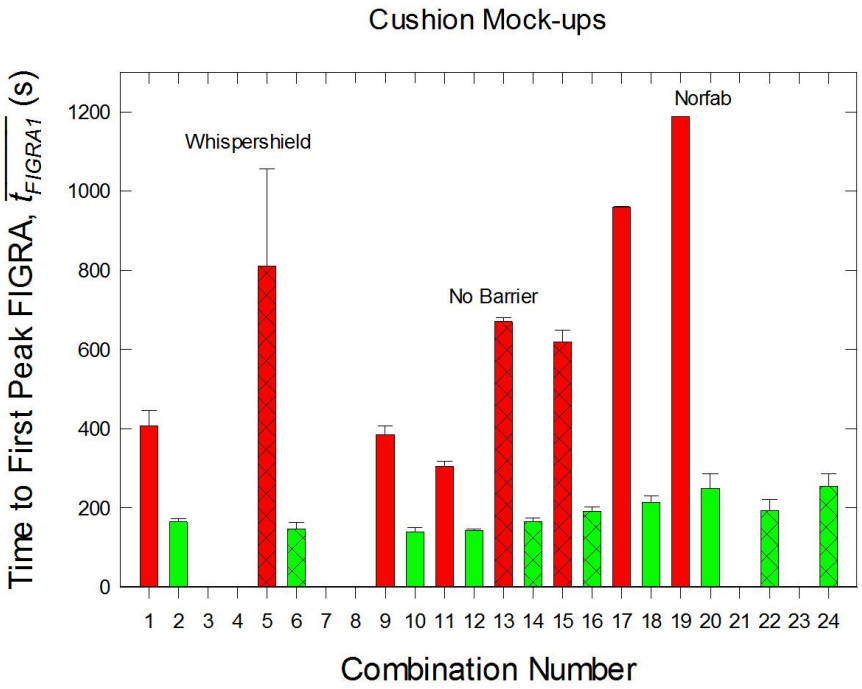

Figure 41. Averages and standard deviations for the periods required to reach an initial FIGRA peak, t_{FIGRA1}, plotted as a function of mock-up combination number.

when the Norfab was covered with 78%PP/22%PE fabric, $\overline{Q_{tot}}$ values increased substantially and were the highest observed among the combinations.

Values of $\overline{Q_{tot}}$ were consistently lower when combinations differing only in FPUF type contained FR foam. The values for mock-ups with FRFPUF also varied with changes in cover fabric in a way that depended on barrier configuration. For combination pairs incorporating no barrier or a Whispershield barrier, $\overline{Q_{tot}}$ were higher for those covered with cotton fabric. In contrast, for combinations incorporating Norfab, measurable HRRs were recorded for the two combinations covered with thermoplastic fabric, but were nearly zero when covered in cotton. Relatively low, comparable values of $\overline{Q_{tot}}$ were recorded for Combinations 6 and 24, which had 78%PP/22%PE fabric over Whispershield and Norfab (over PEFW) barrier fabrics. Videos of these fires suggest that most of the observed HRR was due to burning of the cover fabric. Combination 5, which included the Whispershield barrier material covered by cotton, showed mixed behavior. In one of the three tests no measurable HRR was recorded, while two of the tests gave relatively high values of $\overline{Q_{tot}}$. This explains the large standard deviation recorded for this combination.

5.5 FIGRA

The FIGRA parameter was computed for the various tests by dividing the HRR by the time since ignition. Temporal plots of FIGRA are included in Appendix A. Various parameters were defined in order to characterize these temporal profiles including the value of and time to reach an initial FIGRA peak ($FIGRA_{peak1}$ and t_{FIGRA1}) and the corresponding values for the maximum FIGRA ($FIGRA_{max}$ and $t_{FIGRAmax}$).

The average times and standard deviations needed to reach the initial FIGRA peak are plotted in Figure 41 as a function of combination number. Comparison with the corresponding plot for HRR in Figure 26 shows that the two times are nearly identical for a given combination. Any differences between individual tests were found to be only a few seconds. This is the expected result if the initial HRR peaks are relatively sharp. Average and standard deviations for $FIGRA_{peak1}$ are shown in Figure 42. The corresponding plot for HRR is shown in Figure 27. The relative variations in $\overline{HRR_{peak1}}$ and $\overline{FIGRA_{peak1}}$ with combination number

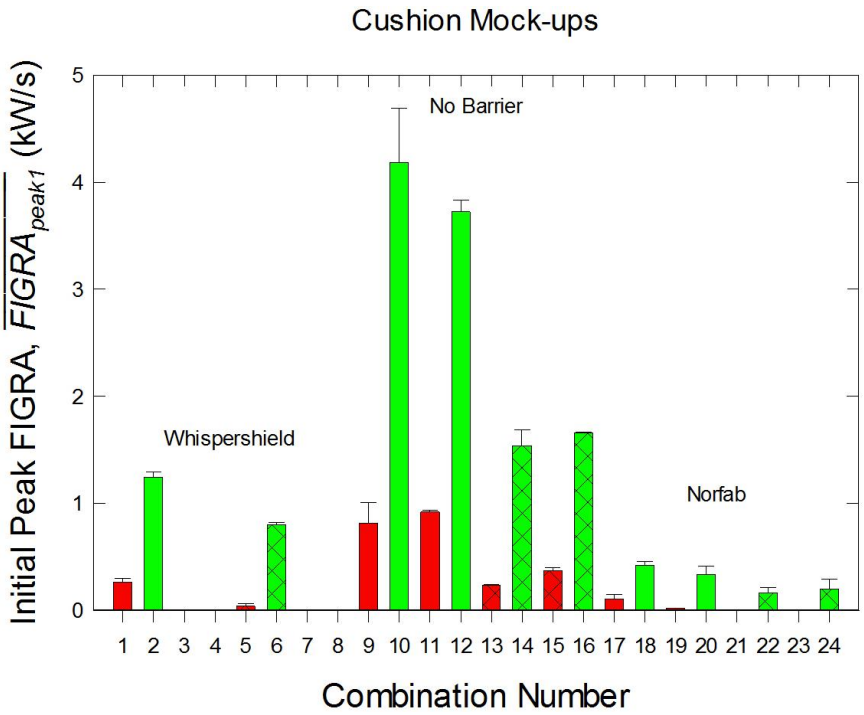

Figure 42. Averages and standard deviations for the initial FIGRA peak plotted as a function of mock-up combination number.

have similar appearances. Consider first the results for cushions covered with thermoplastic upholstery material, i.e., even-numbered combinations. The variations in the relative magnitudes of the two parameters are similar for the ten combinations. The same is true for the ten combinations covered with cotton fabric. The primary difference between the two plots is the larger decrease in the relative values of $\overline{FIGRA_{peak1}}$ when similar combinations covered with cotton are compared to those covered with 78%PP/22%PE fabric. This shift is associated with the longer times needed to reach HRR_{peak1} when cotton is the cover fabric (see Figure 26).

Figure 43 shows a bar plot of the averages and standard deviations for the times required to reach the maximum FIGRA. The corresponding plot for $\overline{t_{max}}$ is shown in Figure 28. While many of the $\overline{t_{FIGRAmax}}$ for a given combination are very similar to those for $\overline{t_{max}}$, there are several combinations for which the FIGRA values are markedly lower. These include Combinations 1, 2, 13, 19, and 22. A review of the HRR temporal profiles for these combinations shows that each had multiple HRR peaks of comparable magnitude. The time shifts occurred when the FIGRA value of a later peak that corresponded to the maximum HRR was lowered below that of an earlier peak as the HRR was divided by time.

Average and standard deviation values for $FIGRA_{max}$ are plotted as a function of combination number in Figure 44. Corresponding values for $\overline{HRR_{max}}$ are shown in Figure 34. Comparison of the two figures reveals substantial shifts in the relative values for the two parameters. Unlike the case for values of $\overline{FIGRA_{peak1}}$, relative shifts in the magnitudes of $\overline{FIGRA_{max}}$ occur for combinations covered with the same upholstery fabric. For instance, values of $\overline{HRR_{max}}$ for Combinations 18 and 20 are greater than those for Combinations 14 and 15, but the opposite was observed for $\overline{FIGRA_{max}}$. The cushions in these mock-ups were covered with 78%PP/22%PE fabric. A similar, but less pronounced shift, can be seen for the corresponding combinations covered with cotton.

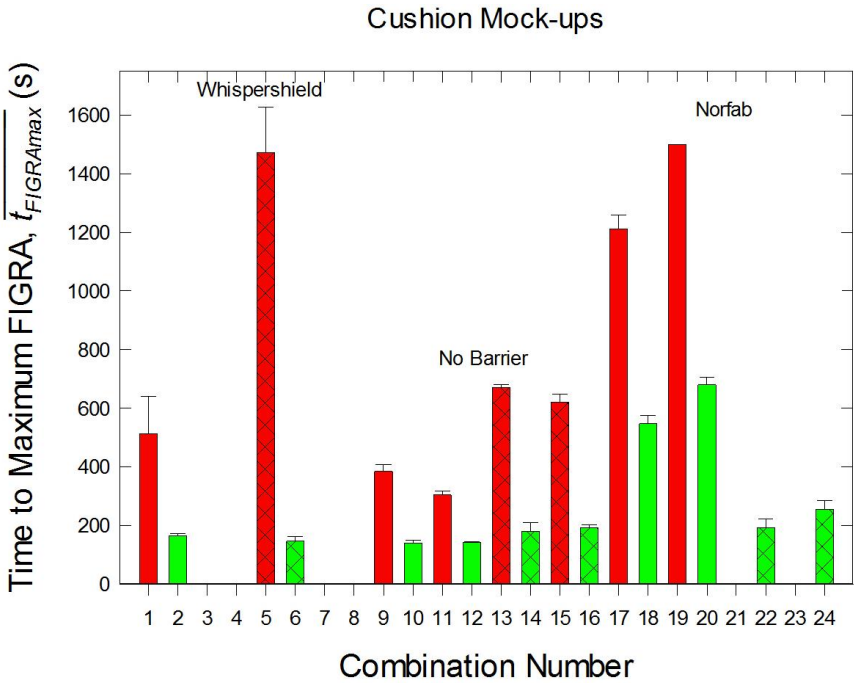

Figure 43. Averages and standard deviations of the times required for fires on the mock-ups to grow to the maximum FIGRA are plotted as a function of mock-up combination number.

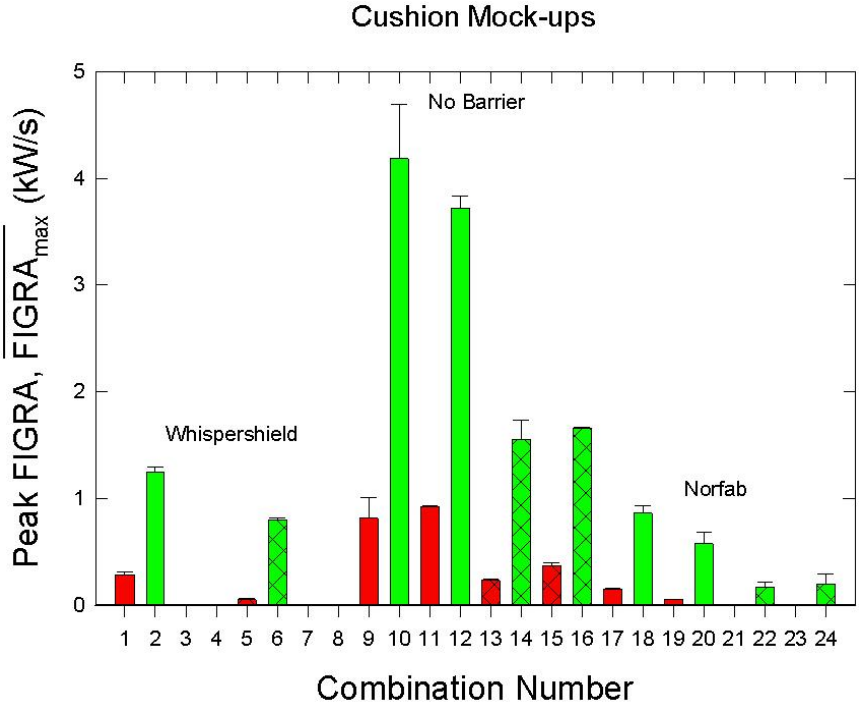

Figure 44. Average and standard deviation values of the maximum FIGRA are plotted as a function of mock-up combination number.

The use of FIGRA values accentuates differences between the combinations compared to those for HRR. For instance, relative differences between combinations including the two types of fabrics are much larger in the FIGRA results. Similarly, when considering combinations with a given type of upholstery fabric, $\overline{FIGRA_{max}}$ vary consistently with the type of barrier used. The highest values are associated with cushions

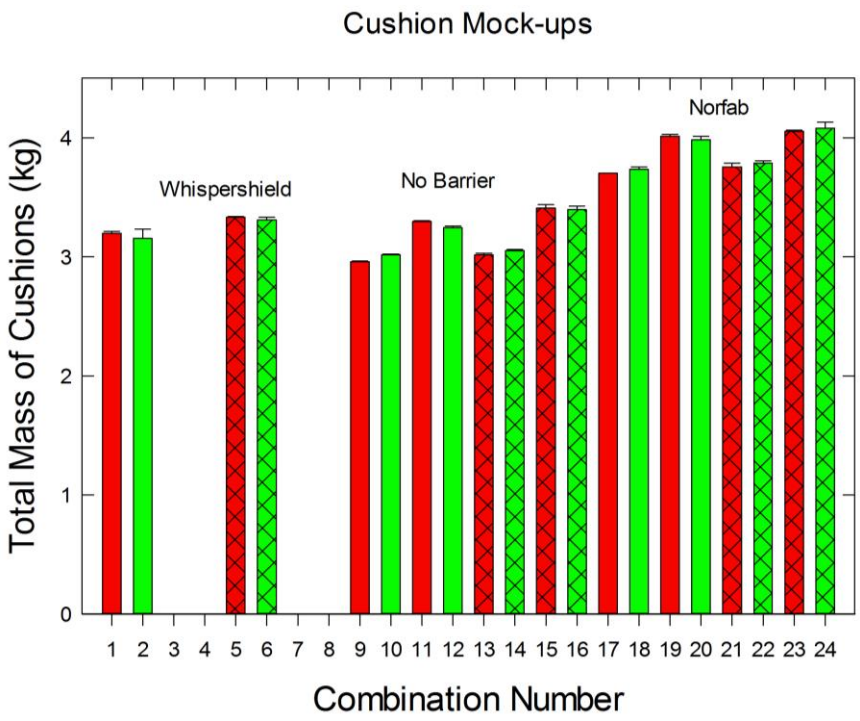

Figure 45. Average total masses and standard deviations for the materials in a mock-up are plotted as a function of mock-up combination number.

having no barrier. Addition of a barrier fabric reduces $\overline{FIGRA_{max}}$, with larger reductions observed with Norfab as compared to Whispershield. Such differences are not as apparent in the HRR plots.

5.6 Mass Measurements

Masses for the individual components (upholstery, barrier fabric, PEFW, and FPUF) of each cushion were measured during assembly. The upholstery was weighted after sewing, so its mass includes that of a zipper and sewing thread. The same is true for the Norfab barrier fabric. The Whispershield barrier material and PEFW were weighted prior to stapling, so the mass of the staples is not included in the totals for these individual materials.

In order to compare the total masses of different mock-ups, the masses of individual components within the four cushions forming a given mock-up were totaled. Average total masses and their standard deviations are shown as a function of combination number in Figure 45. The standard deviations are generally small, indicating good reproducibility within a combination. The total mass varied from a low of 3.0 kg up to 4.1 kg.

Measurements summarized in Section 3.4.2 indicated that the cotton fabric had a slightly greater (≈ 9 %) areal density than the 78%PP/22%PE fabric. The density of the FRFPUF was also slightly higher (≈ 3 %) than the NFR version. Mass variations between combinations where only the upholstery fabric or FPUF type was varied are generally consistent with these expected small differences. Larger changes of mass are associated with adding additional materials such as a barrier and/or PEFW to base cushions formed only from upholstery fabric and FPUF. Recall that when WhisperShield or PEFW were used, the volume of foam was reduced slightly (see Section 3.4.6).

A stacked bar chart indicating the masses of individual components within a given combination is shown for the first repeated test of each combination in Figure 46. For all combinations, FPUF represents the

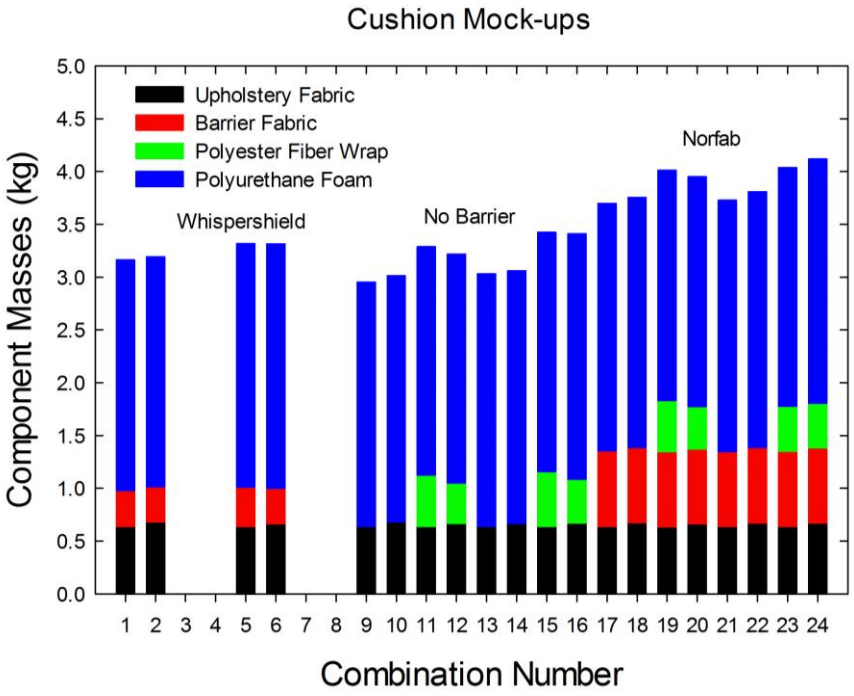

Figure 46. Masses for the various components of mock-ups as a function of component number are plotted as stacked bar charts.

largest mass component in the mock-up. However, it is clear that the fraction of total mass that is foam varies as additional components are included in the cushions. The large masses associated with mock-ups incorporating Norfab are due both to the addition of the Norfab and to its relatively high aerial density.

Averages and standard deviations of the mass of FPUF in the mock-ups are plotted as a function of combination number in Figure 47. This plot indicates that the variations in the masses for repeated tests are small. The effects of changing foam volumes and FPUF type, are more easily identified than in the total mass plot of Figure 45. It should be noted that variations in the amount of foam present in the mock-ups were less than 10 %.

The mass of the mock-up was recorded continuously during a fire test. As discussed in Section 3.5, the load cell used during the initial test matrix malfunctioned sporadically. This resulted in mass measurements that were either non-physical, e.g., either increasing or abrupt changes, or were offset in mass (identified by comparison with earlier measurements) by a constant amount. The notes associated with the tests in Appendix A identify individual tests for which the mass measurements were corrupted and whether or not the measurements were excluded or adjusted. In cases where the mass was offset, the temporal curve was corrected by setting the initial mass to the sum of the masses for the four cushions recorded prior to testing.

Plots of mock-up mass as a function of time are included in Appendix A. By comparing the curves with the corresponding HRR curves for a given mock-up, it is evident that the mass loss is highest during periods of substantial HRR. This correspondence will become more evident when the mass loss rate curves are discussed below.

When the mass loss curves for different mock-up combinations are compared, it is evident that the fraction of original mass loss during a fire test varied substantially. In order to quantify these differences, the fraction of total mass loss was calculated as the final mass reading for a test normalized by the mass prior to ignition. Fractional values were recorded for all tests where mass measurements judged to be valid were

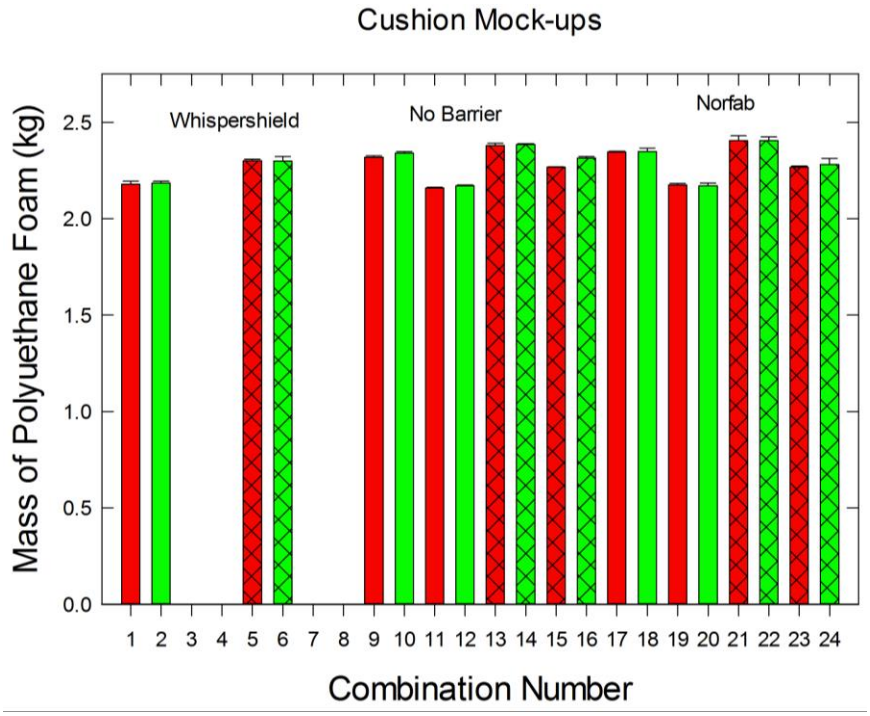

Figure 47. Average masses and standard deviations for the FPUF in the mock-ups are plotted as function of mock-up combination number.

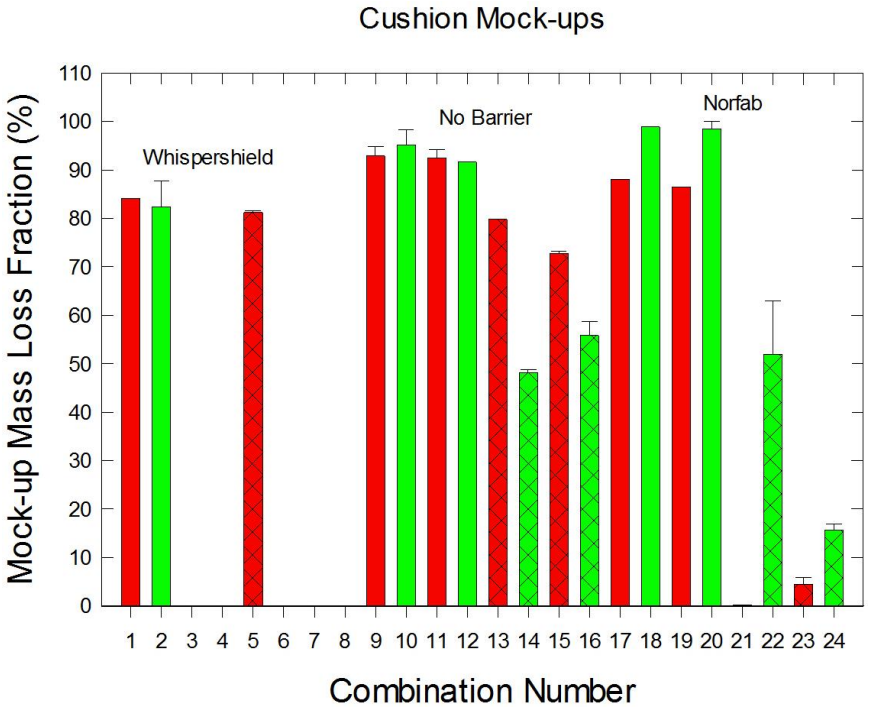

Figure 48. Average and standard deviation values for percentage of mass loss during tests are plotted against combination number.

available. Average and standard deviation values for the percentage of total mock-up mass loss are plotted against combination number in Figure 48. It should be kept in mind that results for several individual tests are missing. The error bars representing the standard deviation are missing for several of the combinations.

This is generally due to there being only one valid mass measurement for that combination. Note that satisfactory mass measurements were unavailable for Combination 6. A review of the mass time records for these two tests indicated that mass losses on the order of 0.4 kg occurred for each. This corresponds to percentage total mass losses of roughly 12 % for this combination. This is comparable to the percentage mass loss values for Combination 24, which differs from Combination 6 by the replacement of the Whispershield barrier fabric with Norfab.

Several trends are evident in the total mass loss results. The average mass loss exceeds 80 % for all mock-ups that contained NFRFPUF, irrespective of whether or not a barrier fabric and/or PEFW was included. Generally, mock-ups with the NFRFPUF replaced by the FR version had reduced mass loss percentages. When no barrier fabrics were used, the reductions were relatively modest. Interestingly, the relative reductions were somewhat greater when the upholstery cover fabric was the 78%PP/22%PE blend as opposed to the cotton.

Combining barrier fabrics with FRFPUF gave mixed results. When Norfab was used, the percentage mass loss was significantly reduced compared to cases with the NFR foam, but the mass loss percentage for Combination 22 was comparable to mock-ups without a barrier fabric, Combination 14, while the values for Combination 24 were much reduced from those for Combination 16. The mass loss percentages for two of the three tests with Combination 5 mock-ups, which combined cotton upholstery with a Whispershield barrier and FRFPUF, were very close to those observed for Combination 1, which contained NFRFPUF. However, it needs to be noted that one of the Combination 5 tests did not become fully involved, and the mass loss percentage for this test was quite low. As discussed earlier, even though mass measurements are not available for Combination 6, the mass loss percentages were quite low. This differs from the corresponding Combination 2 results, which had total mass losses in excess of 80 %.

Plots of MLR as a function of time are included in Appendix A for experiments where reliable mass measurements were available. These plots were generated from mass values as a function of time that were smoothed utilizing the Savitzky-Golay filter to reduce random noise and noise introduced by the limited resolution of the measurements. Comparison showed that plots of mass as a function of time for smoothed and unsmoothed data were nearly indistinguishable. Similar plots for the MLR revealed that while the temporal behaviors were generally similar, data derived using the unsmoothed mass had substantial high frequency fluctuations associated with the mass steps introduced by the limited resolution, while values determined from the smoothed mass values were slowly varying with limited high frequency components. Some smoothing of the mass values was evident at times of rapid mass change, such as when an ignition source was abruptly applied or removed from a mock-up. Associated recovery times were on the order of ten seconds. Since such abrupt changes in mass were generally not observed during burning, it is concluded that application of the digital filter to the mass data resulted in relatively minor changes in measured mock-up mass behaviors.

The plots of MLR were generally smooth. Often there was an initial peak near zero time associated with the application of Ignition Source 1 or 2 to the mock-up. The strength of these peaks varied from nonexistent to levels comparable to peaks associated with the burning behaviors. These differences suggest there were variations in the manner that the ignition source was applied.

Temporal profiles for HRR and MLR for individual tests can be compared in Appendix A. Such comparisons reveal that the two types of curves generally have similar appearances, e.g., regions of high HRR and MLR are highly correlated. It is also evident that higher frequency variations are much greater in the HRR data than for the MLR results calculated using smoothed mass measurements. Due to the nature of the measurement methods, the time response for the mass measurements should be considerably faster based on the time response of the load cell (on the order of seconds) compared to that for the HRR

Table 14. Summary of observed effective heat of combustion temporal behaviors for the material combinations.

Combination	Observed Temporal Behaviors
1	Test 1_3 initially ≈ 17.5 MJ/kg and increased to ≈ 25 MJ/kg
2	Tests 2_1 and 2_2 remained roughly constant at 25 MJ/kg
5	Tests 5_2 and 5_3 initially ≈ 15 MJ/kg and increased to ≈ 20 MJ/kg when HRR increased, Test 5_2 had a short period when EHOC was ≈ 25 MJ/kg
6	Reliable mass measurements were not available for this combination
9	Tests 9_1 and 9_3 initially ≈ 20 MJ/kg, increased to between 25 MJ/kg and 30 MJ/kg
10	Tests 10_1 and 10_3 initially ≈ 30 MJ/kg and then dropped to ≈ 20 MJ/kg
11	Tests 11_1 and 11_2 initially ≈ 15 MJ/kg, increased slowly to ≈ 25 MJ/kg before dropping back to ≈ 20 MJ/kg
12	Test 12_1 initially ≈ 30 MJ/kg and then dropped to ≈ 15 MJ/kg
13	Tests 13_1 and 13_2 initially ≈ 15 MJ/kg and then increased to ≈ 25 MJ/kg
14	Tests 14_1 and 14_2 initially ≈ 15 MJ/kg, increased to ≈ 25 MJ/kg, and then decreased to ≈ 18 MJ/kg
15	Tests 15_1 and 15_2 remained ≈ 15 MJ/kg for a long period and then rapidly increased to ≈ 20 MJ/kg
16	Tests 16_1 and 16_2 initially ≈ 20 MJ/kg during rapid burning and then fell to ≈ 15 MJ/kg during long HRR tail
17	Test 17_2 initially ≈ 15 MJ/kg during slow burning period and increased to ≈ 22 MJ/kg as HRR increased, dropped near end of fire
18	Test 18_1 initially near 30 MJ/kg and then remained at ≈ 22 MJ/kg during much of the burning period before falling during the HRR tail
19	Test 19_2 initially ≈ 15 MJ/kg and then remained at ≈ 20 MJ/kg over the burning period from 900 s to 2300 s
20	Tests 20_2 and 20_3 remained at ≈ 22 MJ/kg over much of the long burning period before falling as the HRR dropped near the end of the test
21	Tests 21_1 and 21_2 HRRs and MLRs were too low to calculate EHOC
22	Tests 22_2 and 22_3 remained at ≈ 20 MJ/kg before slowly falling off over a long period of time to ≈ 15 MJ/kg
23	Tests 23_1 and 23_2 HRRs and MLRs were too low to calculate EHOC
24	Tests 24_1 and 24_2 values are noisy, seem to cluster near ≈ 25 MJ/kg during period of intense burning and then drop to ≈ 15 MJ/kg

measurements using oxygen depletion (on the order of tens of seconds). These observations suggest that the intrinsic relative noise levels were considerably higher in the HRR measurements.

5.7 Effective Heat of Combustion

The instantaneous HRR divided by the MLR yields the EHOC with units of MJ/kg. Plots of EHOC as a function of time are included in Appendix A for the tests where reliable mass measurements are available. Review of these curves provided the general observations listed in Table 14.

During periods when HRR values were unmeasurable or very low; often observed immediately following ignition or near the end of an experiment, but also during experiments in which the HRR remained low; calculated EHOCs were generally quite noisy and often fell below zero, i.e., a non-physical result. This noise is associated with high frequency noise present in the HRR measurements. As the HRR rose during an experiment, the relative noise in the HRR measurements decreased, and the EHOC also began to increase

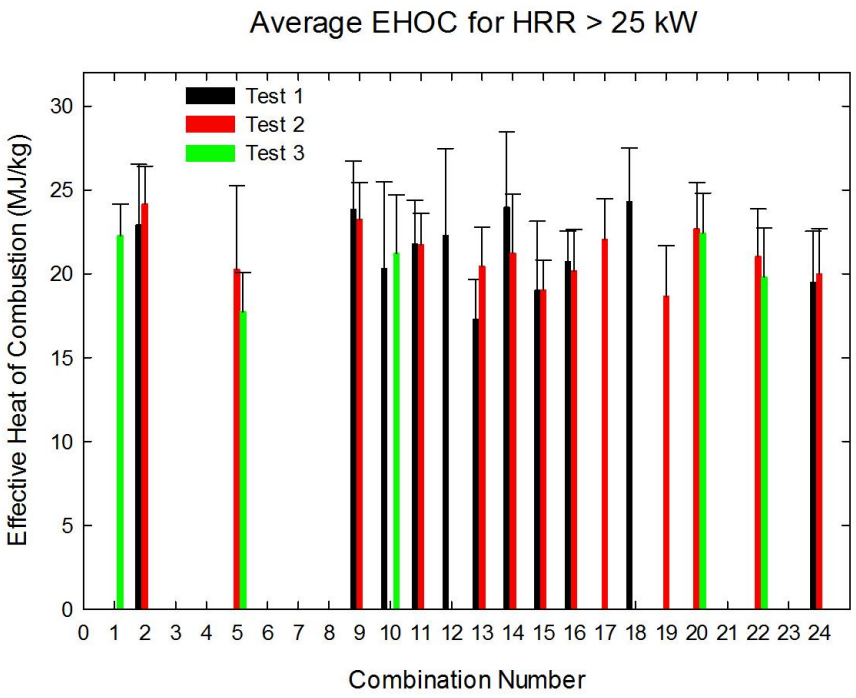

Figure 49. Values of EHOC averaged over the period when HRRs were greater than 25 kW are plotted as a function of combination number for cases where mass measurements were available. Test numbers for individual combination are color coded. Error bars represent the standard deviations due to temporal EHOC fluctuations.

and smooth out. Even though lower frequency fluctuations were still evident, it became feasible to identify approximate levels of EHOC and general behaviors in the temporal variations of the values.

EHOC values observed during the various tests ranged from roughly 15 MJ/kg up to 35 MJ/kg. Some general trends are evident in the gross features of the temporal variations summarized in Table 14. For combinations in which only the upholstery fabric was varied, initial values of EHOC were lower for the combinations including cotton. At later times following ignition, EHOCs were generally somewhat higher for combinations containing NFRFPUF as compared to those with FRFPUF. The observations are not detailed enough to allow conclusions to be drawn concerning the role of barrier fabrics, sewing thread, or the addition of PEFW on EHOCs.

Values of EHOC reported in the literature are frequently averaged over the test. In order to reduce the effect of noise in the EHOC measurements, values were averaged over the period when the HRRs were higher than 25 kW. Results for such averaging are shown in Figure 49 for experiments where mass measurements were available. Average values varied between 17.3 MJ/kg and 24.3 MJ/kg, with standard deviations between 1.8 MJ/kg and 5.2 MJ/kg. The relatively large size of the fluctuations reflects both noise in the HRR measurements and variations in values of EHOC over the averaging periods. The only trend evident in the data, albeit a weak one, is a decrease in the average EHOC for mock-ups containing FRFPUF as compared to those with NFRFPUF. Values for the NFRFPUF cluster around 23 MJ/kg while those for FRFPUF are closer to 20 MJ/kg.

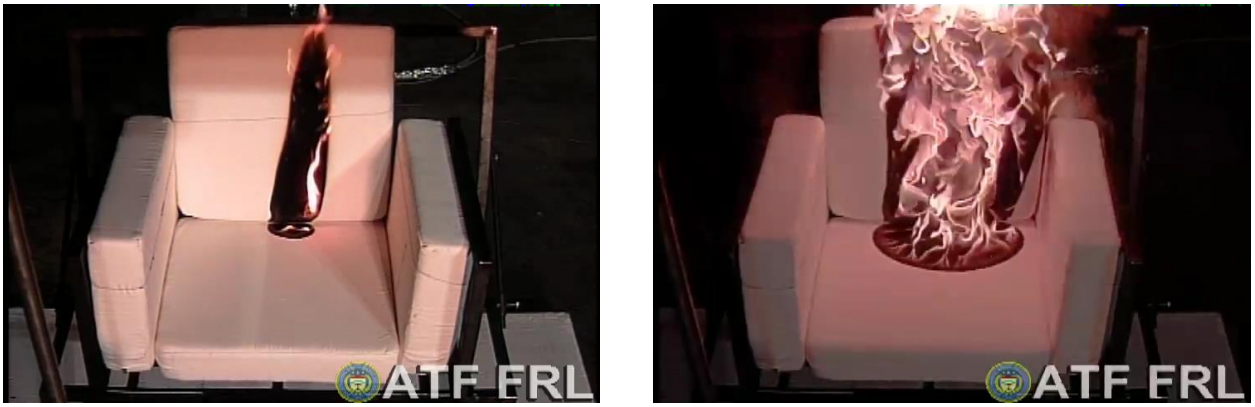

Figure 50. Two frames from a video of Test 9_2 show the burned areas on the seat and back cushions 94 s and 239 s following ignition.

5.8 Flame Spread Contours

Flame front locations were identified using the approach described in Section 4. Plots of flame front contours as a function of time are included in Appendix A. When multiple ignition sources were used, separate contours are shown for cases where substantial flame spread occurred.

A range of flame spread behaviors was observed for the different mock-up combinations. One common type involved the flames spreading rapidly upward on the back cushion in a narrow band to the top, while spreading laterally away from the ignition point in both directions on the seat and back cushions at a much slower rate. Note that for some of these fires only the back cushion was initially ignited by application of Ignition Source 1, with the fire spreading to the top of the back cushion, followed by extinguishment. In these cases ignition of the seat cushion followed by lateral flame spread on the seat and back cushions occurred following the application of Ignition Source 2.

Frequently, the fire on the seat cushion would spread transversely from the ignition location at roughly the same rate as it was moving in the two lateral directions, which resulted in an approximate semicircle-shaped burned area on the seat cushion with a radius that increased with time. Meanwhile, the flames on the back cushion would spread in the lateral directions at roughly constant rates from the bottom to the top of the cushion. These general trends would continue until the spreading flames reached the arms of the mock-up. At this time, the flames had spread over most of the back cushion, while the burned area on the seat cushion was approximately semi-circular with a radius equal to half of the cushion width. Once the arm cushions became involved, the burned area on the seat developed a more rectangular shape as it continued to spread toward the unburned region on the side opposite the ignition point.

Figure 50 and Figure 51 show frames taken from Camera #3 videos of flames spreading over the seat and back cushions of cotton- and 78%PP/22%PE-covered mock-ups, respectively. The left-hand images were recorded just after the flames had spread to the top of the back cushion. At these times lateral flame spread was limited. The right-hand frames correspond to times when the laterally spreading flames were approaching the mock-up arms. It is evident that the flames on the seat and back cushions have been spreading laterally in both directions at roughly the same rates. The nearly vertical edges of the fire contours on the back cushions and the roughly semi-circular shape of the burned areas on the seats are visible. The appearance of these two fires spreading across the seat cushions shortly after the arm cushions became involved are shown in Figure 52. The fire fronts on the seat cushion are nearly perpendicular to the transverse fire spread direction as they approach the near edges of the cushions.

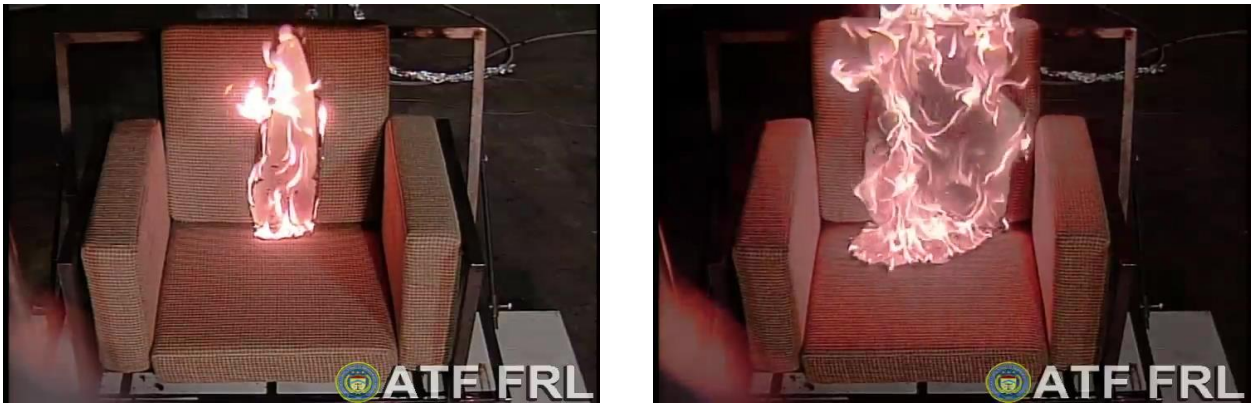

Figure 51. Two frames from a video of Test 10_1 show the burned areas on the seat and back cushions 45 s and 79 s following ignition.

Figure 52. Frames from Camera #3 videos of Test 9_2 313 s after ignition (left) and Test 10_1 104 s after ignition (right) are shown.

Mock-up combinations with at least one test displaying the above type of burning behavior included Combinations 1, 2 (Test 2_1), 5 (Tests 5_2 and 5_3), 9, 10, 11, 12, 15, 17 and 23 (see Appendix A). All four of the Combinations (9-12) having cushions stuffed with NFRFPUF and having no barrier fabric are included. With the exception of Combination 2, the remaining combinations included cotton upholstery fabric over either barrier fabric, PEFW, or FRFPUF.

A second frequently observed type of flame spread differed from that described above in that the initial spread on the back cushion only progressed upward over a fraction of the cushion height before temporarily halting. Lateral flame spread on the seat and back cushions was similar to that already described so that the burned area on the back initially only covered the lower portion of the cushion nearest the crevice. Figure 53 and Figure 54 show frames taken from Camera #3 videos of two fires that displayed this type of flame spread. Eventually, as the burning area on the seat grew larger, the flames typically spread rapidly upward and covered the entire surface of the back cushion. Late-stage flame spread over the seat cushion was similar to that described earlier.

Mock-ups for which at least one test displayed this type of flame spread include Combinations 2 (Test 2_2), 6, 13 (Test 13_2), 14, 16, 18, 20, 22, and 24. With the exception of Test 13_2 (Test 13_1 displayed a different type of flame spread discussed below), all of the mock-ups with this type of flame spread were covered with the 78%PP/22%PE fabric. All combinations, except those in which the thermoplastic fabric directly covered NFRFPUF, are represented.

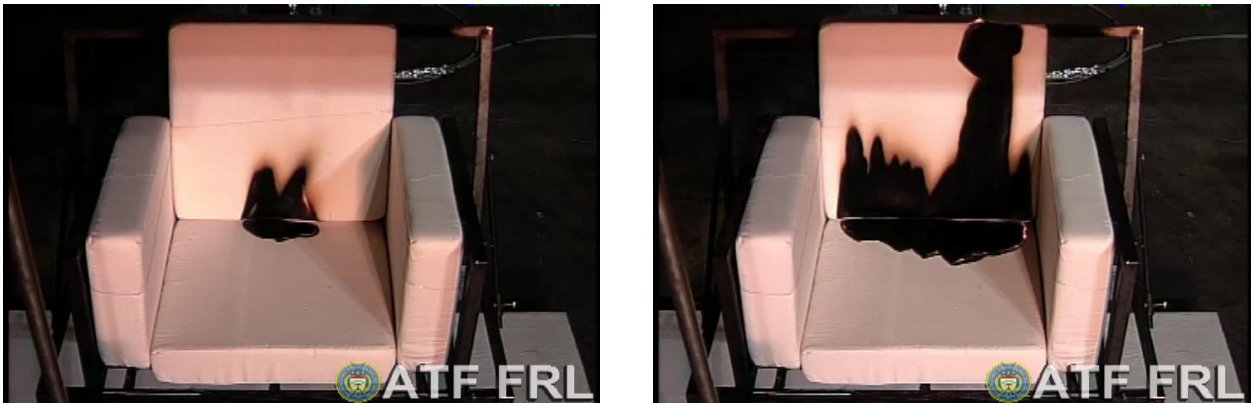

Figure 53. Two frames from a video of Test 13_2 show the burned areas on the seat and back cushions 164 s and 364 s following ignition.

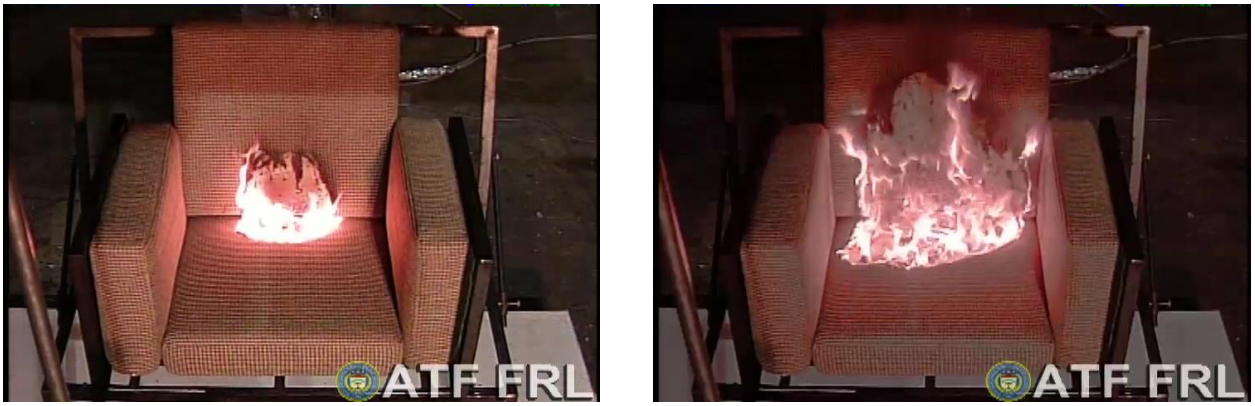

Figure 54. Two frames from a video of Test 16_2 show the burned areas on the seat and back cushions 64 s and 110 s following ignition.

Most of the tests displayed one of the two flame spread types summarized above. Note that both types were observed for Combination 2 mock-ups. The flame spread during Test 5_1 was somewhat different. Following the application of Ignition Source 1, rapid flame spread to the top of the seat back was observed, but the seat cushion did not ignite (see Figure A-26). When the flames reached the top of the back cushion extinguishment did not occur, but lateral flame spread developed along a base that moved upward during the fire spread. This resulted in a burned area that was quite narrow at the bottom of the cushion but covered the entire width at the top. Eventually, a slow-moving flame front spread from the right edge and filled in the unburned area on the right side at the base of the cushion. The unburned area on the left remained when the fire died down. Application of Ignition Source 2 ignited the seat cushion, and the subsequent flame spread over the seat cushion filled in the unburned area on the lower left side of the back cushion. The latter flame spread was similar to that observed during Tests 5_2 and 5_3 which were ignited by Source 1.

The flame spread behavior for Test 13_1 was similar to Test 5_1. Ignition Source 1 only ignited the back cushion. After spreading rapidly to the top, a slow lateral spread developed on either side of the burned area along a base located well above the bottom of the cushion. The base increased in width as the flames moved away from the ignition location. By the time extinguishment occurred, the fire had covered the entire width of the cushion at the top. Unlike Test 5_1, unburned areas remained at lower positions on both sides of the back cushion. Ignition Source 2 ignited the seat cushion, and the resulting flame spread covered the remaining unburned areas on the back as well as the entire seat cushion. As noted above, the flames spread during Test 13_2 such that only the lower portion of the back cushion was involved as the flames spread laterally.

The flame spread behaviors observed during the two tests with mock-ups including Combination 19 cushions differed substantially from those discussed thus far. In both tests only the back cushion was ignited during the application of Ignition Source 1. In each case the flames spread upward to the top of the cushion and then extinguished. During Test 19_1 the width of the burned area did not change appreciably as the flames spread upward, while moderate broadening was evident during Test 19_2. The seat and back cushions were ignited following application of Ignition Source 2 during Test 19_1. However, the resulting fire only broadened the burned area on the left side of the previously burned area on the back cushion, and the flames on the seat cushion spread only a short distance to the right along the crevice formed by the two cushions before extinguishing. An Ignition Source 5 wood crib was also applied during Test 19_1. Some flame spread was observed in both directions along the crevice between the seat and back cushions, but the fire extinguished well before it reached the edges of either the seat or back cushions. The flames did not propagate substantially in the transverse direction on the seat. During Test 19_2 Ignition Source 2 resulted in a fire that initially spread over both cushions in the lateral direction only to the right. After reaching the right-hand edge of the seat cushion, the fire then propagated over a narrow region located along the crevice formed by the seat and right arm. After a long period, flames appeared in the corner formed by the seat, back, and left-arm cushions. The video from Camera #4 shows this fire spreading from left to right along the seat-back crevice on the outside of the mock-up, with flames appearing on the mock-up interior after reaching the right edge on the outside. These flames eventually spread to cover the entire interior areas of the seat and back cushions. This was the only test where this type of flame spread behavior was observed.

The flame spread behaviors observed for Combination 23 tests also warrant additional comment. For both tests only the back cushion ignited following application of Ignition Source 1. These fires spread to the top of the cushions and extinguished. When Ignition Source 2 was applied, the resulting fires spread laterally in both directions on the two cushions along the crevice formed by their intersection. On the back cushions the flames spread to cover most of the surface area, but small unburned areas remained along the edges. The flames on the seat cushions spread to the edges, but since flame spread in the lateral directions was somewhat slower, the burned areas on the seat at these times were more rectangular in shape than the semicircular shape seen in many of the other tests. After reaching the arms, the fires continued burning away from the intersection of the seat and back cushions, but in both tests extinguished well before reaching the far edge of the seat cushions. The leading edge for the fire during Test 23_1 was more irregular in shape at extinguishment than that for Test 23_2.

5.9 Flame Spread Rates

In most past studies RUF and real-scale mock-up flame spread behaviors have not been quantified. As a result, little guidance was available for quantifying and comparing measurements. As described in Section 4, four characteristic flame spread rates were defined. These were for upward, u_{bv}, and lateral, u_{bl}, flame spread over the interior surface of the mock-up back cushion and lateral, u_{sl}, and transverse, u_{st}, flame spread over the seat cushion. Keep in mind that these are characteristic velocities based on flame spread over the periods between times when flame contours were determined. Plots of the spread rates as a function of time following application of an ignition source are included in Appendix A.

An example of the results for Test 9_1 was shown in Figure 23. It is evident that upward flame spread was accelerating at a nearly constant rate, while values for the characteristic lateral spread rates on the seat and back and the transverse rate on the seat were nearly the same and remained roughly constant with time. Note that based on the definitions of the characteristic lateral flame spread rate on the seat as the average of the spread rates away from the central ignition point, equal values of u_{sl} and u_{st} imply a roughly semicircular shape with an increasing radius for the burned area on the seat. Such a shape was one of the flame contour types described in the previous section.

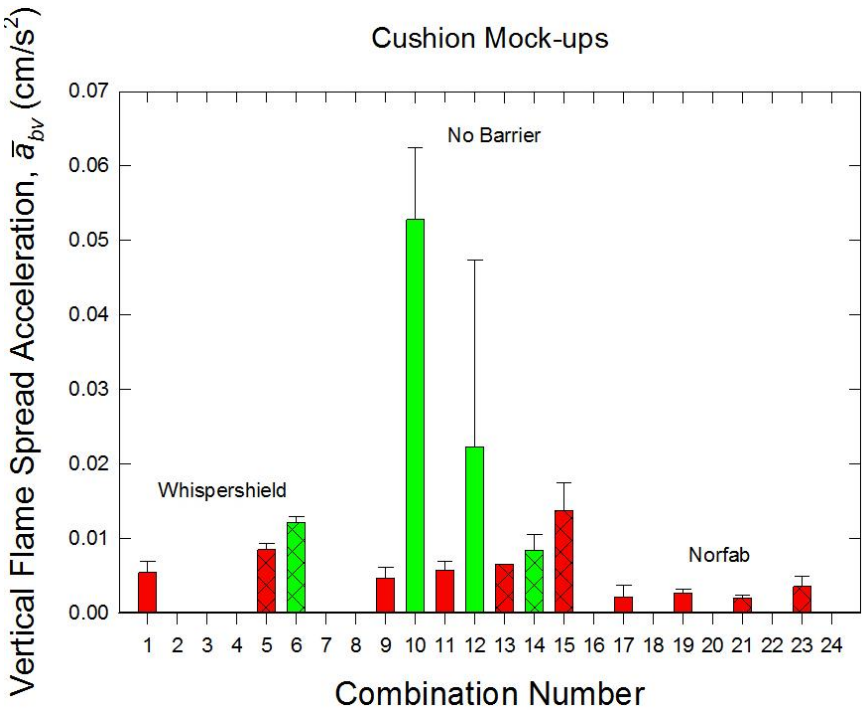

Figure 55. Values of the acceleration in flame spread rate for fires spreading upwards on the back cushion are plotted as a function of mock-up combination number.

Review of the flame spread rate plots in Appendix A showed that for many of the tests an upward spreading flame front on the back cushion undergoing constant acceleration was a good approximation. An appropriate parameter for characterizing this type of flame spread is the acceleration value, a_{bv}, defined as the slope for a plot of u_{bv} versus time with units of cm/s^2. Values of a_{bv} were obtained from linear least squares curve fits to the data. Results for individual tests are listed in Table B-1 and averaged values and standard deviations for combination are provided in Table B-2. Bar plots of the averaged a_{bv} values and their standard deviations as a function of combination number are shown in Figure 55 for those tests in which the increase in the flame spread rate was roughly linear. Most of the combinations are the same as those identified earlier as displaying a rapid flame spread to the top of the back cushion, followed by slower lateral flame spread. However, the overlap is not perfect. There were cases, e.g., tests with Combination 5 materials, where even though flames spread relatively quickly to the top of the back cushion, the acceleration was not constant. Conversely there were other combinations, i.e., Combinations 6, 13, 14, 19, and 21, which showed a roughly linear acceleration of the upward flame spread even though the lateral flame spread did not behave in the manner described earlier.

By far, the highest acceleration values for upward flame spread were observed for the two Combination 10 mock-ups with cushions that contained only NFRFPUF and 78%PP/22%PE upholstery fabric. The second highest flame front accelerations were measured for the same upholstery fabric and FPUF combination with the addition of PEFW in the cushions (Combination 12). The test-to-test variations of a_{bv} for Combinations 10 and 12 were substantial, as indicated by the large error bars in Figure 55. This makes conclusions uncertain, but it appears that the addition of the PEFW somewhat reduced the upward flame spread acceleration.

The upward flame spread acceleration over cushions upholstered with cotton over NFRFPUF (Combination 9) and with included PEFW (Combination 11) were of comparable magnitude to each other, but were greatly reduced from those recorded for Combinations 10 and 12. Since the error bars for these two tests were relatively small, this provides strong evidence that vertical flame spread acceleration over

the thermoplastic-covered cushions was much faster than over cotton-covered ones containing the same interior materials. The inclusion of the PEFW had a minimal effect on the flame spread acceleration for cotton-covered cushions.

Replacing the NFRFPUF with FR foam in cushions without a barrier resulted in substantial reductions in flame spread acceleration when the cushions were upholstered with the 78%PP/22%PE fabric. Note that results for Combination 16 tests are not included in Figure 55 since videos showed that upward flame spread actually halted for a period of time before the fire on the seat cushion grew sufficiently to induce additional spread over the back cushion. In contrast, the results in Figure 55 suggest that replacing the NFRFPUF in cotton-covered cushions had minimal effects on flame spread acceleration for cushions stuffed only with polyurethane foam, while the flame spread actually accelerated faster when a layer of PEFW was included over the foam.

Upward flame spread behaviors for back cushions incorporating Whispershield barriers also showed interesting changes with variations in cover fabric and FPUF type. Increases in u_{bv} for cotton-upholstered cushions were similar to those measured for cushions without a barrier when the NFRFPUF was used and somewhat higher for cushions with FRFPUF. The results for cushions covered with the thermoplastic fabric are less clear. For cushions containing both types of FPUF, videos showed that upward flame spread rates were comparable to lateral flame spread rates, i.e., upward flame spread was not typical of a rapidly accelerating vertical fire. Nonetheless, results for Combination 6 had flame spread rates that increased with time. The acceleration was similar to other combinations incorporating FRFPUF or Whispershield barriers.

The smallest vertical flame spread accelerations were recorded for the four combinations with cotton upholstery over a Norfab barrier. Values of a_{bv} for these combinations had comparable values. When the cotton fabric was replaced with thermoplastic upholstery, vertical flame spread was inhibited relative to lateral spread, and vertical flame acceleration was not evident.

Plots of the characteristic velocities u_{bl}, u_{sl}, and u_{st} are included in Appendix A for each test. Review of these plots as well as the corresponding videos for the fires showed that values of u_{bl} and u_{sl} were roughly constant and nearly equal until laterally spreading flames reached the arms of the mock-up. Averaged values u_{bl} and u_{sl}, denoted $\bar{u}_{bl}$ and $\bar{u}_{sl}$, along with their standard deviations, u'_{bl} and u'_{sl}, for individual tests are included in Table B-1. Individual values of both rates were averaged together over the period between ignition and when the fire ignited an arm cushion to provide an average characteristic lateral flame spread velocity, u_l for each test. These values are also included in Table B-1. Values of u_l for a given combination were averaged together to provide a single characteristic value. These values along with their standard deviations are listed in Table B-2. A bar plot of $\bar{u}_l$ values and associated standard deviations as a function of combination number is shown in Figure 56. Note that no value is included for Combination 19 due to the limited early flame spread observed for these materials. The value for Combination 21 is based solely on Test 21_1 following application of Ignition Source 5. Only limited flame spread was observed for Test 21_2 following application of all three ignition sources.

It is immediately obvious for each pair of combinations for which only the upholstery fabric was varied that the values of $\bar{u}_l$ for cushions covered with 78%PP/22%PE fabric were substantially greater than for those covered with cotton. The ratios of $\bar{u}_l$ for combinations in which only the upholstery fabric was varied are plotted versus combination pair in Figure 57 and range from 2.8 to 7.4. A few trends can be identified in these results. For combinations with Whispershield, replacing NFRFPUF with FRFPUF increased the ratio, suggesting a synergistic effect between barrier fabric and FPUF type. For combinations without a barrier fabric, adding a layer of PEFW tended to decrease the ratio, while FPUF type had little effect. Conclusions concerning combinations with Norfab barriers are less certain, but keeping in mind that values for $\bar{u}_l$ are missing due to the limited flame spread observed, which implies a high value of the $\bar{u}_l$ ratio for Combinations 19 and 20, it can be surmised that adding the Norfab barrier to combinations without a barrier

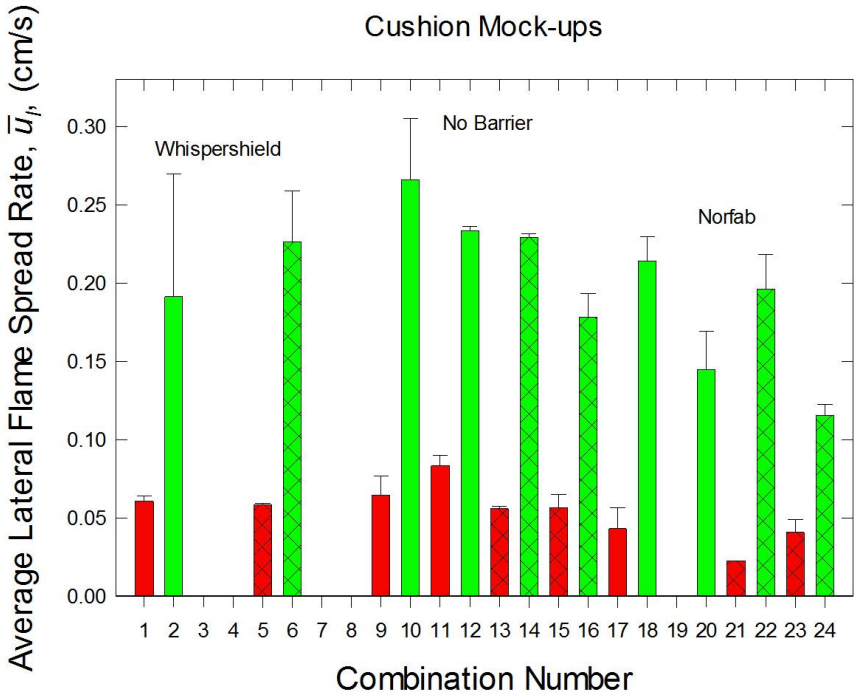

Figure 56. Averages and standard deviations of characteristic lateral flame spread velocities, $\bar{u}_l$, calculated as means of u_{bl} and u_{sl} recorded between the time of ignition and when the spreading fires reached the mock-up arms are plotted as a function of up combination number.

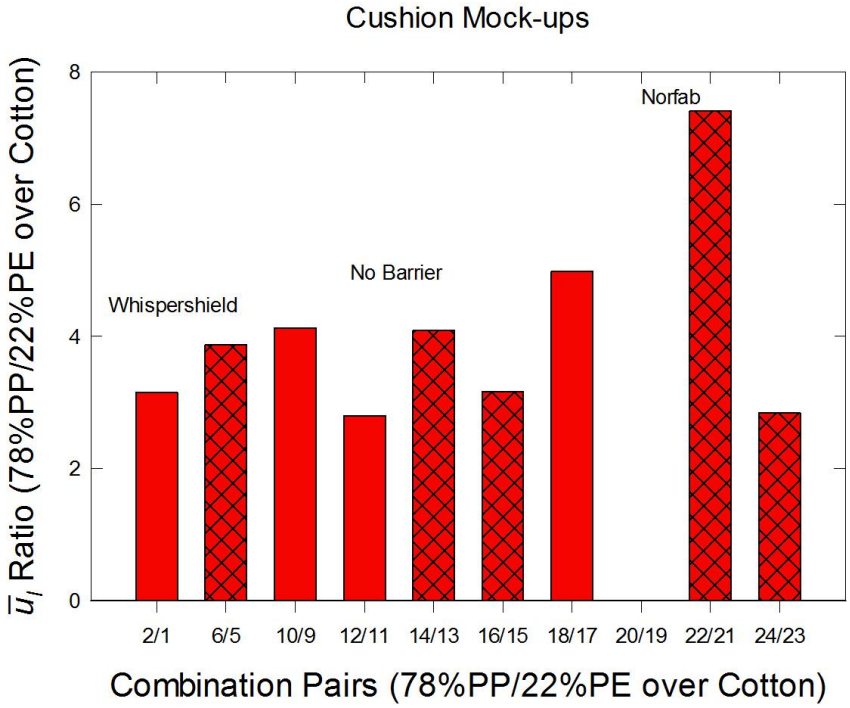

Figure 57. Ratios of $\bar{u}_l$ for mock-ups that differed only in upholstery fabric (78%PP/22%PE) are plotted versus paired combination numbers.

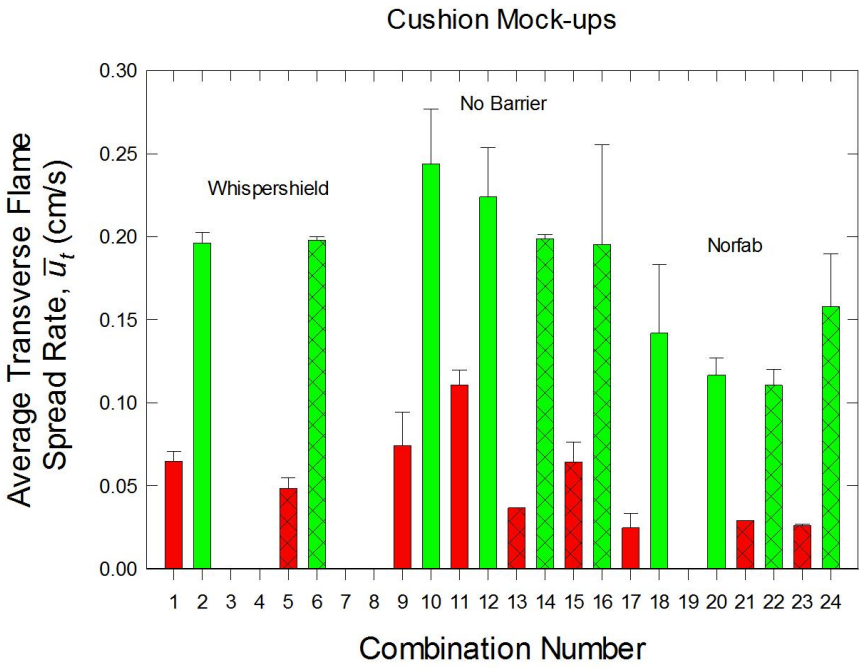

Figure 58. Averages and standard deviations of average transverse flame spread velocities, $\bar{u}_t$, calculated as means of u_{st} recorded between the time of ignition and when the spreading fires reached the mock-up arms are plotted as a function of mock-up combination number.

resulted in higher $\bar{u}_l$ ratios. Interestingly, the highest ratios seem to be associated with cushions containing a Norfab barrier, NFRFPUF, and PEFW (Combinations 19 and 20) and Norfab barrier and FRFPUF (Combinations 21 and 22).

In addition to the strong effect of upholstery fabric on $\bar{u}_l$ values, additional trends are identifiable in the results in Figure 56. For combinations without a barrier, replacing NFRFPUF with the SI-1324 foam resulted in moderate reductions in $\bar{u}_l$. In contrast, the effect of FPUF type on $\bar{u}_l$ values for cushions with added fire barriers was minimal, if present at all. No consistent effects of adding PEFW to cushions without a barrier is apparent.

Transverse characteristic flame spread rates on the seat cushions also tended to be constant over the periods that flames were spreading laterally toward the arm cushions, as can be seen in the plots of flame spread velocities included in Appendix A. For a given test, values of u_{st} during the period between ignition and when a mock-up arm became involved were averaged to yield a characteristic transverse flame spread velocity on the seat, denoted $\bar{u}_{st}$. Values of $\bar{u}_{st}$ and associated standard deviations are included in Table B-1. Individual values of $\bar{u}_{st}$ were then averaged to provide an overall value, denoted $\bar{u}_t$, for a combination. These averages and standard deviations are summarized in Table B-2. Figure 58 shows a bar plot of $\bar{u}_t$ versus combination number with standard deviation values indicated by the error bars. Both the magnitudes and variation with combination number are similar to those for $\bar{u}_l$ shown in Figure 56.

Even though the bar plots for $\bar{u}_l$ and $\bar{u}_t$ have similar appearances, inspection shows that there are differences between the two parameters for given mock-up combination numbers. Ratios of $\bar{u}_l$ and $\bar{u}_t$, denoted as R_u and included in Table B-2, can be used as a means for characterizing these differences. A bar plot of R_u values against mock-up combination number is shown in Figure 59. A perfect semi-circular fire spread area would correspond to a ratio of one (indicated by the horizontal line on the plot). Measured ratios fall above and below this value.

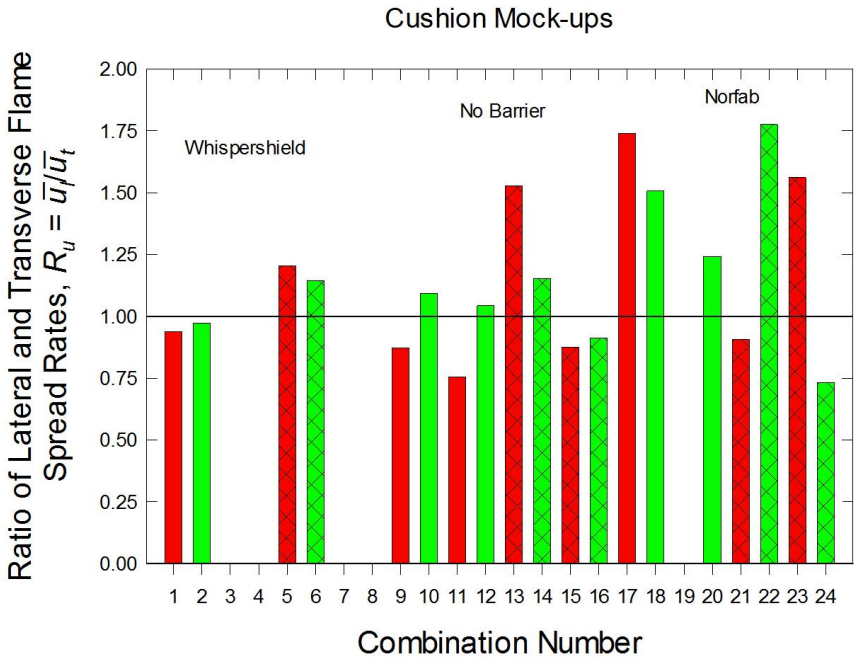

Figure 59. Ratios of characteristic lateral and transverse flame spread rates, $R_u = \bar{u}_l/\bar{u}_t$, are plotted as a function of mock-up combination number.

It is possible to identify some qualitative correlations between observed seat cushion burned area shapes shown in Appendix A and the values of R_u. Combinations 1 and 2 have ratios that fall just below one. After accounting for the uneven flame fronts observed for cushions covered with the 78%PP/22%PE fabric, the flame shapes on the seat fabrics for these two combinations can be approximated well as semicircles with their bases along the intersection of the seat and back cushions. Combinations 5 and 6 have R_u values that are somewhat greater than one. Nonetheless, the flame contours for the three tests with Combination 5 materials had similar well-defined smooth semicircular shapes. The flame fronts for the two Combination 6 tests were highly irregular, but the contours could also be classified as distorted semicircles.

Combinations 9 and 11 had cushions covered with cotton upholstery over NFRFPUF and only differed by the addition of PEFW to Combination 11. The flame contours for both combinations had approximate circular shapes even though both R_u values are considerably less than one. A review of the associated flame contours in Appendix A suggests the reason for the low ratios. Unlike the seat flame spread contours discussed above, the centers for the circular shapes were positioned away from the seat/back crevice for tests with these two material combinations. As a result, the contours curved inward as they approached the back. Since the flames along the crevice were spreading at roughly the same rates, the different definitions for u_{sl} and u_{bl} result in smaller u_{bl} values. This difference is identifiable in the plots for the flame spread rates. Since $\bar{u}_l$ is based on averaged results for both u_{sl} and u_{bl}, the effect is to reduce $\bar{u}_l$, which results in reduced ratios of R_u. The tests with Combination 15 cushions developed similar contours and also yielded R_u values less than one. An unusual burning behavior observed during Test 15_1 should be mentioned. When Ignition Source 1 was initially applied, the back began burning, but the seat failed to ignite. Well after the fire had spread to the top of the back cushion, the fire jumped from the back cushion to the seat cushion at a location well to the right of where the ignition source had been applied and began to spread from this point. This offset is evident for the flame spread contours on the seat shown in Figure A-110.

The R_u for Combinations 10 and 12 were both only slightly greater than one. However, the flame fronts on the seat cushions moving away from the back cushions were much flatter than those for the more circular shapes discussed thus far. The shapes of these burned areas might be better characterized as distorted

rectangles. Similar contour shapes were observed during fires in which Combination 14 and 16 cushions were used. The R_u ratios indicate that lateral flame spread was faster than transverse on the Combination 14 cushions, as was true for Combinations 10 and 12. The opposite was the case when Combination 16 cushions were tested.

Still another type of flame spread behavior was observed on the seat when Combination 13 cushions were used. Initially the burned areas appeared similar to the semicircular shapes discussed above, and the spreading edges were smooth. As the fires spread further, the contours began to flatten, with the fires spreading faster in the lateral directions. This is reflected in the R_u values, which exceeded 1.5. At later times the contours began to lose their "smooth" appearance, and the flame front developed undulations. This behavior can be contrasted with the flame contours observed on the seats of mock-ups with Combination 9 cushions, which only differ from Combination 13 cushions by the replacement of NFRFPUF with the SI-1324 foam.

Flame spread over the Combination 17 seat cushions, which incorporated a Norfab barrier under cotton upholstery, was similar to that observed with Combination 13 cushions. The initial flame spread was roughly semicircular, but as time passed lateral flame spread began to dominate, and the circle became flattened. The high value of roughly 1.75 for R_u reflects this change in spreading behavior. The flame fronts in these tests also developed similar undulations.

Values of R_u were similar for mock-up tests with Combination 17 and Combination 18 cushions. However, the flame shapes for Combination 18 were more rectangular, as observed for Combinations 10, 12, 14, and 16, all of which also included the thermoplastic upholstery material. Similar flame spread shapes were observed when Combination 20, 22, and 24 cushions were included in the mock-ups. Consistent with Combination 18 burning, large values of R_u indicated that lateral flame spread was favored during tests with Combinations 20 and 22, but that the opposite was the case when Combination 24 cushions were used. The latter observation is consistent with that observed for Combination 16 cushions.

Lateral and transverse flame spread over the seat cushions seemed to be strongly inhibited on Combination 19 mock-ups. Even though upward flame spread developed on the backs during both tests following application of the Ignition Source 1 flame, seat cushion ignition was not observed until Ignition Source 2 was used. Flame spread on the seats was exceedingly slow and erratic for both tests. During Test 19_1 the fire only spread a short distance before extinguishing. During Test 19_2 the flames first spread slowly towards the right, before spreading slowly over most of the seat cushion during a period approaching 30 minutes. An Ignition Source 5 wood crib was applied during Test 19_1, but only induced minimal additional flame spread, primarily in the lateral directions.

Flame spread behaviors for mock-ups with Combination 21 cushions were similar to those seen on Combination 19 mock-ups. Ignition Source 1 only ignited the back cushions with subsequent upward spread. For Test 21_1 Ignition Source 2 also failed to ignite the seat cushions. During Test 21_2 ignition of the seat did occur, but the fire only spread a limited distance to the right. Ignition Source 5 wood cribs were used during both tests. Lateral and transverse flame spread was observed during Test 21_1. Even though the value of R_u was close to one, the flame front was very asymmetric and strongly undulating. The flames only covered a portion of the seat cushion before extinguishing. The value of R_u included in Figure 59 is based on this test. For Test 21_2, the wood crib only resulted in limited flame spread before slowly extinguishing.

Ignition Source 1 also failed to ignite the seat cushions for mock-ups formed from Combination 23 cushions. However, for both tests, some lateral and transverse flame spread developed following the application of Ignition Source 2. The flame shapes on the seat cushions developed a rough rectangular shape. Flame spread in the lateral directions was much faster than in the transverse direction, which is

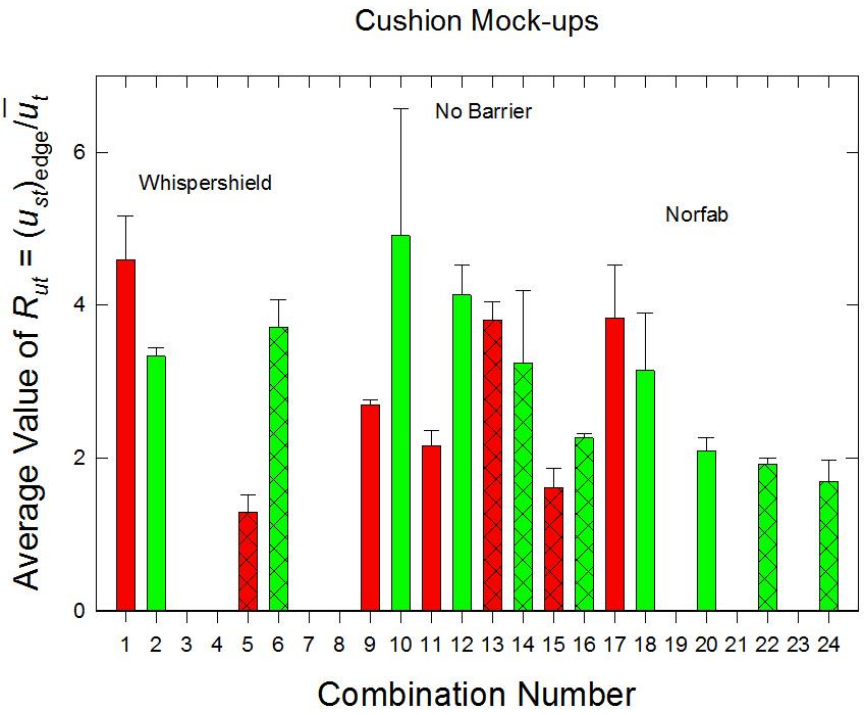

Figure 60. Averages and standard deviations of the transverse flame spread rate as a fire approached the outer edge of the seat cushion normalized by the averaged transverse flame spread velocity at earlier times, $R_{ut} = (u_{st})_{edge}/\bar{u}_t$, are plotted as a function of mock-up combination number.

consistent with the value of $R_u > 1.5$ in Figure 59. For both tests, the flames stopped spreading before covering the entire interior seat cushions surface.

Review of the various videos showed that for many of the material combinations there was a noticeable increase in fire size following flame spread onto the arm cushions. The increasing fire size was often accompanied by an apparent increase in the transverse flame spread rate, u_{st}, across the remaining unburned portion of the seat cushion. These increases in spread rate can be quantified by considering the temporal behaviors of u_{st} after the flames had spread laterally to the arm cushions and then continued to spread to the far side of the seat cushion. Review of the flame spread rate data plots in Appendix A confirms the acceleration of the flame front, with values of u_{st} increasing at later times.

In order to provide a rough quantification of this acceleration, the value of u_{st} for each test recorded as the spreading flames approached the outer edge of the seat cushion, denoted $(u_{st})_{edge}$ was divided by $\bar{u}_t$, the characteristic transverse flame spread rate at early times before the arms ignited. Values of $(u_{st})_{edge}$ and the ratio, denoted R_{ut}, are included in Table B-1. Table B-2 lists averaged values of R_{ut} and standard deviations as a function of combination number. The results are shown in Figure 60. For most combinations, it is evident that the flames were spreading substantially faster over the cushion as they approached the outer edge of the seat with values of $\overline{R_{ut}}$ between 1.5 and 5. Most of the exceptions were combinations withcotton as the upholstery fabric, including Combinations 19, 21, and 23, for which the flames spread erratically and did not cover the entire seat cushion surface. Combination 5, which also had a cotton cover, yielded a R_{ut} average close to one, suggesting a roughly constant u_{st} over the entire seat cushion. A similar value was measured for Combination 22, which had thermoplastic fabric over the Norfab barrier fabric and included PEFW over the FRFPUF. It is difficult to discern clear trends in the data as the fabric type or foam type was varied between otherwise similar mock-ups. In general, the ratios seemed to be somewhat reduced when the Norfab barrier was incorporated into the mock-ups.

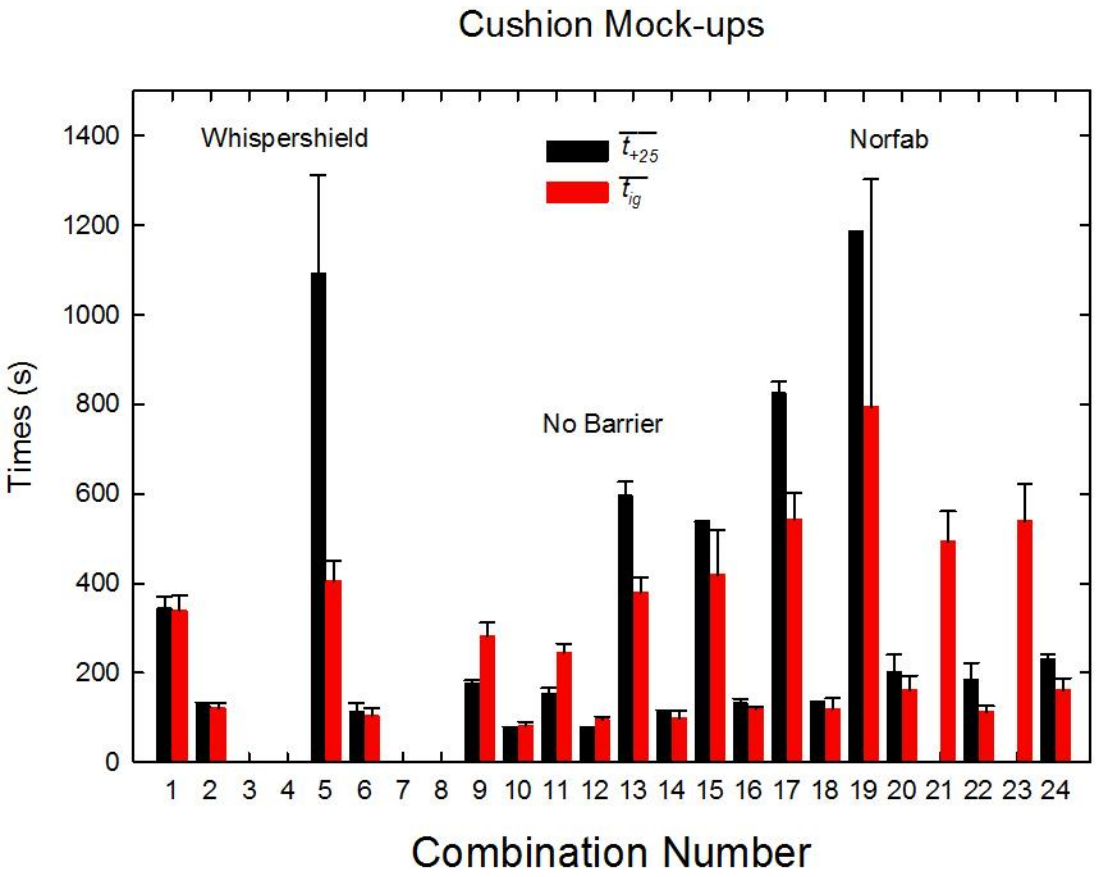

Figure 61. Average values of characteristic times for the ignition of mock-up arms are compared with the average times required to attain a 25 kW HRR for the twenty mock-up combinations. Error bars represent standard deviations.

5.10 Arm Ignition Times

As discussed in Section 5.9, it was observed empirically that during many tests there was a substantial increase in fire size shortly after the spreading flames reached and ignited the arm cushions. Using the videos, it was possible to obtain values for times when flames initially appeared on the arm cushions. Table B-1 in Appendix B lists the ignition times for the left, t_{igl}, and right, t_{igr}, arms for each of the tests.

The two arms typically ignited at different times, but the two events were usually close together. A characteristic ignition time, t_{ig}, for a given test was obtained by averaging the two values. In order to allow comparison of results for mock-ups formed from different combinations of materials, the characteristic times for an individual combination were averaged together, denoted $\overline{t_{ig}}$, and the standard deviation determined. These results are listed in Table B-2 and plotted in Figure 61 as a function of combination number. For later comparison purposes, Figure 61 also includes the average time, $\overline{t_{+25}}$, and standard deviation values for the period required for the HRR to first reach 25 kW. These results were shown earlier in Figure 25 and are listed in Table B-4. Recall that the HRRs for Combinations 21 and 23 never reached 25 kW and could therefore be represented as requiring an infinite time.

Since the arm ignition times are expected to depend on the lateral flame spread rates from the central ignition location, the inverse of $\overline{t_{ig}}$ offers a possible surrogate for lateral flame spread rates on the mockups. Comparison of $\overline{t_{ig}}$ included in Figure 61 with the plot of $\bar{u}_l$ shown in Figure 56 reveals that there is indeed a rough inverse relationship between the two values. Generally, the effects of changing materials are more

easily discerned in the arm ignition times. The strong dependence on upholstery fabric (odd versus even combination numbers) is evident for both parameters, but the effects of adding or changing a barrier fabric or replacing NFRFPUF with the FR version are more distinguishable in Figure 61.

Since rapid increases in fire size, i.e., HRR, were frequently observed when spreading flames ignited the arms, it might be expected that values of $\overline{t_{+25}}$ would have a similar dependence on combination number as $\overline{t_{ig}}$. This is why both parameters are included in Figure 61. Indeed, similar variations in values of $\overline{t_{ig}}$ and $\overline{t_{+25}}$ with mock-up combination number are apparent. For the four combinations (9 to 12) containing NFRFPUF and no barrier (with or without PEFW) the HRRs grew to 25 kW before the arms ignited, while for the remaining combinations the two parameters were nearly equal or the arms ignited well before the HRR reached this value. For combinations covered with the 78%PP/22%PE fabric and which contained a barrier and/or FRFPUF, the fires grew to 25 kW shortly after the arms became involved. A similar behavior was observed for Combination 1, which incorporated the cotton upholstery fabric over a Whispershield barrier that surrounded the NFRFPUF. The inclusion of the barrier in Combination 1 did increase both times compared to cases without a barrier (Combinations 9 and 11). For the remaining combinations, which included cotton fabric over FRFPUF or a Norfab barrier with NFRFPUF, the fires grew to 25 kW well after the mock-up arms became involved, keeping in mind that HRRs for Combinations 21 and 23 never reached this level.

5.11 Seat and Back Burned Areas as a Function of Time

Plots of the burned areas on the seat and back cushion surfaces as a function of time are included in Appendix A and Appendix C. Data for each of the repeated tests for a given mock-up combination are included on a common plot. For cases where multiple ignition sources were applied, the burned areas following the application of each source are shown on separate plots. It is important to keep in mind that flame spread over the two cushions generally took place during the early development of a fire. As a result, the burned areas are more indicative of early fire growth than the ultimate burning behavior of the mock-ups. Since the flame areas are calculated based on the contour plots of flame edges, determined as described in Section 4, the entire area defined as burned may not necessarily be flaming at a given time. It is even possible; particularly for mock-ups covered with the thermoplastic cover fabric, which tended to recede from a nearby fire, that flames may not had yet even passed over the surface near the edge of a given contour.

In general, it proved easy to correlate the changes in fire areas with time with the fire contours that are also included in Appendix A. The temporal behaviors of the burned areas provide indications of how fires developed on the mock-ups. For instance, it was immediately evident when a cushion was not ignited by the ignition source or when fires spread over only a fraction of a given cushion. The period required to cover a given fraction of a cushion is generally related to the overall average flame spread rate, while the variation of the growth rate with time of a burned area depended on how the fire was growing. For example, when a fire accelerated as it spread upward on the back cushion, the plot of burned area versus time curved upwards during this period. In cases where the fire reached the top of the back cushion and began to spread laterally at a constant rate, the area grew roughly linearly with time. Similarly, when a fire on the seat cushion spread at a constant rate from the ignition point, it formed a semi-circle, and the flame area had a time-squared dependence. Deviations from these idealized behaviors resulted in different types of time dependencies for the burned areas.

Several characteristics of the burning behaviors made numerical analysis of the time profiles difficult. For instance, in cases where multiple ignitions of mock-ups were required. Portions of a cushion might already be burned when the next ignition source was applied. Of course, this made comparison with tests in which the application of Ignition Source 1 was sufficient to ignite the mock-up difficult. This problem was exacerbated by the observation that areas of flame spread following the initial application of Ignition

Source 1, and sometimes Ignition Source 2, in which the flames did not spread to fully cover the seat and back cushions could vary widely from experiment to experiment for a given mock-up combination.

The burned area data for the two Combination 13 mock-ups provide an example of such complicated Test behaviors. The flame contours for these tests were discussed in Section 5.8. The application of Ignition Source 1 during Test 13_1 ignited only the back cushion. As the flame contours in Figure A-89 show, the flames initially spread upward on the cushion in a narrow band before beginning to spread horizontally and covering much of the width of the cushion. By the time this fire extinguished, it had spread over roughly 60 % of the surface area of the back cushion as can be seen in Figure A-95. When Ignition Source 2 was subsequently applied, the seat cushion ignited, and the fire spread to cover both the seat cushion and the remaining portion of the back cushion as revealed by the flame contours in Figure A-91 and the burned area plot in Figure A-96. Application of Ignition Source 1 to the Combination 13_2 mock-up ignited both cushions. As can be seen in Figure 53 and the contours shown in Figure A-93, most of the initial flame spread on the back cushion was along the lower portion of the cushion toward the sides, while tracking the lateral flame spread on the seat. As a result, the flame area growth on the rear cushion paused for nearly 200 s before growing rapidly to cover the remainder of the cushion when the fire grew rapidly. Interestingly, the flame area growth on the seat cushion was very similar to that observed during Test 13_1 following application of Ignition Source 2. This is an indication that flame spread on the seat cushion for this combination of materials was independent of the flame spread on the back cushion.

The temporal profiles of burned area for the two fires on Combination 15 mock-ups also differed substantially. For Test 15_1 (see Figure A-114) the burned area on the back cushion first grew relatively quickly, but then remained nearly constant for roughly 150 s before increasing more rapidly. Meanwhile, the burned area on the seat did not begin to increase until nearly 200 s after ignition. As mentioned in Section 5.9, the seat cushion in Test 15_1 did not ignite until roughly 185 s after the ignition source was applied. At this point the fire began to grow on the seat. Once the flames on the seat spread sufficiently along the crevice formed by the seat and back cushion, they began to act as pilots for flame spread on the back cushion, and more rapid flame area growth resumed there. During Test 15_2 the seat and back cushions were ignited simultaneously by the application of Ignition Source 1, and the burned area plots developed smoothly from the ignition time.

The burned area plots for the two Combination 19 tests shown in Figure A-167, Figure A-168 and Figure A-169 also differed substantially. This is not surprising because Ignition Source 2 successfully ignited Combination 19_2, which ultimately developed a substantial HRR, while application of each of the three ignition flame types failed to ignite the Combination Test 19_1 mock-up.

Even though some irreproducibility was present in flame area measurements for repeated tests of the same combination, it was possible to identify some general characteristics of the time-dependent burned area curves by inspection of the of the results included in Appendix A. In most cases the growth curves increased continuously with time. Generally, the individual curves for a given combination were in close agreement for mock-ups covered with cotton fabric while more scatter was evident in the mock-ups with 78%PP/22%PE fabric. The curves also tended to be “smoother” with less “jumps” for the cotton-covered mock-ups. These differences are likely associated with the flame spread behaviors. As described above, flame spread over the cotton fabric tended to occur with well-defined, relatively smooth flame fronts, while flames on cushions with the thermoplastic fabric tended to spread stochastically in a manner determined by non-continuous recession of the fabric away from the spreading flames.

To provide quantification of the results, the burned area plots as a function of time were reviewed to derive estimates for the periods required for flames to spread completely over the seat (t_{seat}) and back cushion (t_{back}) surfaces. There are inherent errors in the measurements due to the lack of continuous data as well as the fact that the curves approached full coverage at different rates. Reasonable uncertainty estimates are

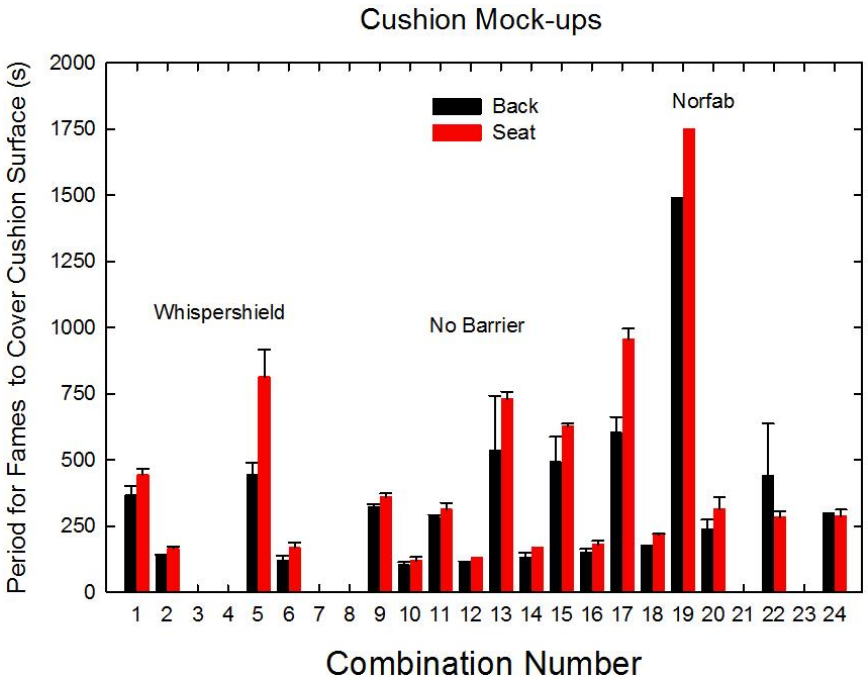

Figure 62. The average periods required for flames to spread over the surfaces of the seat ($\overline{t_{seat}}$) and back ($\overline{t_{back}}$) cushions are plotted as a function of mock-up number. The error bars represent the standard deviations for test-to-test variations.

± 15 s for rapidly spreading flames and tens of seconds for slowly spreading flames. The estimates for individual tests are included in Table B-1 and averages with standard deviations for combinations are tabulated in Table B-2. Average values and standard deviations as a function of mock-up combination number are plotted in Figure 62.

Keeping in mind that flames did not spread sufficiently to fully cover the cushions for Combinations 21 and 23, it is immediately evident that much longer periods were required for flames to spread over the seat and back cushions only differing in cover fabric when covered with cotton, reconfirming the strong effect of cover fabric on flame spread rate. For most combinations, the periods required to spread over the seat cushion were slightly longer than those required to cover the back cushions. This is likely associated with the observation that flame spread on the back cushions was usually piloted by flames spreading laterally on the seat cushion. As a result, flames covered the entire back surfaces before complete transverse flame spread occurred on the seat surfaces. The only exceptions were for Combinations 22 and 24. Recall that complete upward flame on these cushions covered with 78%PP/22%PE fabric over Norfab barrier material only took place following development of more intense mock-up burning when multiple cushions became involved.

The effects of adding barrier fabrics to otherwise similar mock-ups on $\overline{t_{seat}}$ and $\overline{t_{back}}$ were complex. For mock-ups with added Whispershield barrier, the periods were increased slightly from those for mock-ups without the barrier. The increased periods were somewhat greater when Norfab was included in mock-ups covered with the thermoplastic cover fabric. By far, the largest increases were observed when Norfab was added to the mock-ups covered with cotton. Recall that for Test 19_1 flames did not spread over cushion surfaces, while the longest measured period was recorded for Test 19_2. Flames did not fully cover the cushions for Combinations 21 and 23.

The effect of replacing NFRFPUP with the flame-retarded foam generally resulted in longer periods being required for flames to spread over the seat and back cushions. The one exception was for cushions

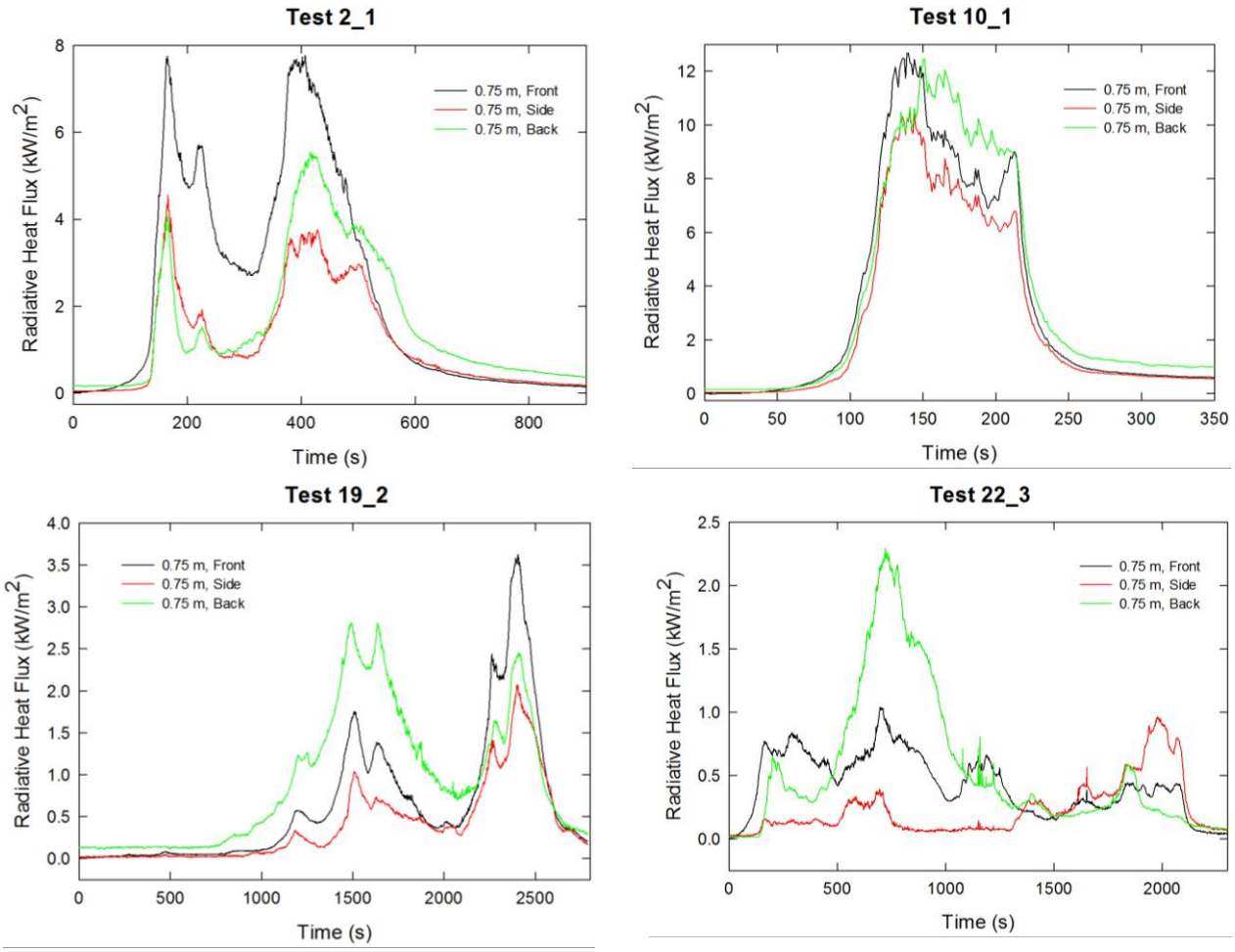

Figure 63. Heat fluxes as a function of time recorded simultaneously by gauges located 0.75 m from the front, side and rear of the upholstered furniture mock-up are compared for four different fire tests.

constructed with 78%PP/22%PE fabric over a Whispershield barrier, where changing the foam type had minimal effects on the values of $\overline{t_{seat}}$ and $\overline{t_{back}}$.

5.12 Heat Flux Measurements

The heat fluxes for each test recorded by six gauges located 0.75 m and 1.5 m from the front, right edge, and rear of the mock-ups are plotted as a function of time in Appendix A. Comparison with the corresponding HRR curve for a given test shows that the curves had similar time dependencies, but that the time variations were not identical. Similarly, different temporal responses were observed for gauges viewing a fire from different directions and even between the two gauges viewing the mock-ups from the same direction at different distances.

Examples of different temporal responses for gauges located 0.75 m from the mock-ups along the three measurement directions are shown in Figure 63 for tests with four different mock-ups. It can be seen that not only did the relative magnitudes of heat flux vary, but the relative ordering of the heat-flux magnitudes could change during a test. Generally, differences in temporal variations in relative heat flux values recorded by gauges located in different directions or distances from the mock-ups could be attributed to integrated variations in the distance and orientation between where a fire was located on the mock-up and

a given heat flux gauge and also to temporally varying view factors for the flames associated with the mock-up geometry and changes it underwent during a fire.

Review of videos of the fires allows some of these effects to be identified in the heat flux data shown in Figure 63. As a fire began to grow on the interiors of the seat and back cushions, the heat flux gauges located to the front generally had unobstructed views of the flames, while a fraction of the flame radiation was blocked by the mock-up arm cushion to the side and to an even larger extent to the rear by the back cushion. This effect explains why the initial heat flux increases were observed towards the front of the mock-ups for the four sets of data. Similarly, the first heat flux maximum evident during Test 2_1 occurred when the interior surfaces of the seat, back, and arms of the mock-up were covered with flames. At this time the mock-up geometry was little changed from that prior to the fire, and the arm and back cushions still partially shielded the side and back gauges from the flames. As a result, the highest heat fluxes were recorded in the forward direction. Heat flux values to the side and rear were similar even though the back was intact and covered a larger area than the right arm. Videos showed that the flame heights were highest near the back cushion closest to the rear heat flux gauges. This increased the view factor for the rear gauges and balanced out the radiation blocked by the back. After falling off for a period, the heat fluxes rose to a second maximum at roughly 400 s after ignition. Videos at this time showed the fire was still located primarily on the interior of the mock-up, which had retained much of its original shape. The primary difference in the fire was that intense burning had developed on the outside of the back cushion. This intense burning near the rear heat flux gauge is the apparent reason for the higher heat flux observed toward the rear of the mock-up as compared to the side. The largest heat flux was still recorded by the front gauge which had an unencumbered view of the mock-up interior.

Variations between heat flux levels recorded in the three directions during Test 10_1 were much smaller. For this mock-up, fire growth was very rapid. Videos showed that the mock-up was mostly intact when the highest heat flux was recorded by the front heat flux gauge roughly 135 s after ignition. At this time heat fluxes to the side and rear were somewhat lower due to thermal radiation blockage by the cushions. Within seconds after the maximum on the front gauge was reached, flames appeared on the outside of the back cushion, and it began to collapse. As it collapsed, the heat flux recorded by the rear gauge increased, while that observed by the front gauge decreased. This demonstrates the effects that changes in mock-up geometry can have on measured radiative heat flux. By 190 s following ignition, all of the cushions had collapsed, and an intense pool fire had developed to the rear of the support stand. Differences in measured heat flux during this period were primarily due to relative variations in flame location and burning intensity.

The heat flux temporal profiles shown in Figure 63 for Test 19_2 are somewhat unusual in that the highest heat fluxes for the initial maximum were recorded just prior to 1500 s by the rear gauge. Review of the videos for this fire showed that relatively intense flaming was present on the outside of the back cushion at this time, while burning on the interior surfaces of the mock-up was localized near the junctures of the seat, back, and arm cushions. This suggests that the high values recorded to the rear of the mock-up were due primarily to the smaller distance between the flames and the gauge in this direction. Flame levels were relatively low at this time, and there was little burning on the right arm, so it is not surprising that heat flux levels to the right side were the lowest. The second heat flux peak was associated with intense burning located on the interior seat surface near the left arm of the mock-up. At this time (≈ 2400 s) the arms had partly caved inward, but the original mock-up structure was largely intact, and the relative ordering of the heat flux levels is consistent with the flame location and partial blockage of the flame radiation by the back and right-arm cushions.

The heat flux variations between the three gauges during Test 22_3 were quite erratic. Review of the associated videos revealed that this was due to the burning behavior. Instead of burning as a unit, areas of relatively intense burning tended to move around on the mock-up. The large heat flux peak recorded by the rear heat flux gauge at ≈ 715 s was associated with strong burning that developed on the rear cushion

with flames primarily visible on the outer side of the cushion. Similarly, the peak recorded by the side heat flux gauge at ≈ 1980 s occurred at a time after most of the mock-up was already burned, but during which relatively intense burning developed on the right arm cushion.

The discussion thus far has focused on variations in heat flux for gauges located at the same distances, 0.75 m, from the edges of a mock-up. Since data are available for each direction for two gauges located at different distances, it is possible to obtain some insights into the dependence of the radiative heat flux on distance from a mock-up. Review of the heat flux data included in Appendix A shows that, as expected, instantaneous values of heat flux recorded 1.5 m from the mock-up are always considerably less than those recorded at 0.75 m. If the thermal radiation from the flames could be treated as a point source located at the edge of the mock-up, the heat flux would be expected to fall off as the square of the distance, and the value at 0.75 m from the mock-up would be four time higher than that at 1.5 m. Of course, the flames are not a point source, and the effective origin for the source is unlikely to be located at the edge of the mock-up. The ratios for the heat fluxes at the two distances are expected to vary with both of these parameters.

In order to obtain insights into the roles of effective source location and the finite area of flames on the fall off of thermal radiation with distance from the upholstered furniture mock-ups, values for the ratio of heat fluxes recorded at 0.75 m and 1.5 m were plotted as a function of time. For comparison purposes, the time dependence of the ratios for the same tests considered in Figure 63 are plotted for the front, side, and back heat flux gauge pairs in Figure 64. It is apparent that the ratios vary substantially with time and direction relative to the mock-up. Consideration of the heat flux behaviors shown in Figure 63 as well as the heat flux plots included in Appendix A provides some insights into the correlation of the temporal heat variations with the observed fluctuations in the ratios for measurements along the three measurement directions.

Calculated ratios tend to be relatively constant with values between 0.25 and 1.5 when measured heat fluxes are close to zero, but vary substantially with measurement direction and from test to test. These variations appear to be most closely associated with varying baselines for the heat flux gauge outputs. As the heat fluxes increase, the ratios of the heat fluxes at the two distances for given directions also increase. During these periods of higher HRR, heat flux ratios tend to fall between 2.5 and 4.0, but it is not unusual to observe values exceeding 4.0 for short periods. During these times temporal variations in the ratios with time are evident, but relative variations are much smaller than those observed in the HRRs over the same periods. Similarly, there does not appear to be strong correlations between the heat flux ratio fluctuations and variations in the HRRs. This suggest that the heat flux ratios depend more strongly on other parameters such as thermal radiation blockage due to mock-up geometry and the location of burning on a mock-up relative to the heat flux gauges.

Based on the above discussion, it is clear that heat fluxes recorded in different directions from mock-ups depend on a large number of variables, but that measured fluxes are consistent with visualized burning behaviors. This suggests that there is unlikely to be a perfect correlation of heat fluxes and a single parameter such as the HRR. In order to obtain insight into potential variations, values of heat flux recorded by the front heat flux gauges located 0.75 m and 1.5 m from the mock-up when the HRR was a maximum are plotted against values of HRR_{max} in Figure 65 and Figure 66, respectively. While there are obvious fluctuations in the data, there appears to be a roughly linear dependence of the maximum heat flux on HRR at both distances. Linear least squares curve fits were used to determine the best lines passing through the origins of the plots, which can be expressed as

$$(q_{max})_z = m_z(HRR_{max})_z, \quad (1)$$

where q_{max} is the maximum heat flux recorded by the total heat flux gauge, z is the distance from the front edge of the burning item to the gauge, and m_z is the slope of the line.

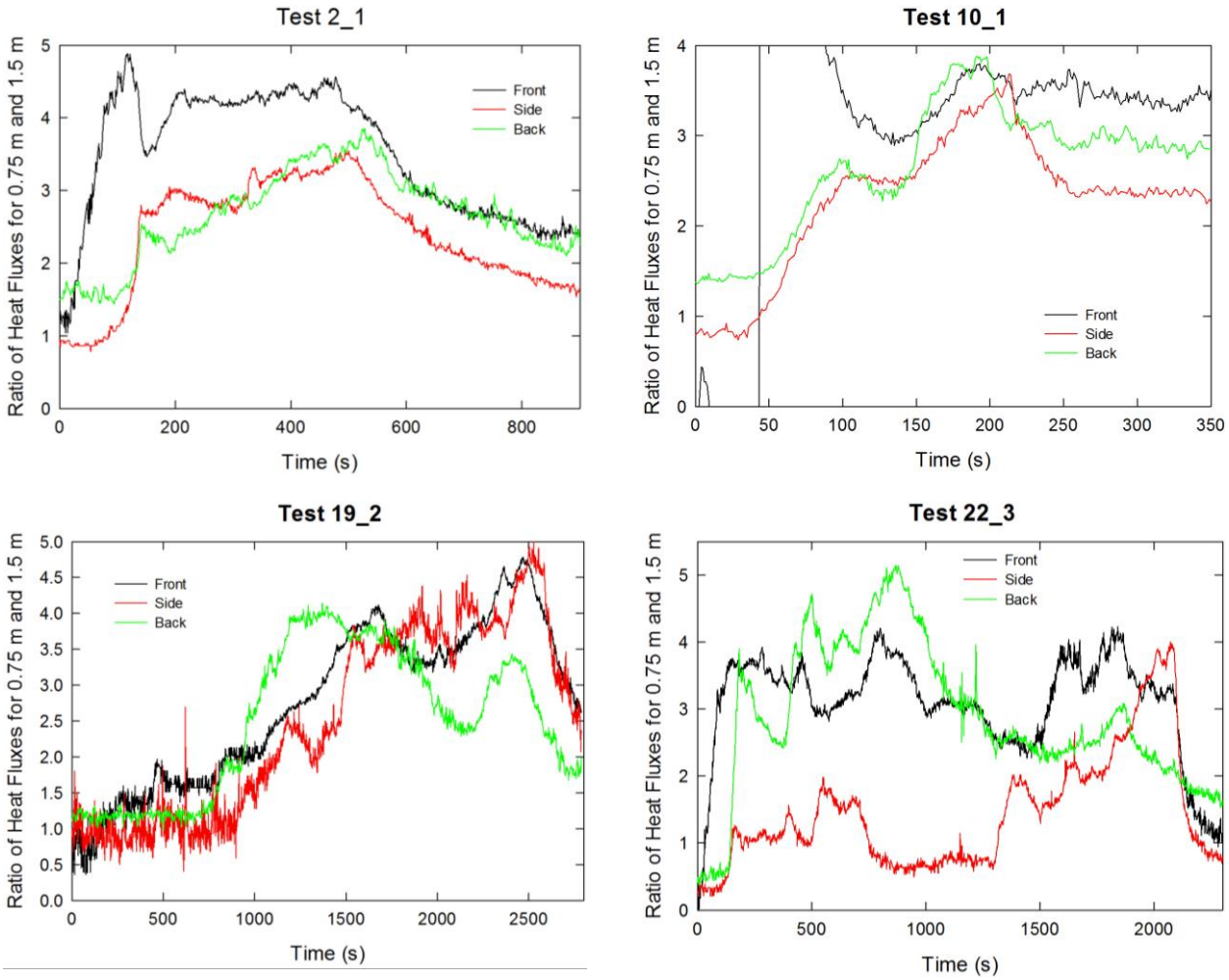

Figure 64. Ratios of heat fluxes recorded by gauges positioned at distances of 0.75 m and 1.5 m to the front, side, and rear of the furniture mock-ups are plotted as a function of time for the four fire tests indicated.

In the following, coefficients of determination, R^2, are based on the best line fit to the data with variable y-intercept, while the slopes are for lines passing through the origin. Thus, R^2 values provide only qualitative indications for nonlinearity and fluctuations of the results about the line. The data in both plots are well represented by straight lines (R^2 = 0.92, $m_{0.75}$ = 0.0230 m^2 at 0.75 m; R^2 = 0.96, $m_{1.5}$ = 0.00726 m^2 at 1.5 m), but there is considerable scatter about the lines, which is likely attributable primarily to the sources of heat flux variations discussed above for the temporal profiles. Nonetheless, the results indicate that a rough estimate for the expected heat flux for a given HRR should be feasible at both distances.

The ratio of the slopes at the two distances should provide an average value for the ratio of the heat fluxes at 0.75 m and 1.5 m. The result is 3.2, which is consistent with the range of instantaneous values discussed above for this parameter.

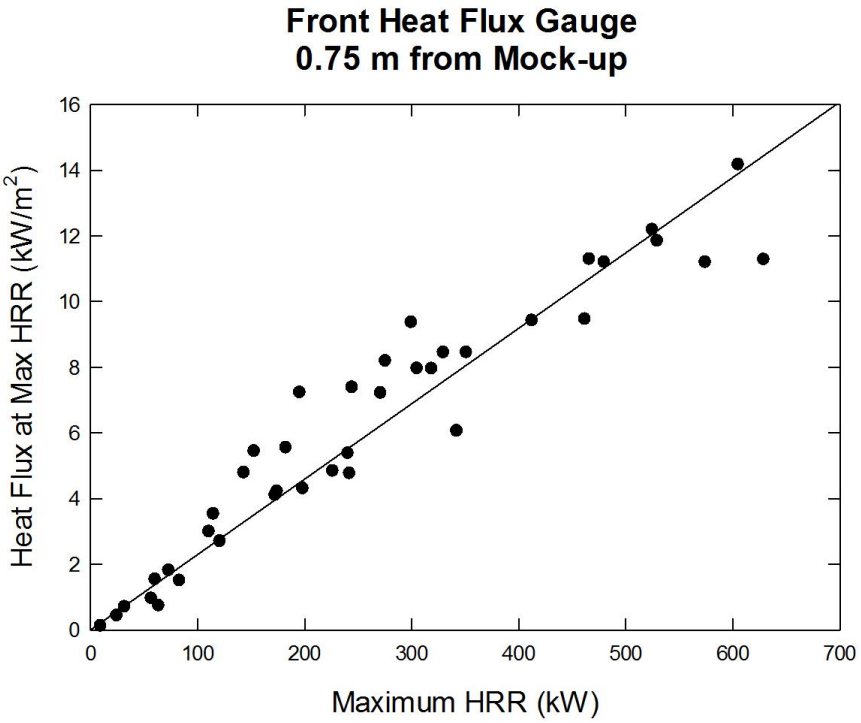

Figure 65. Values of heat flux recorded by the front gauge located 0.75 m from the mock-up at the time of maximum heat release rate (HRR_{max}) are plotted against HRR_{max} for each test. The straight line is the result of a linear least squares curve fit of the data forced to pass through the origin.

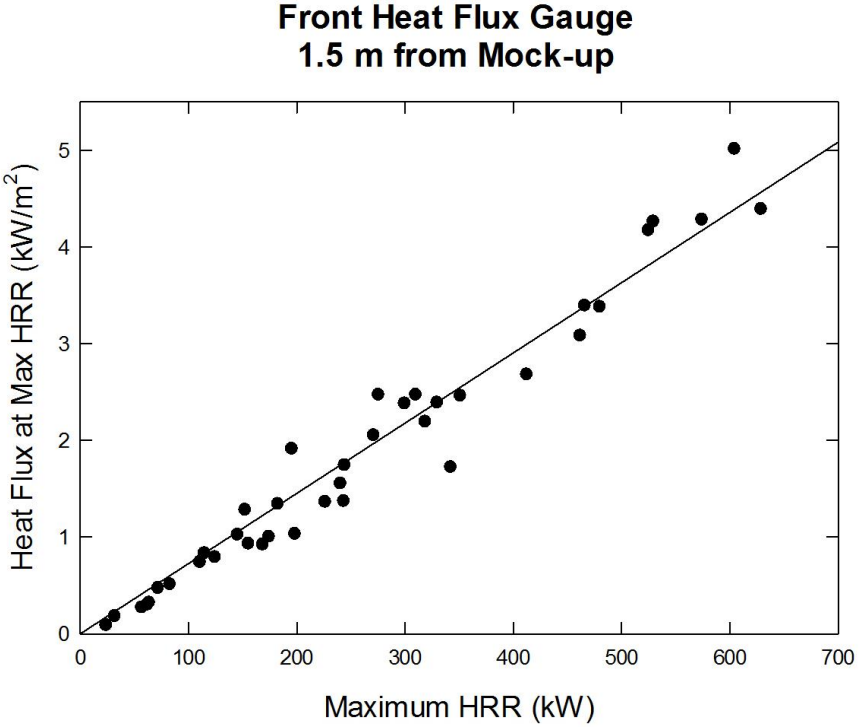

Figure 66. Values of heat flux recorded by the front gauge located 1.5 m from the mock-up at the time of maximum heat release rate (HRR_{max}) are plotted against HRR_{max} for each test. The straight line is the result of a linear least squares curve fit of the data forced to pass through the origin.

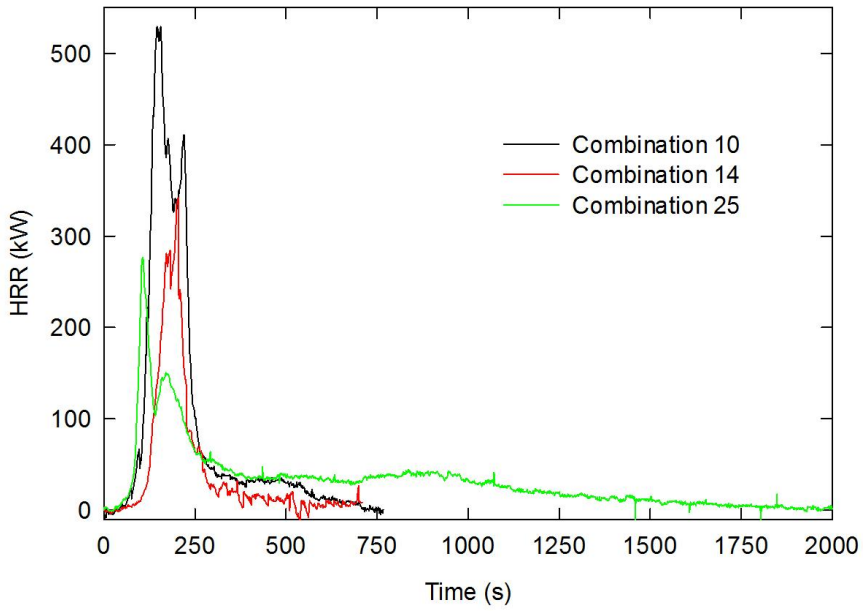

Figure 67 Heat release rate temporal profiles for mock-ups containing Combination 10 (Test 10_1), 14 (Test 14_1) and 25 (Test 25_1) cushions are compared.

6 Results for Supplemental Tests of Mock-ups

A limited number of tests were carried out to provide specific information concerning the role of FPUF on the burning behavior of the mock-ups. The identification numbers and materials used in these mock-ups are summarized in Section 3.14 and Table 11.

A single experiment was performed to test the effectiveness of an experimental fire retardant coating applied to the FPUF slabs. The coating was formed by alternately soaking the FPUF slabs in dilute water solutions containing poly (acrylic acid) mixed with sodium montmorillonite clay and polyethyleneimine to form a coating with 2.5 layers. Details concerning the coating preparation are available elsewhere. [103] The total mass of the four FPUF slabs was increased ≈ 10 % (2.328 kg before, 2.563 kg after) by the coating. The four coated FPUF slabs, covered with the 78%PP/22%PE upholstery fabric, were used to form the Combination 25 mock-up. Mock-ups for Combinations 26 and 27 contained only FR and NFR foam slabs, respectively. Data plots summarizing the measurements for these tests are included in Appendix C.

The coating applied to the cushions for the Combination 25_1 test had a dramatic effect on the burning behavior. Following application of Ignition Source 1, flames spread rapidly on the interior of the back cushion up to the top. After this rapid vertical flame spread, slower spread occurred in the lateral direction on the back and in the lateral and transverse directions on the seat. Even though the flames spread relatively quickly over the mock-up surfaces, the intense burning observed during many of the earlier experiments did not develop. This is apparent in the HRR temporal profiles shown in Figure 67, which compares the HRR curves for Test 25_1 with similar results for Tests 10_1 and 14_1. The HRR for the Combination 25 mock-up fire grew rapidly following ignition, exceeding 275 kW in less than 70 s, before rapidly decreasing. By shortly after 250 s the HRR had fallen to roughly 50 kW and remained near this level for the next 12 min, before falling slowly towards zero over the following 17 min. This HRR burning behavior is in sharp contrast to those observed for mock-ups formed from Combinations 10 and 14 cushions. These two mock-ups were assembled with the same upholstery fabric, but with the NIST-coated FPUF replaced with NFRFPUF and FRFPUF, respectively. The fastest initial HRR growth took place on the mock-up containing the coated FPUF, but even though the HRR_{max} occurred at the earliest time, its value was lower than observed for the other two mock-up types. The long-lived HRR tail observed with the coated foam

Figure 68 Photographs showing mock-ups during Test 14_1 as it was burning out (left) and Test 25_1 (right) after the flames had extinguished.

mock-up lasted much longer than for the other two mock-ups. Review of the videos for these three fires showed that the HRR tails for the mock-ups incorporating NFRFPUF and the FR foam meeting SI-1324 were due to burning that took place primarily on the base under the support stand after the cushions had collapsed, while the much longer HRR tail for the mock-up with coated FPUF was due to low intensity burning that developed on the charred FPUF slabs that remained in place on the test stand.

The different burning behaviors of the cushions with FR and coated FPUF slabs can be seen in Figure 68 where the cushions containing FRFPUF had completely disintegrated as the fire burned while the mock-up that included the coated foam retained much of its initial shape even after the fire had burned out.

Mock-ups for Combinations 26 and 27 were constructed with bare SI-1324 or NFR foam slabs, respectively. Application of Ignition Sources 1 and 2 during Test 26_1 and Test 26_2 resulted in some blackening of the areas on the seat and back in the immediate vicinity of the flame as well as some recession of the foam surface, but there was no evident flame spread away from the flame source. No measurable HRR or mass loss were recorded. Figure 69 (left side) shows a photograph of the Test 26_1 mock-up following the 40 s application of Ignition Source 2. Cavities are visible in the foam where the flame was in close contact with the foam, suggesting the applied heat source caused local pyrolysis. Small dark brown spots are also visible in the blackened area. In our earlier study such areas were attributed to the deposition of a liquid derived primarily from the polyol used in the manufacture of the FPUF following the release of gaseous species derived primarily from the TDI component of the foam. [97]

When the stronger Ignition Source 5 wood crib was applied to the mock-ups, flames were observed spreading away from the immediate vicinity of the wood crib. However, the flames spread only short distances on the seat and back cushions before extinguishing. The crib appeared to sink down into the seat foam slab as it burned. Very low levels of mass loss and HRR (see below) were recorded. The right-hand side of Figure 69 shows the appearance of the Test 26_1 mock-up following the burn out of Ignition Source 5. The increased burned area compared to the photograph on the left is evident, along with the cavities in the slabs formed by the burning.

The burning behaviors of the mock-ups formed with NFRFPUF slabs contrasted sharply with those observed with FRFPUF. Both Combination 27 mock-ups were ignited by Ignition Source 1. Once ignited, the flames spread very rapidly up the center of the back cushion, and then began to spread more slowly in the lateral directions at comparable rates on both the seat and back cushions. As the cushions became fully

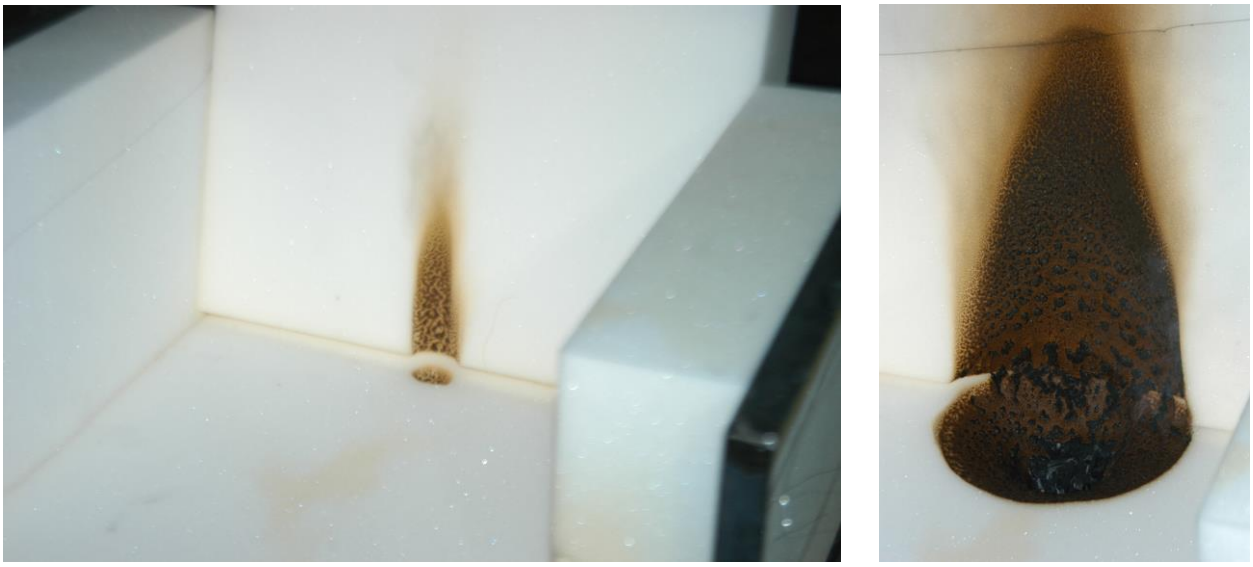

Figure 69. The appearances of Mock-up 26_1 following the application of Ignition Source 2 (left) and Ignition Source 5 (right) are shown.

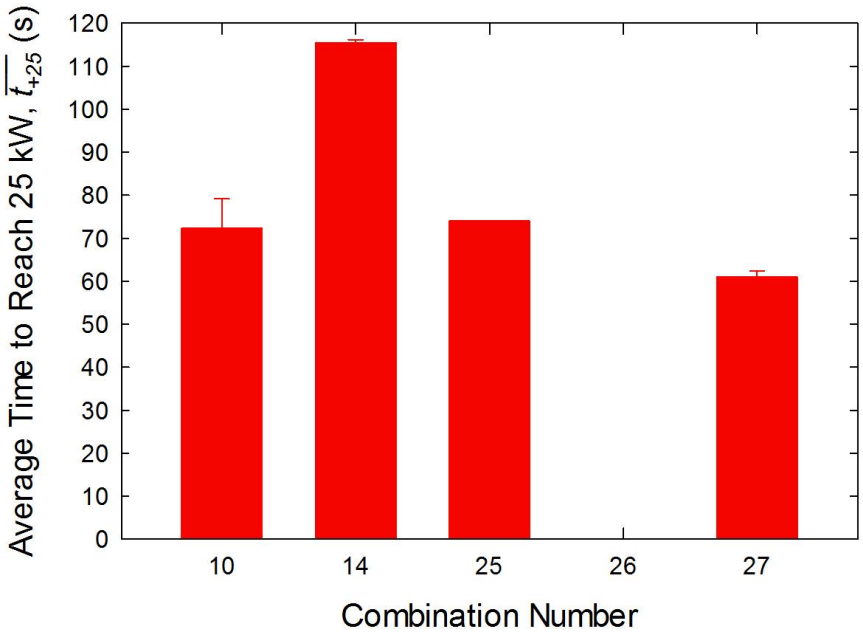

Figure 70. The average periods and associated standard deviations required for the fires to reach 25 kW for the three supplemental combinations are compared with those measured for Combinations 10 and 14.

involved in flames, a substantial amount of liquid poured on to the support stand base, and intense burning developed here as well as on the mock-up.

For comparison purposes, several of the measured parameters based on the HRR time profiles for Combinations 25-27 are compared with those for Combinations 10 and 14 (cushions containing NFR and FRFPUF upholstered with the 78%PP/22%PE fabric) in the following bar graphs. Average values of the periods required to reach HRRs of 25 kW are shown in Figure 70. Keep in mind that Combinations 10, 14, and 25 differed in the type of FPUF cushioning used, while mock-up Combination Pairs 10 and 27 and 14

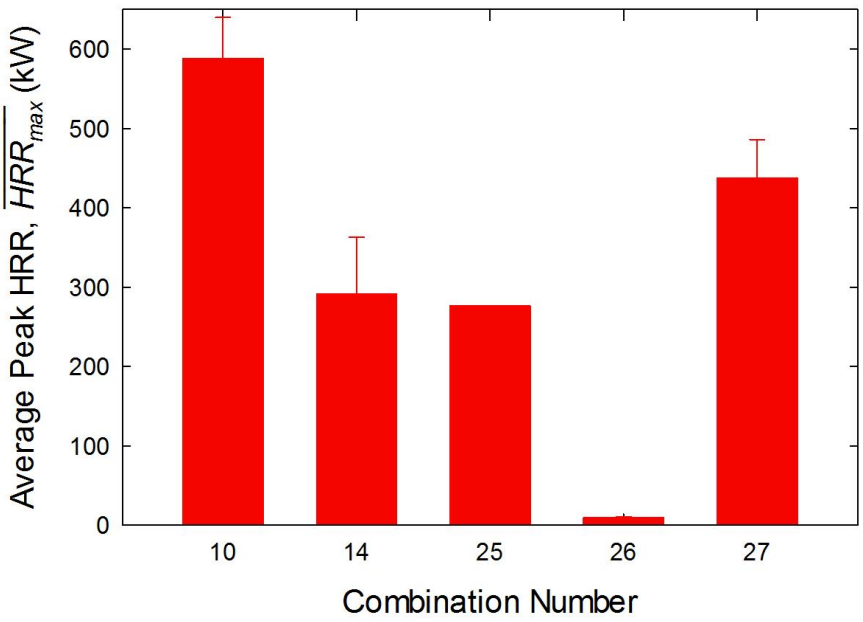

Figure 71. The average peak heat release rates and associated standard deviations for the three supplemental combinations are compared with those measured for Combinations 10 and 14.

and 26 had the same type of foam, but with cushions that were either covered with the thermoplastic fabric or were bare FPUF. Note also that the HRRs for the two Combination 26 tests never reached 25 kW. The initial fire growth behavior for the 78%PP/22%PE-covered cushions filled with NFR- and clay-coated-FPUF were very similar, while the SI-1324 foam seemed to inhibit the initial fire growth. Covering the bare NFRFPUF with thermoplastic fabric slightly increased the values of t_{+25}, while the same modification for mock-ups with FRFPUF changed the burning behavior from one with little fire growth, even after application of Ignition Source 5, to one where significant flame spread and growth took place.

The peak HRR values for the various mock-ups shown in Figure 71 also reflect substantial differences in burning behavior among the mock-up combinations. The largest $\overline{HRR_{max}}$ value was measured for Combination 10 mock-ups. The second highest values were those for Combination 27. Presumably, the roughly 150 kW difference between these mock-up types resulted from the additional heat content of the thermoplastic fabric and, perhaps, more complete burning of the foam. Replacing the NFRFPUF in Combination 10 with either the SI-1324 or clay-coated foams resulted in a roughly factor of two reduction in HRR_{max}. However, the HRR curves shown in Figure 67 suggest that the peak values for the mock-ups with the SI-1324 FPUF resulted from burning of both the foam and upholstery fabric, while the peak value for the mock-up with clay-coated foam was due primarily to fabric burning. Due to the limited flame spread and HRR growth following ignition of the bare FRFPUF mock-ups with Ignition Source 5, the observed maximum HRRs were by far the lowest for the five mock-ups types included in Figure 71.

Total heat release values for the supplemental tests are compared with those for Combinations 10 and 14 in Figure 72. The single value for the Combination 25 mock-up was very similar to those for Combination 10, even though its value of HRR_{max} was much less. This suggests that similar fractions of the FPUF were consumed for both types of mock-up, but that the instantaneous HRRs were much reduced when the foam was clay-coated. The long burning time observed for the Combination 25 mock-up supports this conclusion. In contrast, the relatively low amounts of heat released by Combination 14 mock-ups indicates that a significant fraction of the FRFPUF did not burn. The total heat released by mock-ups constructed with uncovered FRFPUF slabs was barely measurable, while substantial heat was produced when bare NFR slabs were used.

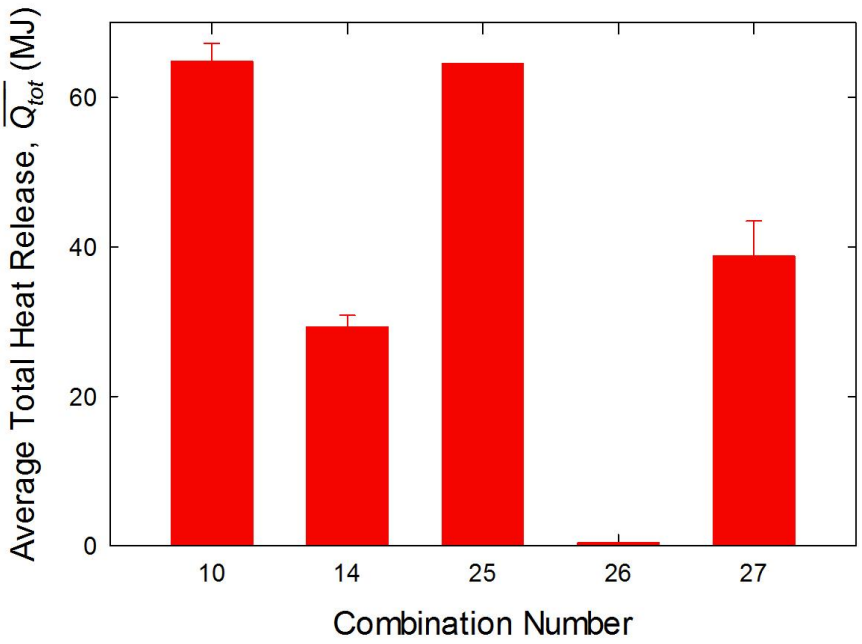

Figure 72. The average total heat release and associated standard deviations for the three supplemental combinations are compared with those measured for Combinations 10 and 14.

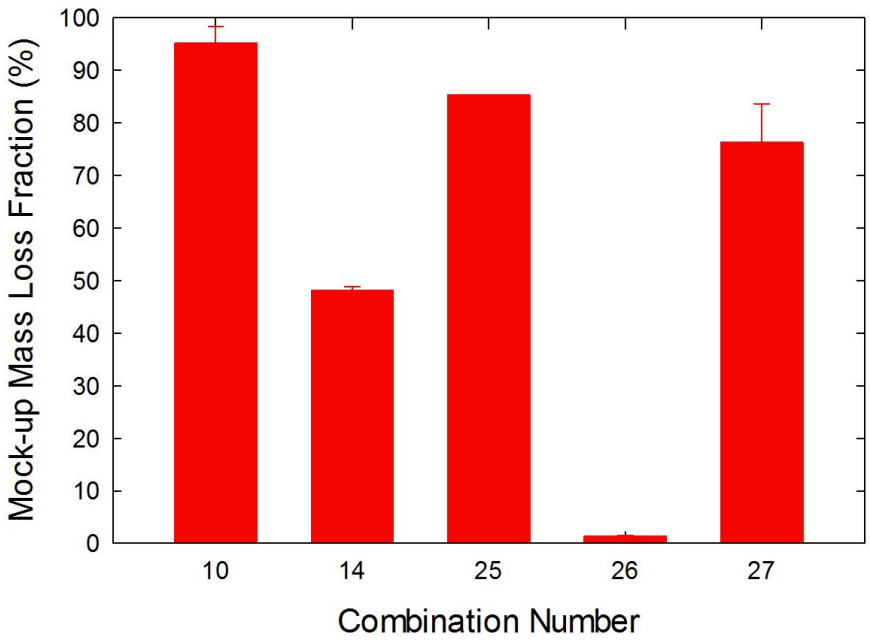

Figure 73. The average percentage of mass loss and associated standard deviations for the three supplemental combinations are compared with those measured for Combinations 10 and 14.

The total mass loss percentages for the five combinations are shown in Figure 73. The highest percentages were for the Combination 10 mock-ups formed with cushions containing NFRFPUF upholstered with thermoplastic fabric. Even though, as shown earlier, there was a charred residue left in the shape of the mock-up following the fire with Combination 25 cushions, the overall mass loss percentage was still 85 %. Recall that the mass of the foam had been increased by roughly 10 % by the application of the coating. This relatively high mass loss is consistent with the high total heat release seen in Figure 72. The mass loss percentages for Combination 27 mock-ups were lower than observed for Combinations 10 and 25. As

Figure 74. Photograph showing the residue on the test stand and support base following Test 14_2.

noted earlier, burning of these mock-ups deposited a large amount of liquid on the base for the support stand. Most of the unburned material following these fires was here, even though substantial burning was observed at this location. Less than half of the total mass was loss when Combination 14 mock-ups with FRFPUF upholstered with the thermoplastic fabric were burned. Figure 74 shows the appearance of the test stand and support base following Test 14_2. Charred material is visible on the test stand, while a substantial amount of brownish liquid-like material and char is located immediately below. Apparently, the fire retardants added to the foam used in this mock-up promoted char formation, while inhibiting burning of the liquid derived from the polyol released by the burning FPUF. A very low mass loss percentage was observed when Ignition Source 5 was applied to mock-ups formed with four slabs of the SI-1324 FPUF.

Average values for the characteristic lateral flame spread velocities, which combine measurements on the seat and back cushions, are plotted in Figure 75 for the five mock-up combinations. The values were similar for Combinations 10, 14, 25, and 27. Only the values for Combination 26, which barely propagated away from Ignition Source 5, were substantially smaller. Note that the $\bar{u}_l$ values for Combinations 10 and 27, which differed in that Combination 10 cushions were covered with the 78%PP/22%PE fabric, had nearly identical rates. This indicates that the thermoplastic fabric does not strongly affect the flame spread rate as compared to flames spreading on bare NFRFPUF.

The characteristic time required to ignite the arms of a mock-up has been shown to be roughly inversely related to the flame spread rate. Values of characteristic arm ignition times for the mock-ups with Combination 10, 14, 25, 26, and 27 cushions are compared in Figure 76. Note that the spreading flames on mock-ups with the bare SI-1324 FPUF slabs (Combination 26) did not spread sufficiently to ignite the arms, and no value is shown. With the exception of the mock-ups including bare FRFPUF, $\overline{t_{lg}}$ were nearly the same within the observed experimental variations, even though some small differences are evident. The longest arm ignition times were recorded for the SI-1324 foam cushions covered with the thermoplastic upholstery fabric (Combination 14), while the corresponding fires on cushions without fabric did not spread to the arm cushions. The characteristic arm ignition time for the clay-coated cushions covered with 78%PP/22%PE fabric were nearly identical to those for fires spreading over bare cushions of NFRFPUF and slightly less than those for cushions covered with the thermoplastic, suggesting the coating had no effect or resulted in a slightly enhanced flame spread rate compared to the untreated foam.

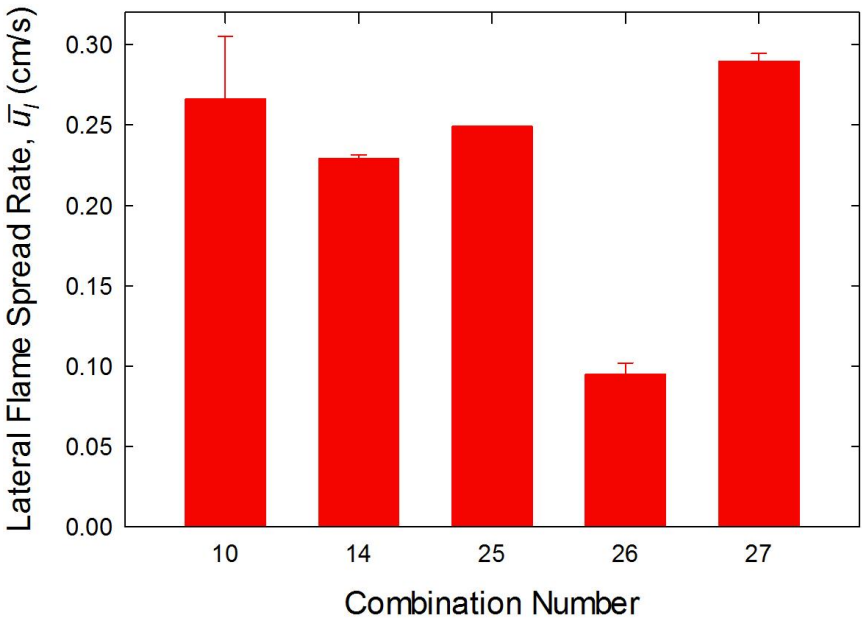

Figure 75. Average characteristic lateral flame spread rates and standard deviations for the three supplemental combinations are compared with those measured for Combinations 10 and 14.

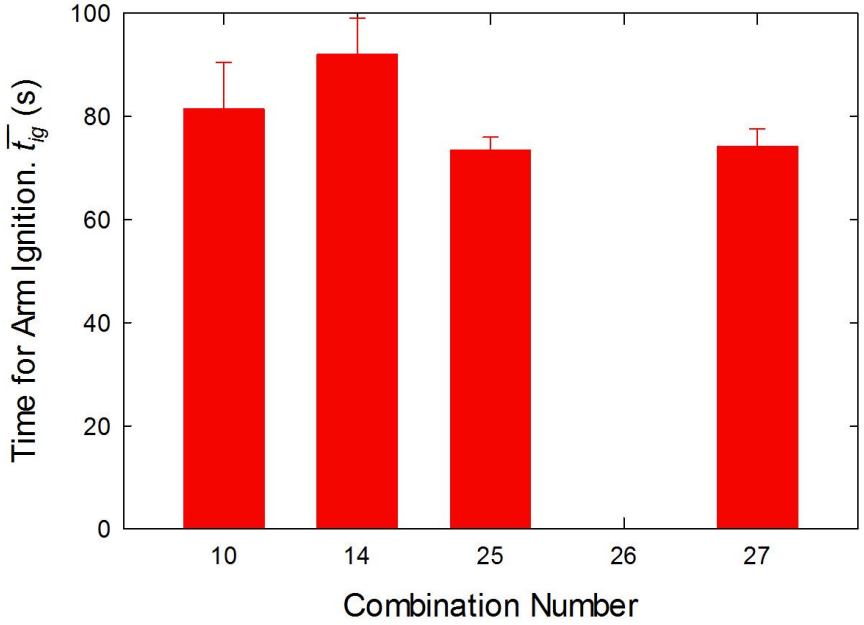

Figure 76. Average times and standard deviations for the characteristic times required to ignite the mock-up arms for the three supplemental combinations are compared with those measured for Combinations 10 and 14.

Table 15. Factors, materials, levels and abbreviations used for statistical analysis.

Factor	Material	Levels	Abbreviation
X1	Barrier	Whispershield	WS
		none	NoB
		Norfab	NF
X2	Foam	non-fire-retarded	NFR
		fire-retarded	FR
X3	Polyester Fiber Wrap	not included	NW
		incorporated	W
X4	Upholstery Fabric	cotton	C
		78%PP/22%PE	P
X5	Sewing Thread	nylon	N
		Kevlar	K

7 Statistical Analysis

7.1 Experimental Factors and Responses

The statistical design of this experiment discussed in Section 2 allows the experimental responses-of-interest to be tested for sensitivity to variations in the types of materials (statistically referred to as "factors") incorporated in the mock-ups. The five factors, in this section indicated by an "X" followed by the factor number, are described in Section 2 and include the

1. type of barrier (X1),
2. type of polyurethane foam (X2),
3. presence or absence of a polyester fiber wrap around the polyurethane foam (X3),
4. type of upholstery fabric (X4), and
5. type of thread used to sew the cushions (X5).

As discussed in Section 2, all of the factors except X1 have two levels as detailed in Table 3. Factor X1 has three levels. Table 15 lists the factors along with their levels and abbreviations used for the levels in this section.

Thirteen responses which focus on the flame spread and HRR growth behaviors of the fires on the RUF mock-ups were chosen for statistical analysis. This total set of 13 responses is identified as Y1 to Y13 in Table 16, along with response definitions, symbols, and abbreviations used in the statistical analysis section.

Ten of these responses (Y1 to Y10) are derived from the HRR temporal profiles. Figure 77 shows the raw HRR traces resulting from each burn--note the consistency of the replications within a given combination. Most combinations had 2 or 3 replicates. A total of 20 out of 24 of the design combinations were tested (recall that combinations including both Whispershield and PEFW were excluded from the test matrix).

In addition to the 10 HRR-derived responses, three additional responses (Y11 to Y13) related to flame spread behavior have been considered.

For each of the 13 responses, a battery of statistical tests is applied to assess whether or not a given response has a statistically significant dependence on the various factors. The factors which affect the response are then ranked in terms of their magnitude. A second series of statistical tests are then used to determine the presence and magnitude of interactions between the various factors. Finally, an analysis is performed to

Table 16. List of responses and corresponding parameters with symbols and abbreviations.

Response	Parameter	Symbol	Abbreviation
Y1	Time required to reach 25 kW	t_{+25}	T25kW
Y2	Time of first HRR maximum	t_{peak1}	T1PHRR
Y3	Value of first HRR maximum	HRR_{peak1}	1PHRR
Y4	Time of maximum HRR	t_{max}	TMaxHRR
Y5	Value of maximum HRR	HRR_{max}	MaxHRR
Y6	Total heat released	Q_{tot}	TotHR
Y7	Time of first FIGRA maximum	t_{FIGRA1}	T1Figra
Y8	Value of first FIGRA maximum	$FIGRA_{peak1}$	1Figra
Y9	Time of maximum FIGRA	$t_{FIGRAmax}$	T2Figra
Y10	Value of maximum FIGRA	$FIGRA_{max}$	2Figra
Y11	Characteristic lateral flame spread velocity	$\bar{u}_l$	LatVel
Y12	Right arm ignition time	t_{igr}	RtArmIT
Y13	Left arm ignition time	t_{igl}	LtArmIT

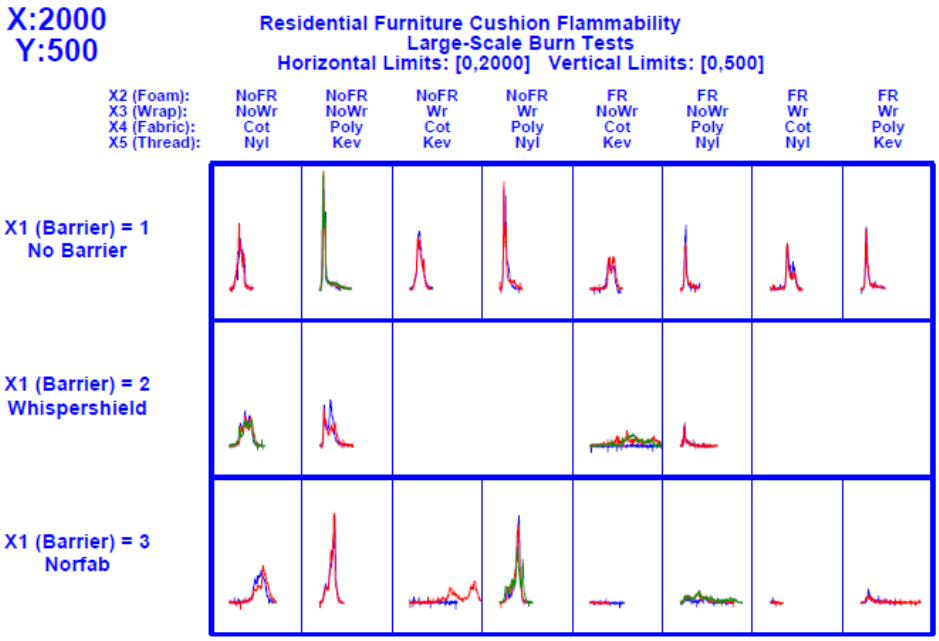

Figure 77. Raw HRR time traces (with replication) as a function of the five factors. The vertical axis is HRR (0 kW to 2000 kW) and the horizontal axis is time (1 s to 2500 s).

determine the best settings for the various factors. The analysis is broken into three subsections entitled:

7.2 Testing Factor Significance,
7.3. Interactions, and
7.4. Optimization.

7.2 Testing Factor Significance

This section reports on our findings with respect to factor significance on the 13 flammability characteristics referred to as "responses." Four questions are addressed:

1. For each of the individual 13 responses, what is the relative importance (that is, what is the ranking) of the five factors under study?

2. For each of the individual responses, which (if any) of the five factors are statistically significant?
3. Globally across all 13 responses, what is the relative importance of the five factors?
4. Globally, what factors are statistically significant?

To address these questions, we carry out formal tests of significance based on two graphical data analysis procedures: the main effects plot and the block plot, and then apply (in the Optimization Section) yet another graphical technique (the ordered data plot) to further confirm our factor conclusions. Our final assessment about the relative importance of the five factors will thus be carried out using six different analysis methodologies:

1. the Main Effects Plot ANOVA (Figure 78 to Figure 91, and Table 22),
2. the Block Plot sign test (Figure 92 to Figure 96, Appendix E, and Table 28),
3. the Block Plot t-test (Figure 92 to Figure 96, Appendix E, and, Table 29),
4. the Ordered Data Plot number of runs (Figure 97 to Figure 109, and Table 38), and
5. the Ordered Data Plot length of the longest run (Figure 97 to Figure 109, and Table 38),
6. the Ordered Data Plot number of consistent settings at the optimum (Figures 97 to 109, and Table 39).

It will be seen that the first three of these methodologies (which focus specifically on the sensitivity analysis question) will all yield the same conclusions about the relative importance of the five factors, and that all six of these methods (sensitivity and optimization) will be consistent in reaffirming the fact that factor X4 (Fabric) is the most important factor—hence such conclusions will be deemed as both rigorous and robust.

7.2.1 Main Effects Plot Analysis for Y5 (= MaxHRR)

The main effects plot is the primary statistical graphics tool for carrying out a general sensitivity analysis with the generic goal of determining the most important factors in a multifactor system. For a given response, the main effects plot shows the mean response (vertically) versus each of the five factors and their two (or three) settings (horizontally). The main effects plot graphically juxtapositions the means of the levels from the five individual scatter plots (one scatter plot per factor). Interpretationally, factors which have (relatively) large differences ("effects") between the mean responses within a factor are deemed (and then tested) to be "important". When this difference of means exceeds a certain threshold (as dictated by statistical criteria and the natural variation of the response with a given setting of that factor), then the factor becomes not just "important", but "statistically significant".

Further, for a given response and a given factor, it is useful to augment the basic main effects plot with relevant summary statistics such as the mean difference between the settings and the relative mean difference percent (= 100 × (the mean difference) / (the grand mean of all the data)). In addition, the outcome of the relevant statistical test--the one-way ANOVA (Analysis of Variance)--is summarized by its p-value for the ANOVA F-statistic. If the difference in the means is large relative to the natural variation of the response within a level of a factor, then the ANOVA F-statistic will yield p-values which are near 0 (with significance declared if the p-value is less than the usual 0.05 value).

As an example, Figure 78**Error! Reference source not found.** illustrates the main effects plot for response Y5 = HRMAX = Max Heat Release Rate. Note visually from Figure 78**Error! Reference source not found.** that the relative ranking of the factors is X1 (Barrier), followed closely by X2 (Foam) and X4 (Fabric), and then distantly by X3 (Wrap) and finally X5 (Thread) with no apparent effect.

Quantitatively, the summary statistics for the results listed at the bottom of the plot support the same ranking. These statistics are reproduced in Table 17 (where the relative effect = the effect / the mean of the data (= 227.95)). The red cells indicate that a factor is statistically significant (based on a p-value ≤ .05).

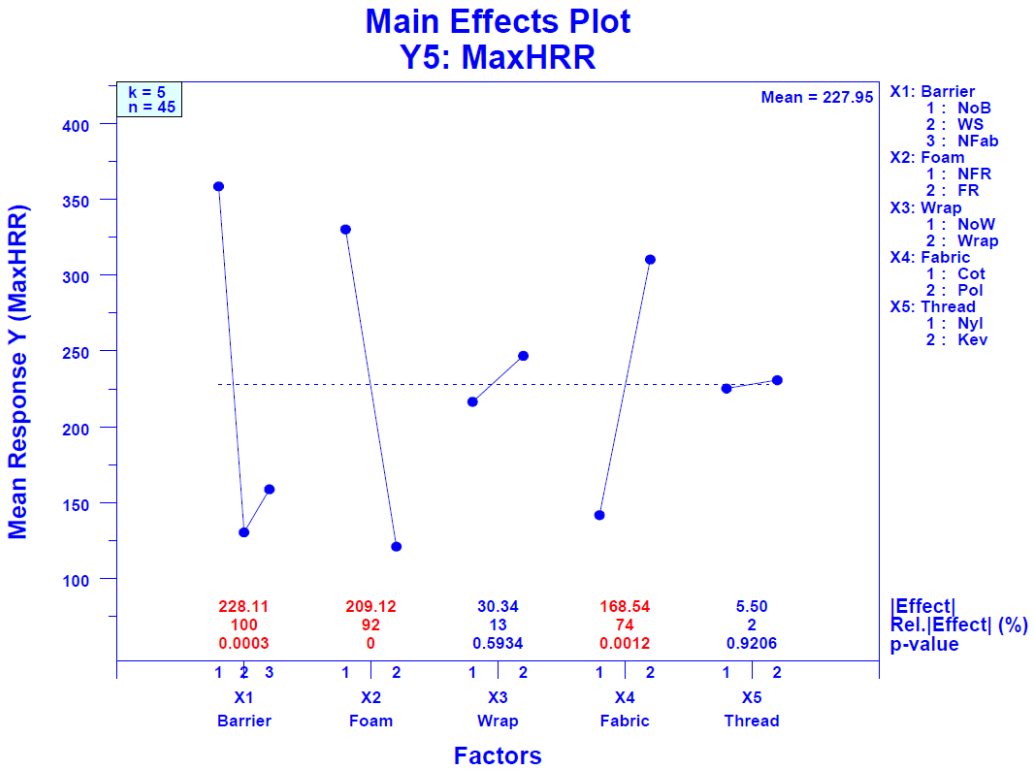

Figure 78. Sensitivity Analysis showing the means for response Y5 = MaxHRR plotted versus each of the five factor levels.

Table 17. Sensitivity analysis for response Y5 = HRMAX showing the effects (= maximum – minimum), the relative effect (= the effect / the mean 227.95), and the 1-way ANOVA p-value for each of the five factors.

		X1	X2	X3	X4	X5
		Barrier	Foam	Wrap	Fabric	Thread
	Effect:	228.11	209.12	30.34	165.54	5.5
Relative Effect:		100%	92%	13%	74%	2%
	p-value:	0.0003	0.0000	0.5934	0.0012	0.9206

Table 18. Sensitivity analysis for response Y5 = HRMAX ranking thefive factors based on the magnitude of the effects (with relative effect and p-value also provided).

		Effect:	Relative Effect:	p-value:
X1	Barrier	228.11	100%	0.0003
X2	Foam	209.12	92%	0.0000
X4	Fabric	165.54	74%	0.0012
X3	Wrap	30.34	13%	0.5934
X5	Thread	5.50	2%	0.9206

For Y5 = HRMAX, the resulting ranked list of the five factors (based on effect and relative effect magnitude) included in Table 18 is thus consistent with what the main effects plot itself graphically

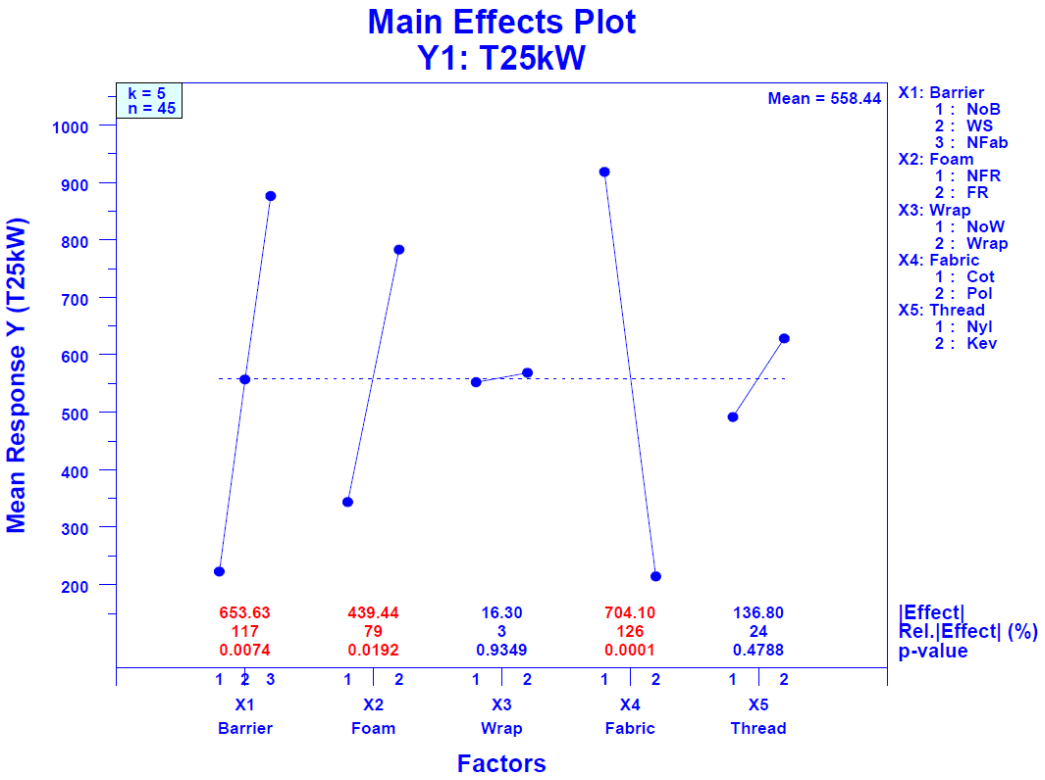

Figure 79. Sensitivity analysis showing the means for response Y1 = T25kW versus each of the five factor levels. Significant: X4 (Fabric), X1 (Barrier), and X2 (Foam).

suggested, with the first three factors X1 (Barrier), X2(Foam), and X4(Fabric) being statistically significant at the 0.05 level.

This ranking is for Y5 = MaxHRR. Does this ranking robustly hold for all 13 responses? To answer this question, an expanded analysis is needed, which is the topic of the next section.

7.2.2 Main Effects Plot Analysis for All 13 Responses

In a similar fashion to the analysis for Y5= HRMAX, Figure 79 to Figure 91 show the main effects plots for all 13 responses.

From the figures, note the varying (but general) dominance of the factors X4 (Fabric), X1 (Barrier), and X2 (Foam). In particular, out of the 13 responses, X4 (Fabric) is statistically significant (note the red) in 12 out of 13 cases, X1 (Barrier) in nine out of 13, X2 (Foam) in six out of 13, and the remaining two factors X3 (Wrap) and X5 (Thread) in none of the 13. This statistical significance issue will be discussed in more detail later, but first an analysis is presented based on effect magnitudes.

Table 19 is a matrix of sensitivity analysis results for the five factors and 13 responses, it summarizes the 13 main effects plots and highlights the most important factors (as defined by their magnitude of the effect). The red cells in this table indicate that the factor effect is the largest over the entire row, that is, is the most important factor for this particular response, while the cells with asterisks indicate statistically significant effects. Note that again only three factors turn out to be most important, namely, X1 (Barrier), X2 (Foam), and X4 (Fabric), with factors X3 (Wrap) and X5 (Thread) never most important for any of the 13 responses. Within the three important factors, X4 (Fabric) is dominant (being most important in seven out of the 13 responses), followed by X1 (Barrier) (five out of 13), and X2 (Foam) (one out of 13).

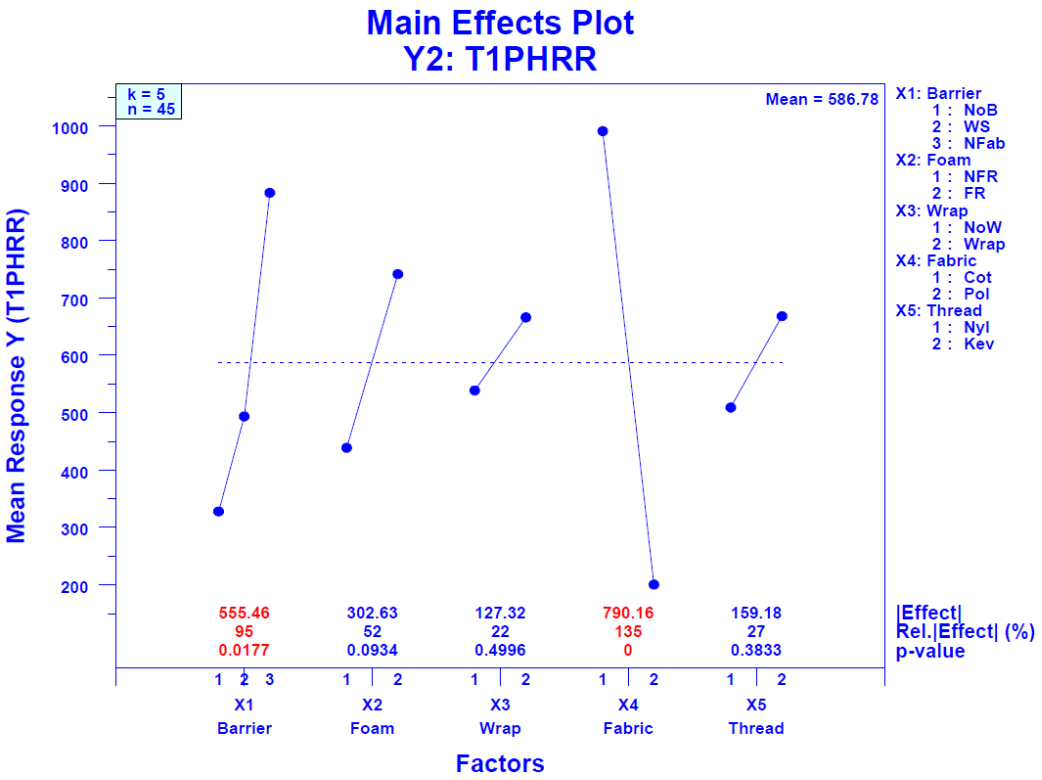

Figure 80. Sensitivity analysis showing the means for response Y2 = T1PHRR versus each of the five factor levels. Significant: X4 (Fabric) and X1 (Barrier).

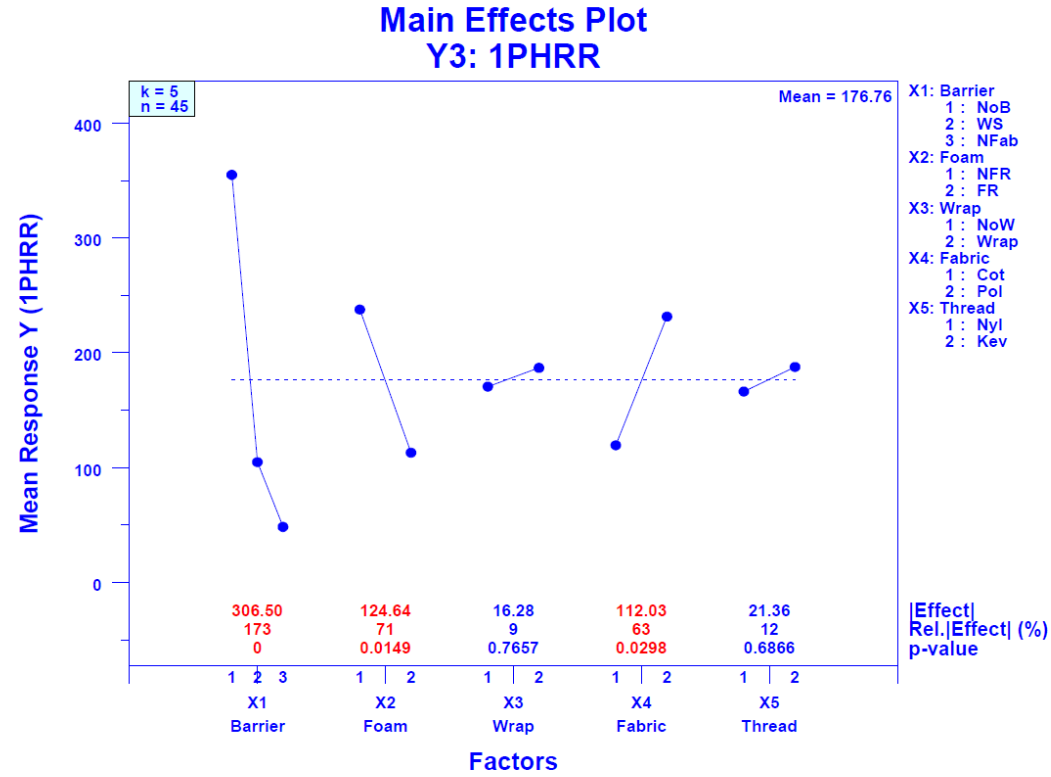

Figure 81. Sensitivity analysis showing the means for response Y3 = 1PHRR versus each of the five factor levels. Significant: X1 (Barrier), X2 (Foam), and X4 (Fabric).

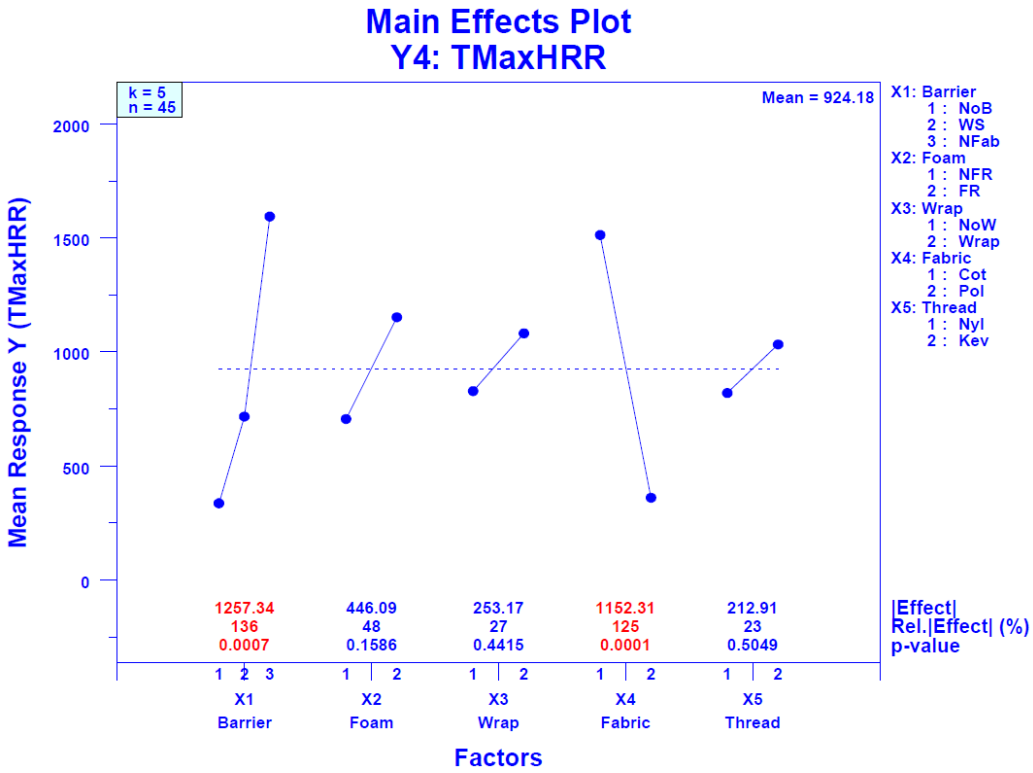

Figure 82. Sensitivity analysis showing the means for response Y4 = TMaxHRR versus each of the five factor levels. Significant: X1 (Barrier) and X4 (Fabric).

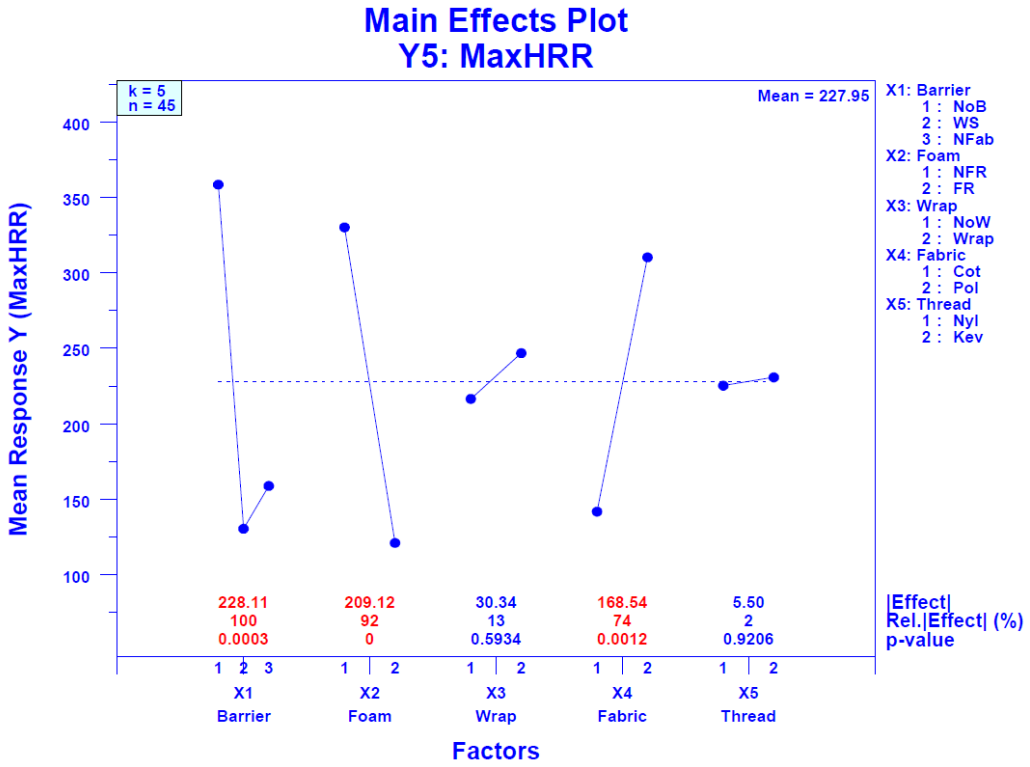

Figure 83. Sensitivity analysis showing the means for response Y5 = MaxHRR versus each of the five factor levels. Significant: X1 (Barrier), X2 (Foam), and X4(Fabric).

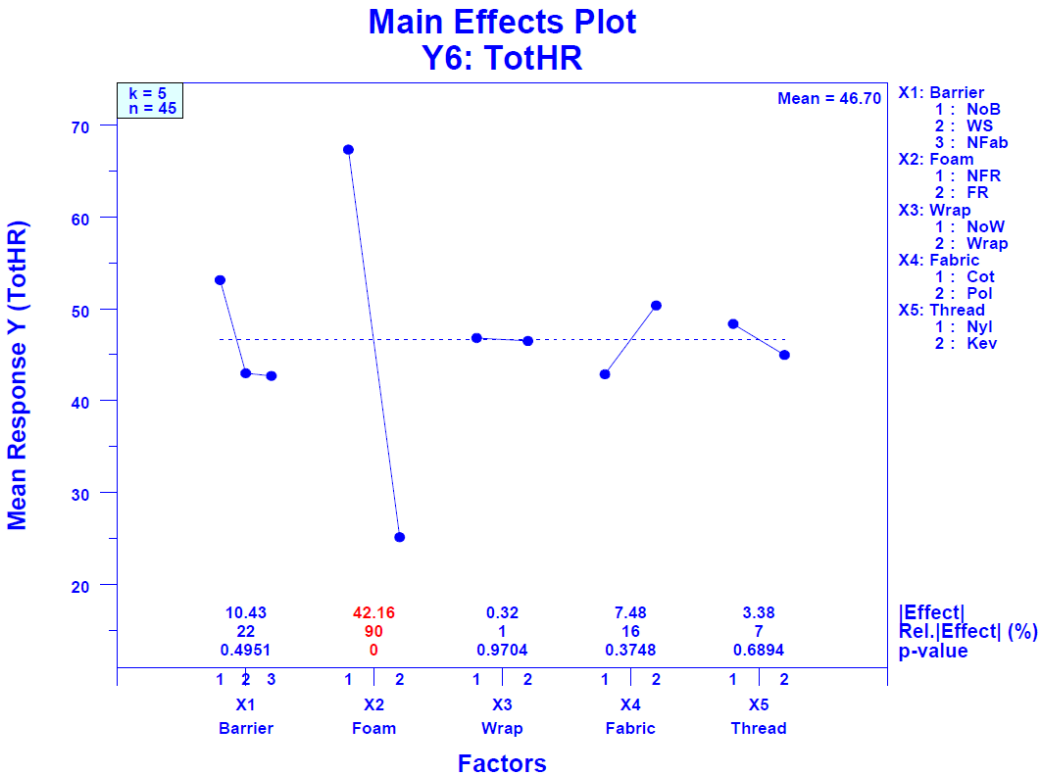

Figure 84. Sensitivity analysis showing the means for response Y6 = TotHR versus each of the five factor levels. Significant: X2 (Foam).

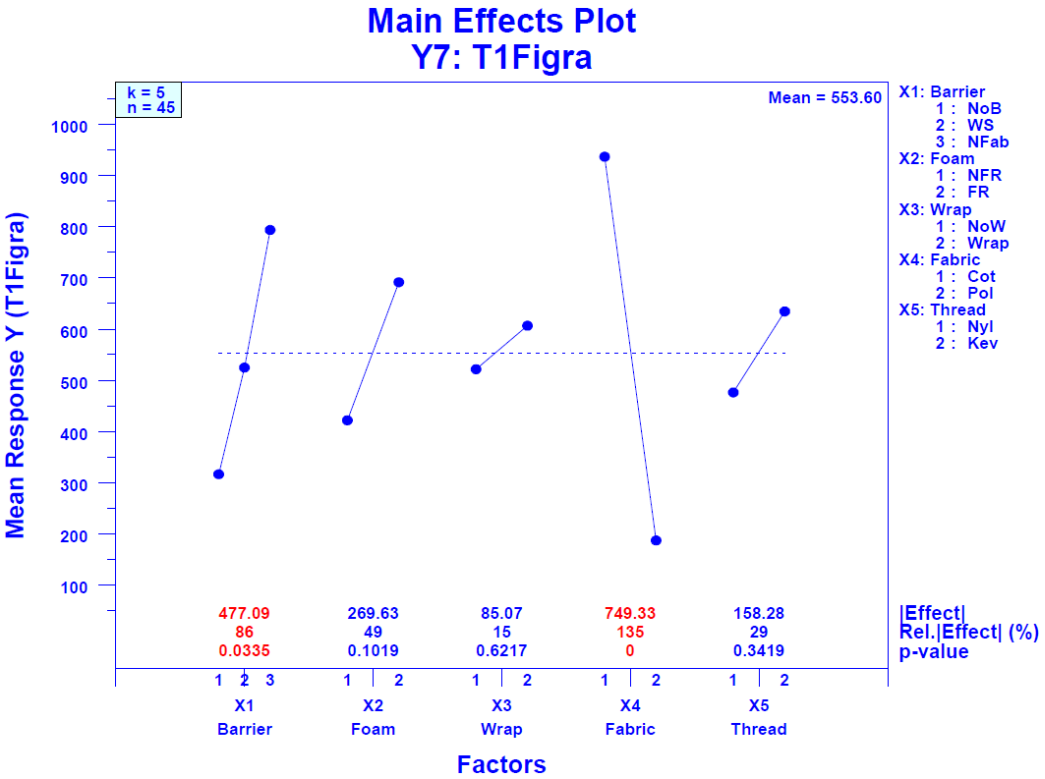

Figure 85. Sensitivity analysis showing the means for response Y7 = T1Figra plotted versus each of the five factor levels. Significant: X4 (Fabric) and X1 (Barrier).

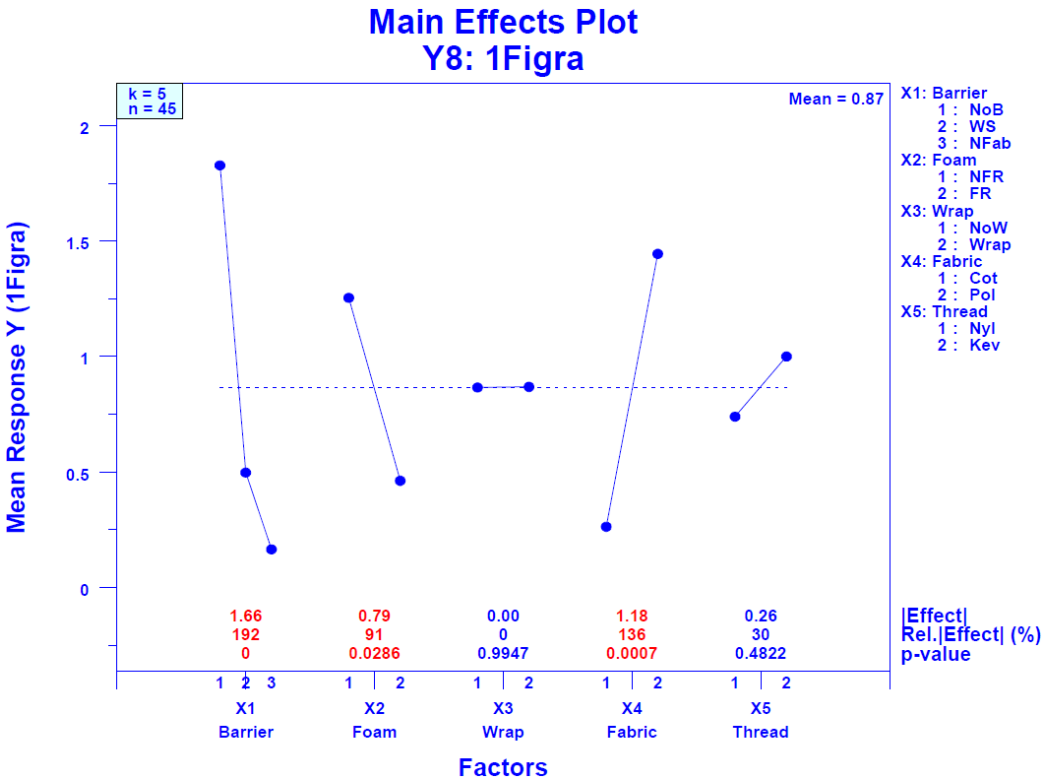

Figure 86. Sensitivity analysis showing the means for response Y8 = 1Figra versus each of the five factor levels. Significant: X1 (Barrier), X4 (Fabric), and X2 (Foam).

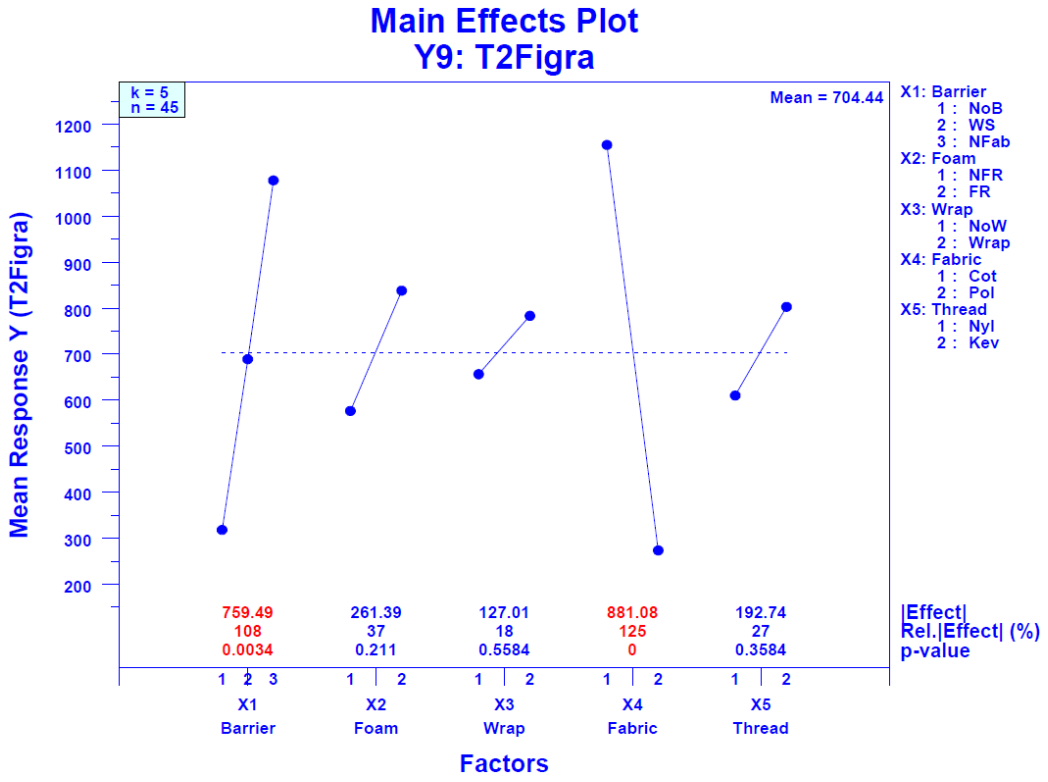

Figure 87. Sensitivity analysis showing the means for response Y9 = T2Figra versus each of the five factor levels. Significant: X4 (Fabric) and X1 (Barrier)

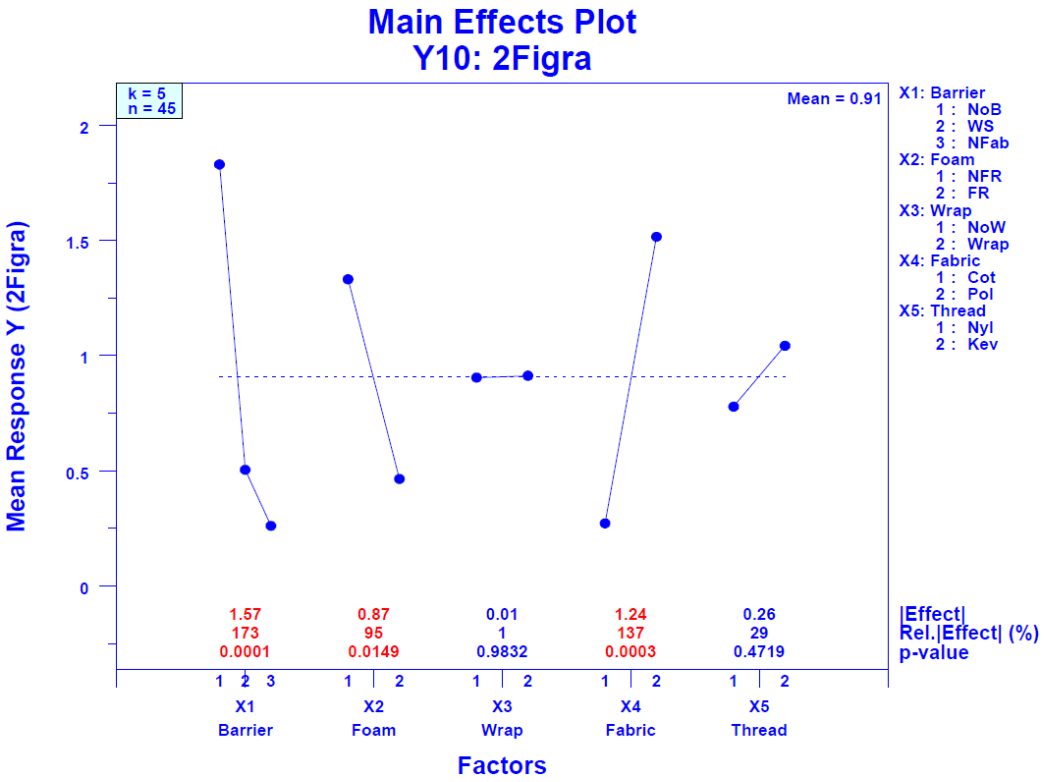

Figure 88. Sensitivity analysis showing the means for response Y10 = 2Figra versus each of the five factor levels. Significant: X1 (Barrier), X4 (Fabric), and X2 (Foam).

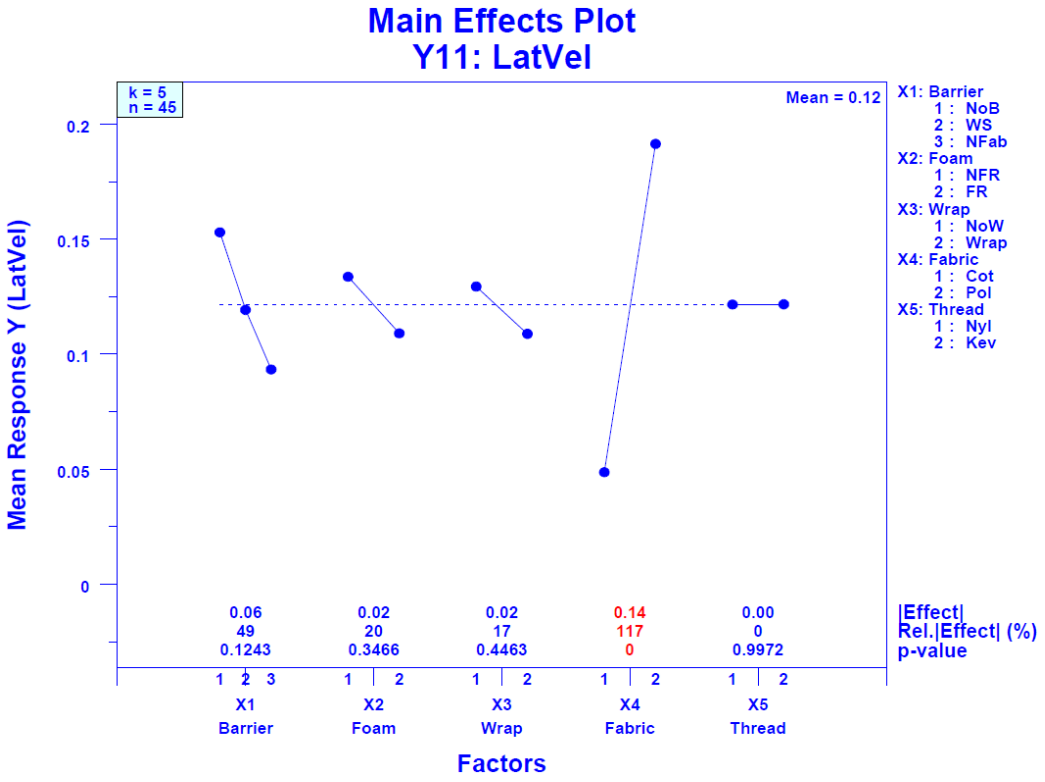

Figure 89. Sensitivity analysis showing the means for response Y11 = LatVel versus each of the five factor levels. Significant: X4 (Fabric).

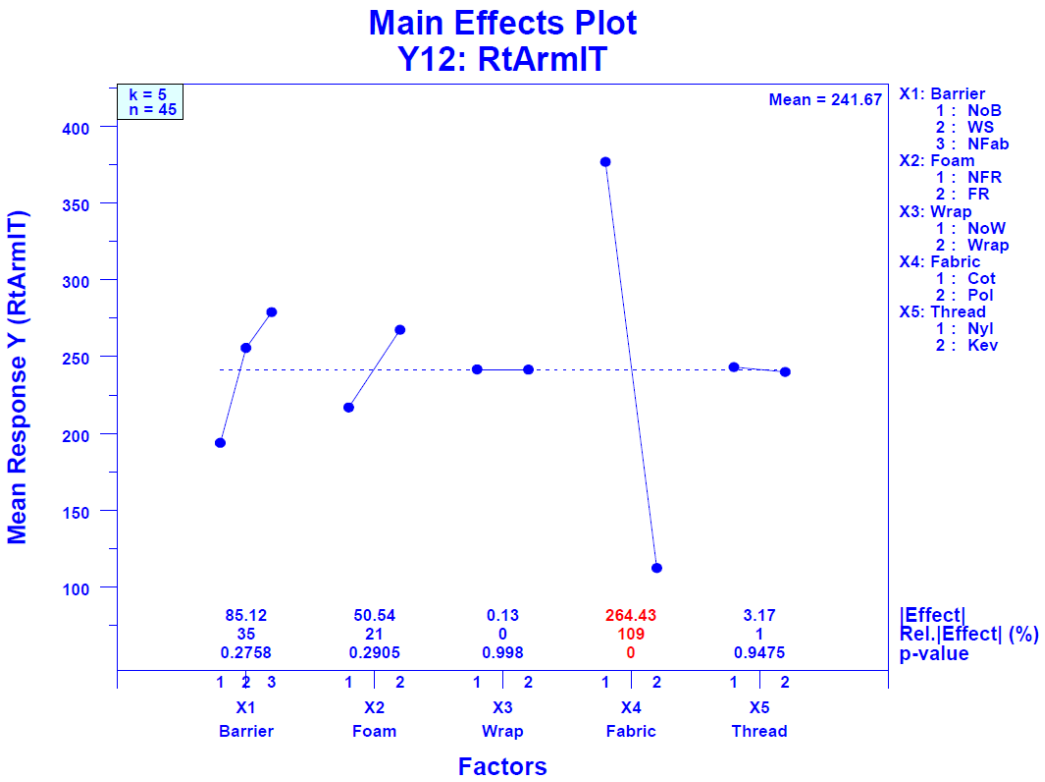

Figure 90. Sensitivity analysis showing the means for response Y12 = RtArmIT versus each of the five factor levels. Significant: X4 (Fabric).

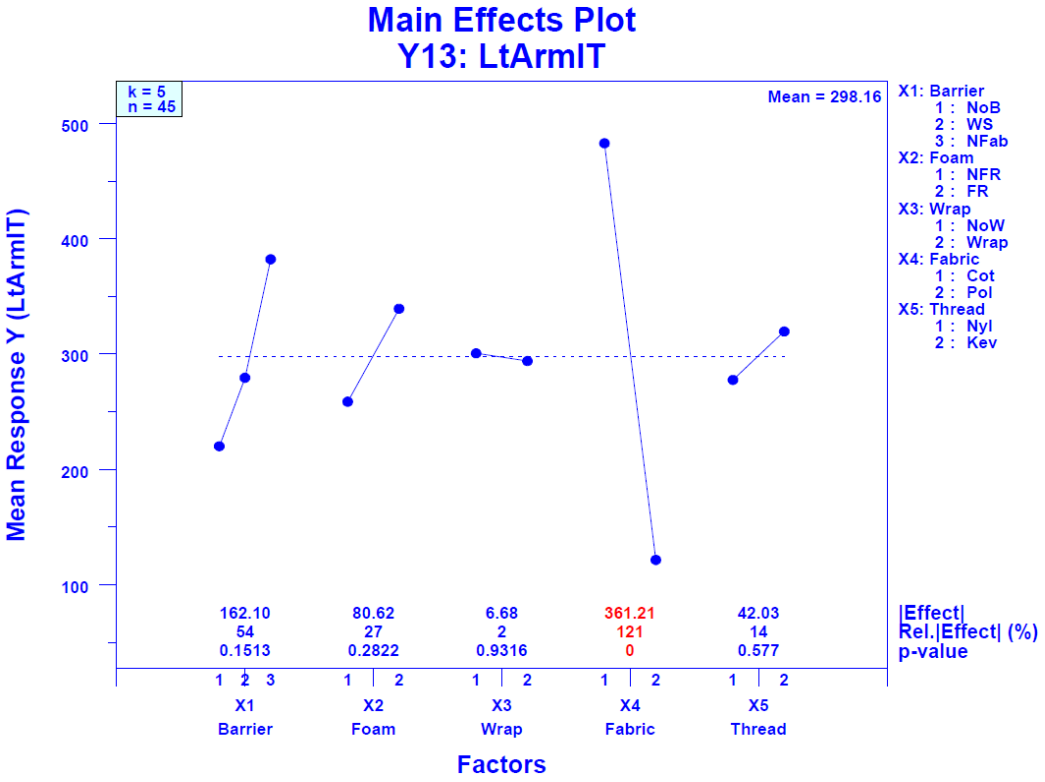

Figure 91. Sensitivity analysis showing the means for response Y13 = LtArmIT versus each of the five factor levels. Significant: X4 (Fabric).

Table 19. Sensitivity analysis for each of the 13 responses showing the effects (= maximum – minimum) for each of the five factors. The largest factor effects are indicated by red cells. Statistically significant factor effects are indicated by asterisks.

		|Main Effects|				
Response		X1 Barr	X2 Foam	X3 Wrap	X4 Fab	X5 Thr
Y1	T25kW	654*	439*	16	704*	137
Y2	T1PHRR	555*	303	127	790*	159
Y3	1PHRR	307*	125*	16	112*	21
Y4	TMaxHRR	1257*	446	253	1152*	213
Y5	MaxHRR	228*	209*	30	169*	6
Y6	TotHR	10	42*	0.3	7	3
Y7	T1Figra	477*	270	85	749*	158
Y8	1Figra	1.66*	0.79*	0	1.18*	0.26
Y9	T2Figra	759*	261	127	881*	193
Y10	2Figra	1.57*	0.87*	0.01	1.24*	0.26
Y11	LatVel	0.06	0.02	0.02	0.14*	0.00
Y12	RtArmig	85	51	0	264*	3
Y13	LtArmig	162	81	7	361*	42
	# Times Max	5	1	0	7	0
	# Times Signif.	9	6	0	12	0

The relative effects of the material parameters on the experimental responses summarized above are global in nature. As noted, the two factors responsible for the largest changes in the responses are the two fabric and the three barrier conditions. The effects of these two factors on the responses are roughly equal. While not a global conclusion, it is possible to derive some additional detail concerning the role of Fabrics, Barrier, and Foam factors on the responses using results summarized in Table 20 and Table 21.

Table 20 translates the effect values into rankings, that is, for a given response, what factor has the largest |effect| (thus yielding rank 1) down to what factor has the smallest |effect| (thus yielding rank 5). For a given row (= response) in this table, red cells highlight the factor with the top ranking. First looking at the highlighted row 5 of the table, (the row for Y5 = HRMAX that we previously examined) we see that the ranking of the five factors is X1, X2, X4, X3, X5, with factor X1 (Barrier) the most important locally (that is, for Y5).

Globally, summarizing the information in Table 20 may be done in two ways. A first method is to compute the average rank. Values of average ranking are included in Table 21 for the five factors. In this case, we see that Factor X1 (Barrier) is best with an average rank of 1.62, followed (very) closely by Factor X4 (Fabric) with a rank of 1.69. The observed reversal is because X1 (Barrier) is ranked no lower than 2 forall 13 responses, while X4 (Fabric) has rank 3 for a few responses. By this criterion, X1 (Barrier) is robustly the most important factor over all 13 responses.

A second way is to note the number of times a factor achieves rank 1. By this criterion, Factor X4 (Fabric) is (as before) globally most important because it achieves the top rank in seven out of the 13 cases, which in turn is closely followed by Factor X1 (Barrier) which is ranked highest in five out of the 13 cases (see

Table 20. Sensitivity analysis for each of the 13 responses showing the ranking of the five effects (where Rank 1 = largest effect) for each of the five factors.

Ranking Based on |Main Effects|

Response		X1 Barr	X2 Foam	X3 Wrap	X4 Fab	X5 Thr
Y1	T25kW	2	3	5	1	4
Y2	T1PHRR	2	3	5	1	4
Y3	1PHRR	1	2	5	3	4
Y4	TMaxHRR	1	3	4	2	5
Y5	MaxHRR	1	2	4	3	5
Y6	TotHR	2	1	5	3	4
Y7	T1Figra	2	3	5	1	4
Y8	1Figra	1	3	5	2	4
Y9	T2Figra	2	3	5	1	4
Y10	2Figra	1	3	5	2	4
Y11	LatVel	2	3	4	1	5
Y12	RtArmig	2	3	5	1	4
Y13	LtArmig	2	3	5	1	4
	Mean Rank	1.62	2.69	4.77	1.69	4.23
	Rank	1	3	5	2	4
	# Times Rank 1	5	1	0	7	0
	Rank	2	3	4	1	5

Table 21. Sensitivity analysis ranking the five factors based on average rank and on the number of times (out of the 13 responses) the factor effect was ranked first.

		Average Rank	# Times Rank 1
X4	Fabric	1.69	7
X1	Barrier	1.62	5
X2	Foam	2.69	1
X3	Wrap	4.77	0
X5	Thread	4.23	0

Table 21). Thus either Fabric or Barrier is first for every response except Y6 (TotHR); for Y6, Foam ranked first followed by Barrier and Fabric.

In summary across the two methods, Fabric and Barrier are thus seen to be the two most important factors, globally—with the ordering depending on criteria used.

A third criteria that can be utilized is that of the computed ANOVA p-value. Continuing with the issue of statistical significance of the five factors (across the 13 responses), Table 22 presents the p-values for the five individual one-way ANOVAs for each of the 13 responses. Red cells in the table indicate statistical significance at the 0.05 level.

Table 22. Sensitivity analysis for each of the 13 responses showing the one-way ANOVA p-values for each of the five factors.

		p-value based on one-way ANOVA				
		X1	X2	X3	X4	X5
		Barrier	Foam	Wrap	Fabric	Thread
Y1	T25kW	**0.0074**	**0.0192**	**0.9349**	**0.0001**	**0 .4788**
Y2	T1PHRR	**0.0177**	**0.0934**	**0.4996**	**0.0000**	**0.3833**
Y3	1PHRR	**0.0000**	**0.0149**	**0.7657**	**0.0298**	**0.6866**
Y4	TMaxHRR	**0.0007**	**0.1586**	**0.4415**	**0.0001**	**0.5049**
Y5	MaxHRR	**0.0003**	**0.0000**	**0.5934**	**0.0012**	**0.9206**
Y6	TotHR	**0.4951**	**0.0000**	**0.9704**	**0.3748**	**0.6894**
Y7	T1Figra	**0.0335**	**0.1019**	**0.6217**	**0.0000**	**0.3419**
Y8	1Figra	**0.0000**	**0.0286**	**0.9947**	**0.0007**	**0.4822**
Y9	T2Figra	**0.0034**	**0.211**	**0.5584**	**0.0000**	**0.3584**
Y10	2Figra	**0.0001**	**0.0149**	**0.9832**	**0.0003**	**0.4719**
Y11	LatVel	**0.1243**	**0.3466**	**0.4463**	**0.0000**	**0.9972**
Y12	RtArmIT	**0.2758**	**0.2905**	**0.998**	**0.0000**	**0.9475**
Y13	LtArmIT	**0.1513**	**0.2822**	**0.9316**	**0.0000**	**0.5770**
	# Times Signif.	**9**	**6**	**0**	**12**	**0**

Table 23. Sensitivity analysis ranking the five factors based on the number of times (out of the 13 responses) a factor is ranked first (which is here identical to the number of times the one-way ANOVA p-value is statistically significant (i.e., ≤ 0.05)).

		Average	**# Times**	**# Times**
		Rank	**Rank 1**	**Stat Sig**
X4	**Fabric**	1.69	7	12
X1	**Barrier**	1.62	5	9
X2	**Foam**	2.69	1	6
X3	**Wrap**	4.77	0	0
X5	**Thread**	4.23	0	0

From Table 22 it is seen that Factor X4 (Fabric) is dominant and statistically significant in 12 out of the 13 responses—missing only the response Y6 (TotHR). The next most important factor globally is Factor X1 (Barrier): nine responses, followed by Factor X2 (Foam): five responses. Factors X3 (Wrap) and X5 (Thread) are not statistically significant for any of the 13 responses. These results are summarized in Table 23.

7.2.3 Main Effects Plot Analysis Conclusions

In summary, based on the three criteria, which are in turn based on the Main Effects Plot Analyses, the following global conclusions are reached:

1. X4 (Fabric) affects the 13 burn-characteristic responses the most,
2. followed closely by X1 (Barrier), and then
3. X2 (Foam),
4. with negligible contributions from X3 (Wrap) and
5. X5 (Thread).

Up to this point the statistical analysis for the 13 responses has not considered any natural groupings of the 13 responses that may exist. However, it is instructive to look at Table 19 and Table 20 results in more detail. The responses where Fabric was the largest factor include Y1 (T25kW), Y2 (T1PHRR), Y11 (LatVel), Y12 (RtArmIT), and Y13 (LtArmIT) as well as two responses based on FIGRA measurements. Earlier, we differentiated between flame spread and fire growth processes, with flame spread describing the growth in flame area and fire growth being characterized by HRR behavior. The most explicit flame spread parameters are Y11, Y12, and Y13. As can be seen in Table 19 and Table 20, each of these factors was heavily dominated by X4 (Fabric). Recall from Section 5.10 that for most tests the period required to reach 25 kW was closely tied to the mock-up arm ignition times. It is thus consistent that X4 (Fabric) ranks first for this response. Based on similar arguments, the time to reach an initial peak in HRR might be expected to depend most strongly on X4 (Fabric), as observed. Thus, for the responses expected to depend most strongly on flame spread behavior, X4 (Fabric) was the dominant factor.

In contrast, the two parameters that are expected to be most representative of fire growth, Y3 (1PHRR) and Y5 (MaxHRR) are dominated by the Barrier factor. The factor Y4 (TMaxHRR) was also most dependent on X1(Barrier). Since this parameter is associated with the maximum HRR, it is likely to be most dependent on fire growth as opposed to flame spread behavior. Thus the dominant factor for the three responses tied most closely to fire growth is X1 (Barrier).

Responses based on FIGRA might be expected to have a more complicated dependence on the factors since this parameter is formed by dividing the HRR by time. For the four FIGRA responses considered, those involving maximum values, Y8 (1Figra) and Y10 (2Figra) were most dependent on X1 (Barrier) while those based on times, Y7 (T1Figra) and Y9 (T2Figra) were most sensitive to Y4 (Fabric). While not as clear cut as above, these results are consistent with the conclusion that flame spread was most dependent on the X4 (Fabric) factor, while fire growth was more sensitive to the X1 (Barrier).

Y6 (TotHR) was the only response where X2 (Foam) was the largest factor. Experimentally it was observed that either there was minimal loss of foam during an experiment or that nearly all of the foam mass was lost. Since the densities, and thus the total mass of foam in mock-ups with cushions having the same remaining materials, were similar for NFRFPUF and FRFPUF, it is expected that the total HRR would depend primarily on foam EHOC. As discussed in Section 5.7, measured EHOCs were lower when the foam was fire retarded, consistent with the lower TotHRs measured for the mock-ups with FRFPUF that differed only in FPUF type.

7.2.4 Block Plot Analysis for Y5 (= MaxHRR)

It is good statistical practice to carry out alternative statistical estimation and testing procedures to ensure that our scientific conclusions are not dependent on the particular statistical methodology being used. In the previous sections we examined three such methodologies—all based on main effects plots and one-way ANOVA. In this section we shall expand our analysis further to ensure that our conclusions are methodology-independent, to increase statistical rigor, and to maximize engineering insight. In our present case, the parallel analysis to be carried out is based on the "block plot" approach. [107]

As before, an analysis for Y5 = MaxHRR is selected as an initial example. In the main effects plot of Section 7.2.1 (see Figure 78), there were 11 points plotted vertically within the plot, namely the mean responses for the three levels of factor X1 and the mean responses for the two levels of each of the remaining factors: X2, X3, X4, and X5. Note, however, that in the main effects plot, the plotted mean for a given setting of a given factor (e.g., X1 = No Barrier versus Whispershield versus Norfab) does indeed convey information about that factor and its setting but also has imbedded latent information from all of the other settings of all of the other factors in the system, with the net effect that this tends to add noise to the plotted mean values for a given factor. This characteristic potentially degrades our ability to differentiate the levels of a factor for that plot.

In this regard, consider the following key points, which in turn will lead to an alternative (= block-plot-based) statistical analysis that will reaffirm our previous conclusions and will provide additional valuable information about interactions:

Design Balance: From an experimental design point of view, when the design is balanced (i.e., every level within each factor appears the same number of times across the totality of runs), this latent information is spread evenly across all factors, and, as a result, our single-factor interpretations are valid (with caution given to the weaker factors). For severely unbalanced experimental designs, however, unambiguous conclusions about single factors may be severely compromised. For this reason, the experimental design constructed for this experiment was purposely chosen to possess such balance. Although certain experimental conditions were lost/impossible due to practical considerations, the resulting final design was sufficiently near-balanced to yield confidence in the final factor effect estimates and statements.

1-Way ANOVA Testing: In any event, the latent imbedded information in the calculated factor and setting means has the net effect of making the above main effects plot / one-way ANOVA approach fairly conservative (which is good in the sense that when a factor is noted to be important and significant--like X4 (Fabric)--then that importance assessment is robustly persistent in spite of the noise and potential contamination from all of the other factors). On the other hand, for small-effect factors such as X3 (Wrap), one reason for concluding that an effect is small is that the large contributions from other "noisy" factors may have the net effect that a potentially small (but real) factor effect is "washed out" due to induced variation from more-dominant factors. The estimate for the factor effect is still valid and unbiased, but the apparent underlying "pseudo-replication" variation may be large, with the net effect that a factor with a small (but real) factor effect may incorrectly be deemed as statistically insignificant. Note that this is an issue of whether or not a factor is declared "statistically significant"; it is not an issue of changing the relative ranking of the five factors—that remains unchanged.

Block Plot: To address (and detect) this potential loss of resolution for the less dominant factors, it is of interest to utilize a second statistical methodology, the block plot [107], to explicitly assess the effect of a single factor locally for each (and then every) combination of all of the remaining factors, and then subsequently (and cumulatively) form a global conclusion of significance from the series of local conclusions. In effect, if a factor exhibits similar behavior across a large number of localized subsets, then that consistent, repeated manifestation is sufficient in itself to be statistically significant.

The block plot is a general statistical graphics tool for carrying out comparative analyses of the settings across a single factor, with the goal of determining whether that single factor is statistically significant, and then determining whether that significance robustly holds over all the other settings of all the other factors in the system.

Unlike the main effects plot, which (for a single response out of the 13) can simultaneously portray the effect of all factors on a single graphic, the block plot requires multiple plots—one plot for each of the five factors under study. That is a complication, but is minor compared to the additional insight on effects and interactions that the block plot typically brings to light.

For a given response, the block plot for a given factor is by definition a plot of the mean response (vertically) for each setting of that single factor versus each (and every) level of each (and every) remaining factor (horizontally). In essence, the block plot examines the behavior of the levels of the factor of interest for a single subset made up of the specific joint settings of the remaining factors and then does so for all possible such combinations of settings (subsets).

Primary and Robustness Factors: In block-plot terminology, the factor of interest is referred to as the "primary factor", and the remaining factors in the system are referred to as "robustness factors". For a

given robustness factors subset (= a given fixed combination of robustness factor settings), a primary factor will be deemed "locally important" if the mean responses for each of its own settings differ "considerably". More importantly, if the responses associated with the primary factor settings differ in a consistent fashion across all of the robustness factor settings, then that primary factor will be deemed to be "globally important", "robustly important", or simply "important".

Sign Test: Such comparisons—though sounding subjective—are in fact backed up by associated rigorous statistical hypothesis tests, namely, the binomial distribution sign test. For example, if the primary factor has two settings, and if the response for one primary factor setting is consistently higher than the response for the second primary factor setting, for all (or almost all) robustness factor subsets, then that is evidence of global statistical significance. Additionally, if the difference between the means for the primary factor settings consistently exceeds a certain threshold (as dictated by natural data variation) then that too categorizes a primary factor as not just being significant, but as statistically significant, and more strongly, being robustly statistically significant.

To illustrate by way of a concrete example, consider the question as to which of the five factors are important for the specific response Y5 = HRMAX. We have already examined this question in Section 7.2.1 in the context of a main effects plot analysis (Figure 78 and Table 17); let us redo the analysis via a block-plot methodology. To do so, we need five block plots—one for each of the five factors under study. The vertical axis will be the mean response (for each primary factor setting) for each robustness factor condition. The first such plot has X1 (Barrier) as the primary factor and the remaining four factors (X2, X3, X4, X5) as the robustness factors. A second such block plot would have X2 (Foam) as the primary factor and the remaining four factors (X1, X3, X4, X5) as the robustness factors, and so on.

Analysis of Block 1: For the given response Y5 = HRMAX, let us consider specifically the first such block plot, which will have X1 (Barrier) as the primary factor. The Barrier factor has three levels: None, Whispershield, and Norfab. The corresponding four robustness factors (X2, X3, X4, X5) have two levels each, and, as a result, for a full factorial design, the block plot would incorporate the mean response (vertically) for each of the three settings of X1 versus each (and every) one of the $2 \times 2 \times 2 \times 2 = 16$ combinations of settings of the four remaining factors X2 to X5 (horizontally). Each of these 16 combinations creates a "block", and we are very much interested in the mean behavior of the three settings of the primary factor of interest (X1) within—not between—such blocks. The plot will in toto contain $3 \times 16 = 48$ points, 16 blocks, and three mean responses per block. In order to emphasize the goal of scrutinizing within-block-behavior (as opposed to between-block-behavior), a box (block) is drawn around the three primary factors responses for each of the 16 robustness factor setting subsets, hence the name "block" plot.

In essence, the block plot graphically juxtapositions the responses for the three settings of primary factor X1 within each given combination of settings of the four robustness factors (X2, X3, X4, X5). Again, if X1 is important, then it will have relatively large differences within each block, and (ideally) these large differences will (robustly) persist over all (or most) of the 16 blocks. This, in turn allows us—block by block—to develop a valid and rigorous global conclusion about the importance of X1. On the other hand, if X1 is in truth unimportant (= no effect), then the ordering of the primary factor levels within each block will be "random" in appearance, with no consistent behavior and, hence, no robustly-global effect.

Estimation & Testing: These within-block differences are, in reality, a local estimate of the primary factor (X1) effect—local to the particular robustness factor subset. The block plot as a whole examines the collection of these local effects and determines if their behavior is consistent and repeatable with what might be expected under the null hypothesis of "no primary factor effect",

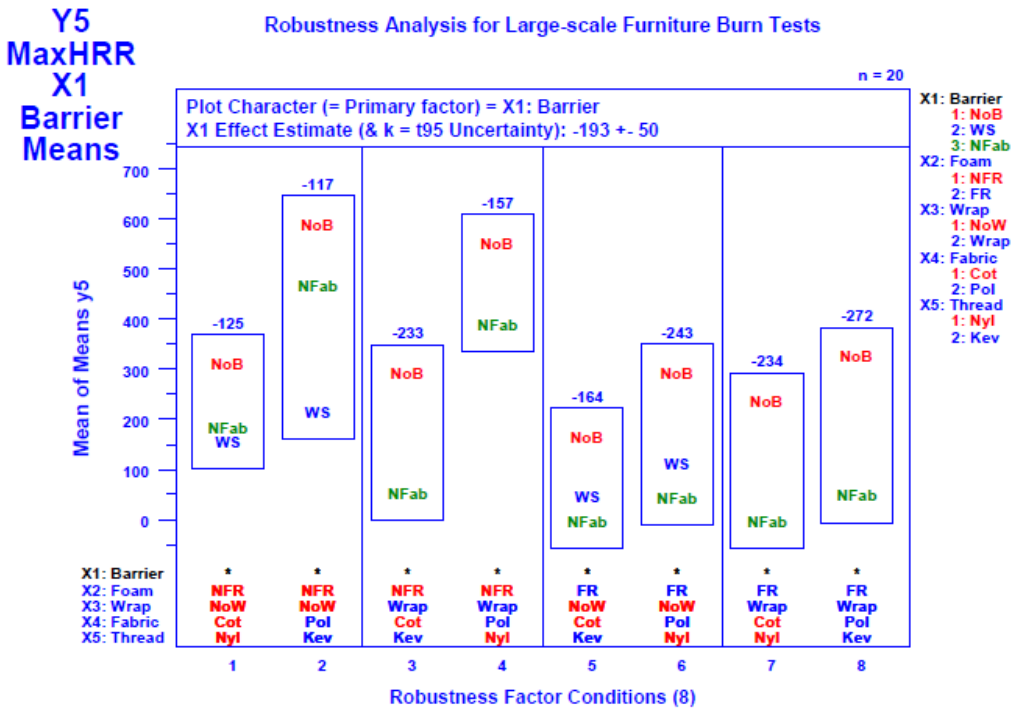

Figure 92. Response Y5 = MaxHRR Block Plot Robustness Analysis showing the means for each of the three levels of the primary factor X1 = Barrier plotted vertically versus each combination of the remaining four robustness factors plotted horizontally.

H0: Primary factor effect = 0, that is,
The response for primary factor (X1) setting 1 is statistically equivalent to the responses for primary factors setting 2 and setting 3—in other words: the factor X1 has no effect and hence is not statistically significant.

After the block plot is formed, two statistical tests may then be used to rigorously test the above null hypothesis, H0:

1. The persistency (and direction) of the response differences suggests a sign-test binomial basis for formally testing factor significance, while
2. The magnitude of the response differences suggests a paired-comparison t-test basis for formally testing factor significance.

We shall use both of these tests in our analysis, and we will compare the results with those obtained by the main effects plots (and ANOVA tests), as presented earlier.

Interactions: In addition to formal testing of significance of a primary factor, it is to be noted that another benefit accrues from use of the block plot methodology; namely, that certain patterns in the differences (that is, factor effects) across the blocks provide insight into the existence (and nature) of potential dependencies between the primary factor and one or more robustness factors—this will serve as the basis for the formal interactions analysis in Section 7.3.

Block Plot for Y5=HRMAX: Figure 92 is a block plot for Y5 = HRMAX (a response of particular engineering interest) and primary factor = X1 (Barrier). Note that although 16 robustness factor setting subsets are theoretically possible (as from the full-factorial design), due to practical constraints, the total number of runs for the full-factorial design was too expensive, and so a balanced fractionated design was

in fact executed. The positive aspect of the fractional design was that the total number of runs became affordable; the negative aspect was that "confounding" of effects (i.e., (known) multiple factors contributing to an estimated effect value) was induced (though this confounding was limited and controllable). In this case, the fractional design resulted in a net of only eight (out of the 16) unique subsets being formed. However, due to the orthogonal nature of the executed design, these eight subsets still provide a representative sampling of the robustness factor space, and so were used as the levels of the horizontal axis in the block plot. We thus will come to conclusions about the effect on Y5 within each subset, and then determine if the same conclusion is reached over all eight subsets.

In the block plot the vertical axis is the mean response for the three levels of Y5, and the horizontal axis is the eight robustness factor conditions. Thus each of the eight blocks has three computed mean values—one for each level of the primary factor X1 (Barrier). Notice that four of the blocks do indeed have three levels, but that four others have only two. The missing values are due to the design decision to exclude cushions containing both the Whispershield barrier and polyester fiber wrap from the test matrix.

Block-by-Block Interpretation: Note that for the first (= leftmost) robustness factor subset block (NFR, NoW, Cot, Nyl), that is,

X2 (Foam) = NFR (= NFRFPUF)
X3 (Wrap) = NoW (= no wrap)
X4 (Fabric) = Cot (= cotton)
X5 (Thread) = Nyl (= nylon),

the primary factor setting NoB (= No Barrier) has the highest average MaxHRR (~ 310 kW), while NFab (= Norfab) is lower (~ 180 kW) and WS (= Whispershield) is lowest (~ 150 kW).

Note also that for the second robustness factor subset/condition (NFR, NoW, Pol, Kev), the block as a whole has shifted up (it is a different condition after all)—but such between-block shifting is of no consequence to our goal of assessing X_1 (that is, within-block) differences. Here we see that the within-block pattern for block 2 is the same as that for block 1: NoB high, NFab mid, and WS low.

Scanning across the remaining six robustness blocks, we see similar—but not identical—patterns, some of which are caused by missing data, and others of which are caused by the primary factor responding differently to (that is, interacting with) different robustness factor conditions.

A close scrutiny across all of the eight robustness factor conditions does, however, identify the pattern that NoB is consistently higher than NFab for all eight combinations. Is this statistically significant? What is the chance of this happening by chance, that is, what is the chance that this persistent eight out of eight pattern could result if the three primary factor settings were in reality equivalent? (This will be addressed below).

The values listed at the tops of the boxes in Figure 92 are the differences between the average values for NFab and NoB. It would also be possible to consider similar differences between NFab and NoB with WS as with-in block effects, but we have chosen to focus only on the NFab and NoB primary factors. This definitional modification of within-block effects was adopted because data for the WS condition is missing for four of the eight blocks, while data for NoB and NFab exists for all eight blocks.

Paired-Comparison Sign Test: If the null hypothesis were true (that is NoB = NFab), then we would expect NoB to exceed NFab about half the time (= four out of eight cases), and NFab to exceed NoB about half the time. That is not the observed case here. To assess whether the observed eight out of eight is statistically significant, we note that H0 (= no effect) is probabilistically equivalent to an eight-time coin

Table 24. Response Y5 (= HRMAX): Block Plot Paired-Comparison one-tailed Sign Test p-values for Primary factor = X1 (= Barrier).

		p-value based on binomial				
		X1	X2	X3	X4	X5
		Barrier	Foam	Wrap	Material	Thread
Y5	MaxHRR	0.0039				

flip of a fair coin. The equivalent probability question is that if we flip a fair coin, note that it is something (heads, say), and then note that the remaining seven coin flips are also the same as the first flip (= heads), then what is the probability of this happening by chance? Is that probability less than the usual p-value cutoff of 0.05 commonly employed in scientific studies?

The relevant statistical test described here is the "sign test", and the underlying reference distribution is the binomial distribution with (n = eight trials and p = probability of success = 0.5). The outcome for this test is that the observed identical "NoB higher than NFab" pattern for all eight robustness subsets is $(½)^8$ or $(½)^{(8-1)}$, depending on whether the pattern is defined before observing the data or after observing the first block of data. For these cases, the probabilities are 1/256 = 0.0039 and 1/128 = 0.0078 for one-tailed and two-tailed distributions, respectively. By default and for simplicity (and with no change in conclusions), we shall use the $(½)^8$ results.) Note that both values are < 0.05 and so in this case both are statistically significant. For the case at hand, namely, Y5 (=HRMAX), the sign test thus yields the global conclusion that the factor X1 (Barrier) is statistically significant—and robustly so.

Note that the sign test is sensitive to directionality only, not to magnitude—we are counting how many times NoB > NFab, not how much larger NoB is than NFab. This makes the test conservative: if significance is concluded for a factor, we can have high confidence that the factor is in fact significant and important. On the other hand, if the test for a factor yields the conclusion "not significant", the question remains open as to whether that conclusion is reached because the factor is in reality not important or because the test is conservative? For such a case, we may prefer to use a less-conservative test (via a different approach or via more assumptions) to more aggressively test the "not significant" conclusion. The downside of approaches with more assumptions is that the validity of the conclusions is dependent on the validity of the assumptions, and so the additional task of testing such assumptions becomes a necessity. The virtue of conservative tests is that such assumptions (and the testing of such) are kept to a minimum.

The net conclusion (see Table 24) from the sign test for Y5 = HRMAX is that the primary factor X1 (Barrier) is statistically significant, and that this statement is robustly true over the observed eight settings of the four robustness factors (X2, X3, X4, X5).

Paired-Comparison t-Test: The second test (which is less conservative) takes into account the magnitude of the differences between levels of the primary factor X1 and is referred to as the "paired-comparison t-test". We visually note from Block 1 in Figure 92 that the difference between NFab (~ 180 kW) and NoB (~ 310 kW) is ~ -130 kW. Similarly, from block 2 the difference NFab - NoB is ~ 460 kW - ~ 580 kW = ~ -120 kW, from block 3 ~ 60 kW - ~ 290 kW = ~ -230 kW, and so on. If there were, in fact, no differences between NoB and NFab, then the average difference across the eight blocks would be near-zero. A (paired-comparison) t-test on these differences may be carried out to provide a second test of statistical significance for this primary factor X1 (Barrier). Note that the visual approximations (~ -130, ~ -120, ~ -230, etc.) are made exact (to the closest integer) across the top of the blocks in Figure 92, namely, -125, -117, -233, etc.)

As reported in the upper panel of the block plot in Figure 92, the average of the actual eight differences is -193 with an uncertainty of ±50. Computational details are as follows: The average (to four decimal places) is -193.1250. The computed standard deviation of the eight differences is 59.2318. The computed standard

Table 25. Response Y5 (= HRMAX): Block Plot Paired-Comparison one-tailed t-test p-values for Primary factor = X1 (= Barrier)

		P-value based on t(delta)				
		X1	X4	X2	X5	X3
		Barrier	Material	Foam	Thread	Wrap
Y5	MaxHRR	0.0000				

deviation of the average difference (= standard deviation of the eight differences / sqrt(8)) is 20.9416. The reported uncertainty (based on the 95 % confidence interval) for the average is computed as the standard deviation of the average × the 97.5 percent point for a t distribution with (8-1) degrees of freedom = 20.9416 * 2.3645 = 49.5185, then rounded to 50 as given at the top of Figure 92.

From a hypothesis testing point of view as to whether the true difference could be 0, the appropriate t-statistic = (stat – 0) / SD(stat) = (average – 0) / SD(average) = -193.1250 / 20.9416 = -9.221. This indicates that the observed mean difference of –193.1250 between NFab and NoB is more than nine standard deviations away from 0. Under the null hypothesis of no difference, this may of course happen by chance, but the probability of such is extremely small (~ 0 %). Thus the (paired-comparison) t-test here yields the (robust) conclusion that for Y5 = HRMAX, the factor X1 (Barrier) is statistically significant.

The net conclusion (see Table 25) from the paired-comparison t-test for Y5 = HRMAX is the same as that from the paired-comparison sign test (see Table 24), namely, that the primary factor X1 (Barrier) is statistically significant, and that this significance is robustly true over all of the observed eight settings of the four robustness factors (X2, X3, X4, X5). Beyond the usual main effects plot and ANOVA, this persistent behavior within the block plot, along with the block-plot-based sign- and t-tests, provides powerful support for the importance of the Barrier factor.

Other Factors for Y5: For response Y5 = MaxHRR, the next step is to generate four additional block plots to assess the significance of primary factors X2 (foam), then X3 (Wrap), then X4 (Fabric), and finally X5 (Thread), respectively. These plots are presented in Figure 93 to Figure 96.

The interpretation of most of the other factors is straightforward in the same fashion as described above. On the other hand, a minor complication does arise which bears discussion. Close inspection of Figure 93 reveals that the levels (Nyl, Kev) for the last robustness factor (thread) appear as overstrikes. This is due to an artifact of the statistical confounding intrinsic to the fact that a full-factorial design was not used. The utilized fractional-factorial design reduced the number of runs required by half but introduced such confounding effects. The net effect is that it is not possible from the Block Plot Analysis to derive explicit conclusions regarding the effect (or its interactions) of changing X5 (Thread) on Y5 (MaxHRR). Similar overstriking for thread is evident in Figure 94 and Figure 95 for primary factors Wrap and Fabric, respectively. Interestingly, in Figure 96 where the means for MaxHRR are plotted for primary factor X5 (fabric), the confounding appears for the third robustness factor (Wrap).

For each of these four figures, a block-plot-based analysis (involving a paired-sign test and a paired-t-test) was carried out in the same fashion as described above (for Barrier) to assess the significance (and robustness) of each of the additional four factors: Foam, Wrap, Fabric, and Thread. For the sign test, the results of the analysis are shown in Table 26, and the results of the t-test are shown in Table 27. As before, red indicates statistical significance at the 5 % level. Beyond the already-noted significance of X1 (Barrier), note from both tables the significance of X2 (Foam) and X4 (Fabric), and the insignificance of X3 (Wrap) and X5 (Thread).

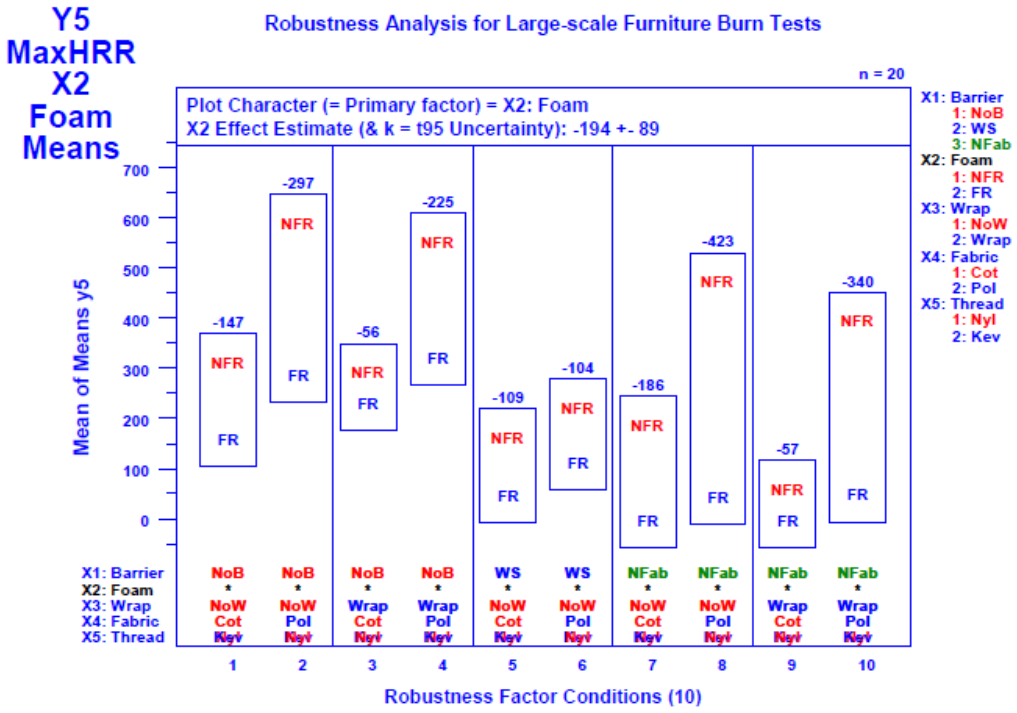

Figure 93. Response Y5 = MaxHRR Block Plot Robustness Analysis showing the means for each of the two levels of the primary factor X2 = Foam plotted vertically versus each combination of four robustness factors plotted horizontally.

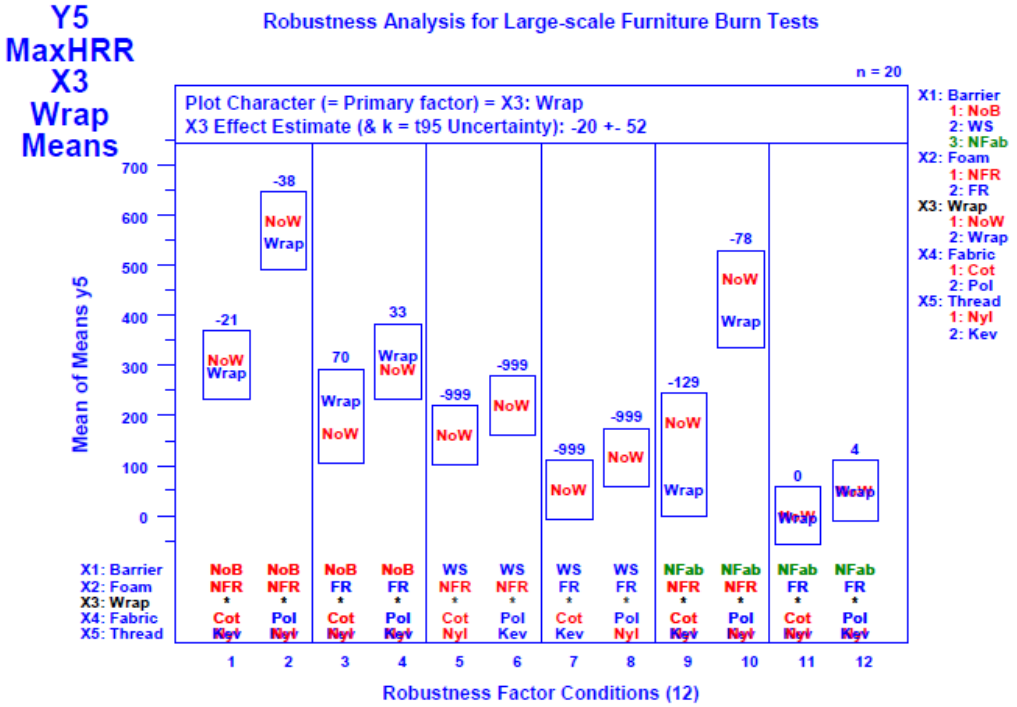

Figure 94. Response Y5 = MaxHRR Block Plot Robustness Analysis showing the means for each of the two levels of the primary factor X3 = Wrap plotted vertically versus each combination of four robustness factors plotted horizontally.

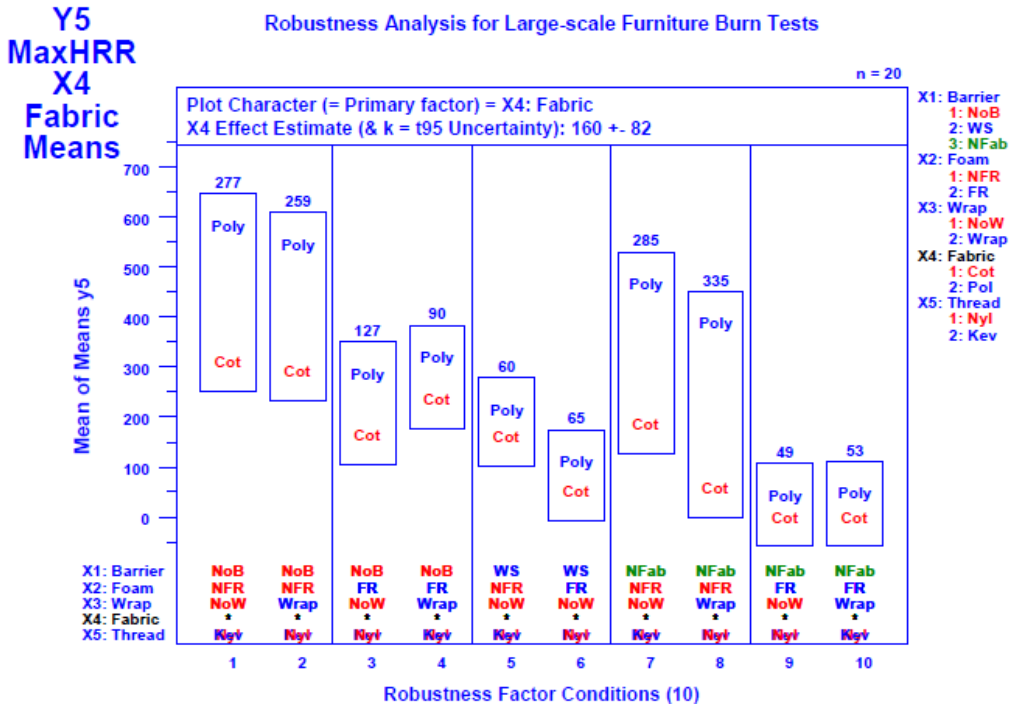

Figure 95. Response Y5 = MaxHRR Block Plot Robustness Analysis showing the means for each of the two levels of the primary factor X4 = Fabric plotted vertically versus each combination of four robustness factors plotted horizontally.

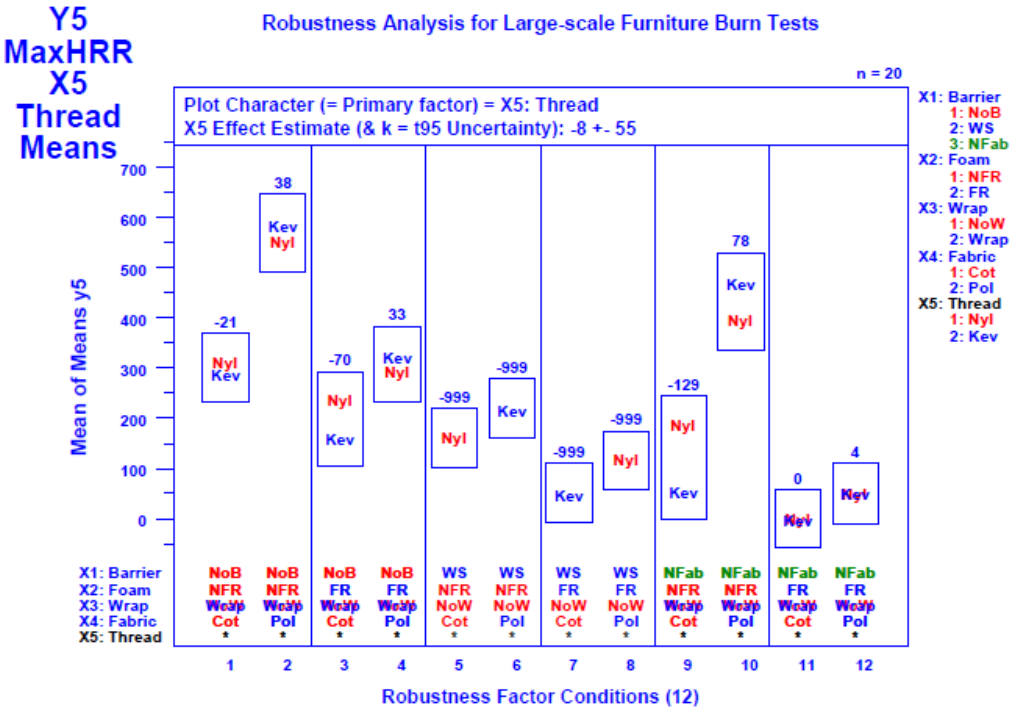

Figure 96. Response Y5 = MaxHRR Block Plot Robustness Analysis showing the means for each of the two levels of the primary factor X5 = Thread plotted vertically versus each combination of four robustness factors plotted horizontally.

Table 26. Response Y5 (= MaxHRR): Block Plot Paired-Comparison one-tailed Sign Test *p*-values for all five Primary Factors.

		P-value based on binomial				
		X1	X2	X3	X4	X5
		Barrier	Foam	Wrap	Material	Thread
Y5	MaxHRR	0.0039	0.0010	0.6367	0.0010	0.6563

Table 27. Response Y5 (= MaxHRR): Block Plot Paired-Comparison one-tailed t-Test *p*-values for all five Primary Factors.

		P-value based on t(delta)				
		X1	X4	X2	X5	X3
		Barrier	Material	Foam	Thread	Wrap
Y5	MaxHRR	0.0000	0.0004	0.1999	0.0009	0.3621

Y5 (MaxHRR) Conclusions:

X1 (Barrier):

1. Compared to NFab (Norfab barrier), NoB (no-barrier) has higher MaxHRR in all eight (X2, X3, X4, X5) cases. This (by the one-tailed sign test) is statistically significant with a p-value = 0.0039.
2. On average, the MaxHRR for NoB exceeds that of NFab by 193 kW, which (by the one-tailed t-test) is also statistically significant with a p-value < 0.0001.

X2 (Foam):

1. Compared to FR (FRFPUF), NFR (NFRFPUF) has higher MaxHRR in all 10 (X1, X3, X4, X5) cases. This (by the one-tailed sign test) is statistically significant with a p-value = 0.0010.
2. On average, the MaxHRR for NFR exceeds that of FR by 194 kW, which (by the one-tailed t-test) is also statistically significant with a p-value = 0.0004.

X3 (Wrap):

1. Compared to Wr (wrapped), NoW (no wrap) has a higher MaxHRR in four out of the eight (X1, X2, X4, X5) cases where both are present. This is not sign-test statistically significant (*p*-value = 0.6367).
2. On average, the MaxHRR for Wr exceeds that of NoW by only 20 kW, which is also not t-test statistically significant (p-value = 0.1999).

X4 (Fabric):

1. Compared to Cot (cotton), Poly (78 % polypropylene/22 % polyester) has higher MaxHRR in all 10 (X1, X2, X3, X5) cases. This (by the sign-test) is statistically significant (p-value = 0.0010).
2. On average, the MaxHRR for Poly exceeds that of Cot by 160 kW, which (by the t-test) is also statistically significant (p-value = 0.0009).

X5 (Thread):

1. Compared to Nyl (nylon), Kev (Kevlar) has higher MaxHRR in three out of eight (X1, X2, X3, X4) cases. This is not sign-test statistically significant (p-value = 0.6563).
2. On average, the MaxHRR for Kev exceeds that of Nyl by only 12 kW, which is also not t-test statistically significant (p-value = 0.3621).

Table 28. Sensitivity Analysis for each of the 13 responses showing the across-block sign test p-values for each of the five factors.

		P-value based on binomial				
		X1	X2	X3	X4	X5
		Barrier	Foam	Wrap	Material	Thread
Y1	T25kW	0.0039	0.0107	0.3633	0.0010	0.6563
Y2	T1PHRR	0.0039	0.0107	0.1445	0.0010	0.6563
Y3	1PHRR	0.0039	0.0010	0.6367	0.0107	0.6563
Y4	TMaxHRR	0.0039	0.0547	0.3633	0.0010	0.6563
Y5	MaxHRR	0.0039	0.0010	0.6367	0.0010	0.6563
Y6	TotHR	0.6367	0.0010	0.3633	0.3770	0.6563
Y7	T1Figra	0.0039	0.0547	0.1445	0.0010	0.6563
Y8	1Figra	0.0039	0.0010	0.3633	0.0010	0.3438
Y9	T2Figra	0.0039	0.1719	0.1445	0.0010	0.6563
Y10	2Figra	0.0039	0.0010	0.3633	0.0010	0.3438
Y11	LatVel	0.0039	0.0547	0.3633	0.0010	0.6563
Y12	RtArmIT	0.0039	0.1719	0.1445	0.0010	0.1094
Y13	LtArmIT	0.0352	0.0547	0.3633	0.0010	0.1094
	# Times Signif.	**12**	**7**	**0**	**12**	**0**

These conclusions are in accord with the graphical and ANOVA results of the Y5 (MaxHRR) Main Effects plot of Figure 78.

7.2.5 Main Effects and Block Plot Analyses for All 13 Responses

Factor Significance: In combination with the Main Effects analysis given in Section 7.2.1, the above section (Section 7.2.4) completes our sensitivity analysis for how each of the five factors affects the response Y5 = MaxHRR (= Max Heat Release Rate). In a similar fashion, we note what the Main Effects Plot analysis (Figure 78 to Figure 91) says about each of the remaining 12 response variables, and we carry out a detailed block-plot analysis for each of the 12 responses (Y1 to Y4, and Y6 to Y13), and (within each response) each of the five primary factors X1 to X5. This entails the generation of 12 × 5 = 60 block plots. These detailed plots yield much insight about what factors affect what responses (and how). The entire collection of 13 × 5 = 65 Block Plots is presented in Appendix E.

In like-fashion to the above, we have quantified the 13 Main Effects plots of Section 7.2.2 and the 65 block plots of Appendix E by means of p-values from three separate statistical tests:

1. Main Effects plot One-Way ANOVA test,
2. Block plot paired-comparison sign-test, and
3. Block plot paired comparison t-test.

The first such table (Main Effects plot One-Way ANOVA) was presented as Table 22 in Section 7.2.3. The Block plot sign-test results are shown in Table 28, and the t-test results are shown in Table 29.

Even though the statistical basis of the three tests is different (that is, each test is sensitive to slightly different statistical characteristics of the data), note the remarkable similarity in the conclusions across the 13 responses and the five factors. This robustness is reassuring in that it protects against the scientific conclusions being analysis-methodology-dependent. In particular, from Table 22, Table 28, and Table 29, it is concluded from all three statistical tests that:

Table 29. Sensitivity Analysis for each of the 13 responses showing the across-block paired comparison p-values for each of the five factors.

		P-value based on t(delta)				
		X1	X2	X3	X4	X5
		Barrier	Foam	Wrap	Material	Thread
Y1	T25kW	0.0055	0.0058	0.4208	0.0013	0.1901
Y2	T1PHRR	0.0133	0.0153	0.1861	0.0013	0.1858
Y3	1PHRR	0.0001	0.0024	0.4845	0.0026	0.3242
Y4	TMaxHRR	0.0083	0.0581	0.2621	0.0045	0.1912
Y5	MaxHRR	0.0000	0.0004	0.1999	0.0009	0.3621
Y6	TotHR	0.1440	0.0001	0.1718	0.2000	0.2326
Y7	T1Figra	0.0127	0.0156	0.1840	0.0007	0.2075
Y8	1Figra	0.0073	0.0178	0.3347	0.0048	0.1733
Y9	T2Figra	0.0055	0.0851	0.1549	0.0016	0.2534
Y10	2Figra	0.0057	0.0095	0.2192	0.0029	0.1397
Y11	LatVel	0.0005	0.0681	0.0674	0.0000	0.4118
Y12	RtArmIT	0.0030	0.0221	0.4255	0.0000	0.1049
Y13	LtArmIT	0.0196	0.0475	0.2658	0.0002	0.0349
	# Times Signif.	**12**	**10**	**0**	**12**	**1**

Fabric (X4) is most important and is significant for almost all responses,
Barrier (X1) is nearly as important and is significant across most responses,
Foam (X2) is next in importance and is significant across many responses,
Wrap (X3) is not important and is not significant for any response, and
Thread (X5) is least important and is not significant for any response.

Factor Effect Size: For each response, it is important to estimate the magnitude and direction of the five factor effects. We have already seen such effect estimates at the bottom of the Main Effects Plots (Figure 79 to Figure 91). We here present factor effect estimates from a Block-Plot-based analysis which confirms the factor-effect estimates based on the Main-Effects Plots. Since the Block Plot provides an estimate of the primary factor effect for each block, these local estimates may be combined to yield a consensus estimate for that primary factor effect over all of the blocks. Mathematically, the two methods (main effects and block plot) are similar, but one is in essence an average while the other is a weighted average, and since the (few) missing data points lead to unequal sample size differences within a block, the two averages may not always be identical. In any event, it is of no consequence since both methods lead to the same factor rankings and the same factor significance conclusions. In general, the Block-Plot-based estimates are more conservative and robust and hence are to be preferred. For each of the 13 responses, Table 30 presents the complete list of Block-Plot-based main effect estimates.

For each response, the five factor effects are then ranked (1 = largest in magnitude to 5 = smallest in magnitude). For each response, these rankings are presented in Table 31. Note again the dominance of Factors X4 (Fabric) and X1 (Barrier), followed next by X2 (Foam), with X3 (Wrap) and X5 (Thread) showing no importance.

7.2.6 Joint Main Effects Plot and Block Plot Analyses Conclusions

Based on the plots and the p-value tables of Sections 7.2.4 and 7.2.5, the following global sensitivity analysis conclusions about the five-factor main effects are derived for this study:

Table 30. Block-Plot-based Sensitivity Analysis for each of the 13 responses showing the robust absolute effect (= the mean absolute effect across all blocks) for each of the five primary factors. The most important factor for each response is highlighted in red.

		|Delta| =|Mean Effect|				
		X1	X2	X3	X4	X5
		Barrier	Foam	Wrap	Material	Thread
Y1	T25kW	694	392	24	730	115
Y2	T1PHRR	624	288	81	819	110
Y3	1PHRR	293	113	1	106	12
Y4	TMaxHRR	1356	421	160	1223	287
Y5	MaxHRR	193	194	20	160	12
Y6	TotHR	11.7	42.3	5.3	6.4	5.2
Y7	T1Figra	538	249	65	767	81
Y8	1Figra	1.53	0.70	0.03	1.15	0.09
Y9	T2Figra	828	237	93	902	85
Y10	2Figra	1.43	0.78	0.06	1.21	0.12
Y11	LatVel	0.058	0.020	0.021	0.145	0.004
Y12	RtArmIT	95	47	5	267	38
Y13	LtArmIT	185	80	37	370	25

Table 31. Block-Plot-based Sensitivity Analysis for each of the 13 responses showing the ranking of the robust absolute effects (where rank 1 = largest absolute effect) for each of the five primary factors.

		Ranking Based on |Mean Effect|				
		X1	X2	X3	X4	X5
		Barrier	Foam	Wrap	Material	Thread
Y1	T25kW	2	3	4	1	5
Y2	T1PHRR	2	3	5	1	4
Y3	1PHRR	1	2	5	3	4
Y4	TMaxHRR	1	3	5	2	4
Y5	MaxHRR	2	1	4	3	5
Y6	TotHR	2	1	4	3	5
Y7	T1Figra	2	3	4	1	5
Y8	1Figra	1	3	5	2	4
Y9	T2Figra	2	3	4	1	5
Y10	2Figra	1	3	5	2	4
Y11	LatVel	2	4	3	1	5
Y12	RtArmIT	2	3	5	1	4
Y13	LtArmIT	2	3	5	1	4
	Mean Rank	1.69	2.69	4.46	1.69	4.46
	Rank	1.5	3	5	1.5	4
	# Times Rank 1	4	2	0	7	0
	Rank	2	3	4.5	1	4.5

ANOVA Test: For the Main Effects Plot ANOVA test (Table 22), X4 (Fabric) is most important (being statistically significant for 12 out of 13 responses), followed by X1 (Barrier) (nine out of 13), and X2 (Foam) (six out of 13); X3 (Wrap) and X5 (Thread) are not important (0 out of 13).

Sign Test: For the Block Plot sign test (Table 28), X4 (Fabric) and X1 (Barrier) are of equal importance (being statistically significant for 12 out of 13 responses), followed by X2 (Foam) (seven out of 13); X3 (Wrap) and X5 (Thread) are not important (0 out of 13).

t-Test: For the Block Plot t-test (Table 29), the same ranking exists: X4 (Fabric) and X1 (Barrier) are of equal importance (being statistically significant for 12 out of 13 responses), followed by X2 (Foam) (10 out of 13); with X5 (Thread) and X3 (Wrap) not important (1 and 0 out of 13, respectively).

General: In summary:

X4 (Fabric) is most important,
followed closely by X1 (Barrier),
and more distantly by X2 (Foam), with
X5 (Thread) not important, and
X3 (Wrap) not important.

7.3 Interactions

7.3.1 Definition and Types of Interactions

Beyond the above sensitivity analysis, it is also of interest (for each of the 13 responses) to determine if interactions exist. A sensitivity analysis yields a ranked list for the five factors based on the magnitude of the estimated effects for each of the factors. An analysis based on the block plots also allows a determination as to whether interactions play a major role.

Interactions: By definition, no interaction between two factors Xi and Xj exists if the effect (= average change in the response) for factor Xi does not depend on the settings of factor Xj. That is, the factor Xi effect is (statistically) the same for each (and every) setting of factor Xj. We may thus speak of the factor Xi effect being approximately the same (that is, consistent and robust) regardless of the setting of Xj. Further, if no interaction between Xi and Xj exists, then the benefit accrues that the joint effect for changing both factors Xi and Xj will be additive, that is, the joint effect will be a simple addition of the Xi effect + the Xj effect.

Conversely, an interaction exists between two factors Xi and Xj if the effect for factor Xi does indeed change depending on the setting of factor Xj (and conversely the effect for Xj will change depending on the factor Xi setting). Such interactions may be small, moderate, or large; may be additive or subtractive; and may be statistically insignificant or significant.

No Interaction Example, X4*X3 (Fabric*Wrap): For a particular response, to determine if a X4*X3 interaction exists it is insightful to visually examine the X4 effect in concert with each X3 setting. For example, for response Y5 (MaxHRR), in order to determine if a X4*X3 interaction exists--a plot such as that shown in Figure 95 is of interest. Thisplot consists of 10 blocks—one for each unique combination of the robustness factors X1 (Barrier), X2 (Foam), X3 (Wrap), and X5 (Thread). This plot focuses on the primary factor X4 (Fabric), and its two levels of fabric (Cotton and Poly) are shown within each block as the mean response for the two fabrics for each of the 10 robustness factor combinations.

Let us first pose the narrow question: Does there exist an X4*X3 (Fabric*Wrap) interaction based only on the first two blocks?

As annotated above the first block, the Fabric effect (rounded to the closest integer) for this block is 277; that is, as the fabric changes from cot to poly, then the average response (MaxHRR) changes by 277 units. For the second block, the fabric effect is 259. Thus as we proceed from block 1 to block 2, the X4 = Fabric Effect changes from 277 to 259, that is, the change in the fabric effect is -18.

As it turns out, the annotation at the bottom of the horizontal axis tells us that blocks 1 and 2 both have the same X1: Barrier (namely, No Barrier), and the same X2: Foam (namely, No Fire Retardant), but differ only in that block 1 has X3: Wrap = No Wrap, while block 2 has X3: Wrap = Wrap. Note that no conclusions are possible for X5 (Thread) due to the confounding from the use of a fractional-factorial experimental design, as discussed earlier. Thus the -18 represents the change in the X4 = Fabric Effect as the X3 = Wrap Factor changes from No Wrap to Wrap; in short, -18 is the estimated X4*X3 (Fabric*Wrap) interaction based on blocks 1 and 2.

Further, it is of interest to compare the local X4*X3 effect (-18) to the grand mean of the data (~ 300) to produce a relative interaction effect. The change of -18 units thus translates into a relative change of 100*(-18/300) ~ -6 %. This is relatively small, especially when compared to the relative size of some of the main effects (such as Fabric itself with an effect of 160 (= 53.3 %))—approximately 9 times larger).

It is thus concluded that based on this first pair of blocks (blocks 1 and 2): where (X1 = Barrier = NoB = None) and (X2 = Foam = NFR = Non Fire Retardant), there is no evidence of an X4*X3 interaction.

Let us now pose the broader question: Does there exist an X4*X3 (Fabric*Wrap) interaction based on all the blocks?

Note from Figure 95 that blocks 1 and 2 are not the only pair of blocks that will yield X4*X3 (Fabric*Wrap) interaction information. In particular, X4*X3 interactions can also be estimated from:

blocks 3 and 4 (for fixed (X1,X2) = (No Barrier, Fire Retardant FPUF)),
blocks 7 and 8 (for fixed (X1,X2) = (NorFab, No Fire Retardant FPUF)), and
blocks 9 and 10 (for fixed (X1,X2) = (Norfab, Fire Retardant FPUF)).

We thus have four independent estimates of the X4*X3 interaction based on the four pairs of subsets:

blocks 1 and 2: 259 – 277 = -18 (-6.0 %),
blocks 3 and 4: 90 – 127 = -37 (-12 %),
blocks 7 and 8: 335 – 285 = 50 (17 %), and
blocks 9 and 10: 53 – 49 = 4 (1 %).

with full-precision values being -17.427, -37.250, 50.767, and 4.000.

(Note that blocks 5 and 6 were not used here because X3 = Wrap happened to not change for these two blocks—a (negative) by-product of the (positive) highly-efficient fractionated design that was utilized.)

Visual inspection of blocks 1 and 2 suggests that the vertical block size (that is, the X4 effect) is about the same for both blocks. Similarly, blocks 3 and 4 are nearly the same, as are blocks 7 and 8, as well as blocks 9 and 10. The visuals thus suggest the conclusion that the X4*X3 interaction is relatively small and relatively unimportant.

This is confirmed quantitatively: the global estimate of the X4*X3 interaction is the mean of the above $n = 4$ full-precision values (= 0.0225) (0.01 %).. These four values have a standard deviation of $s = 37.7913$, and a standard deviation of the mean = $sm = s/\text{sqrt}(n) = 37.7913/2 = 18.8957$. The 95 % confidence interval expansion factor t (based on n-1 = 4-1 = 3 degrees of freedom) is 3.1824. The uncertainty (based on a 95 % confidence interval) of this mean is $t*sm = 60.1344$. The global estimate for the X4*X3 interaction and the α = 95 % uncertainty thus becomes:

X4*X3 ± Unc (X4*X3) = 0.0225 ± 60.1344.

Since this interval does in fact cover 0, the usual t-test concludes (for this response Y5 = MaxHRR) that X4*X3 is not statistically significant. This is an example, therefore, of a no interaction case.

Interaction Details: On the other hand, by definition, an interaction between factors Xi and Xj does exist if the effect for factor Xi does indeed change markedly depending on the settings of factor Xj; that is, the factor Xi effect differs considerably for some (any, or many) of the settings of factor Xj. We may thus speak of the factor Xi effect being non-robust over the settings of Xj. The existence of interactions complicates our understanding of a physical phenomenon (such as fire), but the ability to estimate such interactions adds immeasurably to a complete understanding of the physical phenomenon under study. In a worst-case scenario, if a phenomenon has interactions, and if the analyst neglects to pursue, detect, and estimate such interactions, then the analyst's insight (and predictability) of the phenomenon will be severely limited (and inaccurate), even to the point of invalidating the formal conclusions of a study.

Further, from a mathematical perspective, if an interaction between Xi and Xj is real, then the joint response will not be additive, that is, will not be a simple summation of the Xi effect and Xj effect, and, as a result, a knowledge base limited to the main effects will be inadequate for high-accuracy, scientific prediction. Both repercussions are sufficiently serious to dictate the necessity of aggressively (and routinely) estimating/understanding system interactions.

Interaction Example: X4*X2 (Fabric*Foam): To this end, let us determine if statistically significant interactions between X4 and X2 exist for the Y5 (MaxHRR) response. In particular, in order to determine if a X4*X2 (Fabric*Foam) interaction exists let us again refer to Figure 95.

As before, let us first pose a narrow question:

Does there exist an X4*X2 (Fabric*Foam) interaction based only on blocks 1 and 3?

Blocks 1 and 3 were chosen because they both have the same X1: Barrier (No Barrier), the same X3: Wrap (no Wrap), and uniquely differ only in X2: (Foam); block 1 has Foam = Non-Fire-Retardant, but block 3 has Foam = Fire-Retardant. As before, no conclusions are possible concerning thread type.

For the first block, the X4 = Fabric effect is (as before) 277; that is, as the fabric changes from cot to poly, then the average response (MaxHRR) changes by 277 units. Note that for the third block, the fabric effect is 127. As we proceed from block 1 to block 3, the X4 = Fabric Effect changes from 277 to 127; that is, the change in the fabric effect is -150. As a point of reference, when compared to the grand data mean of ~ 300, the -150 change is roughly 50 % of the mean, which in itself is quite large, especially considering the fact that the Fabric effect itself was 160 (= 53.3 %). This suggests that the X4*X2 interaction overall may turn out to be large.

As for the broader question:

Does there exist an X4*X2 (Fabric*Foam) interaction based on all the blocks?

We note from Figure 95 that blocks 1 and 3 are not the only pair of blocks that will yield X4*X2 interaction information. In particular, a X4*X2 interaction can also be estimated from

blocks 2 and 4 (for fixed (X1,X3) = (No Barrier, Wrap)),
blocks 7 and 9 (for fixed (X1,X3) = (NorFab, No Wrap)), and
blocks 8 and 10 (for fixed (X1,X3) = (Norfab, Wrap))

Note again that blocks 5 and 6 yield no X4*X2 interaction information.

Visual inspection of blocks 1 and 3 suggests that the vertical block size (that is, the X4 effect) differs considerably across the two blocks. Similarly, blocks 2 and 4 are quite different, as are blocks 7 and 8, as well as blocks 9 and 10. The visuals thus suggest the conclusion that the X4 effect does change with (and hence does depend on) the X2 setting; that is, the X4*X2 interaction is large and important.

To confirm this, we compute the four independent estimates of the X4*X2 interaction based on the four pairs of subsets:

blocks 1 and 3: 127 - 277 = -150 (-50 %)
blocks 2 and 4: 90 - 259 = -169 (-56 %)
blocks 7 and 9: 49 - 285 = -236 (-79 %)
blocks 8 and 10: 53 - 335 = -282 (-96 %)

Exact values are -149.450, -169.273, -236.150, and -282.917.

This is confirmed quantitatively: the global estimate of the X4*X2 interaction is the mean of the above $n = 4$ values (= -209.4475) (-69.82 %). These four values have a standard deviation of $s = 61.4396$, and a standard deviation of the mean = $sm = s/\text{sqrt}(n) = 61.4396/2 = 30.7198$. The 95 % confidence interval expansion factor t (based on n-1 = 4-1 = 3 degrees of freedom) is 3.1824. The uncertainty (based on a 95 % confidence interval) of this mean is $t*sm = 97.7641$. The global estimate for the X4*X2 interaction and the α = 95 % uncertainty thus becomes:

X4*X2 ± Unc(X4*X2) = -209.4475 ± 97.7641.

Since this interval does not cover 0, then the usual t-test concludes (for this response Y5 = MaxHRR) that X4*X2 do in fact interact, are statistically significant, and the effect is -209.4475.

In summary:

For Y5 = MaxHRR, the X4 (Fabric) effect (Cot to Poly) depends on the Foam; specifically, the X4 (Fabric) effect decreases 209.4475 MaxHRR units (that is, 69.82 % on average) as we proceed from the X2 (Foam) setting of Non-Fire Retardant to the setting Fire-Retardant.

Other Two-Term Interactions Involving X4 (Fabric): For Y5 (= MaxHRR) and with focus on X4 (Fabric), the above discussion showed how two interactions (X4*X3 and X4*X2) can be interpreted and computed. Continuing in this same fashion from Figure 95, we may examine the remaining two two-term interactions involving X4, namely X4*X1 (Fabric*Barrier) and X4*X5 (Fabric*Thread).

Estimating the X4*X1 interaction involves examining each of the four pairs of blocks: 1 and 7, 2 and 8, 3 and 9, and 4 and 10. Visually, there appears to have been little change in the X4 (Fabric) effect between these four pairs. Quantitatively, it is seen that the X4 (Fabric) effect resulted in the following changes:

blocks 1 and 7: 285 – 277 = 8 (3 %)
blocks 2 and 8: 335 - 259 = 76 (25 %)
blocks 3 and 9: 49 - 127 = - 78 (26 %)
blocks 4 and 10: 53 - 90 = -37 (12%)

Exact values are 7.850, 76.044, -78.850, -36.750.

The global estimate of the X4*X1 interaction is the mean of the above n = 4 values (= -7.9265) (-2.64 %). These four values have a standard deviation of s = 66.2341, and a standard deviation of the mean = sm = s/sqrt(n) = 66.2341/2 = 33.1171. The 95 % confidence interval expansion factor t (based on n-1 = 4-1 = 3 degrees of freedom) is 3.1824. The uncertainty (based on a 95% confidence interval) of this mean is t*sm = 105.3933. The global estimate for the X4*X1 interaction and the α = 95 % uncertainty thus becomes

X4*X1 ± Unc(X4*X1) = -7.9265 ± 105.3933.

This interval covers 0, and so the t-test leads to the conclusion (for this response Y5 = MaxHRR) that X4*X1 is not statistically significant.

X4*X5 (Fabric*Thread) Interaction: The remaining two-term interaction involving X4 (Fabric) is X4*X5 (Fabric*Thread). Due to a confounding by-product of the design's fractionation, we cannot estimate the X4*X5 interaction from Figure 95 directly. As an alternative, we here utilize the plot shown in Figure 96, which has the primary factor = X5 (Thread) and has the 12 combinations of the remaining four factors on the horizontal axis.

To estimate the X4*X5 interaction (which is conceptually identical to X5*X4 interaction), we compute the change in the X5 factor effect as the X4 (Fabric) factor proceeds from Cot to Poly; from Figure 96:

blocks 1 and 2: 38 - (-21) = 59 (19 %)
blocks 3 and 4: 33 - (-70) = 103 (34 %)
blocks 9 and 10: 78 - (-129) = 207 (69 %)
blocks 11 and 12: 4 - 0 = 4 (1 %)

Exact values are 59.027, 103.150, 207.033, 4.000.

The global estimate of the X4*X5 = X5*X4 interaction is the mean of the above n = 4 values (= 93.3025) (31.10 %). These four values have a standard deviation of s = 85.9871 and a standard deviation of the mean = sm = s/sqrt(n) = 85.9871/2 = 42.9936. The 95 % confidence interval expansion factor t (based on n-1 = 4-1 = 3 degrees of freedom) is 3.1824. The uncertainty (based on a 95 % confidence interval) of this mean is t*sm = 136.8247. The global estimate for the X4*X5 interaction and the α = 95 % uncertainty thus becomes:

X4*X5 ± Unc(X4*X5) = 93.3025 ± 136.8247.

This interval does cover 0, and so the t-test leads to the conclusion (for this response Y5 = MaxHRR) that X4*X5 is not statistically significant.

In summary, we have for response Y5 = MaxHRR the following results for those two-term interactions involving X4 (Fabric):

Table 32. For Response Y5 (= MaxHRR): block-plot-based estimates (rounded to two place) of the 10 unique two-term interactions for the five primary factors.

Effect	95% Unc	Significant? (yes/no)
X2*X4	-209.45 ± 97.76	yes
X2*X3	93.30 ± 39.91	yes
X1*X3	-61.79 ± 56.43	yes
X4*X5	93.30 ± 136.82	no
X1*X2	-70.34 ± 95.53	no
X1*X5	-6.74 ± 126.17	no
X1*X4	-8.14 ± 105.59	no
X3*X4	0.02 ± 60.13	no
X2*X5	0.02 ± 144.03	no
X3*X5	non-estimable	

Table 33. For response Y5 (= MaxHRR): block-plot-based estimates (with highlights) of the five main effects and the 10 unique two-term interactions for the five primary factors. Statistically significant effects are highlighted in red.

		Main Effects					2-Term Interactions									
		1	2	3	4	5	12	13	14	15	23	24	25	34	35	45
		Barr	Foam	Wrap	Fab	Thr										
Y5	Effect	-193	-194	-20	160	-8	-70	-62	-8	-7	93	-209	0	0	na	93
	Unc(Effect)	50	89	52	82	55	96	56	106	126	40	98	144	60	na	137

X4*X2 (Fabric*Foam): -209.4475 ± 97.7641 (is statistically significant),
X4*X5 (Fabric*Thread): 93.3025 ± 136.8247 (not statistically significant)
X4*X3 (Fabric*Wrap): 0.0225 ± 60.1344 (not statistically significant)
X4*X1 (Fabric*Barrier): -7.9265 ± 105.3933 (not statistically significant)

In a similar fashion, just as the above approach estimated the four (two-term) interactions involving X4 (Fabric), so too, the four (two-term) interactions involving X1 (Barrier) can be estimated, as well as the four interactions involving X2 (Foam), the four interactions involving X3 (Wrap), and the four interactions involving X5 (Thread).

There are thus five factors × four two-term interactions per factor = 20 two-term interactions in toto. On the other hand, since the Xi*Xj interaction is identical to the Xj*Xi interaction, there are only 10 two-term interactions which are unique.

For the response Y5 = MaxHRR, the 10 interactions are derived from the five block plots of Figure 92 to Figure 96 and are presented in Table 32.

An alternate tabular summary of the Y5 results is shown in Table 33 which includes not only the 10 two-term interactions, but also the five main effects. The top line is the effect estimate. The bottom line is the α = 95 % uncertainty. Statistically significant effects are indicated in red.

7.3.2 Block Plot Interactions Analysis for All 13 Responses

An interaction analysis for the remaining 12 responses is carried out in a similar fashion. For each response, five Block Plots (one for each of five primary factors) are generated. The 5×13 = 65 Block Plots are shown in Appendix E and summary tables for each response similar to Table 32 are provided in Appendix F. For

Table 34. Main effects and two-term interaction effects (and uncertainties) for all 13 responses. For a given response, the first row is the estimated effect and the second row is the estimated 95 % confidence interval. Cells highlighted in red are statistically significant at the 5% level.

	Main Effects						2-Term Interactions									
	1	2	3	4	5	Response	12	13	14	15	23	24	25	34	35	45
	Barr	Foam	Wrap	Fab	Thr											
Effect	694	392	24	-730	22	Y1	282	79	-930	18	-329	-364	-263	-263	na	-329
Unc(Effect)	479	281	277	403	277	T25kW	580	819	580	831	585	89	603	585	na	604
	624	288	81	-819	90	Y2	215	215	-1076	168	-158	-507	-104	-104	na	-158
	527	255	201	447	198	T1PHRR	602	544	626	598	539	622	600	566	na	575
	-293	-113	-1	106	-7	Y3	138	-39	-145	-17	77	-80	17	17	na	77
	102	69	44	66	43	1PHRR	177	74	183	98	53	175	91	69	na	79
	1356	421	160	-1223	160	Y4	498	411	-1919	279	-608	-943	-468	-468	na	-608
	1024	548	565	833	565	TMaxHRR	1657	1577	1664	1672	1306	1410	1429	1315	na	1420
	-193	-194	-20	160	-8	Y5	-70	-62	-8	-7	93	-209	0	0	na	93
	50	89	52	82	55	MaxHRR	96	56	106	126	40	98	144	60	na	137
	-12	-42	-5	6	-6	Y6	-35	-17	34	-15	7	-14	6	6	na	7
	24	15	12	16	12	TotHR	28	29	28	32	36	35	37	36	na	37
	538	249	65	-767	68	Y7	107	181	-939	140	-111	-415	-67	-67	na	-111
	449	221	160	386	159	T1Figra	455	451	465	498	439	454	491	449	na	481
	-1.53	-0.70	-0.03	1.15	0.07	Y8	1.33	-0.01	-1.94	-0.13	0.21	-0.97	-0.14	-0.14	na	0.21
	1.12	0.64	0.16	0.8	0.15	1Figra	1.55	0.42	1.57	0.34	0.40	1.56	0.31	0.46	na	0.22
	828	237	93	-902	71	Y9	-14	243	-1147	153	-174	-676	-80	-80	na	-174
	571	360	200	513	207	T2Figra	894	533	868	636	523	862	629	477	na	664
	-1.43	-0.78	-0.06	1.21	0.09	Y10	1.14	-0.07	-1.79	-0.08	0.26	-1.11	-0.18	-0.18	na	0.26
	1	0.62	0.18	0.76	0.17	2Figra	1.24	0.28	1.26	0.26	0.37	1.28	0.34	0.43	na	0.27
	-0.06	-0.02	-0.02	0.15	0	Y11	0.006	-0.009	-0.035	-0.004	0.022	-0.045	-0.043	-0.043	na	0.022
	0.03	0.03	0.03	0.03	0.03	LatVel	0.080	0.076	0.035	0.077	0.075	0.033	0.079	0.019	na	0.107
	95	47	-5	-267	-25	Y12	-32	-24	-106	-41	49	-82	77	77	na	49
	58	45	55	61	51	RtArmIT	85	115	112	98	123	119	93	143	na	58
	185	80	-37	-370	41	Y13	13	-94	-296	141	-67	-176	128	128	na	-67
	173	97	132	148	131	LtArmIT	349	416	359	369	373	309	324	383	na	312

na: not available

each set of five, the main effects (as discussed in Section 7.2.5 is a "free" Block Plot by-product) may be estimated but will be near-identical to the Main Effects results, but this section rather focuses on and discusses what two-term interaction effects may exist. (Note that the minor differences in the presented effects are due to algorithmic nuances and rounding, but have no effect on our significance conclusions about the factors and interactions.) From Appendix F we extend the Y5 (MaxHRR) summary tables above (Table 33) to derive the summary table shown in Table 34, which encompasses all 13 responses.

7.3.3 Block Plot Interactions Analysis Conclusions

The main conclusions from Table 34 and Section 7.3 are as follows:

1. The interaction between X1 (Barrier) and X4 (Fabric) is most important. The Barrier*Fabric interaction is statistically significant for nine out of the 13 responses. In 10 out of the 13 responses, Barrier*Fabric is the dominant interaction and is statistically significant in seven out of those 10.

2. The interaction between X2 (Foam) and X4 (Fabric) is the next most important. The Foam*Fabric interaction is statistically significant in three out of the 13 cases. For two (Y5 and Y11) out of the 13 responses, Foam*Fabric is most important, and both of these cases are statistically significant.

3. The common element in both of the above interaction pairs is Fabric. The presence of one Fabric or the other leads to changes (mostly significant) in the Barrier effect and/or the Foam effect for almost all of the 13 responses.

4. The five-factor system is dominated both in interactions and main effects by the triad (X4: Fabric, X1: Barrier, and X2: Foam). Of their three two-term interactions, X4*X1 is most important, X4*X2 is next most important, and X1*X2 is least important.

7.4 Optimization

It is of interest to determine the best (and worst) settings for the five factors, and to determine general characteristics of those best settings with respect to the already-known dominance of three of the five factors (Barrier, Foam, Fabric). From the sensitivity analysis of the Main Effects Plots of Section 7.2 not only were the most important factors determined, but it is also possible to identify what the best settings (based on the averages) would be and whether these best average settings agree with the best settings (based on the observed data base). This the focus of the following.

7.4.1 The Design

To this end (for each of the 13 responses), we examined the individual response values for each of the 45 burns conducted during this experimental series. This total (= 45) number of tests was arrived at as summarized here: each experiment was based on the settings of five factors: barrier, foam, wrap, fabric, and thread, with one of the factors (barrier) having three levels, and all of the remaining factors having two. A full-factorial design (no replication) would have required $3 \times 2 \times 4 = 48$ distinct combinations, but this was judged to be unachievable due to both physical and time constraints. A balanced- (half-) fractional factorial design was chosen which reduced the number of combinations from 48 to 24.

Further, prior to the execution of the experiments, a decision was made to exclude combinations incorporating both a high-loft fire barrier and the polyester fiber wrap, with the result that of the 48 possible combinations, a total of 20 distinct combinations were considered.

In addition, in deference to the intrinsic natural variability in the responses, replication (ideally three reps) in the design was deemed a necessity. Again, in order to reduce the total number of tests, the number of reps was limited in many cases to two. Ultimately, 15 of the 20 unique conditions were repeated twice, while five conditions had three replications (an extra experiment was preformed when no valid mass measurements were available from the initial two tests), thus yielding the total number of experiments of $15 \times 2 + 5 \times 3 = 45$. These 45 burns were conducted in a constrained-random fashion over two test periods, with the original planned forty test completed over a three-week time frame and the final five tests performed roughly four months later over a single week.

For each of the 45 tests, 13 variables were chosen as potentially characterizing both fire spread and fire growth behaviors were chosen for statistical analysis, and hence a summary data matrix was formed consisting of 45 rows and 13 columns. These 45 rows represented a near-orthogonal sampling of the five original factors.

For a given response, the following optimization questions can be asked:

1. What were the best run combinations (out of the 45) and hence the best factor combinations (out of the 20)? (Similarly, what were the worst?), and, based on the answers for question 1,

2. Do any of the factor settings (and combinations of factor settings tend to robustly dominate—across all 13 responses—these best (worst) combinations?

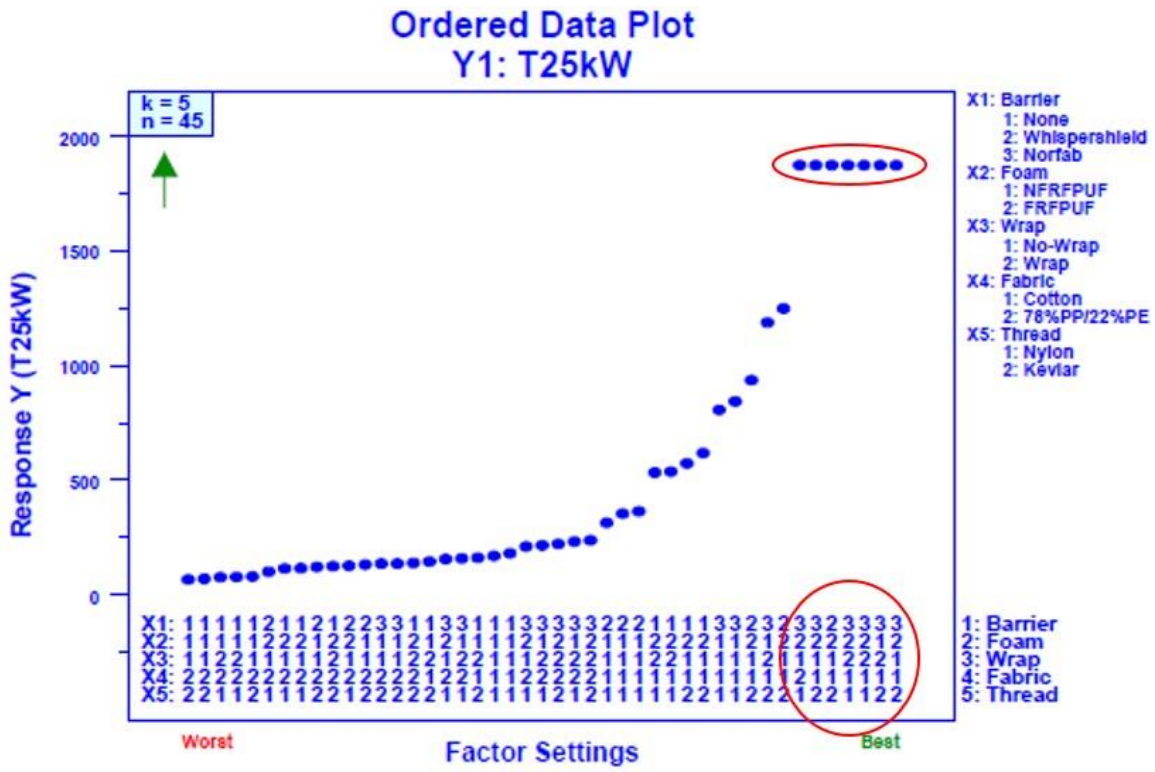

Figure 97. Response Y1 = T25kW Ordered Data Plot to determine the optimal settings of the five factors (and secondarily, to assess important factors).

7.4.2 Ordered Data Plot Analysis for All 13 Responses

For question 1 (for a given response what was the best run?), we employ a Pareto-chart-related graphical methodology which consists of the ordering (smallest to largest) of the response for the 45 runs (and five-factor settings) as shown in Figure 97 for the Y1 (= T25kW) response.

The vertical axis is the measured response; the horizontal axis is the corresponding "carry-along" factor settings for the 45 combinations. For a given response we first define and note what is "best"—large values or small values. For some responses (e.g. Y1 = T25kW = time required to reach a HRR of 25 kW), large values (= long times) would be best because it suggests a slower developing fire. For other responses (e.g., Y5 = MaxHRR = maximum heat release rate) small values (= smaller max HRR) would be better because it suggests a smaller fire. For a given response, this optimum direction (large or small) is indicated by a green arrow (up or down) inside the left margin of the plot. Figure 97 indicates an up arrow for the response Y1 (T25kW).

Given this optimal (up/down) direction, we then determine the best combination that yields the single best value out of the 45. We compare this best response setting with the best (on-the-average) settings that were obtained from the Main Effects Plot analysis of Section 7.2.2. We also note not only the best single setting, but also the characteristics of the settings in the best (and near-best) neighborhood. In particular, we note if any single factor setting yielded the best response, the best five responses, or the best 10 responses. In a similar fashion, we note the best consistent (if existent) combination of factors (pairs and triples) that may yield near-best responses. We also note the same for the worst responses and compare to see if the factor settings are opposite one another, best to worst.

Response Y1 (T25kW) For the response Y1 = T25kW of Figure 97, the largest observed value is Y1 ~ 1800. Seven settings tied for this best Y1 setting (see the upper circle in Figure 97). It should be

recalled that this value was assigned to tests in which minimal burning was observed, and HRRs did not attain 25 kW. In effect, the actual values could be considered to be infinity. From this figure we note one such factor (rightmost column) setting is (3,2,1,1,2), that is:

(X1=3, X2=2, X3=1, X4=1, X5=2) or
(Norfab Barrier, FRFPUF Foam, No-Wrap, Cotton Fabric, Kevlar Thread).

We also note the seven Y1 ~ 1800 responses are dominated by X1 (= 3 = Norfab Barrier), X2 (= 2 = FRFPUF Foam), and X4 (= 1 = Cotton Fabric), with six X1 = 3 occurrences, six X2 = 2 occurrences, and six X4 = 1 occurrences, respectively. Thus, in short, Barrier, Foam, and Fabric were the controlling factors in optimizing Y1, with the best settings being

(X1 = Norfab Barrier, X2 = FRFPUF Foam, X4 = Cotton Fabric)

Similarly, the worst (= smallest T25kW) setting is from

(X1=1, X2=1, X3=1, X4=2, X5=2) in particular, and
(X1=1, X2=1, X4=2) in general, that is,
(No Barrier, NFRFPUF Foam, 78%PP/22%PE Fabric).

Note further the consistency of factors X1, X2, and X4 in this worst neighborhood, with (X1, X2, X4) = (1,1,2) prevailing. Finally, note especially the dominance of X4 = 2, which occurs for the worst 15 Y1 responses.

Hence the best response is dominated by (X1=3, X2=2, X4=1), and the worst response is dominated by the same three factors but with opposite settings: (X1=1, X2=1, X4=2).

Visual inspection allowed us to derive these "important-factor" conclusions. Two quantitative methods may also be used to confirm these conclusions:

1. Method 1 = number of runs and
2. Method 2 = length of longest run,

where a run is a string of contiguous identical settings of a factor, as we proceed left to right across the factors settings.

Method 1. Number of Runs: For each of the five factors, compute the number of runs out of the 45, thus, for example, in Figure 97, the sequence of runs for X1 is five 1's, followed by a 2, followed by two 1's, followed by a 2, followed by a 1, followed by two 2's, followed by two 3's, etc., which in toto yields 20 such "runs". Factor X4 is simpler: 15 2's, followed by a 1, followed by two 2's, followed by three 1's, followed by five 2's, followed by 12 1's, followed by a 2, followed by six 1's, thus yielding a total of eight runs. Interpretationally, unimportant factors tend to have a large number of runs; important factors tend to have a low number of runs. The maximum possible number of runs is 45, the minimum possible number of runs is 2 (or three for Barrier). From Figure 97 for Y1 (= T25kW), the ordered (best to worst) observed number of runs is:

X4 (Fabric): 8 = number or runs,
X3 (Wrap): 17,
X1 (Barrier): 20 (even with three levels),
X5 (Thread): 21, and
X2 (Foam): 22.

Table 35. Assessing dominant factors for response Y1 = T25kW: number of runs and length of longest run for each of the five factors.

	Number of Runs (Out of 45)					Length of Longest Run (Out of 45)				
Y Response	**X1 Barrier** (3)	**X2 Foam** (2)	**X3 Wrap** (2)	**X4 Fabric** (2)	**X5 Thread** (2)	**X1 Barrier** (3)	**X2 Foam** (2)	**X3 Wrap** (2)	**X4 Fabric** (2)	**X5 Thread** (2)
Y1: T25kW	20	22	17	8	21	5	6	5	15	5

From this list, it is clear that this statistic suggests that X4 (Fabric) dominates Y1, which is consistent with our visual inspection.

Method 2. Length of Longest Run: For each of the five factors, compute the length of the longest run. Unimportant factors tend to oscillate much and hence have a short length of longest run. Important factors tend to oscillate little and hence have a longer length of longest run. From Figure 97, the ordered factor list based on the length of the longest run (best to worst) would be:

X4 (Fabric): 15 = length of longest run,
X2 (Foam): 6,
X1 (Barrier): 5,
X3 (Wrap): 5, and
X5 (Thread): 5.

As before, this list also suggests that the dominant factor for Y1 is X4 (Fabric).

With regard to the question of the relative importance of the five factors on Response Y1 (= T25kW), the visual inspection of Figure 97 along with both statistical methods indicate that factor X4 = Fabric was most important via the fact it had the longest run (= contiguous values) (15) and the fewest number of runs (8)—both of which are indicators of importance and both of which are statistically significant. These findings are summarized in Table 35 with the red circles indicating the statistically significant results.

Thus, in summary for Y1, the most important factor which drives T25kW is X4 (Fabric), and the best single factor for producing high T25kW is Fabric = 1 = Cotton.

Response Y2 (T1PHRR): Figure 98 shows a similar analysis for response Y2 (T1PHRR). In this case five settings tied for best setting (~ 2000). Of these five best settings, all five had X1 = 3, four of five had X2 = 2, and all five had X4 = 1, that is, Barrier, Foam, and Fabric were (again) controlling factors for optimizing Y2 and

(X1 = Norfab Barrier, X2 = FRFPUF Foam, and X4 = Cotton Fabric)

were their best settings, with Wrap and Thread being unimportant.

Note also that the 21 highest settings for Y2 have factor X4 = Fabric = 1 = Cotton, thus indicating that Fabric is the most important factor and Cotton is the better of the two.

As for Y1, the worst setting for Y2 was (X1 = 1, X2 = 1, X3 = 1, X4 = 2, X5 = 2), that is,

(No Barrier, NFRFPUF, No-Wrap, 78%PP/22%PE Fabric, Kevlar Thread).

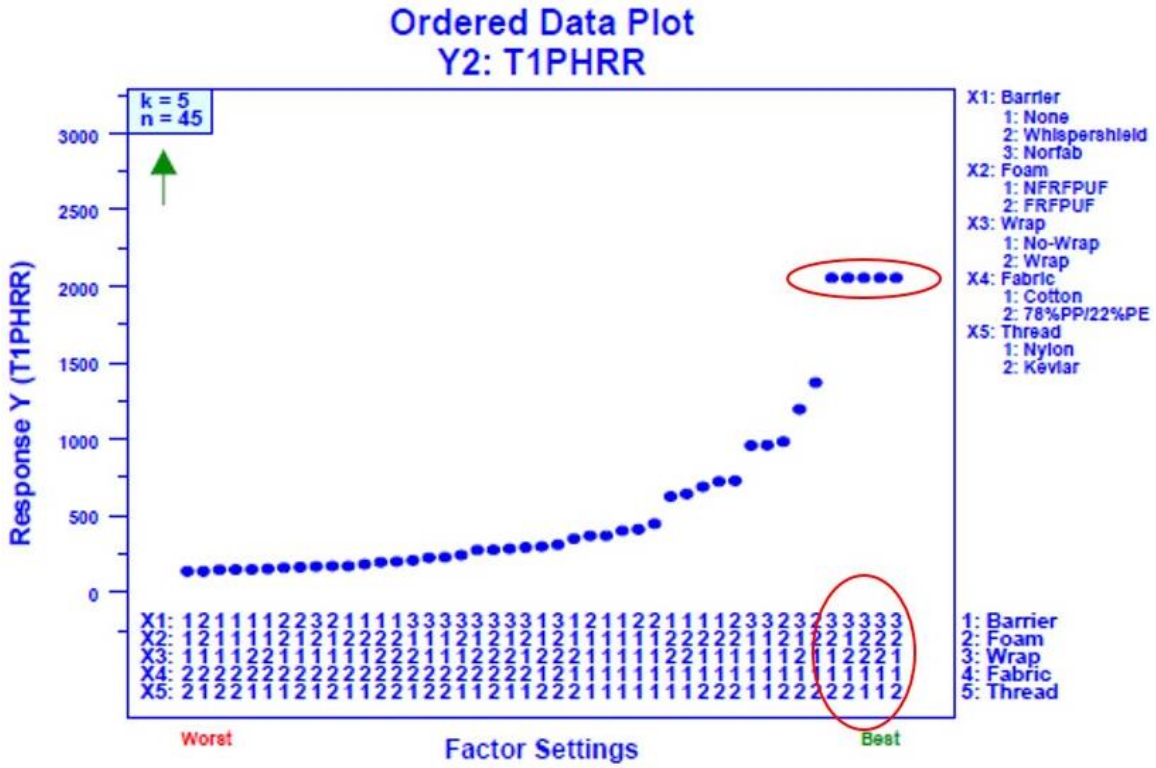

Figure 98. Response Y2 = T1PHRR Ordered Data Plot to determine the optimal settings of the five factors (and secondarily, to assess important factors).

The six worst settings had five out of six with X1 = 1, five out of six with X2 = 1, and six out of six with X4 = 2, and hence were dominated by

(X1 = 1 = No Barrier, X2 = 1 = NFRFPUF , and X4 = 2 = 78%PP/22%PE Fabric),

with Wrap and Thread being unimportant, as before.

Regarding the relative importance of the five factors, note again that factor X4 was most important as evidenced by the fact that out of the 45 data points, factor X4 = Fabric had only four changes and had a longest run of 22--both statistically significant.

The run statistics for responses Y1 and Y2 are summarized in Table 36.

Responses Y3 to Y13: Ordered data plots for the remaining 11 responses are shown in Figure 99 to Figure 109. Values for the number of runs and the length of longest run are summarized in Table 37 for each of the five factors and the 13 responses.

For Table 37, in the Number of Runs section, when the number is small, this implies factor significance. We have encircled those cases (6 responses) where the number of runs was extremely small (≤4). Note that in five out of these six, the smallest values were for Factor X4 (= fabric).

In the Length of the Longest Run section, factor significance is implied when such lengths are large. In Table 37 those cases (9) with extremely long run lengths are circled in red. In seven out of these nine cases, they occurred for Factor X4 (Fabric).

Table 36. Assessing dominant factors for response Y1 = T25kW and Y2 = T1PHRR: number of runs and length of longest run for each of the five factors.

	Number of Runs (Out of 45)					Length of Longest Run (Out of 45)				
Y Response	X1 Barrier (3)	X2 Foam (2)	X3 Wrap (2)	X4 Fabric (2)	X5 Thread (2)	X1 Barrier (3)	X2 Foam (2)	X3 Wrap (2)	X4 Fabric (2)	X5 Thread (2)
Y1: T25kW	20	22	17	8	21	5	6	5	15	5
Y2: T1PHRR	21	24	15	4	21	8	6	6	22	7

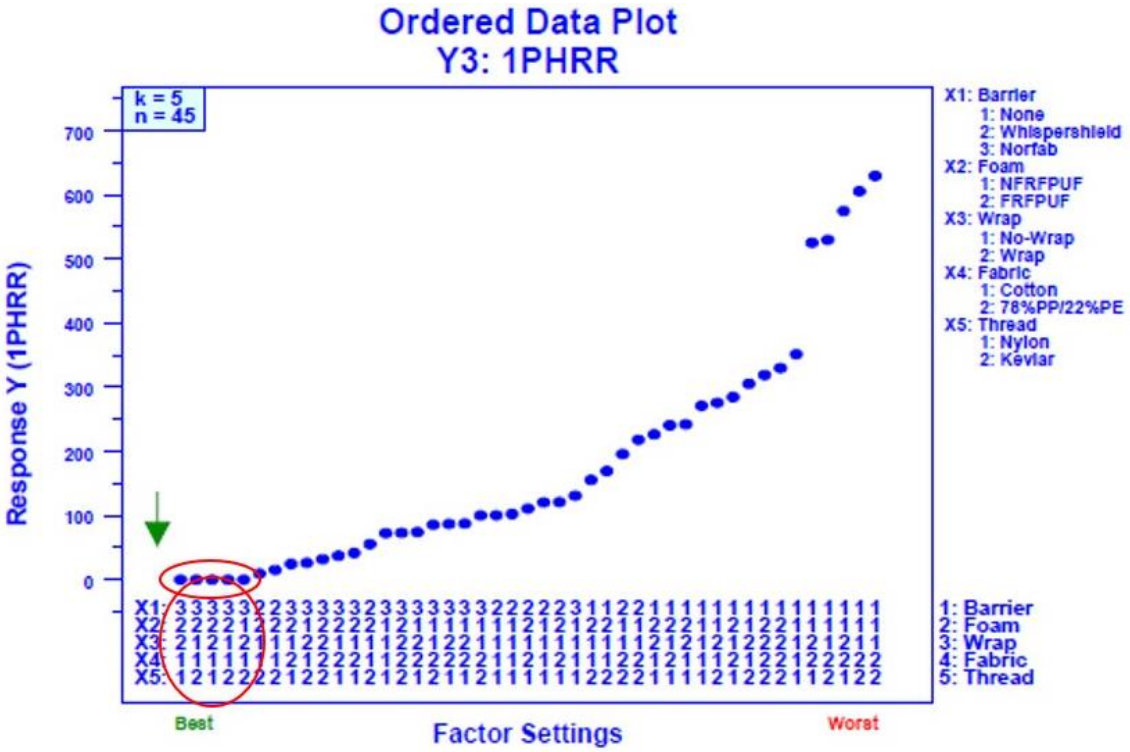

Figure 99. Response Y3 =1PHRR Ordered Data Plot to determine the optimal settings of the five factors (and secondarily, to assess important factors).

In Table 38 the results in Table 37 have been resorted based on the ordering of values for the dominant factor X4 (Fabric). For the Number of Runs Section, Fabric is the dominant factor in 10 out of the 13 responses, and especially so for Y7 (T1Figra), Y11 (LatVel), Y2 (T1PHRR), Y12 (RtArmIT), Y13 (LtArmIT) Y9 (T2Figra) and Y1 (T25kW). A notable exception was Y6 (TotHR), which had X2 (Foam) as the dominant factor.

When the Length of Longest Run was ordered in the same way, the values for Fabric were largest (again) in 10 out of the 13 responses, and especially so for Y7 (T1Figra), Y11 (LatVel), Y2 (T1PHRR), Y12 (RtArmIT) Y13 (LtArmIT), and Y9 (T2Figra). As before, Y6 (TotHR) was an exception in that it was dominated by X2 (Foam).

The best settings for each factor for each response are given in Table 39.

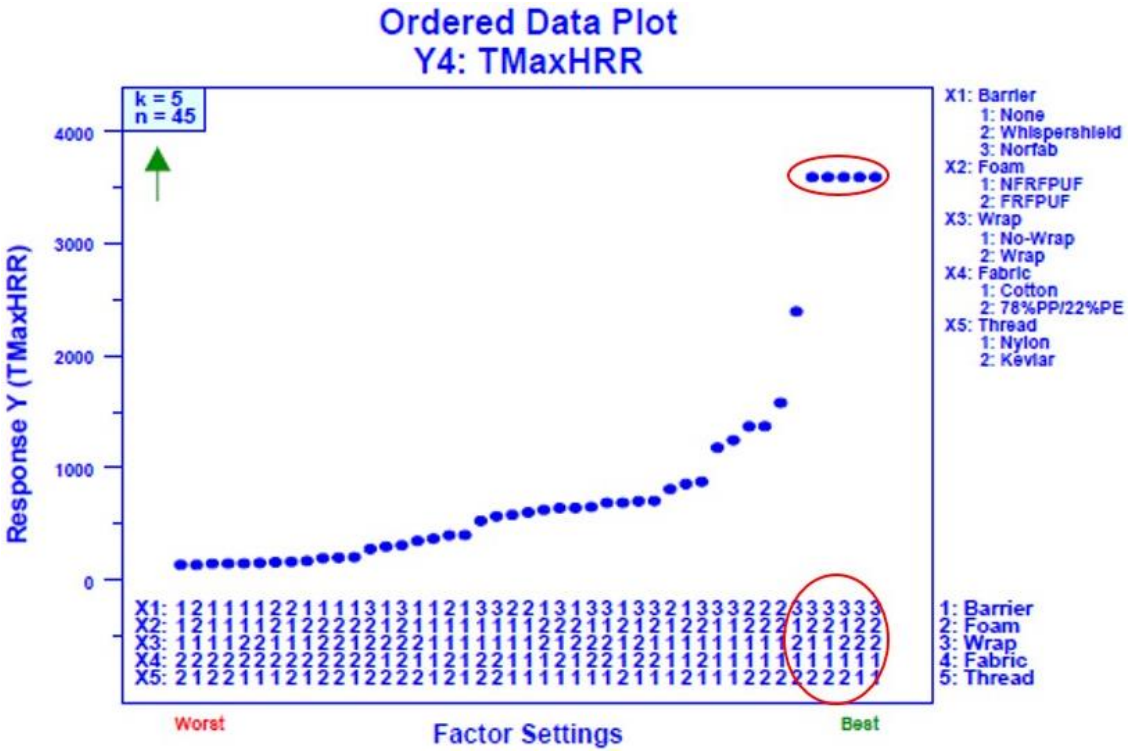

Figure 100. Response Y4 = TMaxHRR Ordered Data Plot to determine the optimal settings of the five factors (and secondarily, to assess important factors).

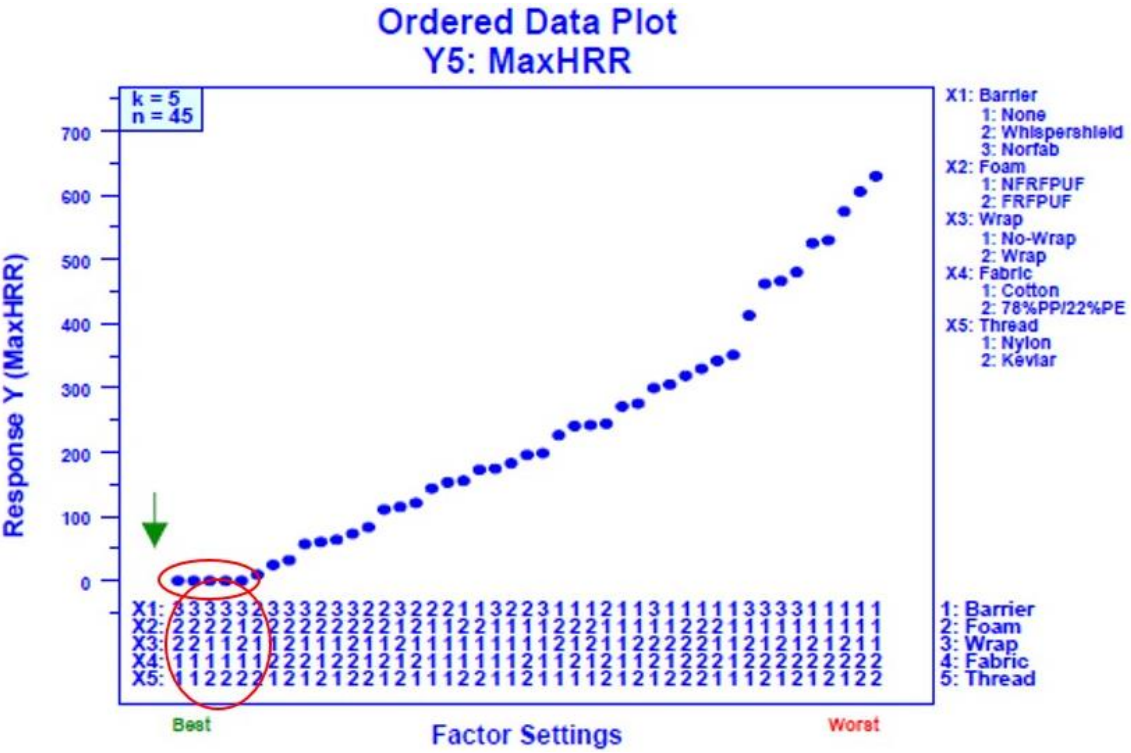

Figure 101. Response Y5 = MaxHRR Ordered Data Plot to determine the optimal settings of the five factors (and secondarily, to assess important factors).

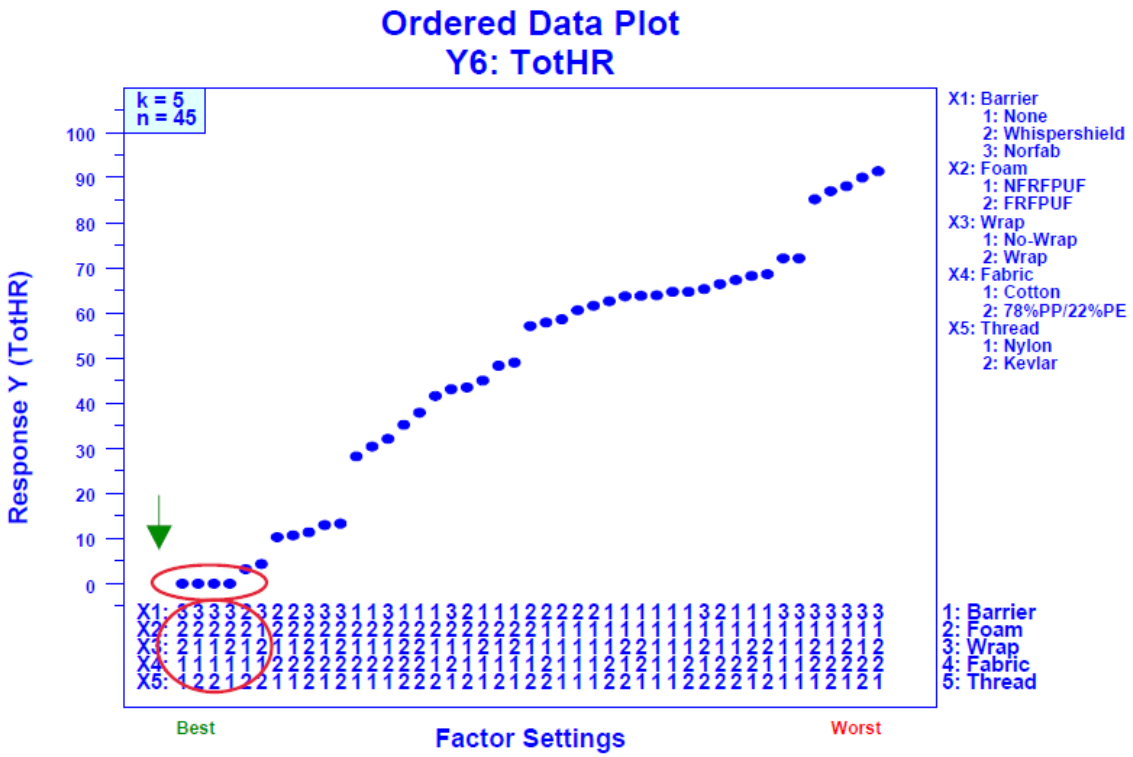

Figure 102. Response Y6 = TotHR Ordered Data Plot to determine the optimal settings of the five factors (and secondarily, to assess important factors).

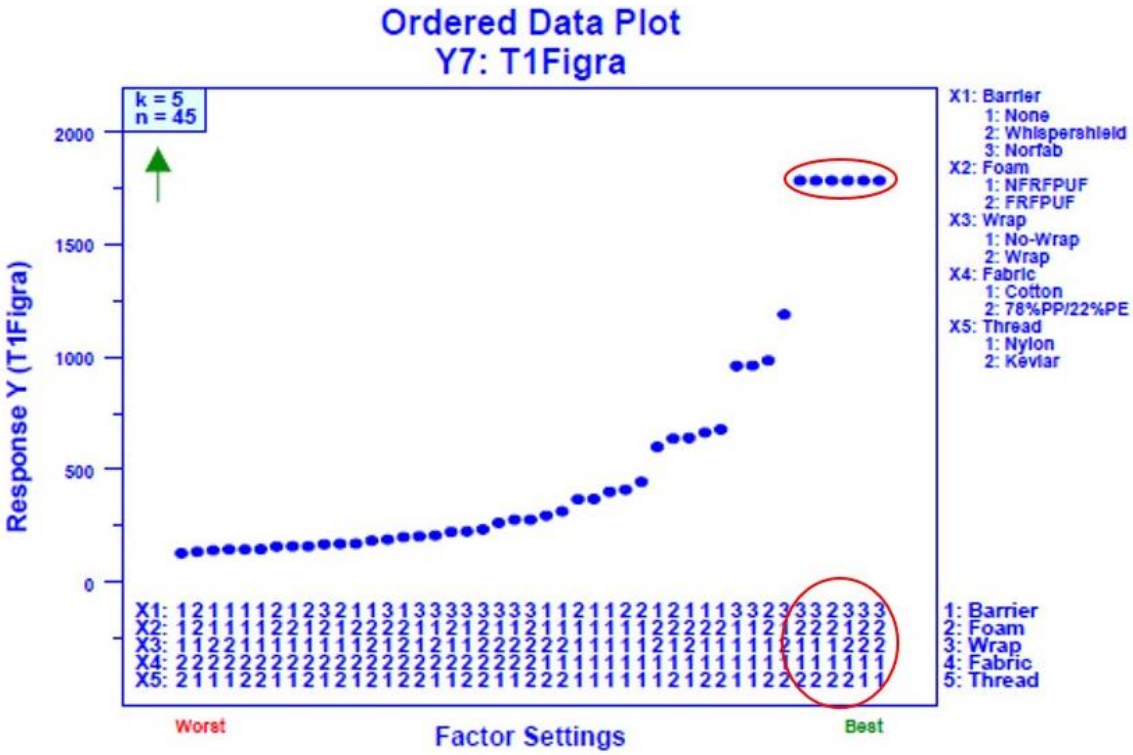

Figure 103. Response Y7 = T1Figra Ordered Data Plot to determine the optimal settings of the five factors (and secondarily, to assess important factors).

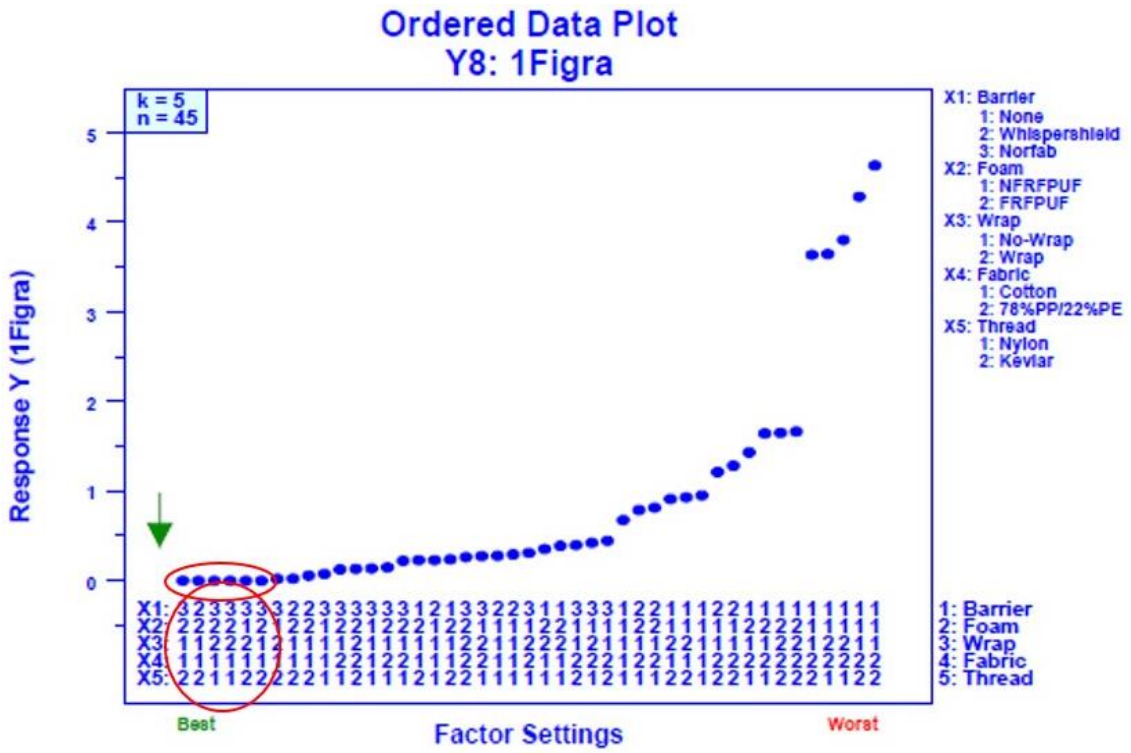

Figure 104. Response Y8 = 1Figra Ordered Data Plot to determine the optimal settings of the five factors (and secondarily, to assess important factors).

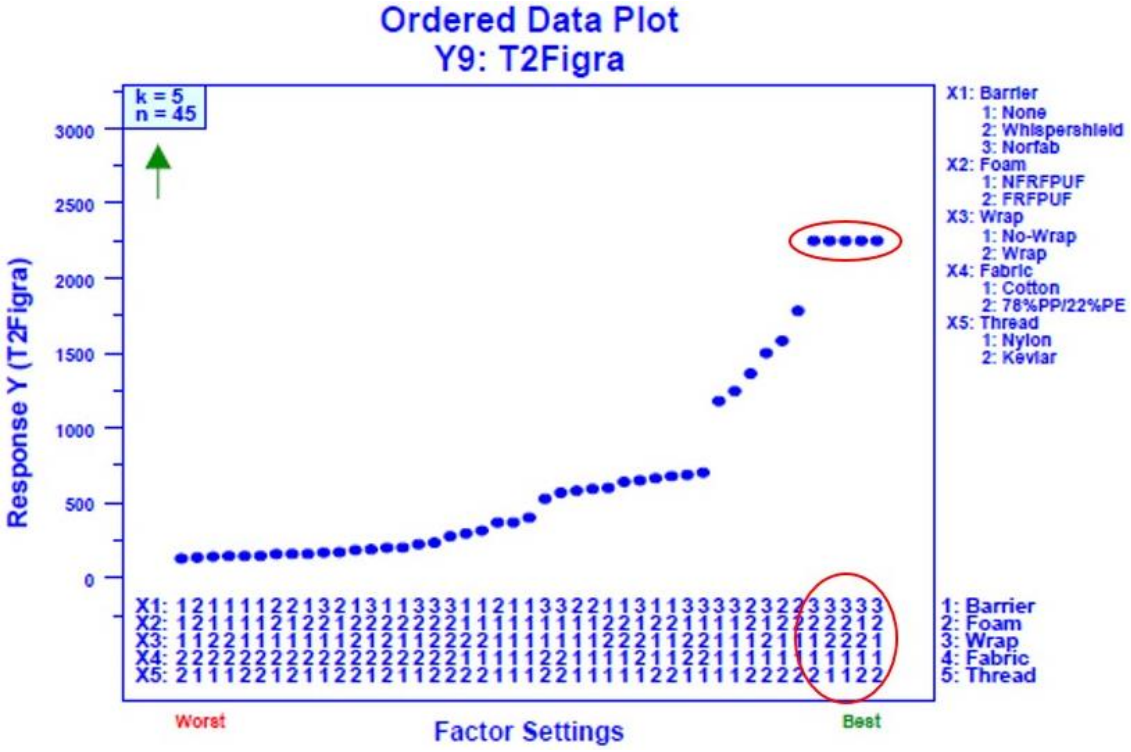

Figure 105. Response Y9 = T2Figra Ordered Data Plot to determine the optimal settings of the five factors (and secondarily, to assess important factors).

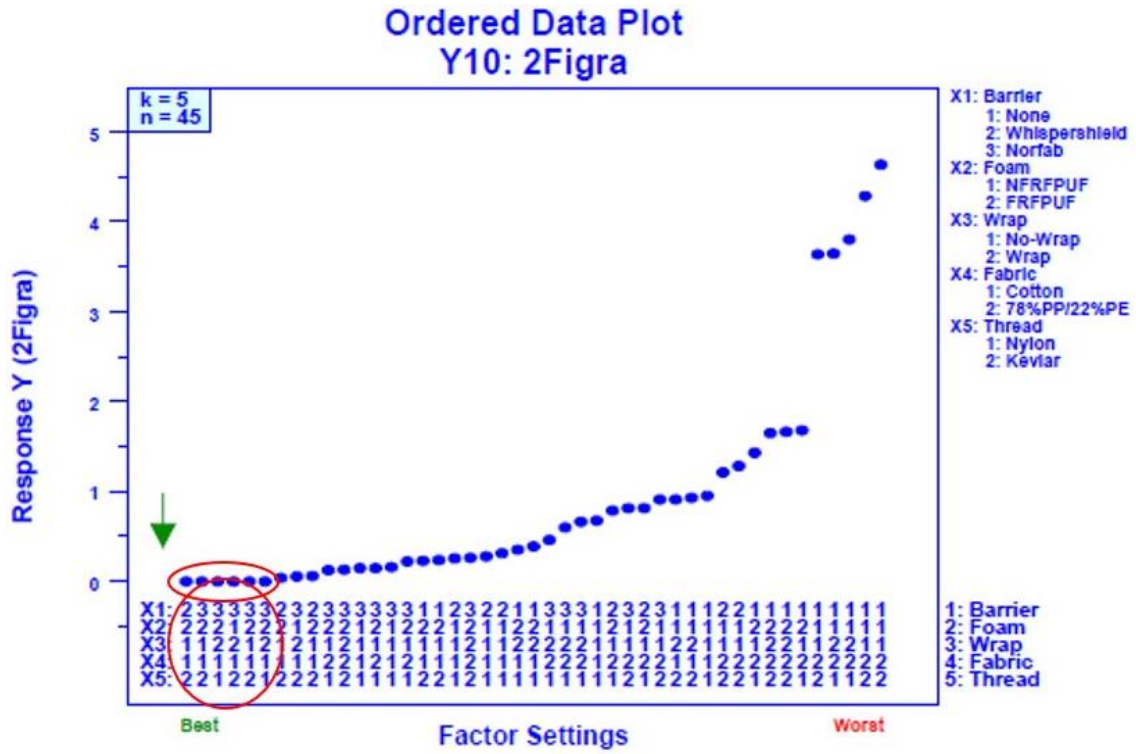

Figure 106. Response Y10 = 2Figra Ordered Data Plot to determine the optimal settings of the five factors (and secondarily, to assess important factors).

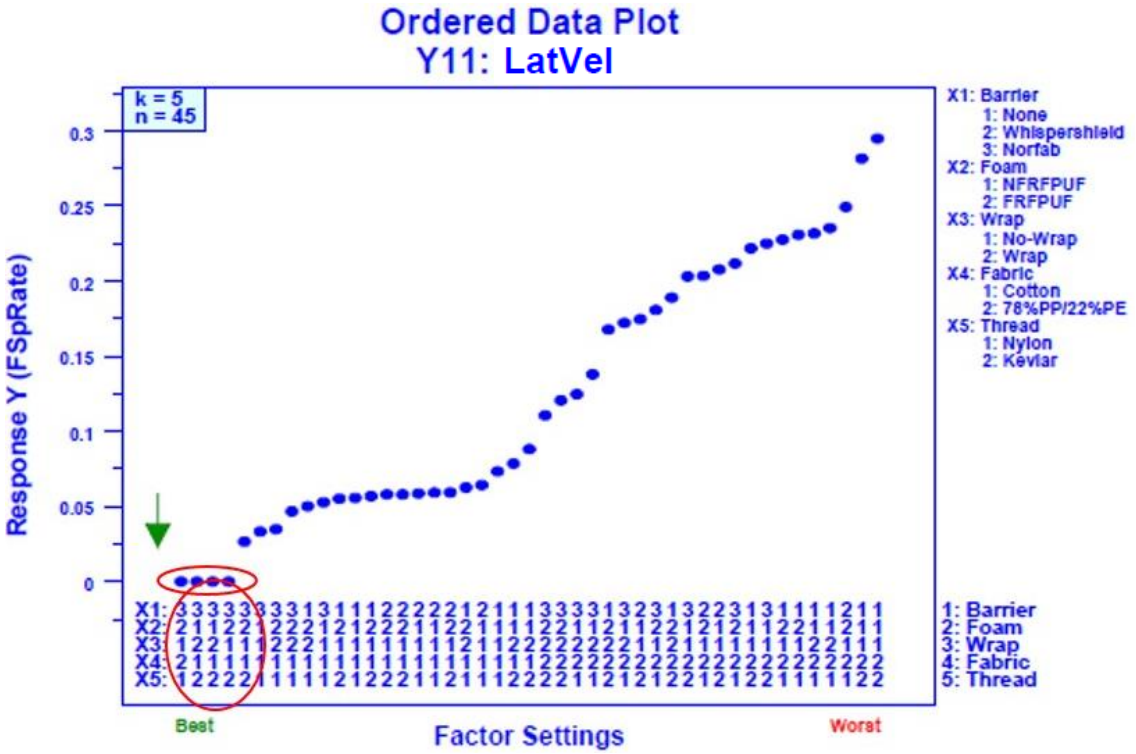

Figure 107. Response Y11 = LatVel Ordered Data Plot to determine the optimal settings of the five factors (and secondarily, to assess important factors).

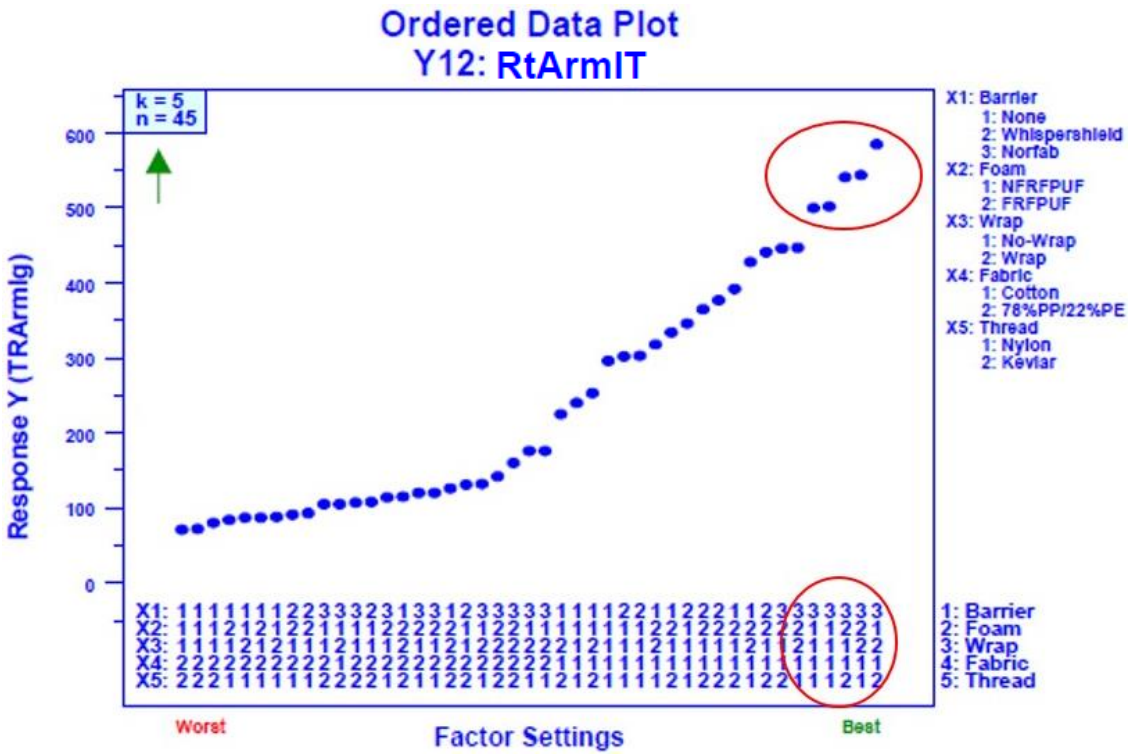

Figure 108. Response Y12 = RtArmIT Ordered Data Plot to determine the optimal settings of the five factors (and secondarily, to assess important factors).

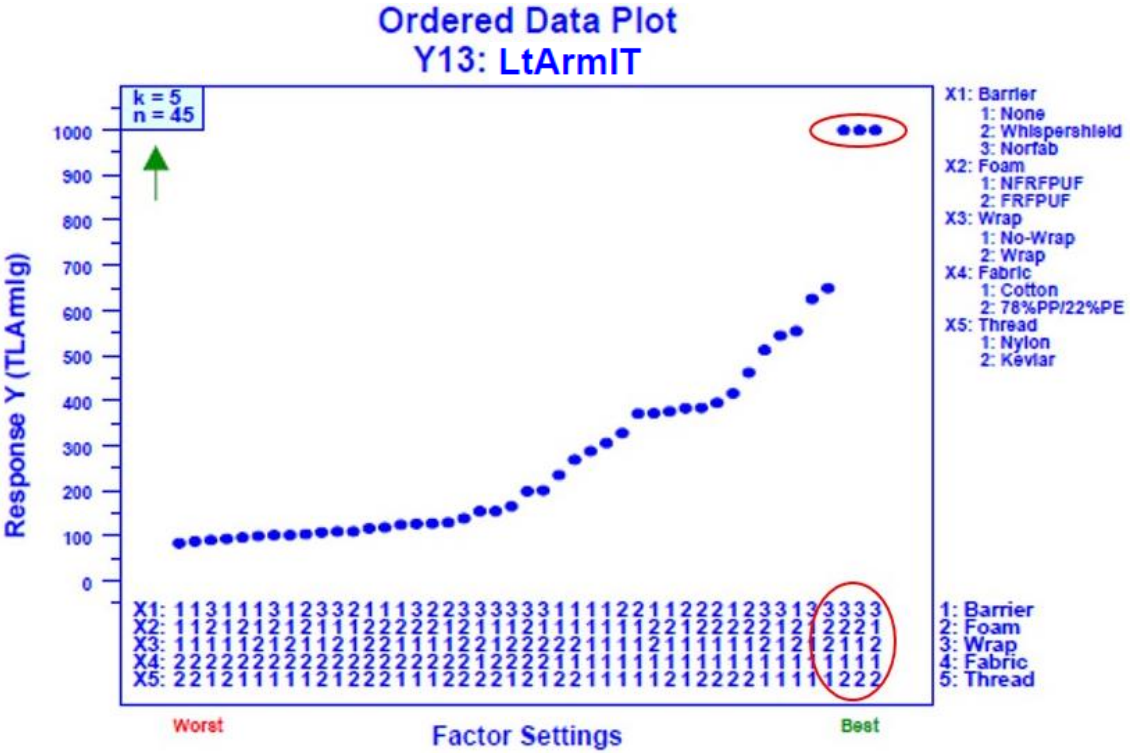

Figure 109. Response Y13 = LtArmIT Ordered Data Plot to determine the optimal settings of the five factors (and secondarily, to assess important factors).

Table 37. Assessing dominant factors for all 13 responses: number of runs and length of longest run for each of the five factors.

	Number of Runs (Out of 45)					Length of Longest Run (Out of 45)				
Y Response	X1 Barrier (3)	X2 Foam (2)	X3 Wrap (2)	X4 Fabric (2)	X5 Thread (2)	X1 Barrier (3)	X2 Foam (2)	X3 Wrap (2)	X4 Fabric (2)	X5 Thread (2)
Y1: T25kW	20	22	17	8	21	5	6	5	15	5
Y2: T1PHRR	21	24	15	4	21	8	6	6	22	7
Y3: 1PHRR	10	20	24	20	24	15	7	11	7	6
Y4: TMaxHRR	24	22	16	16	20	6	8	9	13	7
Y5: MaxHRR	19	12	24	20	28	5	10	9	9	4
Y6: TotHR	17	4	27	16	27	7	22	6	10	4
Y7: T1Figra	24	22	18	2	22	8	7	8	23	6
Y8: 1Figra	18	18	19	14	21	9	5	6	11	6
Y9: T2Figra	24	18	17	8	19	5	9	7	18	5
Y10: 2Figra	20	20	19	14	23	9	6	7	11	9
Y11: LatVel	22	26	13	3	22	8	4	9	22	5
Y12: RtArmIT	17	17	22	4	23	7	8	6	21	6
Y13: LtArmIT	21	23	22	4	19	6	7	6	21	5

Table 38. Assessing dominant factors for all 13 responses: number of runs and length of longest run for each of the five factors—ordered by X4 (Fabric).

	Number of Runs (Out of 45)						Length of Longest Run (Out of 45)				
Y Response	X1 Barrier (3)	X2 Foam (2)	X3 Wrap (2)	X4 Fabric (2)	X5 Thread (2)	Y Response	X1 Barrier (3)	X2 Foam (2)	X3 Wrap (2)	X4 Fabric (2)	X5 Thread (2)
Y7: T1Figra	24	22	18	2	22	Y7: T1Figra	8	7	8	23	6
Y11: LatVel	22	26	13	3	22	Y11: FSpRate	8	4	9	22	5
Y2: T1PHRR	21	24	15	4	21	Y2: T1PHRR	8	6	6	22	7
Y12: RtArmIT	17	17	22	4	23	Y12: TRArmIg	7	8	6	21	6
Y13: LtArmIT	21	23	22	4	19	Y13: TLArmIg	6	7	6	21	5
Y9: T2Figra	24	18	17	8	19	Y9: T2Figra	5	9	7	18	5
Y1: T25kW	20	22	17	8	21	Y1: T25kW	5	6	5	15	5
Y8: 1Figra	18	18	19	14	21	Y4: TMaxHRR	6	8	9	13	7
Y10: 2Figra	20	20	19	14	23	Y8: 1Figra	9	5	6	11	6
Y4: TMaxHRR	24	22	16	16	20	Y10: 2Figra	9	6	7	11	9
Y6: TotHR	17	4	27	16	27	Y6: TotHR	7	22	6	10	4
Y5: MaxHRR	10	20	24	20	24	Y5: MaxHRR	5	10	9	9	4
Y3: 1PHRR	19	12	24	20	28	Y3: 1PHRR	15	7	11	7	6

It is seen that (for example) for response Y1 (= T25kW), the optimal direction is up (= large T25kW), and the maximal value (from Figure 97) was seen to be approximately 1800 and that there were seven conditions that yielded this maximal value. For these seven conditions:

Table 39. Determining optimal settings for the five factors for all 13 responses. Setting (number of occurrences in optimal group).

Y Response	Optimum Direction	# Conditions in Optimal Group	X1 Barrier	X2 Foam	X3 Wrap	X4 Fabric	X5 Thread
Y1: T25kW	up	7	3 (6)	2 (6)	1 (4)	1 (6)	2 (4)
Y2: T1PHRR	up	5	3 (5)	2 (4)	2 (3)	1 (5)	2 (3)
Y3: 1PHRR	down	5	3 (5)	2 (4)	2 (3)	1 (5)	2 (3)
Y4: TMaxHRR	up	5	3 (5)	2 (4)	2 (3)	1 (5)	2 (3)
Y5: MaxHRR	down	5	3 (5)	2 (4)	2 (3)	1 (5)	2 (3)
Y6: TotHR	down	4	3 (4)	2 (4)	2 (2)	1 (4)	2 (2)
Y7: T1Figra	up	6	3 (6)	2 (5)	2 (3)	1 (6)	2 (4)
Y8: 1Figra	down	6	3 (5)	2 (5)	2 (3)	1 (6)	2 (4)
Y9: T2Figra	up	5	3 (5)	2 (4)	2 (3)	1 (6)	2 (3)
Y10: 2Figra	down	6	3 (5)	2 (5)	2 (3)	1 (6)	2 (4)
Y11: LatVel	down	4	3 (4)	2 (2)	1 (3)	1 (4)	2 (4)
Y12: RtArmIT	up	5	3 (5)	2 (3)	1 (3)	1 (5)	1 (3)
Y13: LtArmIT	up	3	3 (3)	2 (2)	1 (2)	1 (3)	2 (3)

Factor X1 (Barrier) was 3 (= Norfab) for six out of these seven conditions;
Factor X2 (Foam) was 2 (= FRFPUF) for six out of the seven conditions;
Factor X3 (Wrap) had a most prevalent setting of 1 (= No Wrap)—but for only four out of the seven conditions;
Factor X4 (Fabric) was 1 (= Cotton) for six out of the seven conditions;
Factor X5 (Thread) had a most prevalent setting of 2 (= Kevlar)—but for only 4 out of the 7 conditions.

In general, therefore, note from Table 39 that:

1. For factor X1 (= Barrier), the optimal setting was 3 (= Norfab) for all 13 responses, and this Norfab setting yielded the optimal response in all (or near-all) 13 responses (see red highlighting).
2. From Table 39, it is seen that X2 (= Foam) has an optimal value of 2 (= FRFPUF) for all 13 responses, and with overwhelming counts (see red) in 10 out of the 13 responses.
3. For factor X3 (Wrap), no single setting was optimal over the 13 responses, and none of these settings were overwhelming in the optimal group.
4. For factor X4 (Fabric), the optimal setting was 1 (= Cotton) for all 13 responses and had a large preponderance in the optimal group (highlighted in red).
5. Finally, for fabric X5 (Thread), the optimal setting was 2 (= Kevlar) in 12 out of 13 responses, but was dominant in only one out of the 13 responses.

In summary, the main conclusions from Table 39 and this Optimization Section are:

1. The dominant factor was X4 = Fabric with optimal setting = Cotton.
2. A close second important factor was X1 = Barrier with optimal setting = Norfab.
3. The next dominant factor was X2 = Foam with optimal setting = FRFPUF.
4. A distant unimportant factor was X5 = Thread with a preferred setting = Kevlar.
5. The least important factor was X3 = Wrap with preferred setting = Wrapped.

A final note is that during the course of deriving results for this Optimization Section, three additional techniques were utilized which not only had the effect of providing best-settings information, but also provided additional insights into the most-important-factors question. We thus have in toto six different analysis methodologies (some more conservative in their statistical assumptions than others):

1. Main Effects Plot 1-way ANOVA p-values (Table 22)
2. Block Plot sign test p-values (Table 28)
3. Block Plot t-test p-values (Table 29)
4. Ordered Data Plot number of runs (Table 38)
5. Ordered Data Plot length of longest run (Table 38)
6. Ordered Data Plot number of consistent settings at the optimum (Table 39).

Though not universal, there was a preponderance of evidence across the six methods—and especially so for the first three methods which focused on the sensitivity analysis question--as to the relative ranking of the five factors:

X4 and X1, followed by
X3, followed distantly by
X5 and X3.

On the other hand, there was in fact consistent and robust agreement across all six methods about factor X4 (Fabric) being the most important.

8 Discussion

The experiments described here were designed to characterize flame spread and fire growth on four-cushion mock-ups arranged in a geometry representative of an upholstered chair. The ultimate goal is to explore the feasibility of predicting the real-scale burning behaviors utilizing the results of small-scale experiments performed in a cone calorimeter. This is Part 1 of a three-part series of reports. Part 2 will summarize the results of the corresponding small-scale experiments, and Part 3 will consider the feasibility of predicting the real-scale experiments based on the small-scale results.

Five types of materials—fire barrier, FPUF, presence or absence of polyester fiber wrap, cover fabric, and sewing thread—used in the cushions forming the mock-ups were varied in the experiments. Materials were chosen to increase the likelihood of observing changes in burning behavior when varied.

There were many possible ways to characterize the burning behavior of the mock-ups studied here. It was necessary to make choices on what parameters to use to provide quantitative measures suitable for statistical analysis and for comparison with small-scale experimental results. A wide variety of measures were considered before settling on the thirteen parameters based on heat release rate time behavior, total heat released, the fire growth rate (FIGRA) time behavior, and early flame spread rate behaviors listed in Table 16.

The reduced-factorial design allowed assessment of whether changes in the materials resulted in statistically significant changes in a range of flammability properties used to characterize mock-up burning behavior. The results of the statistical analyses were described in Section 7. In this section, we review the results and discuss the behaviors in terms of observed burning behaviors. Where appropriate, the results are compared with previous literature findings. The experiments also provided insights into additional aspects of burning behavior that were not the primary focus of the current study. These include observations concerning mock-up ignition by the different ignition source flames, heats of combustion, and the measurements of thermal radiation from the burning mock-ups at two distances along three directions to the front, side, and rear. These results are discussed to provide additional insights into mock-up (and RUF) burning behavior.

8.1 Heat Release Rate

Heat release rate has been identified as the most important variable for determining fire hazard. [106] Its measurement and characterization has come to play the central role in fire studies, in general, and in flammability studies related to RUF, in particular. The vast majority of recent studies of real-scale RUF flammability have utilized HRR for characterizing burning behavior.

The experimental HRR analysis and results were summarized in Section 5.3. HRR temporal profiles are included in Appendix A and Appendix C for the individual tests. One challenge in utilizing HRR is the identification of characteristic parameters appropriate for relating HRR behavior to actual fire hazard. Most previous studies have used the time to and maximum HRR as the primary parameters for characterizing the HRR curves. Recall that various times such as when the ignition source was first applied or when a threshold value of HRR was reached have been used as “zero times”. These two parameters seem most appropriate when the HRR curves display a single well-defined peak, but become more problematic when the shapes of the HRR temporal profiles are more complicated.

In an effort to characterize the HRR curves observed in this study, the thirteen parameters included in Table 13 were introduced. These included parameters intended to characterize the initial HRR growth rate, the time to and value of an initial HRR peak, the time to and maximum value of HRR, the total amount of heat released, and a group of parameters designed to characterize the shape of the HRR curves during the most the intense burning period. These parameters were chosen based on experimental observations that the HRR curves frequently showed more than one peak and that a wide variety of shapes were observed ranging

from single sharp peaks to cases where roughly constant HRRs were measured over relatively long periods of time.

For the purposes of the statistical analysis the number of parameters derived solely from the HRR curves was reduced from the thirteen shown in Table 13 to the first six listed in Table 16. The factors chosen are typical of those used in past research studies to characterize HRR behavior in RUF studies, but were extended somewhat by allowing for two peaks in the HRR curves, i.e., an initial peak and a maximum peak. It should be kept in mind that considering two HRR peaks did introduce ambiguity since in some cases there was only a single peak, and in others the initial HRR peak and maximum HRR peak were the same. The seven HRR parameters not included in the analysis deal in some way with the HRR curve shapes during periods of more intense burning when values were above 25 kW. These included a measure for the length of time of intense burning and the introduction of measures designed to characterize the overall shapes of the HRR curves. These parameters bear some similarity to parameters introduced by Janssens (summarized in Section 1) to characterize HRR curves with single peaks. [63] While judged to be of interest, we recognized that such measurements have not been widely used to characterize HRR behaviors in the past, that variations in the values with mock-up cushion composition were not as clear as for the other parameters, and that the relationship between such parameters and RUF flammability hazard are not well understood. For these reasons, such measures were not included in the current statistical analysis.

Details and results concerning the statistical analysis were discussed in Section 7. Consider first the five responses derived from the time-resolved HRR curves. The results for the integrated curves, i.e., Q_{tot}, are discussed in the following section. Three statistical tests, one based on Main Effects Plots and two based on Block Plot Analyses were used to identify primary factors having statistically significant effects on the experimental responses. Each type of principle effect analysis showed that statistically significant changes in these responses were associated with changes in the Fabric, Barrier, and Foam factors. The five analysis approaches agreed that changes in Barrier and Fabric resulted in statistically significant effects for all five HRR responses. The conclusions concerning the role of Foam differed slightly depending on analysis type. All three approaches agreed that foam type had statistically significant effects on Y1 (t_{+25}), Y3 (HRR_{peak1}), and Y5 (HRR_{max}). The approaches also agreed that there was no significant effect of Foam on Y4 (t_{max}). The result based on Main Effects Plot analysis also found no significant effect for Y2 (t_{peak1}), but the two approaches based on Block Plot analysis yielded the opposite conclusion. The results indicated that factors X1 (Barrier) and X4 (Fabric) had the largest (roughly comparable) effects on the five responses followed by a weaker dependence on X2 (Foam). No statistically significant effects of X3 (Wrap) and X5 (Thread) were identified for any of the responses.

Three approaches based on Ordered Data Plot analysis (see Section 7.4.2) also provided insights into the roles of the factors on the experimental HRR responses. In agreement with the results above, roughly comparable strong effects were identified for X1 (Foam) and X4 (Fabric) with a weaker effect of X2 (Foam). No effects associated with X3 (Wrap) or X5 (Thread) were evident. The good agreement between the six types of analysis provides a high level of confidence in the conclusions.

The strongest primary effects were associated with the type of upholstery fabric. The strength of these effects are evident in the data plots for the five parameters shown in Figure 25 ($\overline{t_{+25}}$), Figure 26 ($\overline{t_{peak1}}$), Figure 27 ($\overline{HRR_{peak1}}$), Figure 28 ($\overline{t_{max}}$), and Figure 34 ($\overline{HRR_{max}}$). Combinations for which the materials in the cushions only differ by the upholstery fabric are adjacent to each other with cotton (red) on the left and 78%PP/22%PE (blue) on the right. Recognizing that longer times and lower HRRs represent improved flammability characteristics, it is immediately evident that the cotton-covered cushions provided better fire performance following open flame ignition with regards to the five parameters derived from the HRR plots. The only exception was for the Combination 17/Combination 18 pair in the $\overline{HRR_{peak1}}$ plot for which the average value was slightly higher for combinations with the cotton fabric.

Numerous earlier studies have identified upholstery fabric as playing an important role in RUF flammability behavior, in general, and HRR behavior, in particular. The advantage of cellulosics, such as the cotton fabric tested in this study, over modern thermoplastic fabrics, such as the 78%PP/22%PE fabric used here, with regard to RUF flammability were identified in studies during the 1970s. [30, 32, 108] Later studies reaching similar conclusions include [38, 41, 43, 47, 109].

It has not been common in the literature on RUF burning to carry out tests to determine statistical significance. Three such studies were identified in Section 1. Using data taken from a study by Metha [60], Miller concluded that fabric type did not result in a statistically significant change in the initial peak in the HRR curves for a series of chairs in which four types of cotton fabric were used. [61] A strong effect of fabric type was identified when the time to initial peak HRR was considered. Janssens used statistical analysis to identify statistically significant effects in his RUF mock-up tests, but fabric type was not included as a variable. [63] Miller also performed a statistical analysis from a study of RUF chair burning experiments performed by Fansler and Lock [66] using both flaming and smoldering ignition sources. [67] For these experiments three fabrics were considered: two different weight cottons and a 56% rayon/34% polyester/10% cotton blend. The statistical analysis showed varying the fabric had a statistically significant effect on both time-to-peak HRR and peak HRR when the flaming ignition source was used.

Even though the qualitative difference in flammability between upholstery covered with cellulosic and thermoplastic fabrics appears to be well documented, it is more difficult to develop a picture of the quantitative reproducibility of the temporal HRR curves between the current experiments and the large number of earlier experiments. This difficulty can be traced to the wide range of experimental variables that can affect the burning behavior of RUF and RUF mock-ups. Factors such as cushion size, geometry, number of cushions, ignition source, and ignition location vary widely between experiments. Quantitative comparisons between different experiments are only appropriate when such factors are the same or only changed slightly. Such variations not only limit direct comparisons between different experiments, but also limit conclusions concerning changes in burning behavior due to such factors as upholstery fabric type and aerial density, effectiveness of a barrier material, and the presence or absence of PEFW.

The second strongest primary effect identified in Section 7.2 was due to the absence or presence of a Norfab barrier within the cushions. Recall that a similar analysis comparing the effect of adding a Whispershield barrier was not carried out due to the reduced number of combinations incorporating this barrier. As was true for the fabric factor, it is possible to easily visually identify the improvement in flammability behavior in the bar plots for the five HRR parameters when the Norfab barrier was added. Combinations differing only in barrier condition are those with numbers separated by eight, e.g., Combination 1 (Whispershield), Combination 9 (no barrier), and Combination 17 (Norfab). Comparisons show that incorporating Norfab into otherwise similar cushions without a barrier resulted in improved flammability behavior for the five responses in all possible combinations.

Similar graphical comparisons between combinations with and without added Whispershield reveal more complicated behaviors. The addition of this barrier clearly improved the burning behavior when characterized in terms of HRR_{peak1} and HRR_{max}. Similar improvements, as indicated by increases in the periods when Whispershield was added to the cushions, are evident when the results for Combinations 5 and 13 are compared for $\overline{t_{+25}}$, $\overline{t_{peak1}}$, and ($\overline{t_{max}}$). Similar comparisons of Combinations 1 and 9 and 2 and 10 generally show much smaller or limited improvement for these three responses. When Combinations 6 and 14 are compared, the periods for the combination with Whispershield are found to decrease. The likely reason for this difference was discussed in Section 5.3, where it was noted that the HRR maxima for Combination 6 mock-ups occurred during flaming of the cover fabric and that the FRFPUF did not become strongly involved. In contrast, the maxima for Combination 14 mock-ups occurred when the foam became involved. This conclusion shows that it is possible for a response to indicate poorer flammability behavior even though the overall burning behavior is improved.

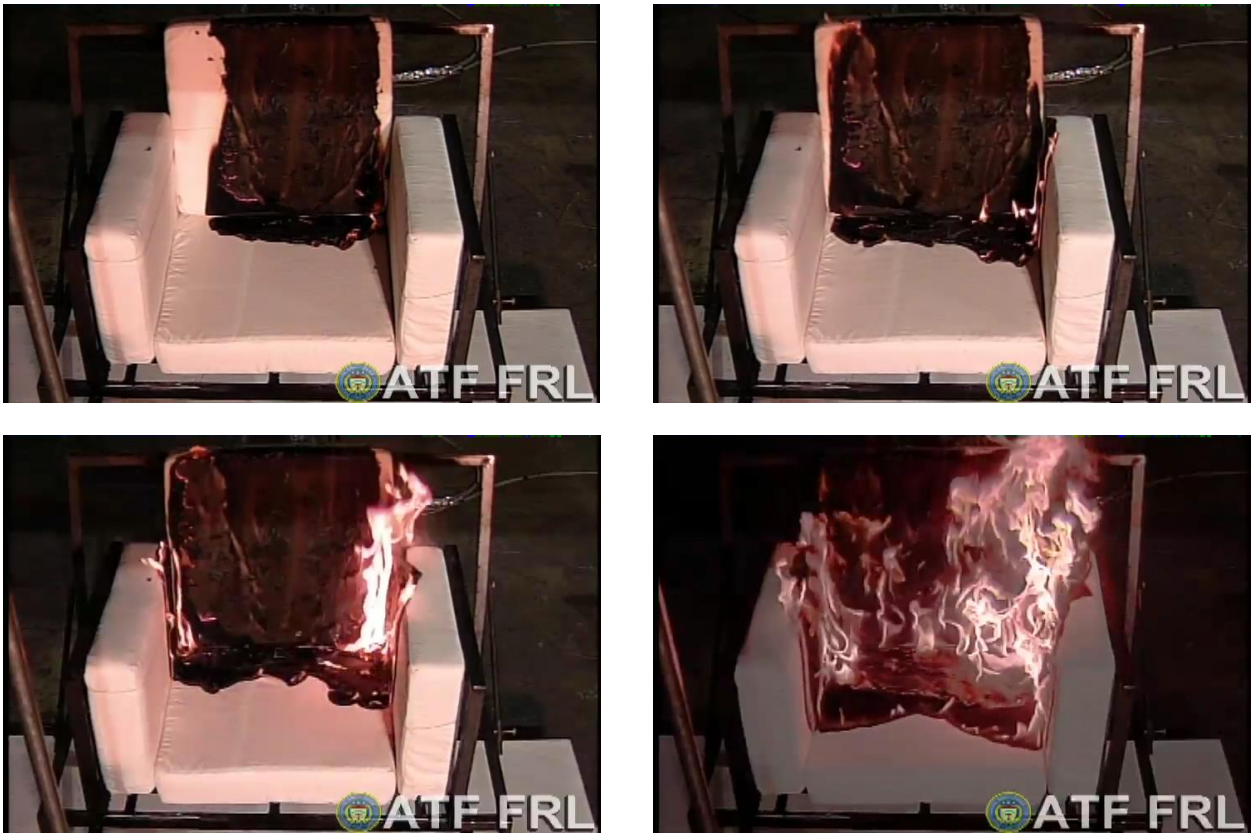

Figure 110. Four frames recorded by Camera #3 show a fire burning on a Combination 17 mock-up during Test 17_2 at 494 s, 614 s, 710 s, and 913 s following application of Ignition Source 2.

Differences were also discernable when the flammability behaviors for mock-ups in which Whispershield and Norfab barrier fabrics were exchanged (combination numbers differing by 16). For each of the four mock-up pairs where comparisons are possible for $\overline{t_{+25}}$, $\overline{t_{peak1}}$, $\overline{HRR_{peak1}}$, and $\overline{t_{max}}$, use of the Norfab fabric provided improved flammability behavior. Only the results for HRR_{max} did not follow this pattern. As seen in Figure 34, values of $\overline{HRR_{max}}$ for combinations with NFRFPUF and a Whispershield barrier (Combinations 1 and 2) were generally lower than those for the corresponding mock-ups with the Norfab barrier (Combinations 17 and 18). Recall that the $\overline{HRR_{max}}$ values for Combinations 18 and 20 were among the highest observed during the test series. The opposite $\overline{HRR_{max}}$ dependence was found when mock-ups which included FRFPUF and Whispershield (Combinations 5 and 6) were compared with those with the Norfab barrier (Combinations 21 and 22).

Review of videos and observations from the tests provides a likely explanation for the higher values of $\overline{HRR_{max}}$ observed for combinations with a Norfab barrier and NFRFPUF. Recall that both the upholstery fabric and the Norfab barrier fabric covers incorporated aluminum zippers to provide access to their interiors. The tape for the zipper was nylon, which in turn was sewn to the upholstery fabric. Since aluminum can melt when exposed to heating from flames and nylon is a thermoplastic, such zippers represent likely areas of weakened fire resistance. Some of the mockups were sewn with nylon thread, and the opening of these seams was also a possibility. Four images of the fire growing on a mock-up with cushions formed from standard FPUF wrapped by layers of Norfab and the cotton fabric during Test 17_2 are shown in Figure 110. The HRR as a function of time for this test is included in Figure A-127. It shows that during most of the period covered by the images the HRR remained under 15 kW, but starting around 825 s after ignition, began to grow more rapidly and by 913 s was approaching 75 kW. It is clear from the images that the fire did not develop substantially until it had spread into the corners formed by the seat,

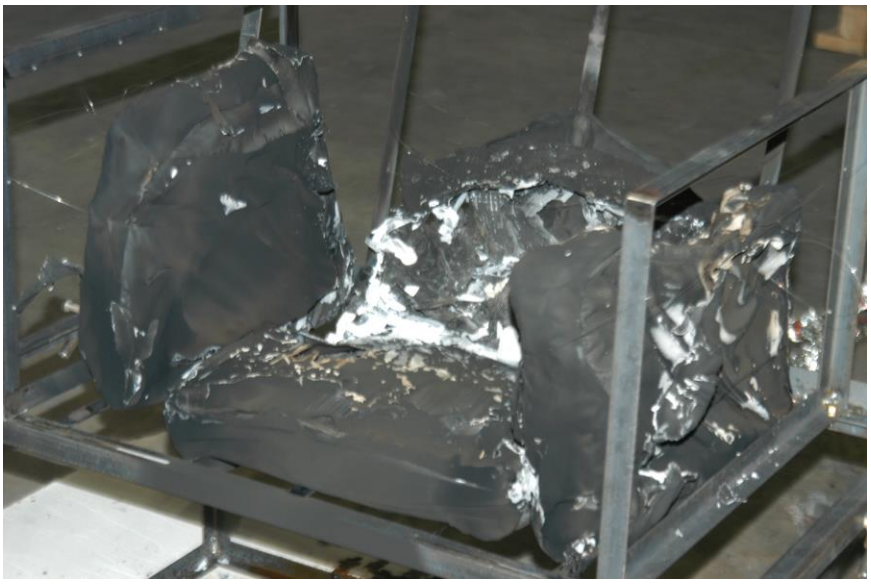

Figure 111. Photograph showing the mock-ups residue following Test 17_1.

back, and arms, with the initial growth occurring on the right-hand side followed by the left side. By 913 s flaming is apparent along the entire crevice formed by the back and seat cushions, as well as the nearby arms.

The video of the fire recorded from the rear of the mock-up by Camera #4 showed intense flames appearing near the base of the back cushion at comparable locations at roughly the same times. The videos suggest a transition in which increased fuel levels were suddenly delivered at the base of the back cushion. As the fire grew, the top of the back cushion moved downward, suggesting FPUF was being lost at the base. These observations can be explained by assuming the fuel was released at the base of the cushion, presumably through openings created by failure of both the cushion cover and barrier fabric seams and/or zippers. The most likely fuel would have been the liquid released by pyrolysis of the FPUF, which is primarily derived from the original polyol used in the manufacture of the foam. This burning scenario requires that there was sufficient heating of the seams or zippers to open both the cover fabric and barrier fabric and that sufficient heat passed through both covers to pyrolyze substantial FPUF. The observations suggest that this occurred after the flames on the outer surface first reached the corners and began to intensity. Once initiated, the growing fire provided positive feedback to accelerate the process. Ohlemiller and Shields described a similar mechanism for barrier failure, which they referred to as a "basal melt fire," in which "melt" from the FPUF supported burning at the base of a vertical cushion. [41] It differed somewhat from the current experiments in that the liquid passed through a porous barrier.

Figure 111 shows a photograph of the mock-up residue following Test 17_1. The back cushion has fully collapsed and the Norfab barrier appears to be partially destroyed. The barriers for the other cushions have maintained their shapes and appear to be mostly intact. There is some evidence that some seams were partially open. Inspection of the residue showed that the barriers were open where the zippers had been located and that the cushioning material inside the barrier had been totally consumed. These observations support the conclusion that substantial fires on Combination 17 mock-ups likely developed following barrier penetration at weak points created by the seams and/or zippers. Ohlemiller and Shields reached similar conclusions concerning the weakness of seams sewn with thermoplastic thread and covers incorporating nylon zippers. [41] They reported that such zippers failed in tests with nonwoven aramid barriers in cushions used to form chair mock-ups. Subsequently, they eliminated the zippers and sewed the openings closed with aramid thread, which was also used for other seams, to alleviate the problem.

Figure 112. A frame taken from a video recorded by Camera #8 672 s following ignition shows the fire burning on the test stand base and the remaining mock-up during Test 20_1.

As already noted, HRR_{max} values for Combinations 18 and 20 were among the highest observed during the test series. The cushions in these mock-ups included the thermoplastic cover fabric over Norfab barrier with NFRFPUF. The HRR curves in Figure A-141 and Figure A-171 indicate that HRRs remained below 100 kW for several minutes before rising to sharp peaks with values between 300 kW and 500 kW. Videos of these fires showed that the rapid increases in HRR were associated with simultaneous burning that developed on both the test stand base, following release of a liquid material from the cushions, and the partially intact mock-up. Figure 112 shows an example of this type of burning observed 672 s after ignition during Test 20_1. It was recorded very close to the time of HRR_{max}. It is noteworthy that the flames on the test stand base are in the form of a "u" shape with the liquid fuel located directly below the original locations of the cushion zippers in the cover fabric and the Norfab barrier fabric. These observations are consistent with the fire breeching the barrier along either the cushion seams or zippers and releasing a liquid product from the pyrolysis of the interior FPUF.

Note that the cushion seams in Combination 18 were sewn with Kevlar thread and therefore would have been less likely to open than those for Combination 20, which were sewn with nylon thread. This difference could explain the slightly longer times required for HRRs to begin their sharp increases for fires on Combination 18 mock-ups, but definite conclusions are not possible since Combination 20 cushions also included PEFW, and it unclear what effect this material would have had on the burning behavior. A photograph showing the residue following the Test 20_1 fire is shown in Figure 113. The charred barrier is considerably more damaged than seen in Figure 111 for Test 17_1, where a similar mock-up with a cotton cover fabric did not develop the intense burning on the test stand base.

The effectiveness of barrier materials in improving the flammability behavior of RUF and RUF mock-ups following flaming ignition has been widely studied in the literature in studies going back to the 1970s. [32, 34, 41-43, 60, 62, 65, 66] Table 40 lists the types of barriers investigated and the types of measurements used to characterize the burning behavior. The review by Nazaré and Davis includes a discussion of the types of barriers that have been used to protect filling materials in soft furnishings. [98] The properties that are expected to determine barrier effectiveness and tests for characterizing these types of materials have been discussed by Nazaré et al. [99]

Figure 113. Photograph showing the mock-ups residue following Test 20_1.

Each of the above studies on barrier effectiveness concluded that inclusion of a barrier material in RUF or RUF mock-ups improved the flammability behavior following flaming ignition. This is consistent with the observations in the current study. Due to the wide variation in types of experiments performed, uncertainties concerning the barrier materials used, and variations in the sizes and configurations of RUF studied, it has proven impossible to directly compare the current results with literature findings. This inability is unfortunate because it limits our ability to draw conclusions concerning the relative effectiveness of different types of barriers and to predict the effectiveness of adding a particular barrier fabric to upholstery in an attempt to reduce the flammability.

Miller concluded, based on the experimental finding of Metha [60], that including a barrier in the cushion resulted in a highly statistically significant effect in flammability characteristics of time to and maximum HRR. [61] Miller reached the same conclusion concerning barrier effectiveness based on the CPSC follow-up study [66]. [67]

A third material-type variation, FPUF type used in the mock-ups (Foam), yielded statistically significant responses for three (t_{+25}, HRR_{peak1}, and HRR_{max}) out of the five HRR-based responses using each of the three approaches based on Main Effects Plots and Block Plots. Mixed results were found for t_{peak1}, with the analysis based the Main Effects Plot indicating a statistically insignificant response and the two Block Plot approaches agreeing there was a statistically significant response. Only the effect on t_{max} was identified as being statistically insignificant by each of the approaches. Generally, the strengths of the effects were less than observed with changes in fabric or barrier.

Review of the bar plots for the five parameters; $\overline{t_{+25}}$, $\overline{t_{peak1}}$, $\overline{HRR_{peak1}}$, $\overline{t_{max}}$, and $\overline{HRR_{max}}$; provide additional insights. It is easily seen in Figure 27 and Figure 34 that both $\overline{HRR_{peak1}}$ and $\overline{HRR_{max}}$ were reduced when NFRFPUF was replaced with the FR version with the other materials held constant. It is not surprising that statistically significant effects were identified in each of the analyses. Such clear-cut distinctions are not as evident in the bar plots for the measures based on times shown in Figure 25, Figure 26, and Figure 28. It should be kept in mind that fires did not develop on Combination 21 and Combination 23 mock-ups, and the times for these tests were set to 150 % of the largest measured value (see Table B-3). While the values of $\overline{t_{+25}}$ and $\overline{t_{peak1}}$ generally increased substantially when NFRFPUF was replaced with FRFPUF in otherwise similar cushions covered with cotton fabric, much smaller relative variations were

Table 40. Examples of studies that examined effects on burning behavior of including barrier fabrics in RUF cushions.

First Author	Barriers Considered					Measurements
Prager [32]	FR cotton	Neoprene-coated cotton	Polyamide/imide fabric	Woven fiberglass	Aluminized cotton	Flame spread, temperatures
Woolley [34]	FR-cotton	Woven fiberglass	Wool batting			Ignition, temperatures
Ohlemiller [41]	Non-woven aramid	Knitted glass/ charring fiber	Woven fiberglass			Fire spread area, max HRR, flame radiation
Parker [42]	Woven fiberglass					Max temperature, max HRR
Sundström [43]	Non-woven aramid	Woven fiberglass	FR glass/cotton system			Max HRR, THR, EHC
Metha [60]	47 % fiberglass/50 % modacrylic/ 3 % polyester					Time to and initial HRR Peak
Fabian [62]	Para-aramid/ polyester/rayon blend	Para-aramid	Coated glass fiber	PAN-PVC copolymer	PAN-PVC copolymer	Mass loss, max HRR, THR, EHC
	PAN-PVC copolymer and cotton	Boric acid treated cotton	Boric acid treated cotton/rayon	Rayon	Boric acid treated cotton/rayon	
	Cotton/polyester/rayon blend					
Storesund [65]	Plain weave fiberglass	Twill weave fiberglass	Plain weave aramid			Max HRR, THR
Fansler [66]	FR-cellulose based	FR-fibrous glass/modacrylic/polyester	FR-modacrylic/silica	FR-rayon/ polyester	FR-rayon/ polyester	Time to and max HRR, time to 200 kW, THR@10 min

evident for similar combinations covered with the thermoplastic material. Apparently, the changes for the cotton-covered cushions were sufficient to yield statistically significant effects overall for $\overline{t_{+25}}$ using the three approaches. Mixed results were found for $\overline{t_{peak1}}$, with the more conservative analysis based on Main Effects Plots indicating no statistical significance, but the two approaches based on Block Plots identifying statistically significant effects. Note that, as discussed further below, that the difference in responses for the two fabrics implies an interaction between Foam and Fabric.

The variations of $\overline{t_{max}}$ values with combination type were more complicated. While the times generally increased for the mock-ups covered in cotton when FRFPUF was substituted for NFRFPUF, the relative increases were somewhat less than observed for $\overline{t_{+25}}$ and $\overline{t_{peak1}}$. The effects of changing the foam type for mock-ups incorporating cushions with the thermoplastic fabric were variable. For the combinations without a barrier, the results of changing from NFRFPUF to FRFPUF were similar to those observed for the other two time-based parameters, i.e., little or no effect on $\overline{t_{max}}$. However, combinations incorporating barriers showed different responses. For the pair containing Whispershield $\overline{t_{max}}$ for Combination 2 was nearly a factor of two higher than for Combination 6 with FRFPUF. Inspection of the HRR time profiles for these two combinations in Figure A-12 and Figure A-37 provides an explanation for this observation. The curves for Combination 2 had long tails with substantial HRRs. For Test 2_1 the maximum HRR occurred as a second peak around 400 s following ignition, while the values of HRR_{peak1} and HRR_{max} were concurrent around 170 s for Test 2_2. The resulting $\overline{t_{max}}$ is included in Figure 28. For the Combination 6 tests shown in Figure A-37, both HRR_{max} values coincided with the first peak associated with fabric burning, and subsequent burning took place at much lower HRRs. Thus, the apparently anomalous $\overline{t_{max}}$ behavior is, in fact, associated with the improved flammability behavior achieved by replacing NFRFPUF with the FR version.

The variation of $\overline{t_{max}}$ with changes in foam type for mock-up pairs including cushions with Norfab and the 78%PP/22%PE cover fabric had an apparent dependence on the presence or absence of PEFW. For the Combination 18/Combination 22 pair $\overline{t_{max}}$ was larger for the combination with FRFPUF (Combination 22), while the opposite was found for the Combination 20/Combination 24 pair with substantial smaller $\overline{t_{max}}$ values recorded for mock-ups with the FRFPUF. Review of the corresponding HRR curves and videos again provides an explanation. The values of t_{max} for the Combination 18 mock-ups were recorded during periods of intense burning, including burning on the test stand platform, that occurred after a relatively long period of slow fire growth (see Figure A-141). The fire behavior was quite different when NFRFPUF was replaced with FR foam. The fires burned gently with HRRs well below 100 kW for long periods of time (see Figure A-203). The maxima are associated with relatively weak HRR peaks in the fluctuating HRRs. For the two combinations that included PEFW, t_{max} was reduced by over a factor of two when NRFFPUF was replaced with the FR version. The HRR curves and videos indicate that the explanation is the same as described above for the mock-ups with a Norfab barrier. The maximum HRRs for Combination 20 occurred when cushioning material became involved in the fire roughly ten minutes after ignition, while the maximum HRR for Combination 24 occurred during burning of the cover fabric with very little apparent involvement of the cushioning material.

The above discussion suggests that even though there were clear effects on $\overline{t_{max}}$ of exchanging the two types of FPUF, the relatively smaller changes for the cotton-covered mock-ups compared to $\overline{t_{+25}}$ and $\overline{t_{peak1}}$ combined with the greater variability observed for mock-ups including the 78%PP/22%PE cover fabric were sufficient to result in the primary effects analysis not meeting the criteria for a statistically significant effect.

As discussed in Section 1, the effectiveness of replacing NFRFPUF with FR foam in reducing the flammability of RUF has been the focus of a great deal of recent interest. Much of the discussion has been driven by the claim that the use of FPUF meeting pre-2013 versions of Cal TB-117, which generally

incorporated FR chemicals, provided little or no improvement in RUF burning behavior, while allowing potentially harmful materials to be released into the environment over long period of time. [83] Numerous studies comparing the flammability behaviors of RUF items with NFR and pre-2013 Cal TB-117 FPUF have been reported. [37, 38, 60, 62, 63] As discussed in Section 1, all but the study of Janssens reached the conclusion that substituting pre-2013 Cal TB 117 foam for NFR FPUF provided little, if any, improvement in RUF flammability behaviors. Janssens did report a substantial reduction in maximum HRR when the FR foam was used. [63]

The FRFPUF used in this study meets the British SI-1324 requirements, which limits burning following application of a BS-5852 Ignition Source 5 wood crib to upholstered materials. This is a considerably more severe exposure than for the pre-2013 Cal TB-117 test, which exposed a small sample of foam to a match-sized flame. In fact, the FRFPUF used in this study resisted ignition by an Ignition Source 5 crib fire placed directly on chair mock-ups formed from four slabs of the foam (Combination 26, see Appendix C.2). This study has shown that the flammability of RUF mock-ups was markedly reduced when the FRFPUF was used as the cushioning material, even though larger differences were associated with changes in cover fabric or the inclusion of a fire barrier. These results show that meaningful reductions in RUF flammability, i.e., improvement in RUF fire safety, are possible by use of FRFPUF with sufficient levels of fire retardants. This conclusion in no way implies that potential human health and environment affects associated with the use of fire retardants do not need to be accounted for when considering the potential benefits of including FRFPUF in RUF.

While numerous previous studies have compared the burning behavior of RUF or RUF mock-ups using NFR and FR foams meeting the pre-2013 Cal TB-117, we were unable to identify any previous studies in which the burning behavior of RUF or RUF real-scale mock-ups containing either NFRFPUF or SI-1324 FPUF were compared. Babrauskas et al. did perform such a comparison for chairs containing NFRFPUF and a very heavily fire-retarded FPUF burning under a furniture calorimeter. [110] The upholstery material was nylon and a 50 kW burner applied for 200 s was used for ignition. HRRs for the two types of chairs had maximum values of 1150 kW and 50 kW, respectively. Thus, the heavily fire-retarded foam was very effective in inhibiting fire growth. In fact, this FRFPUF seems to have been considerably more effective than the SI-1324 FPUF used in the current study.

Two of the materials varied in the current test matrix, namely, the presence or absence of PEFW and sewing thread type, had no statistically meaningful effects on the HRR parameters. This may have had more to do with choices made in designing the experiments than the potential sensitivity of the burning behavior to the actual changes. For the PEFW, the choice was made to not use this material concurrently with Whispershield in the cushions. This eliminated four test combinations that otherwise would have included PEFW. In the combinations that included the Norfab barrier, the PEFW was placed inside the Norfab barrier, which was in turn covered by the upholstery fabric. This may have limited the role of the PEFW in the initial burning process. In the remaining combinations without a barrier fabric, the PEFW was located next to the upholstery fabric, enhancing the likelihood of an effect.

Closer inspection of the bar plots for $\overline{t_{+25}}$ (Figure 25), $\overline{t_{peak1}}$ (Figure 26), $\overline{HRR_{peak1}}$ (Figure 27), $\overline{t_{max}}$ (Figure 28), and $\overline{HRR_{max}}$ (Figure 34) suggests that there may have been relatively small effects of adding PEFW to mock-ups having a given set of other materials. Consider first the mock-ups with no added barrier. The plots show that, with two exceptions, the addition of PEFW to mock-ups covered with cotton fabric resulted in slightly reduced values for all five parameters. Note that in many cases the changes were comparable to the experimental variations within a given combination (indicated by error bars). The exceptions to the general behavior were the two HRR measures, $\overline{HRR_{peak1}}$ and $\overline{HRR_{max}}$, for the mock-ups which incorporated FRFPUF, which were higher for Combination 15 with added PEFW as compared to Combination 13 without the wrap. These results suggest a weak effect on these parameters of adding PEFW

to cushions covered with the cotton fabric as well as the possibility that the effect on the HRR maxima changes sign depending on foam type. A similar comparison for cushions covered with 78%PP/22%PE fabric shows that the values were generally nearly the same and that the signs of the differences appeared to be random.

There is weak evidence for another type of effect resulting from adding PEFW to the mock-ups. Comparison of the values of $\overline{t_{max}}$ and $\overline{HRR_{max}}$ for Combinations 17 and 19 suggests that Combination 19 was somewhat more resistant to fire than Combination 17. In fact, Test 19_1 did not generate a significant HRR following the application of each of the three ignition sources, while the onset of burning of Test 19_2 was significantly delayed following application of Ignition Source 2. In contrast, both tests for Combination 17 developed significant HRRs which were reached at earlier times than in Test 19_2. This suggests that the addition of PEFW provided limited protection for the underlying FPUF. Such a result is not unreasonable since, as discussed above, it is believed that the maximum HRRs occurred after the Norfab barriers were breeched at weak points associated with the presence of zippers and/or seams sewn with nylon thread, and liquid FPUF pyrolyzate was released. It is likely that the presence of the PEFW provided limited additional shielding for the FPUF.

While a careful inspection of the results suggests a weak effect of adding PEFW to the cushions, the overall effect was too small to show up as a statistically significant primary effect. The above discussion also suggests the presence of a weak interaction between fabric and PEFW on the results.

Even though polyester fiber wrap is frequently incorporated into modern RUF, there are relatively few systematic studies of how its use affects the burning behavior. Most investigations that have included PEFW have compared its effect on burning behavior to items incorporating a fire barrier. The only earlier study we identified in which the burning behaviors of RUF items with and without PEFW were compared was that of Fabian. [62] This author found that the addition of PEFW had relatively minor effects on burning, consistent with the current study.

The type of thread used to sew the mock-ups was included in the test matrix because the opening of seams due to heating of thermoplastic thread has been identified as a possible means for flames to penetrate the cover fabric or a barrier of a cushion and reach the underlying cushioning material. [41] The Kevlar thread should resist heating much better than nylon thread. In retrospect, the test matrix utilized here was not appropriate for testing this hypothesis, and it is not surprising that no effect of thread type on burning behavior was statistically verified. In tests without a barrier, flames spread over the cover fabrics on the cushions, and the underlying FPUF was exposed by the failure of the fabric. In the case of the thermoplastic fabric the material pulled away from the flames and exposed the interior, while the cotton fabric first charred and then either split due to stresses or smoldered away (both were observed), again exposing the interior. Since the interiors had already been exposed, a seam opening due to failure of the sewing thread would have had little to no effect on the burning behaviors.

The Whispershield barrier fabric included in the mock-ups was not sewn, so thread was only used to sew the cover fabric, which would open in the manner described above during a fire. Mock-ups that included the Norfab barrier fabric might have been expected to be sensitive to the thread type since this barrier was sewn, and seams would represent a possible weak point in the barrier system. However, as discussed above, the Norfab barriers also included aluminum zippers held in place by nylon webbing, and these locations also represented likely failure points. The Kevlar thread was included in Combinations 18, 19, 21, and 24. As described earlier, Combination 19 contained PEFW and showed an unusual burning behavior, while Combination 21 did not develop a measurable HRR. It is not surprising that no effect of thread type was distinguishable in the statistical analyses.

As described in Section 7.3, the test matrix allowed the effects of interactions between the five factors on the 13 test responses to be assessed. Table 34 includes a summary of the results. A total of eight such interactions had statistically significant effects on the five responses used to characterize the HRR curves. Three of these involved Barrier*Fabric interactions. Interestingly, the three corresponded to the time periods required to reach given HRR levels. The Barrier*Fabric interaction did not have statistically significant effects on the two responses based on HRR magnitudes. It seems reasonable to observe strong interactions between the Barrier and Fabric factors since they had the strongest primary effects on the HRR-based responses.

Two of the statistically significant interactions were between the Fabric and Foam factors. These interactions are between the two factors with the strongest and third-strongest primary effects. The significant interactions involved the initial HRR growth time, t_{+25} and the maximum HRR, HRR_{max}. There is no clear pattern in these results since these two responses would have been expected to have very different dependencies on the factors.

The remaining three statistically significant interactions involve the Fiber Wrap factor interacting with the Barrier and Foam factors. The significance of these interactions is somewhat surprising because they involve a factor, namely, Fiber Wrap, which was not identified as having a statistically significant primary effect on the HRR-based parameters. However, as discussed above, review of the relevant results provided hints that such interactions might exist. Miller reached a similar conclusion during his analysis of the experimental results of Metha [60]. [61] This author reported that despite the fact that fabric type did not have a statistically significant primary effect on peak HRR measurements (recall that the study actually refers to an initial HRR peak), a very strong, statistically-significant Fabric*Barrier interaction was identified. He speculated that the strength of this interaction may have masked a possible primary Fabric effect. A similar explanation may explain the current findings.

The existence of strong interactions between the experimental factors has important implications for developing an understanding of the effectiveness of various approaches for reducing RUF flammability. Not only will it be necessary to understand how individual materials change the burning behavior, but it will also be important to understand how various material changes interact with one another.

Limited discussions of such interaction effects exist in the RUF literature. Only three investigations using statistical analysis have been identified. These were discussed in Section 1. The Miller analysis of the Metha data discussed immediately above found a strong Barrier*Fabric interaction on the peak HHR and the time required to reach this value as the only statistically meaningful interaction. [61] In the current work the same interaction type was found to influence the periods required to reach a given HRR level, but not the HRR values themselves. Janssens did not incorporate interactions into his statistical analysis. [63] Miller also performed a similar interaction term analysis for the experimental results of Fansler and Lock [66]. [67] Based on analyses of the responses for the time required to reach and the value of maximum HRR, only the Barrier*Fabric interaction on the time to reach the HRR maximum was identified as statistically significant. This conclusion is consistent with that reached in the current study.

A few additional comments concerning the temporal behaviors of the HRR curves are warranted. The most widely used approach in the literature for approximating RUF HRR time behaviors can be traced back to the work of Babrauskas and Walton. [111] These authors noted that a variety of qualitatively different HRR temporal profiles had been observed in furniture calorimeter studies of upholstered furniture and mock-ups (see Figure 1 in [111]), but that most could be well approximated as having triangular shapes. These shapes were defined by four parameters: triangle peak height (equal to HRR_{max}), time to peak, triangle base width, and time to start of triangle base. These observations served as the basis for a "design procedure" to predict the maximum HRRs and burning times of upholstered furniture. This procedure was basically a correlation

approach that expressed the maximum HRR and triangle base width in terms of factors that varied with fabric, padding, combustible mass of the item, frame material and upholstered furniture style.

The approach of Babrauskas and Walton was adopted and extended based on results from the CBUF study. [43] The correlating variables were adjusted and new values of the parameters used in the expressions predicting the HRR maximum and the time to HRR peak were determined. This correlation approach has subsequently been tested by a number of investigators. [49, 63, 112] In the most widely used approach, the experimental timeline is adjusted so that the zero time for comparison purposes corresponds to the time when the HRR first reaches 50 kW.

On the basis of a series of ten test burns of chairs incorporating five different foams and two upholstery fabrics (100 % polypropylene and 95 % wool/5 % synthetic), Denize concluded that the HRR temporal curves could be best described by a four-stage time behavior which incorporated a 1) "constant growth HRR" stage to an initial maximum, 2) a "decline in HRR" stage to a minimum HRR, 3) a "rapid growth" stage to a second HRR maximum, and 4) a "decay in HRR" stage in which the HRR fell slowly towards zero. [51] Such time behaviors are very different from the "triangular" temporal profiles described by Babrauskas and Walton. [111]

Denize provided a description of the chair burning behaviors responsible for the shapes of the HRR temporal profiles. Stage 1 was a period of roughly constant HRR growth following the application of the ignition burner that lasted until the seat cushion on the chair began to collapse, releasing liquid pyrolyzate that pooled in the cavity below the cushions. At the end of Stage 1 the covering around the cavity at the base of the chair was still intact and limited the amount of air available to burn the liquid pyrolyzate. As a result, the HRR dropped as Stage 2 burning developed. As burning continued, the fabric surrounding the cavity burned away and allowed additional air to reach the vicinity of the liquid pyrolyzate, and the fire rapidly grew on the liquid pool while also accelerating burning of the remaining soft cushioning materials on the chair frame. This Stage 3 burning resulted in a second HRR maximum. Finally, as the liquid pyrolyzate and cushioning material began to burn out, the fire entered Stage 4 as the HRR decayed.

The temporal HRR profiles observed during the current study were described in Section 5.3. A sufficient number showed multiple peaks that two types of HRR maxima and their associated times were defined, corresponding to the initial HRR peak and the maximum HRR observed. Recall that in some cases HRR_{peak1} and HRR_{max} were identical. The temporal profiles varied significantly from combination to combination, depending strongly on how a given type of mock-up burned. Such variations are evident in the composite plot of HRRs shown in Figure 77. Only a few combinations have shapes that can be easily matched to those suggested by either Babrauskas and Walton or Denize. On this basis, we conclude that there is unlikely to be a common temporal profile that describes the temporal HRR profiles of RUF mock-ups. On the other hand, it should be possible to relate the temporal profiles to the observed flame spread and burning behaviors.

The experimental observations provide additional insights into how changes in materials can alter the effectiveness of including FRFPUF in the cushions for reducing mock-up flammability. As shown in Appendix C.2, the SI-1324 FRFPUF arranged in the mock-up configuration was able to withstand the direct application of a relatively strong BS-5852 Ignition Source 5 wood crib. Nonetheless, mock-ups including cushions with this foam covered only with upholstery fabric (Combinations 17 and 18) were readily ignited by much smaller flames that resulted in fires involving the underlying FPUF capable of generating substantial HRRs. This is a further demonstration of the important role that the burning behavior of upholstery cover fabric play in RUF flammability. Such burning on either cotton or 78%PP/22%PE was more effective at involving the underlying FRFPUF than direct application of the wood crib. The ability of cotton to act in this manner is particularly striking since this cover fabric tended to burn with flames (in the absence of foam involvement) that appeared relatively mild compared to those of a wood crib. Adding

polyester to these mock-ups (Combinations 19 and 20) changed the observed burning behaviors slightly. In particular, substantial burning of the underlying FPUF did not develop during the Combination 19-1 test, while such burning did take place for Combination 19-2 as well as the Combination 20 mock-ups. This may be an indication that the layer of polyester in combination with the overlying cotton fabric provided marginal protection from involvement of the underlying foam.

Incorporating a Whispershield barrier in cushions with FRFPUF (Combinations 5 and 6) had interesting effects on the burning behaviors. Ignition of mock-ups covered with thermoplastic fabric (Combination 6) resulted in fires in which the cover fabric rapidly burned off, but the foam within the barrier did not become substantially involved. On the other hand, for two out of three Combination 5 tests, long-lived, low-HRR fires developed that consumed substantial amounts of the underlying FRFPUF despite the observation that HRR_{max} values were lower than for the Combination 6 fires. Even though the flames associated with burning of the cotton fabric were much less intense than those on thermoplastic fabric, they proved to be more effective in igniting the FRFPUF underlying the barrier. These observations suggest that the effectiveness of this barrier in limiting foam involvement was not only a function of the intensity of the flaming source, but was sensitive to other characteristics of the flaming. In this case, the length of time the flame was present at a given location was likely playing a role.

The effect of adding Norfab barriers also changed the flammability behaviors of the mock-ups with FRFPUF in complicated ways. There was no substantial involvement of the foam for mock-ups covered with cotton fabric in contrast to the results when Whispershield was used as the barrier fabric. For the three tests with Combination 22 mock-ups, substantial amounts of the FPUF were consumed by long-lasting, low-HRR fires. These results indicate that burning of the 78%PP/22%PE cover fabric was sufficient to generate fires sustained by foam burning (again in contrast to the findings for mock-ups incorporating Whispershield). As discussed earlier, the development of such burning was likely assisted by the fire breeching the cushions at locations where the zippers were located. The addition of a layer of polyester fiber wrap inside the barrier fabric (Combination 24) resulted in much less involvement of the underlying foam. Apparently, the polyester provided additional protection in the area of the zipper.

The above discussion indicates that whether or not the soft-cushioning materials of upholstered items will contribute in an important way to the HRR behavior of the item can depend in complicated ways on the materials and their possible interactions used as covers. Quite complex burning behaviors can play important roles.

8.2 Total Heat Release

The integration of a HRR curve over the entire burning period yields the total heat release, Q_{tot}, for the test. Here we have differentiated between the five responses based on the HRR curves and Q_{tot}. The averages and standard deviations for Q_{tot} are shown as a function of mock-up combination number in Figure 40. The appearance is very different from the corresponding plot for $\overline{HRR_{max}}$ in Figure 34. Different dependencies due to changes in cover fabric, FPUF, and barriers are evident.

The three primary effect analyses summarized in Table 22, Table 28, and Table 29 agree that only the Foam factor had a statistically significant primary effect on Q_{tot}. This contrasts sharply with results for the five measures based on the HRR curves, which showed statistically significant effects for the Fabric, Barrier, and Foam factors.

Several features in Figure 40 are worthy of discussion. First, note that Combinations 1, 2, 9, 10, 11, 12, 17, and 19, all containing NFRFPUF, have $\overline{Q_{tot}}$ values around 60 MJ. Recall that limited burning was observed for Test 19_1, and the value in Figure 40 is only for Test 19_2. Post-test checks showed that the vast majority of NFRFPUF was consumed in these tests. The similar $\overline{Q_{tot}}$ values suggest that the masses of

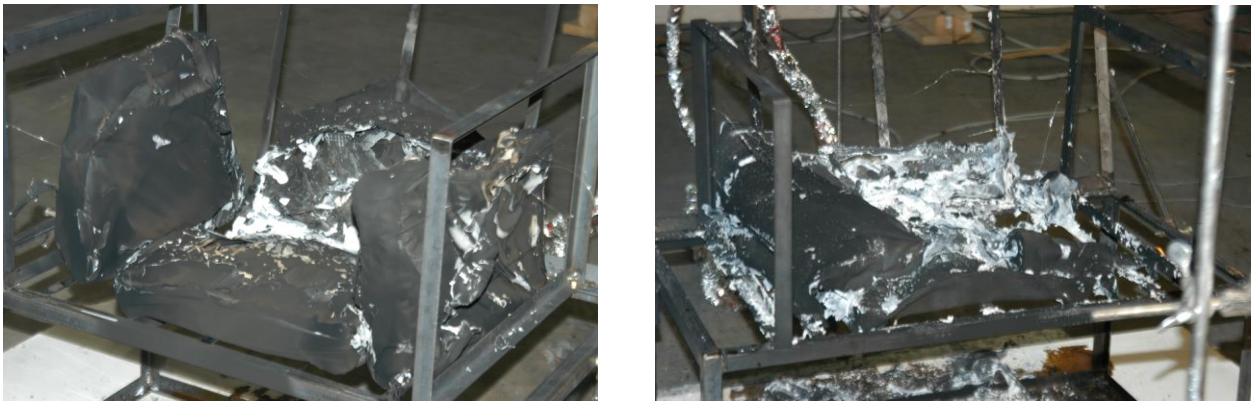

Figure 114. Two images showing the remaining charred material on the mock-up stand following Test 17_1 (left) and Test 18_1 (right).

burned material were roughly the same and that diffeences in heat released by cotton and 78%PP/22%PE were relatively small. The remaining combinations containing NFRFPUF (Combinations 18 and 20) had substantially higher $\overline{Q_{tot}}$. These mock-ups included cushions with the thermoplastic cover fabric, the Norfab barrier fabric, and, in the case of Combination 20, PEFW inside of the barrier. The likely reason for the higher values of $\overline{Q_{tot}}$ for these two combinations is more complete burning of the dense Norfab barrier system along with nearly complete burning of the NFRFPUF. Figure 114 compares photographs of the charred Norfab barriers following Test 17_1 and Test 18_1. The barrier for Test 17_1 still has the shape of the original cushions and shows limited loss of Norfab, while the residue from Test 18_1 is collapsed and has clearly loss more barrier material. It can be concluded that, with the exception of Test 19_1, nearly all of the foam inside mock-ups containing NFRFPUF was consumed regardless of cover fabric, presence or absence of a barrier material, and whether or not PEFW was incorporated.

The differences in $\overline{Q_{tot}}$ between the cotton-covered (Combinations 17 and 19) and 78%PP/22%PE-covered (Combinations 18 and 20) mock-ups in Figure 40 are striking. The higher loss of Norfab barrier fabric is likely attributable to the more intense burning that developed on the mock-ups covered with the thermoplastic fabric. As evident in Figure 34, $\overline{HRR_{max}}$ for these mock-ups were more than a factor of two higher. As discussed earlier (see Section 5.3, Figure 33 and Section 8.1, Figure 112), videos showed that large amounts of liquid from the mock-ups with thermoplastic fabric dumped onto the test stand base and subsequently burned as substantial pool fires. For the mock-ups with cotton cover fabric, only small amounts of liquid dripped down onto the test stand base, and very little burning occurred there.

Mock-ups incorporating FRFPUF generally had Q_{tot} that were less than those measured for mock-ups with NFRFPUF. There was also more variability in the values with changes in cover fabric and barrier usage and type. For the combinations without a barrier and those with a Whispershield barrier, higher values of Q_{tot} were observed for mock-ups with cotton cover fabric as compared to those with the 78%PP/22%PE. Note that Test 5_1 was an exception since it did not develop a measurable HRR following the application of all three ignition sources. This is the reason for the large standard deviation for this combination in Figure 40. Even though Combination 5 mock-ups released considerably more heat than Combination 6 cases, the values of $\overline{HRR_{max}}$ were higher for Combination 6. Review of videos and the individual HRR curves provides an explanation for these observations. When ignited, flames spread relatively rapidly over the thermoplastic covers and underlying barrier, and this burning was responsible for the HRR maximum. Little or no burning of the FRFPUF under the barrier was apparent. In contrast, fires on the Combination 6 mock-ups initially spread very slowly over the cotton cover fabric with little visible flaming and very low HRR. After reaching the intersections of the seat, back, and arm cushions, the burning intensity increased, and relatively weak flames were observed that ultimately spread to cover the various cushion surfaces in a sequential manner. As can be seen in Figure 28, the times required to reach $\overline{HRR_{max}}$ were much longer

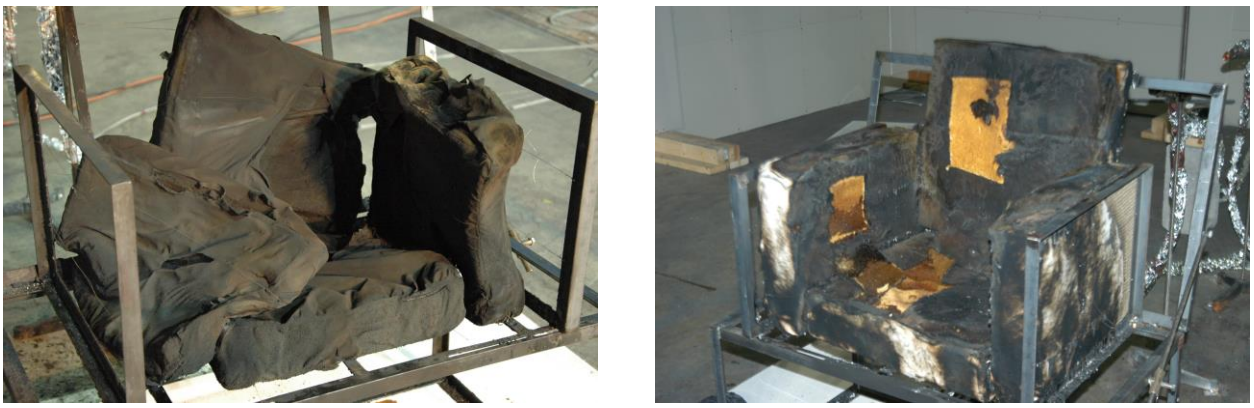

Figure 115. Two images showing the remaining charred material on the mock-up stand following Test 5_3 (left) and Test 6_1 (right). Sections of the cover and barrier fabrics have been cut out to expose the material underneath in the figure on the right.

for the Combination 5 mock-ups. Even though burning on the cotton-covered mock-ups was less intense, the much longer burn periods resulted in higher Q_{tot}.

Two photographs of the mock-ups after Tests 5_3 and 6_1 are shown in Figure 115. Sections of the cover fabric and the underlying barrier fabric have been cut out to expose the cushioning material underneath for Test 6_1. Some darkening of the FRFPUF is evident, but the foam appears to be intact at these locations. There is even some unburned 78%PP/22%PE fabric visible on the outside of the right arm. The appearance of the mock-up originally covered with cotton, Test 5_3, is totally different. While the residue still has the general shape of the four cushions, the cushions appear to be collapsed. There are several openings in the material, and no intact foam is visible inside the cushions. When the residue from the cushions was cut open, a hard, char-like material was found inside that had a much smaller volume than that originally occupied by the FRFPUF. These observations indicate that the small fires responsible for the long duration, low-level HRRs seen in Figure A-21 were fueled by the FRFPUF inside the cushions. It is an interesting observation that the relatively weak flames that grew on the cotton-covered cushions were sufficient to involve the foam inside the cushions, while the much stronger flames spreading over the cushions covered with a thermoplastic material did not.

A similar dependence of $\overline{Q_{tot}}$ on fabric was observed for the mock-ups with no barriers and FRFPUF cushioning (Combinations 13-16). The HRR curves in Figure A-98 and Figure A-116 show that the combinations with 78%PP/22%PE cover fabric developed a single peak, while those with the cotton cover fabric (Figure A-86 and Figure A-107) had double peaks of roughly comparable magnitudes. Comparison of the HRR curves with videos of the fires provided an explanation. Following ignition of Combinations 14 and 16, which were covered with thermoplastic fabric, flames spread rapidly over the entire mock-up, and a relatively large fire developed. After a short time, a significant amount of liquid poured onto the base of the mock-up stand as the thermoplastic covering gave way. Some flaming developed on the base, but it was not nearly as intense as observed for corresponding fires with NFRFPUF cushioning (e.g., compare Figure 29 and Figure 31). When the cotton-covered mock-ups were ignited, the flames spread more slowly, but eventually covered the entire interior surfaces of the seat, back, and arms, and a substantial fire developed that was responsible for the first HRR maximum. After a period on the order of one or two minutes, the fires began to die down. Somewhat later, the back and arm cushions were observed to collapse down on the seat cushions. When this occurred, the fires flared back up, leading to the second HRR peak. Very limited liquid was observed dripping down onto the test stand base, presumably being prevented from doing so by the intact cotton fabric. The higher $\overline{Q_{tot}}$ values for the cotton-covered mock-ups seem to have been due to more efficient burning of polyol-derived liquid trapped in the cushions as opposed to that deposited on the test stand base when the thermoplastic fabric opened up and released the liquid.

Figure 116. Images showing the remaining charred material on the mock-up stand following Test 22_2. The seat cushion has been removed, and the Norfab fabric on the left arm has been cut to expose the FRFPUF underneath. The partially collapsed back cushion is located to the right of the arm cushion.

Comparison of the results for Combinations 13 and 14 with those for Combination 15 and 16 indicates the inclusion of a layer of PEFW had little, if any, effect on $\overline{Q_{tot}}$.

The burning behaviors of the mock-ups with cushions that included FRFPUF and a Norfab barrier differed from those observed when a Whispershield barrier were used. For the mock-ups with Norfab barriers, essentially no HRR was measured when the upholstery fabric was cotton, while values of $\overline{Q_{tot}}$ for Combination 22 mock-ups were greater than and those for Combination 24 were close to those for Combination 6 (see Figure 40).

HHR and Q_{tot} temporal profiles are shown in Figure A-203 for Combination 22 tests. Review of videos for these tests showed that the initial HRRs measured for the mock-ups covered with thermoplastic fabric were due to the flames spreading and burning on the cover fabric, but at later times materials inside the cushions became involved. Later burning was relatively gentle but lasted for long periods. Flames were located primarily at locations where the cushions had zippers. Even though some of the cushioning material was involved, inspection of the materials remaining at the ends of the fires showed that substantial amounts of FRFPUF were present even though there was evidence of pyrolysis and charring. Figure 116 shows a view of the residue remaining after Test 22_2. During the fire, the back cushion shrank and partially collapsed. It is evident in the photograph that the bottom of the cushion partially opened during the fire and that a substantial amount of material was lost from the interior. The left-arm cushion visible in the photograph, with the Norfab barrier fabric slit open to expose the interior, was much more intact, even though there is evidence of heavy pyrolysis and charring near the bottom. At upper locations of the cushions there was some evidence of heating on the FRFPUF surface, but the material was essentially intact. When the foam was cut open, it appeared to be pristine on the interior.

The fires on Combination 24 mock-ups initially burned similarly to those on Combination 22, but there was considerably less loss of material from the cushion interiors and the long-lasting, low-HRR fires seen for Combination 22 did not develop. As discussed earlier, this may be associated with some limited protection provided by the PEFW surrounding the FRFPUF in these cushions. The similar $\overline{Q_{tot}}$ values for

Combination 6 and Combination 24 are the result of the fires on both cushion types involving primarily burning of the thermoplastic cover fabric.

The above discussion provides additional evidence that the effectiveness of a given barrier fabric is dependent on it interactions with the burning exterior cover fabric and other materials included in the cushions, in addition to the physical mechanisms responsible for its fire resistance.

While no discussions were identified in the literature which directly addressed the somewhat surprising observation that Q_{tot} values were higher for mock-ups that included cotton-covered cushions with either no barrier or a Whispershield barrier and FRFPUF than for the corresponding mock-ups with cushions covered with the 78%PP/22%PE fabric, there is evidence for a similar effect in the CSIRO results summarized by Firestone. [47] As discussed in Section 1, this study considered mock-ups with cushions covered with either a cotton/linen blend or polypropylene fabric combined with NFRFPUF or one of two FRFPUFs. Unlike the current study, it was reported that while mock-ups incorporating the non-FR foam and the polypropylene cover fabric had higher maximum HRRs than the corresponding cases with the cellulosic fabric, the opposite was the case when either of the FRFPUFs were used. HRR curves included in the report support Firestone's conclusion that the FRFPUF in the cushions covered with polypropylene did not become involved in the fires, while the foam did burn in cushions covered with cotton/linen fabric. By comparing HRR curves in the report, it is clear that the total amounts of heat released were much higher for mock-ups with cushions containing FRFPUF when covered with the cellulosic fabric than for those covered with polypropylene. [47] This is consistent with the conclusion reached in the current study. The conflicting results with regard to HRR_{max} between the two studies may be due differences in areal densities of the cover fabrics used, which were roughly 50 % higher in the CSIRO study.

As noted above, the statistical analysis indicated that only the Foam factor had a statistically significant effect on Q_{tot}. The strong dependence on foam type is consistent with the observations discussed above. Even though the measurements also indicated that the mock-ups that included FRFPUF had Q_{tot} which depended on cover and barrier fabrics, the variations were apparently not sufficient to result in statistically significant primary effects. Interestingly, these two factors do appear in the two two-term interactions, Barrier*Foam and Barrier*Fabric, which are identified as having statistically significant effects in Table 34. As discussed above, it is possible that a particularly strong primary effect has masked the primary effects of other variables, which can nonetheless appear in statistically significant two-term interactions.

A review of the literature dealing with burning of RUF and RUF mock-ups revealed that even though total heat release is often reported for real-scale experiments, the effects of changes in materials are infrequently assessed or discussed. As an example, no studies were identified that included statistical analysis of the effects of variables on the total heat release response. More recent studies have discussed the effects of foam type, use of polyester fiber wrap, and/or including barriers in cushions on the total heat release. [62, 65] Fabian reported that replacing standard FPUF with FRFPUF meeting TB-117 in his three-cushion mock-ups reduced the total heat release by 23 % and including PEFW increased the total heat release by 15 % to 20 %. [62] The effects of including barriers were variable, with some barriers leading to higher total heat release and others reducing the total heat release to values close to zero. Storesund et al. reported similar variability in total heat release due to the inclusion of barriers in similar mock-up with measured values either remaining roughly unchanged or decreasing significantly. [65]

As for the responses based on HHR, it is difficult to directly compare the total heat release results of the current study with the earlier findings. While general trends such as the impact of including PEFW, reduced values when standard FPUF is replaced with FRFPUF, and highly variable responses when barrier fabrics are included in the mock-ups are evident, detailed comparisons are limited by a lack of knowledge concerning materials used and different geometric configurations. As a result, the quantitative understanding of these variables on the total heat release of RUF and RUF mock-ups remains elusive.

8.3 FIGRA

The fire growth rate (FIGRA) parameter is defined as the HRR normalized by the measurement time. FIGRA is a relatively new parameter that was introduced in the European single burning item test. [105] While not a fundamental measurement, it does incorporate the ratio of two parameters HRR and time (which can be viewed as inversely related to the fire growth rate), judged to be important for characterizing flammability. Since improved flammability behavior is associated with lower HRRs and slower fire growth rates, i.e., longer times, a lower value of FIGRA implies better fire performance. Many years earlier Wooley et al. defined a parameter they called the "temperature index" as the square of maximum temperature in the upper layer of a fire divided by the time required to reach this value. [34] While clearly not equivalent to the FIGRA, it is interesting that these authors attempted to combine a property related to the fire intensity by normalizing it with a property inversely related to the fire growth rate.

As utilized here, FIGRA is a time-dependent parameter. Characteristic values derived from the FIGRA time records, namely, t_{FIGRA1}, $FIGRA_{peak1}$, $t_{FIGRAmax}$, and $FIGRA_{max}$, are analogous to those based on the HRR time records. Comparisons of the plots for parameters based on FIGRA with the corresponding plots based on HRR were discussed in Section 5.5. In general, relative variations with combination number were very similar for the two initial peak times (compare Figure 26 and Figure 41). This is not surprising since the initial HRR and FIGRA peak times for most combinations were nearly identical. Larger variations occurred when the maxima for relatively flat peaks were shifted to shorter times. The corresponding plots based on the times for maximum values, Figure 28 and Figure 43, also have similar appearances, even though the values of $t_{FIGRAmax}$ for a limited number of the combinations were reduced considerably from those for t_{max}. As an example, consider the values of t_{max} (2391 s) and $t_{FIGRAmax}$ (1500 s) for Combination 19_2 tests listed in Table B-3 and Table B-5, respectively. Comparison of the time plots of HRR and FIGRA in Figure A-152 and Figure A-153 shows that converting HRR to FIGRA resulted in the maximum peak shifting from the third peak in the HRR curve to the second in the FIGRA curve, thus explaining the large difference between the two values.

The use of FIGRA parameters resulted in increased differentiation between material combinations when the magnitudes of HRR and FIGRA were considered. The bar plots for $\overline{HRR_{peak1}}$ and $\overline{FIGRA_{peak1}}$ included in Figure 27 and Figure 42 reveal that relative differences between mock-up combinations differing only in the cover fabric were much larger and thus better differentiated for $\overline{FIGRA_{peak1}}$. This is the case because the times required to reach the initial peaks were increased substantially when cotton fabric was used. Relative changes due to varying only the foam type or only the barrier type or of simply adding PEFW to a mock-up appear to be minimal. This implies that the fabric type had, by far, the strongest influence on the differences in relative values for HRR_{peak1} and $FIGRA_{peak1}$. This is associated with slower fire spread and growth rates on cushions covered with cotton.

Corresponding plots for the average maximum values of HRR and FIGRA are shown in Figure 34 and Figure 44. Consistent with the results for initial peak magnitudes, large changes in relative differences between $\overline{HRR_{max}}$ and $\overline{FIGRA_{max}}$ are evident for combinations differing only in fabric type. Some additional changes in relative variations due to other cushion material changes are also apparent. For HRR, the third and fourth highest $\overline{HRR_{max}}$ values were recorded for Combinations 18 and 20, which included the 78%PP/22%PE fabric, Norfab barrier, and NFRFPUF. These values are higher than for each of the combinations without a barrier except Combinations 10 and 12. When $\overline{FIGRA_{max}}$ is considered, the relative values for Combinations 18 and 20 are considerably reduced compared to those without Norfab, reflecting the long periods required to reach HRR_{max} for these tests. In fact, the $\overline{FIGRA_{max}}$ values for Combinations 18 and 20 are the lowest observed for any of the combinations which included the thermoplastic cover fabric and NFRFPUF. Changes in the relative ordering of $\overline{HRR_{max}}$ and $\overline{FIGRA_{max}}$ variations with combination number are also evident. As discussed in Section 8.1, $\overline{HRR_{max}}$ values for Combinations 17 and 18, which included Norfab barriers, were somewhat higher than the corresponding

Combinations 1 and 2 with Whispershield barriers. This ordering is reversed when $\overline{FIGRA_{max}}$ values are considered.

The three statistical tests for characterizing main effects significance summarized in Section 7 yielded similar results for the four corresponding responses (times to and values of first peak and maximum peak) based on HRR and FIGRA. The results for statistical significance based on Main Effects Plot Analysis showed a one-to-one correspondence for the HRR and FIGRA paired responses for each of the five experimental factors (see Table 22). The results for the two analyses based on Block Plot Analysis, Sign Test (Table 28) and Paired Comparison Test (Table 29), differed slightly from the Main Effects Plot test (Table 22). While the three approaches agreed that Foam did not have a statistically significant effect on $t_{FIGRAmax}$, the two approaches based on Block Plots also indicated an insignificant effect on t_{FIGRA1}, while the opposite was the case for the Main Effects Plot Analysis. Taken together, the results suggest that primary responses based on the HRR and FIGRA temporal profiles responded similarly to changes in the experimental factors. The relatively minor changes in conclusions between the analysis approaches with regard to the statistically significance of Foam likely result from the relatively weak dependence on this factor identified earlier.

The Block Plot two-term interactions analysis discussed in Sections 7.3.2 and 7.3.3 (see Table 34) found that Barrier*Fabric interactions had statistically significant effects for each of the four responses based on FIGRA temporal profiles. No other two-term interactions resulted in statistically significant responses. As discussed in Section 8.1, Barrier*Fabric interactions were statistically significant for three out of four of the corresponding HRR factors, with t_{peak1} being the exception. It is significant that these two factors were identified as having the strongest effects on the experimental responses by the various main effects analyses. While a statistically significant second-order effect involving Foam*Wrap on HRR_{peak1} was identified, no additional second-order terms were statistically significant for FIGRA. It is likely that the increased strength of the fabric effect for the FIGRA results is the source of this difference.

The current findings suggest that the use of FIGRA results in increased differentiation between different mock-up material confirmations as well as changing the relative effects of various changes in materials. The findings do not provide a clear-cut justification for choosing between parameters based on HRR and FIGRA, and both have been included in the final analysis of results.

8.4 Flame Spread Behavior and Parameters

8.4.1 Qualitative Observations of Flame Spread

Qualitative flame spread behaviors over the seat and back cushions were discussed in Section 5.8, and quantitative measures were provided in Section 5.9. Some of the qualitative behaviors were clearly tied to ignition behavior. For instance, the observed flame spread following application of Ignition Source 1 to cotton-covered mock-ups depended on whether only the back cushion was ignited or both cushions became involved. For cases where both cushions were ignited or when the flames spread from the back cushion onto the seat cushion, the flames generally spread to cover the entire mock-up surface. When only the back cushion was ignited, the flames typically spread upward until they reached the top of the cushion and then died out. These upward spreading flames had a roughly linear acceleration, and upward flame spread was much more rapid than any lateral movement, so the burned area was usually a narrow vertical band when the top of the cushion was first reached. In several cases, no additional lateral movement took place, and only a narrow band remained when Ignition Source 2 was applied. Figure 14 shows an example of such a burn pattern. In other cases, the fire developed a secondary flame spread from a point somewhere above the cushion base and propagated in both directions at angles between vertical and horizontal, and the burned areas would widen with height. This type of flame spread continued until the secondary flame fronts

reached the top of the cushion and extinguished. An example of this type of burn pattern can be seen in Figure 15.

When both the seat and back cushions were ignited for the cotton-covered mock-ups, roughly constant rates of lateral flame spread generally occurred concurrently on each cushion along both directions of the crevice formed by the cushions. Most often the lateral flame spread across the back cushion was such that the burned edges were nearly vertical and moved at the same rates as the spread along the crevice. Examples of this type of burning behavior were shown in Figure 16 and Figure 50. This suggests that the spreading flames in the crevice acted as pilots for rapidly upward spreading vertical flames on the back cushion. When combined with the observation that lateral flame spread on the back cushion when the seat was not involved either did not occur or took place as the result of fires burning at an angle to the vertical indicates that lateral flame spread along the crevice formed by the two cushions spread faster and more reliably than lateral flame spread only on the nearly vertical back cushion.

For the fires on the cotton-covered mock-ups with no barrier or with a Whispershield barrier, the flame spread on the seat cushions initially developed approximately semi-circular shapes irrespective of FPUF type or the presence of PEFW. This was reflected in both the flame contour shapes and in the roughly equal values of characteristic lateral and transverse flame spread rates. For these mock-ups, initial flame spread on the seat cushion was nearly independent of spread direction and took place at a roughly constant rate. Thus, the initial flame spread on the seat cushion in such cases should be predictable given a single characteristic value of linear flame spread rate for the cushion and a pseudo-point source for ignition. Furthermore, since the lateral flame spread on the back cushion seemed to be piloted by the spreading fire on the seat cushion, it should be possible to predict lateral flame spread rates on the back cushion using the same characteristic flame spread rate. The measurement of the acceleration for the flames spreading upward on the back cushion should be sufficient to predict initial flame spread on this surface. Thus, it should be possible to predict the initial flame spread behavior on the seat and back cushions using two experimental parameters for these cotton-covered mock-ups.

The flame spread behavior on cotton-covered mock-ups incorporating a Norfab barrier fabric was clearly more inhibited than when this material was not included. While upward flame spread on the back cushion usually occurred, lateral flame spread on the back and both lateral and transverse flame spread on the seat cushions was more problematic and irregular. In many experiments where flame spread in both directions occurred along the crevice formed by the two cushions, the characteristic lateral spread rate was higher on the seat cushion than the corresponding transverse spread rate. This suggests that for these tests there was some enhancement of flame spread rate due to interaction with burning on the back cushion. In other tests the flame spread occurred along the crevice in only one direction from the ignition location. In a few others, the flames appeared to spread along only one direction, not necessarily the crevice, and developed strongly distorted burn areas. In many cases these fires died out before covering the entire seat cushion. Predicting such complex and complicated burning behaviors will clearly be more difficult than simply using the two flame spread parameters discussed above.

During the initial periods of flame spread over the cotton-covered mock-ups flame heights were generally short and yellow flames were sporadic and widely spaced. Closer inspection showed that there were very small bluish flames at the edges of the burned area where flame spread was occurring. Generally, flames were not as evident behind the flame front until more rapid fire development occurred (see ahead).

The flame spread behaviors observed for the mock-ups covered with the 78%PP/22%PE fabric differed substantially from those covered in cotton. The most obvious difference was that the cotton fabric tended to char and stay in place as flames spread over it, while the thermoplastic fabric tended to melt and pull away unevenly from the approaching fire. The edges of the burned areas for the cotton-covered mock-ups tended to be smooth while those with the thermoplastic were uneven. The melting behavior of the

thermoplastic resulted in the rapid exposure of the materials beneath the fabric, while the charred cotton provided some protection for the materials underneath.

Even though the mock-ups covered by the thermoplastic fabric were easily ignited by Ignition Source 1, variable flame spread behaviors were seen. The largest differences were apparent on the back cushions. For mock-ups formed with cushions containing NFRFPUF and no barrier (Combinations 10 and 12), the flames tended to spread rapidly up the cushions, resulting in a relatively narrow burned area by the time they reached the top of the cushion. Yellow flames were evident on the underlying materials exposed on the cushion by the spreading fire. An example of this type of flame spread was shown in Figure 51. Similar to the fire spread behaviors observed for many of the cotton-covered cushions, the fires tended to spread laterally in both directions at roughly the same rates on the seat and back cushions. The burned areas on the back cushion developed roughly vertical edges as the fires spread transversely, while the areas on the seat cushion were approximately circular. These characteristics are also evident in Figure 51. The edges of the burned areas on both cushions became more irregular as the flaming areas grew larger and heat feedback to the surfaces increased.

The remaining combinations of cushions covered by the thermoplastic, with one exception discussed below, showed a different type of flame spread. Following ignition, the fabric on the back cushion initially melted and receded upward away from the fire. Well before the receding fabric reached the top of the cushion, further upward movement halted until the flames grew substantially larger. As the flames on the seat cushion spread laterally along the cushion crevice, the exposed area on the lower section of the back cushion widened concurrently, and there was a period during which a substantial band of unburned (or melted) fabric remained along the upper portion of the back cushion above an exposed area of non-burning foam having a roughly rectangular shape. An example of this burning behavior was shown in Figure 54.

The first test involving Combination 2 materials was the exception, with flame spread on the back cushion resembling that observed for mock-ups with cushions formed from NFRFPUF covered with thermoplastic fabric. The second test for this combination burned in the alternate way. Figure 117 compares two frames taken from videos of these fires 90 s after ignition where the differences in flame spread behavior can be seen. These images provide an important clue as to the reason for the difference. For Test 2_1 blackening of the surface under the fabric, presumably the underlying Whispershield barrier, is evident all the way to the top of the back cushion. For Test 2_2 similar blackening is only evident in a band above locations where flame spread has taken place on the seat along the crevice with the back cushion. This suggests that flaming on the substrate was necessary for rapid upward flame spread and that the thermoplastic fabric burning alone was insufficient to support upward flame spread. The flames observed on the exposed back surfaces for fires that did spread rapidly to the top of the back cushion, e.g., see Figure 51 (note that the video was time-averaged), are consistent with this conclusion.

The flame spread on the thermoplastic-covered seat cushions containing FRFPUF and/or barrier fabrics also differed from those with no barrier and NFRFPUF. As the flames spread in the lateral directions from the ignition point, the burned areas developed roughly rectangular shapes. Examples of this type of burning behavior on the seat cushions are shown in Figure 118 for Tests 16_2 and 18_1. These shapes indicate that lateral flame spread rates were faster than in the transverse direction. The most likely reason for this observation is that flame spread in the lateral directions was enhanced by concurrent burning on the seat and back cushions along the crevice. It should be emphasized that while lateral flame spread appeared to be favored over transverse, there was no indication that the transverse flame spread paused as observed for upward flame spread over the back cushions. Comparison of Figure 117 and Figure 118 provides an explanation for the difference. As the thermoplastic fabric pulled away from the flames spreading over the seat, burning is evident on the rolls formed by the receding fabric for the two fires shown in Figure 118.Limited flaming is also visible in exposed areas behind the flame fronts. Note that the substrates

Figure 117. Two frames taken from videos recorded by Camera #2 90 s after ignition are shown for Test 2_1 (left) and Test 2_2 (right).

Figure 118. Frames taken from videos recorded by Camera #3 105 s following ignition are shown for Test 16_2 (left) and Test 18_1 (right).

immediately below the fabric were PEFW for Test 16_2 and Norfab for Test 18_1. The heat from the burning fabric edges was apparently sufficient to maintain flame spread over the horizontal surfaces.

Similar burning along the upper edges of exposed areas is not evident on the rear cushions for the fires shown in Figure 117. The difference in burning behavior for the underlying substrate in the exposed areas on the back cushion for these two tests is consistent with the conclusion that nearby burning is required to support upward flame spread over the thermoplastic fabric. Upward flame spread halted when the non-burning fabric pulled a sufficient distance away from the flames below.

The qualitative flame spread behaviors discussed above were highly variable with fabric type, type of foam utilized, and the presence or absence of a barrier. A review of the literature on RUF and RUF mock-ups behaviors did not identify studies where such a range of burning behaviors were described. However, multiple earlier studies have described some of the observations of the current study. As early as 1984 Krasny and Babraukas emphasized the different behaviors of cellulosic and thermoplastic fabrics, including cotton charring in place and polyolefins melting and pulling away from the spreading flames. [38] Similar observations were described by Ohlemiller and Shields [41] and Firestone [47]. Ohlemiller and Shields described a flame spread behavior (see their Figure 27) very similar to one of those observed in the current work where flames initially spread rapidly up the center of the back cushion (for ignition near the center of the crevice formed by the back and seat cushions) followed by slower lateral flame spread on the back cushion and transverse and lateral flame spread on the seat cushion. This was the case even though their

ignition source was much stronger than those employed here. [41] Mehta also discussed a similar flame spread behavior. [60]

8.4.2 Quantitative Measures of Flame Spread

The quantitative measures of flame spread in terms of characteristic upward acceleration and the characteristic lateral and transverse flame spread rate parameters summarized in Section 5.9 depended on the materials used in the cushions. The most dominant factor was upholstery cover fabric. Every value of u_l and u_t included in Figure 56 and Figure 58 for mock-ups covered with the 78%PP/22%PE fabric was higher than for the corresponding mock-ups with cotton fabric when the remaining materials were the same. It was also observed that the highest upward flame spread accelerations on the back cushions were measured for mock-ups upholstered with the thermoplastic fabric and cushioned with NFRFPUF (see Figure 55). However, it should be kept in mind that upward flame spread actually paused briefly on most of the other mock-up combinations upholstered with the thermoplastic. This observation emphasizes the importance of substrate burning behavior on upward flame spread.

The most direct measure of quantitative flame spread rate included in the statistical analysis of Section 7 is the average characteristic lateral velocity derived from the lateral flame spread rates on the seat and back cushions, $\bar{u}_l$. The results of the various analyses for the relative strengths of primary factor effects on $\bar{u}_l$ are included in Table 19, Table 20, and Table 31. In each case, Fabric was identified as the having the strongest effect.

Varying the other materials used in the cushions had smaller effects on the flame spread behaviors than observed for Fabric. Incorporating a barrier between the FPUF (or the FPUF covered with PEFW) had mixed effects on upward flame spread acceleration for cotton-covered back cushions (see Figure 55). Acceleration was faster when Whispershield was used as a barrier, while the presence of Norfab significantly reduced the acceleration. Interestingly, upward accelerations were slightly higher when NFRFPUF was replaced with the SI-1324-compliant foam in combinations with no barrier and those incorporating the Whispershield barrier. Little dependence on foam type was apparent for combinations with the Norfab barrier.

For mock-ups with a given upholstery fabric, it is evident from the $\bar{u}_t$ plot in Figure 58 that there were noticeable, but relatively minor, variations in lateral flame spread rate with changes in the other materials included in the cushions. For example, lateral flame spread rates for mock-ups with NFRFPUF were reduced somewhat when a barrier fabric was included, with combinations incorporating Norfab reducing the spread rate somewhat more than those with Whispershield. Such differences were not as evident for mock-ups that included FRFPUF. For mock-ups that did not include a barrier, the addition of the PEFW to otherwise identical cushions resulted in lower value of $\bar{u}_t$, with greater reductions for the cotton-covered mock-ups. Such changes were not apparent for the mock-ups that included the Norfab barrier.

The tests for statistical significance based on Main Effects Plots and summarized in Table 22 indicated that only Fabric had a significant effect on $\bar{u}_t$. However, the two analyzes based on Block Plot results (see Table 28 and Table 29) also identified Barrier as having statistically significant primary effects on $\bar{u}_t$. No statistically significant effects were identified for $\bar{u}_t$ by any of the analysis approaches when Foam, Fiber Wrap, or Sewing Thread were considered, but it should be noted that the p-values for the Foam factor were only slightly higher than the 0.05 significance level for both Block Plot results.

The tests summarized in Table 34 indicate that the statistically significant interactions involving $\bar{u}_t$ were Barrier*Fabric, Foam*Fabric, and Fiber Wrap*Fabric. All three involve Fabric, which was by far the strongest statistically significant primary factor. The presence of the Barrier*Fabric interaction is reasonable since the results of the two Block Plot analyses identified Barrier as being statistically significant. In contrast, the statistically significant interactions involving Foam Type and Fiber Wrap

include factors that were not statistically significant as main effects. This may be due to the strong dependence of $\bar{u}_t$ on upholstery fabric, which, as discussed earlier, may have obscured the primary effects associated with Foam Type (recall that the results fell just out of the statistically significant range) and Fiber Wrap. The Barrier factor did have a statistically significant main effect for many of the other responses, so the importance of its interaction with fabric for $\bar{u}_t$ may not be too surprising. On the other hand, the effect of Fiber Wrap was not statistically significant as a primary factor for any of the responses. Interestingly, the Fiber Wrap*Fabric interaction was also identified as statistically significant for the t_{+25} response. As discussed in Section 5.10, this response seems to be correlated with flame spread rate. This provides some additional support that a statistically significant Fiber Wrap*Fabric interaction may be a real effect for $\bar{u}_t$.

Even though the values of $\bar{u}_t$ have some dependence on other factors, there are useful insights to be gained by averaging together the results for each upholstery fabric. The results are 0.20 cm/s ± 0.04 cm/s and 0.058 cm/s ± 0.004 cm/s for mock-ups covered with the 78%PP/22%PE and cotton fabrics, respectively. Note that no values for Combinations 19 and 21 are included due to the limited flame spread observed on these cotton-covered mock-ups. Here the standard deviations are based on the variations between different tests with the same fabric. The relatively small variations suggest that the averaged values should provide good approximations for characteristic lateral flame spread rates over upholstered cushions for these two fabrics.

The number of previous investigations involving RUF or RUF mock-ups in which flame spread behavior was quantitatively characterized are surprisingly limited. There appears to be three major reasons for this. The first is that HRR is widely recognized as being the most important parameter for characterizing fire hazard. [106] The second is that flame spread rate measurements are technically challenging and time consuming. The third is the widely-held view that much of the variability in fire development is due to variations in the initial fire growth rate. As a result, it is common to attempt to improve reproducibility by defining the start of a fire as the time the fire reaches some pre-determined level, with 50 kW being the most common choice. [43] As made clear in the current study, flames have often already spread to cover much of the interior seating surface of a RUF item by the time the HRR reaches this level. For the current study we explicitly wanted to investigate flame spread and fire development immediately following ignition, so zero time was defined as the application time of the ignition source. The reproducibility of the experiments was generally good. In cases where substantial differences were observed between tests for a given material combination, they were often associated with variations in ignition effectiveness as opposed to subsequent flame spread behavior.

A few relevant studies of flame spread behavior were summarized by Krasny et al. [2] In an early paper describing flame spread over horizontal upholstered cushions, Lee and Wiltshire reported a flame spread rate over a cushion constructed with cotton having an areal density of 230 g/m^2 covering FPUF. [113] The value estimated from a plot in their paper was 0.067 cm/s, which is in relatively close agreement with the characteristic value of 0.057 cm/s given above. Another study was due to Krasny and Babrauskas. [38] These authors used temporally resolved area measurements of the burned area on the seat cushion as a surrogate for flame spread over four-cushion chair mock-ups following small-flame ignition at a location on the seat centerline 10 cm from the back cushion. The materials used in their cushions included both cotton and olefin cover fabrics having two areal densities as well as NFR- and FR-FPUFs. Unfortunately, it is not possible to relate their measurements directly to flame spread rates. Nonetheless, their conclusions regarding the effects of cushion materials on horizontal flame spread are relevant. They ranked the combinations from slowest to fastest flame spread as 1) heavy cotton fabric-covered assemblies, 2) FRFPUF without fabric, 3) light cotton fabric-covered assemblies, 4) polyolefin fabric-covered assemblies, and 5) ordinary polyurethane foam without fabric. The ordering of the polyolefin and cotton cover fabrics is the same as observed in the current study.

Table 41. Flame spread measurements in the horizontal flame spread test apparatus over fabric/foam composites. [114]

Fabric	Areal Density (g/m^2)	FPUF Type	Flame Spread Rate (cm/s)
Olefin	360	Non-fire-retarded	0.34
Olefin	360	Fire-retarded	0.30
Olefin	560	Fire retarded	0.10
Cotton	110	Fire-retarded	0.06
Cotton	650	Non-fire-retarded	0.01
Cotton	650	Fire-retarded	0
None		Non-fire-retarded	0.37
None		Fire-retarded	0.21

Krasny et al. briefly described a series of unpublished measurements of horizontal flame spread rate on upholstered cushions using an apparatus originally developed by Dilbert [115] to study flame spread on samples subjected to thermal irradiation. [2] A summary of the findings from this study, attributed to Babrauskas, was included in a research proposal prepared by Mark Dietenberger, which is available in the NIST fire research literature collection. [114] Flame spread rates with no applied external thermal radiation, which are relevant to the current study, are listed in Table 41 along with the corresponding cover fabric and areal density and FPUF type. The closest match to the current experiments is the cotton upholstery with an areal density of 120 g/m^2 over NFRFPUF. The fabric used in the current experiments had an areal density of 222 g/m^2. The measured flame spread rate of 0.06 cm/s is very close to the value of 0.058 cm/s ± 0.004 cm/s determined for the characteristic flame spread rate on the mock-ups, which was shown to be primarily the result of flame spread on the horizontal seat cushions. The fabric for the olefin-covered cushion over NFR foam included in Table 41 with an areal density of 360 g/m^2 is somewhat heavier than the 78%PP/22%PE fabric used in the current tests (203 g/m^2). The characteristic flame spread rate from the current measurements (0.20 cm/s) is less than the 0.34 cm/s value included in Table 41. The two values are not in as good agreement as observed for cotton-covered cushions. This may be due to differences in the fabrics or NFRFPUF properties. Note that for identical materials, the current value would have been expected to be the larger based on the expected dependence on fabric areal density (decreasing with areal density) summarized by Krasny et al. [2]

Paul summarized vertical and horizontal flame spread rate measurements on half-scale chairs taken from an unpublished report by Palmer et al. [116] Three fabric/foam combinations were considered including polypropylene over standard FPUF. For the latter combination, measured vertical and horizontal flame spread rates were 1.3 cm/s and 0.17 cm/s, respectively. Comparison of the vertical value with the current findings is not feasible since vertical flame spread on the back cushions of mock-ups formed from NFRFPUF and the 78%PP/22%PE fabric showed strong acceleration as the flames spread upward on the back cushions. The characteristic 0.20 cm/s flame spread rate measured on the seat cushion in the current study is relatively close to the 0.17 cm/s value reported by Paul for horizontal flame spread over the half-scale chair. The small difference could be due to differences in the fabric areal density or FPUF properties.

An interesting study in which fires were ignited in the interior corner formed by the seat, back, and arm cushions of one chair of two nearby chairs arranged side-by-side was summarized by Prager. [117] The ignition corner was on the first chair opposite the second chair. The fires were observed to spread across the initially ignited chair and then jump to the edge of the nearby chair before spreading further. Measurements reported included the lateral flame spread rates for both chairs. Multiple combinations of upholstery fabric, interliners, and cushioning material were tested. For a chair containing NFRFPUF covered with polypropylene, the flame spread rate over the first chair was approximately 0.5 cm/s. This value is more than a factor of two higher than found for the similar combinations of materials tested in the current work. An image (their Figure 13) of a fire burning on one of the chairs included in [117] provides

a probable explanation. The spreading fire is seen to involve all three surfaces in the corner formed by the seat, back, and arm cushions with flame heights higher than the back cushion. The current experiments have shown that transverse flame spread rates accelerated on the seat when such burning developed. It thus appears that igniting in the corner formed by the three cushions substantially altered the quantitative flame spread behavior due to more rapid fire growth. This emphasizes the likely dependence of flame spread behavior on ignition location.

While earlier studies of flame spread rate are limited, comparisons indicate that measurements of the characteristic lateral flame spread rates recorded in this study are in reasonably good agreement with previous results on horizontal upholstered surfaces for conditions where flame spread is not augmented by thermal radiation from tall flames. This suggests that it should be possible to develop tables of characteristic flame spread rates for various material combinations for such cases.

The periods between the application of an ignition source at the center of the mock-up and the ignition of the arms were recorded as an alternate measure of relative flame spread rate. Results plotted in terms of averaged values for the ignition times ($\overline{t_{ig}}$) of the two arms are included in Figure 61. The strong dependence on upholstery fabric is evident by comparing the results for combinations differing only in cover fabric. Keeping in mind that the times for Combinations 21 and 23 are actually infinite since the arms did not ignite, it is apparent that $\overline{t_{ig}}$ values for the mock-ups covered with 78%PP/22%PE were considerably shorter for each pair than those covered with cotton. These results are consistent with the higher values of $\bar{u}_t$ recorded for the thermoplastic fabric since the times required to ignite the arms should be roughly inversely dependent on the flame spread rate. Closer inspection of Figure 61 suggests that values of $\overline{t_{ig}}$ also varied with changes in the barrier condition and foam type.

The flame spread periods required to ignite each arm (responses Y12 and Y13) were included in the three primary effect statistical analyses described in Section 7. The results are summarized in Table 22, Table 28, and Table 29. The factors identified as having statistically significant primary effects on the arm ignition times varied with analysis approach. As was the case for $\bar{u}_t$, Fabric was, by far, the factor with the strongest statistically significant effects on t_{igr} and t_{igl}. As also found for $\bar{u}_t$, the results of the Main Effects Plot analysis identified Fabric as the only statistically significant factor for these responses. In contrast, analysis based on the Block Plot Sign Test (Table 28) also identified Barrier as having statistically significant effects, as was also the case for $\bar{u}_t$. The Block Plot Paired-Comparison analysis (Table 29) not only identified Barrier as having statistically significant effects on the two periods, but also Foam. In contrast, the corresponding analysis for $\bar{u}_t$ indicated that the effect of Foam was not statistically significant. No two-term interactions (Table 34) were identified as statistically significant for these two responses.

Figure 61 includes comparisons of $\overline{t_{ig}}$ with corresponding values of the times required for the fires to grow to 25 kW, $\overline{t_{+25}}$. It is evident that both parameters have similar dependencies on mock-up combination number. As discussed in Section 5.10, the explanation for this observation seems to be that rapid HRR growth was often observed shortly after flames spread into the corners formed by the seat, back, and arm cushions and began to burn on the three nearby surfaces. A correlation with parameters related to fire spread rate is not surprising for small-flame ignition at the of center of the crevice formed by the seat and back cushions. It is likely that the results would be different for ignition at other locations or by a larger dispersed ignition source such as that specified in Cal TB-133. [26]

No studies utilizing arm ignition as a surrogate for flame spread rate on RUF or RUF mock-ups were identified in the literature. The importance of corner burning on the overall fire growth rate also does not seem to have been discussed previously.

The flame spread behaviors discussed thus far are limited to the initial fire growth period between ignition near the center of the seat-back cushion crevice and when a fire had spread laterally in both directions to the arms of the mock-up. As discussed in Section 5.10, in many cases the HRR for such fires had not yet reached 25 kW. However, it was observed that for most of these fires rapid fire growth occurred shortly after the arms became involved along with the seat and back. Generally, the transverse flame spread rates on the seat increased substantially as the flame heights grew in the mock-up corners. As shown in Figure 60, u_{st} increased by as much as a factor of five for mock-ups containing cushions with NFRFPUF covered with 78%PP/22%PE fabric. These fires reached high HRRs very quickly. For most other material combinations, the relative increases in u_{st} were between 2 and 4. For Combination 5 mock-ups there was very little increase in u_{st} after the flames involved the arm cushions. For these tests, the initial peak HRRs recorded were among the lowest observed during the test series. This suggests that a minimum fire size is required to cause acceleration of flame spread in the transverse direction. Note that this conclusion is consistent with observation of constant flame spread rates at early times when fire HRRs were low.

The flame contours allowed quantitative measurements of burned areas on the seat and back cushions of the mock-ups to be made as a function of time as described in Section 5.11. The growth of these areas is clearly related to flame spread behavior. It was shown that the growth of these areas was consistent with the types of flame spread observed. For instance, burned areas increased faster than linearly on the back during periods of rapid upward flame spread acceleration and then became more linear as the flames spread laterally. Due to geometric effects, the roughly constant flame spread rates on the seat resulted in burned area growth that increased with the square of time until the arms become involved. The dependence became more linear as the flames spread across the remainder of the seat cushion up to the point where transverse flame spread acceleration occurred as the fire grew. Apparently, such observations have not been reported in the literature previously.

It should be possible to use the total burned area measurements to correlate with flame spread behavior. In practice, it proved difficult to identify appropriate parameters for characterizing the time behavior of the fire areas due to changes in the time dependence with time. Assumptions are possible, such as the burned area on the seat cushion varies as time squared, that would allow the burned area to be related to the flame spread rate. Since flame spread rates were measured directly, the decision was made to not pursue such analyses further.

The only quantitative measures based on burned cushion surface area discussed in Section 5.11 were the averaged periods required for flames to fully spread over the seat and back cushions ($\overline{t_{seat}}$ and $\overline{t_{back}}$) as a function of combination number. The results are included in Table B-2 and plotted in Figure 62. As discussed in Section 5.11, the periods depended strongly on cover fabric and showed complex dependencies on the barrier and foam types. A strong interaction of fabric and foam was apparent in the results.

Comparison of Figure 61, which shows values of $\overline{t_{ig}}$ and $\overline{t_{+25}}$ plotted as a function of combination number, and Figure 62 shows that the relative variations of $\overline{t_{seat}}$ and $\overline{t_{back}}$ with combination number are similar to those measured for $\overline{t_{ig}}$ and $\overline{t_{+25}}$. This suggests that all four parameters are closely associated with flame spread behavior. Even so, some differences are evident among the four measures. For instance, even though the flames did not spread to fully cover the back and seat cushions and the HRRs did not reach 25 kW for Combinations 21 and 23, arm ignitions were observed. The average period required for the fires to grow to 25 kW on Combination 5 mock-ups were relatively much longer than the corresponding values for arm ignition. The relative values of $\overline{t_{seat}}$ and $\overline{t_{back}}$ were similar to those for $\overline{t_{ig}}$.

The times required for flames to fully spread over the seat cushions were usually the longest of the four types of periods. This is the expected behavior for fires where the flame spread and HRR developed in the most characteristic way identified in this study. Following ignition of both the seat and back cushions,

flames would spread rapidly up the back cushion while slower, roughly constant-rate, flame spread developed on the seat cushion. As the flames spread laterally on the seat, lateral flame spread on the back surface was piloted by the flames spreading over the seat. Arm ignition occurred at roughly the same time the laterally spreading flames reached the edges of the seat and back cushions. As discussed earlier, rapid HRR growth tended to occur when simultaneous burning developed in the corners formed by the seat, back, and arm cushions. As a result, for most fires values of $\overline{t_{+25}}$ were either less than or slightly higher than values of $\overline{t_{ig}}$.

Since the spreading flames on the back surfaces were piloted from below, values of $\overline{t_{back}}$ were typically greater than $\overline{t_{+25}}$ and $\overline{t_{ig}}$. Transverse flame spread rates on the seat were typically roughly equal to or less than the corresponding lateral rates. This usually resulted in substantial fractions of the seat surface being unignited when the three other characteristics periods were reached, thus leading to the values for $\overline{t_{seat}}$ having the largest values.

Tests in which the above ordering was not observed typically involved fires in which flame spread and HRR growth were relatively slow, such as the examples discussed above. This suggests that substantial improvement in burning behavior in terms of slower flame spread rates and reduced HRR are accompanied by changes in the relative order of $\overline{t_{+25}}$, $\overline{t_{ig}}$, $\overline{t_{back}}$, and $\overline{t_{seat}}$

The only earlier studies identified which reported temporally resolved measurements of burned surface area on RUF mock-ups were those of Krasny and Babrauskas [38] and Ohlemiller and Shields [41]. Krasny and Babrauskas estimated the burned area on the seat following small-flame ignition at a location 10 cm removed from the center of the crevice formed by the seat and back cushions. Initial flame spread behavior would be expected to be different than in the current study where ignition was at the crevice. The surface area of the 61 cm × 61 cm cushions was also roughly 1.8 times larger than for the cushions used in the current study (46 cm × 46 cm). The difference in ignition locations along with differences in materials and mock-up geometries make direct comparisons more difficult. Nonetheless, some general observations and even quantitative comparisons are possible.

Plots of burned areas as a function of time are shown in Figure 5 of Krasny and Babrauskas, and values are listed in tables. [38] Cover fabrics tested included moderate-weight (360 g/m^2) and heavy-weight (560 g/m^2) olefins and light-weight (110 g/m^2) and heavy-weight (650 g/m^2) cottons. Two FPUFS, one mildly fire-retarded and one non-fire-retarded, with densities of roughly 20 kg/m^3 were used. The measurements showed that the fastest flame spread occurred on cushions covered with the moderate-weight olefin, with flames spreading rapidly over the entire seat surface following short induction periods during which spread was relatively slow. A shorter period of 95 s was required to burn over the seat cushion with NFR-foam as compared to the mock-up with FRFPUF, 125 s. The values measured for comparable material combinations in the current experiments were somewhat higher $\overline{t_{seat}}$ = 119 s and $\overline{t_{seat}}$ = 170 s for Combination 10 and Combination 14, respectively (see Table B-2). Based simply on seat cushion surface area, the periods required for flames to fully cover the seat cushion would have been expected to be shorter in the current study. The lower areal density of the olefin cover fabric in the current experiments would also have been expected to favor relatively faster flame spread rates, thus also shortening the period needed to spread over the cushion. On the other hand, the higher FPUF density would have been expected to result in lower flame spread rates and increased periods. It is also possible that the cover fabric materials were different between the experiments since only "olefin" was specified by Krasny and Babrauskas. The similar magnitudes of the periods suggest reasonable agreement between the two sets of experiments, but the uncertainties do not allow a more quantitative assessment.

For the heavy-weight cotton fabric-covered cushions the periods required for flames to spread over the seats were 380 s when the cushion contained NFRFPUF and 570 s when FRFPUF was used. Corresponding

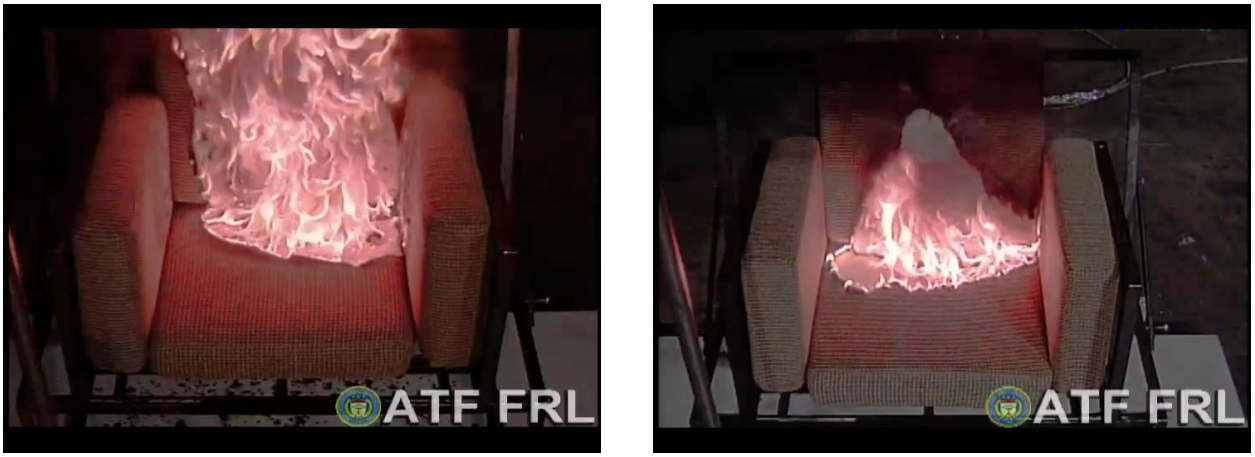

Figure 119. Images captured from Camera 3 videos of Test 10_1 (left) and Test 14_1 (right) are shown 89 s and 95 s following ignition, respectively.

values in the current experiments were $\overline{t_{seat}}$ =360 s and $\overline{t_{seat}}$ =730 s for Combination 9 and Combination 13 mock-ups. Krasny and Babrauskas also reported a value of 230 s for a mock-up with the FRFPUF covered with the light-weight cotton. As was the case for mock-up covered with the olefin fabrics, the periods measured in the two experiments are similar, but the results for the current experiments appear to be higher than expected based on the earlier measurements.

While it is difficult to fully assess the quantitative agreement of the two sets of experiments, the general conclusions that the use of cellulosic fabric in place of a thermoplastic fabric and replacement of NFRFPUF with FRFPUF substantially increased the periods required for flames to fully spread over the seat cushions agree in both studies. The relative increases between the two studies are comparable.

Ohlemiller and Shields used video observations to measure the total burned areas on the inside surfaces of four-cushion mock-ups (seat, back, and two arms) as a function of time. [41] The ignition source was the 18 kW Cal TB-133 burner applied for 80 s. Flame edges on various types of fabric were identified using similar approaches as the current study, e.g., blackening of charring fabrics and edges of rolled back material for thermoplastic fabrics. In addition to burned areas, these authors also reported the visible flaming areas at the same times. FPUF, presumably lightly fire retarded, meeting the pre-2013 Cal TB-117 flammability standard [10] was the cushioning material.

Measurements were shown for three fires having low- (modacrylic-nylon cover fabric, non-woven aramid barrier), medium- (cotton cover fabric, knitted glass charring fiber barrier), and high- (heavy polypropylene cover fabric, non-woven aramid barrier) HRRs. For the two lower HRR fires, flames did not spread to fully cover the interior surfaces, and the actual flaming surface areas rapidly decreased after the ignition burner was removed. For the mock-up covered with the heavy polypropylene cover fabric, the flames rapidly spread to cover the entire interior surface and the flaming area remained a large fraction of the total burned area after the ignition burner was removed.

It is not possible to directly relate the results of Ohlemiller and Shields to the current measurements due the different types of measurements made and the large difference in the strengths of the ignition sources used in the two studies. An aspect of the earlier work, estimates for the actual surface area burning, was not attempted here. However, as discussed earlier, differences between burned area and burning area were observed, and these varied with Combination Number. Figure 119 shows two images taken from Camera 3 videos of Test 10_1 and Test 14_1. The materials for these two tests differed only in FPUF type, with NFR foam used in Combination 10. In the image on the left for Test 10_1 flames are visible burning on edges

of the rolled up 78%PP/22%PE fabric as well as on the surfaces of exposed FPUF behind the edges. This can be contrasted with the image on the right where flames are apparent on the fabric at the edges of the burned area on the seat cushion, but where there appears to be a large unburning area of exposed foam behind the edge on the left side. This effect is more pronounced on the back cushion where the fabric has pulled back from the seat cushion to expose a wide expanse of non-burning foam. This example confirms the care which should be exercised in interpreting the burned area as defined in the current study.

8.5 Additional Flammability Behaviors

This study was specifically designed to investigate flame spread and fire growth on RUF mock-ups as discussed up to this point. However, additional details concerning the flammability behavior of the mock-ups were also characterized. The following subsections discuss observations concerning ignition ease, mock-up mass loss, heat of combustion, and radiative heat flux from mock-ups.

8.5.1 Mock-up Ignition Behavior

As evident from Table 12 and the results summarized in Section 5.2, each of the mock-ups with cushions covered with the 78%PP/22%PE fabric ignited following a single application of the BS-5852 Ignition Source 1 flame. Recall that ignition has been defined as when flames spread to cover a large fraction of the seat and back cushion surfaces. In contrast, for 55 % of the tests involving cotton-covered cushions, Ignition Source 2 flames were applied after fires failed to spread widely over the mock-ups following use of Ignition Source 1. Review of videos showed that for most of these tests the back cushion was ignited by Ignition Source 1 at the bottom, while the seat cushion failed to ignite. The videos also revealed numerous instances (Tests 1_2, 9_1, 11_1, 11_2, 15_1, and 17_1) in which the cotton-covered back cushion initially ignited and only spread to the seat after Ignition Source 1 or Source 2 was removed. Both types of behavior are likely related to the way the ignition source flames were applied (see Figure 13 and Figure 14) to the mock-ups. The burner tube was placed near the seat cushion with the flame base impinging on a small flat area of the seat and the upper, presumably hotter, part of the flame directly impinging on a larger area of the lower edge of the back cushion. As a result, the back was exposed to a higher and more reproducible heat flux. Apparently, the resulting heat fluxes on the cushions were sufficient to reliably ignite the thermoplastic and cotton fabrics on the back of the mock-ups, but only the thermoplastic on the seat.

Only a limited number of mock-ups with the cotton-covered cushions that failed to ignite with the application of Ignition Source 1 incorporated no barrier or the Whispershield barrier. For these tests, a follow-up application of Ignition Source 2 resulted in ignition on both the seat and back of the mock-up. In contrast, when a Norfab barrier fabric was included between the cotton fabric and the interior cushioning materials, application of Ignition Source 1 did not result in substantial flame spread over the mock-ups even though in most tests spreading flames were observed on the back cushion. For three out of four tests with cushions that included NFRFPUF, application of Ignition Source 2 resulted in widely spreading fires on the mock-ups. For the four tests with mock-ups incorporating the FPUF meeting SI-1324, flame spread was limited following applications of both Ignition Source 2 and Ignition Source 5.

The ignition results can be summarized as follows: mock-ups covered with the 78%PP/22%PE fabric were easily ignited by a small flame and varying the other materials utilized during the current test series did not improve the ignition resistance measurably. Replacing the thermoplastic with the cotton upholstery fabric increased the ignition resistance of the mock-ups to the small flame moderately, but mock-ups containing cushions without a barrier or with a Whispershield barrier were still likely to be ignited by the small ignition source flame. The reproducibility of these experiments was not particularly good. The source(s) of the variations was not evident. Possibilities range from test-to-test variations in how Ignition Source 1 was applied to possible variations in cushion construction. Incorporating a Norfab barrier substantially increased the small-flame resistance of the mock-ups, and when the Norfab barrier was used to cover the

FRFPUF, the mock-ups were not only resistant to the small-flame ignition source, but also to the more robust Ignition Sources 2 and 5.

The number of previous studies of ignition behavior of composites of RUF materials is limited. Krasny et al. provided a summary in their book covering studies up to about the year 2000. [2] The most relevant study cited is that of Paul. [116] This author investigated the ignition behavior of a range of mock-ups subjected to BS-5852 ignition sources. In agreement with the current study, it was reported that ignition resistance increased when a cotton fabric replaced polypropylene. Krasny et al. also indicated that the results were improved when an interliner was used. [2] In the current study, the improvement in ignition resistance due to the inclusion of a barrier fabric below the upholstery fabric varied widely from no observable change for cushions with the thermoplastic upholstery fabric to excellent ignition resistance when Norfab was included with fire-retarded FPUF and the cotton cover fabric. Both upholstery fabrics used in the current investigation were relatively light weight compared to those typically used for RUF. There is little information in the literature concerning how ignition resistance varies with fabric areal density.

8.5.2 Mock-up Mass Measurements

As evident in Figure 48, most of the mock-ups for which mass measurements were available lost 80 % or more of their initial mass during a fire. The values exceeded 90 % for mock-ups with NFRFPUF and only an outer upholstery fabric and those with NFRFPUF and Norfab barrier fabric. Those mock-ups with substantially lower percentages of mass loss were generally those with particularly low Q_{tot} values. These included Combinations 6, 14, 15, 16, 21, 22, 23, and 24. Recall that no uncorrupted mass measurements were available for Combination 6, but that values of 15% mass loss were estimated for the two tests. Each of these combinations contained FRFPUF as the cushioning material. These results are consistent with burning behavior observations which revealed that burning of these mock-ups was far from complete, and substantial charred, and in some cases uncharred, foam and fabric residue remained after these fires.

8.5.3 Effective Heat of Combustion

The HRR and mass measurements, which were smoothed and differentiated to provide time-resolved mass loss rate, allowed temporally-resolved EHOC to be calculated. The results for each of the tests where mass measurements were available are included in Appendix A as plots, and Table 14 includes general observations concerning the EHOC temporal profiles for the various combinations tested.

Keeping in mind that there were large noise levels in EHOC values when HRRs were low, the observations suggest that during the initial growth period of the fires EHOCs were considerably lower for mock-ups covered with cotton fabric than for those in which 78%PP/22%PE fabric was used. This conclusion is consistent with heats of combustion of 16.1 MJ/kg, 43.4 MJ/kg, and 22.0 MJ/kg for cotton, polypropylene, and polyester, respectively, taken from the chapter in the SFPE Handbook of Fire Protection Engineering by Tewarson. [118] While EHOCs are not expected to be identical to measured heats of combustion, their magnitudes should be similar. Thus, if only the upholstery cover fabrics were involved in burning of the mock-ups at early times, measured EHOCs of roughly 16.1 MJ/kg and 43.4 MJ/kg would be expected. The EHOCs reported for early times during the majority of fires included in Table 14 are consistent with this conclusion, suggesting that most of the HRR at the earliest times in these fires was indeed associated with burning of the cover fabric.

Average EHOC values recorded during periods when the HRRs were > 25 kW are shown in Figure 49. While a range of values were measured, the most likely values fell between 20 MJ/kg and 25 MJ/kg. For most of the fires, the largest contributor to the HRRs during these periods was expected to be FPUF. For FPUFs, heats of combustion listed by Tewarson for a number of FPUFs range from 23.2 MJ/kg to 27.2 MJ/kg, which is consistent with the measured EHOCs. [118]

EHOCs have been reported in a number of studies of RUF burning. Selected examples are summarized here. In one of the earliest studies, Babrauskas reported EHOCs for furniture of various sizes which incorporated a range of fabrics and FPUF types. [37] Values ranged from 13.9 MJ/kg to 35.1 MJ/kg. The highest value was clearly an outlier and involved a chair that incorporated a polypropylene frame. The remainder of the tests had EHOCs that fell between 13.95 MJ/kg and 20.9 MJ/kg. The chairs were constructed with either polypropylene or cotton fabric and either NFRFPUF or foam meeting pre-2013 Cal TB-117. In general, the lower values of EHOC were associated with furniture covered with the cotton fabric. Notice that the measured EHOCs are somewhat lower than observed in the current experiments.

A large number of EHOC measurements were reported in the CBUF report for both actual RUF and furniture especially constructed for the experiments. [43] With the exception of a few outliers, EHOC values fell between 14 MJ/kg and 25 MJ/kg, with the majority for actual furniture clustered near 20 MJ/kg and those for the especially constructed cases clustering around 17 MJ/kg. These values are reasonably close to those observed in the current study, particularly for the purchased furniture.

Andersson reported a study in which a limited number of upholstered furniture mock-ups were burned in a small room equipped for HRR and mass measurements. [119] Materials used in the mock-ups included NFR and FR FPUF and acrylic, cotton, and wool/rayon upholstery fabrics. Reported EHOC values ranged from 18.4 MJ/kg to 26.7 MJ/kg, with most of the values clustered near 21 MJ/kg. These results are consistent with the current study.

Based on the studies above, it appears that the EHOCs measured for the mock-ups used in the current study were generally consistent with those reported in the literature.

8.5.4 Radiative Heat Fluxes from Flaming RUF Mock-ups

The heat flux measurements included in this study were not part of the effort to characterize flame spread and growth on RUF mock-ups. They were included in the experimental protocol due to the perceived role such heat transfer plays in the ignition of other objects located near a burning item of RUF. The results discussed in Section 5.12 summarize the finding for heat flux measurements recorded at two distances along three directions relative to the mock-ups. The effects of view factors and variations in distance between the flames and the heat flux measurement location were emphasized.

Despite the importance of radiative heat transfer from RUF on fire growth in residences, relatively few measurements of heat flux levels from burning RUF were identified in the literature. Babrauskas and Krasny provided a brief review of work through the mid-1980s in their review on RUF flammability. [1] The most extensive discussion of the topic dates back to a 1981 manuscript of Babrauskas. [120] A variety of furnishings were burned including an acoustical office screen (partition panel), desk, large wooden cabinet filled with paper , and a variety of chairs. Of particular relevance was a test (referred to as F16) in which a traditional easy chair covered with polypropylene fabric was tested. Heat flux values were measured at four heights using gauges mounted on a trolley that was moved to vary the distance between the measurement plane and the burning item. This earlier study was performed before the widespread use of oxygen depletion calorimetry to measure HRR, and the fire intensity was characterized in terms of a maximum measured mass loss rate. Actual heat flux levels were not provided, but instead were extrapolated to maximum distances at which 10 kW/m^2, 20 kW/m^2, and 40 kW/m^2 would be observed. For the easy chair, the maximum MLR of 0.022 kg/s yielded distances of 1.33 m, 0.79 m, and 0.20 m, respectively. A rough estimate for the maximum HRR of this experiment can be obtained by multiplying this MLR by 22 MJ/kg (value based on the discussion in Section 5.7) to give 480 kW. Estimated values of heat flux for this HRR calculated for 0.75 m and 1.5 m using Eq. (1) and the slopes for the lines shown in Figure 65 and Figure 66 are 11.0 kW/m^2 and 3.5 kW/m^2, respectively. Values estimated based on the current mock-up measurements are roughly a factor of two lower than suggested by this seminal paper of Babruaskas.

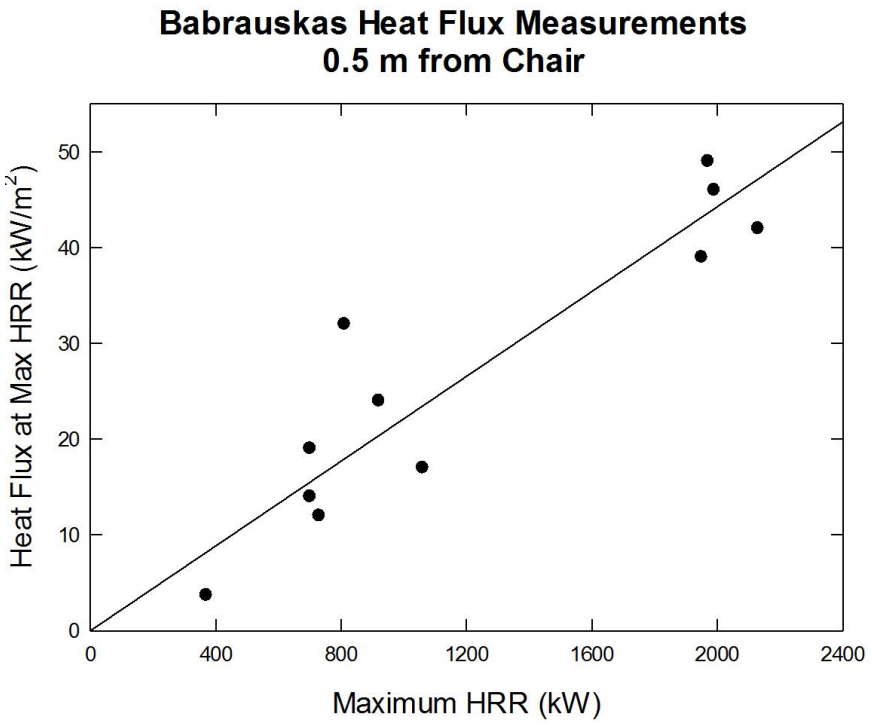

Figure 120. Values of maximum radiative heat flux recorded 0.5 m from the floor and front for a group of burning upholstered chairs plotted against the maximum observed HRR using data taken from Babruaskas. [37] The straight line is the result of a linear least squares curve fit to the data.

For objects at distances greater than 1.3 m from a burning chair, Mizuno and Kawagoe provided the following equation for the heat flux, $(q)_z$ (kW/m^2), as a function of the distance z (m) (for a height of 1 m) from burning used upholstered furniture and the measured MLR, $\dot{m}$ (g/s) [121],

$$(q)_z = 0.312 \frac{\dot{m}}{z^{1.8}}, \tag{2}$$

where the heat flux was shown to have a linear dependence on $\dot{m}$. Recall that a linear dependence of radiant heat flux on HRR was also observed in the current study summarized in Section 5.12. Babrauskas also reported a linear dependence for these parameters in his earlier study. [37] By again assuming an EHOC of 22 MJ/kg, this expression can be rewritten in terms of *HRR* (kW) as

$$(q)_z = 0.0142 \frac{HRR}{z^{1.8}}. \tag{3}$$

For a distance of z = 1.5 m, the slope of a plot of $(q)_{1.5}$ versus *HRR* is predicted to be 0.00684 m^2, which is within 6 % of the value measured for the mock-ups (0.00726 m^2) in the current study. Using the maximum 22 g/s MLR reported in the study of Babrauskas [120], the value of Q_{rad} at 1.33 m is calculated to be 4.1 kW/m^2 compared to the 10 kW/m^2 value provided by Babrauskas. This indicates that there was relatively poor agreement between these two earlier experimental studies.

Babrauskas reported measurements of maximum HRR and heat flux recorded 0.5 m above the floor and to the front of upholstered chairs [37], and Krasny and Babrauskas made similar measurements for upholstered furniture mock-ups [38]. Results from these works are plotted in Figure 120 and Figure 121, respectively. Note that a variety of fabrics and FPUFS were used in the experiments. The data in the figures were fit to Eq. (1) with linear least squares curve fits. The results were R^2 = 0.84, $m_{0.5}$ = 0.0221 m^2 for the chairs and

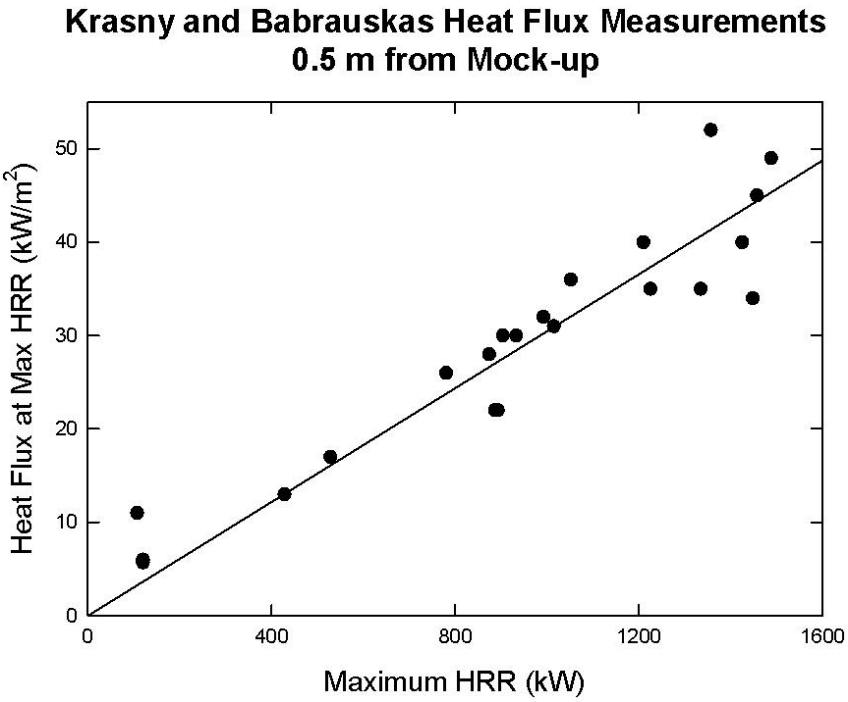

Figure 121. Values of maximum radiative heat flux recorded 0.5 m from the floor and front of a group of burning upholstered chair mock-ups are plotted against the maximum observed HRRs using data taken Krasny and Babrauskas. [38] The straight line is the result of a linear least squares curve fit to the data.

$R^2 = 0.88$, $m_{0.5} = 0.0305$ m^2 for the mock-ups. Even though the data for both plots fall on reasonably good lines, the slopes differ substantially. This suggests that heat fluxes from RUF mock-ups for a given HRR are somewhat higher than for actual RUF items.

If it were possible to determine an expression for the variation of m_z as a function of z it would be possible to estimate values of the heat flux as function of z and HRR. The values of m_z for both mock-ups and actual RUF determined above are plotted as a function of z in Figure 122. While the values clearly suggest the expected fall-off of m_z with increasing z, the results are too scattered to allow an accurate determination of the dependence of m_z on distance from the burning items. While this approach appears to offer a possible means of predicting radiative heat flux from burning RUF and RUF mock-ups, it must be concluded that, at the present time, insufficient measurements of m_z are available to allow effective implementation.

It should be kept in mind that the data in Figure 122 include results for both chair mock-ups and different types of actual upholstered chairs. It is unclear whether or not heat flux levels will have a strong dependence on geometry for similar sized RUF and RUF mock-ups. It does seem likely that large variations in size, such as comparing chair and couches, could lead to substantial variations in heat flux levels as a function of HRR and distance to the gauge.

9 Final Remarks

The results of this study have provided an extensive data base for characterizing flame spread and fire growth on furniture mock-ups. Analysis has shown that three (barrier, foam type, and cover fabric) of the five material variations considered had statistically significant effects on one or more of the 13 factors chosen to characterize the flammability behavior.

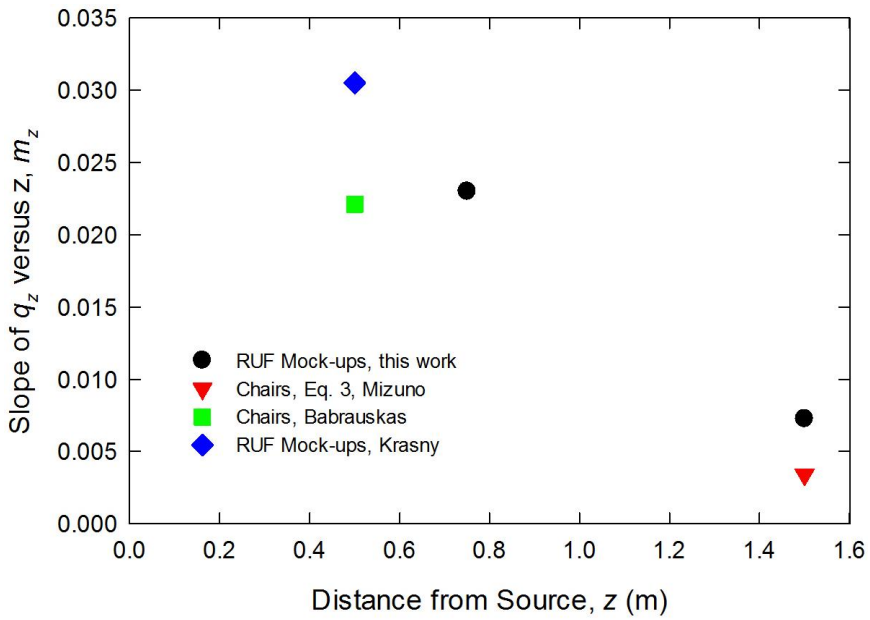

Figure 122. Values of slopes derived from plots of heat flux recorded as a function of HRR are plotted against distance, z, between the heat flux gauge and the burning item. Results are included for measurements taken at z = 0.75 m and z = 1.5 m for the mock-ups used in the current work and in the study of Babrauskas [38] and results for upholstered chairs by Mizuno and Kawagoe [121] and Babrauskas [37].

In addition to meeting the objectives of the study, additional insights have been obtained by characterization of ignition behaviors and measurements of mock-up mass and radiative heat flux. Taken together, the results provide one of the most complete experimental studies and analysis of RUF mock-up burning behavior available.

The second of the three reports in this series will discuss similar data and analysis results for a series of measurements performed in a cone calorimeter on small scale mock-ups with the same material variations.

The final report will then use the findings of the small- and real-scale studies to assess the potential to predict the burning of real-scale RUF mock-ups based on the small-scale results.

Acknowledgements

The completion of this project would not have been possible without the contributions of numerous people. At ATF Jason Ouellette, FRL Laboratory Section Chief, was instrumental in making the arrangements for NIST researchers to perform our experiments in their facility and ensuring that we had all necessary support. Dave Sheppard provided advice on the experimental measurements and details concerning the test facility. Much of the actual experimental work was performed by two outstanding technicians, Jimmy Zurenko, and Dennys Hernandez; with additional support from Laboratory Engineer Jonathan Butta. Mark Whal was responsible for video systems and file maintinace.

Artur Chernovsky of NIST developed the Labview application used to generate videos with time-averaged video frames that proved particularly effective at reducing obscuration due to fluctuating flames. Drs. Mathew Bundy and Anthony Hamins provided helpful suggestions and guidance during planning and analysis of the experiments.

Julie Walker of Vita Cellular Foams (UK) Ltd, Timothy M. McRee of Wm. T. Burnett & Co, Harrish Lilani of Norfab Corporation, and Bob Wertz of American Foam Center provided invaluable advice and help regarding the specification and procurement of materials used in this study. Kevin Johnson of A-B-B-A Upholstering Foam and Futons provided upholstery service and was especially helpful when non standard materials were used.

References

[1] V. Babrauskas and J. F. Krasny, Fire Behavior of Upholstered Furniture, NBS Monograph 173, National Bureau of Standards, Gaithersburg, MD, November 1985, 101 pp.

[2] J. F. Krasny, W. J. Parker and V. Babrauskas, Fire Behavior of Upholstered Furniture and Mattresses, William Andrew Publishig, LLC. Norwich, New York (2001).

[3] F. H. Prager and H. Rosteck, Polyurethane and Fire, Wiley-VCH. Weinheim, Germany (2006).

[4] An Act to Amend the Flammable Fabrics Act to Increase the Protection Afforded Consumers against Injurious Flammable Fabrics, Public Law 90-189, U. S. Congress, U. S. Government Printing Office, Washington, DC, 17 December 1967, 568-574.

[5] Upholstered Furniture: Notice of Finding that Flammability Standard or other Regulation May Be Needed and Institution of Proceedings, United States Consumer Product Safety Commission, Federal Register 37 (230), 25239-25240, Washington, DC (29 November 1972).

[6] J. J. Loftus, Back-up Report for the Proposed Standard for the Flammability (Cigarette Ignition Resistance) of Upholstered Furniture, PFF 6-76, NBSIR 78-1438, National Bureau of Standards, Gaithersburg, MD, June 1978, 239 pp.

[7] White Paper on Upholstered Furniture Flammability, National Fire Protection Associaion, Quincy, MA, September 2013, 37 pp.

[8] Part 1633--Proposed Standard for the Flammability (Cigarette Ignition Resistance) of Upholsterred Furniture (PFF 6-76), National Bureau of Standards, Gaithersburg, MD (21 May 1976).

[9] G. H. Damant and S. Nurbakhsh, Development of Furnishings Flammability Standards for Public Buildings and Private Residences, Journal of Fire Sciences **13** 417-433 (1995). http://dx.doi.org/10.1177/073490419501300601

[10] Requirements, Test Procedure, and Apparatus for Testing and Flame Retardancy of Filling Materials and Fabrics, Technical Bulletin TB-117, Bureau of Home Furnishings, Department of Consumer Affairs, State of California, North Highlands, CA (October 1977).

[11] Flammability of Clothing Textiles, Commercial Standard CS 191-53, United States Department of Commerce, Washington, DC (30 January 1953).

[12] CPSC Staff Recommends Safety Standard for Flammable Upholstered Furniture, Press Release Number: 78092, United States Consumer Product Commission, Bethesda, MD, (20 November 1978), https://www.cpsc.gov/Newsroom/News-Releases/1979/CPSC-Staff-Recommends-Safety-Standard-for-Flammable-Upholstered-Furniture, Accessed: 26 September 2019.

[13] Technical Specifications, Upholstered Furniture Action Council, High Point, NC (April, 1979), online: https://ufac.org/technical-specifications/, Accessed: 25 September 2019.

[14] Standard Test Methods for Cigarette Ignition Resistance of Components of Upholstered Furniture, ASTM E1353-16, ASTM International, West Conshohocken, PA (1 September 2016).

[15] Standard Methods of Tests and Classification System for Cigarette Ignition of Components of Upholstered Furniture 2013 Edition, NFPA 260, National Fire Protection Association, Quincy, MA (17 December 2012).

[16] A. K. Vickers and H. Tovey, Upholstered Furniture in Fire Incidents, NBS Report 10835, National Bureau of Standards, Gaithersburg, MD, 24 April 1972, 49 pp.

[17] F. B. Clarke and J. Ottoson, Fire Death Scenarios and Firesafety Planning, Fire Journal **70** (3), 20-22, 117-118 (1976).

[18] G. Fristrom, Fire Deaths in the United States: Review of Data Sources and Range of Estimates, CIB W14/78/66, National Fire Data Center, National Fire Prevention and Control Administration, Washington, DC, September 1977, 32 pp.

[19] Petition for Promulgation of Upholstered Furniture Fabric Regulations under the Flammable Fabrics Act, FP 93-1, United States Comsumer Product Safety Commission, Bethesda, MD (1993), online: https://web.archive.org/web/20170127233140/https://www.cpsc.gov/PageFiles/80998/3458cd08.pdf, Accessed: 30 September 2019.

[20] 16 CFR Part 1640 Upholstered Furniture; Advance Notice of Proposed Rulemaking; Request for Comments and Information, United States Consumer Product Safety Commission, Federal Register 59 (114), 30735-30738, Washington, DC (15 June 1994).

[21] 16 CFR, Chapter 11, Subchapter D, Ignition of Upholstrered Furniture by Small Open Flames and/or Smoldering Cigarettes; Advance Notice of Proposed Rulemaking; Request for Comments and Information, United States Consumer Product Safety Commission, Federal Register 68 (205), 60629-60632, Washington, DC (23 October 2003).

[22] 16 CFR Part 1634, Standard for the Flammability of Residential Upholstered Furniture (Proposed), United States Consumer Product Safety Commission, Federal Register 73 (43), 11702-11752, Washington, DC (4 March 2008).

[23] Methods of Test for Assessment of the Ignitability of Upholstered Seating by Smouldering and Flaming Ignition Sources, BS 5852:2006, British Standards Institution, London, UK (March 2006).

[24] Furniture and Furnishings (Fire) (Safety) Regulations 1988, Statutory Instrument No. 1324, Department of Trade and Industry (United Kingdom), London, United Kingdom, 26 July 1988,

[25] Flammability Test Procedure for Seating Furniture for Use in High Risk and Public Occupancies, Technical Bulletin TB-133, Bureau of Home Furnishings, Department of Consumer Affairs, State of California, North Highlands, CA (May 1985).

[26] Flammability Test Procedure for Seating Furniture for Use in Public Occupancies, Technical Bulletin TB-133, Bureau of Home Furnishings and Thermal Insulation, Department of Consumer Affairs, State of California, North Highlands, California (January 1991).

[27] T. J. Ohlemiller and K. Villa, Furniture Flammability: An Investigation of the California Bulletin 133 Test. Part II: Characterization of the Ignition Source and a Comparable Gas Burner, NISTIR NISTIR 4348, National Institute of Standards and Technology, Gaithersburg, MD, June 1990, 42 pp.

[28] Standard Test Method for Fire Testing of Upholstered Furniture, ASTM E1537-15, ASTM International, West Conshohocken, PA (1 November 2015).

[29] K. N. Palmer and W. Taylor, Fire Hazards of Plastics in Furniture and Furnishings; Ignition Studies, The Journal of Comsumer Product Flammability **1** 186-220 (1974).

[30] K. N. Palmer, W. Taylor and K. T. Paul, Fire Hazards of Plastics in Furniture and Furnishings: Characteristics of the Burning, BRE 3/75, Her Magistry's Stationary Office, London, England, January 1975, 63 pp.

[31] K. N. Palmer, W. Taylor and K. T. Paul, Fire Hazards of Plastics in Furniture and Furnishings: Fires in Furnished Rooms, BRE 21/76, Her Magistry's Stationary Office, London, England, February 1976, 64 pp.

[32] F. H. Prager, W. C. Darr and J. F. Wood, The Contribution of Upholstered Furniture to Residential Fire Risk, Cellular Polymers **3** 161-194 (1984).

[33] W. J. Wilson, Large Scale Fire Tests, Journal of Fire and Flammability **7** 112-124 (1976).

[34] W. D. Woolley, S. A. Ames, A. I. Pitt and K. Buckland, The Ignition and Burning Characteristics of Fabric Covered Foams, CP30/78, Fire Research Station, Garston, Watford, D2 7R, UK, February 1978, 24 pp.

[35] V. Babrauskas, Full-scale Burning Behavior of Upholstered Chairs, NBS Technical Note 1103, National Bureau of Standards, Washington, DC, August 1979, 86 pp.

[36] D. L. Sensenig, An Oxygen Consumption Technique for Determining the Contribution of Interior Wall Finishes to Room Fires, NBS Technical Note 1128, National Bureau of Standards, Washington , DC, July 1980, 87 pp.

[37] V. Babrauskas, Upholstered Furniture Heat Release Rates - Measurement and Estimation, Journal of Fire Sciences **1** (1), 9-32 (1983). http://dx.doi.org/10.1177/073490418300100103

[38] J. F. Krasny and V. Babrauskas, Burning Behavior of Upholstered Furniture Mockups, Journal of Fire Sciences **2** (3), 205-235 (1984). http://dx.doi.org/10.1177/073490418400200305

[39] V. Babrauskas, Upholstered Furniture Room Fires - Measurements, Comparison with Furniture Calorimeter Data and Flashover Predicitons, Journal of Fire Sciences **2** (1), 5-19 (1984). http://dx.doi.org/10.1177/073490418400200103

[40] B. Andersson and S. E. Magnusson, Fire Behavior of Upholstered Furniture--An Experimental Study, Fire and Materials **9** (1), 41-45 (1985). http://dx.doi.org/10.1002/fam.810090107

[41] T. J. Ohlemiller and J. R. Shields, Behavior of Mock-Ups in the California Technical Bulletin 133 Test Protocol: Fabric and Barrier Effects, NISTIR 5653, National Institute of Standards and Technology, Gaithersburg, MD, May 1995, 77 pp.

[42] W. J. Parker, K.-M. Tu, S. Nurbakhsh and G. H. Damant, Furniture Flammability: An Investigation of the California Technical Bulletin 133 Test. Part III: Full Scale Chair Burns, NISTIR 4375, National Instittute of Standards and Technology, Gaithersburg, MD, July 1990, 43 pp.

[43] B. Sundström (Ed.), CBUF Fire Safety of Upholstered Furniture--The Final Report on the CBUF Research Programme, London, England, Interscience Communication Limited (1995).

[44] J. Söderbom, P. van Hees and P. Meirsschaert, Influence of Ignition Sources on Heat Release Rate in the Furniture Calorimeter, Fire and Materials **20** (2), 61-67 (1996). http://dx.doi.org/10.1002/(SICI)1099-1018(199603)20:2<61::AID-FAM558>3.0.CO;2-6

[45] P. van Hees and P. Meirsschaert, WP9B Furniture Calorimeter Ignition Conditions, Beproevingsverslag No. 7244, Ghent University, Ghent, Belgium, 1993, XX pp.

[46] Furniture - Assessment of the Ignitability of Upholstered Furniture - Part 2: Ignition Source Match Flame Equivalent, EN 1021-Part 2, The European Committee for Standardization, Brussels, Belgium (1 October 1993).

[47] J. Firestone, An Analysis of Furniture Heat Release Rates by the Nordtest, Fire Engineering Research Report 99/7, School of Engineering, University of Canterbury, Christchurch, New Zealand, March 1999, 161 pp.

[48] Upholstered Furniture: Burning Behaviour - Full Scale Test, NT Fire 032, NORDTEST, Esbo, Finland (May 1991).

[49] P. A. Enright, Heat Release and the Combustion Behaviour of Upholstered Furniture, Doctor of Philosophy Thesis, University of Canterbury, Christchurch, New Zealand, June 1999, 191 pp.

[50] P. A. Enright, C. M. Fleischmann and P. Vandevelde, CBUF Model II Applied to Exemplary NZ Furniture (NZ-CBUF), Fire and Materials **25** (3), 105-115 (2001). http://dx.doi.org/10.1002/fam.763

[51] H. R. Denize, The Combustion Behaviour of Upholstered Furniture in New Zealand, Masters Thesis, University of Canterbury, Christchurch, New Zealand, 2000, 140 pp.

[52] N. Girgis, Full-Scale Compartment Fire Experiments on "Upholstered Furniture", Masters Thesis, University of Canterbury, Christchurch, Nw Zealand, February, 2000, 109 pp.

[53] E. A. Young, Standardising Design Fires for Residential and Apartment Buildings: Upholstered Furniture Fires, Masters Thesis, University of Canterbury, Christchurch, New Zealand, April 2007, 191 pp.

[54] A. R. Coles, Flammability of Upholstered Furniture Using the Cone Calorimeter, Fire Engineering Report 2001/1, Canterbury University, Christchurch, New Zealand, March 2001, 104 pp.

[55] F. F. Chen, Radiant Ignition of New Zealand Upholstered Furniture Composites, Fire Engineering Report 2001/2, University of Canterbury, Christchurch, New Zealand, February 2001, 141 pp.

[56] C. R. Wong, Contribution of Upholstered Furniture to Residential Fire Fatalities in New Zealand, Fire Engineering Report 2001/9, University of Canterbury, Christchurch, New Zealand, March 2001, 122 pp.

[57] P. C. R. Collier and P. N. Whiting, Timeline for Incipient Fire Development, Branz Study Report 194, Branz Ltd., Judgeford, New Zealand, 2008, 50 pp.

[58] A. Bwalya, E. Gibbs, G. Lougheed and A. Kashef, Characterization of Fires in Multi-Suite Residential Dwellings: Phase 1 -- Room Fire Experiments with Individual Furnishings, IRC-RR 302, National Research Council Canada, Ottawa, Ontario, Canada, September 2010, 75 pp.

[59] Fire Tests — Full-scale Room Test for Surface Products, ISO 9705:1993, International Organization for Standardization, Geneva, Switzerland (17 June 1993).

[60] S. Mehta, Upholstered Furniture Full Scale Chair Tests – Open Flame Ignition Results and Analysis, Memorandum, Consumer Product Safety Commission, Bethesda, MD, 9 May 2012, 63 pp.

[61] D. Miller, Analysis of Chair Open-Flame Data, Consumer Product Safety Commission, Bethesda, MD, 11 May 2012, 18 pp.

[62] T. Fabian, Upholstered Furniture Flammability, Underwriters Laboratory, Northbrook, IL (31 July, 2013), online: https://slidelegend.com/upholstered-furniture-flammability-ulcom_5a0caec61723dda699a6be19.html, Accessed: 30 September, 2019.

[63] M. L. Janssens, Reducing Uncertainty of Quantifying the Burning Rate of Upholstered Furniture, Document Number 239050, U. S. Department of Justice, Washington, DC, July 2012, 208 pp.

[64] Standard Methods of Fire Tests for Flame Propagation of Textiles and Films, 2015 Edition, NFPA 701, National Fire Protection Association, Quincy, MA (2014).

[65] K. Storesund, A. Steen-Hansen and A. Bergstrand, Fire Safe Upholstered Furniture. Alternative Strategies to the Use of Chemical Flame Retardants, SPFR Report A15 20124:2, SP Fire Research AS, Trondheim, Norway, 18 December 2015, 75 pp.

[66] L. Fansler and A. Lock, Summary Report of Open Flame and Smoldering Tests on Chairs, Consumer Product Safety Commision, Bethesda, MD, 28 January 2016, 75 pp.

[67] D. Miller, Analysis of Chair Open-Flame and Smoldering Data, Consumer Product Safety Commission, Bethesda, MD, 22 January 2016, 21 pp.

[68] National Fire Incident Reporting System, U. S. Fire Administration, Emmitsburg, MD (2015), online: https://www.nfirs.fema.gov/, Accessed: 25 June 2015.

[69] M. Ahrens, Home Fires that Began with Upholstered Furniture, NFPA No. USS 56, National Fire Protection Association, Quincy, MA, February 2017, 70 pp.

[70] M. Ahrens, Home Structure Fires, NFPA No. USS12G, National Fire Protection Association, Quincy, MA, September 2015, 112 pp.

[71] M. Ahrens, Home Structure Fires, NFPA No. USS12G-01, National Fire Protection Association, Quincy, MA, April 2013, 158 pp.

[72] W. M. Pitts, Summary and Conclusions of a Workshop on "Quantifying the Contribution of Flaming Residential Upholstered Furniture to Fire Losses in the United States", NIST Technical Note 1757, National Institute of Standards and Technology, Gaithersburg, MD, 17 September 2012, 134 pp. http://dx.doi.org/10.6028/NIST.TN.1757.

[73] W. M. Pitts, Summary and Conclusions of a Workshop on "Quantifying the Contribution of Flaming Residential Upholstered Furniture to Fire Losses in the United States", NIST Technical Note 1757r1, National Institute of Standards and Technology, Gaithersburg, MD, August 2013, 135 pp. http://dx.doi.org/10.6028/NIST.TN.1757r1.

[74] J. R. Hall, Estimating Fires When a Product is the Primary Fuel But Not the First Fuel, With an Application to Upholstered Furniture, Fire Technology **51** (2), 381-391 (2015). http://dx.doi.org/10.1007/s10694-014-0391-8

[75] A. Blum and B. N. Ames, Flame-Retartant Additives as Possible Cancer Hazards, Science **195** (4273), 17-23 (1977). http://dx.doi.org/10.1126/science.831254

[76] M. D. Gold, A. Blum and B. N. Ames, Another Flame-retardant, TRIS-(1,3-Dichloro-2-Propyl)-Phosphate, and Its Expected Metabolites are Mutagens, Science **200** (4343), 785-787 (1978). http://dx.doi.org/10.1126/science.347576

[77] M. Alaee and R. J. Wenning, Eds, The Significance of Brominated Flame Retardants in the Environment: Current Understanding, Issues and Challenges, Chemosphere **46** (5), 579-796 (2002). http://dx.doi.org/10.1016/S0045-6535(01)00224-7

[78] R. Letcher and P. Behnisch, Eds., The State-of-Science and Trends of BFRs in the Enviroment, Environment International **29** (6), 663-886 (2003). http://dx.doi.org/10.1016/S0160-4120(03)00122-3

[79] Polybrominated Diphenyl Ethers (PBDEs) Project Plan, U. S. Environmental Protection Agency, Washington, DC (2006), online: https://www.epa.gov/sites/production/files/2015-09/documents/proj-plan32906a.pdf, Accessed: 2 July 2015.

[80] M. A. Babick, CPSC Staff Preliminary Risk Assessment of Flame Retardant (FR) Chemical in Upholstered Furniture Foam, U. S. Consumer Product Safety Commission, Bethesda, MD, 21 December 2006, 81 pp.

[81] Furniture Flame Retardancy Partnership: Environmental Profiles of Chemical Flame-Retardant Alternatives for Low-Density Polyurethane Foam: Volume 1, EPA 742-R-05-002A, U. S. Environmental Protection Agency, Washington, DC, September 2005, 153 pp.

[82] Furniture Flame Retardancy Partnership: Environmental Profiles of Chemical Flame-Retardant Alternatives for Low-Density Polyurethane Foam: Volume 2, EPA 742-R-05-002B, U. S. Environmental Protection Agency, Washington, DC, September 2005, 398 pp.

[83] V. Babrauskas, A. Blum, R. Daley and L. Birnbaum, Flame Retardants in Furniture Foam: Benefits and Risks, in: M. Spearpoint Ed., Fire Safety Science--Proceedings of the Tenth International Symposium, International Association for Fire Safety Science, Greeenwich, England, 2011, 265-278.

[84] H. M. Stapleton, S. Sharma, G. Getzinger, P. L. Ferguson, M. Gabriel, T. F. Webster and A. Blum, Novel and High Volume Use Flame Retardants in US Couches Reflective of the 2005 PentaBDE Phase Out, Environmental Science & Technology **46** (24), 13432-13439 (2012). http://dx.doi.org/10.1021/es303471d

[85] P. Callahan and S. Roe, Playing with Fire. Part 1: A Deceptive Campaign by Industry Brought Toxic Flame Retardants into Our Homes and into Our Bodies. And the Chemicals Don't Even Work as Promised., Chicago Tribune, Chicago, IL, 6 May 2012.

[86] P. Callahan and S. Roe, Playing with Fire. Part 2: Big Tobacco's Clout. How Industry and Its Inside Man Steered a Group of Fire Officials to Push Flame Retardant Furniture, Chicago Tribune, Chicago, IL, 8 May 2012.

[87] S. Roe and P. Callahan, Playing with Fire. Part 3: 'Flat-out Deceptice.' Distortion of Science Helped Industry Promote Flame Retardants, Downplay Health Risks, Chicago Tribune, Chicago, IL, 9 May 2012.

[88] M. Hawthorne, Playing with Fire. Part 4: Toxic Roulette. Flame Retardants Get a Pass from Regulators with Little Assessment of Potential Health Risks, Chicago Tribune, Chicago, IL, 10 May 2012.

[89] Governor Brown Directs State Agencies to Revise Flammability Standards, Office of the Governor, Sacramento, CA (18 June 2012), online: https://www.ca.gov/archive/gov39/2012/06/18/news17598/index.html, Accessed: 27 Septembeer 2019.

[90] Requirements, Test Procedure and Apparatus for Testing the Smolder Resistance of Upholstered Furniture (Draft), Technical Bulletin TB-117-2012, Bureau of Electronic & Appliance Repair, Home Furnishings & Thermal Insulation, Department of Consumer Affairs, State of California, Sacramento, CA (July 2012).

[91] Requirements, Test Procedure and Apparatus for Testing the Smolder Resistance of Materials Used in Upholstered Furniture, Technical Bulletin TB-117-2013, Bureau of Electronic & Appliance Repair, Home Furnishings & Thermal Insulation, Department of Consumer Affairs, State of California, Saramento, CA (July 2013).

[92] Are Consumers Adequately Protected from Flammability of Upholstered Furniture? Hearing on the Effectiveness of Furniture Flammability Standards and Flame-Retardant Chemicals, Committee on Appropriations, United States Senate, Senate Hearing 112 (705), 1-77, U.S. Government Printing Office, Washington, DC (12 July 2012).

[93] White Paper on Upholstered Furniture Flammability, National Fire Protections Association, Quincy, MA (September, 2013), online: http://www.nfpa.org/Assets/files/AboutTheCodes/277/2156%20-%20UpholsteredFurnWhitePaper.pdf, Accessed: 15 February, 2017.

[94] R. G. Gann, The Challenge of Realizing Low Flammability Home Furnishing, in: Interflam 2013, Proceedings of the Thirteenth International Conference, Interscience Communications, Greenwich, England, 2013, Electronic version only.

[95] 16 CFR Part 1633. Final Rule: Standard for the Flammability (Open Flame) of Mattress Sets, United States Consumer Product Safety Commission, Federal Register 71 (50), 13472-13523, Washington, DC (15 March 2006).

[96] W. M. Pitts, Applied Heat Flux Distribution and Time Response Effects on Cone Calorimeter Characterization of a Commercial Flexible Polyurethane Foam, Fire Technology **50** (3), 635-672 (2014). http://dx.doi.org/10.1007/s10694-011-0235-8

[97] W. M. Pitts, Role of Two Stage Pyrolysis in Fire Growth on Flexible Polyurethane Foam Slabs, Fire and Materials **38** (3), 323-338 (2014). http://dx.doi.org/10.1002/fam.2183

[98] S. Nazaré and R. Davis, A Review of Fire Blocking Technologies for Soft Furnishings, Fire Science Reviews **1** (1), 1-23 (2012). http://dx.doi.org/10.1186/2193-0414-1-1

[99] S. Nazaré, W. Pitts, S. Flynn, J. R. Shields and R. D. Davis, Evaluating Fire Blocking Performance of Barrier Fabrics, Fire and Materials **38** (7), 695-716 (2014). http://dx.doi.org/10.1002/fam.2210

[100] Technical Reference, Fire Products Collector – 1 MW Square, Technical Reference Number TR011a, Fire Research Laboratory, National Laboratory Center, Bureau of Alcohol, Tobacco, Firearms, and Explosives, Ammendale, MD, 2014, 34 pp.

[101] C. Huggett, Estimation of Rate of Heat Release by Means of Oxygen Consumption Measurements, Fire and Materials **4** (2), 61-65 (1980). http://dx.doi.org/10.1002/fam.810040202

[102] R. A. Bryant, T. J. Ohlemiller, E. L. Johnsson, A. Hamins, B. S. Grove, W. F. Guthrie, A. Maranghides and G. W. Mulholland, The NIST 3 Megawatt Quantitative Heat Release Rate Facility, NIST Special Publication 1007, National Institute of Standards and Technology, Gaithersburg, MD, December 2003, 81 pp.

[103] Y. S. Kim, Y. C. Li, W. M. Pitts, M. Werrel and R. D. Davis, Rapid Growing Clay Coatings to Reduce the Fire Threat of Furniture, ACS Applied Materials & Interfaces **6** (3), 2146-2152 (2014). http://dx.doi.org/10.1021/am405259n

[104] P. A. Gorry, General Least-squares Smoothing and Differentiation by the Convolution (Savitzky-Golay) Method, Analytical Chemistry **62** (6), 570-573 (1990). http://dx.doi.org/10.1021/ac00205a007

[105] Reaction to Fire tests for Building Products – Building Products Excluding Floorings Exposed to the Thermal Attack by a Single Burning Item, EN 13823:2002, European Committee for Standardization, Brussels, Belgium (February 2002).

[106] V. Babrauskas and R. D. Peacock, Heat Release Rate - The Single Most Important Variable in Fire Hazard, Fire Safety Journal **18** (3), 255-272 (1992). http://dx.doi.org/10.1016/0379-7112(92)90019-9

[107] NIST/SEMATECH e-Handbook of Statistical Methods, http://www.itl.nist.gov/div898/handbook, 10/30/2013.

[108] J. F. Wood and F. H. Prager, Full Scale Intestigation of the Fire Performance of Upholstered Furniture. Introduction and Part 1: Two Chair Burn--RAPRA 4, PRC Project 75-1-13, International Isocyanate Institute, INC., December 1977, 33 pp.

[109] J. G. Schuhmann and G. E. Hartzell, Flaming Combustion Characteristics of Upholstered Furniture, Journal of Fire Sciences **7** (6), 386-402 (1989). http://dx.doi.org/10.1177/073490418900700602

[110] V. Babrauskas, R. H. Harris Jr., R. G. Gann, B. C. Levin, B. T. Lee, R. D. Peacock, M. Paabo, W. Twilley, M. F. Yoklavich and H. M. Clark, Fire Hazard Comparison of Fire-Retarded and Non-Fire-Retarded Products, NBS Special Publication 749, National Bureau of Standards, Washington, DC, July 1988, 92 pp.

[111] V. Babrauskas and W. D. Walton, A Simplified Characterization of Upholstered Furniture--Heat Release Rates, Fire Safety Journal **11** (3), 181-192 (1986). http://dx.doi.org/10.1016/0379-7112(86)90061-5

[112] P. A. Enright and C. M. Fleischmann, CBUF Model 1, Applied to Exemplary New Zealand Furniture, in: M. Curtat, Ed., Fire Safety Science--Proceedings of the Sixth International Symposium, International Association of Fire Safety Science, Boston, MA, 2000, 147-158.

[113] B. T. Lee and L. W. Wiltshire, Fire-spread Models of Upholstered Furniture, Journal of Fire & Flammability **3,** 164-175 (1972).

[114] M. A. Dietenberger, Time to Ignition and Flame Spreading on Common Materials. A Proposal to the NBS Research Associate Program, University of Dayton, Dayton, OH, July, 1986, 119 pp.

[115] R. A. Dipert, Application of Flame Spread Modeling to Flame Spread on Horizontal Samples, Masters Thesis, Worcester Polytechnic Institute, Worcester, MA, July 1984, 176 pp.

[116] K. T. Paul, Fire and Upholstered Furniture - Small versus Large-Scale Tests, Fire and Materials **10** (1), 29-39 (1986). http://dx.doi.org/10.1002/fam.810100106

[117] F. H. Prager, The United-Kingdom Upholstered Furniture Fire Safety Regulations 1988 - A Challenge to Fibers, Journal of Fire Sciences **7** (5), 291-309 (1989). http://dx.doi.org/10.1177/073490418900700501

[118] A. Tewarson, Generation of Heat and Gaseous, Liquid, and Solid Products in Fires, in: The SFPE Handbook of Fire Protection Engineering, 4th Ed., National Fire Protection Association, Quincy, MA, (2008) 3-109 - 194.

[119] B. Andersson, Fire Behaviour of Beds and Upholstered Furniture--An Experimental Study (Second Test Series). Part 1., Division of Building Fire Safety and Technology Report LUTVDG (TVBB-3723), Lund Institute of Technology, Lund Sweden, 1985, 53 pp.

[120] V. Babrauskas, Will the Second Item Ignite?, Fire Safety Journal **4** (4), 281-292 (1981). https://doi.org/10.1016/0379-7112(81)90031-X

[121] T. Mizuno and K. Kawagoe, Burning Behavior of Upholstered Chairs: Part 2, Burning Rate of Chairs in Fire Tests, Fire Science and Technology **5** (1), 69-78 (1985). https://doi.org/10.3210/fst.5.69

Appendix A Data Plots for Twenty Mock-up Types in Test Matrix

Results for repeated tests of flame spread and fire growth behavior on real-scale furniture mock-ups for the combinations listed in Table 3 are provided as combined temporal plots of HRR and total HRR, FIGRA and mass, mass loss rate and effective heat of combustion; separate flame spread contours on the back and seat cushions for each repeated test followed by plots of characteristic flame spread rates u_{bv}, u_{bl}, u_{sl}, and u_{st}; combined temporal plots of burned areas as a function of time for each of the tests for a given combination; and combined temporal plots of radiative heat flux recorded at distances of 0.75 m and 1.5 m from the front, right side, and back of the mock-ups. The various plots are repeated when more than one application of an ignition source was required.

A.1 Combination 1

Cotton/Whispershield/NFRFPUF

Notes:

Test 1:

Ignition Source 1 applied at time = 0 s

Initial mass reading (2.99 kg) during the experiment disagreed with an earlier measurement for the mock-up (3.18 kg); mass readings increased during the initial period of the test and showed abrupt jumps; **these mass data were excluded from analysis**.

Test 2:

Ignition Source 1 applied at time = 0 s

Following removal of ignition source seat was blackened, but there was no evident flame spread, flames began spreading at ≈ 65 s.

Initial mass reading (2.87 kg) during the experiment disagreed with an earlier measurement for the mock-up (3.20 kg); adjusting for difference resulted in negative mass values; **these mass data were excluded from analysis**.

Test 3:

Ignition Source 1 applied at time = 0 s

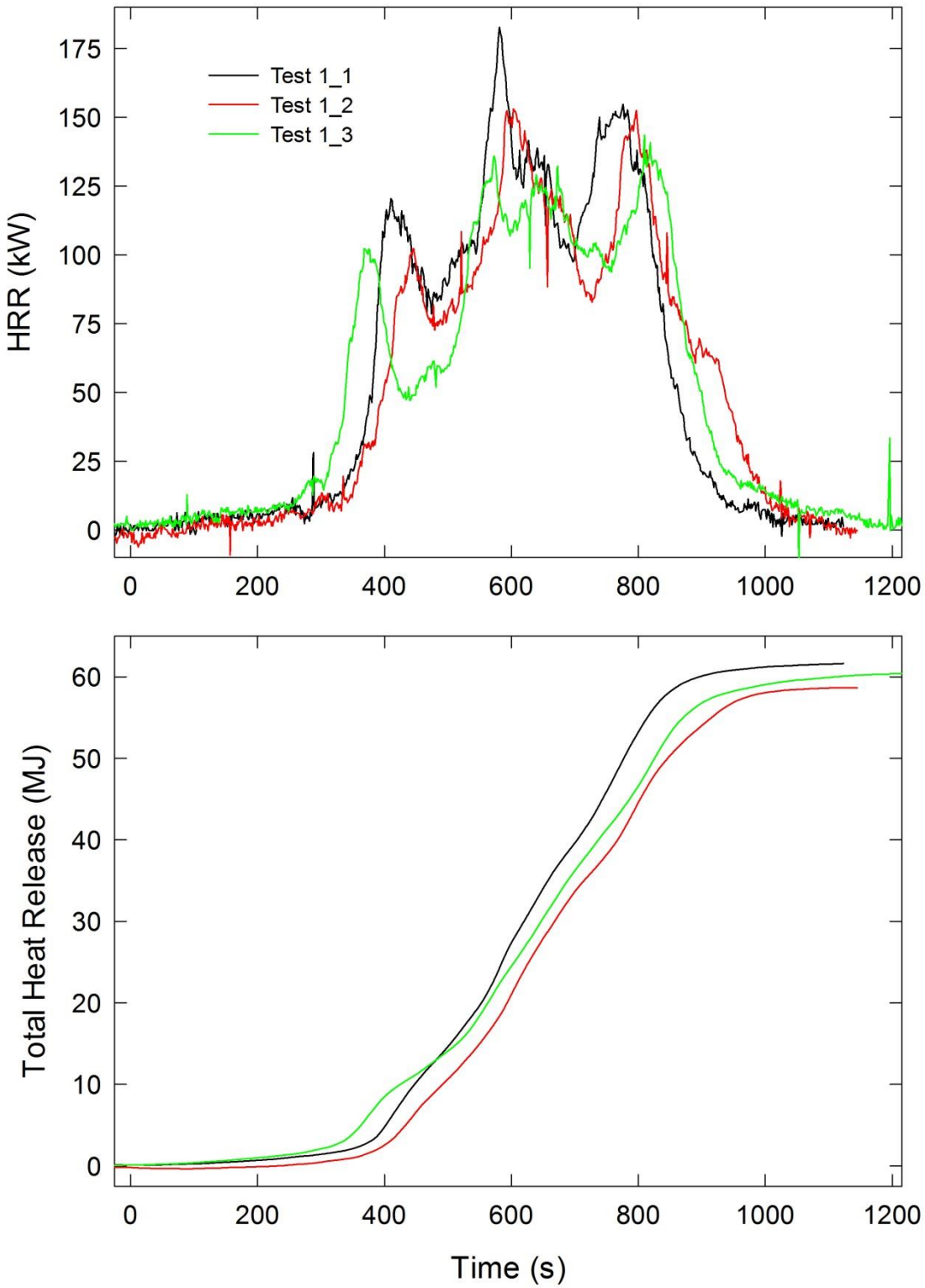

Figure A-1. Temporal profiles of HRR and integrated HRR are shown for Combination 1 tests following application of Ignition Source 1.

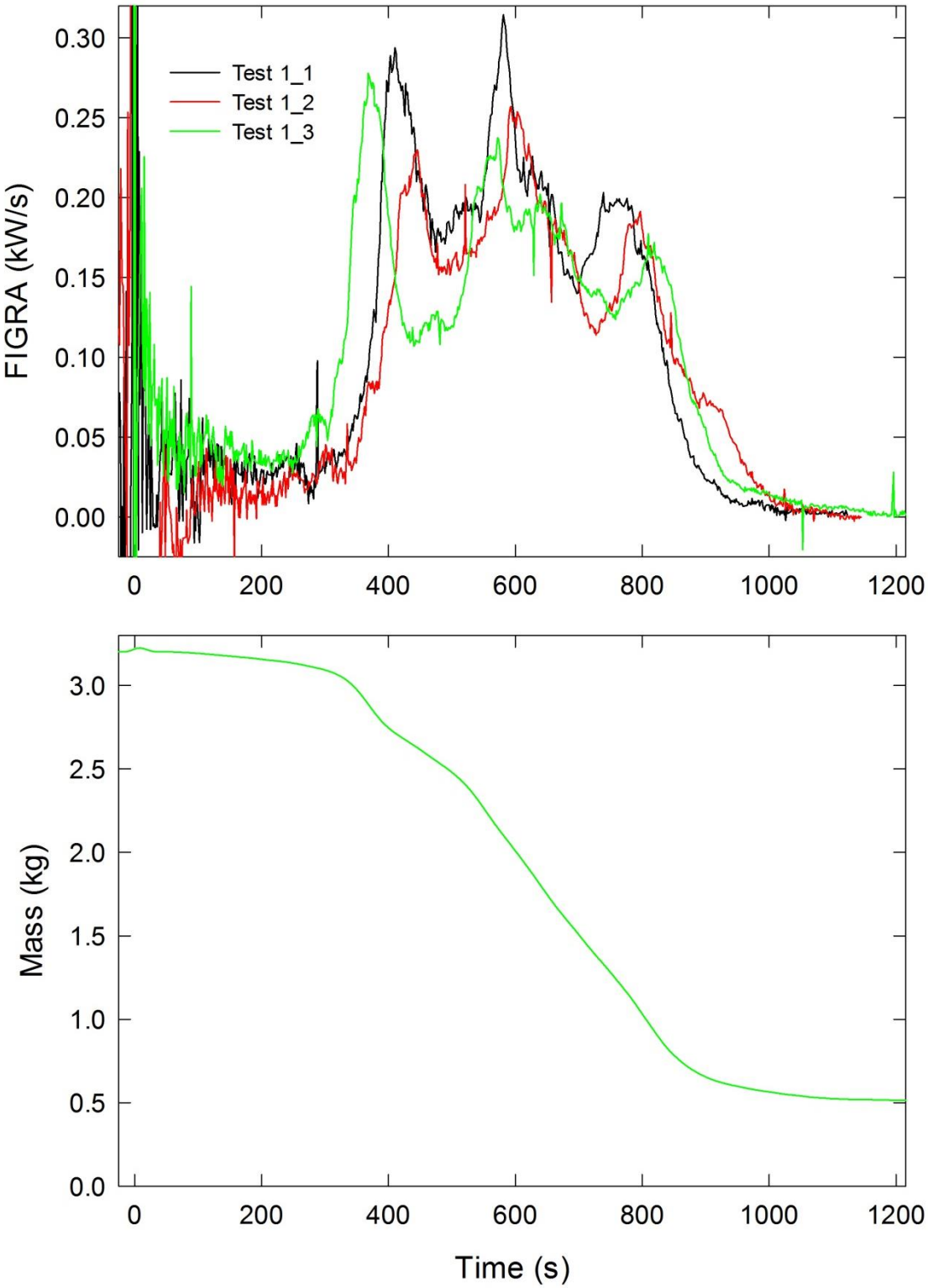

Figure A-2. Temporal profiles of FIGRA for Combination 1 tests and mock-up mass for Test 1_3 are shown following application of Ignition Source 1.

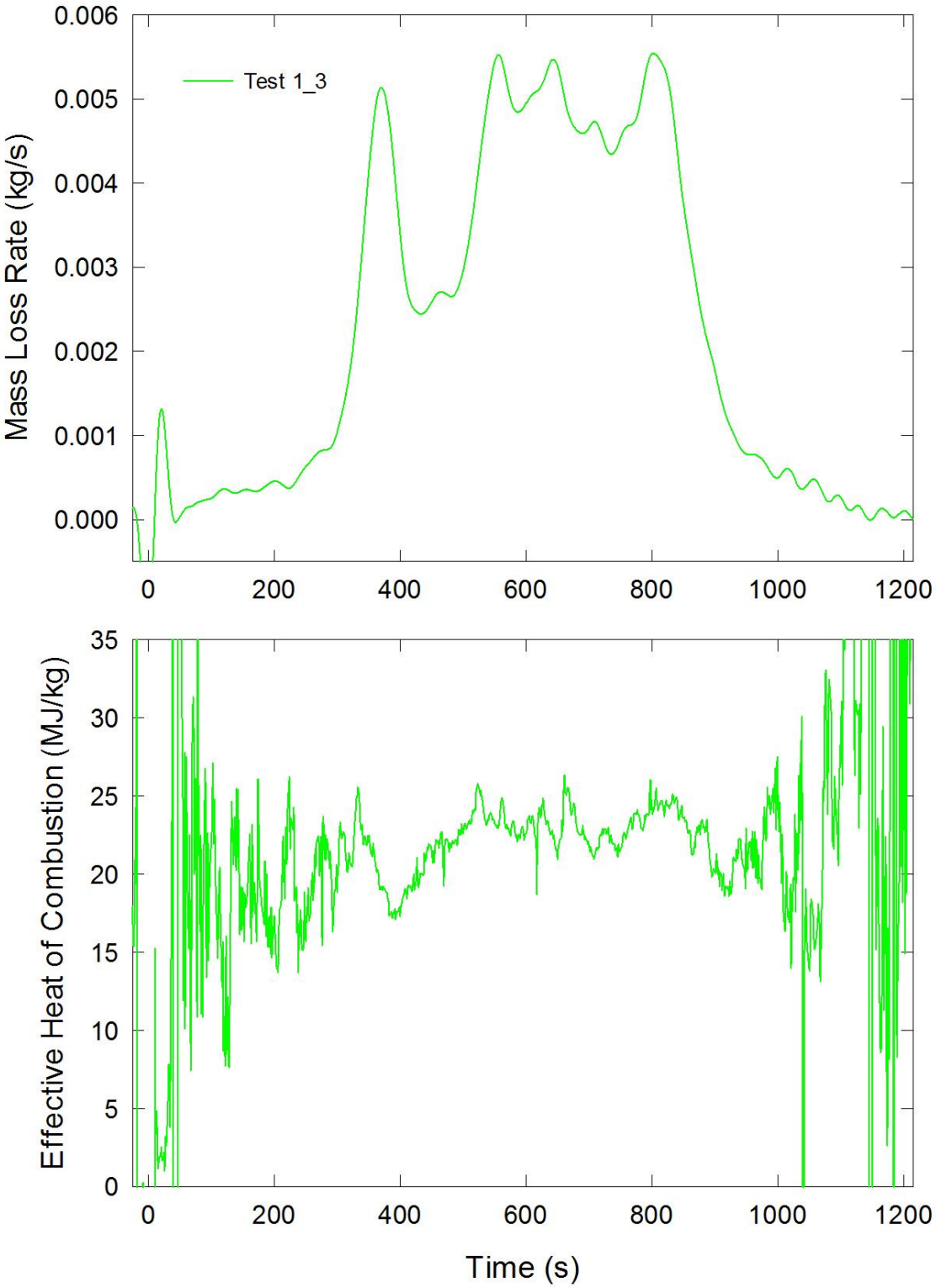

Figure A-3. Temporal profiles of MLR and EHOC are shown for Test 1_3 following application of Ignition Source 1.

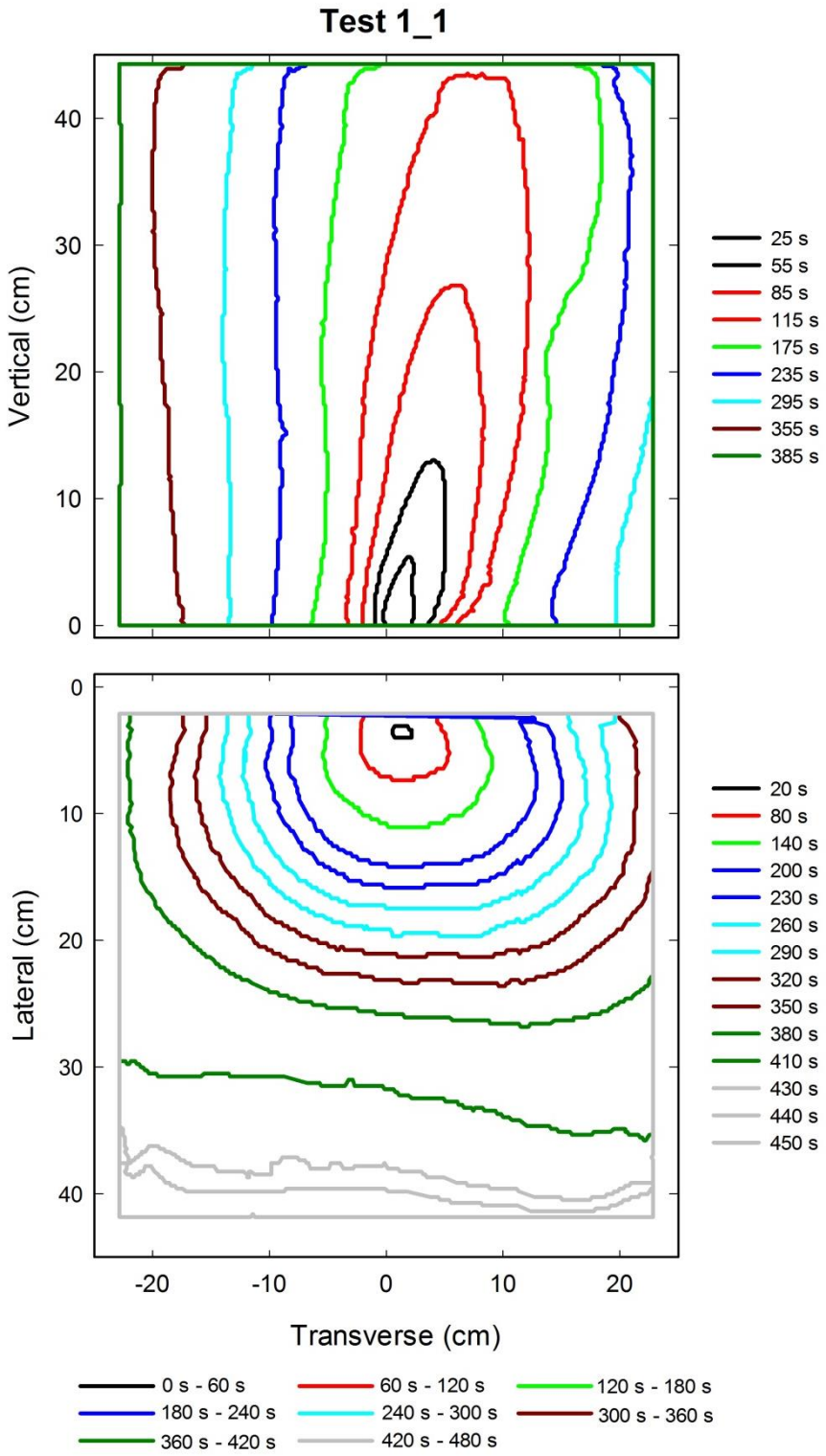

Figure A-4. Flame edge contours on the back (top) and seat (bottom) cushions are plotted as a function of time for Test 1_1 following application of Ignition Source 1.

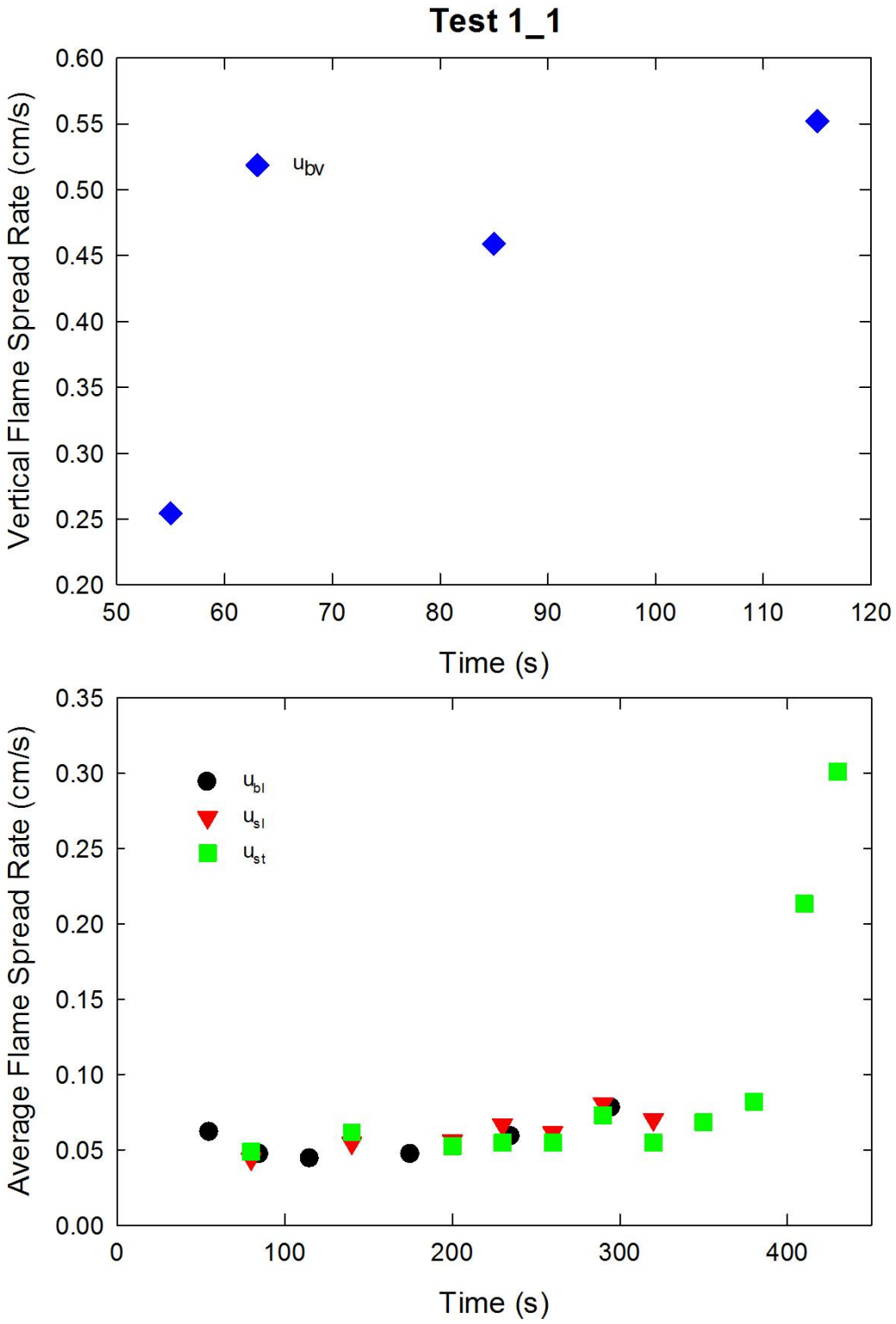

Figure A-5. Vertical flame spread rate on the back cushion (top) and average lateral flame spread rates on the back and seat cushions and transverse flame spread rate on the seat cushion (bottom) are plotted as a function of time for Test 1_1 following application of Ignition Source 1.

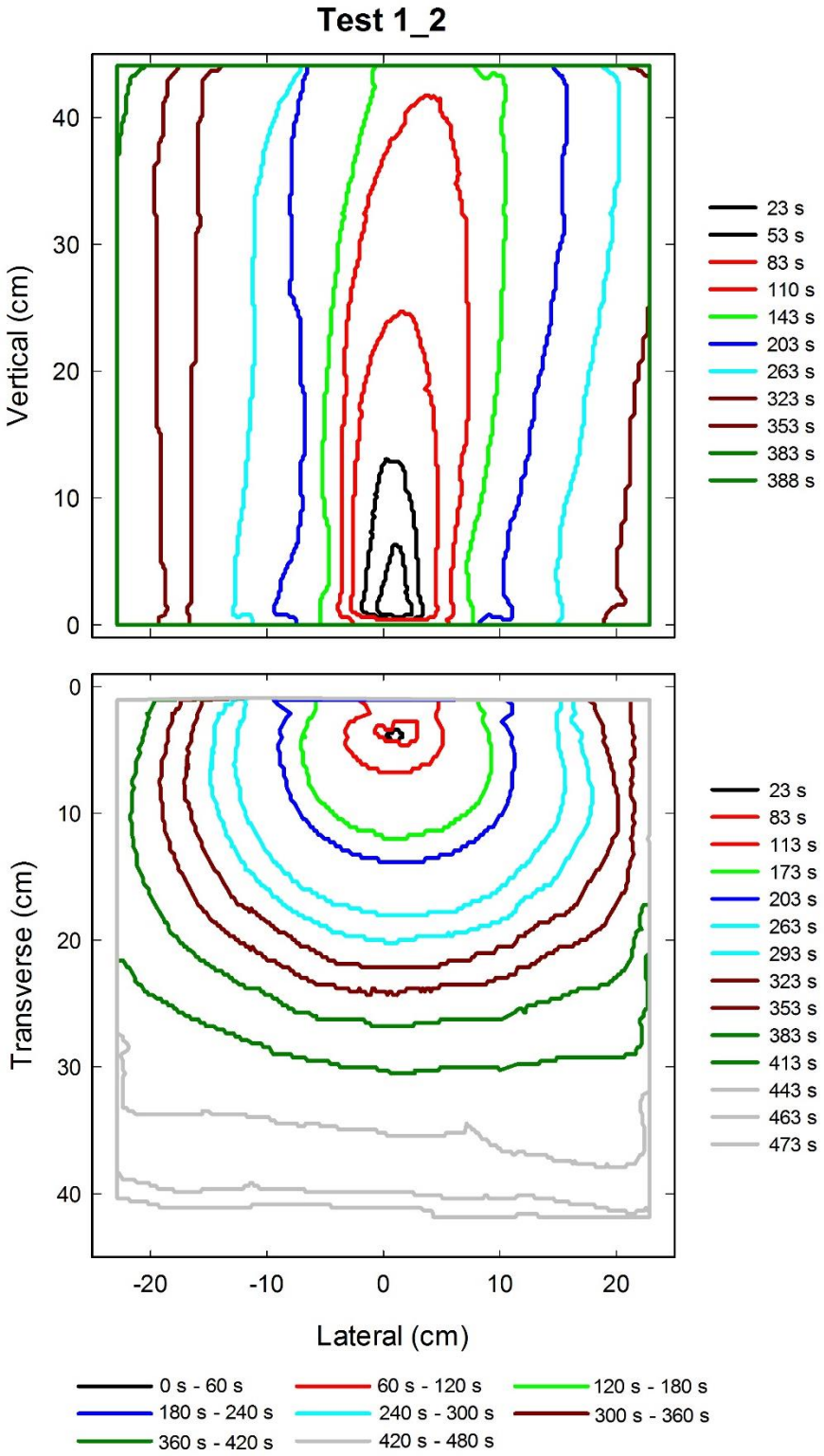

Figure A-6. Flame edge contours on the back (top) and seat (bottom) cushions are plotted as a function of time for Test 1_2 following application of Ignition Source 1.

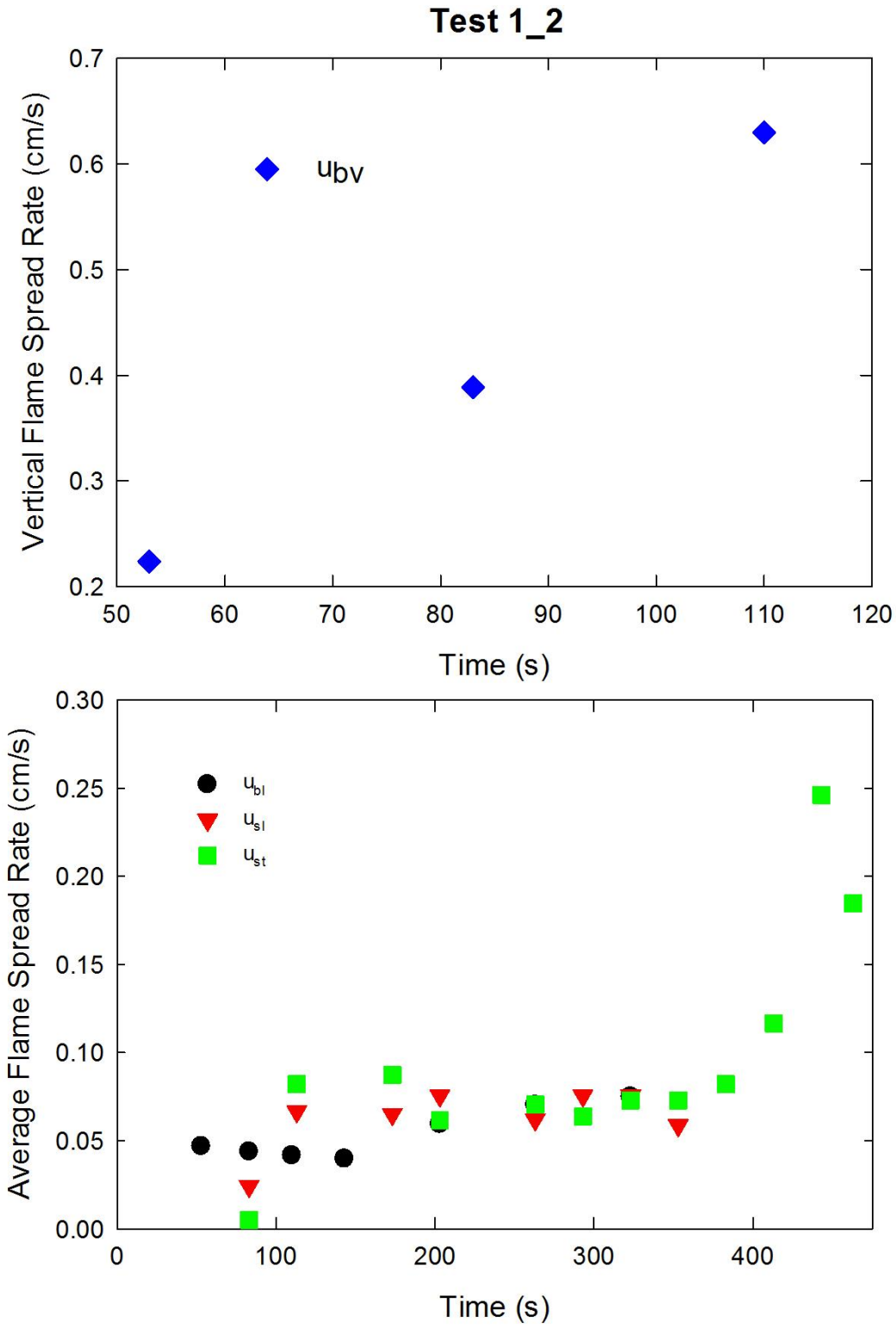

Figure A-7. Vertical flame spread rate on the back cushion (top) and average lateral flame spread rates on the back and seat cushions and transverse flame spread rate on the seat cushion (bottom) are plotted as a function of time for Test 1_2 following application of Ignition Source 1.

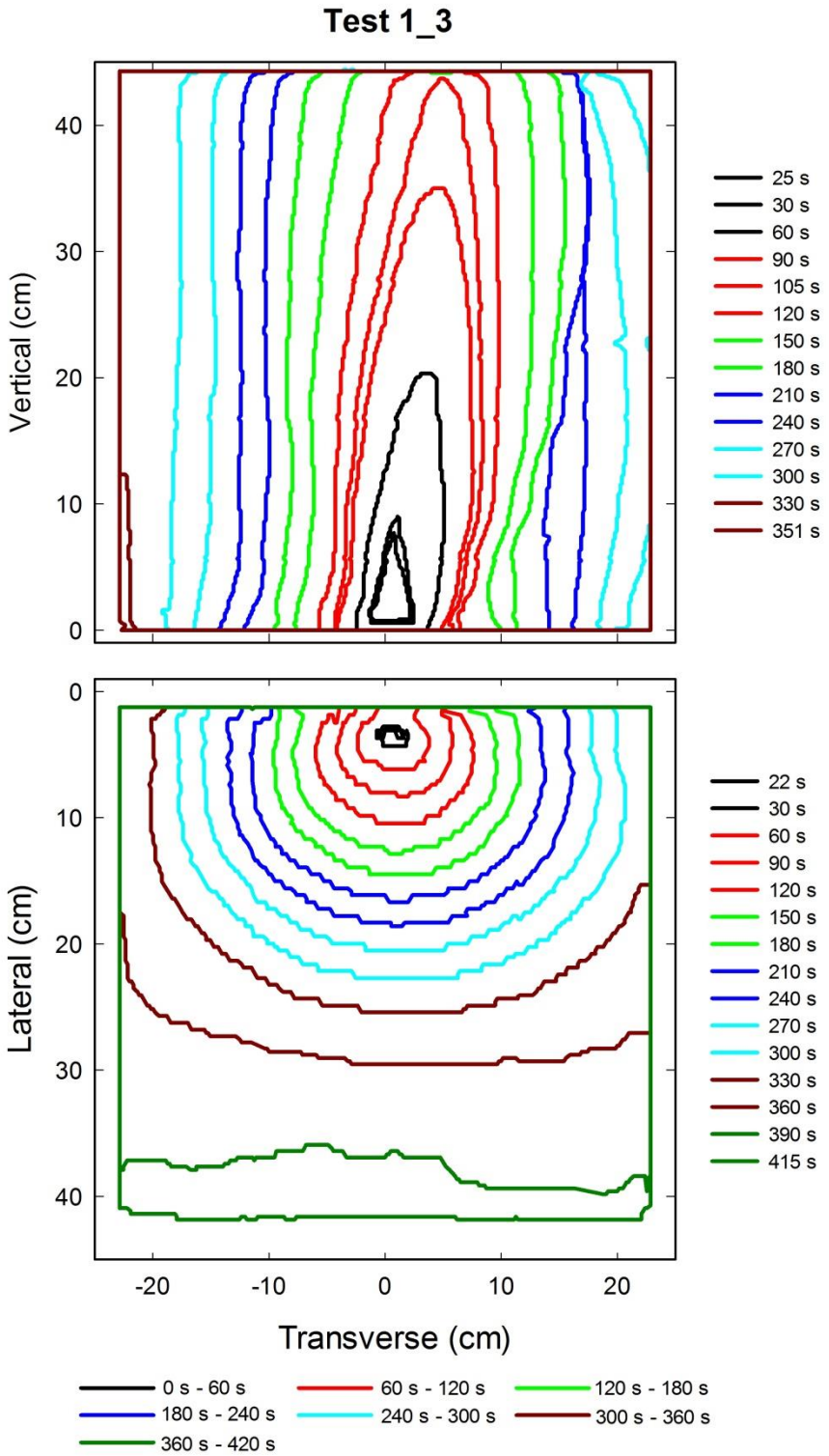

Figure A-8. Flame edge contours on the back (top) and seat (bottom) cushions are plotted as a function of time for Test 1_3 following application of Ignition Source 1.

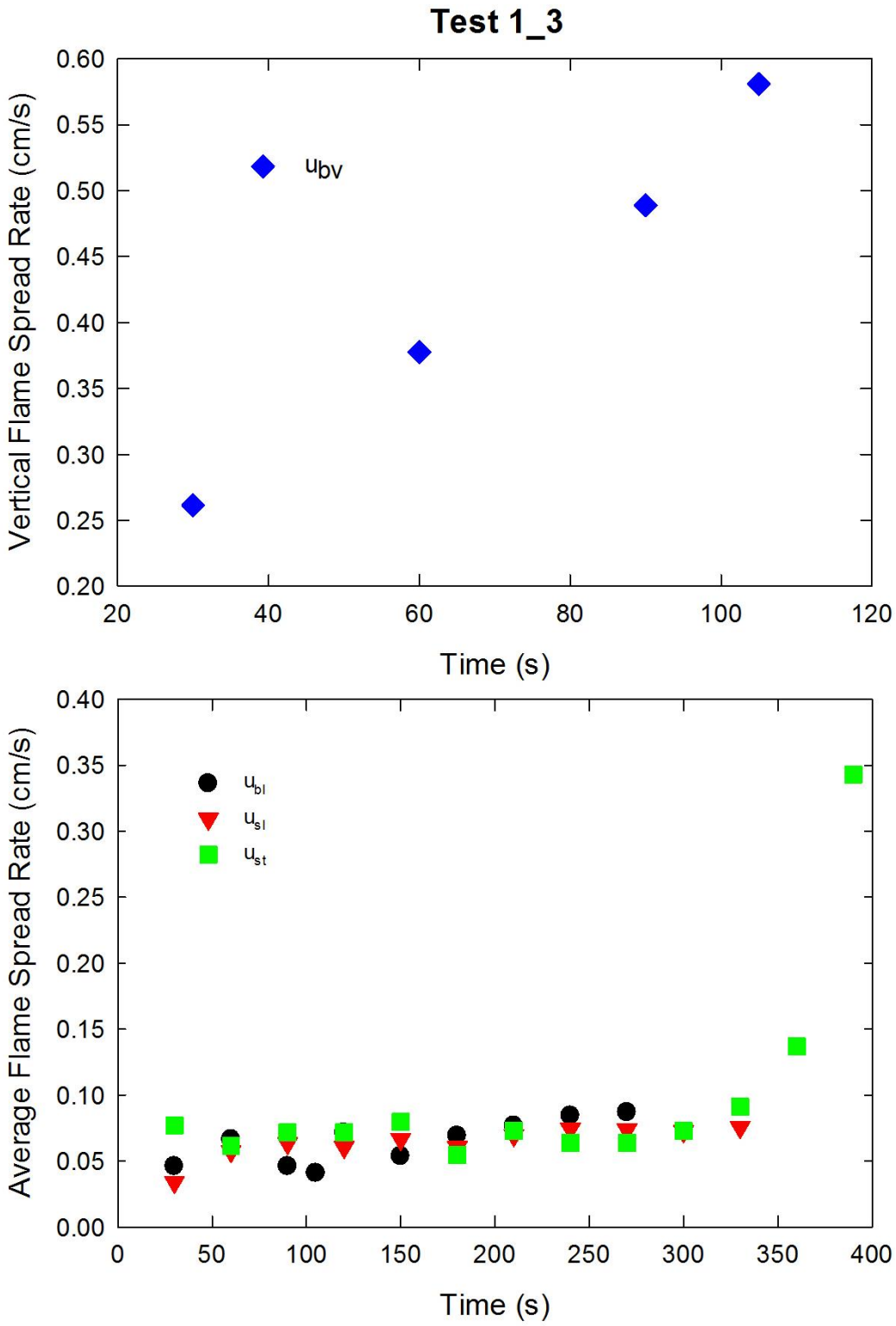

Figure A-9. Vertical flame spread rate on the back cushion (top) and average lateral flame spread rates on the back and seat cushions and transverse flame spread rate on the seat cushion (bottom) are plotted as a function of time for Test 1_3 following application of Ignition Source 1.

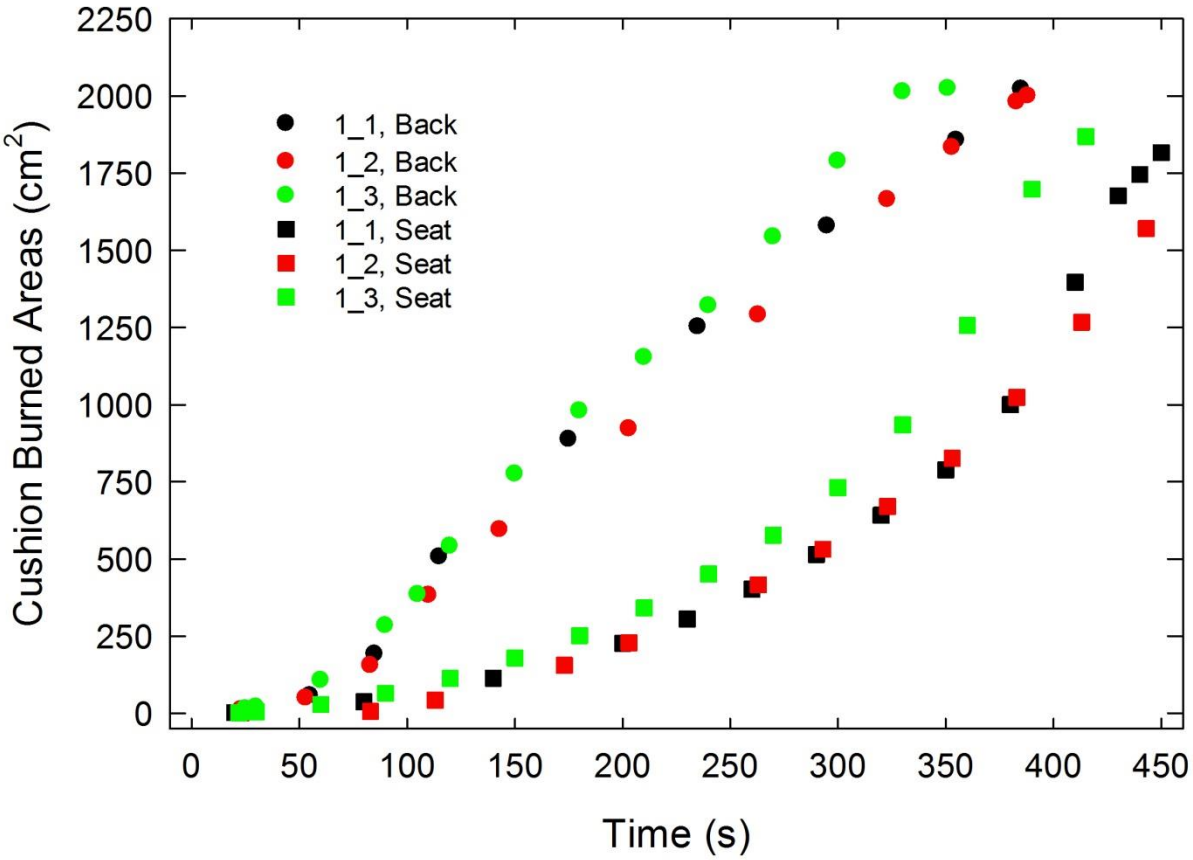

Figure A-10. Burned areas on the seat and back cushions are plotted as a function of time for Combination 1 tests following application of Ignition Source 1.

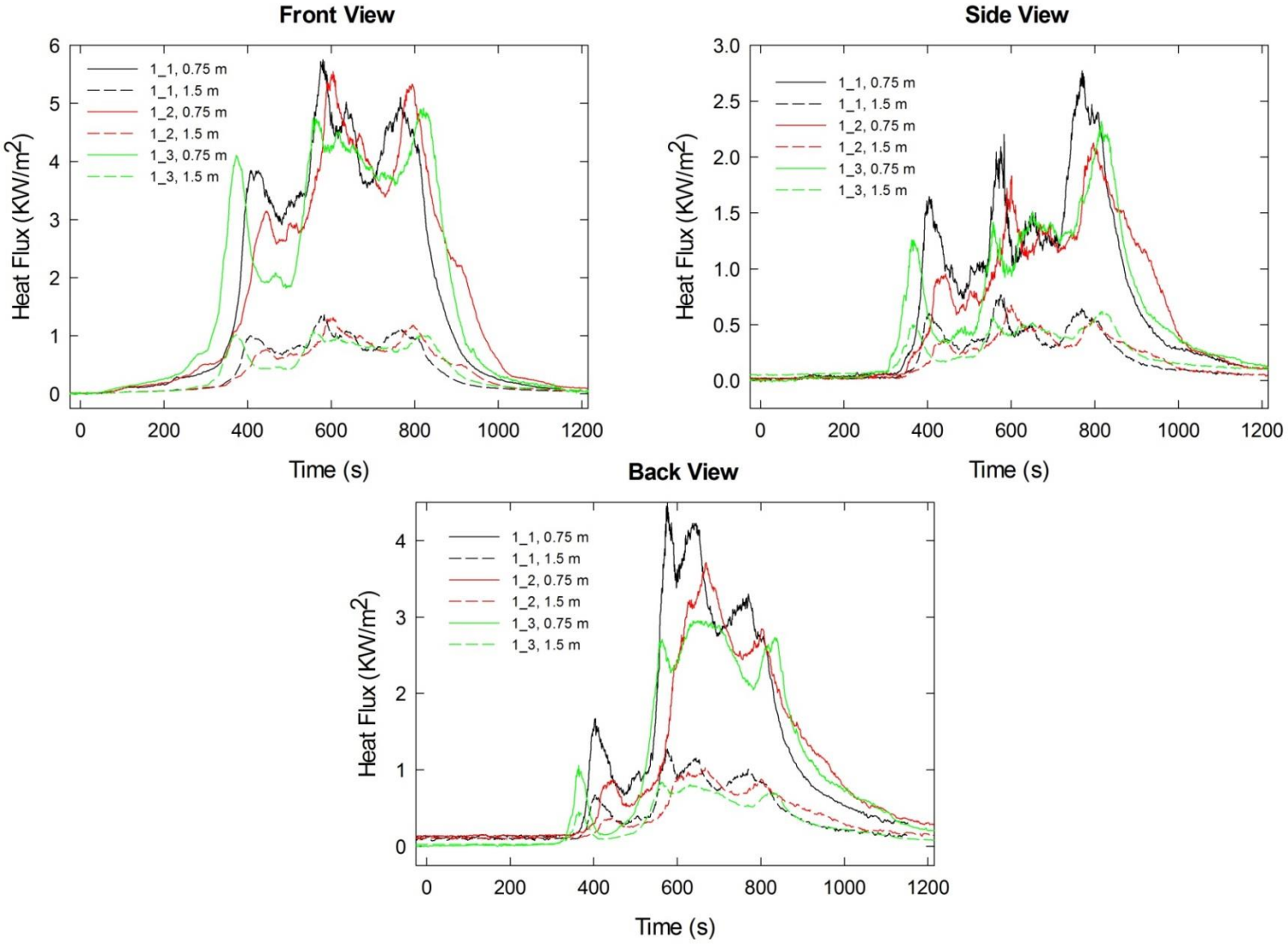

Figure A-11. Heat fluxes recorded at distances of 0.75 m and 1.5 m are plotted as a function of time for locations to the front, side and rear of the mock-up for Combination 1 tests following application of Ignition Source 1.

A.2 Combination 2

78%PP/22%PE/Whispershield/NFRFPUF

Notes:

Test 1

Ignition Source 1 applied at time = 0 s

Test 2:

Ignition Source 1 applied at time = 0 s

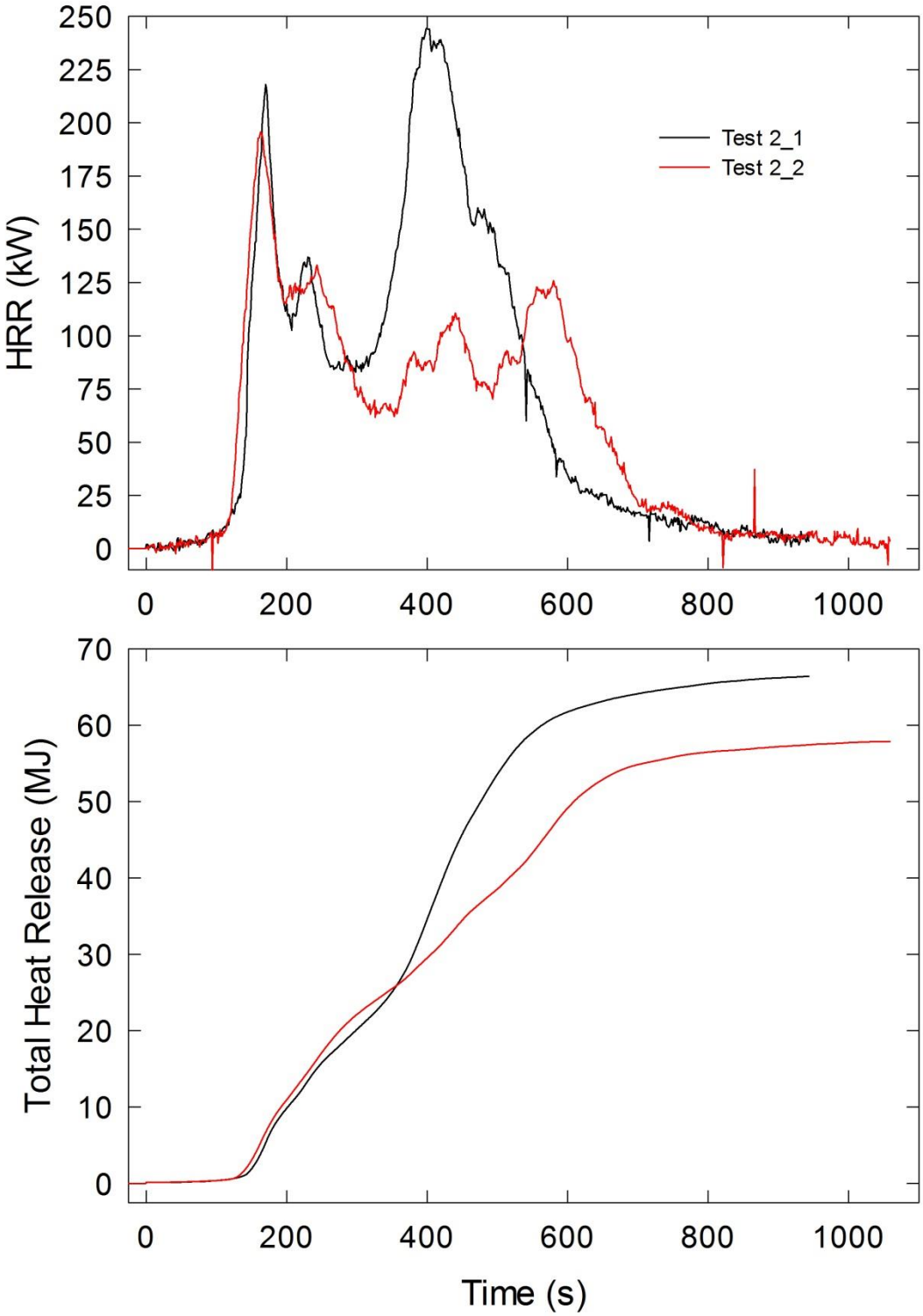

Figure A-12. Temporal profiles of HRR and integrated HRR are shown for Combination 2 tests following application of Ignition Source 1.

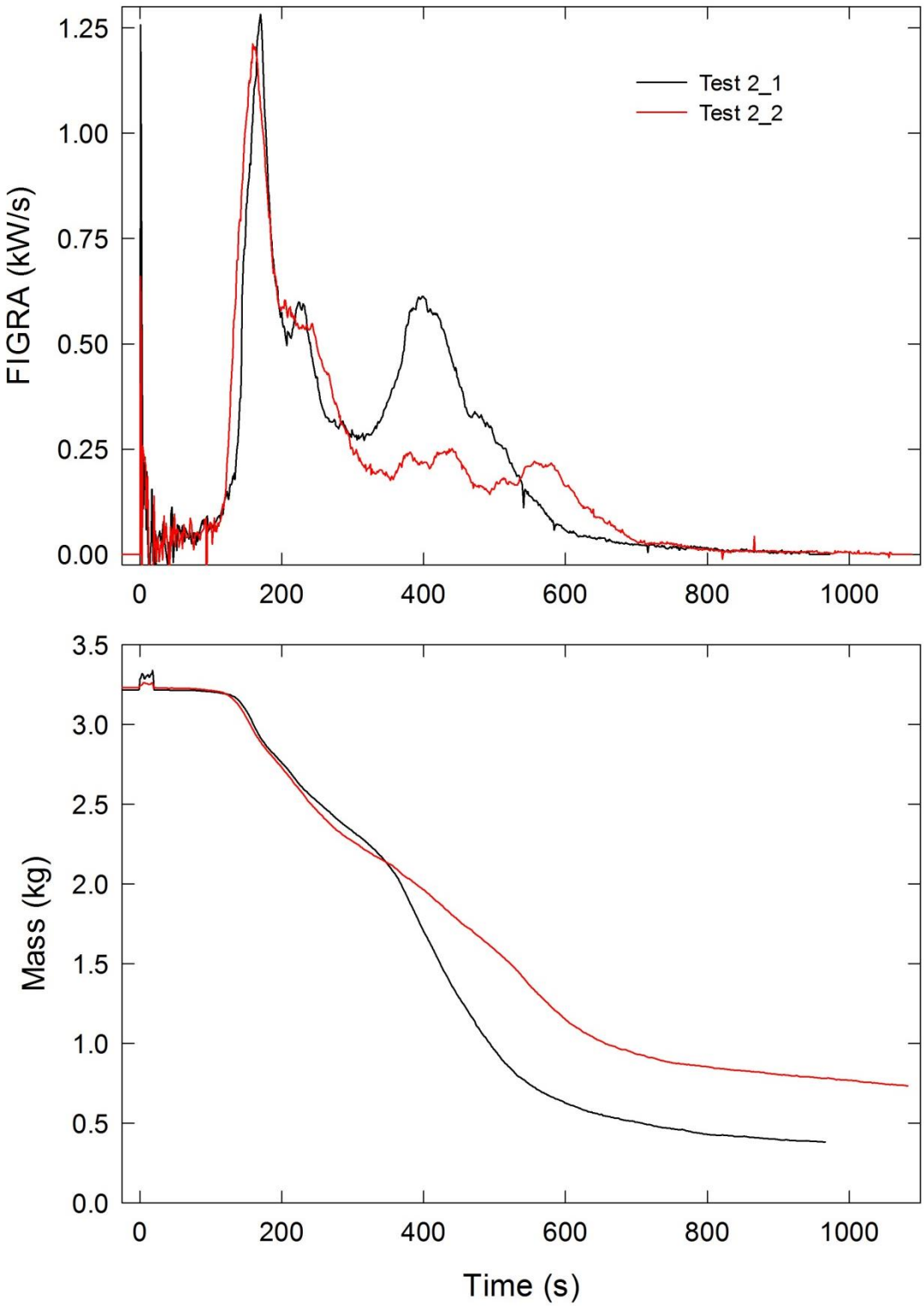

Figure A-13. Temporal profiles of FIGRA and mock-up mass are shown for Combination 2 tests following application of Ignition Source 1.

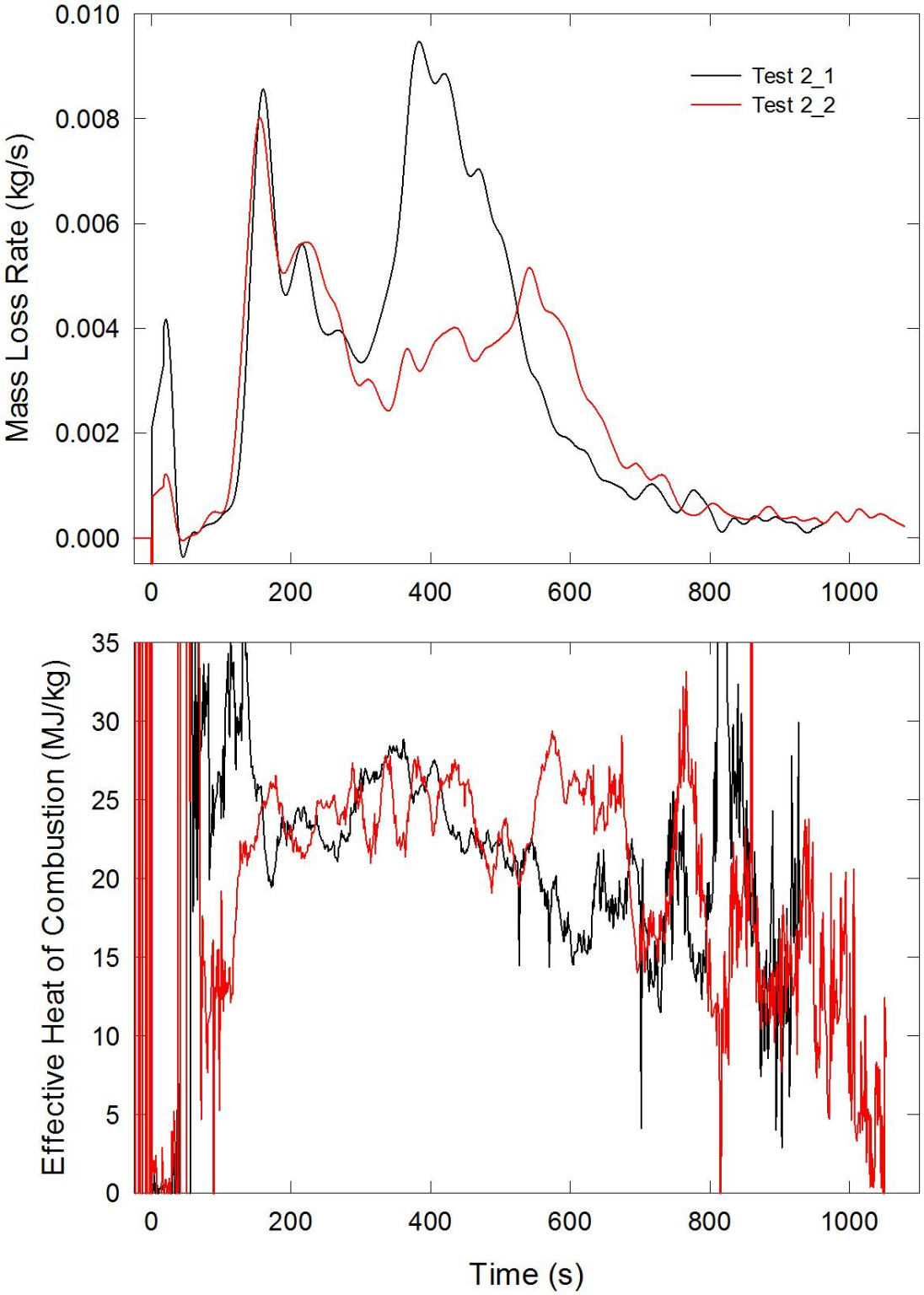

Figure A-14. Temporal profiles of MLR and EHOC are shown for Combination 2 tests following application of Ignition Source 1.

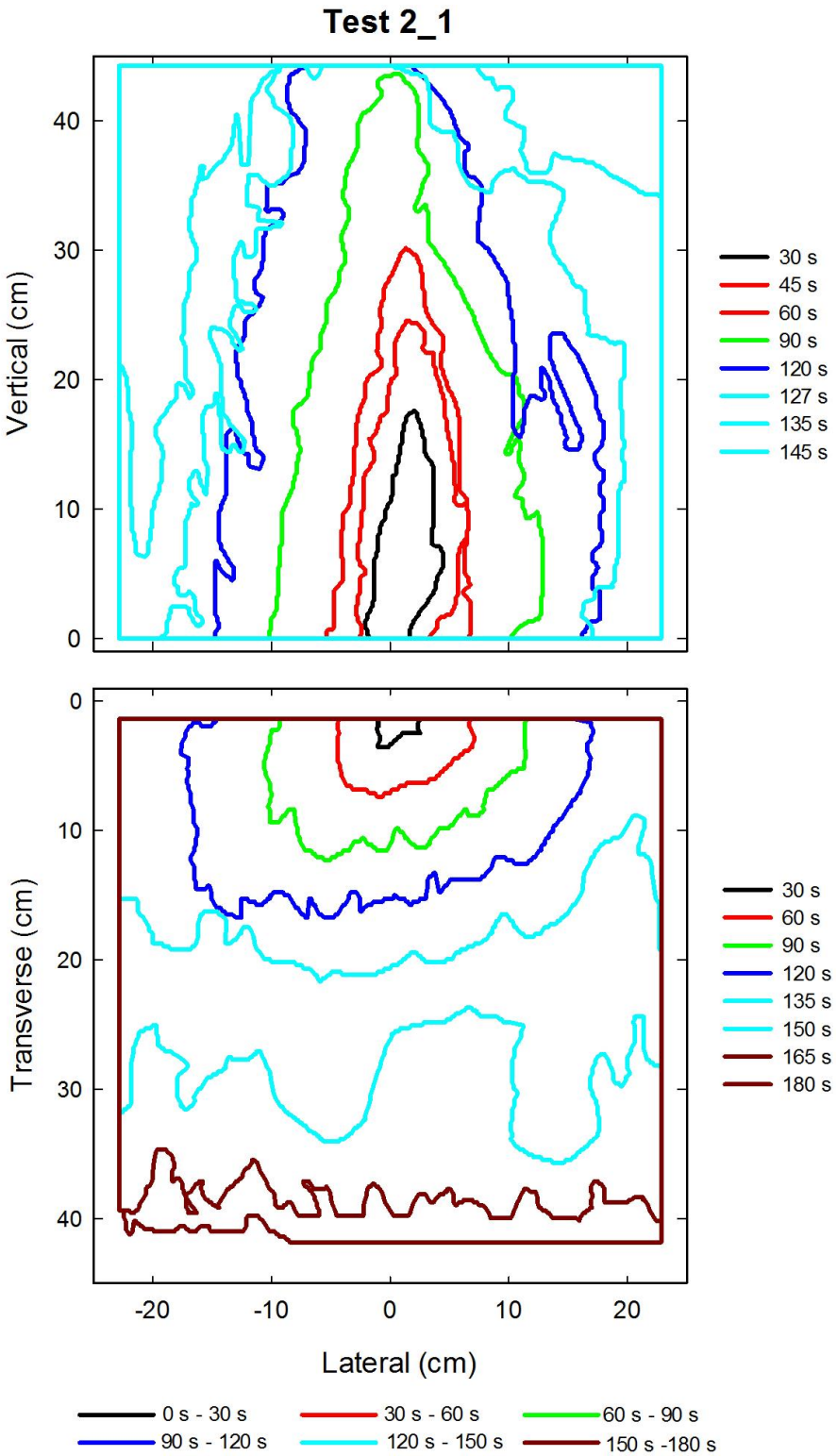

Figure A-15. Flame edge contours on the back (top) and seat (bottom) cushions are plotted as a function of time for Test 2_1 following application of Ignition Source 1.

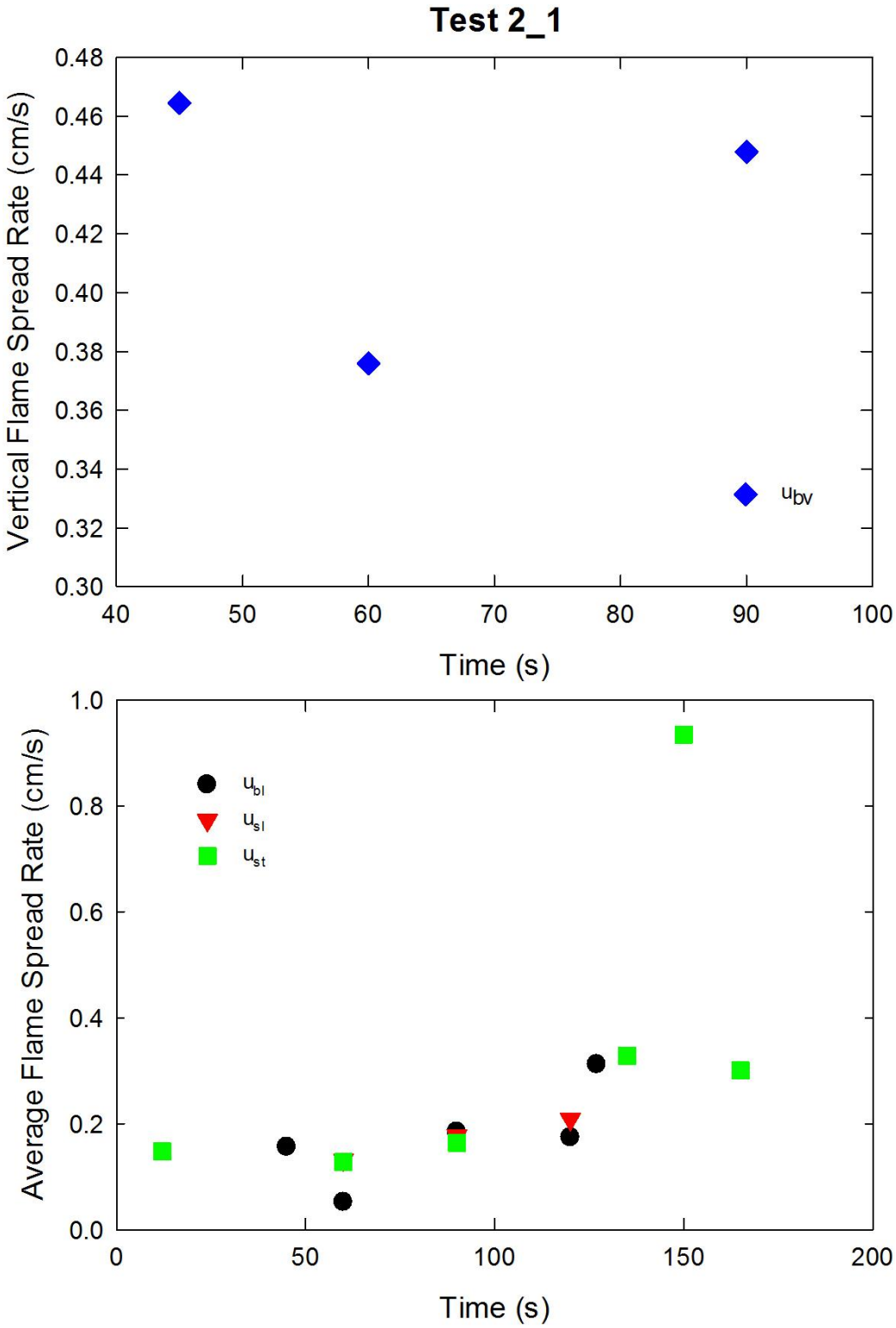

Figure A-16. Vertical flame spread rate on the back cushion (top) and average lateral flame spread rates on the back and seat cushions and transverse flame spread rate on the seat cushion (bottom) are plotted as a function of time for Test 2_1 following application of Ignition Source 1.

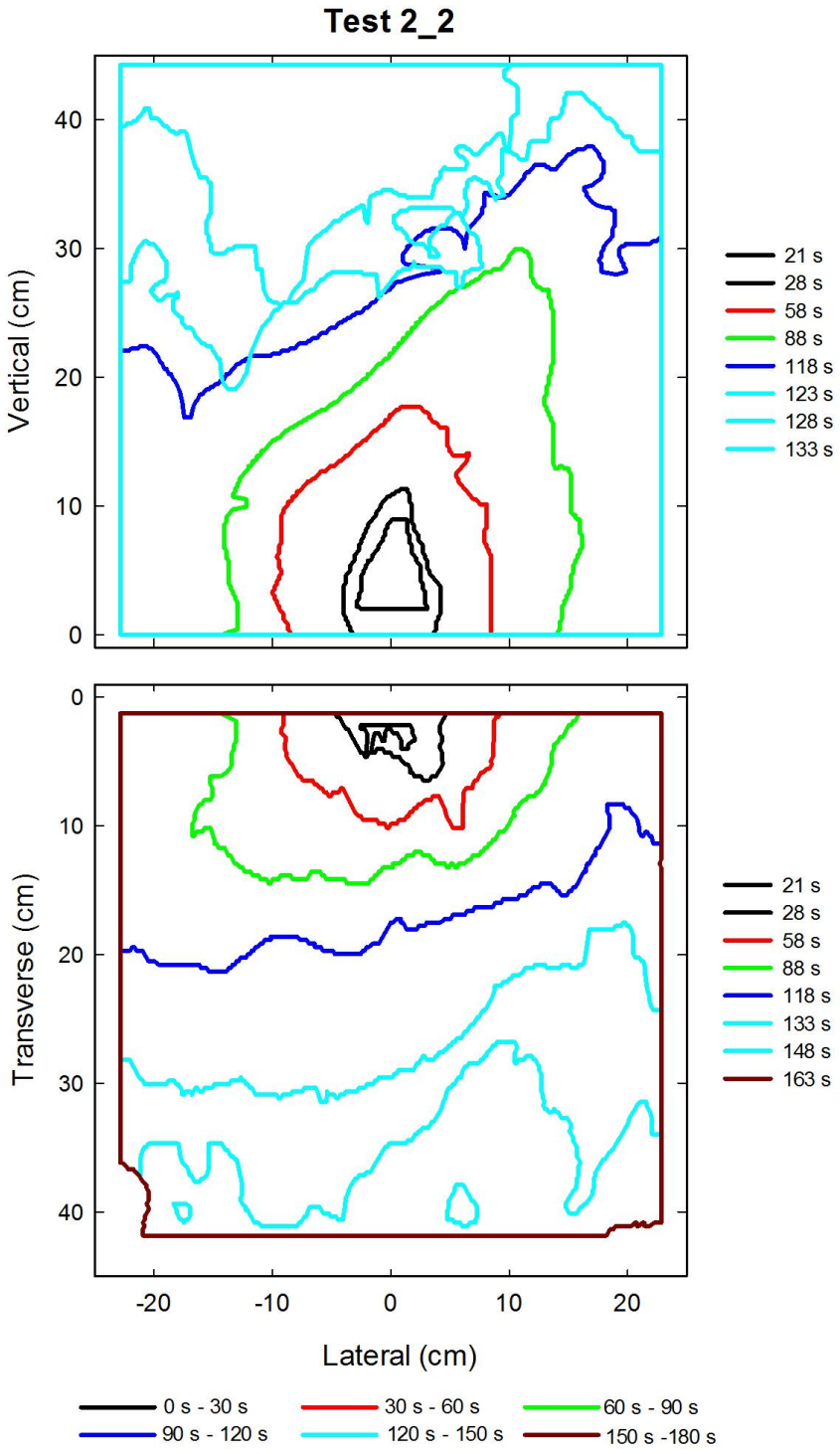

Figure A-17. Flame edge contours on the back (top) and seat (bottom) cushions are plotted as a function of time for Test 2_2 following application of Ignition Source 1.

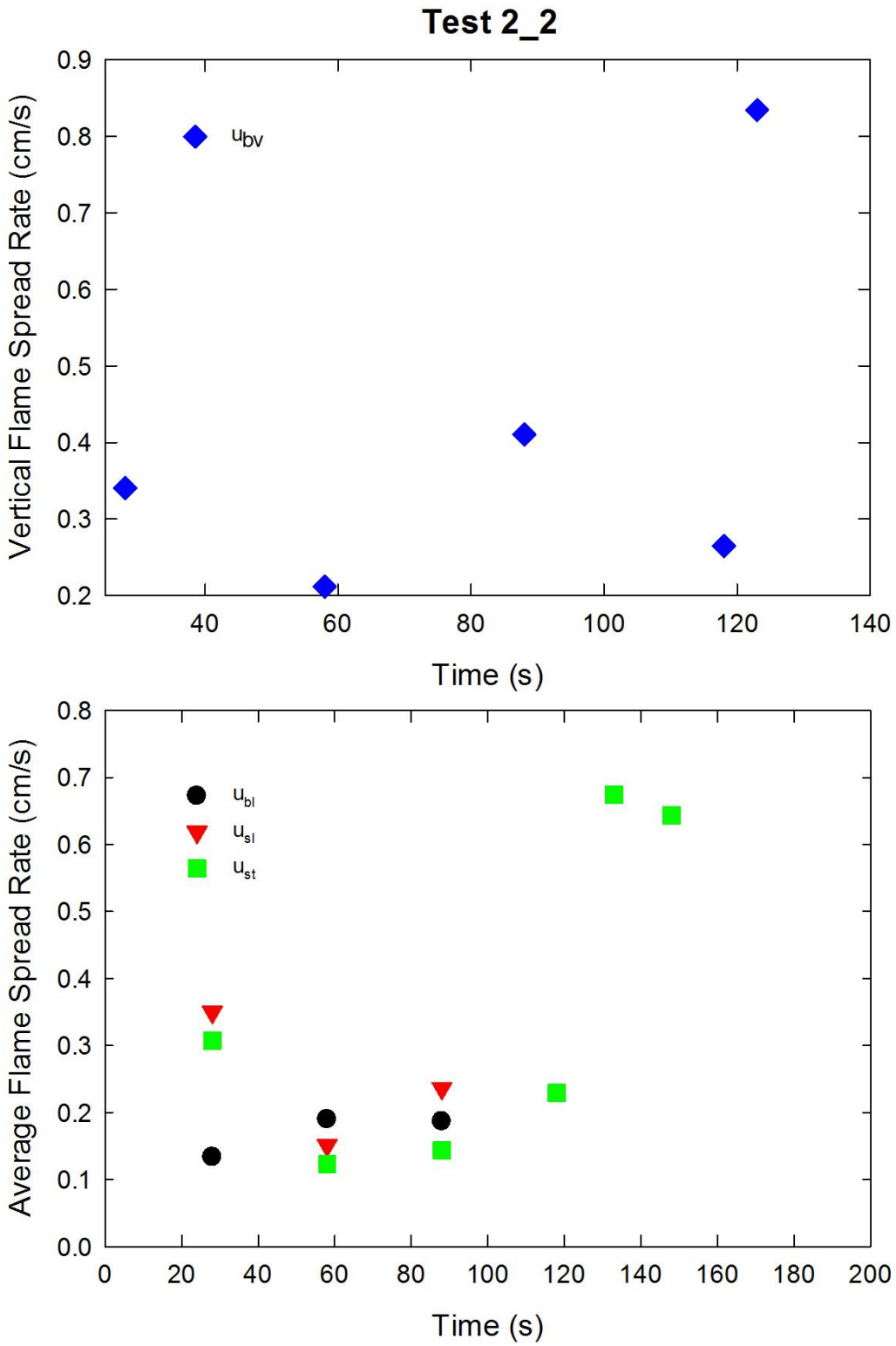

Figure A-18. Vertical flame spread rate on the back cushion (top) and average lateral flame spread rates on the back and seat cushions and transverse flame spread rate on the seat cushion (bottom) are plotted as a function of time for Test 2_2 following application of Ignition Source 1.

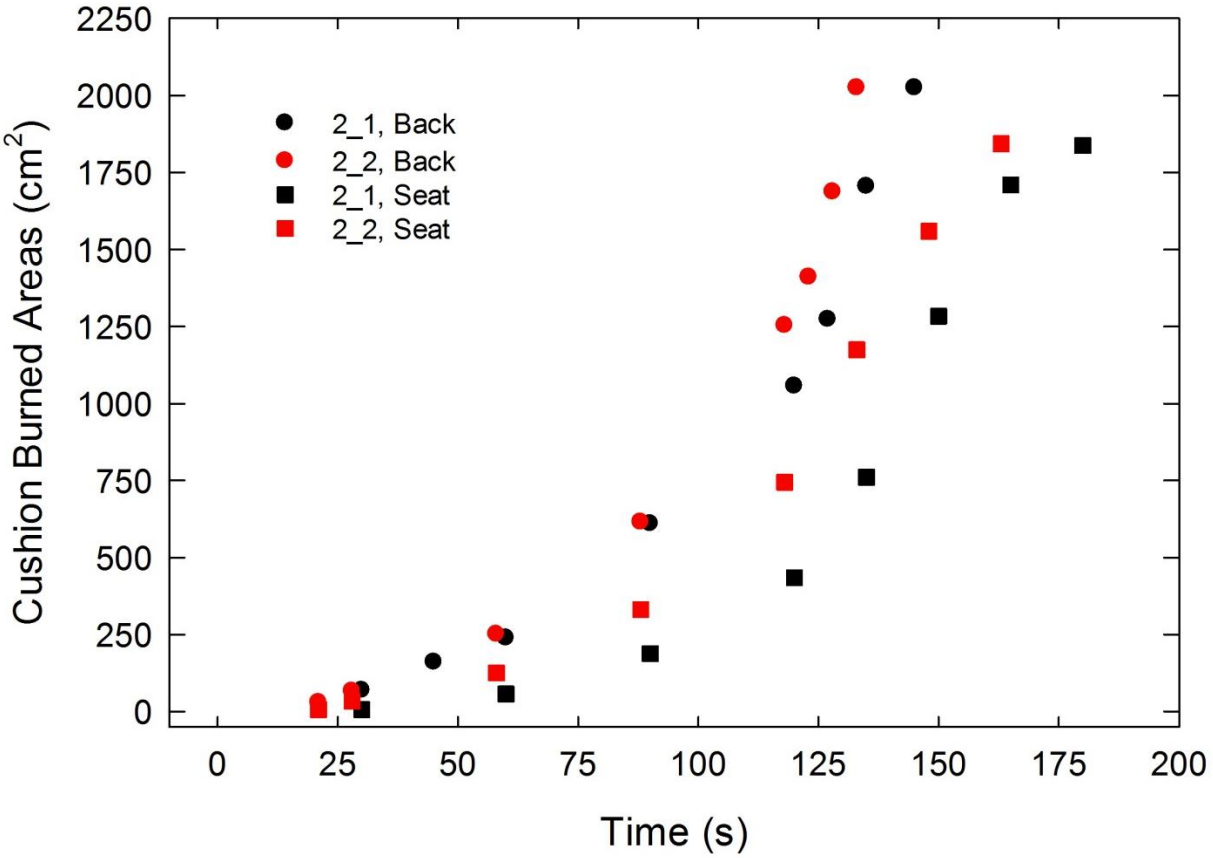

Figure A-19. Burned areas on the seat and back cushions are plotted as a function of time for Combination 2 tests following application of Ignition Source 1.

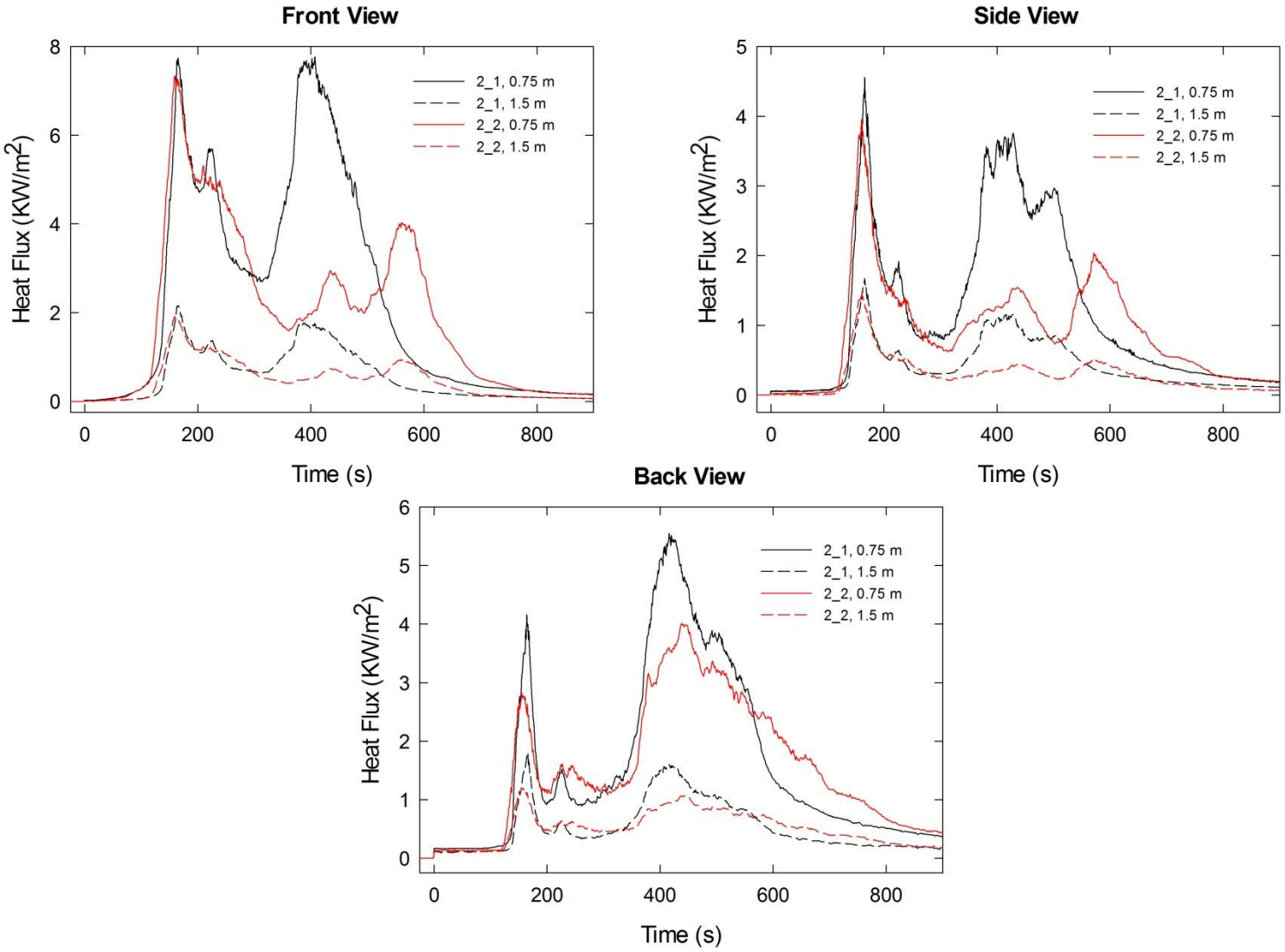

Figure A-20. Heat fluxes recorded at distances of 0.75 m and 1.5 m are plotted as a function of time for locations to the front, side and rear of the mock-up for Combination 2 tests following application of Ignition Source 1.

A.3 Combination 5

cotton/Whispershield/FRFPUF

Notes:

Test 1

Ignition Source 1 applied at time = 0 s; flame spread over only part of back and right-arm cushions.

Ignition Source 2 applied 1647 s after Ignition Source 1; following 40 s application, no obvious blackening of seat surface; within four seconds of flame removal black spot appeared on seat cushion and flames began to spread.

Following application of Ignition Source 2 flames spread over the interior surfaces of the four cushions and the back of the seat cushion, but there was limited flame spread to other locations on the mock-up.

Initial mass reading (3.92 kg) during the experiment disagreed with an earlier measurement for the mock-up (3.33 kg); mass readings increased during initial period of test and showed abrupt jumps; **these mass data were excluded from analysis**.

Test 2:

Ignition Source 1 applied at time = 0 s

Initial mass reading (3.15 kg) during the experiment disagreed with an earlier measurement for the mock-up (3.32 kg); mass readings during test were smooth, physically reasonable and correlated with the HRR; **these mass data were adjusted by adding 0.17 kg to their values and were included in the analysis**.

Test 3:

Ignition Source 1 applied at time = 0 s

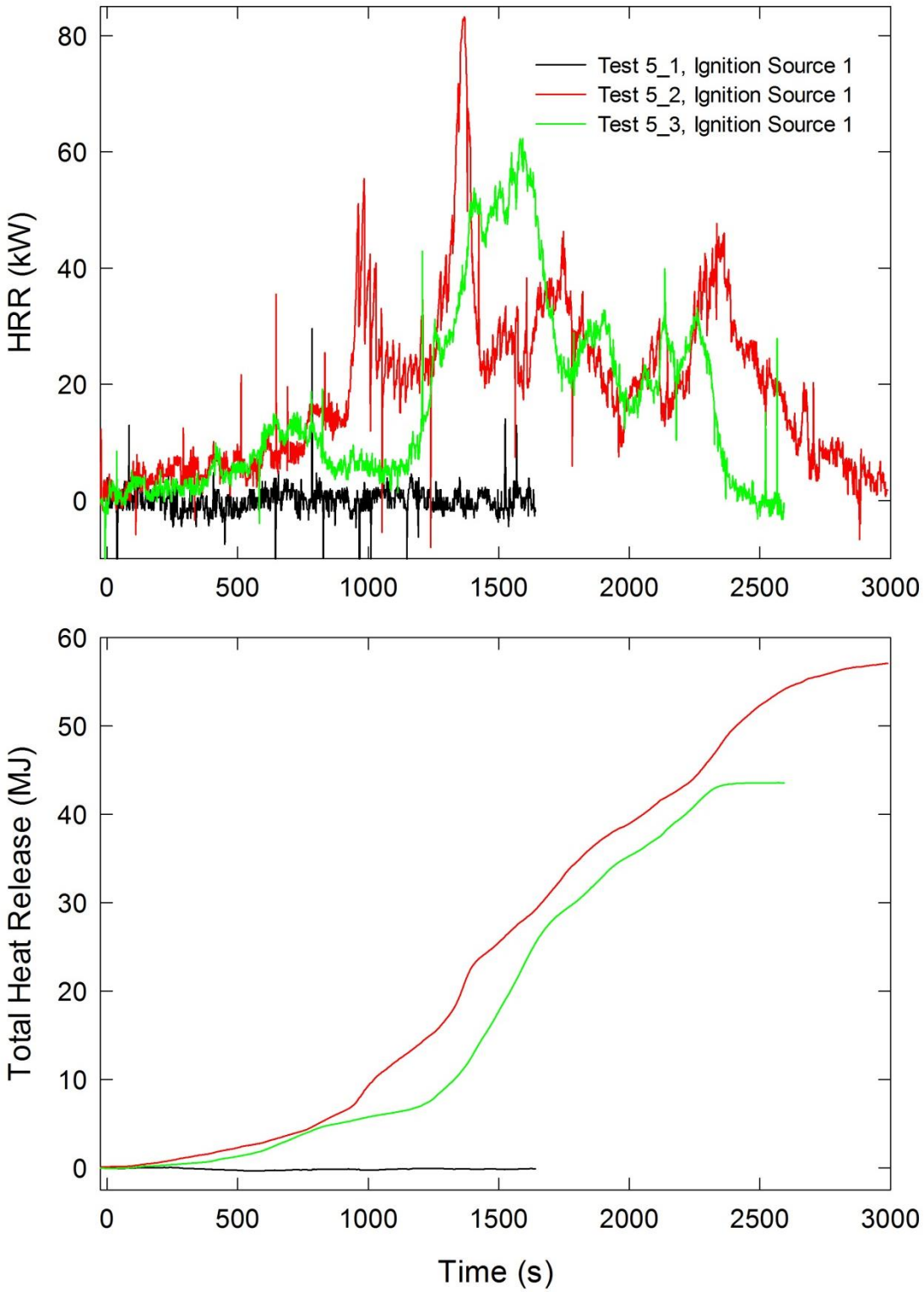

Figure A-21. Temporal profiles of HRR and integrated HRR are shown for Combination 5 tests following application of Ignition Source 1.

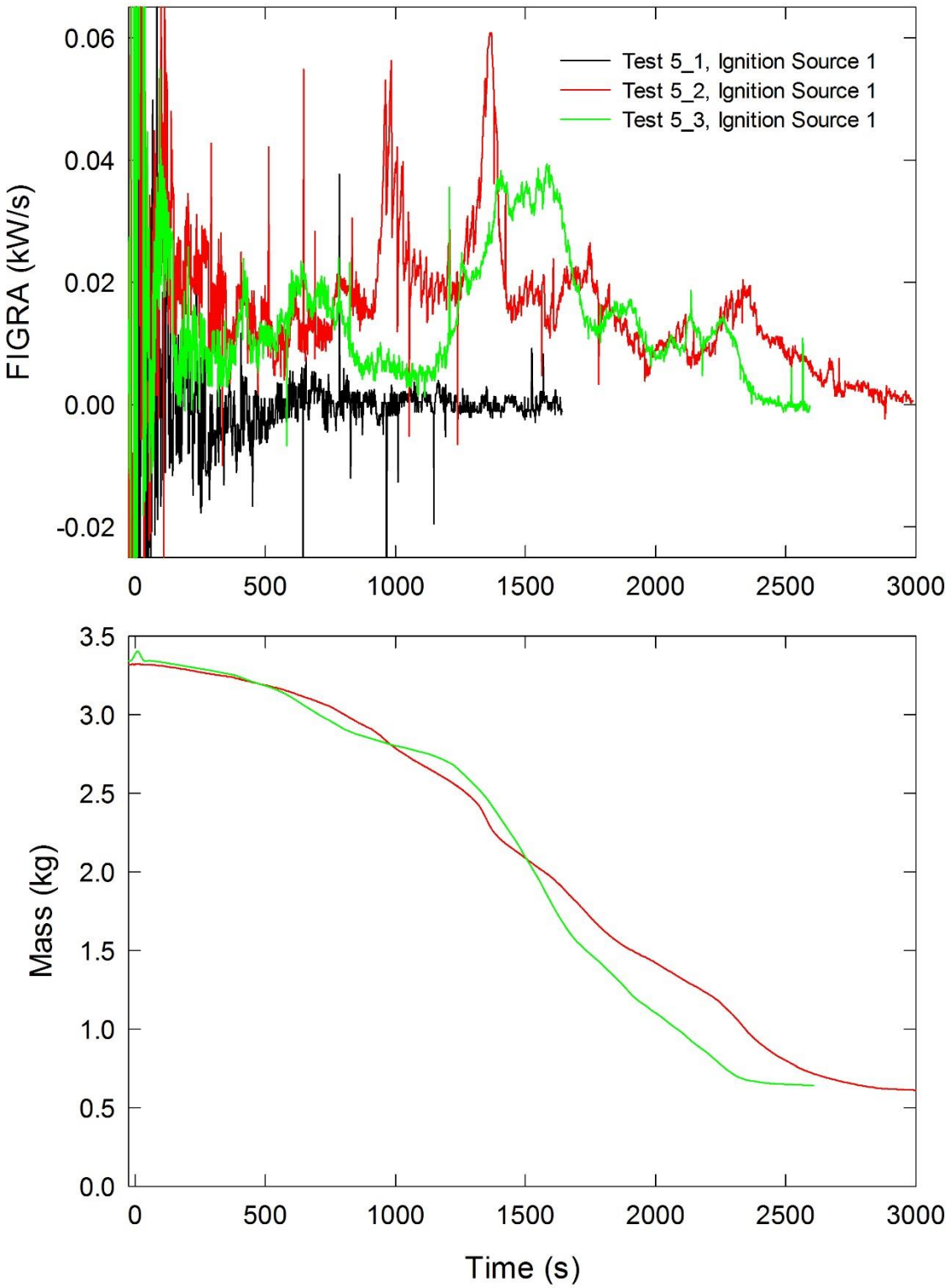

Figure A-22. Temporal profiles of FIGRA for Combination 5 tests and mock-up mass for Test 5_2 and Test 5_3 are shown following application of Ignition Source 1.

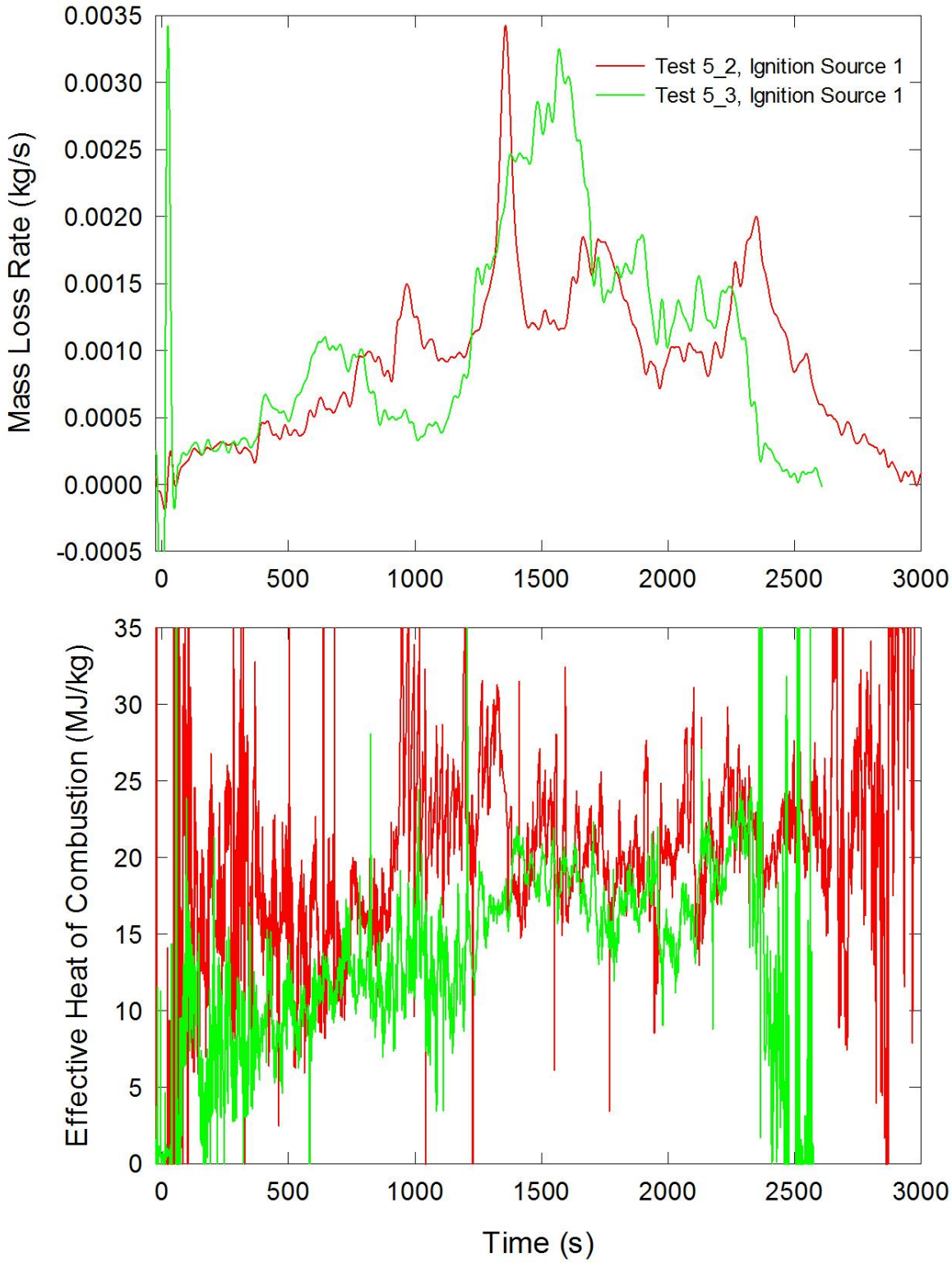

Figure A-23. Temporal profiles of MLR and EHOC are shown for Test 5_2 and Test 5_3 following application of Ignition Source 1.

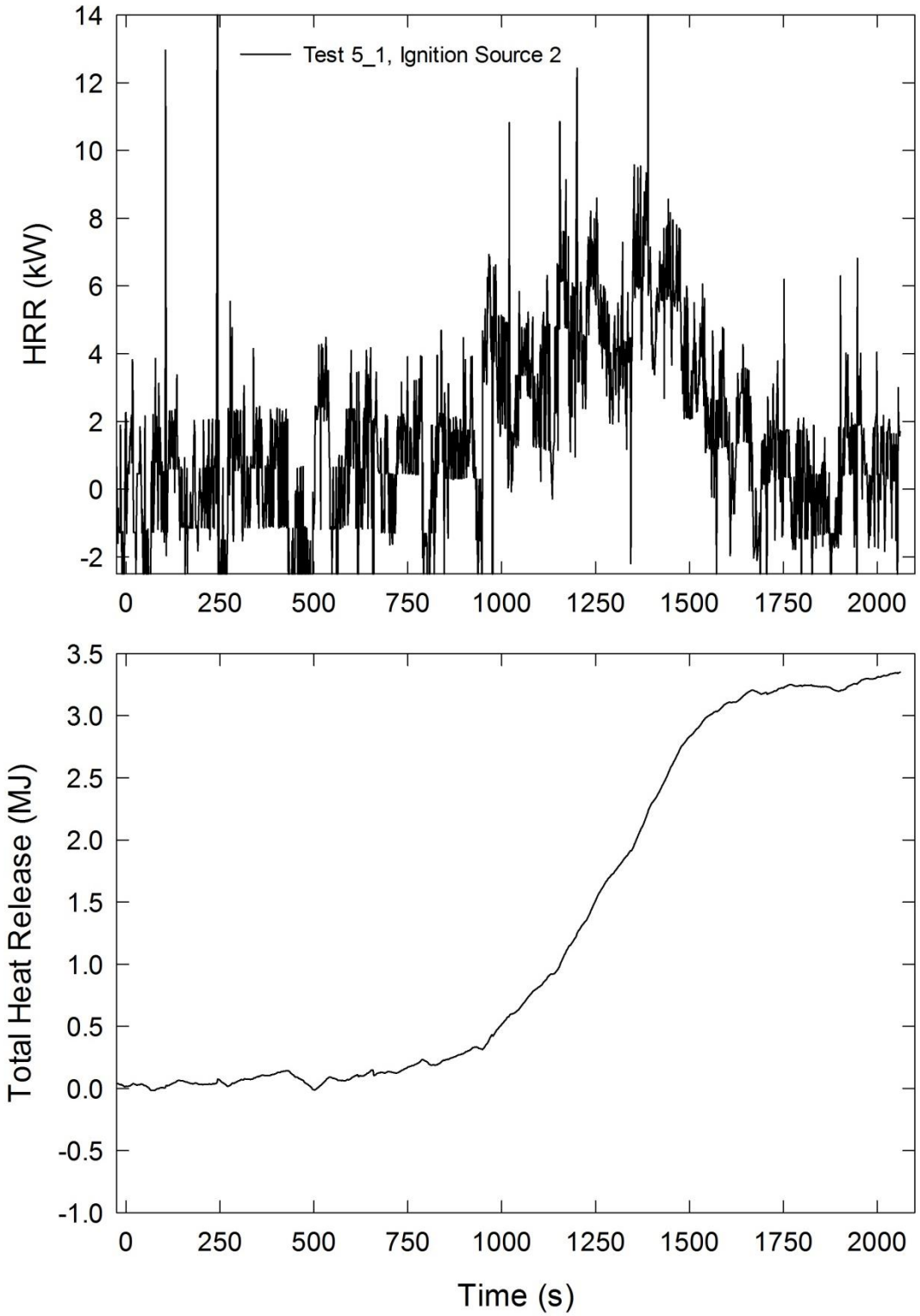

Figure A-24. The temporal profiles of HRR and integrated HRR are shown for Test 5_1 following application of Ignition Source 2.

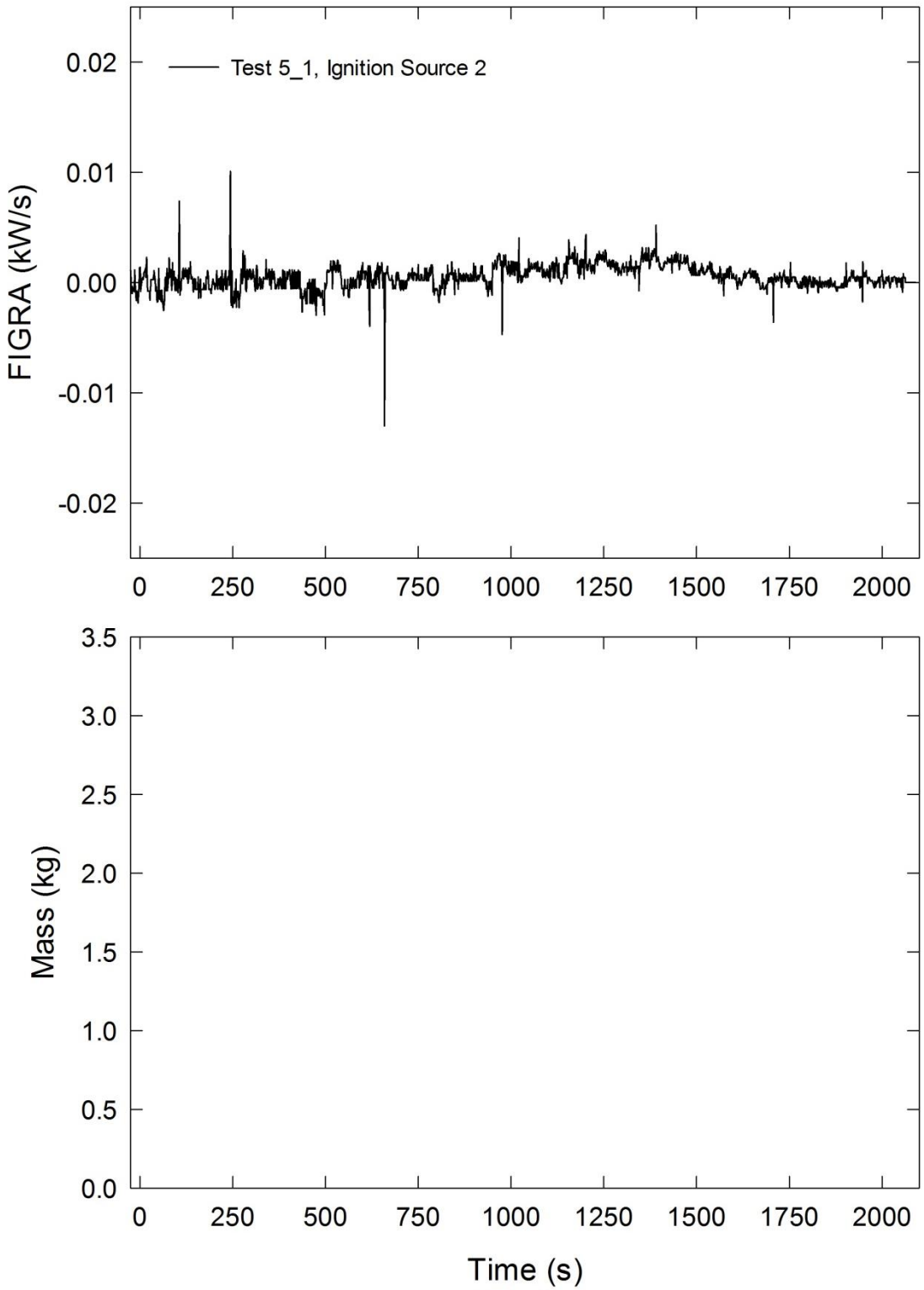

Figure A-25. The temporal profile of FIGRA is shown for Test 5_1 following application of Ignition Source 1.

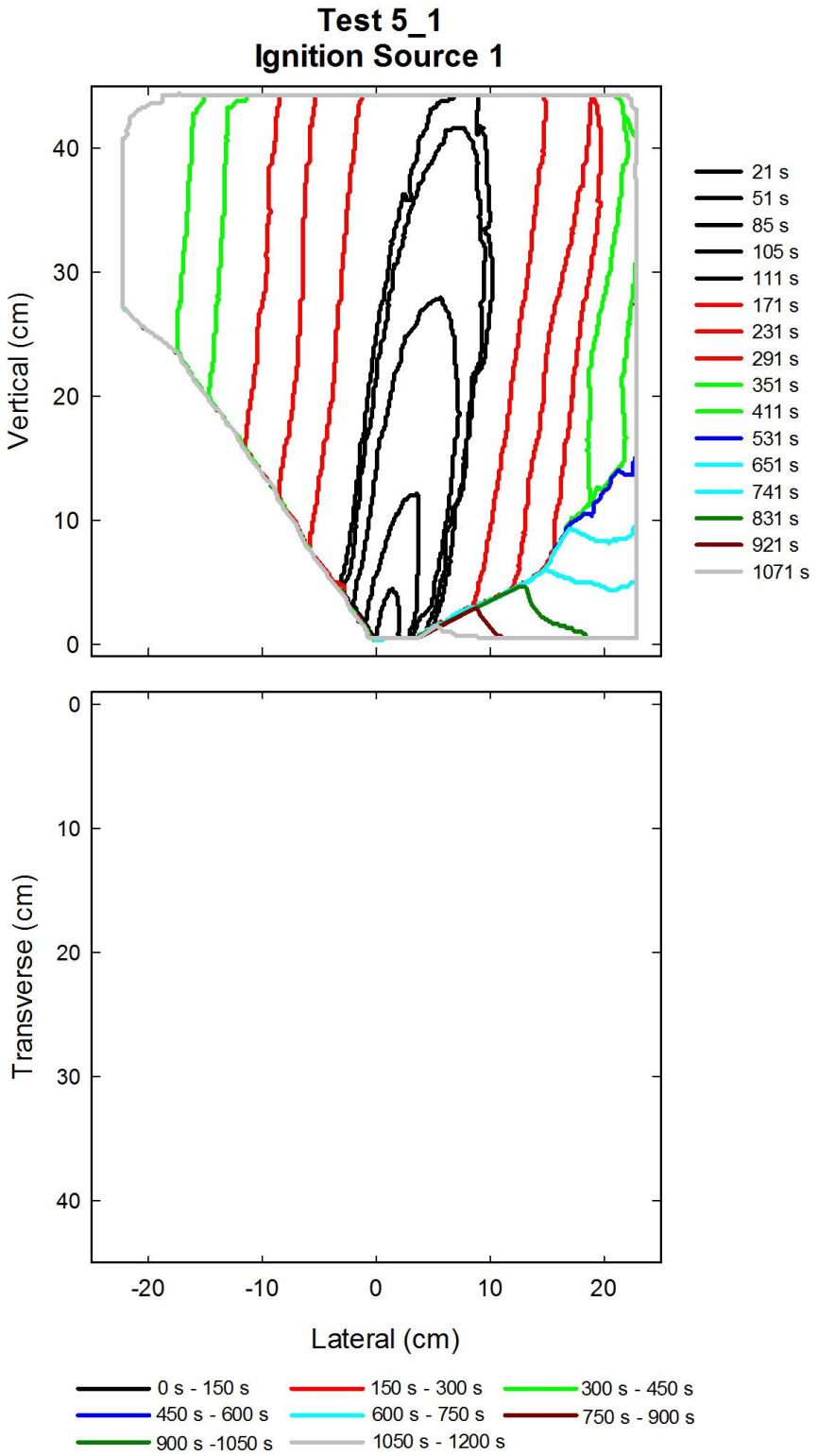

Figure A-26. Flame edge contours on the back (top) and seat (bottom) cushions are plotted as a function of time for Test 5_1 following application of Ignition Source 1.

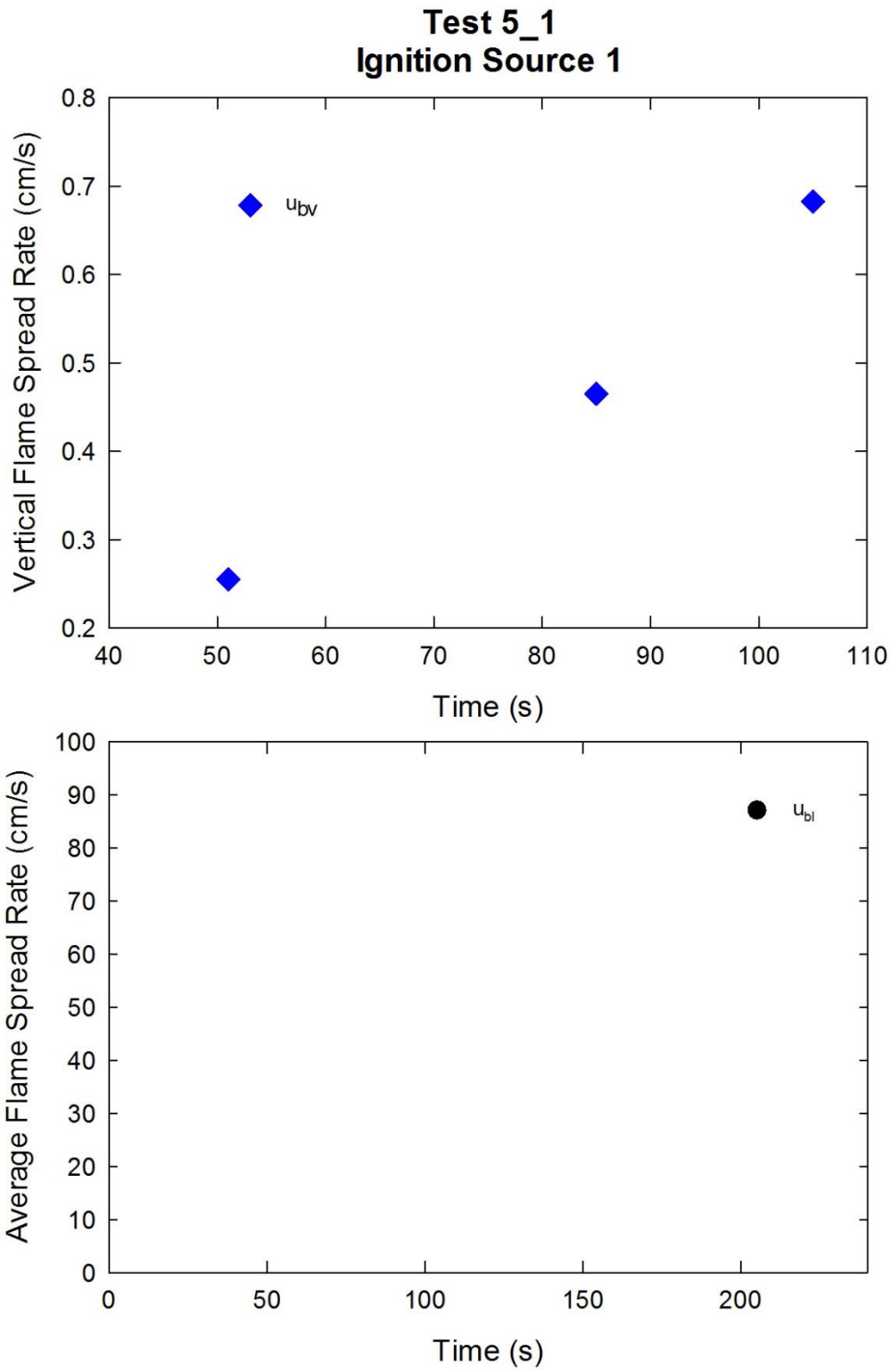

Figure A-27. Vertical flame spread rate on the back cushion (top) and average lateral flame spread rates on the back and seat cushions and transverse flame spread rate on the seat cushion (bottom) are plotted as a function of time for Test 5_1 following application of Ignition Source 1.

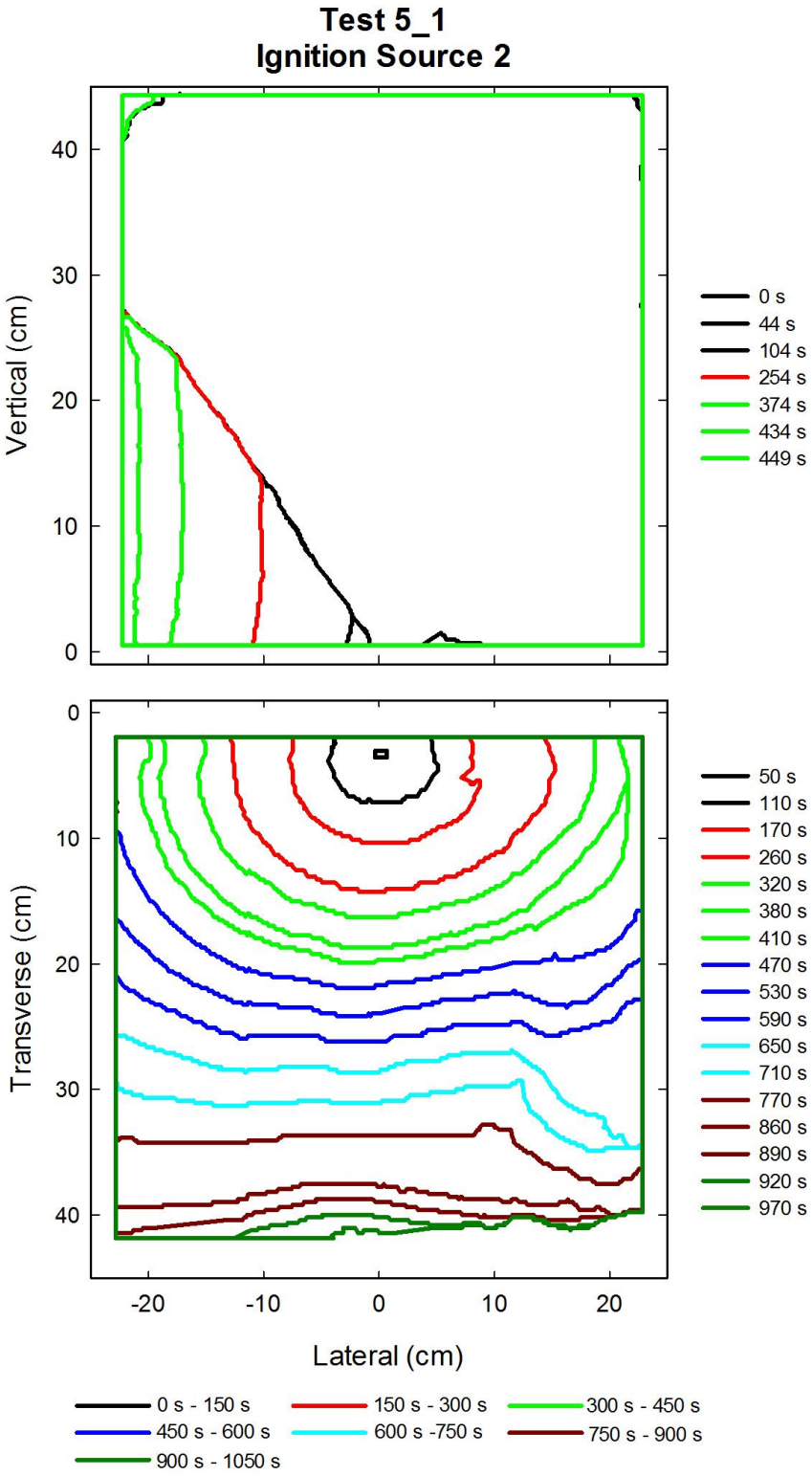

Figure A-28. Flame edge contours on the back (top) and seat (bottom) cushions are plotted as a function of time for Test 5_1 following application of Ignition Source 2.

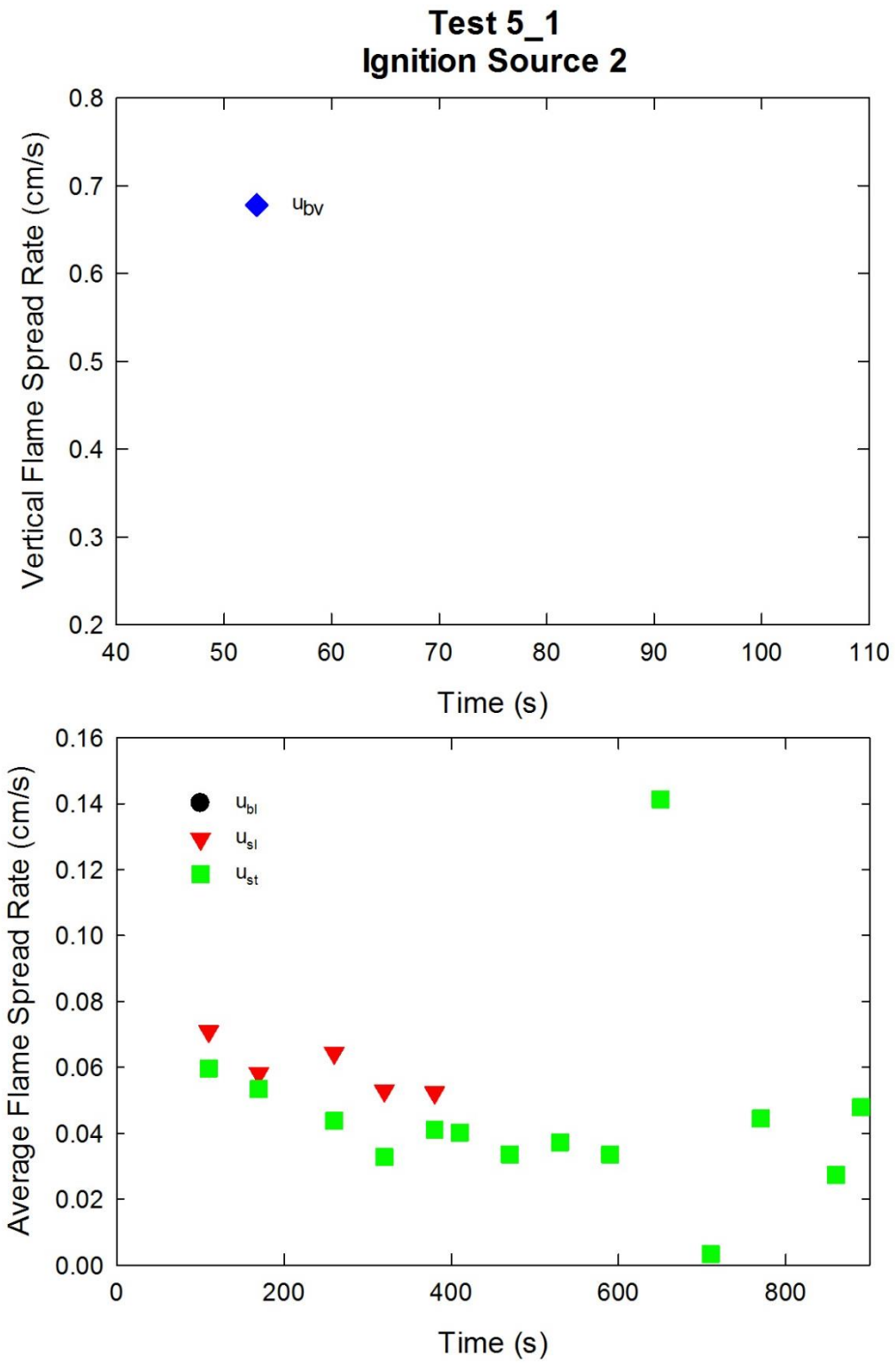

Figure A-29. Vertical flame spread rate on the back cushion (top) and average lateral flame spread rates on the back and seat cushions and transverse flame spread rate on the seat cushion (bottom) are plotted as a function of time for Test 5_1 following application of Ignition Source 2.

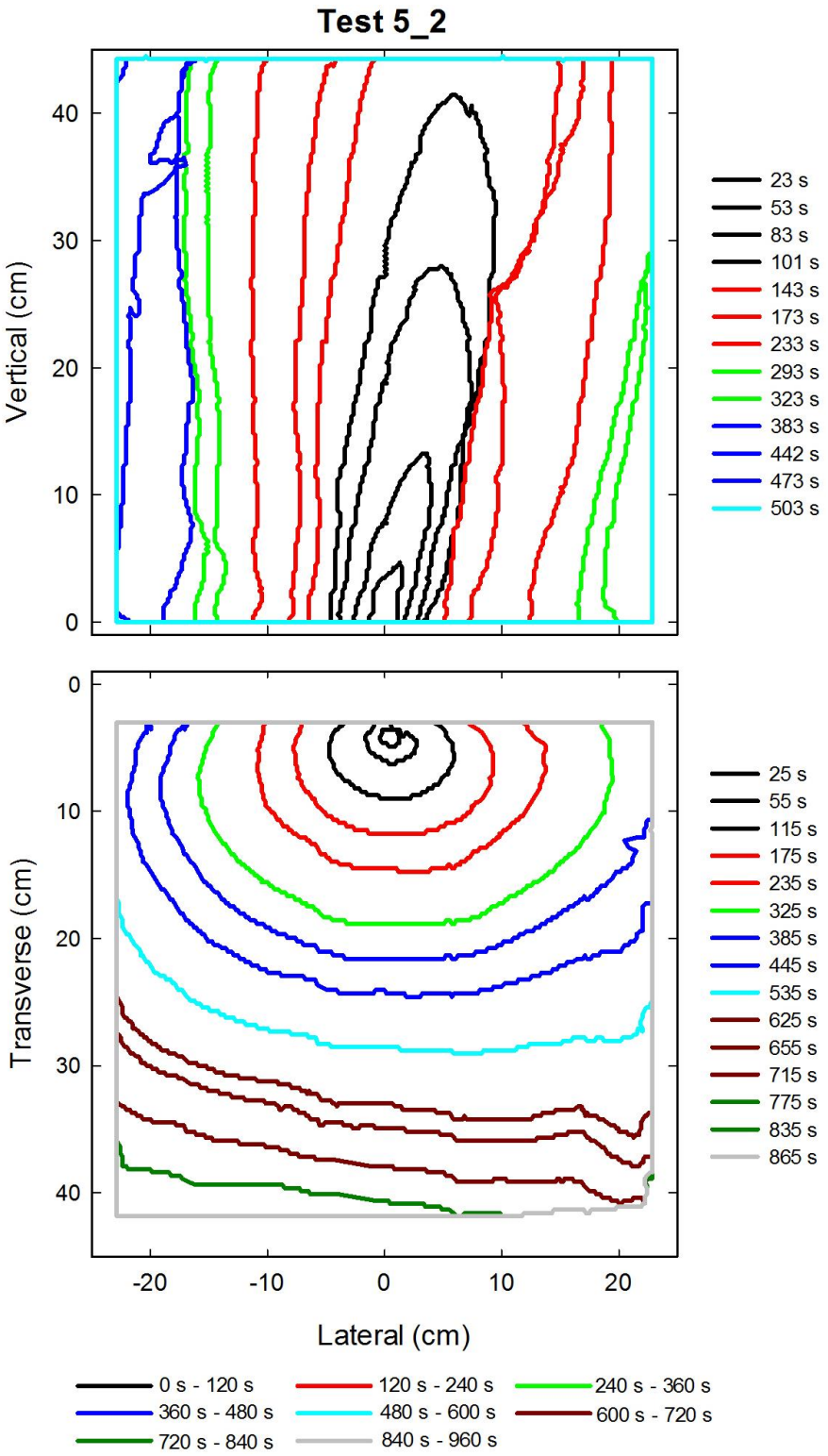

Figure A-30. Flame edge contours on the back (top) and seat (bottom) cushions are plotted as a function of time for Test 5_2 following application of Ignition Source 1.

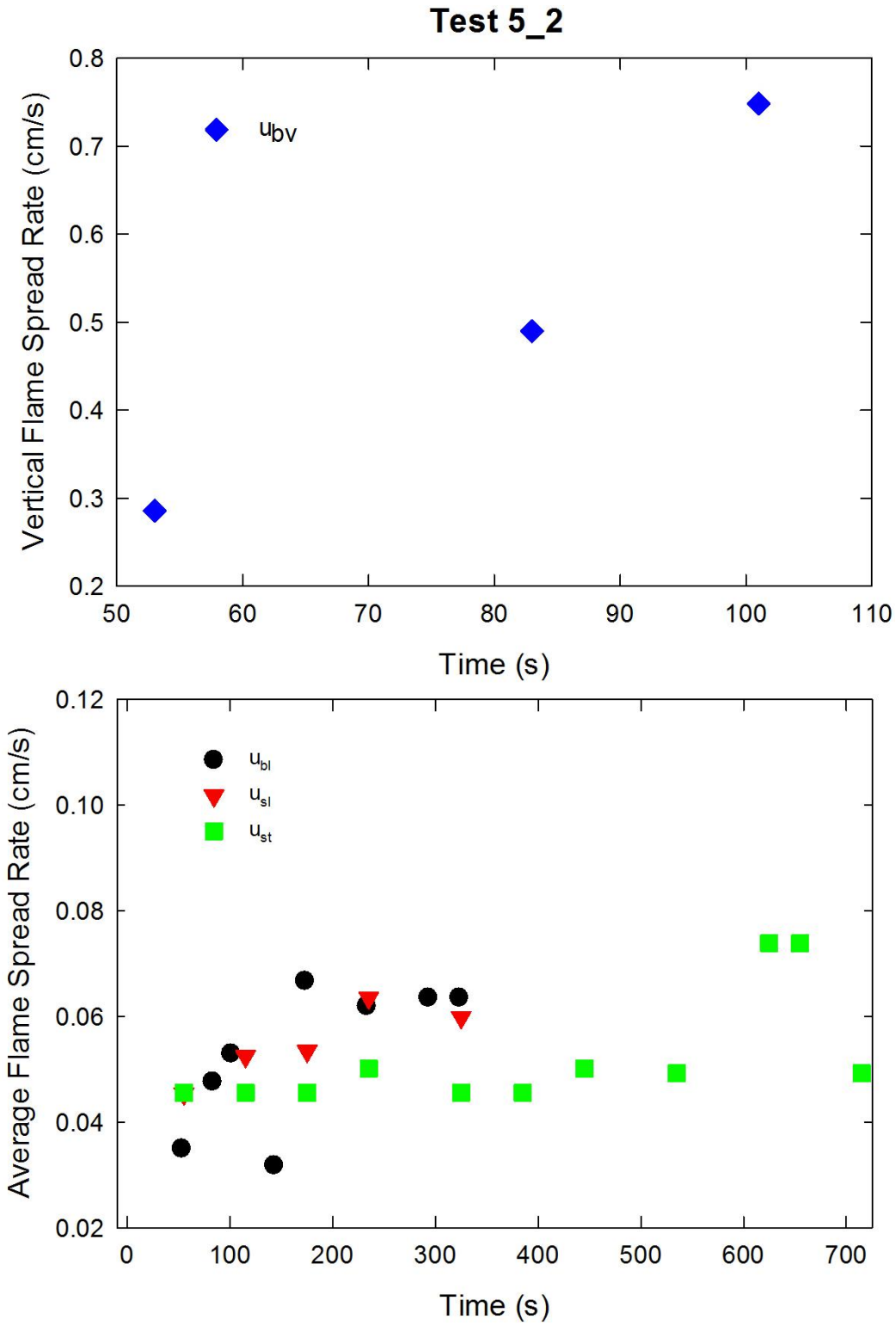

Figure A-31. Vertical flame spread rate on the back cushion (top) and average lateral flame spread rates on the back and seat cushions and transverse flame spread rate on the seat cushion (bottom) are plotted as a function of time for Test 5_2 following application of Ignition Source 1.

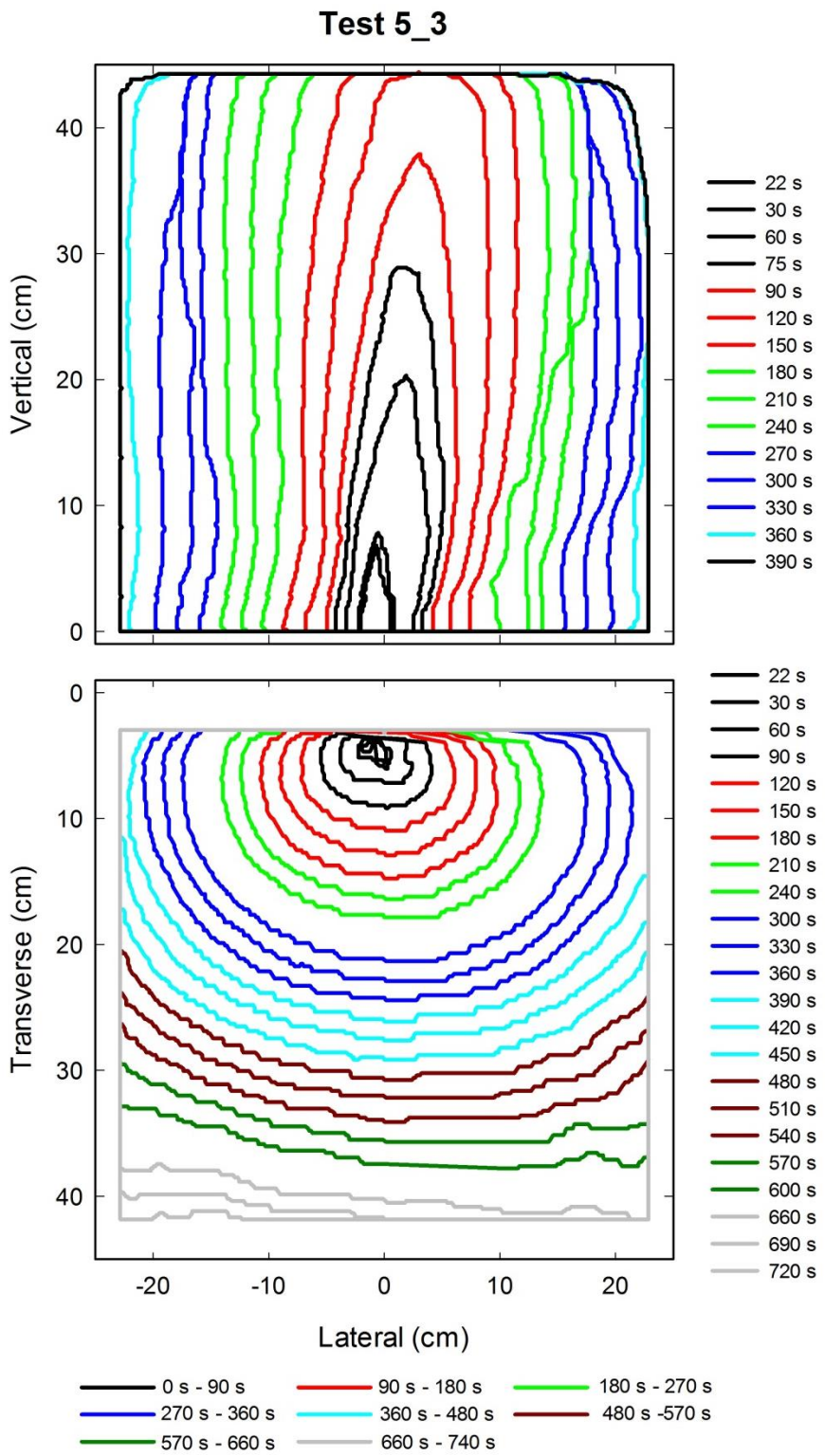

Figure A-32. Flame edge contours on the back (top) and seat (bottom) cushions are plotted as a function of time for Test 5_3 following application of Ignition Source 1.

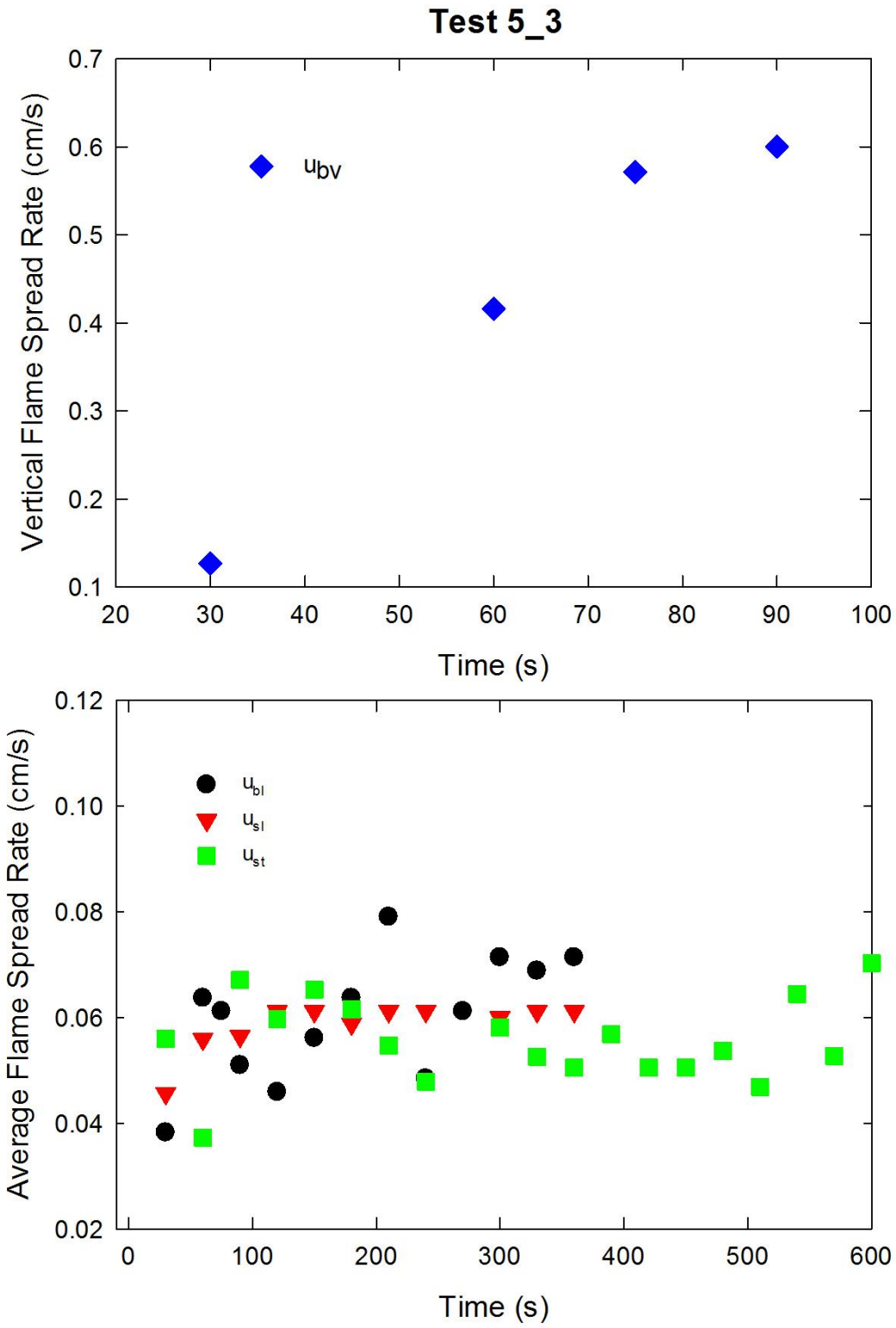

Figure A-33. Vertical flame spread rate on the back cushion (top) and average lateral flame spread rates on the back and seat cushions and transverse flame spread rate on the seat cushion (bottom) are plotted as a function of time for Test 5_3 following application of Ignition Source 1.

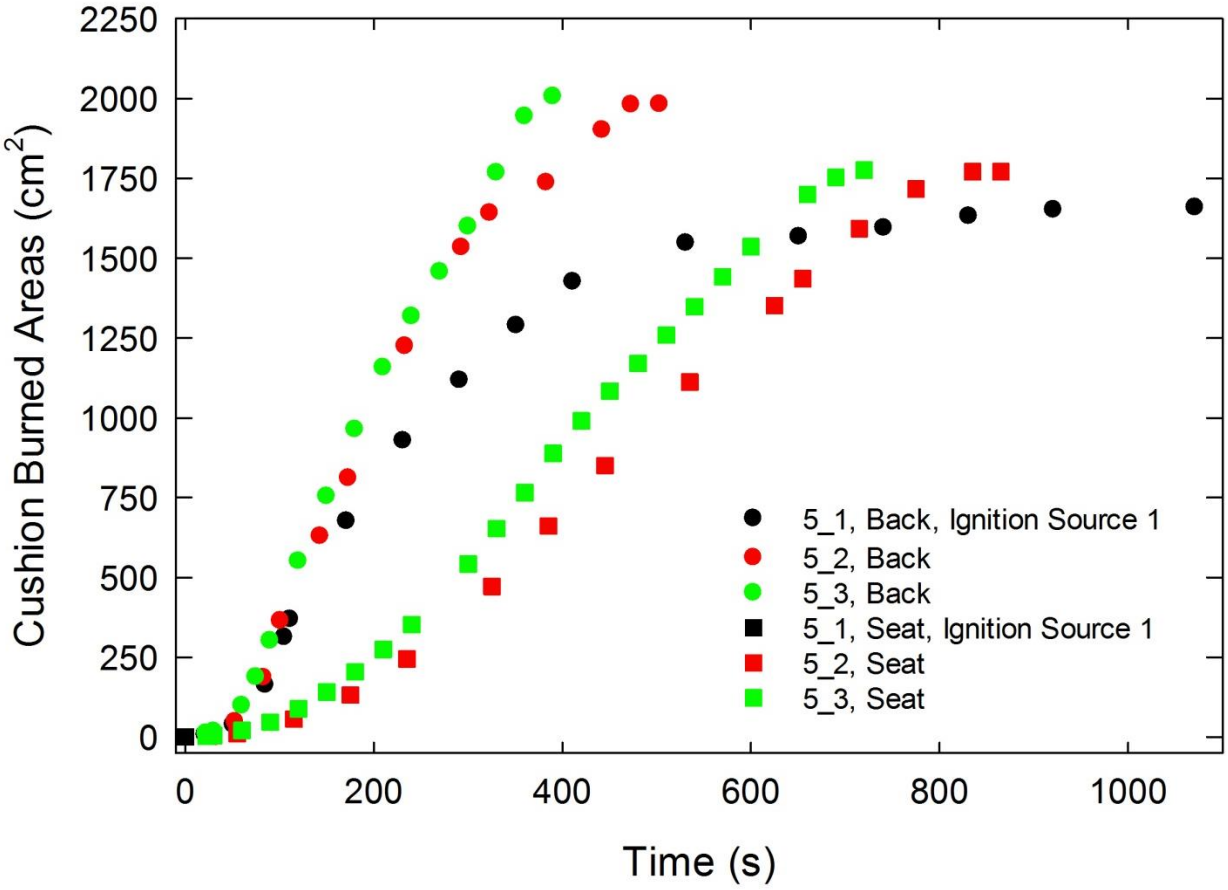

Figure A-34. Burned areas on the seat and back cushions are plotted as a function of time for Combination 5 tests following application of Ignition Source 1.

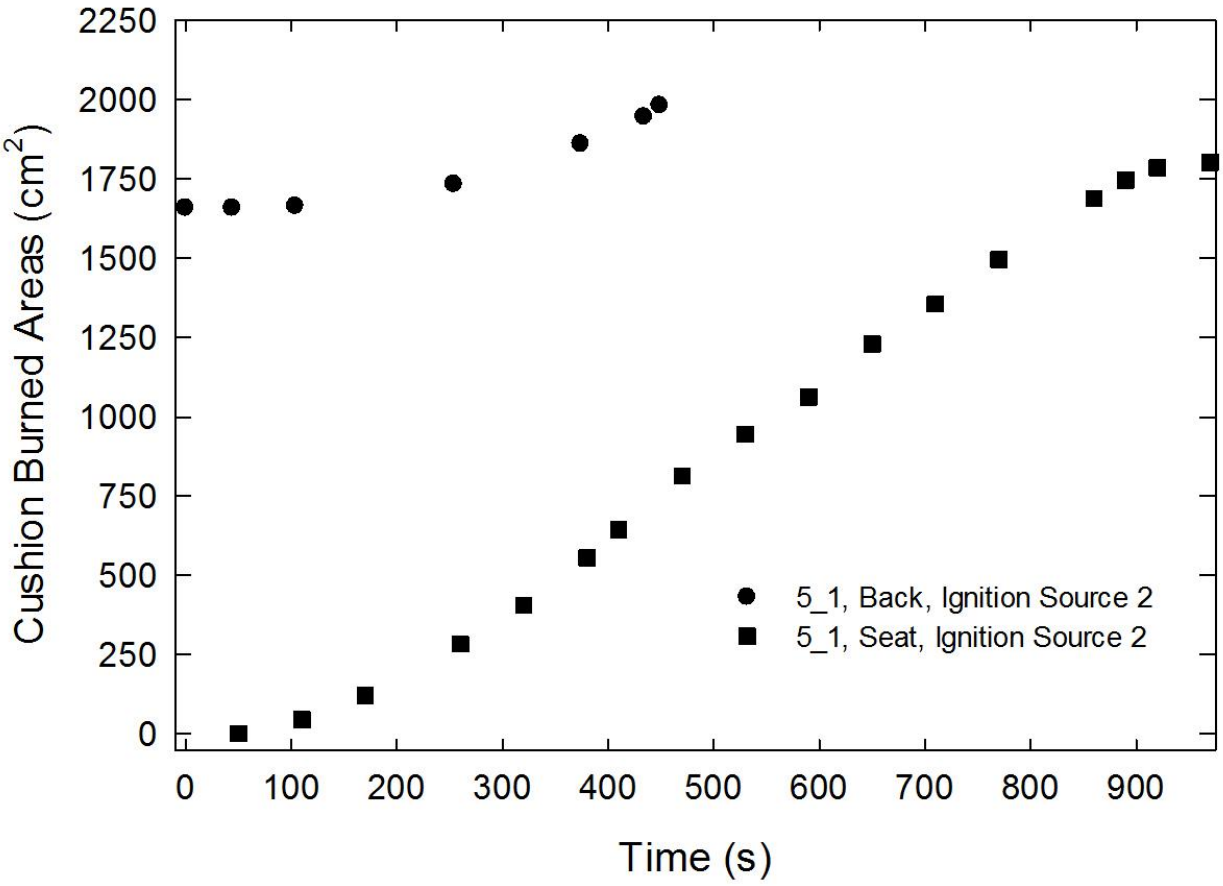

Figure A-35. Burned areas on the seat and back cushions are plotted as a function of time for Test 5-1 following application of Ignition Source 2.

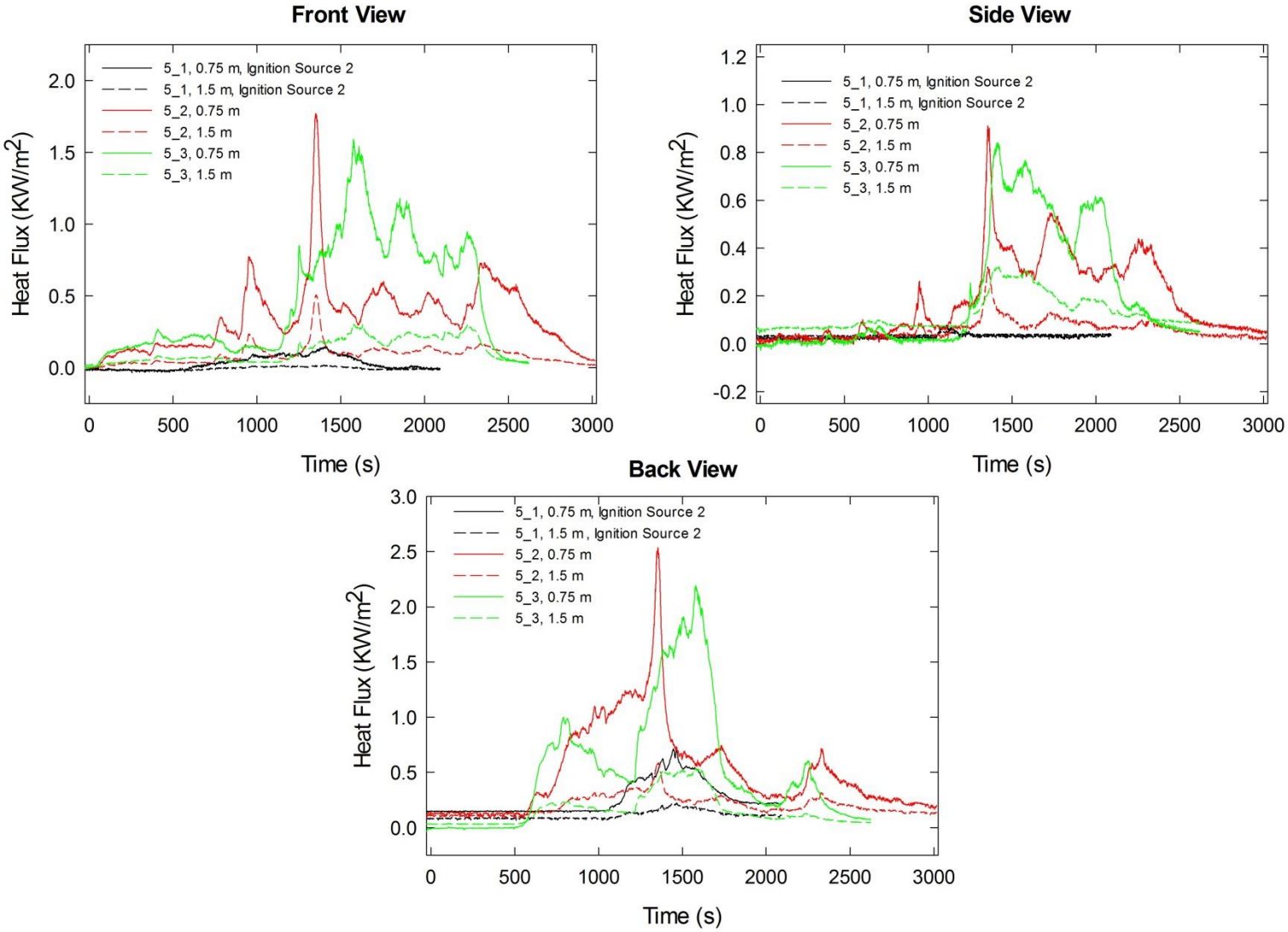

Figure A-36. Heat fluxes recorded at distances of 0.75 m and 1.5 m are plotted as a function of time for locations to the front, side and rear of the mock-up for Test 5_1 following application of Ignition Source 2, Test 5_2 following application of Ignition Source 1, and Test 5_3 following application of Ignition Source 1.

A.4 Combination 6

78%PP/22%PE/Whispershield/FRFPUF

Notes:

Test 1

Ignition Source 1 applied at time = 0 s

Initial mass reading (3.52 kg) during the experiment disagreed with an earlier measurement for the mock-up (3.34 kg); mass readings had periods during which increases were recorded; **these mass data were excluded from analysis**.

Test 2

Ignition Source 1 applied at time = 0 s

Initial mass reading (3.20 kg) during the experiment disagreed with an earlier measurement for the mock-up (3.29 kg); mass readings increased during initial period of test and showed abrupt jumps at later times; **these mass data were excluded from analysis**.

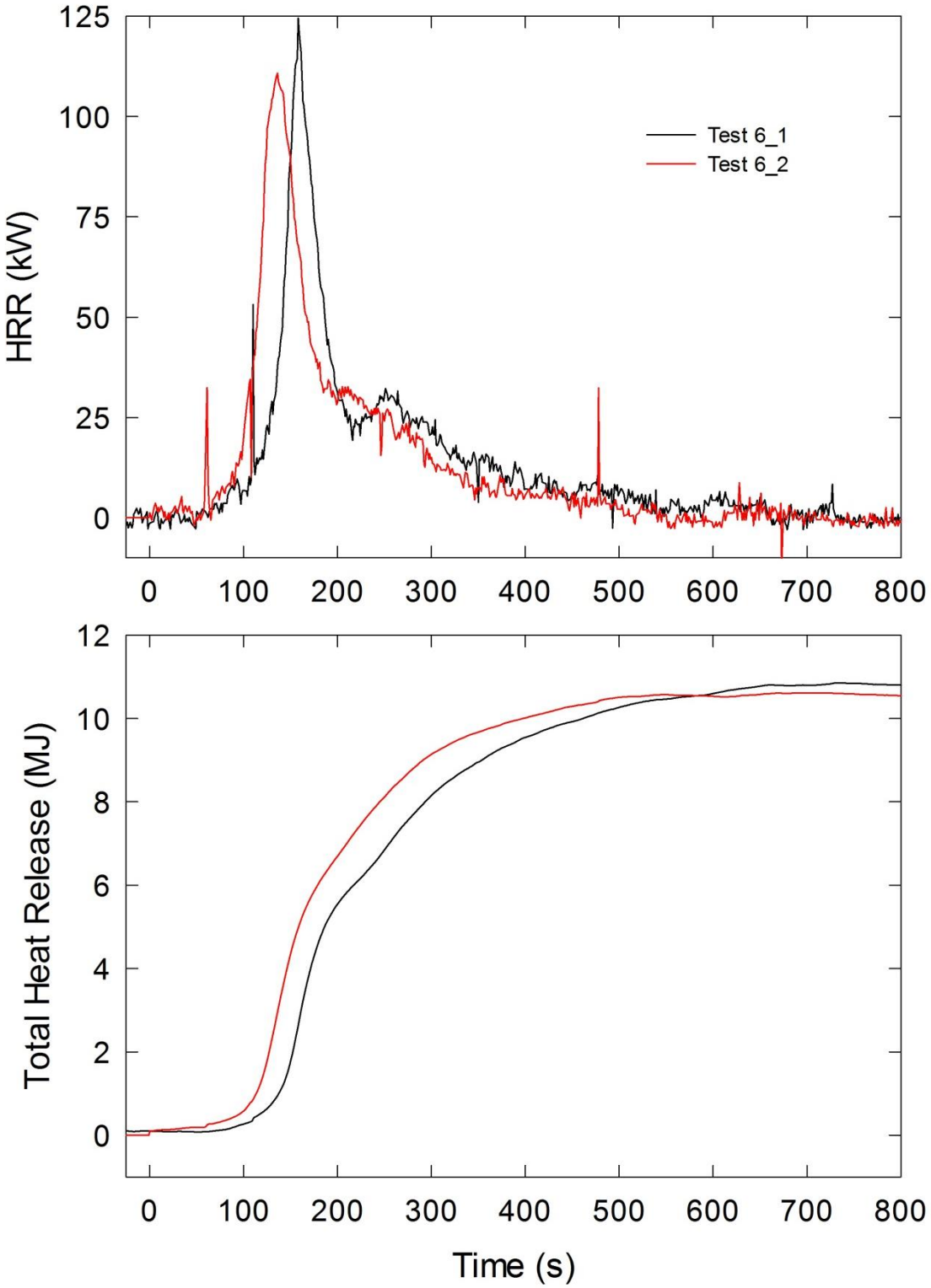

Figure A-37. Temporal profiles of HRR and integrated HRR are shown for Combination 6 tests following application of Ignition Source 1.

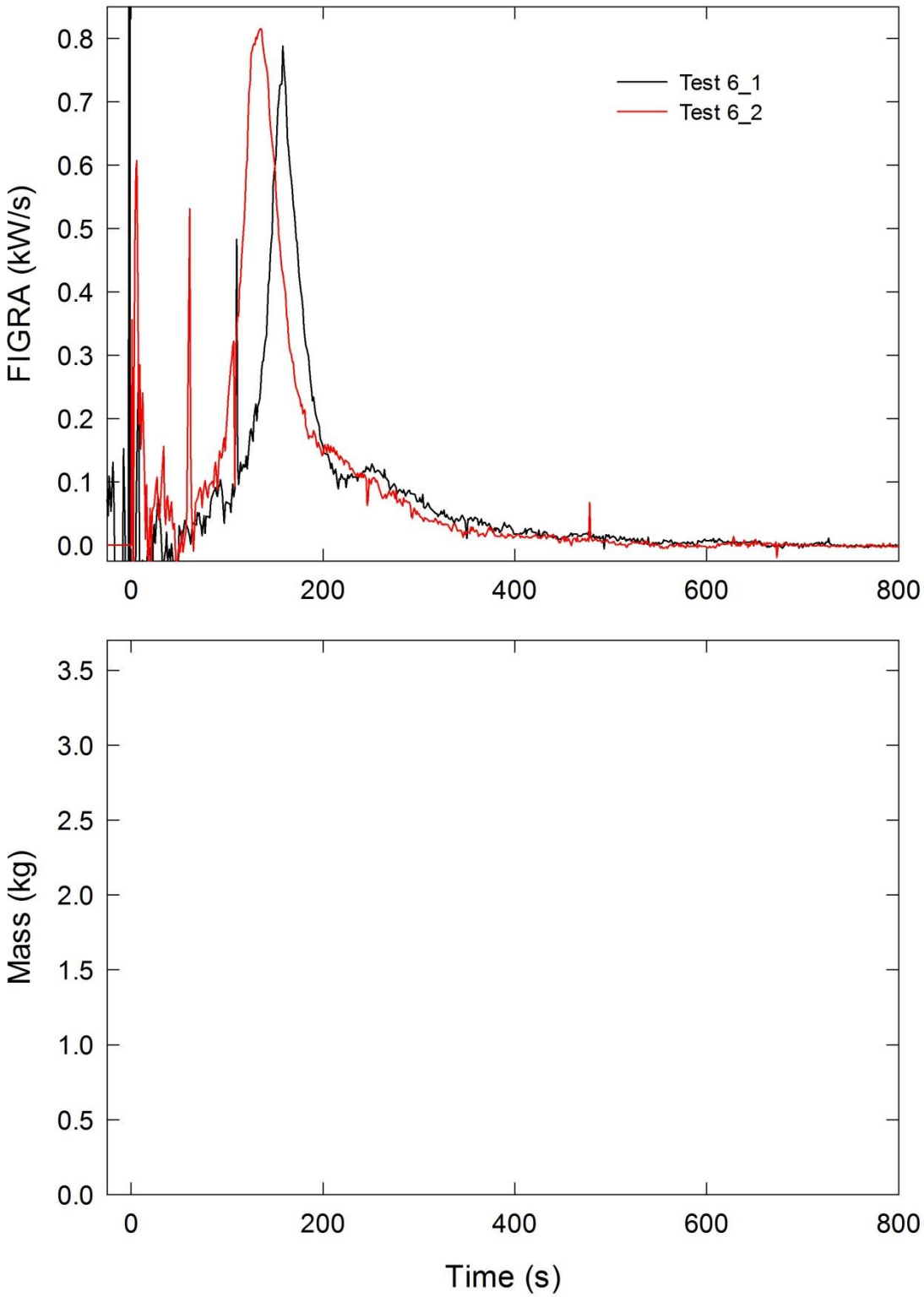

Figure A-38. Temporal profiles of FIGRA are shown for Combination 6 tests following application of Ignition Source 1.

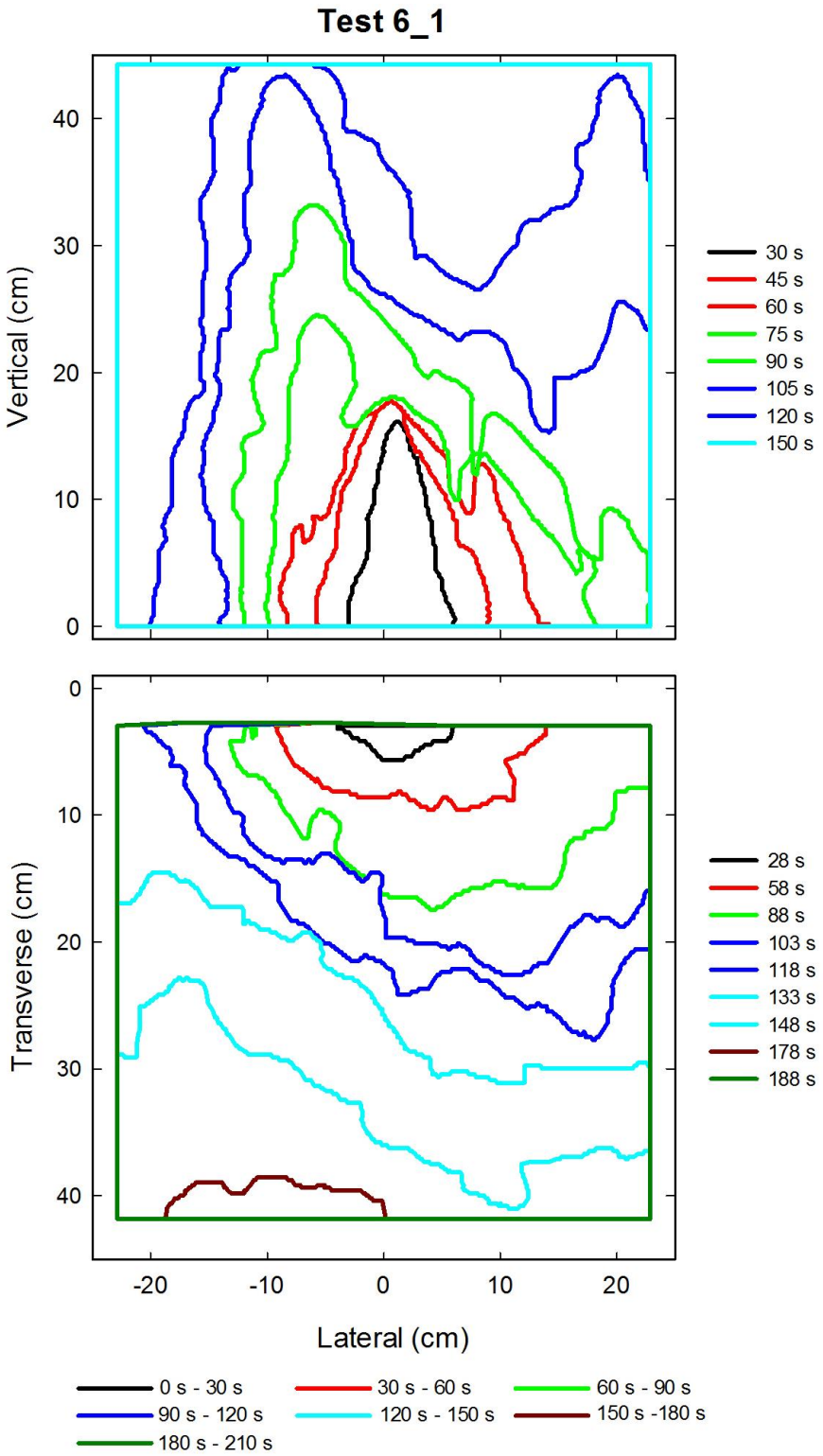

Figure A-39. Flame edge contours on the back (top) and seat (bottom) cushions are plotted as a function of time for Test 6_1 following application of Ignition Source 1.

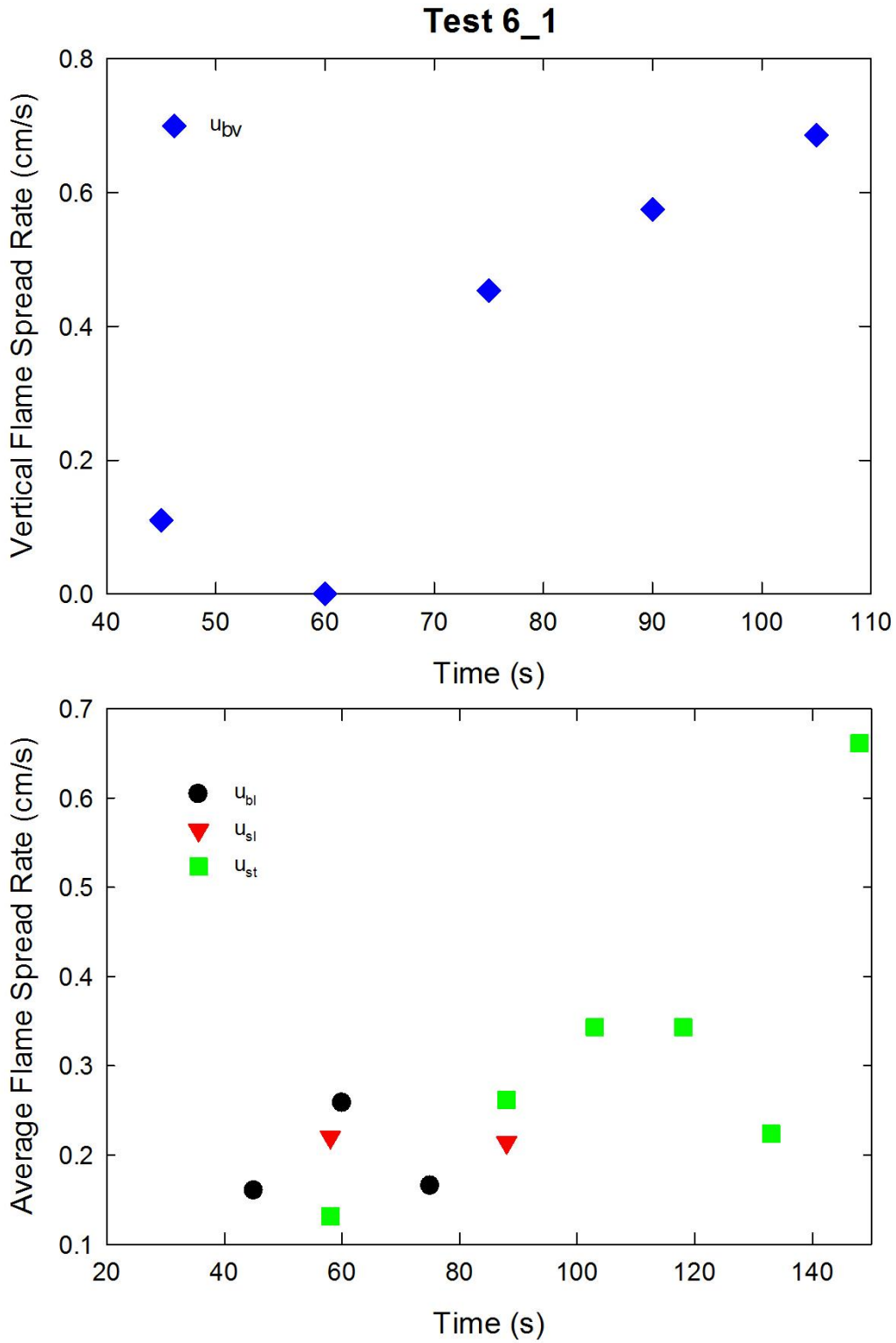

Figure A-40. Vertical flame spread rate on the back cushion (top) and average lateral flame spread rates on the back and seat cushions and transverse flame spread rate on the seat cushion (bottom) are plotted as a function of time for Test 6_1 following application of Ignition Source 1.

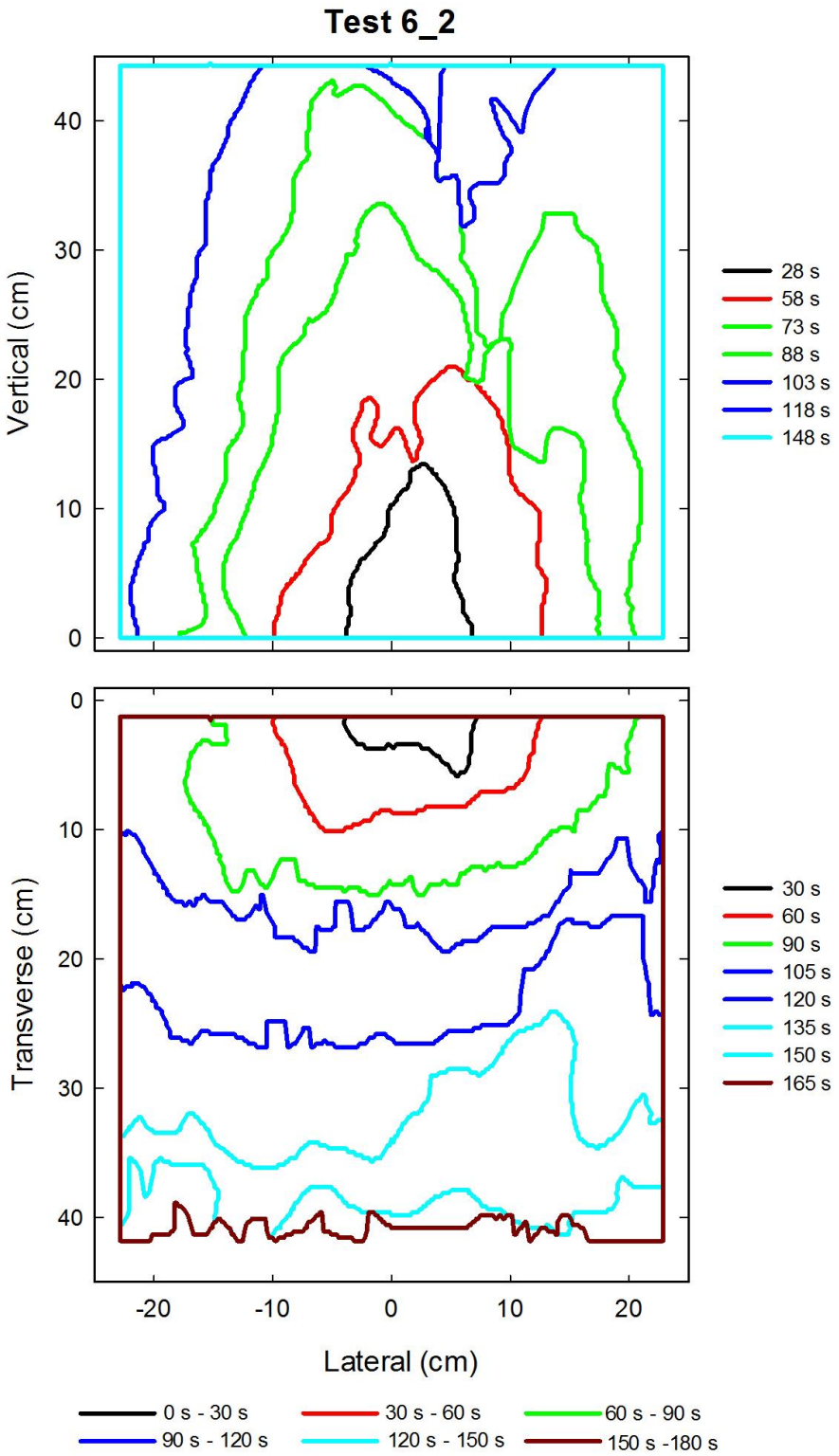

Figure A-41. Flame edge contours on the back (top) and seat (bottom) cushions are plotted as a function of time for Test 2_2 following application of Ignition Source 1.

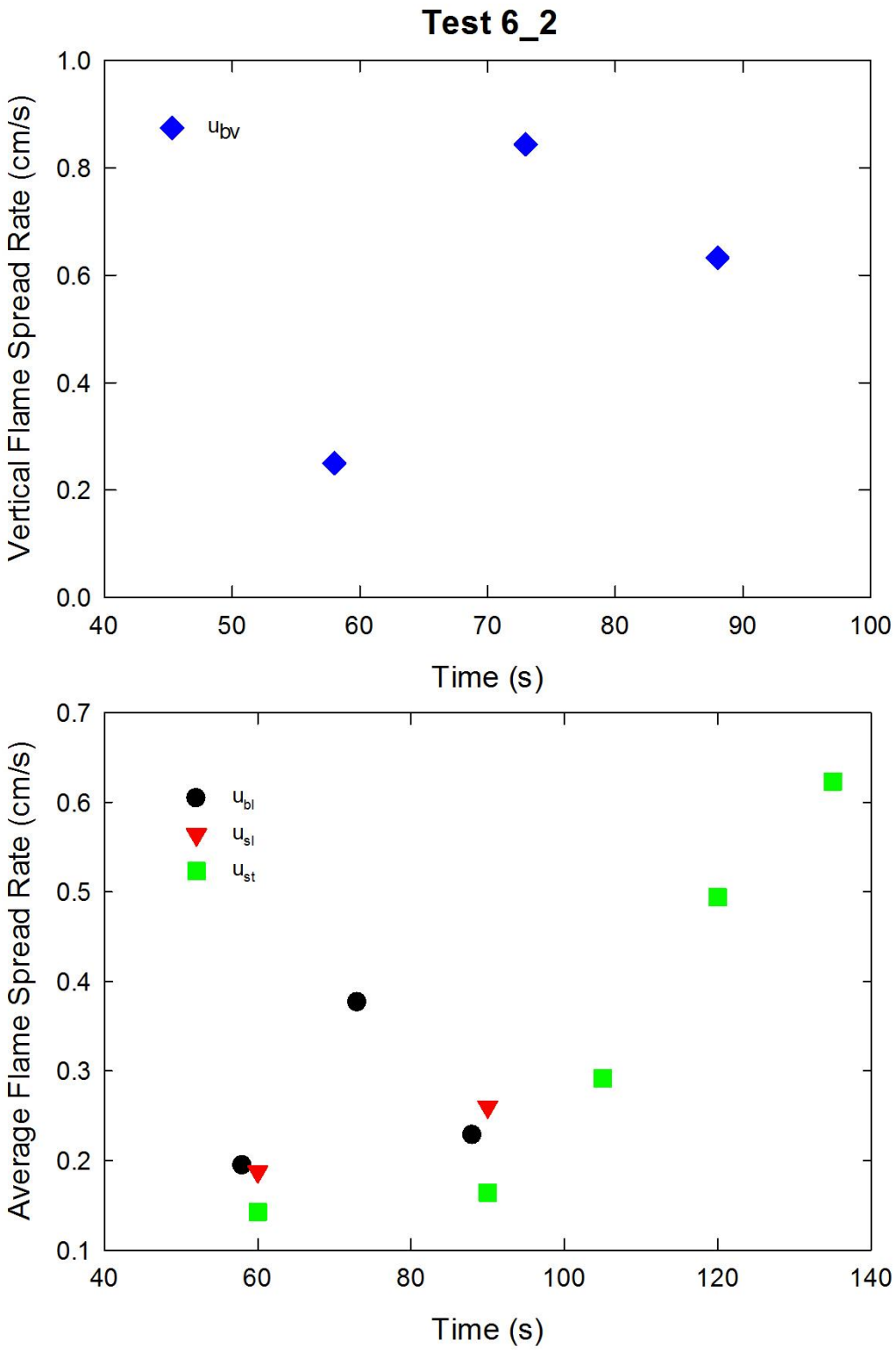

Figure A-42. Vertical flame spread rate on the back cushion (top) and average lateral flame spread rates on the back and seat cushions and transverse flame spread rate on the seat cushion (bottom) are plotted as a function of time for Test 6_2 following application of Ignition Source 1.

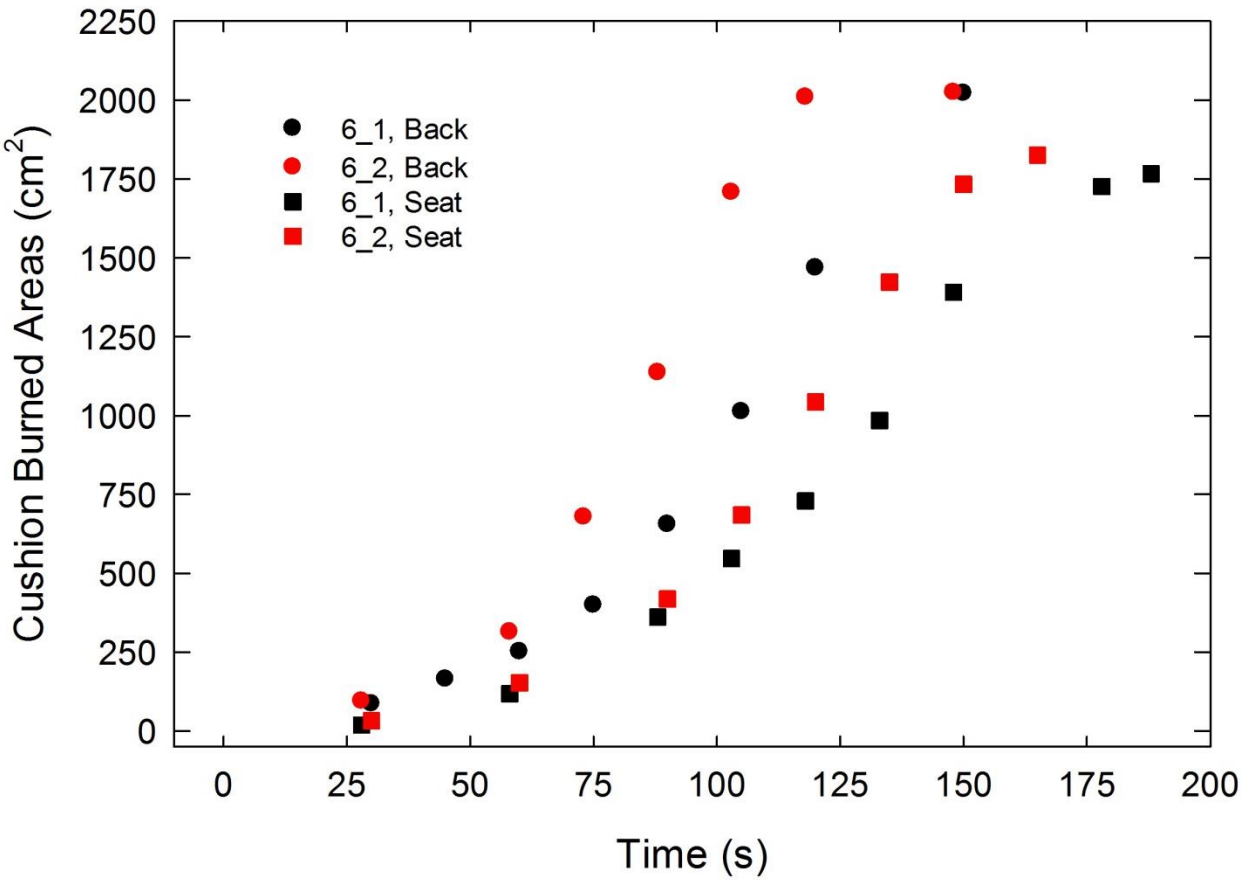

Figure A-43. Burned areas on the seat and back cushions are plotted as a function of time for Combination 6 tests following application of Ignition Source 1.

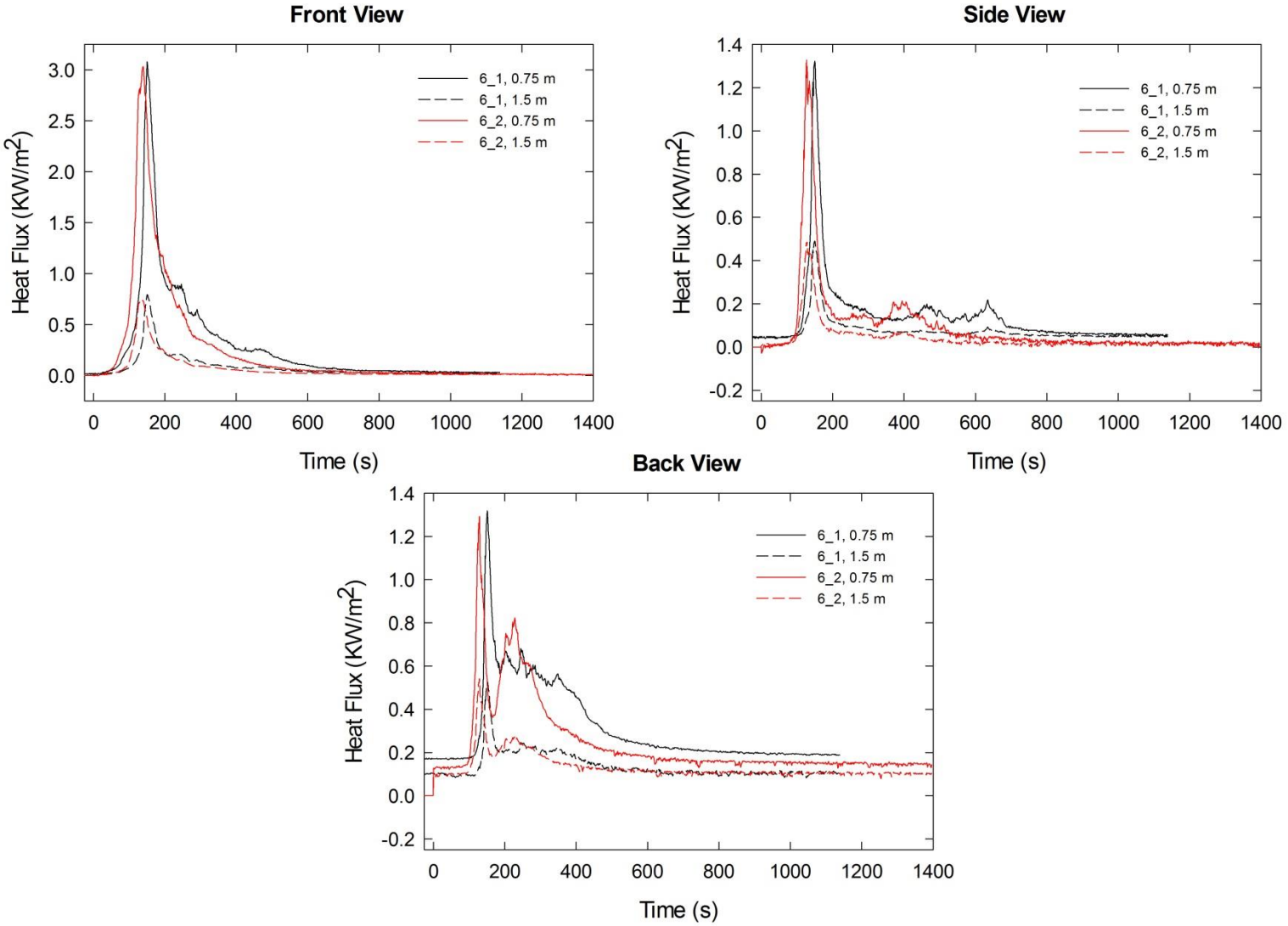

Figure A-44. Heat fluxes recorded at distances of 0.75 m and 1.5 m are plotted as a function of time for locations to the front, side and rear of the mock-up for Combination 6 tests.

A.5 Combination 9

cotton/NFRFPUF

Notes:

Test 1

Ignition Source 1 applied at time = 0 s; following removal of ignition source, there was no evident blackening on seat; a black area appeared at ≈ 50 s and began to spread.

Test 2

Ignition Source 1 applied at time = 0 s, black marks present on both the seat and back cushion surfaces, but no obvious flame spread.

Ignition Source 2 applied 120 s after Ignition Source 1.

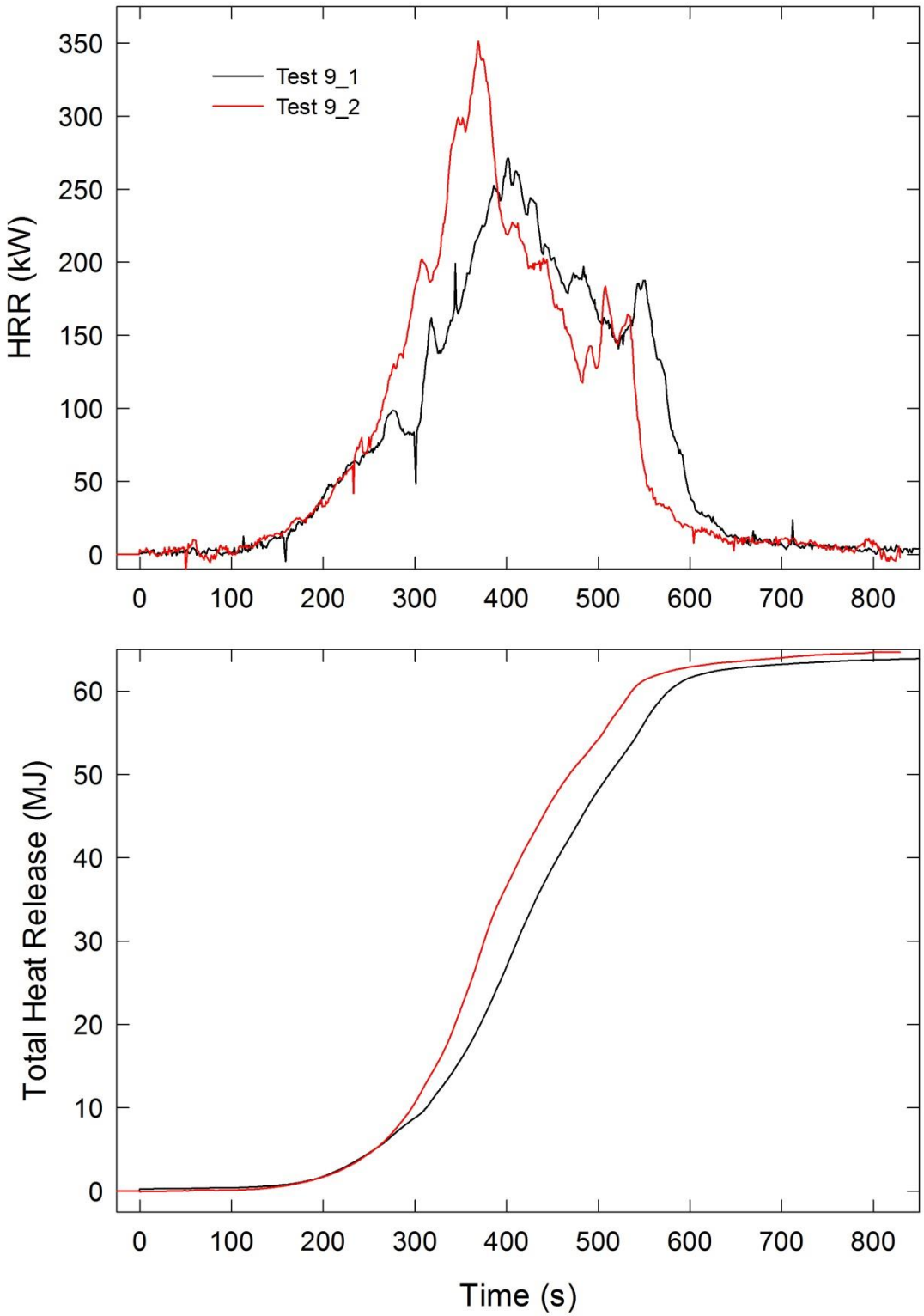

Figure A-45. Temporal profiles of HRR and integrated HRR are shown for Test 9_1 following application of Ignition Source 1 and Test 9_2 following application of Ignition Source 2.

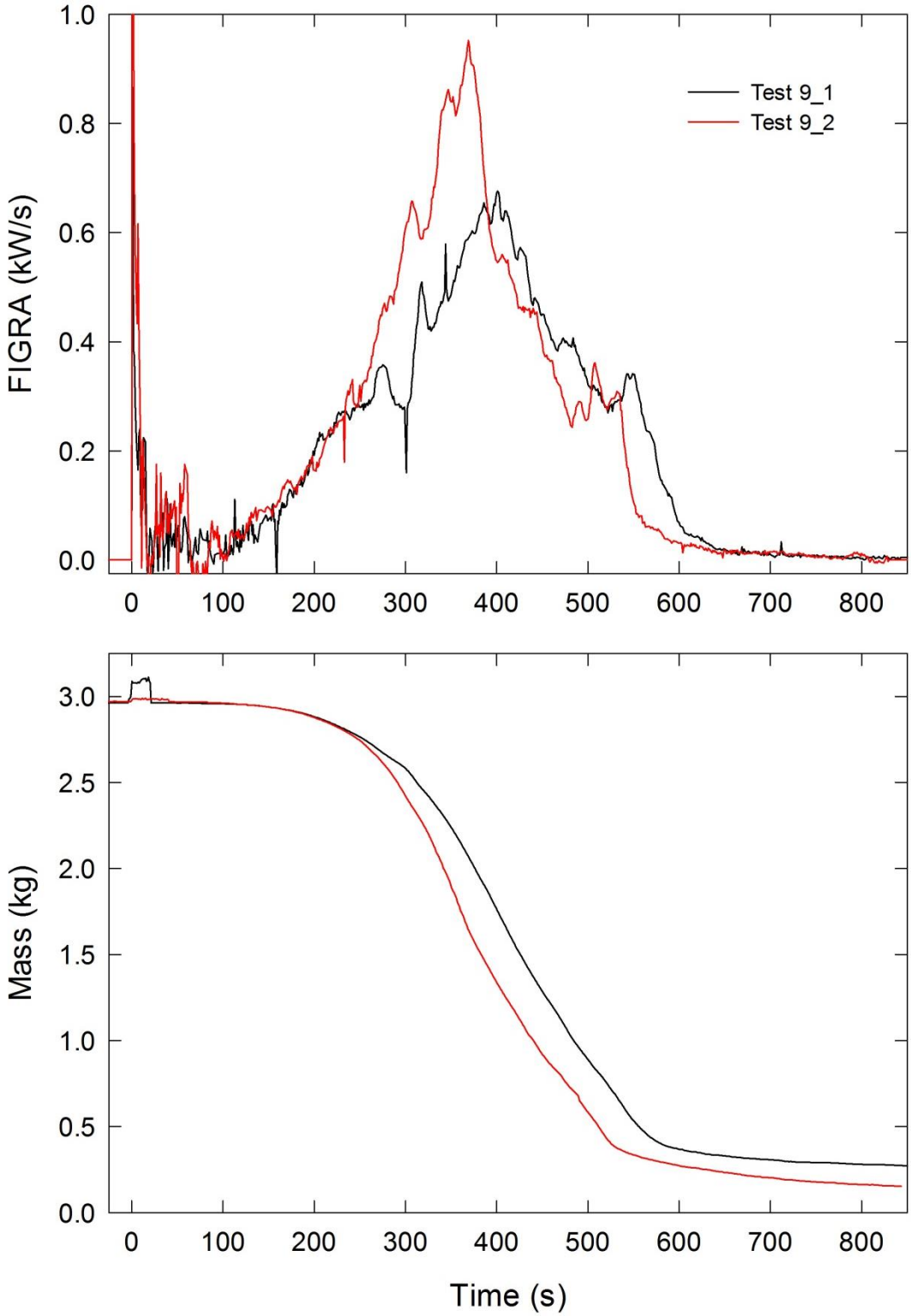

Figure A-46. Temporal profiles of FIGRA and mock-up mass are shown for Test 9_1 following application of Ignition Source 1 and Test 9_2 following application of Ignition Source 2.

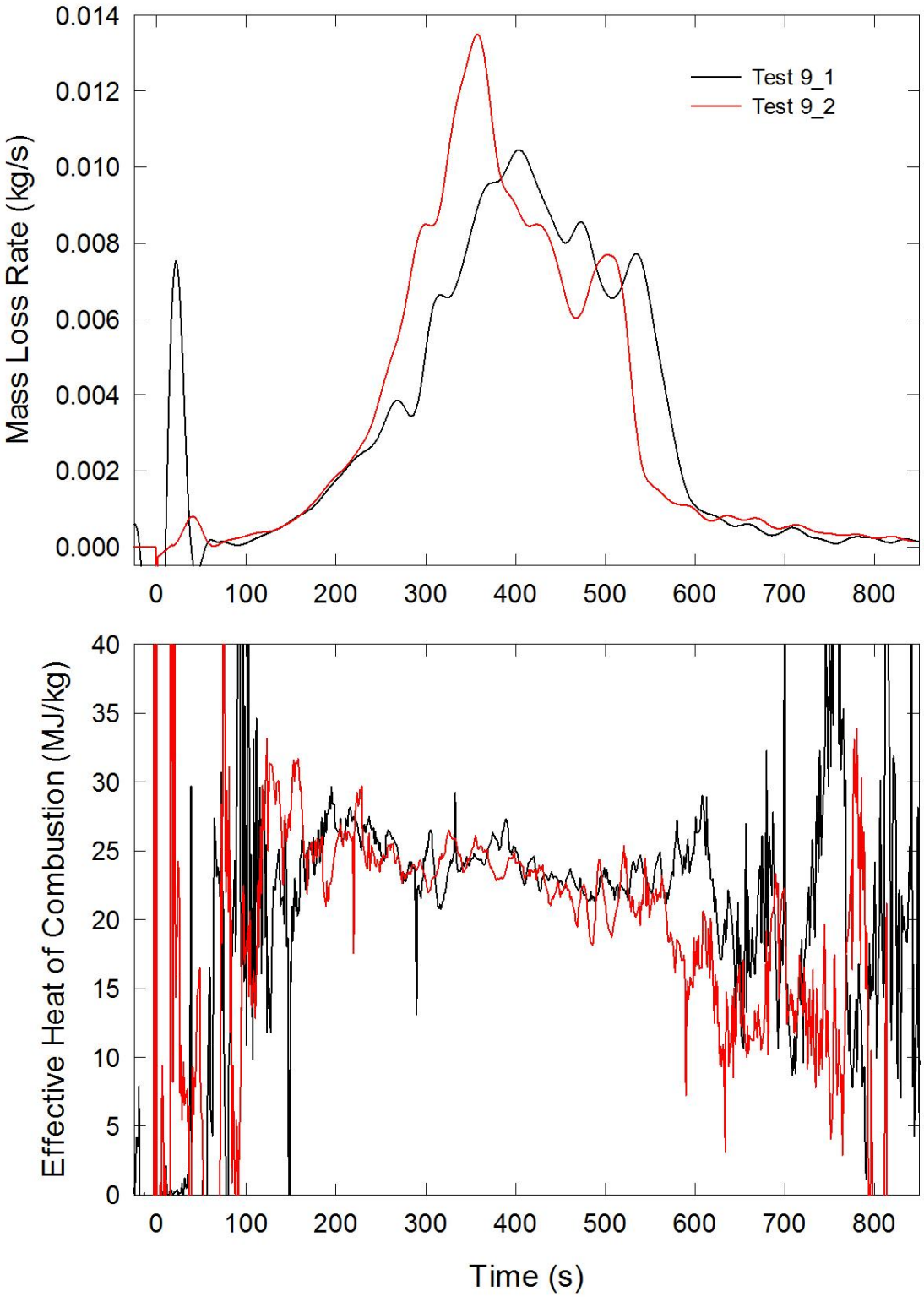

Figure A-47. Temporal profiles of MLR and EHOC are shown for Test 9_1 following application of Ignition Source 1 and Test 9_2 following application of Ignition Source 2.

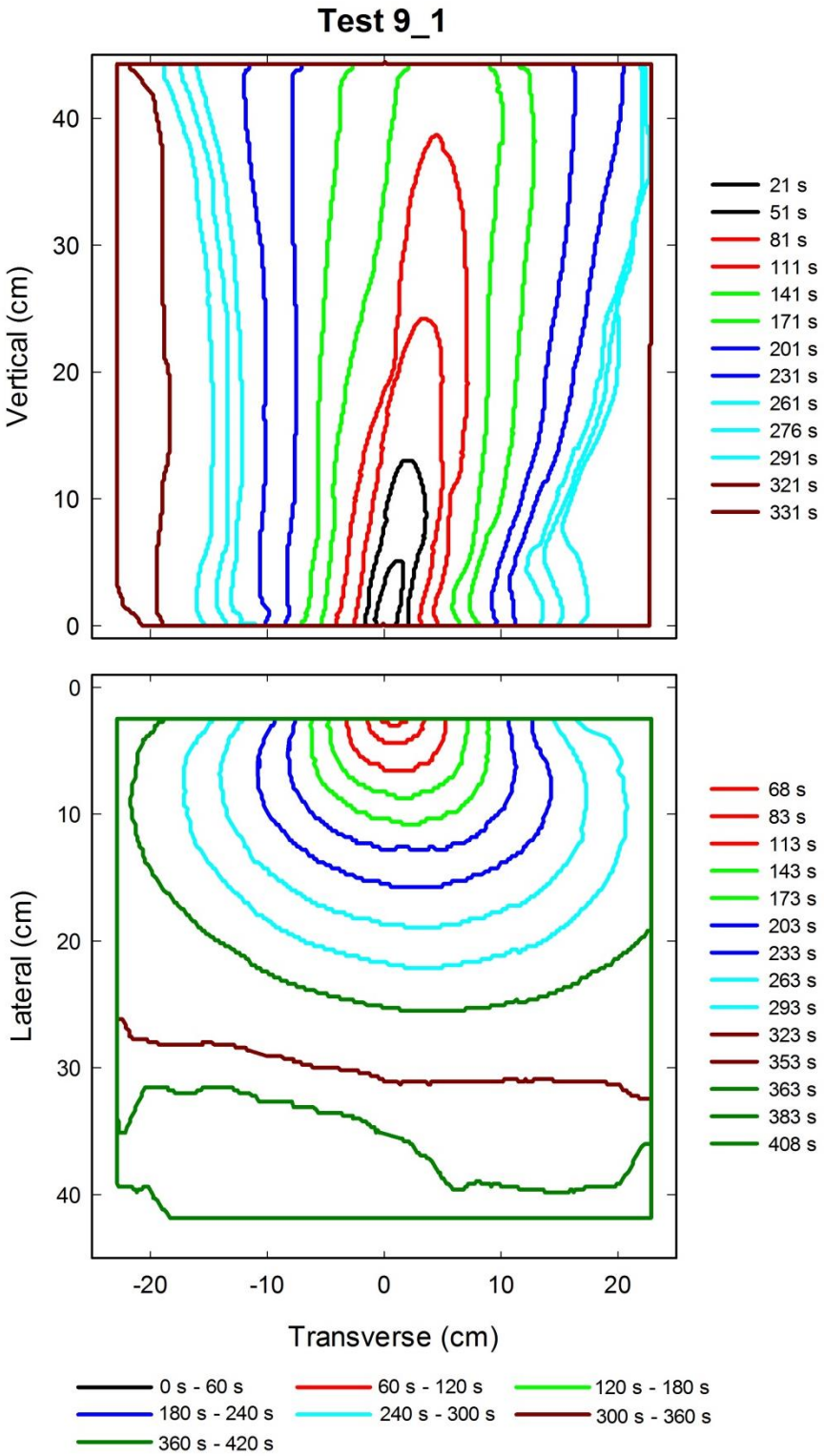

Figure A-48. Flame edge contours on the back (top) and seat (bottom) cushions are plotted as a function of time for Test 9_1 following application of Ignition Source 1.

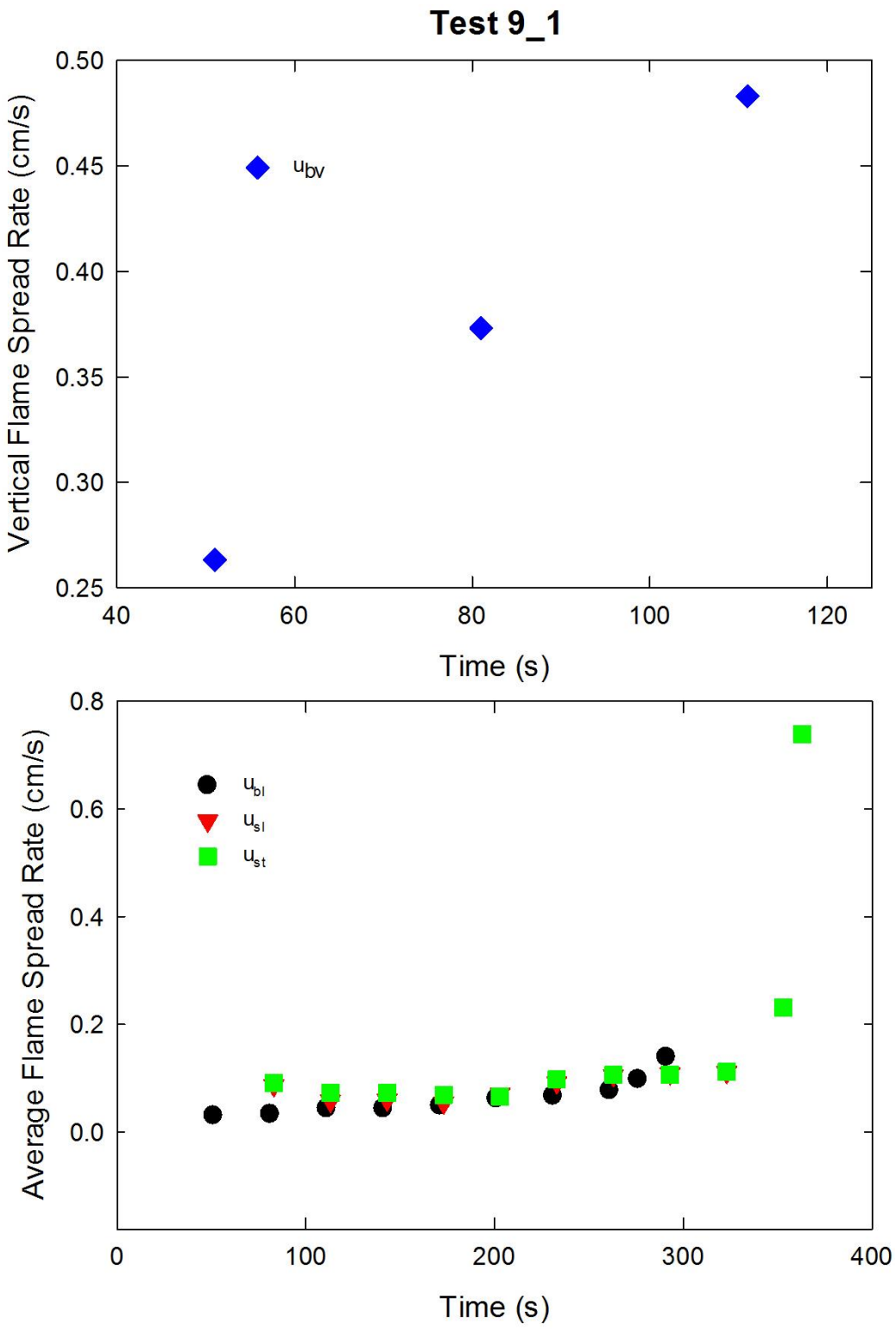

Figure A-49. Vertical flame spread rate on the back cushion (top) and average lateral flame spread rates on the back and seat cushions and transverse flame spread rate on the seat cushion (bottom) are plotted as a function of time for Test 9_1 following application of Ignition Source 1.

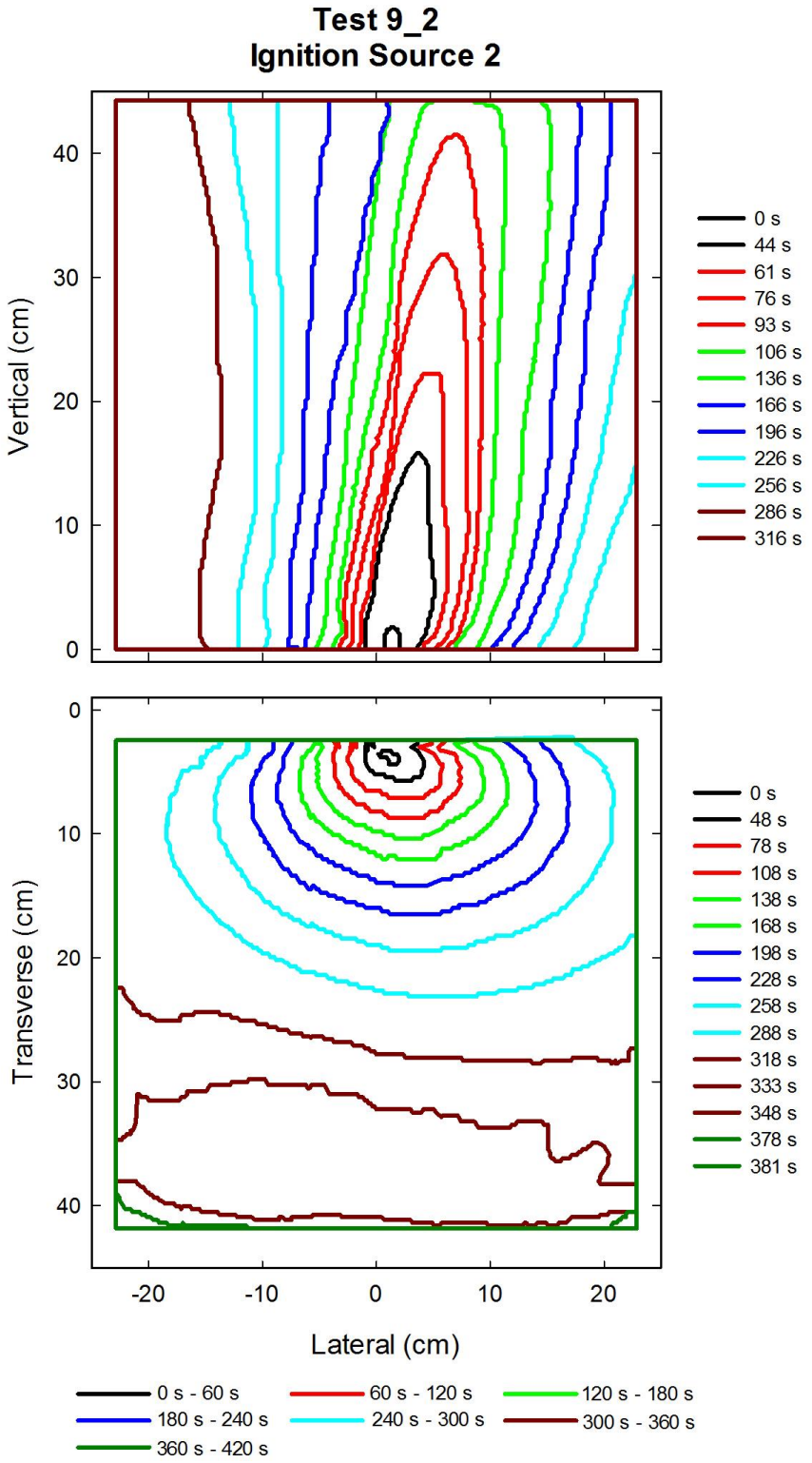

Figure A-50. Flame edge contours on the back (top) and seat (bottom) cushions are plotted as a function of time for Test 9_2 following application of Ignition Source 2.

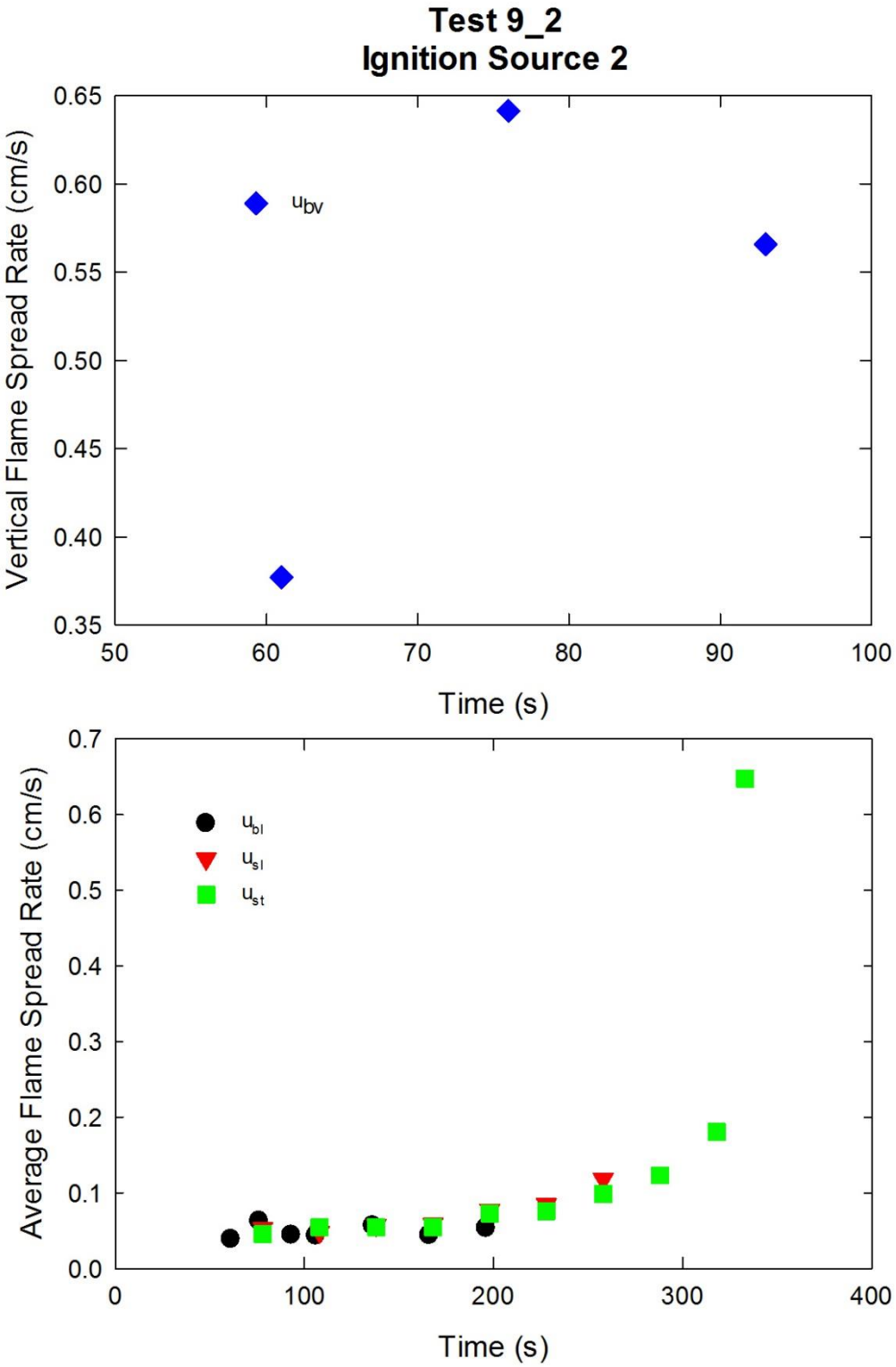

Figure A-51. Vertical flame spread rate on the back cushion (top) and average lateral flame spread rates on the back and seat cushions and transverse flame spread rate on the seat cushion (bottom) are plotted as a function of time for Test 9_2 following application of Ignition Source 2.

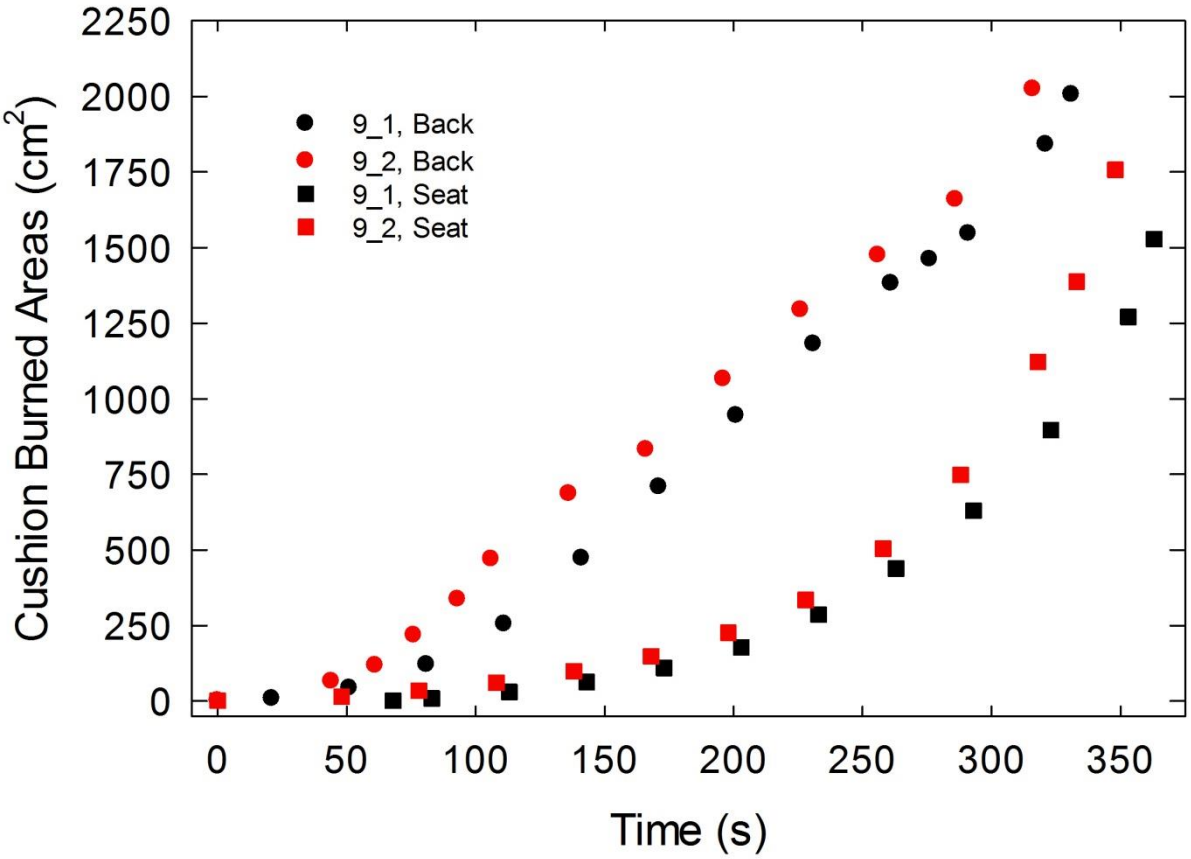

Figure A-52. Burned areas on the seat and back cushions are plotted as a function of time for Test 9_1 following application of Ignition Source 1 and for Test 9_2 following application of Ignition Source 2.

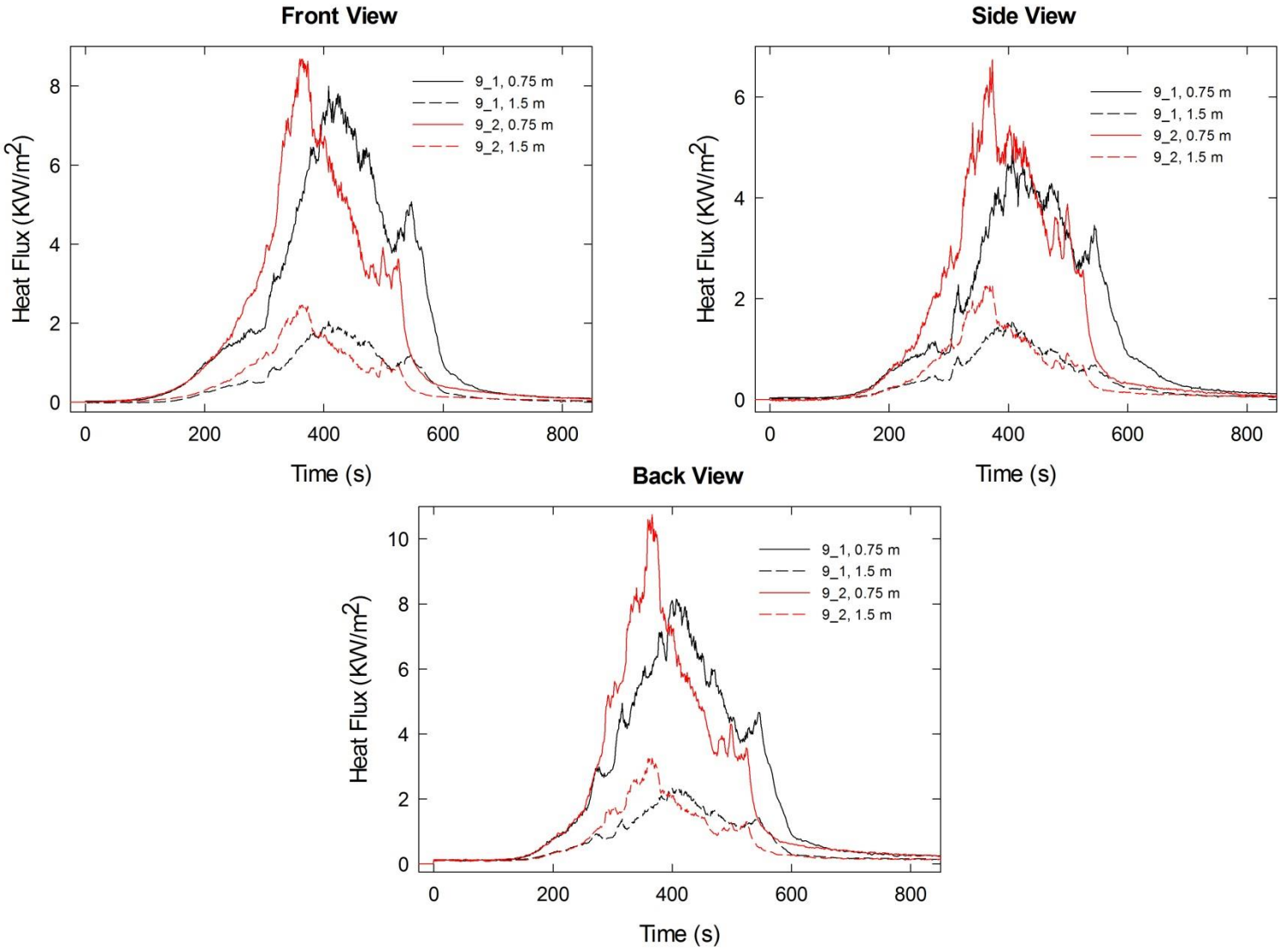

Figure A-53. Heat fluxes recorded at distances of 0.75 m and 1.5 m are plotted as a function of time for locations to the front, side and rear of the mock-up for Test 9_1 following application of Ignition Source 1 and Test 9_2 following application of Ignition Source 2.

A.6 Combination 10

78%PP/22%PE/NFRFPUF

Notes:

Test 1:

Ignition Source 1 applied at time = 0 s

Initial mass reading (2.81 kg) during the experiment disagreed with an earlier measurement for the mock-up (3.01 kg); mass readings during test were smooth, physically reasonable and correlated with the HRR; **these mass data were adjusted by adding 0.200 kg to their values and were included in the analysis**.

Test 2:

Ignition Source 1 applied at time = 0 s

Initial mass reading (3.02 kg) during the experiment agreed with an earlier measurement for the mock-up (3.04 kg); mass readings increased during initial period of test as well as at a later time and also had non-physical abrupt jumps; **these mass data were excluded from analysis**.

Test 3:

Ignition Source 1 applied at time = 0 s

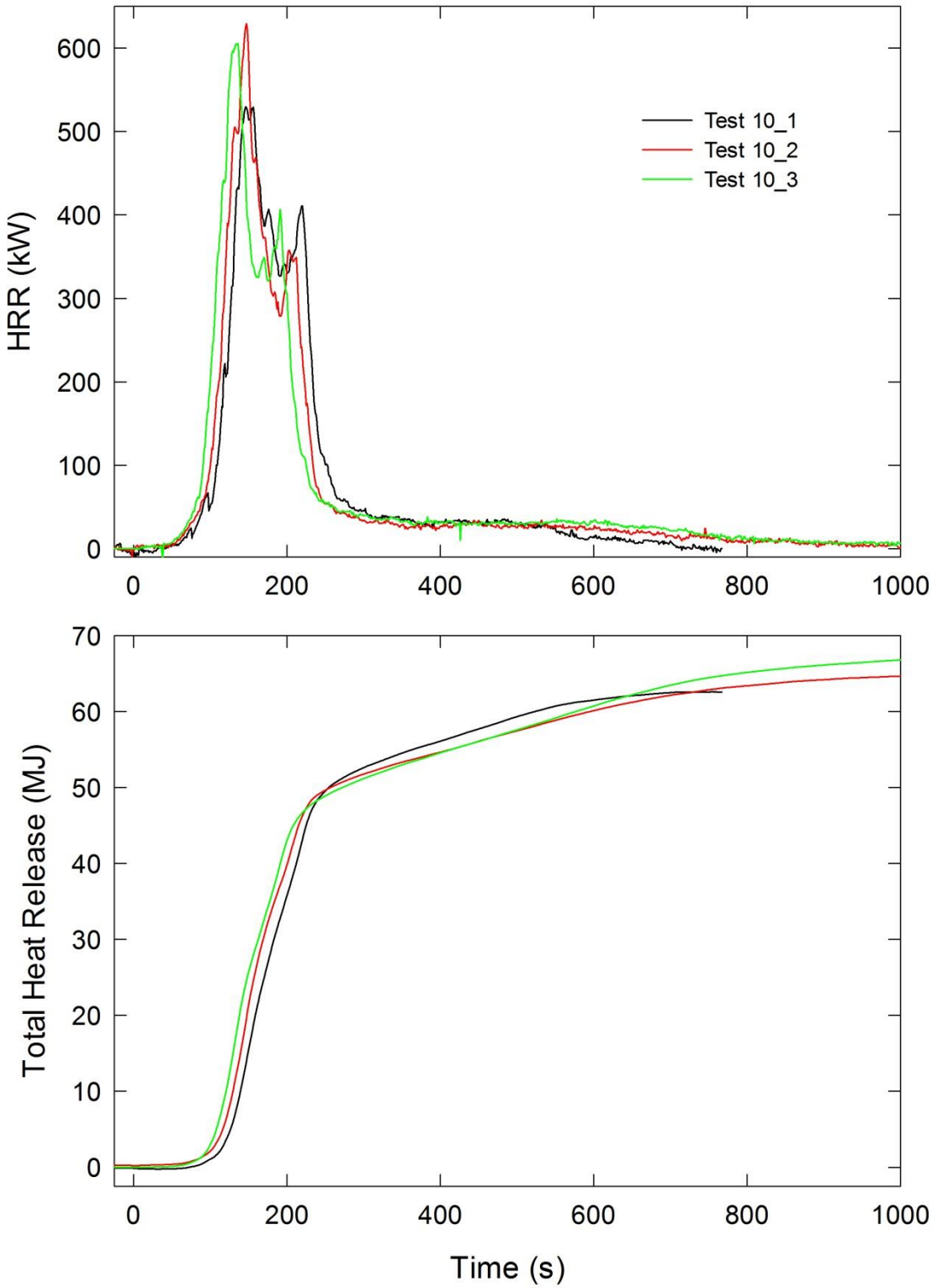

Figure A-54. Temporal profiles of HRR and integrated HRR are shown for Combination 10 tests following application of Ignition Source 1.

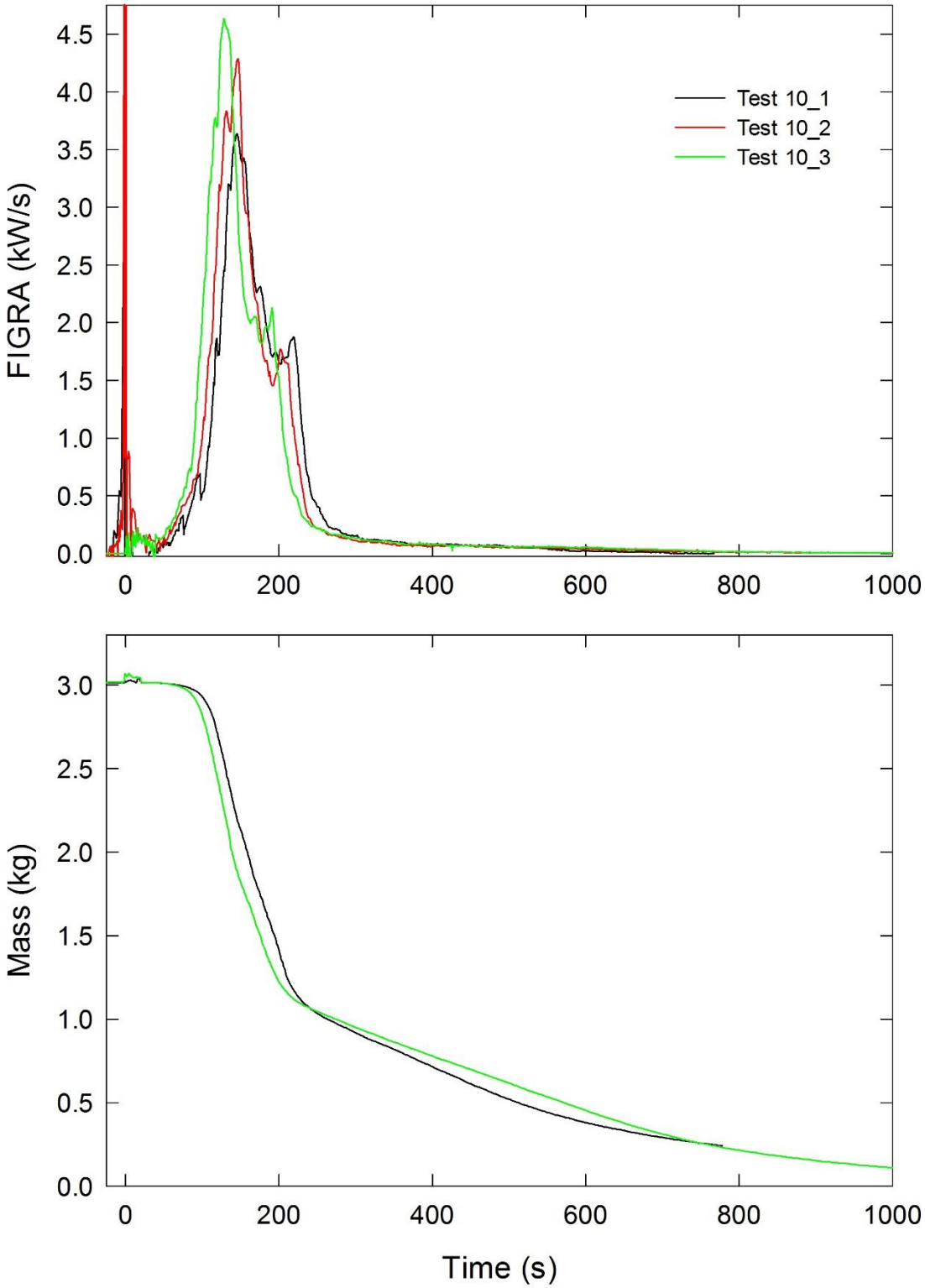

Figure A-55. Temporal profiles of FIGRA for Combination 10 tests and mock-up mass for Test 10_1 and Test 10_3 are shown following application of Ignition Source 1.

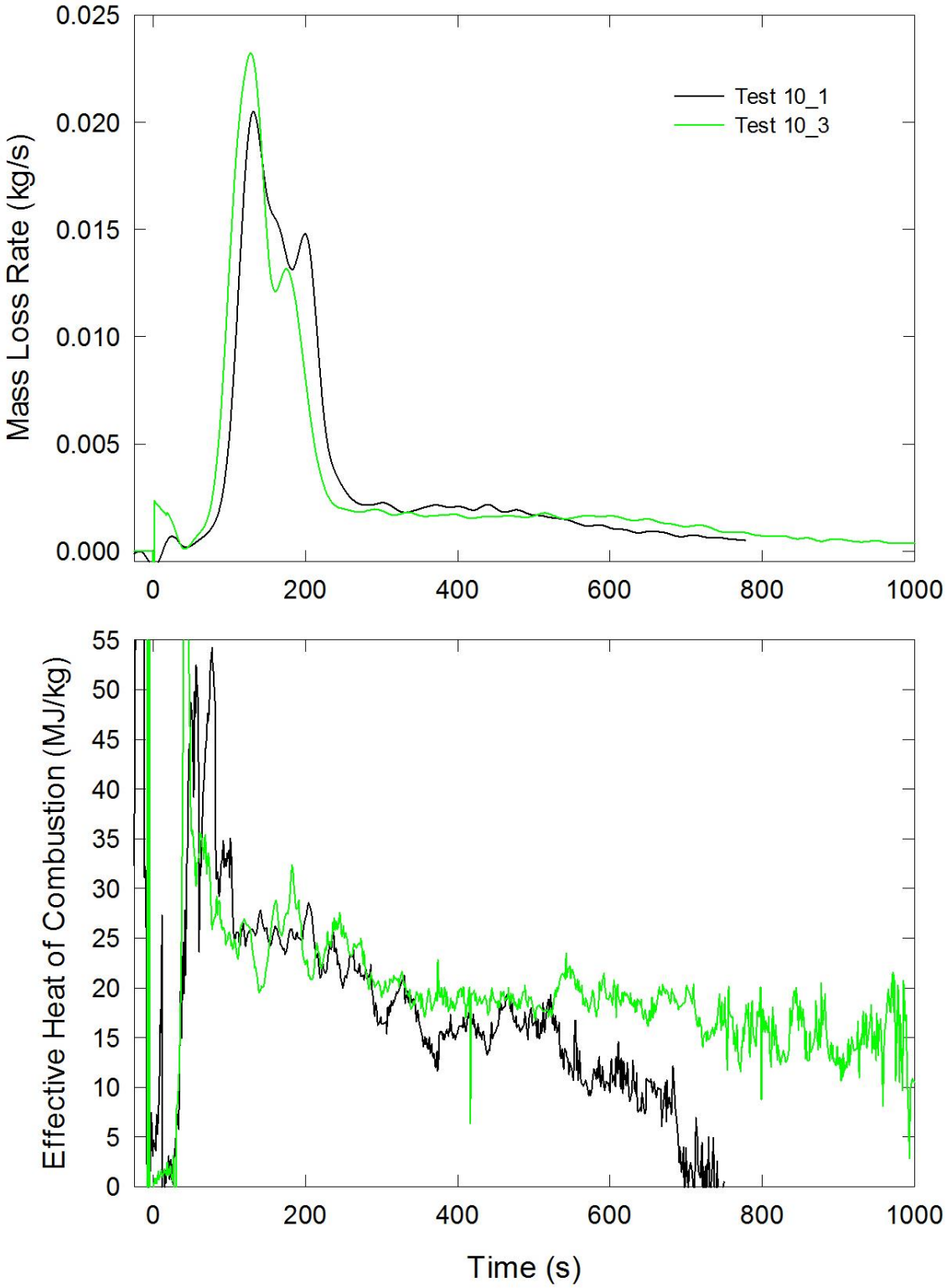

Figure A-56. Temporal profiles of MLR and EHOC are shown for Test 10_1 and Test 10_3 following application of Ignition Source 1.

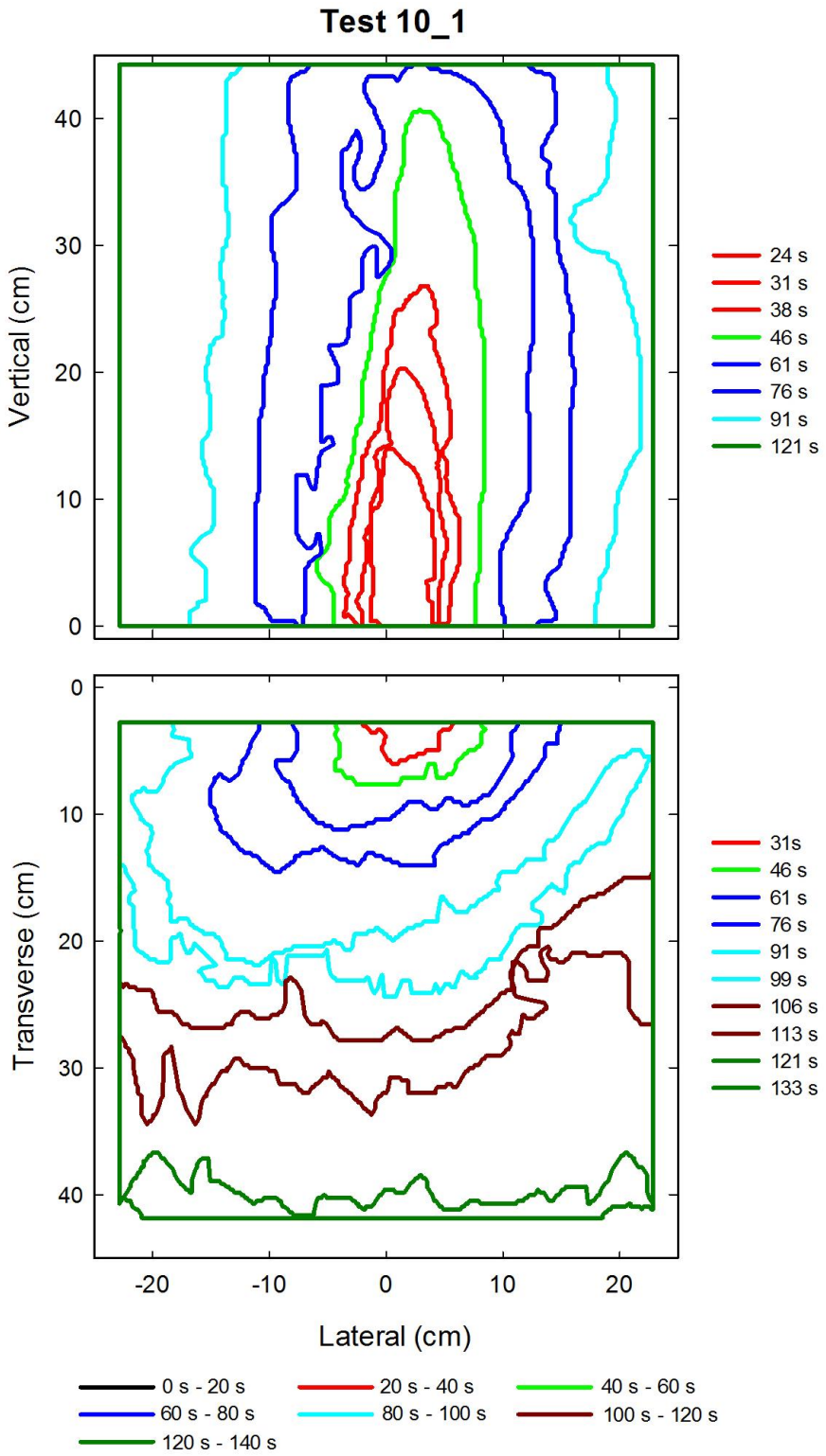

Figure A-57. Flame edge contours on the back (top) and seat (bottom) cushions are plotted as a function of time for Test 10_1 following application of Ignition Source 1.

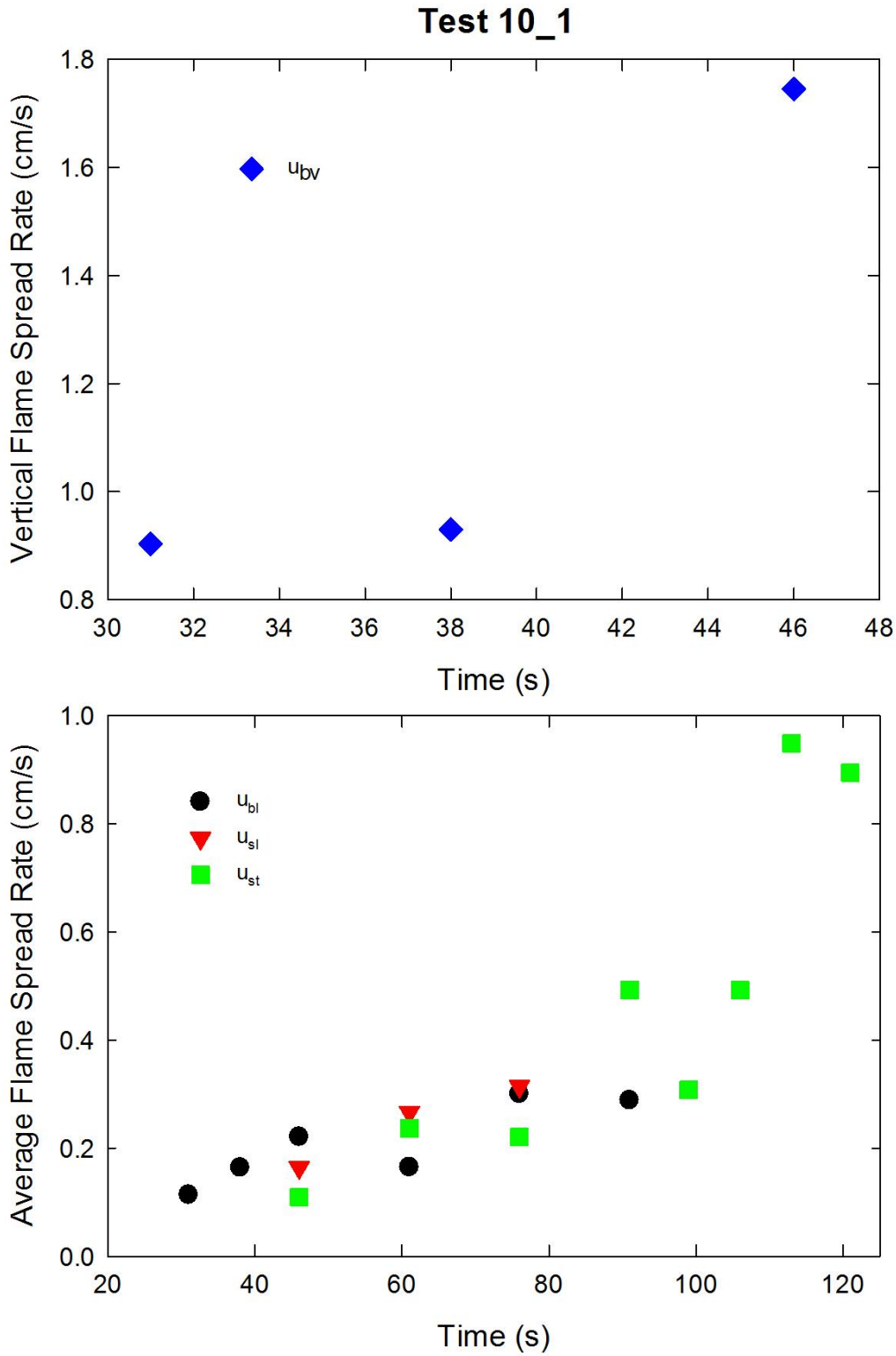

Figure A-58. Vertical flame spread rate on the back cushion (top) and average lateral flame spread rates on the back and seat cushions and transverse flame spread rate on the seat cushion (bottom) are plotted as a function of time for Test 10_1 following application of Ignition Source 1.

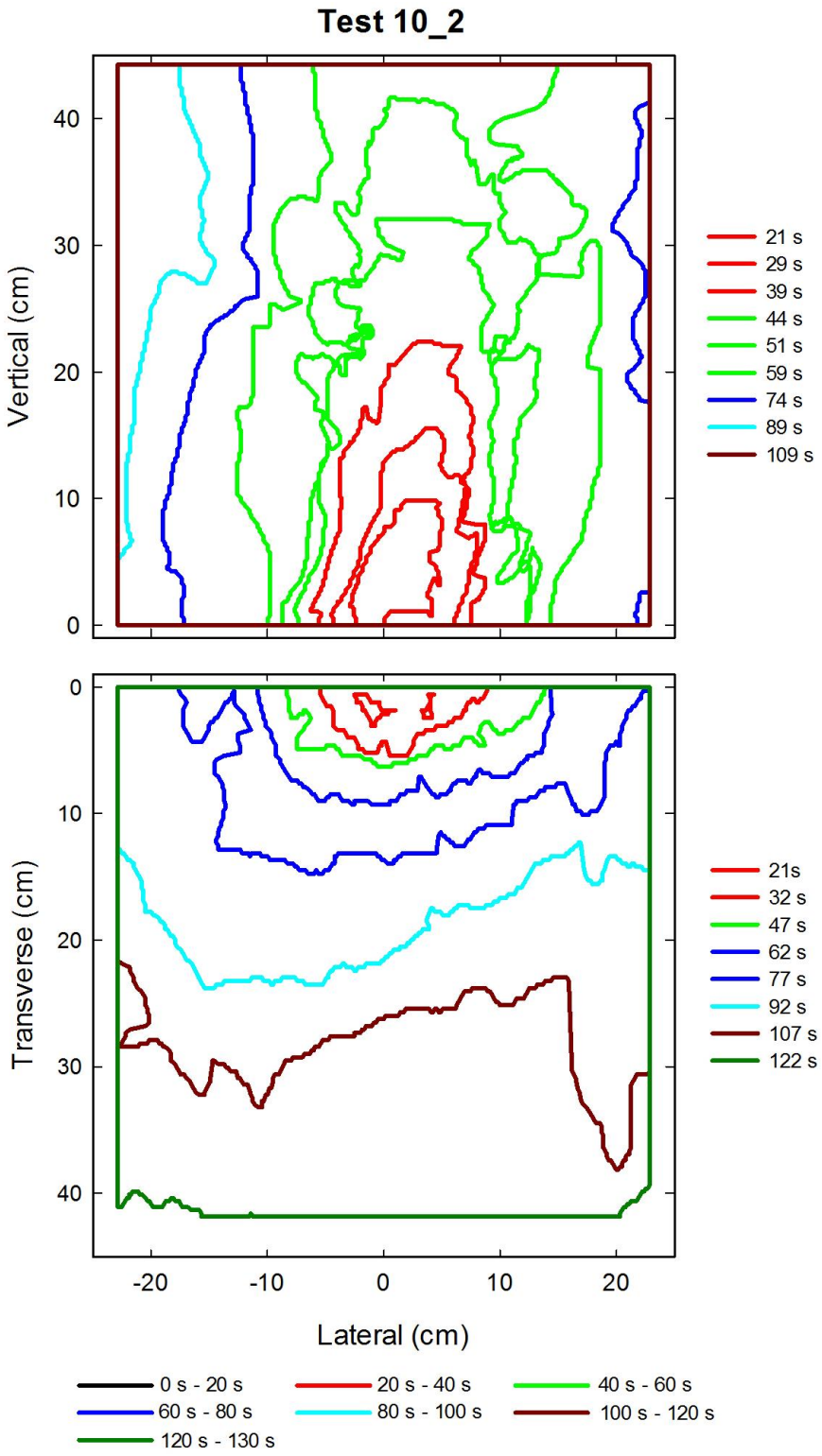

Figure A-59. Flame edge contours on the back (top) and seat (bottom) cushions are plotted as a function of time for Test 10_2 following application of Ignition Source 1.

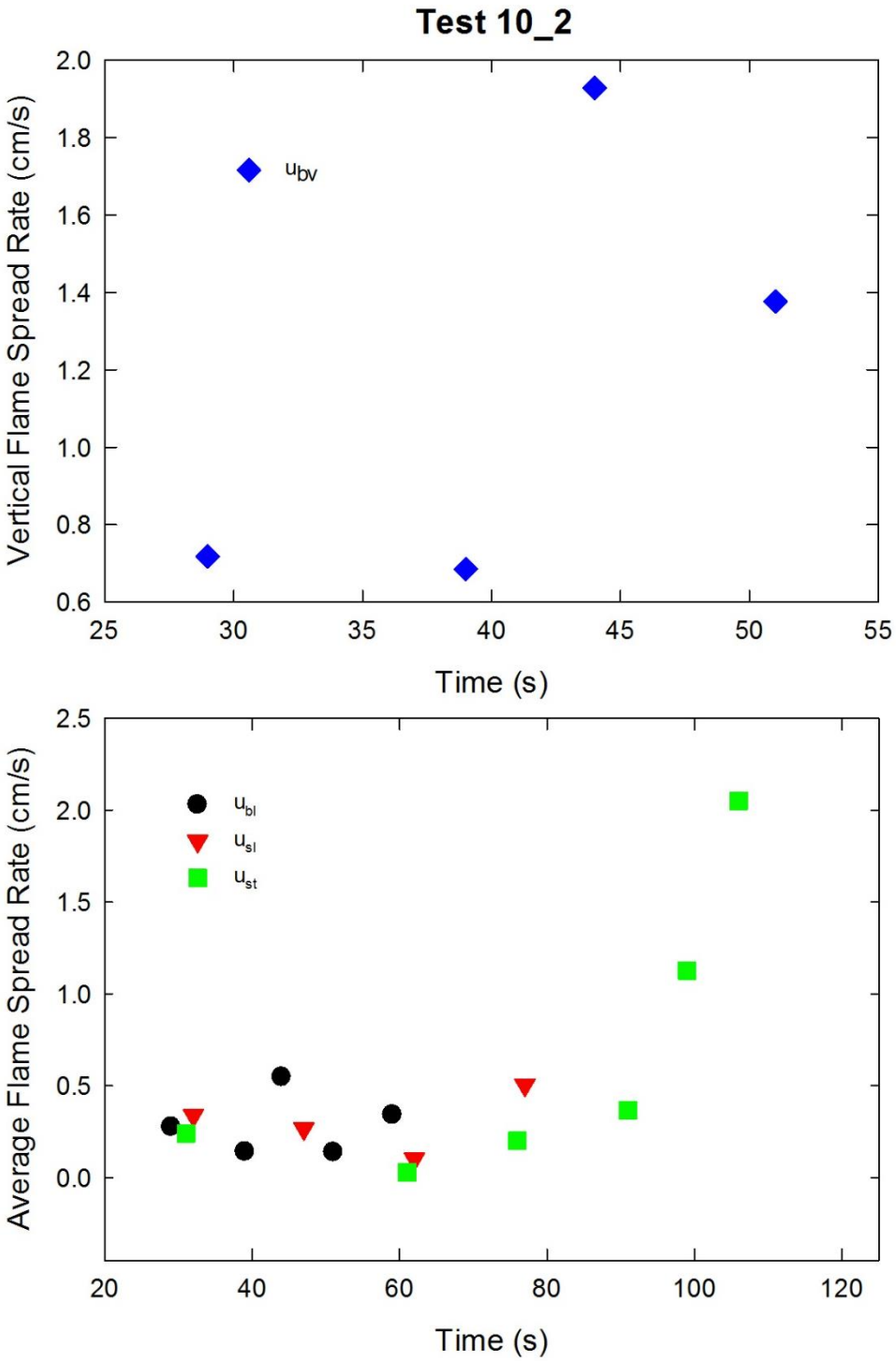

Figure A-60. Vertical flame spread rate on the back cushion (top) and average lateral flame spread rates on the back and seat cushions and transverse flame spread rate on the seat cushion (bottom) are plotted as a function of time for Test 10_2 following application of Ignition Source 1.

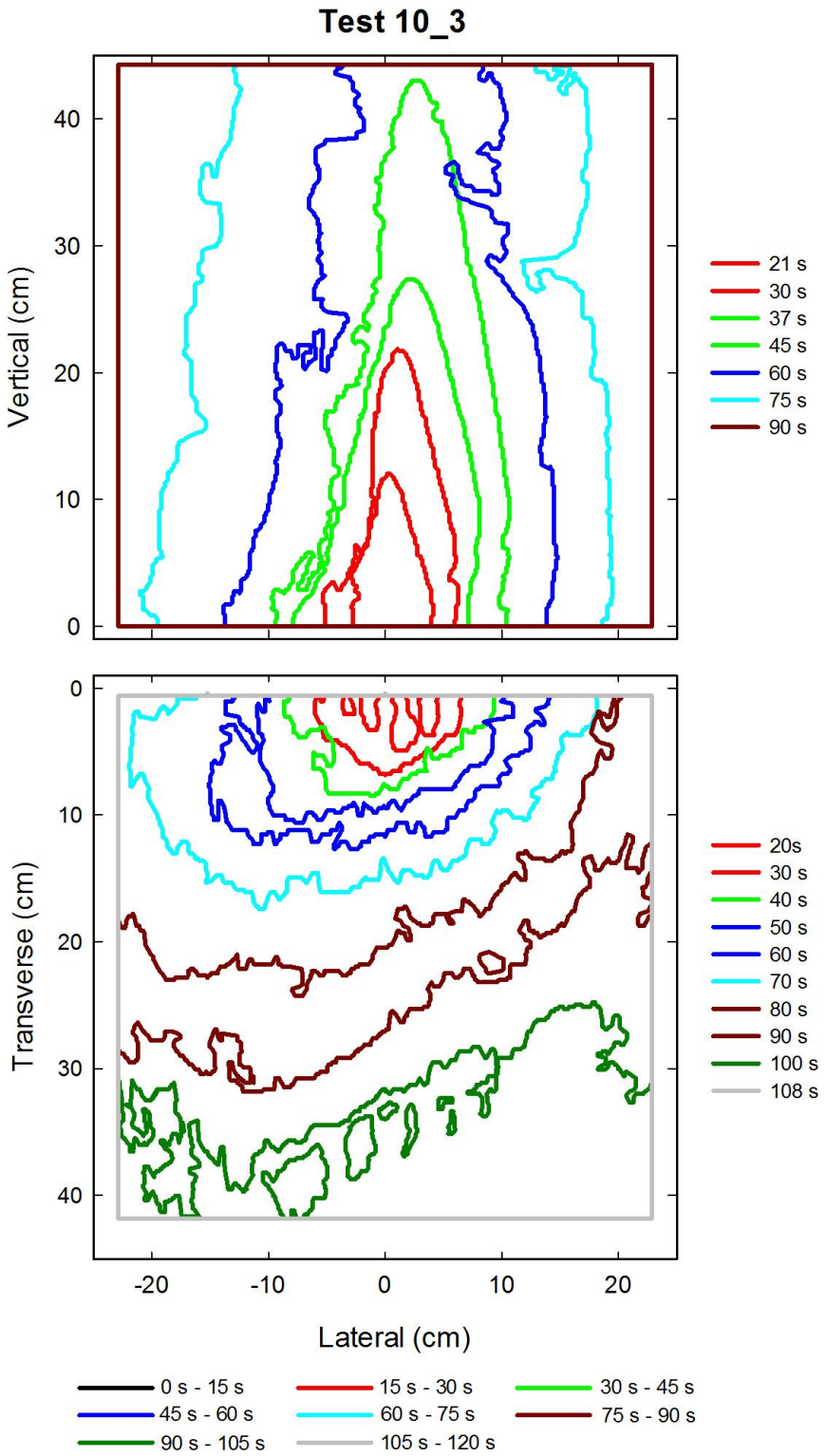

Figure A-61. Flame edge contours on the back (top) and seat (bottom) cushions are plotted as a function of time for Test 10_3 following application of Ignition Source 1.

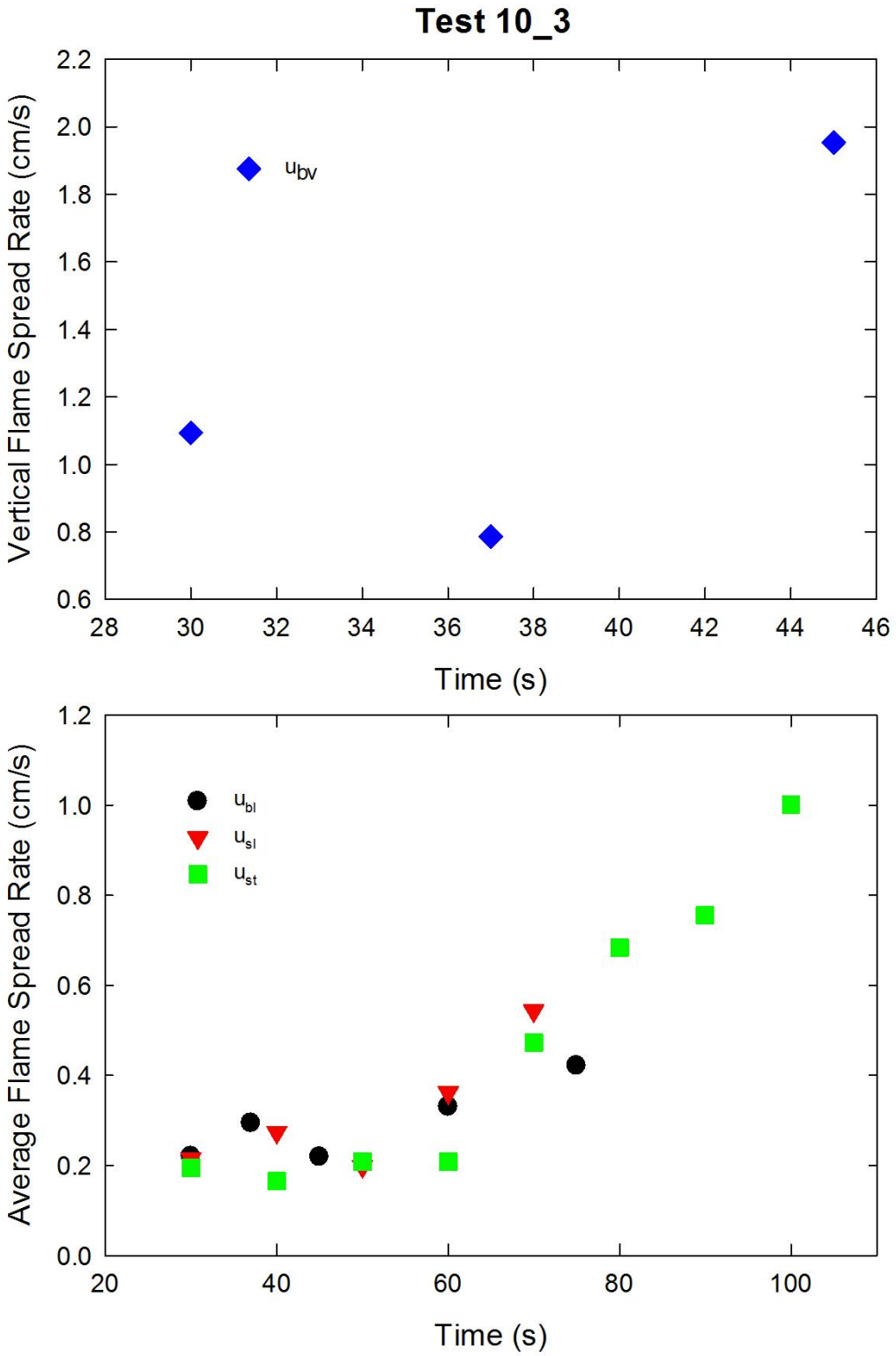

Figure A-62. Vertical flame spread rate on the back cushion (top) and average lateral flame spread rates on the back and seat cushions and transverse flame spread rate on the seat cushion (bottom) are plotted as a function of time for Combination 10 tests following application of Ignition Source 1.

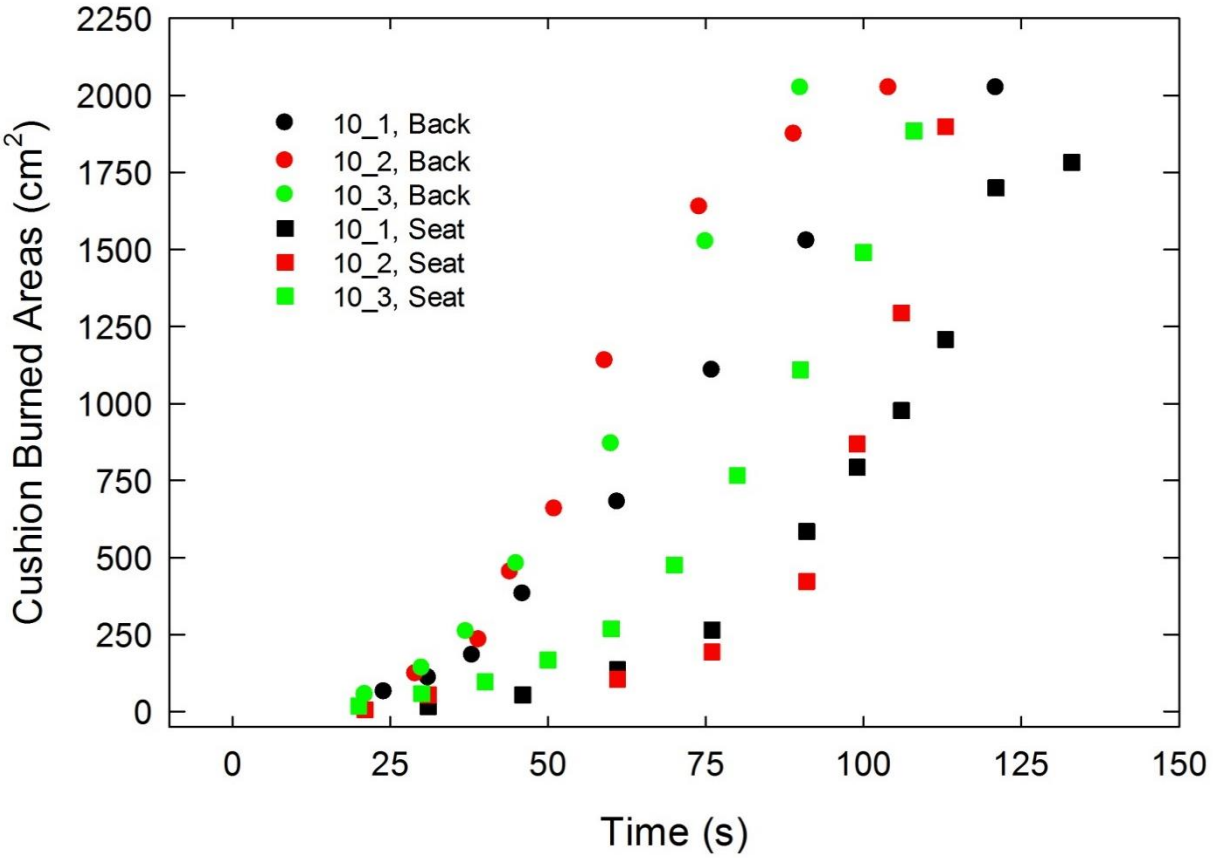

Figure A-63. Burned areas on the seat and back cushions are plotted as a function of time for Combination 10 tests following application of Ignition Source 1.

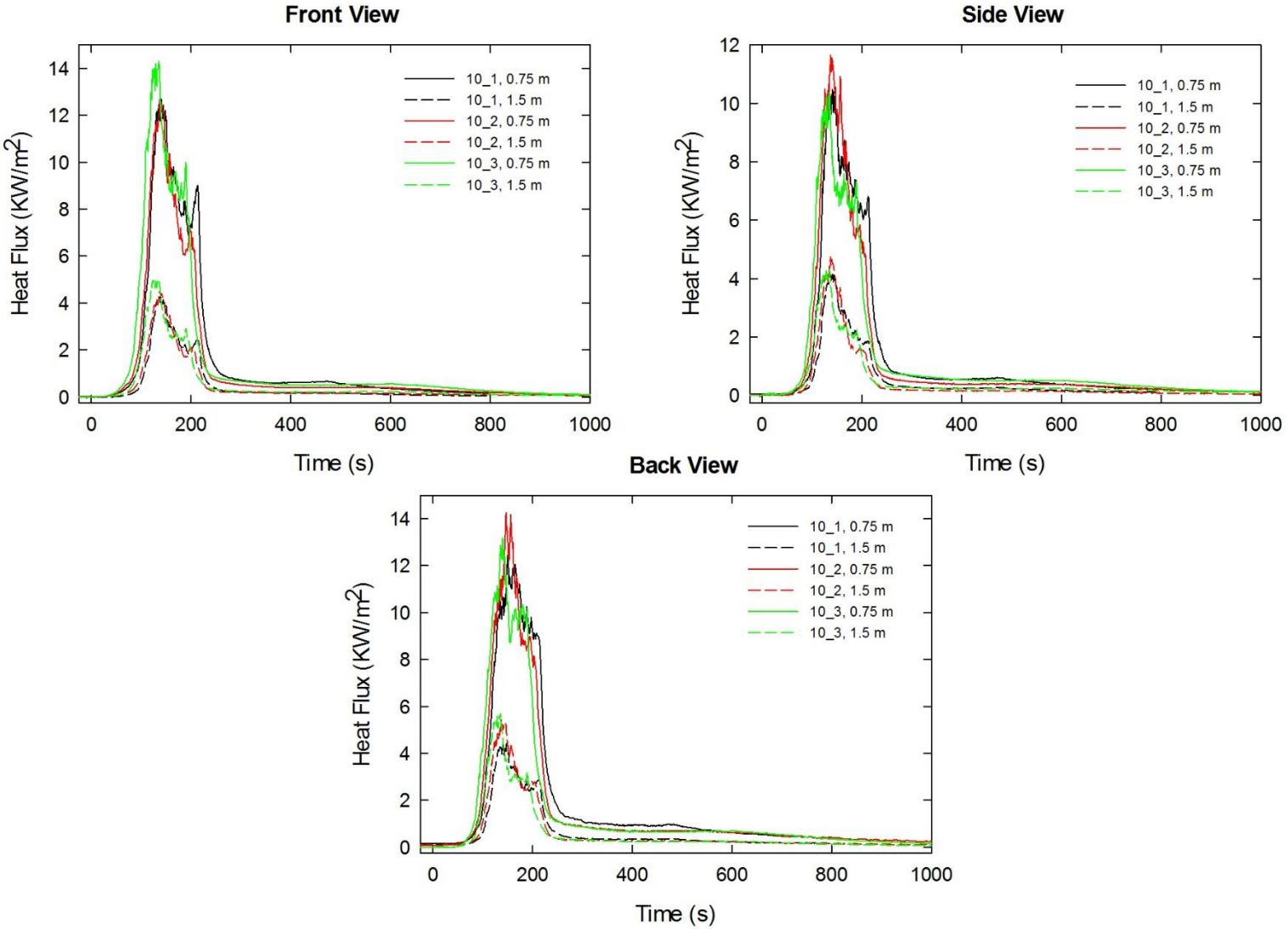

Figure A-64. Heat fluxes recorded at distances of 0.75 m and 1.5 m are plotted as a function of time for locations to the front, side and rear of the mock-up for Combination 10 tests following application of Ignition Source 1.

A.7 Combination 11

cotton/PEFW/NFRFPUF

Notes:

Test 1

Ignition Source 1 applied at time = 0 s; following removal of ignition source, there was upward flame spread on the back cushion and a small black circle on the seat cushion, but with no flame spread; a black area appeared on the seat ≈ 2.5 cm to right of flame application point at ≈ 62 s and began to spread.

Test 2

Ignition Source 1 applied at time = 0 s, following removal of ignition source, there was upward flame spread on the back, but no discoloration on seat; at ≈ 65 s a small black mark appeared on the seat at the ignition point and began to spread.

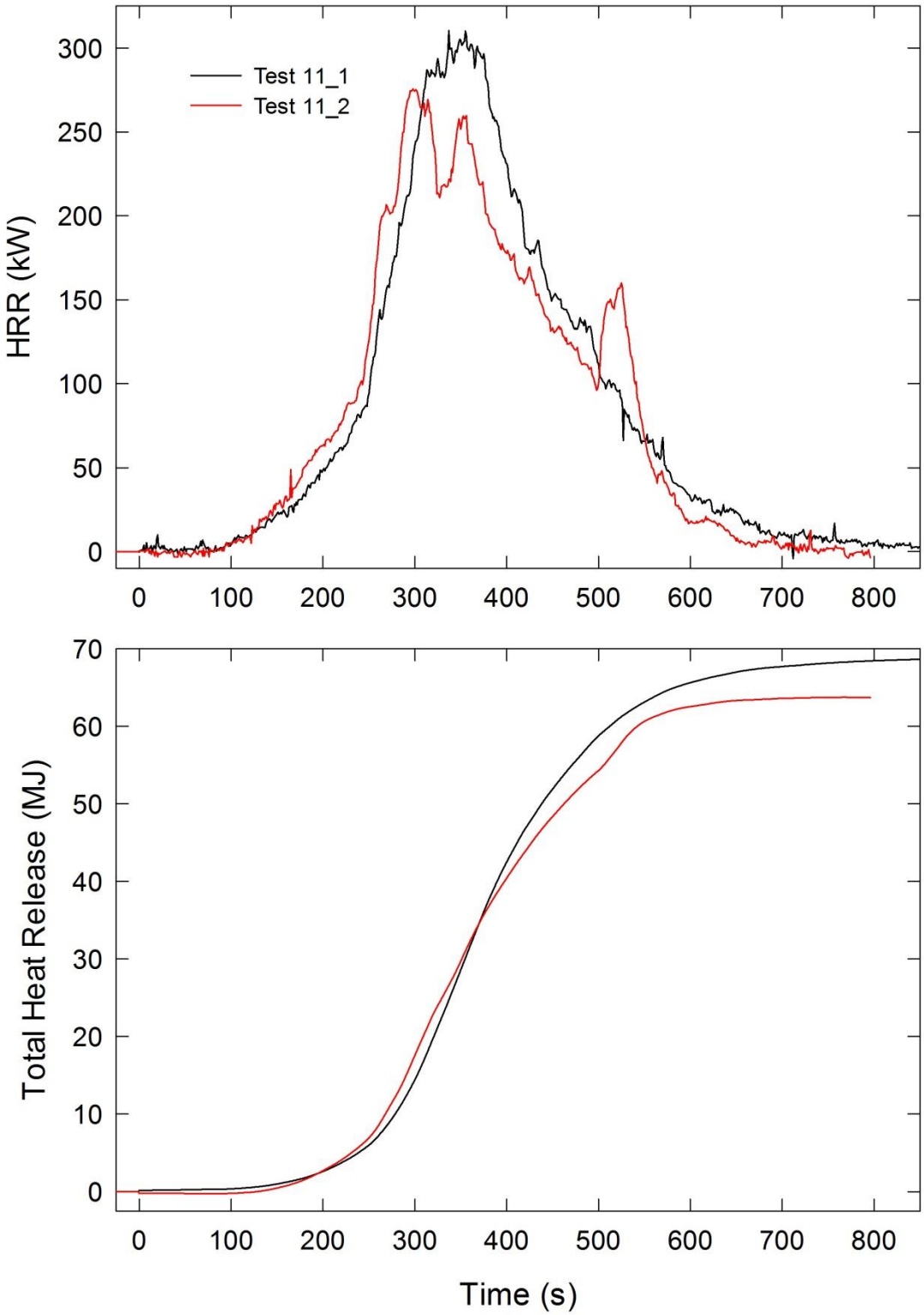

Figure A-65. Temporal profiles of HRR and integrated HRR are shown for Combination 11 tests following application of Ignition Source 1.

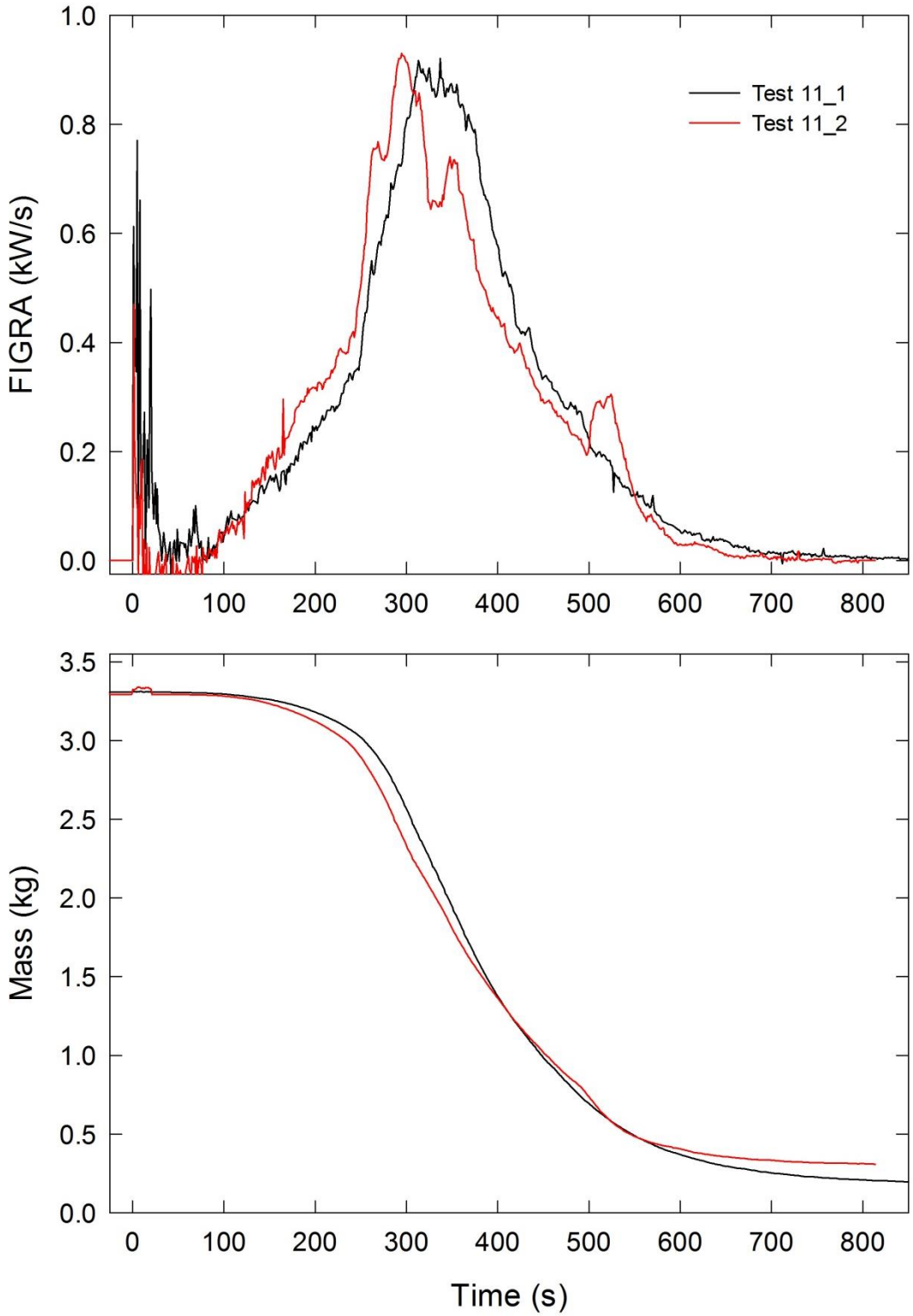

Figure A-66. Temporal profiles of FIGRA and mock-up mass for Combination 11 tests are shown following application of Ignition Source 1.

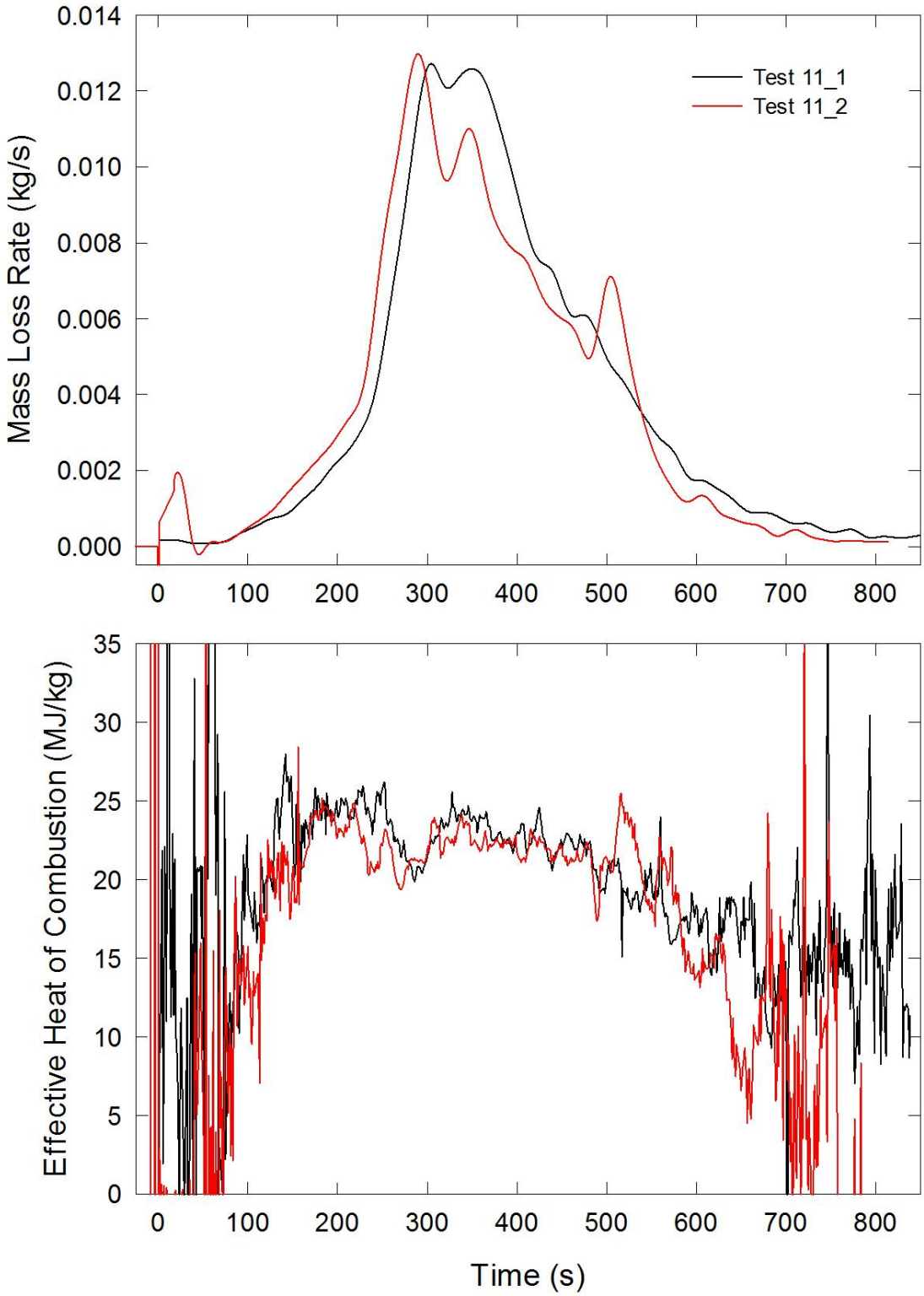

Figure A-67. Temporal profiles of MLR and EHOC are shown for Combination 11 tests following application of Ignition Source 1.

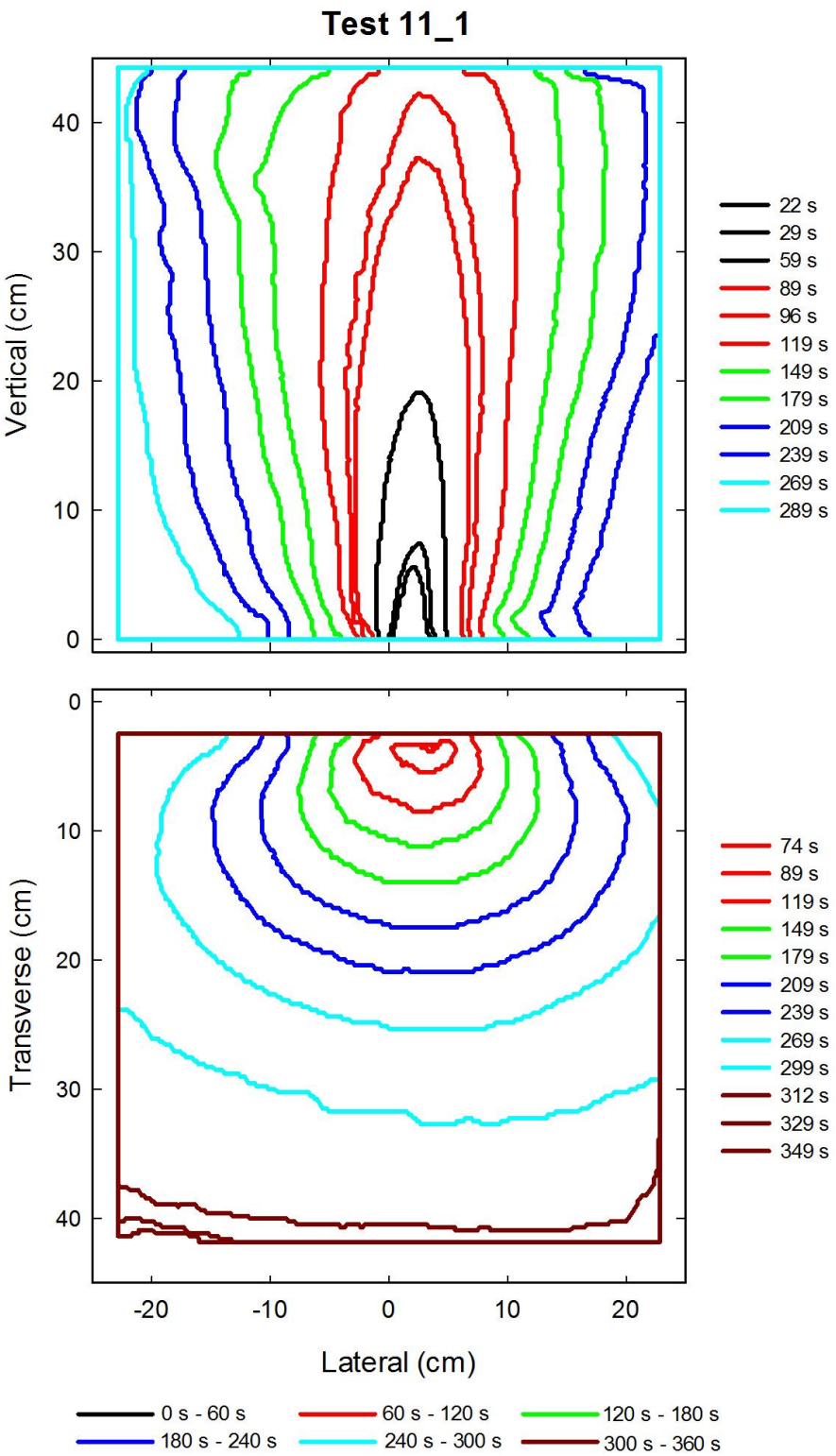

Figure A-68. Flame edge contours on the back (top) and seat (bottom) cushions are plotted as a function of time for Test 11_1 following application of Ignition Source 1.

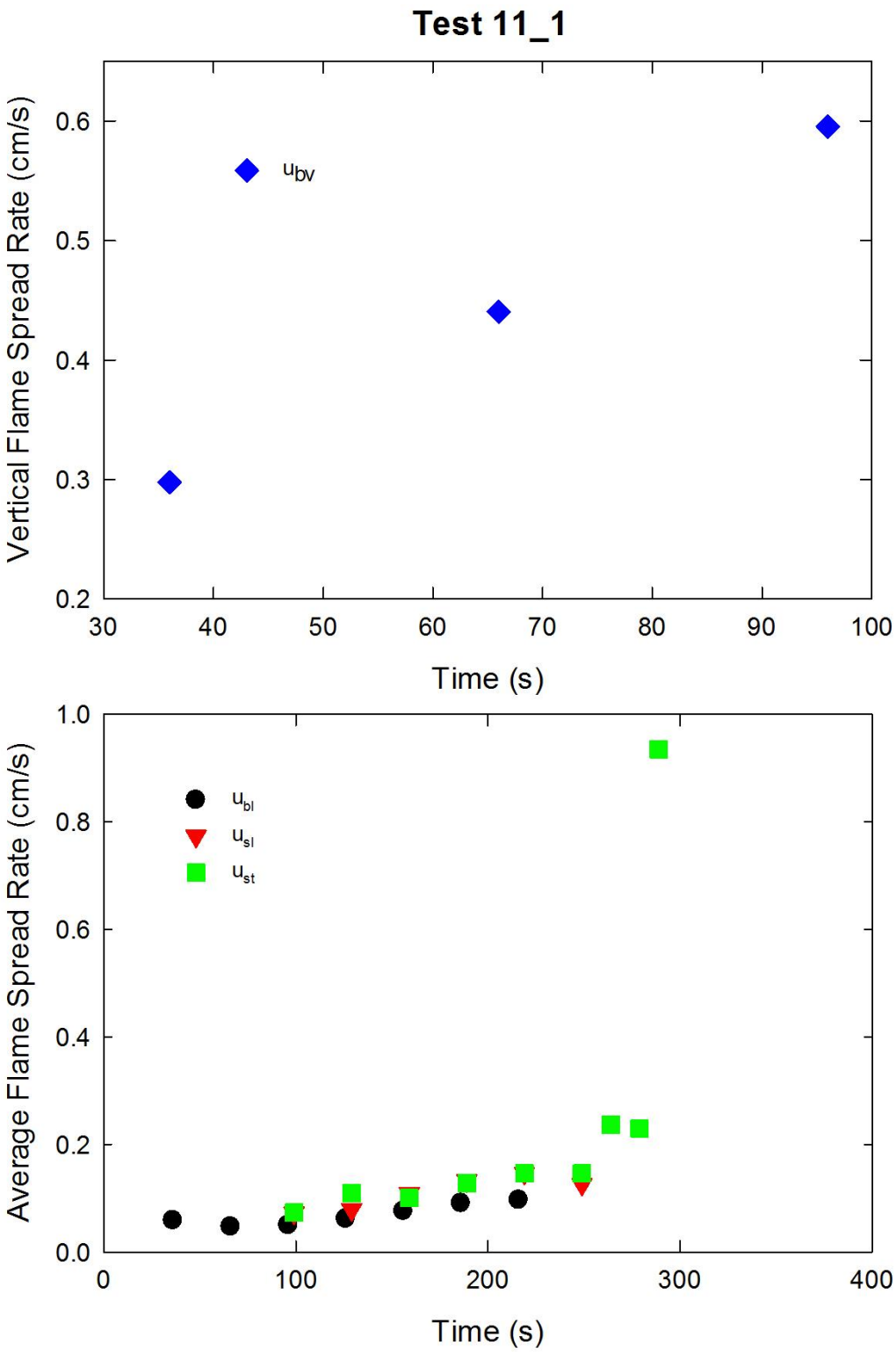

Figure A-69. Vertical flame spread rate on the back cushion (top) and average lateral flame spread rates on the back and seat cushions and transverse flame spread rate on the seat cushion (bottom) are plotted as a function of time for Test 11_1 following application of Ignition Source 1.

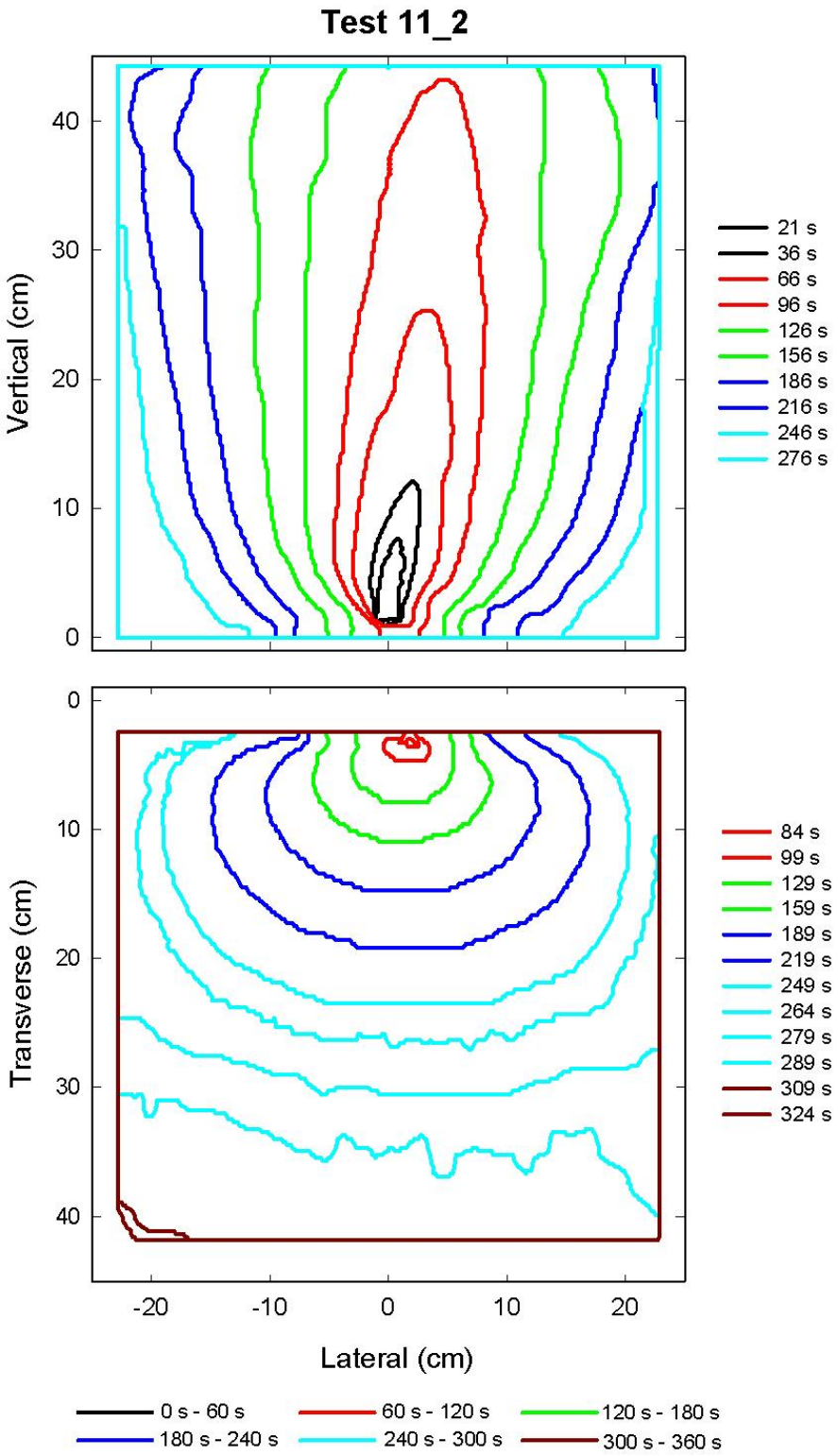

Figure A-70. Flame edge contours on the back (top) and seat (bottom) cushions are plotted as a function of time for Test 11_2 following application of Ignition Source 1.

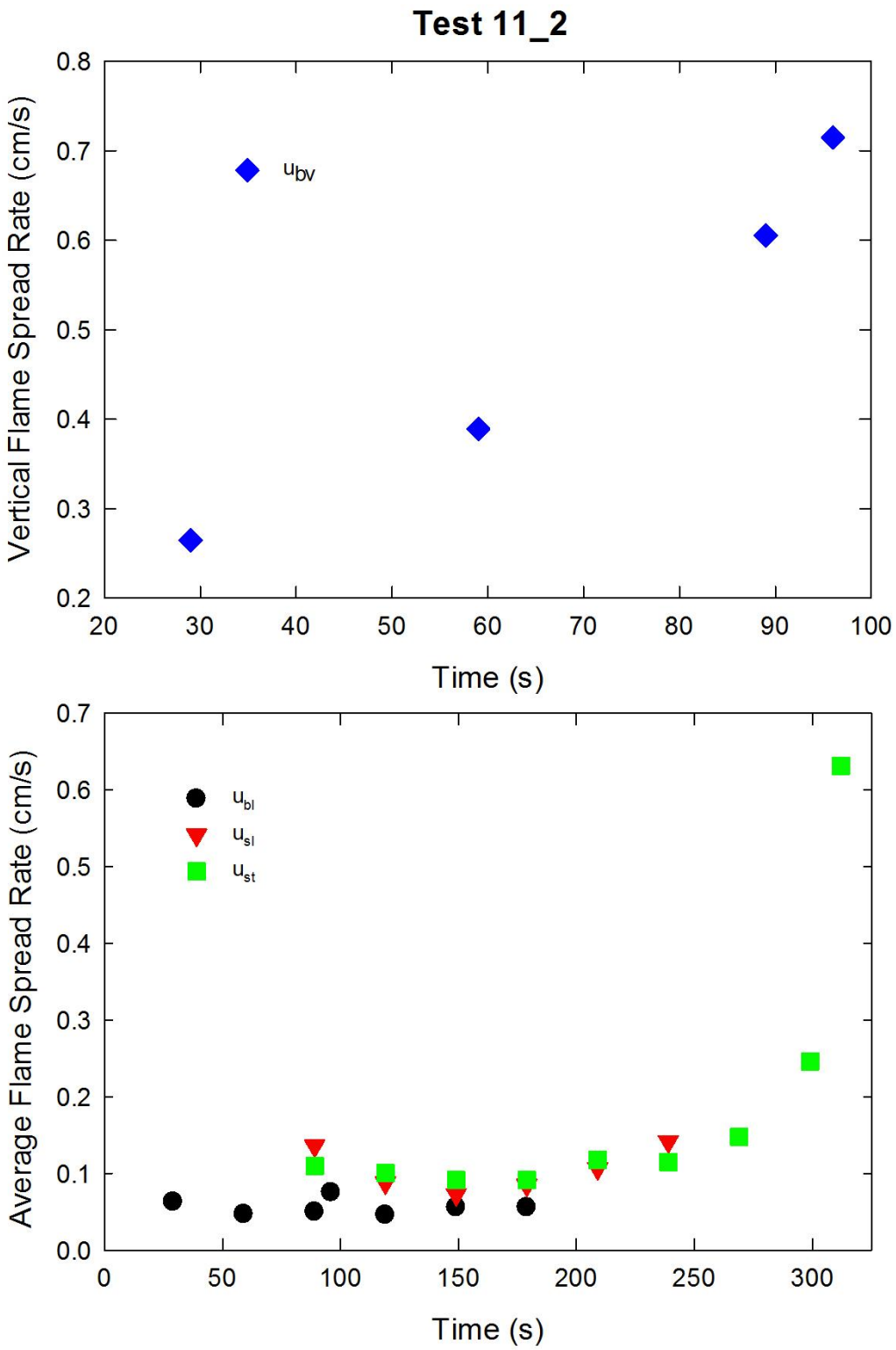

Figure A-71. Vertical flame spread rate on the back cushion (top) and average lateral flame spread rates on the back and seat cushions and transverse flame spread rate on the seat cushion (bottom) are plotted as a function of time for Test 11_2 following application of Ignition Source 1.

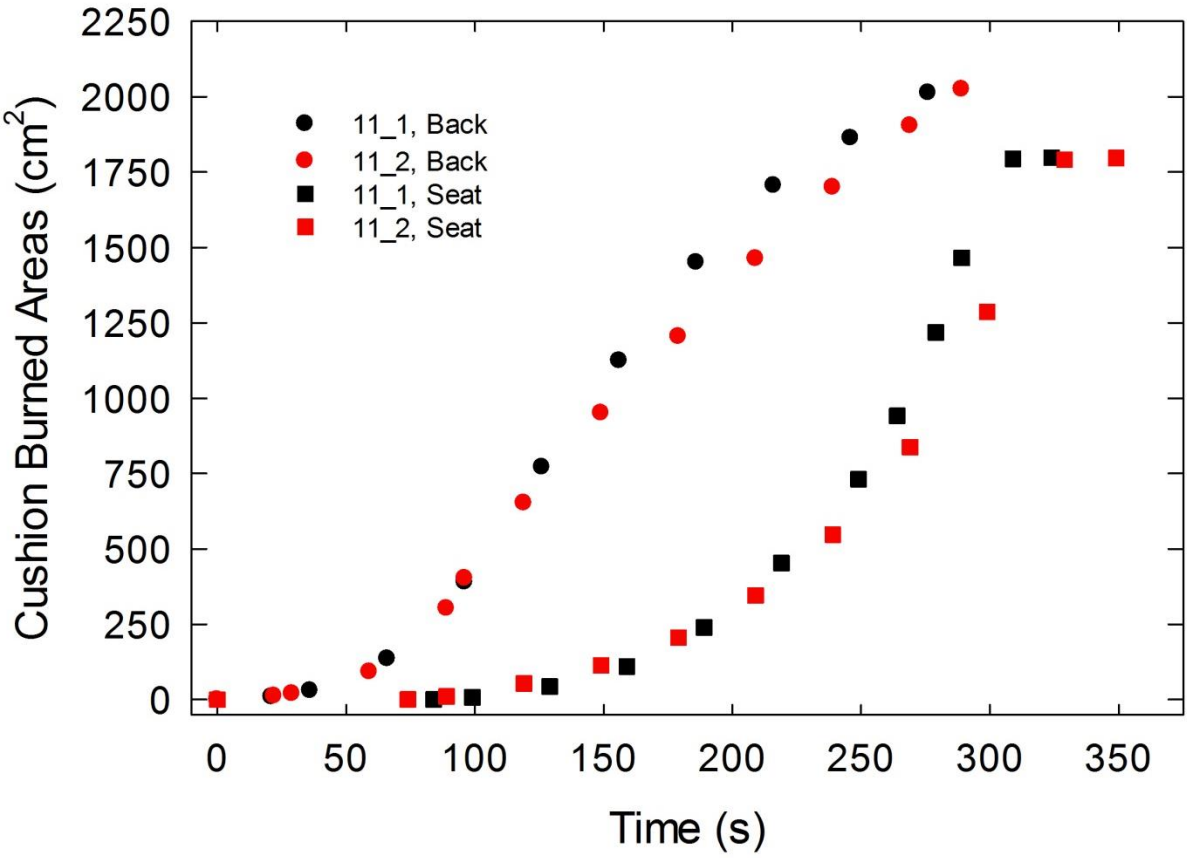

Figure A-72. Burned areas on the seat and back cushions are plotted as a function of time for Combination 11 tests following application of Ignition Source 1.

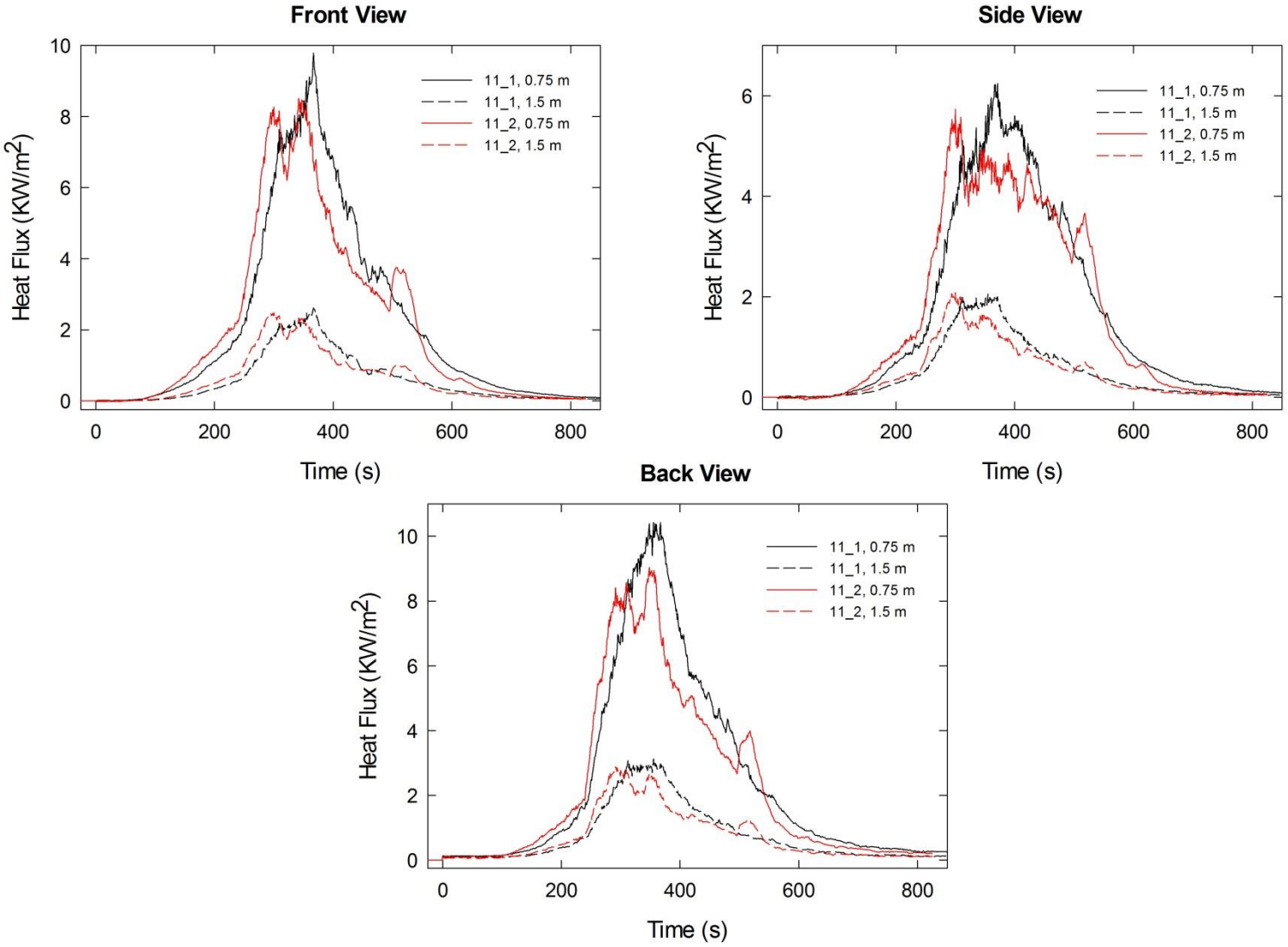

Figure A-73. Heat fluxes recorded at distances of 0.75 m and 1.5 m are plotted as a function of time for locations to the front, side and rear of the mock-up for Combination 11 tests following application of Ignition Source 1.

A.8 Combination 12

78%PP/22%PE/PEFW/NFRFPUF

Notes:

Test 1:

Ignition Source 1 applied at time = 0 s

Test 2:

Ignition Source 1 applied at time = 0 s

Initial mass reading (3.26 kg) during the experiment agreed with an earlier measurement of mock-up (3.26 kg); mass readings during initial period of test looked normal, but at later times there were periods of increasing mass and non-physical abrupt jumps; **these mass data were excluded from analysis**.

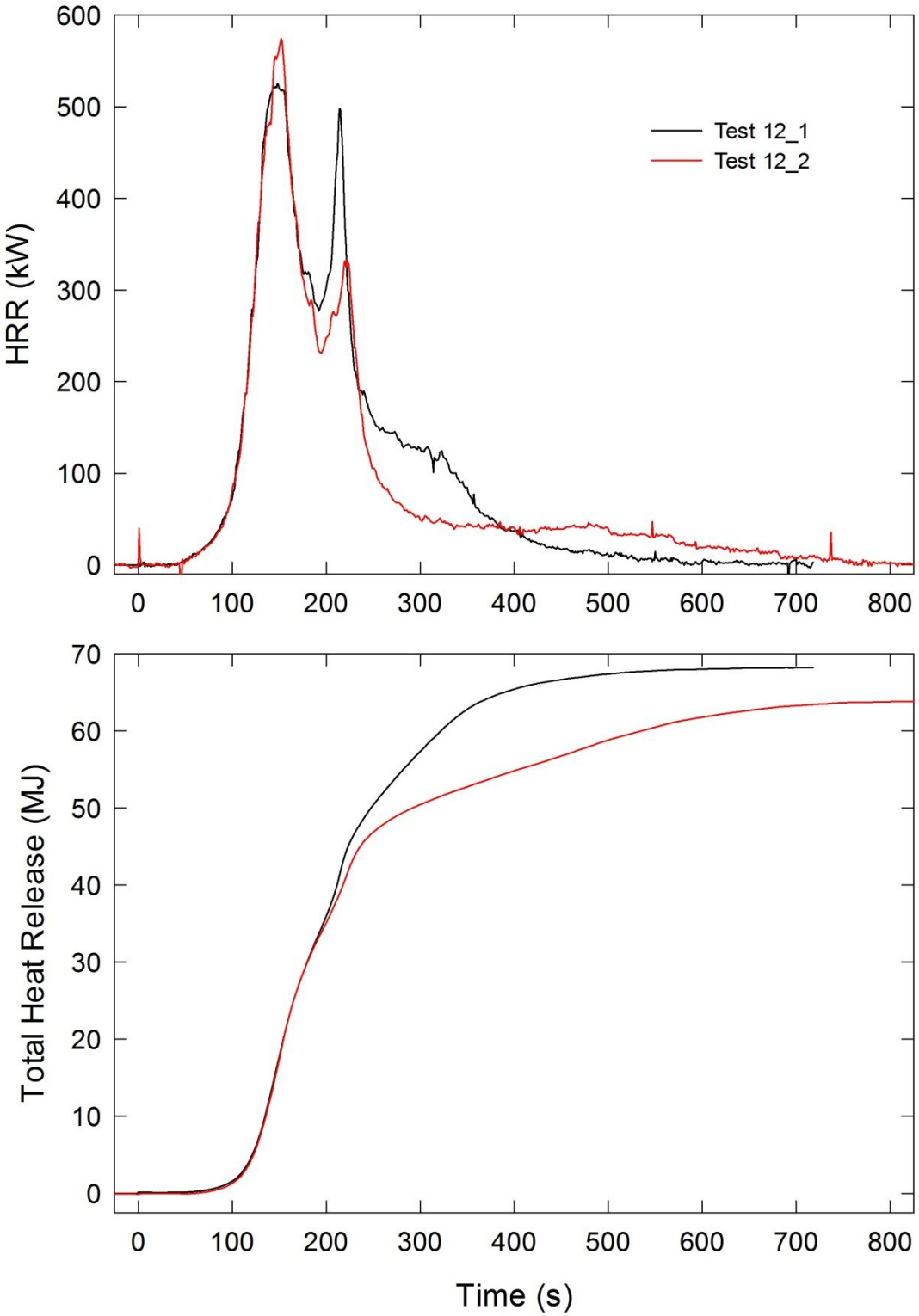

Figure A-74. Temporal profiles of HRR and integrated HRR are shown for Combination 12 tests following application of Ignition Source 1.

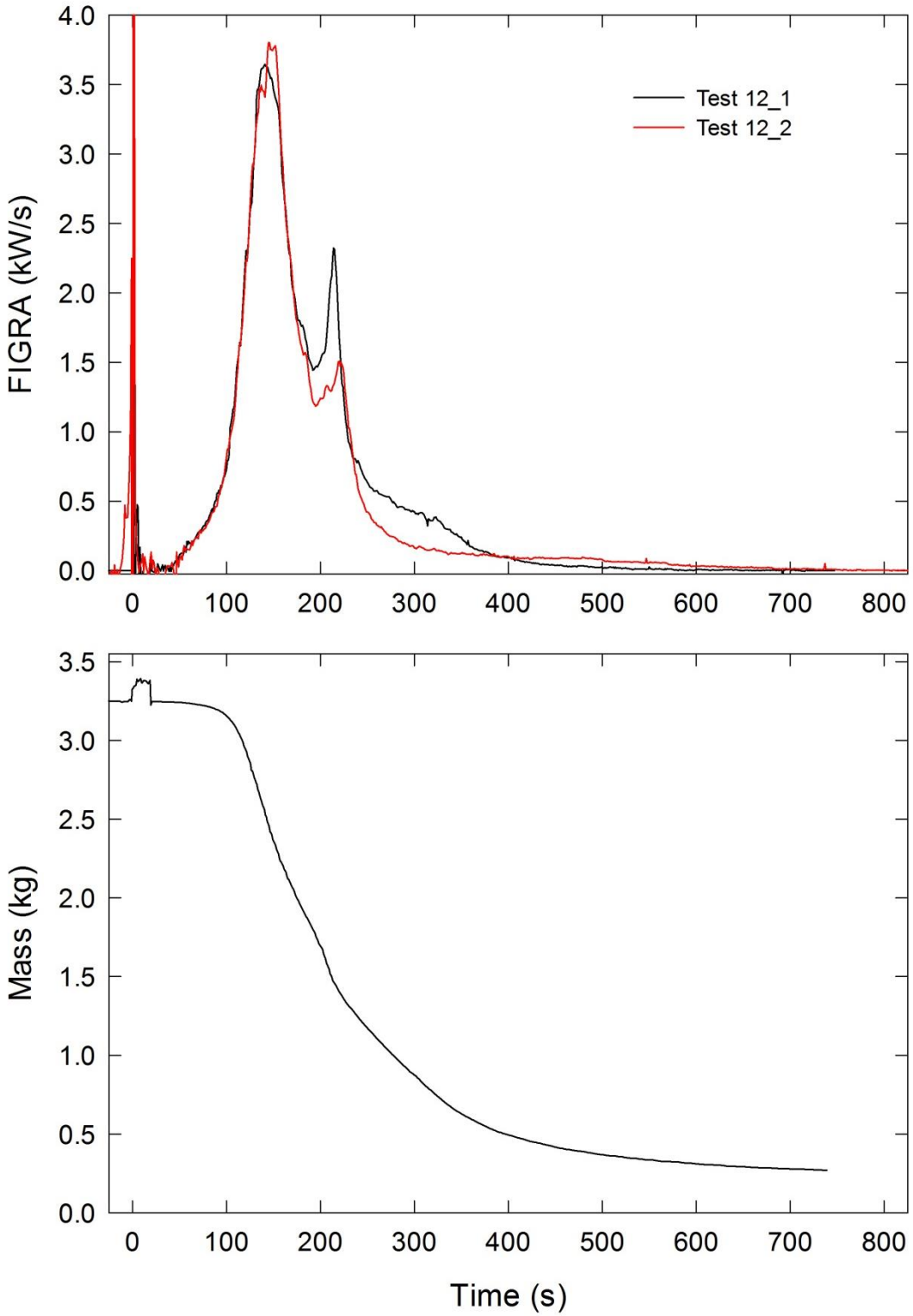

Figure A-75. Temporal profiles of FIGRA for Combination 12 tests and mock-up mass for Test 12_1 are shown following application of Ignition Source 1.

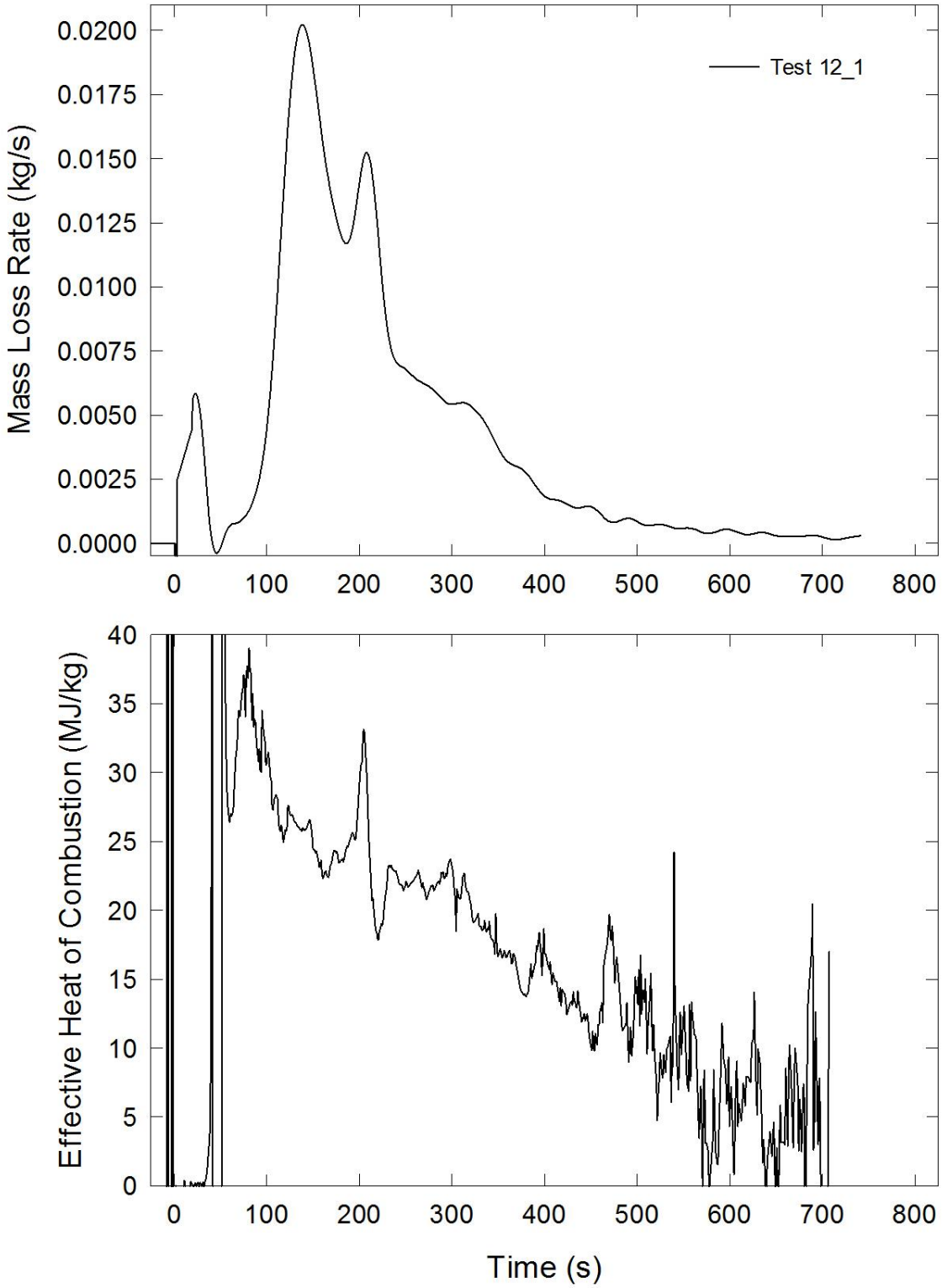

Figure A-76. Temporal profiles of MLR and EHOC are shown for Test 12_1 following application of Ignition Source 1.

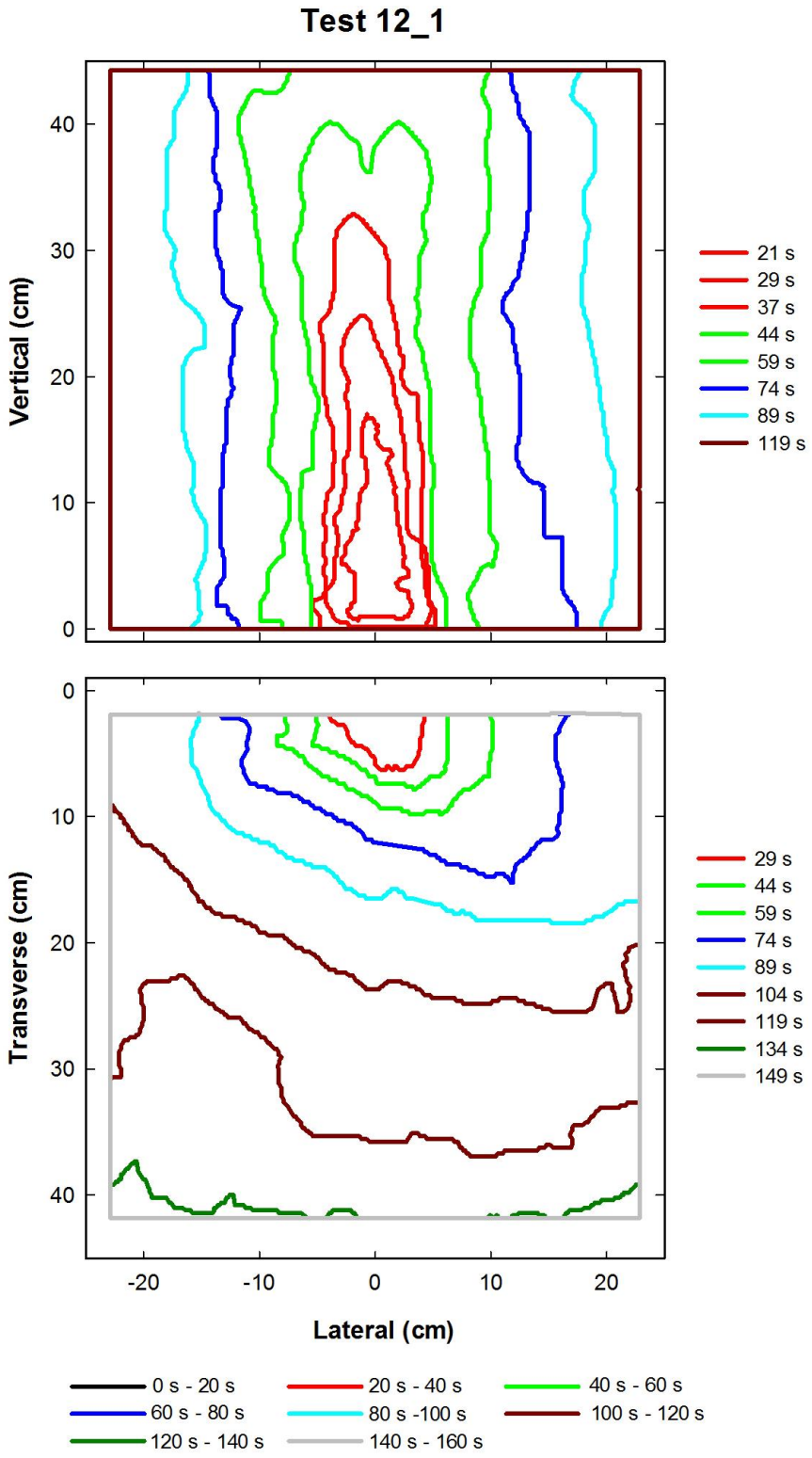

Figure A-77. Flame edge contours on the back (top) and seat (bottom) cushions are plotted as a function of time for Test 12_1 following application of Ignition Source 1.

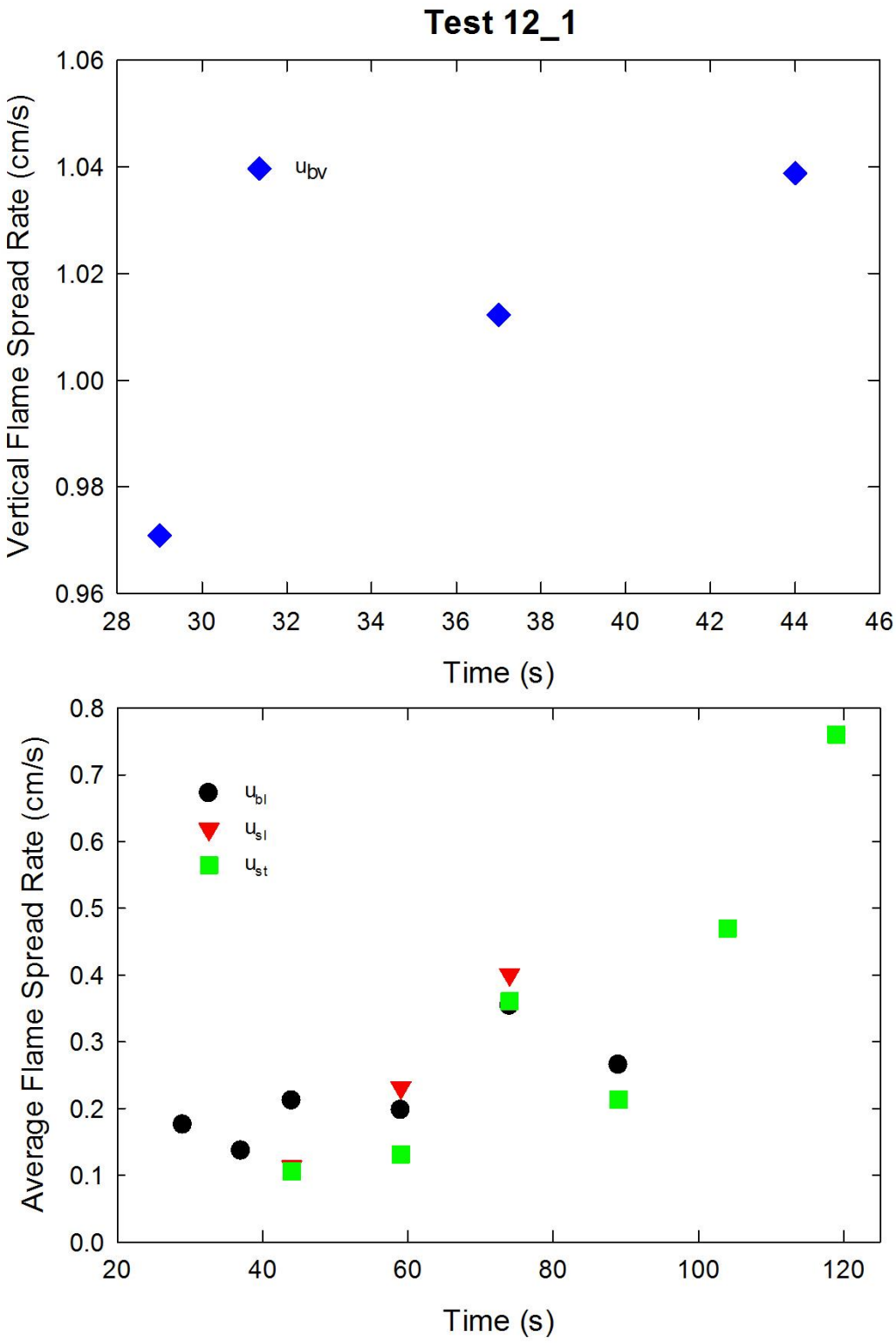

Figure A-78. Vertical flame spread rate on the back cushion (top) and average lateral flame spread rates on the back and seat cushions and transverse flame spread rate on the seat cushion (bottom) are plotted as a function of time for Test 12_1 following application of Ignition Source 1.

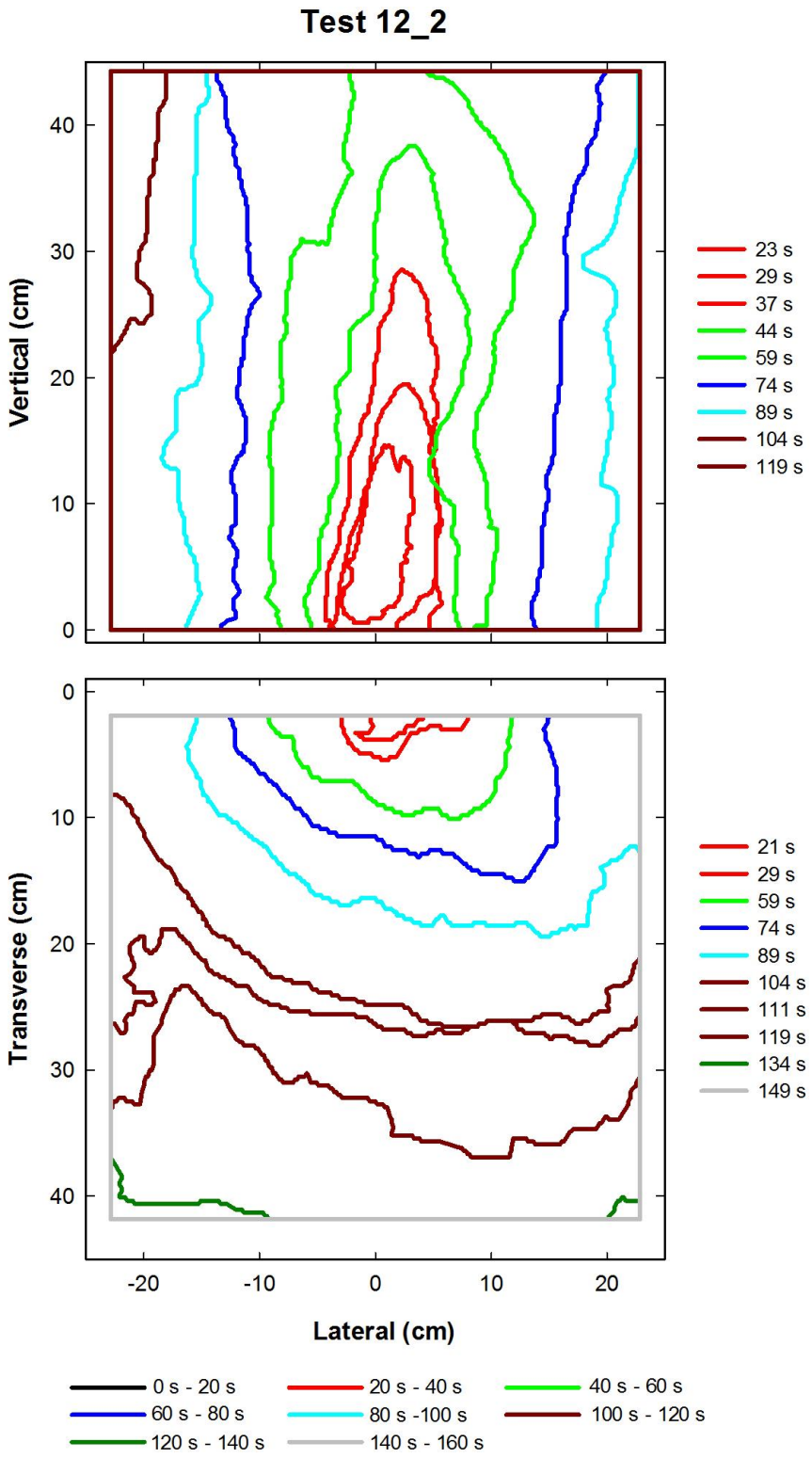

Figure A-79. Flame edge contours on the back (top) and seat (bottom) cushions are plotted as a function of time for Test 12_2 following application of Ignition Source 1.

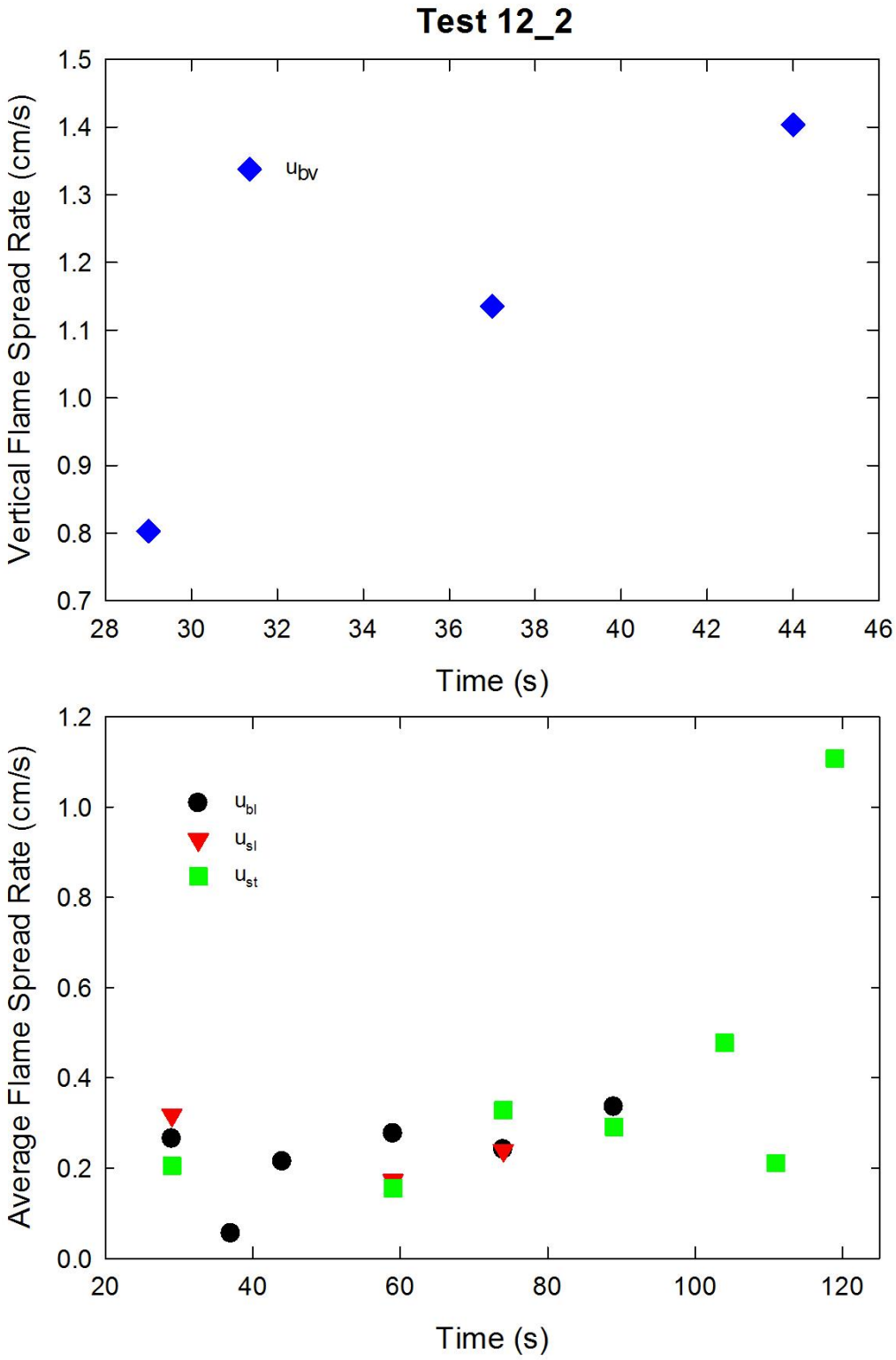

Figure A-80. Vertical flame spread rate on the back cushion (top) and average lateral flame spread rates on the back and seat cushions and transverse flame spread rate on the seat cushion (bottom) are plotted as a function of time for Test 12_2 following application of Ignition Source 1.

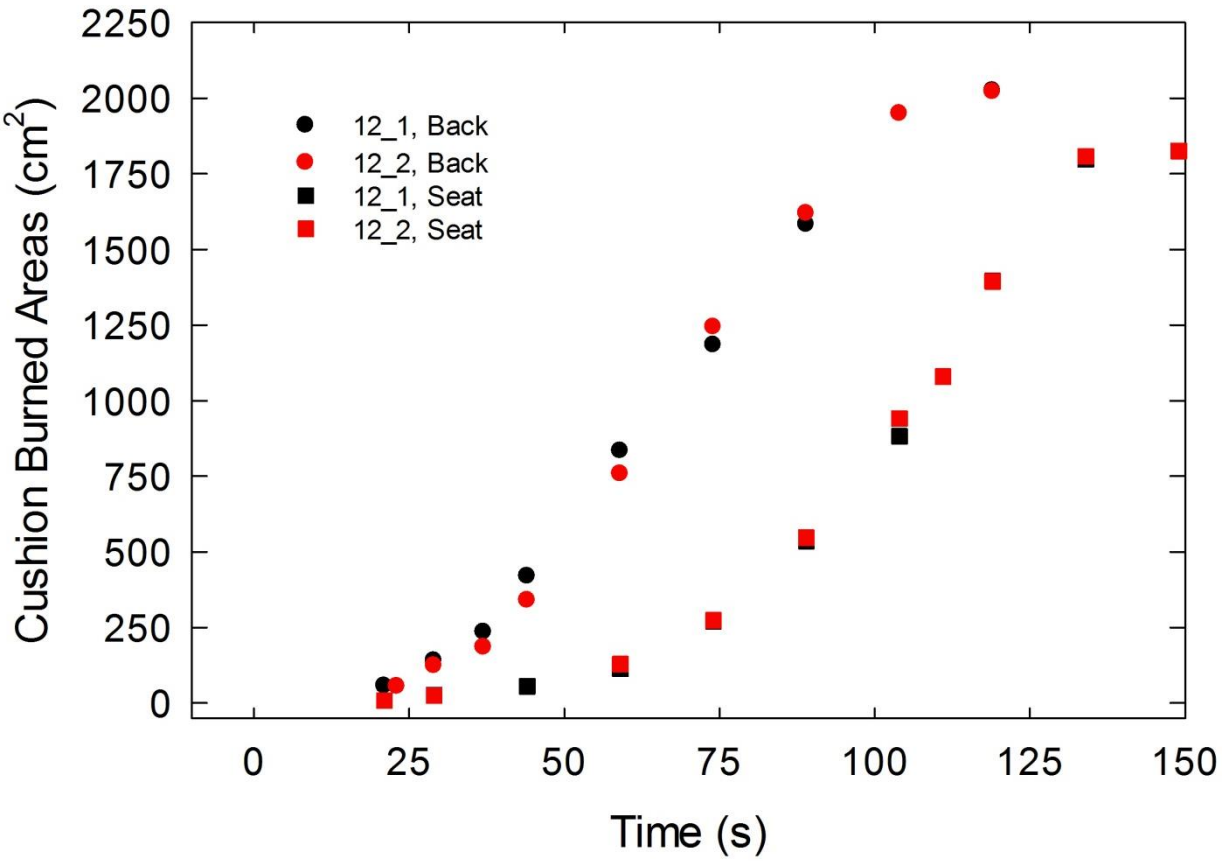

Figure A-81. Burned areas on the seat and back cushions are plotted as a function of time for Combination 12 tests following application of Ignition Source 1.

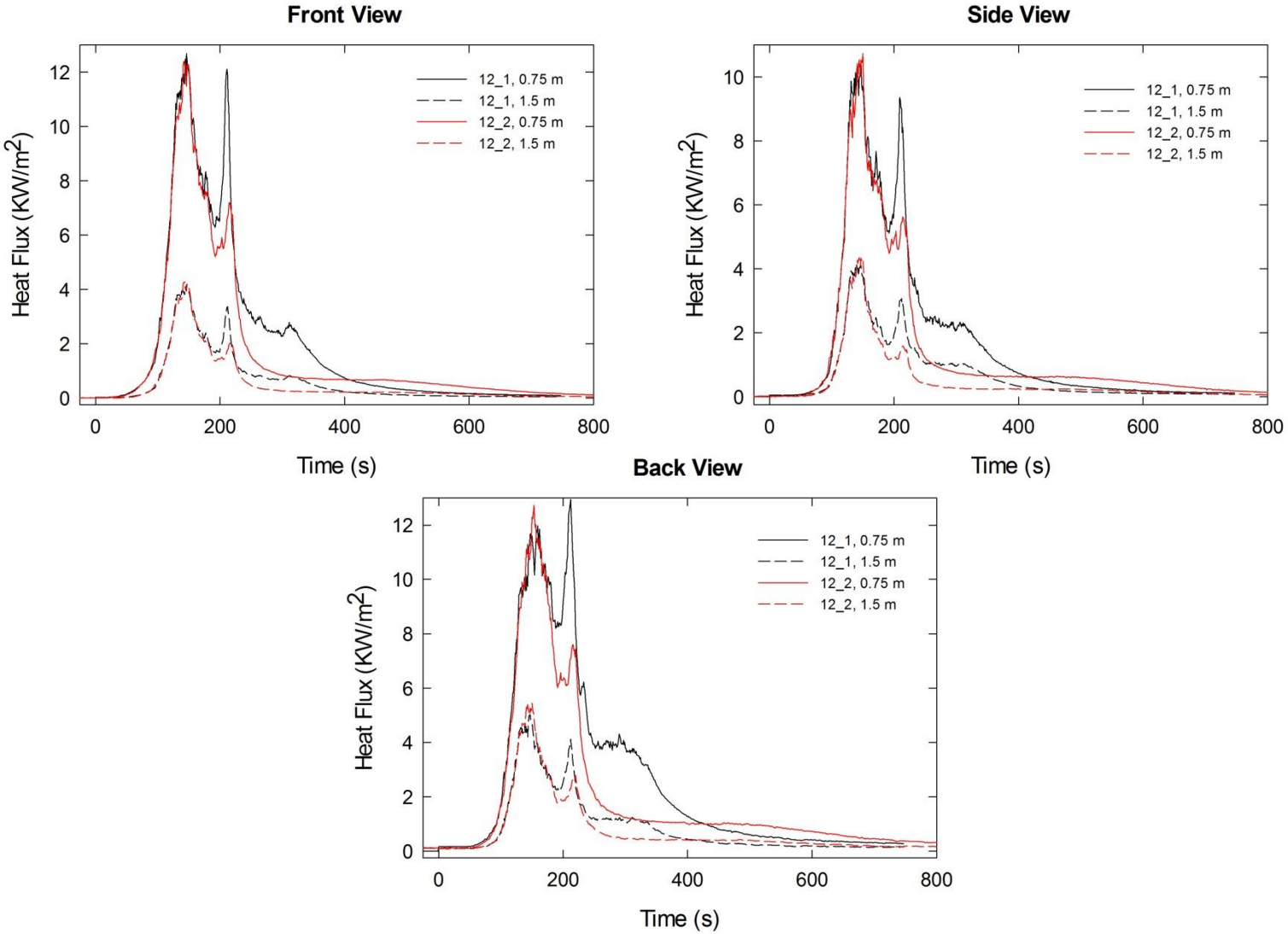

Figure A-82. Heat fluxes recorded at distances of 0.75 m and 1.5 m are plotted as a function of time for locations to the front, side and rear of the mock-up for Combination 12 tests following application of Ignition Source 1.

A.9 Combination 13

cotton/FRFPUF

Notes:

Test 1:

Ignition Source 1 applied at time = 0 s; flame spread over only part of back and top of right-arm cushion; no blackening on seat cushion.

Ignition Source 2 applied 1434 s after Ignition Source 1.

Heat release rate measurement gave negative readings at end of test.

Test 2:

Ignition Source 1 applied at time = 0 s

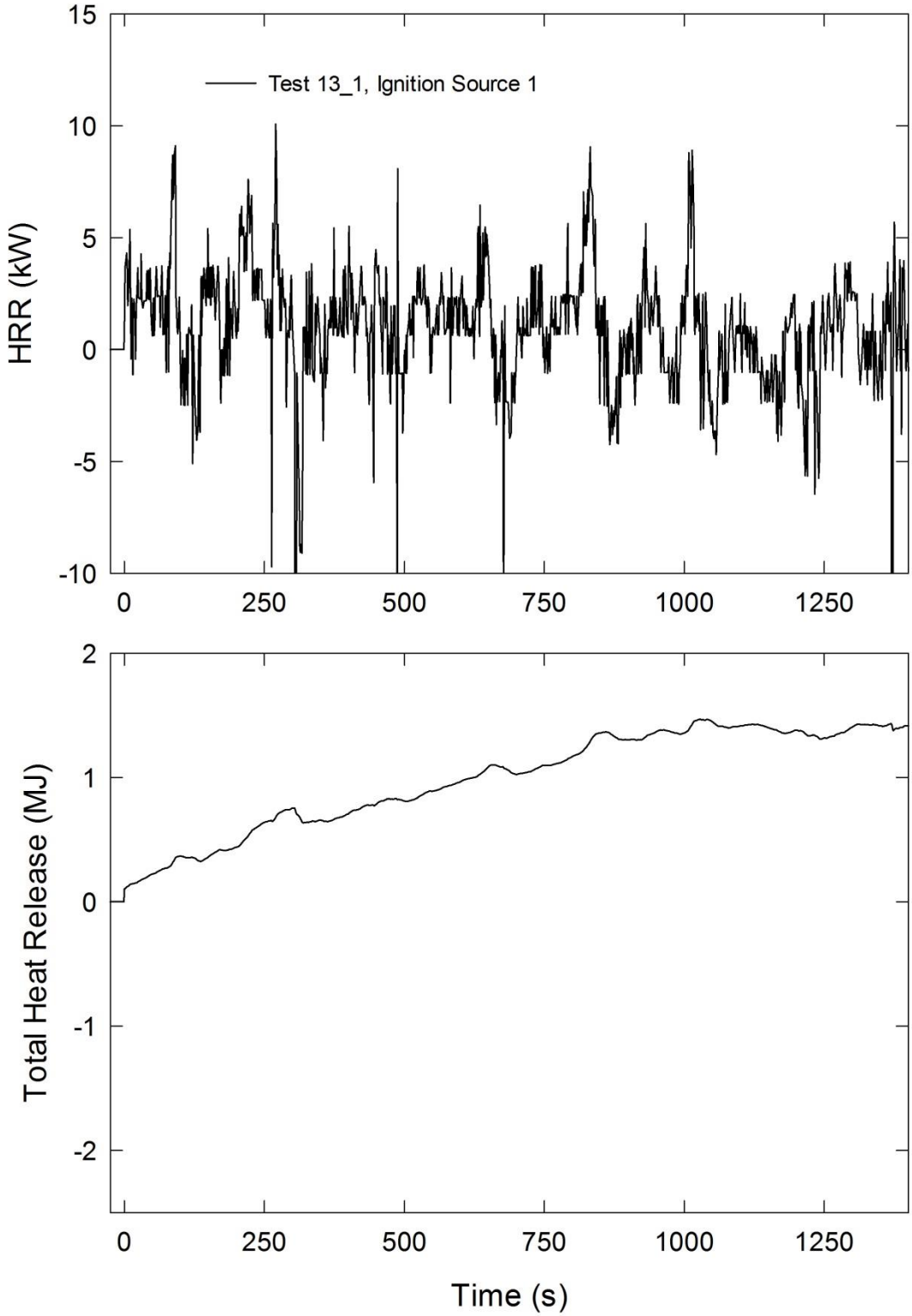

Figure A-83. Temporal profiles of HRR and integrated HRR are shown for Test 13_1 tests following application of Ignition Source 1.

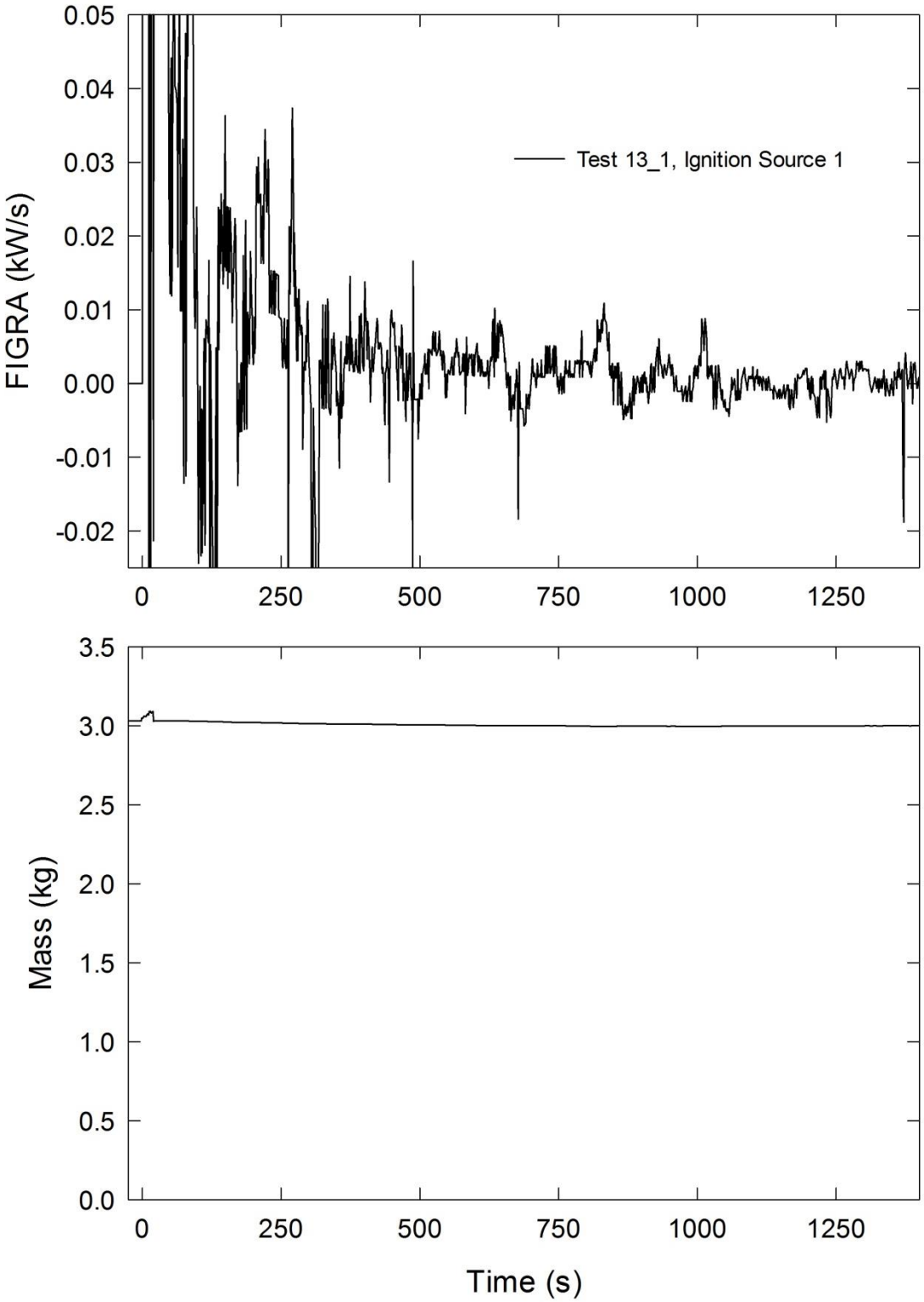

Figure A-84. Temporal profiles of FIGRA and mock-up mass are shown for Test 13_1 following application of Ignition Source 1.

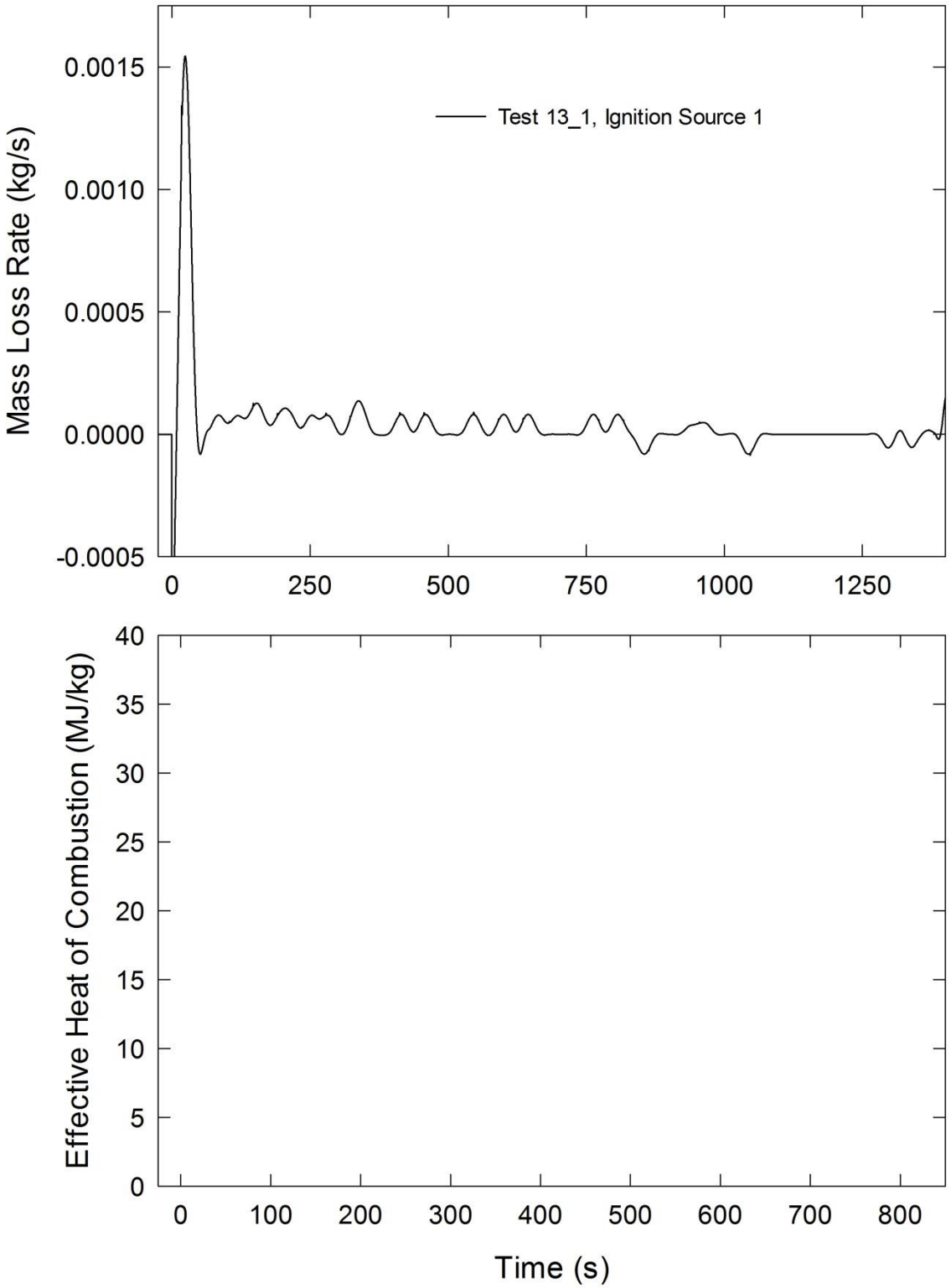

Figure A-85. The temporal profile of MLR is shown for Test 13_1 following application of Ignition Source 1.

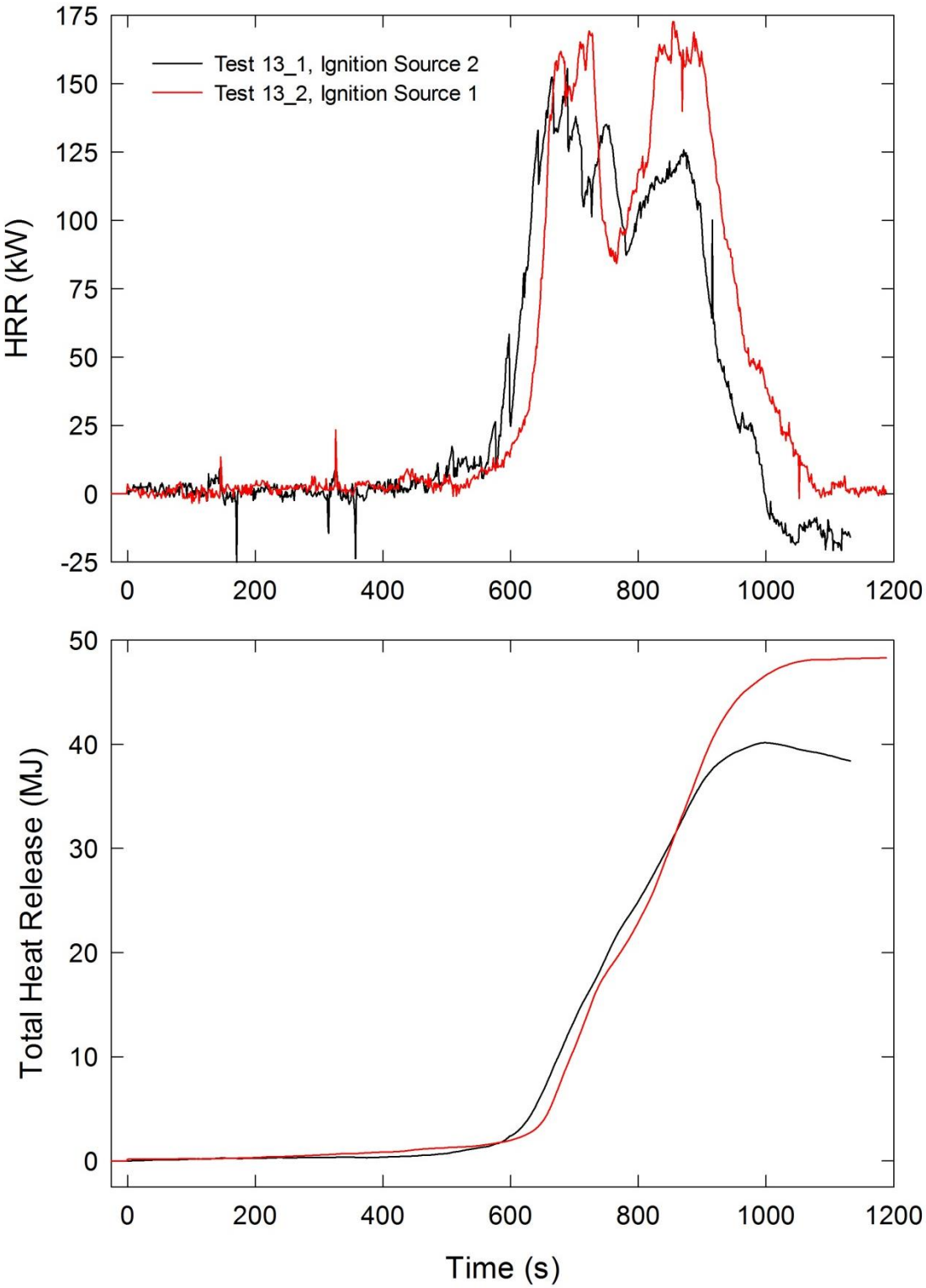

Figure A-86. Temporal profiles of HRR and integrated HRR are shown for Test 13_1 following application of Ignition Source 2 and Test 13_2 following application of Ignition Source 1.

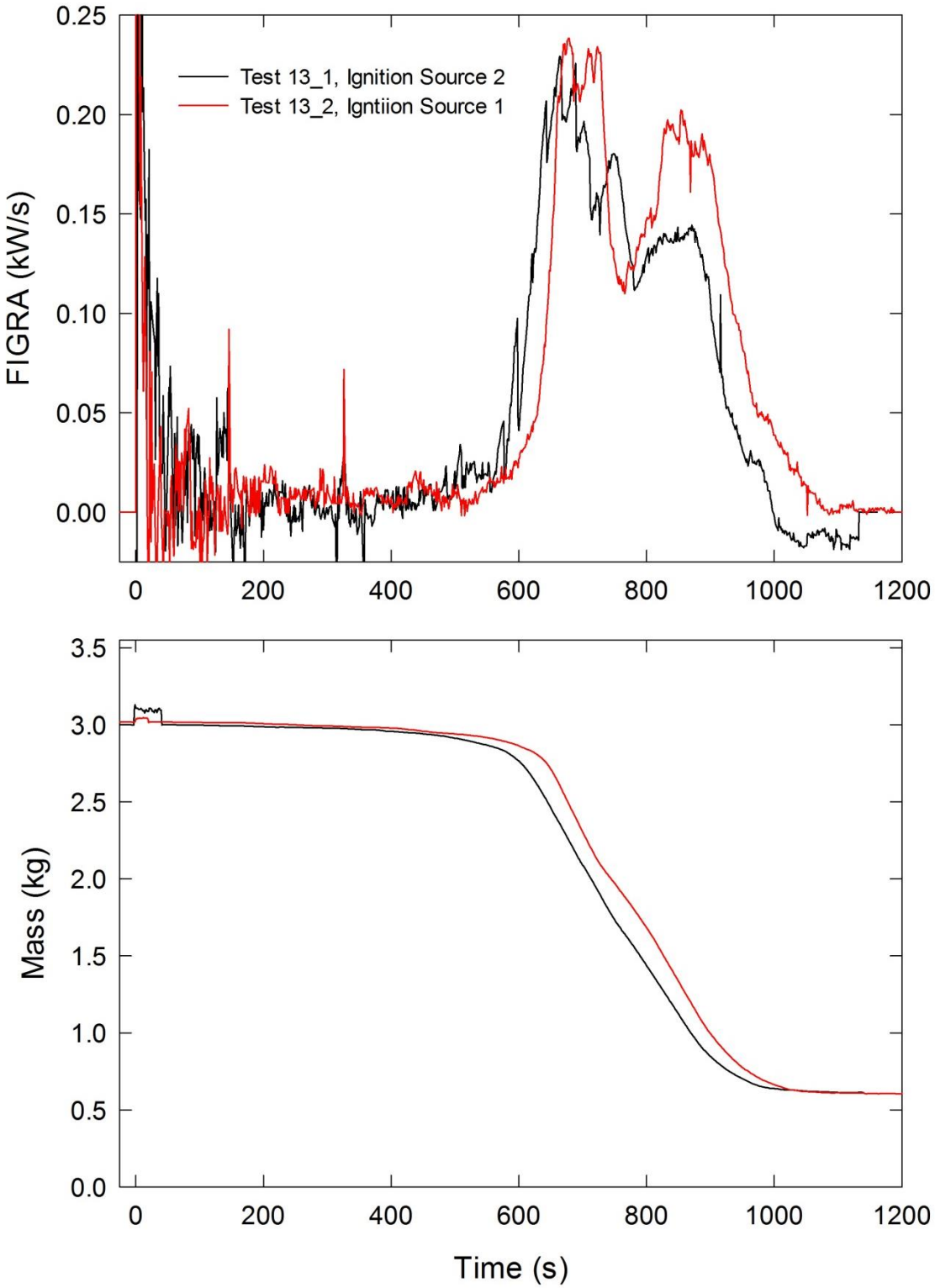

Figure A-87. Temporal profiles of FIGRA and mock-up mass are shown for Test 13_1 following application of Ignition Source 2 and Test 13_2 following application of Ignition Source 1.

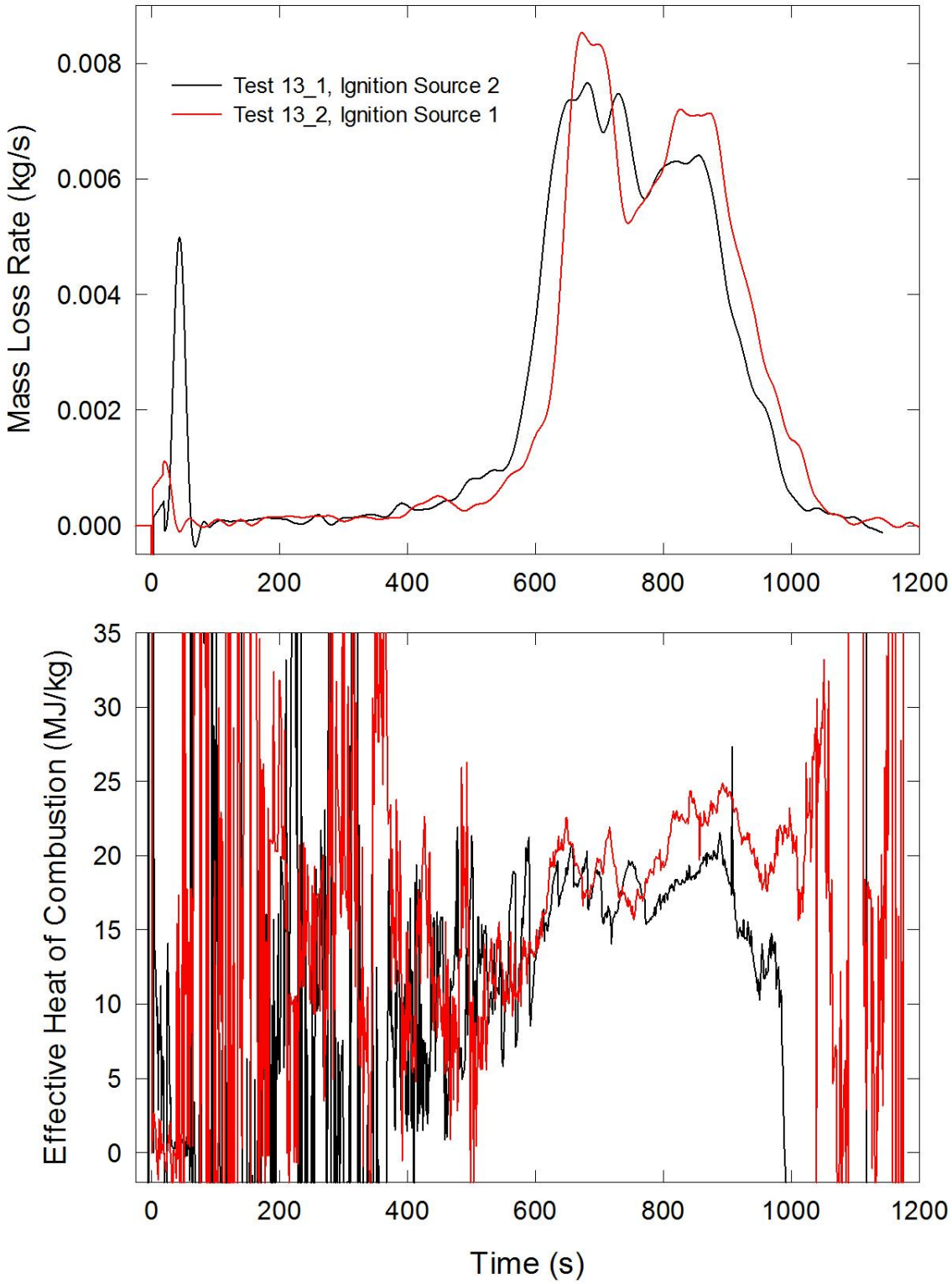

Figure A-88. Temporal profiles of MLR and EHOC are shown for Test 13_1 following application of Ignition Source 2 and Test 13_2 following application of Ignition Source 1.

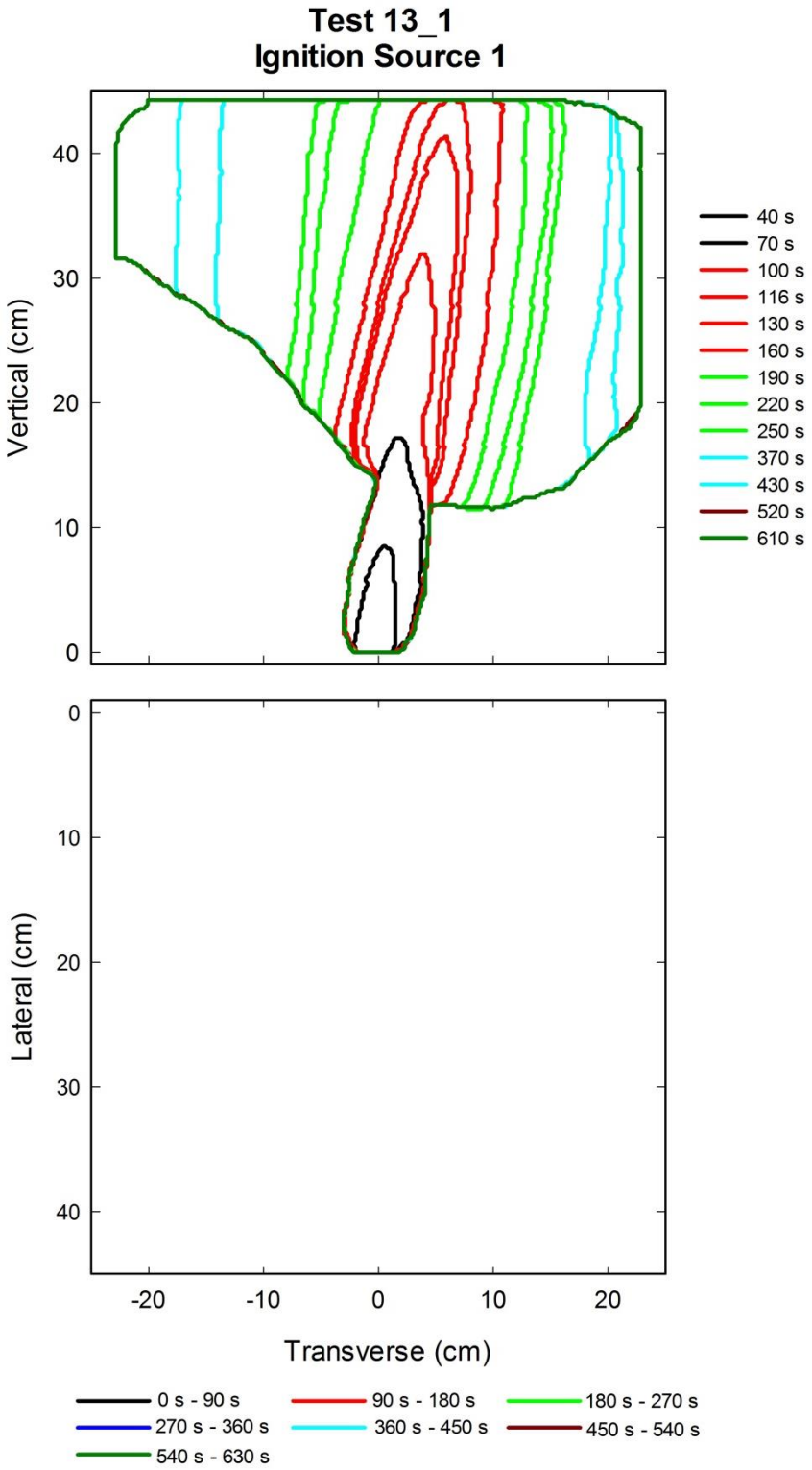

Figure A-89. Flame edge contours on the back (top) and seat (bottom) cushions are plotted as a function of time for Test 13_1 following application of Ignition Source 1.

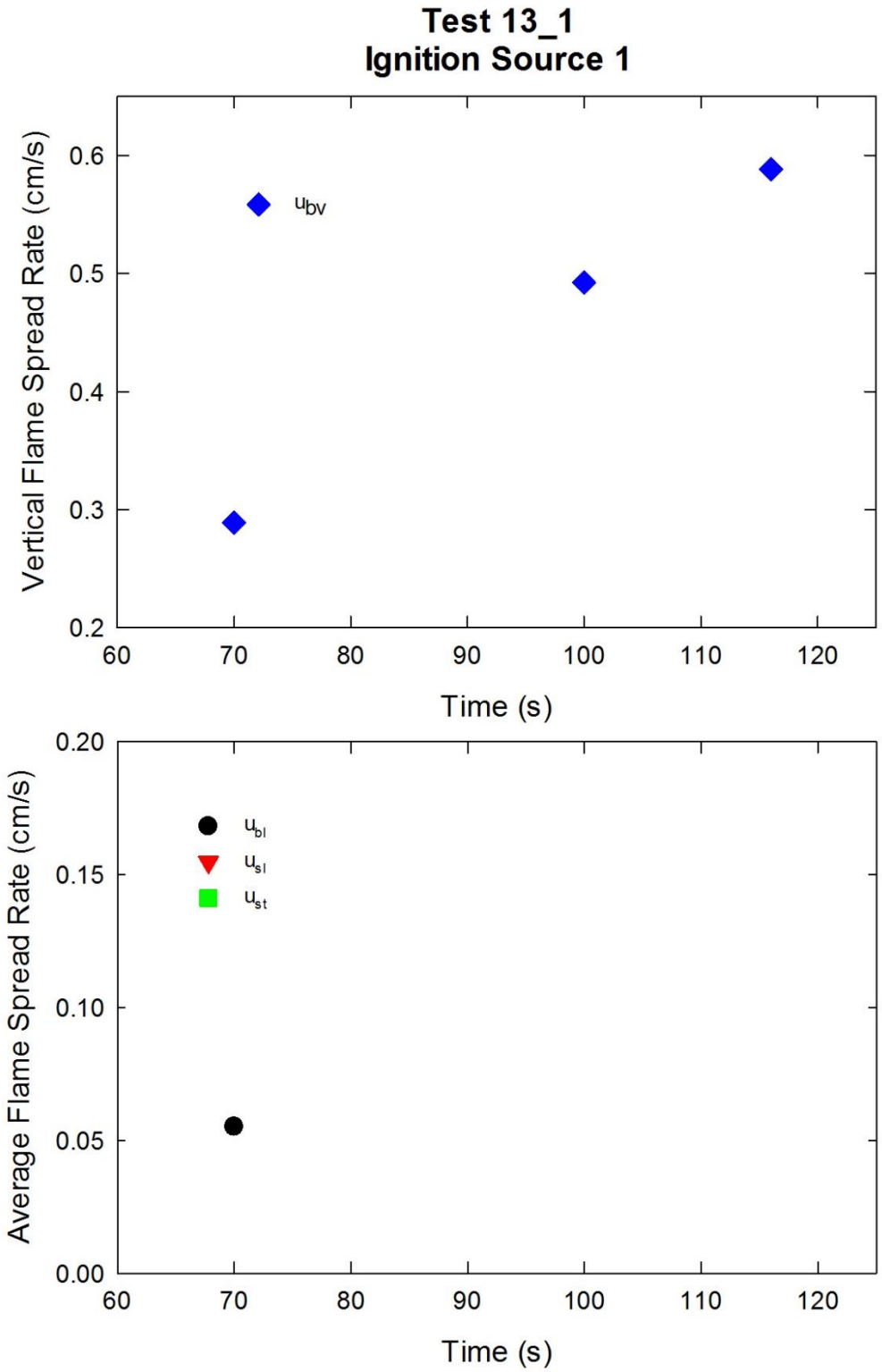

Figure A-90. Vertical flame spread rate on the back cushion (top) and average lateral flame spread rates on the back and seat cushions and transverse flame spread rate on the seat cushion (bottom) are plotted as a function of time for Test 13_1 following application of Ignition Source 1.

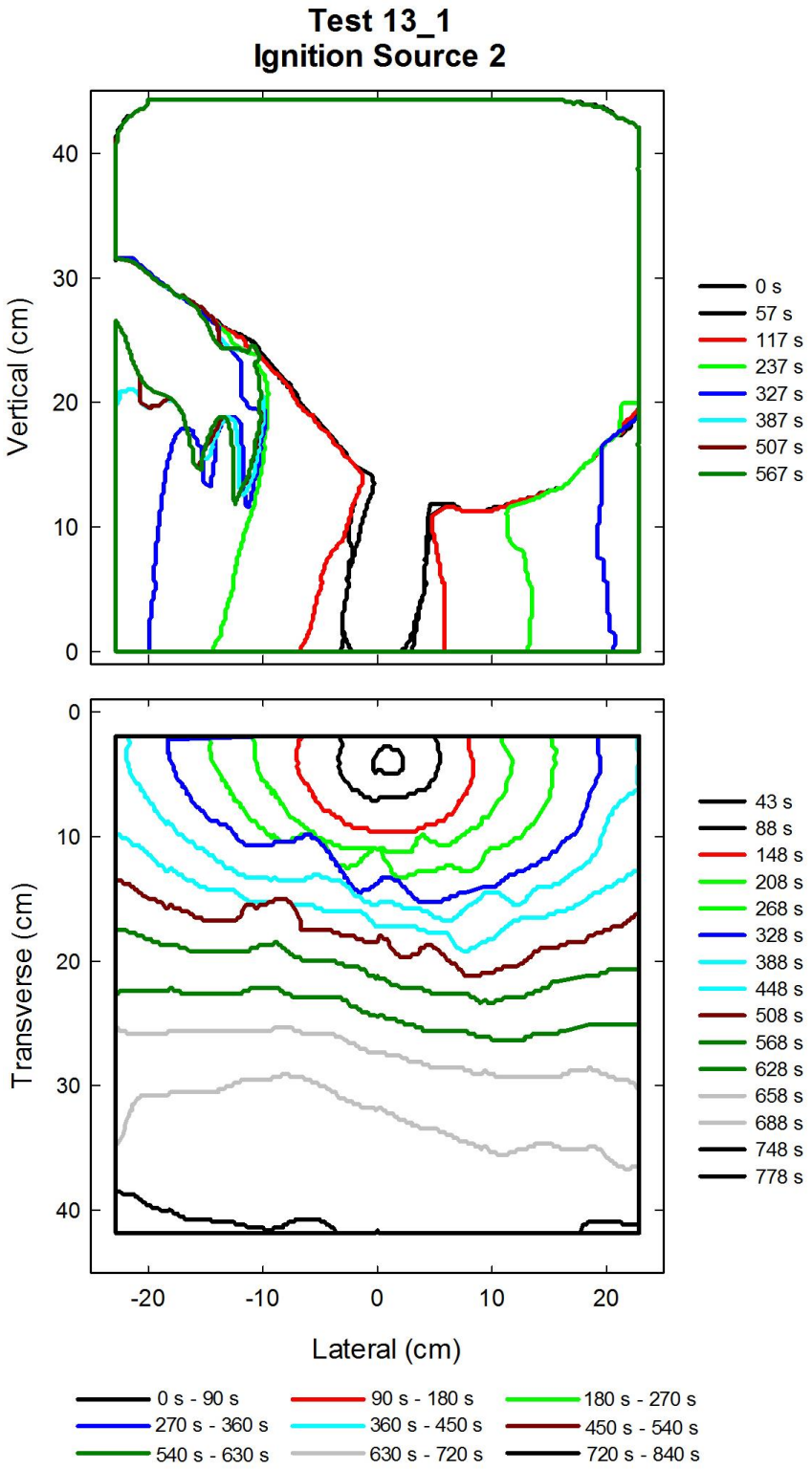

Figure A-91. Flame edge contours on the back (top) and seat (bottom) cushions are plotted as a function of time for Test 13_1 following application of Ignition Source 2.

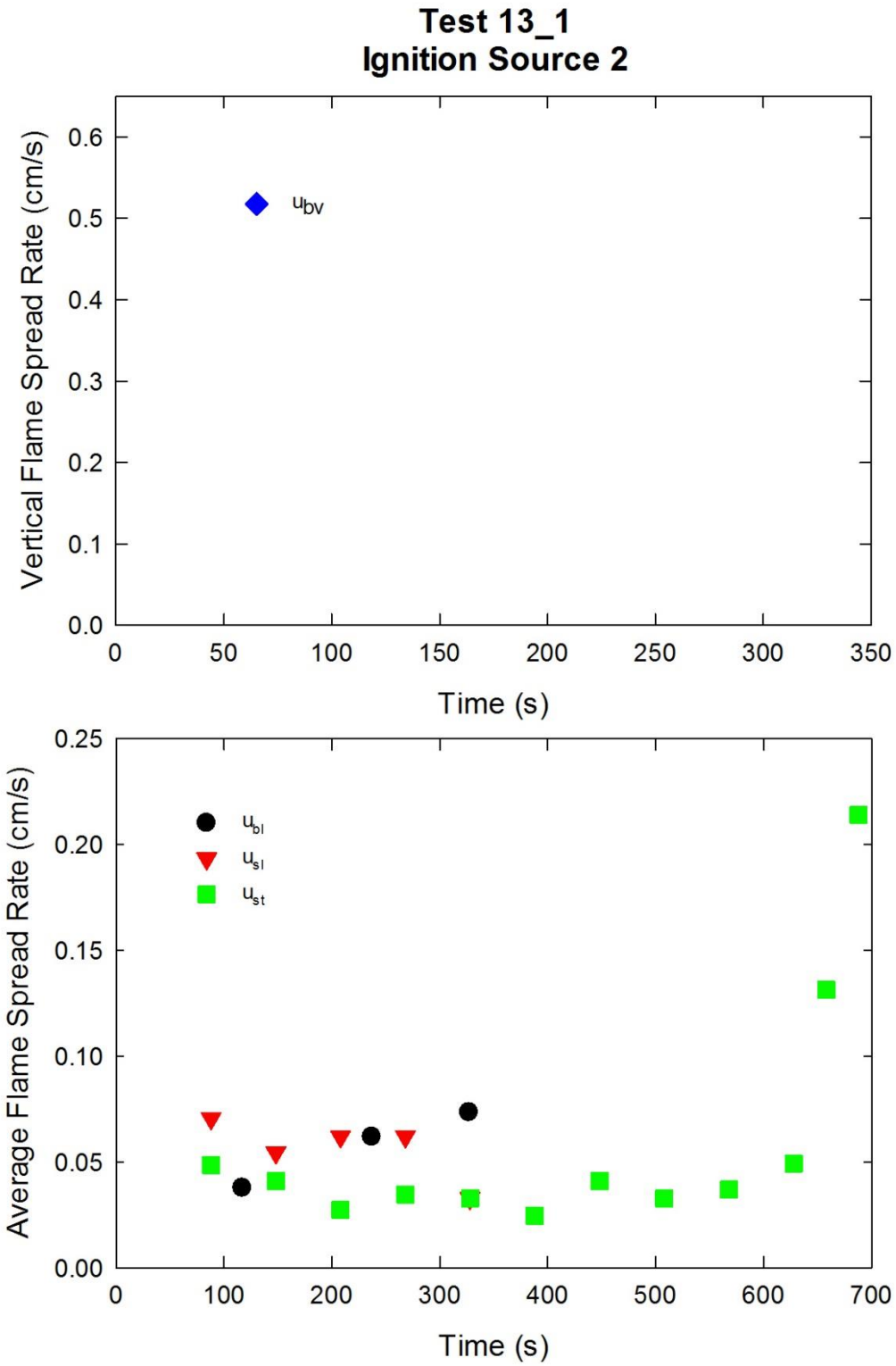

Figure A-92. Vertical flame spread rate on the back cushion (top) and average lateral flame spread rates on the back and seat cushions and transverse flame spread rate on the seat cushion (bottom) are plotted as a function of time for Test 13_1 following application of Ignition Source 2.

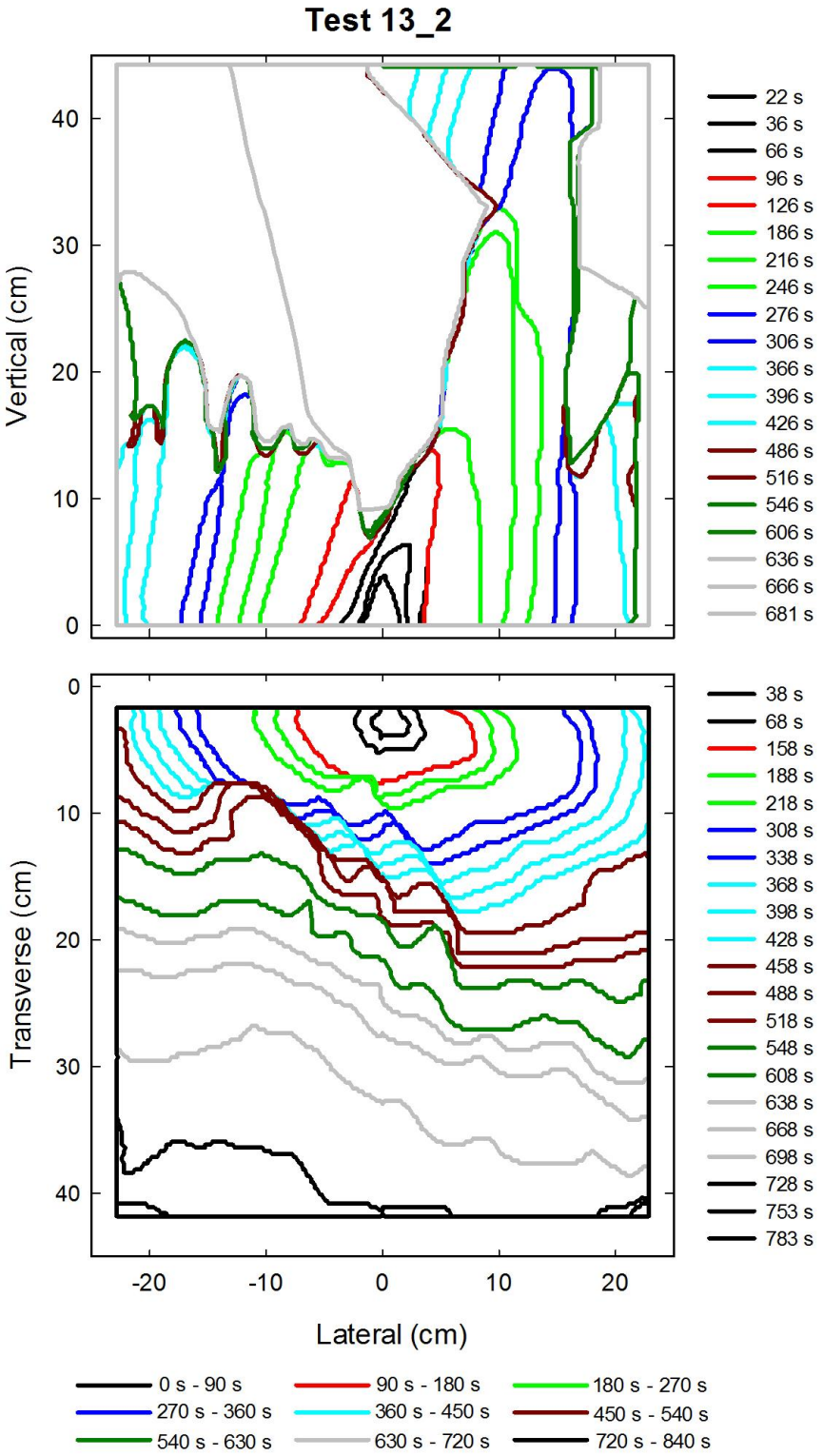

Figure A-93. Flame edge contours on the back (top) and seat (bottom) cushions are plotted as a function of time for Test 13_2 following application of Ignition Source 1.

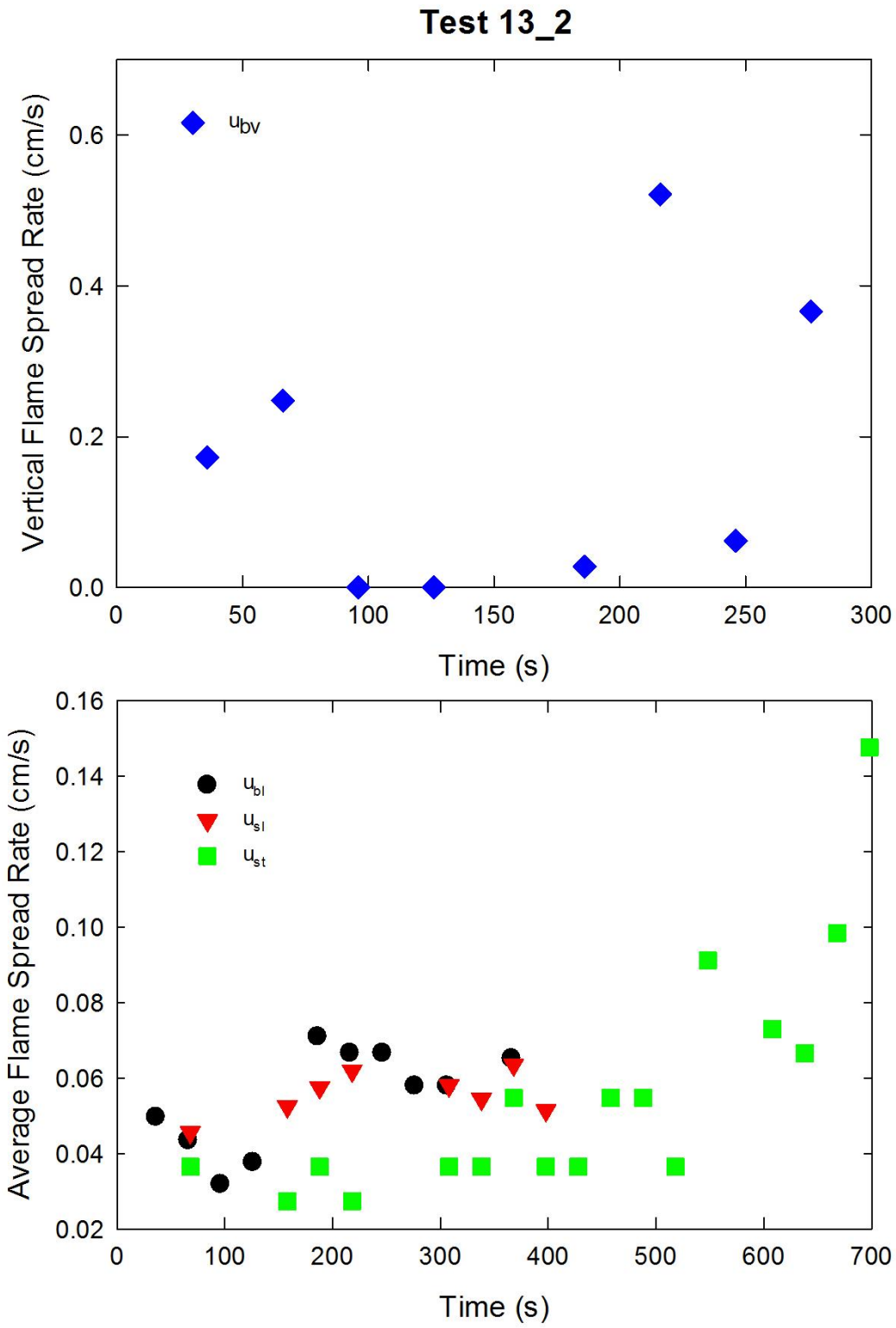

Figure A-94. Vertical flame spread rate on the back cushion (top) and average lateral flame spread rates on the back and seat cushions and transverse flame spread rate on the seat cushion (bottom) are plotted as a function of time for Test 13_2 following application of Ignition Source 1.

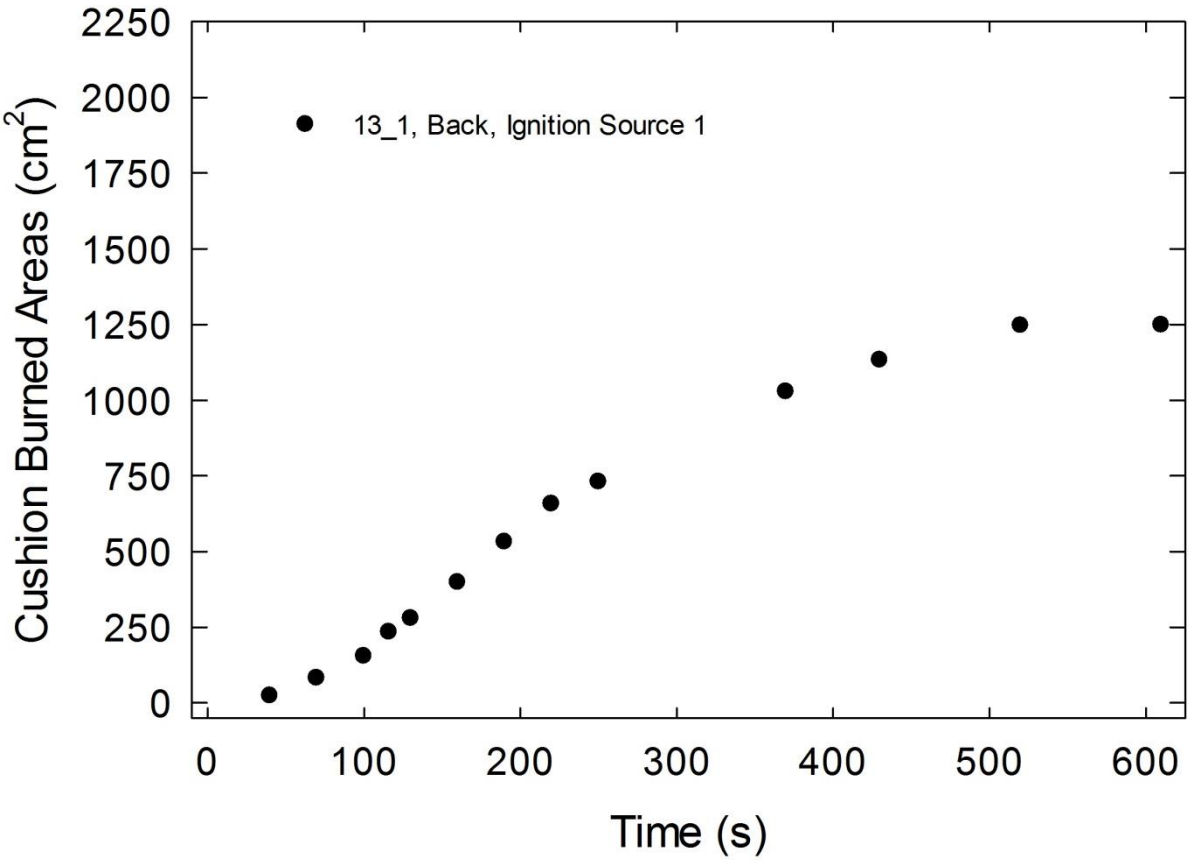

Figure A-95. Burned areas on the back cushion are plotted as a function of time for Test 13_1 following application of Ignition Source 1.

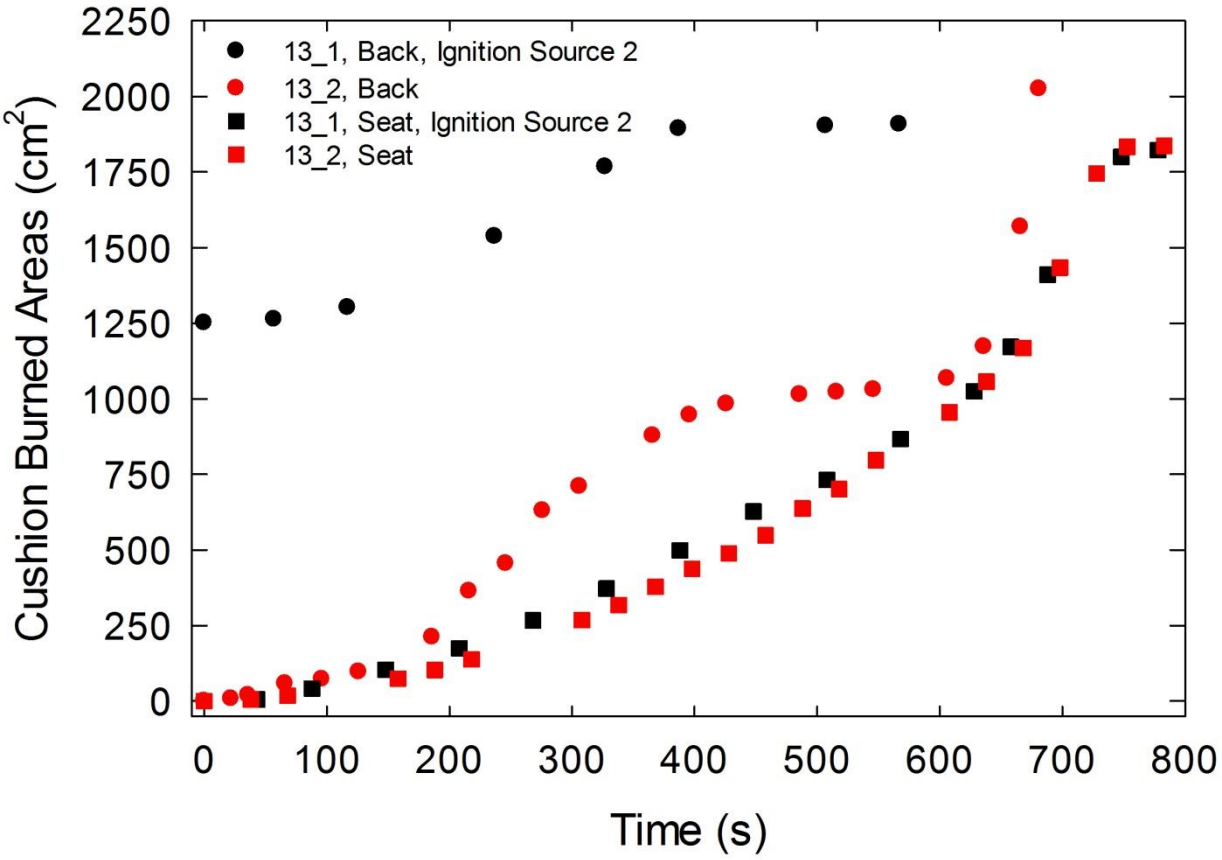

Figure A-96. Burned areas on the seat and back cushions are plotted as a function of time for Test 13_1 following application of Ignition Source 2 and Test 13_2 following application of Ignition Source 1.

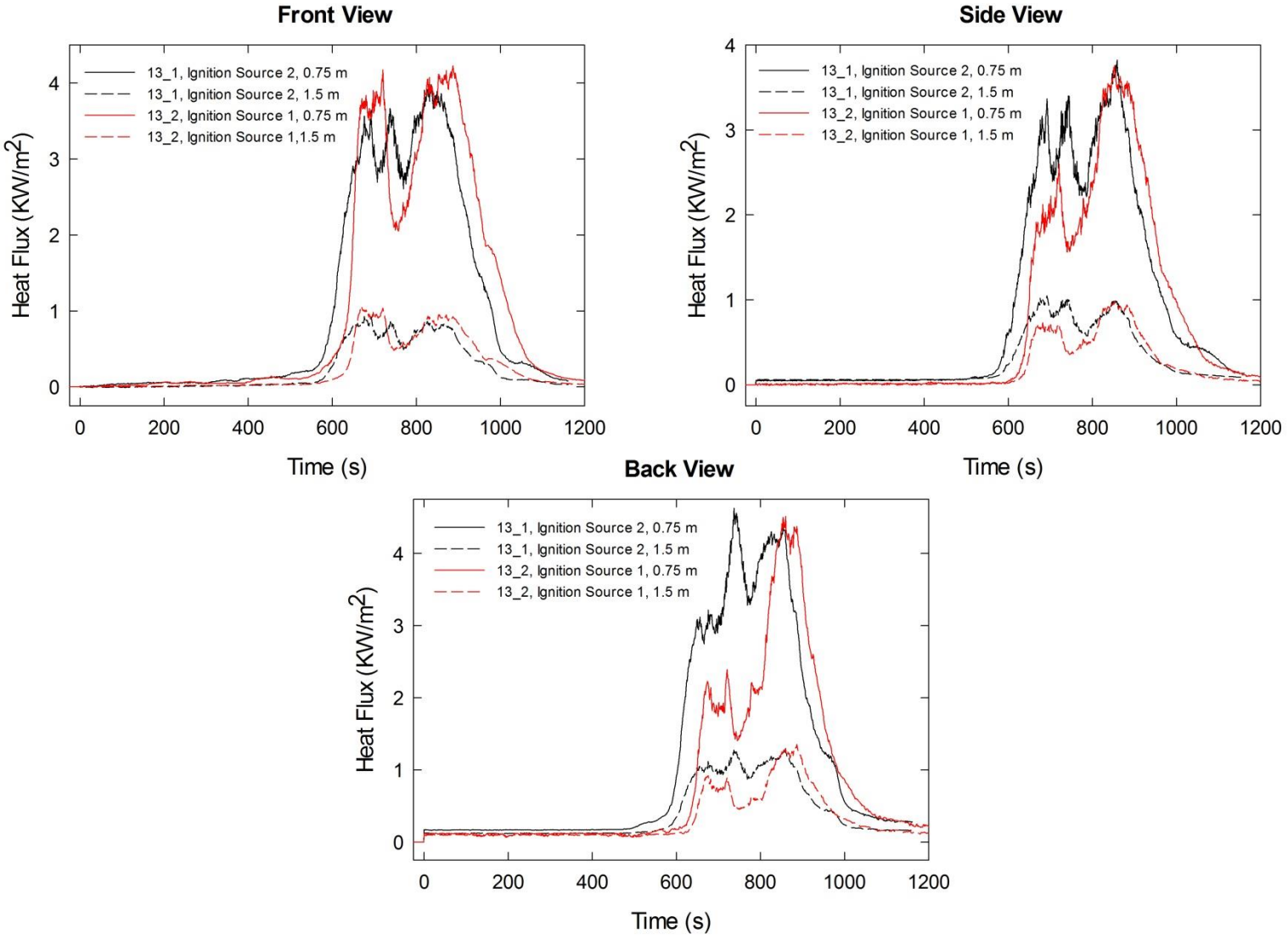

Figure A-97. Heat fluxes recorded at distances of 0.75 m and 1.5 m are plotted as a function of time for locations to the front, side and rear of the mock-up for Test 13_1 following application of Ignition Source 2 and Test 13_2 following application of Ignition Source 1.

A.10 Combination 14

78%PP/22%PE/FRFPUF

Notes:

Test 1:

Ignition Source 1 applied at time = 0 s

Test 2:

Ignition Source 1 applied at time = 0 s

Initial mass reading (3.35 kg) during the experiment disagreed with an earlier measurement for the mock-up (3.04 kg); mass readings during the test were smooth, physically reasonable, and correlated with the HRR; **these mass data were adjusted by subtracting 0.303 kg from their values and were included in the analysis**.

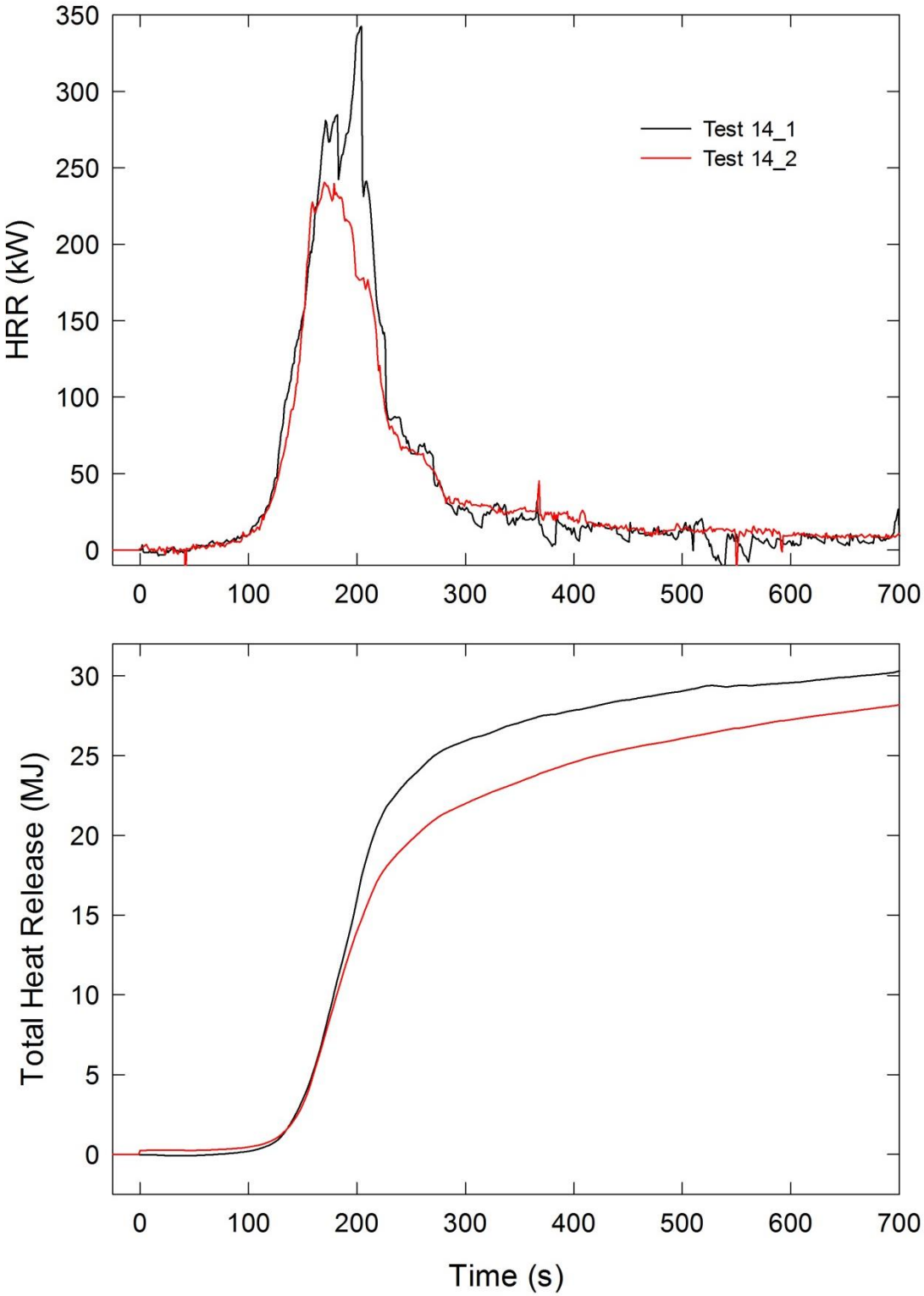

Figure A-98. Temporal profiles of HRR and integrated HRR are shown for Combination 14 tests following application of Ignition Source 1.

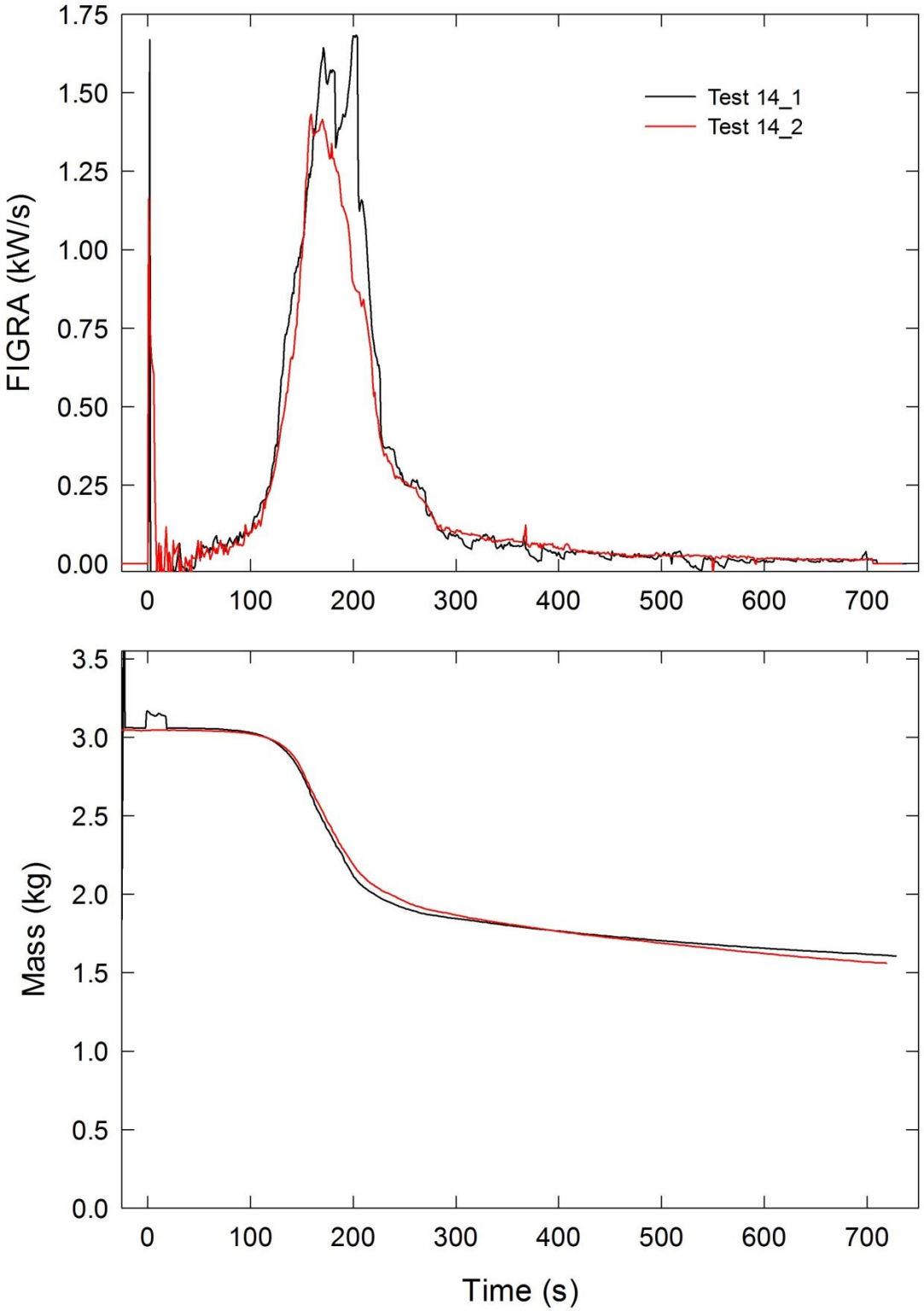

Figure A-99. Temporal profiles of FIGRA and mock-up mass for Combination 14 tests are shown following application of Ignition Source 1.

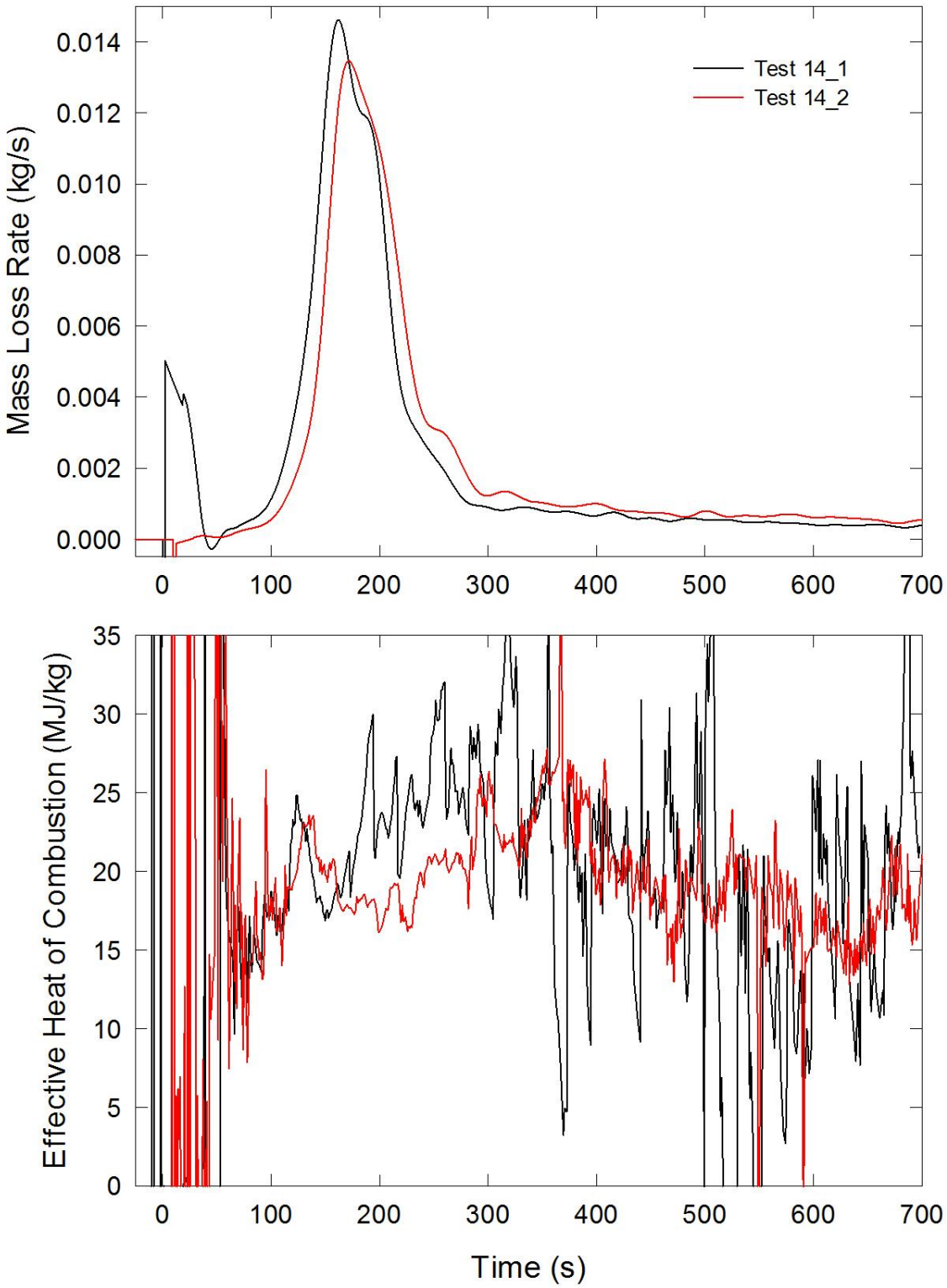

Figure A-100. Temporal profiles of MLR and EHOC are shown for Combination 14 tests following application of Ignition Source 1.

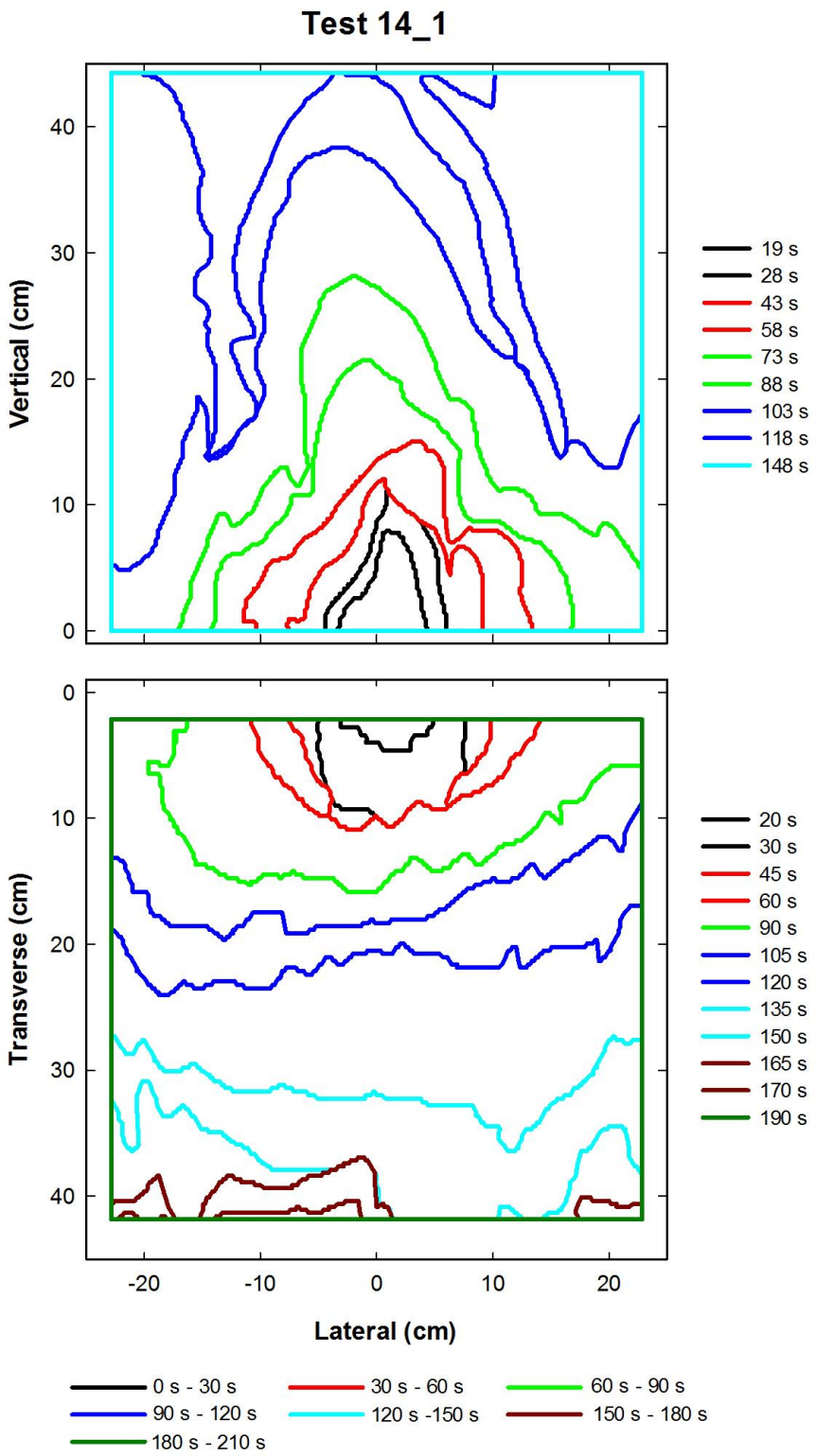

Figure A-101. Flame edge contours on the back (top) and seat (bottom) cushions are plotted as a function of time for Test 14_1 following application of Ignition Source 1.

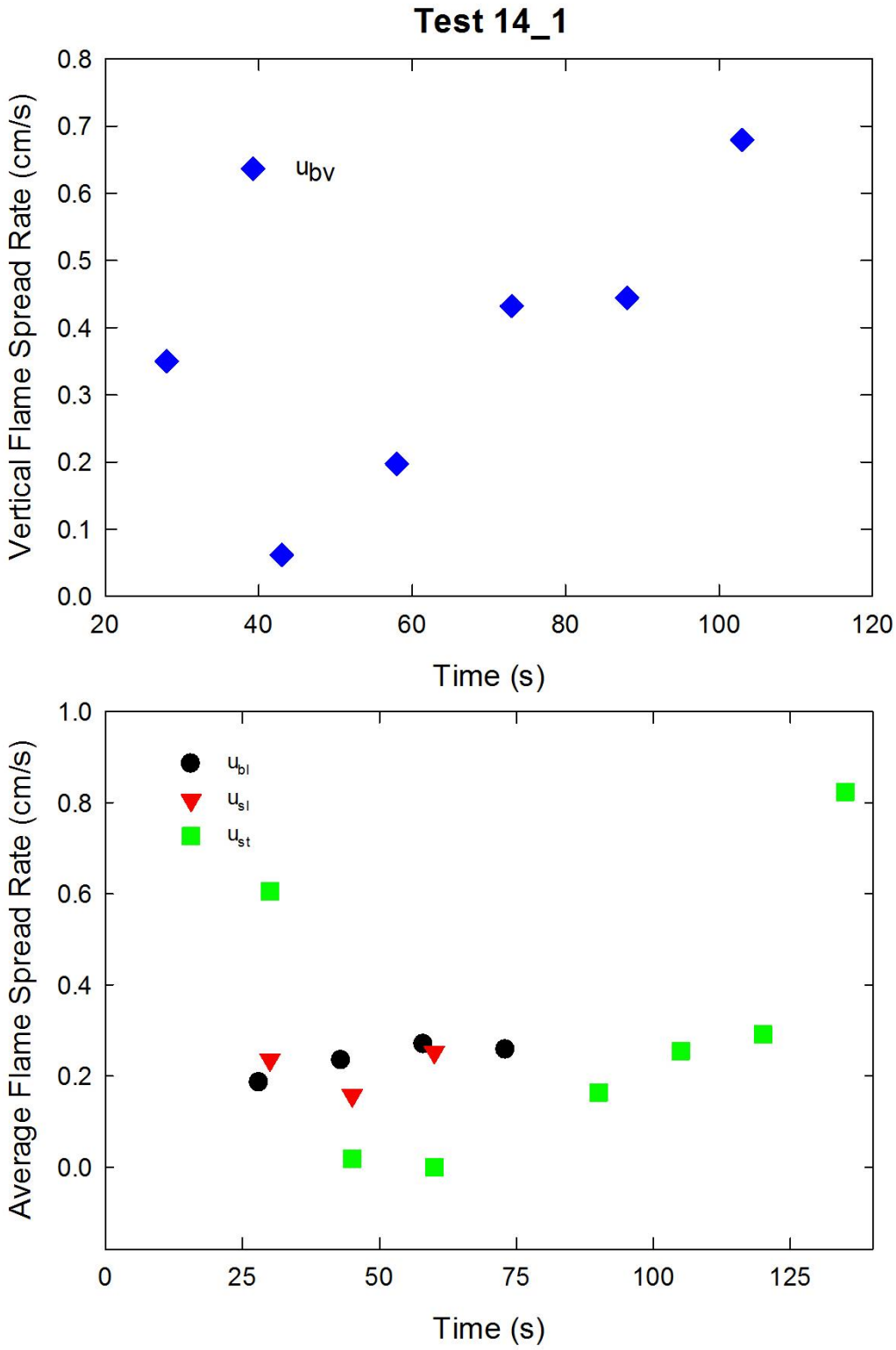

Figure A-102. Vertical flame spread rate on the back cushion (top) and average lateral flame spread rates on the back and seat cushions and transverse flame spread rate on the seat cushion (bottom) are plotted as a function of time for Test 14_1 following application of Ignition Source 1.

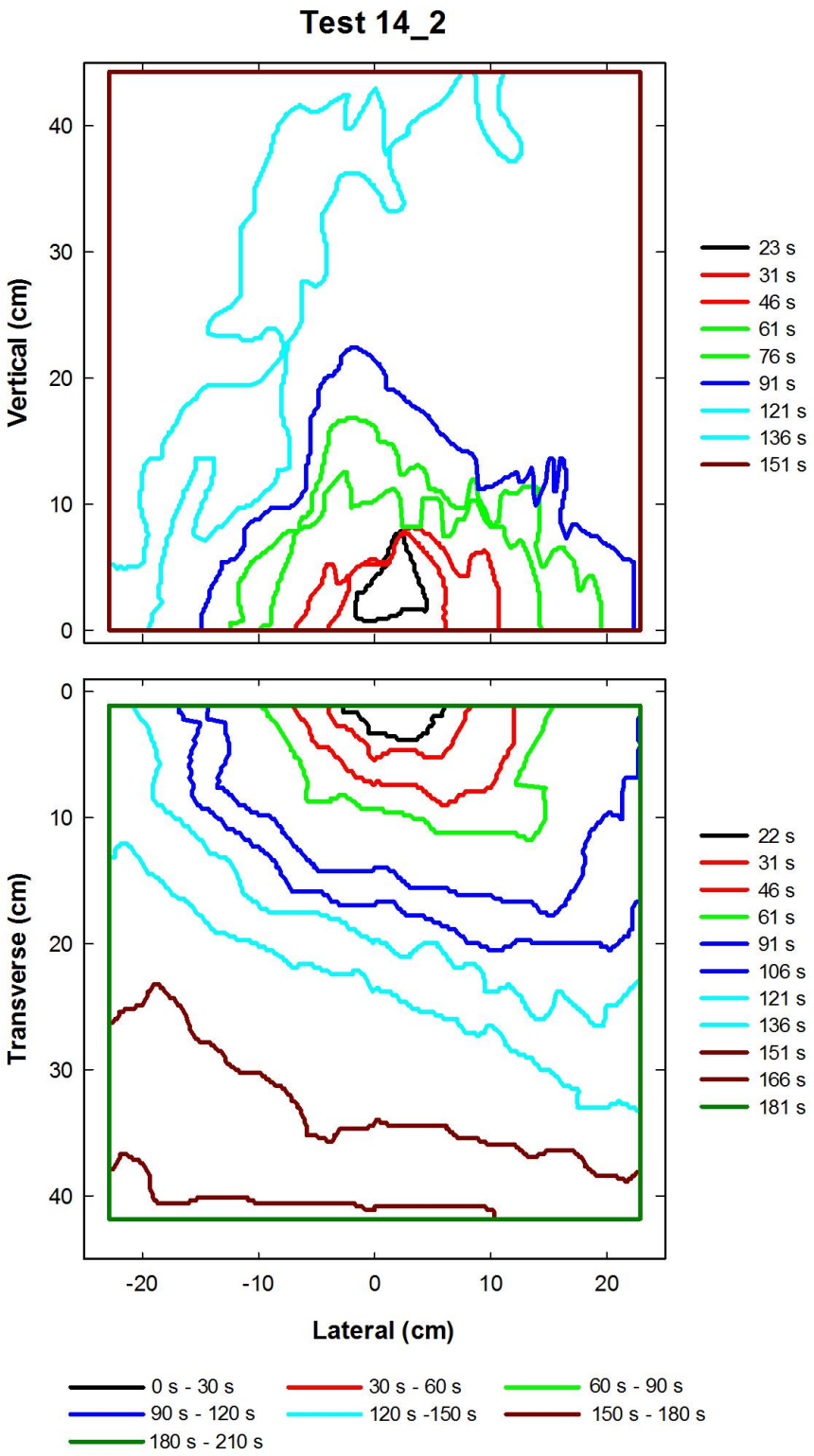

Figure A-103. Flame edge contours on the back (top) and seat (bottom) cushions are plotted as a function of time for Test 14_2 following application of Ignition Source 1.

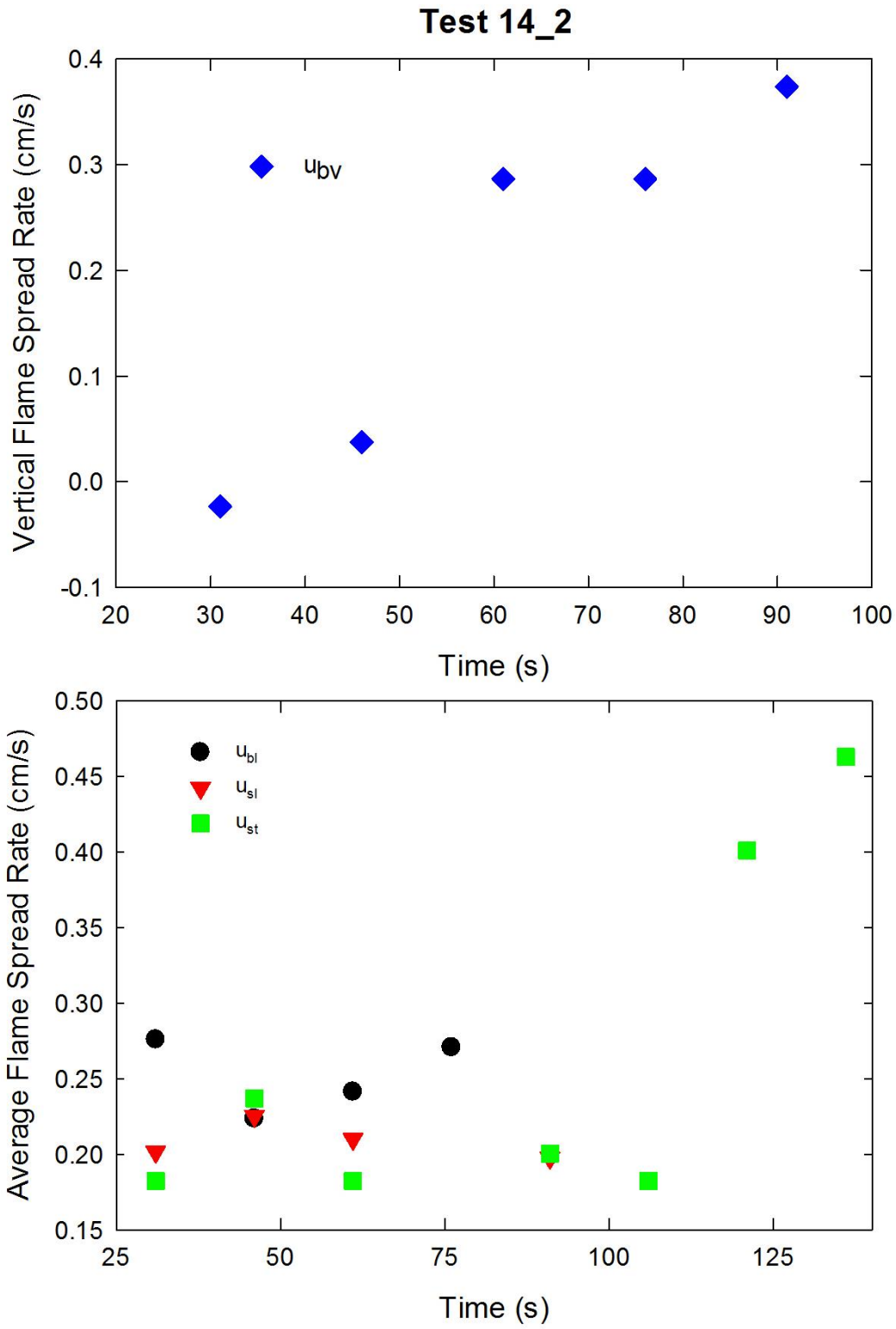

Figure A-104. Vertical flame spread rate on the back cushion (top) and average lateral flame spread rates on the back and seat cushions and transverse flame spread rate on the seat cushion (bottom) are plotted as a function of time for Test 14_2 following application of Ignition Source 1.

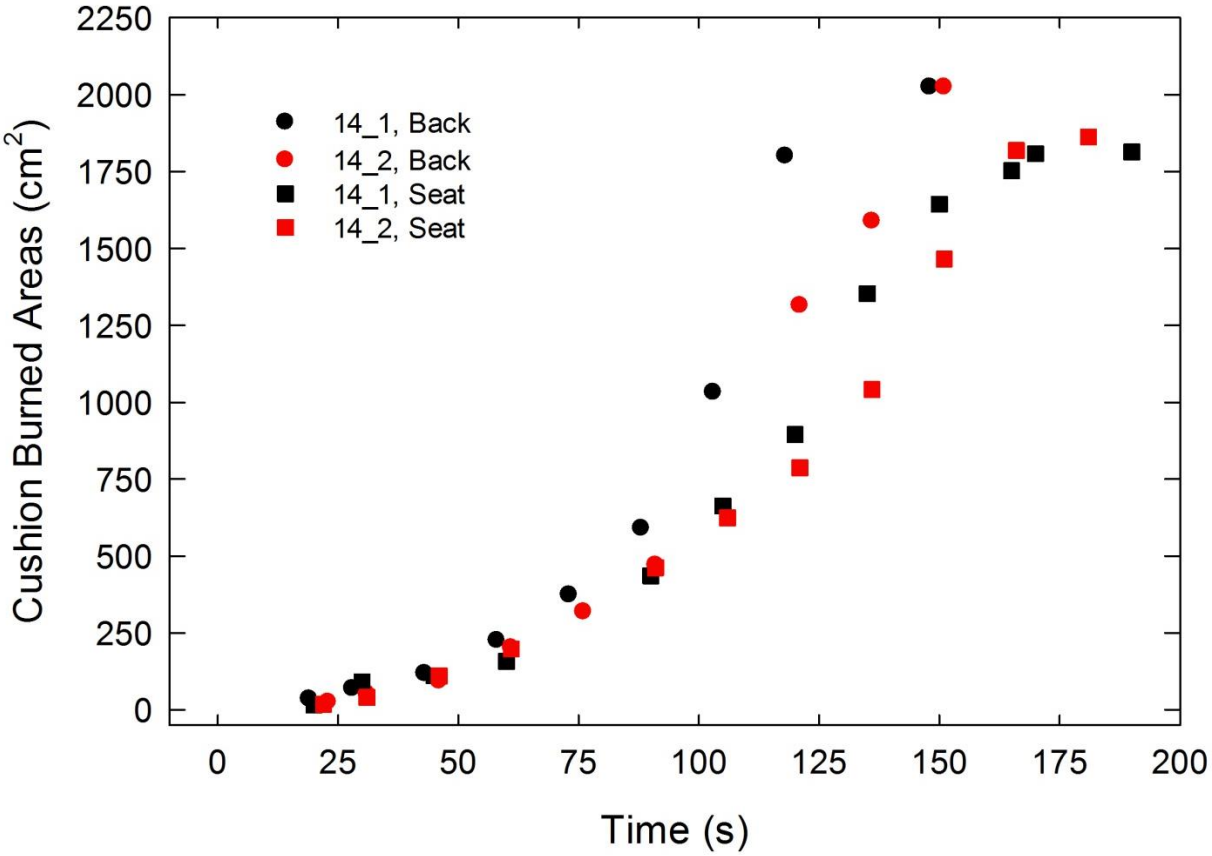

Figure A-105. Burned areas on the seat and back cushions are plotted as a function of time for Combination 14 tests following application of Ignition Source 1.

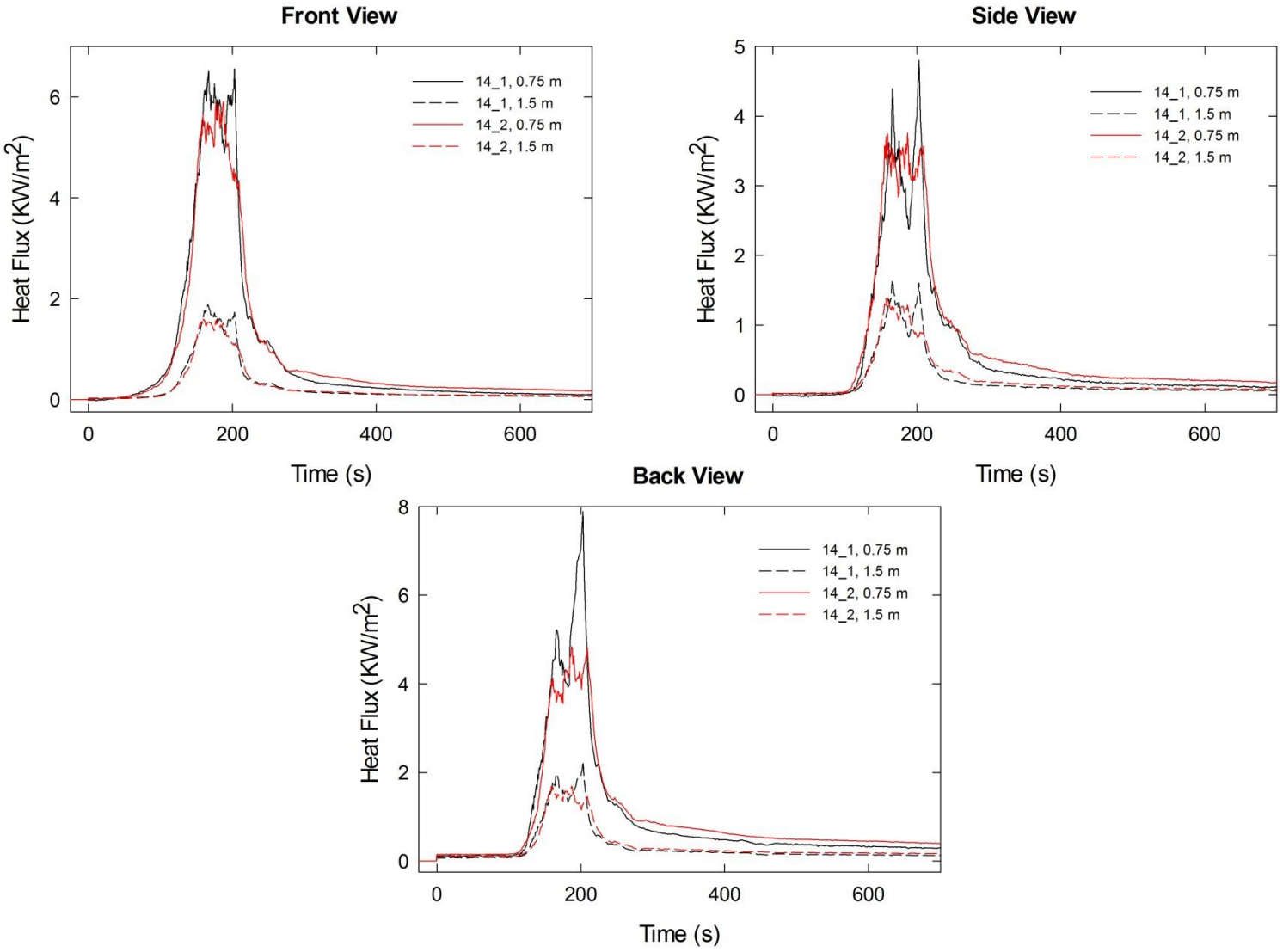

Figure A-106. Heat fluxes recorded at distances of 0.75 m and 1.5 m are plotted as a function of time for locations to the front, side and rear of the mock-up for Combination 14 tests following application of Ignition Source 1.

A.11 Combination 15

cotton/PEFW/FRFPUF

Notes:

Test 1:

Ignition Source 1 applied at time = 0 s; following removal of ignition source, upward and slower lateral flame spread on back cushion, but no darkening on seat cushion; a black area appeared on seat ≈ 3.8 cm to right of flame application point at ≈ 195 s and began to spread.

Test 2:

Ignition Source 1 applied at time = 0 s; black marks present on both the seat and back cushion surfaces, but no obvious flame spread.

Ignition Source 2 applied 87 s after Ignition Source 1.

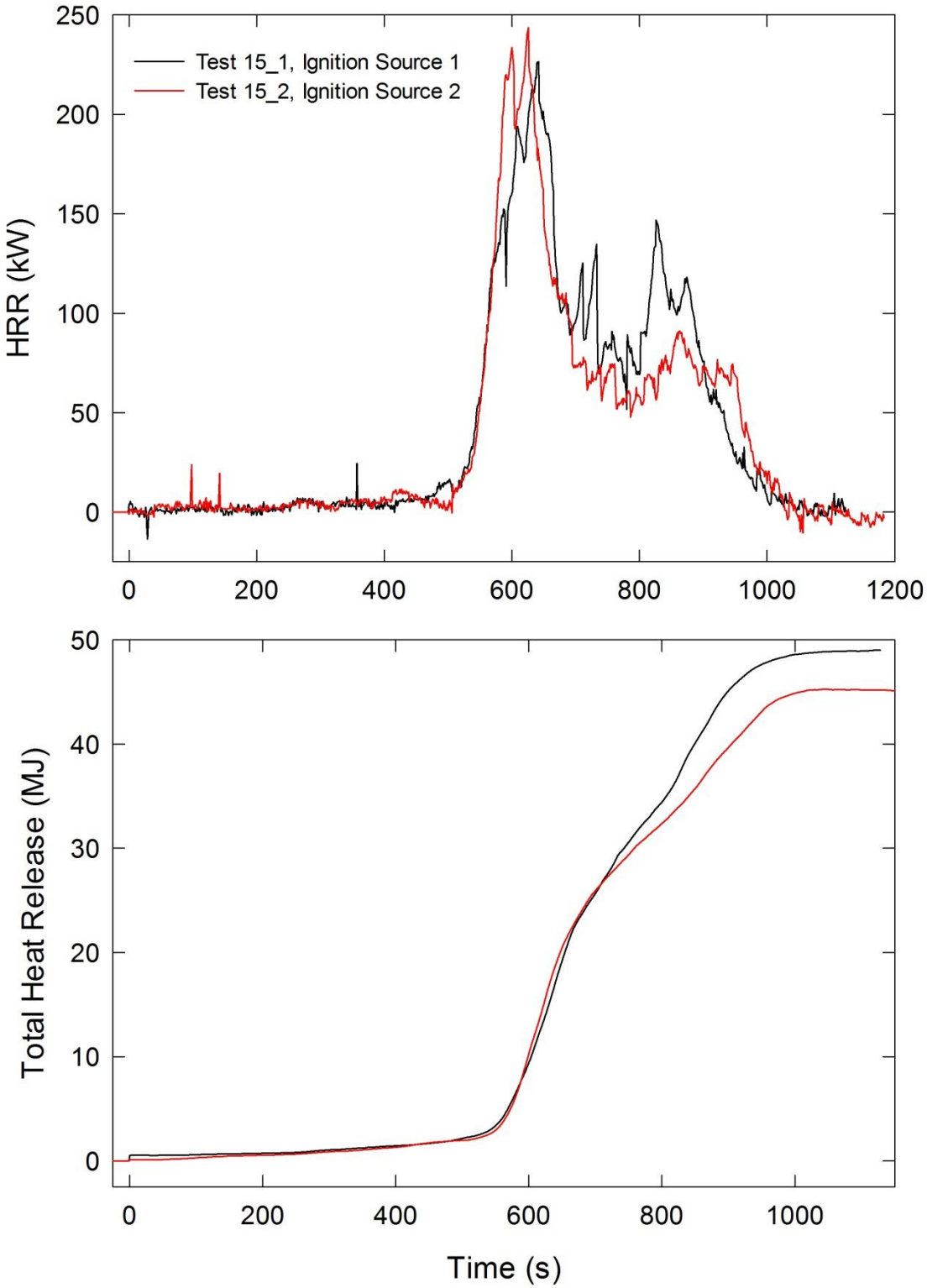

Figure A-107. Temporal profiles of HRR and integrated HRR are shown for Test 15_1 following application of Ignition Source 1 and Test 15_2 following application of Ignition Source 2.

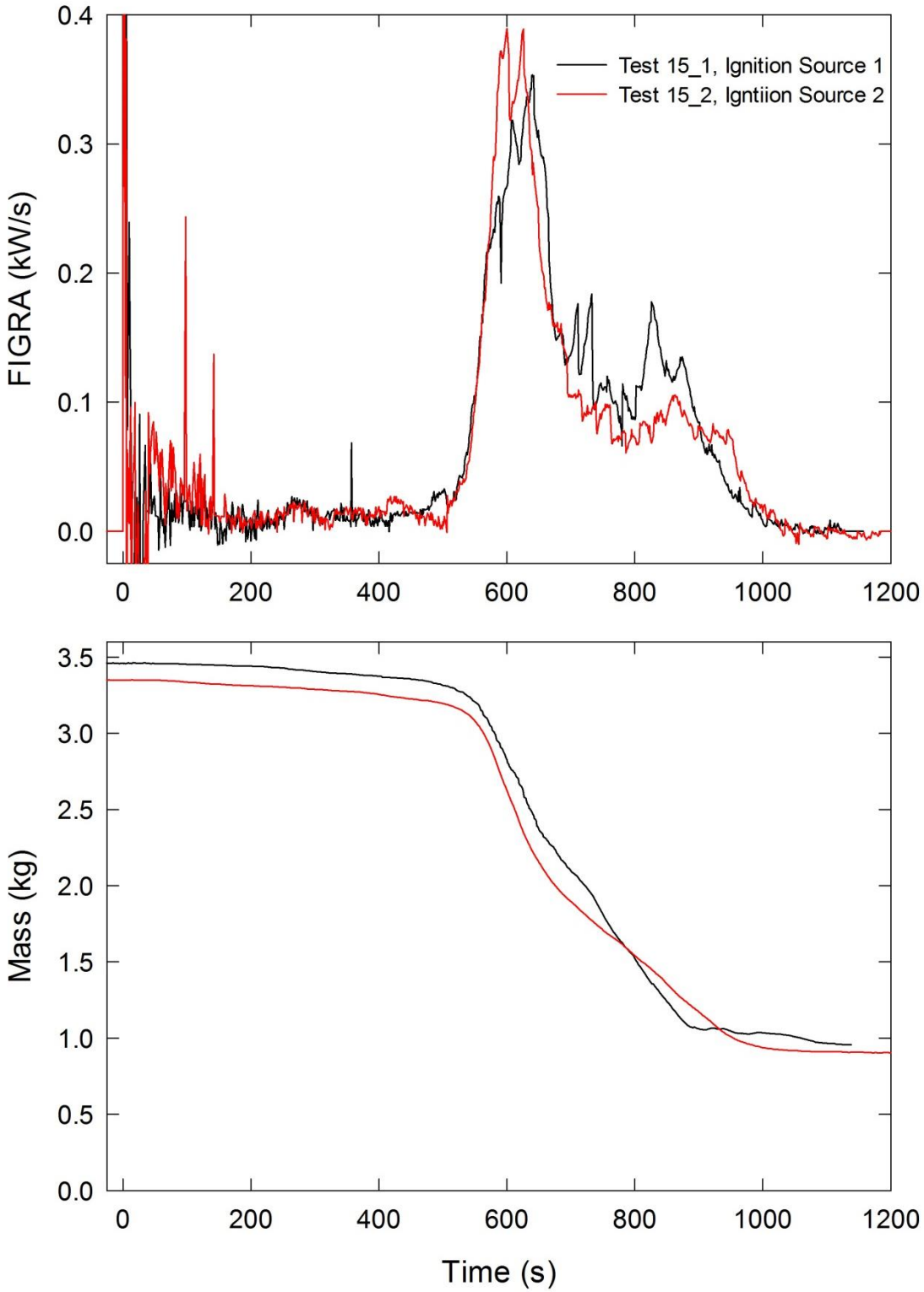

Figure A-108. Temporal profiles of FIGRA and mock-up mass are shown for Test 15_1 following application of Ignition Source 1 and Test 15_2 following application of Ignition Source 2.

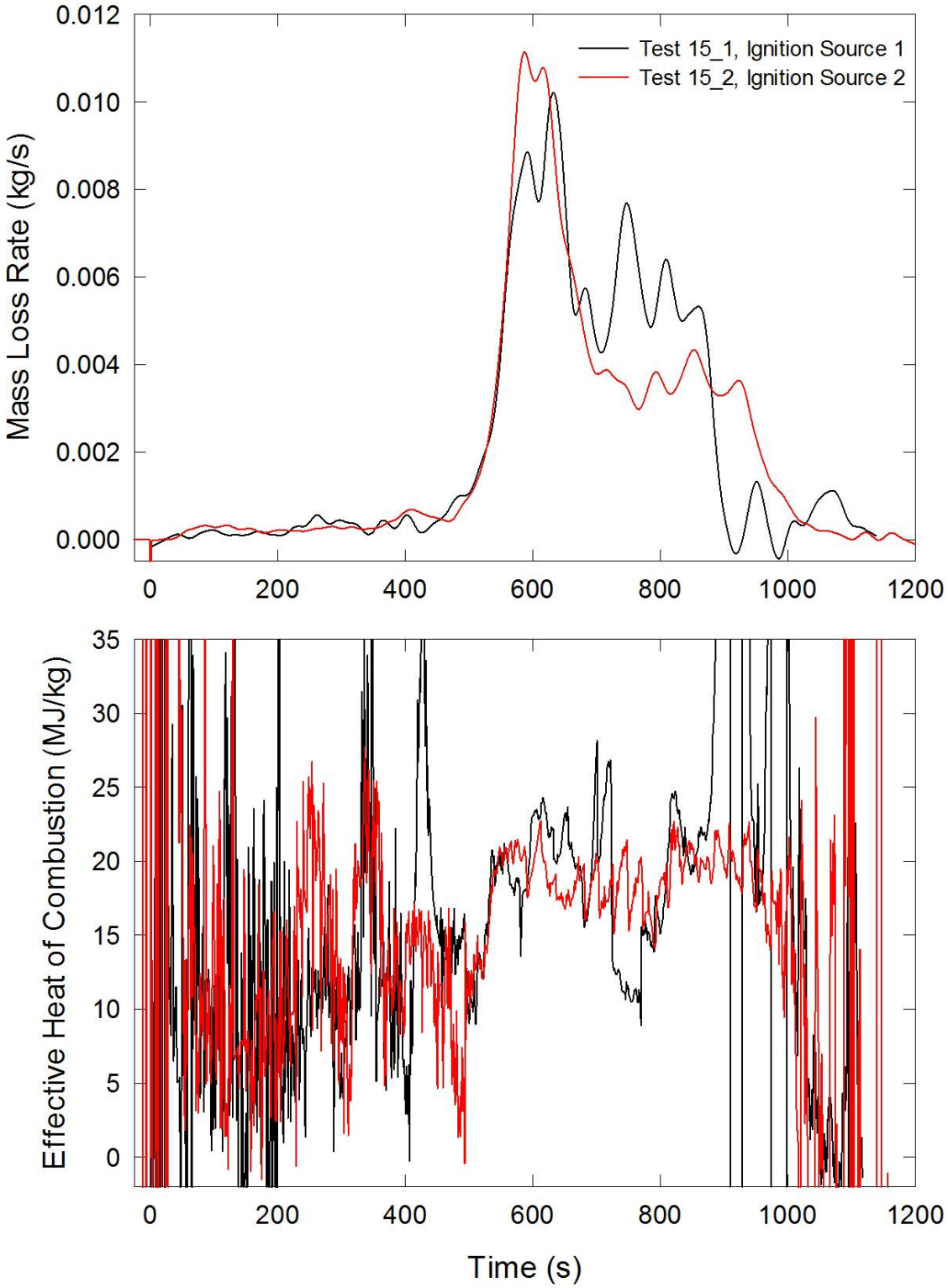

Figure A-109. Temporal profiles of MLR and EHOC are shown for Test 15_1 following application of Ignition Source 1 and Test 15_2 following application of Ignition Source 2.

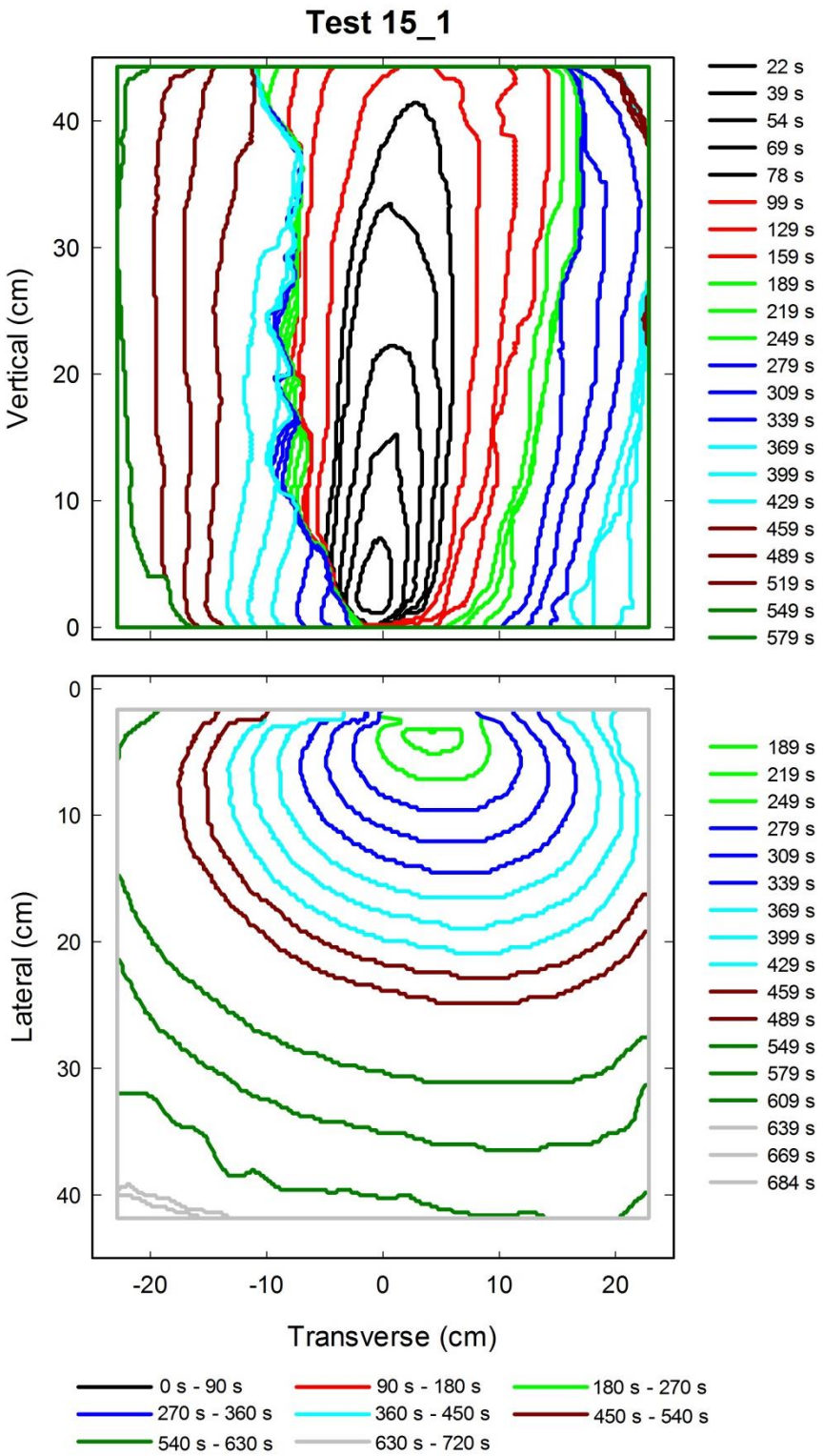

Figure A-110. Flame edge contours on the back (top) and seat (bottom) cushions are plotted as a function of time for Test 15_1 following application of Ignition Source 1.

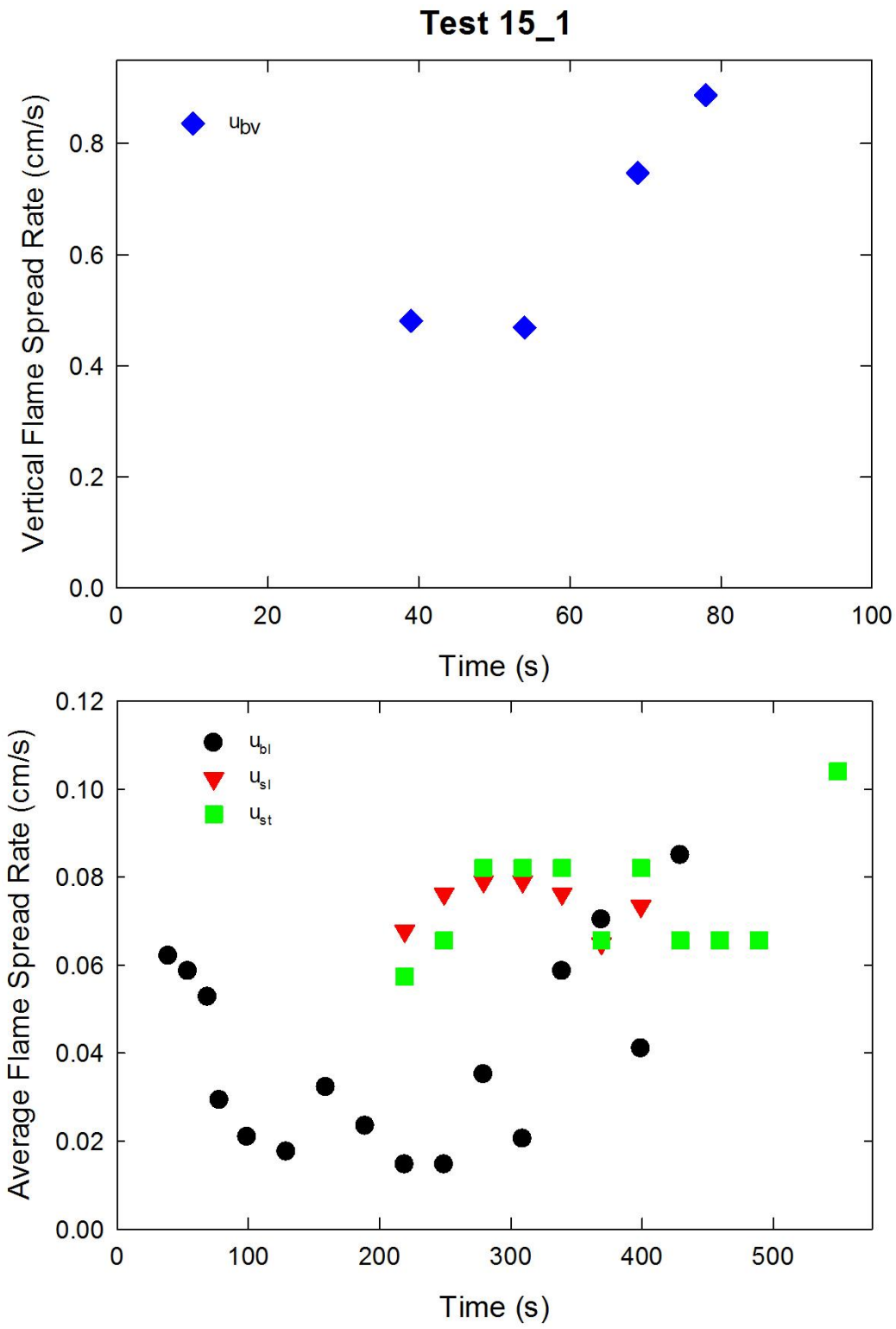

Figure A-111. Vertical flame spread rate on the back cushion (top) and average lateral flame spread rates on the back and seat cushions and transverse flame spread rate on the seat cushion (bottom) are plotted as a function of time for Test 15_1 following application of Ignition Source 1.

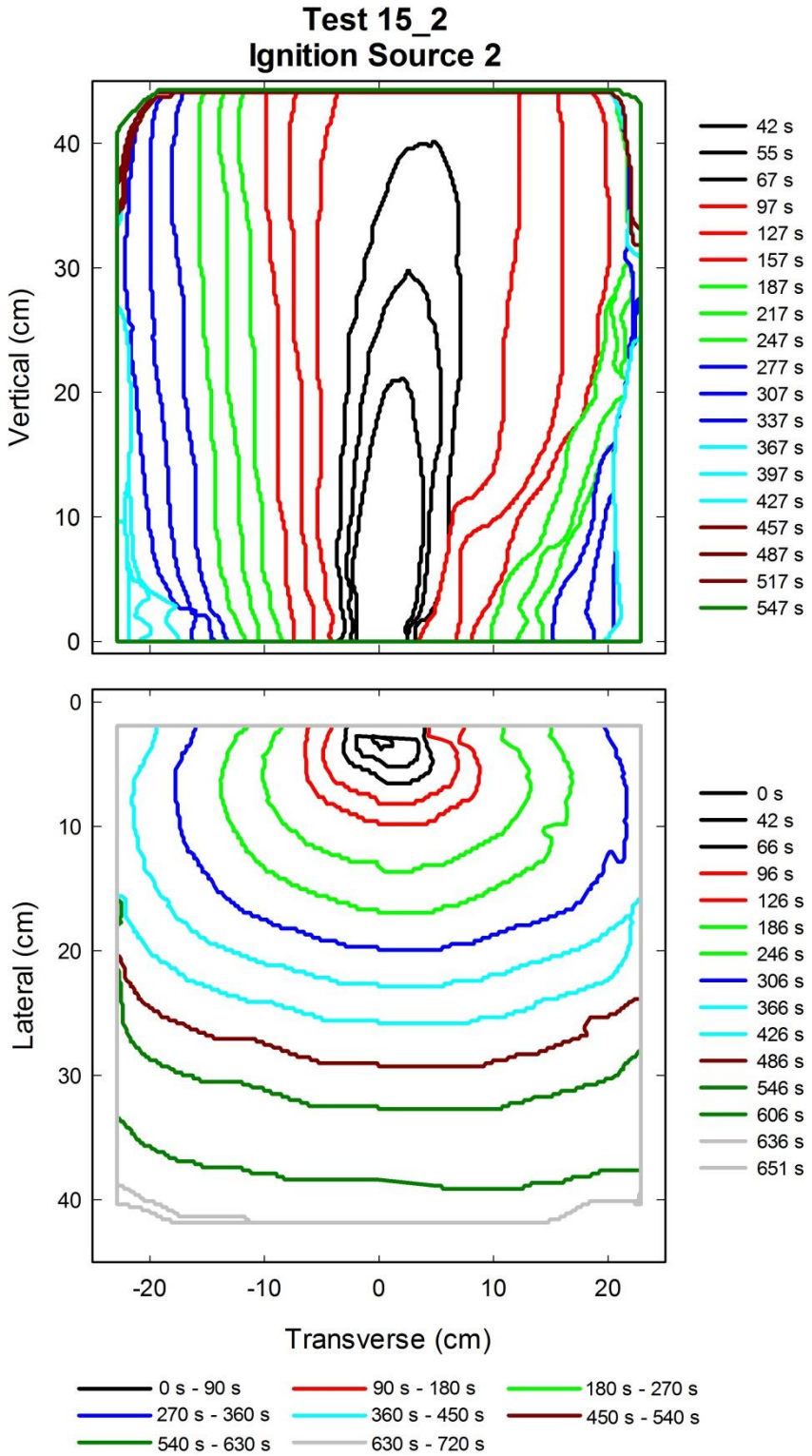

Figure A-112. Flame edge contours on the back (top) and seat (bottom) cushions are plotted as a function of time for Test 15_2 following application of Ignition Source 2.

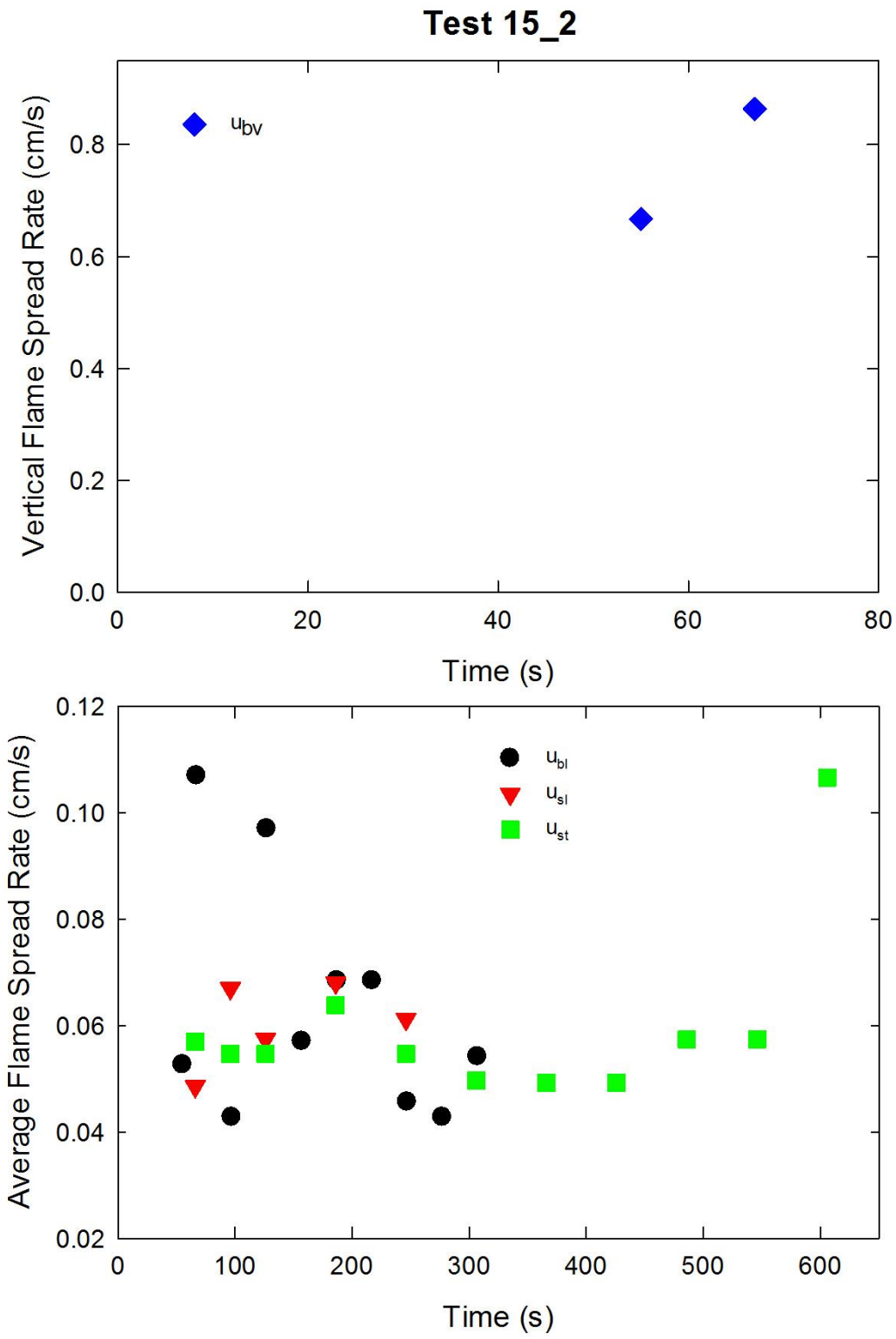

Figure A-113. Vertical flame spread rate on the back cushion (top) and average lateral flame spread rates on the back and seat cushions and transverse flame spread rate on the seat cushion (bottom) are plotted as a function of time for Test 15_2 following application of Ignition Source 2.

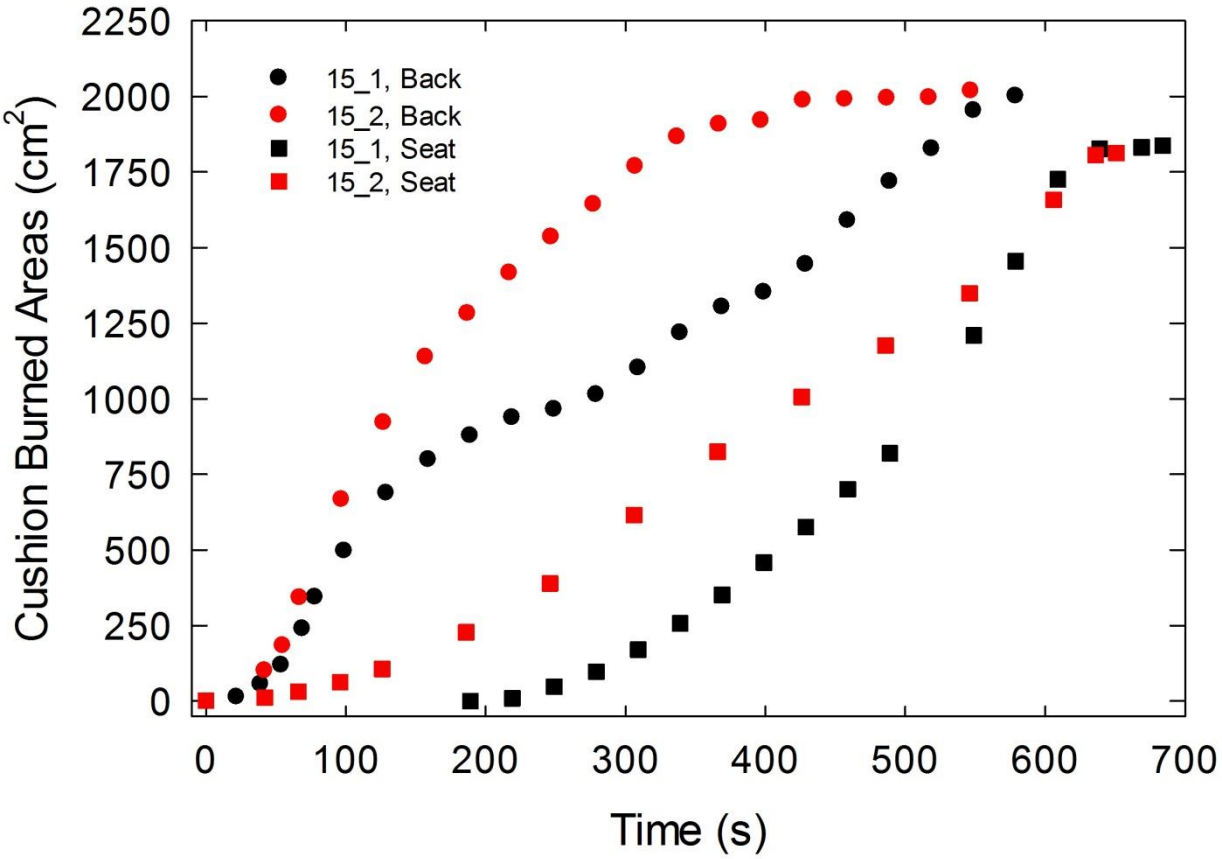

Figure A-114. Burned areas on the seat and back cushions are plotted as a function of time for Test 15_1 following application of Ignition Source 1 and Test 15_2 following application of Ignition Source 2.

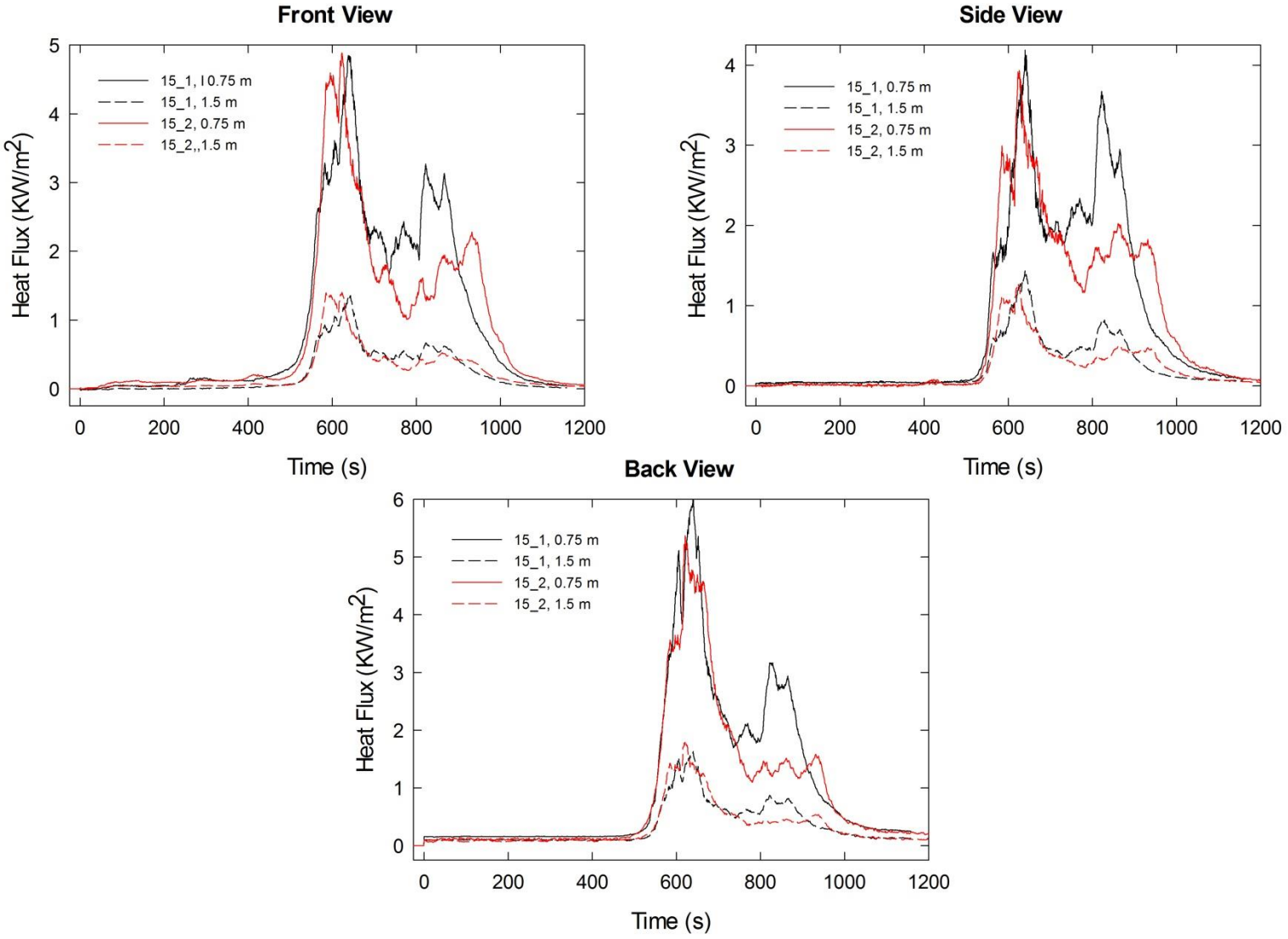

Figure A-115. Heat fluxes recorded at distances of 0.75 m and 1.5 m are plotted as a function of time for locations to the front, side and rear of the mock-up for Test 15_1 following application of Ignition Source 1 and Test 15_2 following application of Ignition Source 2.

A.12 Combination 16

78%PP/22%PE/PEFW/FRFPUF

Notes:

Test 1:

Ignition Source 1 applied at time = 0 s

Test 2:

Ignition Source 1 applied at time = 0 s

Initial mass reading (2.52 kg) during the experiment disagreed with an earlier measurement for the mock-up (3.37 kg); mass readings during the test were smooth, physically reasonable and correlated with the HRR; **these mass data were adjusted by adding 0.849 kg to their values and were included in the analysis**.

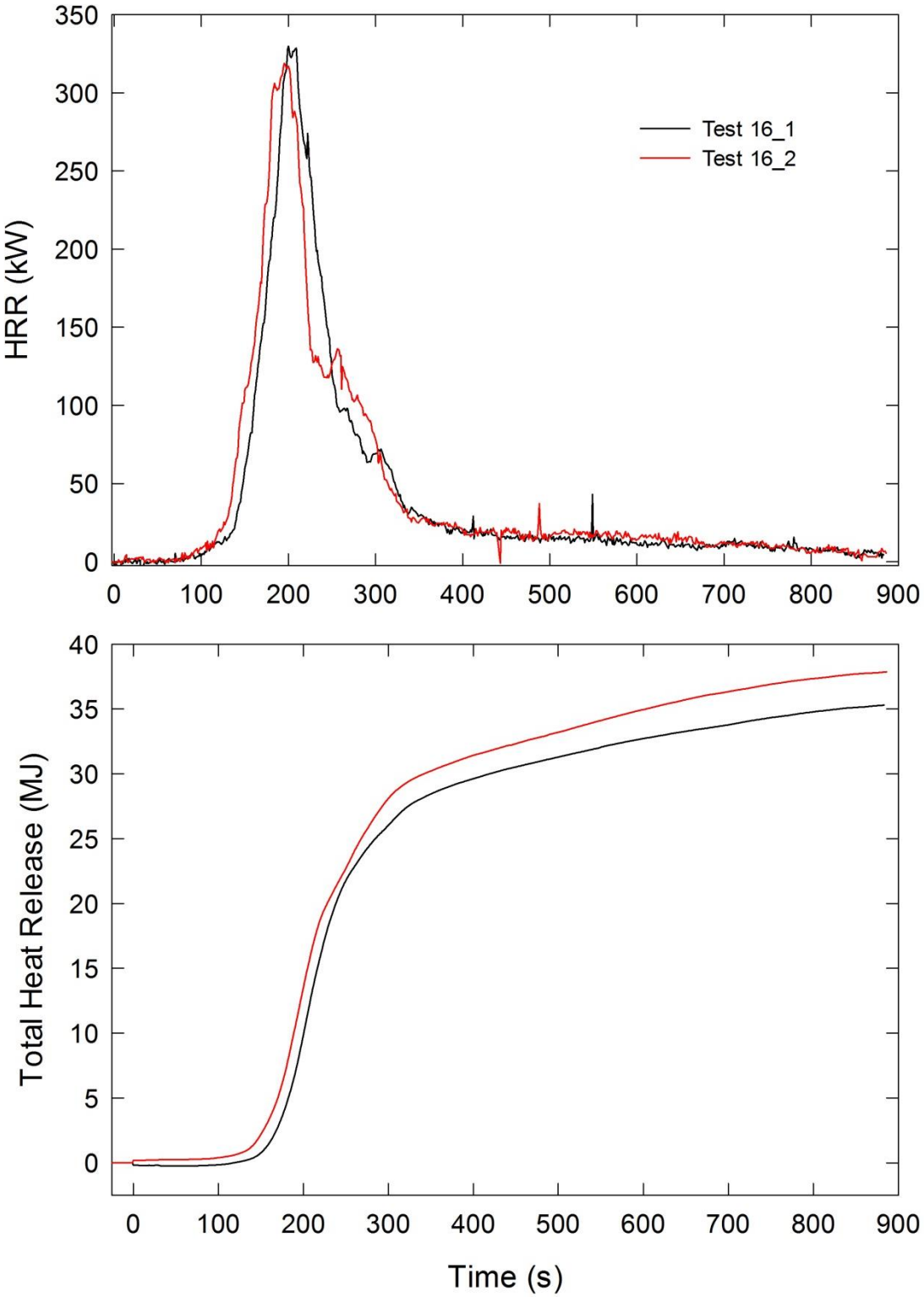

Figure A-116. Temporal profiles of HRR and integrated HRR are shown for Combination 16 tests following application of Ignition Source 1.

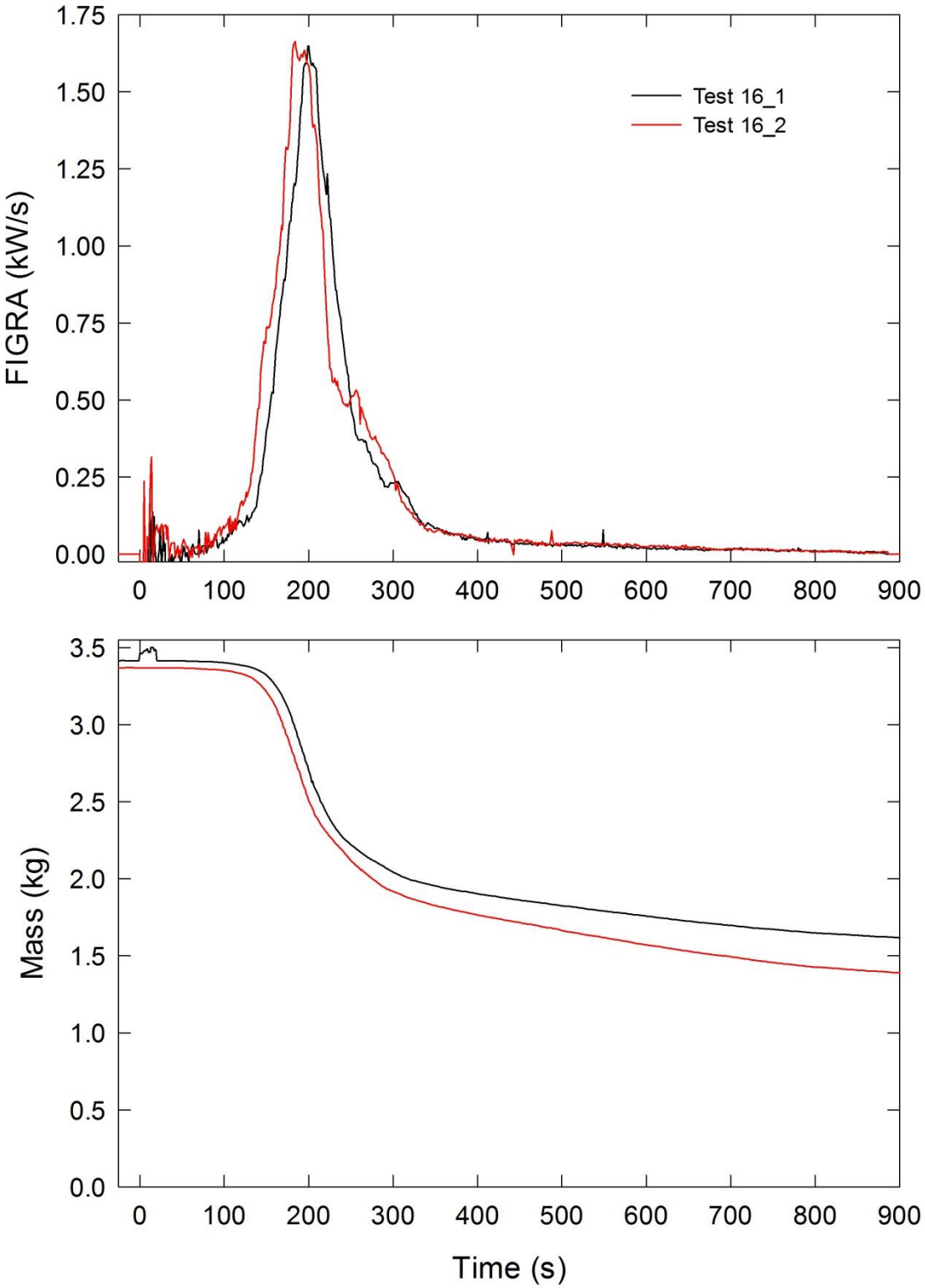

Figure A-117. Temporal profiles of FIGRA and mock-up mass are shown for Combination 16 tests following application of Ignition Source 1.

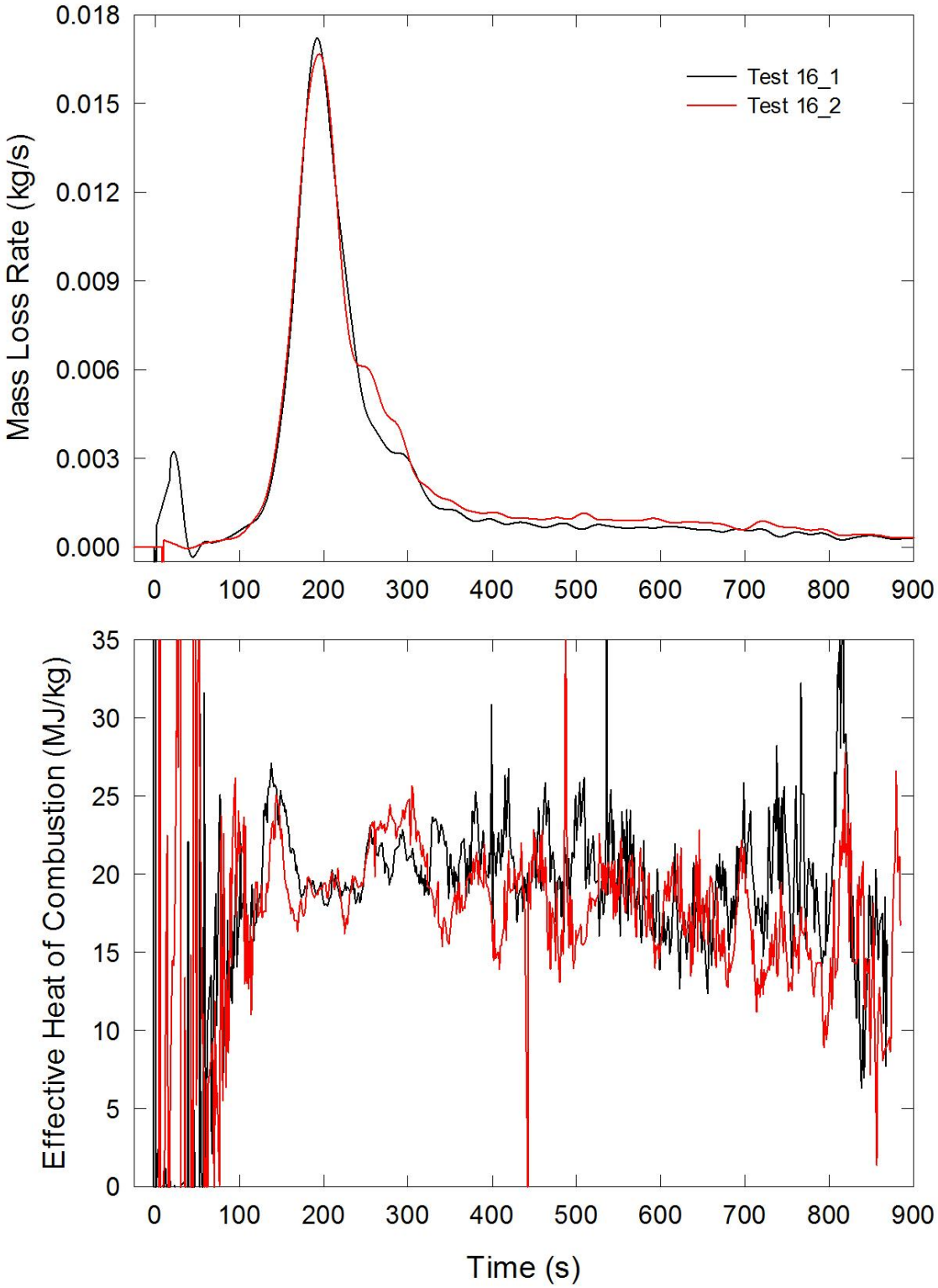

Figure A-118. Temporal profiles of MLR and EHOC are shown for Combination 16 tests following application of Ignition Source 1.

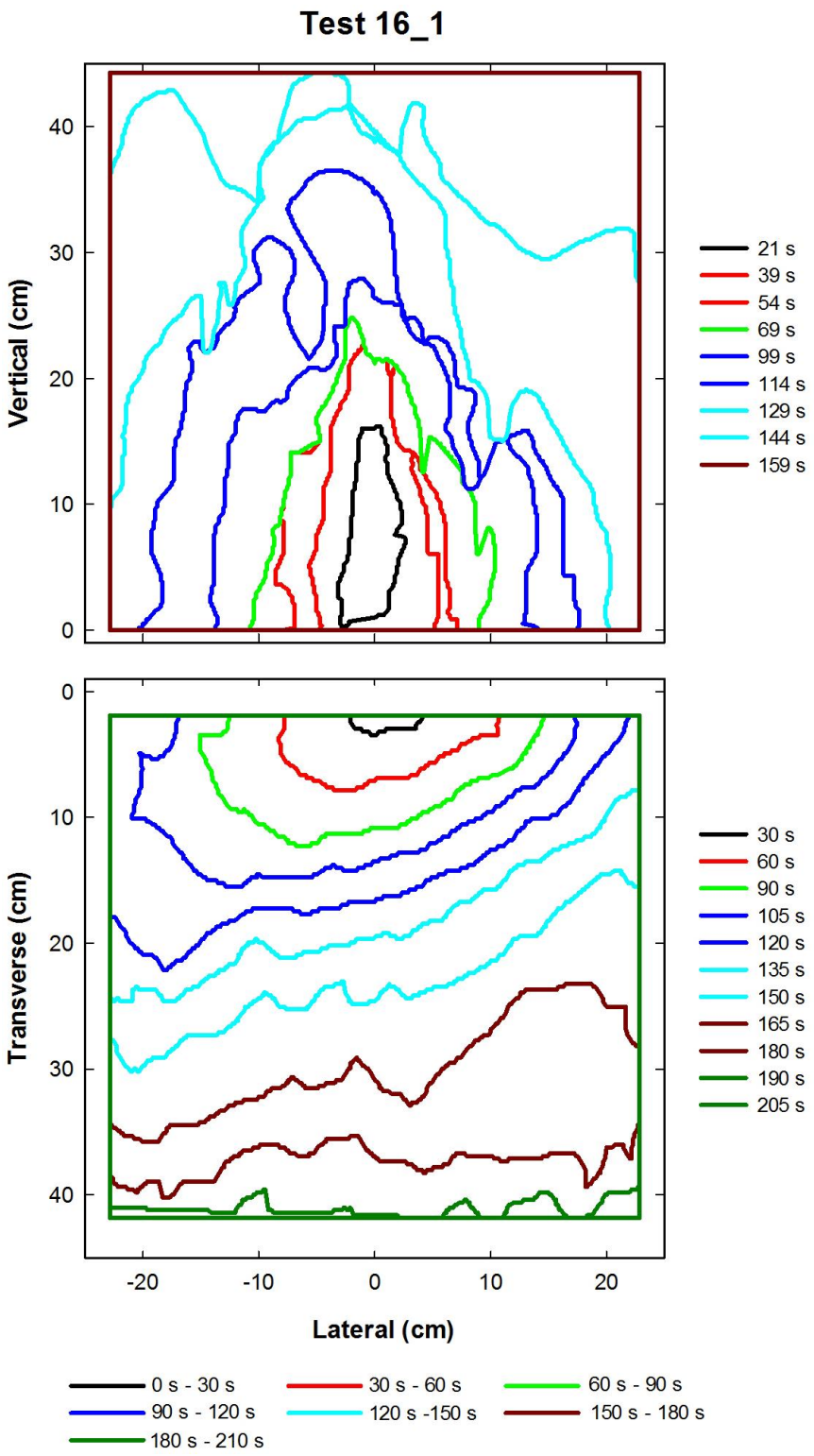

Figure A-119. Flame edge contours on the back (top) and seat (bottom) cushions are plotted as a functionof time for Test 16_1 following application of Ignition Source 1.

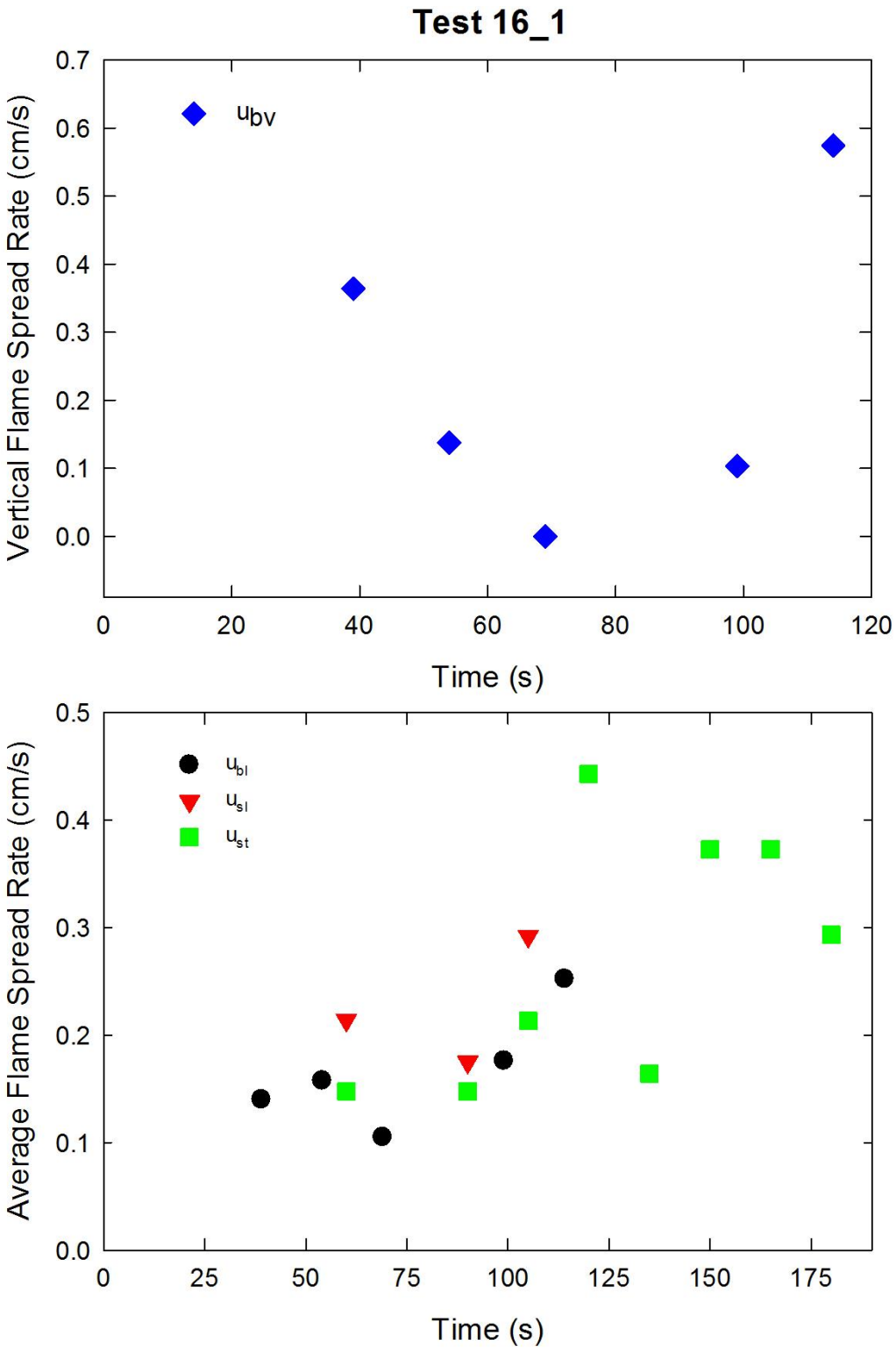

Figure A-120. Vertical flame spread rate on the back cushion (top) and average lateral flame spread rates on the back and seat cushions and transverse flame spread rate on the seat cushion (bottom) are plotted as a function of time for Test 16_1 following application of Ignition Source 1.

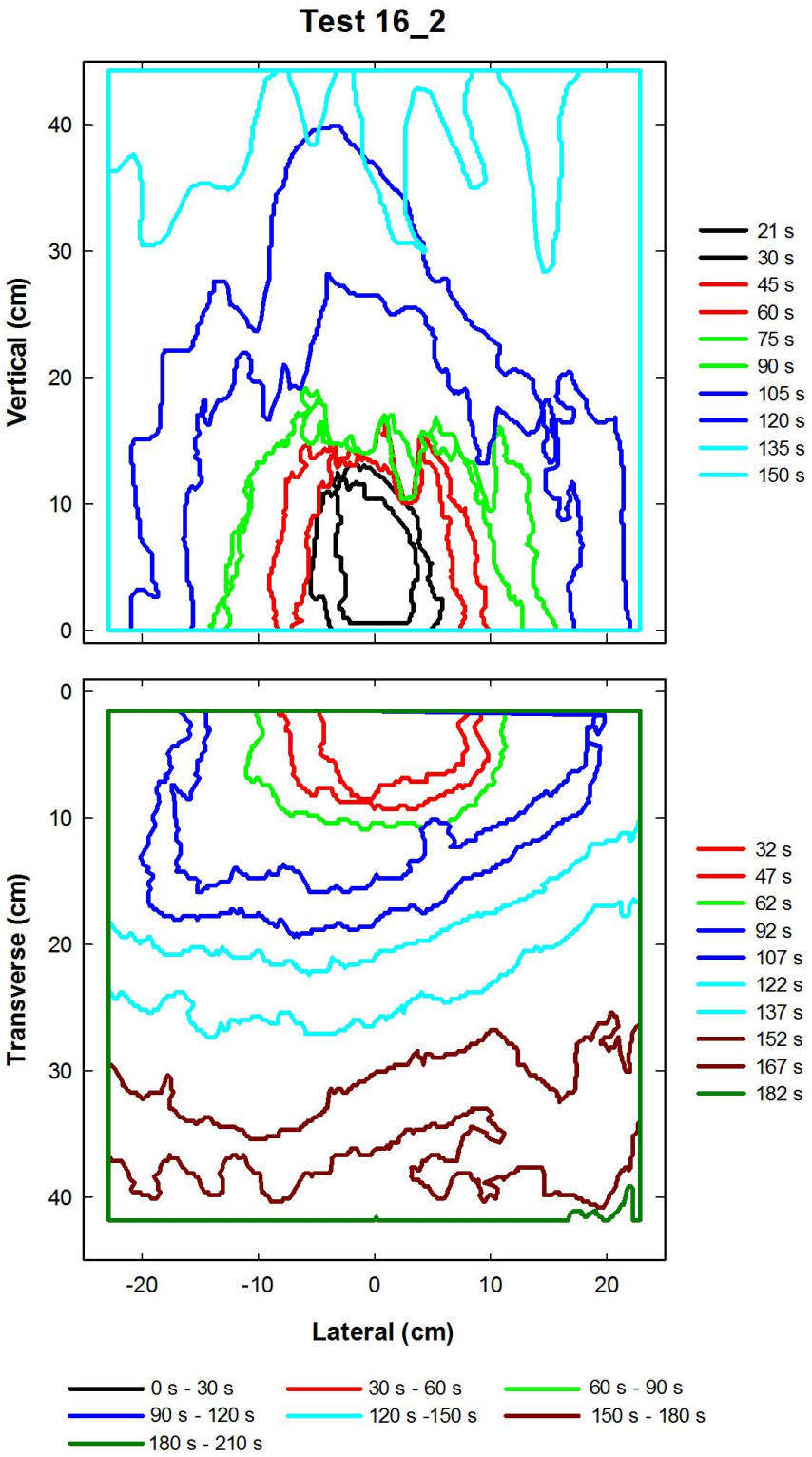

Figure A-121. Flame edge contours on the back (top) and seat (bottom) cushions are plotted as a function of time for Test 16_2 following application of Ignition Source 1.

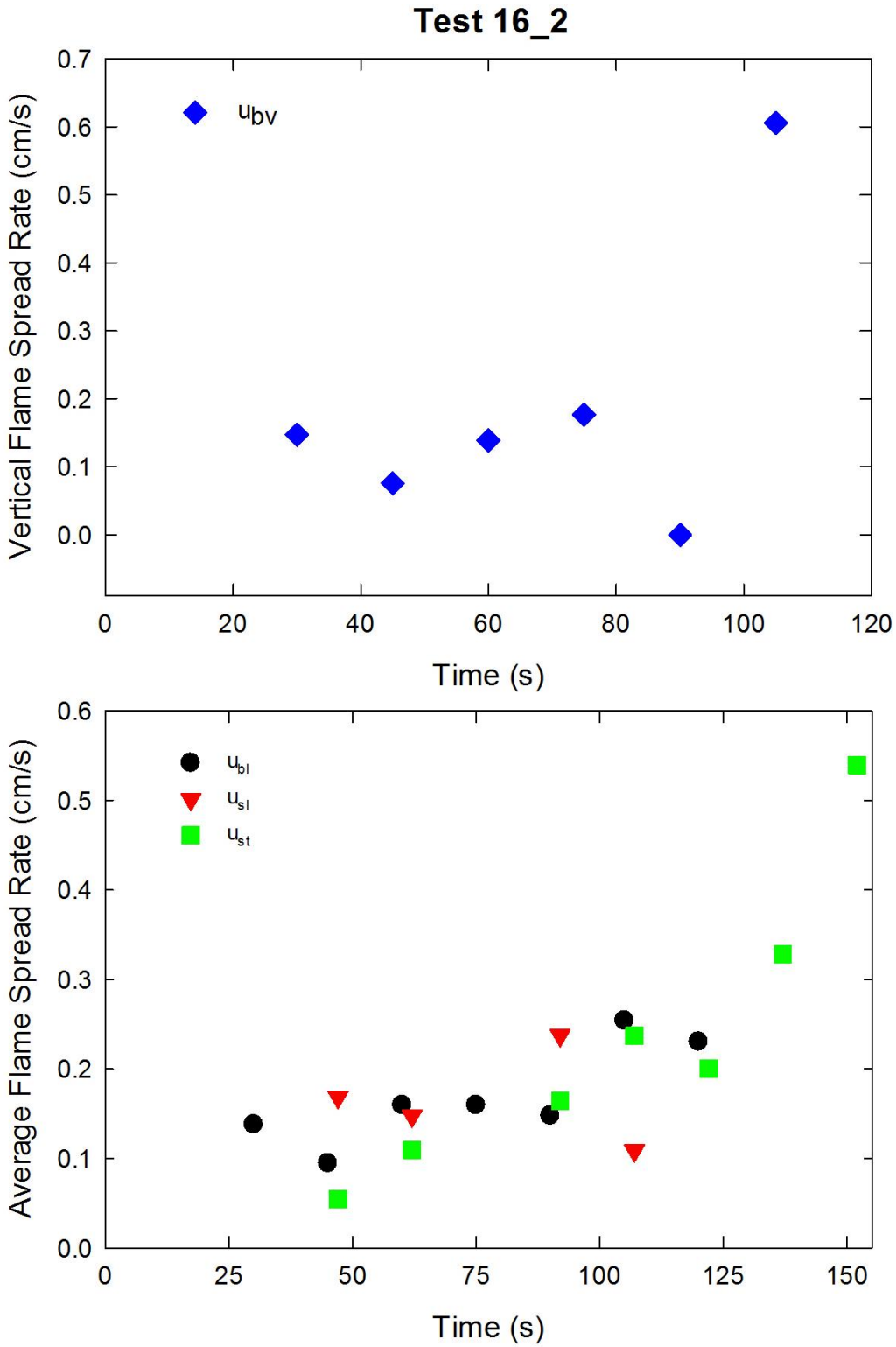

Figure A-122. Vertical flame spread rate on the back cushion (top) and average lateral flame spread rates on the back and seat cushions and transverse flame spread rate on the seat cushion (bottom) are plotted as a function of time for Test 16_2 following application of Ignition Source 1.

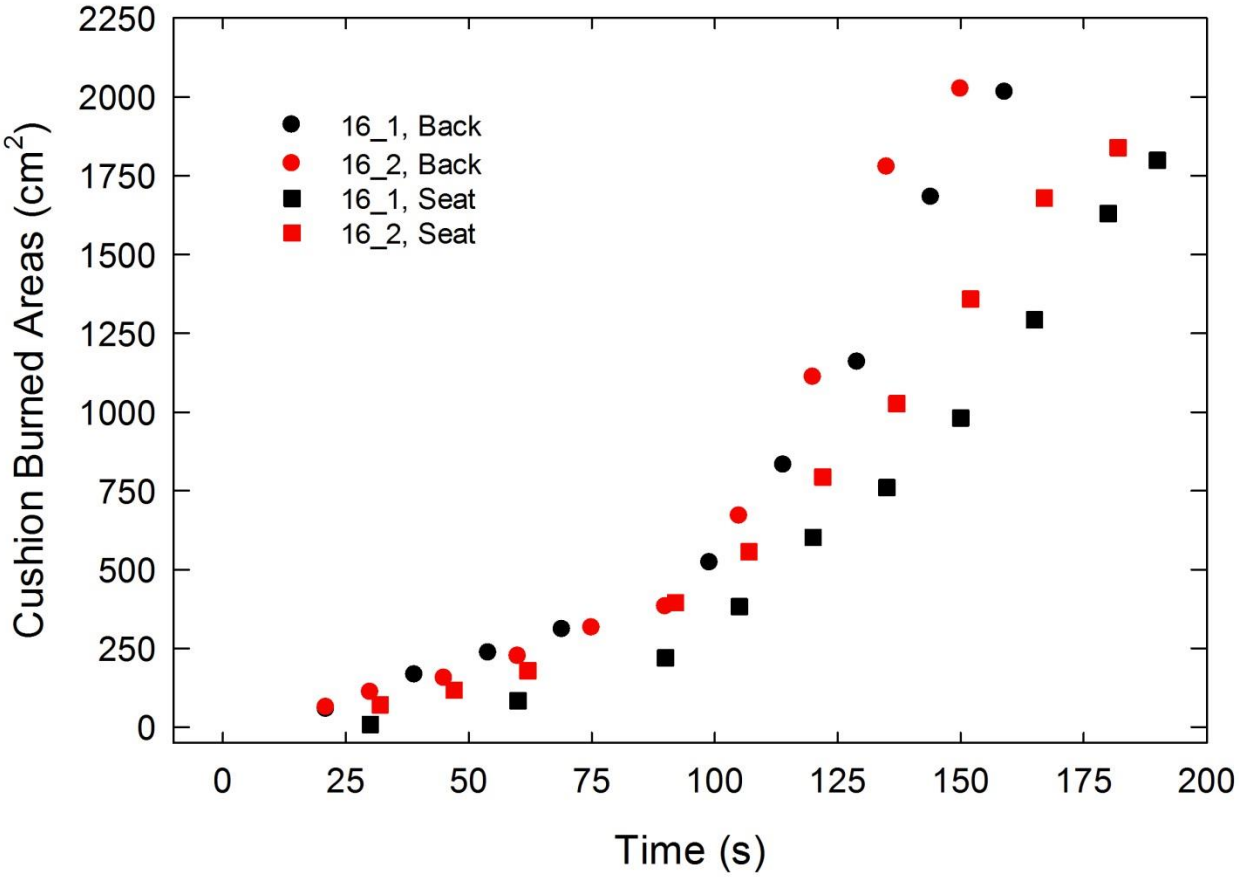

Figure A-123. Burned areas on the seat and back cushions are plotted as a function of time for Combination 16 tests following application of Ignition Source 1.

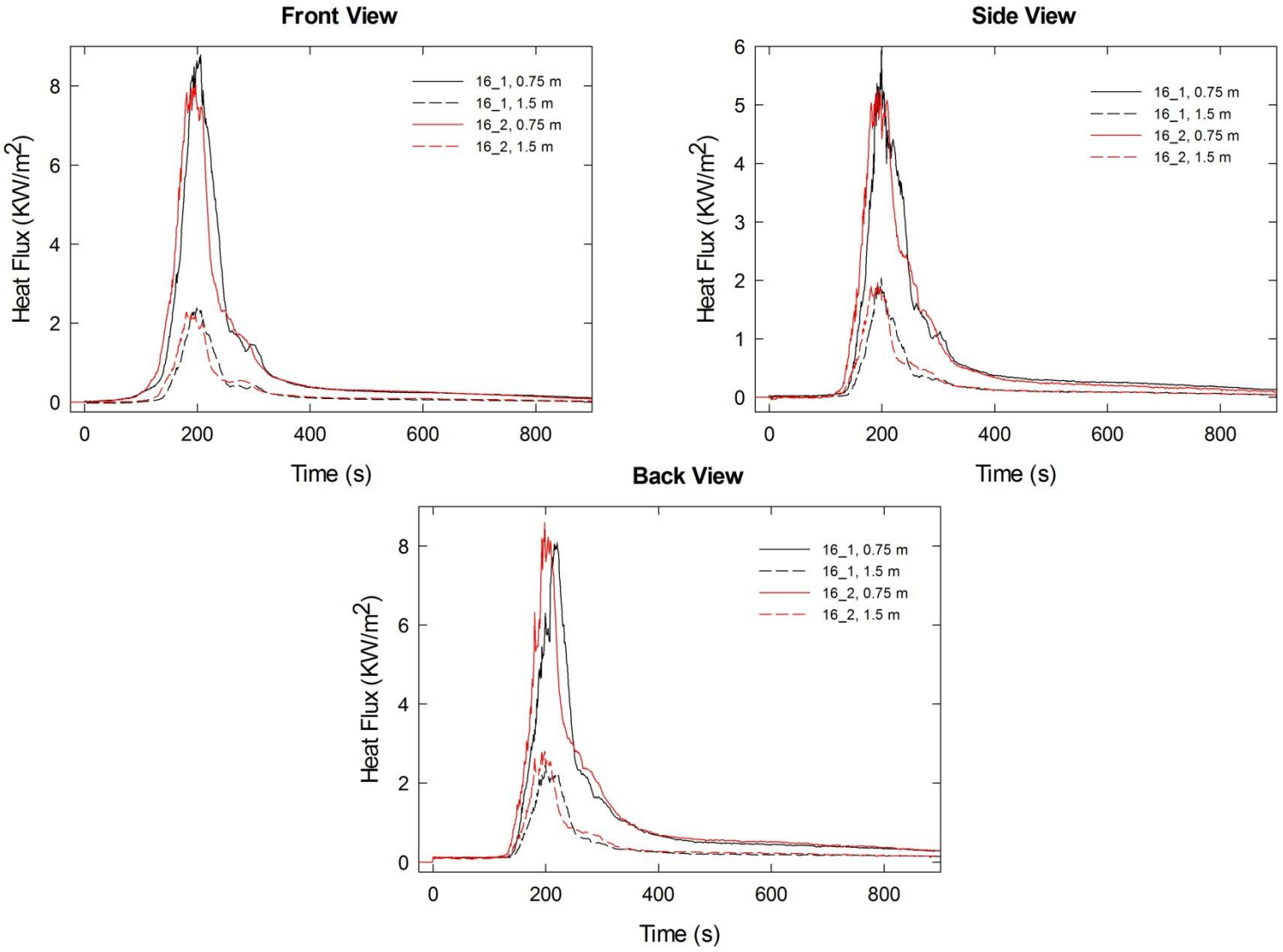

Figure A-124. Heat fluxes recorded at distances of 0.75 m and 1.5 m are plotted as a function of time for locations to the front, side and rear of the mock-up for Combination 16 tests following application of Ignition Source 1.

A.13 Combination 17

cotton/Norfab/NFRFPUF

Notes:

Test 1:

Ignition Source 1 applied at time = 0 s; following removal of ignition source, upward flame spread with little lateral spread on back cushion; no darkening on seat cushion.

Ignition Source 2 applied 369 s after Ignition Source 1; following removal of ignition source, limited lateral spread at the base of the back cushion; no darkening on seat cushion; spreading dark area appeared on seat cushion at ignition location ≈ 44 s after flame removed.

Initial mass reading (3.77 kg) during the experiment disagreed with an earlier measurement for the mock-up (3.70 kg); mass readings displayed numerous non-physical, abrupt jumps; **these mass data were excluded from analysis**.

Test 2:

Ignition Source 1 applied at time = 0 s; following removal of ignition source, upward flame spread with some lateral spread on back cushion; no darkening on seat cushion.

Ignition Source 2 applied 767 s after Ignition Source 1.

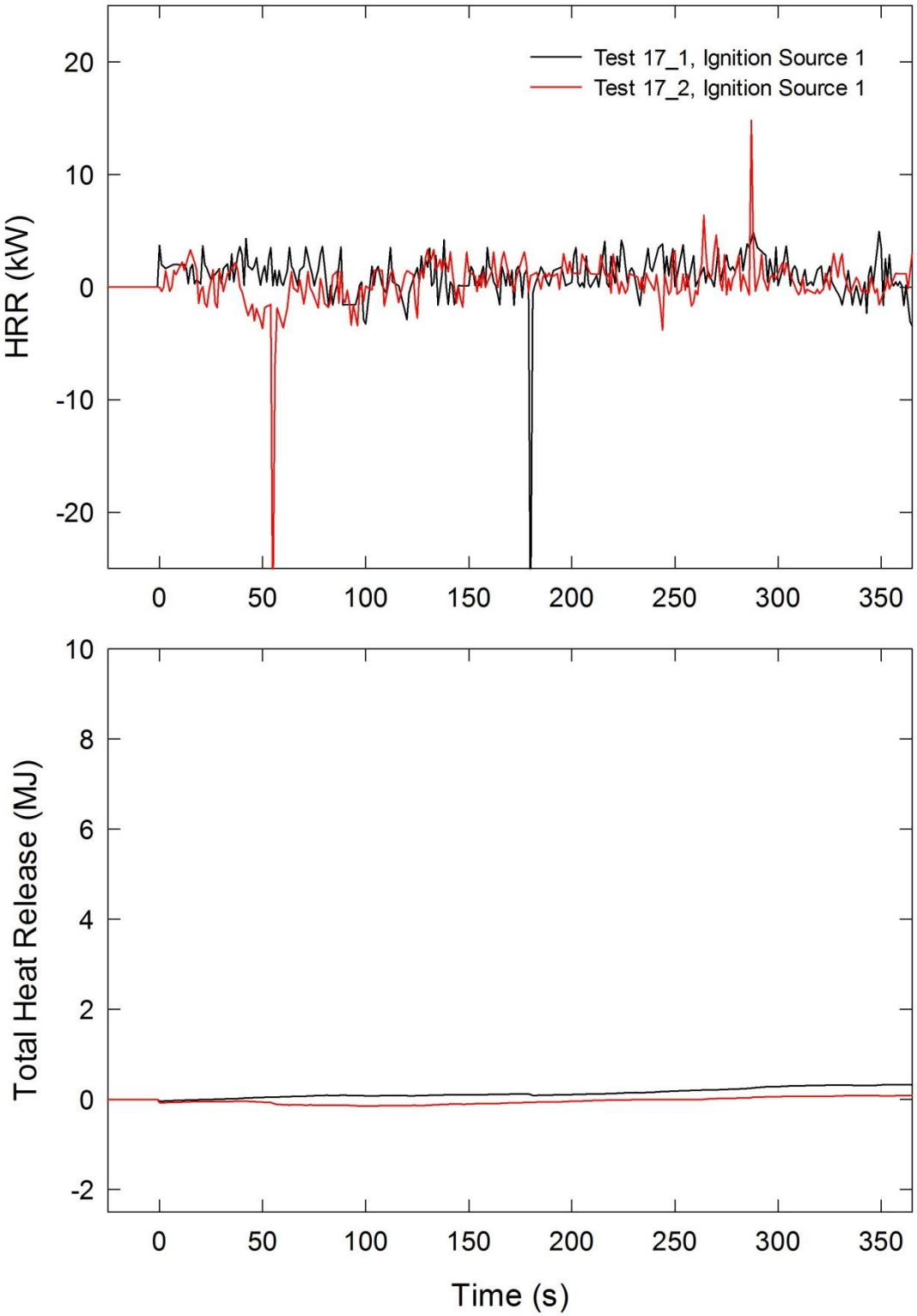

Figure A-125. Temporal profiles of HRR and integrated HRR are shown for Combination 17 tests following application of Ignition Source 1.

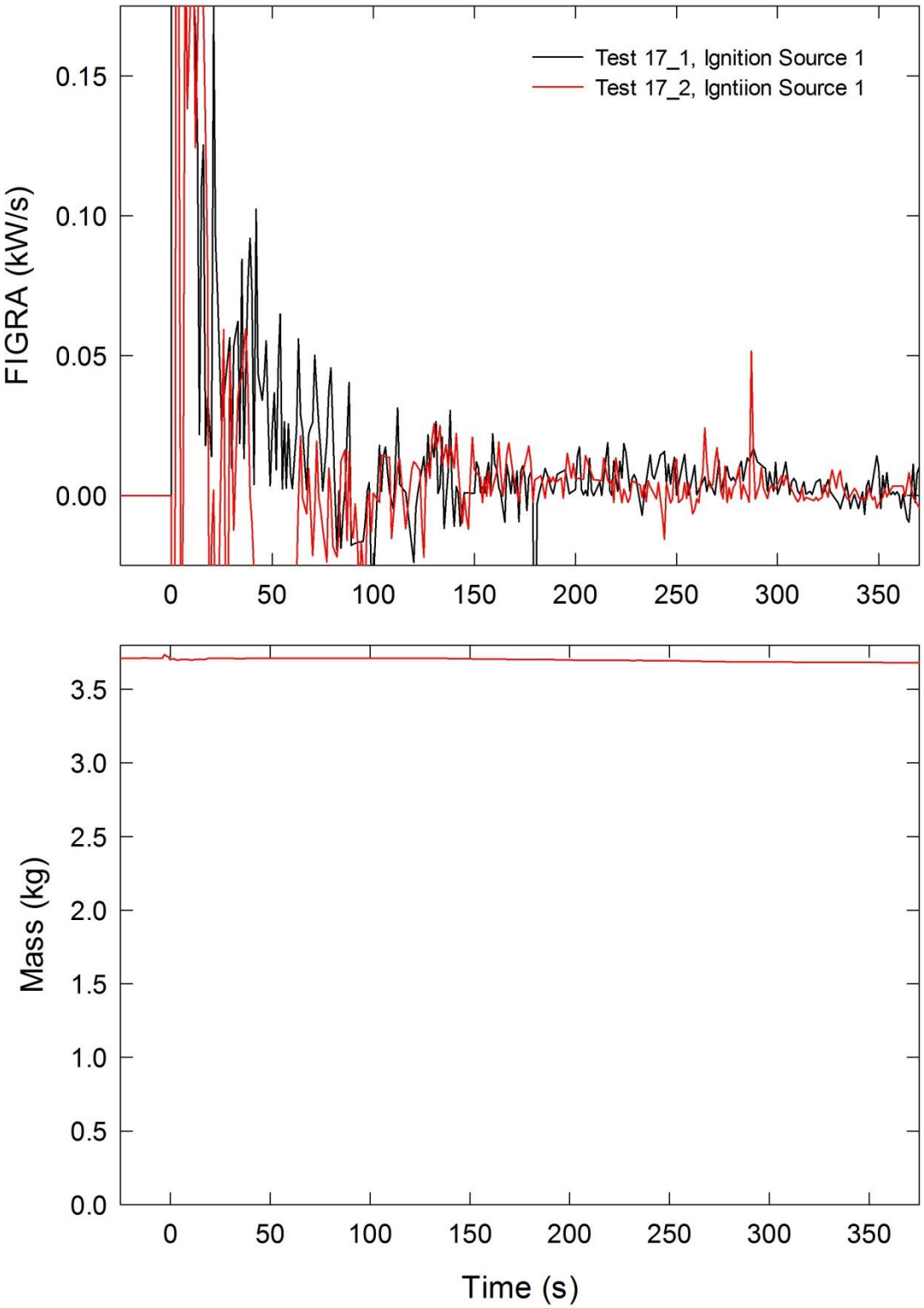

Figure A-126. Temporal profiles of FIGRA are shown for Combination 17 tests and mock-up mass for Test 17_2 following application of Ignition Source 1.

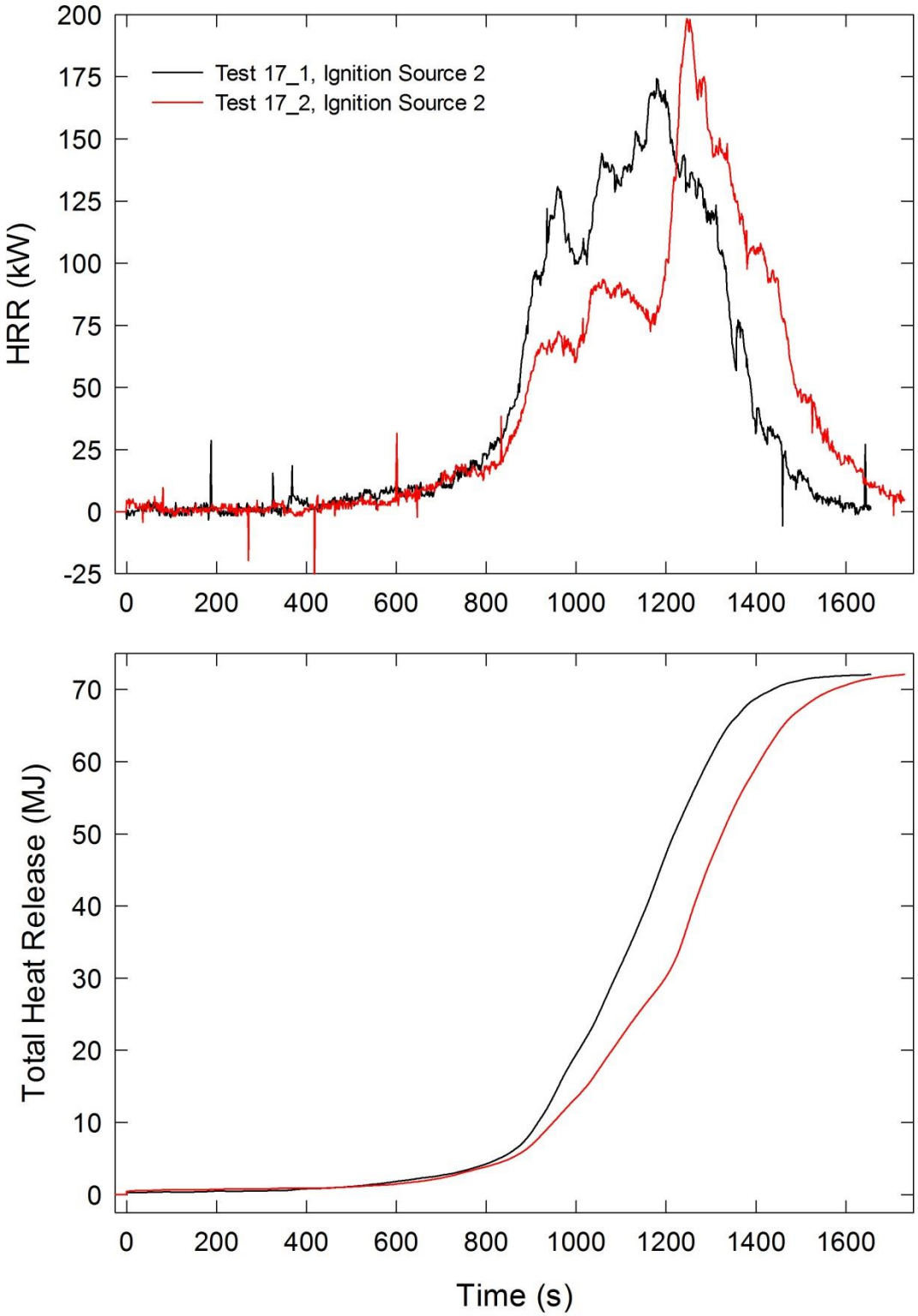

Figure A-127. Temporal profiles of HRR and integrated HRR are shown for Combination 17 tests following application of Ignition Source 2.

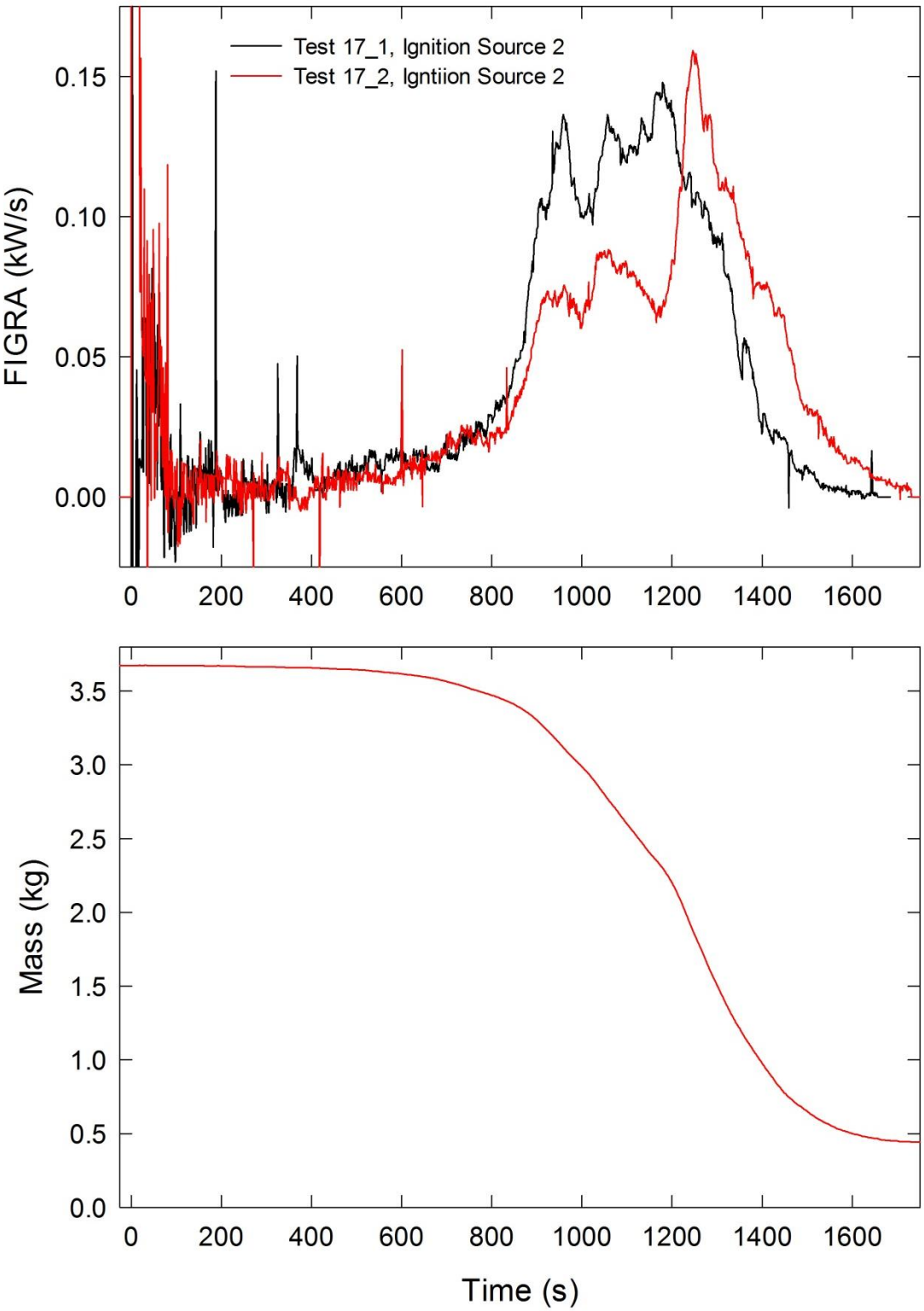

Figure A-128. Temporal profiles of FIGRA are shown for Combination 17 tests and mock-up mass for Test 17_2 following application of Ignition Source 2.

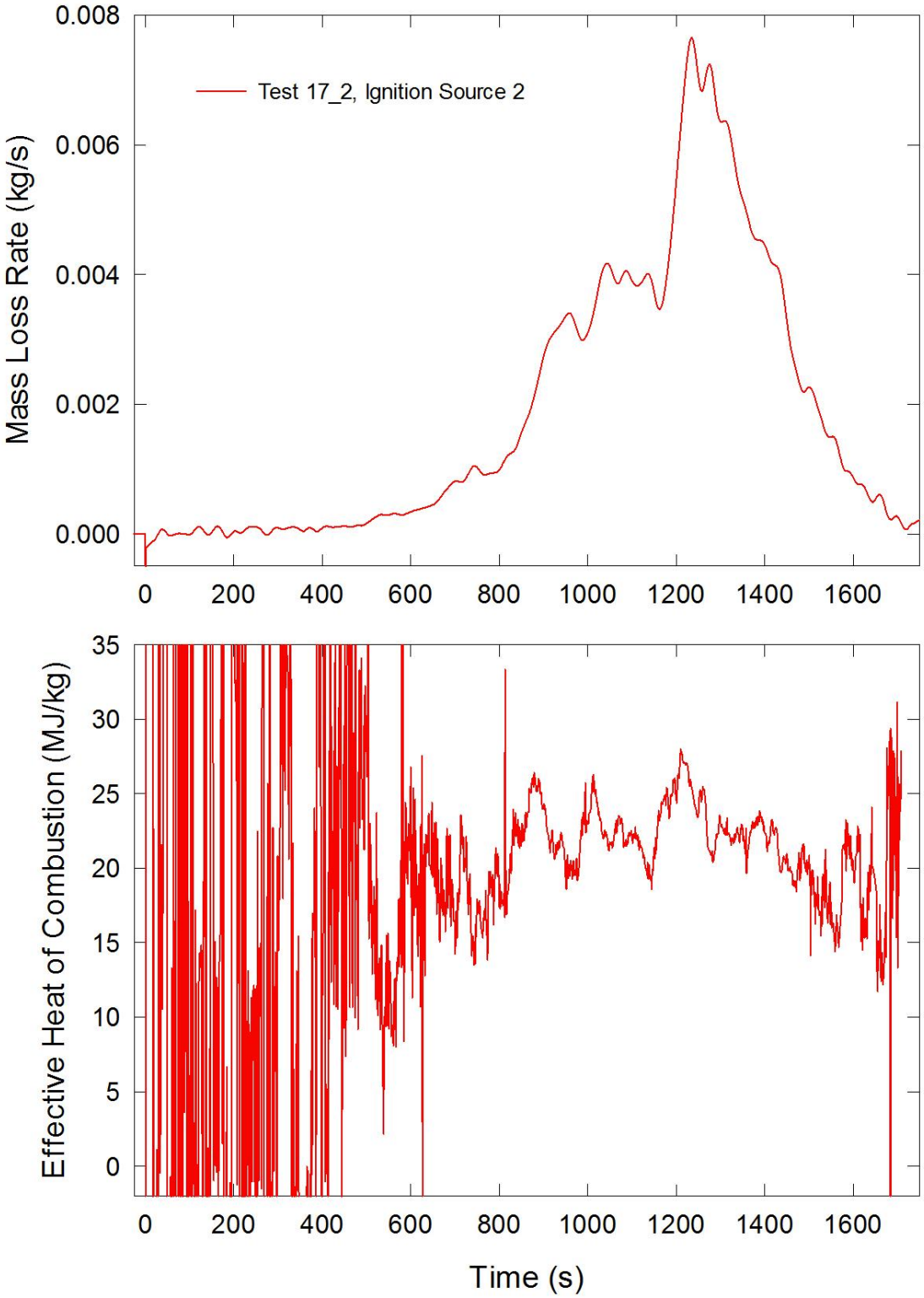

Figure A-129. Temporal profiles of MLR and EHOC are shown for Test 17_2 following application of Ignition Source 2.

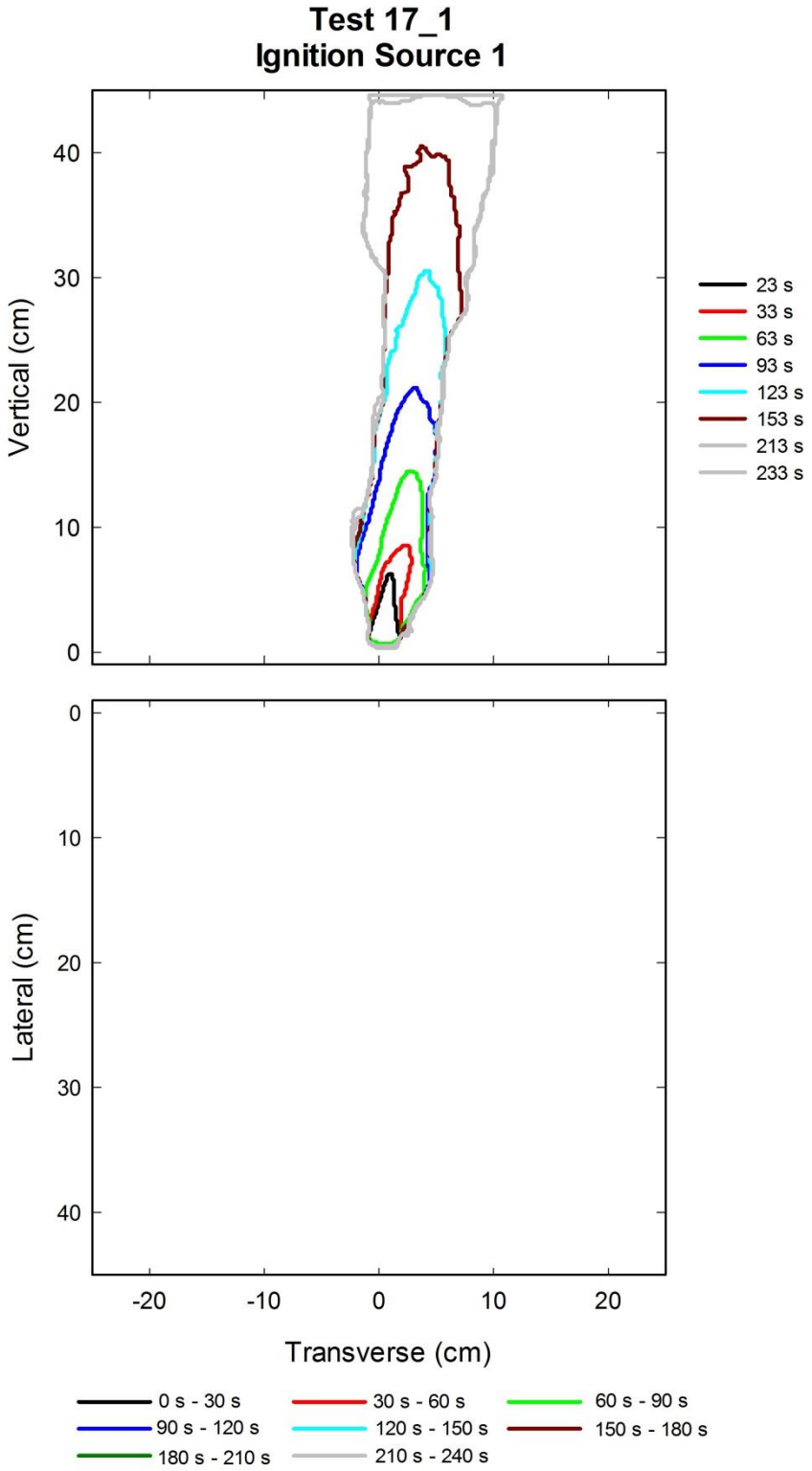

Figure A-130. Flame edge contours on the back (top) and seat (bottom) cushions are plotted as a function of time for Test 17_1 following application of Ignition Source 1.

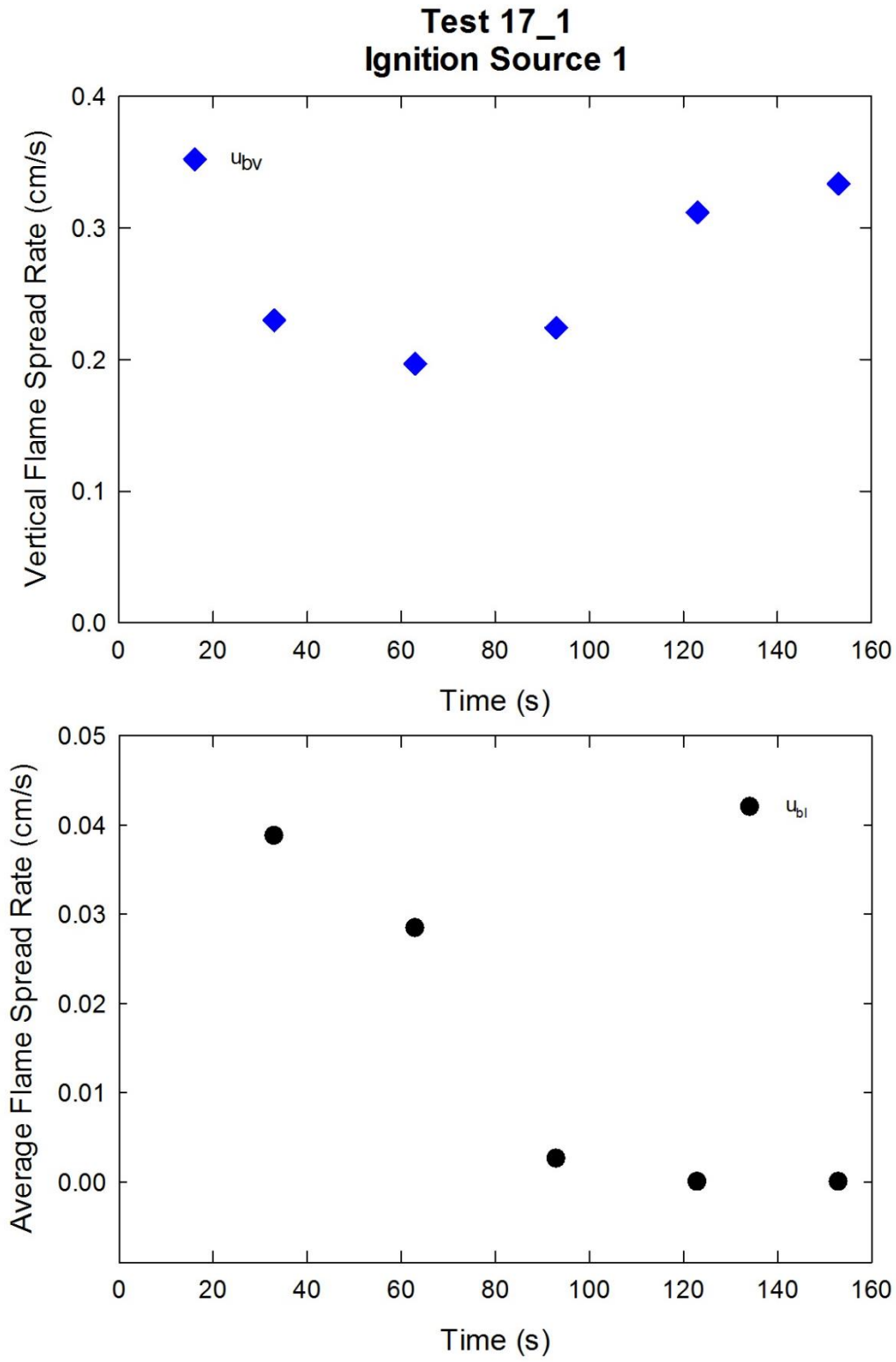

Figure A-131. Vertical flame spread rate on the back cushion (top) and average lateral flame spread rates on the back and seat cushions and transverse flame spread rate on the seat cushion (bottom) are plotted as a function of time for Test 17_1 following application of Ignition Source 1.

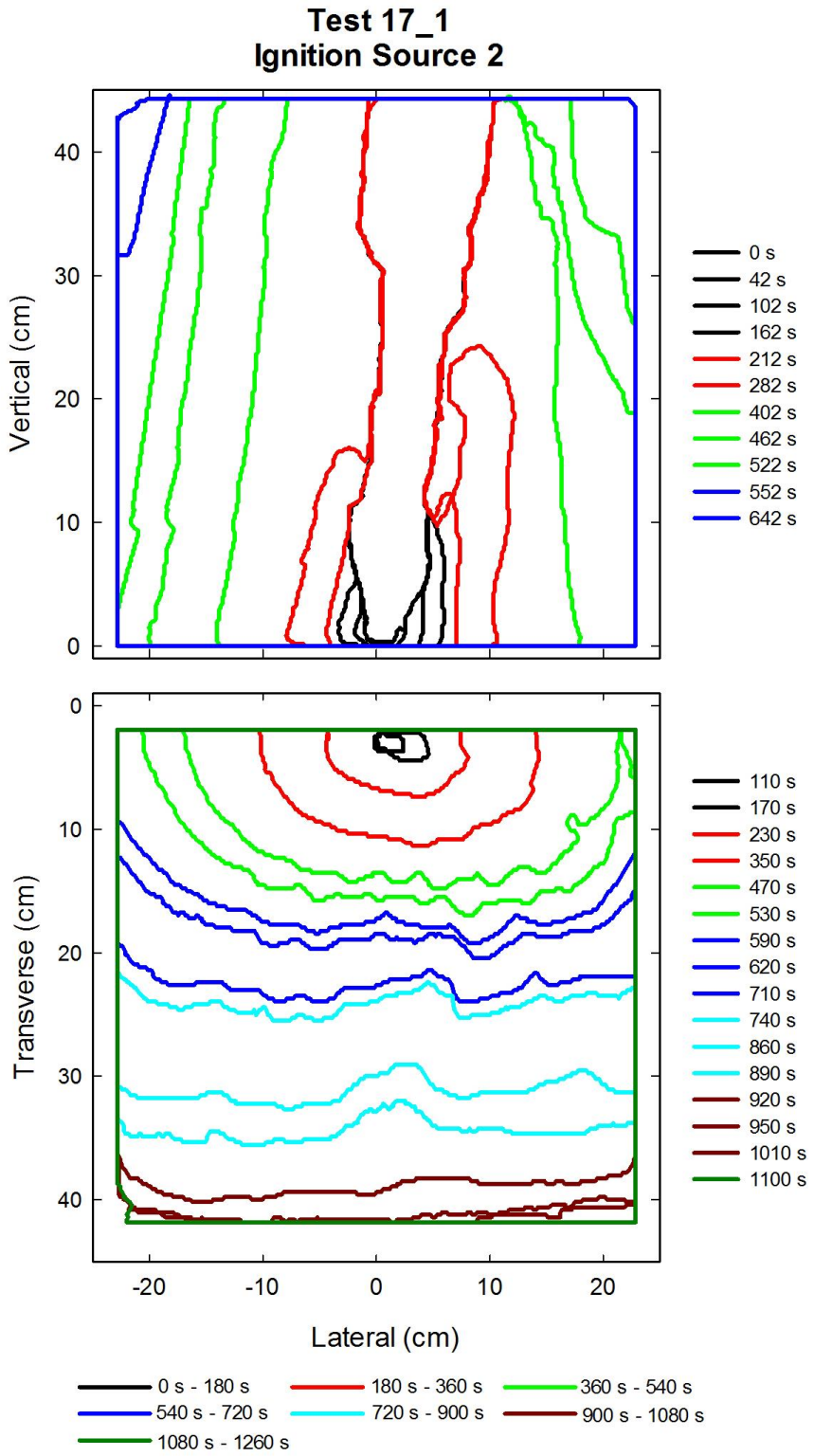

Figure A-132. Flame edge contours on the back (top) and seat (bottom) cushions are plotted as a function of time for Test 17_1 following application of Ignition Source 2.

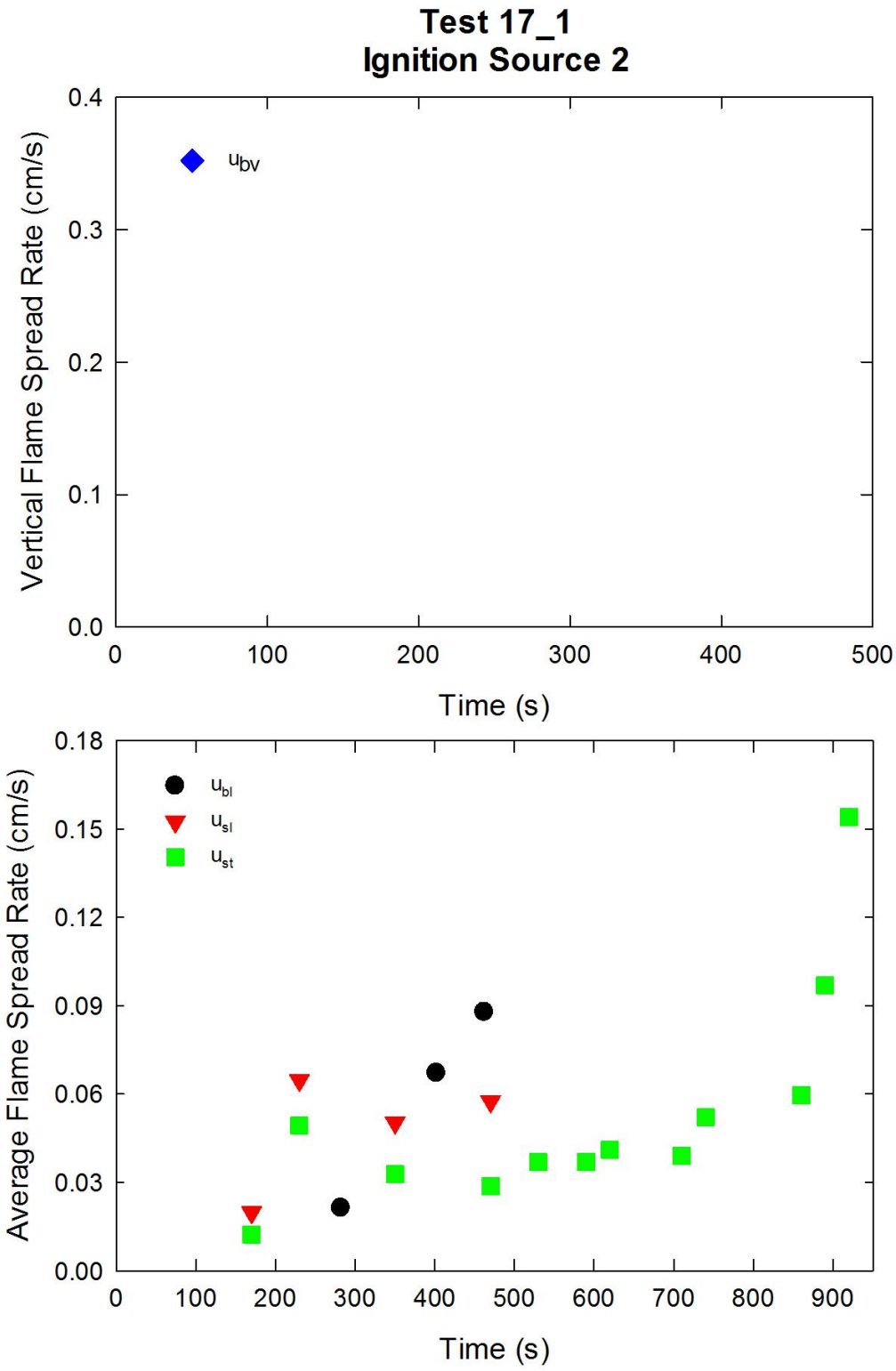

Figure A-133. Vertical flame spread rate on the back cushion (top) and average lateral flame spread rates on the back and seat cushions and transverse flame spread rate on the seat cushion (bottom) are plotted as a function of time for Test 17_1 following application of Ignition Source 2.

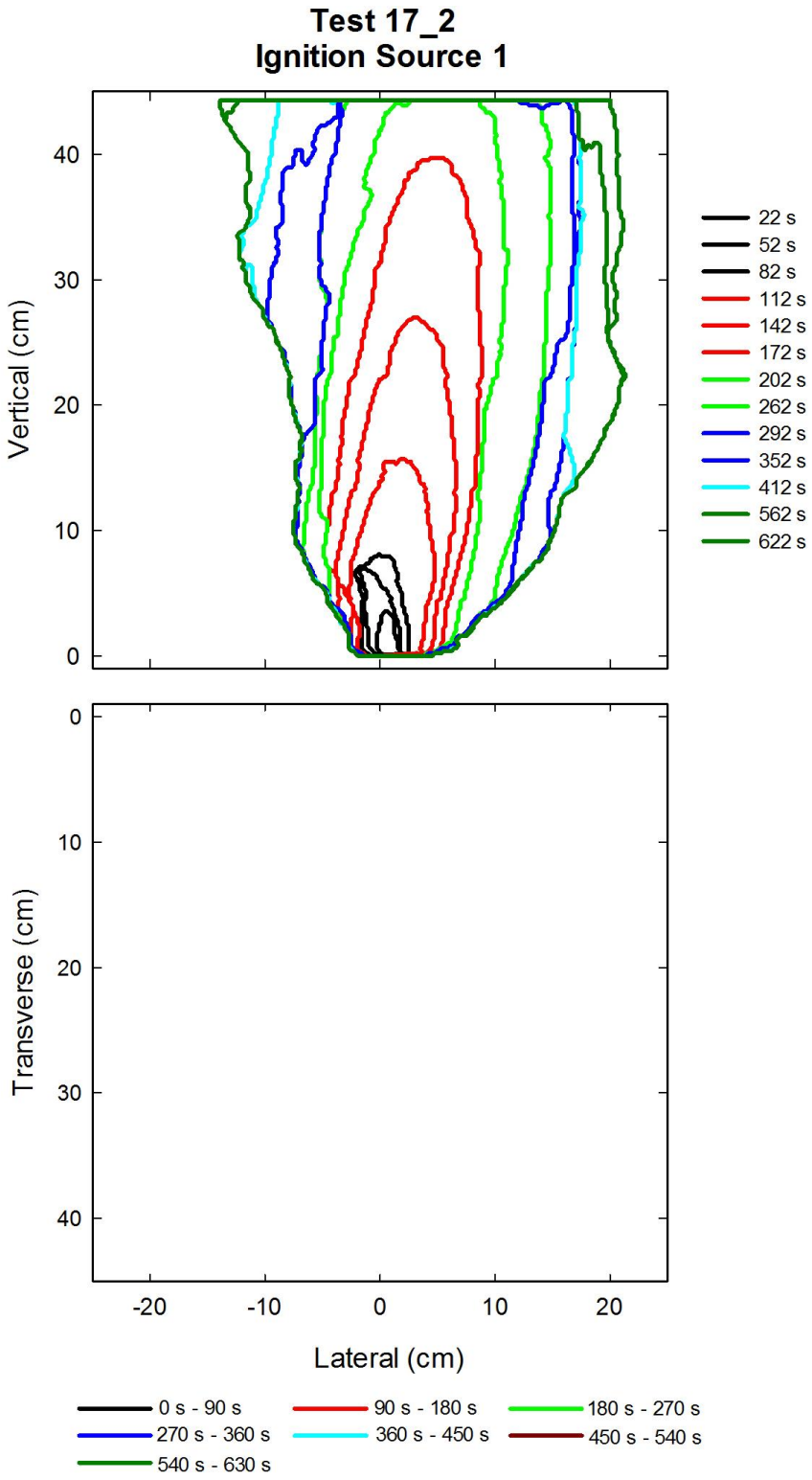

Figure A-134. Flame edge contours on the back (top) and seat (bottom) cushions are plotted as a function of time for Test 17_2 following application of Ignition Source 1.

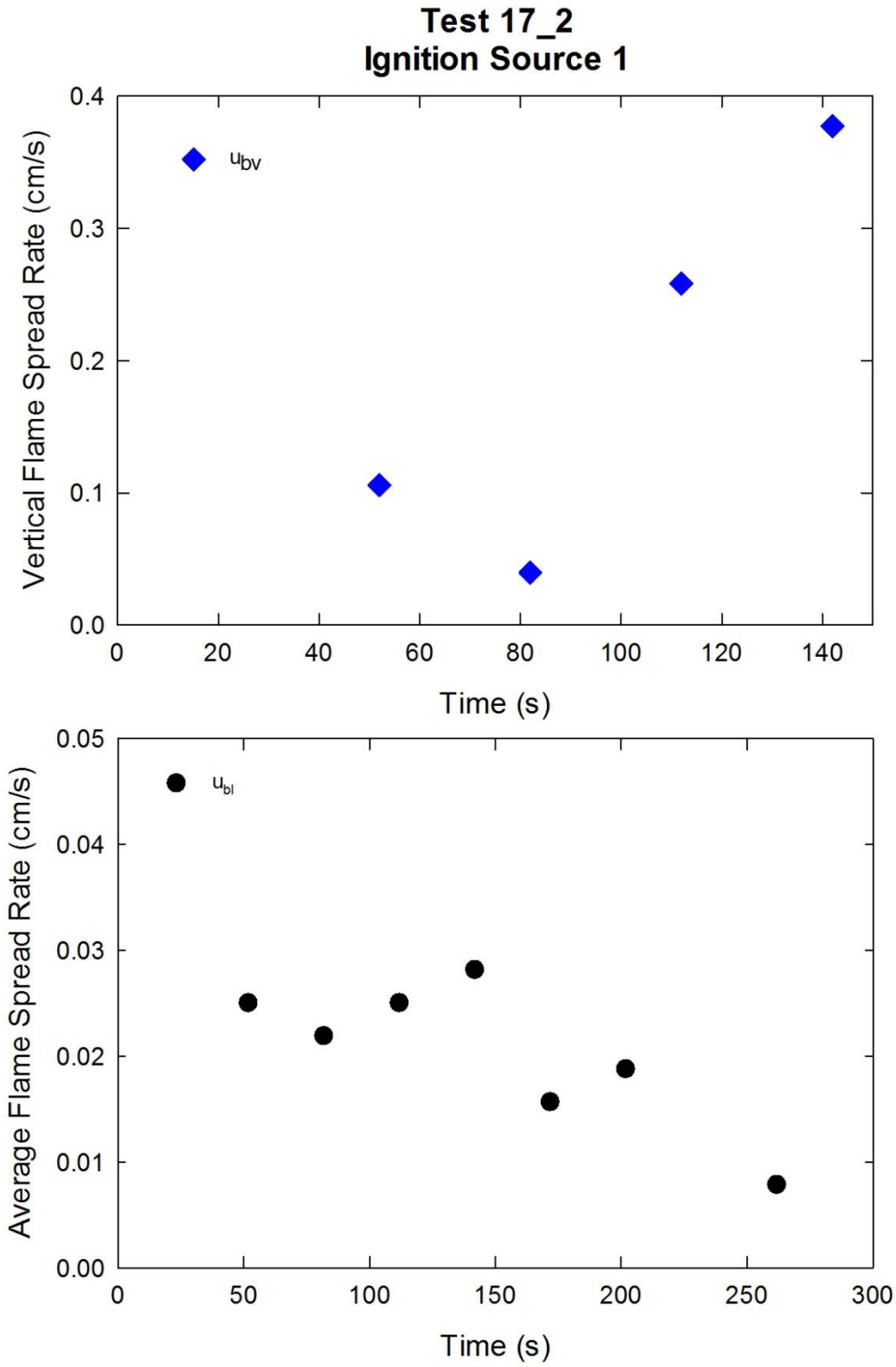

Figure A-135. Vertical flame spread rate on the back cushion (top) and average lateral flame spread rates on the back seat cushion (bottom) are plotted as a function of time for Test 17_2 following application of Ignition Source 1.

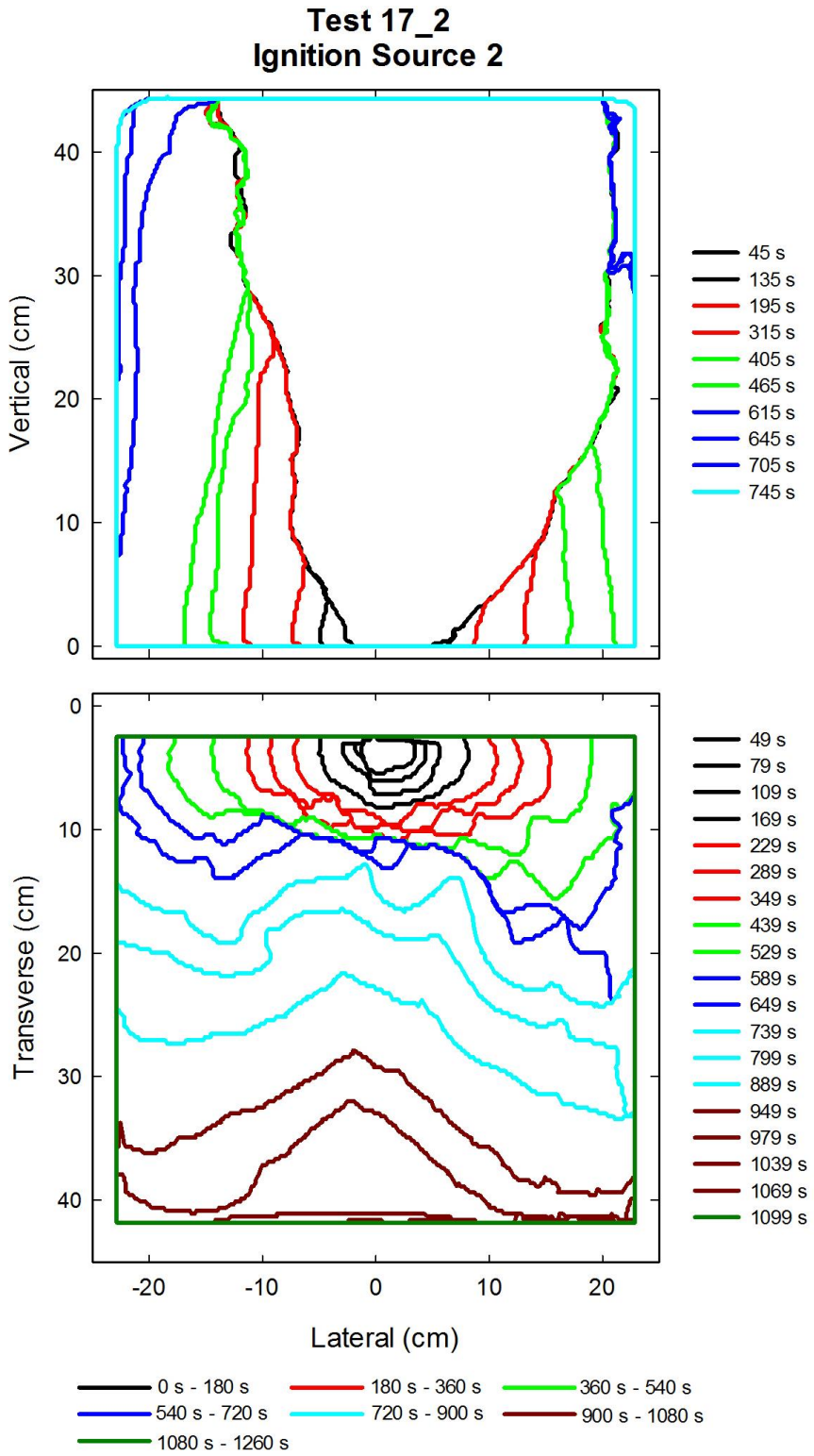

Figure A-136. Flame edge contours on the back (top) and seat (bottom) cushions are plotted as a function of time for Test 17_2 following application of Ignition Source 2.

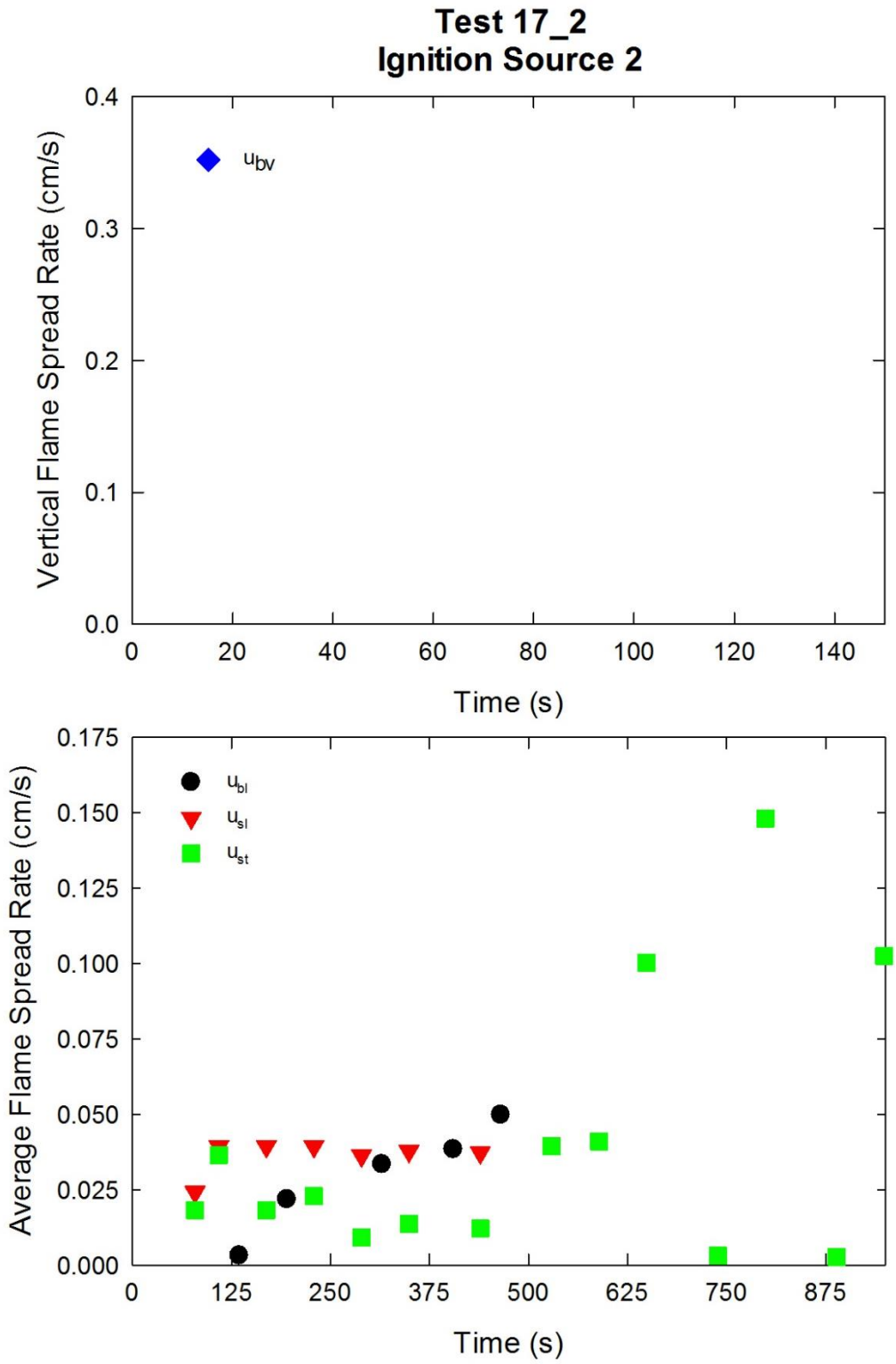

Figure A-137. Vertical flame spread rate on the back cushion (top) and average lateral flame spread rates on the back and seat cushions and transverse flame spread rate on the seat cushion (bottom) are plotted as a function of time for Test 17_2 following application of Ignition Source 2.

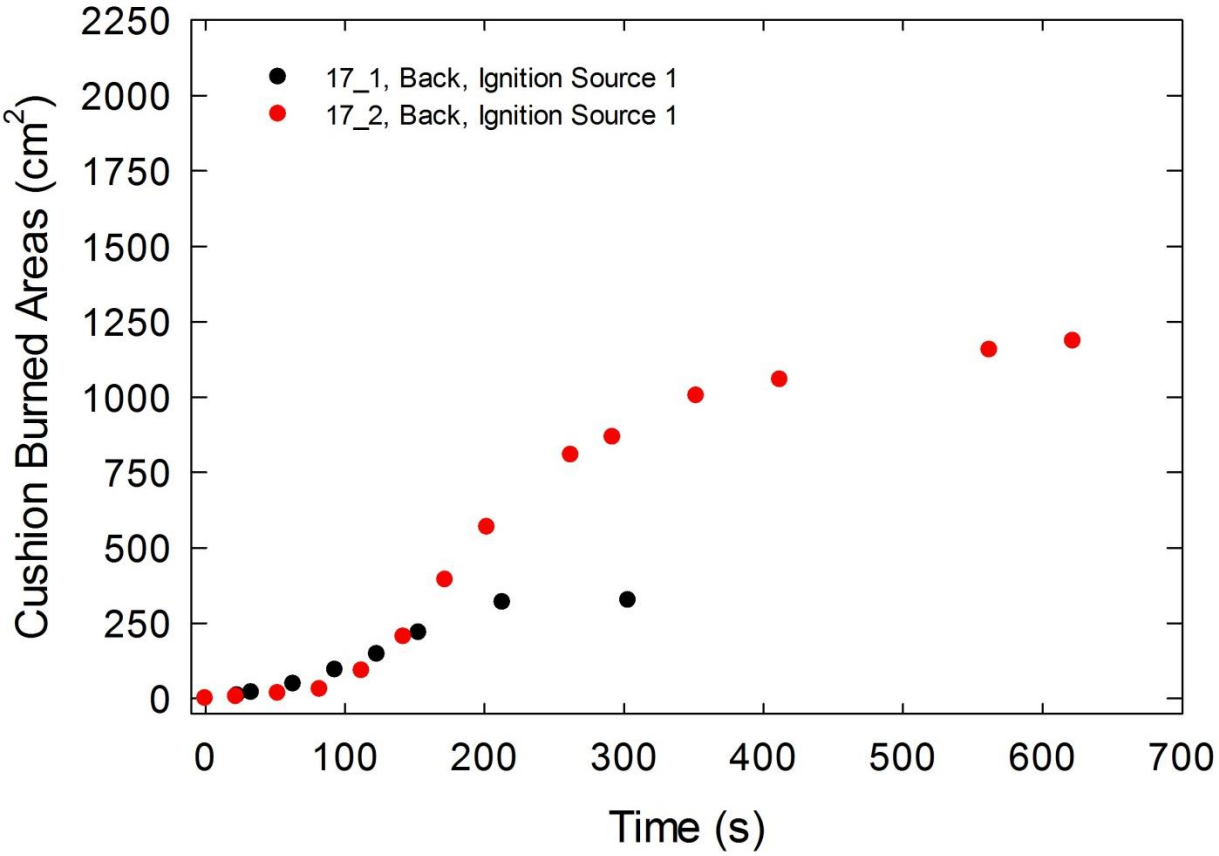

Figure A-138. Burned areas on the back cushion are plotted as a function of time for Combination 17 tests following application of Ignition Source 1.

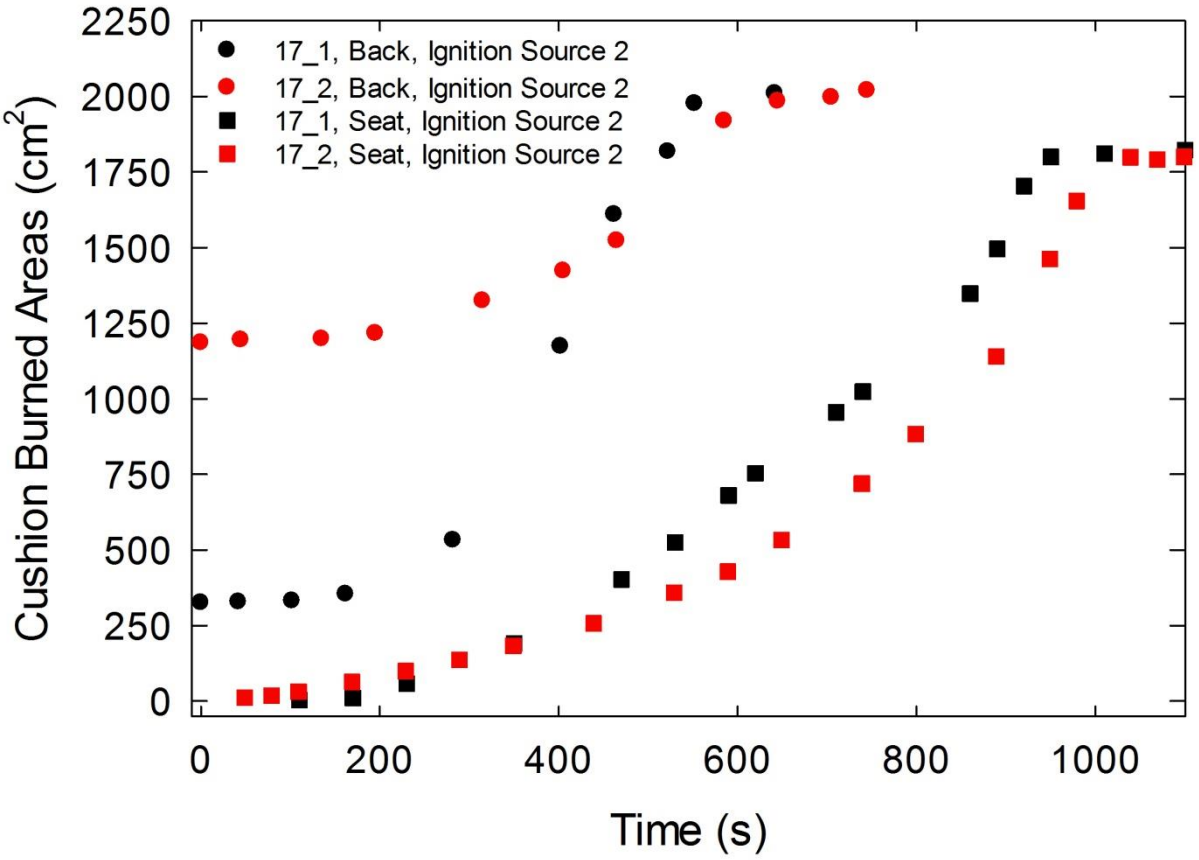

Figure A-139. Burned areas on the seat and back cushions are plotted as a function of time for Combination 17 tests following application of Ignition Source 2.

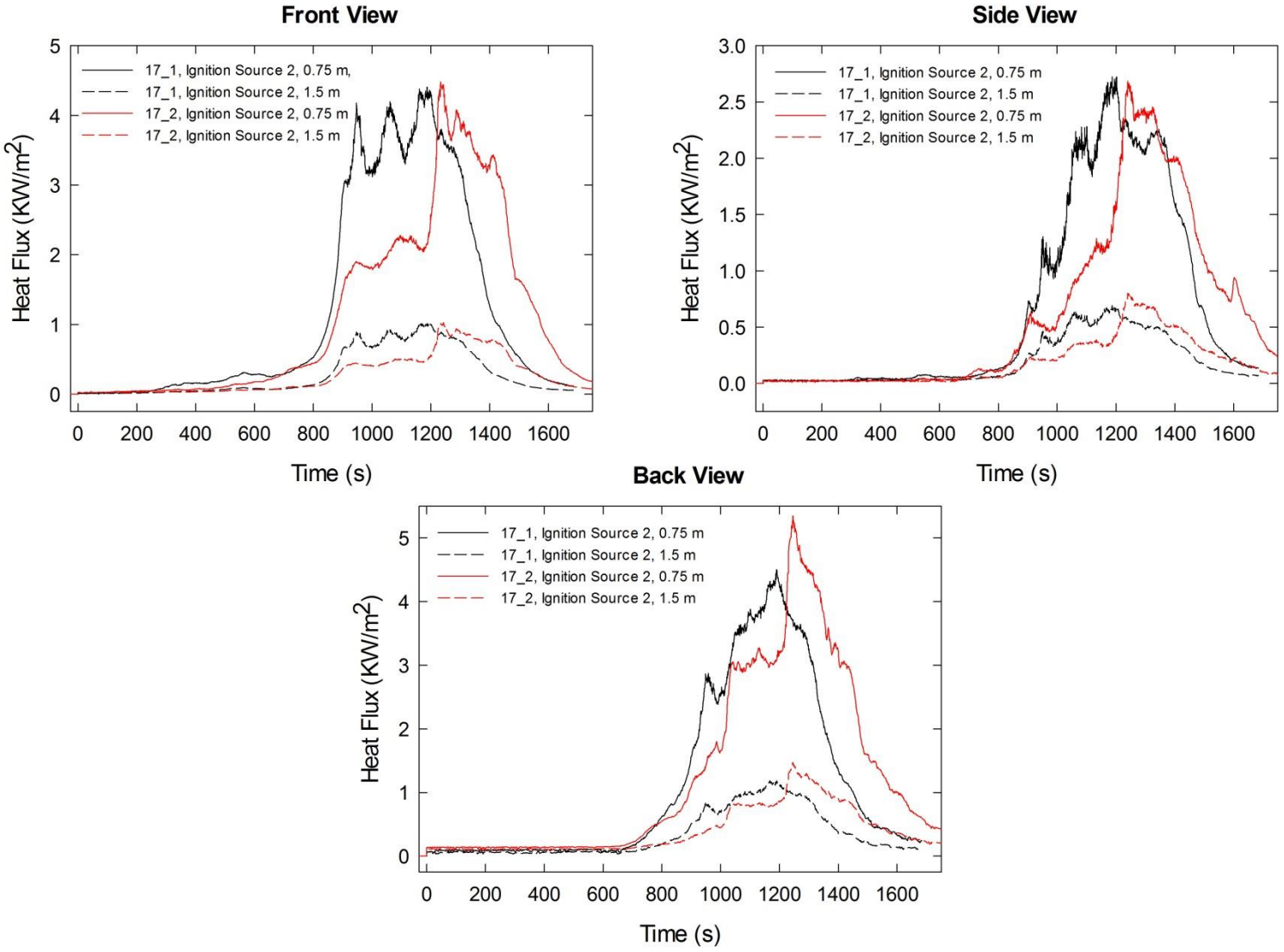

Figure A-140. Heat fluxes recorded at distances of 0.75 m and 1.5 m are plotted as a function of time for locations to the front, side and rear of the mock-up for Combination 17 tests following application of Ignition Source 2.

A.14 Combination 18

78%PP/22%PE/Norfab/NFRFPUF

Notes:

Test 1:

Ignition Source 1 applied at time = 0 s.

Test 2:

Ignition Source 1 applied at time = 0 s.

Initial mass reading (3.66 kg) during the experiment agreed with an earlier measurement for the mock-up (3.72 kg); mass readings increased during initial period of test, showed periods with no change, and displayed non-physical abrupt jumps; **these mass data were excluded from analysis**.

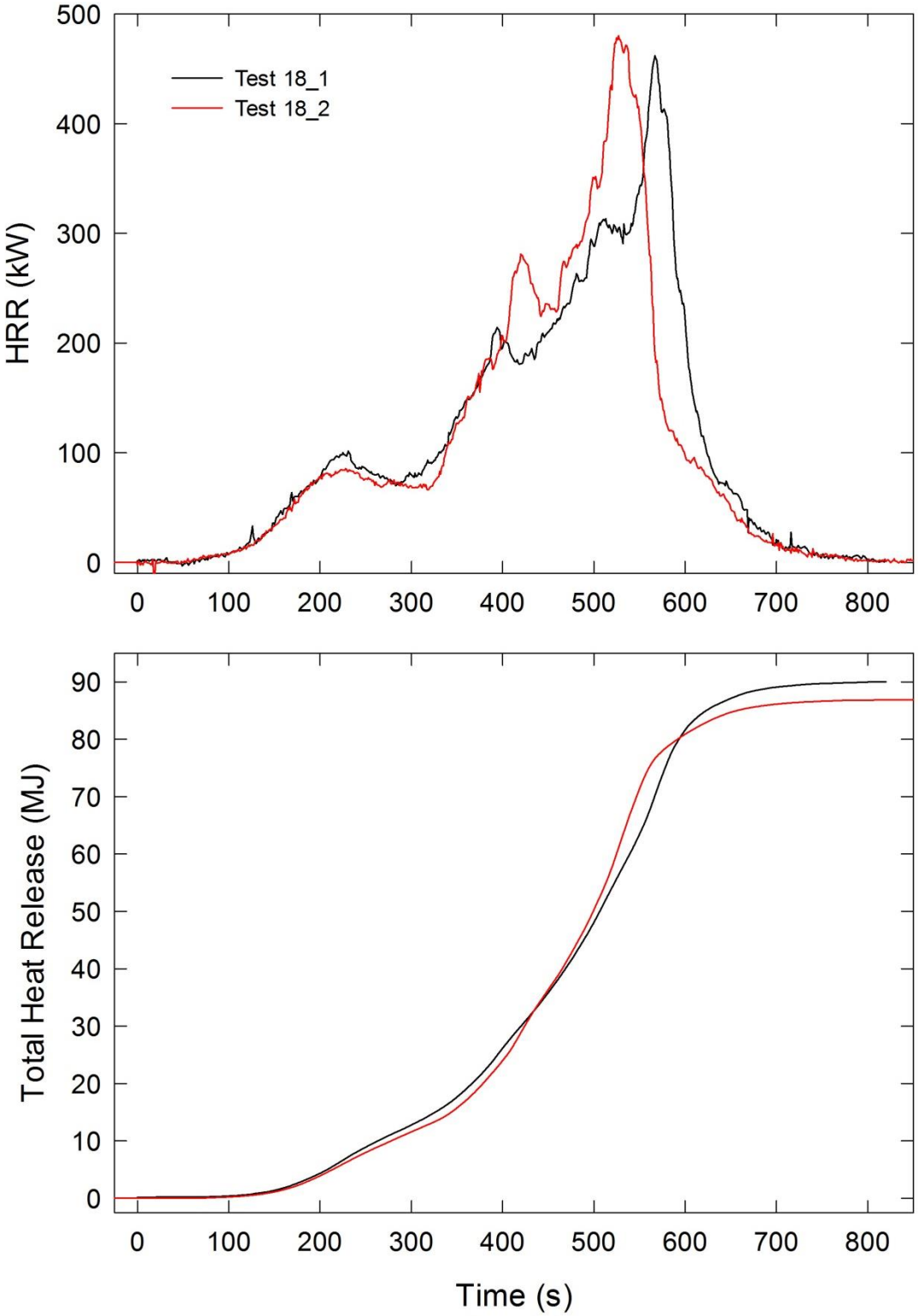

Figure A-141. Temporal profiles of HRR and integrated HRR are shown for Combination 18 tests following application of Ignition Source 1.

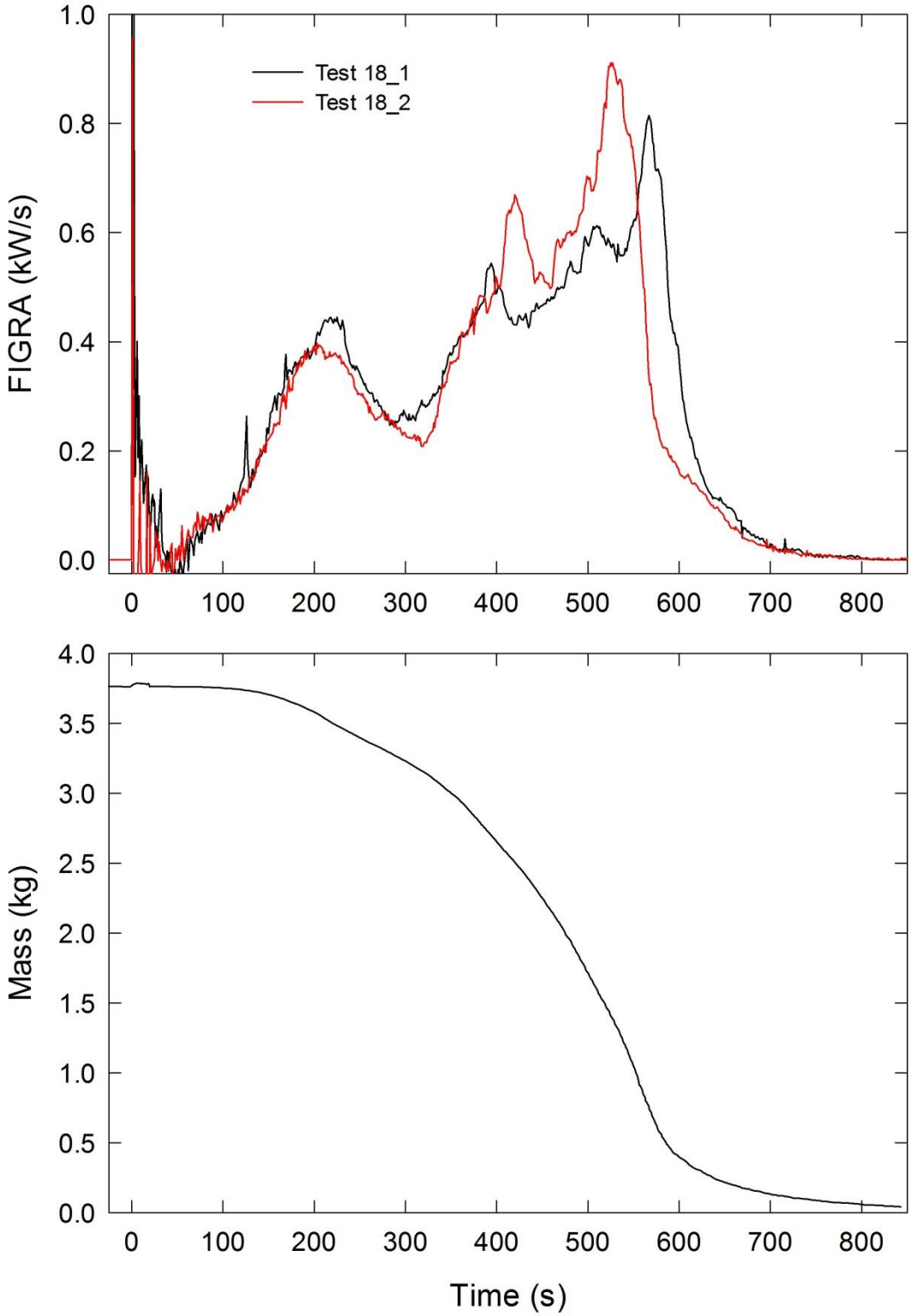

Figure A-142. Temporal profiles of FIGRA for Combination 18 tests and mock-up mass for Test 18_1 are shown following application of Ignition Source 1.

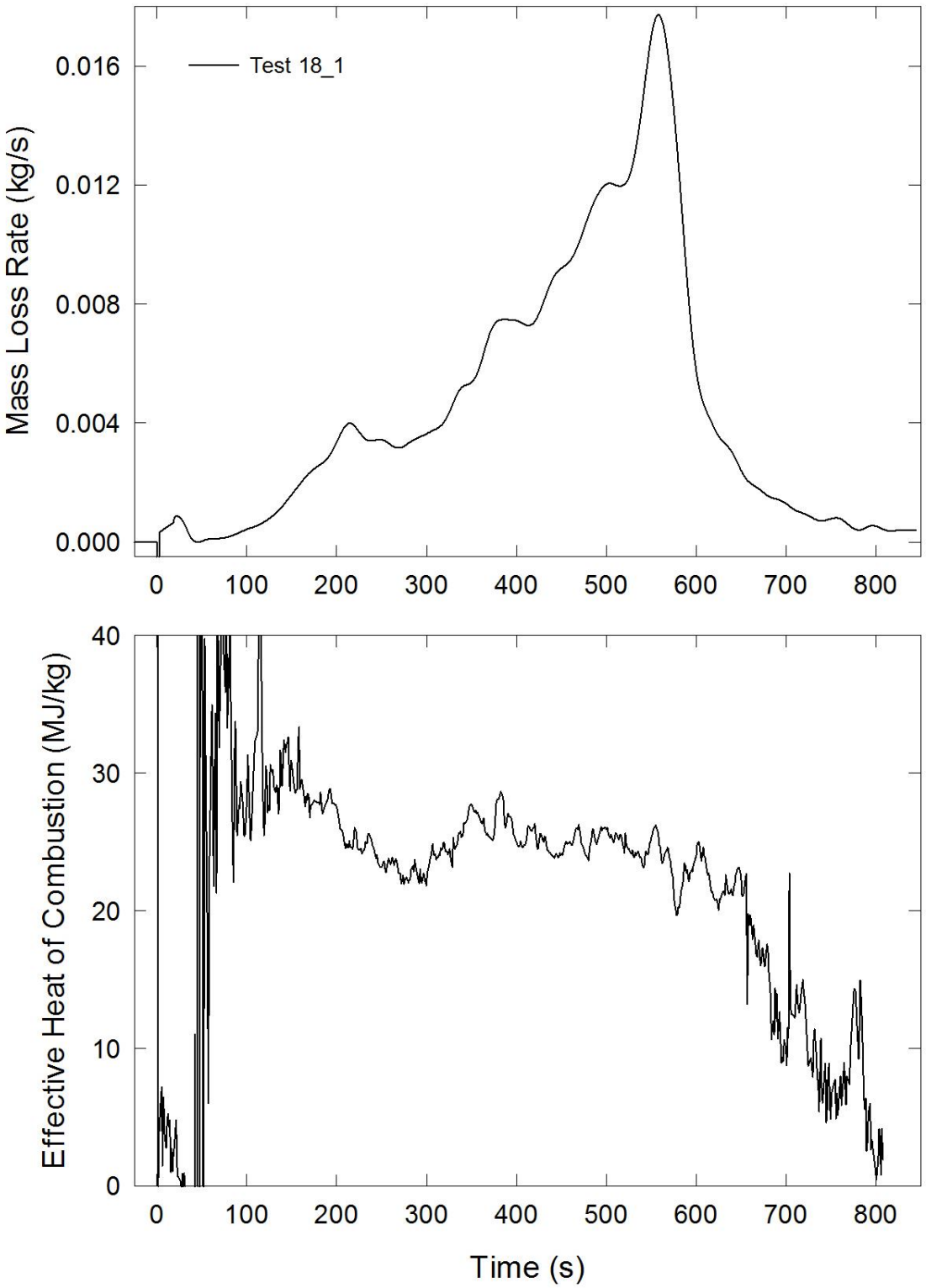

Figure A-143. Temporal profiles of MLR and EHOC are shown for Test 18_1 following application of Ignition Source 1.

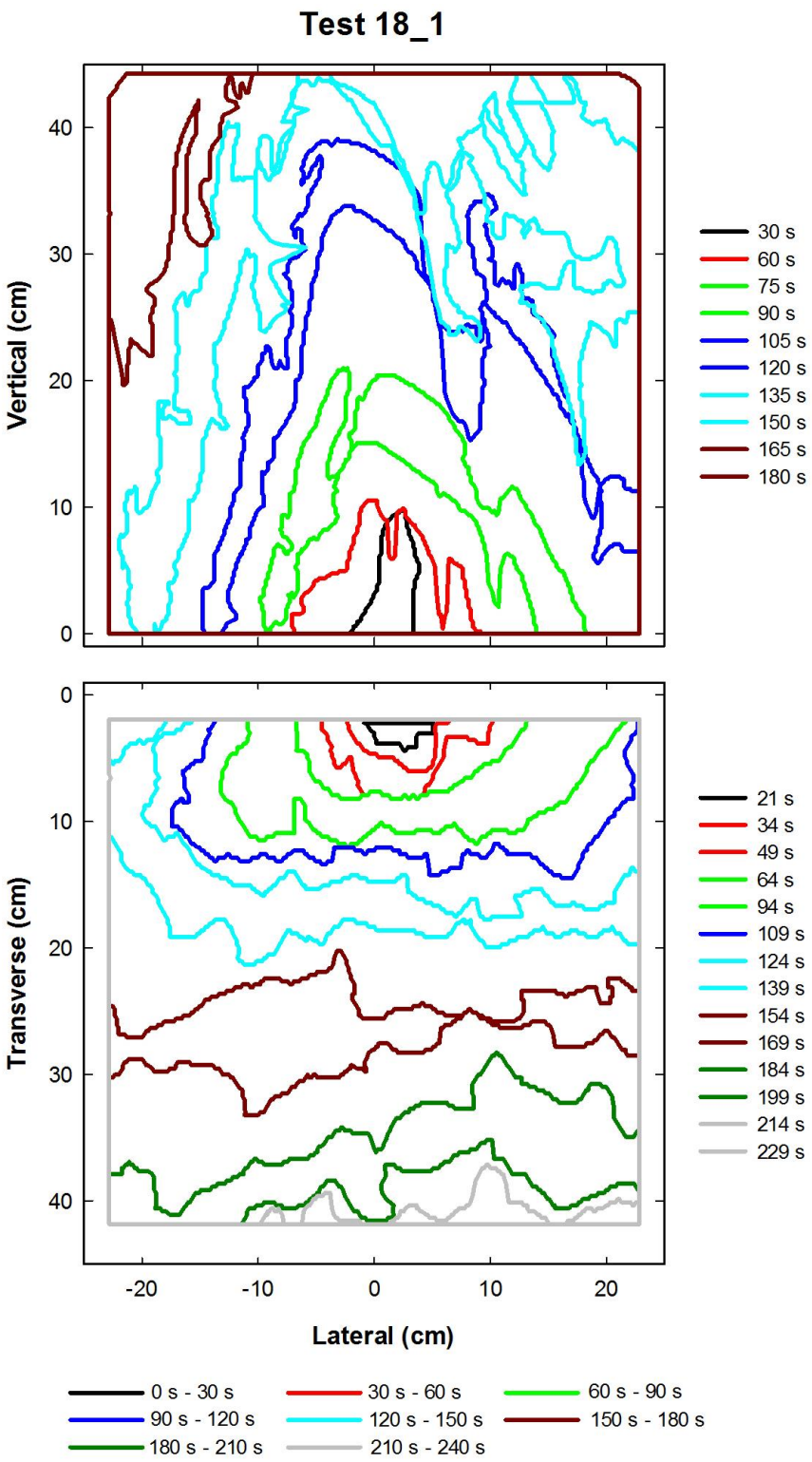

Figure A-144. Flame edge contours on the back (top) and seat (bottom) cushions are plotted as a function of time for Test 18_1 following application of Ignition Source 1.

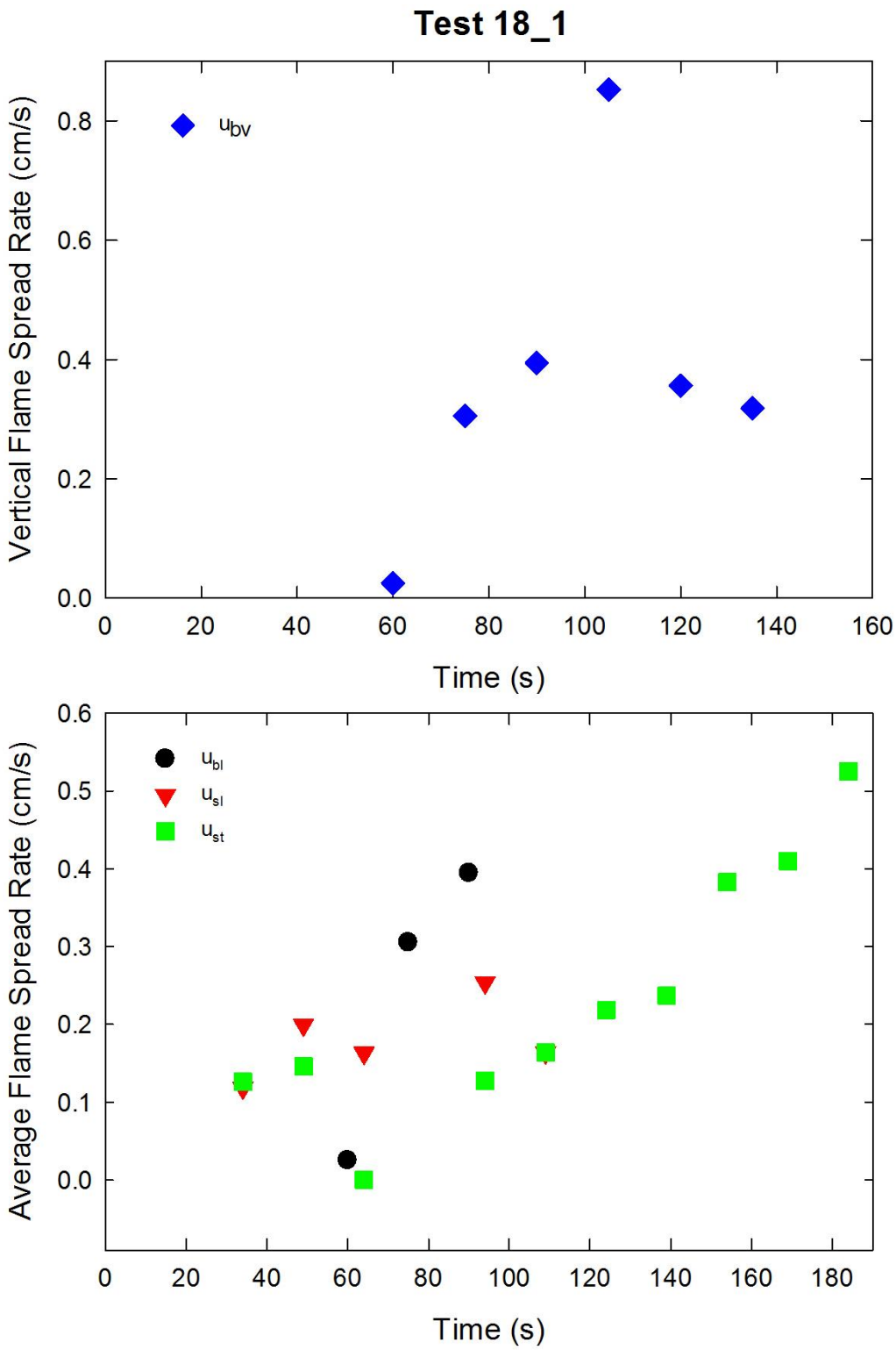

Figure A-145. Vertical flame spread rate on the back cushion (top) and average lateral flame spread rates on the back and seat cushions and transverse flame spread rate on the seat cushion (bottom) are plotted as a function of time for Test 18_1 following application of Ignition Source 1.

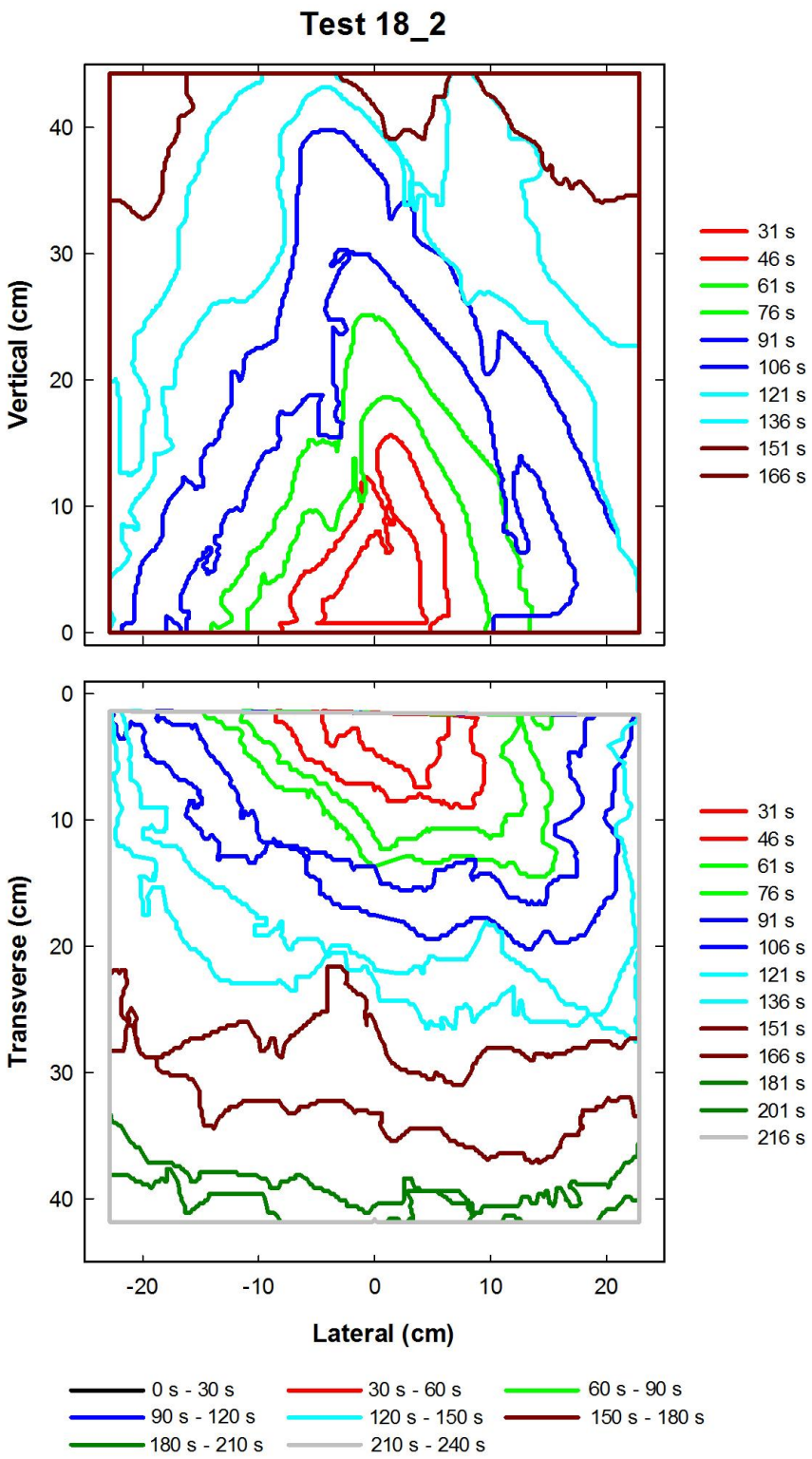

Figure A-146. Flame edge contours on the back (top) and seat (bottom) cushions are plotted as a function of time for Test 18_2 following application of Ignition Source 1.

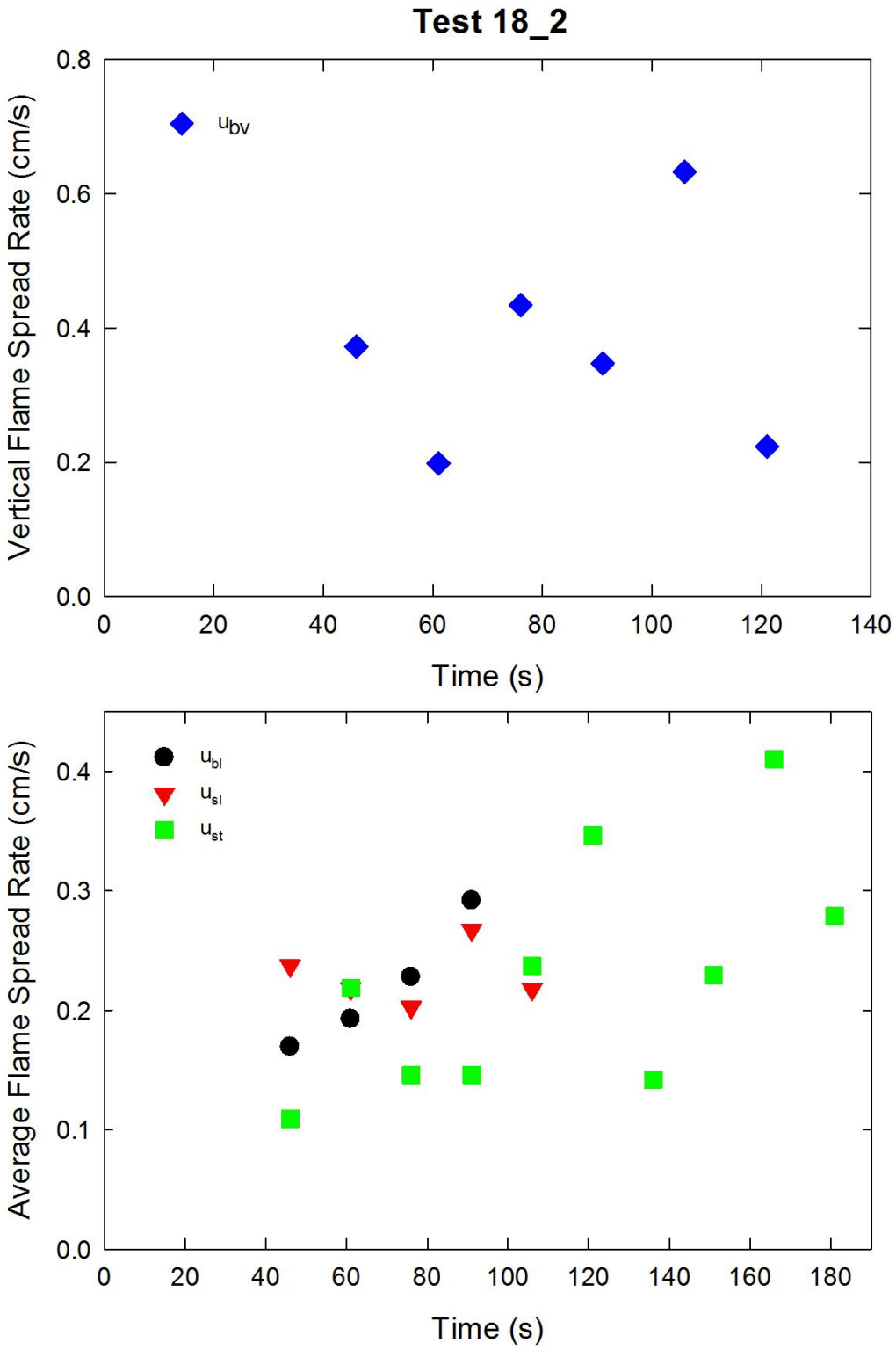

Figure A-147. Vertical flame spread rate on the back cushion (top) and average lateral flame spread rates on the back and seat cushions and transverse flame spread rate on the seat cushion (bottom) are plotted as a function of time for Test 18_2 following application of Ignition Source 1.

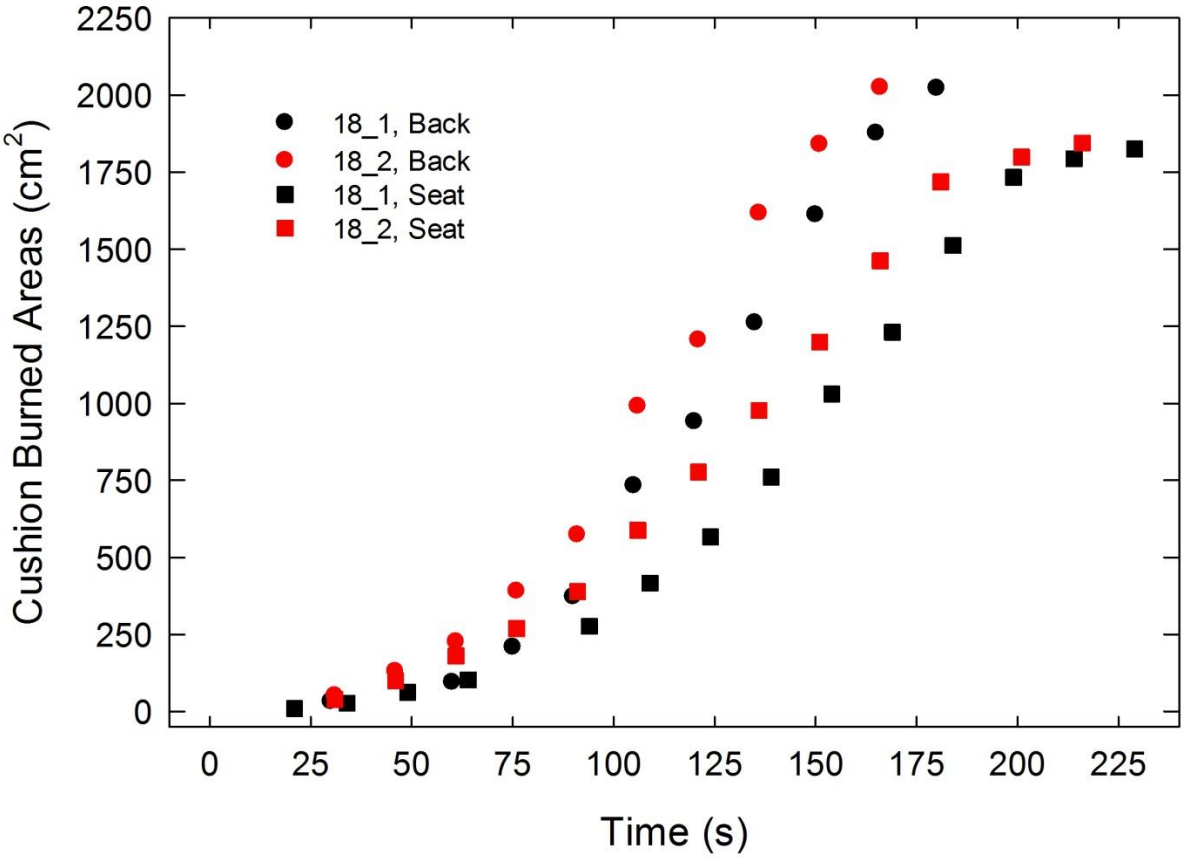

Figure A-148. Burned areas on the seat and back cushions are plotted as a function of time for Combination 18 tests following application of Ignition Source 1.

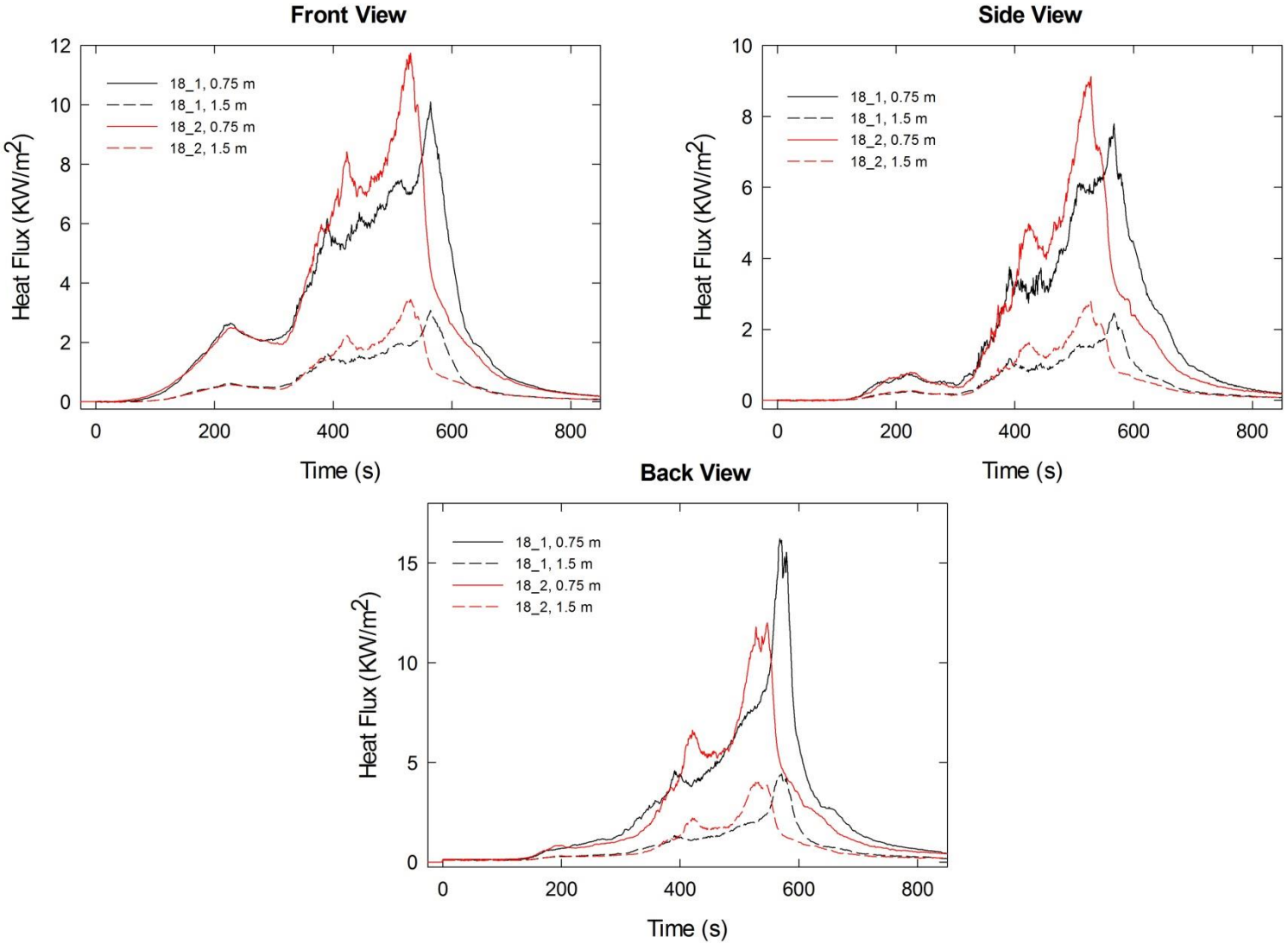

Figure A-149. Heat fluxes recorded at distances of 0.75 m and 1.5 m are plotted as a function of time for locations to the front, side and rear of the mock-up for Combination 18 tests following application of Ignition Source 1.

A.15 Combination 19

cotton/Norfab/PEFW/NFRFPUF

Notes:

Test 1:

Ignition Source 1 applied at time = 0 s; small triangle-shaped blackened area on back cushion, no evident flame spread; very small darkened area on seat cushion, no flame spread.

Ignition Source 1 was reapplied 63 s after removal; flame spread to the top of the back cushion with very little lateral flame spread; very small darkened area on seat cushion, no flame spread.

Ignition Source 2 applied 335 s after second Ignition Source 1 removed; following removal of ignition source, limited flame spread on the back and seat cushions.

Ignition Source 5 ignited 1085 s after Ignition Source 2 removed; limited additional flame spread on back and seat cushions.

Test 2:

Ignition Source 1 applied at time = 0 s; following removal of ignition source, upward flame spread with limited lateral spread on back cushion; small darkened area on seat cushion with no flame spread.

Ignition Source 2 applied 490 s after Ignition Source 1 removed; following slow flame spread on the right sides of the seat and back cushions, full mock-up became involved.

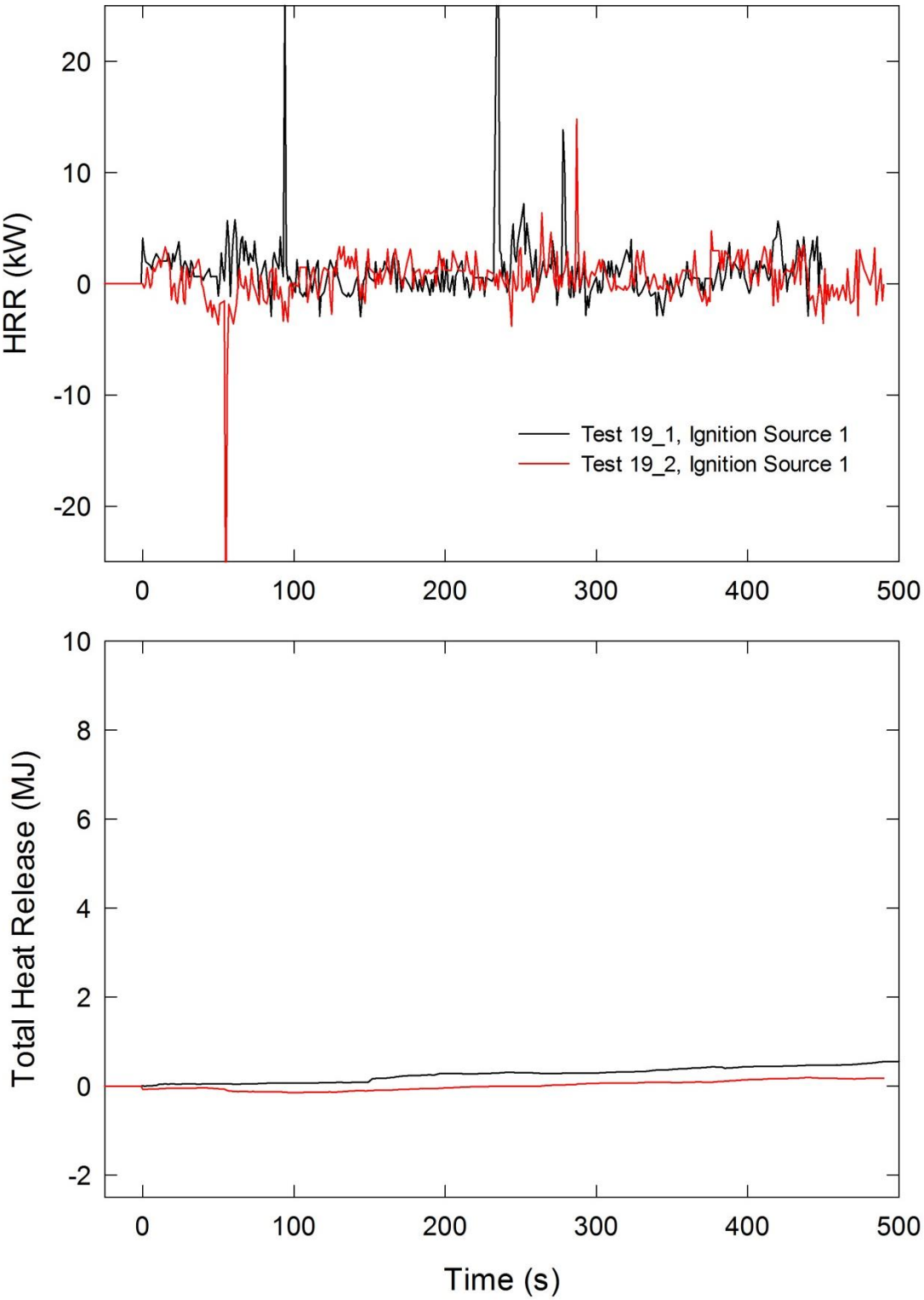

Figure A-150. Temporal profiles of HRR and integrated HRR are shown for Combination 19 tests following application of Ignition Source 1.

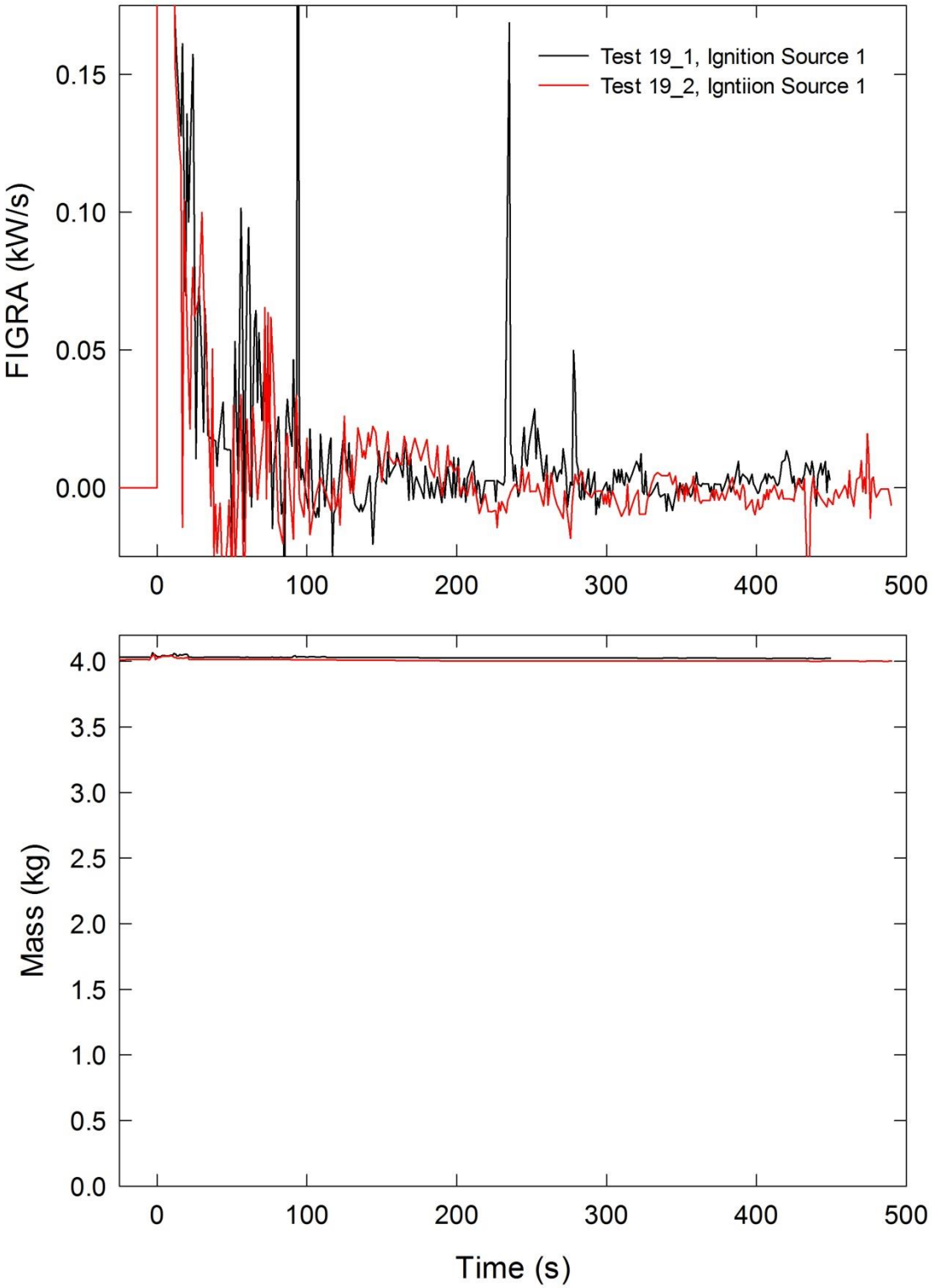

Figure A-151. Temporal profiles of FIGRA and mock-up mass are shown for Combination 19 tests following application of Ignition Source 1.

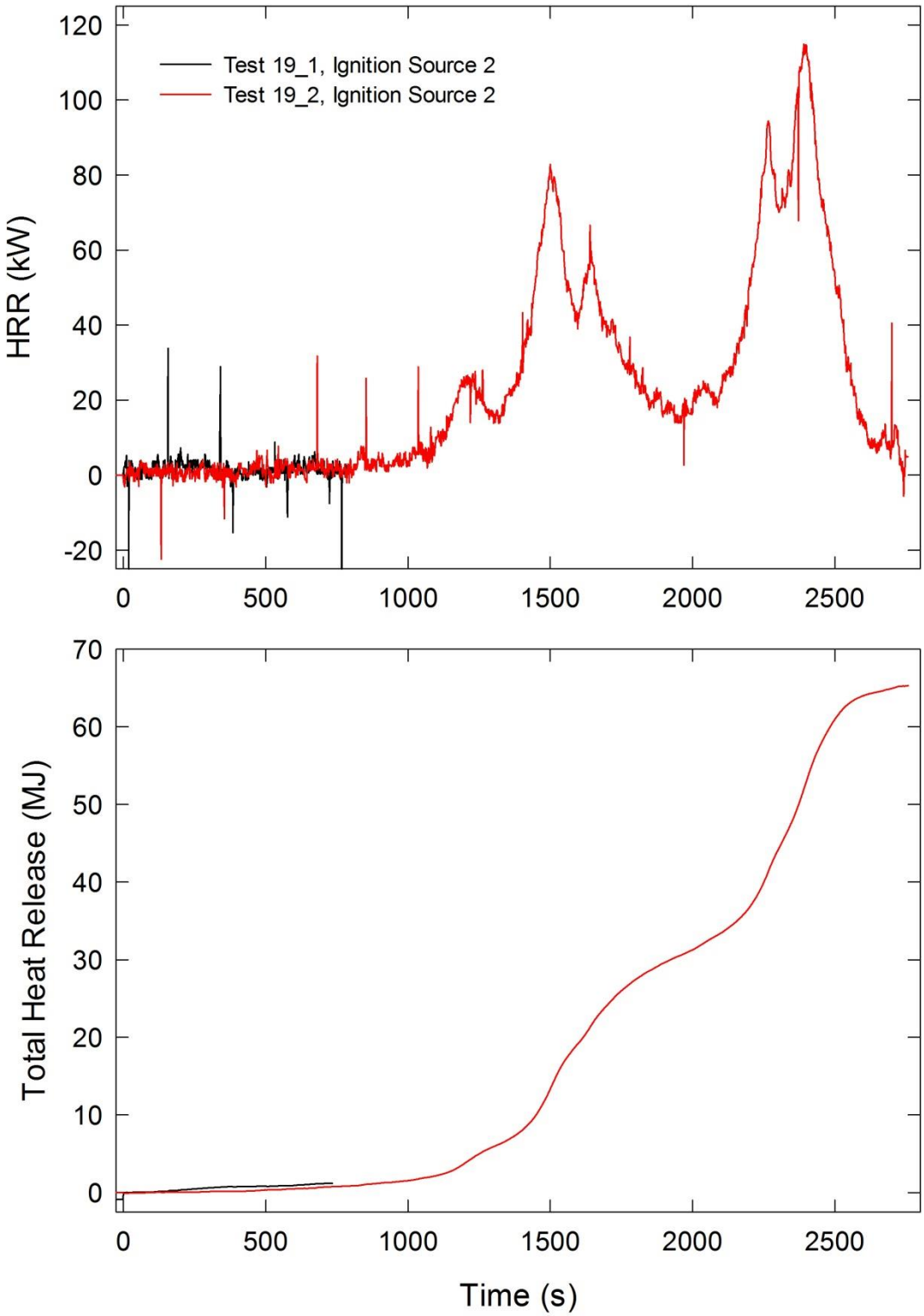

Figure A-152. Temporal profiles of HRR and integrated HRR are shown for Combination 19 tests following application of Ignition Source 2.

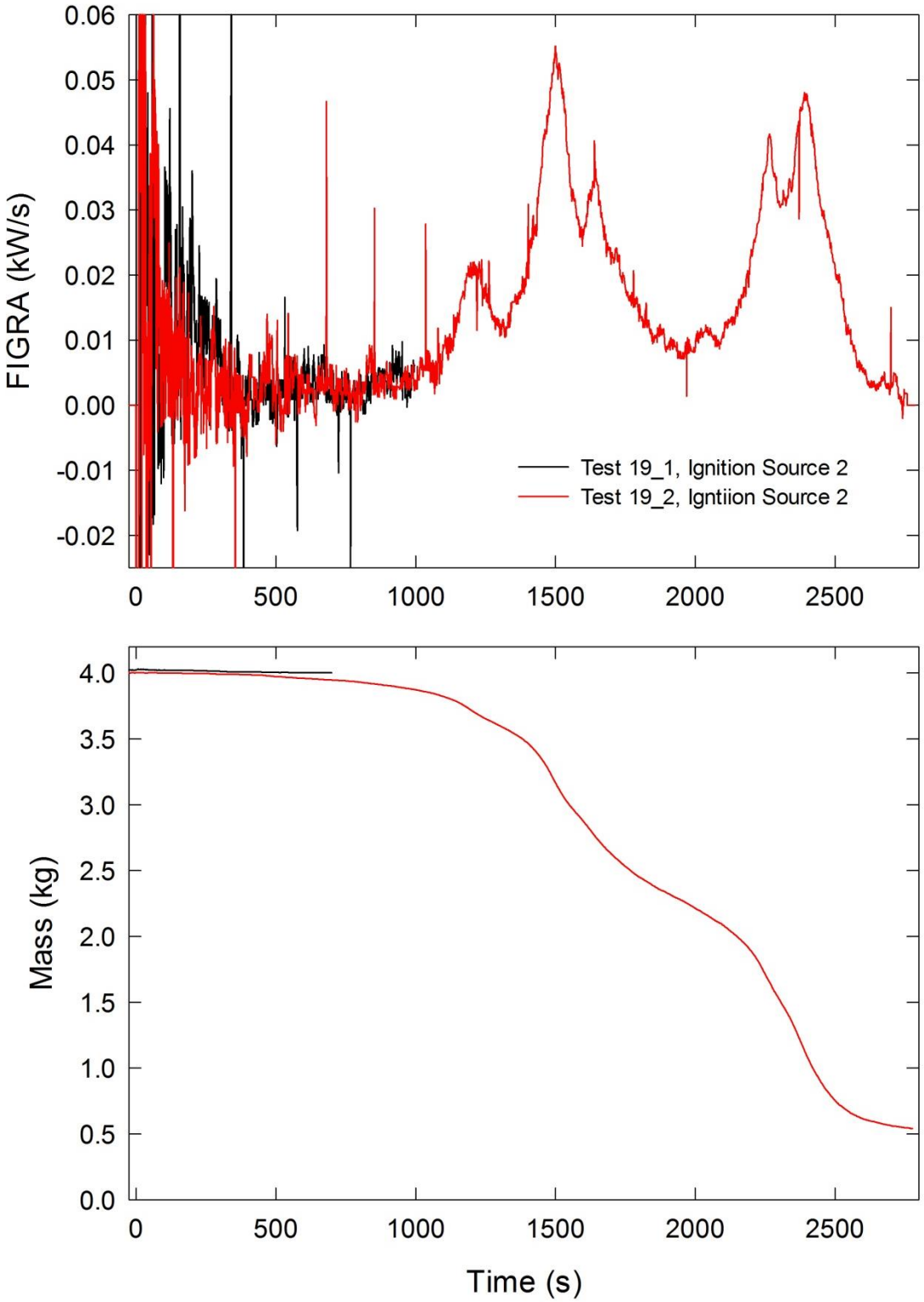

Figure A-153. Temporal profiles of FIGRA and mock-up mass are shown for Combination 19 tests following application of Ignition Source 2.

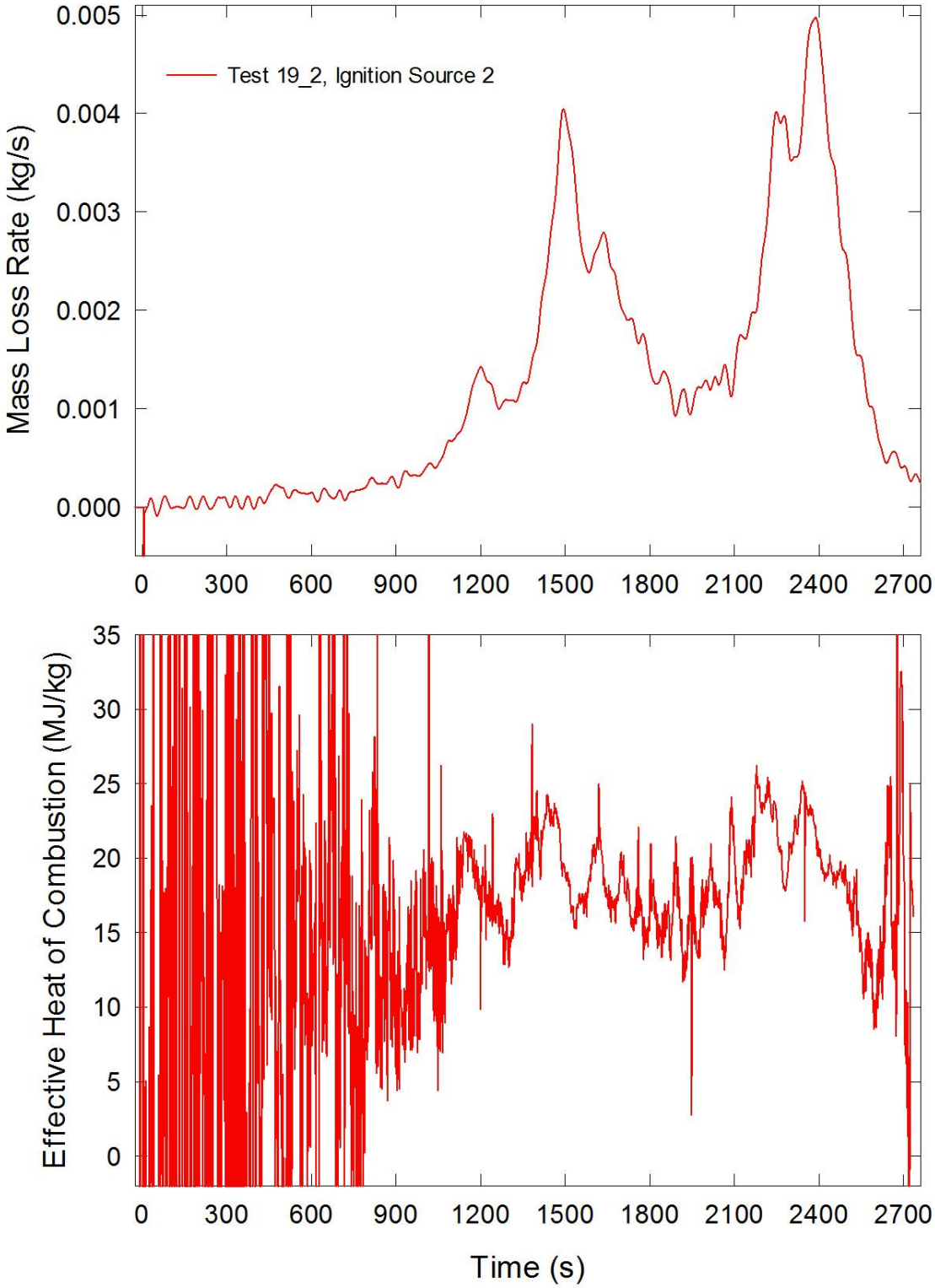

Figure A-154. Temporal profiles of MLR and EHOC are shown for Test 19_2 following application of Ignition Source 2.

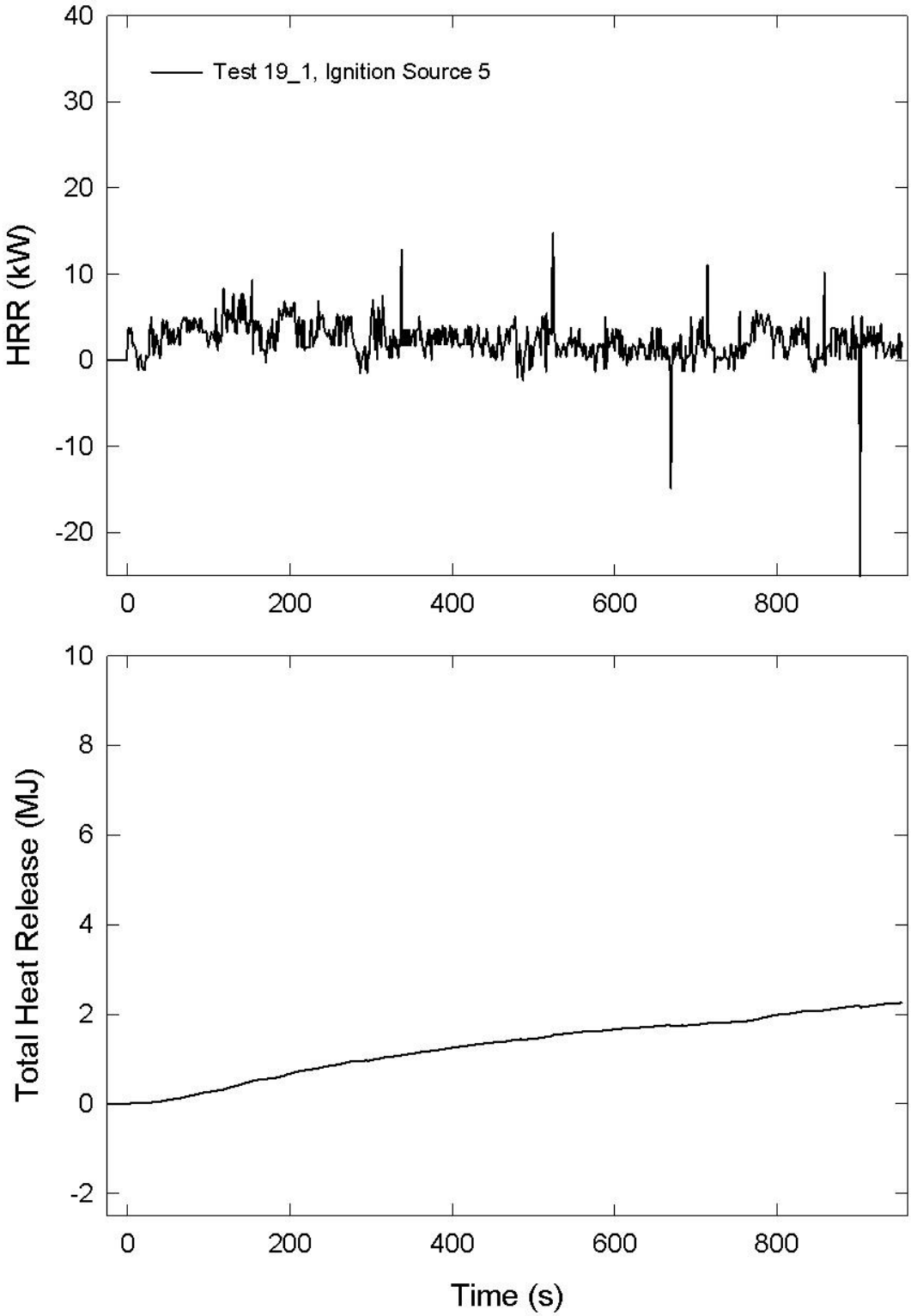

Figure A-155. Temporal profiles of HRR and integrated HRR are shown for Test 19_1 tests following application of Ignition Source 5.

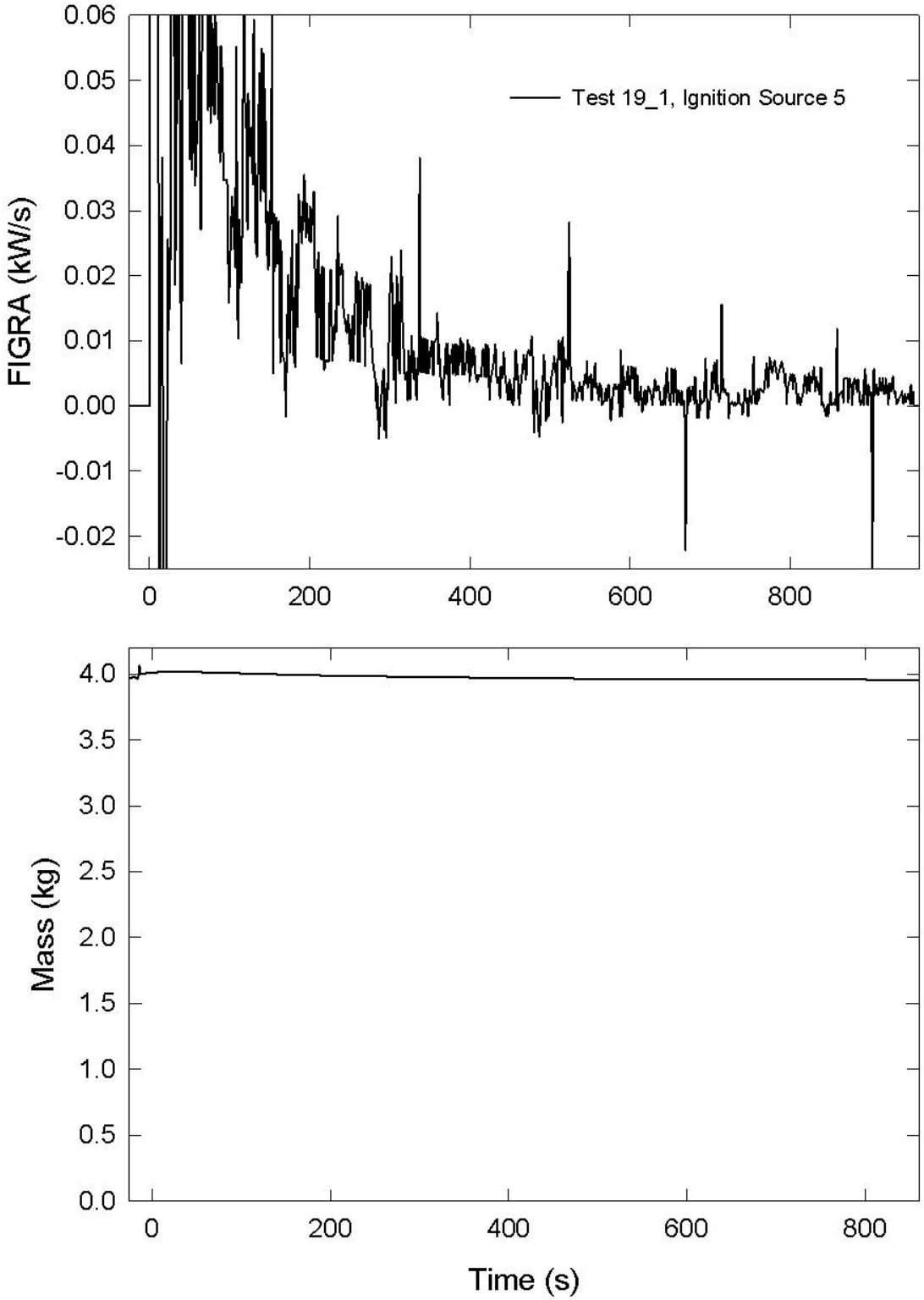

Figure A-156. Temporal profiles of FIGRA and mock-up mass are shown for Test 19_1 following application of Ignition Source 5.

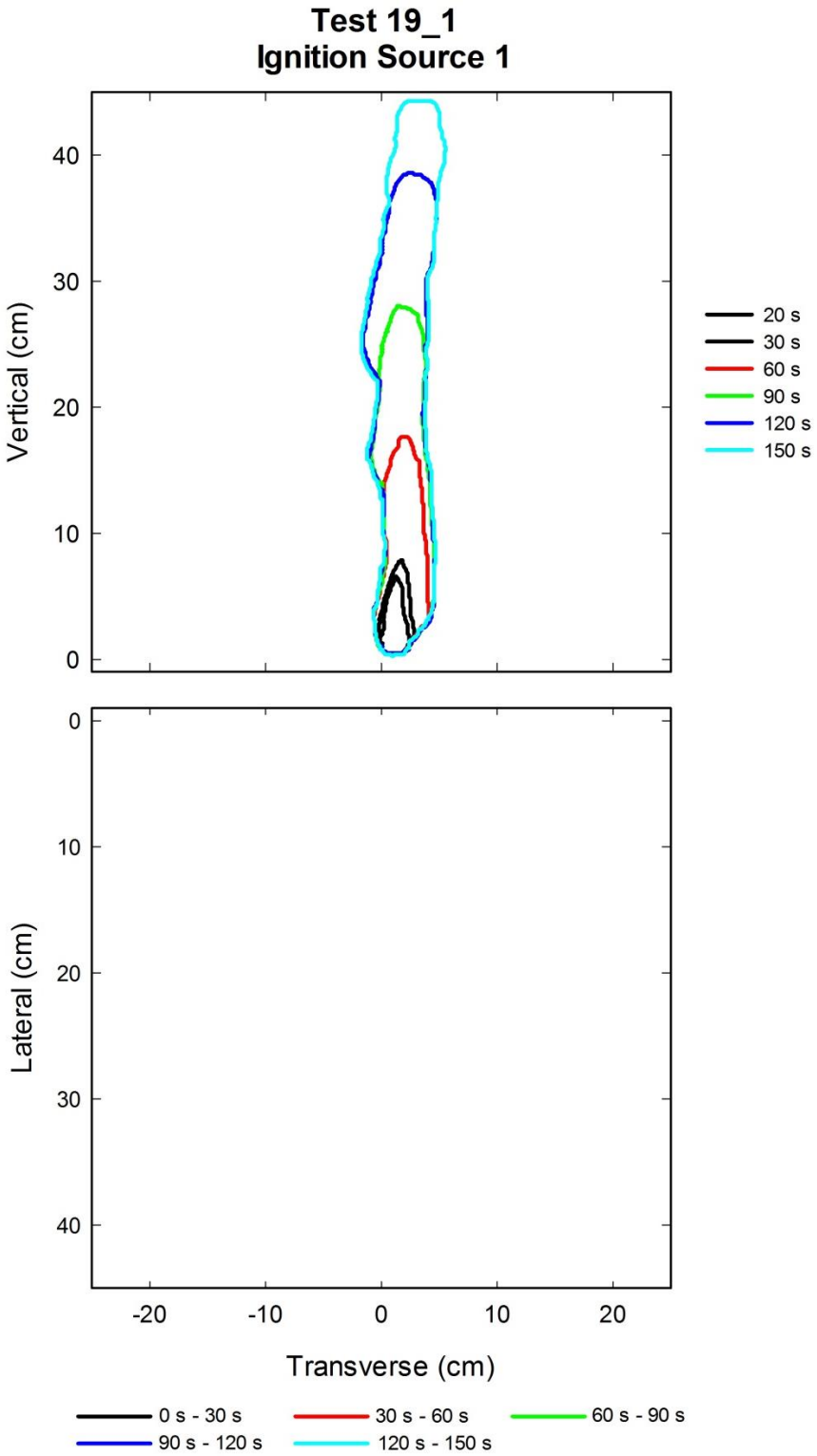

Figure A-157. Flame edge contours on the back (top) and seat (bottom) cushions are plotted as a function of time for Test 19_1 following application of Ignition Source 1.

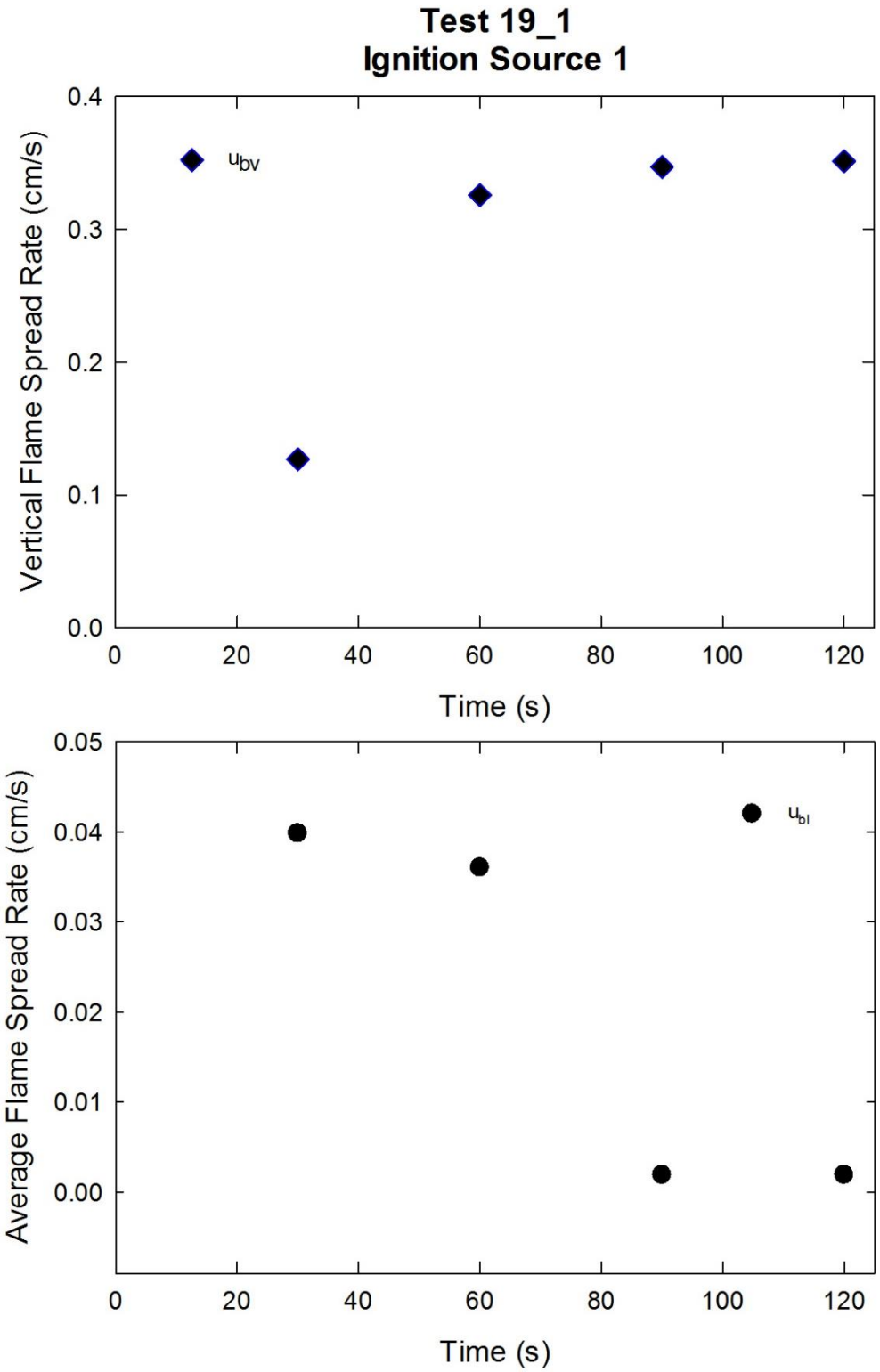

Figure A-158. Vertical flame spread rate on the back cushion (top) and average lateral flame spread rate on the back cushion (bottom) are plotted as a function of time for Test 19_1 following application of Ignition Source 1.

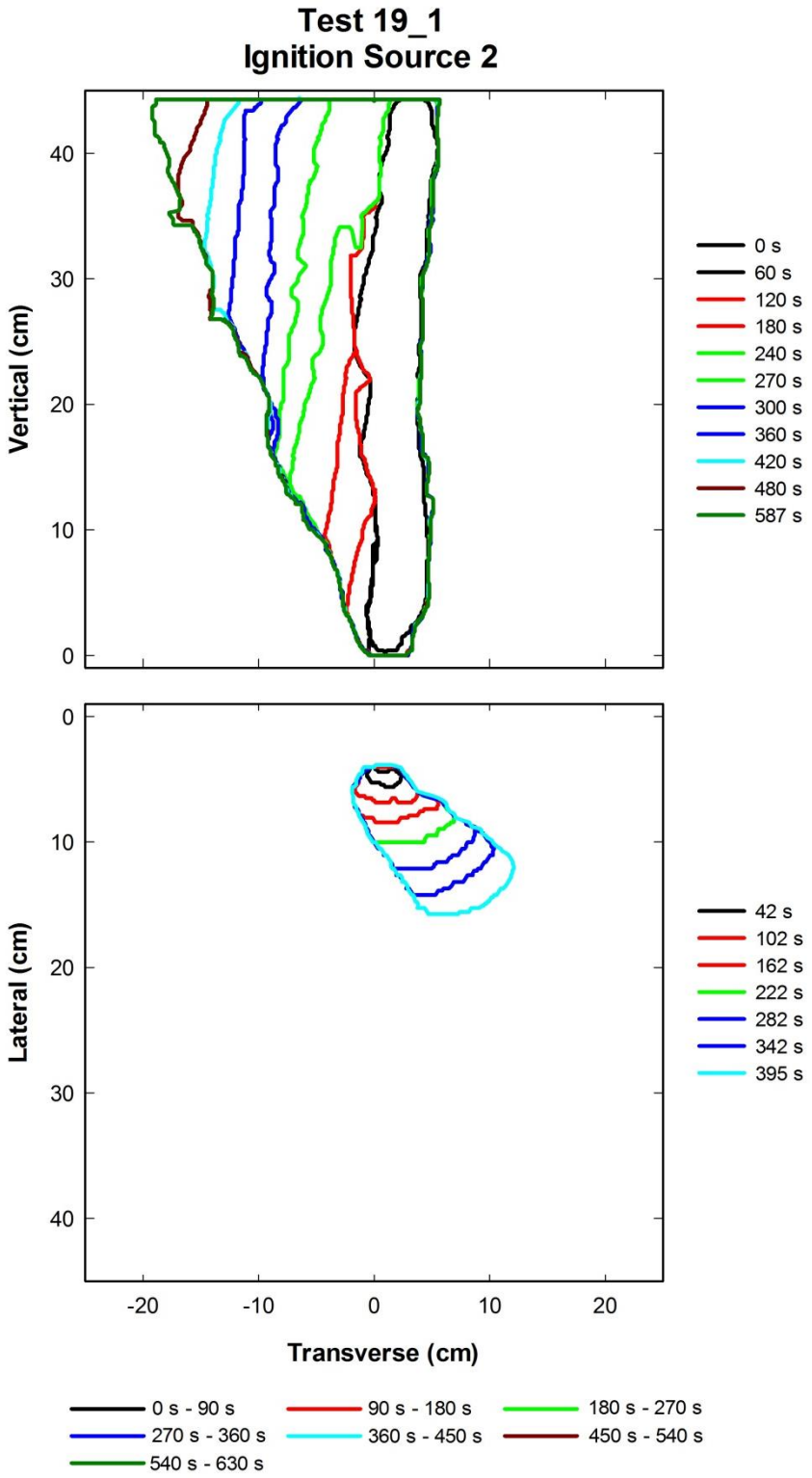

Figure A-159. Flame edge contours on the back (top) and seat (bottom) cushions are plotted as a function of time for Test 19_1 following application of Ignition Source 2.

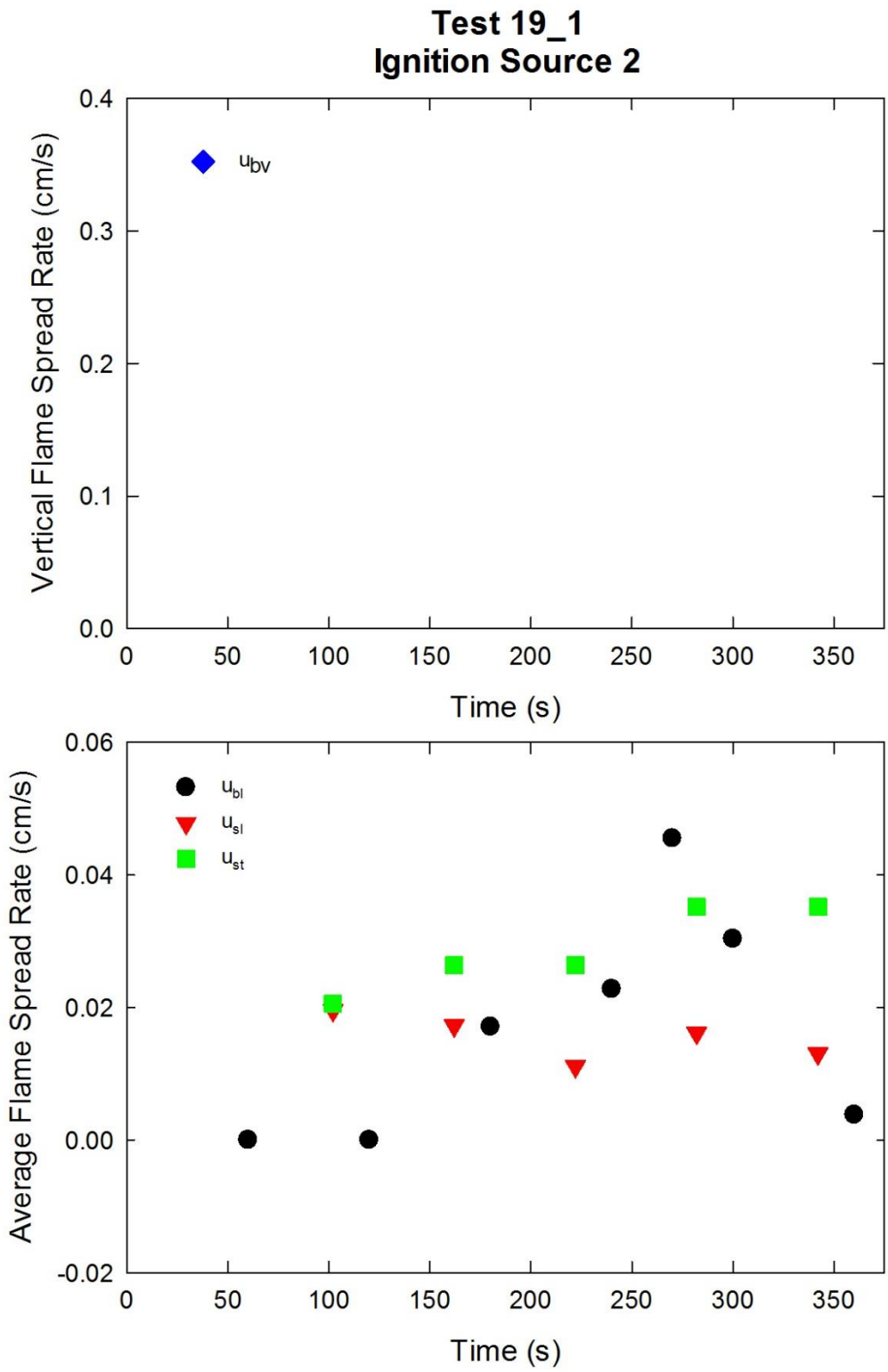

Figure A-160. Vertical flame spread rate on the back cushion (top) and average lateral flame spread rates on the back and seat cushions and transverse flame spread rate on the seat cushion (bottom) are plotted as a function of time for Test 19_1 following application of Ignition Source 2.

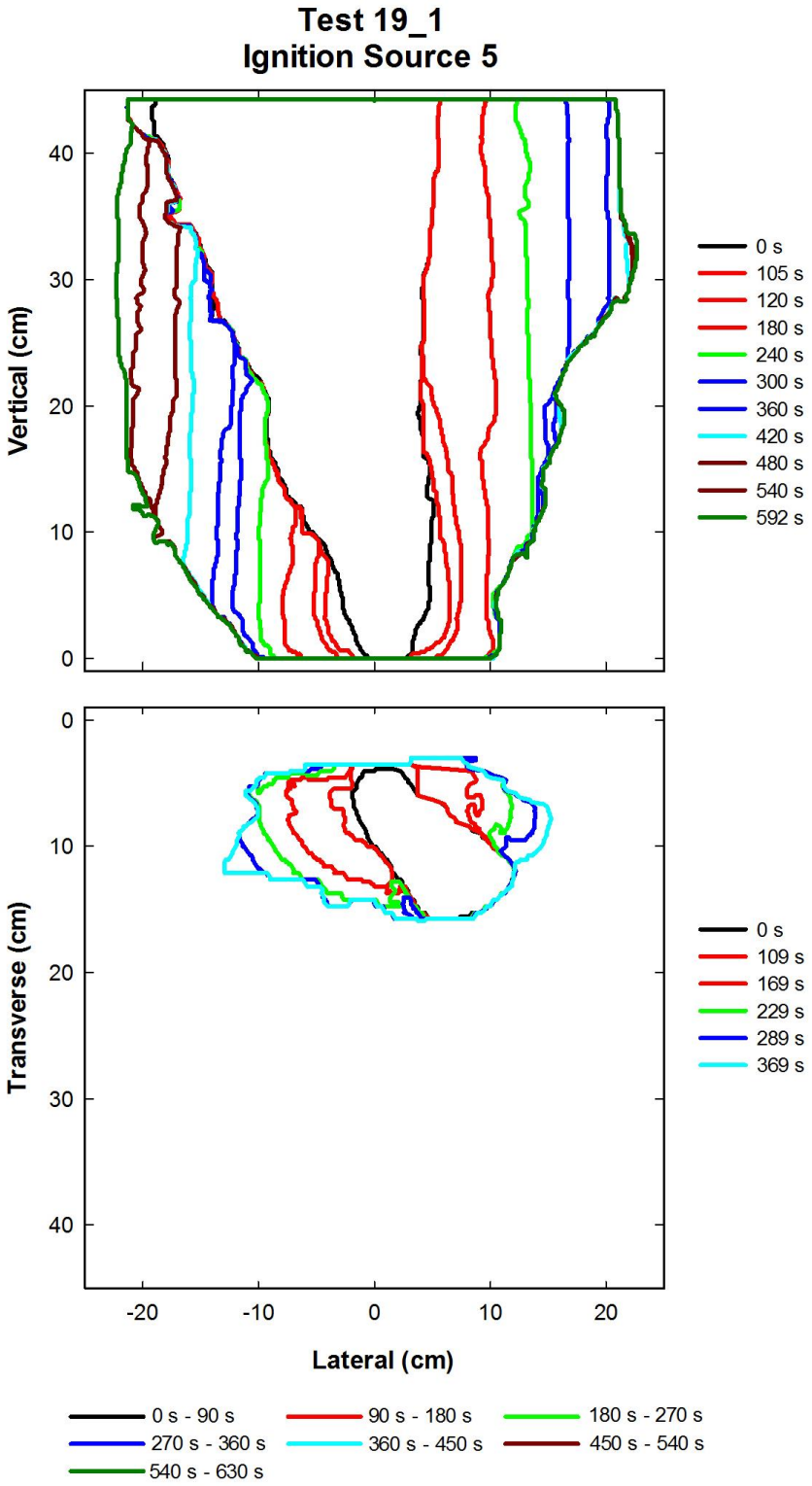

Figure A-161. Flame edge contours on the back (top) and seat (bottom) cushions are plotted as a function of time for Test 19_1 following application of Ignition Source 5.

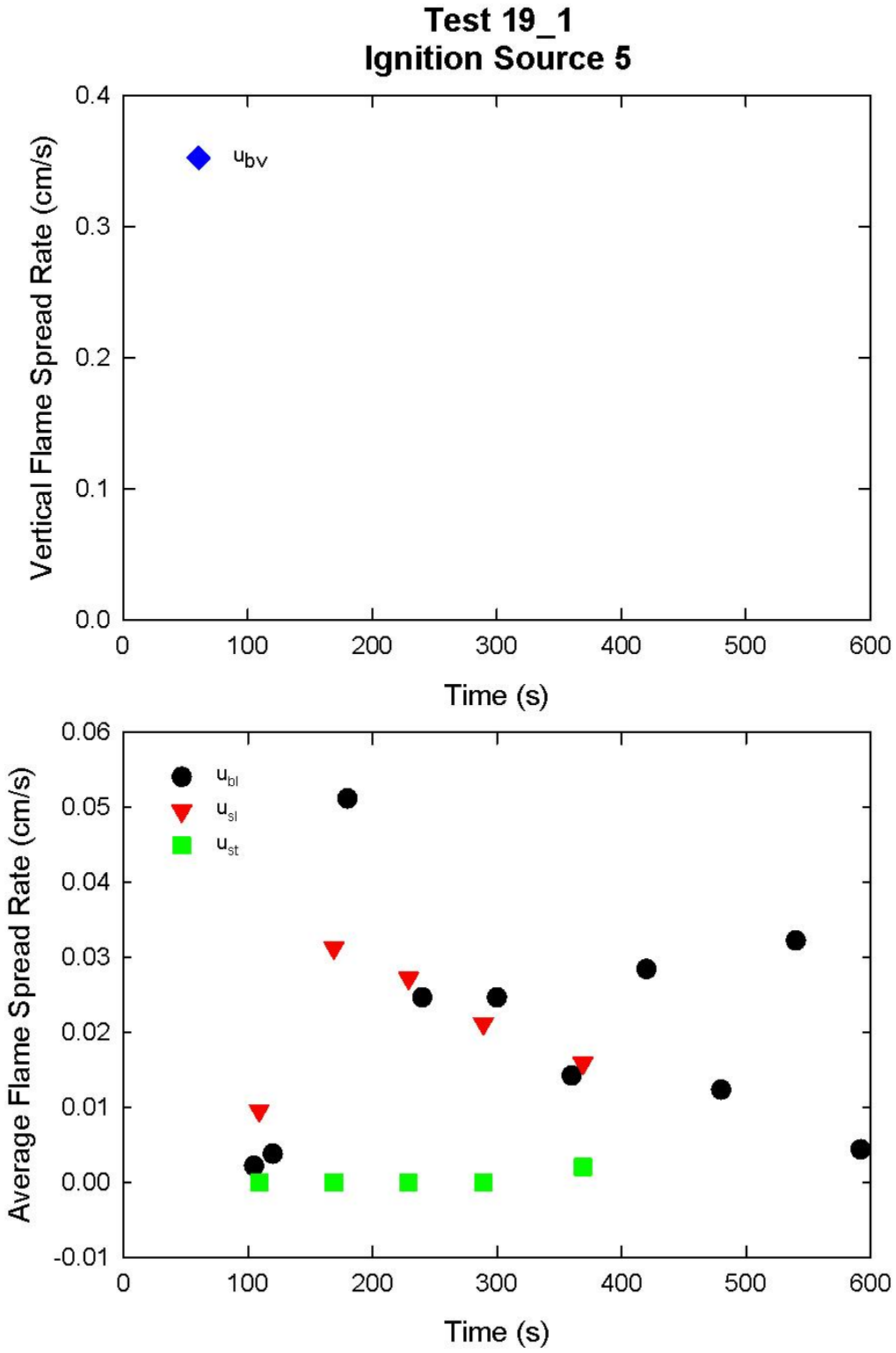

Figure A-162. Vertical flame spread rate on the back cushion (top) and average lateral flame spread rates on the back and seat cushions and transverse flame spread rate on the seat cushion (bottom) are plotted as a function of time for Test 19_1 following application of Ignition Source 5.

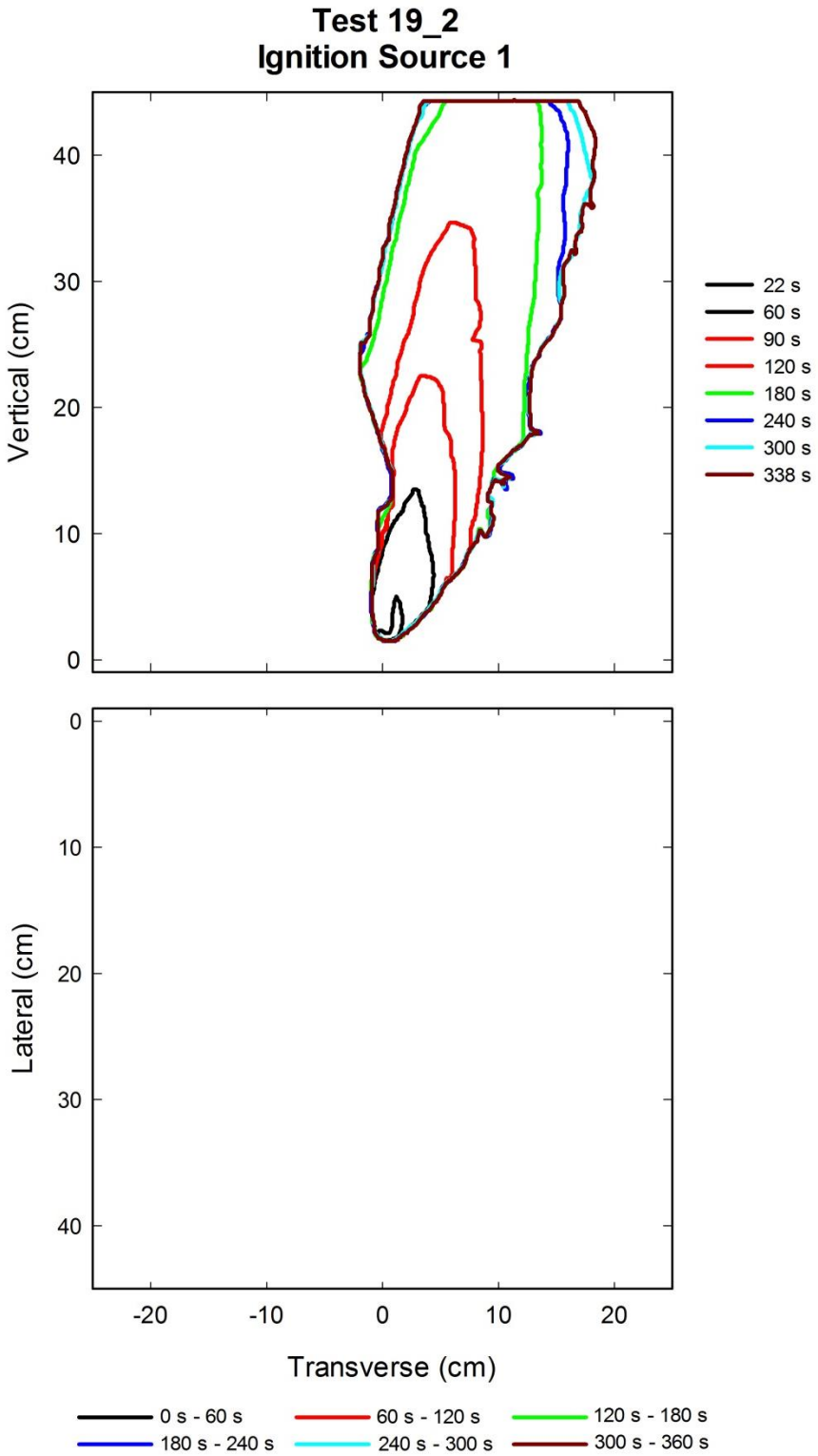

Figure A-163. Flame edge contours on the back (top) and seat (bottom) cushions are plotted as a function of time for Test 19_2 following application of Ignition Source 1.

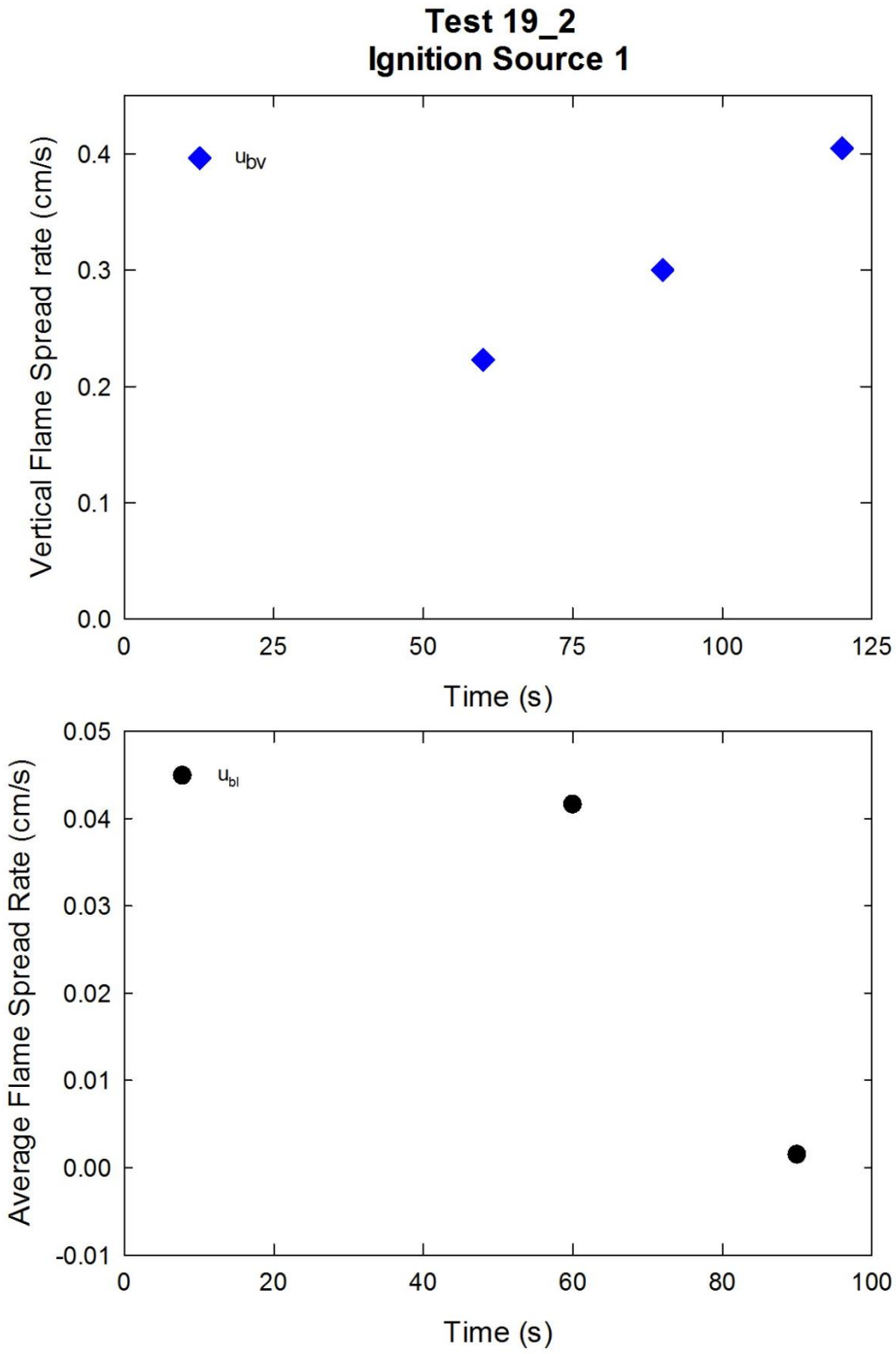

Figure A-164. Vertical flame spread rate on the back cushion (top) and average lateral flame spread rate on the back cushion (bottom) are plotted as a function of time for Test 19_2 following application of Ignition Source 1.

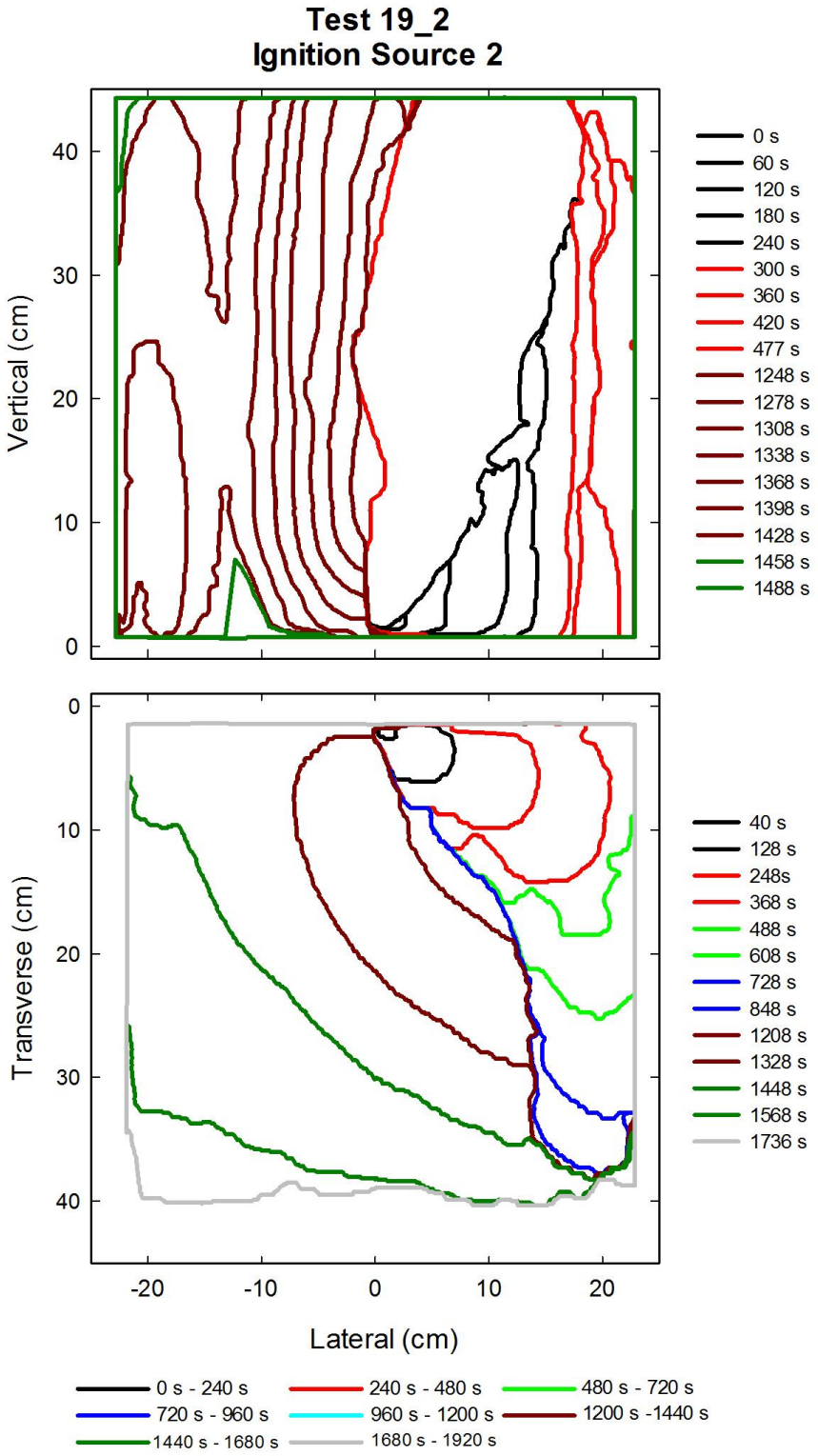

Figure A-165. Flame edge contours on the back (top) and seat (bottom) cushions are plotted as a function of time for Test 19_2 following application of Ignition Source 2.

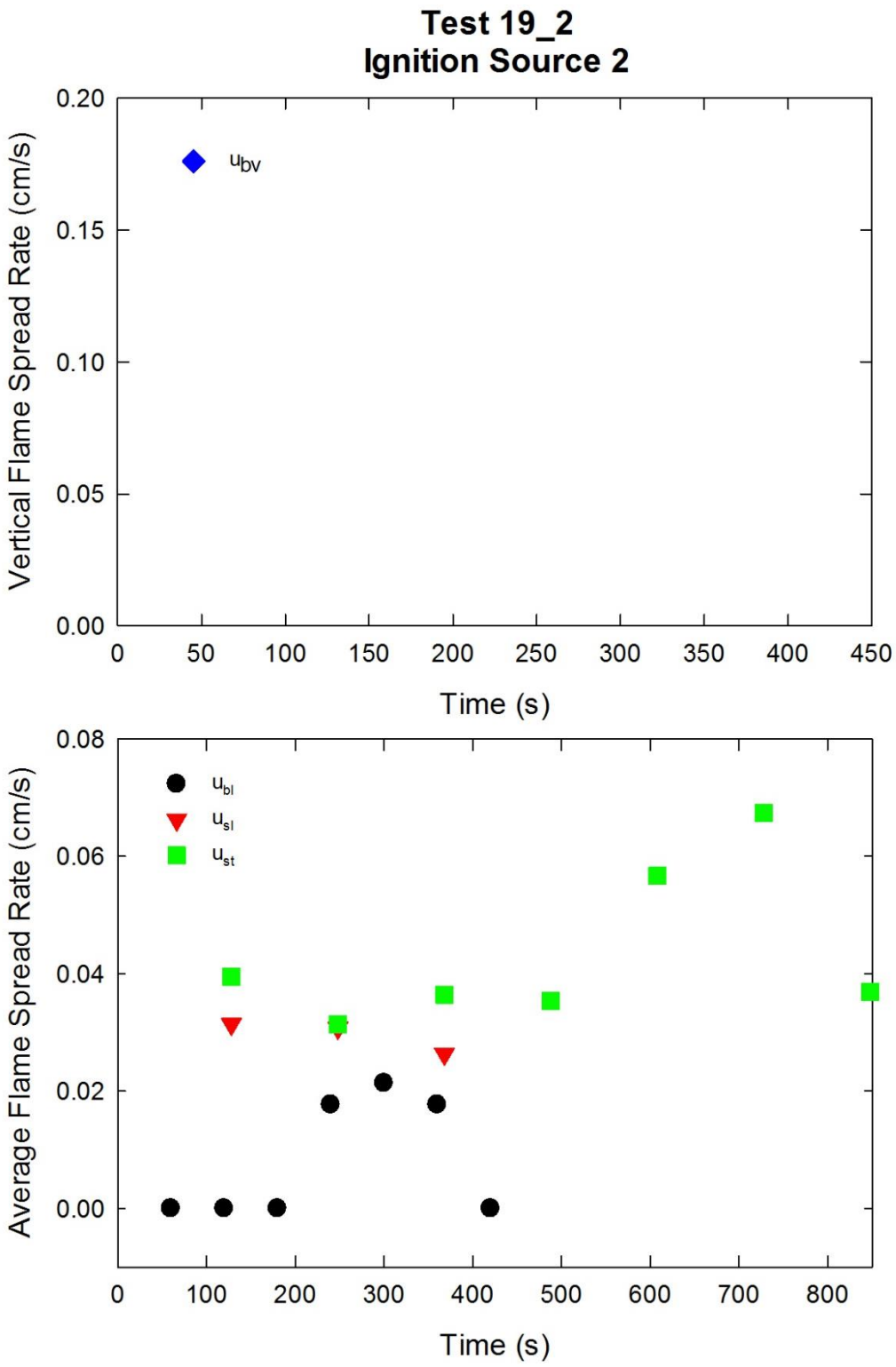

Figure A-166. Vertical flame spread rate on the back cushion (top) and average lateral flame spread rates on the back and seat cushions and transverse flame spread rate on the seat cushion (bottom) are plotted as a function of time for Test 19_2 following application of Ignition Source 2.

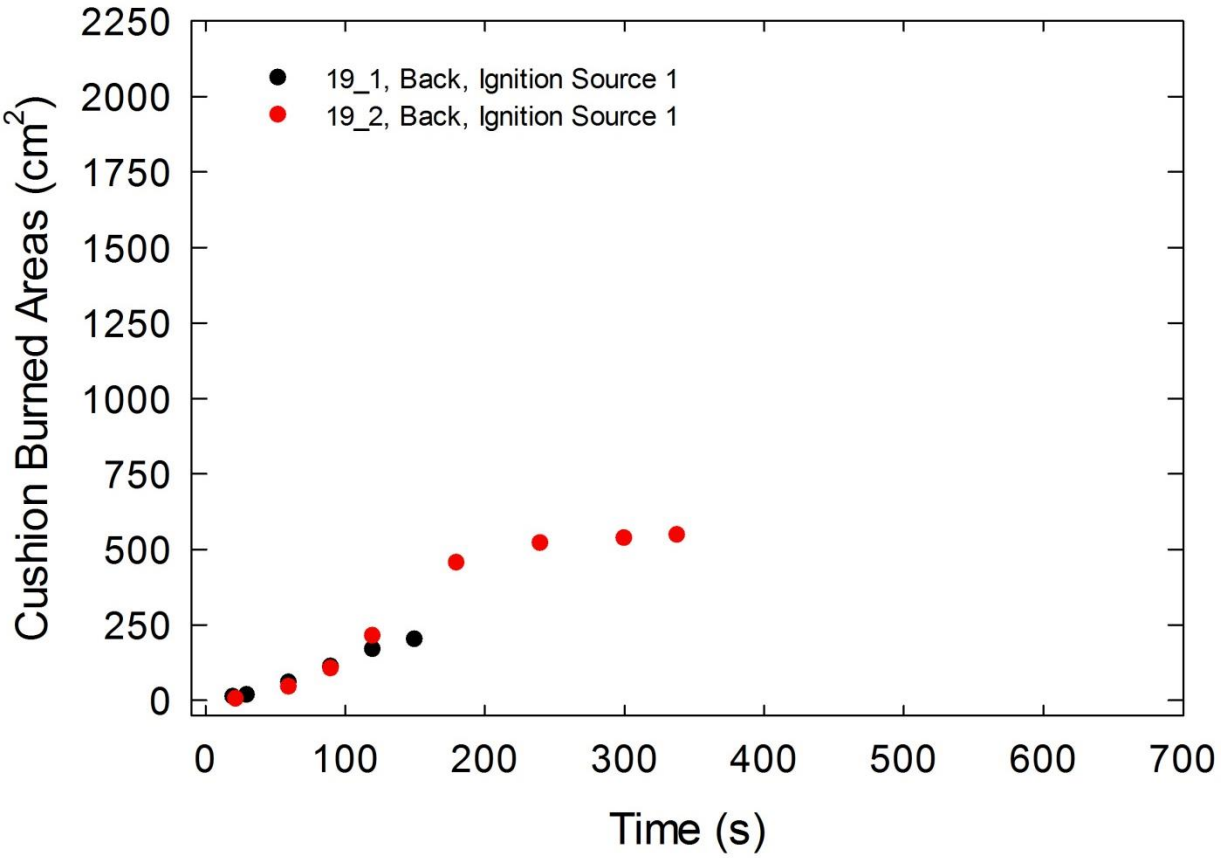

Figure A-167. Burned areas on the seat cushions are plotted as a function of time for Combination 19 tests following application of Ignition Source 1.

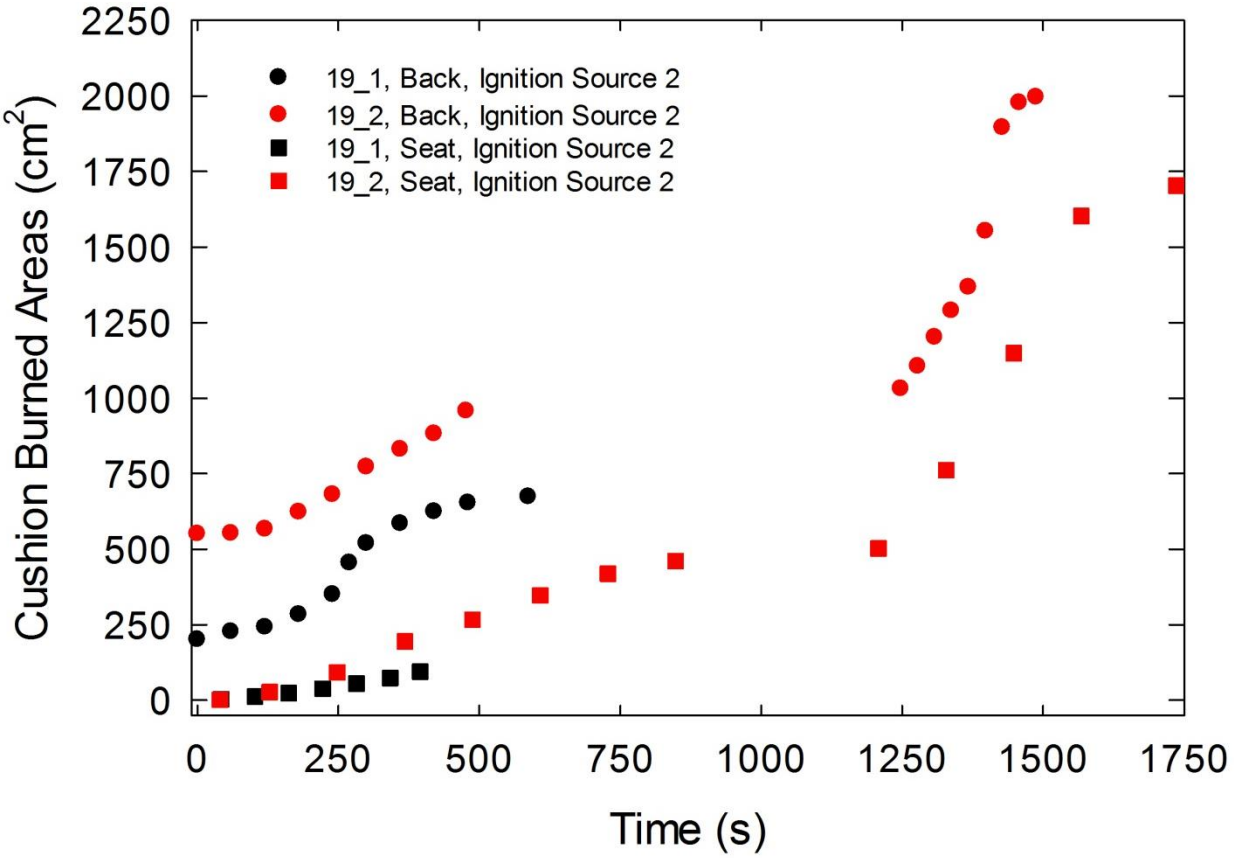

Figure A-168. Burned areas on the seat and back cushions are plotted as a function of time for Combination 19 tests following application of Ignition Source 2.

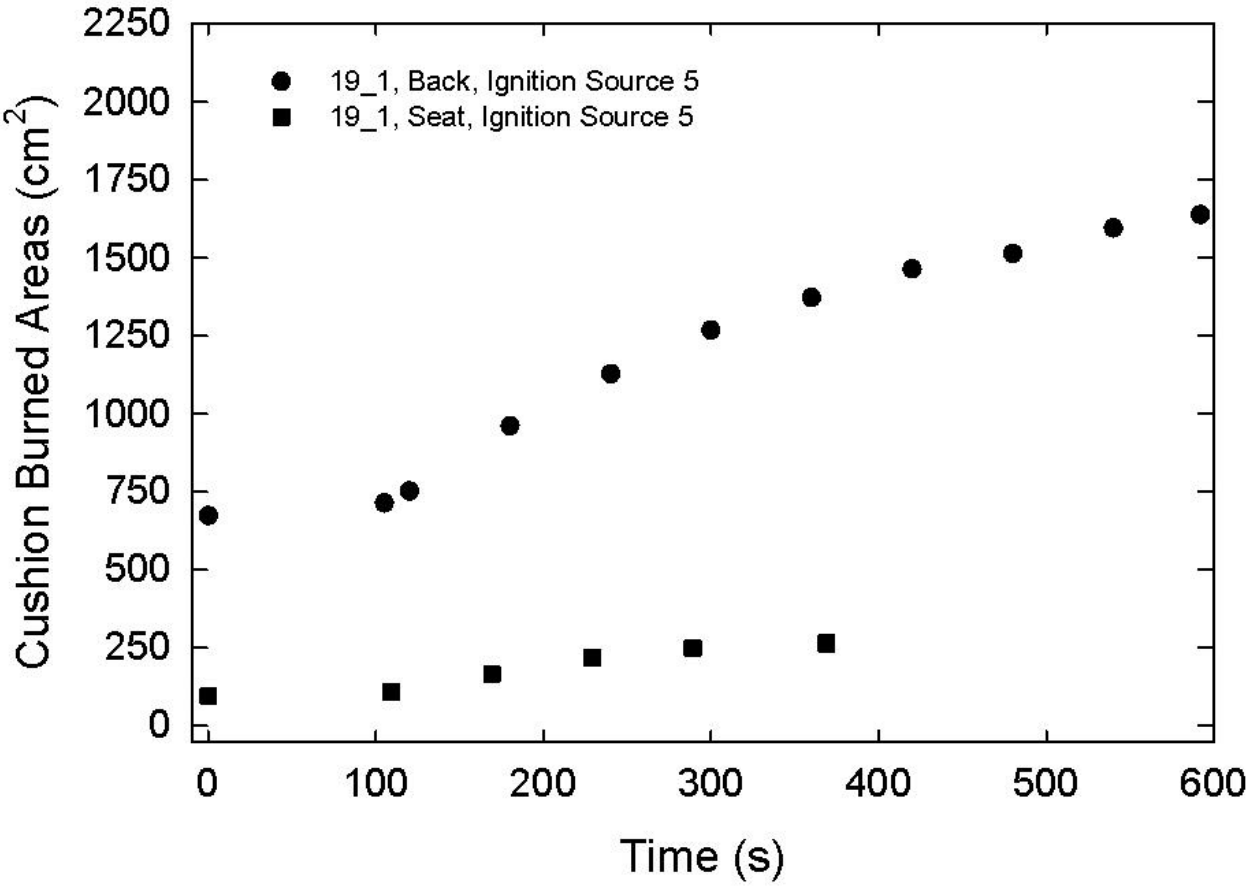

Figure A-169. Burned areas on the seat and back cushions are plotted as a function of time for Test 19_1 following application of Ignition Source 5.

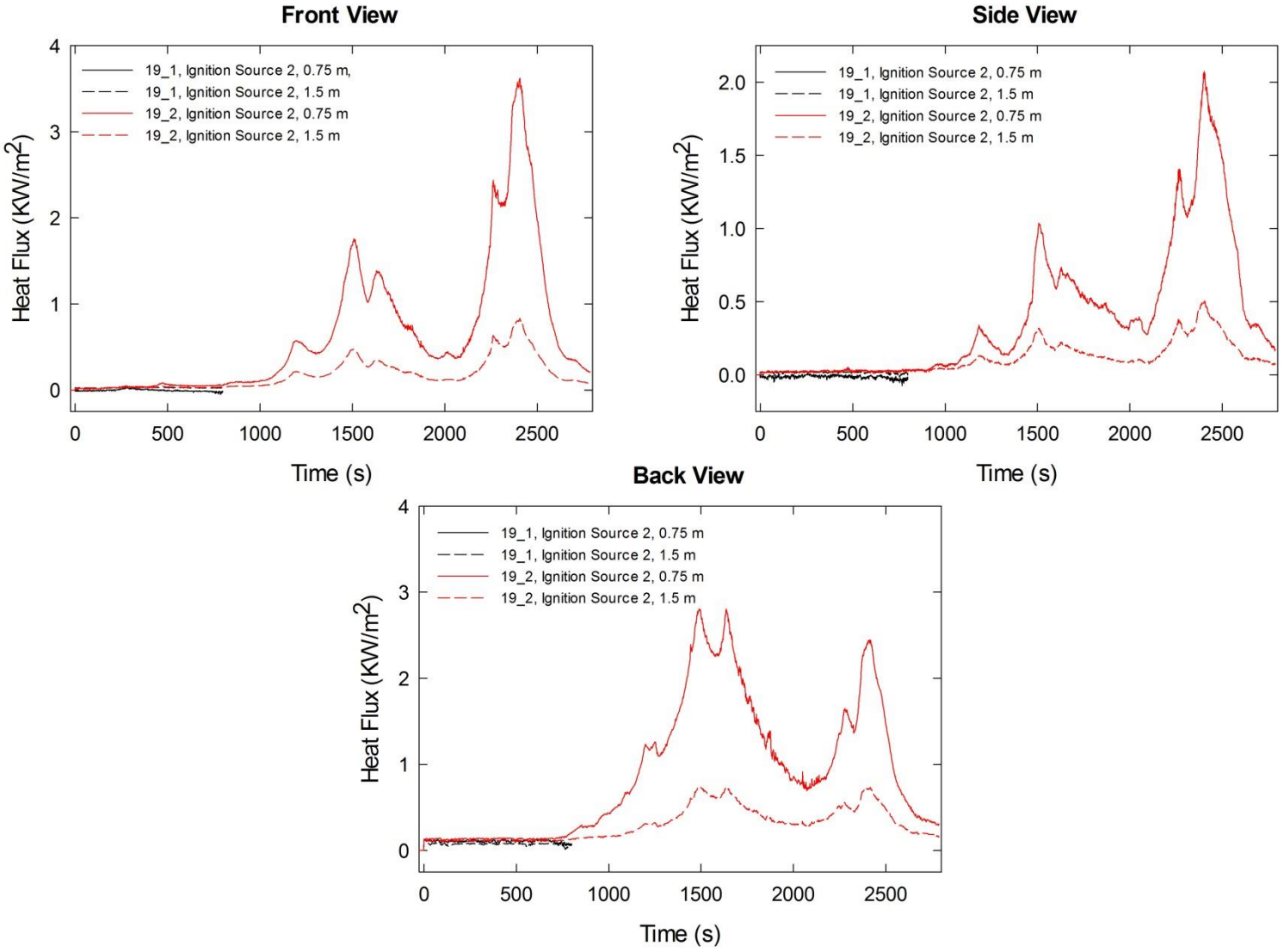

Figure A-170. Heat fluxes recorded at distances of 0.75 m and 1.5 m are plotted as a function of time for locations to the front, side and rear of the mock-up for Combination 19 tests following application of Ignition Source 2.

A.16 Combination 20

78%PP/22%PE/Norfab/PEFW/NFRFPUF

Notes:

Test 1:

Ignition Source 1 applied at time = 0 s.

Initial mass reading (3.45 kg) during the experiment disagreed with an earlier measurement for the mock-up (3.97 kg); mass readings remained constant during the initial period of the test and showed a period of increasing mass; **these mass data were excluded from analysis**.

Test 2:

Ignition Source 1 applied at time = 0 s.

Initial mass reading (3.19 kg) during the experiment disagreed with an earlier measurement for the mock-up (3.96 kg); mass readings were negative at the end of the test, but during the test were smooth, physically reasonable and correlated with the HRR; **these mass data were adjusted by adding 0.770 kg to their values and were included in the analysis**.

Test 3

Ignition Source 1 applied at time = 0 s.

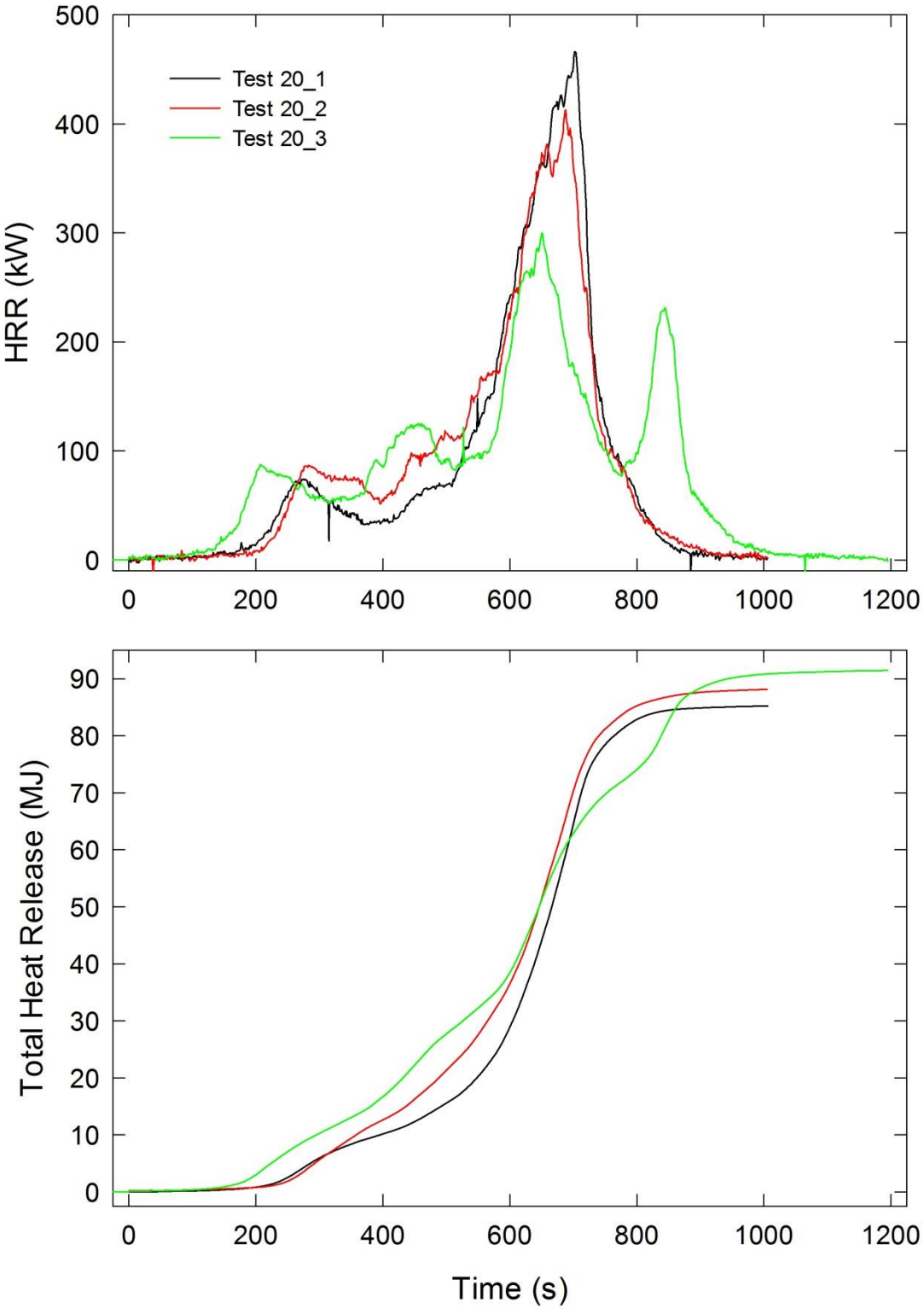

Figure A-171. Temporal profiles of HRR and integrated HRR are shown for Combination 20 tests following application of Ignition Source 1.

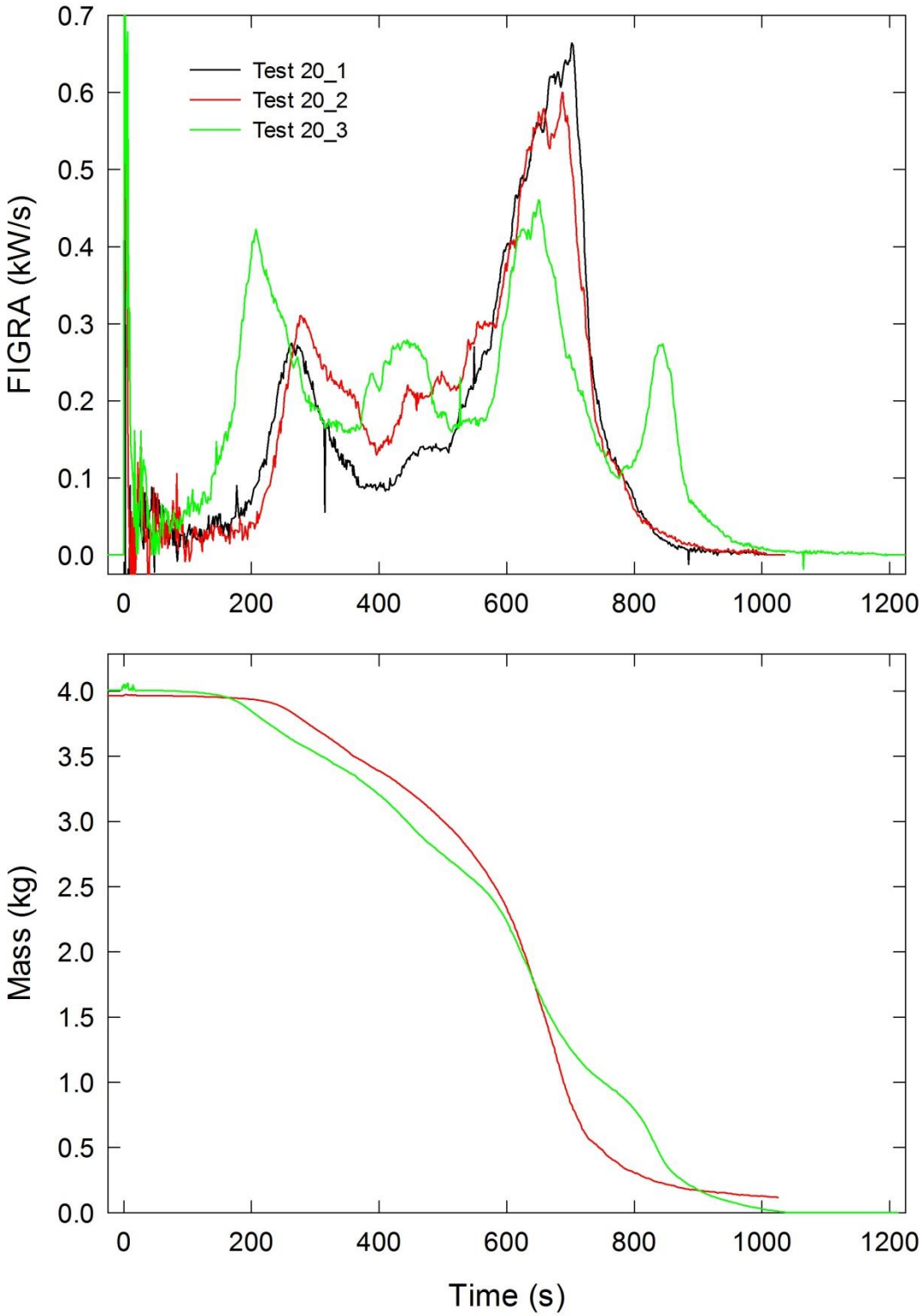

Figure A-172. Temporal profiles of FIGRA for Combination 20 tests and mock-up mass for Test 20_2 and Test 20_3 are shown following application of Ignition Source 1.

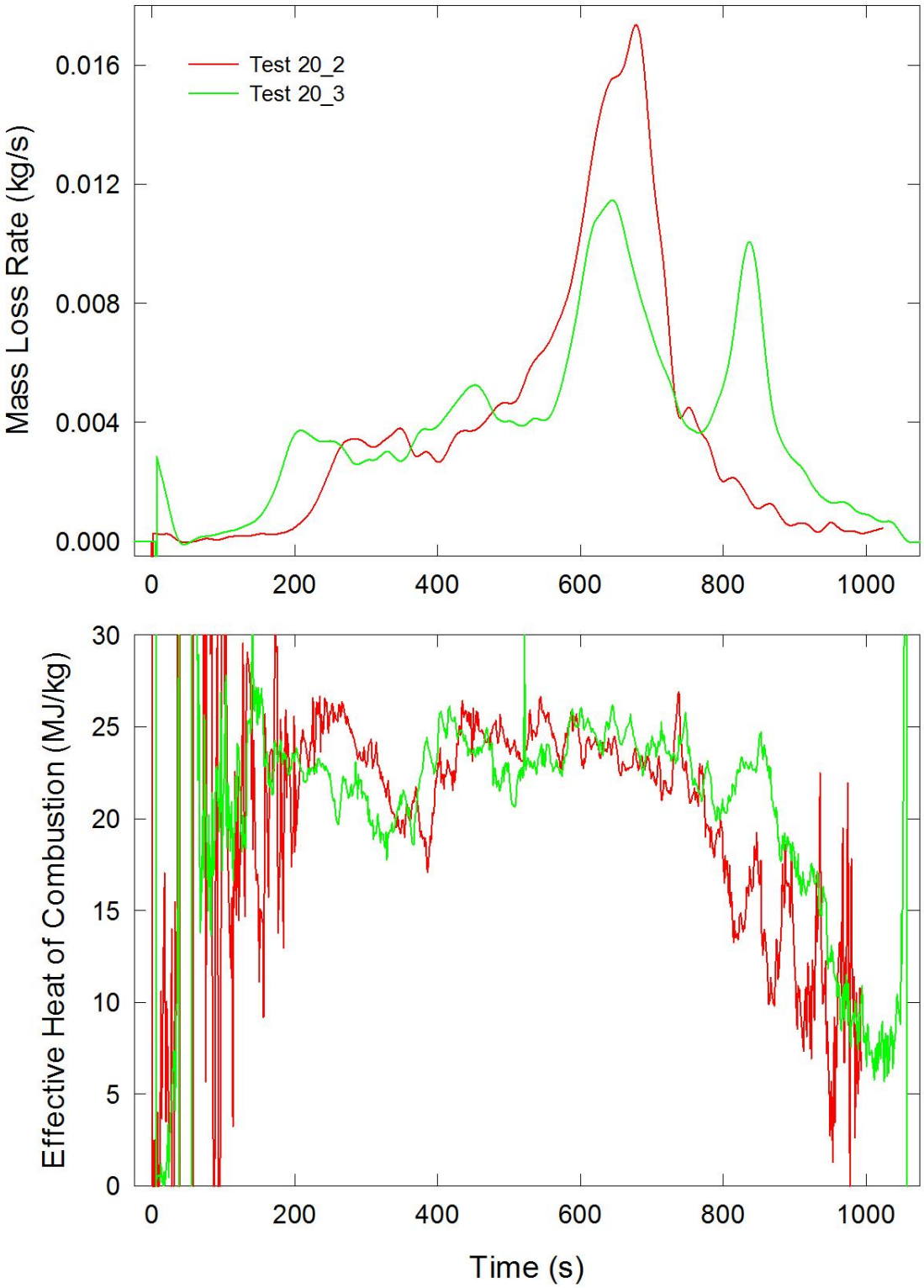

Figure A-173. Temporal profiles of MLR and EHOC are shown for Test 20_2 and Test 20_3 following application of Ignition Source 1.

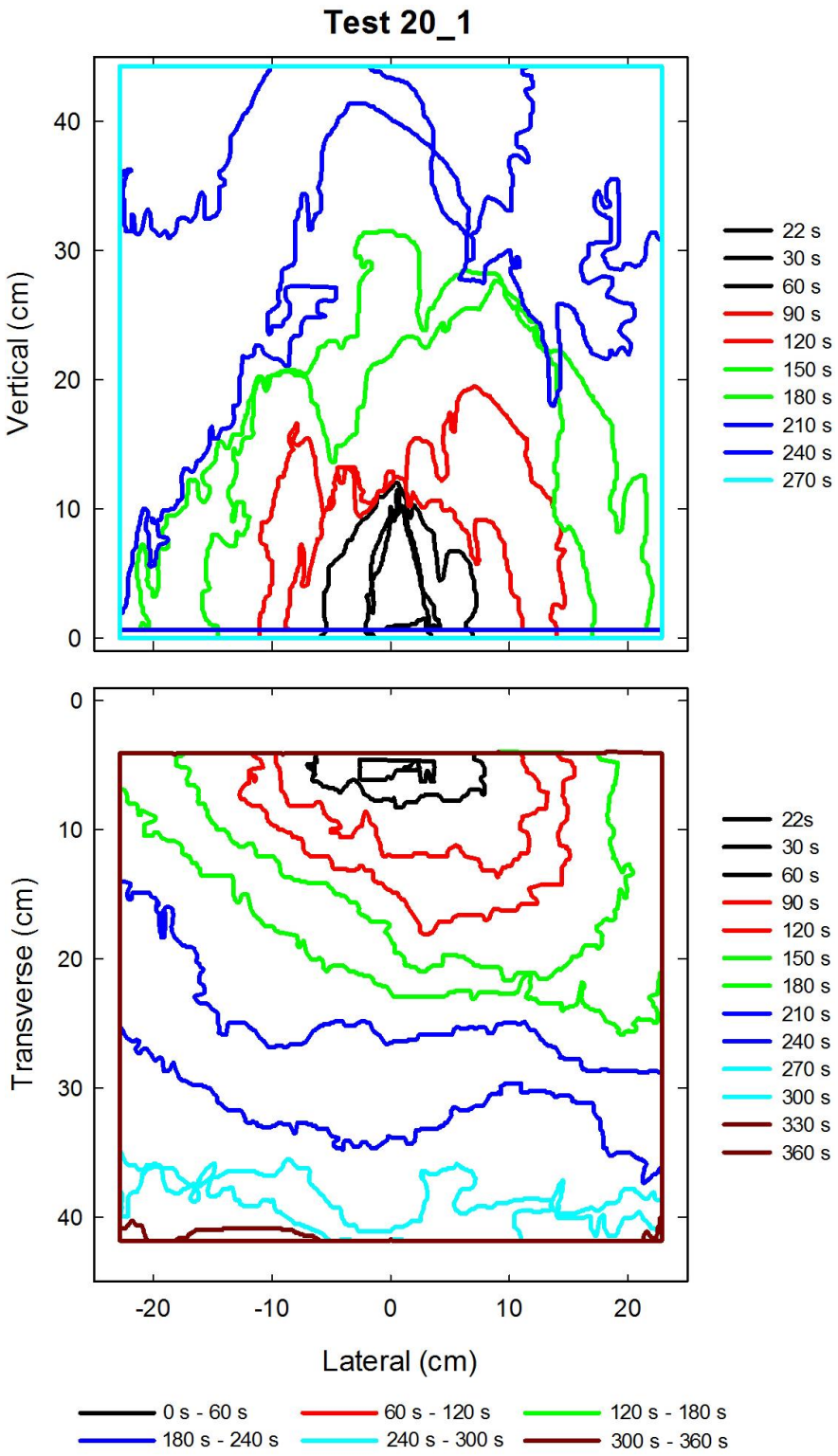

Figure A-174. Flame edge contours on the back (top) and seat (bottom) cushions are plotted as a function of time for Test 20_1 following application of Ignition Source 1.

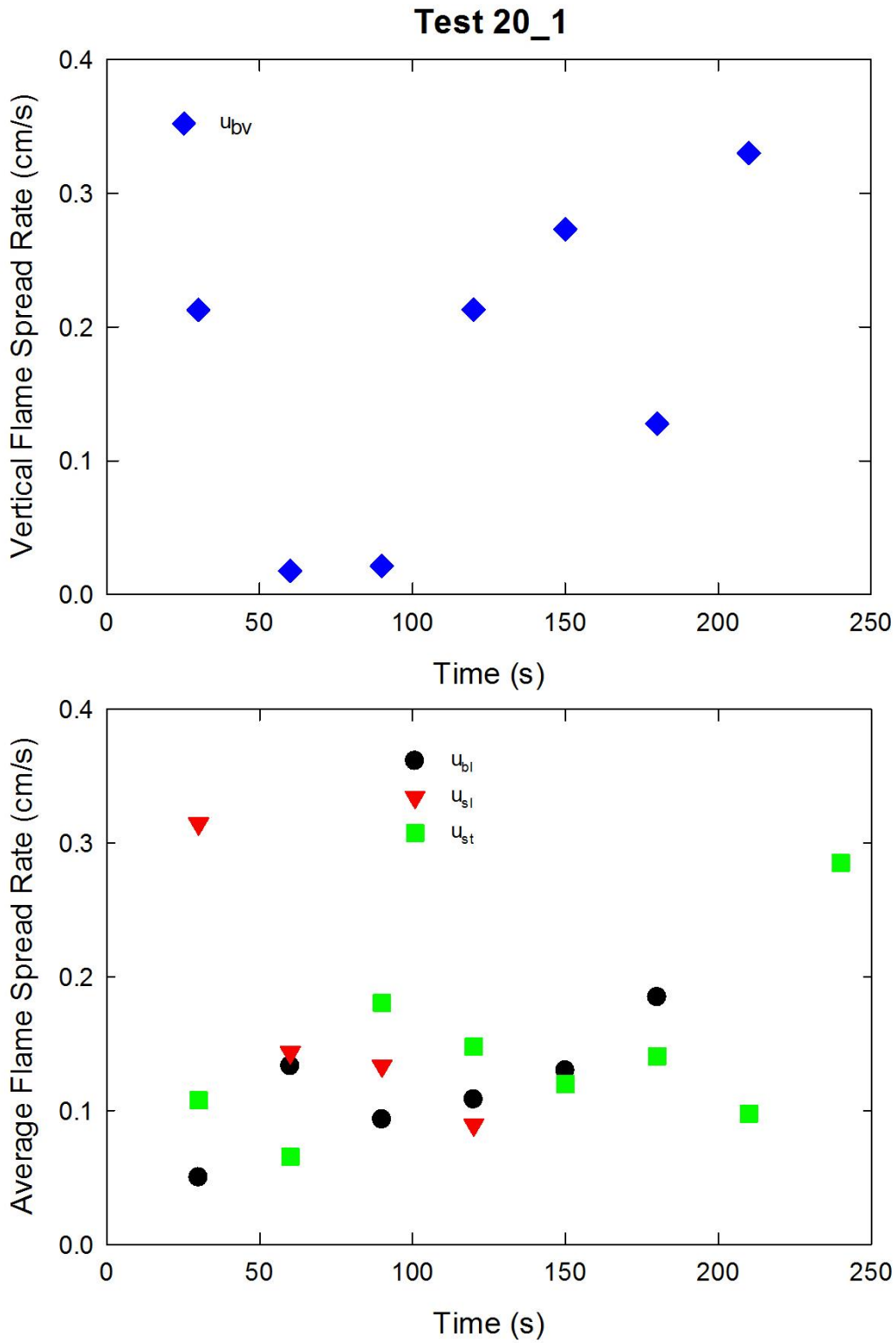

Figure A-175. Vertical flame spread rate on the back cushion (top) and average lateral flame spread rates on the back and seat cushions and transverse flame spread rate on the seat cushion (bottom) are plotted as a function of time for Test 20_1 following application of Ignition Source 1.

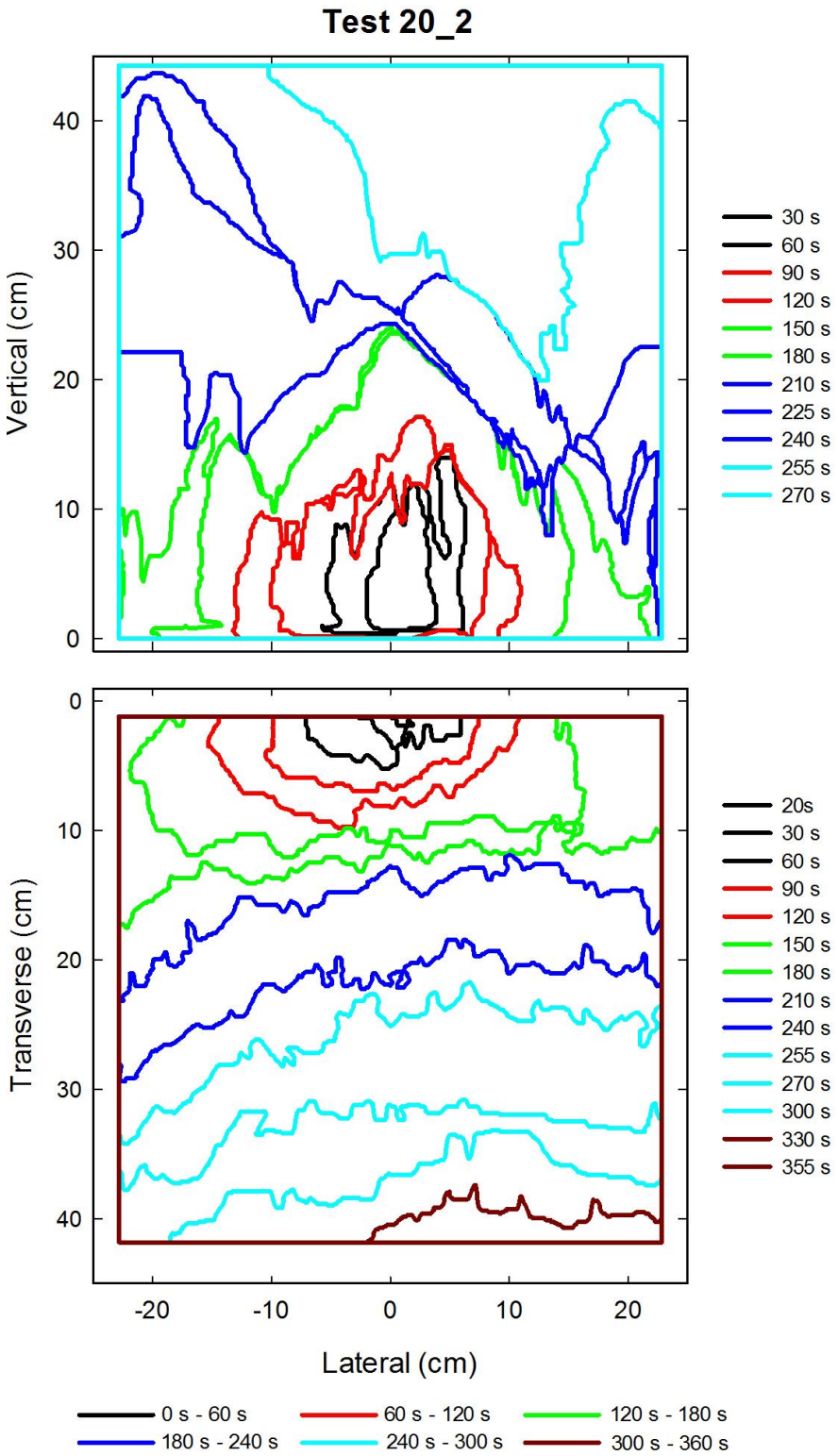

Figure A-176. Flame edge contours on the back (top) and seat (bottom) cushions are plotted as a function of time for Test 20_2 following application of Ignition Source 1.

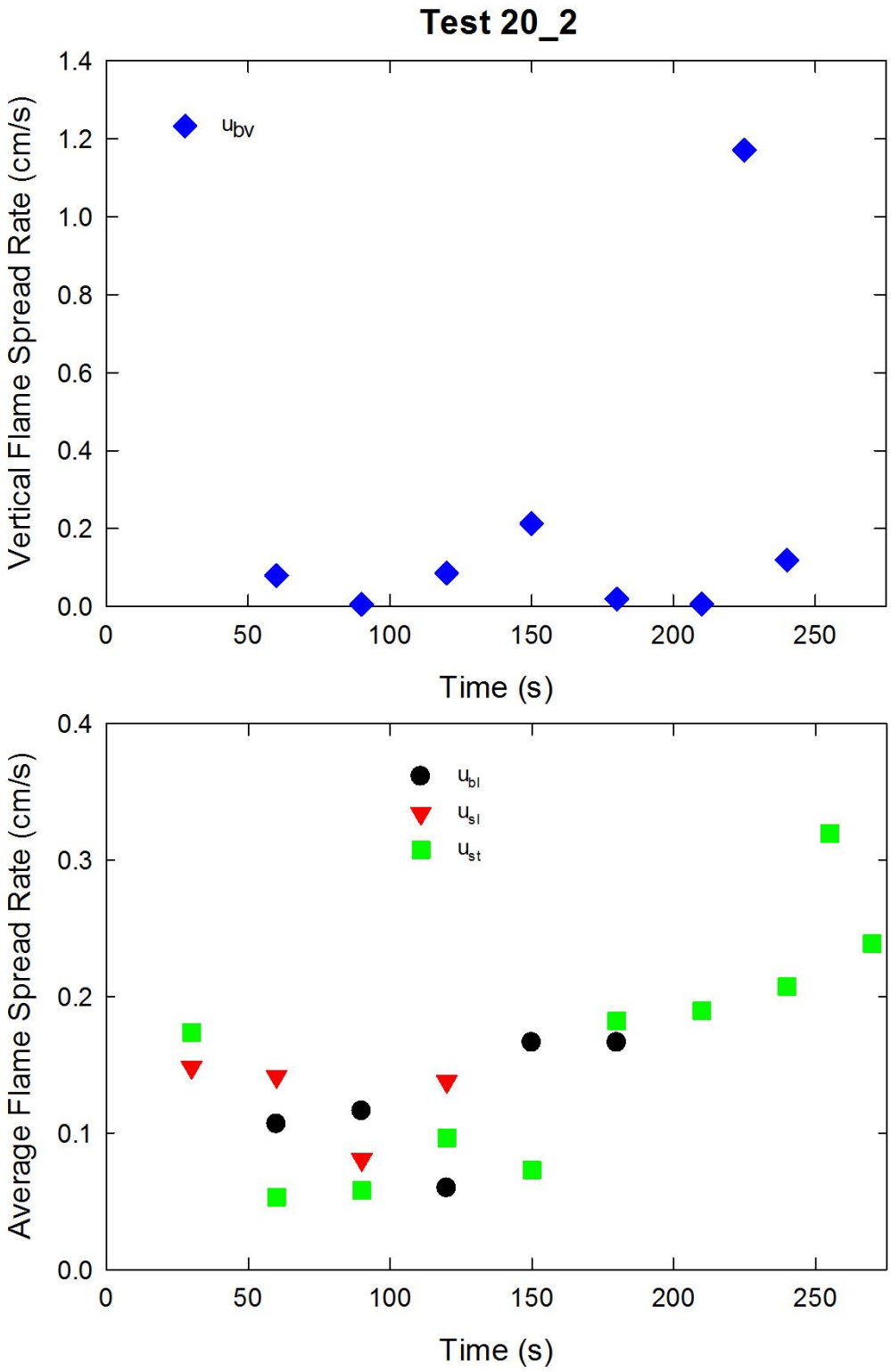

Figure A-177. Vertical flame spread rate on the back cushion (top) and average lateral flame spread rates on the back and seat cushions and transverse flame spread rate on the seat cushion (bottom) are plotted as a function of time for Test 20_2 following application of Ignition Source 1.

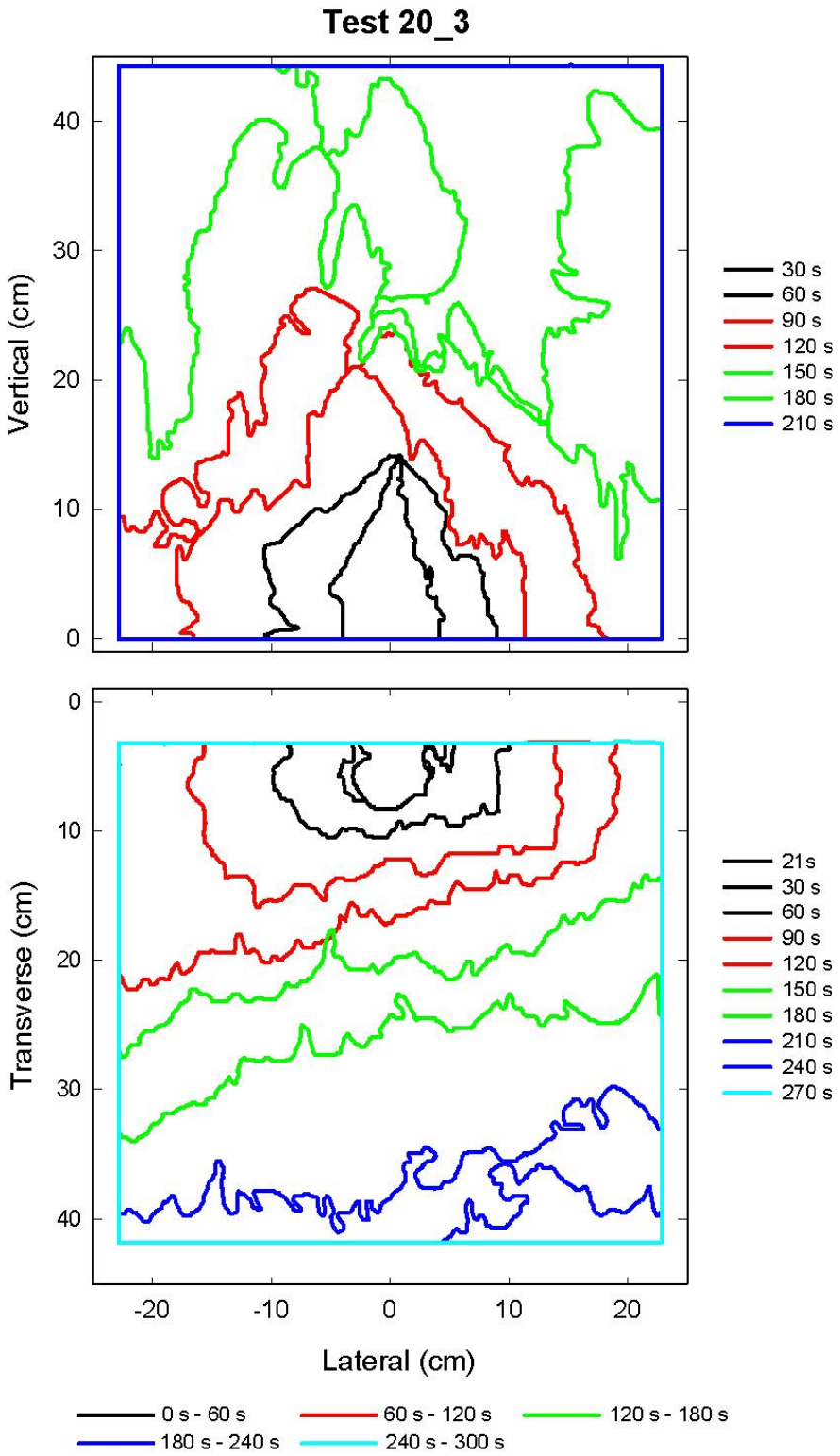

Figure A-178. Flame edge contours on the back (top) and seat (bottom) cushions are plotted as a function of time for Test 20_3 following application of Ignition Source 1.

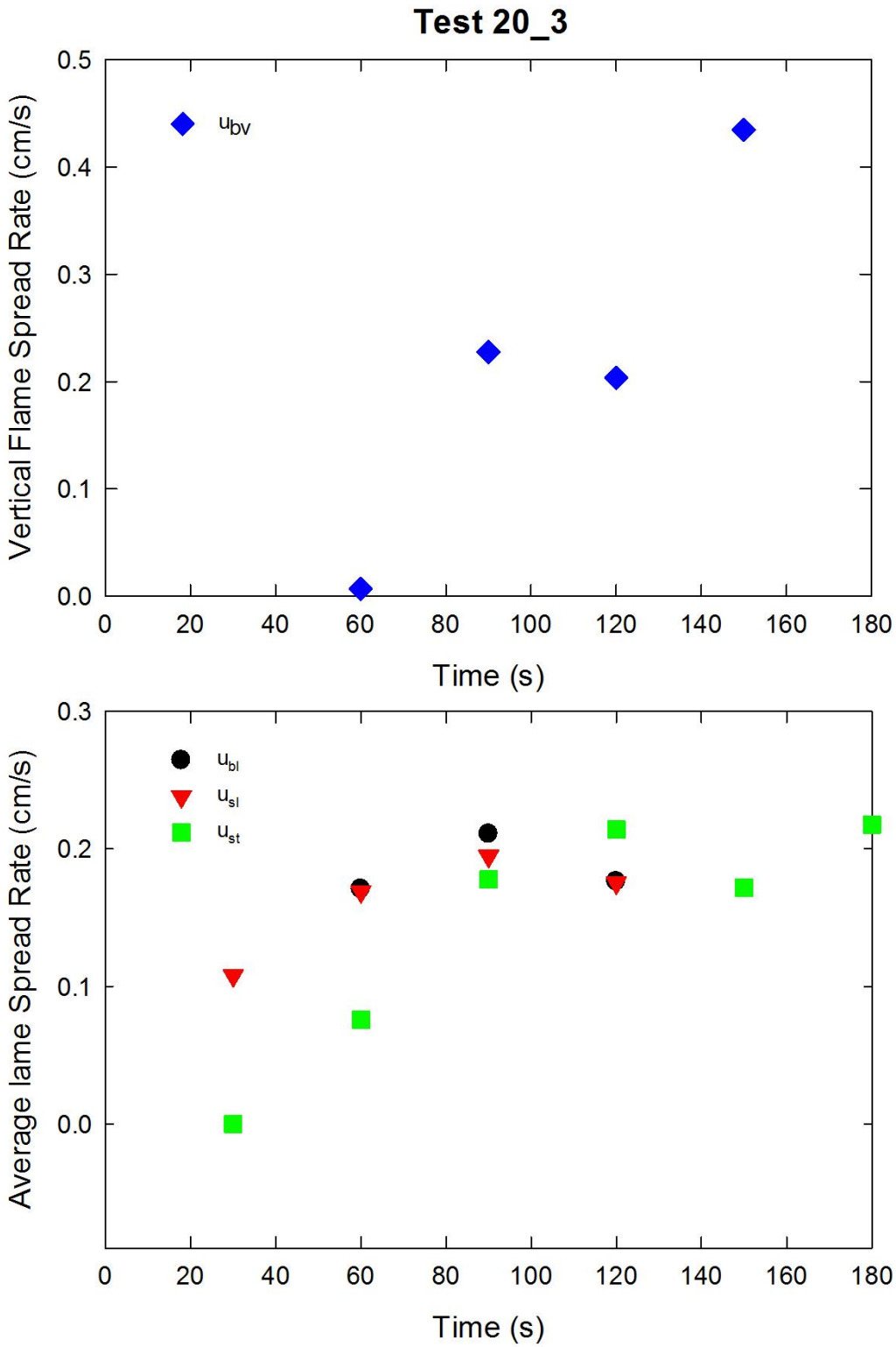

Figure A-179. Vertical flame spread rate on the back cushion (top) and average lateral flame spread rates on the back and seat cushions and transverse flame spread rate on the seat cushion (bottom) are plotted as a function of time for Test 20_3 following application of Ignition Source 1.

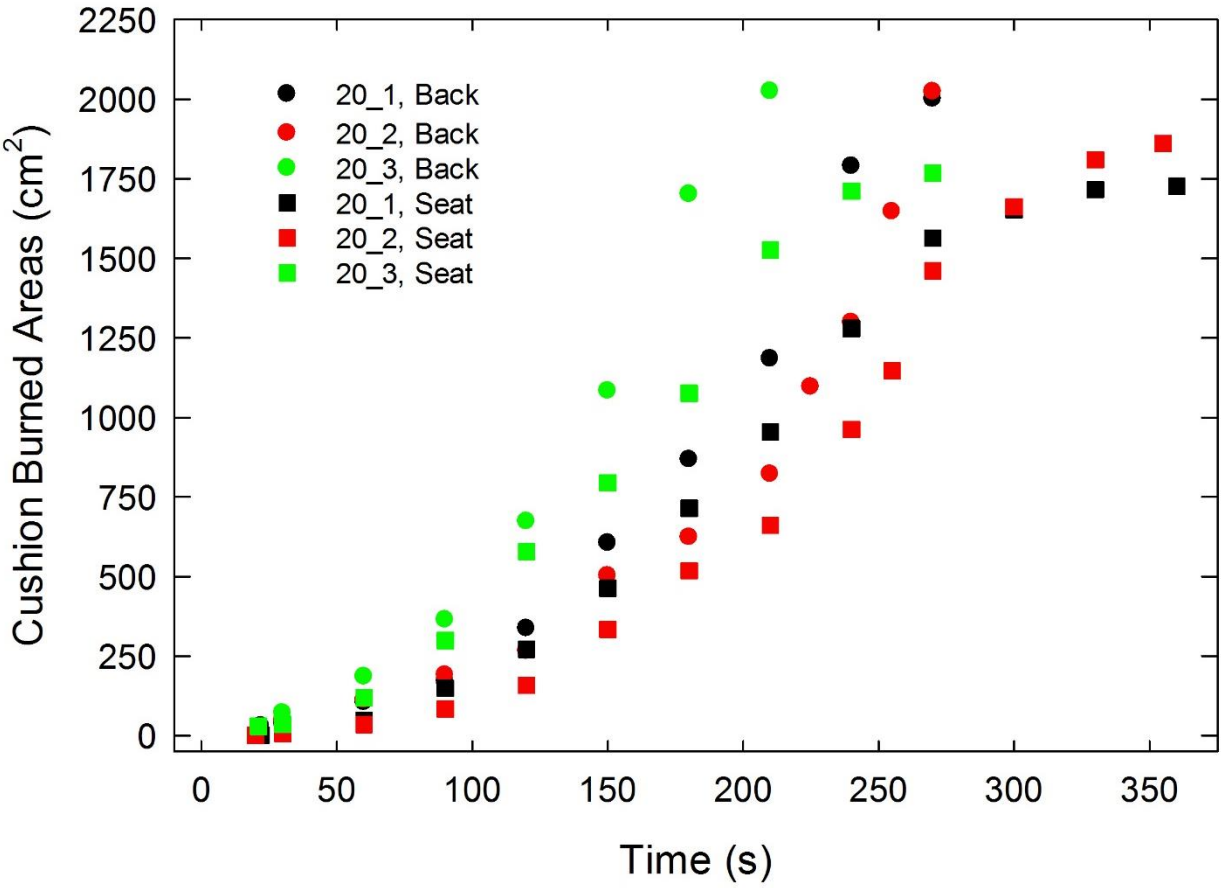

Figure A-180. Burned areas on the seat and back cushions are plotted as a function of time for Combination 20 tests following application of Ignition Source 1.

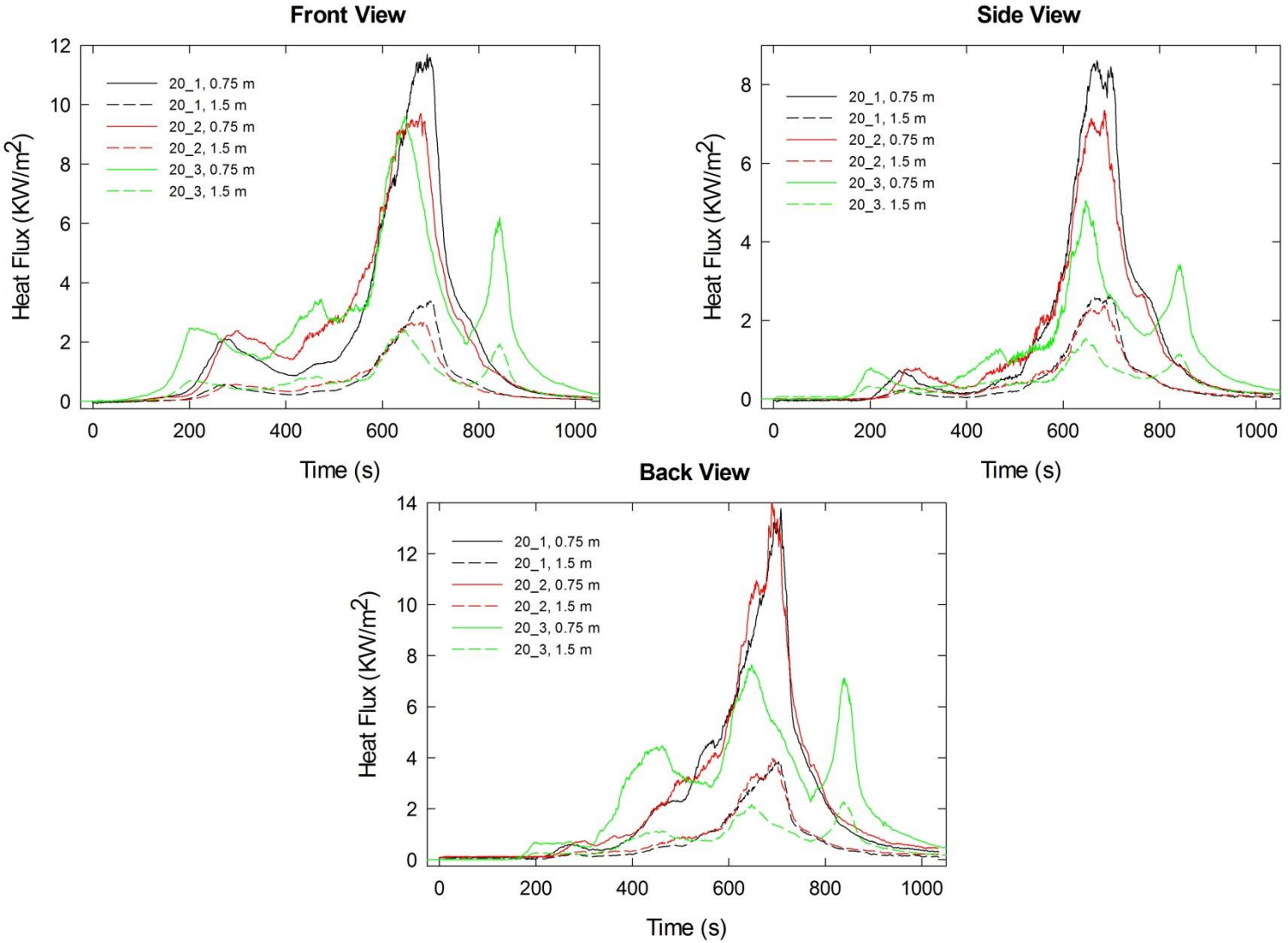

Figure A-181. Heat fluxes recorded at distances of 0.75 m and 1.5 m are plotted as a function of time for locations to the front, side and rear of the mock-up for Combination 20 tests following application of Ignition Source 1.

A.17 Combination 21

cotton/Norfab/FRFPUF

Notes:

Test 1:

Ignition Source 1 applied at time = 0 s; some flame spread over part of back cushion, with lateral spread becoming wider at top; no sign of blackening or flame spread on seat cushion.

Ignition Source 2 applied 890 s after Ignition Source 1 removed; following removal of ignition source limited flame spread at base of back cushion; some darkening on seat cushion with no sign of flame spread.

Ignition Source 5 ignited 268 s after Ignition Source 2 removed; limited additional flame spread on back, seat, and right-arm cushions.

Test 2:

Ignition Source 1 applied at time = 0 s; following removal of ignition source, upward flame spread with lateral spread near top on back cushion, small darkened area on seat cushion with no flame spread.

Ignition Source 2 applied 858 s after Ignition Source 1 removed; slow flame spread on the right sides of seat and lower-back and right-arm cushions.

Ignition Source 5 ignited 1320 s after Ignition Source 2 removed; limited additional flame spread on back, seat, and right-arm cushions.

Initial mass reading (4.29 kg) during the experiment disagreed with an earlier measurement for the mock-up (3.79 kg); mass readings increased after Ignition Source 1 removed and during much of the test; **these mass data were excluded from analysis**.

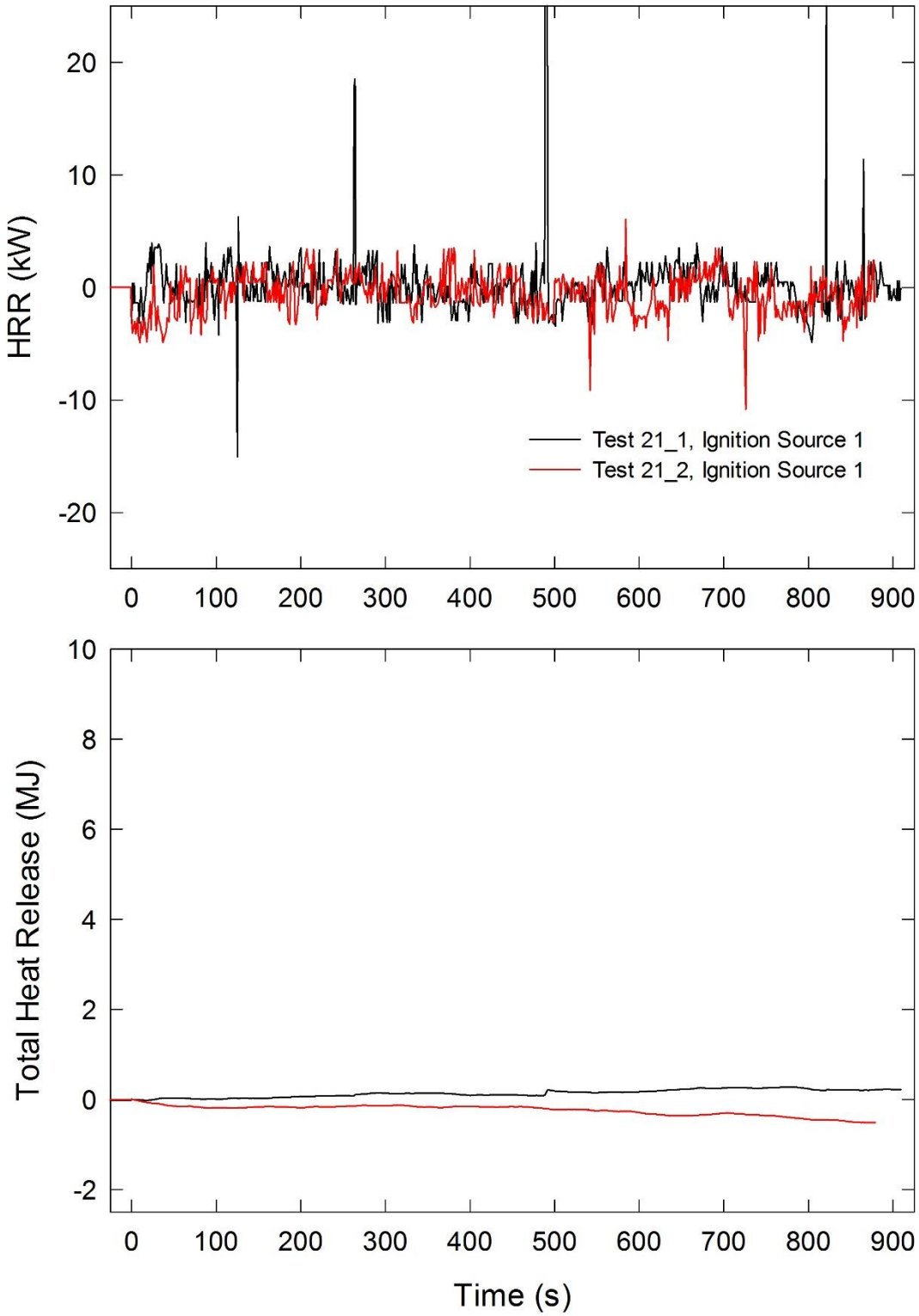

Figure A-182. Temporal profiles of HRR and integrated HRR are shown for Combination 21 tests following application of Ignition Source 1.

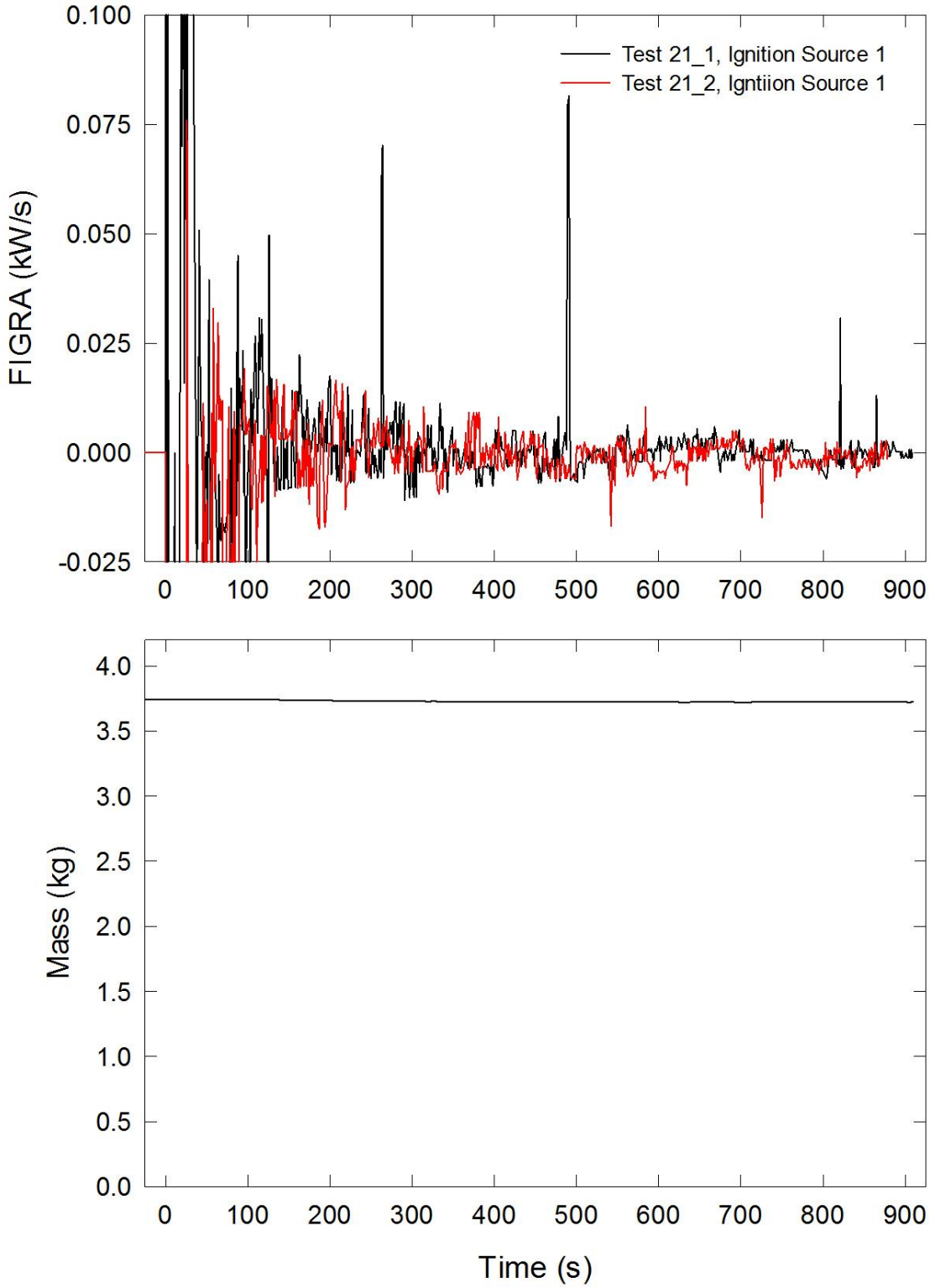

Figure A-183. Temporal profiles of FIGRA for Combination 21 tests and mock-up mass for Test 21_1 are shown following application of Ignition Source 1.

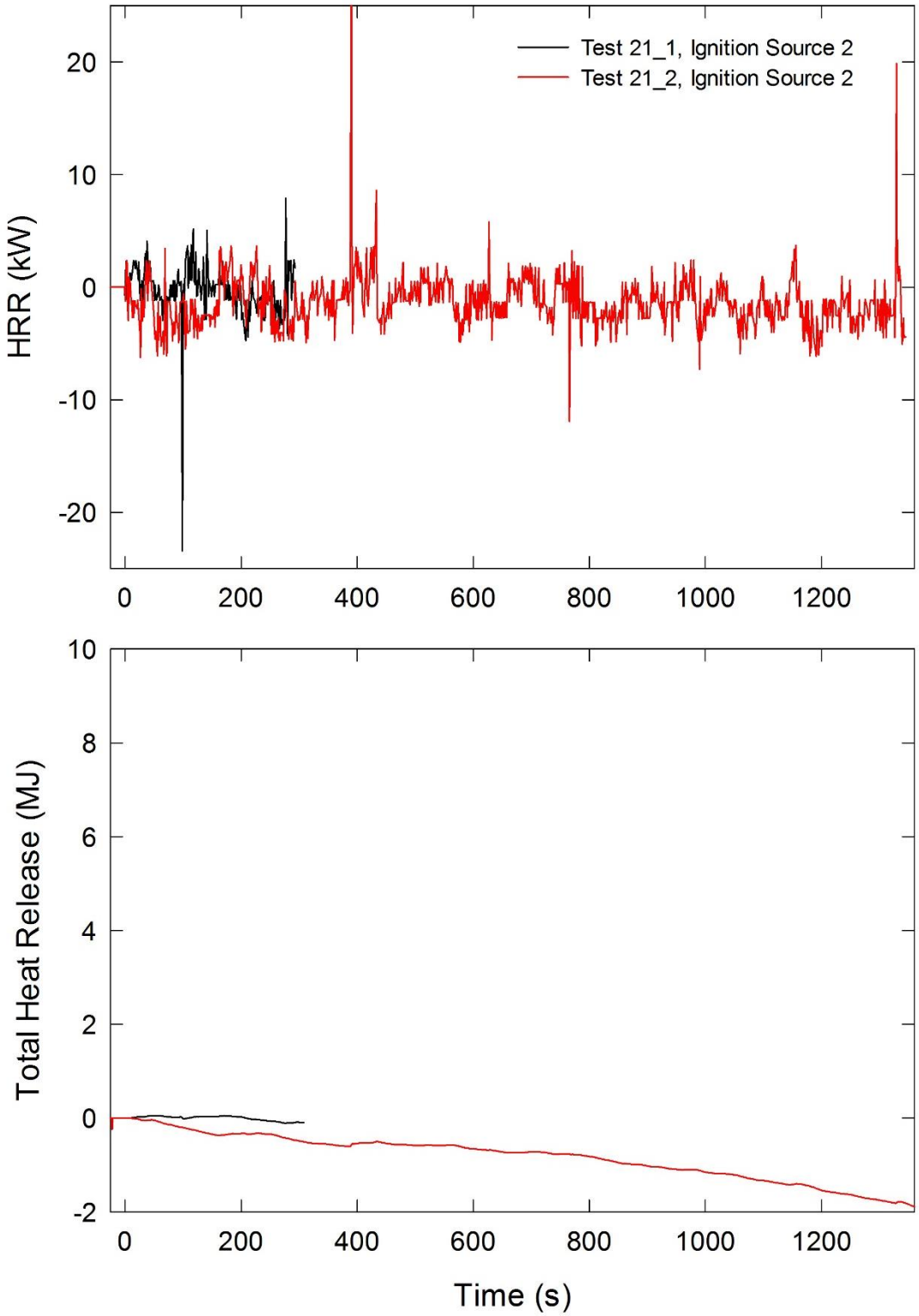

Figure A-184. Temporal profiles of HRR and integrated HRR are shown for Combination 21 tests following application of Ignition Source 2.

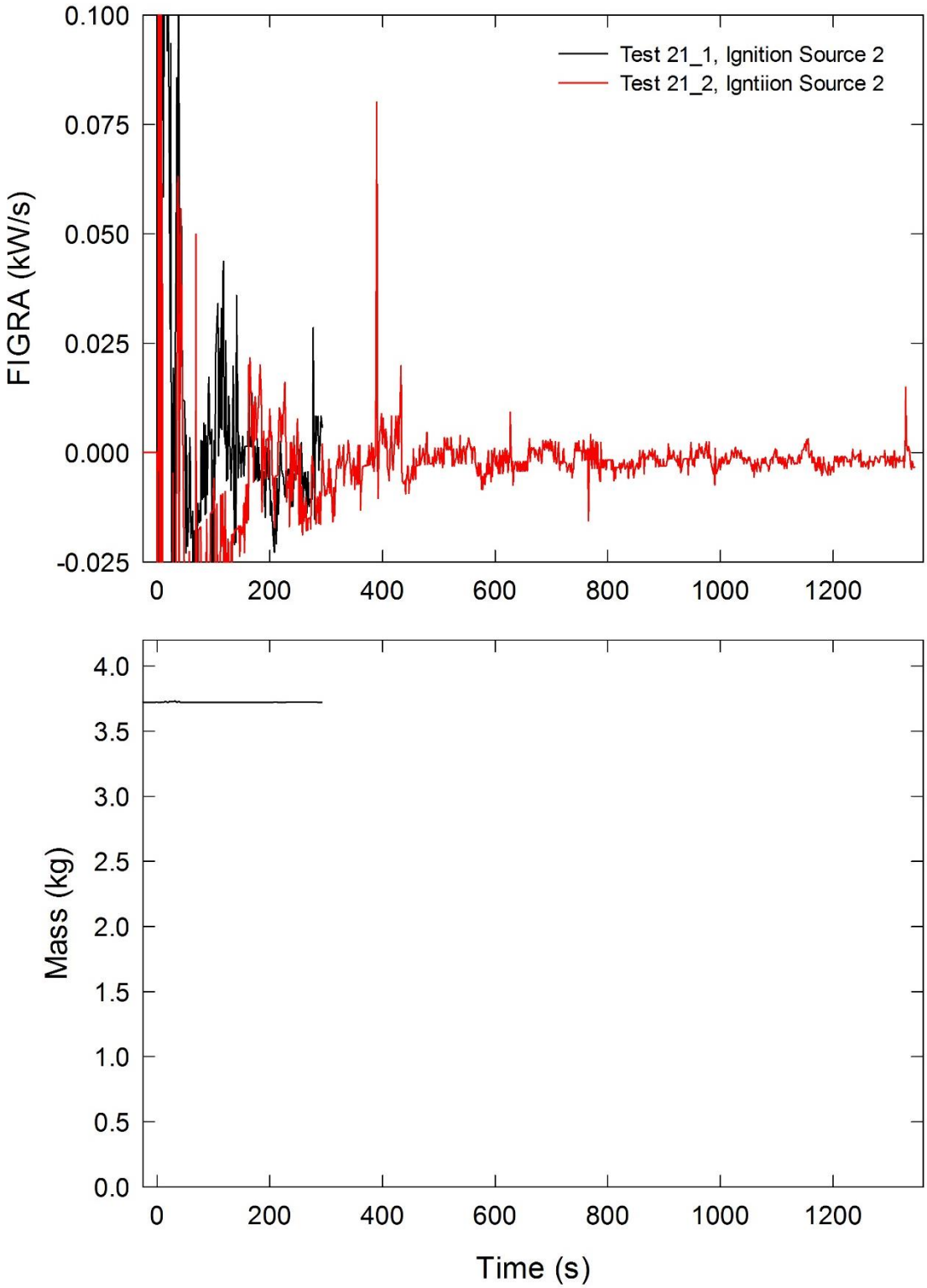

Figure A-185. Temporal profiles of FIGRA for Combination 21 tests and mock-up mass for Test 21_1 are shown following application of Ignition Source 2.

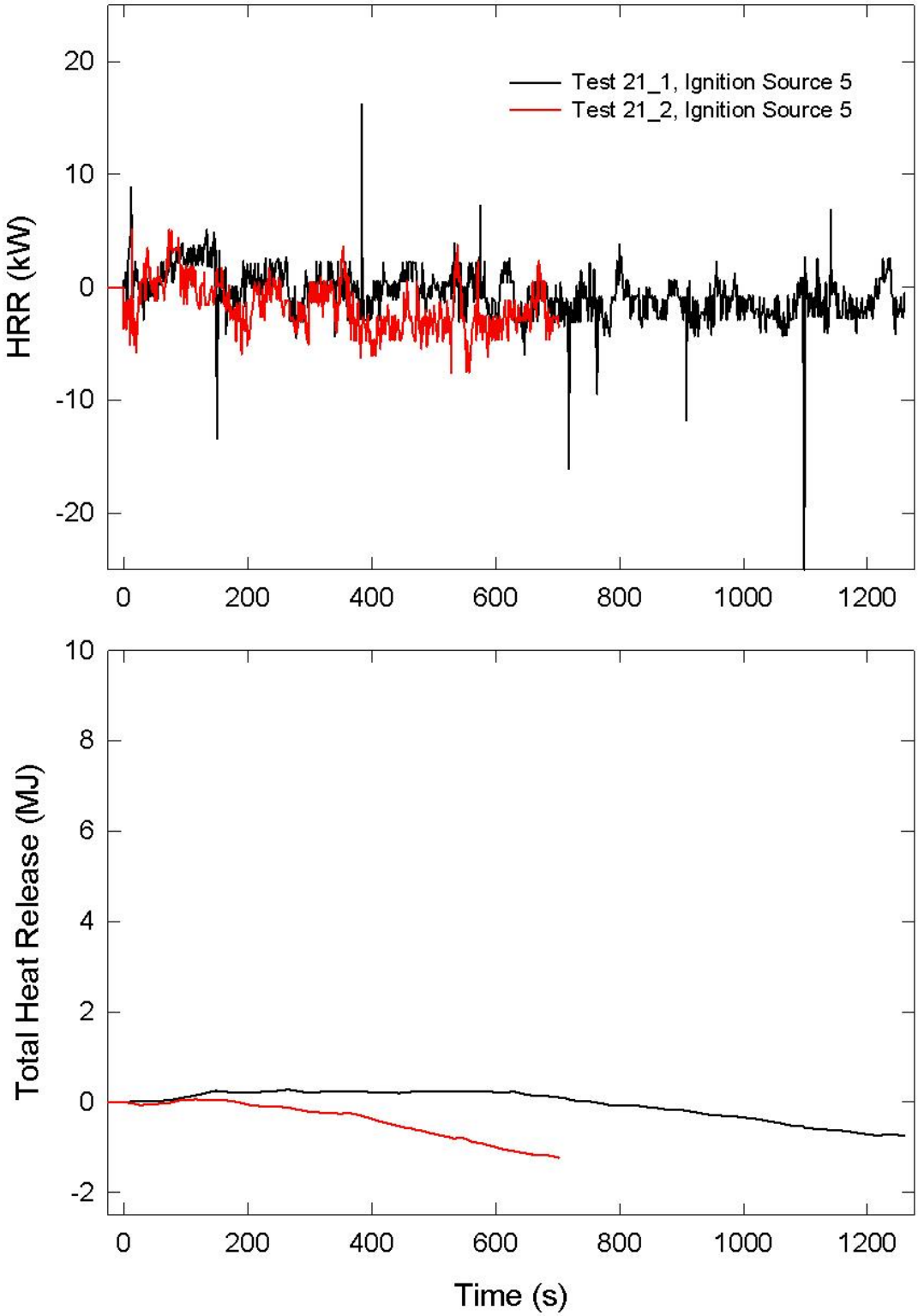

Figure A-186. Temporal profiles of HRR and integrated HRR are shown for Combination 21 tests following application of Ignition Source 5.

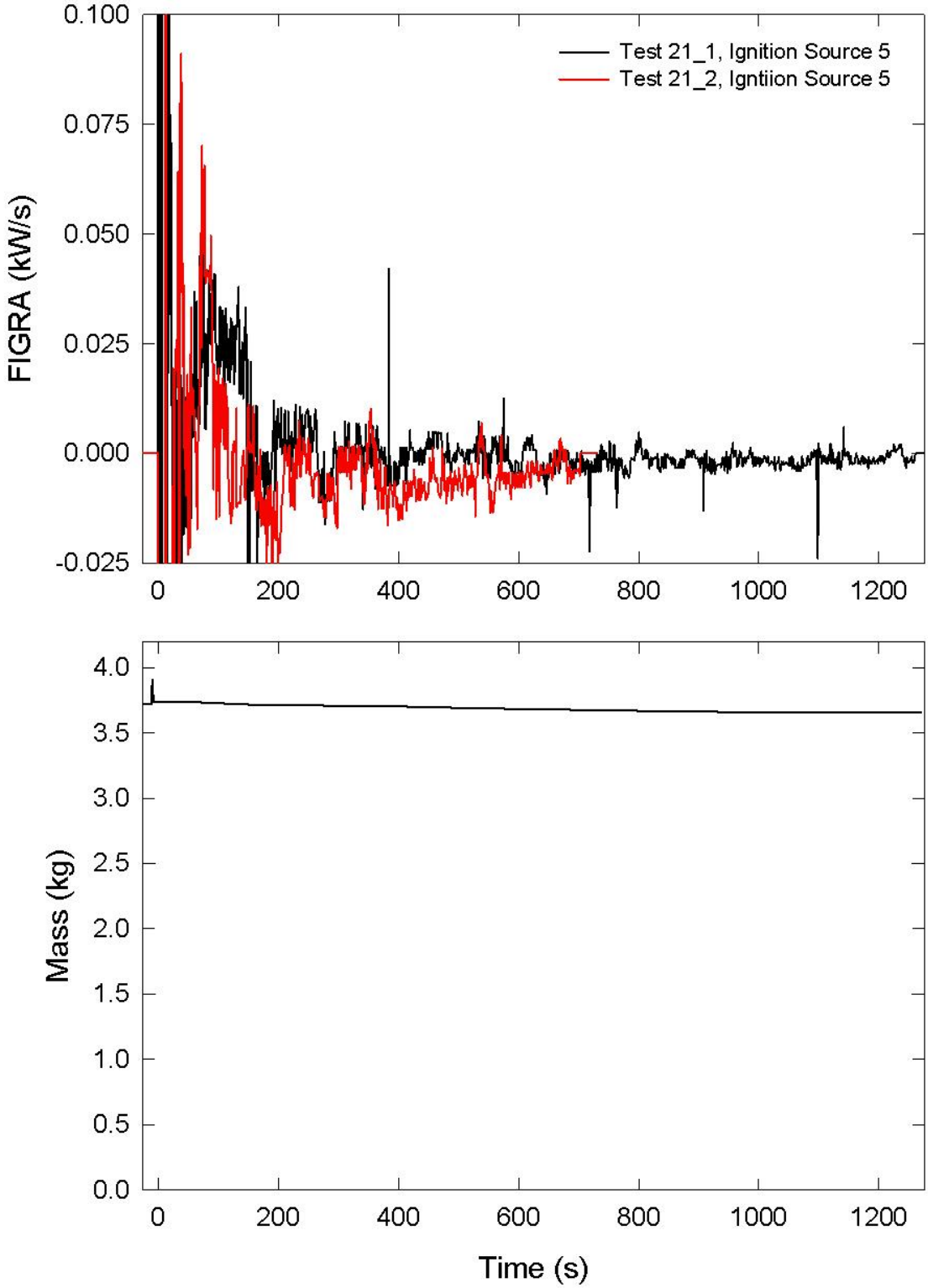

Figure A-187. Temporal profiles of FIGRA for Combination 21 tests and mock-up mass for Test 21_1 are shown following application of Ignition Source 5.

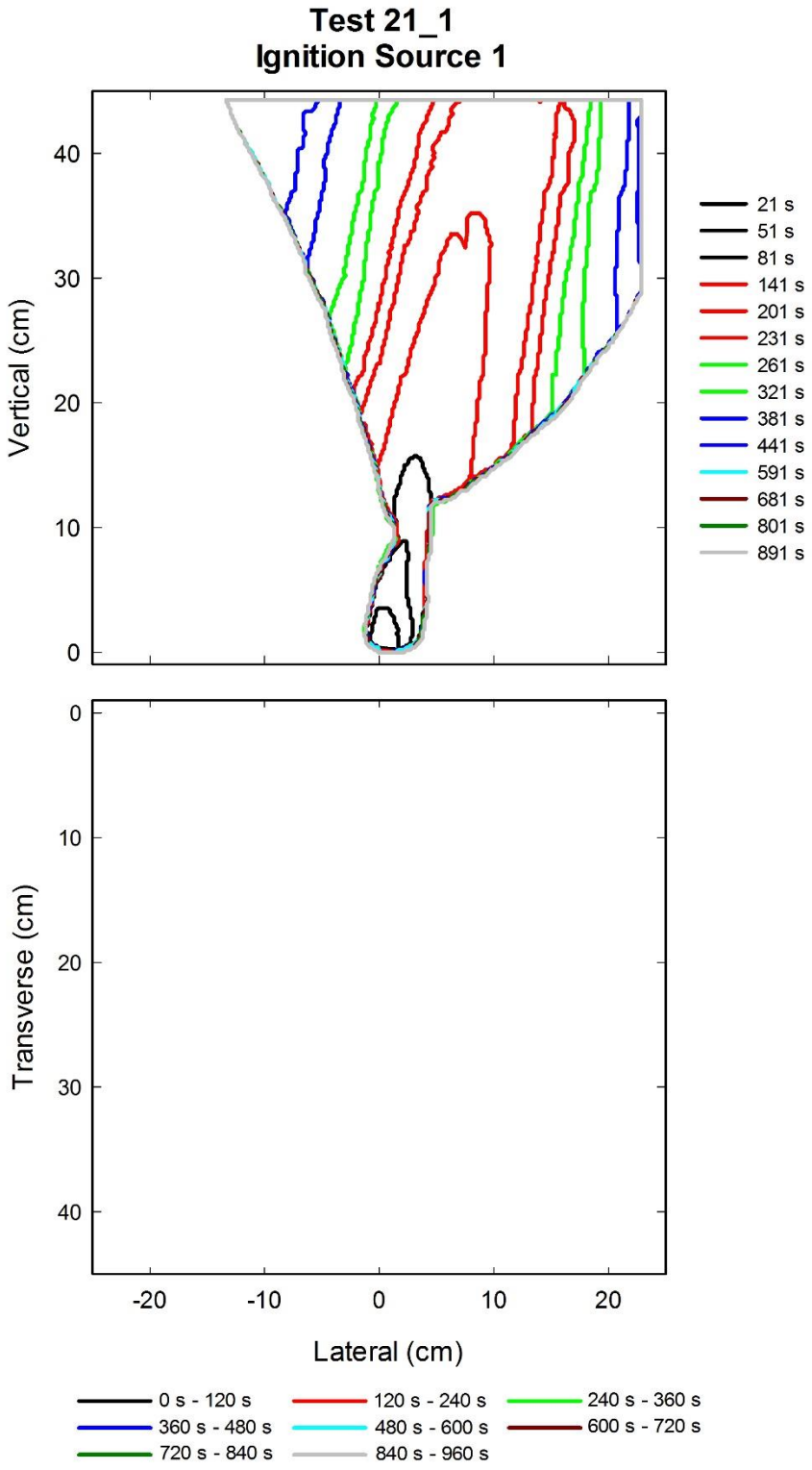

Figure A-188. Flame edge contours on the back (top) cushion are plotted as a function of time for Test 21_1 following application of Ignition Source 1.

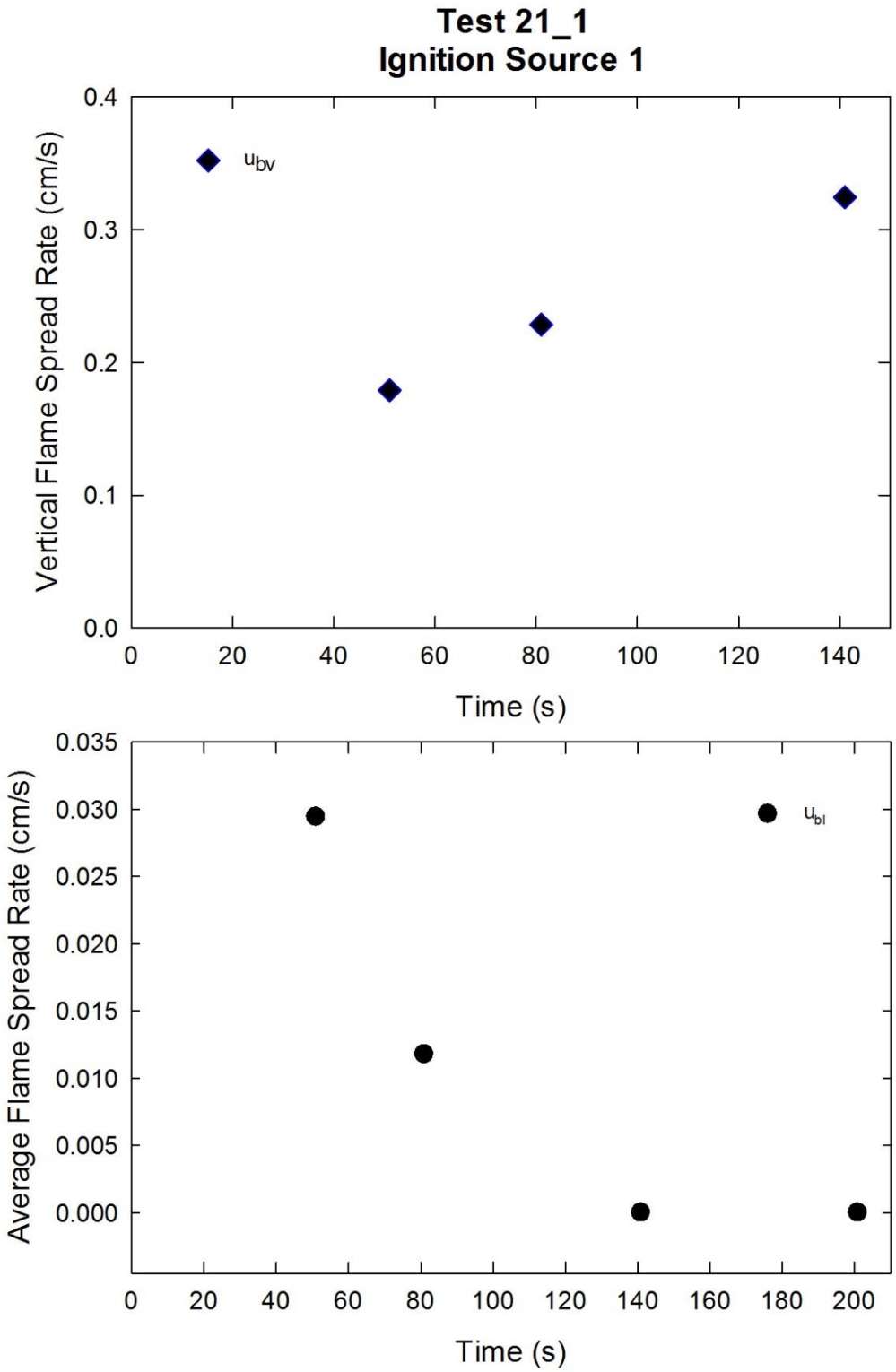

Figure A-189. Vertical flame spread rate (top) and average lateral flame spread rate (bottom) on the back cushion are plotted as a function of time for Test 21_1 following application of Ignition Source 1.

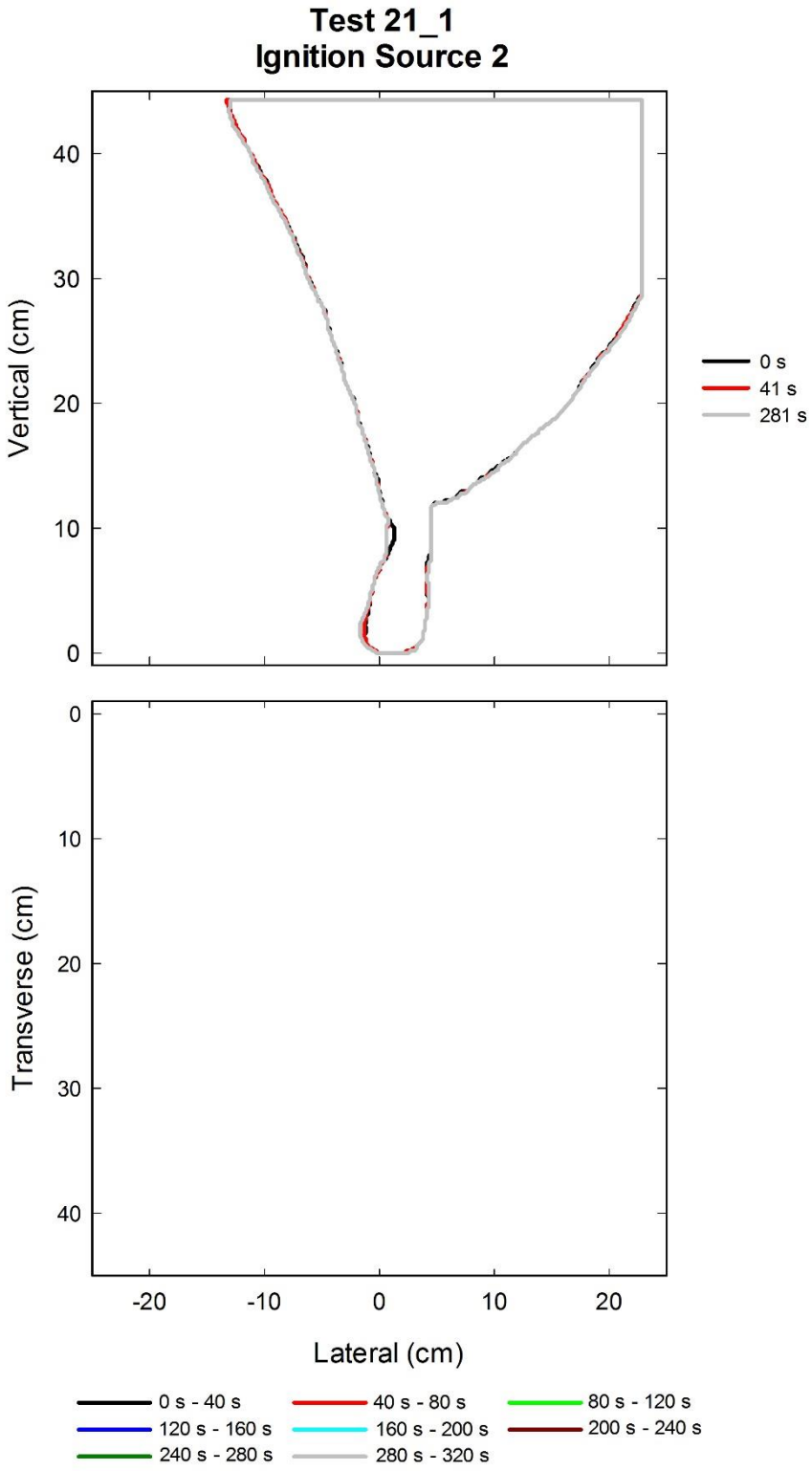

Figure A-190. Flame edge contours on the back (top) cushion are plotted as a function of time for Test 21_1 following application of Ignition Source 2.

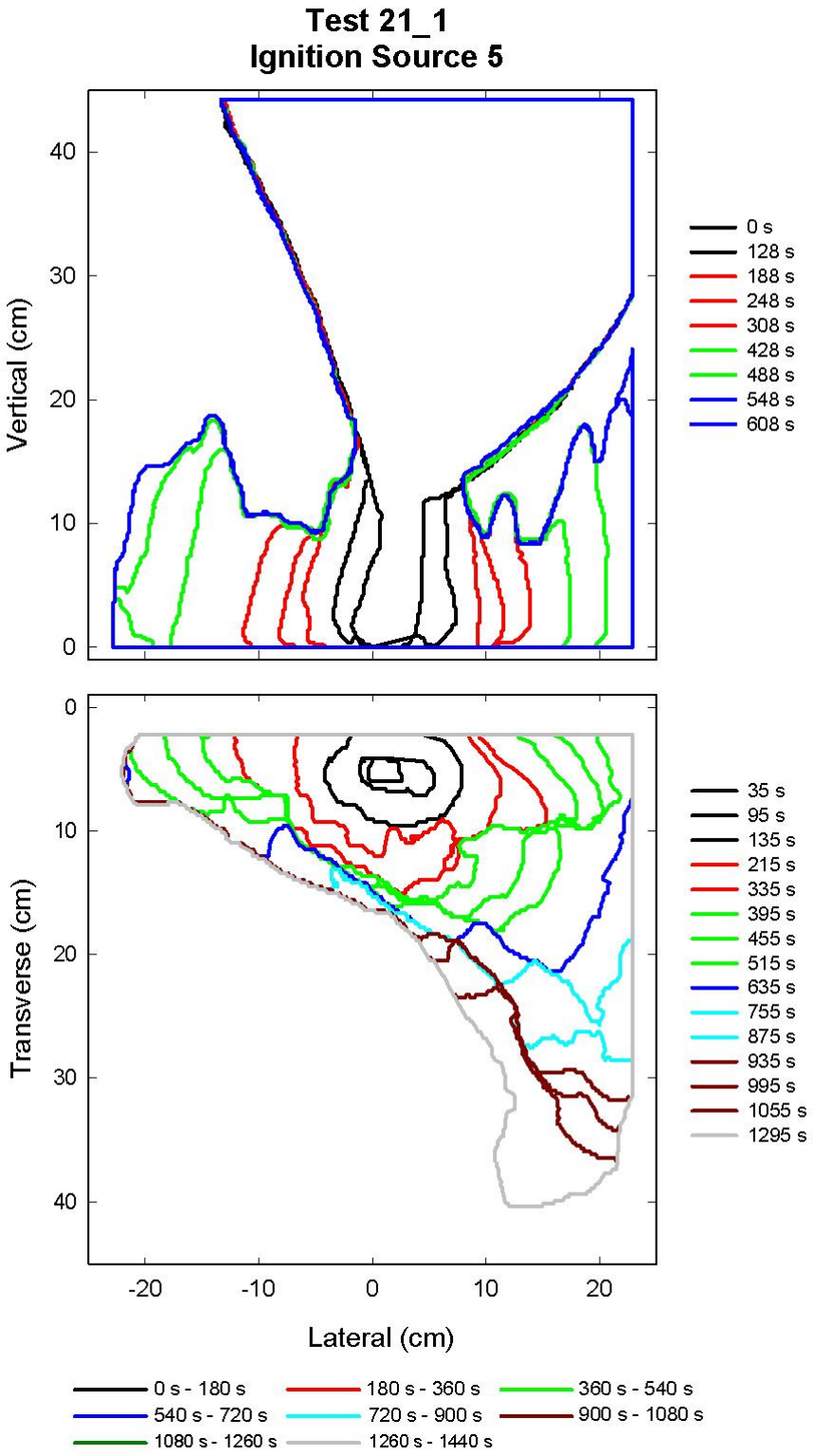

Figure A-191. Flame edge contours on the back (top) and seat (bottom) cushions are plotted as a function of time for Test 21_1 following application of Ignition Source 5.

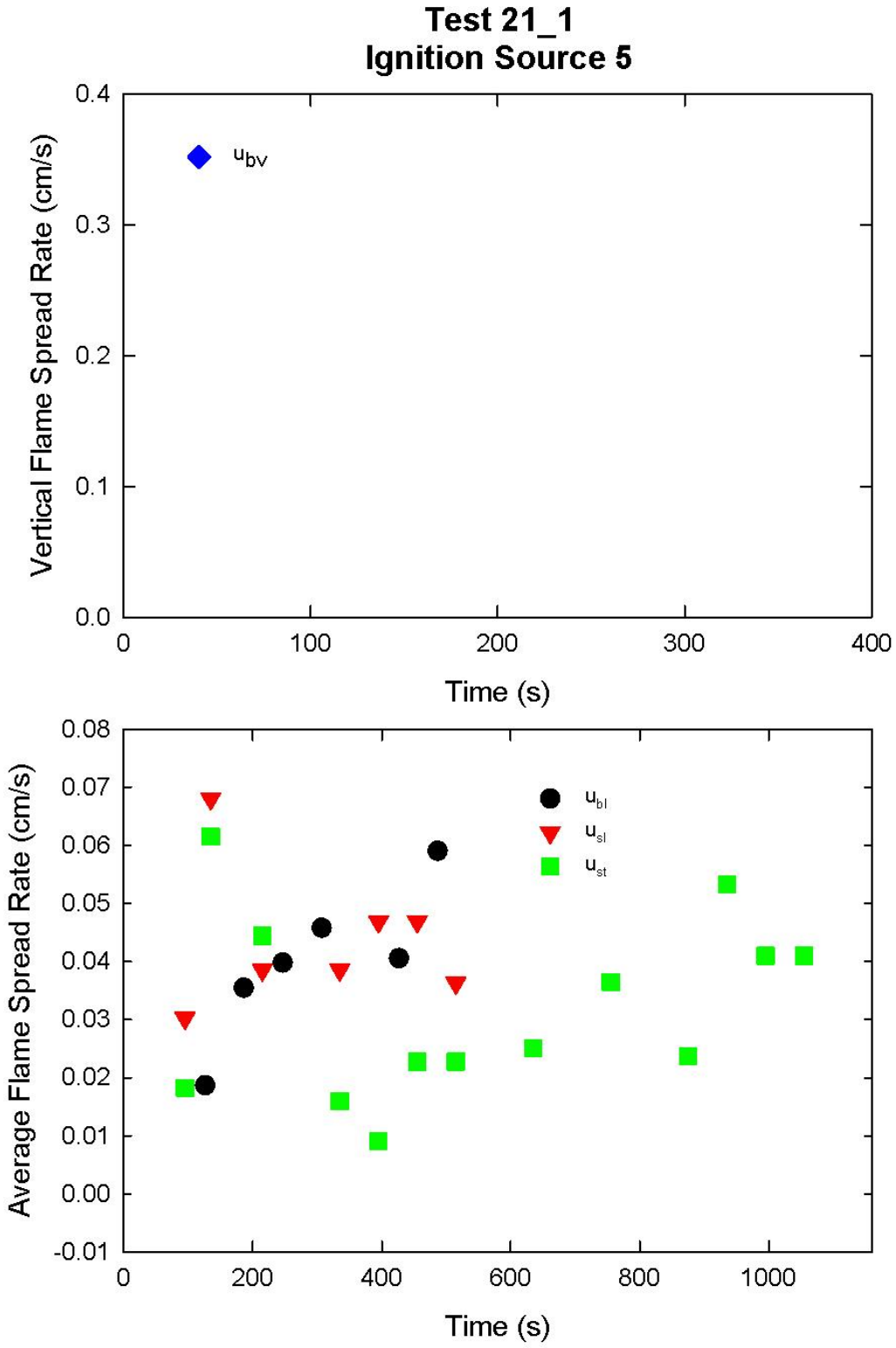

Figure A-192. Average lateral flame spread rate on the back and seat cushions and transverse flame spread rate on the seat cushion (bottom) are plotted as a function of time for Test 21_1 following application of Ignition Source 5.

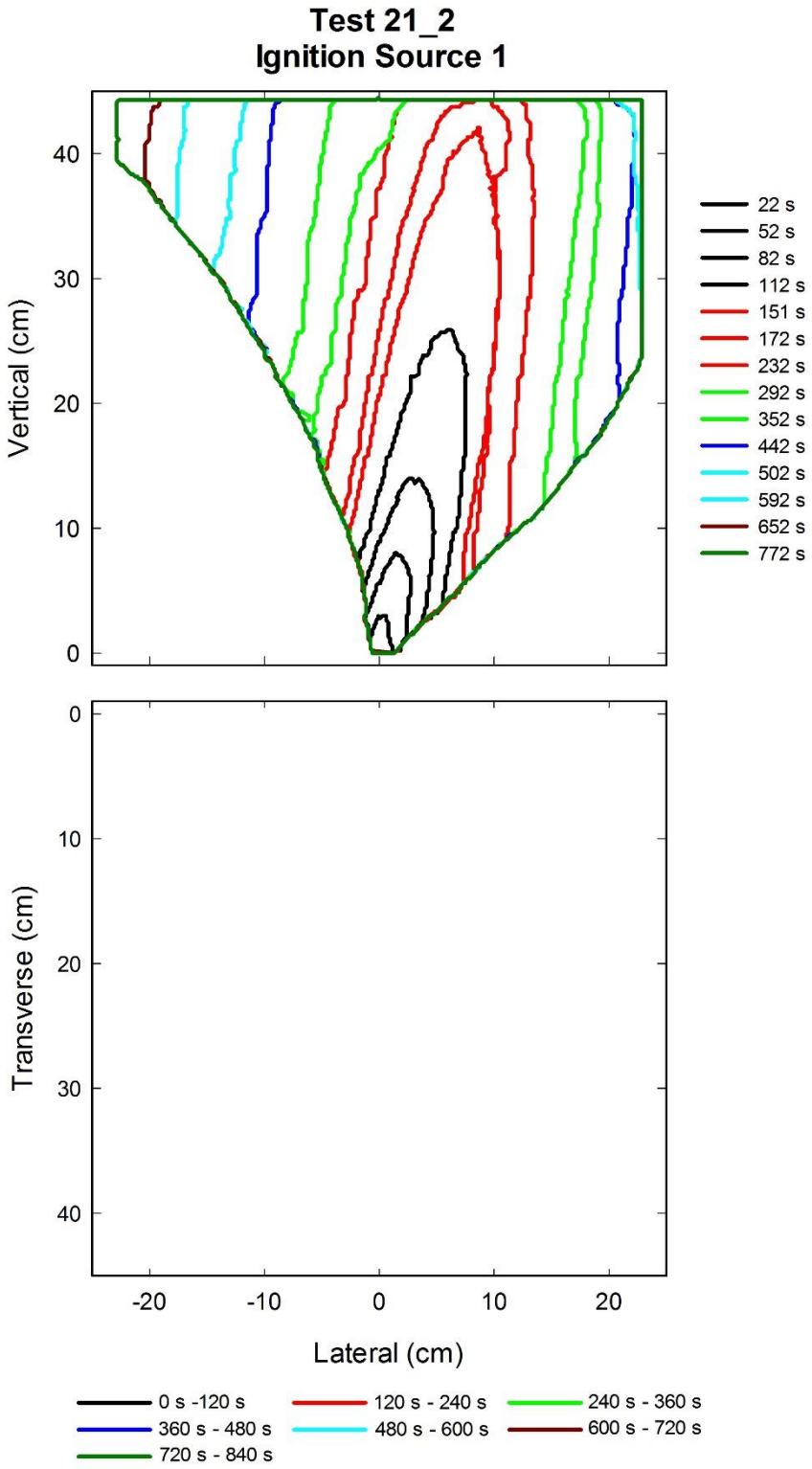

Figure A-193. Flame edge contours on the back cushion (top) are plotted as a function of time for Test 21_2 following application of Ignition Source 1.

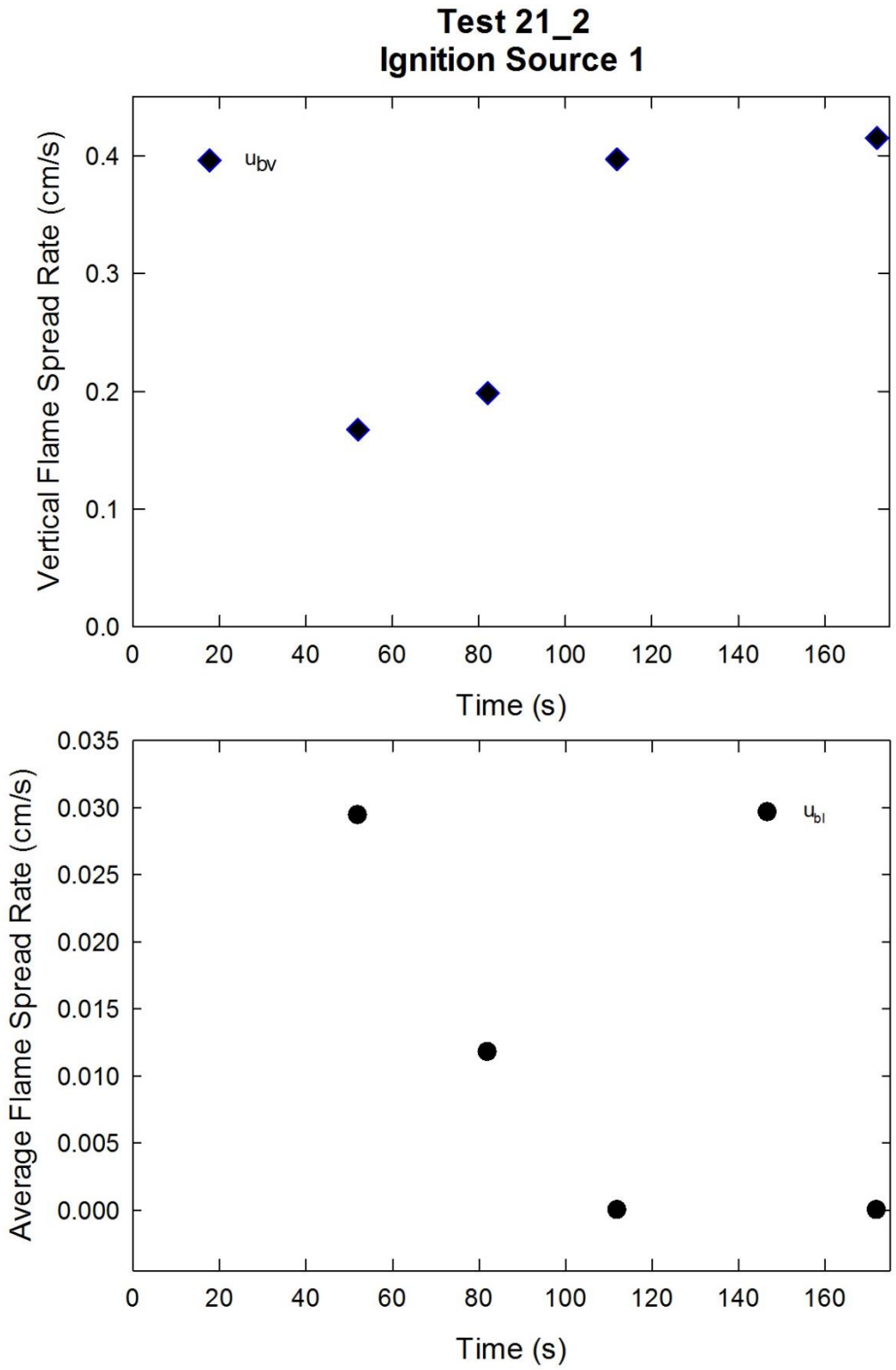

Figure A-194. Vertical flame spread rate (top) and average lateral flame spread rate (bottom) on the back cushion are plotted as a function of time for Test 21_2 following application of Ignition Source 1.

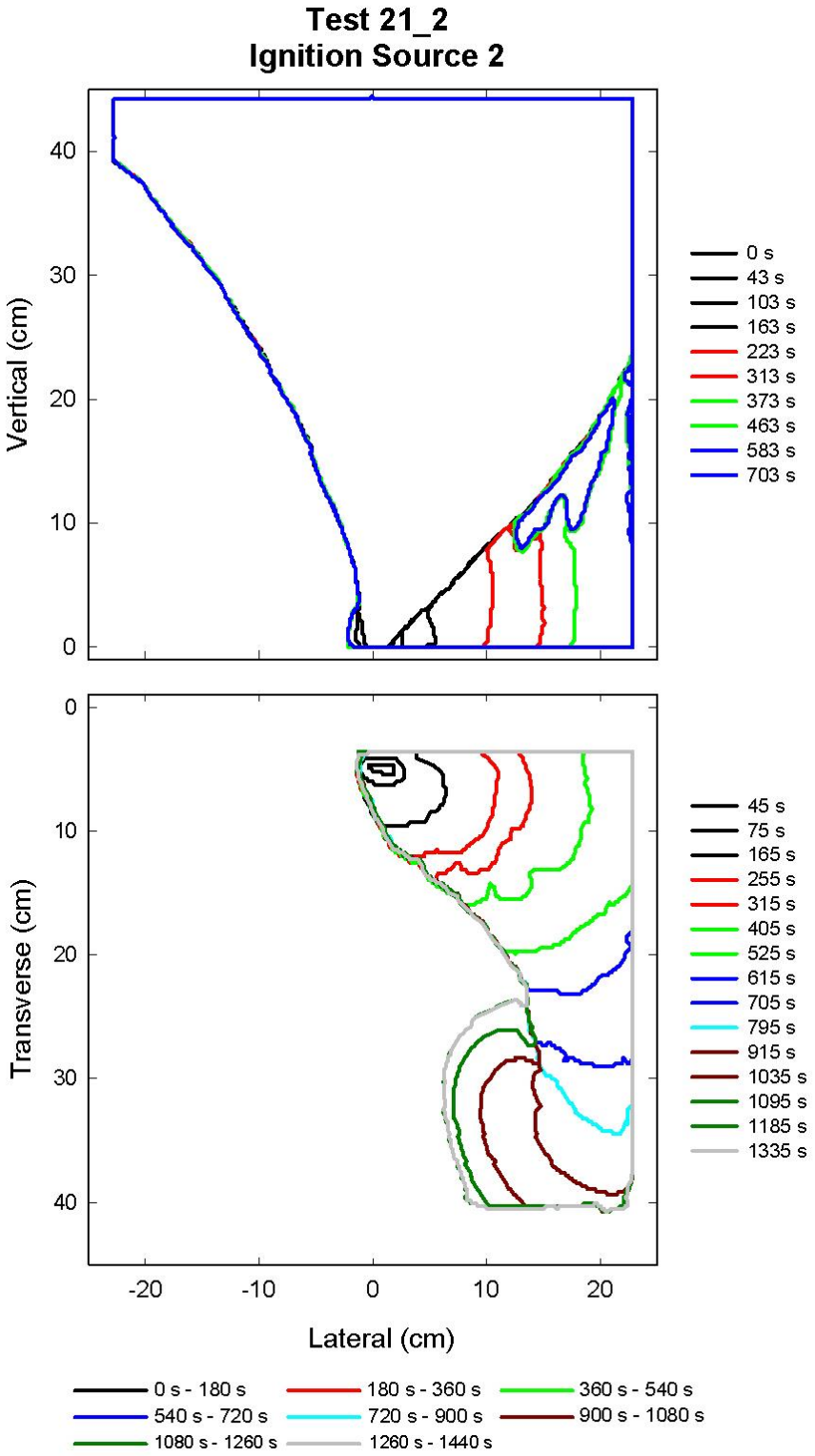

Figure A-195. Flame edge contours on the back (top) and seat (bottom) cushions are plotted as a function of time for Test 21_2 following application of Ignition Source 2.

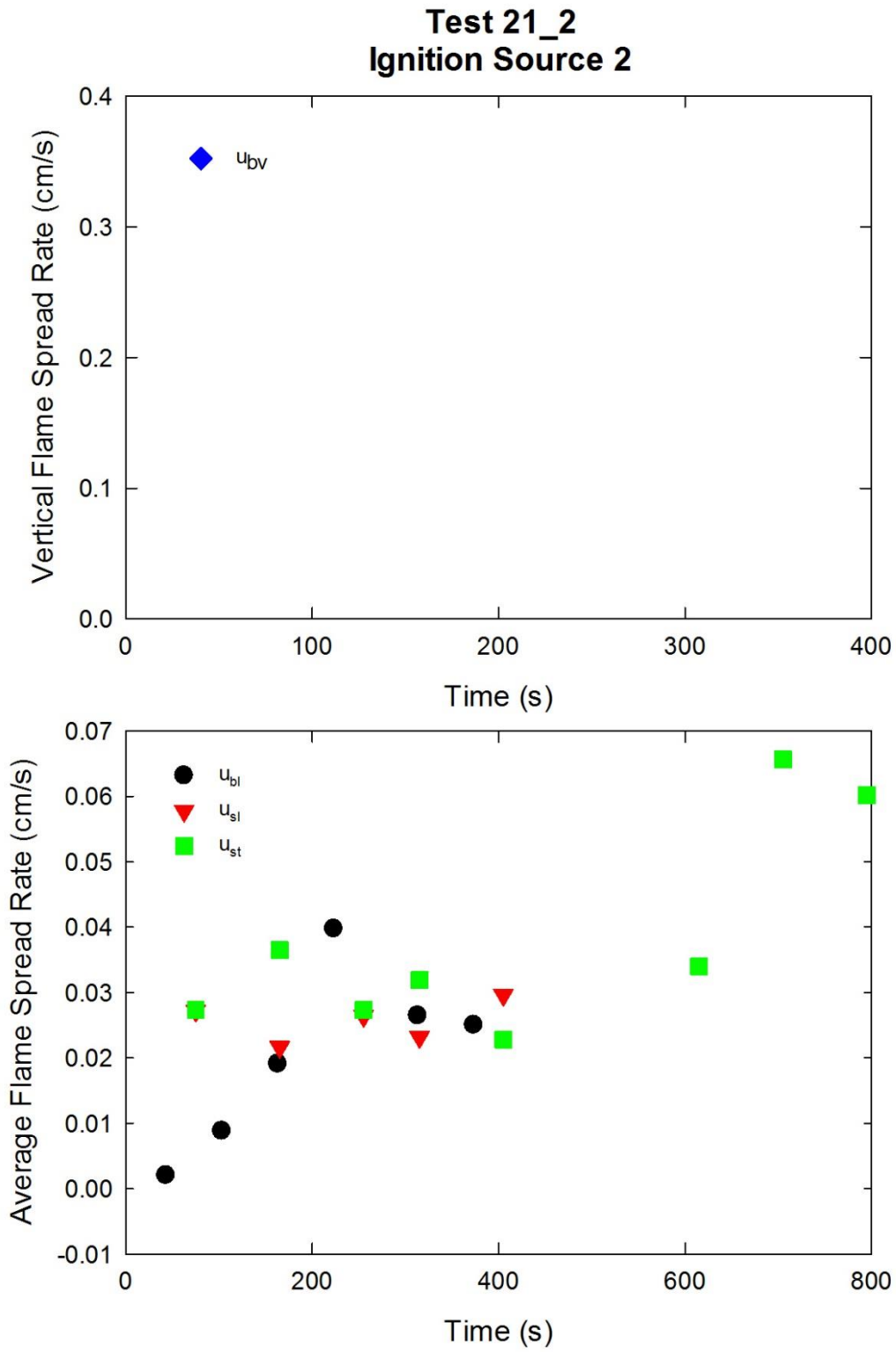

Figure A-196. Average lateral flame spread rates on the back and seat cushions and transverse flame spread rate on the seat cushion (bottom) are plotted as a function of time for Test 21_2 following application of Ignition Source 2.

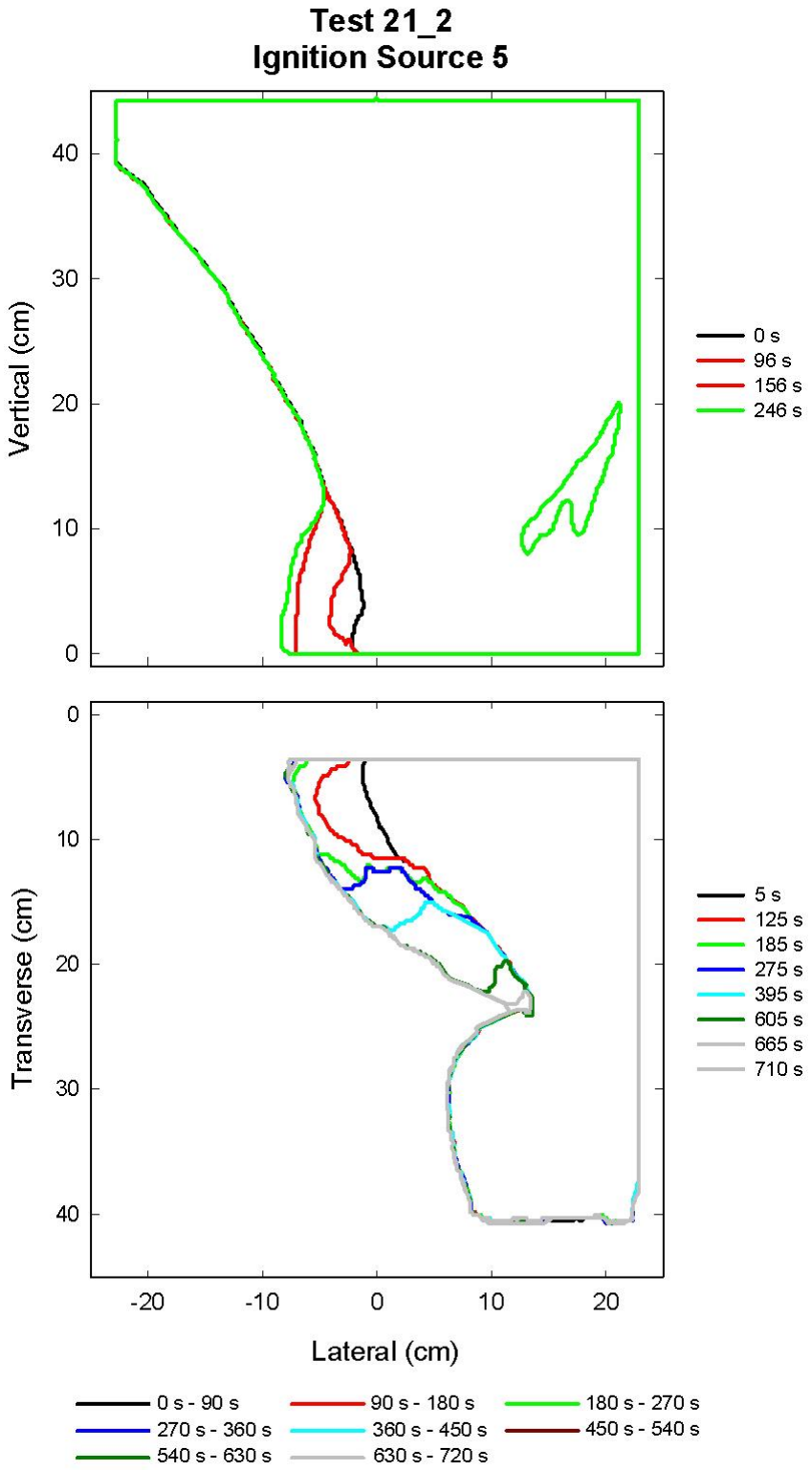

Figure A-197. Flame edge contours on the back (top) and seat (bottom) cushions are plotted as a function of time for Test 21_2 following application of Ignition Source 5.

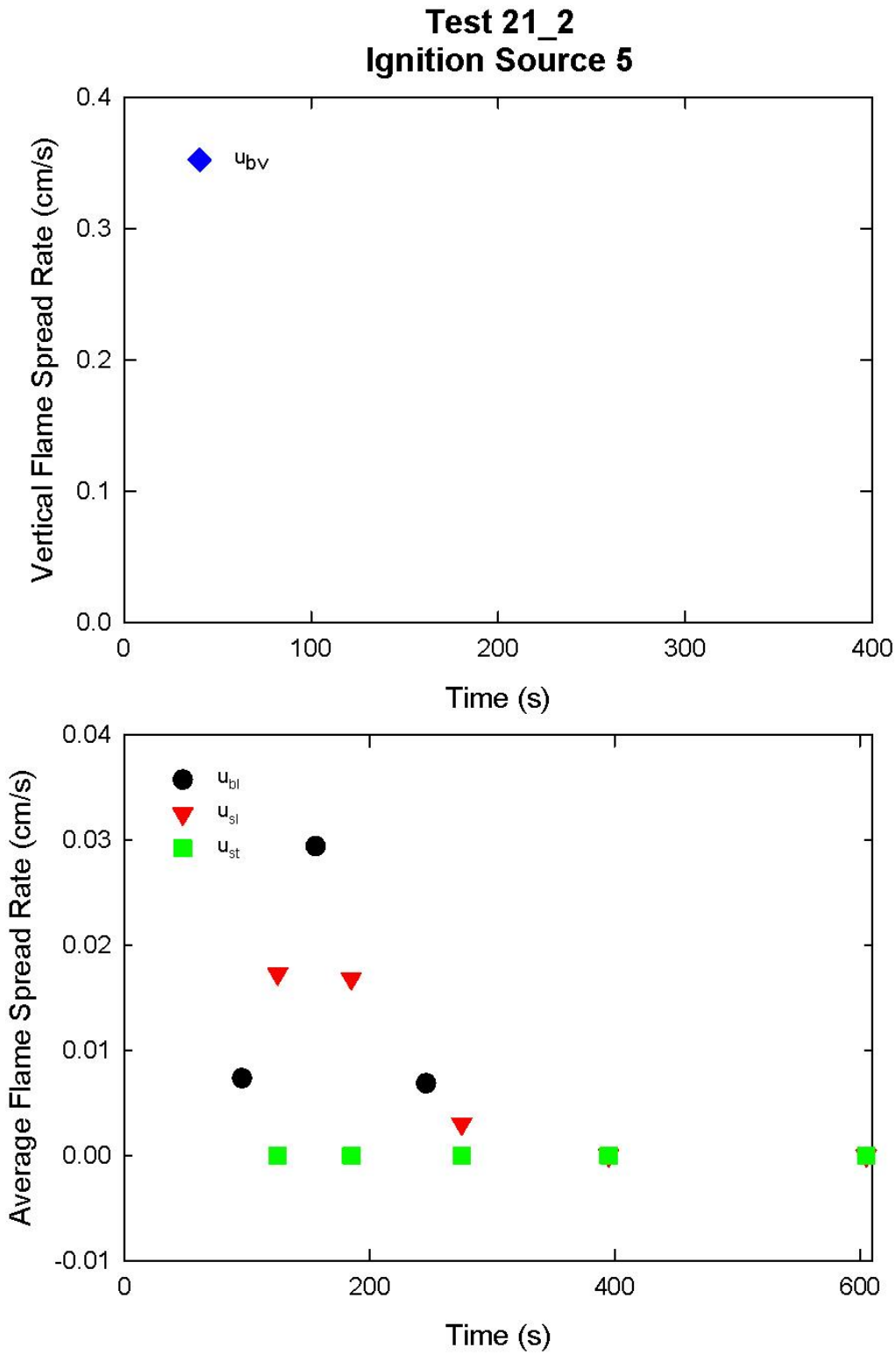

Figure A-198. Average lateral flame spread rates on the back and seat cushions and transverse flame spread rate on the seat cushion (bottom) are plotted as a function of time for Test 21_2 following application of Ignition Source 5.

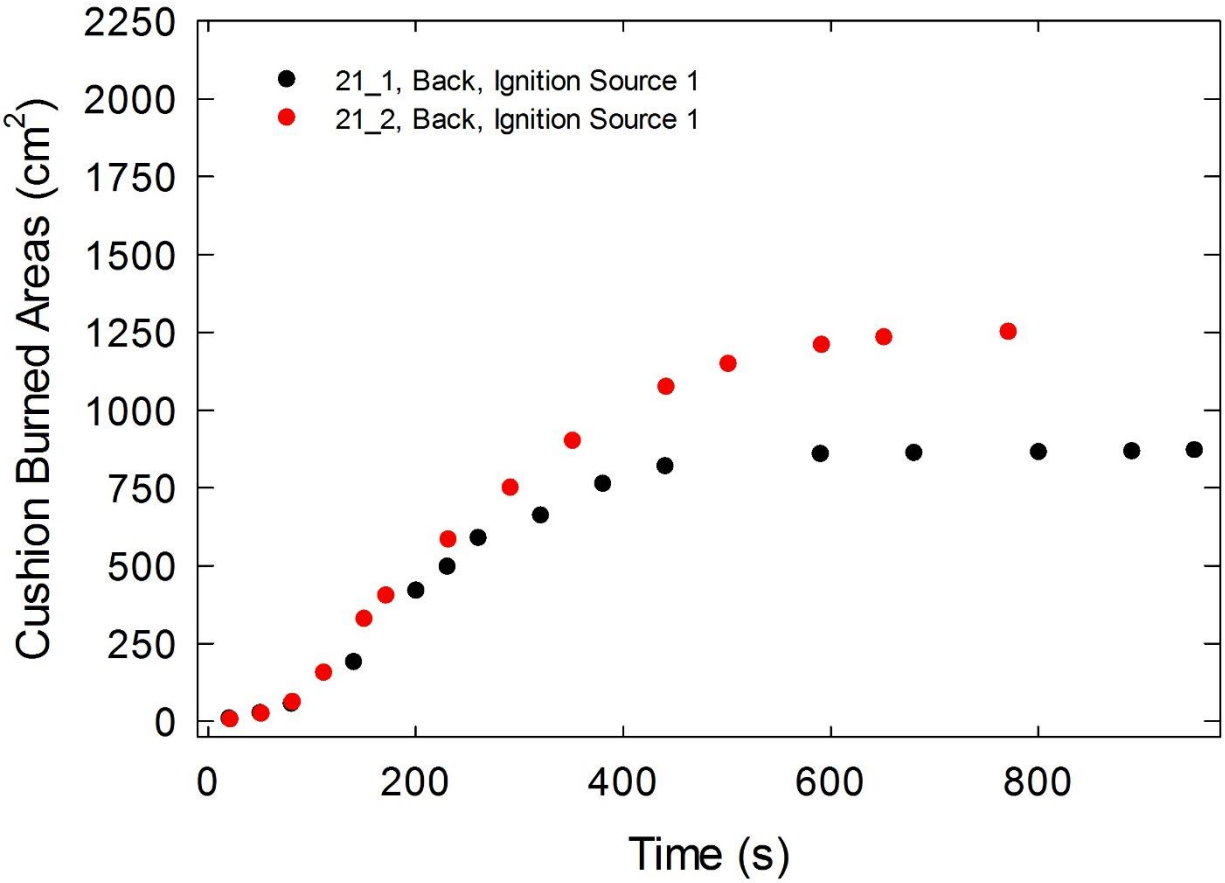

Figure A-199. Burned areas on the back cushion are plotted as a function of time for Combination 21 tests following application of Ignition Source 1.

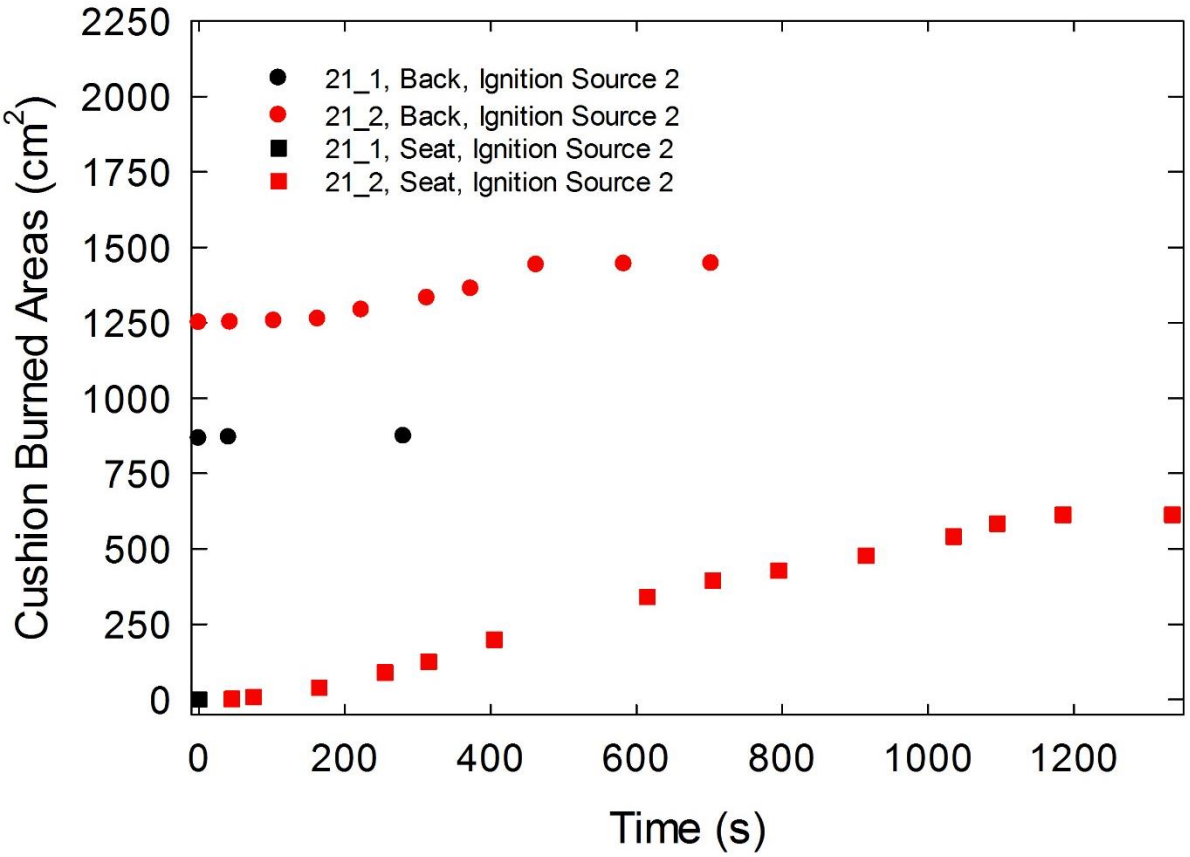

Figure A-200. Burned areas on the seat and back cushions are plotted as a function of time for Combination 21 tests following application of Ignition Source 2.

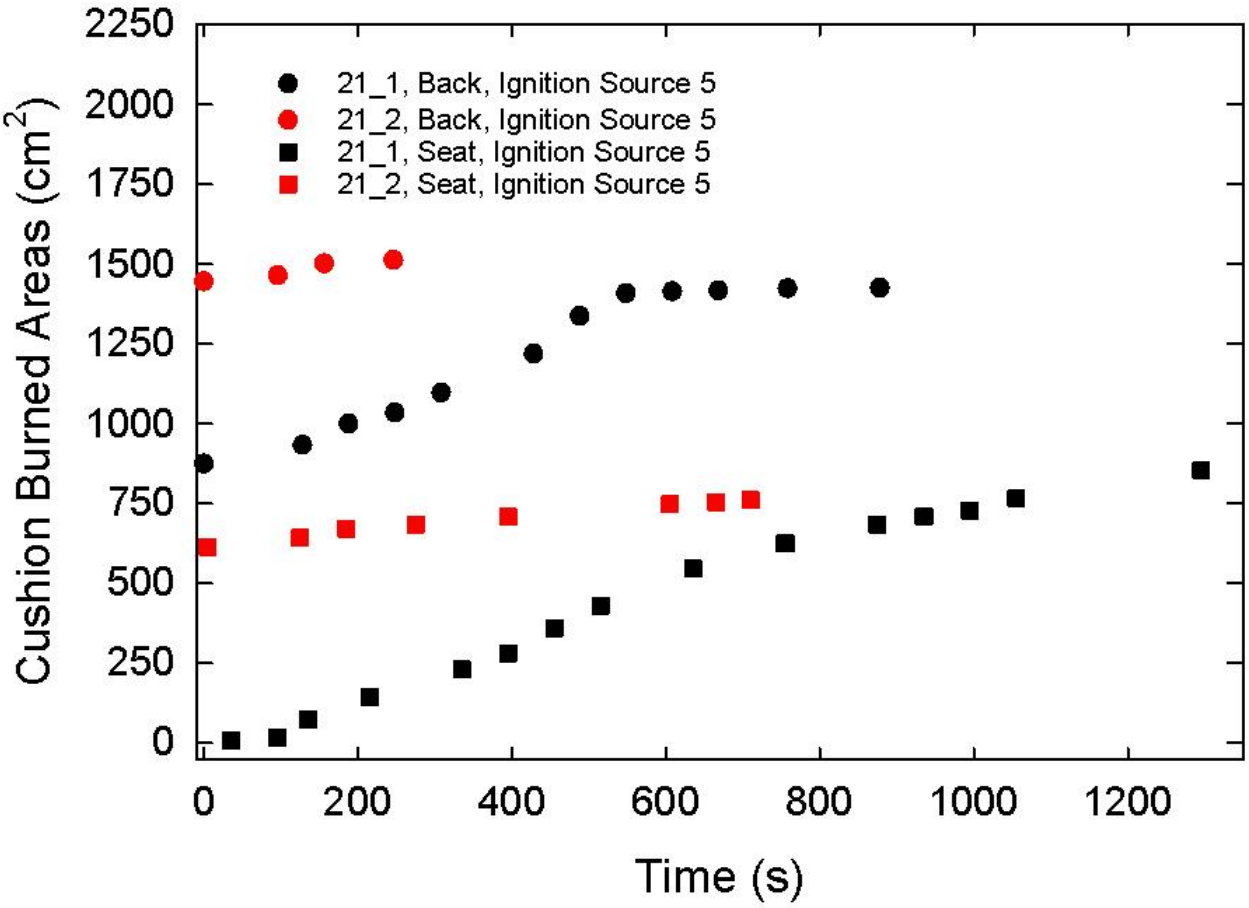

Figure A-201. Burned areas on the seat and back cushions are plotted as a function of time for Combination 21 tests following application of Ignition Source 5.

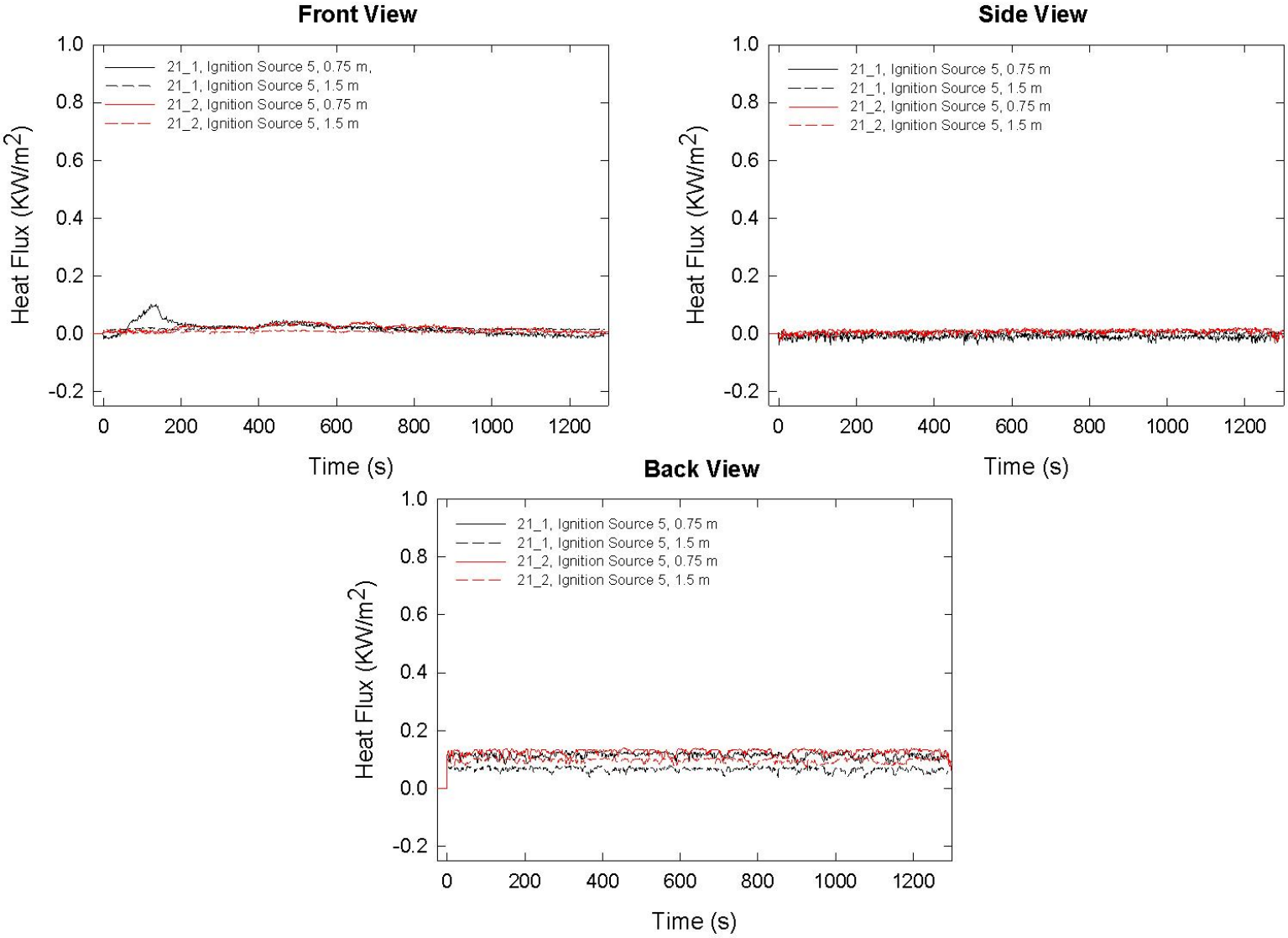

Figure A-202. Heat fluxes recorded at distances of 0.75 m and 1.5 m are plotted as a function of time for locations to the front, side and rear of the mock-up for Combination 21 tests following application of Ignition Source 5.

A.18 Combination 22

78%PP/22%PE/Norfab/FRFPUF

Notes:

Test 1:

Ignition Source 1 applied at time = 0 s.

Initial mass reading (4.94 kg) recorded during the test disagreed with an earlier measurement for the mock-up (3.81 kg); mass readings were highly erratic and nonphysical; **these mass data were excluded from analysis**.

Test 2:

Ignition Source 1 applied at time = 0 s.

Test 3:

Ignition Source 1 applied at time = 0 s.

Front-view (Camera #2) video is not available.

Back cushion was placed in the mock-up with zipper facing right side

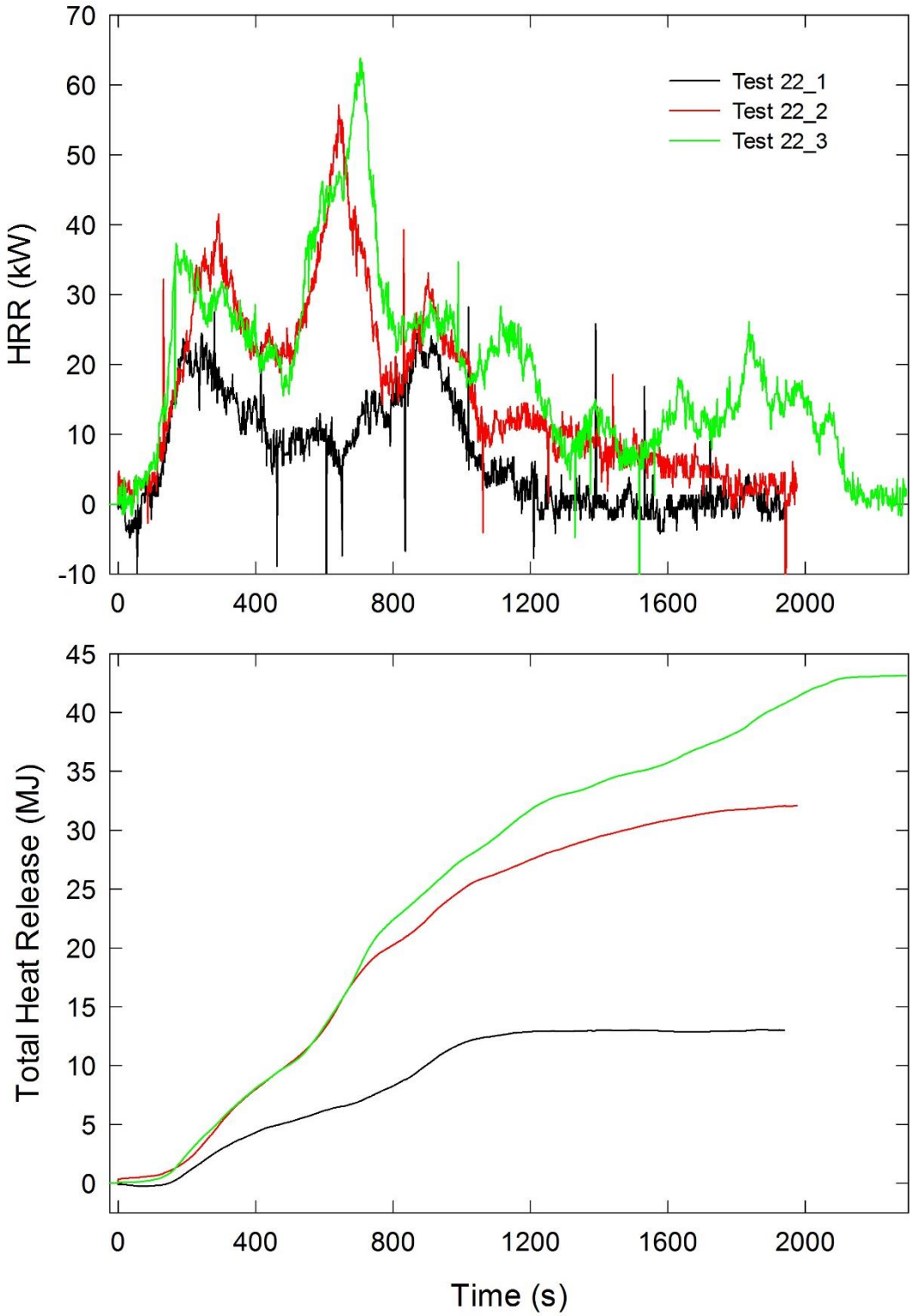

Figure A-203. Temporal profiles of HRR and integrated HRR are shown for Combination 22 tests following application of Ignition Source 1.

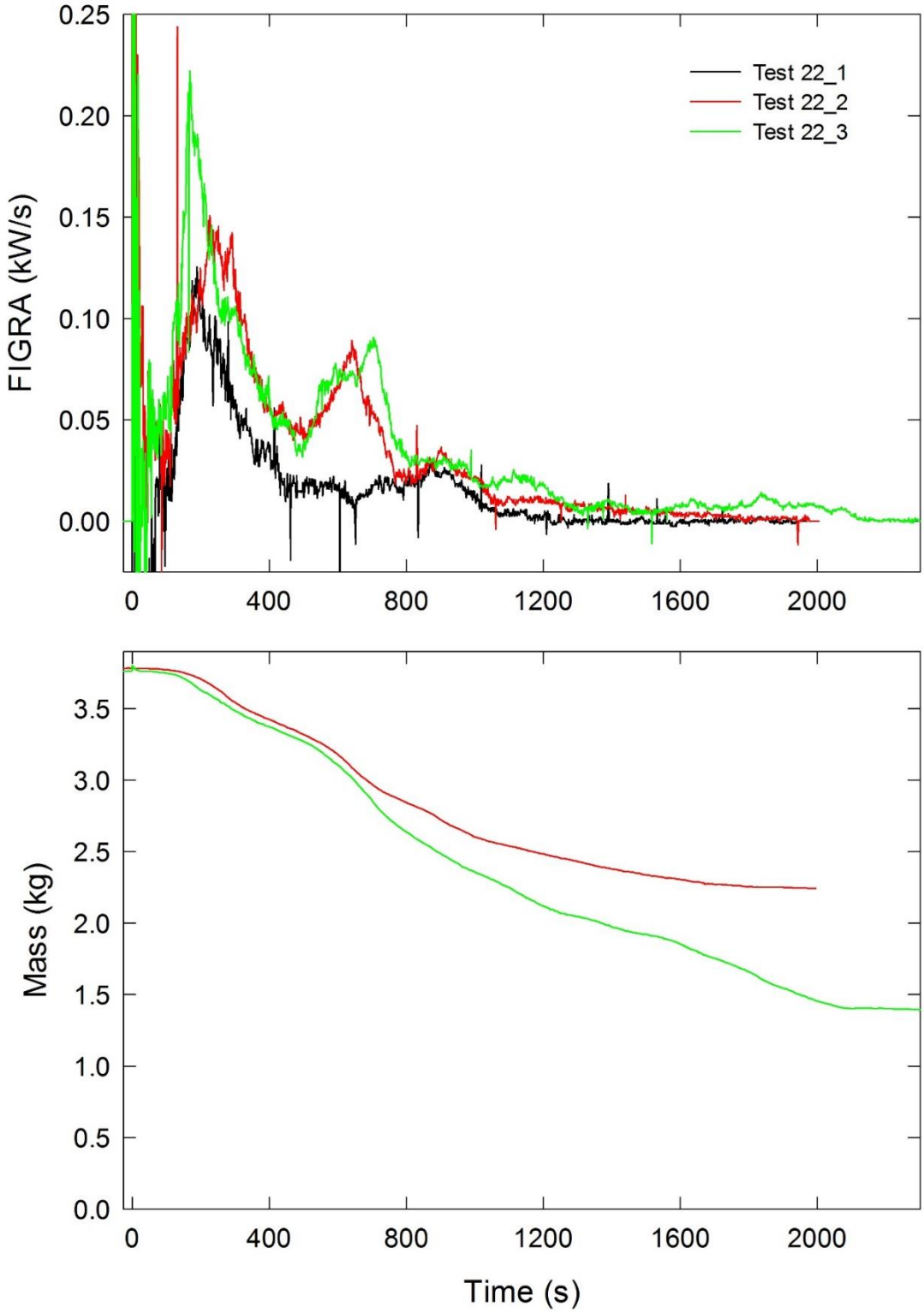

Figure A-204. Temporal profiles of FIGRA for Combination 22 tests and mock-up mass for Test 22_2 and Test 22_3 are shown following application of Ignition Source 1.

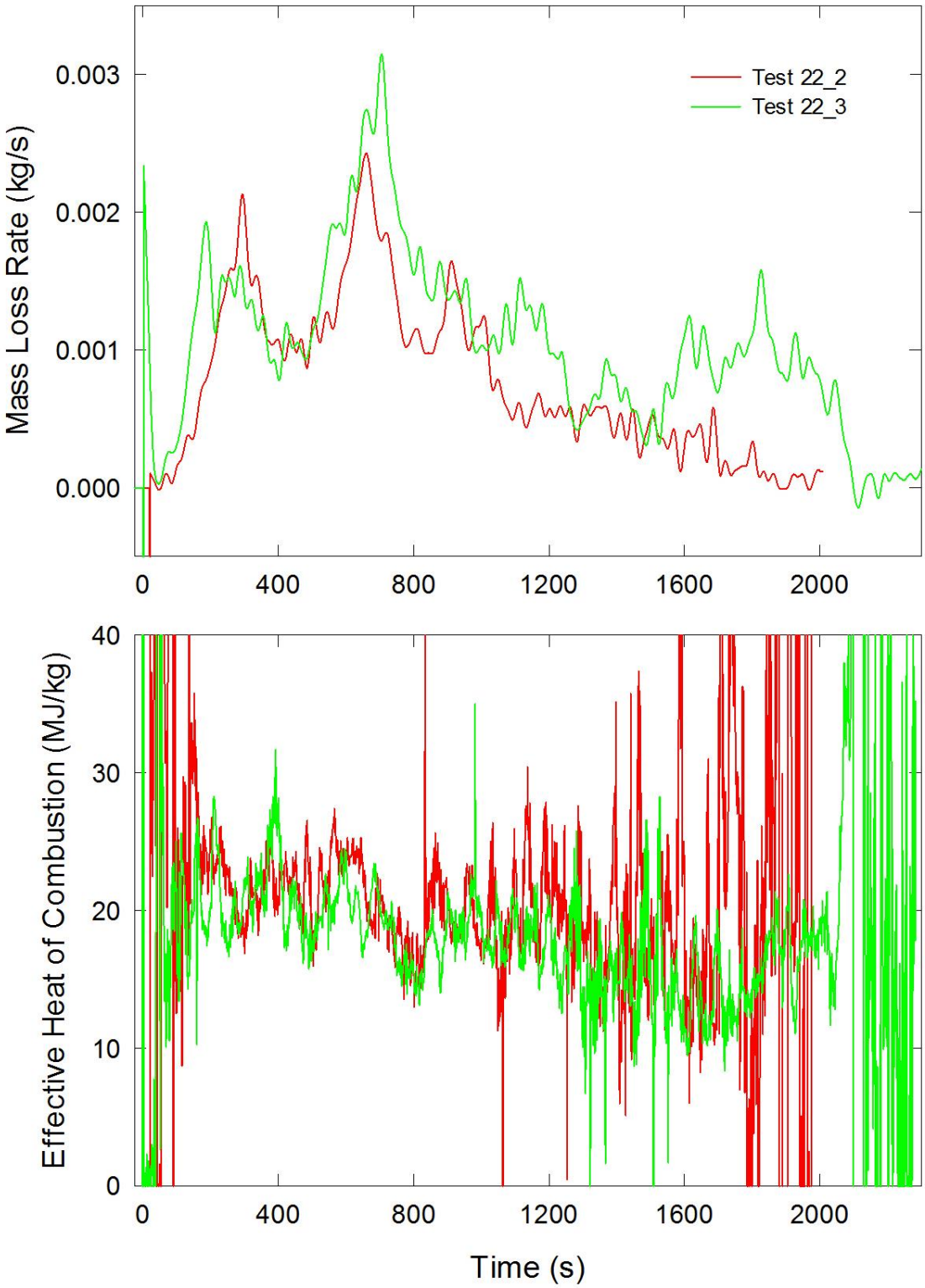

Figure A-205. Temporal profiles of MLR and EHOC are shown for Test 22_2 and Test 22_3 following application of Ignition Source 1.

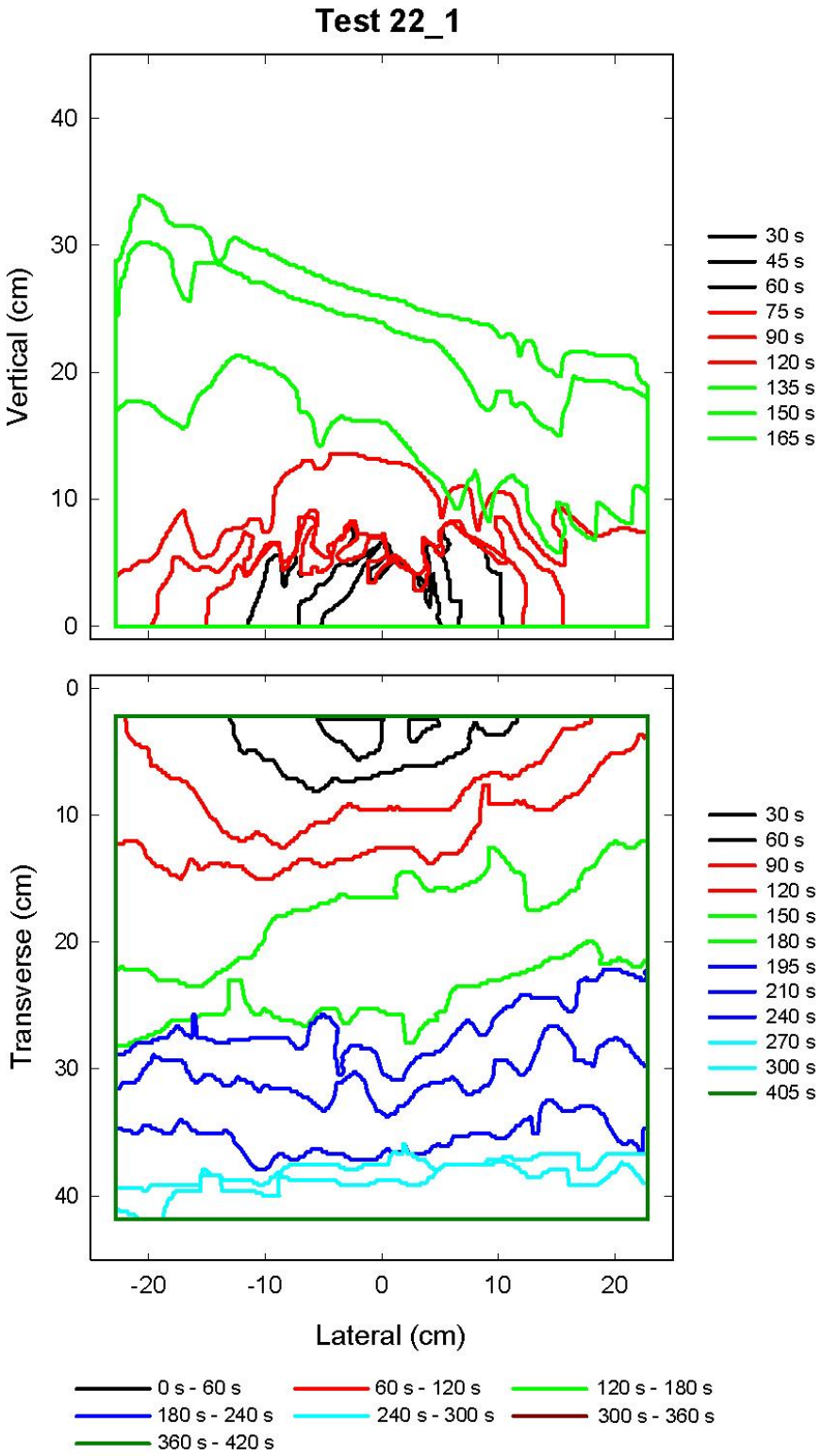

Figure A-206. Flame edge contours on the back (top) and seat (bottom) cushions are plotted as a function of time for Test 22_1 following application of Ignition Source 1.

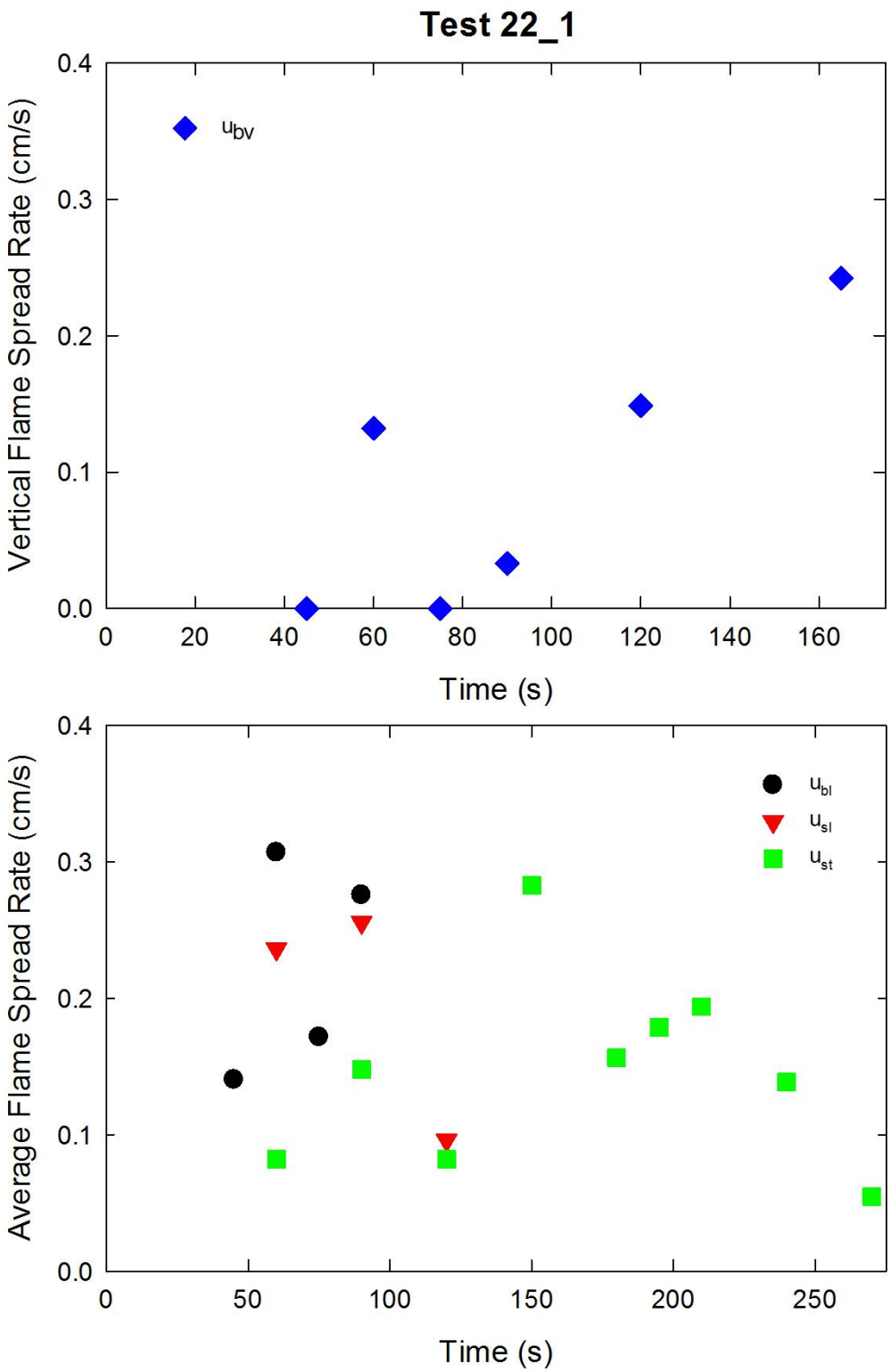

Figure A-207. Vertical flame spread rate on the back cushion (top) and average lateral flame spread rates on the back and seat cushions and transverse flame spread rate on the seat cushion (bottom) are plotted as a function of time for Test 22_1 following application of Ignition Source 1.

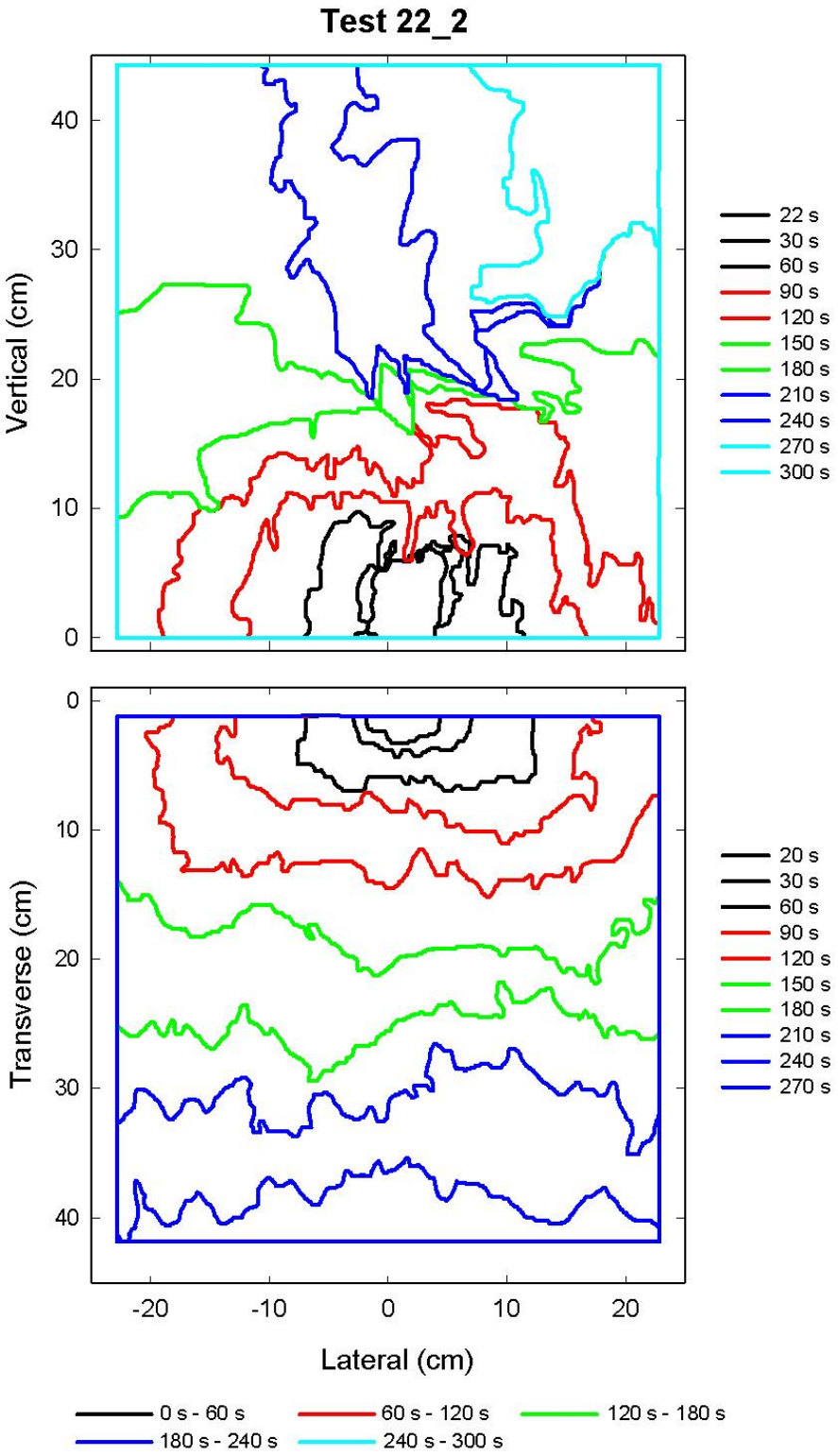

Figure A-208. Flame edge contours on the back (top) and seat (bottom) cushions are plotted as a function of time for Test 22_2 following application of Ignition Source 1.

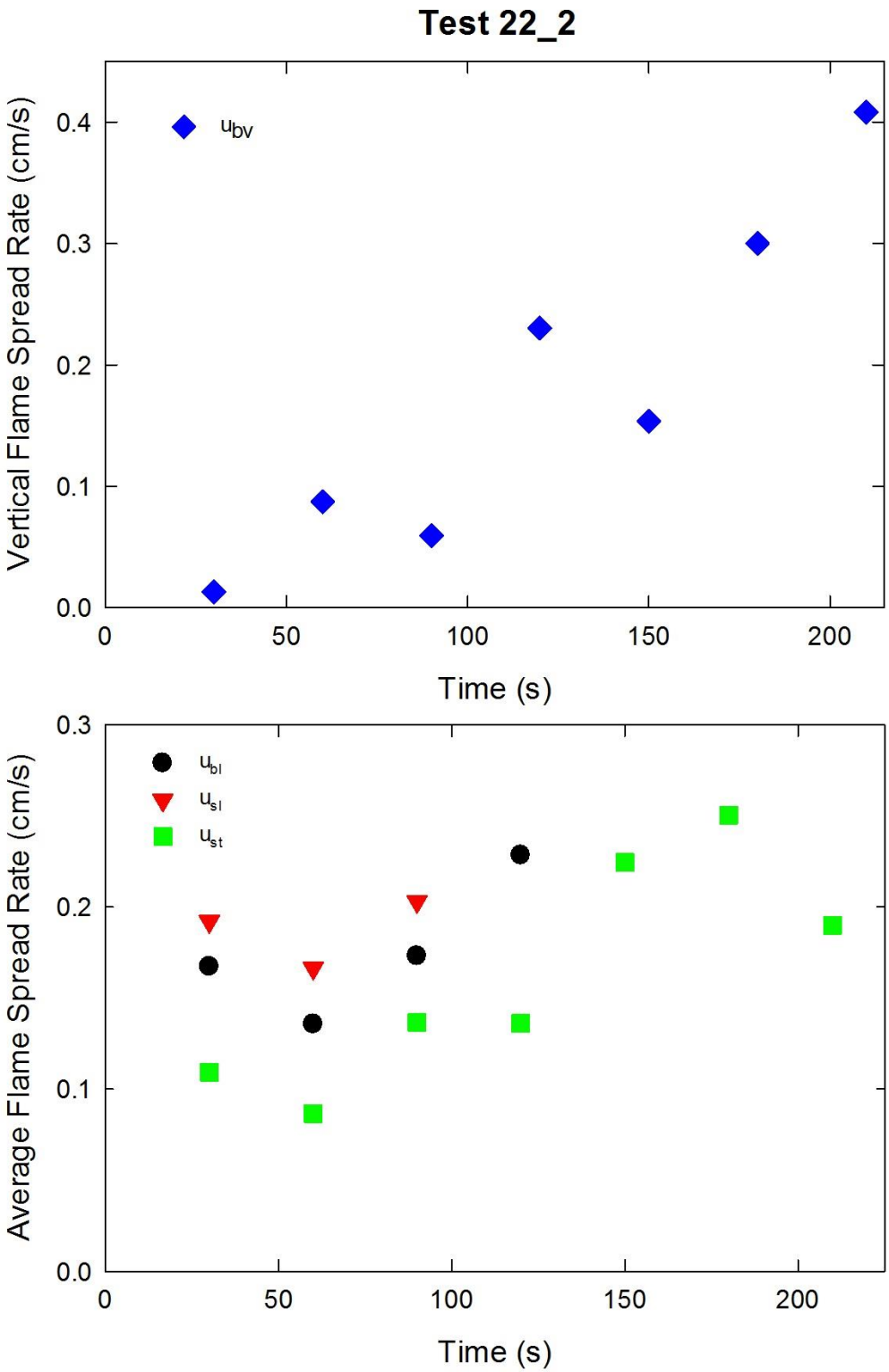

Figure A-209. Vertical flame spread rate on the back cushion (top) and average lateral flame spread rates on the back and seat cushions and transverse flame spread rate on the seat cushion (bottom) are plotted as a function of time for Test 22_2 following application of Ignition Source 1.

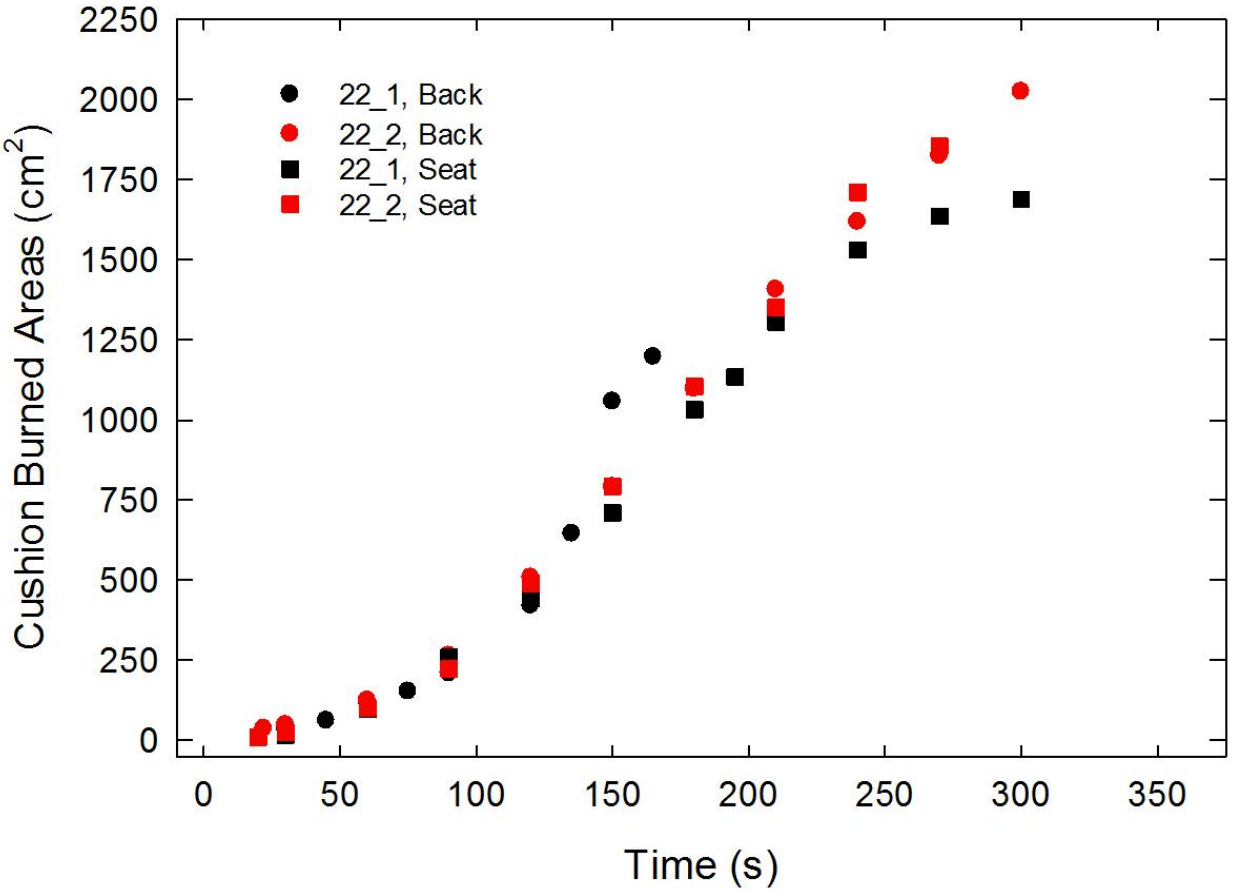

Figure A-210. Burned areas on the seat and back cushions are plotted as a function of time for Test 22_1 and Test 22_2 following application of Ignition Source 1.

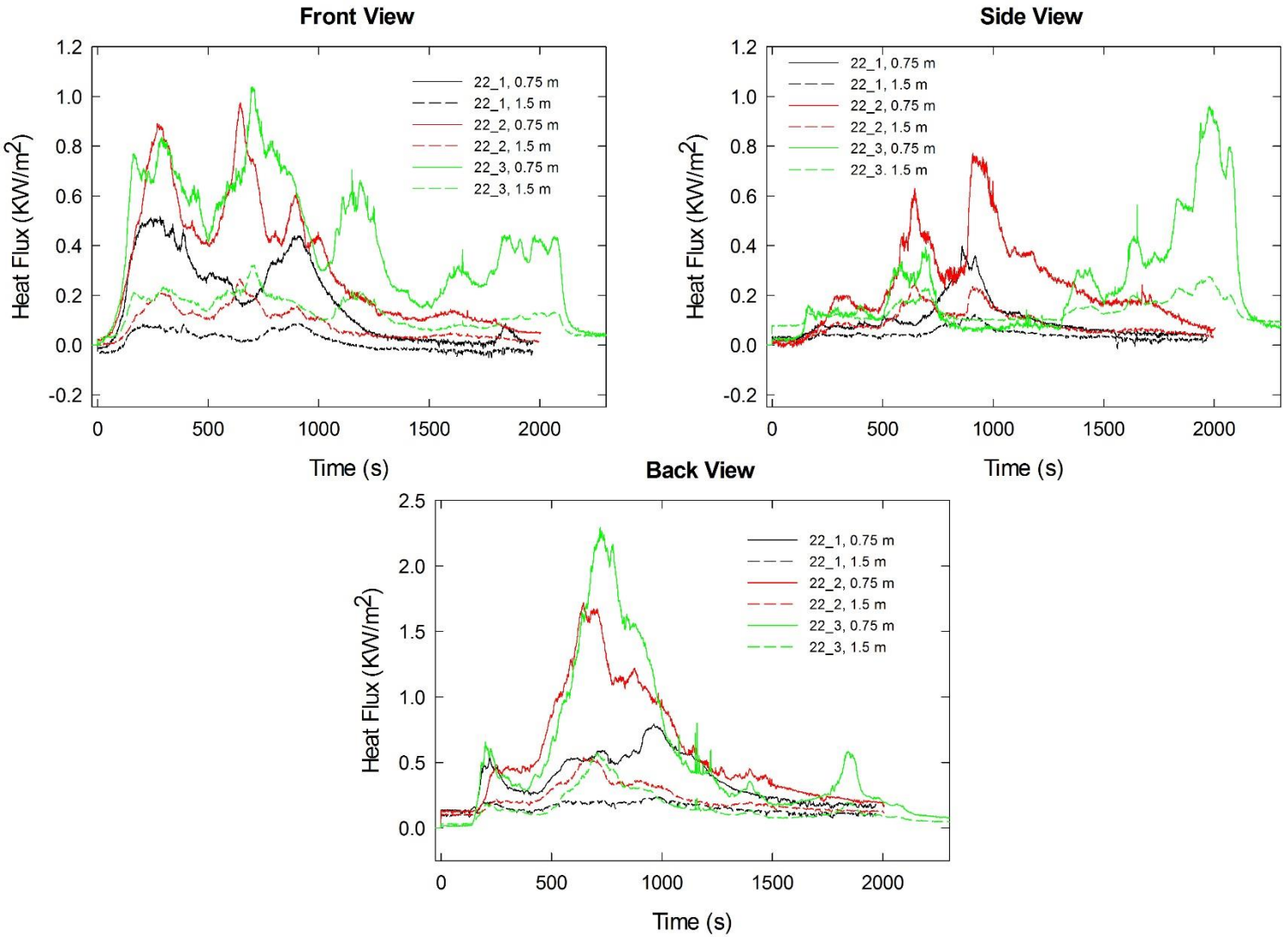

Figure A-211. Heat fluxes recorded at distances of 0.75 m and 1.5 m are plotted as a function of time for locations to the front, side and rear of the mock-up for Combination 22 tests following application of Ignition Source 1.

A.19 Combination 23

cotton/Norfab/PEFW/FRFPUF

Notes:

Test 1:

Ignition Source 1 applied at time = 0 s; vertical flame spread to top of back cushion with little lateral spread; no sign of blackening or flame spread on seat cushion.

Ignition Source 2 applied 319 s after Ignition Source 1 removed; flame spread over most of back cushion and parts of the seat and arm cushions; some smoldering of char on seat still evident when Ignition Source 5 applied.

Ignition Source 5 ignited 1587 s after Ignition Source 2 removed; no additional flame spread.

Test 2:

Ignition Source 1 applied at time = 0 s; upward flame spread on back cushion with little lateral spread; small darkened area on seat cushion with no flame spread.

Ignition Source 2 applied 466 s after Ignition Source 1 removed; slow flame spread covered most of the back, seat, and interiors of arm cushions.

Ignition Source 5 ignited 2181 s after Ignition Source 2 removed; no additional flame spread.

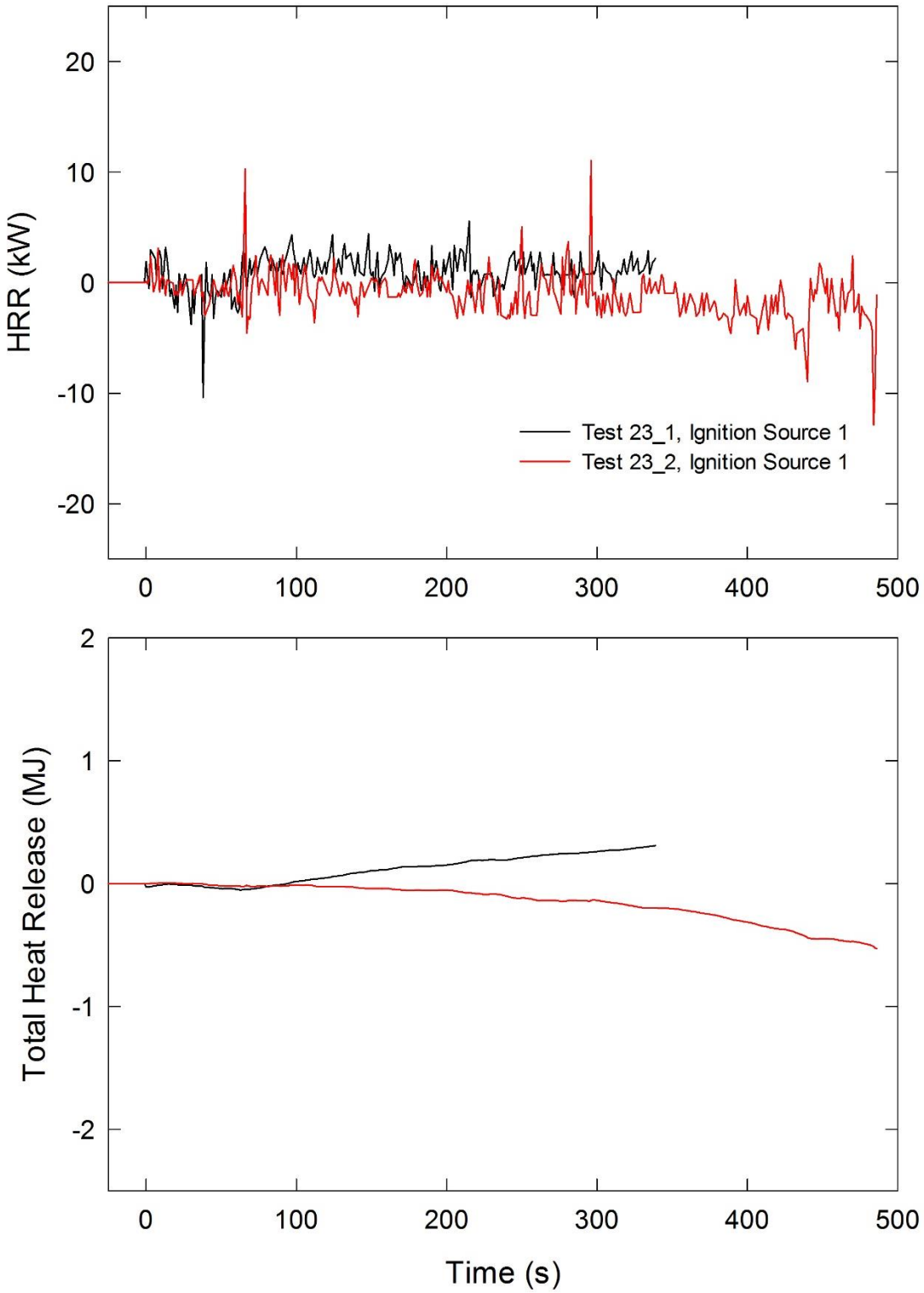

Figure A-212. Temporal profiles of HRR and integrated HRR are shown for Combination 23 tests following application of Ignition Source 1.

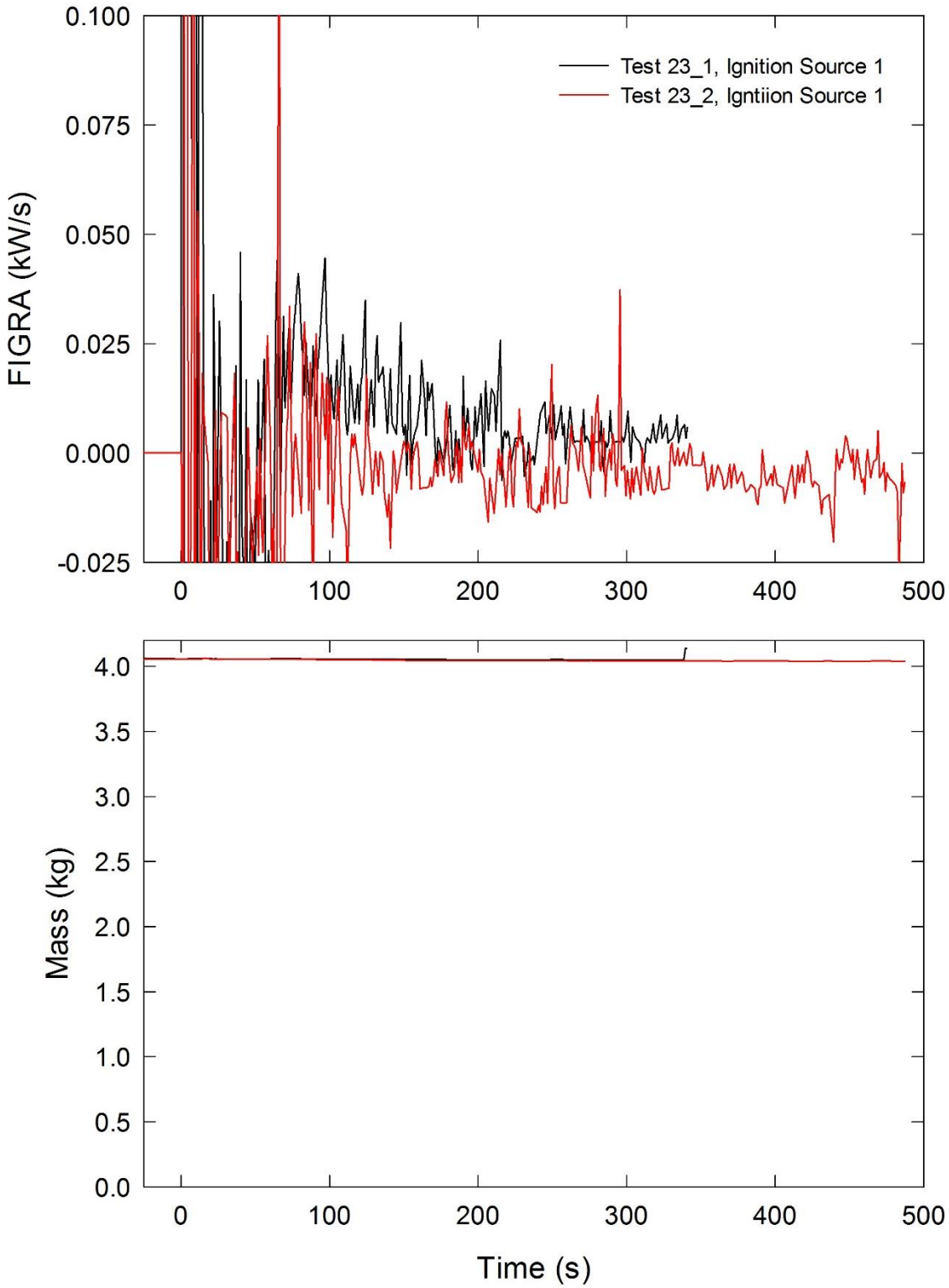

Figure A-213. Temporal profiles of FIGRA and mock-up mass for Combination 23 tests are shown following application of Ignition Source 1.

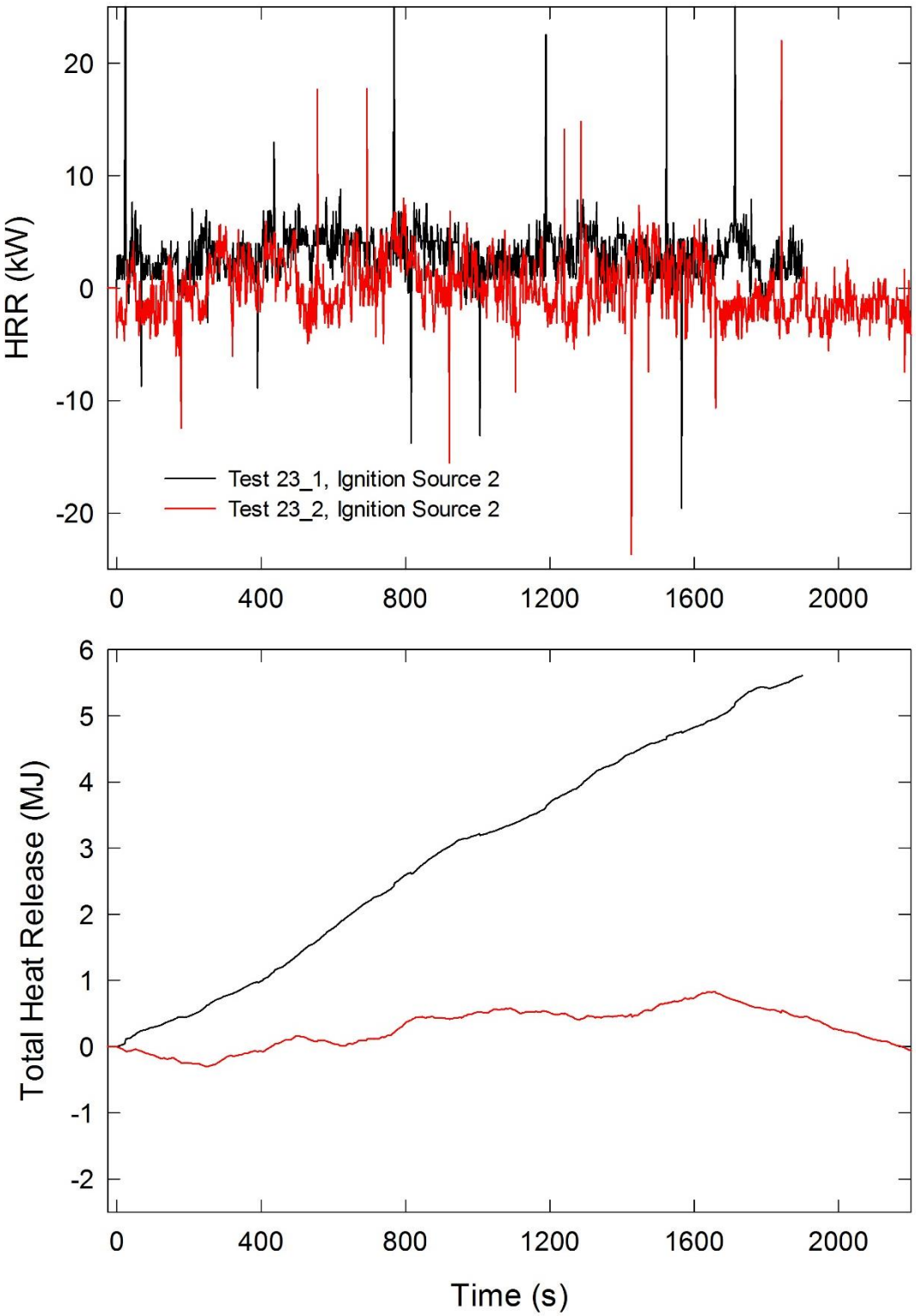

Figure A-214. Temporal profiles of HRR and integrated HRR are shown for Combination 23 tests following application of Ignition Source 2.

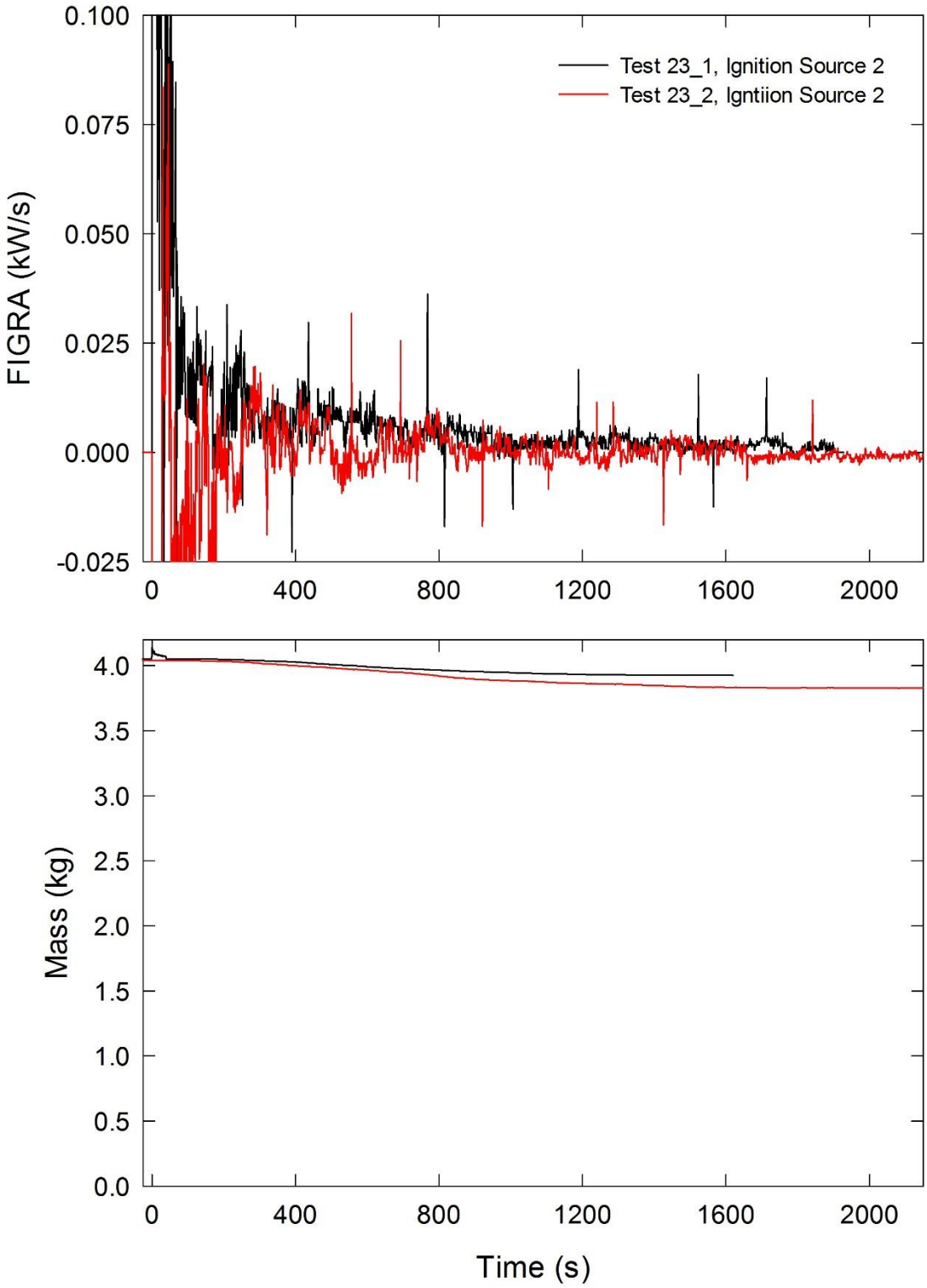

Figure A-215. Temporal profiles of FIGRA and mock-up mass for Combination 23 tests are shown following application of Ignition Source 2.

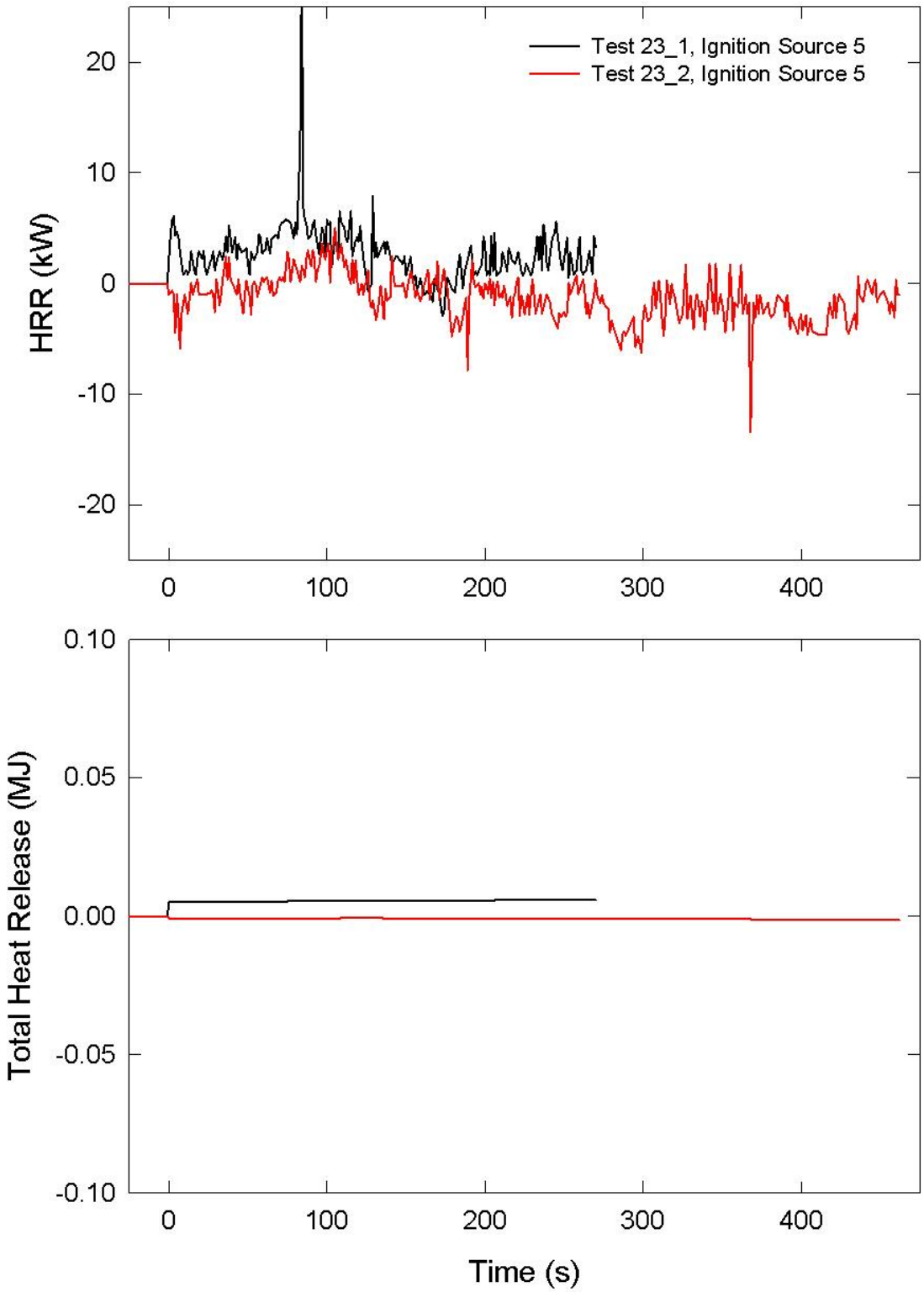

Figure A-216. Temporal profiles of HRR and integrated HRR are shown for Combination 23 tests following application of Ignition Source 5.

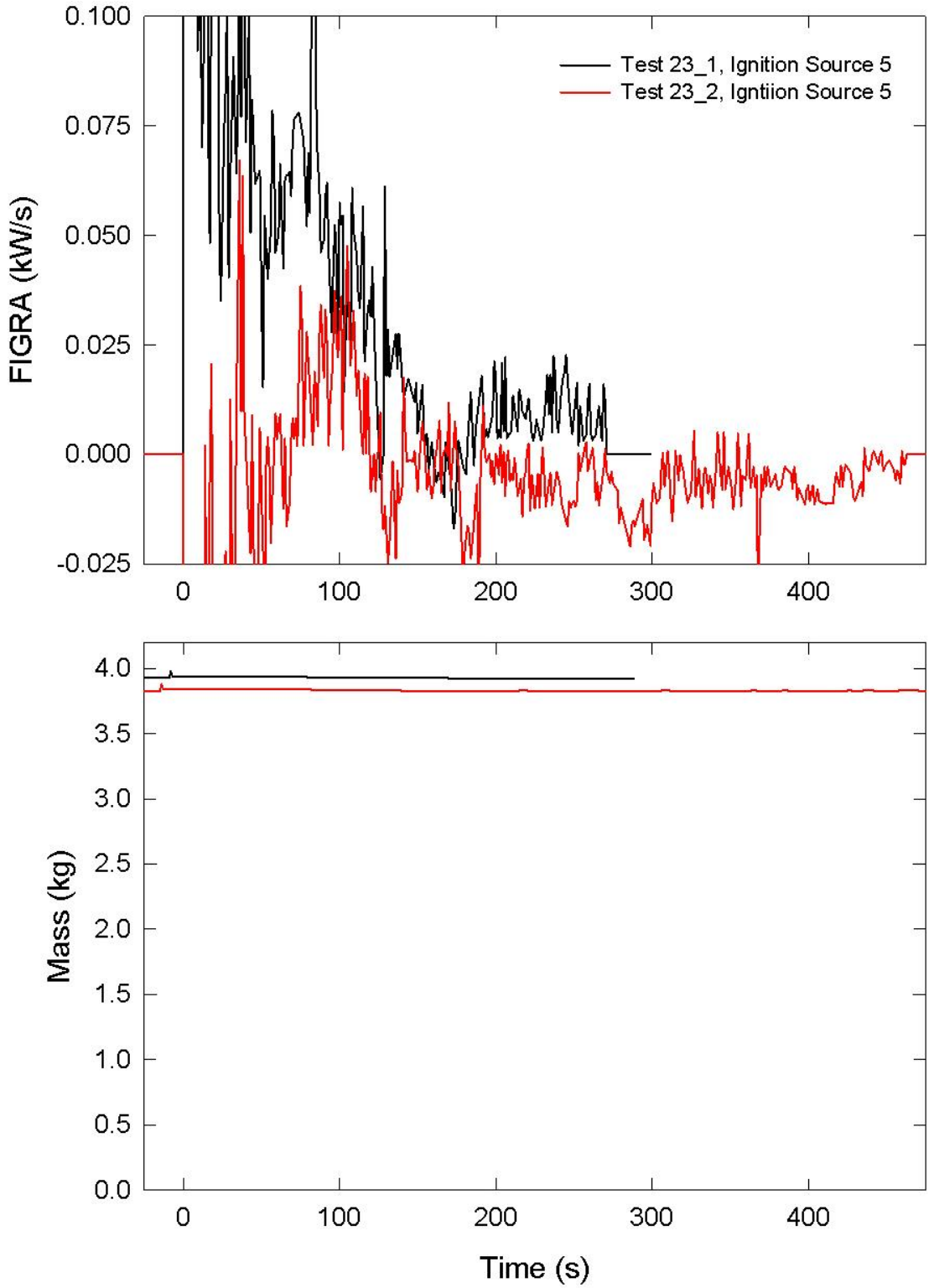

Figure A-217. Temporal profiles of FIGRA and mock-up mass for Combination 23 tests are shown following application of Ignition Source 5.

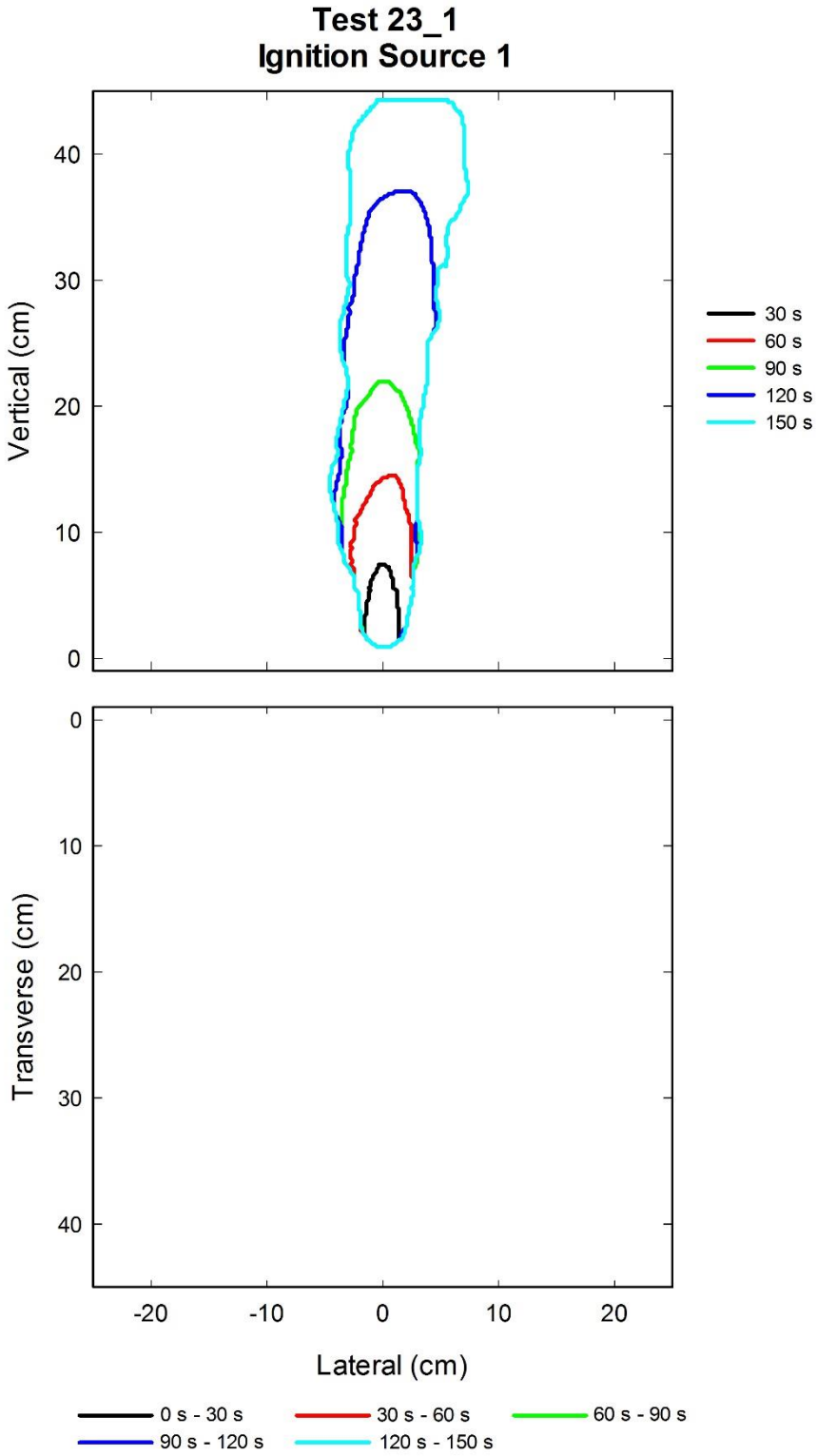

Figure A-218. Flame edge contours on the back (top) cushion are plotted as a function of time for Test 23_1 following application of Ignition Source 1.

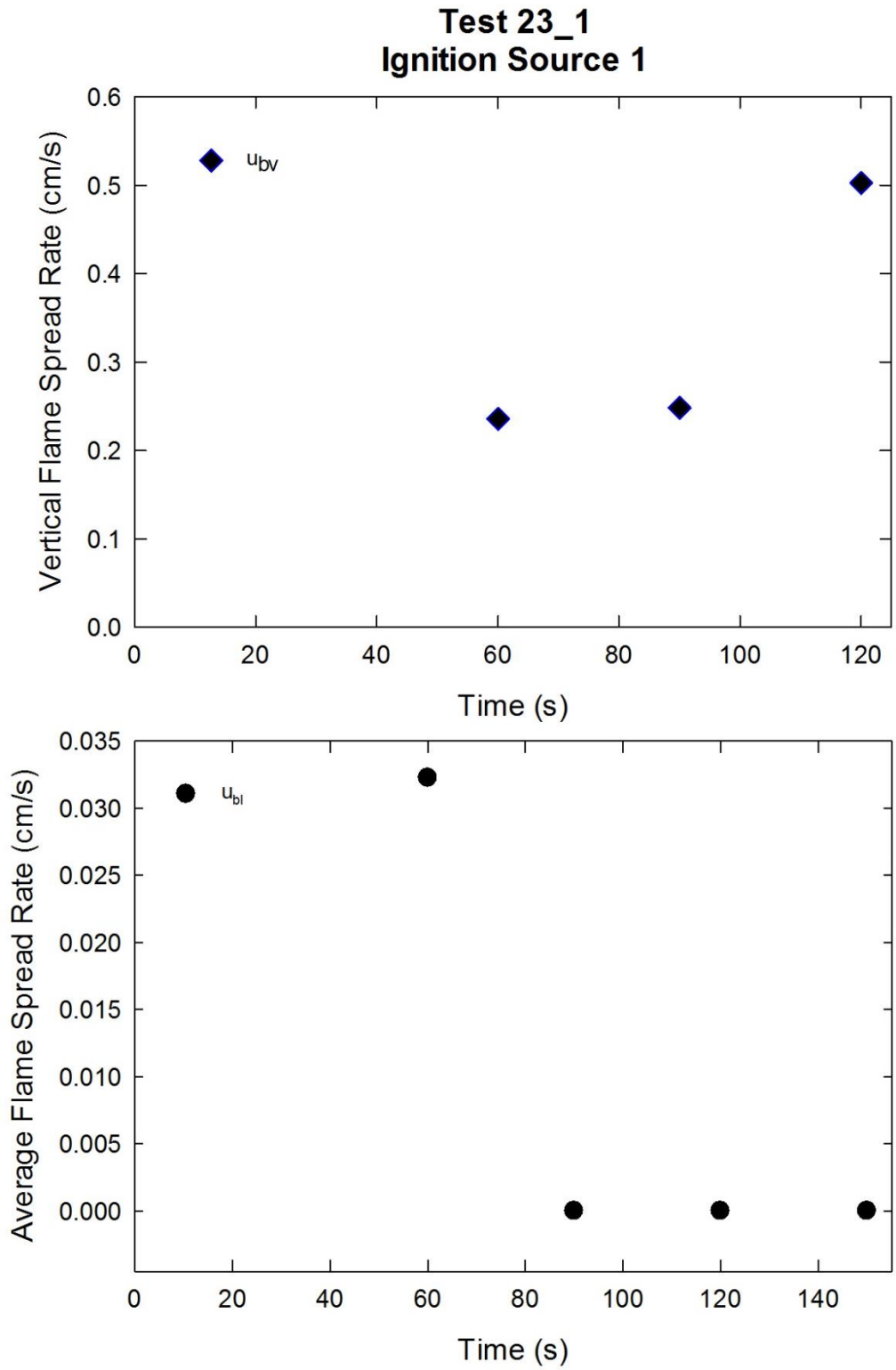

Figure A-219. Vertical flame spread rate (top) and average lateral flame spread rate (bottom) on the back cushion are plotted as a function of time for Test 23_1 following application of Ignition Source 1.

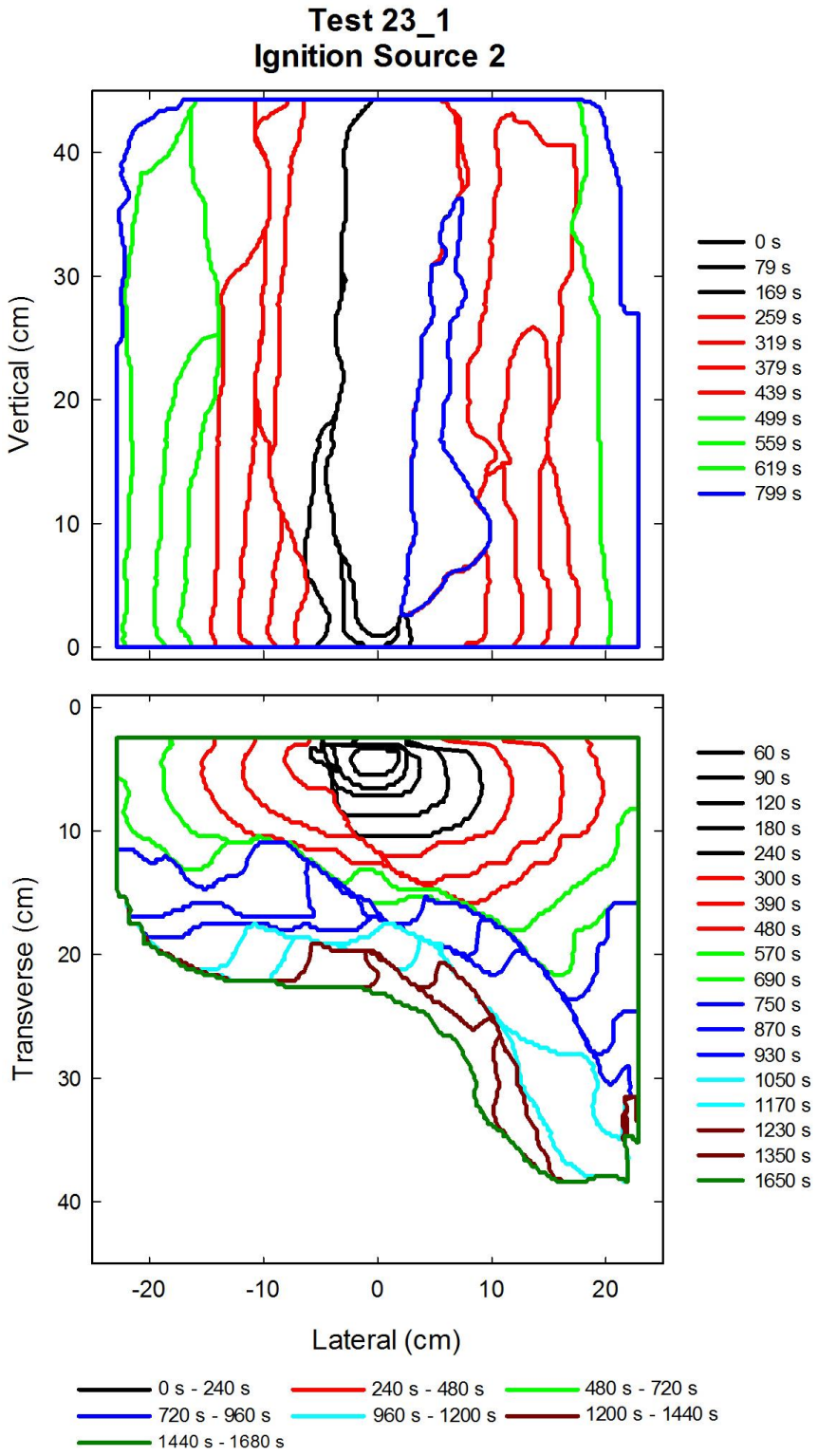

Figure A-220. Flame edge contours on the back (top) and seat (bottom) cushions are plotted as a function of time for Test 23_1 following application of Ignition Source 2.

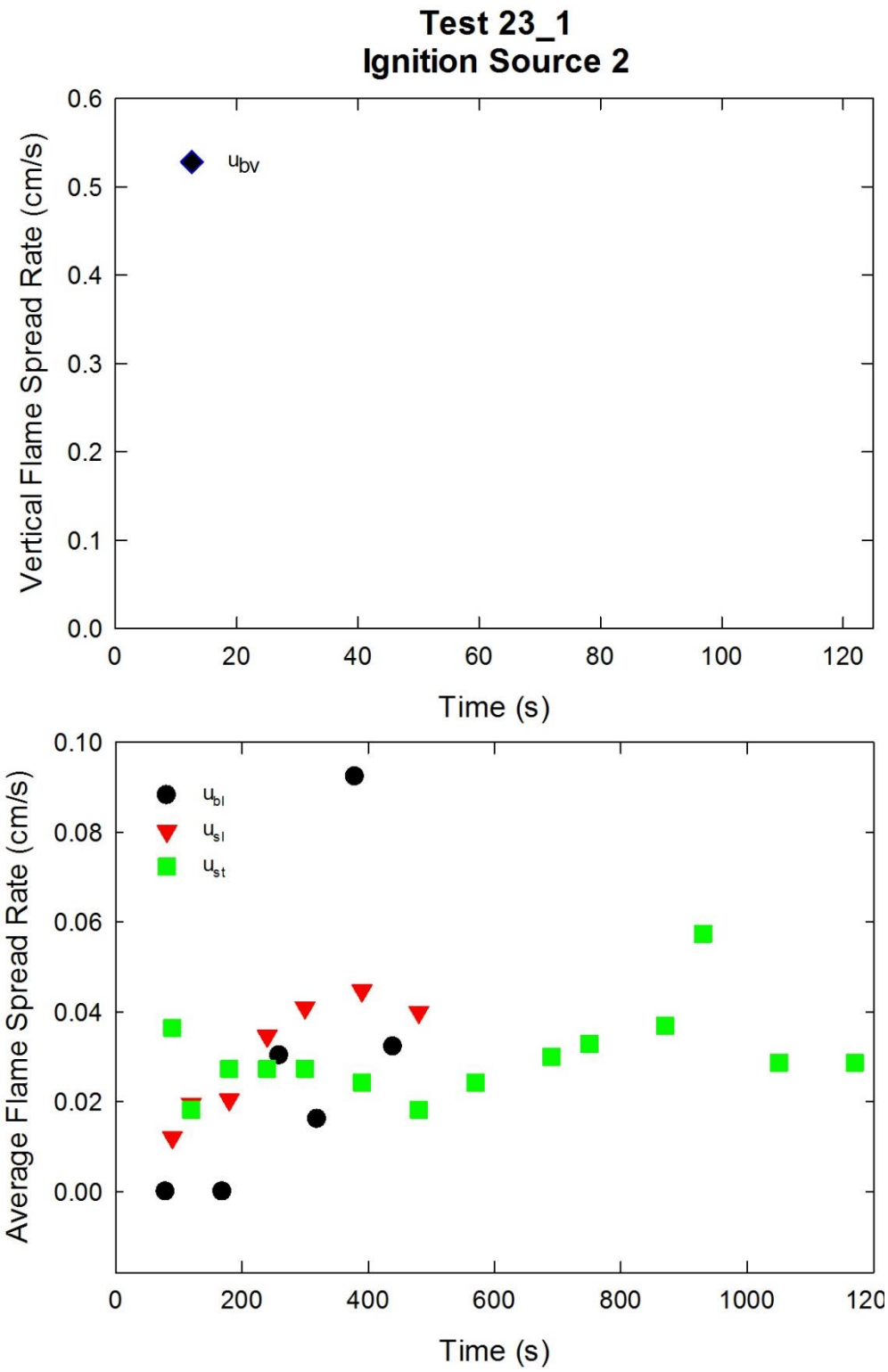

Figure A-221. Average lateral flame spread rate on the back and seat cushions and transverse flame spread rate on the seat cushion (bottom) are plotted as a function of time for Test 23_1 following application of Ignition Source 2.

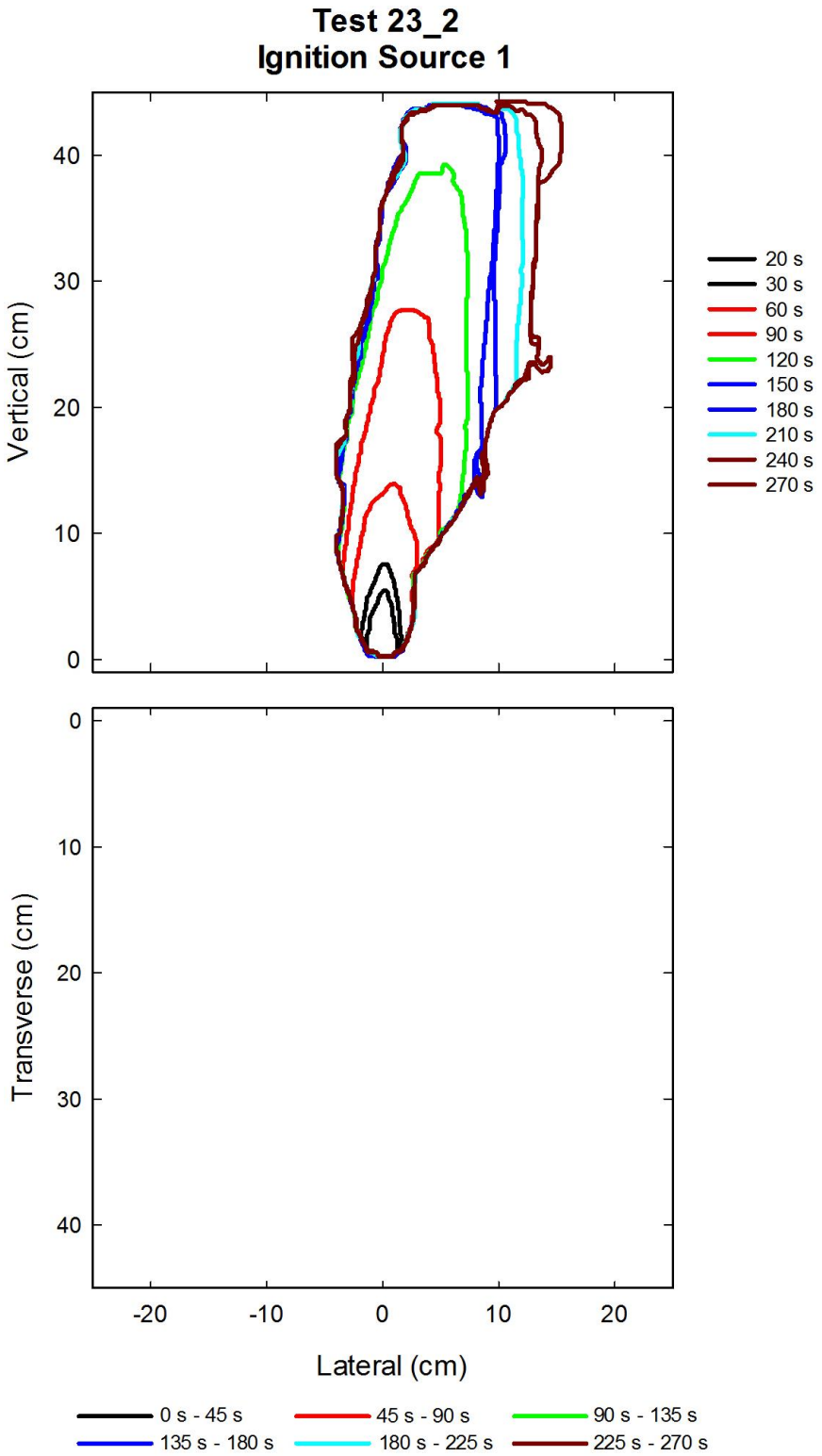

Figure A-222. Flame edge contours on the back cushion (top) are plotted as a function of time for Test 23_2 following application of Ignition Source 1.

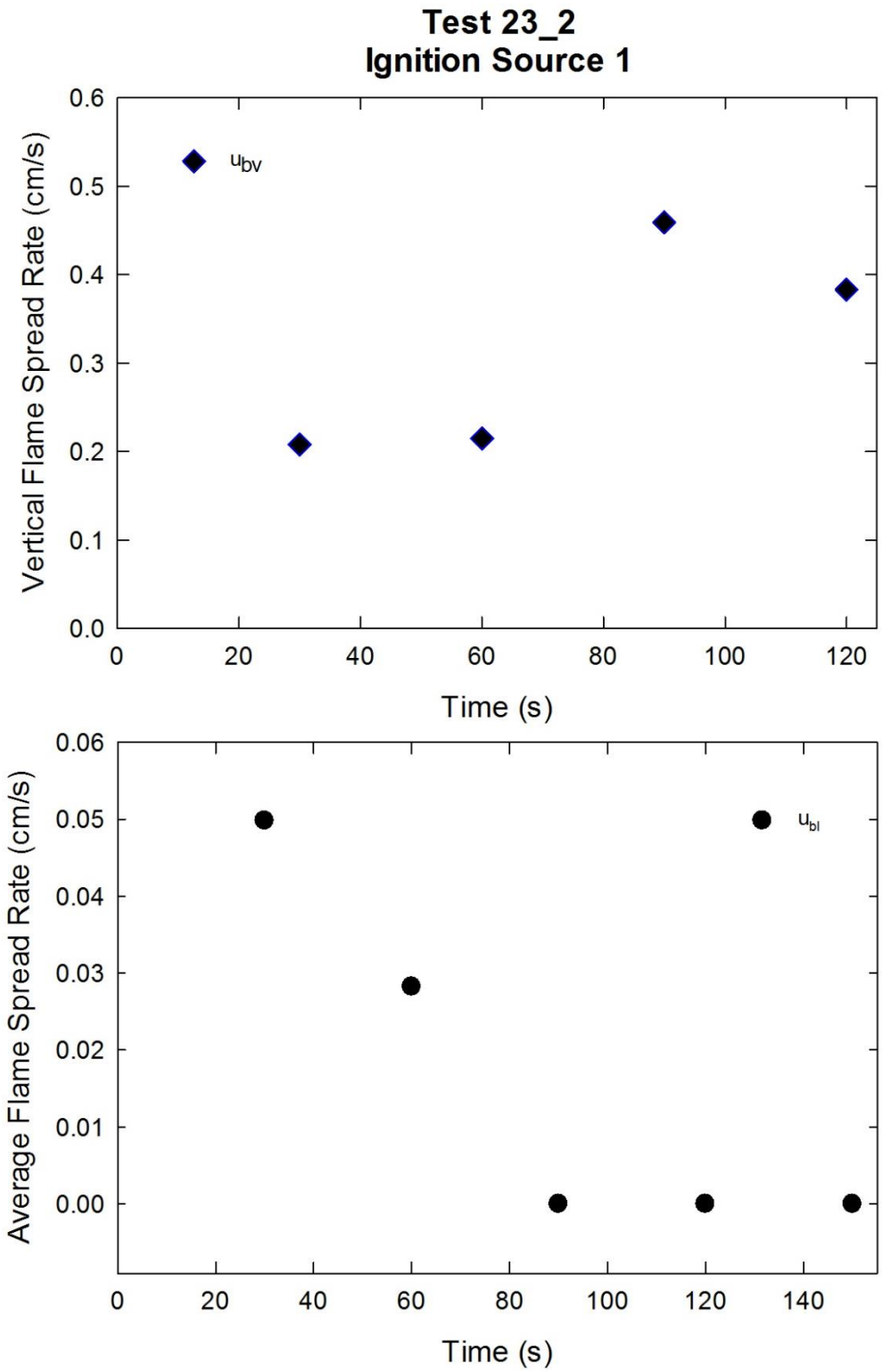

Figure A-223. Vertical flame spread rate (top) and average lateral flame spread rate (bottom) on the back cushion are plotted as a function of time for Test 23_2 following application of Ignition Source 1.

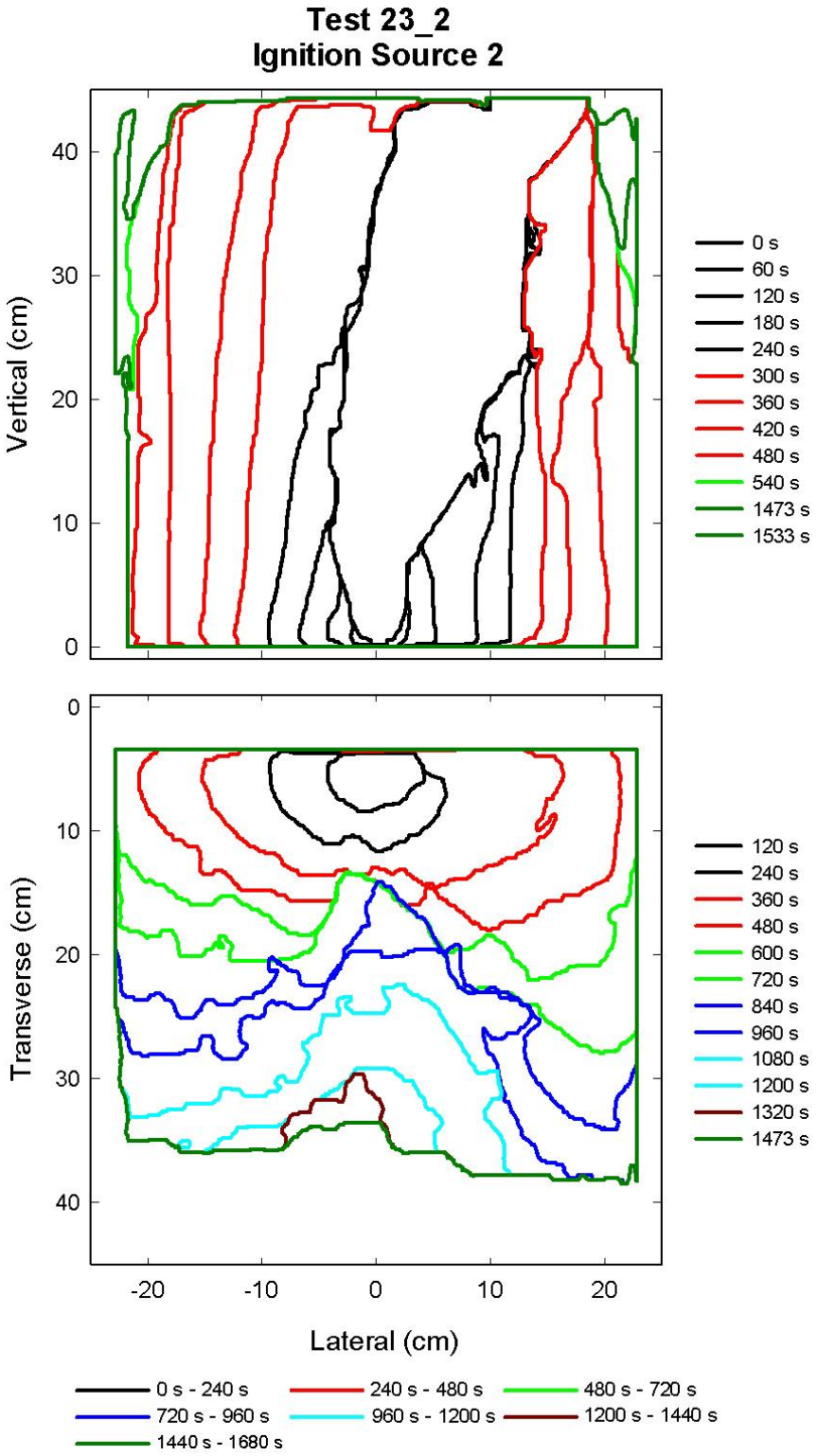

Figure A-224. Flame edge contours on the back (top) and seat (bottom) cushions are plotted as a function of time for Test 21_2 following application of Ignition Source 2.

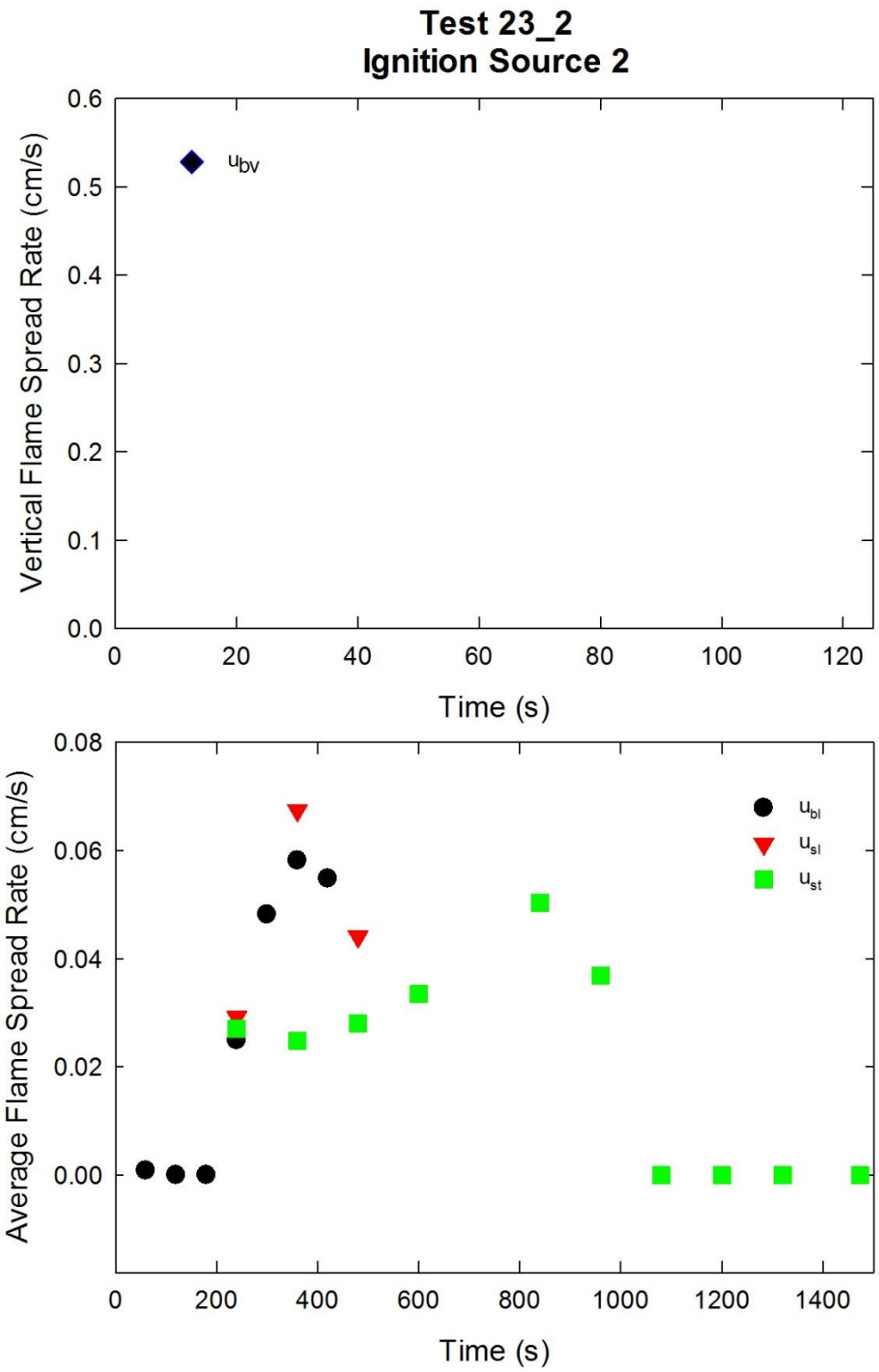

Figure A-225. Average lateral flame spread rate on the back and seat cushions and transverse flame spread rate on the seat cushion (bottom) are plotted as a function of time for Test 23_2 following application of Ignition Source 2.

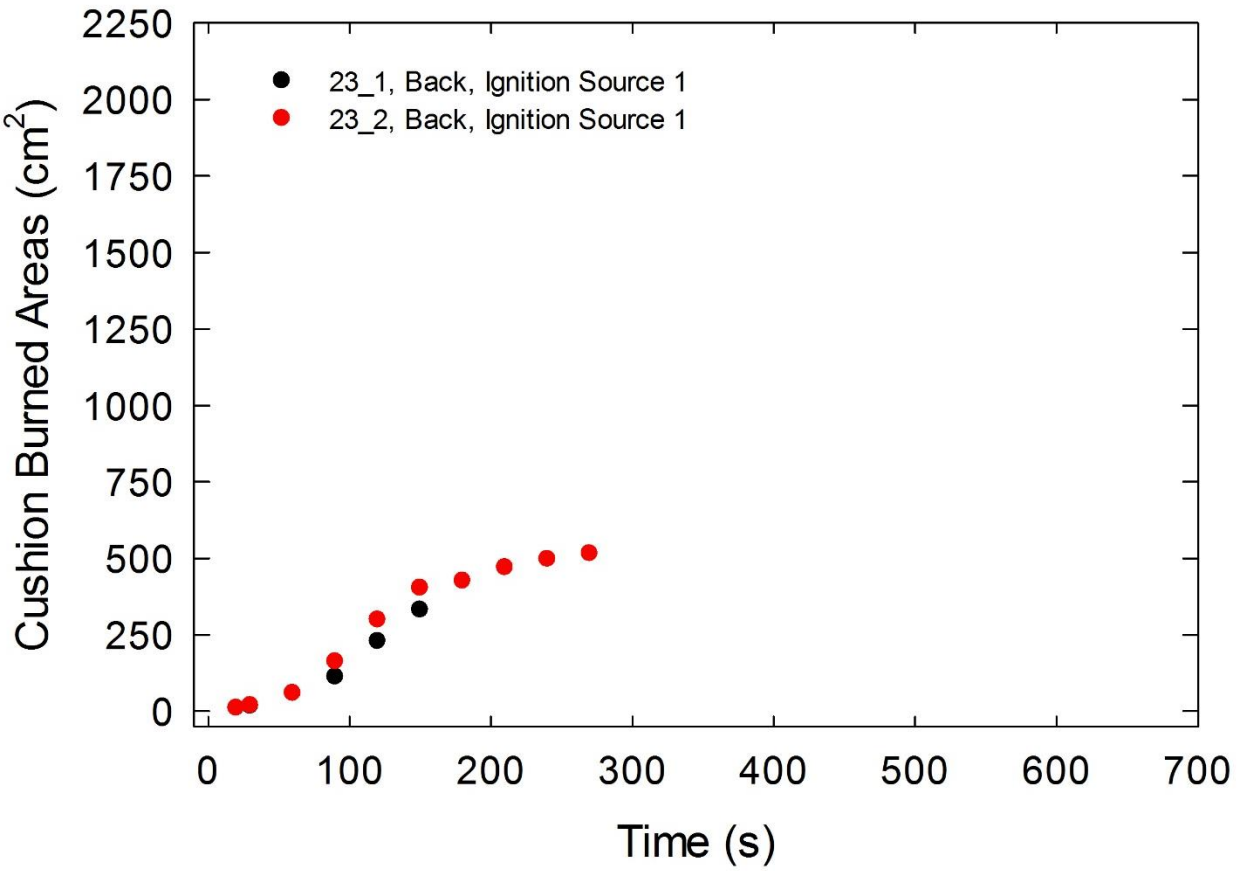

Figure A-226. Burned areas on the back cushion are plotted as a function of time for Combination 23 tests following application of Ignition Source 1.

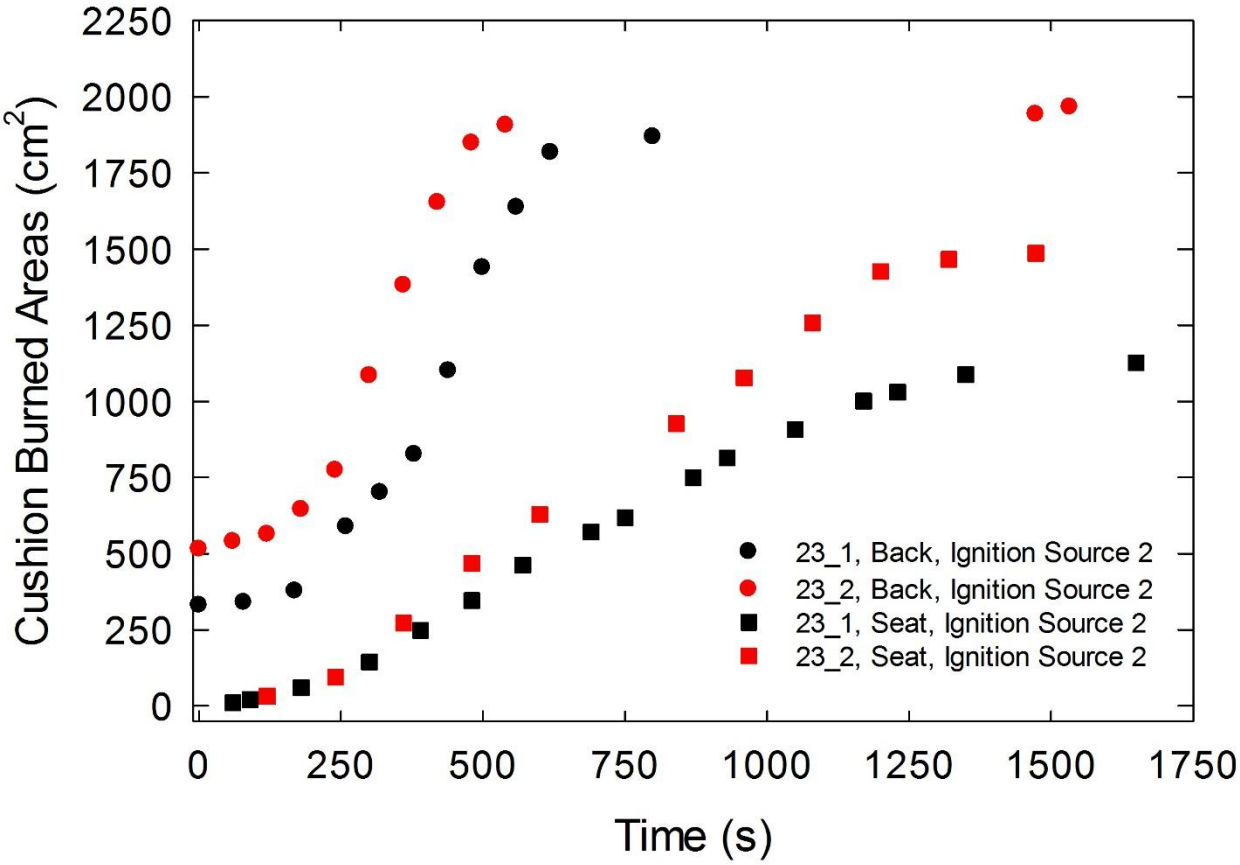

Figure A-227. Burned areas on the seat and back cushions are plotted as a function of time for Combination 23 tests following application of Ignition Source 2.

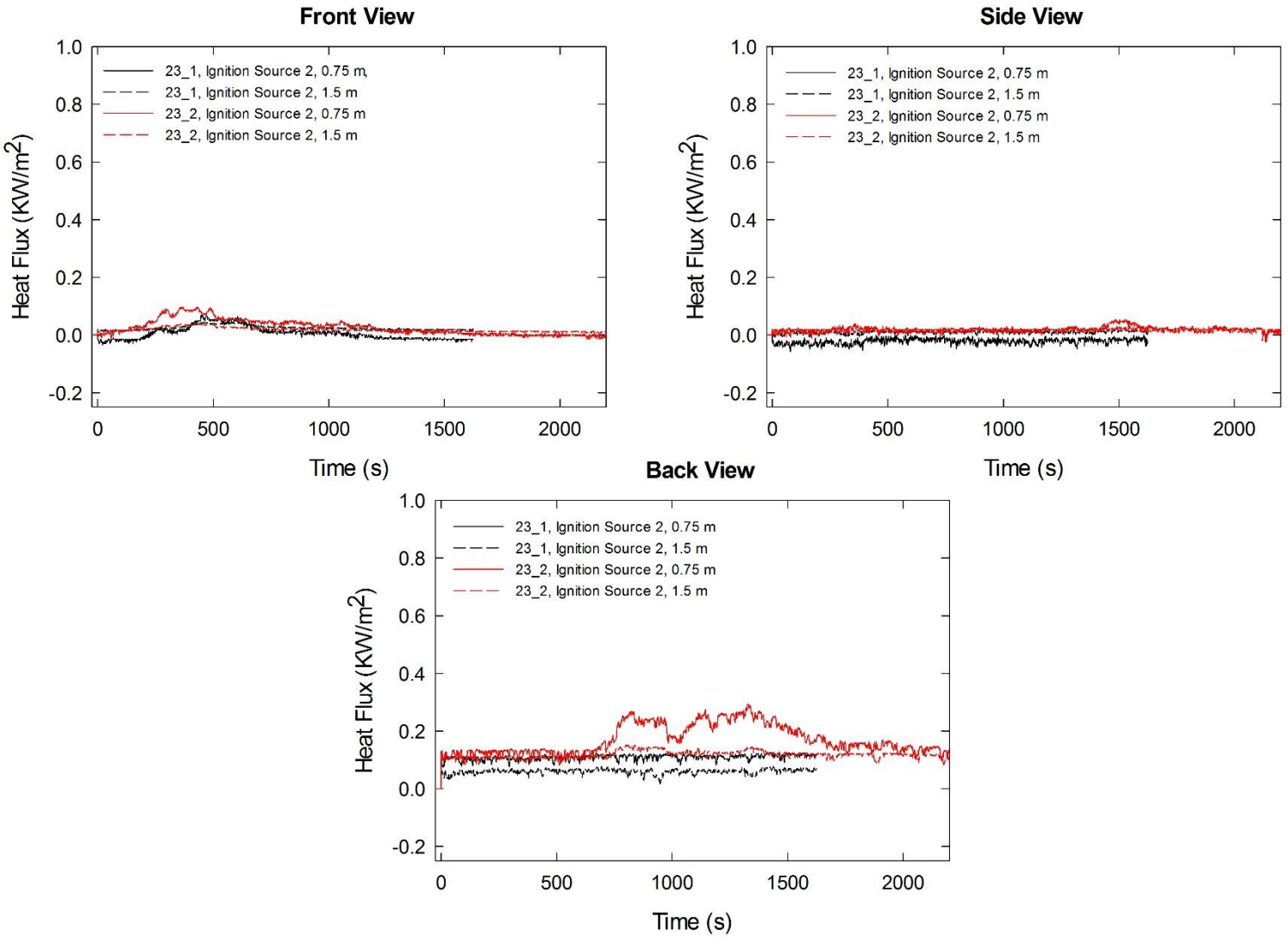

Figure A-228. Heat fluxes recorded at distances of 0.75 m and 1.5 m are plotted as a function of time for locations to the front, side and rear of the mock-up for Combination 23 tests following application of Ignition Source 2.

A.20 Combination 24

78%PP/22%PE/Norfab/PEFW/FRFPUF

Notes:

Test 1:

Ignition Source 1 applied at time = 0 s.

Initial mass reading (4.03 kg) during the experiment disagreed with an earlier measurement for the mock-up (4.15 kg); mass readings during test were smooth, physically reasonable and correlated with the HRR; **these mass data were adjusted by adding 0.082 kg to their values and were included in the analysis**.

Test 2:

Ignition Source 1 applied at time = 0 s.

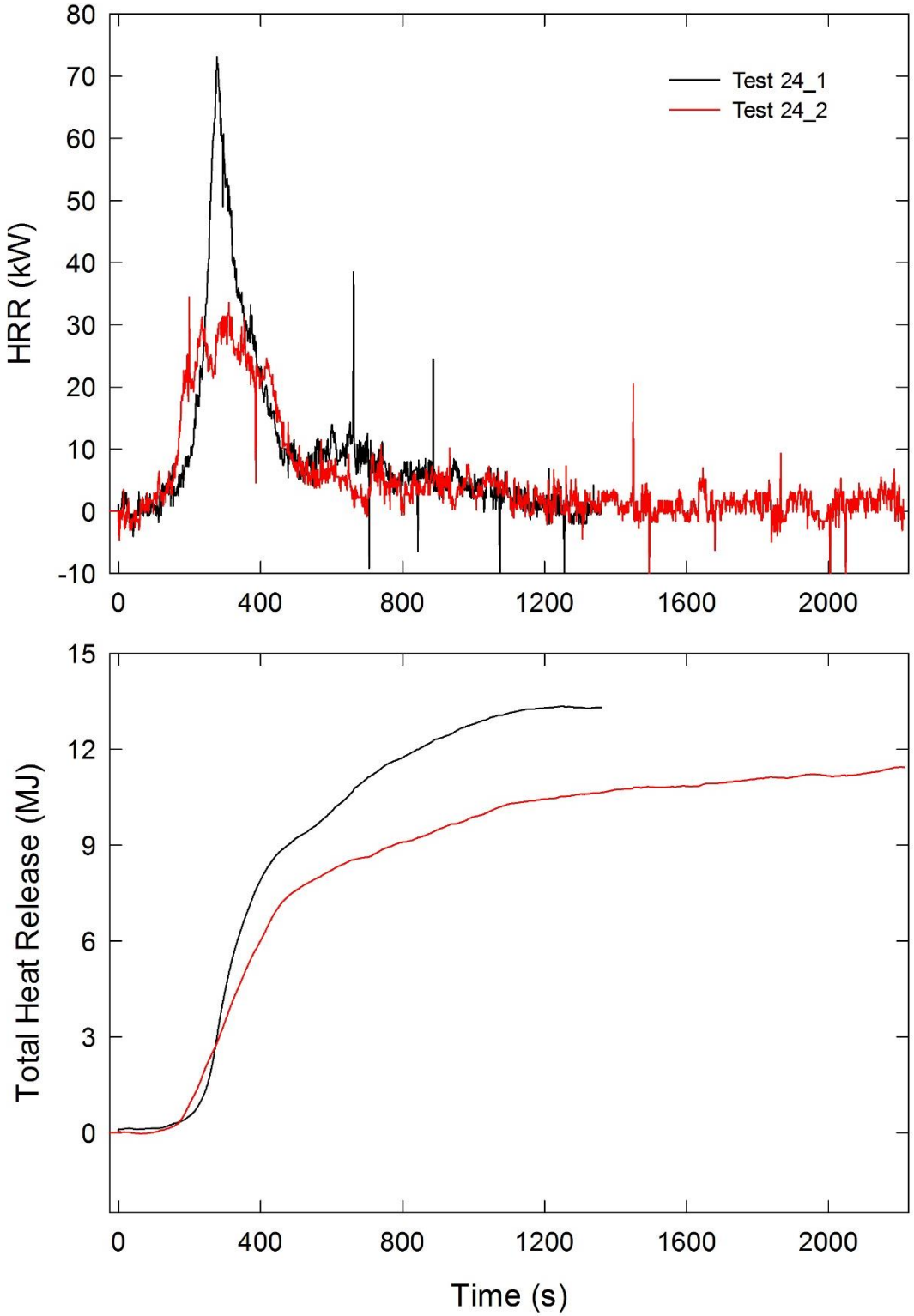

Figure A-229. Temporal profiles of HRR and integrated HRR are shown for Combination 24 tests following application of Ignition Source 1.

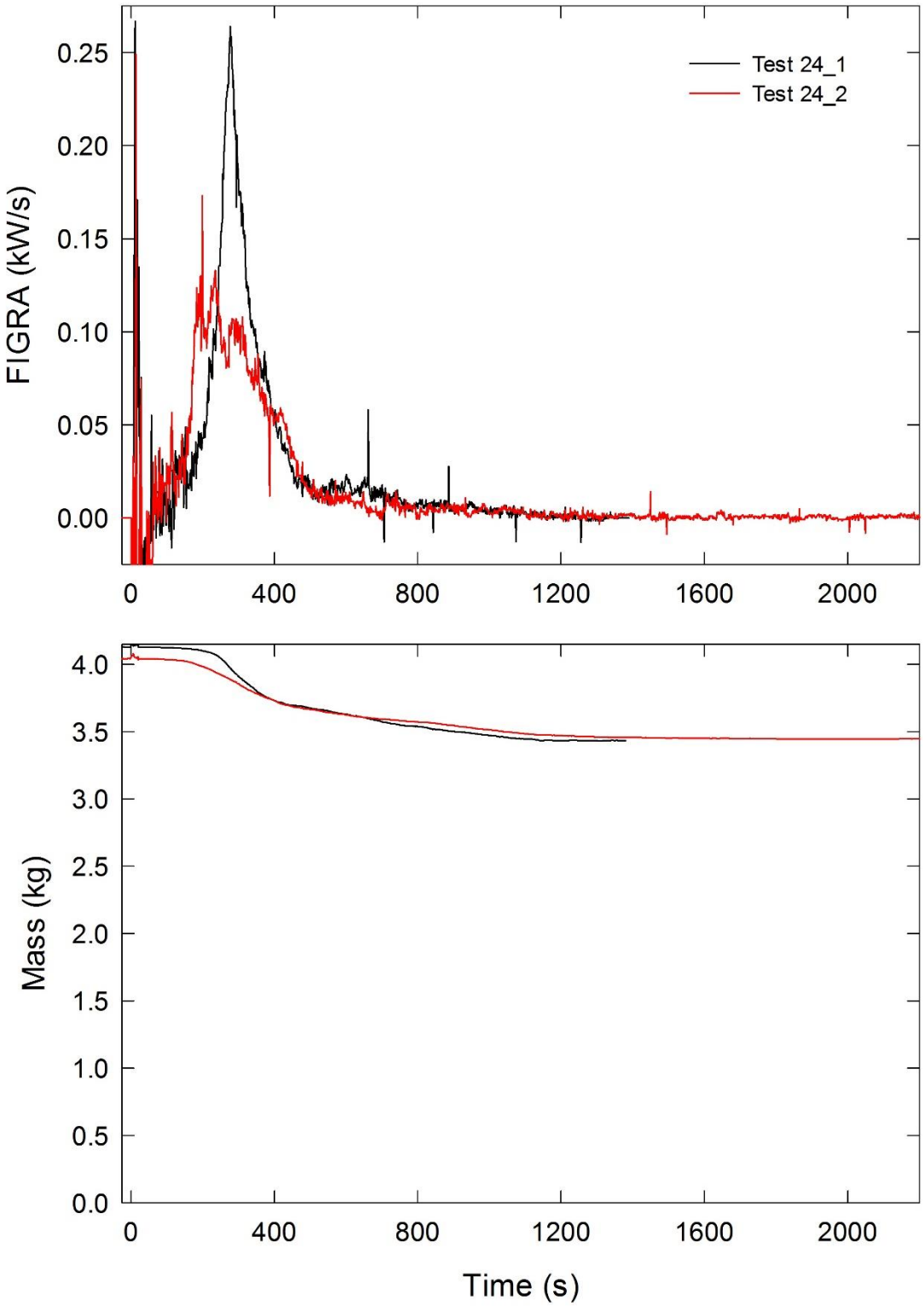

Figure A-230. Temporal profiles of FIGRA and mock-up mass are shown for Combination 24 tests following application of Ignition Source 1.

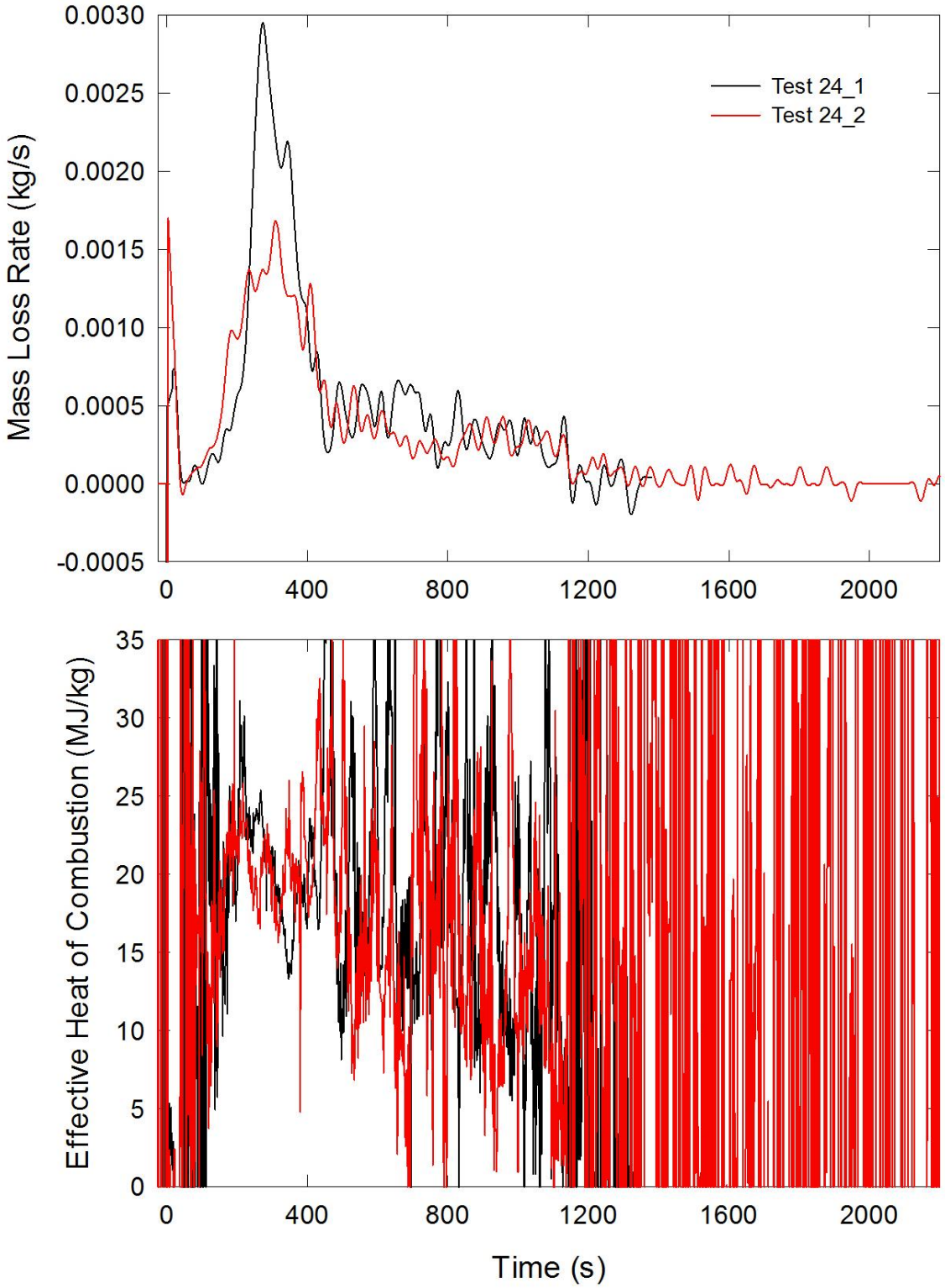

Figure A-231. Temporal profiles of MLR and EHOC are shown for Combination 24 tests following application of Ignition Source 1.

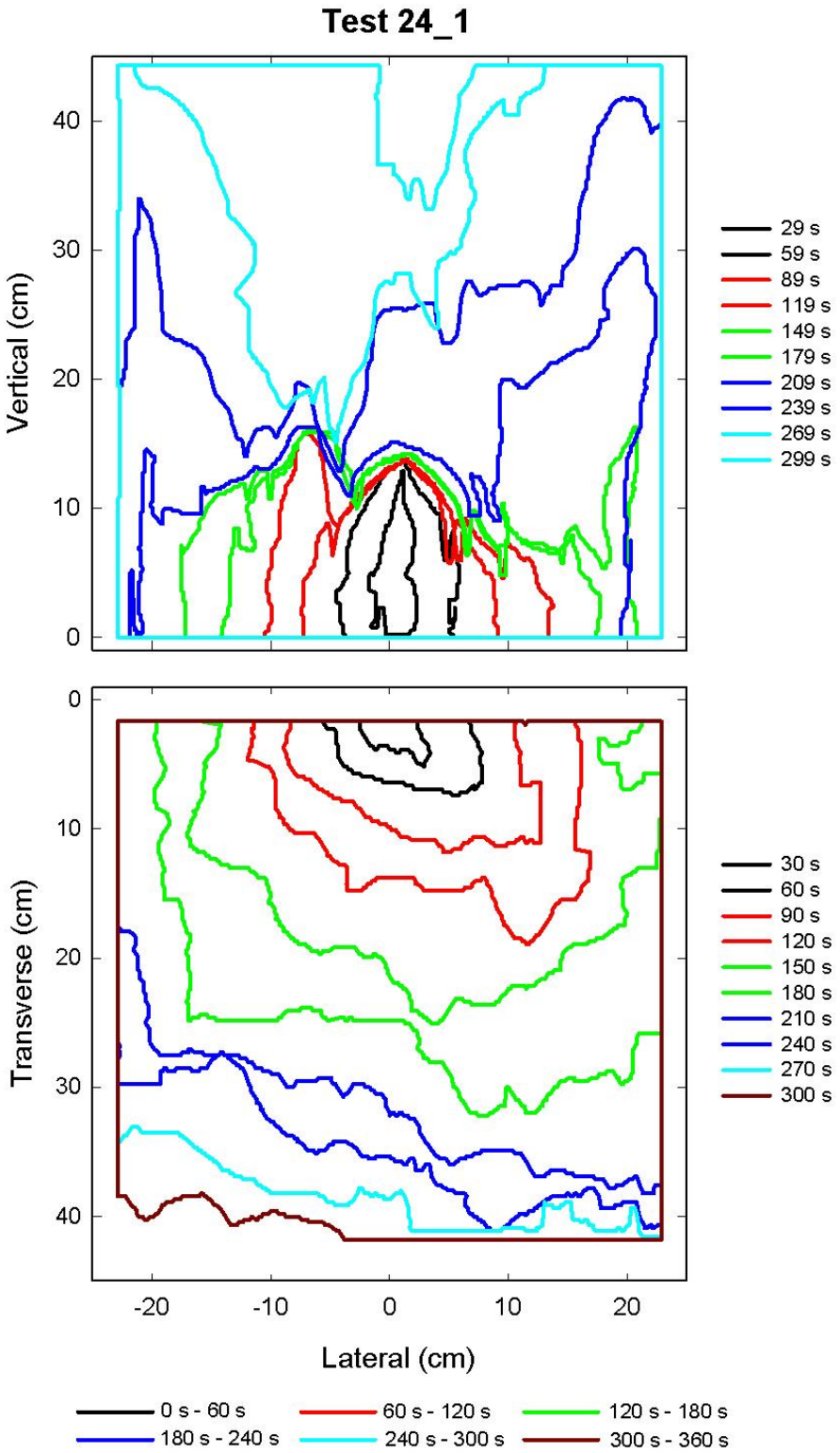

Figure A-232. Flame edge contours on the back (top) and seat (bottom) cushions are plotted as a function of time for Test 24_1 following application of Ignition Source 1.

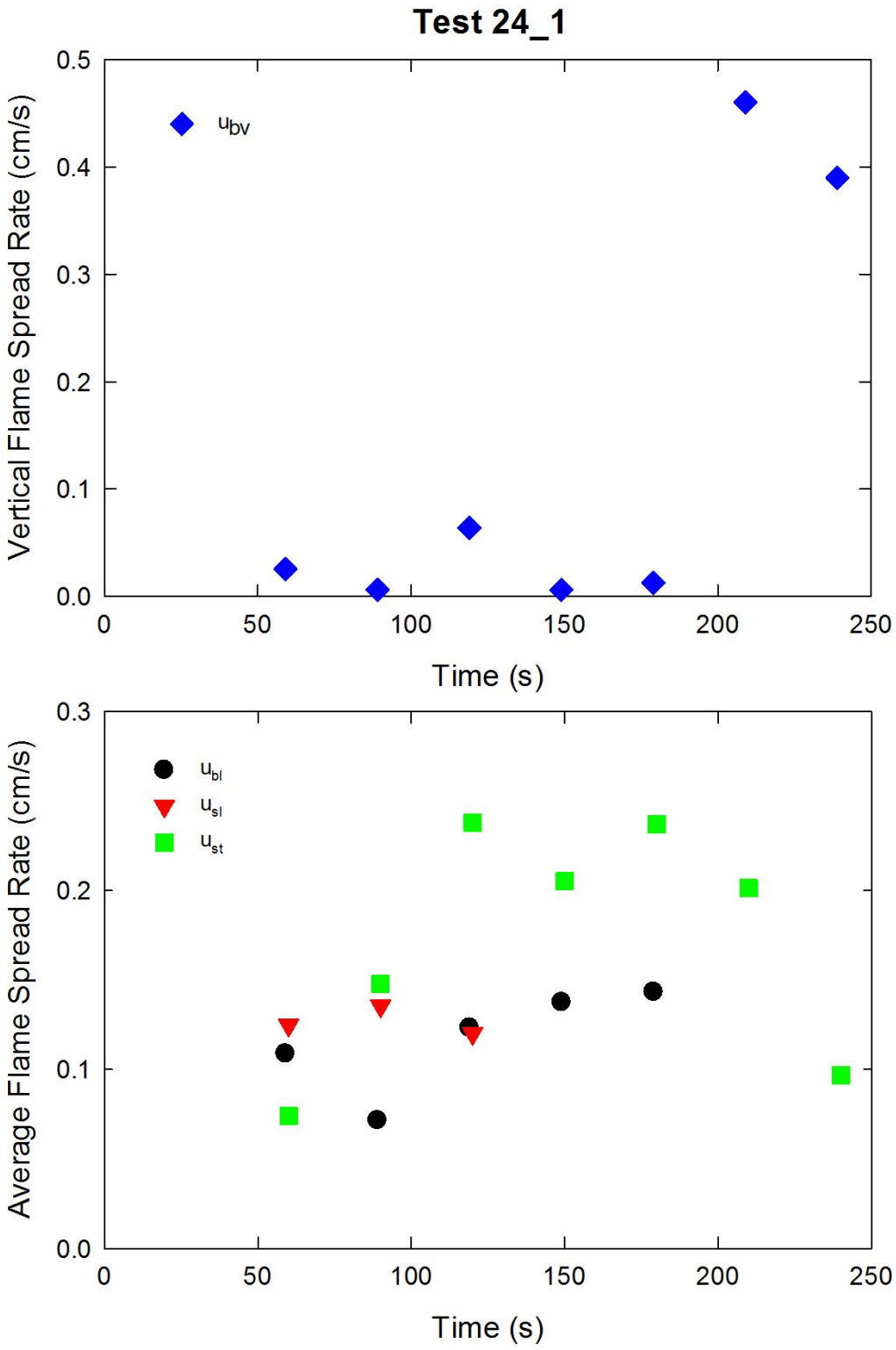

Figure A-233. Vertical flame spread rate on the back cushion (top) and average lateral flame spread rates on the back and seat cushions and transverse flame spread rate on the seat cushion (bottom) are plotted as a function of time for Test 24_1 following application of Ignition Source 1.

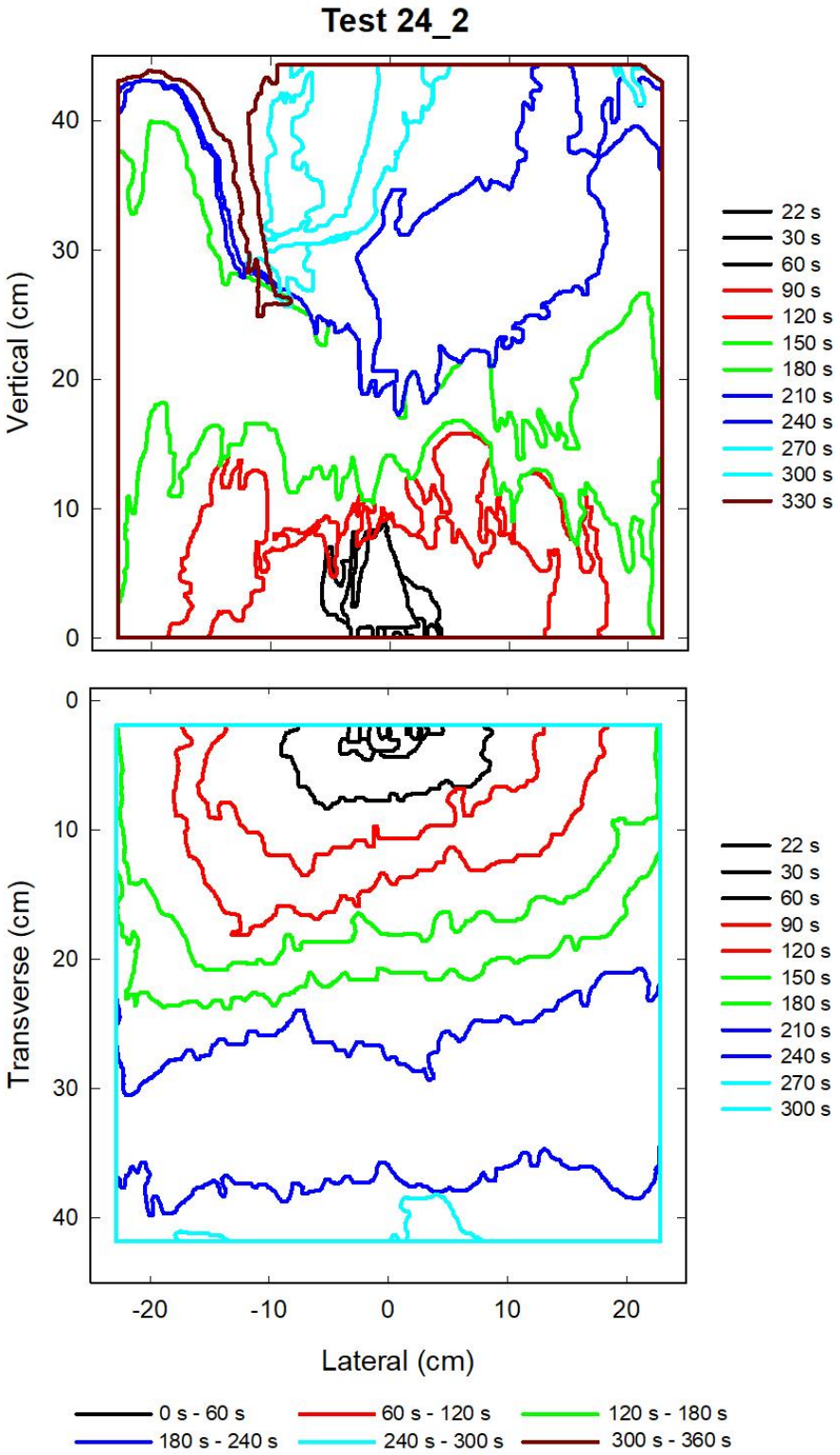

Figure A-234. Flame edge contours on the back (top) and seat (bottom) cushions are plotted as a function of time for Test 24_2 following application of Ignition Source 1.

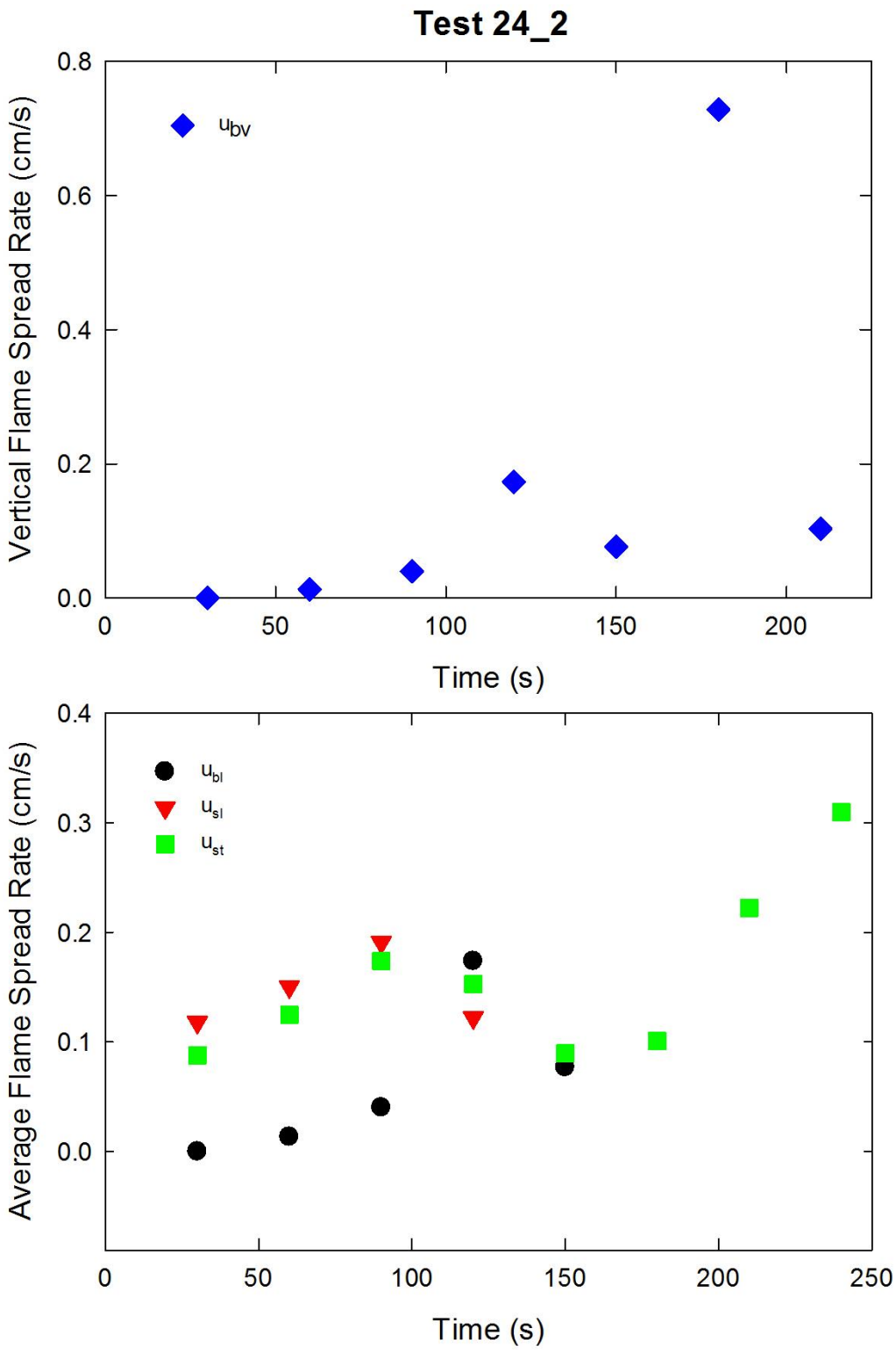

Figure A-235. Vertical flame spread rate on the back cushion (top) and average lateral flame spread rates on the back and seat cushions and transverse flame spread rate on the seat cushion (bottom) are plotted as a function of time for Test 24_2 following application of Ignition Source 1.

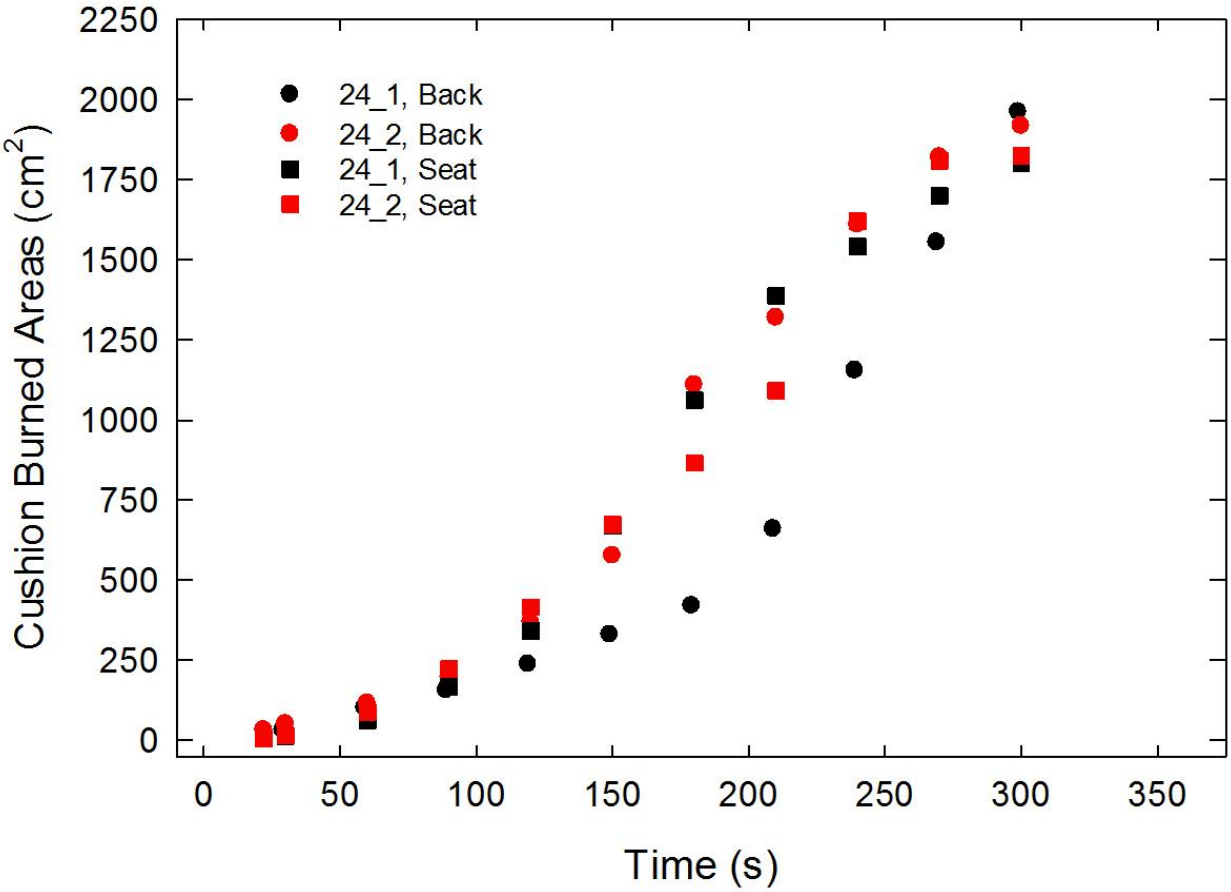

Figure A-236. Burned areas on the seat and back cushions are plotted as a function of time for Combination 24 tests following application of Ignition Source 1.

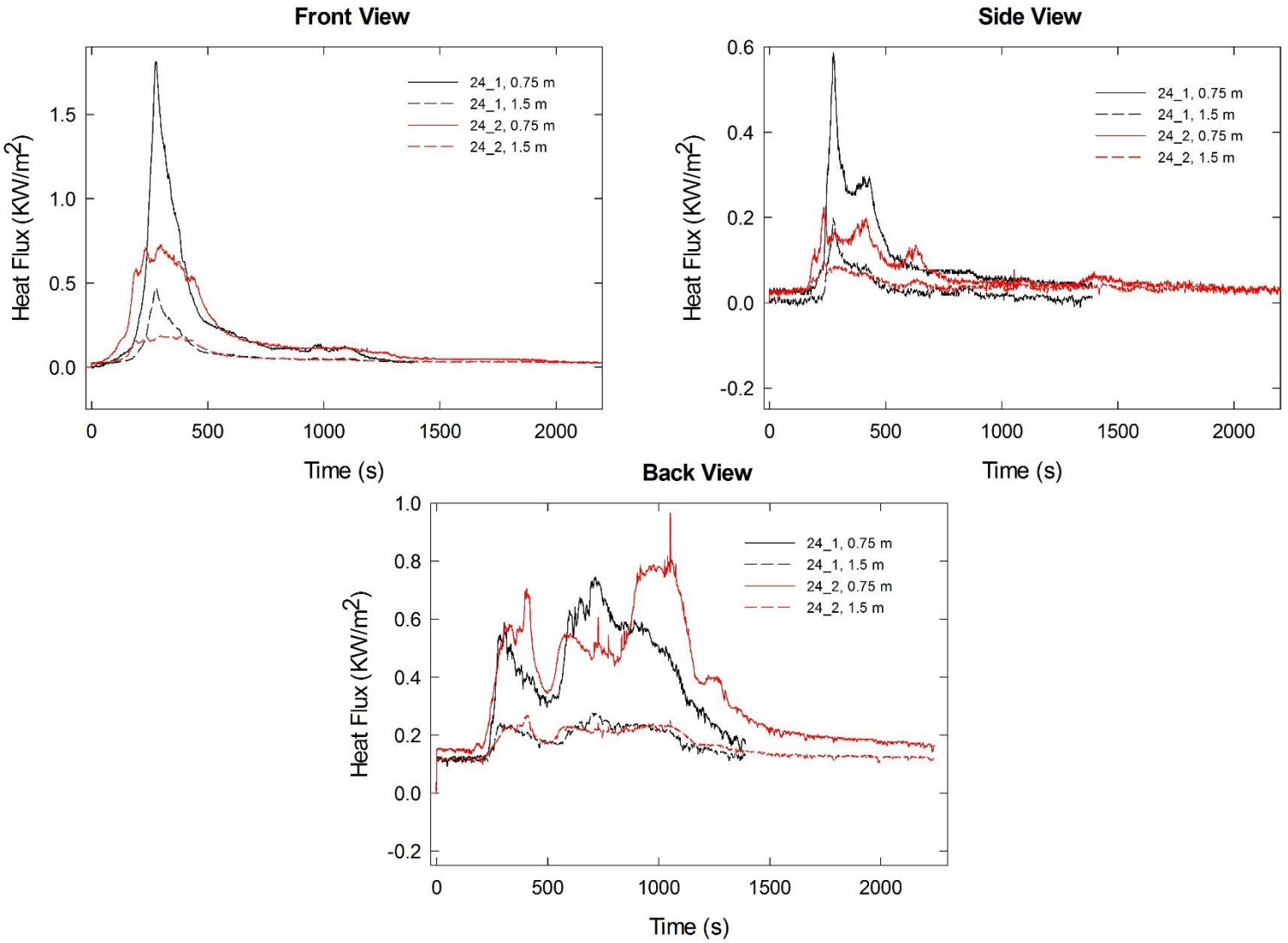

Figure A-237. Heat fluxes recorded at distances of 0.75 m and 1.5 m are plotted as a function of time for locations to the front, side and rear of the mock-up for Combination 24 tests following application of Ignition Source 1.

Appendix B Tabulated Results for Measures Characterizing Flame Spread and Growth on Furniture Mock-ups

The following tables summarize a variety of numerical values chosen to characterize the time behaviors of flame spread and fire growth observed on the twenty types of mock-ups described in Table 3. Note that tables are included for measures based on individual tests as well as for selected grouped measures for the twenty combinations.

Parameters used to characterize flame spread for the individual tests include vertical flame spread acceleration on the back cushion, characteristic lateral flame spread rates on the seat and back cushions (temporal variations characterized by standard deviations), transverse flame spread rate on the seat cushion (temporal variations characterized by standard deviations), and the times of ignition of left- and right-arm cushions and their average. Combined measures characterizing flame spread for the various mock-up combinations include averages and standard deviations for vertical flame acceleration on the back cushion, a measure of lateral flame spread incorporating characteristic lateral flame spread rates on both the seat and back seat cushions, transverse flame spread on the seat cushion, the ratio of lateral and transverse flame spread rates, and left- and right-arm ignition times and their average.

Both HRR and FIGRA are used as measures of fire growth. Numerical measures used to characterize the temporal profiles are tabulated separately. Individual HRR temporal profiles are characterized by values of times required to reach 25 kW, the first peak, the maximum value, the length of time the HRR remained above 25 kW, the initial HRR peak, the maximum HRR, the average value and full width at half maximum while the HRR > 25 kW, total heat released while HRR > 25 kW and overall, and shape factors for the temporal profiles defined in terms of times and HRR factors. Combined measures used to characterize HRR behaviors for the various combinations include averages and standard deviations for results for the individual tests for the periods required to reach 25 kW, the initial HRR peak, and the maximum HRR along with the corresponding HRR values and the total heat released.

Measures used to characterize the individual FIGRA temporal profiles included the times and values for the first FIGRA peak and the highest measured value. Combined measures for the combinations included the averages and standard deviations for the individual measures.

B.1 Measures Characterizing Flame Spread Behavior

Values in Table B-1 with red borders were used for the statistical analyses described in Section 7. Values colored blue were assigned using criteria described in Section 5.

Table B-1. Tabulated measures characterizing flame spread for individual tests

Test	a_{bv} cm/s^2	$\bar{u}_{bl}$ cm/s	u'_{bl} cm/s	$\bar{u}_{sl}$ cm/s	u'_{sl} cm/s	$\bar{u}_{l}$ cm/s	$\bar{u}_{st}$ cm/s	u'_{st} cm/s	$(u_{st})_{edge}$ cm/s	R_{ut}	t_{igr} s	t_{igl} s	t_{ig} s	t_{seat} s	t_{back} s
1_1	0.00496	0.0562	0.0117	0.0618	0.0120	0.0592	0.0585	0.0078	0.301	5.14	303	371	337	455	385
1_2	0.00709	0.0538	0.0134	0.0629	0.0170	0.0586	0.0645	0.0238	0.246	3.82	346	383	365	460	389
1_3	0.00414	0.0642	0.0157	0.0644	0.0119	0.0643	0.0710	0.0095	0.343	4.83	302	328	315	415	330
2_1		0.176	0.083	0.173	0.039	0.1746	0.192	0.080	0.618	3.22	131	130	131	159	140
2_2		0.170	0.026	0.246	0.100	0.2078	0.191	0.083	0.659	3.44	108	110	109	170	133
5_1	0.00773	0.0559	0.0030	0.0597	0.0079	0.0580	0.0461	0.0094	0.048	1.04	441	395	418	925	473
5_2	0.00935	0.0529	0.0127	0.0549	0.0070	0.0580	0.0465	0.0018	0.074	1.59	365	462	414	798	469
5_3	0.0083	0.0600	0.0112	0.0585	0.0047	0.0593	0.0555	0.0081	0.070	1.27	377	384	381	716	393
6_1	0.0115	0.195	0.045	0.217	0.004	0.2035	0.196	0.065	0.661	3.37	91	128	110	182	134
6_2	0.0127	0.266	0.079	0.224	0.051	0.2493	0.153	0.011	0.623	4.07	93	104	99	155	108
9_1	0.00366	0.0646	0.0318	0.0830	0.0227	0.0733	0.0884	0.0173	0.231	2.62	296	306	301	370	330
9_2	0.00567	0.0492	0.0080	0.0711	0.0244	0.0557	0.0652	0.0168	0.180	2.77	240	288	264	349	316
10_1	0.0571	0.209	0.068	0.248	0.077	0.2218	0.273	0.127	0.949	3.47	80	94	87	135	115
10_2	0.0418	0.289	0.151	0.302	0.167	0.2949	0.156	0.092	1.128	7.24	71	88	80	113	103
10_3	0.0595	0.297	0.076	0.319	0.141	0.2816	0.250	0.113	1.002	4.01	72	84	78	108	90
11_1	0.00496	0.0687	0.0182	0.1109	0.0299	0.0881	0.1170	0.0260	0.230	1.96	225	235	230	295	275
11_2	0.00651	0.0560	0.0096	0.1048	0.0284	0.0785	0.1040	0.0106	0.246	2.37	253	269	261	330	289
12_1	0.00454	0.223	0.070	0.248	0.145	0.2317	0.203	0.100	0.761	3.75	87	102	95	130	110
12_2	0.04	0.231	0.087	0.243	0.073	0.2353	0.245	0.069	1.108	4.52	88	100	94	130	115
13_1	0.00654	0.0498	0.0121	0.0564	0.0144	0.0568	0.0369	0.0073	0.131	3.56	334	376	355	710	390
13_2		0.0548	0.0128	0.0556	0.0059	0.0552	0.0365	0.0079	0.148	4.05	392	416	404	750	682

Table B-1. (continued)

Test	a_{bv} cm/s^2	$\bar{u}_{bl}$ cm/s	u'_{bl} cm/s	$\bar{u}_{sl}$ cm/s	u'_{sl} cm/s	$\bar{u}_{l}$ cm/s	$\bar{u}_{st}$ cm/s	u'_{st} cm/s	$(u_{st})_{edge}$ cm/s	R_{ut}	t_{igr} s	t_{igl} s	t_{ig} s	t_{seat} s	t_{back} s
14_1	0.00988	0.237	0.032	0.215	0.051	0.2276	0.197	0.244	0.824	4.19	87	97	92	170	120
14_2	0.00696	0.253	0.021	0.209	0.012	0.2308	0.201	0.022	0.463	2.31	84	125	105	170	145
15_1	0.0111	0.0398	0.0213	0.0738	0.0055	0.0501	0.0765	0.0077	0.104	1.36	428	554	491	620	560
15_2	0.0164	0.0636	0.0212	0.0605	0.0079	0.0626	0.0570	0.0035	0.107	1.87	318	372	345	635	425
16_1		0.166	0.049	0.227	0.060	0.189	0.170	0.031	0.373	2.20	126	117	122	190	160
16_2		0.169	0.051	0.166	0.054	0.1678	0.141	0.067	0.328	2.32	115	119	117	170	140
17_1	0.00108	0.0588	0.0278	0.0481	0.0197	0.0527	0.0308	0.0131	0.097	3.15	502	544	523	925	560
17_2	0.00324	0.0293	0.0159	0.0362	0.0054	0.0333	0.0187	0.0084	0.084	4.52	500	625	563	985	645
18_1		0.242	0.157	0.180	0.050	0.2031	0.113	0.058	0.439	3.90	105	155	130	220	175
18_2		0.220	0.046	0.229	0.025	0.2250	0.171	0.048	0.410	2.39	107	108	108	215	165
19_1	0.00231					0					585	649	585		
19_2	0.00303					0					105	155	130	1750	1490
20_1		0.116	0.041	0.170	0.099	0.1379	0.125	0.043	0.285	2.27	176	201	189	330	245
20_2		0.123	0.040	0.127	0.031	0.1247	0.106	0.053	0.227	2.14	176	166	171	350	270
20_3		0.186	0.018	0.162	0.038	0.1722	0.117	0.084	0.217	1.86	132	110	121	265	195
21_1	0.00161	0.0202	0.0123	0.0256	0.0032	0.0265	0.0292	0.0047			541	649	541		
21_2	0.0022					0					446	649	446		
22_1		0.224	0.069	0.196	0.087	0.2117	0.104	0.031	0.190	1.83	120	102	111	300	580
22_2		0.176	0.033	0.187	0.019	0.1808	0.111	0.020	0.222	2.00	114	127	121	270	300
22_3						0					120	91	106		
23_1	0.00445	0.0285	0.0313	0.0303	0.0127	0.0348	0.0256	0.0058			544	649	597		
23_2	0.00257	0.0267	0.0249	0.0469	0.0193	0.0467	0.0266	0.0014			447	512	480		
24_1		0.117	0.026	0.127	0.008	0.1206	0.153	0.067	0.215	1.40	160	199	180	305	300
24_2		0.0608	0.0622	0.1452	0.0336	0.1106	0.1349	0.0322	0.266	1.97	142	139	141	270	300

Table B-2. Tabulated measures characterizing flame spread behavior for mock-up material combinations

Combination	$\overline{a_{bv}}$ cm/s^2	a'_{bv} cm/s	$\overline{u_l}$ cm/s	u'_l cm/s	$\overline{u_t}$ cm/s	u'_t cm/s	R_u	$\overline{t_{igr}}$ s	t'_{igr} s	$\overline{t_{igl}}$ s	t'_{igl} s	$\overline{t_{ig}}$ s	t'_{ig} s	$\overline{t_{seat}}$ s	t'_{seat} s	$\overline{t_{back}}$ s	t'_{back} s
1	0.00540	0.00152	0.0607	0.0031	0.0647	0.0062	0.94	317	21	361	24	339	34	444	25	368	33
2			0.1912	0.0787	0.1963	0.0063	0.97	120	12	120	10	120	12	165	8	137	5
3																	
4																	
5	0.00846	0.00082	0.0585	0.0007	0.0485	0.0062	1.21	394	33	414	39	406	43	813	105	445	45
6	0.0121	0.00085	0.2264	0.0324	0.1979	0.0020	1.14	92	1	116	12	104	17	169	19	121	18
7																	
8																	
9	0.00467	0.00142	0.0645	0.0125	0.0740	0.0203	0.87	268	28	297	9	283	29	360	15	323	10
10	0.0528	0.0096	0.2661	0.0389	0.2437	0.0331	1.09	74	4	89	4	82	9	119	14	103	13
11	0.00574	0.00110	0.0833	0.0068	0.1105	0.0091	0.75	239	14	252	17	246	19	313	25	282	10
12	0.0223	0.0250	0.2335	0.0025	0.2239	0.0298	1.04	88	1	101	1	94	8	130	0	113	4
13	0.00654		0.0560	0.0012	0.0367	0.0003	1.53	363	29	396	20	380	35	730	28	536	206
14	0.00842	0.00207	0.2292	0.0022	0.1986	0.0026	1.15	86	2	111	14	98	19	170	0	133	18
15	0.0138	0.00375	0.0564	0.0088	0.0643	0.0120	0.88	373	55	463	91	418	101	628	11	493	95
16			0.1784	0.0150	0.1955	0.0599	0.91	121	6	118	1	119	5	180	14	150	14
17	0.00216	0.00153	0.0430	0.0137	0.0247	0.0085	1.74	501	1	585	41	543	58	955	42	603	60
18			0.2141	0.0154	0.1420	0.0414	1.51	107	2	132	23	119	24	218	4	170	7
19	0.00267	0.00051								980	395	793	510	1750		1490	
20			0.1450	0.0245	0.1166	0.0104	1.24	161	21	159	37	160	33	315	44	237	38
21	0.00191	0.00042	0.0265		0.0292		0.91	446	0			494	67				
22			0.1963	0.0218	0.1105	0.0094	1.78	118	3	107	15	112	13	285	21	440	198
23	0.00351	0.001329	0.0407	0.0084	0.0261	0.0007	1.56	496	49	581	69	538	84				
24			0.1156	0.0070	0.1578	0.0318	0.73	151	9	169	30	160	28	288	25	300	0

B.2 Measures Characterizing HRR Temporal Profiles

Values in Table B-3 with red borders were used for the statistical analyses described in Section 7. Values colored blue were assigned using criteria described in Section 5.

Table B-3. Tabulated measures characterizing HRR temporal profiles for individual tests

Test	t_{+25} (s)	t_{peak1} (s)	HRR_{peak1} (kW)	t_{max} (s)	HRR_{max} (kW)	t_{-25} (s)	$t_{>25}$ (s)	$Q_{>25}$ (MJ)	$HRR_{avg>25}$ (kW)	$FWHM_{>25}$ (s)	SF_t	SF_{HRR}	Q_{tot} (MJ)
1_1	354	410	120.4	581	182.7	893	539	59.9	107.0	425	0.788	0.586	61.6
1_2	364	447	100.4	603	153.0	970	606	57.5	92.8	412	0.680	0.606	58.6
1_3	314	368	102.2	810	143.5	927	613	57.7	90.3	507	0.827	0.630	60.6
2_1	132	170	218.0	399	244.4	637	505	62.8	122.8	348	0.689	0.502	66.4
2_2	122	163	195.7	163	195.7	693	571	54.7	94.7	452	0.792	0.484	57.9
5_1	1872	1370	9.5	1370	9.5								3.2
5_2	936	984	55.4	1368	83.2	2437	1501	50.8	29.2	409	0.272	0.351	57.1
5_3	1248	728	15.2	1578	60.4	2294	1046	42.2	32.9	273	0.261	0.545	43.5
6_1	127	159	120.9	159	120.9	269	142	7.4	47.3	28	0.197	0.392	10.7
6_2	101	136	110.8	136	110.8	246	145	8.0	51.2	38	0.262	0.462	10.3
9_1	181	401	271.1	401	271.1	622	441	62.3	138.4	226	0.512	0.511	63.9
9_2	170	369	351.3	369	351.3	583	413	62.5	149.3	143	0.346	0.425	64.7
10_1	80	146	529.6	146	529.6	544	464	60.6	130.2	103	0.222	0.246	62.6
10_2	70	147	629.1	147	629.1	560	490	59.1	119.3	94	0.192	0.190	64.7
10_3	67	136	605.3	136	605.3	658	591	62.4	105.0	90	0.152	0.173	67.3
11_1	162	349	305.2	349	305.2	623	461	66.3	141.1	167	0.362	0.462	68.6
11_2	145	298	275.6	298	275.6	590	445	62.3	139.3	263	0.591	0.505	63.7
12_1	77	148	525.0	148	525.0	423	346	66.1	189.5	105	0.303	0.361	68.2
12_2	78	152	574.5	152	574.5	571	493	61.1	123.4	102	0.207	0.215	63.8
13_1	573	689	155.5	689	155.5								41.6
13_2	618	723	169.3	855	172.6	1022	404	47.4	111.4	278	0.688	0.646	48.3
14_1	115	182	284.6	204	342.2	289	174	25.6	144.7	61	0.351	0.423	30.4
14_2	116	170	240.6	170	240.6	327	211	22.8	104.6	71	0.336	0.435	28.2

Table B-3. (continued)

Test	t_{+25} (s)	t_{peak1} (s)	HRR_{peak1} (kW)	t_{max} (s)	HRR_{max} (kW)	t_{-25} (s)	$t_{>25}$ (s)	$Q_{>25}$ (MJ)	$HRR_{avg>25}$ (kW)	$FWHM_{>25}$ (s)	SF_t	SF_{HRR}	Q_{tot} (MJ)
15_1	533	642	226.4	642	226.4	952	419	47.7	107.4	264	0.630	0.475	49.0
15_2	537	625	242.1	625	242.1	979	442	44.4	94.9	81	0.183	0.392	45.0
16_1	139	200	329.8	200	329.8	361	222	28.8	128.1	64	0.288	0.388	35.2
16_2	125	195	318.9	195	318.9	361	236	30.2	124.8	55	0.233	0.391	37.9
17_1	806	959	130.8	1179	174.3	1457	651	70.6	101.7	401	0.616	0.584	72.1
17_2	843	961	72.5	1246	198.4	1563	720	69.8	90.4	165	0.229	0.455	72.1
18_1	136	225	100.1	567	461.9	692	556	88.9	158.2	120	0.216	0.342	90.0
18_2	136	228	85.6	527	480.1	675	539	85.6	157.5	153	0.284	0.328	87.0
19_1	1872	2055	0	3587	0								4.4
19_2	1187	1196	26.2	2391	114.9	2558	1371	63.2	43.6	984	0.718	0.379	65.3
20_1	216	275	74.1	702	466.1	829	613	84.0	135.2	121	0.197	0.290	85.2
20_2	232	283	86.9	688	412.7	838	606	86.6	140.8	127	0.210	0.341	88.1
20_3	159	207	87.4	651	299.8	939	780	89.9	113.8	273	0.350	0.380	91.4
21_1	1872	2055	0	3587	0		0						0
21_2	1872	2055	0	3587	0		0						0
22_1	1872	242	24.5	876	24.6		0						13.0
22_2	211	292	41.5	641	57.1	934	723	23.4	29.4	71	0.098	0.515	32.1
22_3	156	168	37.3	705	63.8	928	772	25.7	32.0	149	0.193	0.501	43.1
23_1	1872	2055	0	3587	0		0						0
23_2	1872	2055	0	3587	0		0						0
24_1	238	277	73.1	277	73.1	388	150	7.6	43.3	50	0.333	0.593	13.3
24_2	222	310	31.9	310	31.9	334	112	4.5	27.4	60	0.536	0.860	11.4

Table B-4. Tabulated measures characterizing HRR behavior for mock-up material combinations

Combination	$\overline{t_{+25}}$ (s)	t'_{+25} (s)	$\overline{t_{peak1}}$ (s)	t'_{peak1} (s)	$\overline{HRR_{peak1}}$ (kW)	HRR'_{peak1} (kW)	$\overline{t_{max}}$ (s)	t'_{max} (s)	$\overline{HRR_{max}}$ (kW)	HRR'_{max} (kW)	$\overline{Q_{tot}}$ (MJ)	Q'_{tot} (MJ)
1	344	26	408	40	108	11	665	126	160	20	60.3	1.5
2	127	7	167	16	207	16	281	167	220	34	62.2	6.0
3												
4												
5	1092	221	1027	323	27	25	1439	121	51	38	34.6	28.0
6	114	18	148	7	116	7	148	16	116	7	10.5	0.3
7												
8												
9	176	8	385	57	311	57	385	23	311	57	64.3	0.6
10	72	7	143	6	588	52	143	6	588	52	64.9	2.4
11	154	12	324	21	290	21	324	36	290	21	66.2	3.5
12	78	1	150	35	550	35	150	3	550	35	66.0	3.1
13	596	32	706	10	162	10	855		173		48.3	
14	116	1	176	31	263	31	187	24	291	72	29.3	1.6
15	535	3	634	11	234	11	634	12	234	11	47.0	2.8
16	132	10	198	8	324	8	198	4	324	8	36.6	1.9
17	825	26	960	41	102	41	1213	47	186	17	72.1	0.0
18	136	0	227	10	93	10	547	28	471	13	88.5	2.1
19	1187		1196		26		2391		115		34.8	43.1
20	202	38	255	42	81	9	680	26	393	85	88.2	3.1
21												
22	184	39	234	62	34	9	741	121	49	21	29.4	15.2
23												
24	230	11	294	29	53	29	294	23	53	29	12.4	1.3

B.3 Measures Characterizing FIGRA Temporal Profiles

Values in Table B-5 with red borders were used for the statistical analyses described in Section 7. Values colored blue were assigned using criteria described in Section 5.

Table B-5. Tabulated measures characterizing FIGRA temporal profiles for individual tests

Test	t_{FIGRA1} (s)	$FIGRA_{peak1}$ (kW/s)	$t_{FIGRAmax}$ (s)	$FIGRA_{max}$ (kW/s)
1_1	410	0.294	581	0.315
1_2	445	0.230	593	0.257
1_3	368	0.278	368	0.278
2_1	170	1.282	170	1.282
2_2	159	1.212	159	1.212
5_1	1782	0	1782	0
5_2	984	0.056	1363	0.061
5_3	637	0.024	1582	0.039
6_1	158	0.788	158	0.788
6_2	135	0.815	135	0.815
9_1	401	0.676	401	0.676
9_2	369	0.952	369	0.952
10_1	145	3.636	145	3.636
10_2	146	4.285	146	4.285
10_3	128	4.633	128	4.633
11_1	314	0.911	314	0.911
11_2	295	0.930	295	0.930
12_1	141	3.645	141	3.645
12_2	145	3.802	145	3.802
13_1	664	0.229	664	0.229
13_2	678	0.238	678	0.238
14_1	171	1.643	201	1.681
14_2	159	1.431	159	1.431
15_1	640	0.353	640	0.353
15_2	600	0.389	600	0.389
16_1	200	1.649	200	1.649
16_2	184	1.663	184	1.663
17_1	959	0.136	1179	0.148
17_2	961	0.076	1246	0.159
18_1	225	0.445	567	0.815
18_2	203	0.398	527	0.911
19_1	1782	0	2250	0
19_2	1188	0.021	1500	0.055

Table B-5. Tabulated measures characterizing FIGRA temporal profiles for individual tests (continued)

Test	t_{FIGRA1} (s)	$FIGRA_{peak1}$ (kW/s)	$t_{FIGRAmax}$ (s)	$FIGRA_{max}$ (kW/s)
20_1	263	0.275	702	0.664
20_2	277	0.310	687	0.600
20_3	207	0.422	650	0.461
21_1	1782	0	2250	0
21_2	1782	0	2250	0
22_1	189	0.125	189	0.125
22_2	223	0.148	223	0.148
22_3	168	0.222	168	0.222
23_1	1782	0	2250	0
23_2	1782	0	2250	0
24_1	277	0.264	277	0.264
24_2	234	0.131	234	0.131

Table B-6. Tabulated measures characterizing FIGRA behavior for mock-up material combinations

Combination	$\overline{t_{FIGRA1}}$ (s)	t'_{FIGRA1} (s)	$\overline{FIGRA_{peak1}}$ (kW/s)	$FIGRA'_{peak1}$ (kW/s)	$\overline{t_{FIGRAmax}}$ (s)	$t'_{FIGRAmax}$ (s)	$\overline{FIGRA_{max}}$ (kW/s)	$FIGRA'_{max}$ (kW/s)
1	408	39	0.267	0.033	514	127	0.283	0.029
2	165	8	1.247	0.050	165	8	1.247	0.050
3								
4								
5	811	245	0.040	0.023	1473	155	0.050	0.015
6	147	16	0.802	0.019	147	16	0.802	0.019
7								
8								
9	385	23	0.814	0.195	385	23	0.814	0.195
10	140	10	4.185	0.506	140	10	4.185	0.506
11	305	13	0.921	0.014	305	13	0.921	0.014
12	143	3	3.724	0.111	143	3	3.724	0.111
13	671	10	0.234	0.006	671	10	0.234	0.006
14	165	8	1.537	0.150	180	30	1.556	0.177
15	620	28	0.371	0.025	620	28	0.371	0.025
16	192	11	1.656	0.010	192	11	1.656	0.010
17	960	1	0.106	0.043	1213	47	0.154	0.008
18	214	16	0.421	0.033	547	28	0.863	0.068
19	1188		0.021		1500		0.055	
20	249	37	0.336	0.077	695	11	0.575	0.104
21								
22	193	28	0.165	0.050	193	28	0.165	0.050
23								
24	256	30	0.198	0.094	256	30	0.198	0.094

Appendix C Data Plots for Supplemental Mock-up Tests

Results for repeated tests of flame spread and fire growth behavior on mock-ups for the supplemental combinations listed in Table 11 are provided as combined temporal plots of HRR and total HRR, FIGRA and mass, mass loss rate and effective heat of combustion; separate flame spread contours on the back and seat cushions for each repeated test followed by plots of characteristic flame spread rates u_{bv}, u_{bl}, u_{sl}, and u_{st}; combined temporal plots of burned areas as a function of time for each of the tests for a given combination; and combined temporal plots of radative heat flux recorded at distances of 0.75 m and 1.5 m from the front, right side, and back. The various plots are repeated when more than one application of an ignition source was required.

C.1 Combination 25

78%PP/22%PE/NIST Prepared Foam

Notes:

Test 1:

Ignition Source 1 applied at time = 0 s.

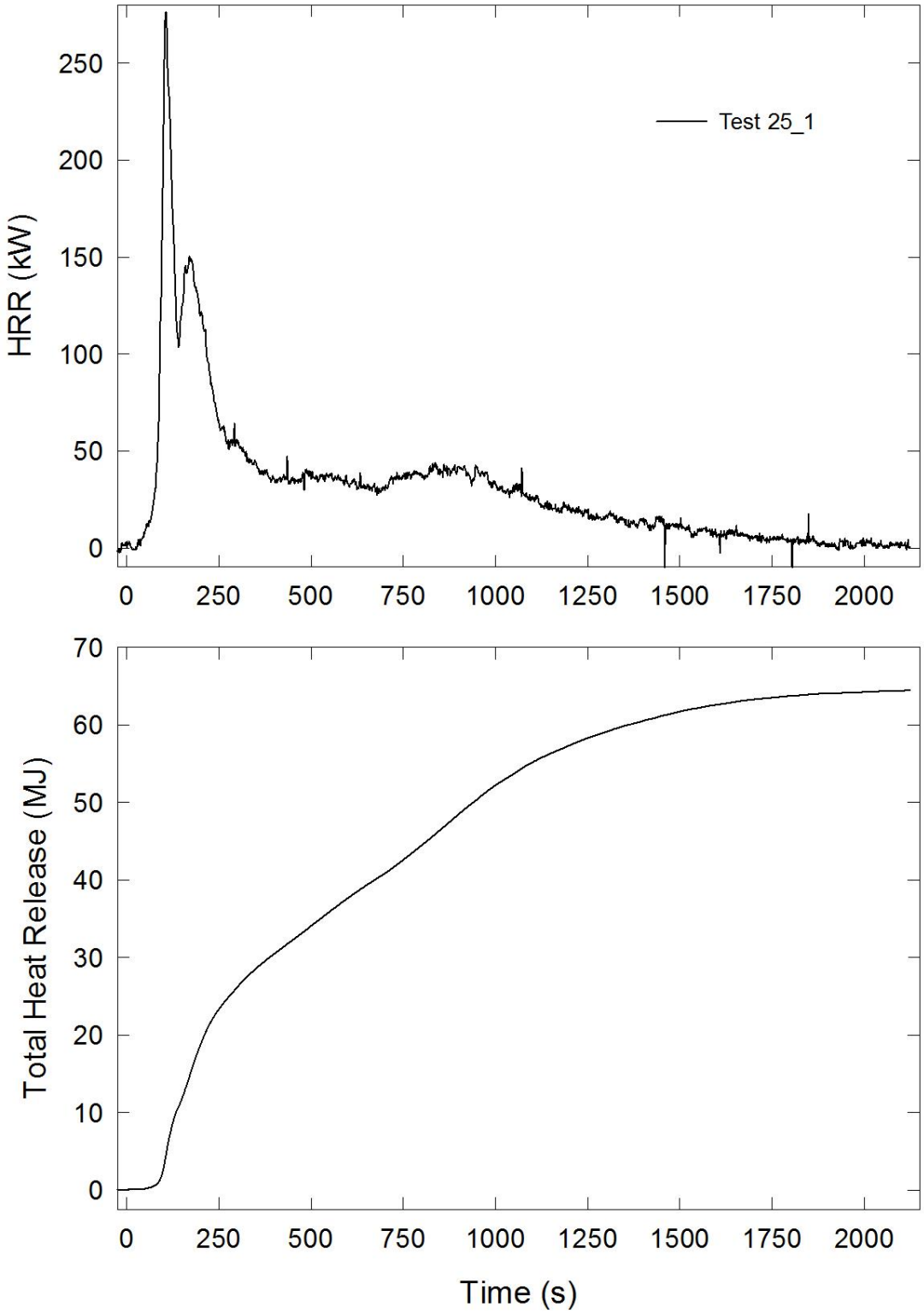

Figure C-1. Temporal profiles of HRR and integrated HRR are shown for Test 25_1 following application of Ignition Source 1.

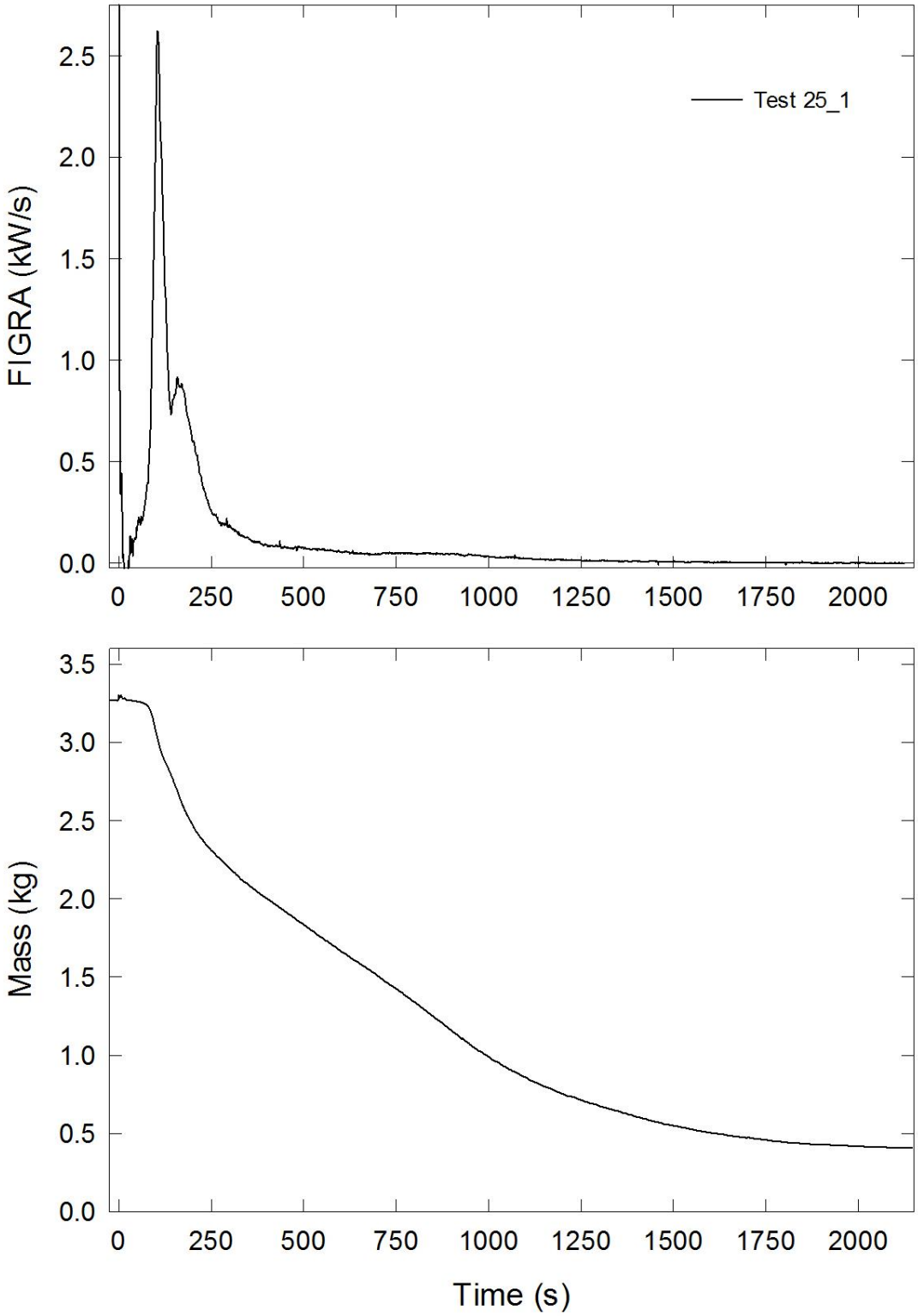

Figure C-2. Temporal profiles of FIGRA and mock-up mass for Test 25_1 are shown following application of Ignition Source 1.

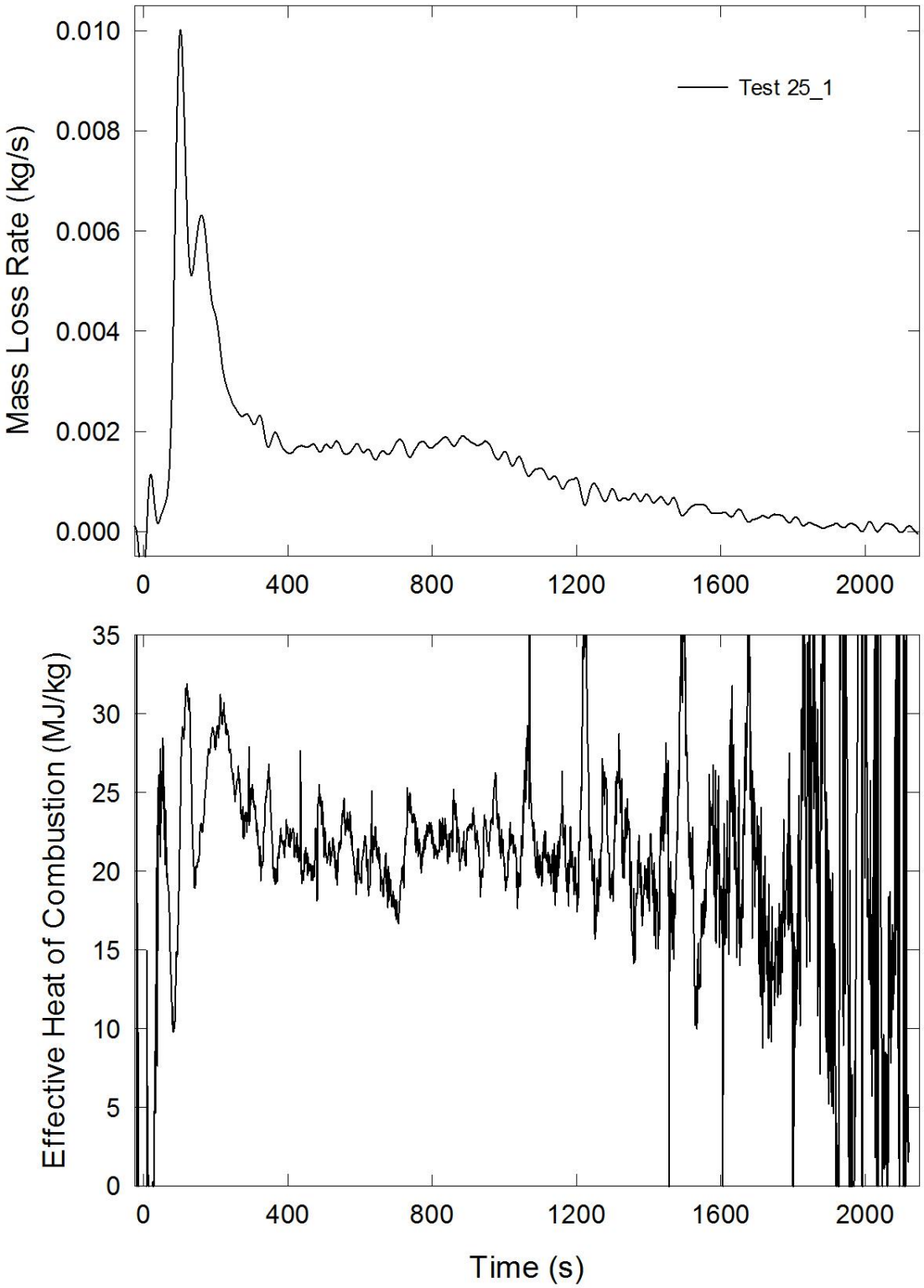

Figure C-3.Temporal profiles of MLR and EHOC are shown for Test 25_1 following application of Ignition Source 1.

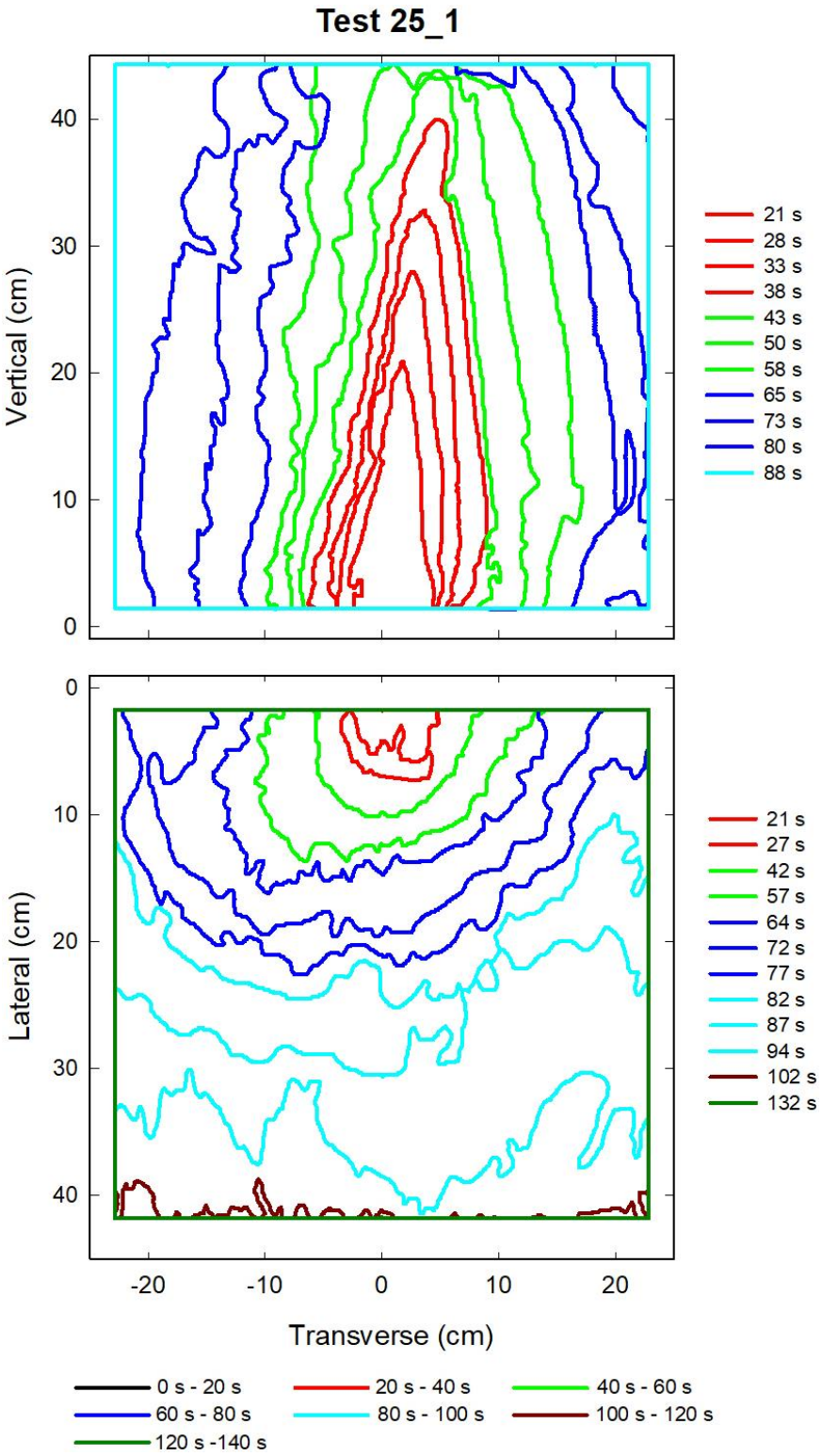

Figure C-4. Flame edge contours on the back (top) and seat (bottom) cushions are plotted as a function of time for Test 25_1 following application of Ignition Source 1.

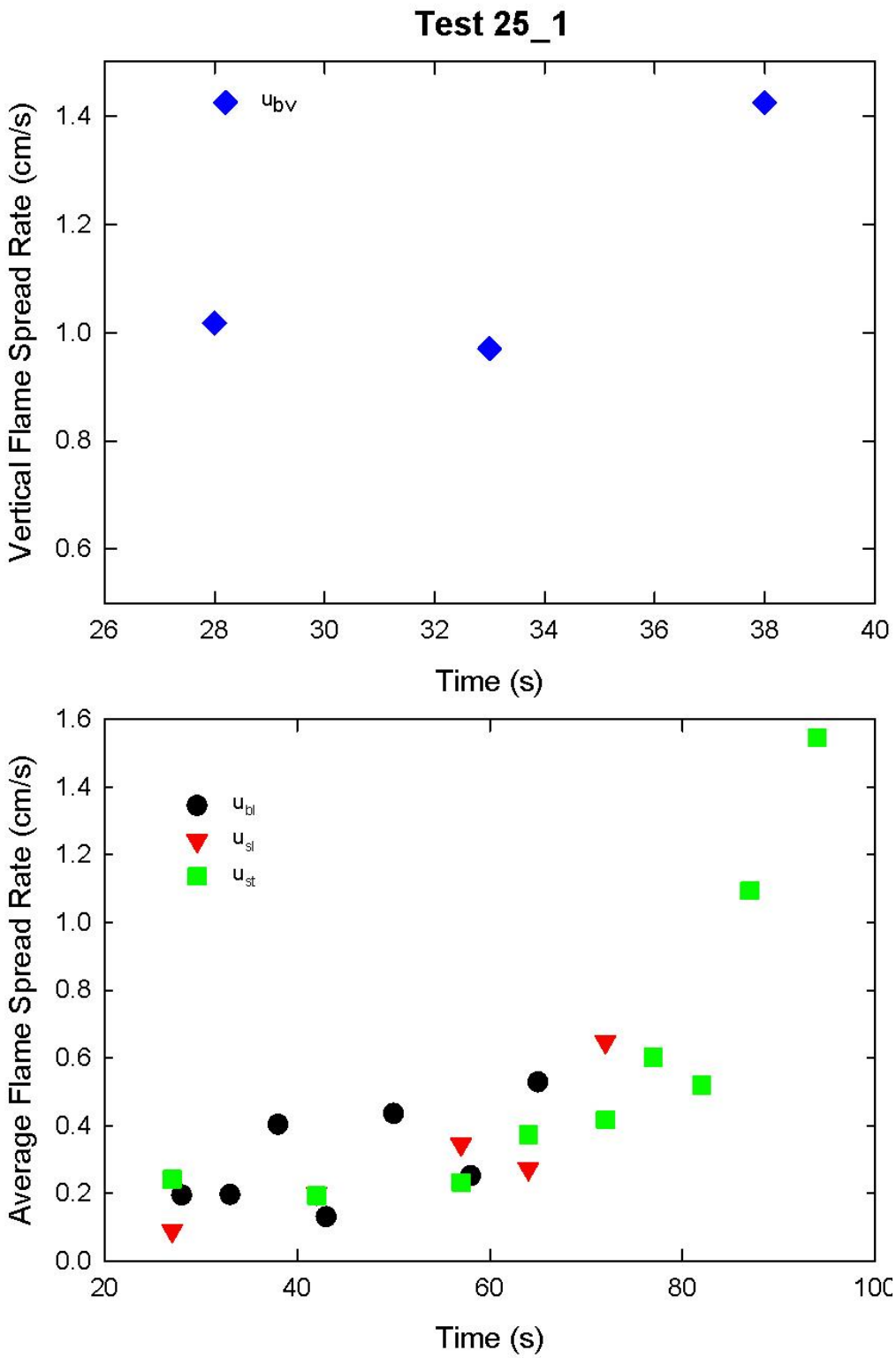

Figure C-5. Vertical flame spread rate on the back cushion (top) and average lateral flame spread rates on the back and seat cushions and transverse flame spread rate on the seat cushion (bottom) are plotted as a function of time for Test 25_1 following application of Ignition Source 1.

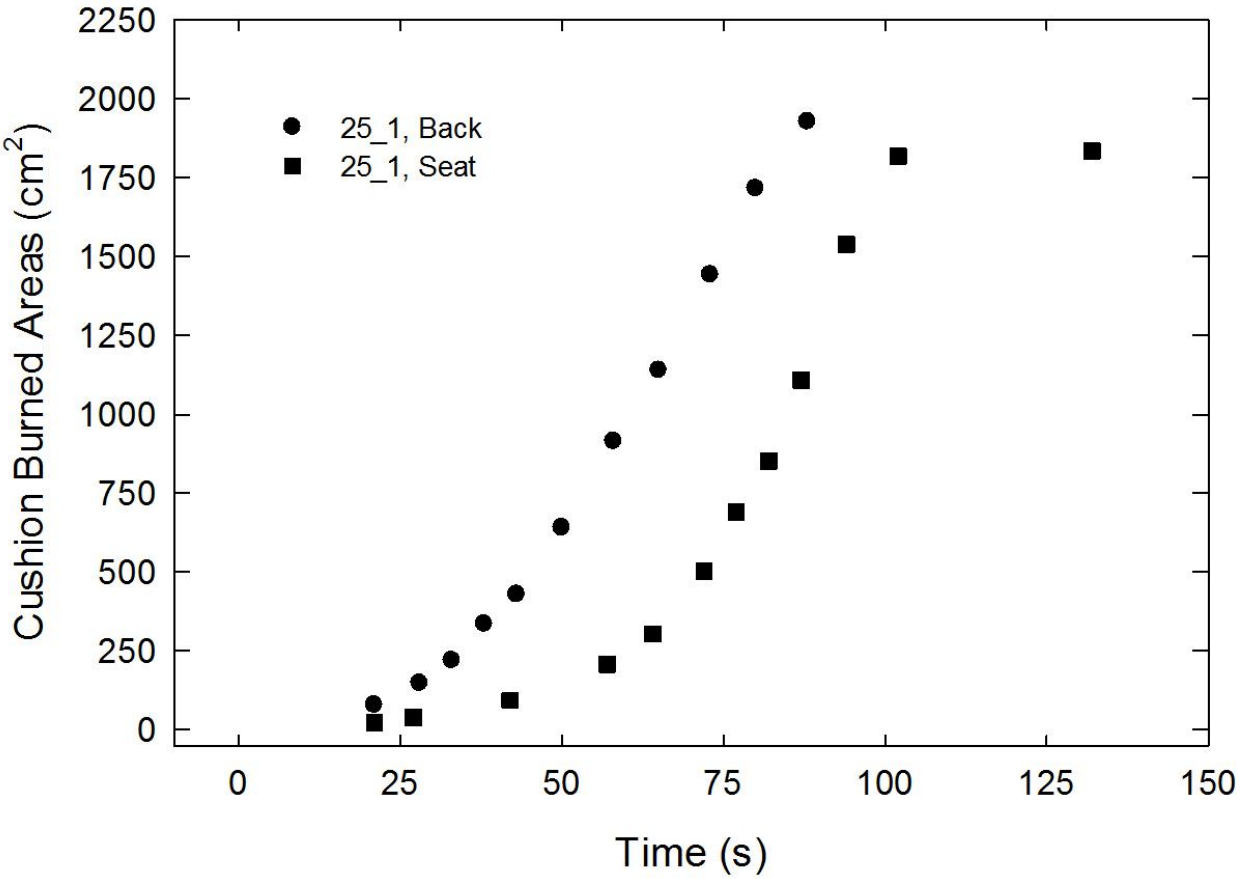

Figure C-6. Burned areas on the seat and back cushions are plotted as a function of time for Test 25_1 following application of Ignition Source 1.

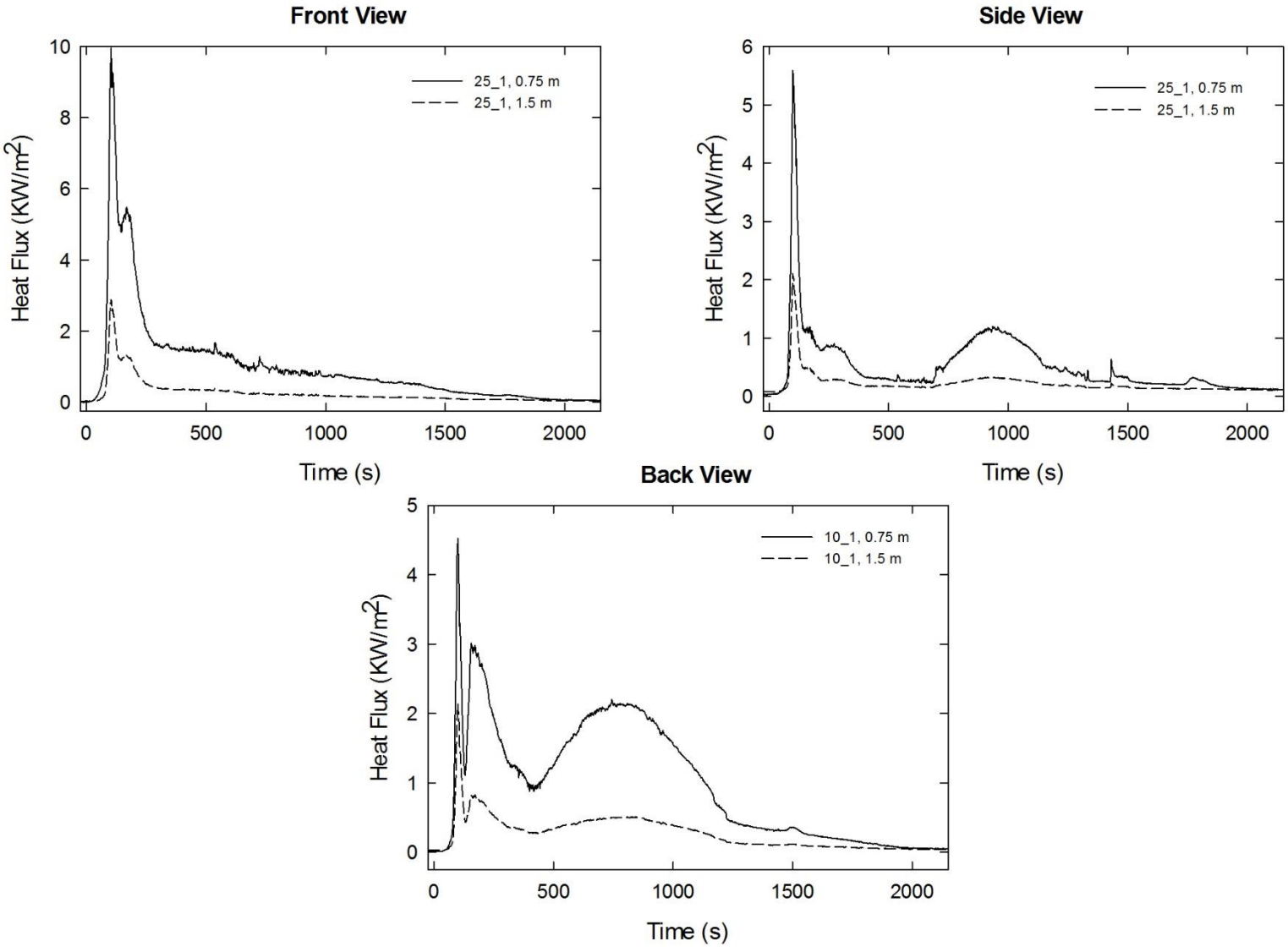

Figure C-7. Heat fluxes recorded at distances of 0.75 m and 1.5 m are plotted as a function of time for locations to the front, side and rear of the mock-up for Test 25_1 following application of Ignition Source 1.

C.2 Combination 26

FRFPUF

Notes:

Test 1:

Ignition Source 1 applied at time = 0 s

Ignition Source 2 applied 85 s after Ignition Source 1 removed

Ignition Source 5 ignited 284 s after Ignition Source 2 removed

Test 2

Ignition Source 1 applied at time = 0 s.

Ignition Source 2 applied 71 s after Ignition Source 1 removed.

Ignition Source 5 ignited 156 s after Ignition Source 2 removed.

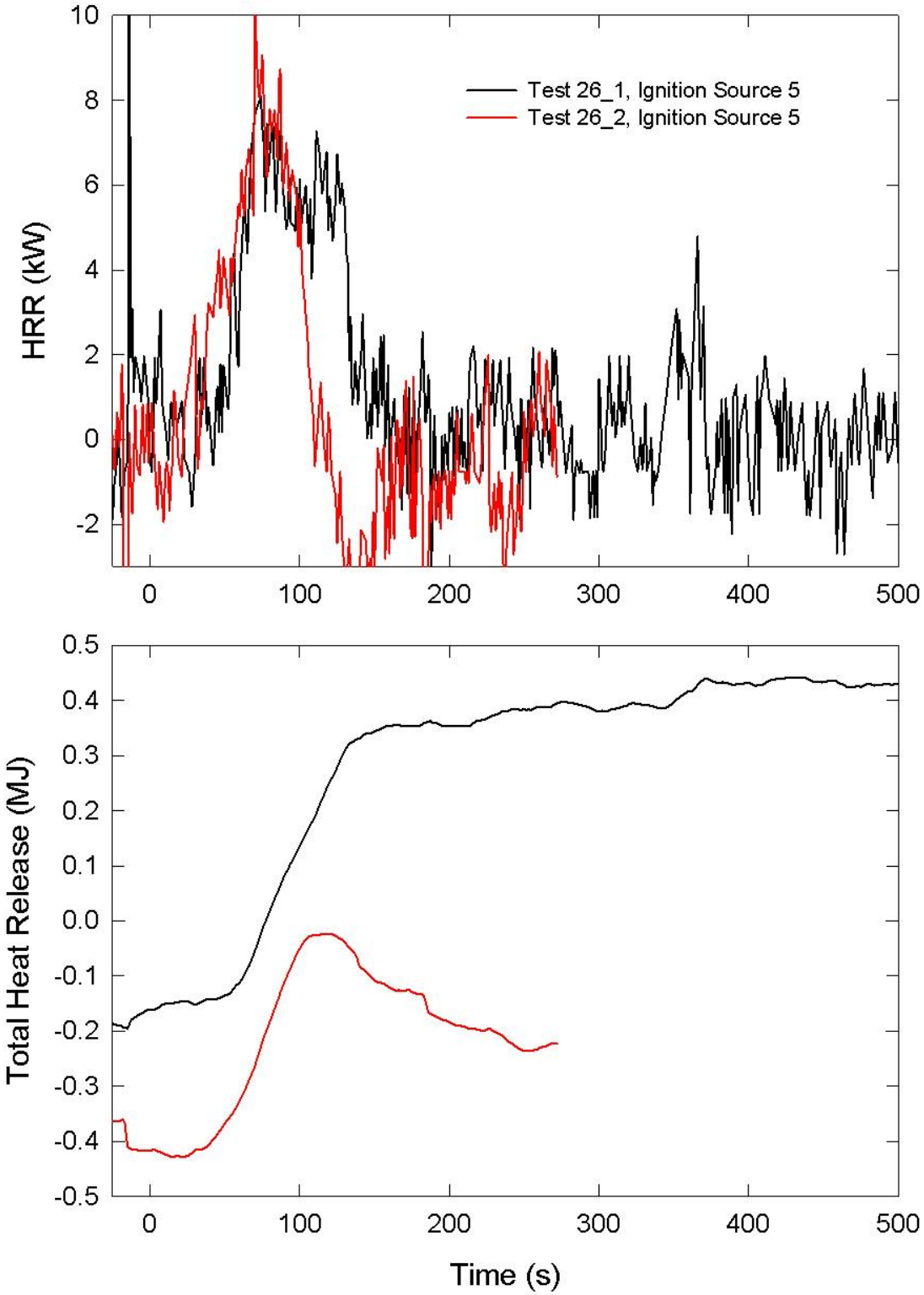

Figure C-8. Temporal profiles of HRR and integrated HRR are shown for Combination 26 tests following application of Ignition Source 5.

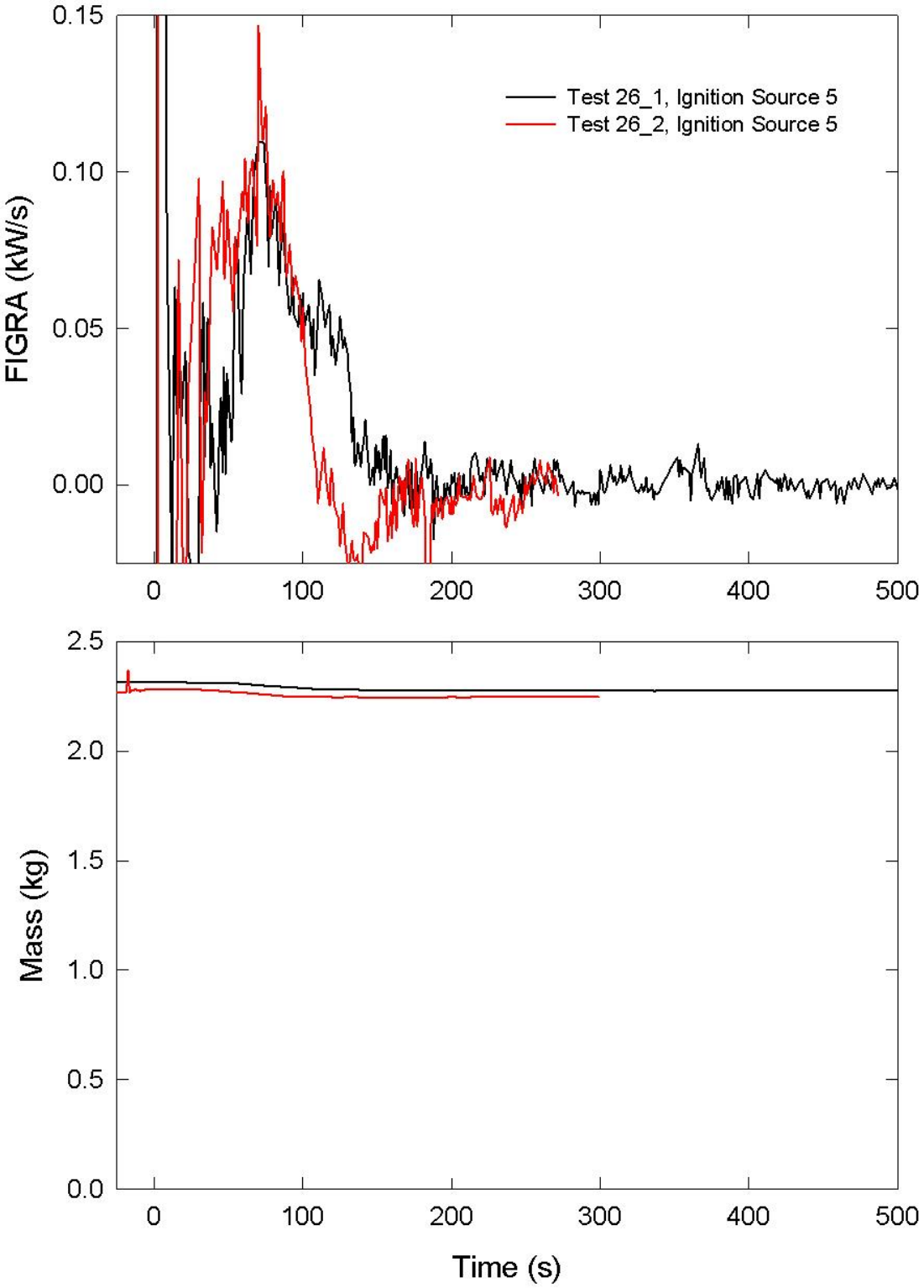

Figure C-9. Temporal profiles of FIGRA and mock-up mass are shown for Combination 26 tests following application of Ignition Source 5.

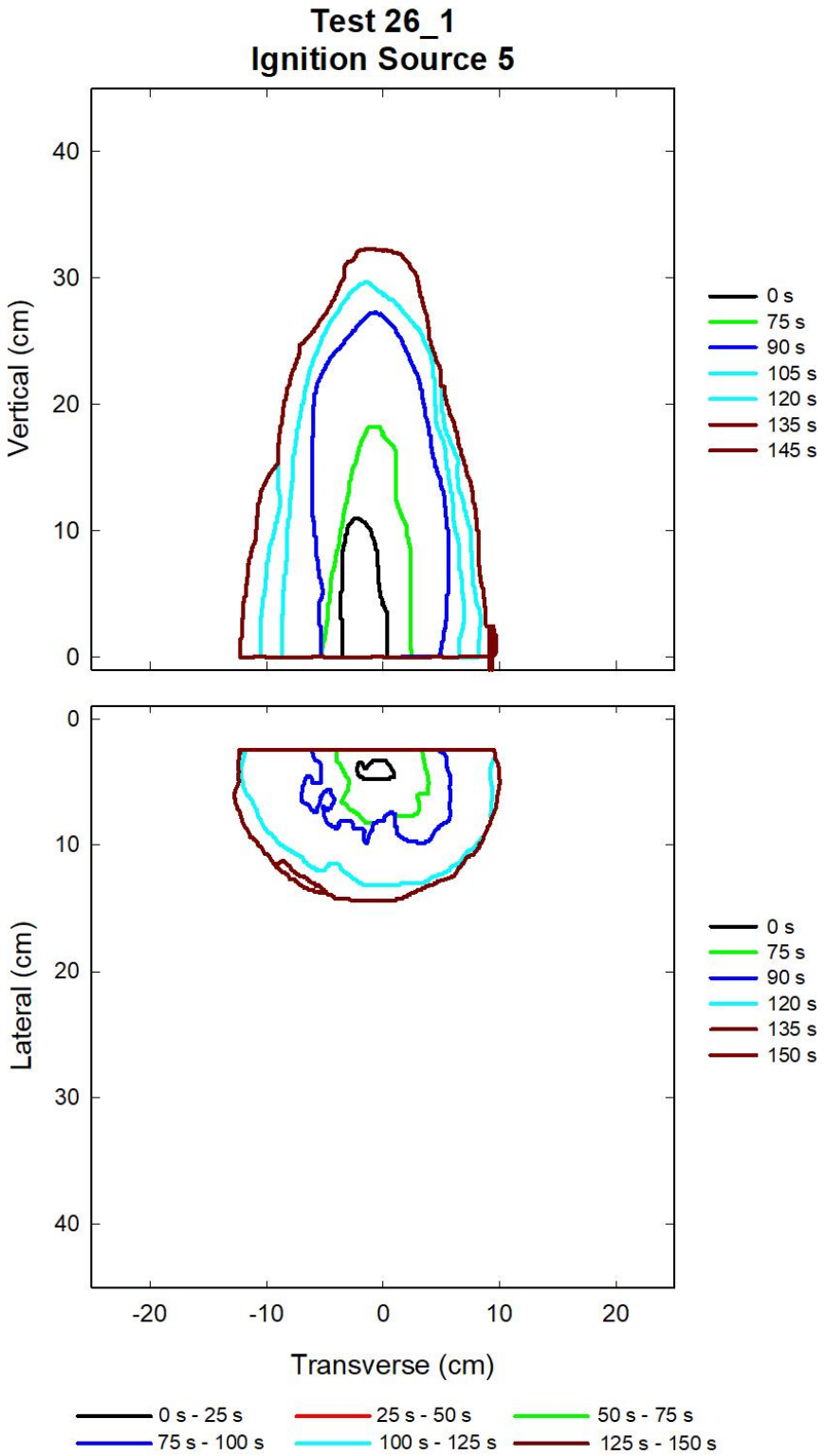

Figure C-10. Flame edge contours on the back (top) and seat (bottom) cushions are plotted as a function of time for Test 26_1 following application of Ignition Source 5.

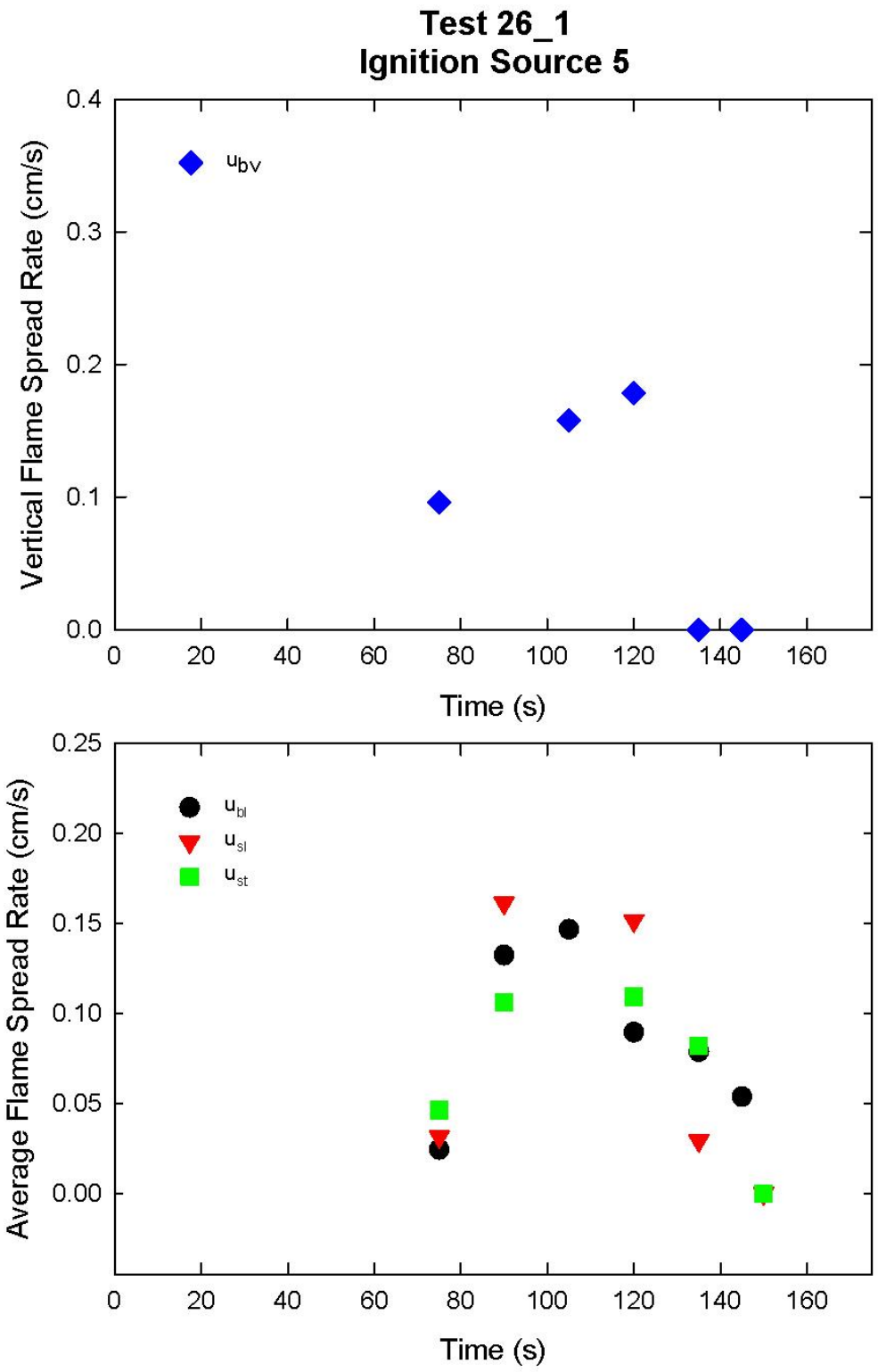

Figure C-11. Vertical flame spread rate on the back cushion (top) and average lateral flame spread rates on the back and seat cushions and transverse flame spread rate on the seat cushion (bottom) are plotted as a function of time for Test 26_1 following application of Ignition Source 5.

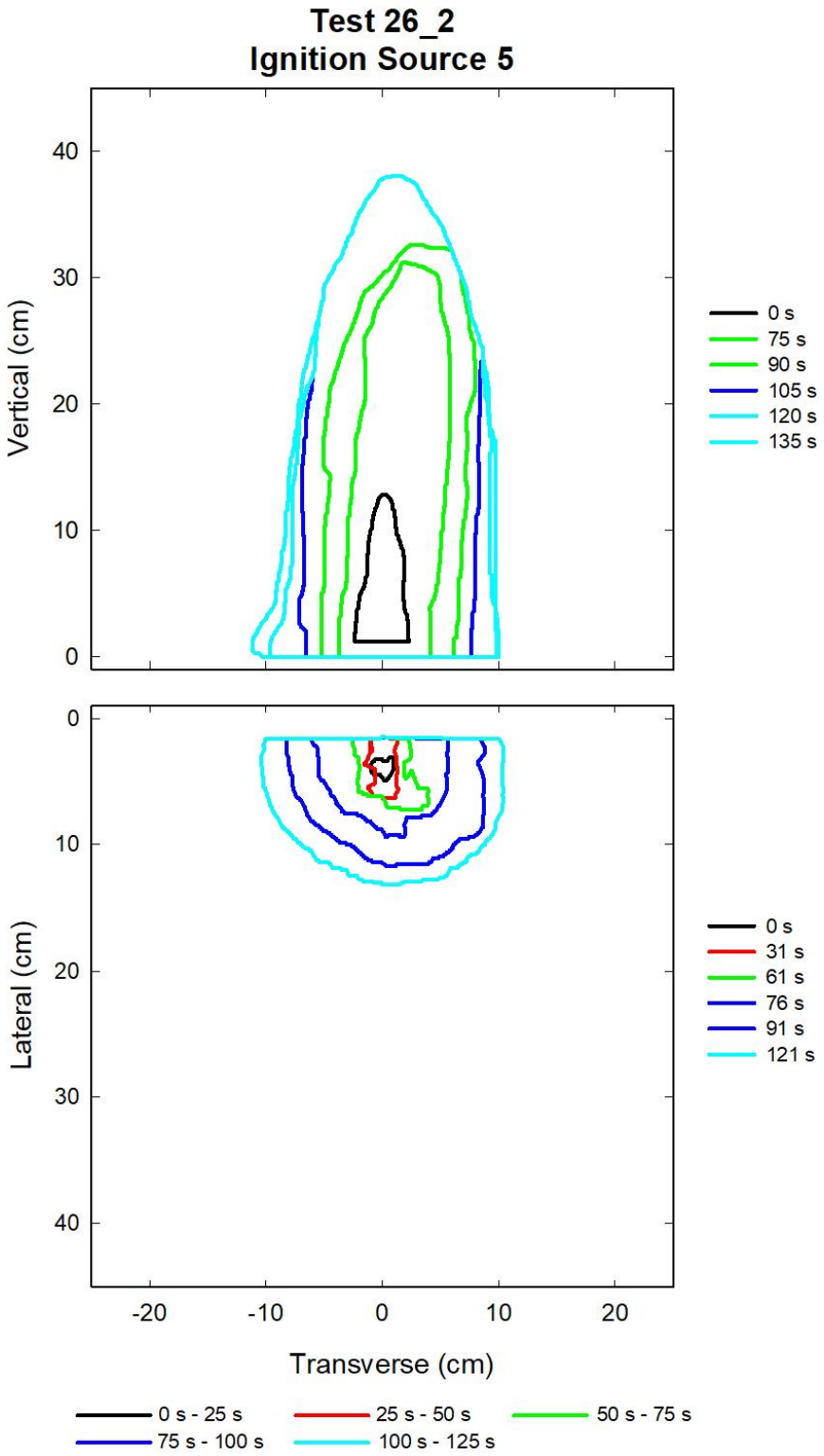

Figure C-12. Flame edge contours on the back (top) and seat (bottom) cushions are plotted as a function of time for Test 26_2 following application of Ignition Source 5.

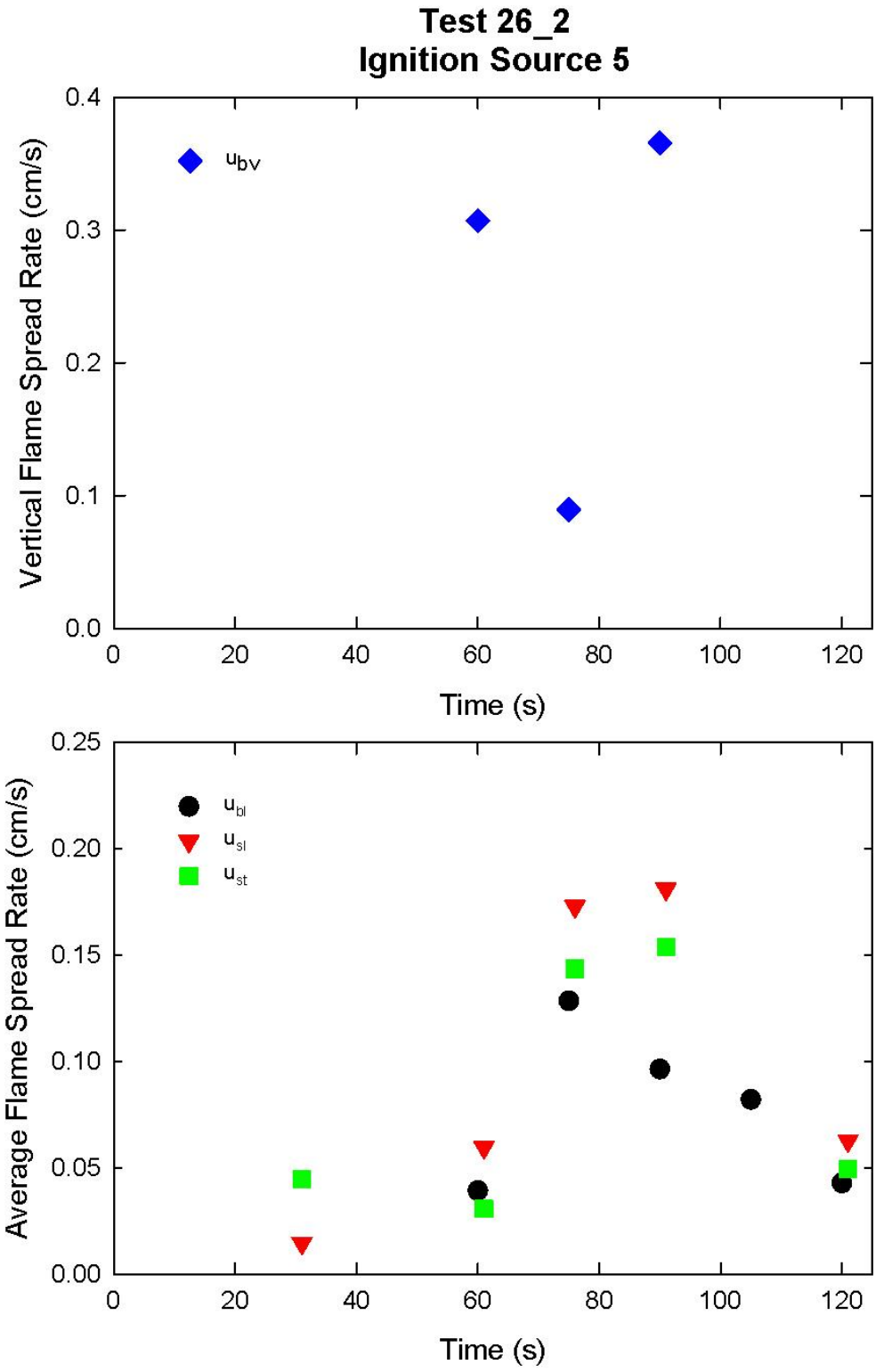

Figure C-13. Vertical flame spread rate on the back cushion (top) and average lateral flame spread rates on the back and seat cushions and transverse flame spread rate on the seat cushion (bottom) are plotted as a function of time for Test 26_2 following application of Ignition Source 5.

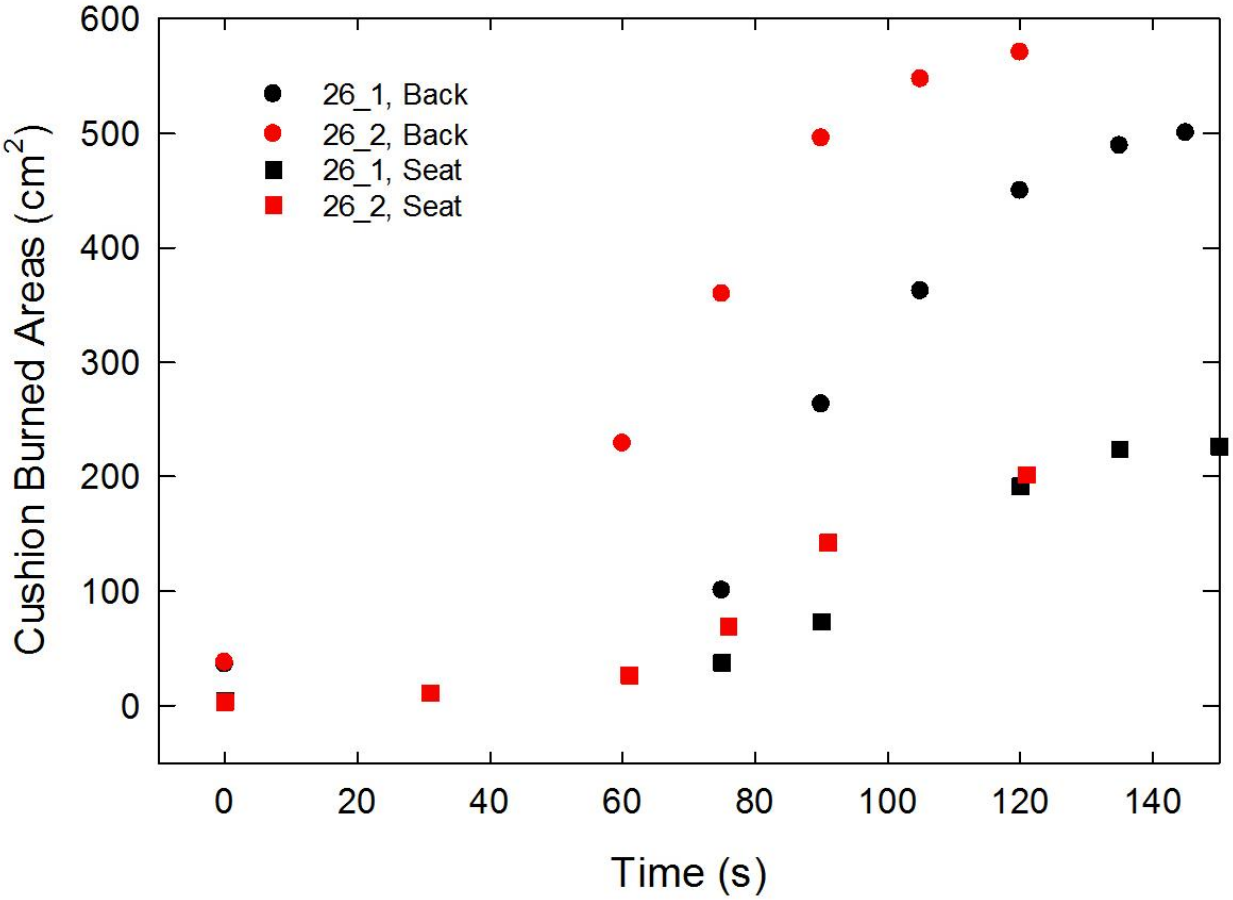

Figure C-14. Burned areas on the seat and back cushions are plotted as a function of time for Combination 26 tests following application of Ignition Source 5.

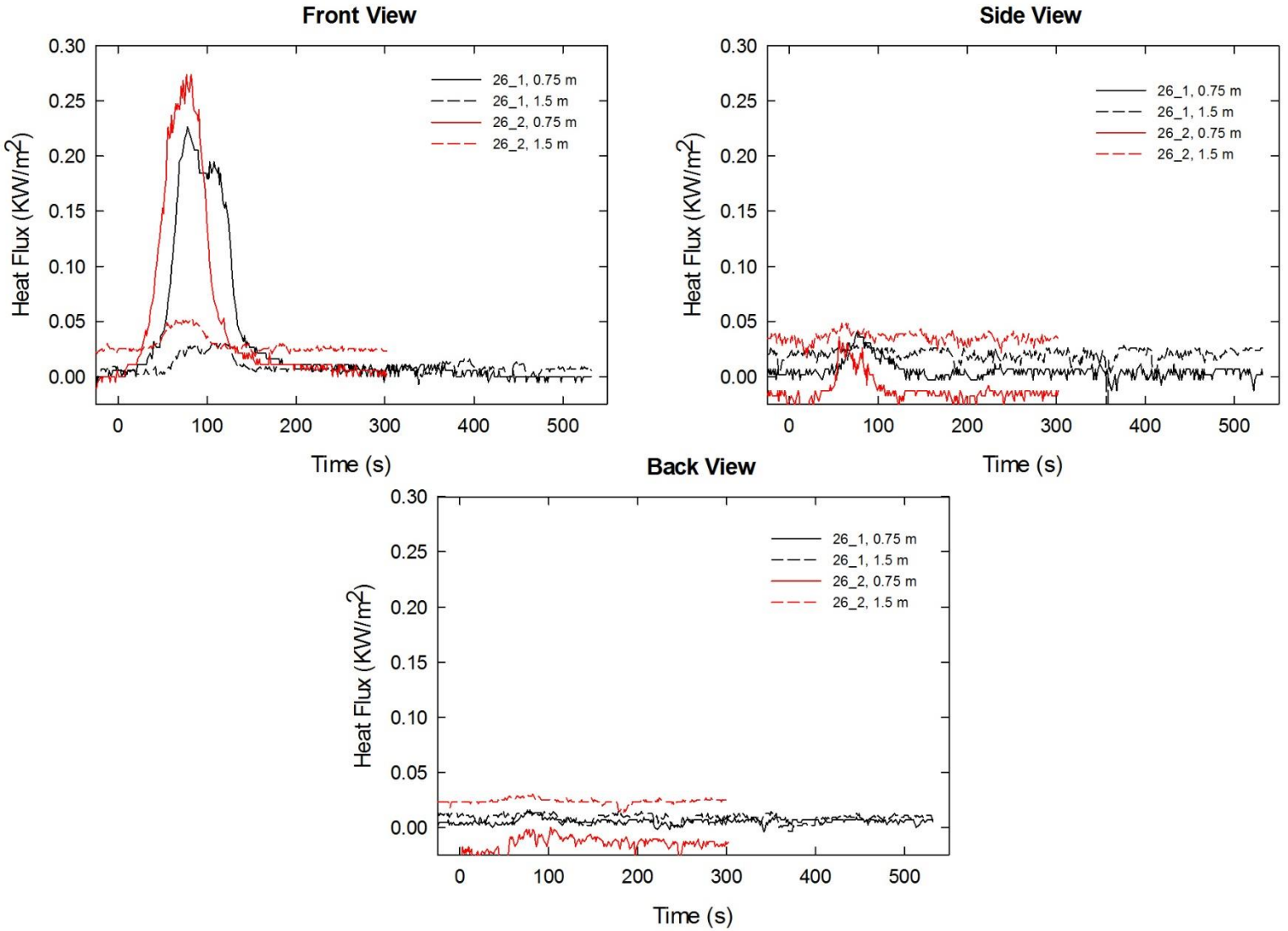

Figure C-15. Heat fluxes recorded at distances of 0.75 m and 1.5 m are plotted as a function of time for locations to the front, side and rear of the mock-up for Combination 26 tests following application of Ignition Source 5.

C.3 Combination 27

FRFPUF

Notes:

Test 1:

Ignition Source 1 applied at time = 0 s

Test 2:

Ignition Source 1 applied at time = 0 s

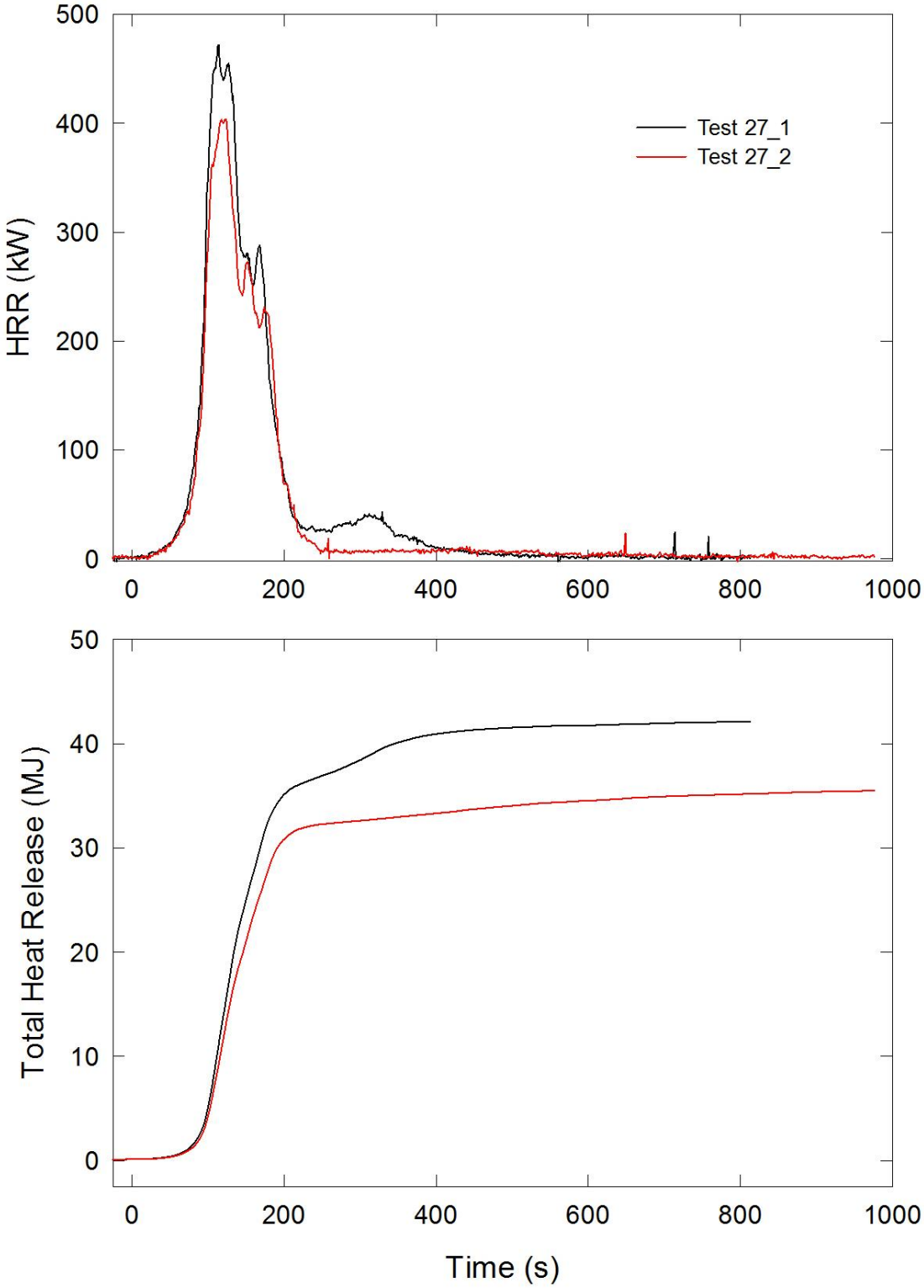

Figure C-16. Temporal profiles of HRR and integrated HRR are shown for Combination 27 tests following application of Ignition Source 1.

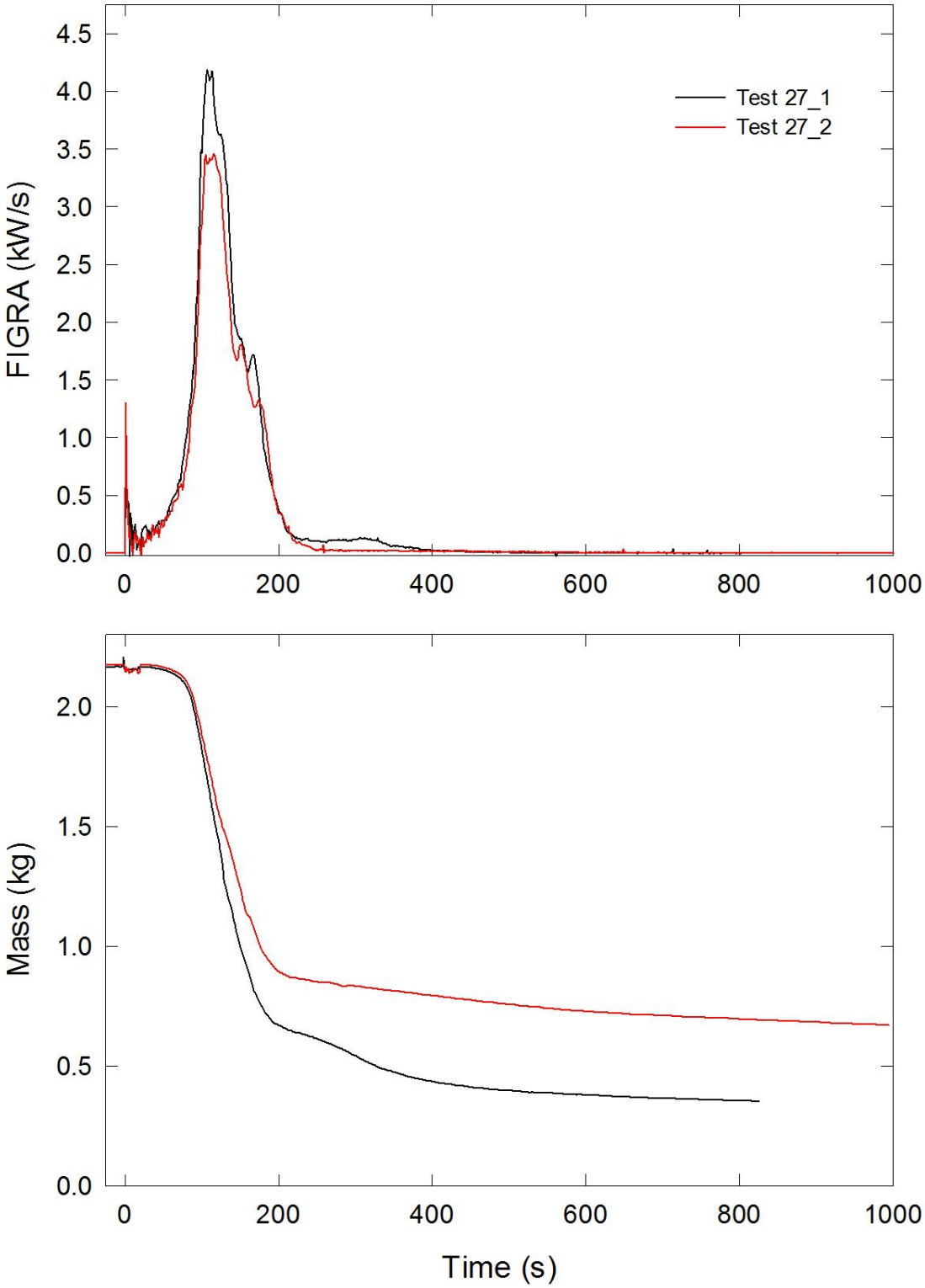

Figure C-17. Temporal profiles of FIGRA and mock-up mass are shown for Combination 27 tests following application of Ignition Source 1.

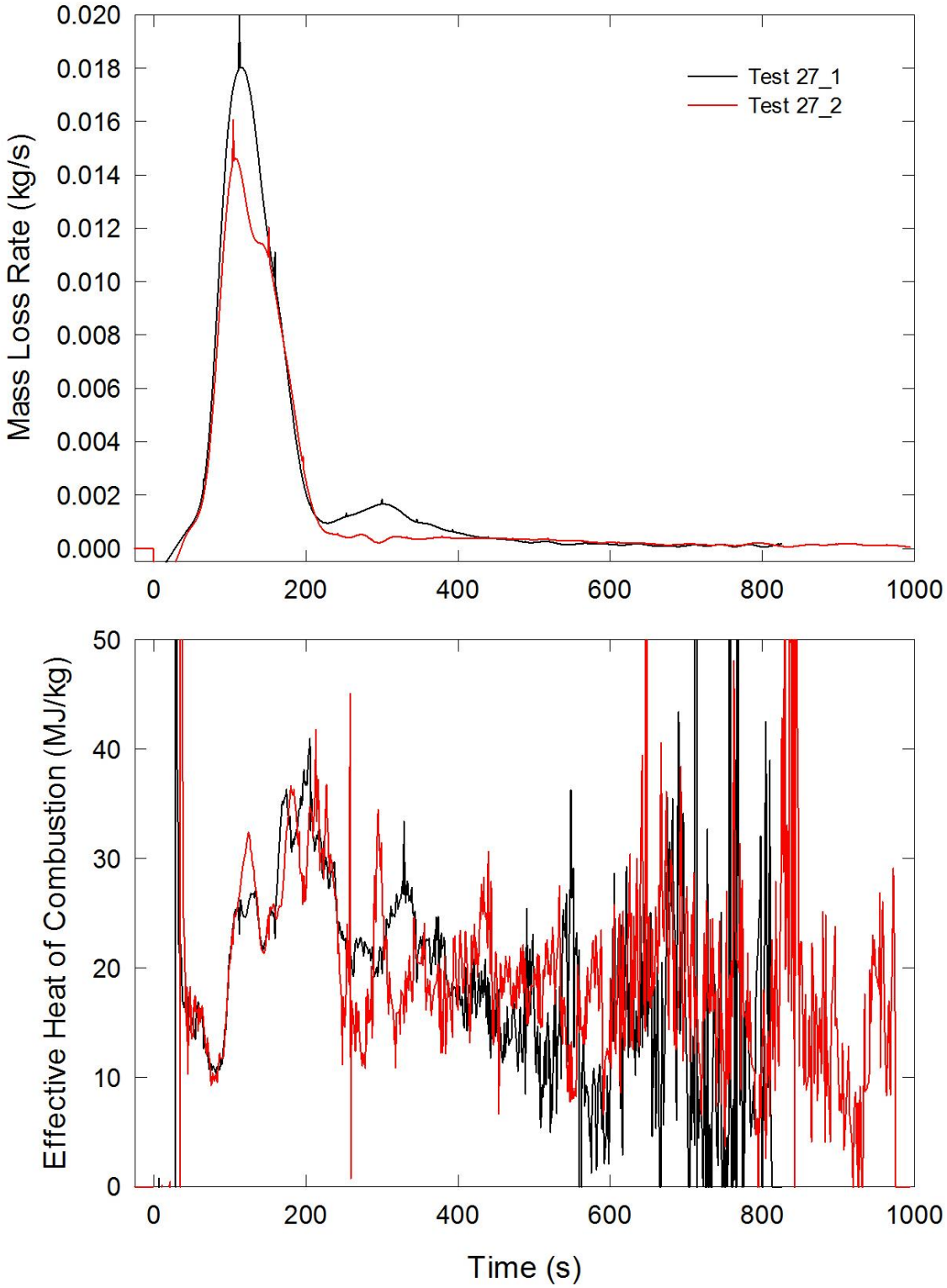

Figure C-18. Temporal profiles of MLR and EHOC are shown for Combination 27 tests following application of Ignition Source 1.

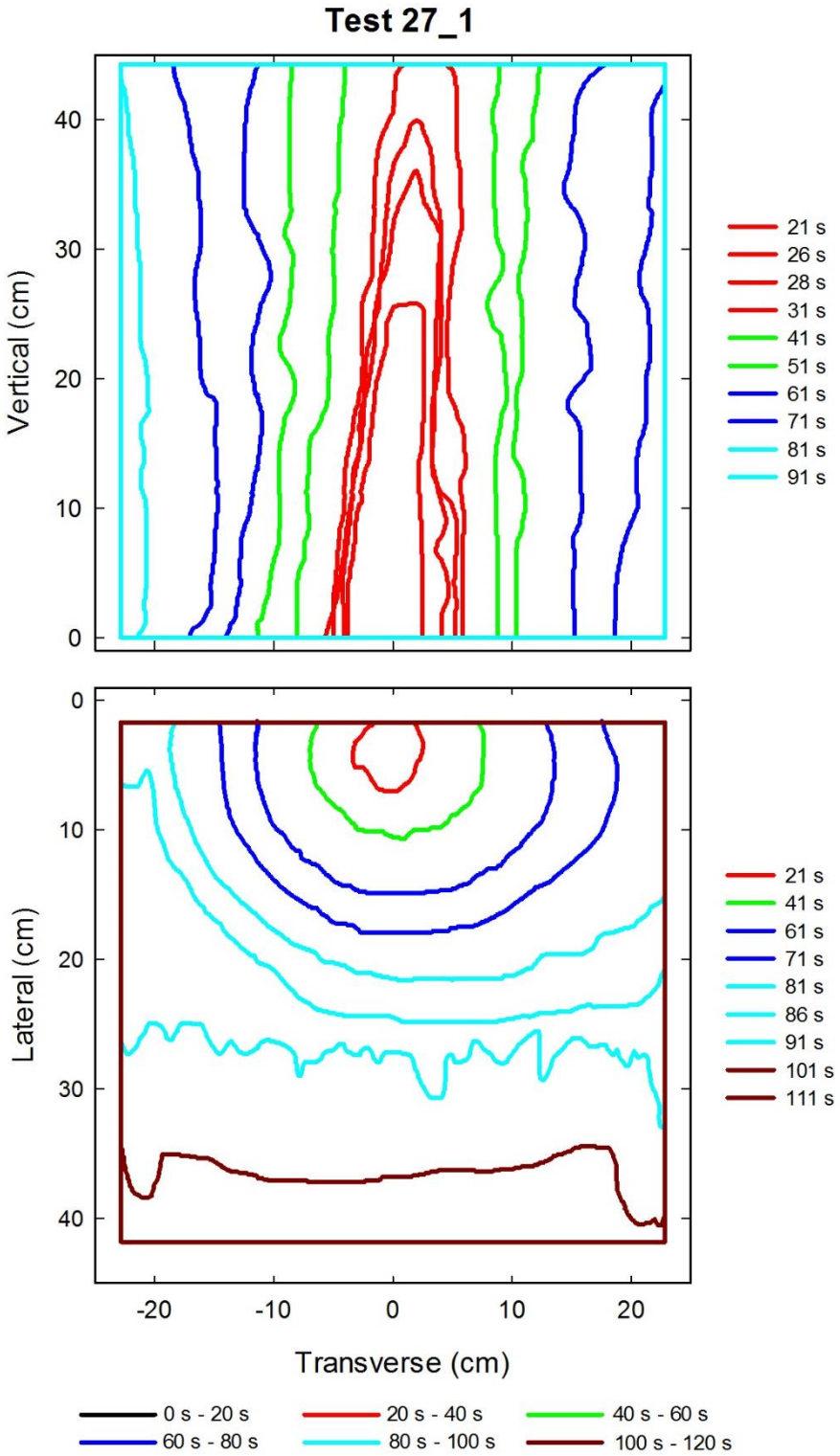

Figure C-19. Flame edge contours on the back (top) and seat (bottom) cushions are plotted as a function of time for Test 27_1 following application of Ignition Source 1.

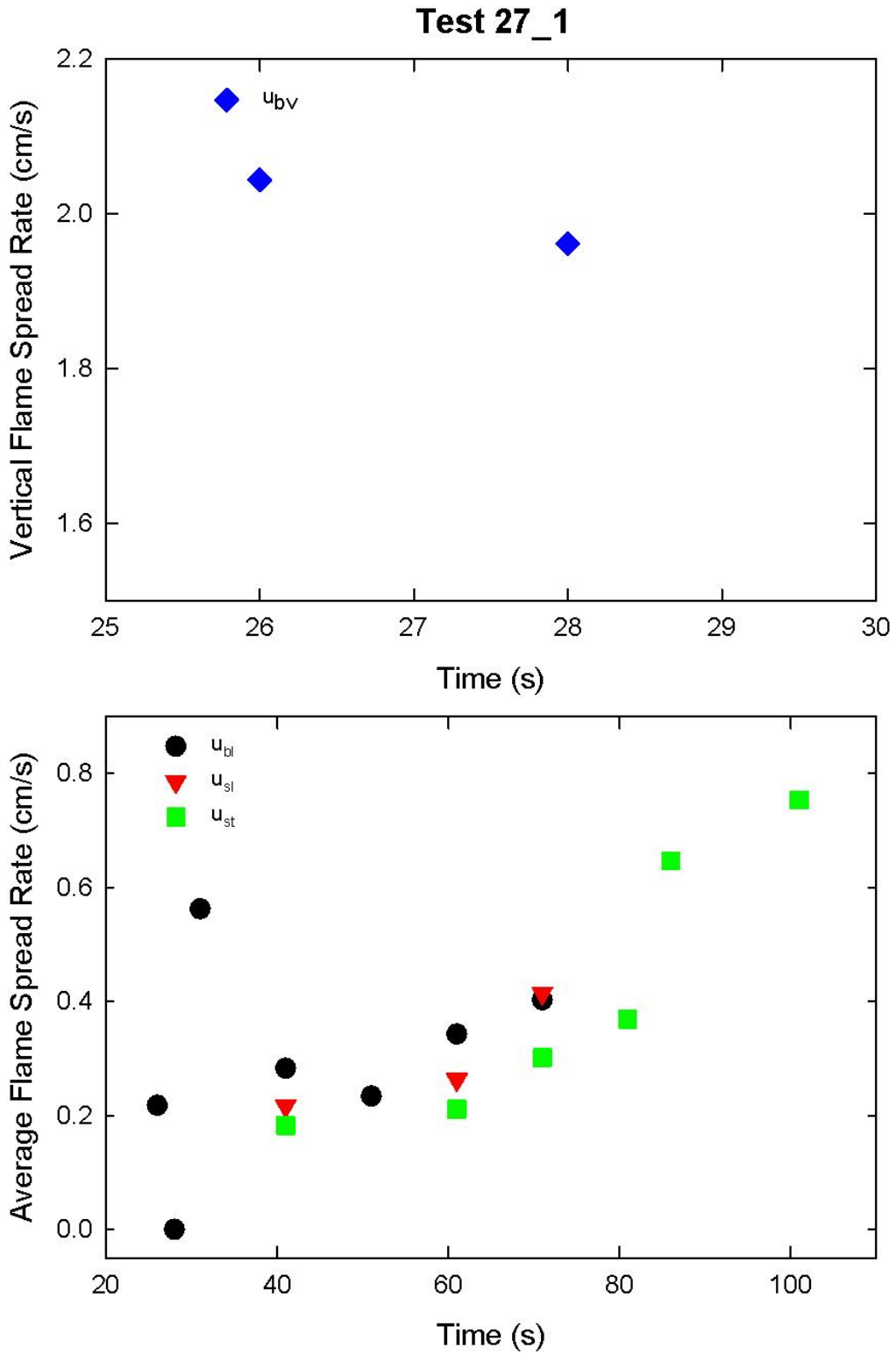

Figure C-20. Vertical flame spread rate on the back cushion (top) and average lateral flame spread rates on the back and seat cushions and transverse flame spread rate on the seat cushion (bottom) are plotted as a function of time for Test 27_1 following application of Ignition Source 1.

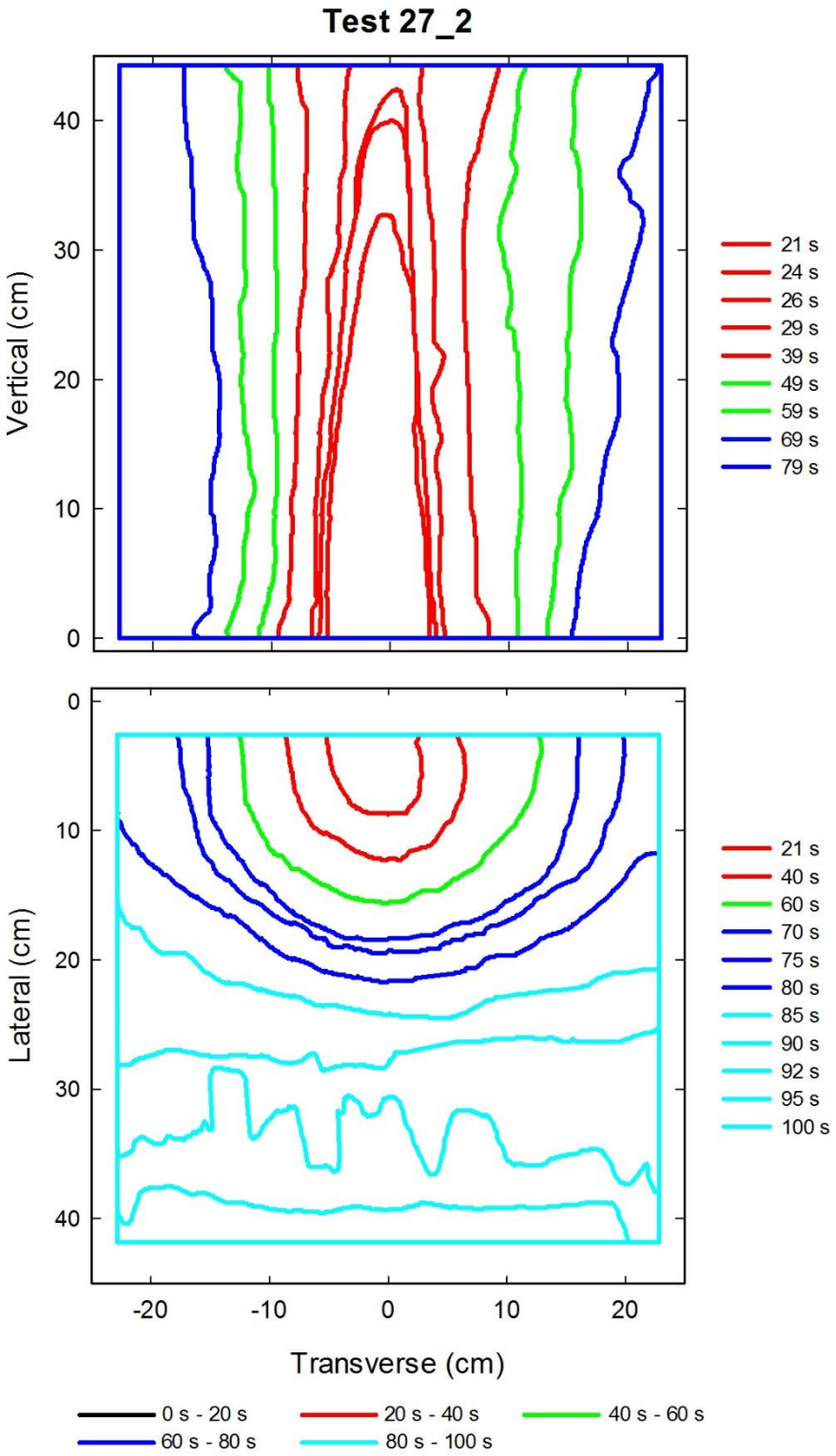

Figure C-21. Flame edge contours on the back (top) and seat (bottom) cushions are plotted as a function of time for Test 27_2 following application of Ignition Source 1.

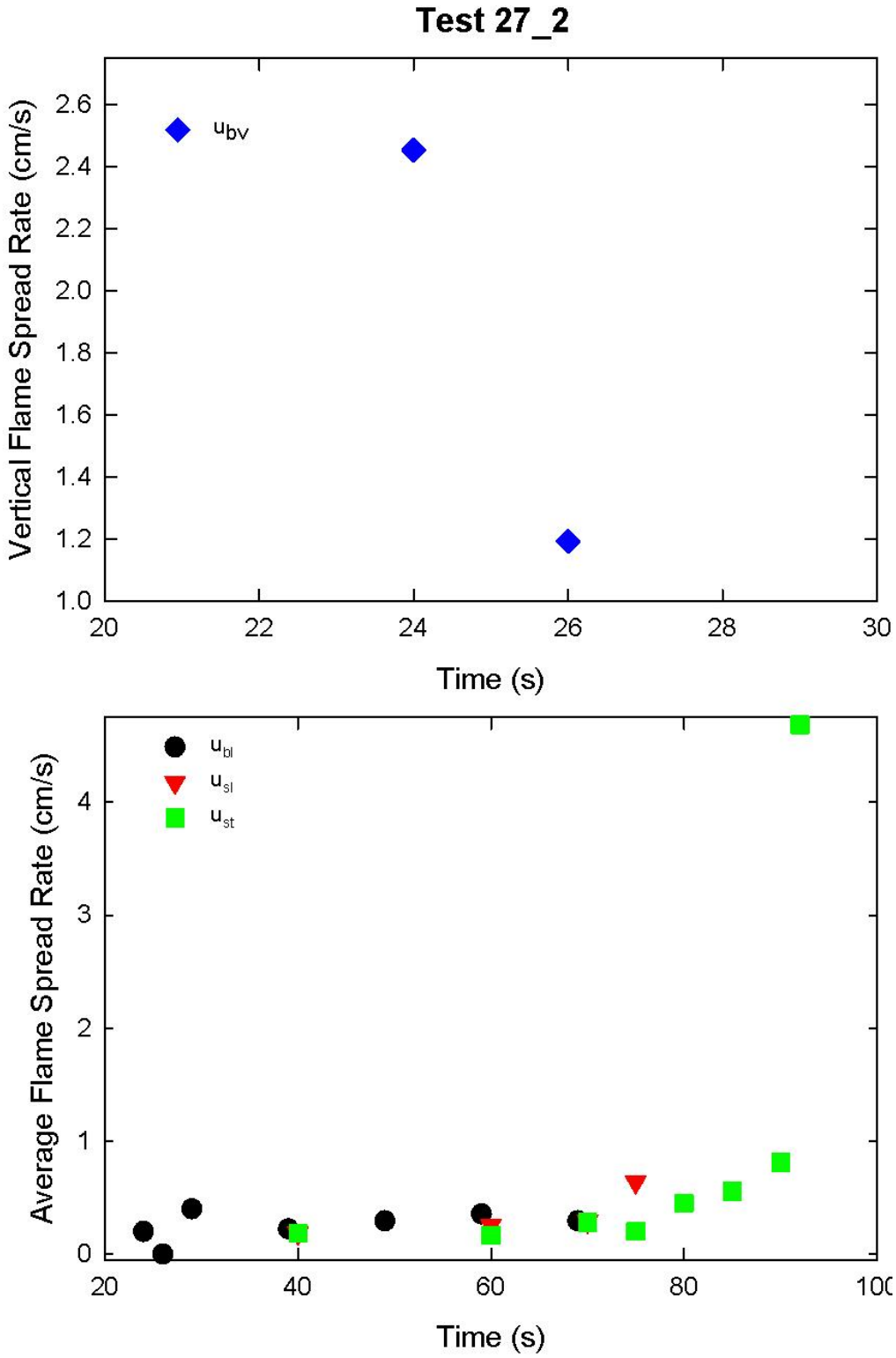

Figure C-22. Vertical flame spread rate on the back cushion (top) and average lateral flame spread rates on the back and seat cushions and transverse flame spread rate on the seat cushion (bottom) are plotted as a function of time for Test 27_2 following application of Ignition Source 1.

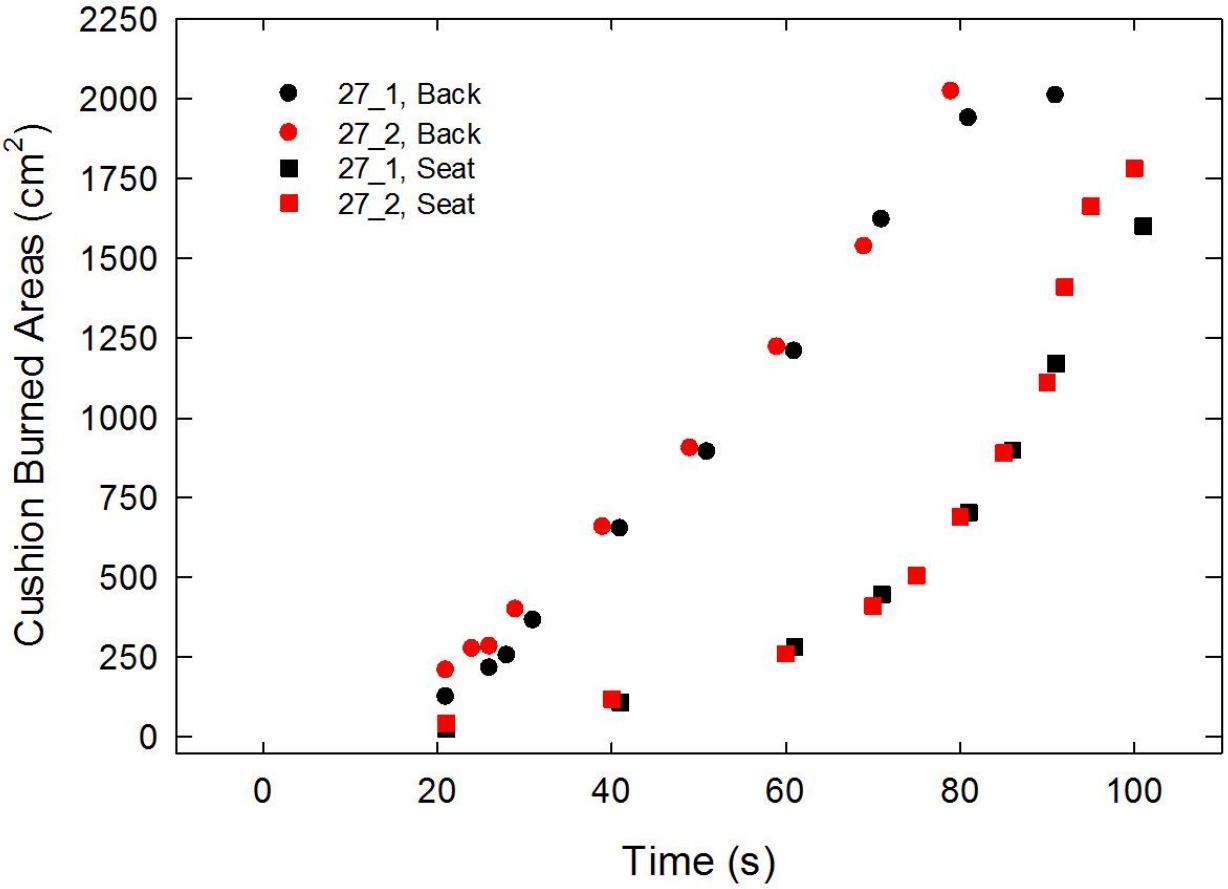

Figure C-23. Burned areas on the seat and back cushions are plotted as a function of time for Combination 27 tests following application of Ignition Source 1.

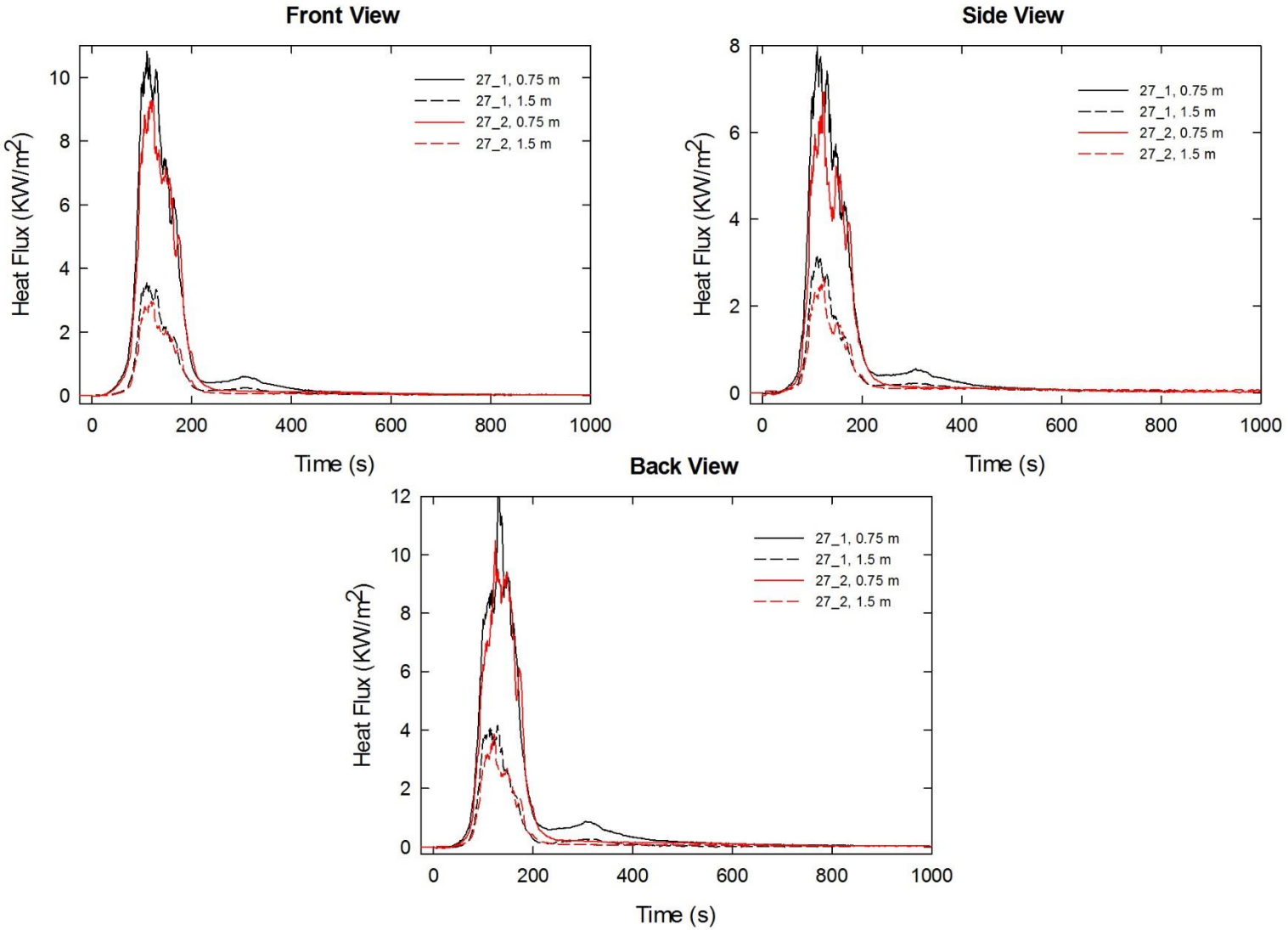

Figure C-24. Heat fluxes recorded at distances of 0.75 m and 1.5 m are plotted as a function of time for locations to the front, side and rear of the mock-up for Combination 27 tests following application of Ignition Source 1.

Appendix D Tabulated Results for Measures Characterizing Flame Spread and Growth on Supplemental Furniture Mock-ups

The following tables summarize a variety of numerical values chosen to characterize the time behaviors of flame spread and fire growth observed on the supplemental mock-ups described in Table 11. Note that tables are included for measures based on individual tests as well as for selected grouped measures.

D.1 Measures Characterizing Flame Spread Behavior

Table D-1. Tabulated measures characterizing flame spread for supplemental tests.

Test	a_{bv} cm/s^2	$\bar{u}_{bl}$ cm/s	u'_{bl} cm/s	$\bar{u}_{sl}$ cm/s	u'_{sl} cm/s	$\bar{u}_{l}$ cm/s	$\bar{u}_{st}$ cm/s	u'_{st} cm/s	$(u_{st})_{edge}$ cm/s	R_{ut}	t_{igr} s	t_{igl} s	t_{ig} s	t_{seat} s	t_{back} s
25_1	0.0407	0.306	0.138	0.311	0.210	0.308	0.291	0.087	1.32	4.53	69	75	72	98	80
26_1															
26_2															
27_1		0.292	0.161	0.343	0.096	0.313	0.342	0.166	1.20	3.50	70	78	74	90	78
27_2		0.253	0.121	0.344	0.201	0.286	0.208	0.043	0.607	2.91	72	77	74.5	91	77

Table D-2. Tabulated measures characterizing flame spread behavior for supplemental mock-up material combinations.

Combination	$\overline{a_{bv}}$ cm/s^2	a'_{bv} cm/s	$\overline{u_l}$ cm/s	u'_l cm/s	$\overline{u_t}$ cm/s	u'_t cm/s	R_u	$\overline{t_{igr}}$ s	t'_{igr} s	$\overline{t_{igl}}$ s	t'_{igl} s	$\overline{t_{ig}}$ s	t'_{ig} s	$\overline{t_{seat}}$ s	t'_{seat} s	$\overline{t_{back}}$ s	t'_{back} s
25	0.0407		0.308	0.291	0.291		4.53	69		75		72		98		80	
26																	
27			0.300	0.019	0.275	0.95	3.21	71.0	1.4	77.5	0.71	74.3	0.35	90.5	0.7	77.5	0.7

D.2 Measures Characterizing HRR Temporal Profiles

Table D-3. Tabulated measures characterizing HRR temporal profiles for individual tests.

Test	t_{+25} (s)	t_{peak1} (s)	HRR_{peak1} (kW)	t_{max} (s)	HRR_{max} (kW)	t_{-25} (s)	$t_{>25}$ (s)	$Q_{>25}$ (MJ)	$HRR_{avg>25}$ (kW)	$FWHM_{>25}$ (s)	SF_t	SF_{HRR}	Q_{tot} (MJ)
25_1	74	106	276	106	276	1117	1043	55.5	52.8	34	.033	.191	64.4
26_1													
26_2													
27_1	60	113	472	113	472	344	284	39.4	138.7	78	0.275	0.294	42.1
27_2	62	124	404	124	404	219	157	31.2	198.7	70	0,446	0.493	35.5

Table D-4. Tabulated measures characterizing HRR behavior for mock-up material combinations.

Combination	$\overline{t_{+25}}$ (s)	t'_{+25} (s)	$\overline{t_{peak1}}$ (s)	t'_{peak1} (s)	$\overline{HRR_{peak1}}$ (kW)	HRR'_{peak1} (kW)	$\overline{t_{max}}$ (s)	t'_{max} (s)	$\overline{HRR_{max}}$ (kW)	HRR'_{max} (kW)	$\overline{Q_{tot}}$ (MJ)	Q'_{tot} (MJ)
25	74		106		276		106		276		64.5	
26									9.2	1.6	0.4	0
27	61.0	1.4	118.5	7.8	438	48	118.5	7.8	438	48	38.8	4.7

D.3 Measures Characterizing FIGRA Temporal Profiles

Table D-5. Tabulated measures characterizing FIGRA temporal profiles for individual tests.

Test	t_{FIGRA1} (s)	$FIGRA_{peak1}$ (kW/s)	$t_{FIGRAmax}$ (s)	$FIGRA_{max}$ (kW/s)
25_1	105	2.62	105	2.62
26_1				
26_2				
27_1	113	4.18	113	4.18
27_2	116	3.45	116	3.45

Table D-6. Tabulated measures characterizing FIGRA behavior for mock-up material combinations.

Combination	$\overline{t_{FIGRA1}}$ (s)	t'_{FIGRA1} (s)	$\overline{FIGRA_{peak1}}$ (kW/s)	$FIGRA'_{peak1}$ (kW/s)	$\overline{t_{FIGRAmax}}$ (s)	$t'_{FIGRAmax}$ (s)	$\overline{FIGRA_{max}}$ (kW/s)	$FIGRA'_{max}$ (kW/s)
25	105		2.62		105		2.62	
26								
27	114.5	2.1	3.82	0.51	114.5	2.1	3.82	0.51

Appendix E Block Plots for Statistical Analysis

Block plots for all 13 responses and five-factor combinations are shown. These plots are part of the statistical analyses included in Section 7.2 and Section 7.3.

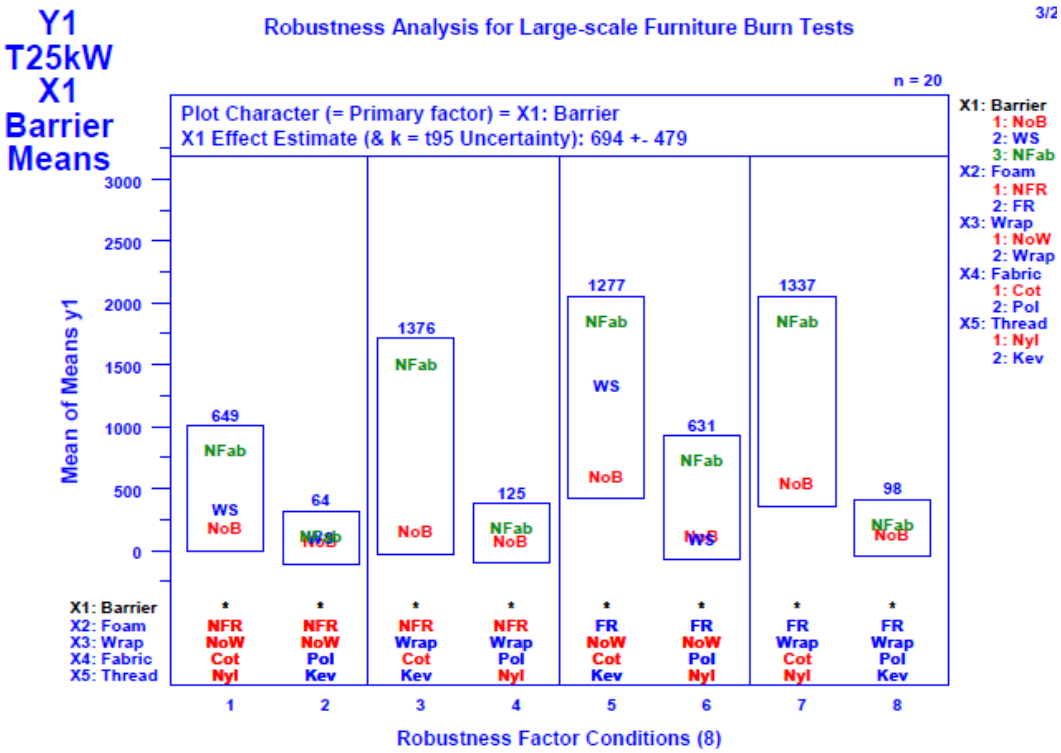

Figure E-1.Robustness Analysis: Mean Response vs. Robustness Factor Combination for Response Y1 = T25kW and Primary Factor X1 = Barrier.

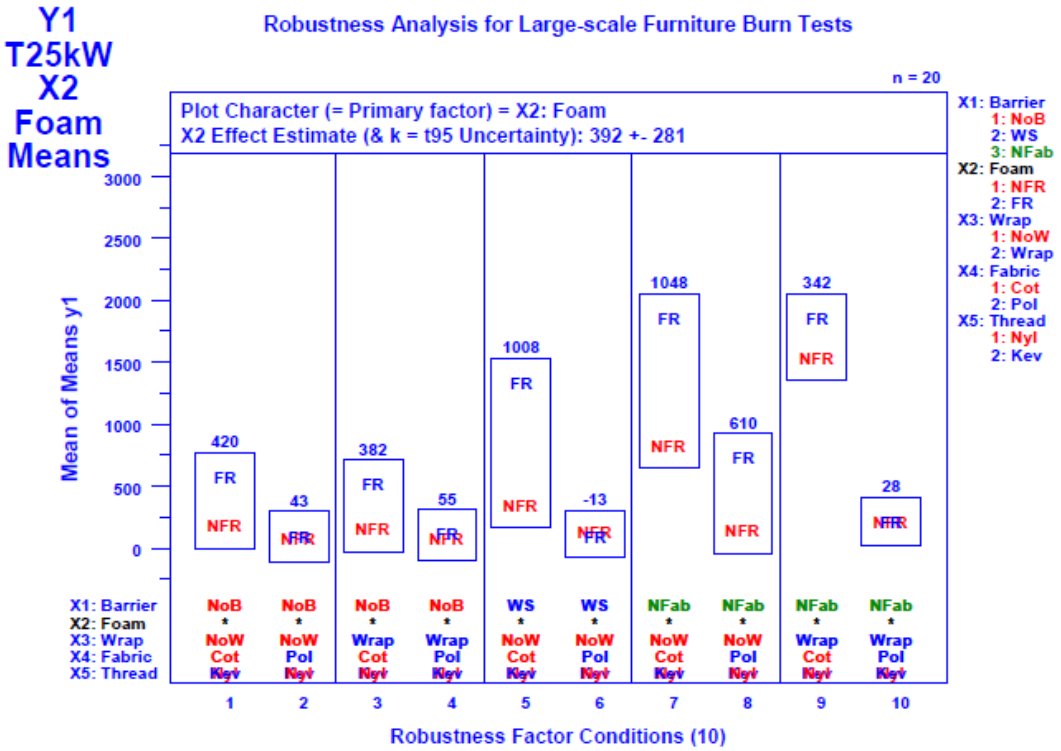

Figure E-2. Robustness Analysis: Mean Response vs. Robustness Factor Combination for Response Y1 = T25kW and Primary Factor X2 = Foam.

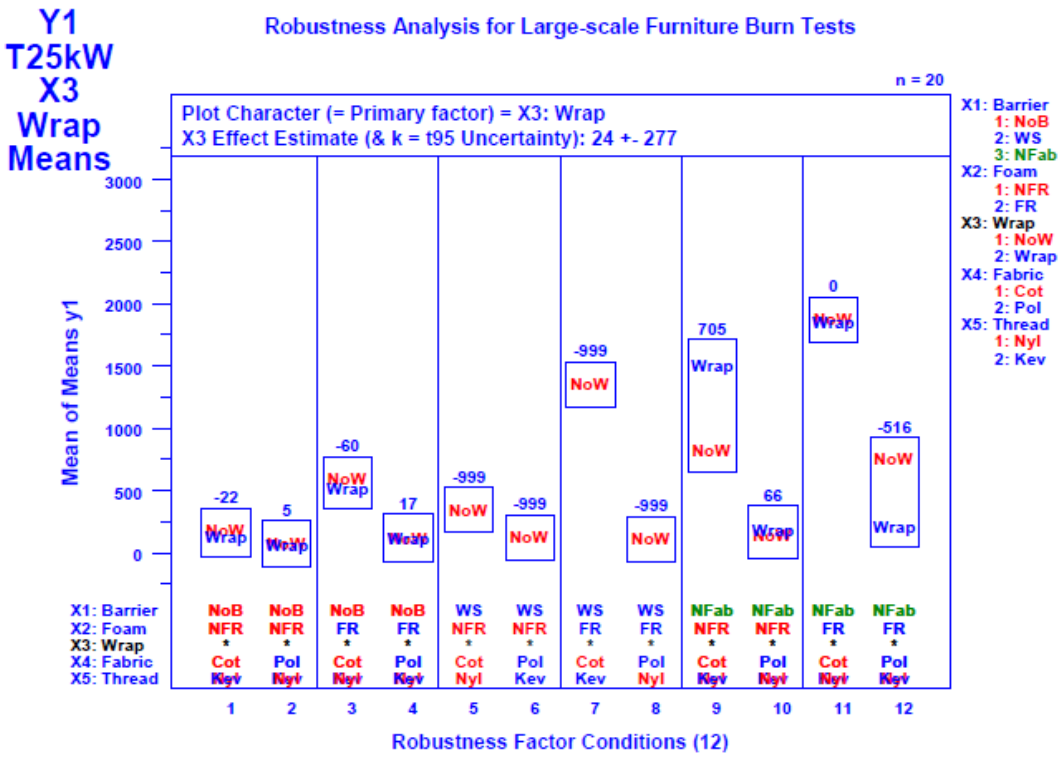

Figure E-3. Robustness Analysis: Mean Response vs. Robustness Factor Combination for Response Y1 = T25kW and Primary Factor X3 = Wrap.

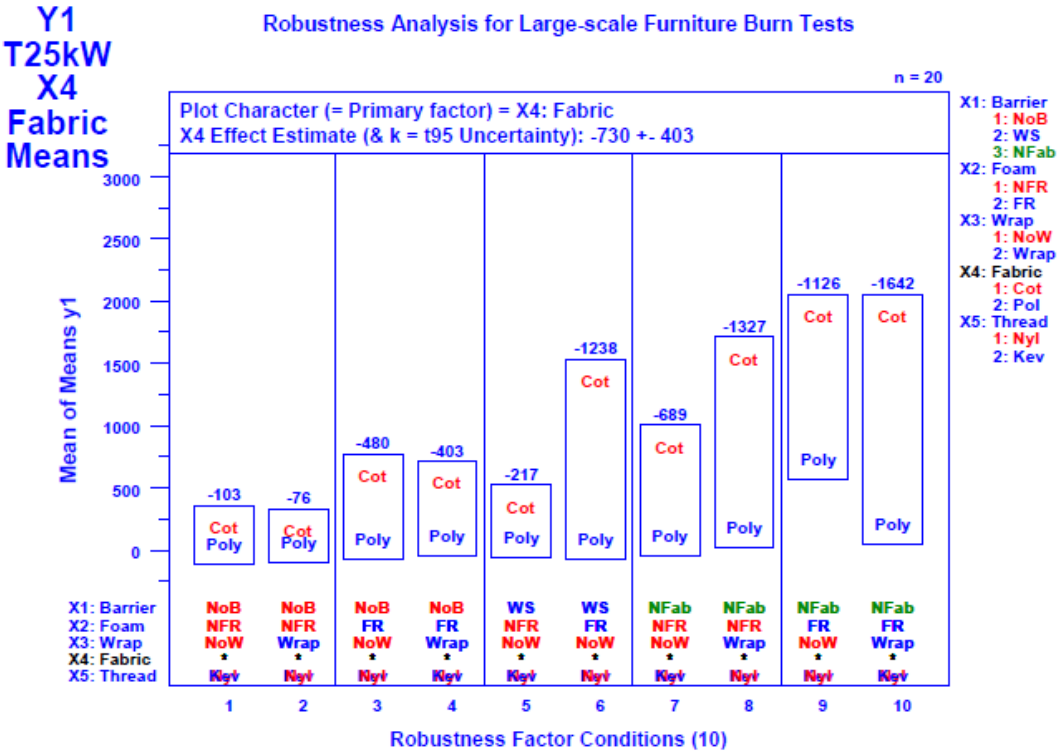

Figure E-4. Robustness Analysis: Mean Response vs. Robustness Factor Combination for Response Y1 = T25kW and Primary Factor X4 = Fabric.

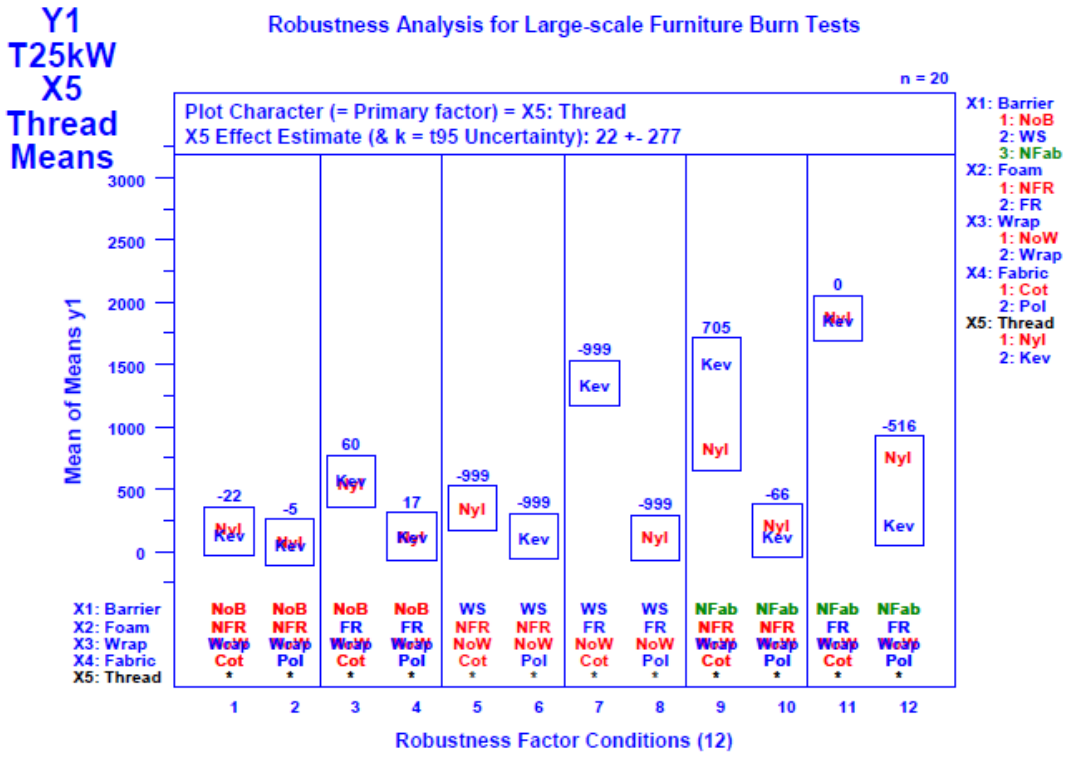

Figure E-5. Robustness Analysis: Mean Response vs. Robustness Factor Combination for Response Y1 = 25kW and Primary Factor X5 = Thread.

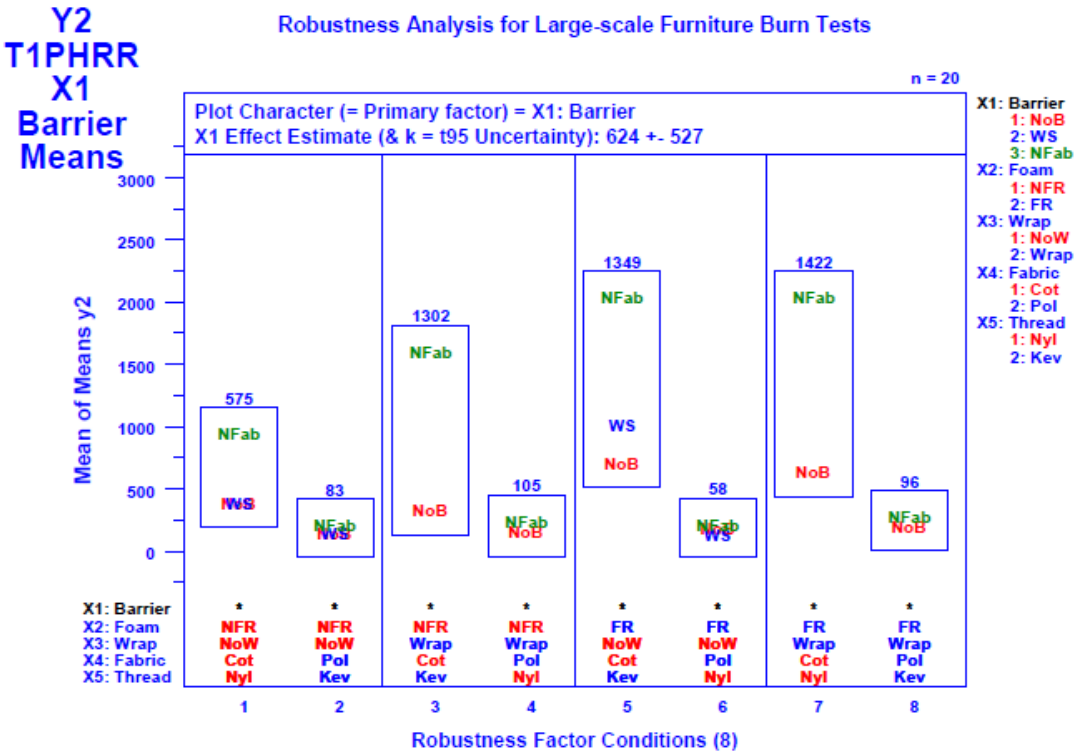

Figure E-6. Robustness Analysis: Mean Response vs. Robustness Factor Combination for Response Y2 = T1PHRR and Primary Factor X1 = Barrier.

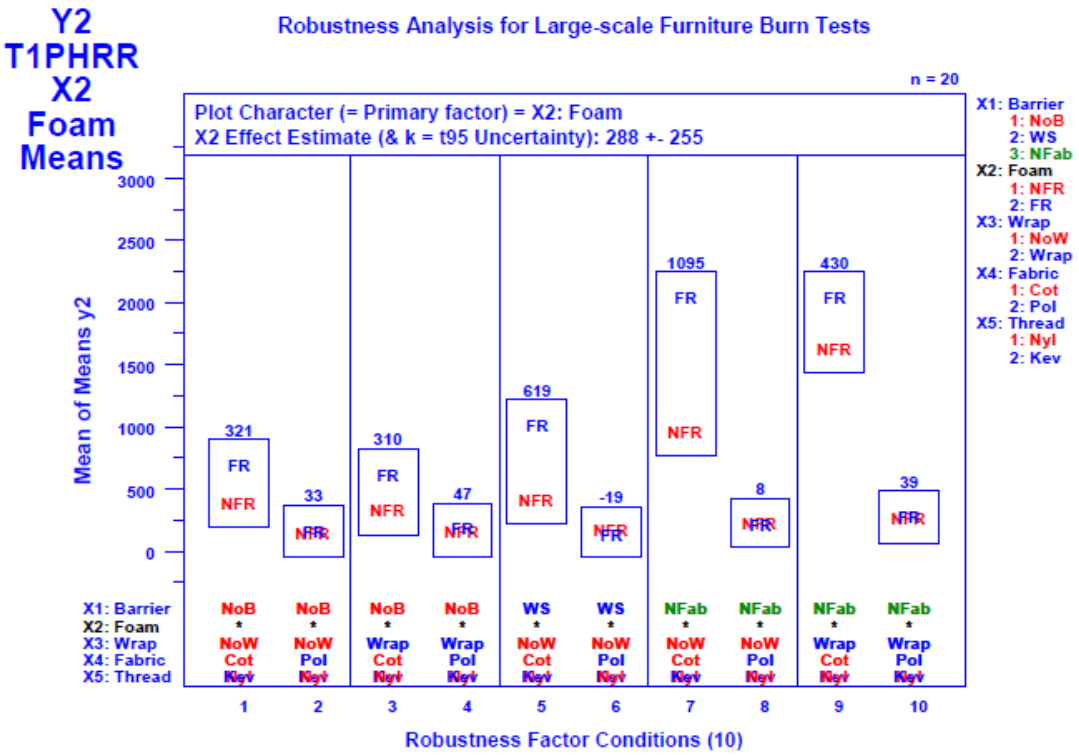

Figure E-7. Robustness Analysis: Mean Response vs. Robustness Factor Combination for Response Y2 = T1PHRR and Primary Factor X2 = Foam.

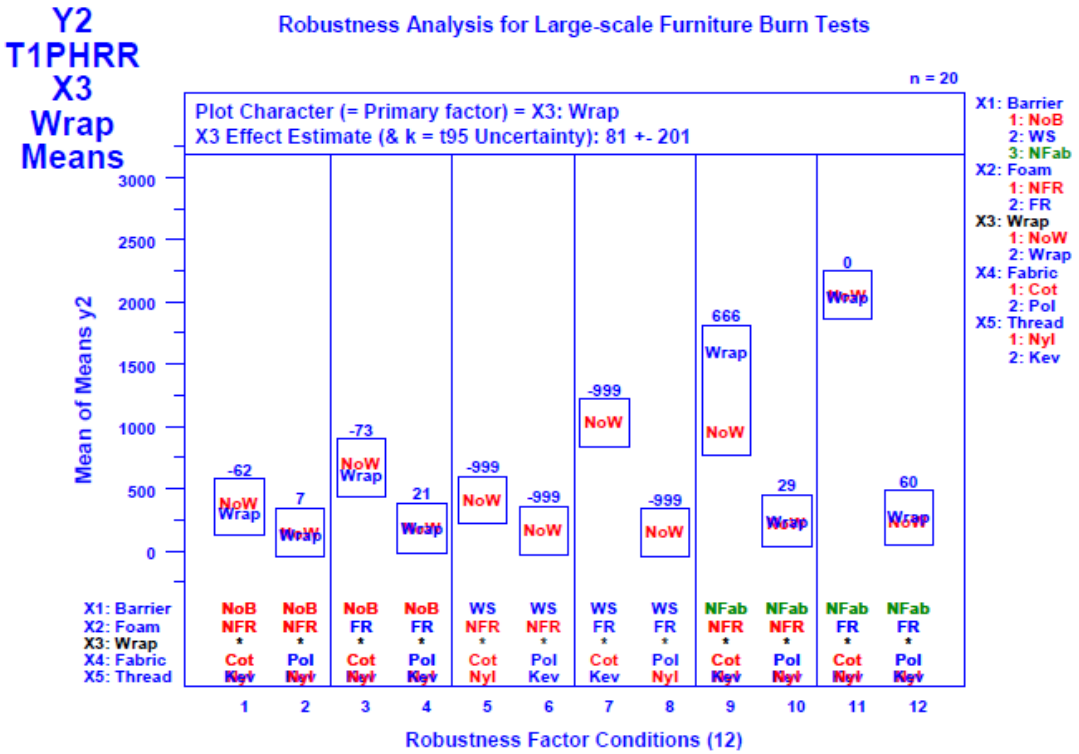

Figure E-8. Robustness Analysis: Mean Response vs. Robustness Factor Combination for Response Y2 = T1PHRR and Primary Factor X3 = Wrap.

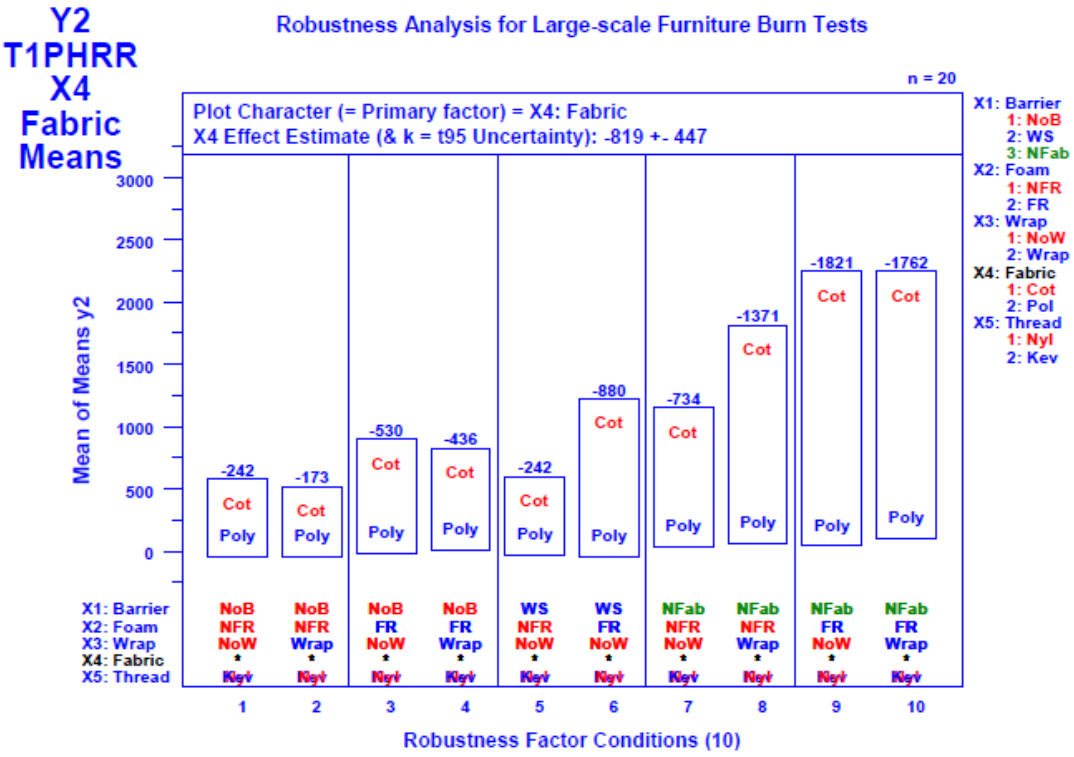

Figure E-9. Robustness Analysis: Mean Response vs. Robustness Factor Combination for Response Y2 = T1PHRR and Primary Factor X4 = Fabric.

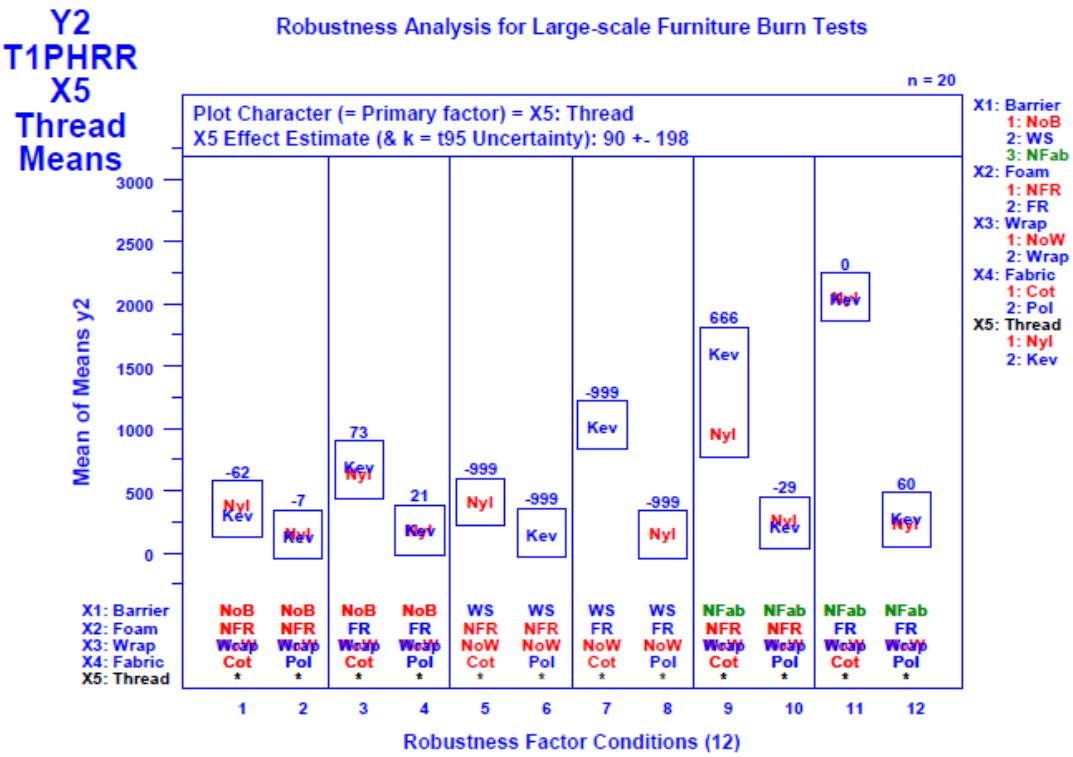

Figure E-10. Robustness Analysis: Mean Response vs. Robustness Factor Combination for Response Y2 = T1PHRR and Primary Factor X5 = Thread.

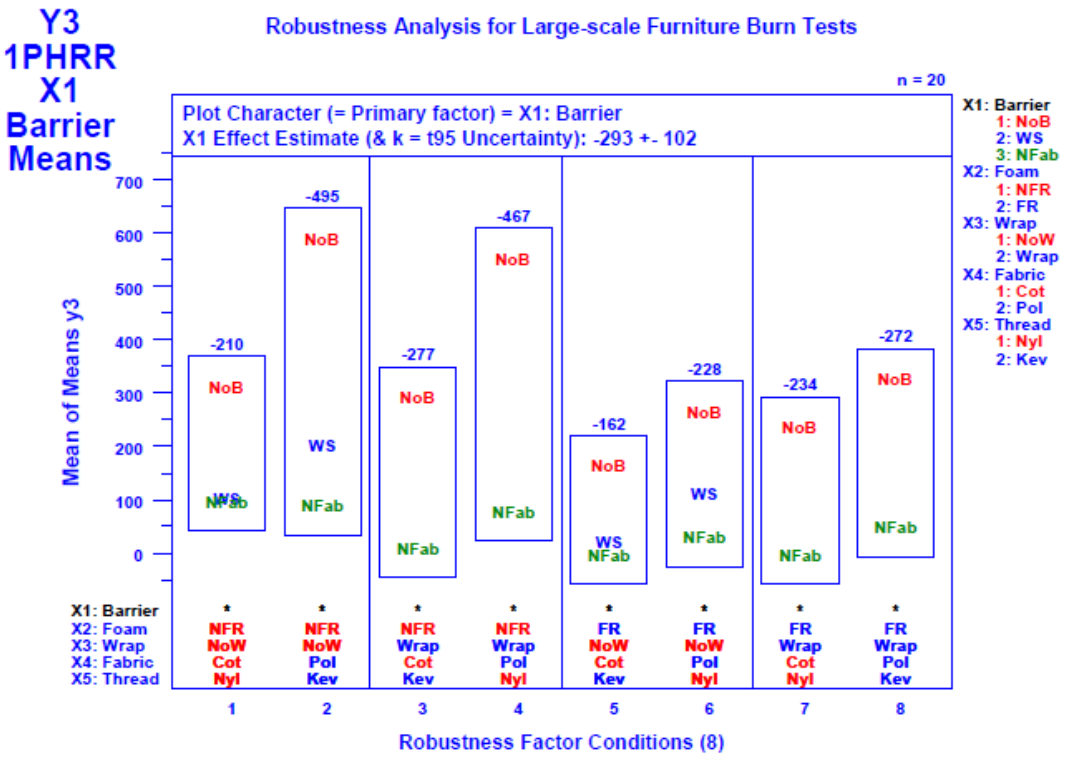

Figure E-11. Robustness Analysis: Mean Response vs. Robustness Factor Combination for Response Y3 = 1PHRR and Primary Factor X1 = Barrier.

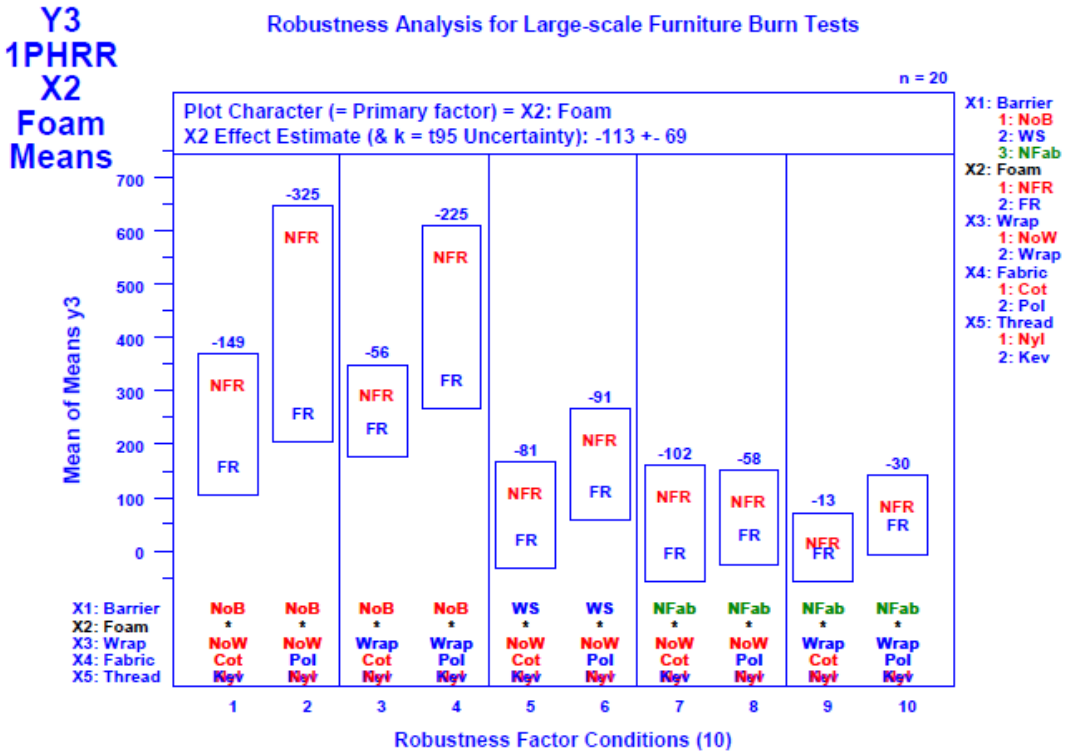

Figure E-12. Robustness Analysis: Mean Response vs. Robustness Factor Combination for Response Y3 = 1PHRR and Primary Factor X2 = Foam.

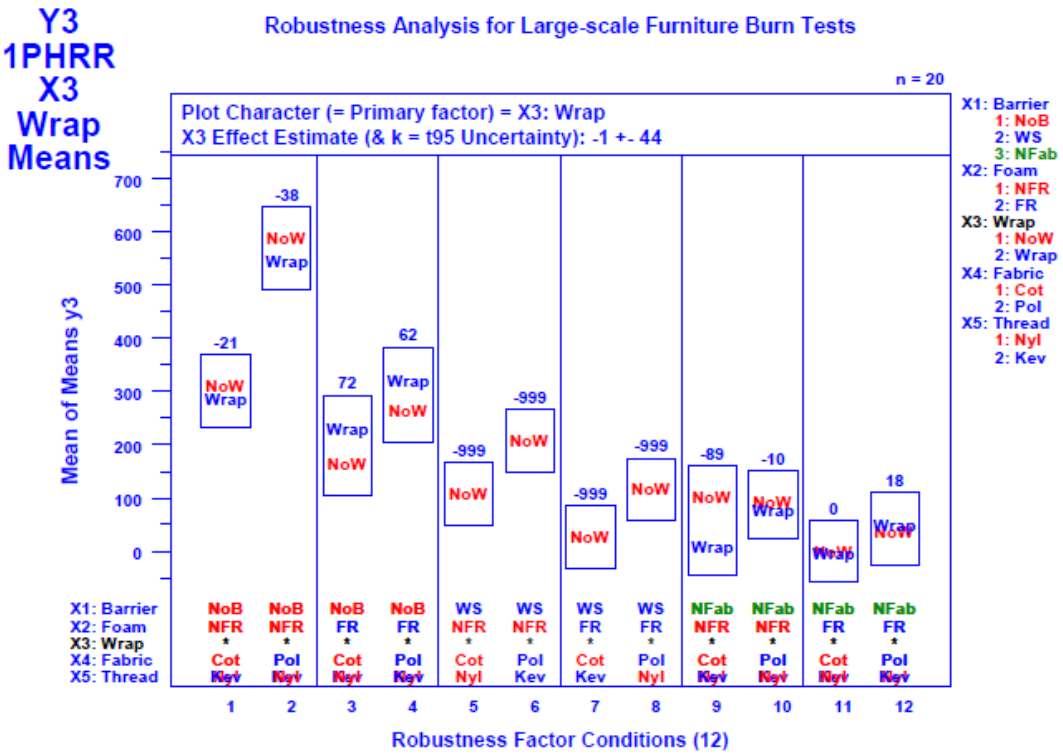

Figure E-13. Robustness Analysis: Mean Response vs. Robustness Factor Combination for Response Y3 = 1PHRR and Primary Factor X3 = Wrap.

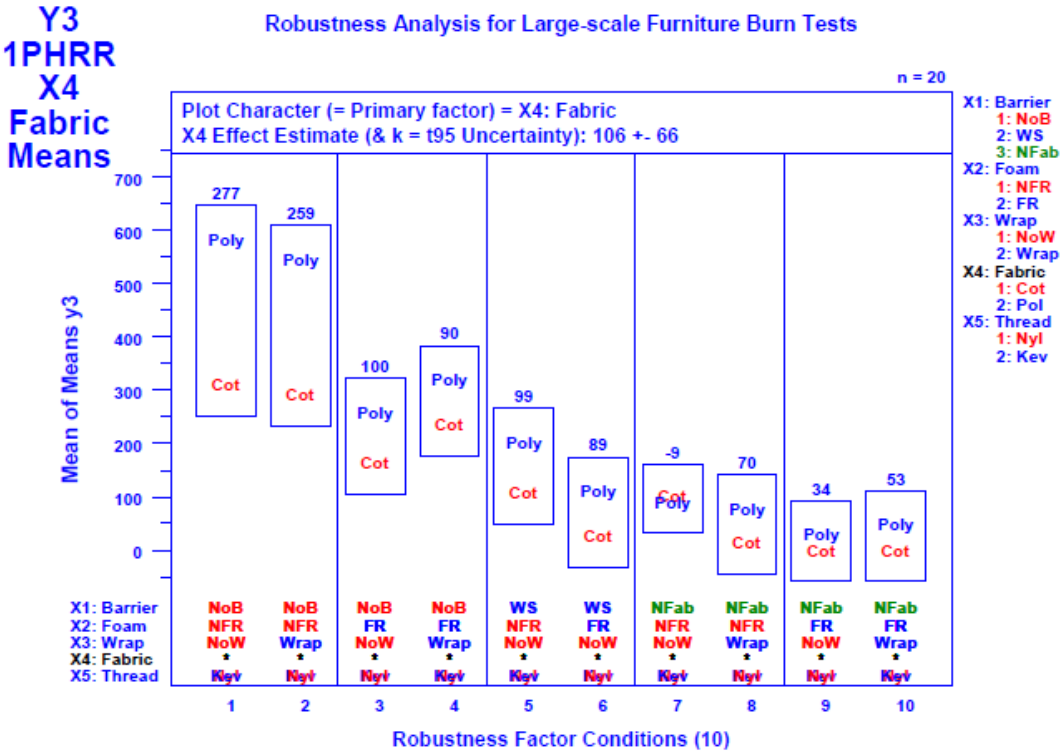

Figure E-14. Robustness Analysis: Mean Response vs. Robustness Factor Combination for Response Y3 = 1PHRR and Primary Factor X4 = Fabric.

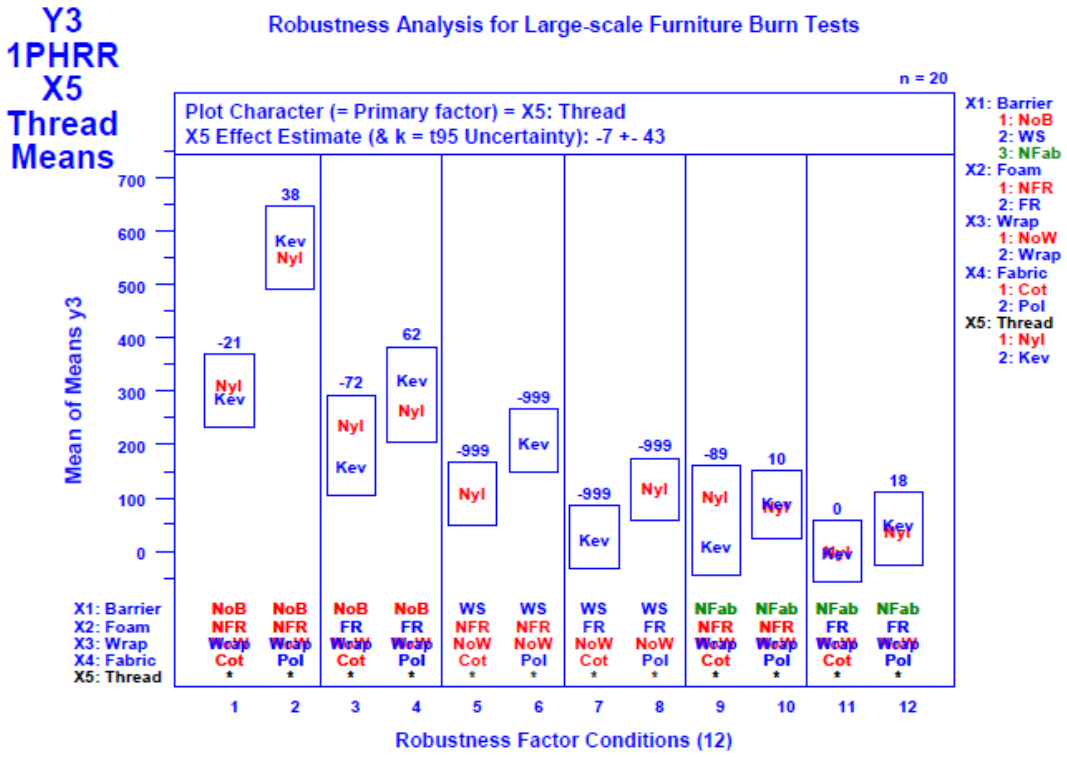

Figure E-15. Robustness Analysis: Mean Response vs. Robustness Factor Combination for Response Y3 = 1PHRR and Primary Factor X5 = Thread.

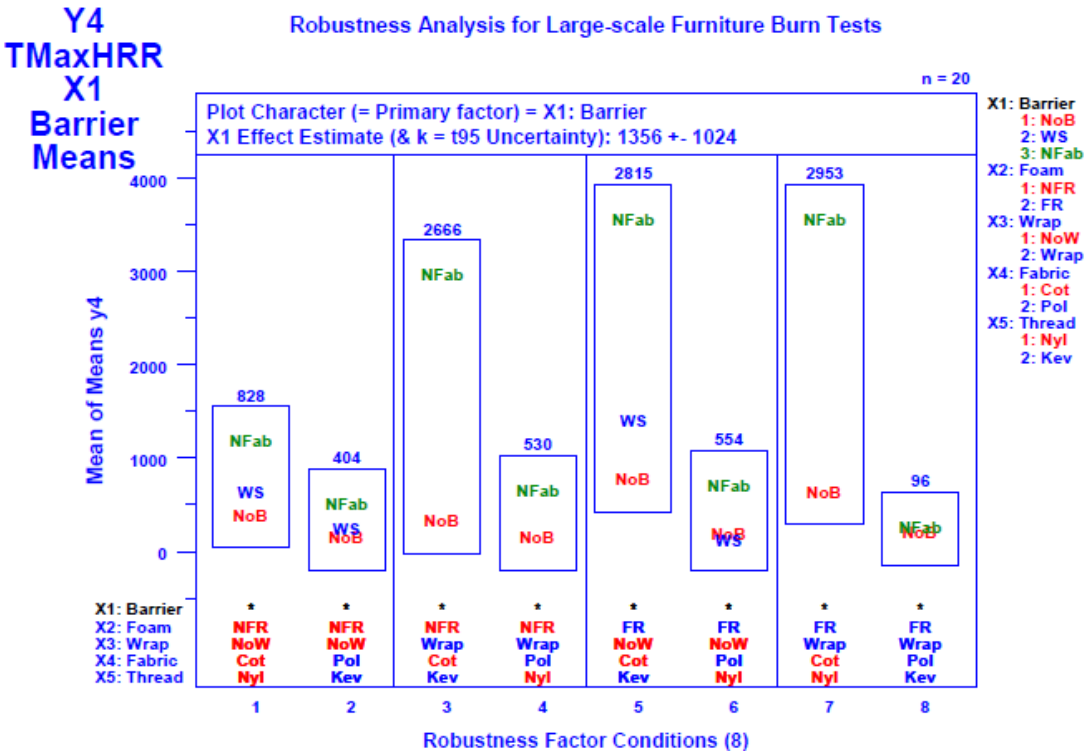

Figure E-16. Robustness Analysis: Mean Response vs. Robustness Factor Combination for Response Y4 = TMaxHRR and Primary Factor X1 = Barrier.

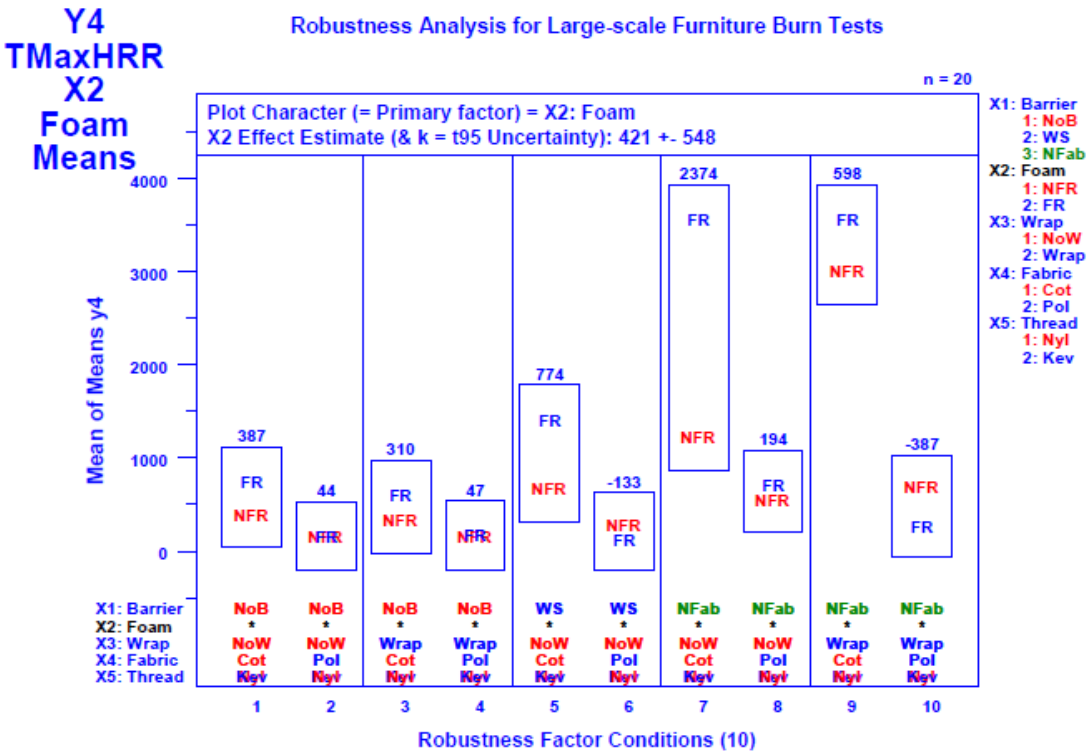

Figure E-17. Robustness Analysis: Mean Response vs. Robustness Factor Combination for Response Y4 = TMaxHRR and Primary Factor X2 = Foam.

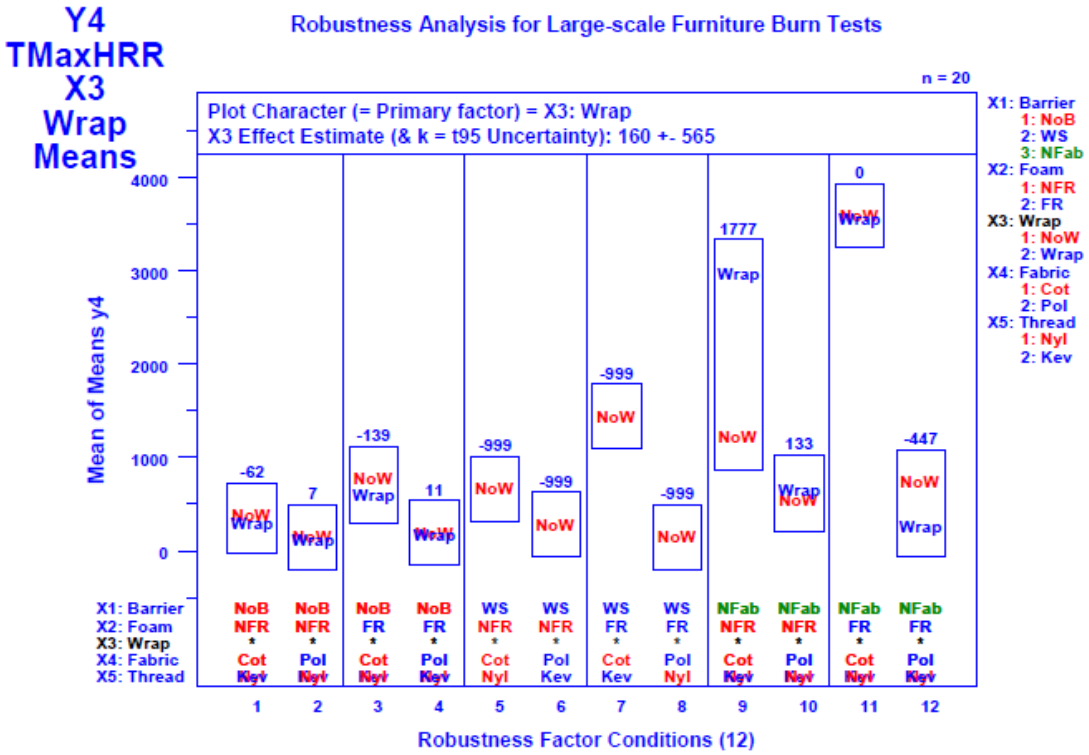

Figure E-18. Robustness Analysis: Mean Response vs. Robustness Factor Combination for Response Y4 = TMaxHRR and Primary Factor X3 = Wrap.

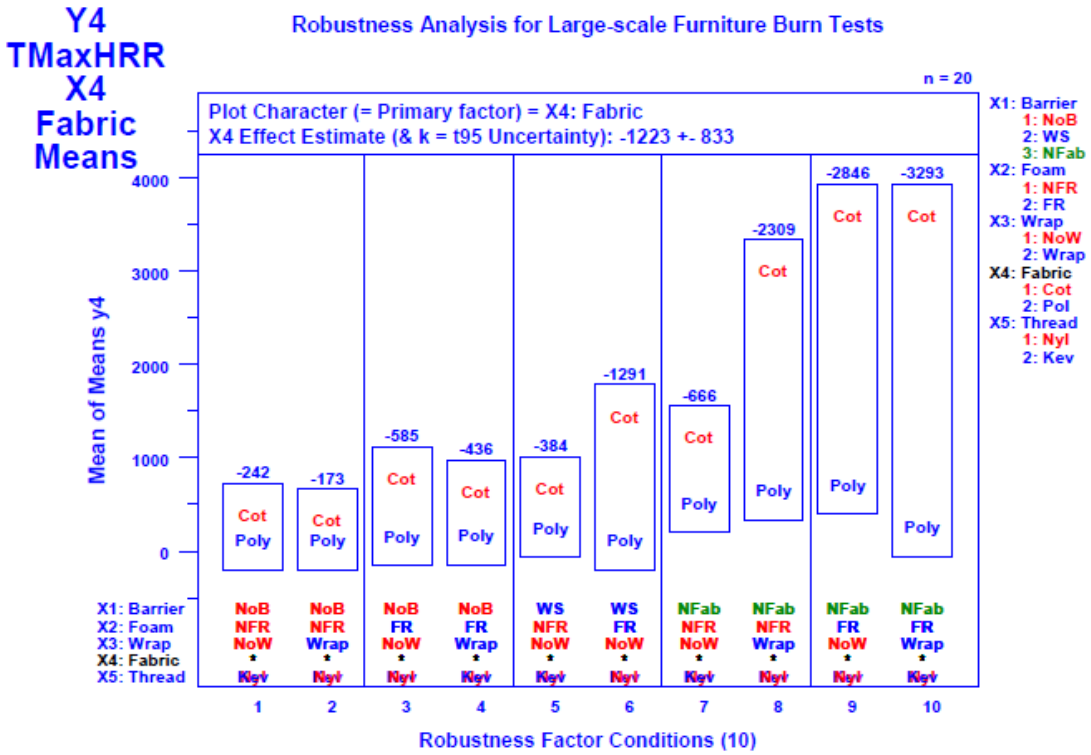

Figure E-19. Robustness Analysis: Mean Response vs. Robustness Factor Combination for Response Y4 = TMaxHRR and Primary Factor X4 = Fabric.

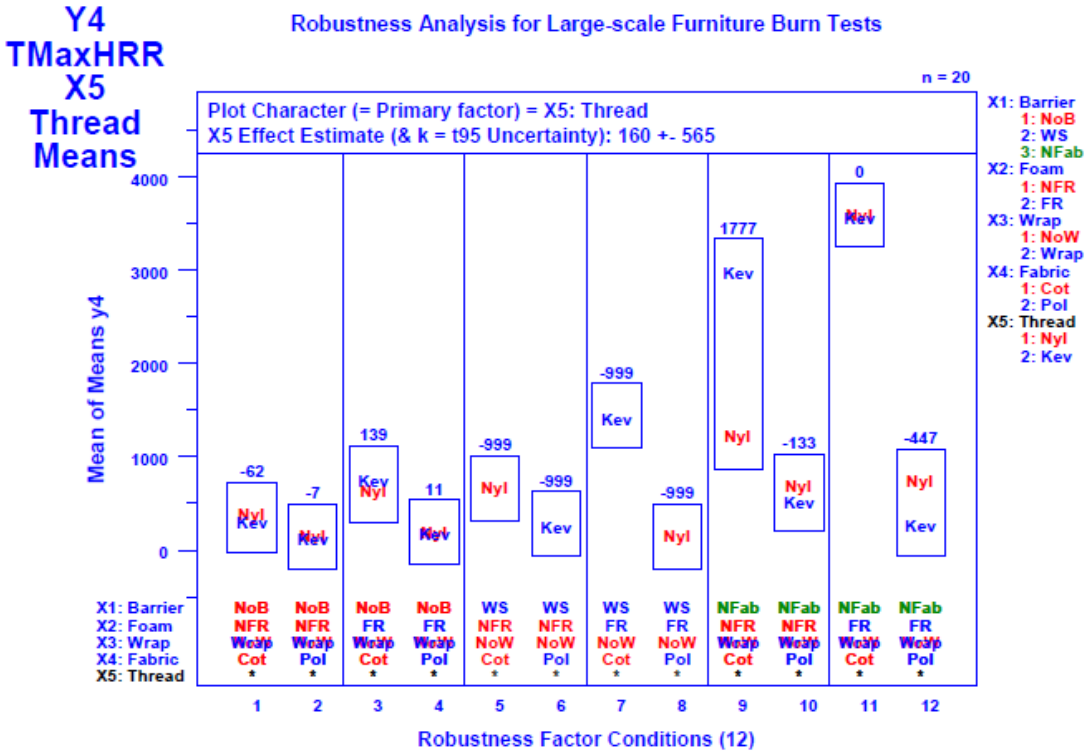

Figure E-20. Robustness Analysis: Mean Response vs. Robustness Factor Combination for Response Y4 = TMaxHRR and Primary Factor X5 = Thread.

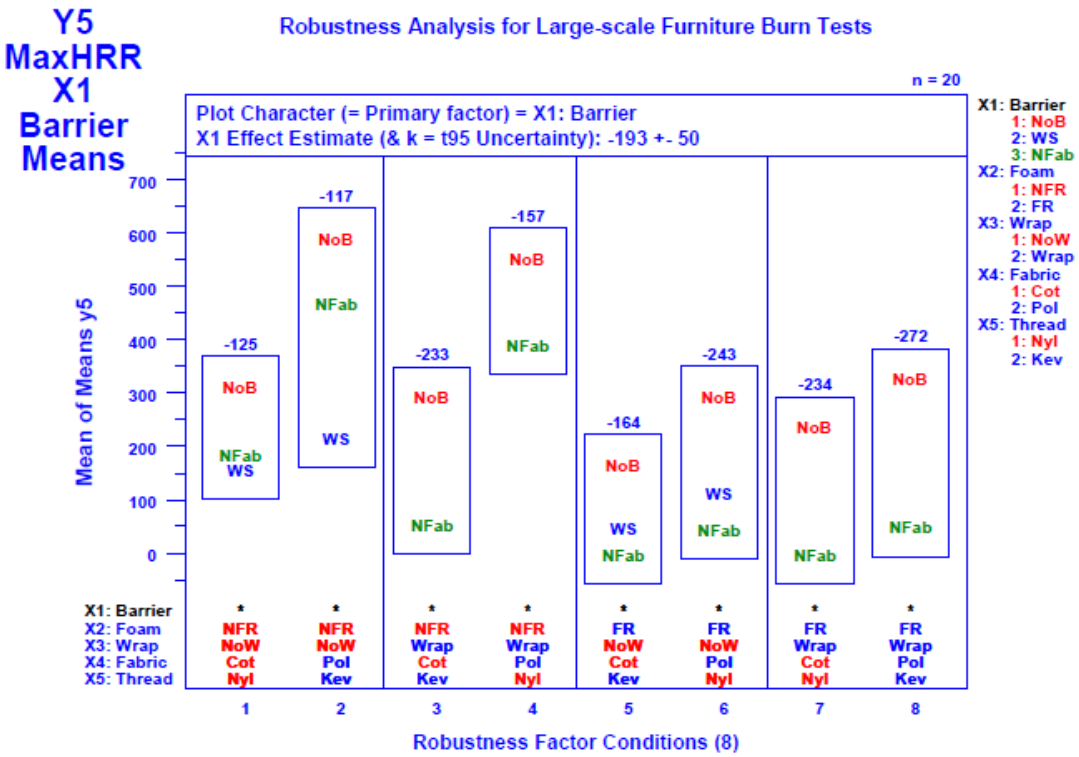

Figure E-21. Robustness Analysis: Mean Response vs. Robustness Factor Combination for Response Y5 = MaxHRR and Primary Factor X1 = Barrier.

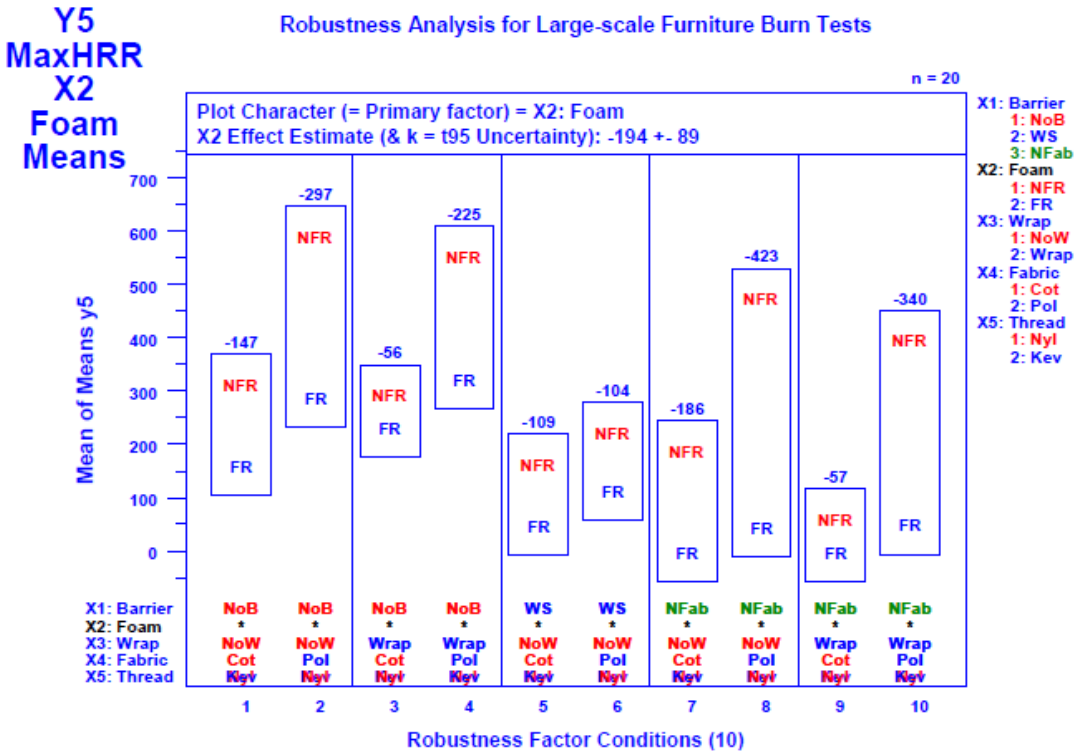

Figure E-22. Robustness Analysis: Mean Response vs. Robustness Factor Combination for Response Y5 = MaxHRR and Primary Factor X2 = Foam.

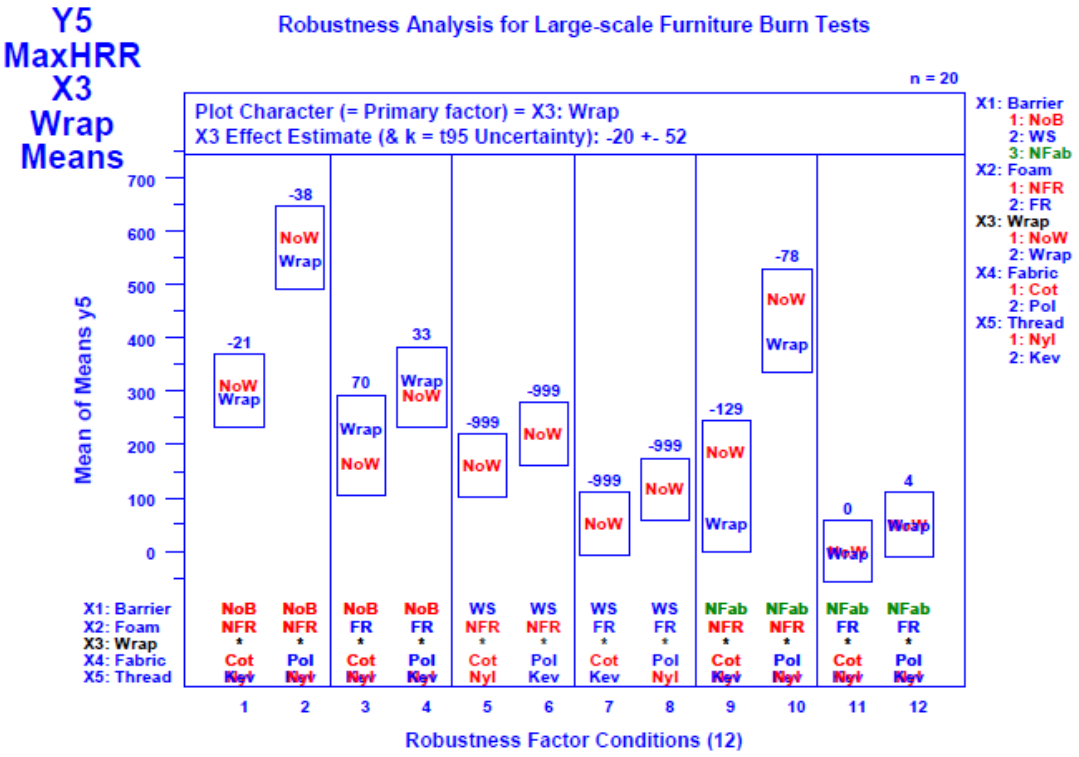

Figure E-23. Robustness Analysis: Mean Response vs. Robustness Factor Combination for Response Y5 = MaxHRR and Primary Factor X3 = Wrap.

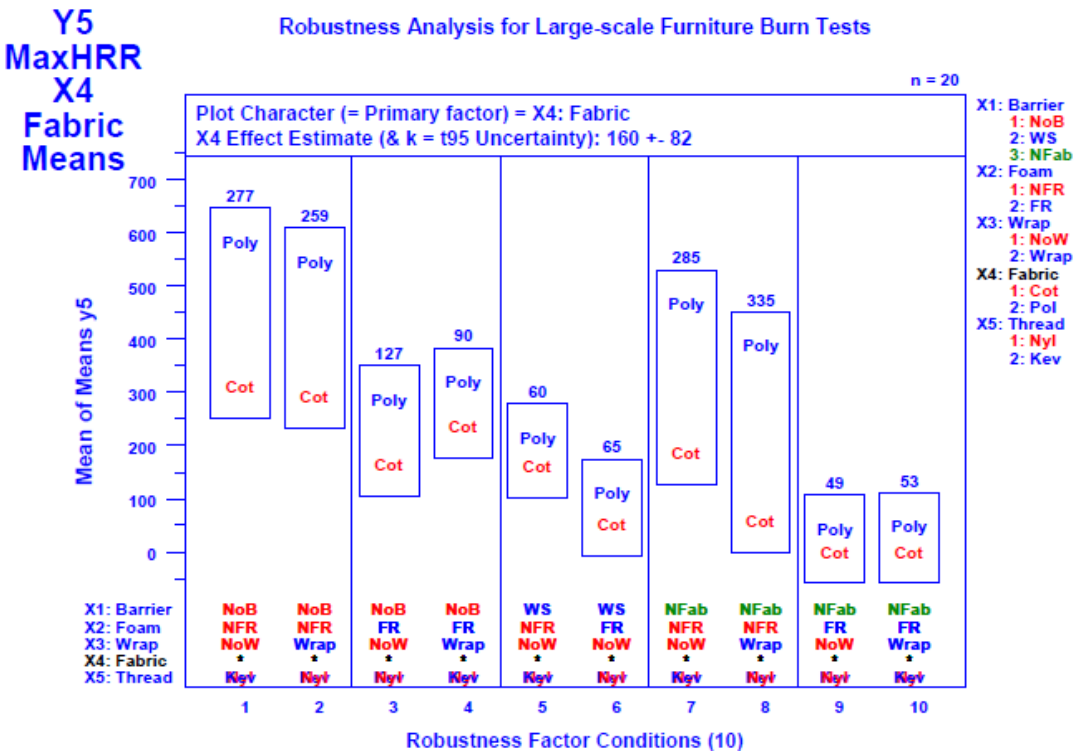

Figure E-24. Robustness Analysis: Mean Response vs. Robustness Factor Combination for Response Y5 = MaxHRR and Primary Factor X4 = Fabric.

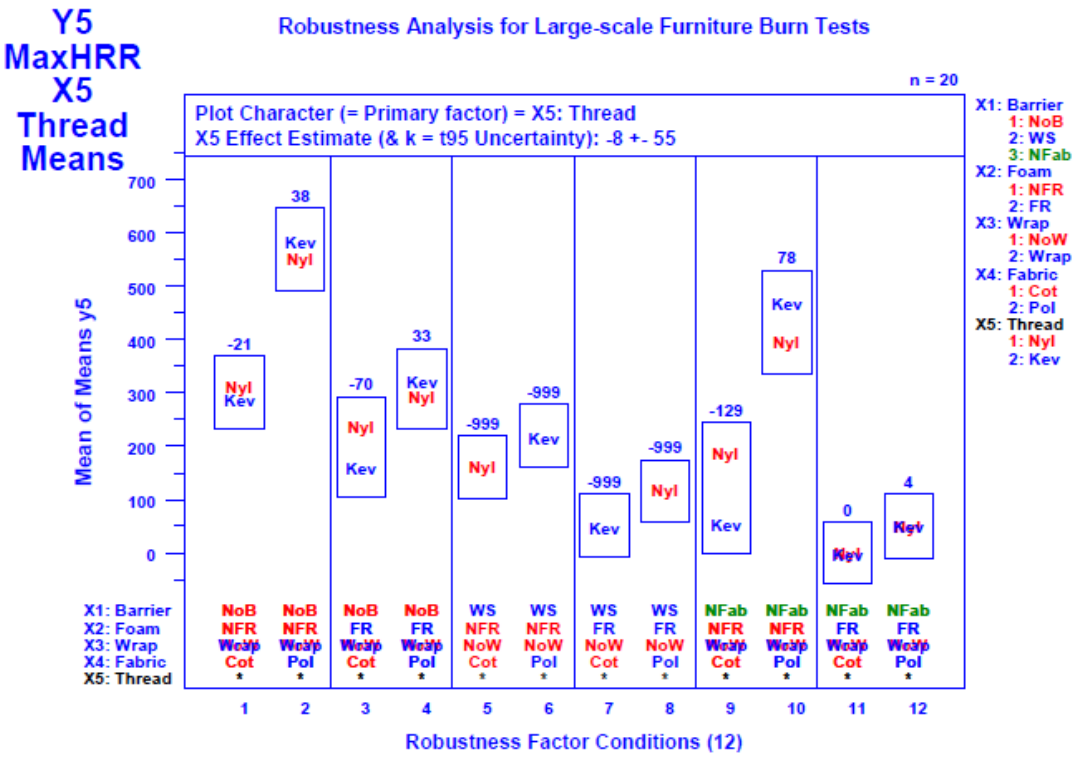

Figure E-25. Robustness Analysis: Mean Response vs. Robustness Factor Combination for Response Y5 = MaxHRR and Primary Factor X5 = Thread.

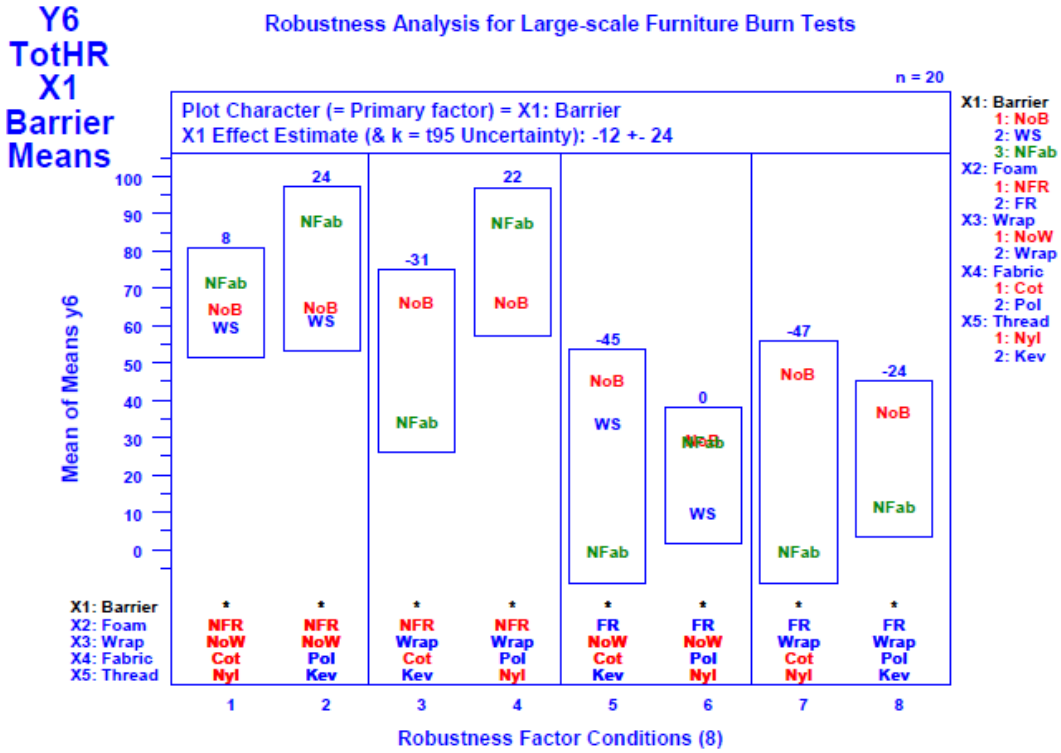

Figure E-26. Robustness Analysis: Mean Response vs. Robustness Factor Combination for Response Y6 = TotHR and Primary Factor X1 = Barrier.

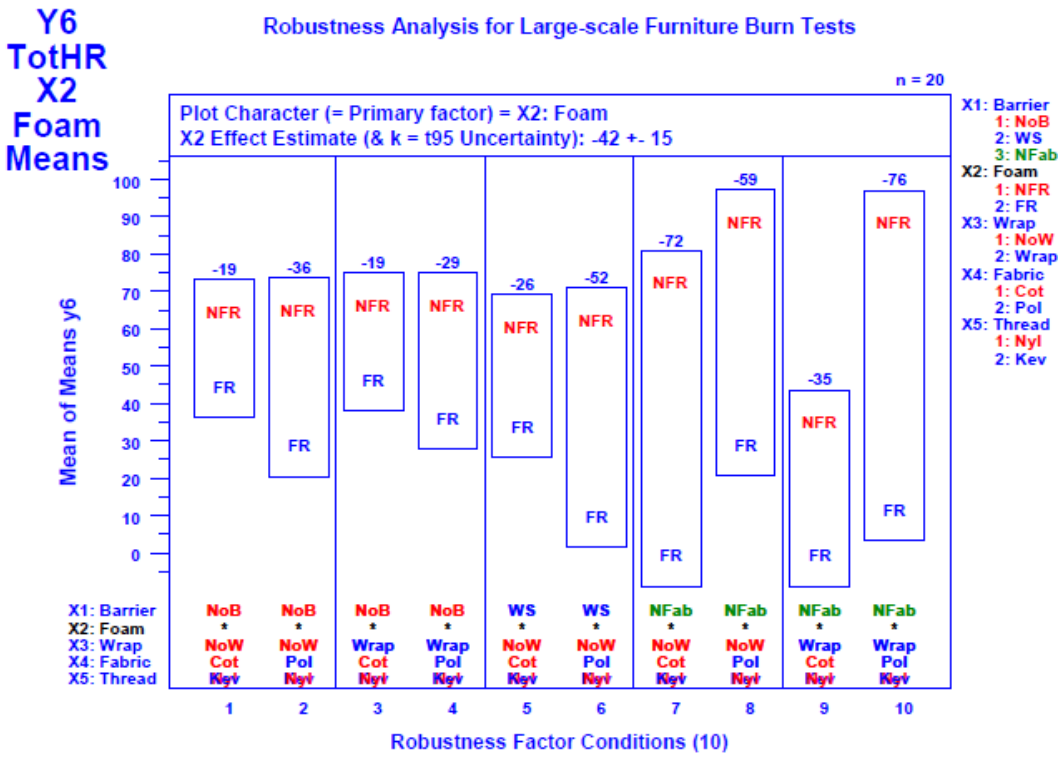

Figure E-27. Robustness Analysis: Mean Response vs. Robustness Factor Combination for Response Y6 = TotHR and Primary Factor X2 = Foam.

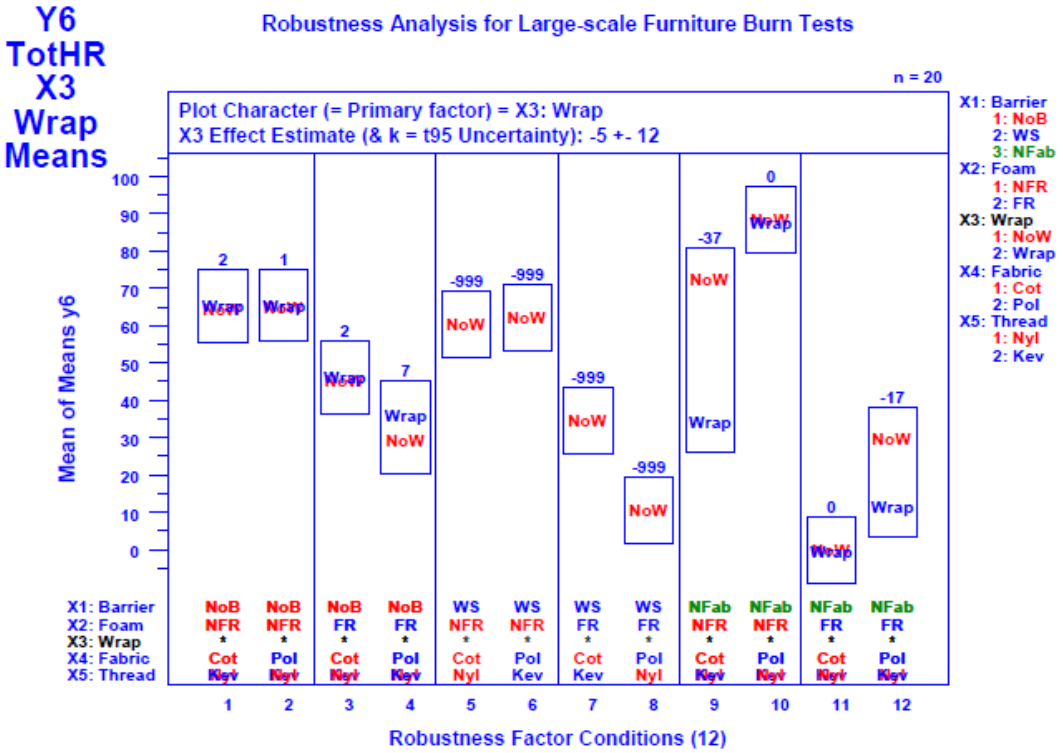

Figure E-28. Robustness Analysis: Mean Response vs. Robustness Factor Combination for Response Y6 = TotHR and Primary Factor X3 = Wrap.

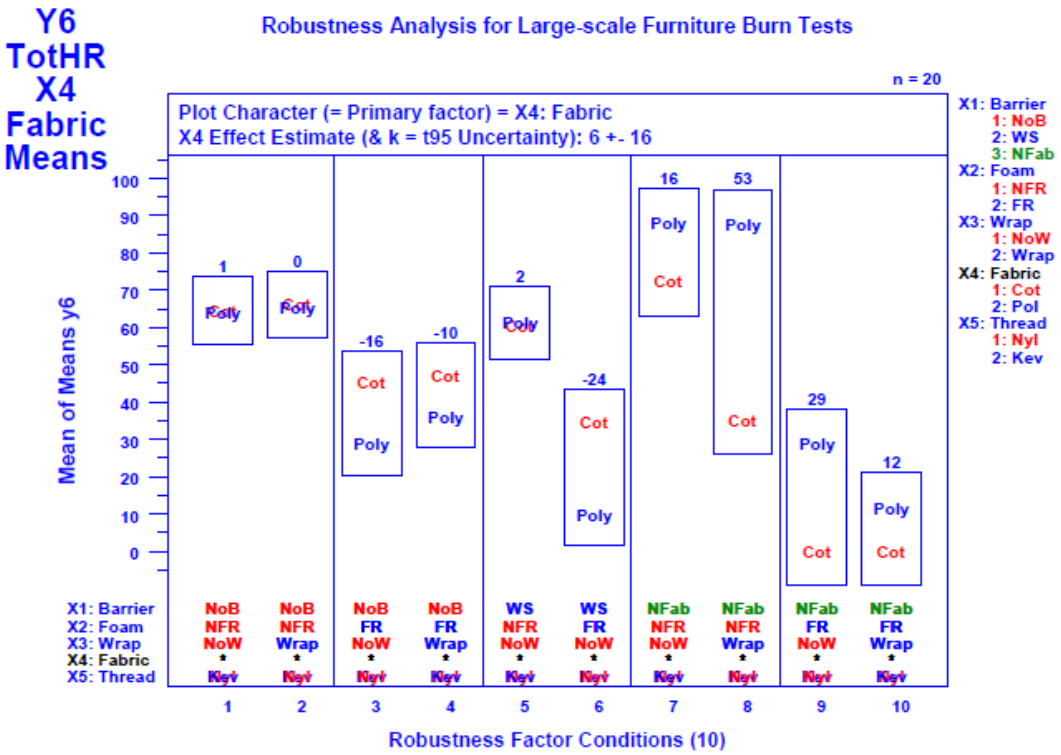

Figure E-29. Robustness Analysis: Mean Response vs. Robustness Factor Combination for Response Y6 = TotHR and Primary Factor X4 = Fabric.

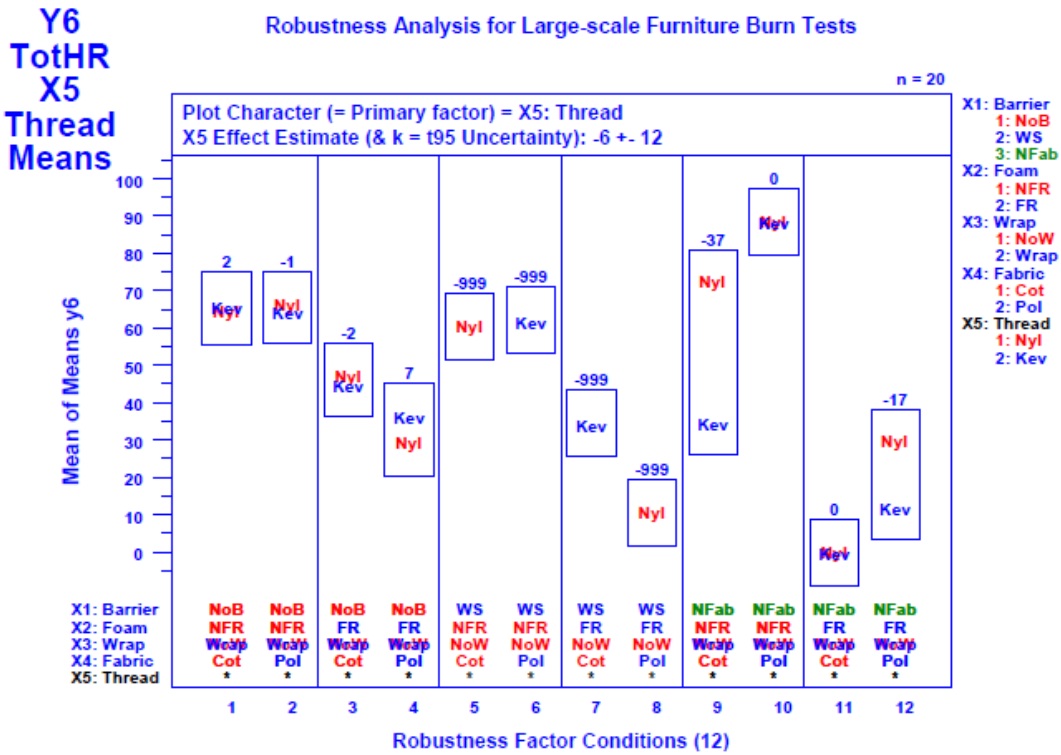

Figure E-30. Robustness Analysis: Mean Response vs. Robustness Factor Combination for Response Y6 = TotHR and Primary Factor X5 = Thread.

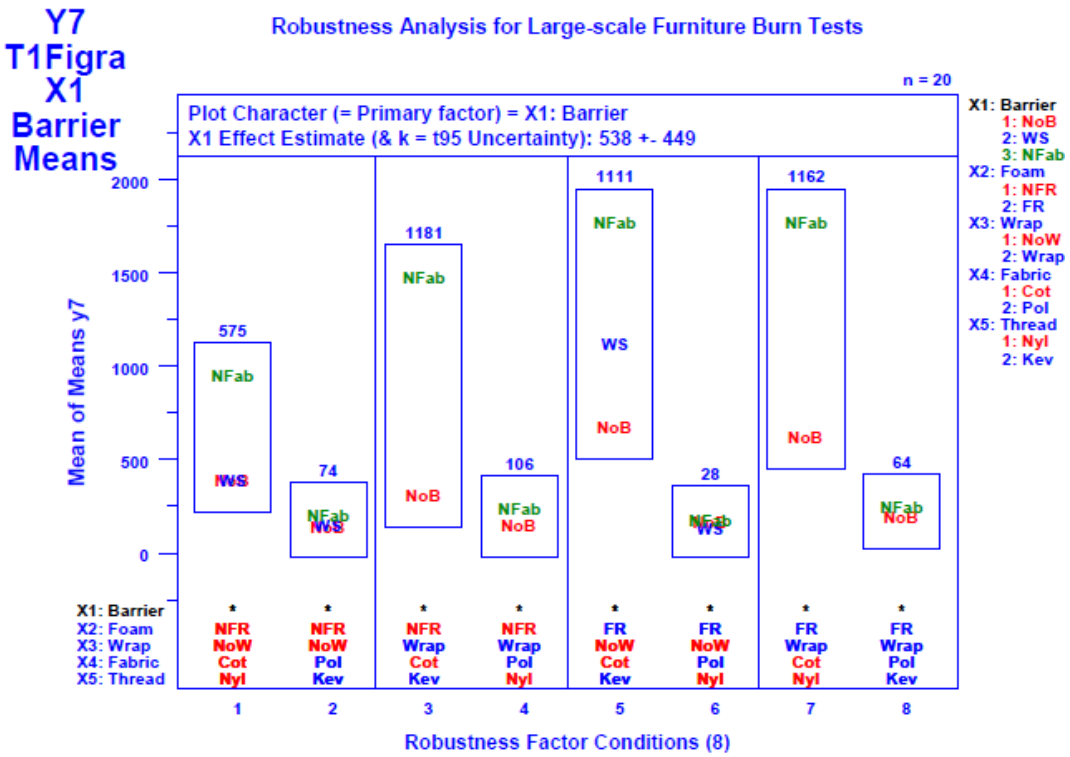

Figure E-31. Robustness Analysis: Mean Response vs. Robustness Factor Combination for Response Y7 = T1Figra and Primary Factor X1 = Barrier.

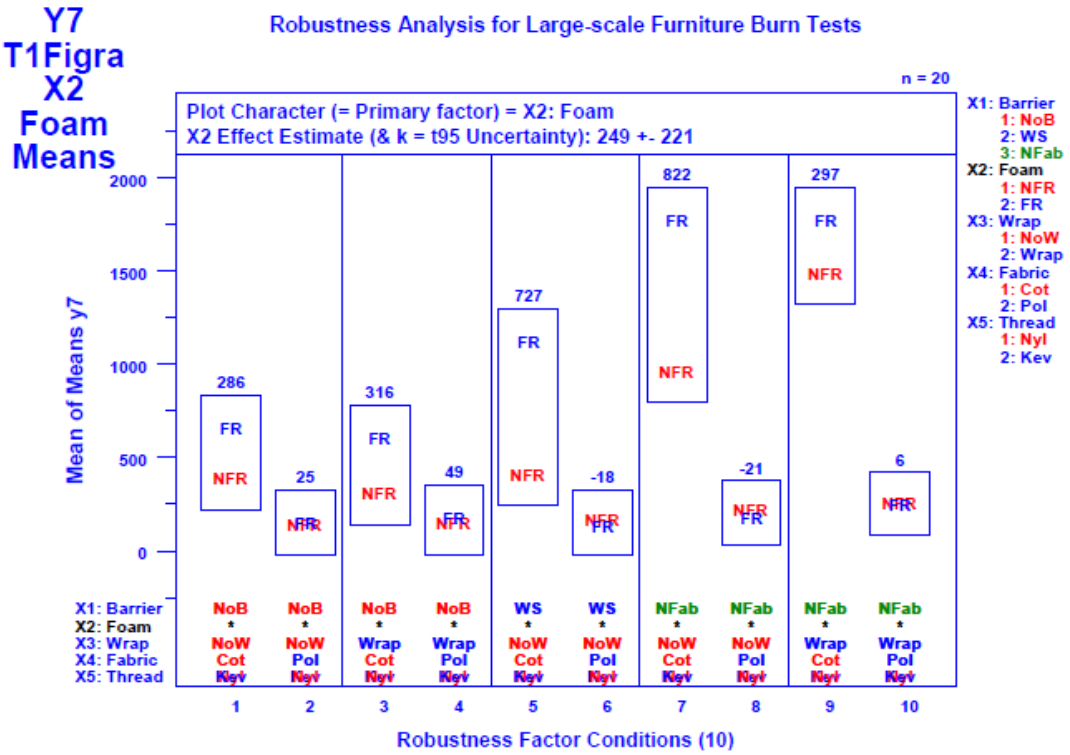

Figure E-32. Robustness Analysis: Mean Response vs. Robustness Factor Combination for Response Y7 = T1Figra and Primary Factor X2 = Foam.

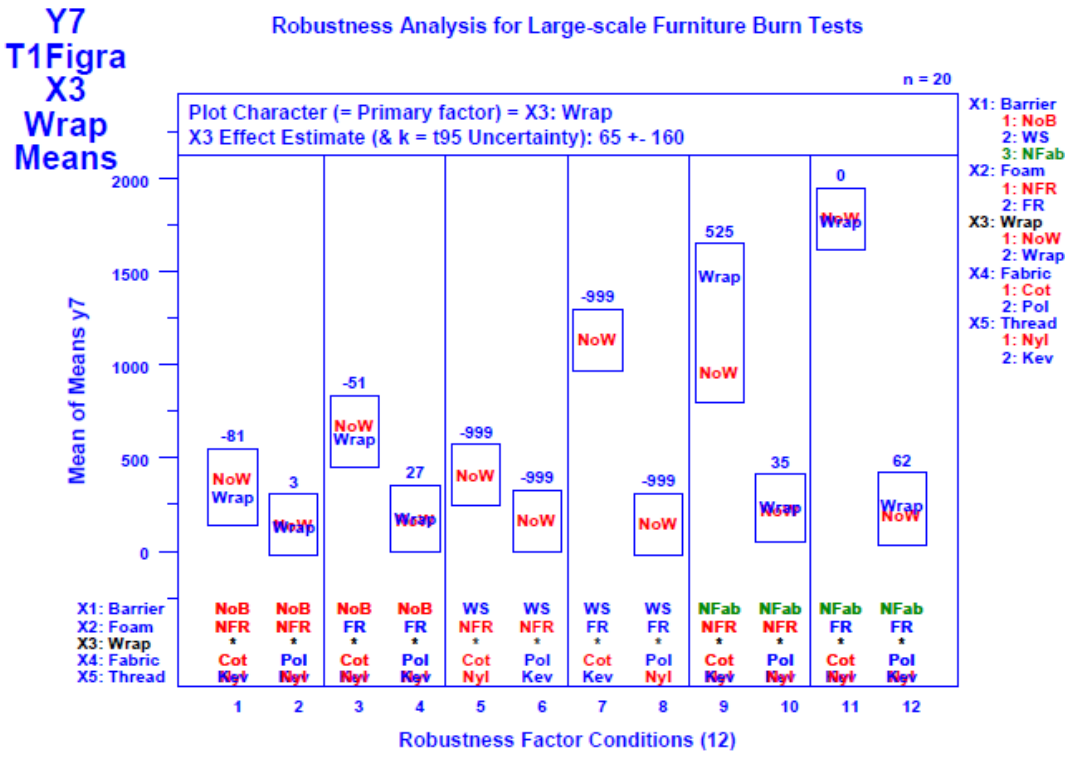

Figure E-33. Robustness Analysis: Mean Response vs. Robustness Factor Combination for Response Y7 = T1Figra and Primary Factor X3 = Wrap.

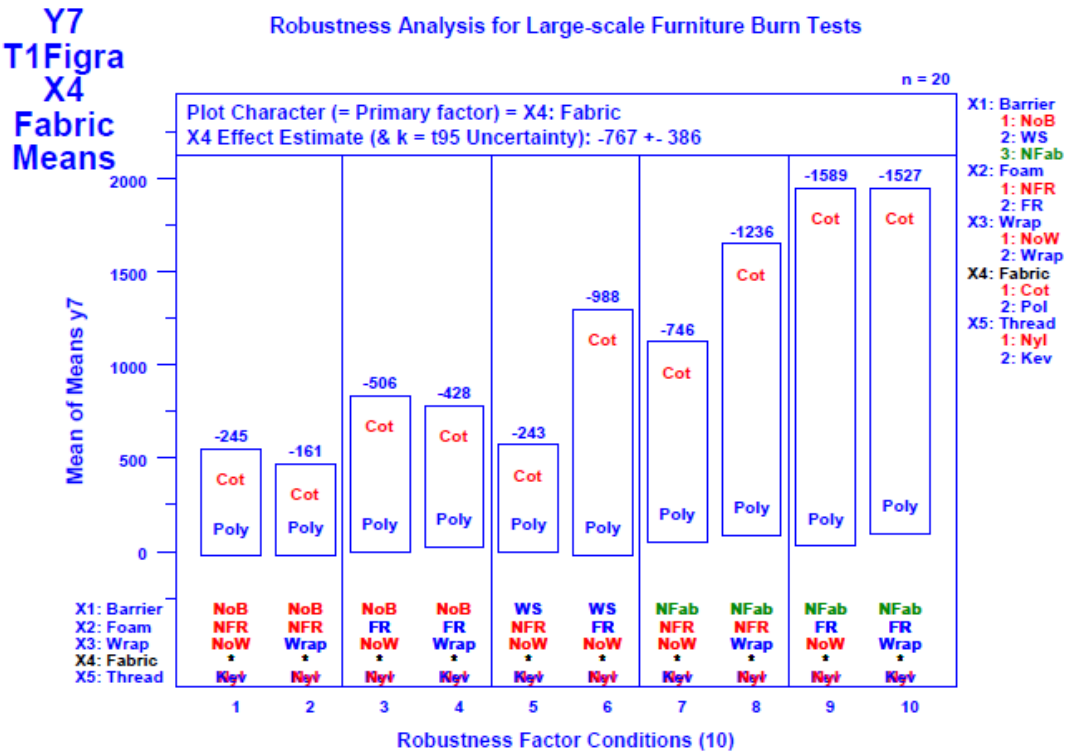

Figure E-34. Robustness Analysis: Mean Response vs. Robustness Factor Combination for Response Y7 = T1Figra and Primary Factor X4 = Fabric.

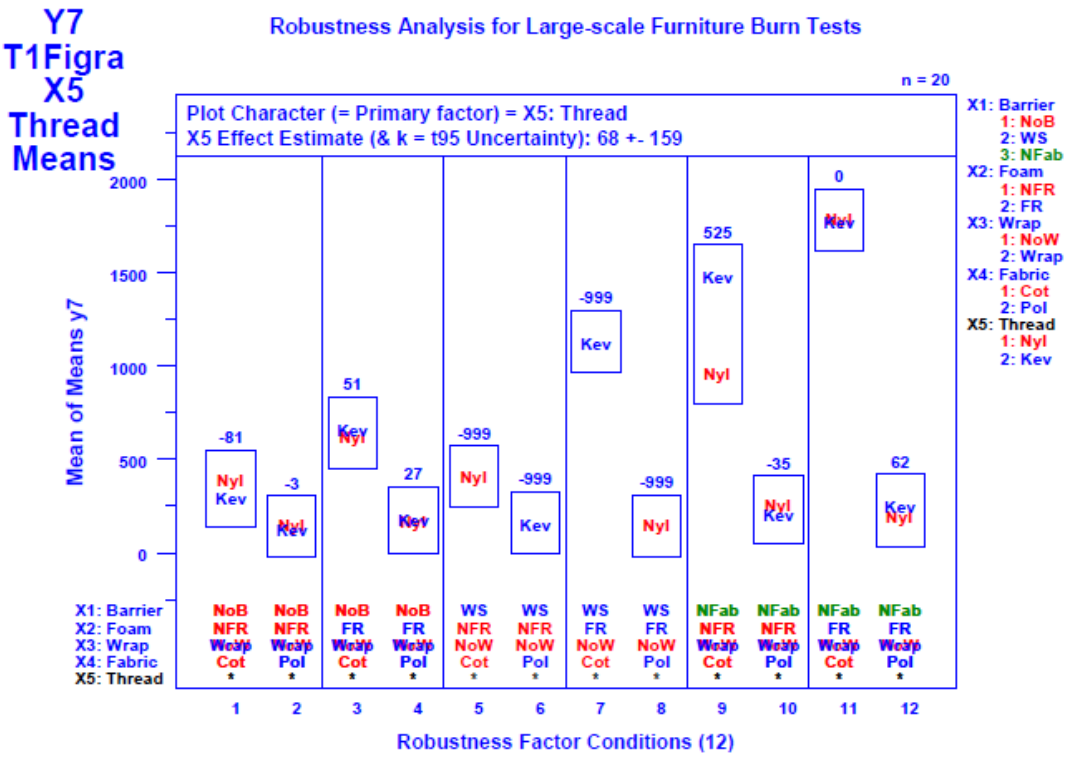

Figure E-35. Robustness Analysis: Mean Response vs. Robustness Factor Combination for Response Y7 = T1Figra and Primary Factor X5 = Thread.

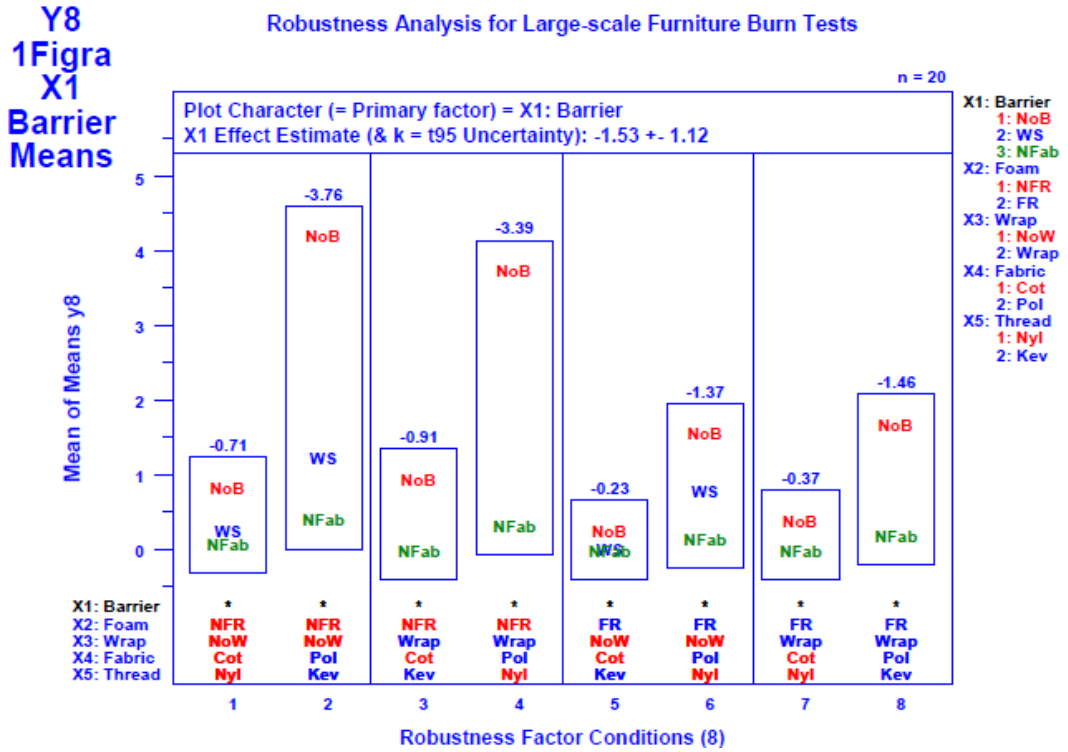

Figure E-36. Robustness Analysis: Mean Response vs. Robustness Factor Combination for Response Y8 = 1Figra and Primary Factor X1 = Barrier.

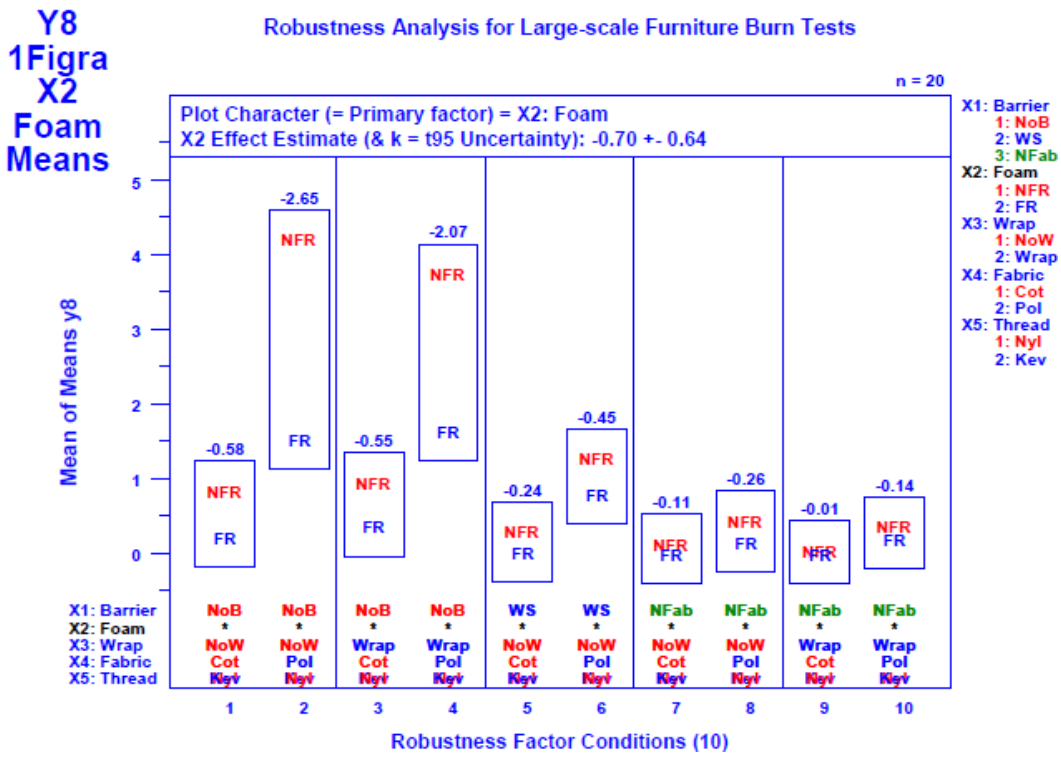

Figure E-37. Robustness Analysis: Mean Response vs. Robustness Factor Combination for Response Y8 = 1Figra and Primary Factor X2 = Foam.

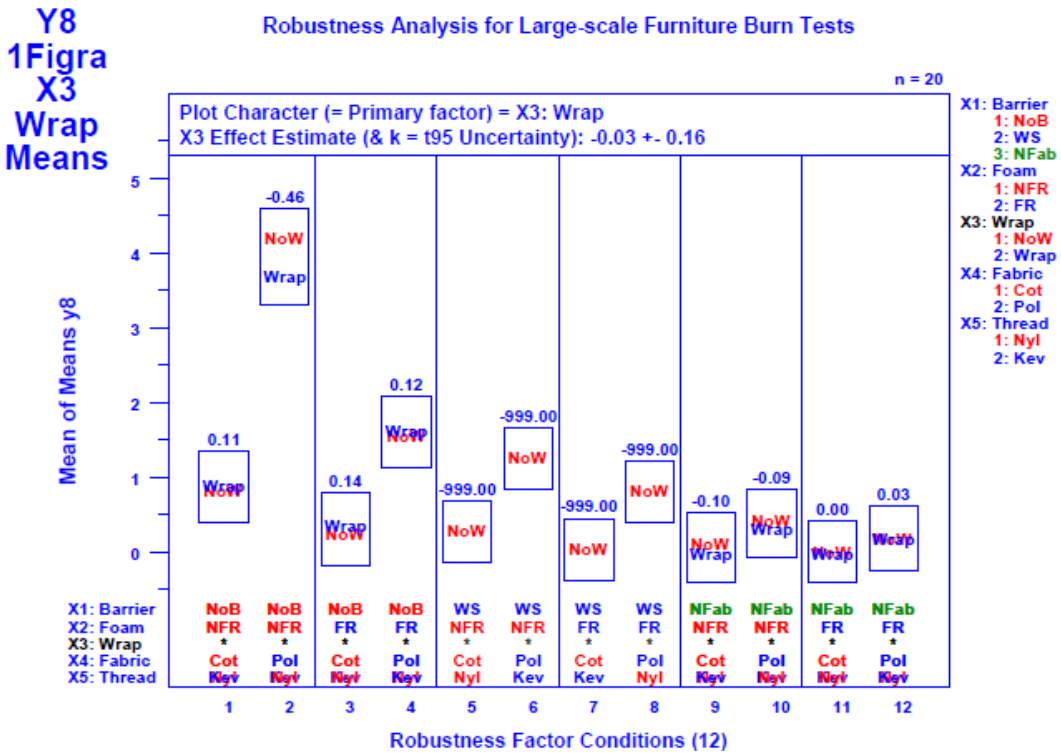

Figure E-38. Robustness Analysis: Mean Response vs. Robustness Factor Combination for Response Y8 = 1Figra and Primary Factor X3 = Wrap.

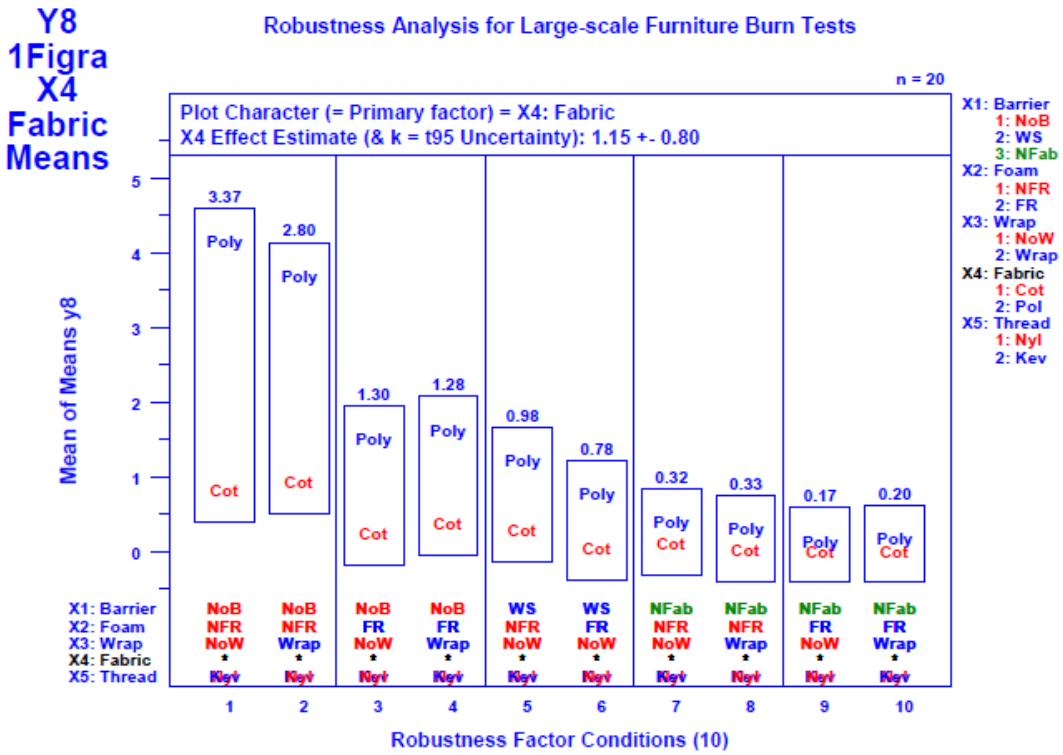

Figure E-39. Robustness Analysis: Mean Response vs. Robustness Factor Combination for Response Y8 = 1Figra and Primary Factor X4 = Fabric.

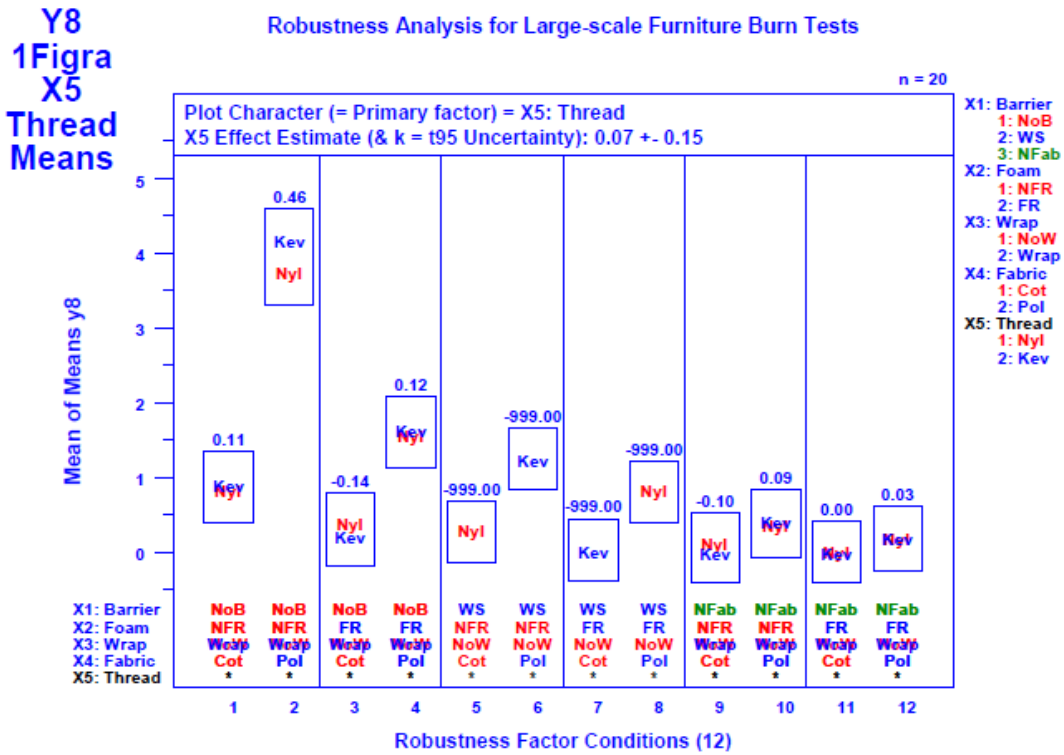

Figure E-40. Robustness Analysis: Mean Response vs. Robustness Factor Combination for Response Y8 = 1Figra and Primary Factor X5 = Thread.

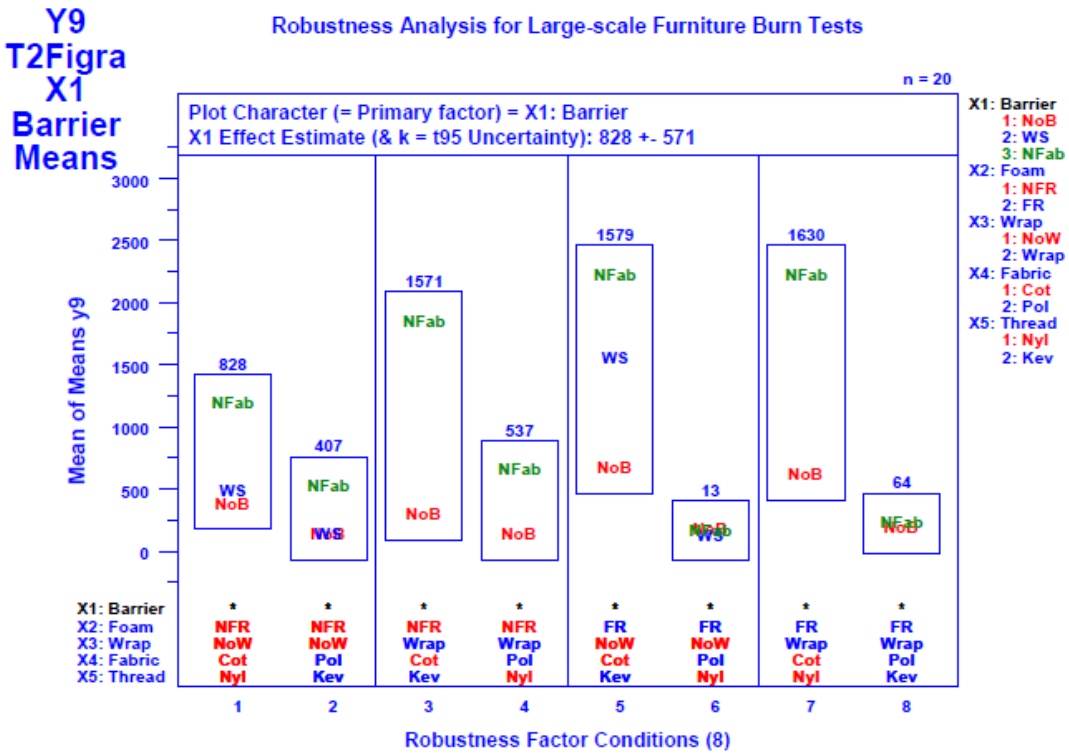

Figure E-41. Robustness Analysis: Mean Response vs. Robustness Factor Combination for Response Y9 = T2Figra and Primary Factor X1 = Barrier.

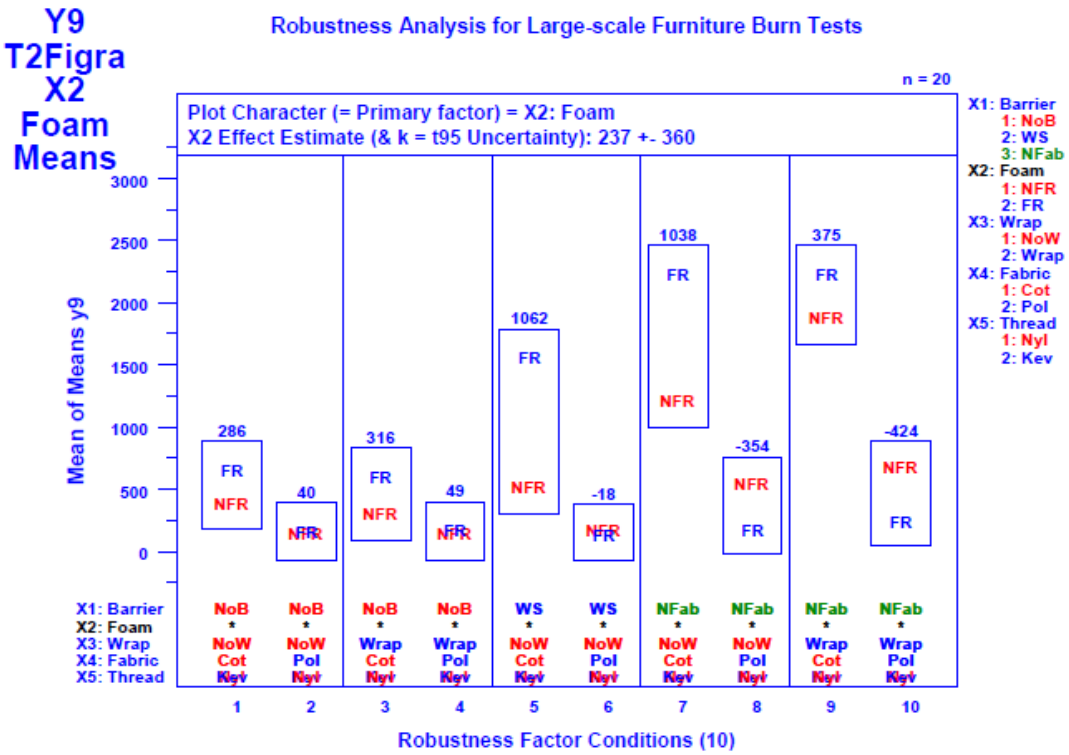

Figure E-42. Robustness Analysis: Mean Response vs. Robustness Factor Combination for Response Y9 = T2Figra and Primary Factor X2 = Foam.

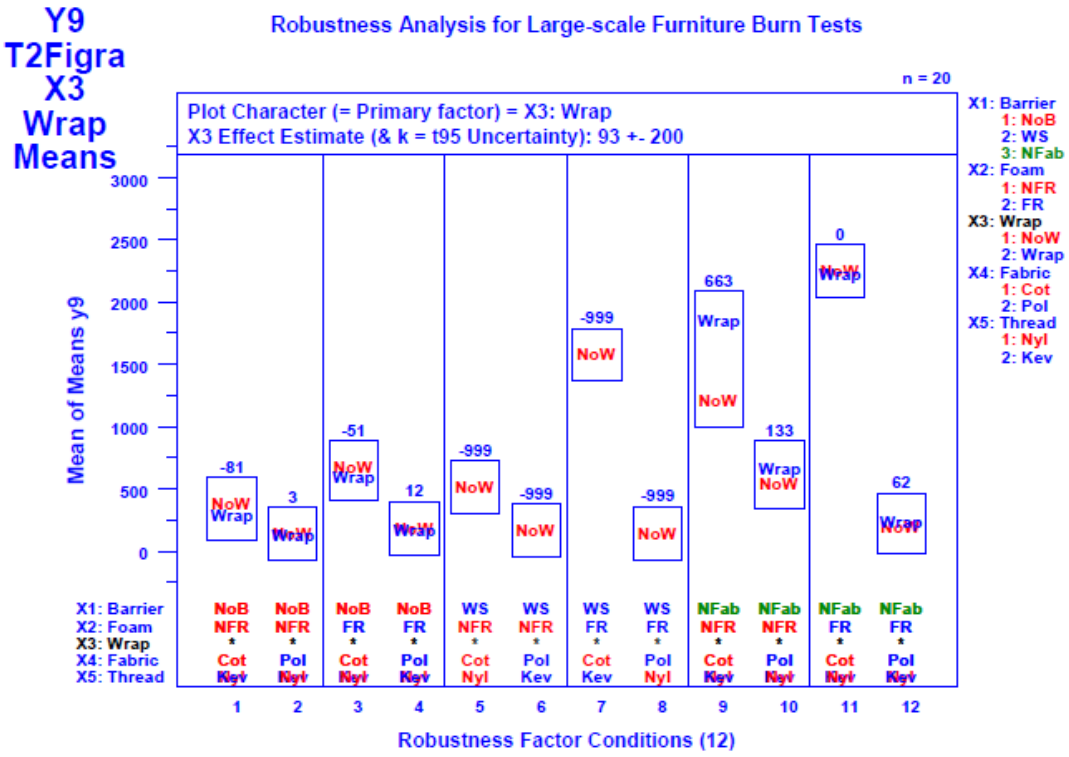

Figure E-43. Robustness Analysis: Mean Response vs. Robustness Factor Combination for Response Y9 = T2Figra and Primary Factor X3 = Wrap.

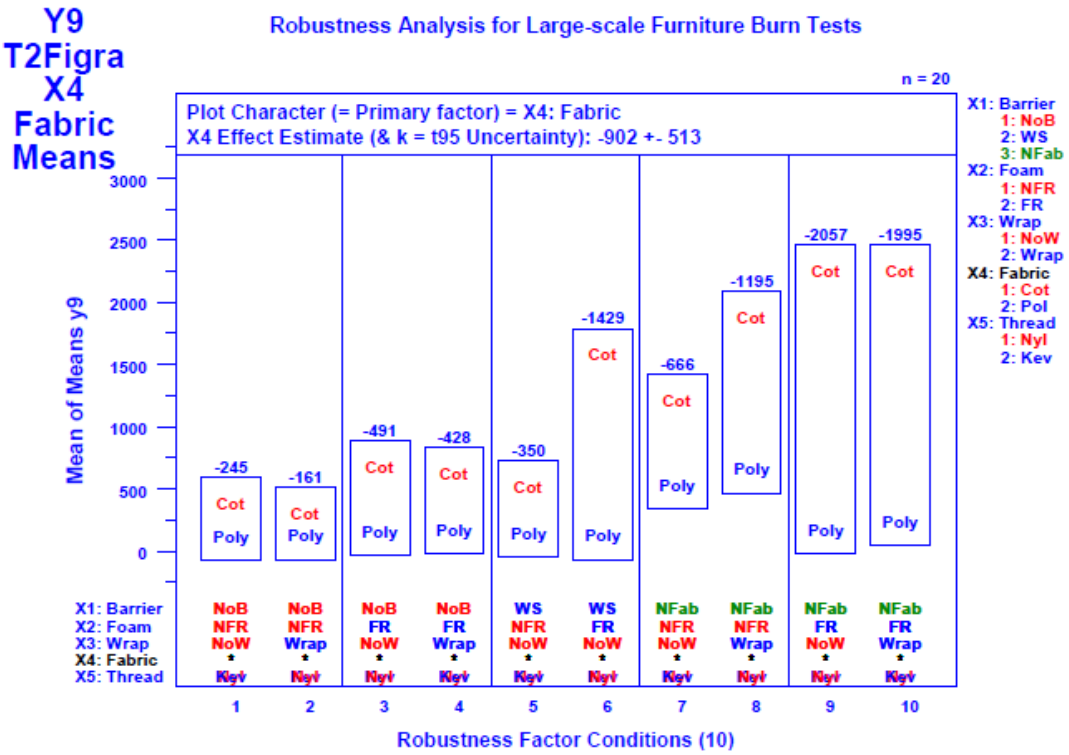

Figure E-44. Robustness Analysis: Mean Response vs. Robustness Factor Combination for Response Y9 = T2Figra and Primary Factor X4 = Fabric.

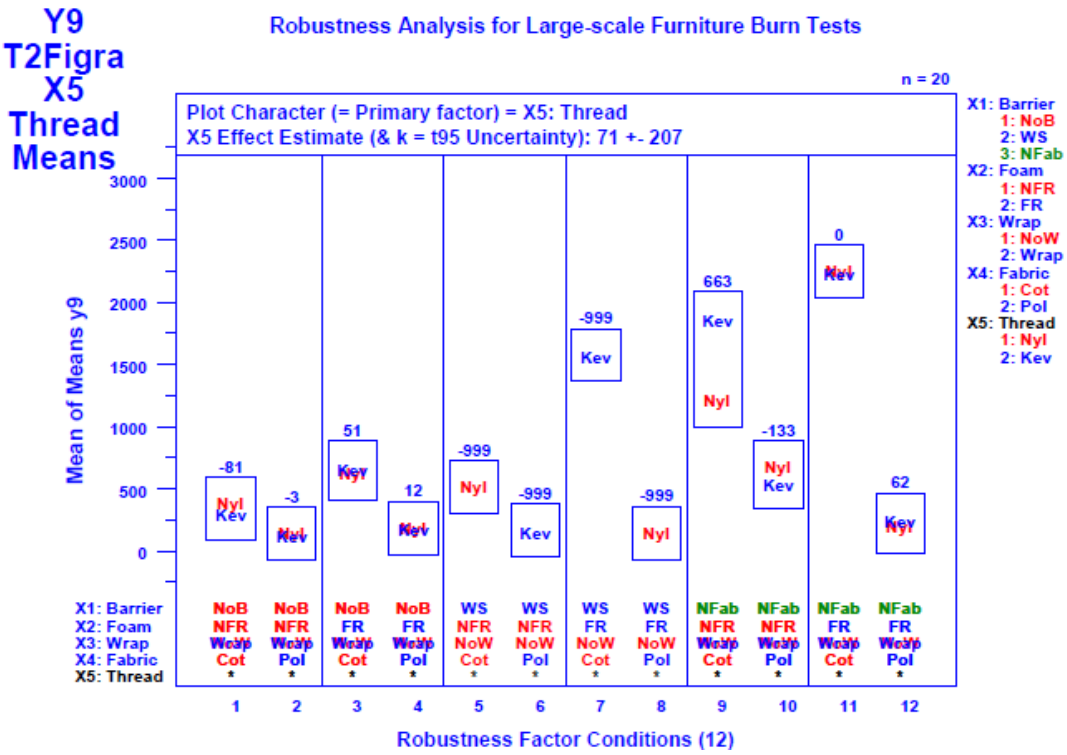

Figure E-45. Robustness Analysis: Mean Response vs. Robustness Factor Combination for Response Y9 = T2Figra and Primary Factor X5 = Thread.

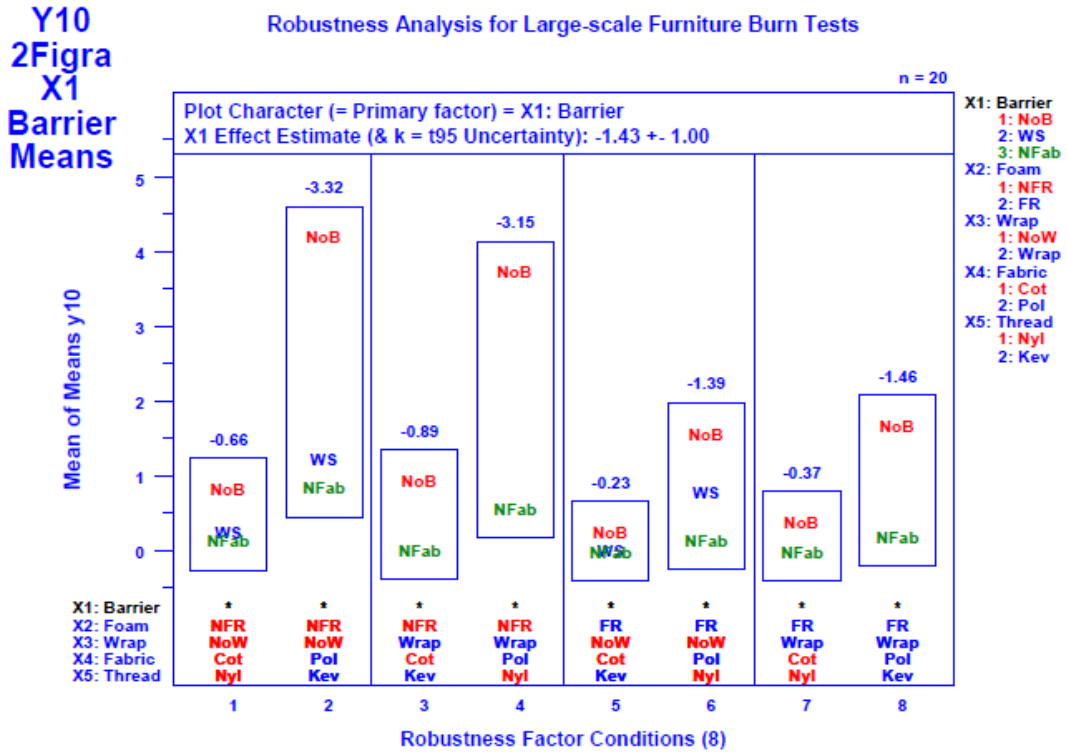

Figure E-46. Robustness Analysis: Mean Response vs. Robustness Factor Combination for Response Y10 = 2Figra and Primary Factor X1 = Barrier.

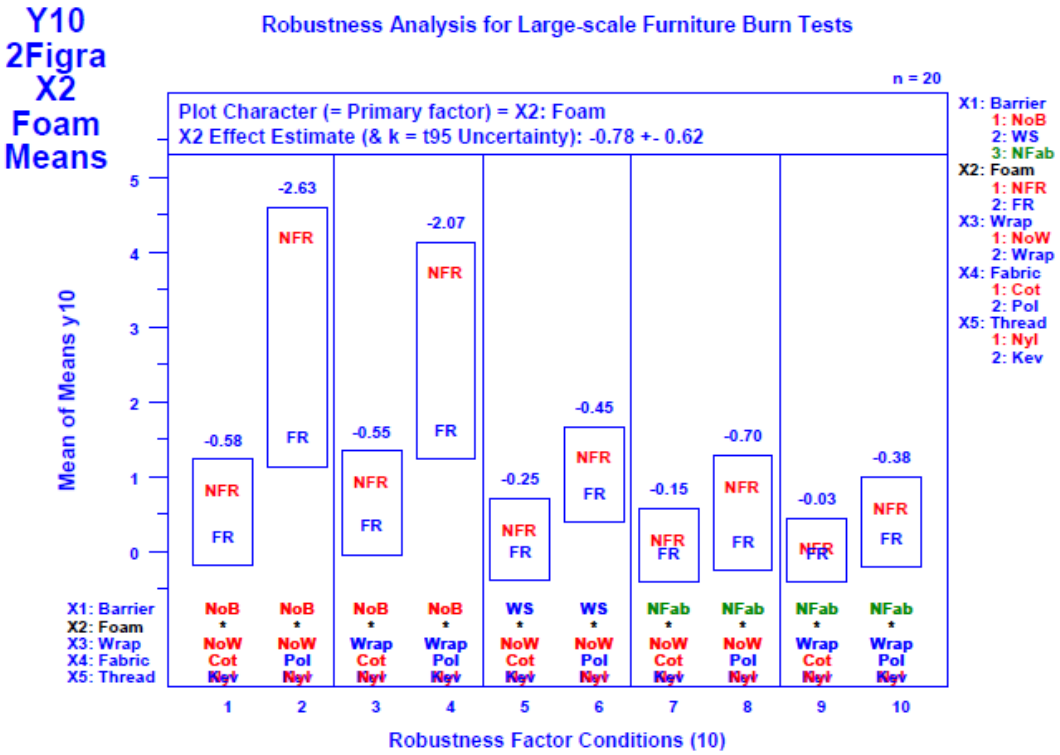

Figure E-47. Robustness Analysis: Mean Response vs. Robustness Factor Combination for Response Y10 = 2Figra and Primary Factor X2 = Foam.

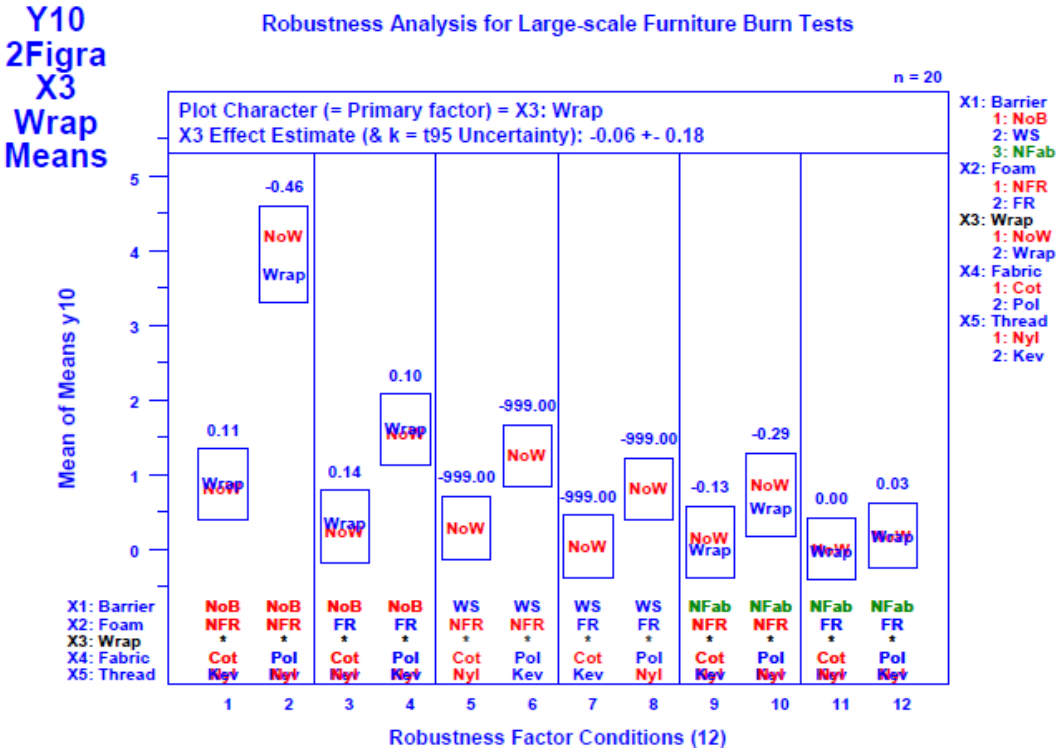

Figure E-48. Robustness Analysis: Mean Response vs. Robustness Factor Combination for Response Y10 = 2Figra and Primary Factor X3 = Wrap.

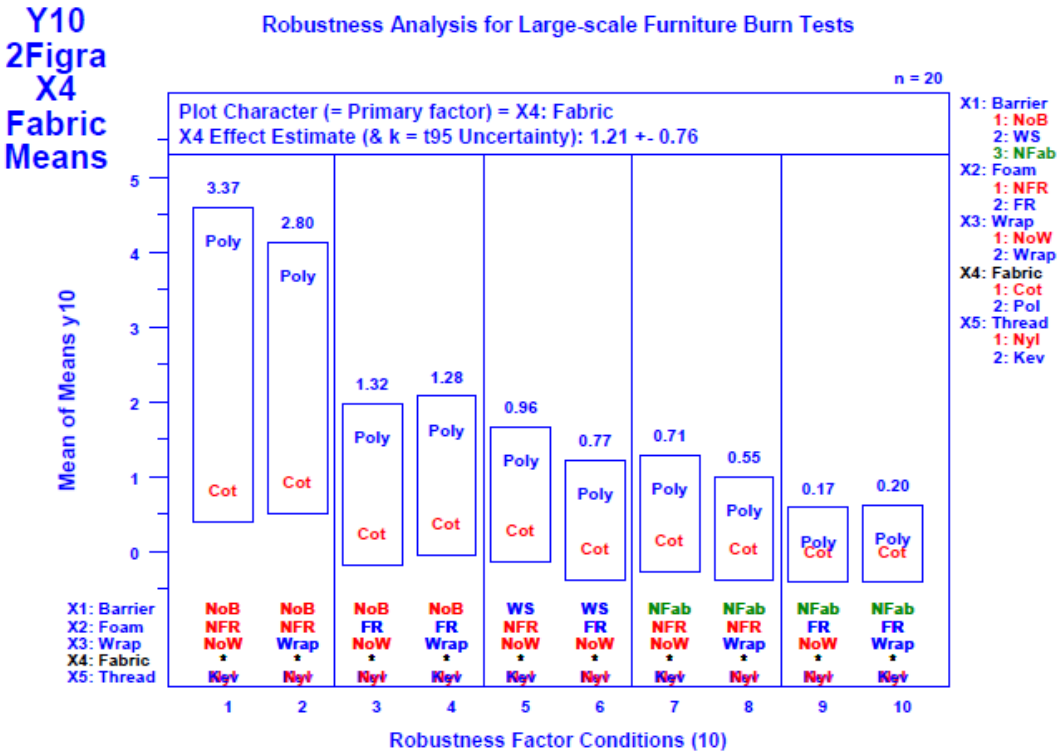

Figure E-49. Robustness Analysis: Mean Response vs. Robustness Factor Combination for Response Y10 = 2Figra and Primary Factor X4 = Fabric.

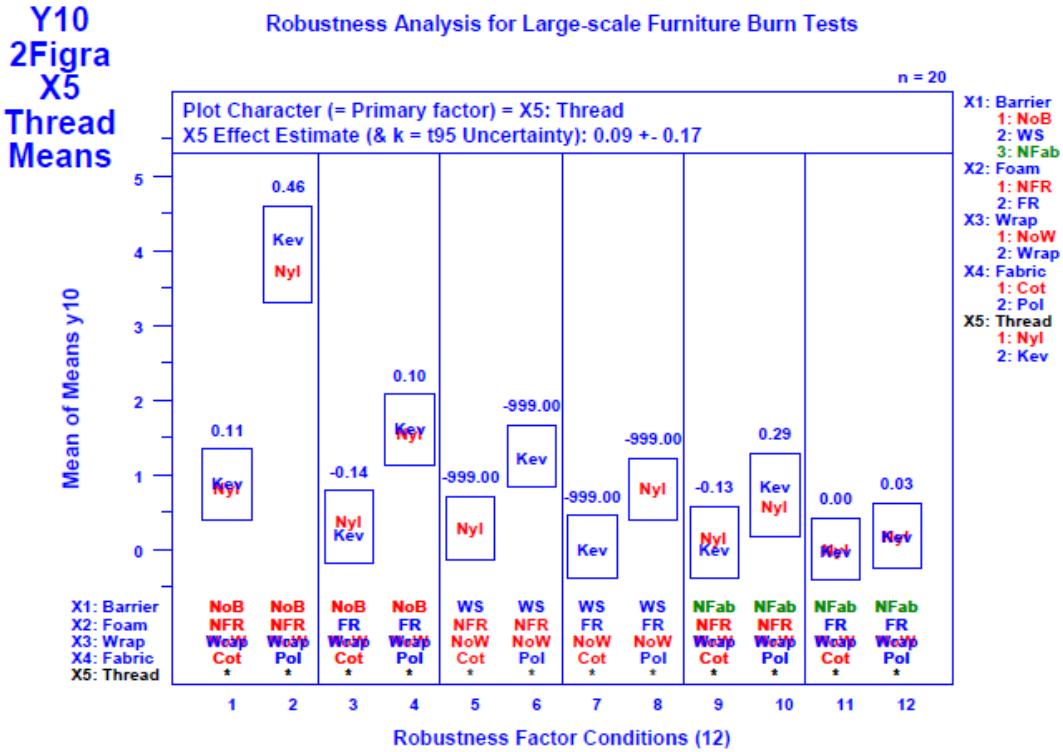

Figure E-50. Robustness Analysis: Mean Response vs. Robustness Factor Combination for Response Y10 = 2Figra and Primary Factor X5 = Thread.

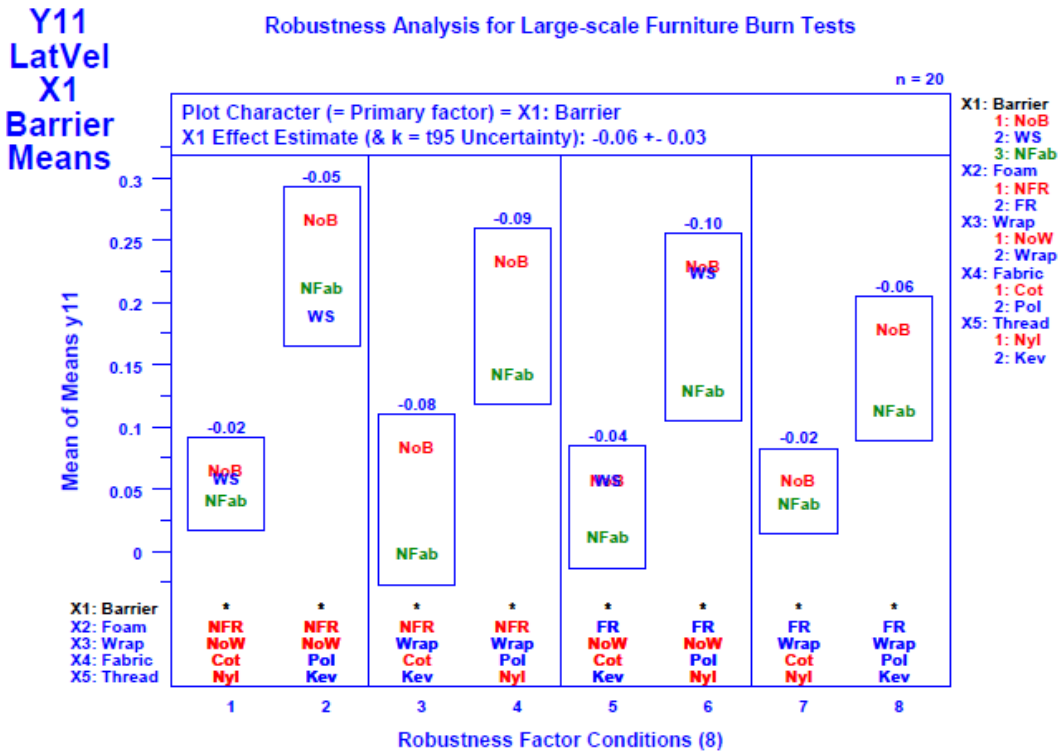

Figure E-51. Robustness Analysis: Mean Response vs. Robustness Factor Combination for Response Y11 = LatVel and Primary Factor X1 = Barrier.

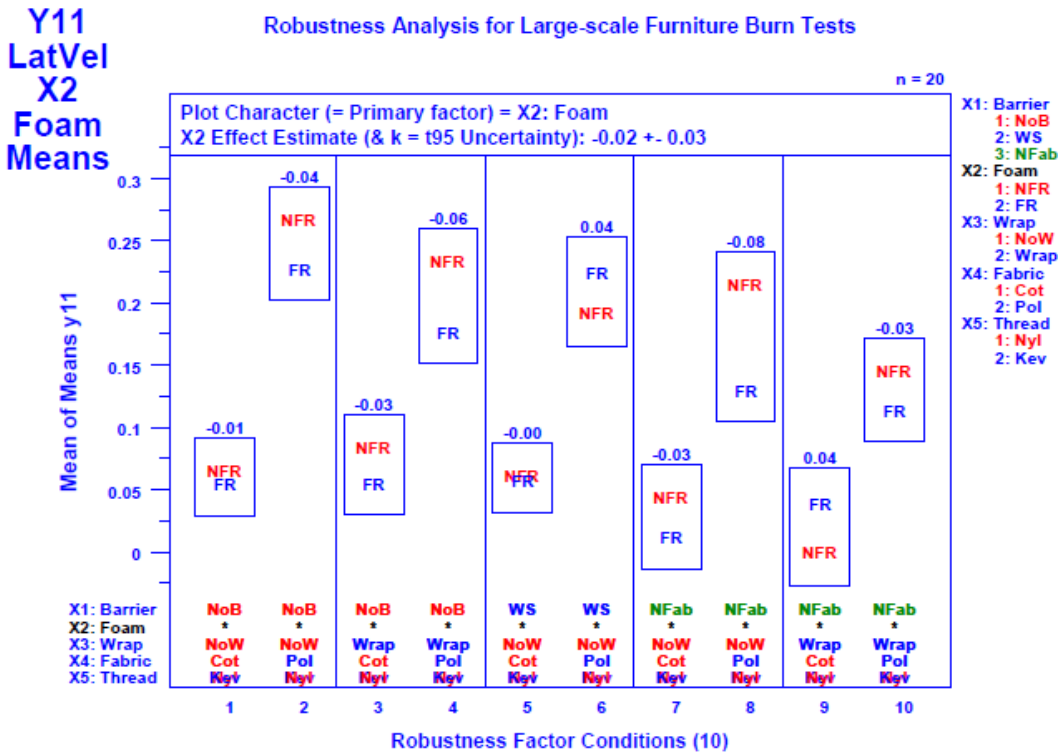

Figure E-52. Robustness Analysis: Mean Response vs. Robustness Factor Combination for Response Y11 = LatVel and Primary Factor X2 = Foam.

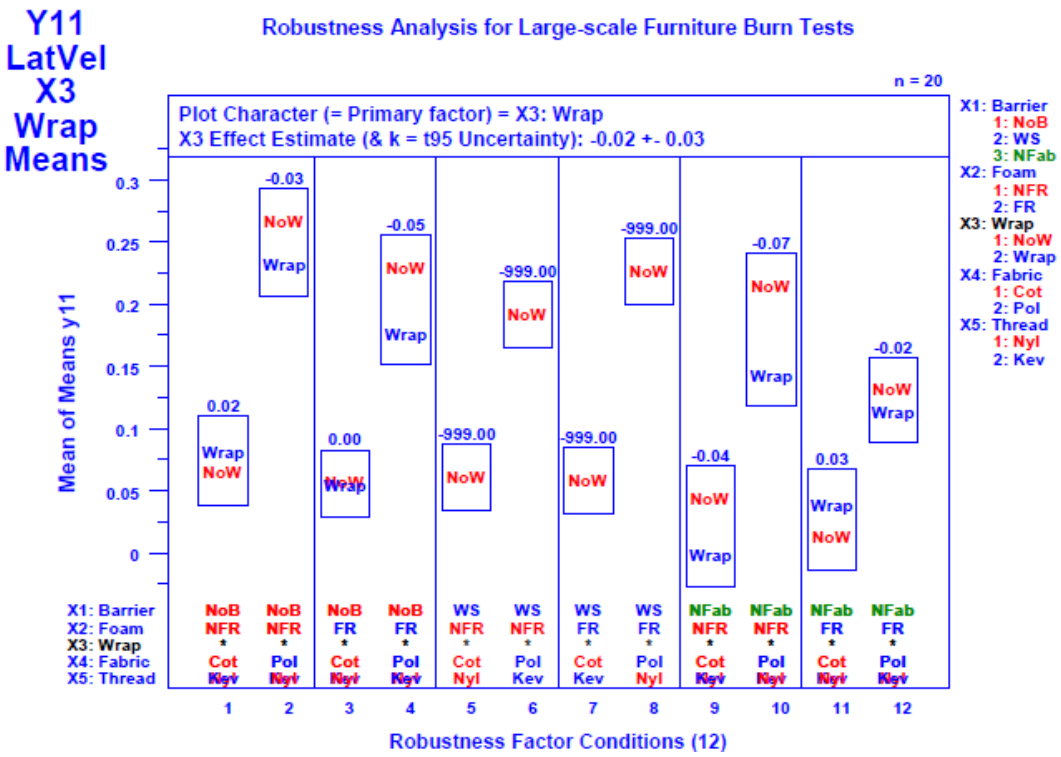

Figure E-53. Robustness Analysis: Mean Response vs. Robustness Factor Combination for Response Y11 = LatVel and Primary Factor X3 = Wrap.

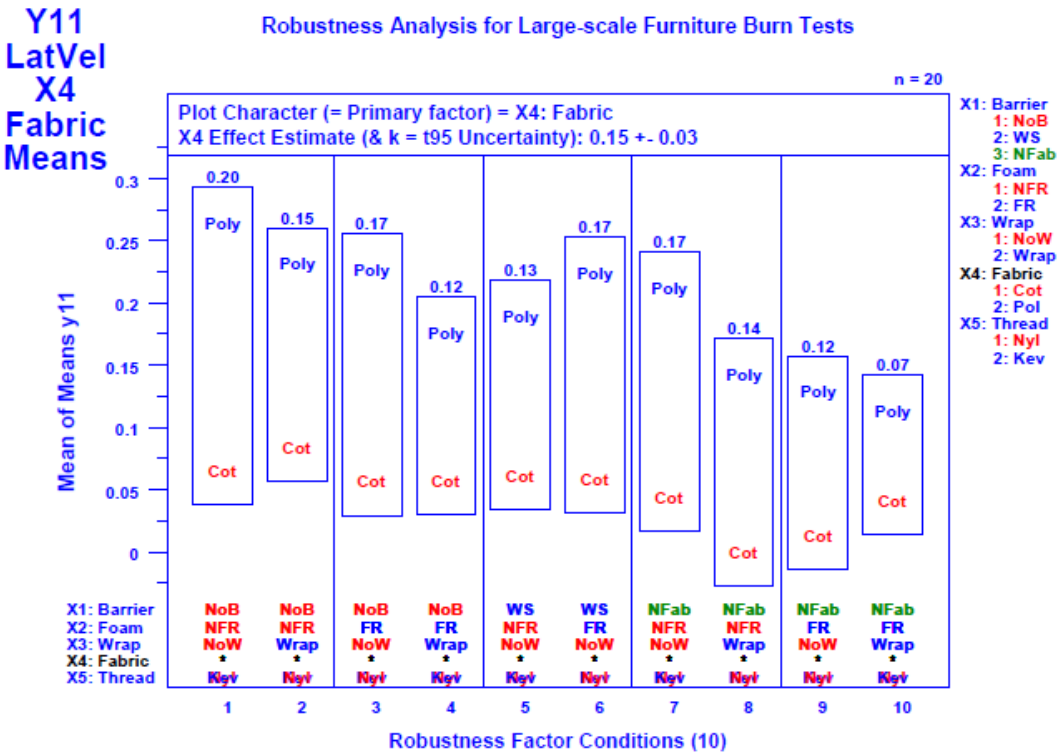

Figure E- 54. Robustness Analysis: Mean Response vs. Robustness Factor Combination for Response Y11 = LatVel and Primary Factor X4 = Fabric.

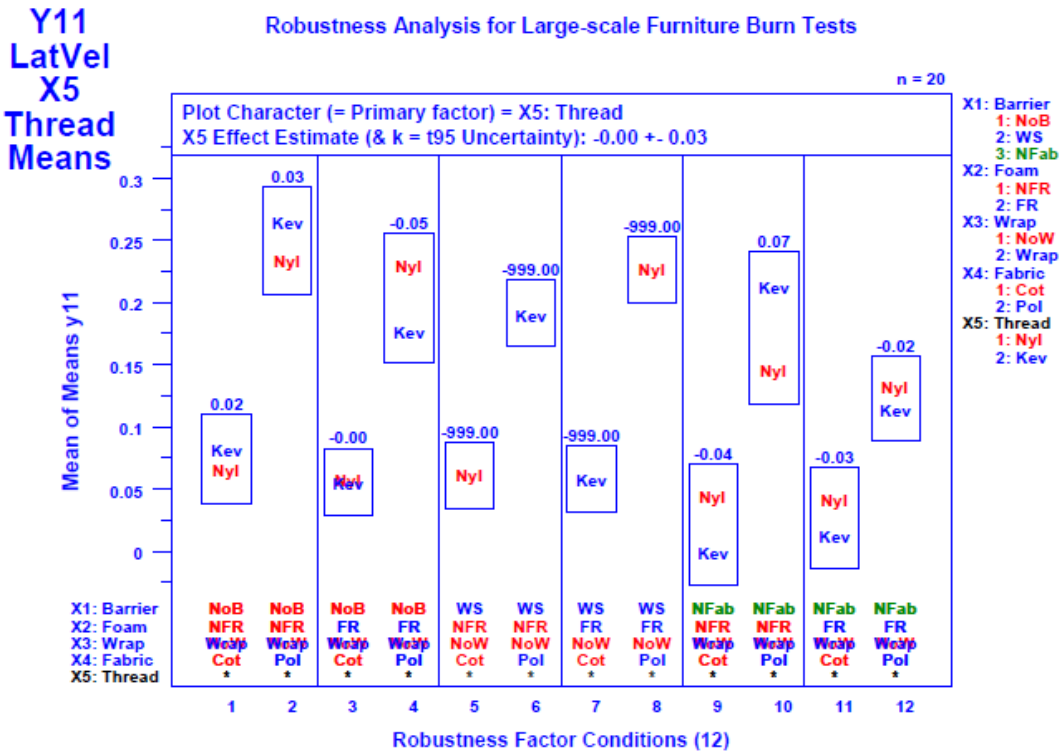

Figure E-55. Robustness Analysis: Mean Response vs. Robustness Factor Combination for Response Y11 = LatVel and Primary Factor X5 = Thread.

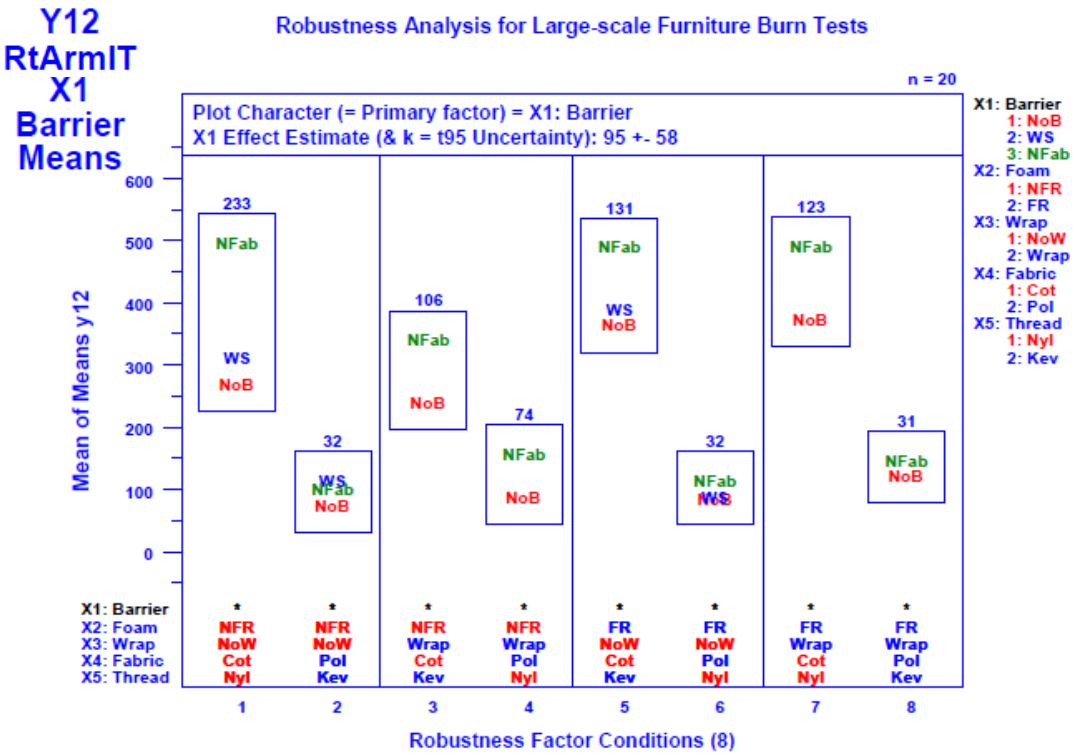

Figure E-56. Robustness Analysis: Mean Response vs. Robustness Factor Combination for Response Y12 = RtArmIT and Primary Factor X1 = Barrier.

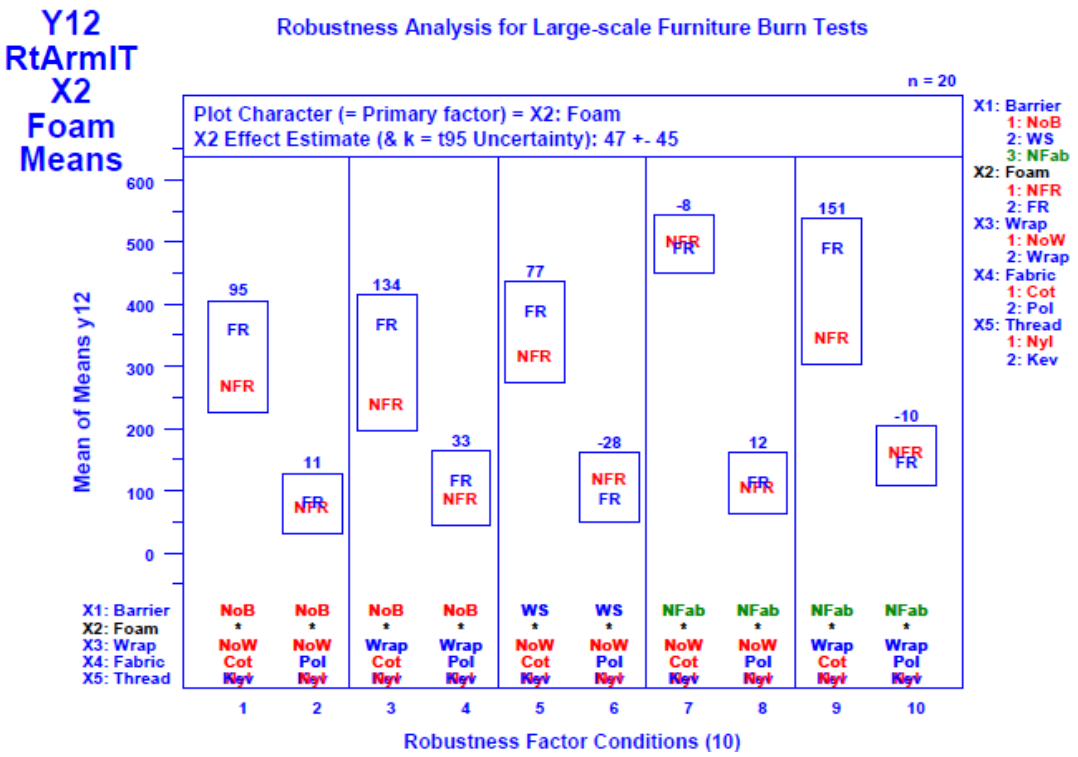

Figure E-57. Robustness Analysis: Mean Response vs. Robustness Factor Combination for Response Y12 = RtArmIT and Primary Factor X2 = Foam.

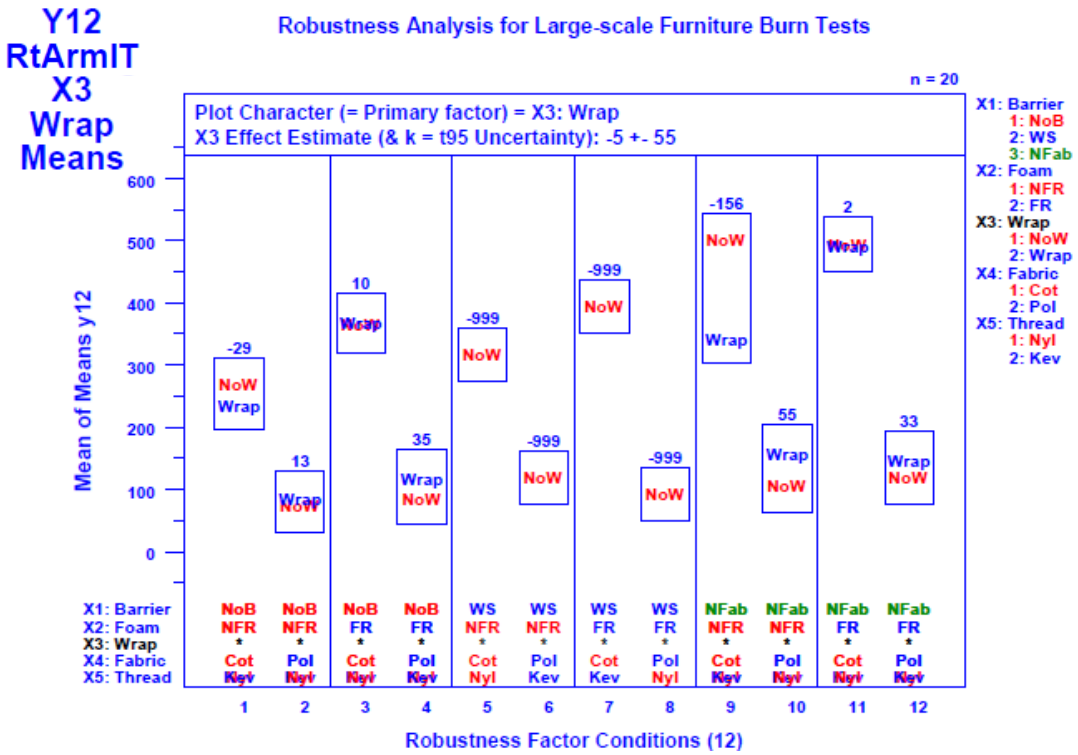

Figure E-58. Robustness Analysis: Mean Response vs. Robustness Factor Combination for Response Y12 = RtArmIT and Primary Factor X3 = Wrap.

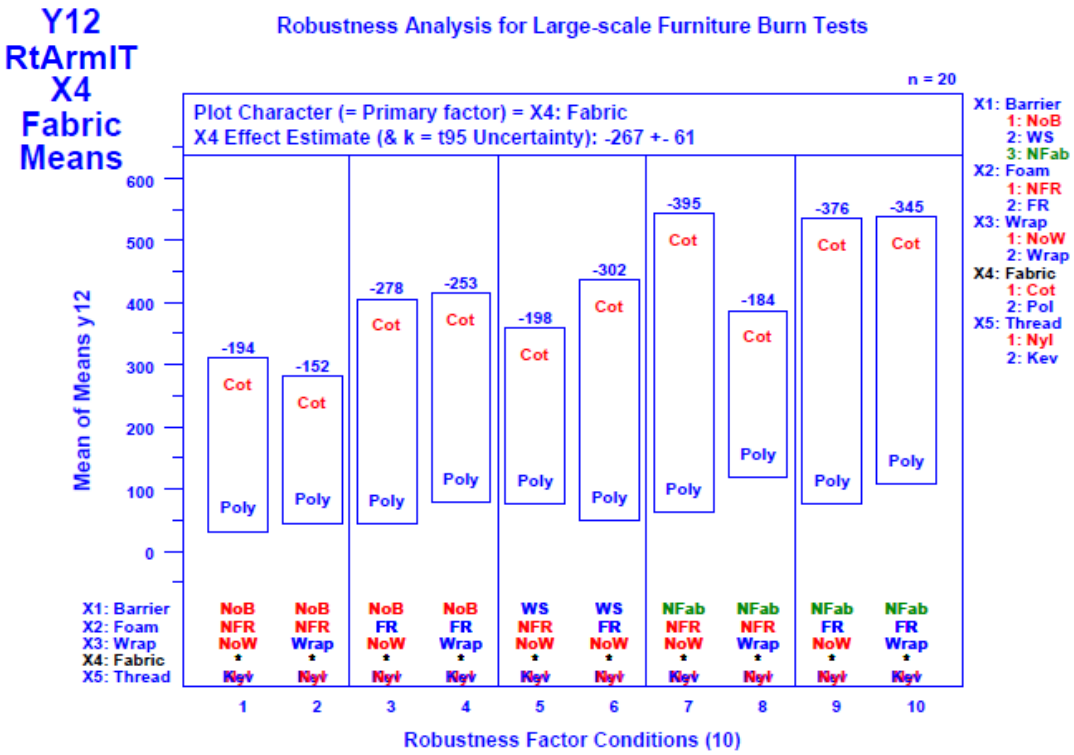

Figure E-59. Robustness Analysis: Mean Response vs. Robustness Factor Combination for Response Y12 = RtArmIT and Primary Factor X4 = Fabric.

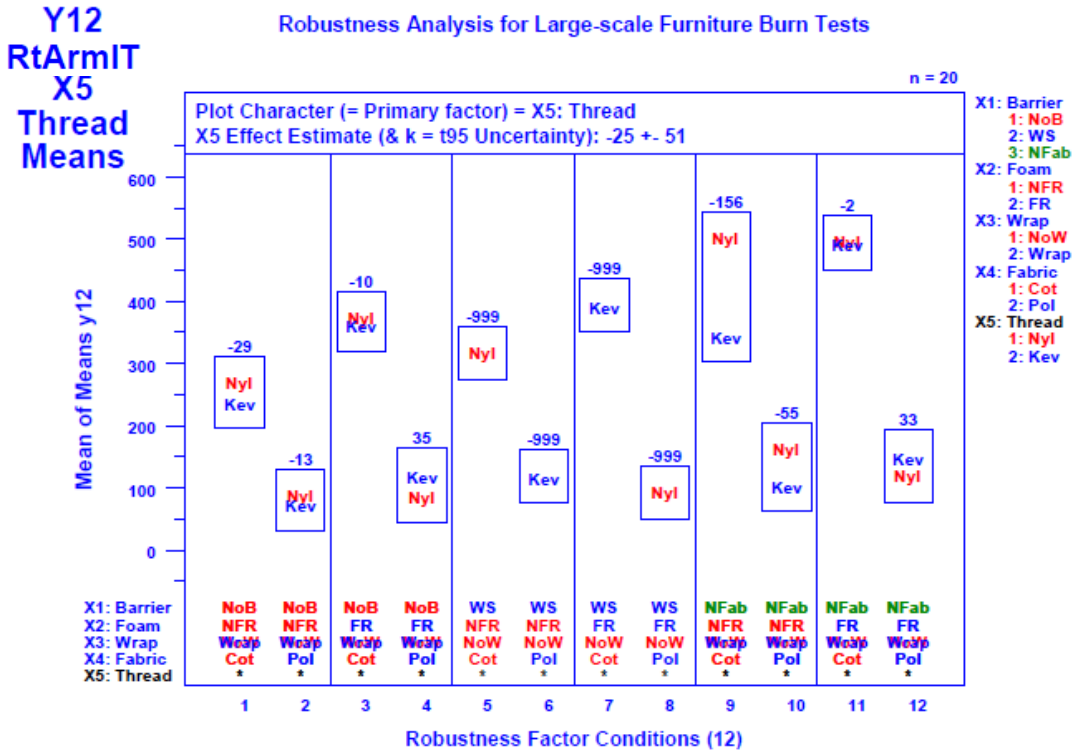

Figure E-60. Robustness Analysis: Mean Response vs. Robustness Factor Combination for Response Y12 = RtArmIg and Primary Factor X5 = Thread.

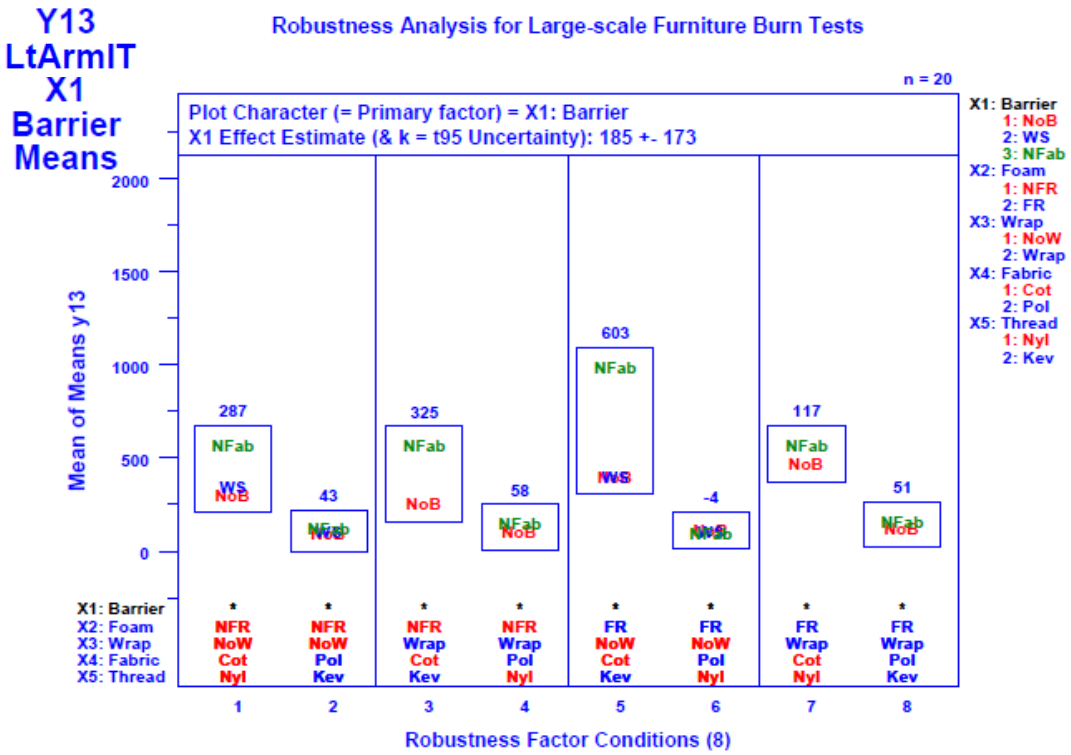

Figure E-61. Robustness Analysis: Mean Response vs. Robustness Factor Combination for Response Y13 = LtArmIT and Primary Factor X1 = Barrier.

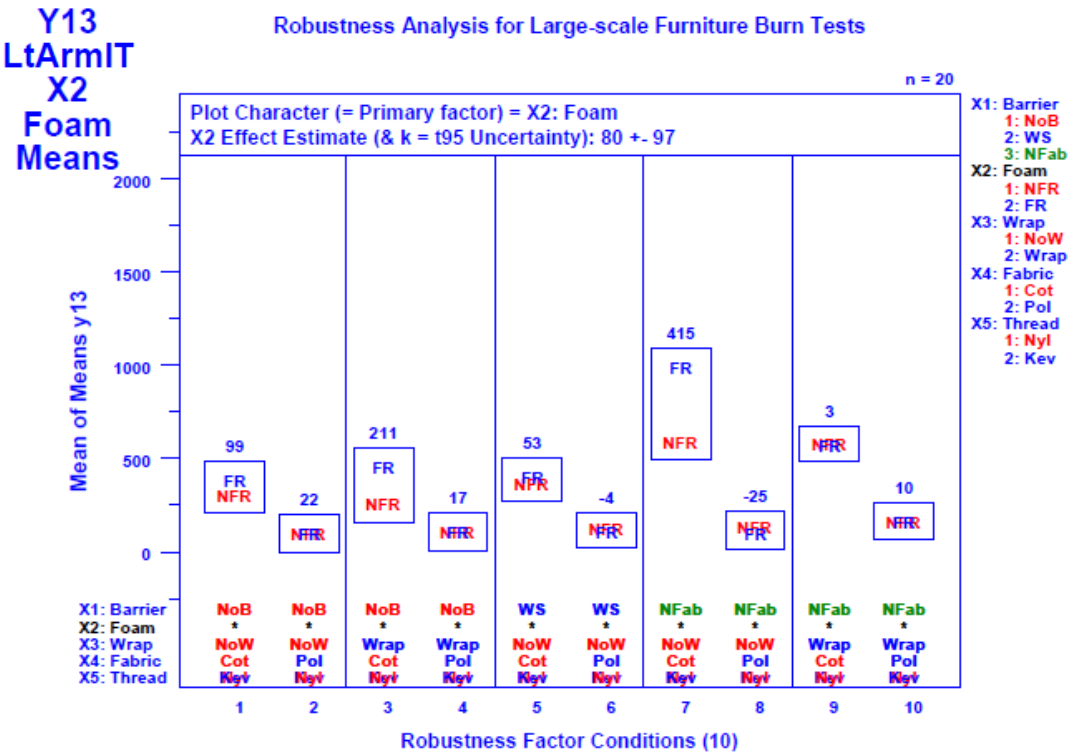

Figure E-62. Robustness Analysis: Mean Response vs. Robustness Factor Combination for Response Y13 = LtArmIT and Primary Factor X2 = Foam.

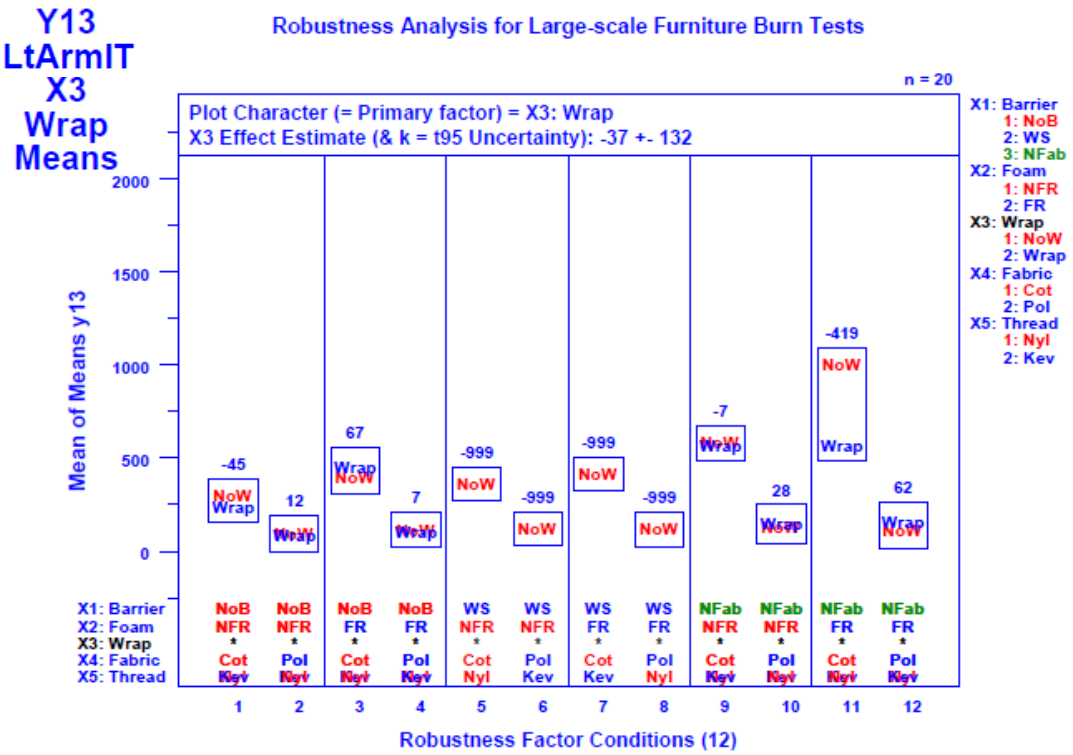

Figure E-63. Robustness Analysis: Mean Response vs. Robustness Factor Combination for Response Y13 = LtArmIT and Primary Factor X3 = Wrap.

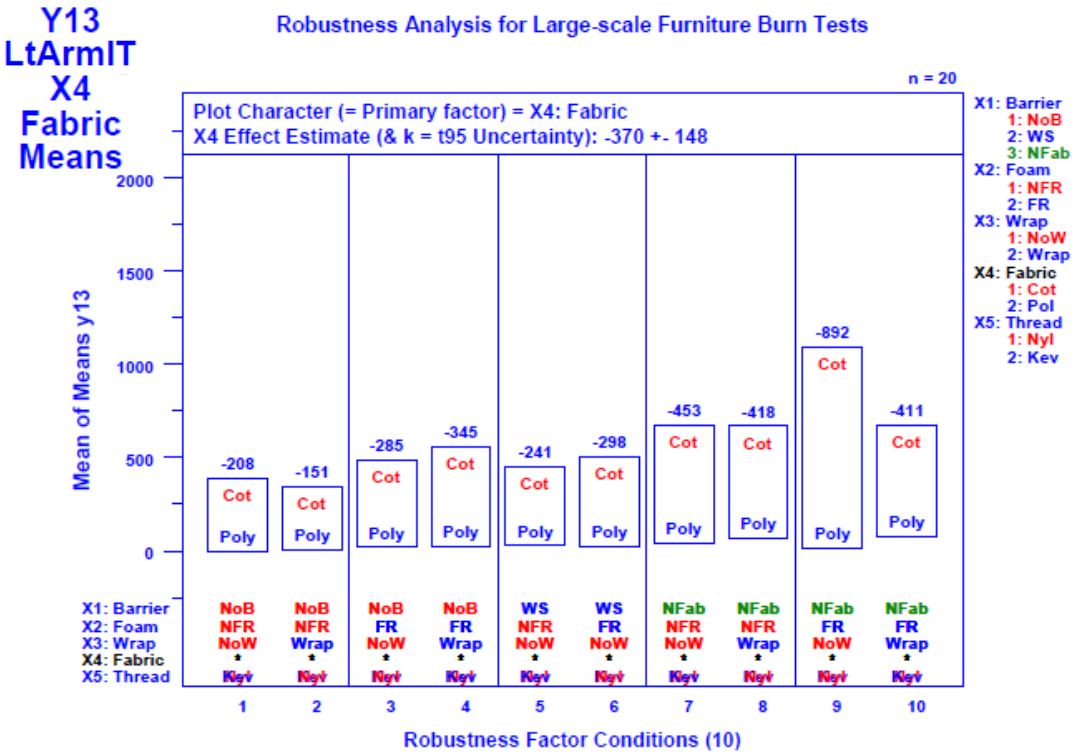

Figure E-64. Robustness Analysis: Mean Response vs. Robustness Factor Combination for Response Y13 = LtArmIT and Primary Factor X4 = Fabric.

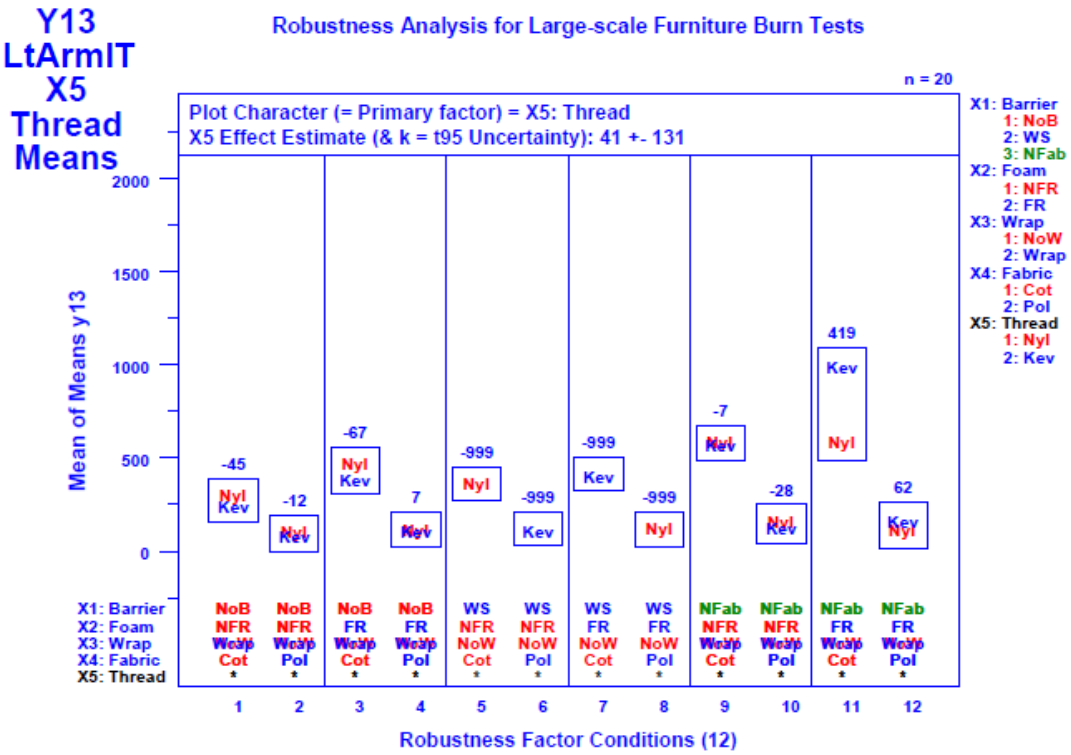

Figure E-65. Robustness Analysis: Mean Response vs. Robustness Factor Combination for Response Y13 = LtArmIT and Primary Factor X5 = Thread.

Appendix F Summary Tables for Factor Interaction Analysis of Thirteen Responses

The following tables summarize the results of analyses designed to determine whether or not statistically significant interactions exist between the five factors considered in the current study with regard to the thirteen responses. Values of the averaged response are compared with the corresponding 95 % estimate of the corresponding uncertainty to derive whether the interaction has a statistically significant effect on the given response.

Table F-1. For Response Y1 (= T25kW): Block-Plot-based Estimates of the 10 Unique Two-term Interactions for the Five Primary Factors

Interaction	Effect	95% Unc	Significant? (yes/no)
X1*X4	-930.29	±579.77	yes
X2*X4	-363.96	±88.62	yes
X2*X	-328.71	±585.33	no
X4*X5	-328.71	±603.53	no
X1*X	282.21	±580.36	no
X3*X4	-262.71	±584.72	no
X2*X5	-262.71	±602.94	no
X1*X3	78.96	±819.08	no
X1*X5	18.13	±831.16	no
X3*X5	unestimable		

Table F-2. For Response Y2 (= T1PHRR): Block-Plot-based Estimates of the 10 Unique Two-term Interactions for the Five Primary Factors

Interaction	Effect	95% Unc	Significant? (yes/no)
X1*X4	-1076.25	± 626.30	yes
X2*X4	-507.25	± 621.85	no
X1*X2	214.75	± 602.16	no
X1*X3	214.75	± 544.45	no
X1*X5	167.75	± 597.60	no
X2*X3	-157.75	± 539.33	no
X4*X5	-157.75	± 574.61	no
X3*X4	-103.75	± 566.16	no
X2*X5	-103.75	± 599.86	no
X3*X5	unestimable		

Table F-3. For Response Y3 (= 1PHRR): Block-Plot-based Estimates of the 10 Unique Two-term Interactions for the Five Primary Factors

Interaction	Effect	95% Unc	Significant? (yes/no)
X2*X3	77.32	±52.74	yes
X1*X4	-144.66	±182.76	no
X1*X2	138.08	±177.12	no
X2*X4	-79.96	±175.35	no
X4*X5	77.32	±79.38	no
X1*X3	-38.78	±73.73	no
X3*X4	17.26	±69.38	no
X2*X5	17.26	±91.28	no
X1*X5	-16.94	±97.69	no
X3*X5	unestimable		

Table F-4. For Response Y4 (= TMaxHRR): Block-Plot-based Estimates of the 10 Unique Two-term Interactions for the Five Primary Factors

Interaction	Effect	95% Unc	Significant? (yes/no)
X1*X4	-1919.38	±1664.13	yes
X2*X4	-942.79	±1410.44	no
X2*X3	-607.63	±1306.37	no
X4*X5	-607.63	±1420.25	no
X1*X2	497.71	±1657.04	no
X3*X4	-468.21	±1315.36	no
X2*X5	-468.21	±1428.52	no
X1*X3	411.29	±1576.89	no
X1*X5	278.88	±1671.86	no
X3*X5	unestimable		

Table F-5. For Response Y5 (= MaxHRR): Block-Plot-based Estimates of the 10 Unique Two-term Interactions for the Five Primary Factors

Interaction	Effect	95% Unc	Significant? (yes/no)
X2*X4	-209.45	±97.76	yes
X2*X3	93.3	±39.91	yes
X1*X3	-61.79	±56.43	yes
X4*X5	93.3	±136.82	no
X1*X2	-70.34	±95.53	no
X1*X5	-6.74	±126.17	no
X1*X4	-8.14	±105.59	no
X3*X4	0.02	±60.13	no
X2*X5	0.02	±144.03	no
X3*X5	unestimable		

Table F-6. For Response Y6 (= TotHR): Block-Plot-based Estimates of the 10 Unique Two-term Interactions for the Five Primary Factors

Interaction	Effect	95% Unc	Significant? (yes/no)
X1*X2	-34.6	±28.32	yes
X1*X4	34.31	±28.46	yes
X1*X3	-16.72	±29.19	no
X1*X5	-14.99	±32.20	no
X2*X4	-13.64	±35.33	no
X2*X3	6.7	±35.92	no
X4*X5	6.7	±36.93	no
X3*X4	6.11	±36.03	no
X2*X5	6.11	±37.04	no
X3*X5	unestimable		

Table F-7. For Response Y7 (= T1Figra): Block-Plot-based Estimates of the 10 Unique Two-term Interactions for the Five Primary Factors

Interaction	Effect	95% Unc	Significant? (yes/no)
X1*X4	-939.08	±465.35	yes
X2*X4	-415.08	±454.05	no
X1*X3	180.83	±450.69	no
X1*X5	139.5	±497.82	no
X2*X3	-111.17	±439.02	no
X4*X5	-111.17	±481.38	no
X1*X2	107.25	±455.24	no
X3*X4	-66.5	±449.49	no
X2*X5	-66.5	±490.96	no
X3*X5	unestimable		

Table F-8. For Response Y8 (= 1Figra): Block-Plot-based Estimates of the 10 Unique Two-term Interactions for the Five Primary Factors

Interaction	Effect	95% Unc	Significant? (yes/no)
X1*X4	-1.94	±1.57	yes
X1*X2	1.33	±1.55	no
X2*X4	-0.97	±1.56	no
X2*X3	0.21	±0.40	no
X4*X5	0.21	±0.22	no
X3*X4	-0.14	±0.46	no
X2*X5	-0.14	±0.31	no
X1*X5	-0.13	±0.34	no
X1*X3	-0.01	±0.42	no
X3*X5	unestimable		

Table F-9. For Response Y9 (= T2Figra): Block-Plot-based Estimates of the 10 Unique Two-term Interactions for the Five Primary Factors

Interaction	Effect	95% Unc	Significant? (yes/no)
X1*X4	-1146.54	±867.84	yes
X2*X4	-675.63	±861.57	no
X1*X3	243.38	±533.29	no
X2*X3	-173.71	±523.03	no
X4*X5	-173.71	±664.34	no
X1*X5	153.21	±636.49	no
X3*X4	-80.21	±477.24	no
X2*X5	-80.21	±628.93	no
X1*X2	-14.04	±893.84	no
X3*X5	unestimable		

Table F-10. For Response Y10 (= 2Figra): Block-Plot-based Estimates of the 10 Unique Two-term Interactions for the Five Primary Factors

Interaction	Effect	95% Unc	Significant? (yes/no)
X1*X4	-1.79	±1.26	yes
X1*X2	1.14	±1.24	no
X2*X4	-1.11	±1.28	no
X2*X3	0.26	±0.37	no
X4*X5	0.26	±0.27	no
X3*X4	-0.18	±0.43	no
X2*X5	-0.18	±0.34	no
X1*X5	-0.08	±0.26	no
X1*X3	-0.07	±0.28	no
X3*X5	unestimable		

Table F-11. For Response Y11 (= LatVel): Block-Plot-based Estimates of the 10 Unique Two-term Interactions for the Five Primary Factors

Interaction	Effect	95% Unc	Significant? (yes/no)
X2*X4	-0.045	±0.033	yes
X1*X4	-0.035	±0.035	yes
X3*X4	-0.043	±0.019	no
X2*X5	-0.043	±0.079	no
X2*X3	0.022	±0.075	no
X4*X5	0.022	±0.107	no
X1*X3	-0.009	±0.076	no
X1*X2	0.006	±0.080	no
X1*X5	-0.004	±0.077	no
X3*X5	unestimable		

Table F-12. For Response Y12 (= RtArmIT): Block-Plot-based Estimates of the 10 Unique Two-term Interactions for the Five Primary Factors

Interaction	Effect	95% Unc	Significant? (yes/no)
X1*X4	-105.88	±111.76	no
X2*X4	-81.54	±119.36	no
X3*X4	77.37	±142.56	no
X2*X5	77.37	±93.02	no
X2*X3	49.13	±122.59	no
X4*X5	49.13	±57.97	no
X1*X5	-40.79	±97.74	no
X1*X2	-32.12	±84.84	no
X1*X3	-23.71	±115.21	no
X3*X5	unestimable		

Table F-13. For Response Y13 (= LtArmIT): Block-Plot-based Estimates of the 10 Unique Two-term Interactions for the Five Primary Factors

Interaction	Effect	95% Unc	Significant? (yes/no)
X1*X4	-296.37	±359.44	no
X2*X4	-175.87	±308.61	no
X1*X5	140.79	±368.76	no
X3*X4	128.29	±382.64	no
X2*X5	128.29	±324.25	no
X1*X3	-94.38	±415.73	no
X2*X3	-67.38	±372.66	no
X4*X5	-67.38	±312.41	no
X1*X2	13.46	±348.80	no
X3*X5	unestimable		